

**PROCEEDINGS
OF
THE NINTH ANNUAL SUMMER
CONFERENCE**



**NASA/USRA UNIVERSITY
ADVANCED AERONAUTICS DESIGN PROGRAM
AND
ADVANCED SPACE DESIGN PROGRAM**

**Hosted by
NASA Lyndon B. Johnson Space Center**

**Houston, Texas
June 14-18, 1993**

WJ/D
~~INFORMATION SCIENCES LIBRARY~~
~~NASA LIBRARY~~
~~AMES RESEARCH CENTER~~
~~MOFFETT FIELD, CALIF.~~

NASA/USRA University Advanced Design Program, Summer Conference

~~TL
858
N27
1993
C.12SL~~

✓
NASA/USRA

UNIVERSITY ADVANCED DESIGN PROGRAM

PROCEEDINGS OF THE
9TH ANNUAL SUMMER CONFERENCE

June 14-18, 1993

Houston, Texas

NASA/USRA UNIVERSITY ADVANCED DESIGN PROGRAM
9TH ANNUAL SUMMER CONFERENCE

Funding for the NASA/USRA University Advanced Design Program is provided by the Office of Advanced Concepts and Technology, the Office of Aeronautics, and the Education Division at NASA Headquarters. The Universities Space Research Association (USRA) administers these funds through a contract (NASW-4435) with NASA's Education Division. Inquiries regarding the program may be directed to:

Dr. Vicki S. Johnson, Program Manager
Advanced Design Program
Universities Space Research Association
3600 Bay Area Boulevard
Houston, Texas 77058-3111
(713)244-2000
FAX (713)244-2006

FOREWORD

The NASA/USRA University Advanced Design Program was established in 1984 as an attempt to add more and better design education to primarily undergraduate engineering programs. The original focus of the pilot program encompassing nine universities and five NASA centers was on space design. Two years later, the program was expanded to include aeronautics design with six universities and three NASA centers participating. This year marks the last of a three-year cycle of participation by forty-one universities, eight NASA centers, and one industry participant.

The Advanced Space Design Program offers universities an opportunity to plan and design missions and hardware that would be of use in the future as NASA enters a new era of exploration and discovery, while the Advanced Aeronautics Design Program generally offers opportunities for study of design problems closer to the present time, ranging from small, slow-speed vehicles to large, supersonic and hypersonic passenger transports. The systems approach to the design problem is emphasized in both the space and aeronautics projects. The student teams pursue the chosen problem during their senior year in a one- or two-semester capstone design course and submit a comprehensive written report at the conclusion of the project. Finally, student representatives from each of the universities summarize their work in oral presentations at the Annual Summer Conference, sponsored by one of the NASA centers and attended by the university faculty, NASA and USRA personnel, and aerospace industry representatives.

As the Advanced Design Program has grown in size, it has also matured in terms of the quality of the student projects. The comprehensive final reports are distributed through the National Technical Information Service. However, the results of the studies reach only a small audience, principally those who attend the Summer Conference. In order to broaden the distribution, a Proceedings volume, which summarizes the project results and roughly parallels the Conference presentations, is published. The present volume represents the student work accomplished during the 1992-1993 academic year reported at the Ninth Annual Summer Conference hosted by NASA Lyndon B. Johnson Space Center, June 14-18, 1993.

ACKNOWLEDGMENTS

We are most grateful to the students, the university faculty, and their teaching assistants for the excellent technical work contained in this volume. We are also indebted to those individuals from NASA Headquarters and from the NASA centers who conceived the program in the beginning, have provided valuable guidance to both USRA and the universities throughout, and through their keen interest in the student projects, are in large part responsible for the boundless enthusiasm of the students.

—USRA Advanced Design Program Office

TABLE OF CONTENTS

Foreword	iii
----------------	-----

AERONAUTICS PROJECTS

ARIZONA STATE UNIVERSITY High-Speed Rotorcraft Design—Rotor/Wing Configurations	3
CALIFORNIA POLYTECHNIC STATE UNIVERSITY, SAN LUIS OBISPO Exploring Subsonic Flight of Advanced Commercial and Military Transports	15
EMBRY-RIDDLE AERONAUTICAL UNIVERSITY The Design of a Primary Flight Trainer Using Concurrent Engineering Concepts	26
GEORGIA INSTITUTE OF TECHNOLOGY—SCHOOL OF AEROSPACE ENGINEERING Integrated Design and Manufacturing for the High Speed Civil Transport	38
UNIVERSITY OF KANSAS Operational Design Considerations for an Oblique All-Wing Supersonic Transport	48
UNIVERSITY OF MICHIGAN Design of an Airborne Launch Vehicle for an Air Launched Space Booster	57
NAVAL POSTGRADUATE SCHOOL Aircraft Design at the Naval Postgraduate School: Tactical Waverider/Long-Range Cargo Aircraft	66
UNIVERSITY OF NOTRE DAME Gaining the Competitive Edge: Design for Manufacturing	81
OHIO STATE UNIVERSITY The Design of Three Experimental Hypersonic Test Vehicles	93
PURDUE UNIVERSITY The Design of an Ultra High Capacity Long Range Transport Aircraft	101
VIRGINIA POLYTECHNIC INSTITUTE AND STATE UNIVERSITY Design of a Vehicle-Based Intervention System to Prevent Ozone Loss	112
WORCESTER POLYTECHNIC INSTITUTE Design and Analysis of a Radio-Controlled Flying Wing Aircraft	124

SPACE PROJECTS

UNIVERSITY OF ALASKA, FAIRBANKS Wireless Space Power Experiment (WISPER)	135
UNIVERSITY OF ARIZONA Autonomous Space Processor for Orbital Debris	147
UNIVERSITY OF CALIFORNIA, LOS ANGELES Planetary and Asteroid Missions—Getting There	156

UNIVERSITY OF CENTRAL FLORIDA	
Design and Testing of a One-Third Scale Soyuz TM Descent Module.....	167
Spartan Conversion Project Super Loki Instrumentation	173
UNIVERSITY OF CINCINNATI	
Design of a Lunar Propellant Processing Facility.....	177
DUKE UNIVERSITY	
Radiation Shielding for Interplanetary Spacecraft.....	189
UNIVERSITY OF FLORIDA	
Bioregenerative Life Support Systems for Microgravity.....	200
FLORIDA A&M /FLORIDA STATE UNIVERSITY COLLEGE OF ENGINEERING	
Umbilical Support, Lunar Surface Emergency Shelter, and Robotic Arm for Lunar Surface Vehicle Projects.....	212
GEORGIA INSTITUTE OF TECHNOLOGY—GEORGE W. WOODRUFF SCHOOL OF MECHANICAL ENGINEERING	
Enabler: A Lunar Work Vehicle	222
UNIVERSITY OF IDAHO	
Wheeled Articulating Land Rover: WALRUS.....	227
IOWA STATE UNIVERSITY OF SCIENCE AND TECHNOLOGY	
Iowa Satellite Project.....	232
KANSAS STATE UNIVERSITY	
Human-Like Robots.....	246
UNIVERSITY OF MARYLAND, COLLEGE PARK	
MOOSE: Manned On-Orbit Servicing Equipment	258
MASSACHUSETTS INSTITUTE OF TECHNOLOGY	
Project Perseus: A Crew Return Vehicle for Space Station Freedom.....	269
UNIVERSITY OF MICHIGAN	
Project Gryphon: Air Launched Space Booster.....	274
Tethered Atmospheric/Ionospheric Research Satellite (AIRSAT).....	286
UNIVERSITY OF MINNESOTA	
Design of a Lunar Transportation System	297
NAVAL POSTGRADUATE SCHOOL	
NATSAT: A Multi-Purpose LEO Bus.....	310
Near-Earth Asteroid Rendezvous	318
OLD DOMINION UNIVERSITY	
Internal Combustion Engines on the Martian Surface	326
PENNSYLVANIA STATE UNIVERSITY	
A Mission to Mercury and A Mission to the Moons of Mars.....	338

UNIVERSITY OF TEXAS, AUSTIN—AEROSPACE ENGINEERING AND ENGINEERING MECHANICS LEO, Lunar, and Mars Projects.....	350
UNIVERSITY OF TEXAS, AUSTIN—MECHANICAL ENGINEERING Space Engineering Projects in Design Methodology.....	363
UNITED STATES NAVAL ACADEMY Remote Universal Naval Transponder.....	374
UTAH STATE UNIVERSITY Wheeled Experimental Surface Lunar Explorer (WESLE).....	298
VANDERBILT UNIVERSITY Stiffening of Deployable Space Booms..... Automated Protein Crystal Growth.....	396 403
VIRGINIA POLYTECHNIC INSTITUTE AND STATE UNIVERSITY Lunar UV/Optical/IR Long-Baseline Interferometric Arrays.....	408
UNIVERSITY OF WASHINGTON Project Hydreus: Mars Sample Return Mission Utilizing <i>in situ</i> Propellant Production.....	421
WEST VIRGINIA UNIVERSITY—ELECTRICAL AND COMPUTER ENGINEERING Various Applications of NASA's Capaciflector Proximity Sensor.....	438
WEST VIRGINIA UNIVERSITY—MECHANICAL AND AEROSPACE ENGINEERING The Preliminary Design of a Universal Martian Lander.....	445
UNIVERSITY OF WISCONSIN, MADISON Jupiter Exploration Using Fusion Rocket Integration (JEFRI)..... UW-3S900 Dark Horse: Joined Wing Global Transport.....	457 471
UNIVERSITY OF WISCONSIN, MILWAUKEE <i>Domus I and Dymaxion</i> : Two Concept Designs for Lunar Habitats.....	479
WORCESTER POLYTECHNIC INSTITUTE Evaluation of the Microgravity Ignition Experiment Prepared for the GASCAN II Project.....	490

Aeronautics Projects

HIGH-SPEED ROTORCRAFT DESIGN—ROTOR/WING CONFIGURATIONS

Arizona State University
Department of Mechanical and Aerospace Engineering
Tempe, AZ

Professors V. L. Wells and D. H. Laananen

Teaching Assistant Jian Shi

Abstract

The Advanced Design Program at Arizona State University has considered the design of high-speed rotorcraft which can take off and land vertically, yet can achieve relatively fast forward velocities. Two design missions were considered—a military ground attack mission and a civil commuter transport mission. The design groups selected the rotor/wing configuration for each of these applications. The design groups utilized their own software to perform design tradeoff studies to determine the optimum design point. Once the design points were determined, more detailed design of the various components was undertaken. The paper outlines the needs for a high-speed VTOL aircraft, and describes the aircraft designed to meet those needs. Several technology areas unique to the rotor/wing design are discussed.

Introduction

All Department of Defense (DOD) services, NASA and commercial enterprises have expressed interest in high-speed, Vertical Take-Off and Landing (VTOL) aircraft. Air Force studies indicate a clear requirement for a special operations aircraft with capabilities not available in any existing vehicle. Navy studies have focussed on the need to disperse air defense aircraft from carriers to smaller combat ships, dictating the need for VTOL capabilities. Additionally, in order to carry out the air defense mission, these aircraft must have the ability to fly high and fast. The reduced-size, future Army will have fewer helicopter assets with which to accomplish virtually the same missions presently assigned, resulting in the need for vehicles with increased speed and capacity for the necessary mobility and self-deployment capability.

NASA has had an interest in high-speed rotorcraft since the mid 1950's and has recently reem-

phasized study of these vehicles. Commercial interest in VTOL aircraft stems from the need to relieve airport congestion and to provide city-center to city-center transportation in a truly cost-effective manner. Such missions call for an aircraft which can hover with helicopter-like efficiency and cruise at speeds of 400 knots or more, well beyond the maximum possible for the V-22 tilt rotor aircraft.

The students involved in the first year of the NASA/USRA Advanced Design Program at Arizona State University have designed and analyzed two high-speed VTOL concepts, one of which satisfies the mission requirements for a civil transport, and the other fulfilling requirements for a military ground-attack vehicle. The mission statements were adapted from the NASA "Technology Needs for High-Speed Rotorcraft" program.

Ten students who expressed keen interest in design were selected from among the top seniors in Aerospace Engineering to participate in a year-long design sequence. These students made up two of the design groups in the aerospace engineering capstone design course in the Fall semester. During the semester, each group completed the conceptual design of an aircraft meeting the requirements for one of the two mission statements. In the spring, these students enrolled in a special design course created for the program. Tasks during the second semester included more detailed design and verification of the suitability of the original design point. In particular, issues unique to the chosen configurations were studied.

Though the mission requirements for the two groups varied, both determined that a rotor/wing configuration best suited their design goals. This type of aircraft has a large, stiff lifting surface which rotates like a helicopter blade for vertical flight, but which can be stopped to act as a fixed wing once the vehicle reaches a certain "conversion" speed. Virtually every aspect of the design of this type of vehicle includes some innovation. Some examples of

those areas which have been studied include: the design and testing of midchord-symmetric airfoils, analysis of the conversion process from vertical to forward flight and *vice versa*, investigation into the characteristics of a convertible engine which can act as both a turboshaft and a turbofan, design of a rotor hub which includes conventional collective and cyclic controls as well as mechanisms for locking out pitching and flapping motions and braking, and the structural design of a hub/rotor combination which must also act as a wing.

The design teams selected the rotor/wing configuration from among several possible solution configurations. Figure 1 shows those concepts considered by the group designing the civil transport aircraft. The groups evaluated each candidate vehicle according to a set of predetermined criteria which had each been assigned a weight function according to perceived importance to the design. The decision matrix resulting from this exercise is given in table 1. As shown in the matrix, the rotor/wing design obtained the highest score, followed fairly closely by the tilt-rotor. The military ground-attack design team followed a similar procedure, evaluating some of the same vehicle concepts and some different ones. Because of the differing missions, the evaluation criteria included such attributes as weapon system integration, survivability, and signature production. Nevertheless, the rotor/wing configuration scored highest in the selection process.

The original rotor/wing appeared in the mid-1960's as the Hughes Rotor/Wing. The concept consisted of a large, roughly circular hub with three stub blades, attached to a fuselage. In order for the aircraft to take off and land vertically, the hub rotated using reaction drive where hot gases exhausted from the turbojet engine were ducted through the hub and out the blade tips, and the blades produced enough lift to raise the vehicle. When the aircraft achieved a high enough velocity, the blade rotation speed was reduced, the hub was locked into place, and the aircraft flew in fixed-wing mode using the now-stationary blades as a wing. During conversion from rotary- to fixed-wing flight, the weight of the aircraft had to be carried by the center hub—not a very efficient lifting device. The Hughes Rotor/Wing never flew, but it was extensively tested in the wind tunnel during its six-year development program.

A similar concept to the rotor/wing was the Navy-sponsored X-Wing. Though the X-Wing looked similar to a rotor/wing, the former aircraft was to utilize a very complex circulation-control system to enact cyclic and pitch control of the blades

during rotary-wing flight, and to aid in the aerodynamic performance of the midchord-symmetric airfoils used on the rotor. The circulation-control system was very complex and ultimately led to cancellation of the X-Wing program.

Recently, McDonnell Douglas Helicopter Company has engaged in the development of a two-bladed rotor/wing aircraft.[1] This vehicle uses reaction drive, as did the former Hughes Rotor/Wing, but it does not rely on the large lifting hub to support the aircraft during conversion. This Canard Rotor/Wing (CRW) has a forward lifting surface (a canard) as well as a large horizontal tail to carry the lift during the conversion process. Thus, the CRW takes advantage of much more efficient lift production than the Hughes Rotor/Wing for conversion, and does not rely on very complex circulation control as did the X-Wing. Figure 2 shows a comparison of the Hughes Rotor/Wing, the X-Wing, and the CRW.

The rotor/wing vehicles designed by the ADP students at ASU differ from all of the above aircraft. Unlike the Hughes Rotor/Wing and the CRW, both ADP designs utilize direct rather than reaction drive. However, unlike the X-Wing, neither of the two new designs have incorporated circulation control, the designers opting instead for conventional helicopter controls. The remainder of this paper outlines the major attributes of each of the aircraft designed by the ADP student groups and then discusses the solution to some unique problems encountered in their design.

Rotor/Wing Designs

Civil Transport

Mark Meyer, group leader, Muhammed Budi Kurnia, Jack Lo, Dan Lohavanijaya, Alex Pozzi

The civil transport VTOL aircraft was designed for the following primary mission:

- Takeoff and hover out of ground effect (HOGE) for 1 minute at sea level international standard atmosphere (SLISA) + 15° C.
- Fly to conversion speed and convert to cruise configuration in 1g flight at SLISA + 15° C.
- Climb to altitude for best range.
- Cruise 600 nautical miles (NM) at 350 NM/hr true air speed (KTAS) at cruise altitude.

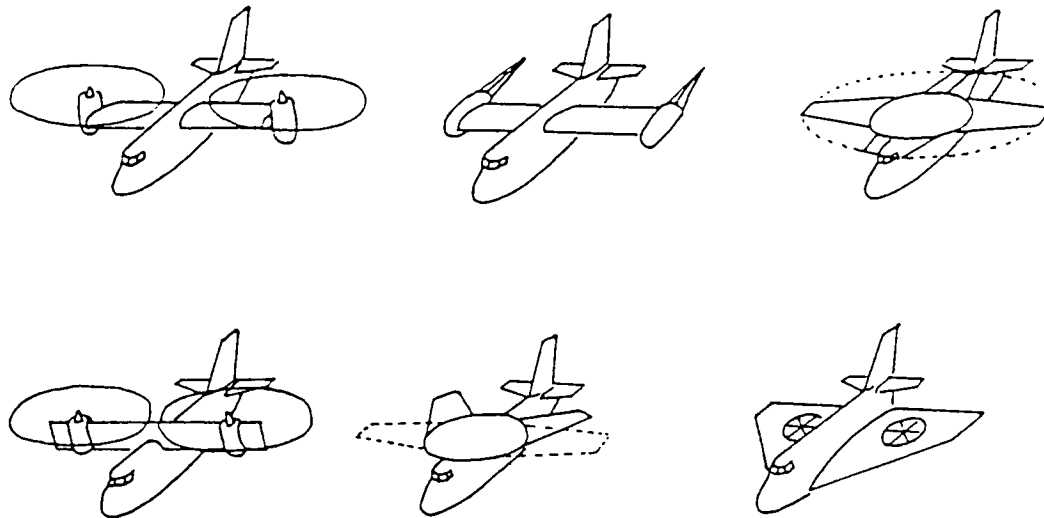


Figure 1: Candidate Configurations

Category	Concept	Tilt Wing	Tilt Rotor	Folding Rotor	Rotor/ Wing	Variable R/W	Rotor-in- Wing
Stability/Control (Conversion) x10		8 80	8 80	8 80	7 70	7 70	10 100
Weight x10		6 60	7 70	7 70	10 100	9 90	3 30
High Speed Performance x10		8 80	7 70	7 70	10 100	10 100	3 30
Aerodynamics x8		8 64	8 64	7 56	10 80	10 80	6 48
Structures x8		8 64	9 72	10 80	6 48	5 40	9 72
Safety x6		7 42	8 48	8 48	9 54	9 54	10 60
Risk x6		10 60	10 60	7 42	7 42	6 36	6 36
Complexity x4		8 32	9 36	9 36	7 28	6 24	10 40
Propulsion x4		10 40	10 40	8 32	8 32	8 32	8 32
Total		522	540	514	554	526	448

Table 1: Decision Matrix for Candidate Configurations

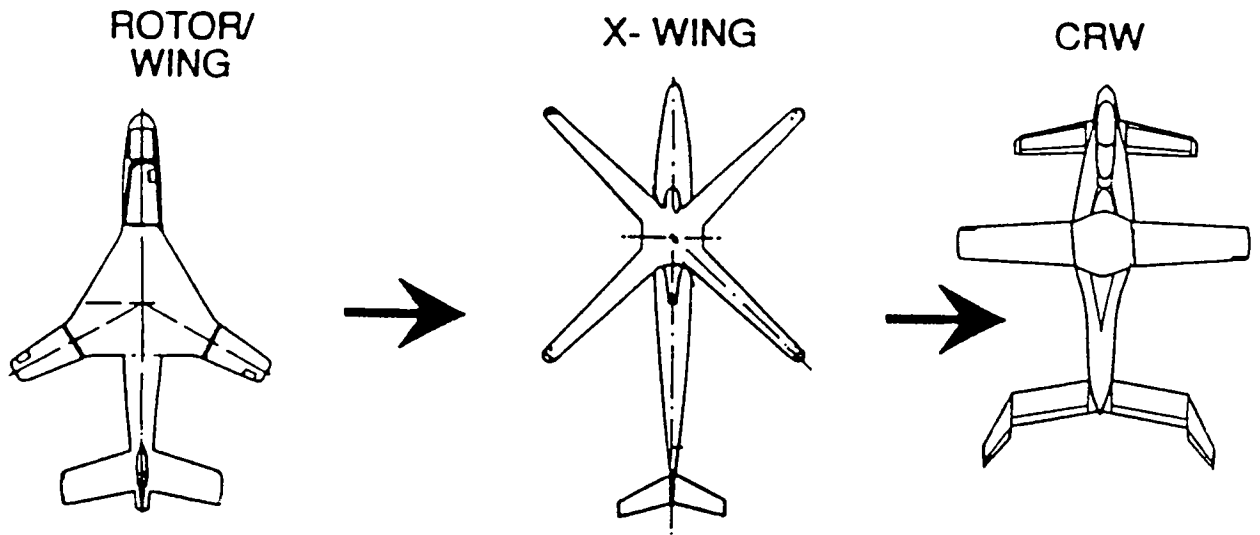


Figure 2: Previously Designed Rotor/Wing-Type Configurations

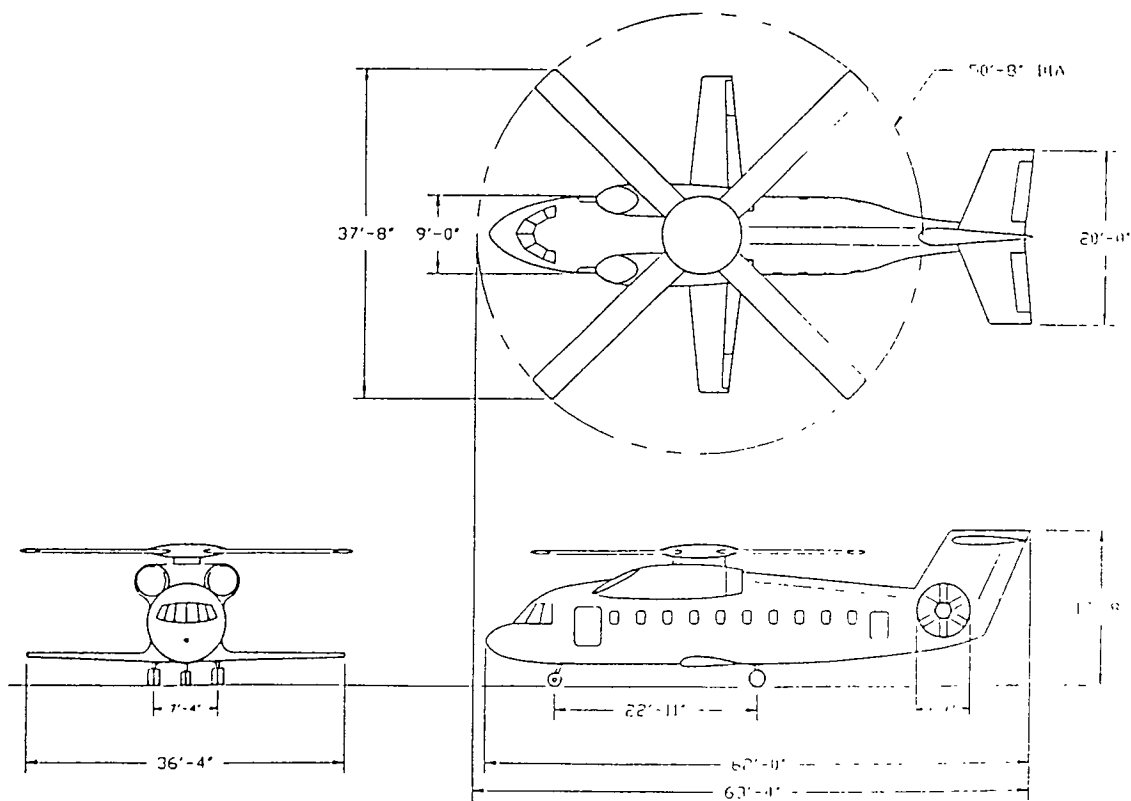


Figure 3: Hummingbird VTOL Commuter Transport

- Decelerate and descend to sea level.
- Fly to conversion speed and convert to hover configuration in 1g flight at SLISA + 15° C.
- Land with 10% mission fuel reserve.

The aircraft must carry:

- 6000 lb. payload (30 passengers)
- Fixed equipment (not including controls) 4000 lbs.
- Avionics 800 lbs.
- Operating items 625 lbs.

In addition to the mission requirement, the aircraft must meet the following performance constraints:

- In hover configuration, SLISA vertical rate of climb (VROC) ≥ 400 ft/min.
- In cruise configuration, perform a 1.5g maneuver at takeoff gross weight, constant cruise airspeed (350 KTAS), and constant cruise altitude.

The *Hummingbird* is a VTOL commuter transport meeting all of the above specifications. The fuselage of the aircraft is similar in size and layout to many common commuter aircraft. The aircraft has a four-bladed rotor/wing mounted on the top of the fuselage which rotates to provide lift for vertical and low-speed forward flight, and acts as a fixed wing for high-speed forward flight. The blades of the rotor/wing have a midchord-symmetric cross section so that the leading and trailing edges are interchangeable. An additional small, low wing is located underneath the rotor. This wing, outfitted with high lift devices, provides the lift required to maintain the aircraft in 1g flight during conversion from one flight mode to the other. The aircraft is powered by two convertible engines capable of producing both shaft horsepower and jet thrust. The engines are mounted near the top of the fuselage close to the transmission and drive system for the rotor/wing. The aircraft has standard horizontal and vertical tails in the T-configuration to provide stability and trim in all flight modes. Anti-torque thrust in rotary-wing mode is provided by a fan built in to the vertical tail surface. Figure 3 shows the main features and dimensions of the *Hummingbird*.

The *Hummingbird* was sized using a Quattro Pro computer model of the aircraft which estimates the component weights, the hover horsepower and cruise

thrust required (engine size), the wing size, the rotor diameter and aspect ratio, the aircraft parasite and induced drag, and the total fuel required for the design mission. The important design parameters, which were varied to determine the best design, include:

- rotor disk loading (gross weight/disk area)
- rotor tip speed
- a measure of rotor blade average lift coefficient, C_T/σ (where C_T is the rotor thrust coefficient and σ is the rotor solidity given by number of blades (B) multiplied by the blade chord (C) divided by π and the blade radius (R))
- wing aspect ratio (wing span squared/wing area)
- wing maximum lift coefficient
- conversion speed

The design code utilizes "rubber" convertible engines based on data provided by McDonnell Douglas Helicopter Company. Losses due to installation, transmission, bleed air, and accessories are estimated at 7% of the total engine power or thrust available. The drag is determined using a standard component drag buildup method described by Raymer[2]. Induced drag is estimated using the biplane equation given by von Kármán and Burgers[3], which depends on the vertical and horizontal separation of the lifting surfaces, the share of the lift carried on each, and the spans of each. The component weights were estimated using several statistically-based sources. These include the method of Raymer[2], the method found in the VASCOMP computer sizing code[4], and a hub/blade weight estimation method supplied by McDonnell Douglas Helicopter Company.

Table 2 shows a component weight breakdown for the *Hummingbird*. As shown in the table, the design gross weight for the vehicle is 40,386 lb. with an empty weight of 28,467lb. To complete the design mission, 5294 lb. of fuel are required.

Military Ground Attack Aircraft

Anthony T. Glinka, group leader, Scott A. Capehart, Daryl J. Hilderbrand, Eric W. Lloyd, Thurston J. Ruggiero

The military ground attack aircraft mission consists of the following:

- Entire mission at 4000 ft. altitude and 95° F.

Weight Breakdown	
Group	Weight (lbs)
Fixed Wing	1082
Main Rotor	3393
Drive System	5097
Tail Fan	679
Engines	2985
Body	5170
Horizontal Tail	352
Vertical Tail	104
Landing Gear	1065
Nacelles	854
Engine Controls	18
Starter	89
Fuel System	265
Flight Controls	2515
Avionics	800
Fixed Equipment	4000
Empty Weight	28467
Payload	6000
Operating Items	625
Mission Fuel	5294
Gross Weight	40386

Table 2: *Hummingbird* Component Weight Breakdown

- Take off and HOGE for 1 minute.
- Fly to conversion speed and convert to cruise configuration in 1g flight.
- Cruise out 150 NM at $V_{99\%}$.
- Dash 50 NM at 400 KTAS and Intermediate Power Rating (IPR).
- Convert to hover mode.
- Nap-of-the-Earth (NOE) maneuver including 15 minutes HOGE and 15 minutes at 40 KTAS.
- Attack target at IRP for 5 minutes without dropping weapons.
- Convert to cruise mode.
- Cruise 200 NM at $V_{99\%}$ back to base.
- Fly to conversion speed and convert to hover configuration in 1g flight.
- HOGE for 1 minute.
- Land with 10% mission fuel reserves.

The aircraft must carry the following:

- Internal payload of 2000 lb. and external payload of 1000 lb.
- Fixed equipment 2000 lb.
- Mission equipment 2900 lb.
- Crew 470 lb.

Other performance requirements include:

- Sustained g loading of -0.5 to 3.5 in helicopter mode and -1.5 to 5.0 in fixed-wing mode.
- Ferry mission of 1260 NM unrefueled.
- VROC 800 ft/min

The AV-13 *Mohave* is a tandem-seat, twin-high-engine attack aircraft which can hover with helicopter-like efficiency, yet achieve dash speeds in excess of 500 kts. Its capabilities dovetail well with the reduced-size, future military, and it meets all requirements outlined above. The aircraft can deliver 3000 lb. of ordnance to a target which is 1200 NM distant without need for refueling. The *Mohave* is a three-surface aircraft, having a canard with flaps, a horizontal tail with flaps and ailerons, and a two-bladed, teetering rotor/wing. The vertical tail has a

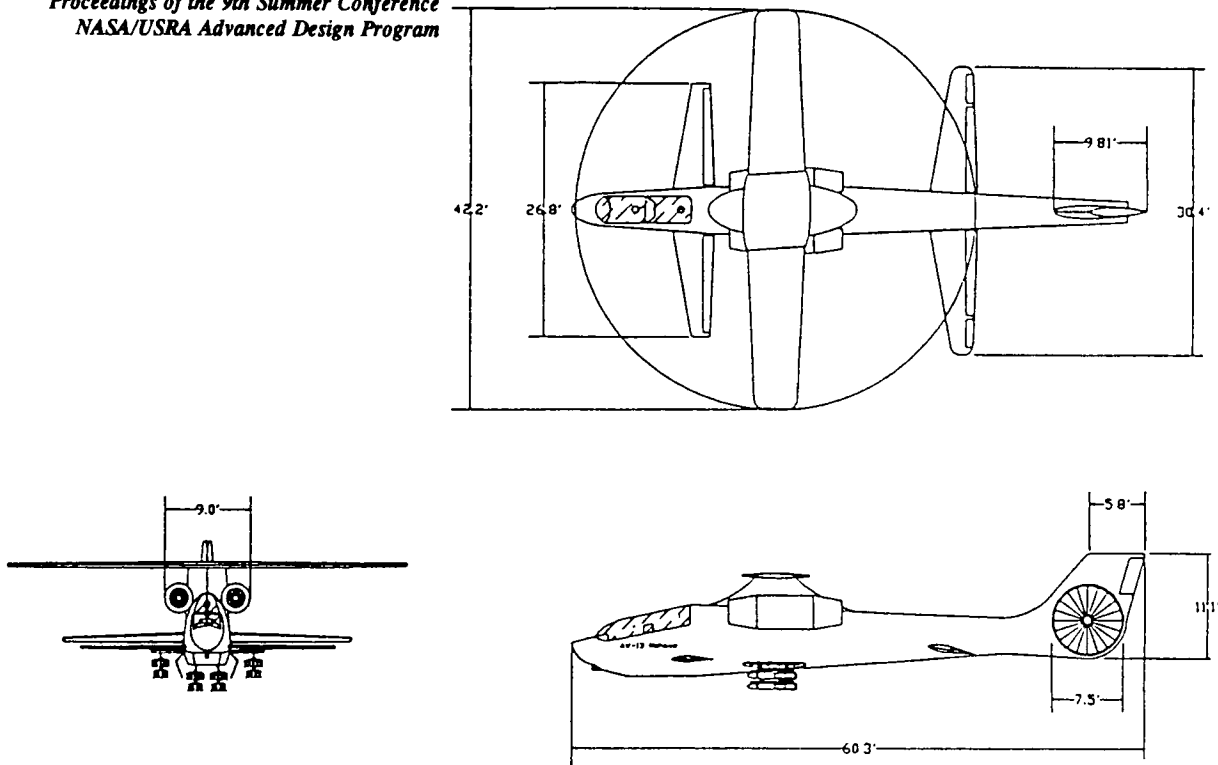


Figure 4: AV-13 *Mohave* Ground Attack Aircraft

conventional rudder and contains within it an anti-torque fan. Figure 4 shows a three-view drawing of the *Mohave*.

The crew compartment houses both pilot and co-pilot and provides easy access to all of the necessary instruments and controls. Measures were taken to give the pilot 15° of over-nose vision, fully satisfying the 11–15° military requirement. Since the *Mohave* must perform as a ground attack aircraft, the cockpit is designed so that the over-the-side vision requirement of 40° is met for the pilot.

The *Mohave* can accommodate a variety of weapon systems. Weapons are located both externally on pylons and internally in a weapons bay. Options for the external weapons include Hellfire air-to-ground missiles, rocket pods, or Maverick missiles. The internal weapons bay may house either rocket pods or Hellfire missiles. The internal storage area can be used as an additional fuel storage compartment for extended-range missions. A 30 mm turreted cannon is located near the nose of the aircraft.

The conceptual design for the *Mohave* was developed through an iteration between configuration layout requirements and a design sizing code written in C. Results of the design code were used to construct carpet plots which designated a feasible design space. By choosing the lowest weight aircraft

within the feasible design space which also satisfies the constraints on configuration layout (such as visibility requirements), the best design for the military ground attack mission was obtained.

The design gross weight for the *Mohave* is 27,972 lb., with a total weight empty of 19,870 lb. The aircraft requires 4631 lb. of fuel to complete the design mission. Table 3 gives a component weight breakdown for the *Mohave*. Table 4 gives the important performance characteristics of the aircraft.

Technology Developments for High-Speed Rotorcraft

Conversion Analysis

One of the most important performance attributes for a successful high-speed rotorcraft is the ability to convert smoothly from rotary-wing to fixed-wing flight and *vice versa*. Both of the ADP designs are intended to convert in a similar manner; the following discussion pertains to the civil transport in particular.

The convertible engines used in this design are one of the key elements in providing the desired smooth conversion. The design point analysis showed that

WEIGHT BREAKDOWN		
COMPONENT	W lbs	PERCENT
STRUCTURES GROUP		
1 ROTOR-WING	2230.6	7.97
2 HUB	1424.7	5.09
3 VERTICAL TAIL + FAN	143.0	0.51
4 HORIZONTAL TAIL	539.9	1.93
5 FUSELAGE + BOOM	3421.7	12.23
6 MAIN LANDING GEAR	596.8	2.13
7 NOSE LANDING GEAR	298.4	1.07
8 ENGINE SECTION	63.7	0.23
9 FIREWALL	90.4	0.32
10 CANARD	356.6	1.27
PROPULSION GROUP		
11 ENGINES	2170.7	7.76
12 DRIVE SYSTEM	2679.3	9.58
EQUIPMENT GROUP		
14 FLIGHT CONTROLS	627.1	2.24
15 FIXED EQUIPMENT	2000.0	7.15
16 AVIONICS	327.8	1.17
17 MISSION EQUIPMENT	2900.0	10.37
TOTAL WEIGHT EMPTY	19870.6	71.04
USEFUL LOAD GROUP		
18 CREW	470.0	1.68
19 FUEL	4631.4	16.56
20 AMMUNITION	1200.0	4.29
21 EXTERNAL WEAPONS	1000.0	3.57
22 INTERNAL WEAPONS	800.0	2.86
TAKEOFF GROSS WEIGHT	27972.0	100.00

Table 3: AV-13 Mohave Component Weight Breakdown

Airplane Mode

Maximum Velocity		
@ Pmax	510.52 kt	861.76 fps
@ IRP	529.25 kt	893.37 fps
Best Range		
Velocity	256.08 kt	411.48 fps
Cruise-climb	1238.90 nmi	
Const. altitude	1177.79 nmi	
Max. Endurance	5.586 hr	
Min. Drag Velocity	194.58 kt	328.84 fps
Stall Speed	150.98 kt	254.83 fps
Lift-off Speed	181.18 kt	305.80 fps
Take-off Distance	1.048 nmi	6367.57 ft
Steepest Climb		
R/C	53.79 fps	3227.4 fpm
Velocity	328.84 fps	194.58 kt
γ	9.42°	
Fastest Climb		
R/C	70.11 fps	4206.6 fpm
Velocity	519.70 fps	307.88 kt
γ	7.75°	
Ceiling	41,654.52 ft	
Helicopter Mode		
Max. Downwash	72.18 fps	
Velocity		
Figure of Merit	0.6956	
Maximum Vertical	13.64 fps	818.23 fpm
Climb Velocity		

Table 4: AV-13 Mohave Performance Characteristics

the engines were sized by the 1.5g maneuver constraint, which means that there is an excess of power available in rotary-wing mode. Therefore, some of the power can be diverted to thrust even while the aircraft is hovering, causing the aircraft to begin forward flight. As the aircraft gains speed, the wing begins to provide lift, which off-loads the rotor and allows even more power to be diverted to thrust. Once the aircraft reaches the conversion speed, the wing carries the entire aircraft weight. At this point, the rotor is disengaged from the driving mechanism, and the gimbaling motion of the hub is locked. The rotor brake is applied, and, once the rotor is stopped, it is locked into place in an X-Wing configuration. At this time, the high-lift devices on the wing are retracted, and the aircraft flies in fixed-wing mode, sharing the lift between the rotor and the wing.

The feasibility of this conversion process was verified by examining the forces acting on the aircraft and the engine output available at all points along the flight trajectory. These computed forces, along with the engine data, were used to determine a suitable schedule for diverting the power into thrust. Figure 5 shows the wing lift and rotor thrust tradeoff as a function of velocity from takeoff to conversion and cruise speed. Figure 6 shows the rotor horsepower required and the jet thrust available vs. velocity for the same conditions.

Hub Design

In order to enact the conversion sequence described above, the rotor hub must be designed to slow and stop the rotor, to disable the teetering mechanism, to lock the rotor in a specified position, and to keep the blades from pitching in fixed-wing mode. Both rotor/wing designs will require similar function from the hub. The following description pertains specifically to the ground attack vehicle.

The disc braking system is hydraulically operated and will stop the rotor within 40 seconds. It is made of steel and weighs a total of 67 lb. The positioning system consists of locking pins which will prevent the rotor from moving during fixed-wing mode, and a sensor which detects the position and speed of the rotor shaft during braking. This positioning system is disengaged during rotary-wing mode, and allows the rotor shaft to spin freely. During braking, the sensor detects a rotor angular velocity of 10 rpm, and then signals the braking system to stop the rotor in its fixed-wing position. Once the rotor angular motion has stopped, locking pins move into "V" shaped slots in the disc brake.

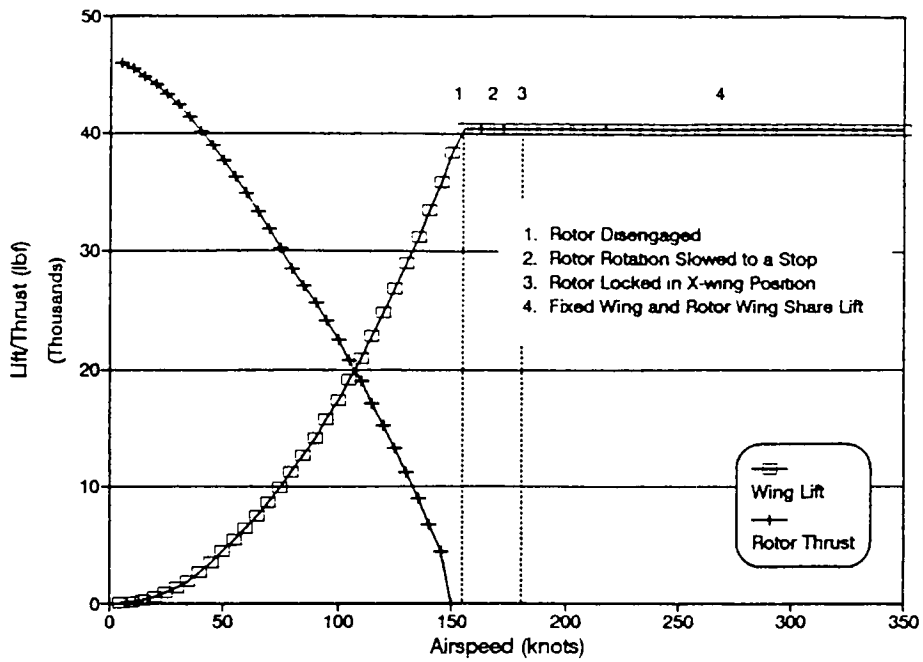


Figure 5: Wing Lift and Rotor Thrust from Takeoff to Cruise

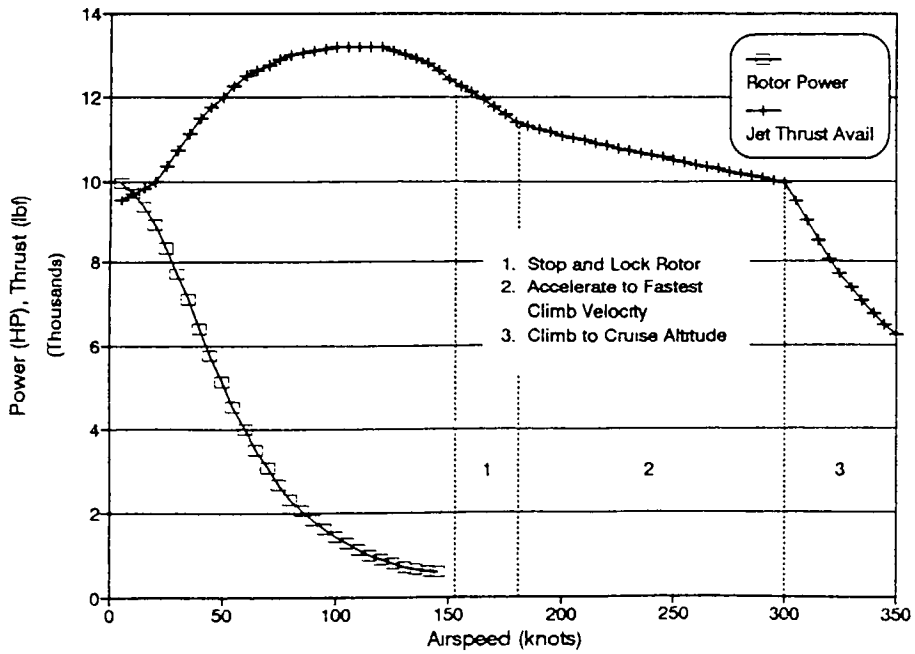


Figure 6: Horsepower Required and Thrust Available from Takeoff to Cruise

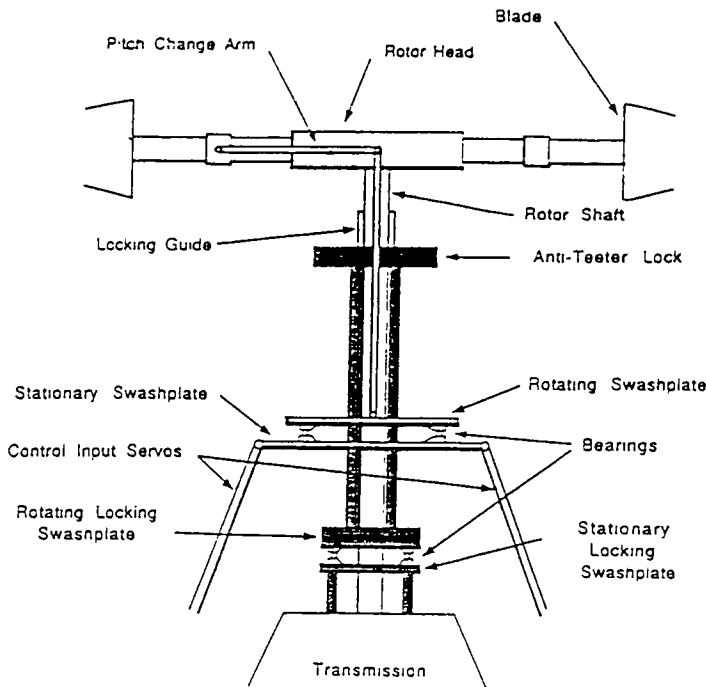


Figure 7: Locking Mechanism (Rotary-Wing Mode), Front View

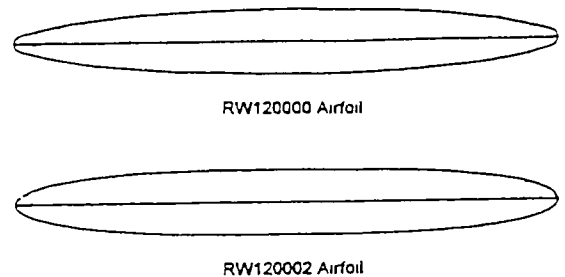


Figure 9: Midchord Symmetric Airfoils

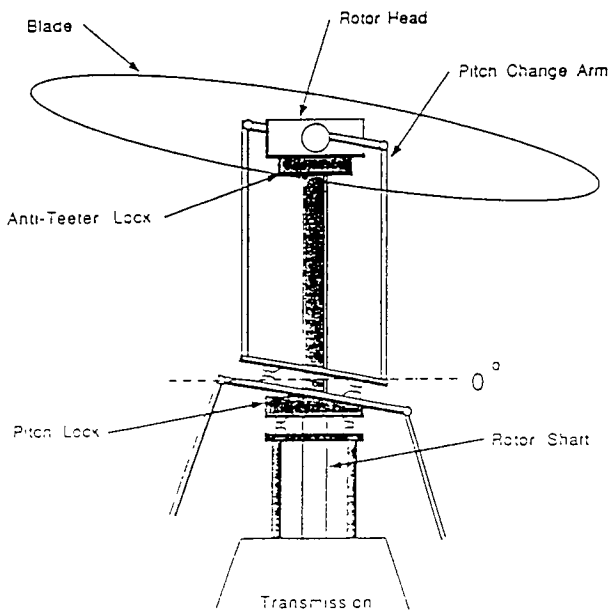
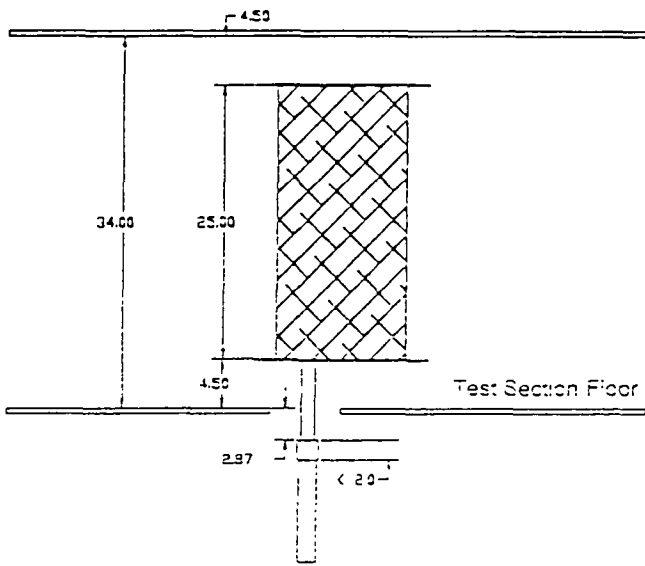


Figure 8: Locking Mechanism (Fixed-Wing Mode), Side View

The anti-teetering and pitching mechanism is designed to prevent the rotor/wing from teetering or pitching, but to allow the rotor to have an angle of attack relative to the fuselage in fixed-wing mode. During rotary-wing mode, the locking mechanism will be in the position shown in fig. 7, which gives a front view of the hub. The anti-teeter lock is a bar which will rotate with the rotor shaft. The anti-teeter lock can also move up and down the shaft by means of the stationary swashplate control arms and the locking guides. The mechanism is designed to allow the rotor head to teeter up to 15° above and below the horizontal with no interference during rotary-wing mode. During fixed-wing flight, the anti-teeter lock will move into the position shown in the side view of the hub depicted in fig. 8. The anti-teeter lock is positioned against the rotor head and prevents the hub from teetering. The rotating and stationary swashplates are fixed at the zero degree position by means of the pitch lock. This allows the rotor blades to symmetrically pitch relative to the fuselage utilizing the cyclic control.

Midchord-Symmetric Airfoil Analysis

In order for the rotor/wing to operate as both a rotating and a fixed lifting surface, its airfoil must be



Dimensions are in inches

Figure 10: Schematic of Airfoil Model in the Wind Tunnel

symmetric about the midchord. Little information is available concerning midchord-symmetric airfoils, so wind tunnel testing and numerical analysis were scheduled in order to determine the characteristics of these sections. The tested airfoil was a 12% thick ellipse, designated the RW120000. A modified ellipse with increased bluntness of the leading and trailing edges is scheduled for future testing. Figure 9 shows the profiles of these two airfoils, along with the locations of the pressure taps on the wind tunnel models. Figure 10 represents the model in the Department of Aeronautical Technology Wind Tunnel at ASU. The models were tested at an average velocity of 150 ft/sec, an average Reynolds number of 790,000, and a Mach number of .13.

Figure 11 shows lift coefficient vs. angle of attack for the RW120000 airfoil. The wind tunnel data is from both a force balance and the pressure taps. The numerical data comes from a Navier-Stokes solver. The computations predict a higher $c_{l,max}$ than does the wind tunnel. Some possible reasons for this are that the model has some flaws, particularly around the leading edge which could greatly affect the behavior at high angles of attack. In addition, there was some evidence of three-dimensional flow on the model which could

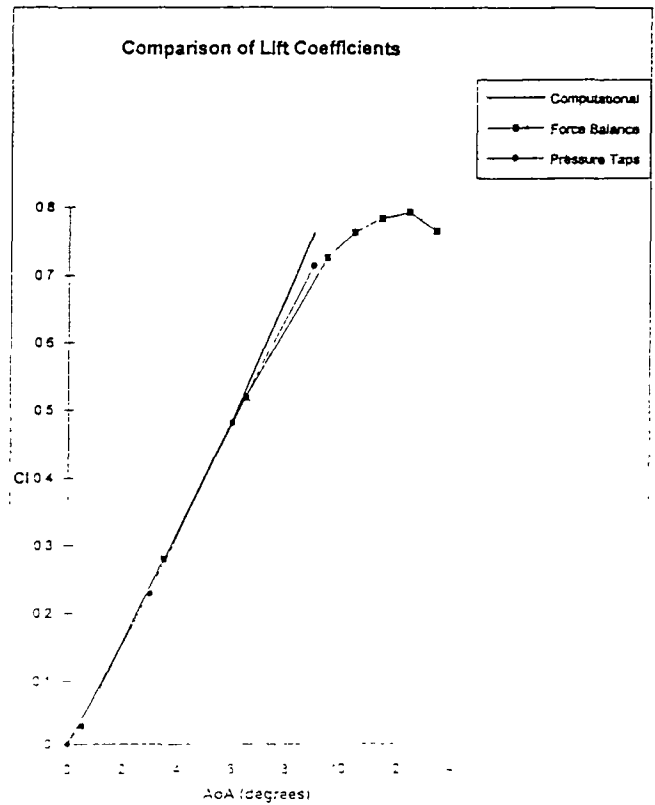


Figure 11: Lift Coefficient vs. Angle of Attack, 12% Ellipse

also reduce the maximum lift.

Conclusions

Two rotor/wing aircraft have been designed, one which satisfies the mission requirements for a military ground attack aircraft, and one which meets the specifications for a civil commuter transport. Both aircraft can hover with near helicopter-like efficiency, but can also cruise at speeds up to twice as fast as the most swift helicopter. Several specific technology areas have been addressed—these represent problem areas unique to rotor/wing aircraft. Further development is necessary in order to proceed to the manufacturing of such aircraft, but the analysis indicates a good probability that the technological barriers—such as conversion from one flight mode to the other—can be overcome. The rotor/wing represents a useful and viable concept which should be considered further for high-speed VTOL missions.

Acknowledgements

The NASA/USRA Advanced Design Program is gratefully acknowledged for their support. Dr. Jack Rutherford of McDonnell Douglas Helicopter Company provided invaluable and continuous support in the form of lectures, material, design mentoring, and constructive criticism. The class could not have succeeded without him. The students of the Mechanical Engineering design course, MAE 443, provided help in the hub design. Mr. Bill Crossley of MDHC and ASU provided advice and support, particularly in areas relating to rotor/wing weight estimation. Also, the ASU Advanced Design Program would like to thank Dr. Robert Stroub of NASA Ames Research Center for acting as our NASA Center representative.

References

- [1] Rutherford, John W, O'Rourke, M., Lovenguth, M., and Mitchell, C., Conceptual Assessment of Two High-Speed Rotorcraft, *Journal of Aircraft*, Vol. 30, March-April 1993, pp. 241-247.
- [2] Raymer, D. P., *Aircraft Design: A Conceptual Approach*, AIAA Press, 1989.
- [3] von Kármán, Th. and Burgers, J. M., General Aerodynamic Theory—Perfect Fluids, In Du-

rand, W. F., editor, *Aerodynamic Theory, Volume II*, Guggenheim Fund for the Promotion of Aeronautics, 1934.

- [4] Schoe, Allen H., Rosenstein, Harold, Stanzione, Kaydon, and Wisniewski, John S., *User's Manual—VASCAMP II*, Boeing Vertol, 1980.

EXPLORING SUBSONIC FLIGHT OF ADVANCED COMMERCIAL AND MILITARY TRANSPORTS

California Polytechnic State University, San Luis Obispo
Aeronautical Engineering Department
San Luis Obispo, California

Professor Robert van't Riet
Danielle Soban and Ty Hoang, Teaching Assistant

Abstract

This year Cal Poly challenged 37 students (six design teams) with four modern subsonic transport projects. Two groups chose to tackle the Boeing 737 and McDonnell Douglas MD-90 series replacement. One group took the challenge for a new mid-size (Boeing 767) commercial transport. A fourth group attempted to market an 800 plus passenger (PAX) aircraft that would rival Boeing's and Airbus' upcoming mega-transport. Finally, the next two groups were given the problem of designing a global range military transport with a 800,000 pounds cargo capacity.

Their solution includes ample use of low and high risk technologies. These include: higher usage of composites, more efficient propulsion units, high lift devices and unique configurations.

Introduction

The six design project presented in this paper is a culmination of Cal Poly's 1992/1993 Flight Vehicle Design senior design class. The design class' project varies from year to year. This year the students were given the task of designing the next generation of commercial and military subsonic transport. Summaries of the six design projects are presented in this report, from small to large commercial transports to the heavy military lifters.

The 100-150 Passenger Solution

The AC-120 Advanced Commercial Transport

Design Team: AeroCom

Aircraft Name: AC-120

Team Members: David Duran, Ernest Griffin, Saul Mendoza, Son Nguyen, Clemm Noernberg, and Tim Pickett.

The main objective of this design is to fulfill the need for a new airplane to replace the aging 100 to 150

passenger, 1500 nautical mile aircraft such as the Douglas DC9 and Boeing 737-100 airplanes. After researching the future aircraft market, conducting extensive trade studies and analysis of different configurations, a final design was achieved. The AC-120's (Figures 1 and 2) main design features include the incorporation of a three lifting surface configuration which is powered by two turboprop engines. The AC-120 is an economically sensitive aircraft which meets the new FAA Stage 3 noise requirements, and has lower NOx emissions than current turbofan engine airplanes. The AC-120 also improves on contemporary aircraft in passenger comfort, ease of manufacturing, and lower operating costs.

The AC-120 is a commercial transport which has the distinct feature of using a three lifting surface design. This configuration was chosen to allow for a reduction in wetted surface area and trim drag. The entire span of the canard is flapped which helps achieve higher lift coefficients and smaller control surface areas. The plane cruises at a speed of Mach .68 at an altitude of 29,000 feet.

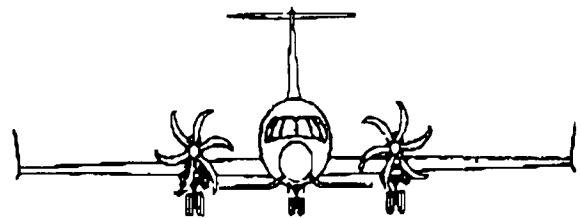


Figure 1: Front View

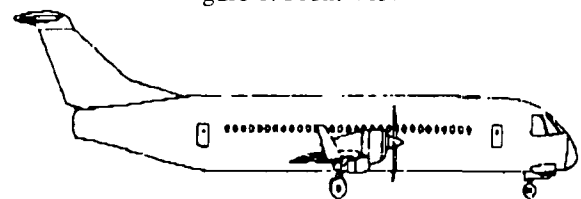


Figure 2: AC-120 Side View

The AC-120 uses a supercritical airfoil and has wing aspect ratio of 9, with a wing loading of 98.6 pounds per square foot. The airfoil chosen allows for a larger fuel volume and gives the plane a range (with maximum cargo) of 1550 nautical miles. This range allows the AC-120 to fly from Los Angeles to Chicago non-stop, giving it the flexibility to not only be a short range aircraft but also capable of flying longer ranges.

The wing span (Figure 3) is 97.7 feet and has 0 degrees of sweep at the quarter chord. The leading edge sweep is 3.18 degrees and has no leading edge lift devices to keep manufacturing cost low. Single slotted Fowler flaps are used along with outboard ailerons. The placement of the ailerons, the outboard sections of the wing allow the pilots to use them for the purposes of trim and lateral control when the auto pilot is engaged. Spoilers are used to during landing to increase the aircraft's decent into crowded airspace or when landing in urban areas.

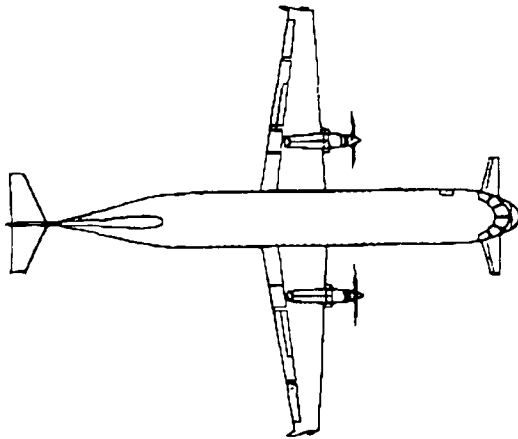


Figure 3: AC-120 Top View

The propulsion for this aircraft is provided by two turboprop engines using swept-blades. Currently there is no turboprop engine capable of producing the horsepower required (8,500 HP) to power a twin engine transport the size of the AC-120. Several engines do exist which possible derivatives could be created, such as the Allison GMA 2100 Turboprop. A predicted derivative of the GMA 2100 needed to power the AC-120 would need to have an engine diameter of 54 inches, a length of 140 inches, dry weight of 2010 pounds, and operate with a specific fuel consumption of .41 lbs/hp/hr. The propeller diameters and engine RPM at cruise were determined by using Hamilton Standard propeller performance charts, with the tip Mach number scaled down by the cosine of the tip sweep. Estimated propeller diameters were found to be 12-14 feet and engine RPM

at cruise to be 1200 ~ 1500 with an efficiency of 0.8. The reason for the selection of turboprops was due to the advantages they have over turbofans. Examples of these advantages are lower emissions, reduced ground handling expense and reduced maintenance and acquisition cost.

The AC-120 comes in two different passenger seating arrangements; a mixed and an all tourist configuration. The mixed class layout is configured to 110 passengers, 10 seats in business class and 100 in tourist for a tourist arrangement. The business class seats are situated in an a four abreast arrangement and are in a 36 inch pitch width seats being 21 inches wide and have 25 inch aisles. This arrangement provides a comfort equal to that of the Boeing 747-400 first class seating. The economy seats are 18.5 inches wide, have 18 inch wide aisles and are at a 31 inch seat pitch arranged six abreast. The 120 passenger layout is arranged in 20 rows of seats in a 6 abreast configuration and are in a 31 inch seat pitch. The seat width is similar to those in the mixed class configuration. At a width of 18.5 inches and 18 inch aisles, the all tourist class layout provides the widest economy seats available, comparable to only the economy seats to be found in the Boeing 777.

The acquisition cost for the AC-120 is 24.5 million dollars. This price kept low due to the aircraft's use of inexpensive aluminum and avoided the use of expensive composites. Currently the AC-120 operates at cost of 6 cents per passenger mile (USD) for a 1500 nautical mile and the cost rises to 7 cents for a 800 nautical mile mission.

The AC-120 use of swept blade technology allows it to beat existing turbofans with a fuel savings of 30%. Along with the low drag to the three lifting surface design, high passenger comfort, low unit and operating cost makes the AC-120 a strong player in already crowded aircraft market.

The SA-150 Advanced Commercial Transport

Design Team: Weasel Works

Aircraft Name: SA-150

Team Members: Kevin Alkema, Mike Comeaux, Tim Gilbert, Victor Para, and George Toepfer.

The Weasel Works design team was presented with a request for proposal (RFP) at the beginning of September, 1992. This RFP required that a new aircraft be designed in the 100 to 150 passenger range entering

service by the year 2000. The new aircraft also needed to meet all current FAR parts 25 and 121 requirements and the more stringent emissions requirements and stage IV noise requirements. This new aircraft was limited to take-off on a 5000 ft runway at 95°F at sea level. With these restrictions in mind, the aircraft had to operate up to an altitude of 40,000 ft with a cruise speed of Mach .76 traveling up to 1500 nautical miles with international fuel reserves while carrying full passengers and baggage with 20% overage.

The Weasel Works design team decided that in order to assure salability, the new aircraft would have to outperform Boeing's 737-500 model aircraft as well as meet the RFP requirements. Thus the goals for design became a comparable unit cost, lower direct operating costs, and an increased comfort level to help achieve a higher load factor for the airlines.

As is the custom, price was the bottom line. When all was said and done, Weasel Works came up with a product that will cost 30 million 1993 dollars assuming a production of 800 units. This is higher than the 737 price of about 25 million dollars. However, much of this cost is incurred due to the use of composites in the wing and the use of a fly-by-wire system. If the price of composites and manufacturing processes of composites lowers as the years pass, which they should as more becomes known about them, then the price of the SA-150 should drop. This is not true of the fly-by-wire system, however, since as the price of the equipment decreases, more and more software will be added to the system which seems to be ever increasing in cost.

The SA-150 is much less sensitive to fuel prices than the competition. With fuel prices at 65 cents per gallon, the 737-500 has an estimated direct operating cost of 4.17 cents per available seat mile (ASM) while the SA-150 has a DOC of 4.21 ASM. However, with an increase of just 4.2 cents per gallon the SA-150 and the 737-500 will have an equal DOC. Any larger increase will make the SA-150 more profitable to run. This event seems quite probable with the current Clinton administrations attempt to increase fuel taxes.. So with higher fuel prices in mind, the Weasel Works design team felt that the SA-150 would be a winner. The aircraft's end design incorporates several distinctive features (Figures 4, 5, and 6)) and creative design concepts which are described below.

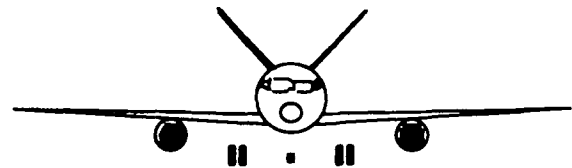


Figure 4. SA-150 Front View

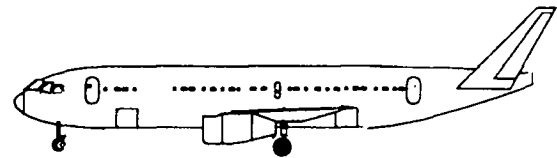


Figure 5. SA-150 Side View

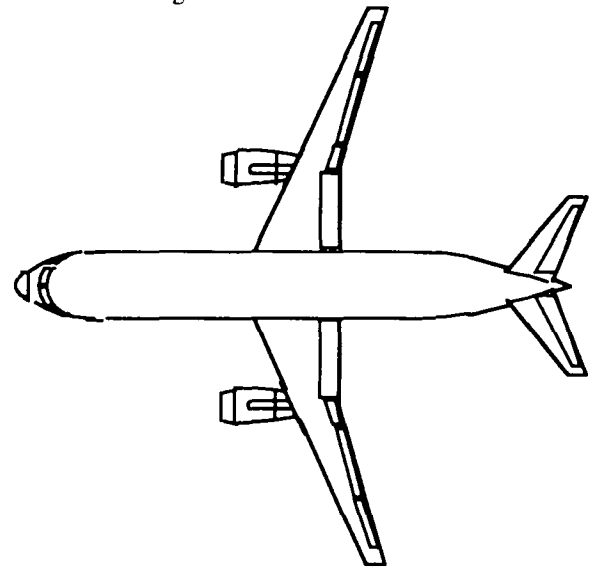


Figure 6. SA-150 Top View

The most outstanding features of the aircraft are the "V" tail and the high aspect ratio wing. The "V" tail was originally chosen in order to reduce surface area and to decrease drag. In order to avoid porting drag by moving the entire tail surface for trim this function will be performed by fuel pumping. Double hinged control surfaces were used to achieve the control power required, however, due to the need for even more control power during one engine out operations the reduced tail surface area was not realized. Instead, the wetted surface area had to be increased causing an increase in skin friction drag. Yet all was not lost, for only two surfaces mate with the fuselage instead of three which causes less interference drag. This reduction in interference drag cancels out the increase in skin friction drag leaving a no gain and no loss situation in comparison with a conventional tail. Two benefits were realized. One being a distinctive appearance which would help in marketing. The other advantage is that the two surfaces are identical and symmetrical which lessens the cost of

manufacture.

The other distinctive feature of the SA-150 is the 12 aspect ratio wing. This is a substantial increase over the Boeing 737-500 which uses an aspect ratio of approximately 8. At the same time, the wing was constrained to a wingspan of 107 ft to ensure that the aircraft fits into existing gateways and maintenance facilities. The high aspect ratio was chosen in order to reduce induced drag. Induced drag comprises a majority of the total aircraft drag in all flight regimes. It was thought lowering this value would have a large effect on DOC during cruise and thus generate a superior product. The problem with the high aspect ratio is its susceptibility to aeroelastic flutter effects. In order to compensate for this, the Weasel Works design team utilized the directional strength qualities of composite materials. This had the additional advantage of lowering the weight of the wing which then allowed for downsizing and fuel reduction further reducing aircraft gross weight. In order to utilize the inherent advantages of composite materials, we eliminated the traditional twin spar design of conventional aluminum wings and used a one piece structure. This structure lends itself well to an automated manufacturing process which will ensure consistent quality and reduce labor costs. However, the cost of the structure will still be more expensive than conventional designs at this time.

The wing sits about 7.5 ft off the ground at the root location with landing gear deployed and flat tires. The SA-150 fuselage rests 5.3 ft above the ground under these conditions which provides for easy one person servicing. These dimensions are a direct result of the engine size and tip over requirements. The engines mounted under the wing are Rolls-Royce/BMW BR-700-17 engines which provide our required 16,000 lbf thrust requirements (determined by second stage climb). Weasel Works design team felt that it would be cost prohibitive to have an engine designed to our own specifications so the BR-700 was selected from available engines in this thrust range as the best option. With the lowest specific fuel consumption, an acceptable fan diameter of 53 inches and a low weight (675 lbf lower than the CFM56-3), no other engine currently compares to it. Rolls-Royce has also guaranteed it to be 30% below stage III noise requirements which we believe will be more than adequate to satisfy proposed Stage IV requirements.

The length of the fuselage is 107 ft which (with a diameter of 13.2 ft) results in a fineness ratio of about 8.

This is considered optimum for drag considerations. In an attempt to further reduce manufacturing costs of the aircraft, the fuselage will be built with the frames and stringers far apart than usual. The skins will then have to be thicker in order to provide the necessary strength. This reduces the number of fasteners required which has a direct effect on manufacturing cost. An additional advantage is that fail safe tear straps will not be needed providing a slight weight savings. Without an secondary structure to take the loads in case of a failure additional testing will be required to insure safety of the design.

The SA-150 aircraft has three passenger configurations, a 108 dual class, a 118 single class, and a 124 high density class. In comparison, the 737-500's three passenger configurations consist of a 108 dual class, 120 normal class, and 126 high density class seating arrangement with an interior cabin diameter of 11 ft 7 inches. However, the SA-150 surpasses the 737-500 with an inner cabin diameter of 12 ft 8 inches and overall roomier seat pitches (33 inches being the normal class seat pitch). The larger cabin diameter allows for wider arm rests which hold fold out trays removing the need for seat back trays (which tend to shake the seats and are considered annoying). With the higher seat pitch, the larger cabin diameter, and wider arm rests, the SA-150 carries about the same amount of passengers for the same ticket price as the Boeing 737-500 yet provides a more comfortable and roomier atmosphere for the passenger. This will allow the airlines to sell a superior product and build a good reputation, thus increasing their load factors. The resulting bottom line is increased profits for the airlines.

With its high efficiency, enhanced passenger comfort, and distinctive appearance, the SA-150 will meet the needs of the airlines in the 21st century.

The 250-350 Passenger Solution

The JB-300 Advanced Commercial Transport

Design Team: TAC Team

Aircraft Name: JB-300

Team Members: Gilles de Brouwer, Katherine Graham, Jim Ison, Vince Juare, Steve Moskalik, Jon Pankonin, and Arnold Weinstein

In the fall of 1992, the TAC Team was presented with a Request for Proposal (RFP) for a mid-size (250-350 PAX) commercial transport. The result was an aircraft

that is highly competitive in the areas of passenger comfort, performance, environmental and economic aspects.

By using fly by wire, a high aspect ratio supercritical wing, a new type of Very High By-pass Ratio (VHBR) turbofan engine, an optimized, low drag configuration, and mild use of composites the JB-300 (Figure. 7), offers a significant performance improvement. It is an economically viable choice to the airlines with an total operating cost as low as 1.76 ¢/PAX/mile.

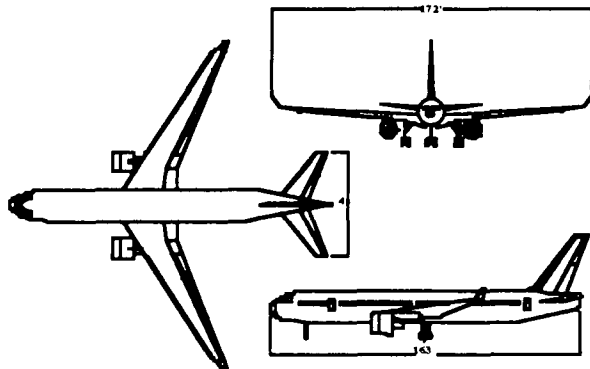


Figure 7 JB-300 Three-View

Introduction. The design philosophy of the TAC Team, was to design a highly competitive, technologically advanced aircraft with low operational cost and development risk, that is compatible with technological advancements and restrictions, and economical over the life of the aircraft. This was achieved by several means. First, a fly by wire control system was incorporated to improve performance and design flexibility. Second, a high aspect ratio supercritical wing with a low wing loading, sweep, and winglets provided a cruise lift to drag ratio of 21. A Pratt & Whitney VHBR turbofan engine known as the Advanced Ducted Propulsion (ADP) provided a cruise SFC of .45 lbf/lbt/hr, and low noise levels. A conventional structure made of primarily aluminum alloy, with moderate use of composites minimized risk and cost while still allowing a takeoff and empty weight of 286000 lbs, and 141000 lbs respectively. The maximum payload and range of up to 75000 lbs and 7000 NM are highly competitive with competing aircraft. Finally, an optimized conventional configuration was used to achieve a good balance between cost, aerodynamic and structural efficiency.

Fly by Wire Flight Control System. The JB-300 has a triple redundant and electro-hydraulic digital fly-by-wire flight control system. This system was chosen

primarily because of its weight reduction, and it's stability augmentation capability. It also improves the ride quality associated with low wing loading, high aspect ratio wing designs by providing active gust alleviation.

Supercritical Wing. The supercritical wing allowed the sweep to be reduced by 7.5°, 2000 ft higher cruising altitudes, a 1.8% increase in L/D, and a 4% decrease in fuel and takeoff weight due to decreased wing weight and drag. The current wing design has an aspect ratio of 10.5, a 31 degree sweep, a total area of 2900 sqft, a 173 ft span, winglets, a 15.5 % thickness ratio at the root tapering down to 10 % near the tip, and a design cruise lift coefficient of 0.51. At Mach .82 this wing has 8 to 13 counts of cruise compressibility drag.

The main advantage of this wing is that it allows the JB-300 to have up to 44 % less induced drag than a Boeing 767 during cruise. This improvement comes from the aircraft having a 25 % lower span loading (lbs/ft wing span), as induced drag is proportional to the span loading squared. The wing's 36 % increase in weight fraction (0.15) over currently flying design's is completely offset by reduced structural weight due to decreased fuel loads.

Propulsion System. The Pratt & Whitney ADP was selected primarily for it's low SFC of .45 and low noise output. Using a low thrust version, 46000 lbs thrust, also eliminated the weight penalty and minimized the size penalty as shown in Table 1.

This resulted in a cruise SFC penalty of only 3% caused by the engine operating at a higher than optimum cruise thrust. This engine is also expected to provide a 5 to 10 dB decrease in noise contributing to the lower overall noise levels in indicated in the noise section of this paper.

Table 1 Airframe/ Engine Combination Comparison

Airframe/ engine	767-300 PW4056	A300-600 CF-6-80C2	JB-300 ADP
Thrust (lbs)	56000	59000	46000
Diam. (ft)	9.2	9.8	10.8

Aircraft Configuration. The JB-300 has the low risk and cost associated with a conventional configuration yet has a major improvement in performance over current competitors. The final design, Figure. 7 was arrived at by optimizing the preliminary design. Several specific changes were required to minimize trim drag associated

with a supercritical wing. These included adding a centerline main landing gear, a tail fuel trim tank, and repositioning the wing. These changes improved the overall performance without significantly increasing cost. The optimum wing loading was found by investigating a family of configurations with different wing areas. Wing sweep and thickness were also adjusted as needed for optimum performance. The result was that the current designs low wing loading, and span loading configuration provides a 4.5% fuel weight savings, compared to a 23 % higher wing loading case, while not affecting the gross weight. It also has lower noise levels by reducing thrust required during the takeoff and landing phases as shown in Table 2 below.

Table 2 JB-300 and Certification Noise Levels

Flight Condition	FAR 36-8 Stage 3 (EPNdB)	Anticipated Stage 4 (EPNdB)	JB-300 Predicted +/-2.5 dB (EPNdB)
Approach	102.3	99.3	94.1
Sideline	99.0	96.0	83.9
Takeoff	94.5	91.5	75.6

Conclusions. The JB-300 has several distinct advantages that make it more efficient and cost effective than the competition. It successfully integrates 24 % more fuel efficient VHBR engines that are currently being developed, and has reduced noise. The engine's large diameter also prevents them from being incorporated by current aircraft at a later time.

The JB-300's low cost conventional configuration would allow for a \$53 million dollar acquisition cost, based on 1993 dollars for a production run of 505. Its high fuel efficiency, and low cost design resulted low direct operating costs and total operating cost as low as 1.76 ¢/PAX/mile.

Given a demand for 505 aircraft, the JB-300 provides an economic alternative to the Boeing 767, and the Airbus 300, 330, and 340. It does this with greatly reduced environmental impact, fuel use, and fuel price sensitivity.

The 800 Plus Passenger Solution

The VLCT-13 Advanced Commercial Transport

Design Team: Aeroheads
Aircraft Name: VLCT-13
Team Members: Wilfredo Balanon, Pamela Beal,

Matthew Cotton, Manuel Parayo, Terri Sowels, and Hitoshi Takahashi

Introduction. Boeing and members of Airbus have joined together in a feasibility study of a new long-haul commercial transport with a capacity of 600 - 800 passengers (PAX). The market for the proposed design would be the Transpacific. By 2001, 30 million passengers are expected to travel the Pacific Rim, corresponding to a growth of 8%. Typical city pairs include Los Angeles to Sydney and Chicago to Hong Kong, a trip of about 16 hours. With such a long trip, a philosophy of passenger comfort at an economical price controlled the VLCT-13 design (Figure 8).

Weight. The maximum payload for the VLCT-13 would be 200,000 pounds. This is based on 800 PAX weighing 175 pounds with 40 pounds of baggage, 30,000 pounds of cargo. Along with 500,000 pounds of fuel and reserves to travel 7,000 NM, the maximum takeoff weight of the VLCT-13 is 1.4 million pounds. The operational empty weight of the VLCT-13 is 600,000 pounds. A tried and true, conventional configuration resulted; this is shown in Figure 8.

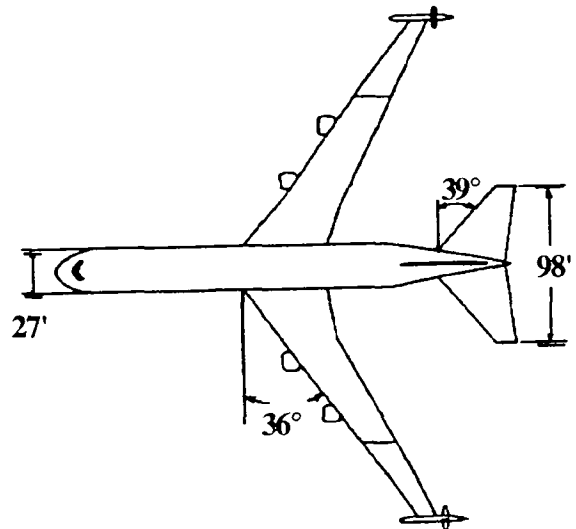


Figure 8 Top View of the VLCT-13

Performance. The thrust required for takeoff is 400,000 pounds; the aircraft is powered by four engines, each producing 100,000 pounds of thrust. A wing loading of 155 lb/sqft gave the VLCT-13 a wing area of 8000 ft². Since most of VLCT's time is spent in cruise, a high aspect ratio is desired; 11.63 was chosen. In cruise, VLCT-13 has a lift-to-drag ratio of 21.5. From a payload-range calculation, the VLCT-13 can fly 9,000

nautical miles at maximum takeoff weight. A ferry range is 14,000 nautical miles.

Cost. An airplane market price of \$190 million based in 1993 dollars. The current Boeing 747-400 market price is \$151 million. The VLCT-13 carries twice the number of passengers for only 1.3 times the market price. This savings is passed on in terms of cost per available seat-mile, only 2.8 cents per available seat-mile with 800 PAX. In the growth version, 2.3 cents per available seat-mile can be attained.

Interior. The fuselage diameter is 27 feet. The main deck has ten across seating of business class. This Business class is the VLCT-13's Tourist class in keeping with the design philosophy. The upper deck has seven across seating representing the Business 1st class which has a 40" pitch. This two class arrangement accommodates 852 PAX. The growth version does not require buying a new airplane; changing the seat size to 20" by 32" pitch and retaining 96 Business 1st seats will accommodate 1012 PAX. There are 16 Type A emergency exits; both the upper and main decks have four exits on either side. An estimated 1030 passengers can be evacuated from the VLCT-13. The emergency exits on the upper deck have tube slides since the door is 27 feet above the ground and passengers may feel uncomfortable seeing such a long drop.

Landing Gear. The VLCT-13 requires 28 tires. The nose gear has four tires which are steerable. The main gear struts have six tires. There are two wing gear and two fuselage gear. The fuselage gear telescope up to facilitate storage. The main gear carry 76% of VLCT-13's weight. With an LCN of 112, the VLCT-13 can land in any existing international airport.

Extras. A folding wing option is offered with the VLCT-13. By reducing the wing span 100 feet, the VLCT-13 can fit into B747 loading bays. A unique concept for this airplane is the vortex turbine. This turbine uses the vortex produced by the aerodynamics of the wing to produce an estimated 400 hp. This extra power can be used to power PAX computers, galley microwaves, etc. An added aerodynamic benefit is a 6% drag reduction.

Conclusion. A very large commercial transport is required to support 800 - 1000 PAX comfortably for about 16 hours. The VLCT-13 can carry 1000 PAX without growing the airplane. Recommendations for further study include: passenger egress, landing gear, the

vortex turbine and airport compatibility.

The VLCT-13 uses existing technology and a tried and true configuration at only 1.3 times the market price of Boeing's 747-400. With the expected growth in passenger travel along the Pacific Rim, an aircraft of this size is required.

The 800,000 lb Global Range Military Solution

The Cetaceopteryx Heavy Military Airlift

Design Team: Hydra

Aircraft Name: Cetaceopteryx

Team Members: Chad Brivkalns, Nicole English, Tahmeneh Kazimi, Kim Kopel, Seth Kroger, Edmund Ortega

Introduction. The Hydra Cetaceopteryx is a global range military transport aircraft. The Hydra team found that the changing role of the military was very influential in the design philosophy of the Cetaceopteryx. With the current wave of closures of US. bases on foreign soil, America's transport aircraft will face longer ranges with less refueling. The amount of distributed supplies is also dwindling, leaving the bulk of American military equipment and manpower stationed on domestic soil. The Cetaceopteryx is faced then with being a large expensive aircraft carrying large expensive payloads over incredibly long distances. The obvious cost and vulnerability of this type of mission, dictates that the Cetaceopteryx not be used as a tactical lifter delivering cargo to combat areas. It will fly instead from a main supply base in the US. to a large airport transfer point and distribute its cargo to smaller tactical lifters such as the McDonnell Douglas C-17. These smaller aircraft will then fly directly to combat areas.

Because the Cetaceopteryx is a cargo aircraft, the cargo bay was considered to be of the utmost importance in the overall design. Initially the cargo bay was designed as short and wide. This was done in order to ease loading and unloading of the aircraft. However, the resulting ovalar shape was found to be structurally inefficient. A longer thinner, more circular fuselage was then adopted because of its structural and aerodynamic benefits. To compensate for its loading shortfalls, a nose door was added. The floor was designed wide enough to load two tanks concurrently side by side. The above dimensional requirements also allow the Cetaceopteryx to hold four full McDonnell Douglas C-17 loads situated two loads across and two loads longitudinally. This was

a consideration for the rapid deployment of cargo to awaiting tactical aircraft. The two hundred combat troops were placed on the upper deck of the plane. They were spaced at a seat pitch of forty inches so that they could attach their packs to the seat directly in front of them.

In the initial phase of design, the Hydra team realized that in order to fulfill the strenuous requirements of the request for proposal (RFP), a very efficient, high lift, low drag wing would be necessary. Due to the sheer size requirements of the aircraft, a conventional wing was soon found to be a structural hindrance. The high aspect ratios required by the aircraft were too structurally demanding for the conventional wing approach. The alternatives that were considered were tandem, forward swept, joined wing, and various three surface configurations. It was found that the joined wing was an excellent compromise between structural and aerodynamic characteristics. The joined wing is comprised of two wings in the configuration shown below. (Figure 9). The front wing was chosen to be a high wing in order not to interfere with the cargo bay which was situated low in the fuselage. The rear wing joins the front wing at seventy percent of the semi-span. The Cetaceopteryx does not have a conventional horizontal tail but relies instead on the rear wing for control. A canard was also incorporated for control and for lift at takeoff for rotation.

The Cetaceopteryx joined wing has three main advantages over a conventional wing with similar parameters. Firstly, the wing structure is lighter than that of an aerodynamically equivalent cantilever wing-tail configuration. Secondly, wings of higher than normal aspect ratio, which with conventional design are structurally unfeasible, can be used with very good structural and aerodynamic efficiency. And lastly, the elongated wing box structure allows for larger fuel volume storage than a conventional wing would allow.

The specific joined wing configuration chosen by the Hydra group was a compromise between aerodynamic and structural considerations. For aerodynamics to be optimized, the wings must be joined at the tips, so that both wings have the same span. Unfortunately this configuration tends to be more structurally inefficient than a cantilever design. For structural optimization, the wings must attach at approximately one third the semi-span of the front wing. With this configuration however, all aerodynamic advantages of the joined wing are lost.

The Hydra team found that a rear to front wing span ratio of 0.7 was a good compromise between the above extremes. Structurally, the wing was forced to become heavier due to the reduced support encountered at the larger span ratio. Aerodynamically, the Oswald efficiency factor was cut from a possible 1.15 to approximately 1.0. Even with these compromises, the joined wing was still a much more attractive solution than the conventional wing.

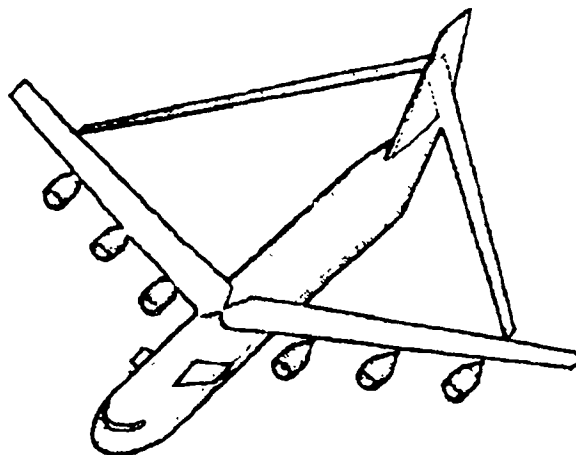


Figure 9- Cetaceopteryx Isometric View

Composites were used as the primary structural material in the Cetaceopteryx. This decision was made because strict range requirements required as light an aircraft as possible. Composites are being used increasingly in industry and given the technological limitations in aluminum, seem to be the material of the future. The Hydra team used composites in ways that are currently being manufactured. The non-circular fuselage structure was made with an isogrid back bone. The isogrid is a series of ribs forming a grid of isometric triangles glued to the inside of a composite skin. The grid was arranged so that one direction of ribs ran parallel to the longitudinal direction of the fuselage. This was done to allow the maximum resistance to bending in that direction.

Advantages of the isogrid over conventional frame and stringer construction are twofold. Firstly, the isogrid is a more efficient structure distributing loads more evenly throughout its mass. Secondly, isogrid construction is easier to manufacture, requiring less manpower and material. The wings were designed in such a way as to be easy to manufacture using extrusion, automatic tape laying and filament winding methods. There was one area of the aircraft where composites were not used. In general, the large loads being transmitted through each

side of the rear wing tend to equal each other causing compressive loads in the wing. If however, one side of the wing happens to stall and lose its lift, all of the lateral loads from the lifting wing are transmitted into the vertical tail. These loads would cause a rigid structure made of composites to fail. Therefore a less rigid aluminum material was used in the vertical tail structure.

Propulsion for the Cetaceopteryx was accomplished with six General Electric GE90 high bypass ratio engines each producing over 100,000 pounds of thrust. GE sources verified that this number would be attainable in production engines by the manufacture date of this aircraft. The engines were initially mounted beneath the rear wing. This was done because at the time, the front wing was mounted low on the fuselage for aerodynamic reasons and there wasn't enough room below the wing for the twelve foot diameter engines. This decision was reconsidered when it was realized that because of the large anhedral and the height of rear wing root, maintenance on the engines would be next to impossible. The front wing was then moved to a high position on the fuselage and the engines mounted underneath. The GE90 engine was chosen over the Pratt & Whitney PW4084 because it met the thrust requirements with a minimal number of engines. The GE90 also had a low SFC, met stringent noise requirements, and had low emissions.

The idea behind designing the landing gear for the Cetaceopteryx, was to use the fewest amount of wheels and struts in order to minimize size and weight, while retaining the ability to operate under the huge required operating loads. To achieve these goals, large high pressure tires were chosen for the highest load carrying capability distributed among as few tires as possible. The same tires were used for both the nose and main landing gear. The nose gear is comprised of six wheels arranged into two triple bogies placed at the edge of the fuselage in pods. The main gear consists of thirty-six wheels arranged in two rows of six struts each holding three wheels. The same struts, bogies, tires, and retraction sequence were used for both the nose and main gear. The main gear can rotate 20 degrees to the left and right of the centerline. This feature was added to reduce the turning radius of the aircraft. In flight controlled tire inflation was added so that stresses on paved intermediate runways could be minimized. The unusually high ACN rating of 110 at maximum gross takeoff weight would require that, the initial home base runway, where the aircraft will be heaviest would have to have a specially reinforced surface. Once the plane has

reached its intermediate point however, the ACN rating falls to 87 due to the weight loss from fuel burn. This rating is low enough for normal runway operations. Two extendible supports were added to help distribute the loading stresses more evenly onto the landing surface during nose loading.

The Cetaceopteryx uses new ideas in aircraft design to provide a unique solution to a complex problem. Using advanced materials and new research, it attains capabilities that have previously been unattainable. Designed for the role of global range strategic transport, the Cetaceopteryx uses a joined wing to improve upon conventional wing design in weight savings, structural efficiency, and longer range. The Cetaceopteryx provides a feasible solution to the changing needs of global military operations for decades to come.

The Ostrich Heavy Military Airlift

Design Team: Trash Haulers

Aircraft Name: Ostrich

Team Members:

Introduction. Recent studies have shown an increased need for a global range military transport capable of carrying large numbers of troops and equipment from the continental United States to anywhere in the world. This is due in part to the reduction in the number of US bases abroad, as well as the changing world political climate.

The Ostrich, which is shown in Figure 10, is a multibody military transport capable of carrying 800,000 pounds of payload 6,500 NM, and returning without refueling.

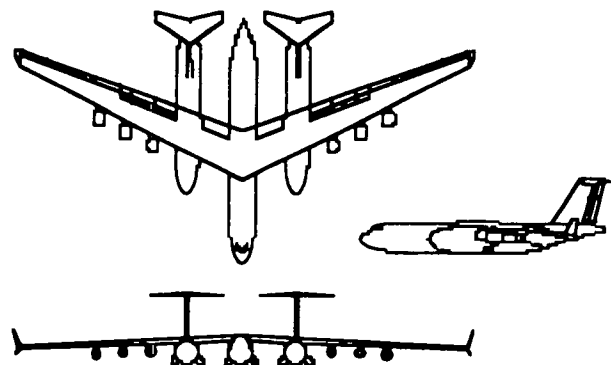


Figure 10 Three View of the Ostrich

Two main factors guided the design of the Ostrich. The first was a need to keep the size to a minimum. Size

was important because of the large range and long range. The other factor was the cost. Reductions in cost were achieved by using existing technologies in the design of the Ostrich including existing McDonnell Douglas C-17 fuselages with slight modifications. The results of the preliminary sizing process are given in Table 3.

Table 3. Weight sizing results for the Ostrich

WEIGHTS	POUNDS
Payload weight	800,000
Mission fuel weight	839,000
Operating empty weight	650,000
Trapped fuel/oil weight	5,000
Crew weight (6 crew)	1,200
Empty weight	640,000
Fuel fraction (ff)	0.61
Gross take-off weight	2.3 million

The aircraft was sized for a Mach number at cruise of 0.73 and flight altitude of 35,000 ft. The required C_{LmaxTO} was determined to be 2.6. Because the C_{LmaxTO} was so high, it was important to develop a low drag, high lift system for the take-off configuration. The C_{LmaxL} was established from the design point to be 2.2, but the aircraft was designed with a C_{LmaxL} of 3.2, in order to obtain a slower approach speed.

A specific fuel consumption of 0.4 was projected to be attainable by the technology availability date of 2010. It was found that the take-off weight increased with Mach number. The design Mach number of 0.73 was a compromise between speed, drag, and structural weight.

The configuration of the Ostrich aircraft was selected after the consideration of several different designs. Weight, aerodynamic efficiency, loadability and cost were the primary concerns in the selection of a configuration. The three body fuselage design was selected after comparing this design to other designs such as a flying wing and single fuselage.

Studies have shown that a multibody aircraft configuration offers many of the advantages of a span-distributed-load aircraft while retaining configuration and operational characteristics much like those of conventional transport aircraft. Reduced wing bending moment is accomplished by distributing the load along the wing. This in turn reduces the overall weight of the wing. The overall cost of the multibody aircraft can be reduced by using existing fuselages instead of designing a single fuselage that is capable of handling the same size

payload. A further reduction in cost is obtained from part commonality associated with the use of multiple fuselages and empennages. The three-body configuration, because it has multiple cargo loading doors, offers reduced loading and unloading times.

The lateral placement of the fuselages was a compromise between wing bending moment relief, maneuverability and runway capability. The outer fuselages were placed at a spacing of 100 feet from centerline to centerline (23% semi-span), which gives the Ostrich about ten feet of clearance between the landing gear and the edge of a 150 ft. wide runway.

In order to obtain a high L/D ratio, a wing of enormous span is necessary. An aspect ratio of 13 was chosen to reduce the induced drag produced by the wing. A total wing area of 12,600 sq. ft. was needed to produce the necessary lift for the Ostrich. This resulted in a wingspan of 410 ft. The sweep was set at 25 degrees at the quarter chord position to delay drag divergence during normal flight operations. Winglets were placed on the wing tips to reduce induced drag. Fowler flaps were used at the trailing edge of the wing to obtain high lift at take off and landing. The flaps run 80% span and with a flap chord ratio of 0.30. The airfoil selection for the Ostrich was a derivative of the supercritical MS-86 airfoil.

Laminar Flow Control (LFC) suction capability is used on the leading edge and top of the wing. LFC is implemented to increase the L/D by sucking the shear layer through a porous titanium skin, and thereby reducing the skin friction drag by delaying transition. Projections are that by the year 2010, LFC will produce a 20% increase in L/D. The LFC consists of a titanium skin placed on the leading edge and top surface of the wing and suction units.

With a thrust-to-weight ratio of 0.24, the required thrust for the Ostrich was 560,000 lbs. The engine chosen for the aircraft is a derivative of the General Electric GE 90, which is currently producing over 100,000 lbs of thrust. With this thrust, the Ostrich requires six engines. The placement of the Ostrich's six engines on the outboard portion of the wing was determined to be the most advantageous position after considering several other configurations.

The landing gear for the Ostrich consists of sixteen main bogeys with three wheels each and three nose gear bogeys with two wheels each. The three wheel main

bogeys are identical to those used on the McDonnell Douglas C-17 and was chosen for compatibility with the C-17 fuselages. Each of the main gears rotate 90 degrees when retracted for a low pod frontal area. The three-body configuration, because of its shorter fuselage lengths, allows for a shorter landing gear strut resulting in reduced weight and compatibility with existing loading equipment. Flotation for the Ostrich is comparable to that of the C-17. The nose gear loading which range from 8% to 11% of the gross take-off weight provides sufficient friction for steering.

The entire structure of the Ostrich is 56% composites allowing for a 30% reduction in the empty weight. The remaining structure is aluminum. The wing structure is entirely composites except for the titanium skin on the upper surface and hinges for the control surfaces. The titanium skin is needed for the laminar flow control system. Composites are also used for the empennages, nacelles, pylons, nose cones, and the center fuselage tailcone.

The maximum lift to drag coefficient for cruise in the clean configuration was calculated to be approximately 24. The maximum L/D ratio for take-off with landing gear retracted is approximately 20, and the maximum L/D for landing with landing gear deployed is approximately 12.

The Ostrich has an airplane estimated price, AEP, of \$1.2 billion for a 100 unit production quantity assuming a 15 year operation cycle, 700 flight hours per year utilization rate and a fuel cost of \$0.60 per gallon. The total life cycle cost of the Ostrich was estimated to be \$162 billion.

In conclusion, the Ostrich is an innovative approach to the need to rapidly transport large amounts of cargo and troops to problem areas around the world without refueling. By incorporating existing and advanced technologies, the Ostrich can serve it's mission both effectively and efficiently.

THE DESIGN OF A PRIMARY FLIGHT TRAINER USING CONCURRENT ENGINEERING CONCEPTS

Embry-Riddle Aeronautical University
Aerospace Engineering Department
Daytona Beach, Florida

Dr. James G. Ladesic
Professor Charles N. Eastlake
Nicholas H. Kietzmann Jr., Teaching Assistant

Abstract

Concurrent Engineering (CE) concepts seek to coordinate the expertise of various disciplines from initial design configuration selection through product disposal so that cost efficient design solutions may be achieved. Integrating this methodology into an undergraduate design course sequence may provide a needed enhancement to engineering education. The Advanced Design Program (ADP) project at Embry-Riddle Aeronautical University (ERAU) is focused on developing recommendations for the general aviation Primary Flight Trainer (PFT) of the twenty first century using methods of CE. This project, over the next two years, will continue synthesizing the collective knowledge of teams composed of engineering students along with students from other degree programs, their faculty, and key industry representatives. During the past year (Phase I), conventional trainer configurations that comply with current regulations and existing technologies have been evaluated. Phase I efforts have resulted in two baseline concepts, a high-wing, conventional design named Triton and a low-wing, mid-engine configuration called Viper. In the second and third years (Phases II and III), applications of advanced propulsion, advanced materials, and unconventional airplane configurations along with military and commercial technologies which are anticipated to be within the economic range of general aviation by the year 2000, will be considered.

Introduction

Concurrent Engineering is presently receiving a great deal of attention in many segments of industry due to the significant reductions in development costs that can be realized with its implementation. It has long been recognized that ninety percent of all product development costs are locked in during the initial concept phase of preliminary design¹. CE departs from the long standing approach to design as being a sequential activity. CE requires the combination of every function involved in the development of a product. This would include functions like engineering, procurement, marketing, sales and user

support groups, all involved in design decision making early on in the design phase.

Why is CE important to engineering education programs? For one reason it is believed that the U.S. is losing its dominance in several industries as a result of engineering graduates who are poorly prepared in design and product development². In fact, industry's view of engineering design education is that American engineering schools are producing great scientists but mediocre engineers. In other words, many universities do not view design as a credible research discipline. Thus, there has been an increasing number of engineering graduates specialized in theoretical and analytical methods, but with minimal design experience. Integrating CE into engineering education would help universities keep pace with the needs of industry and play more vital roles in a competitive U.S. design strategy.

Professional organizations such as the American Institute of Aeronautics and Astronautics (AIAA), and the Society of Automotive Engineers (SAE) strongly emphasize design activity at the university level; this may be the reason that the U.S. still lead in aerospace engineering by a thin margin. However, this dominance is continuing to erode from 73% of the market share in 1985 to 60% currently.³ This trend may be linked to problems within the general aviation (GA) industry. GA makes up a large portion of the U.S. air transportation system.

Most of the primary flight trainers flying today are aging, almost to the critical point. Very few new designs (none from the U.S.) are being manufactured to fill the trainer roll. Most student pilots are being trained with pre-1980 aircraft. A poll of central Florida flight schools confirms the aging aircraft problem. All schools reported that at least 80 percent of their fleet are more than ten years old.⁴

Some of the more common aircraft used as trainers include the Cessna models 152 and 172 (both introduced in the 1950's), the Grumman AG-5B Tiger (introduced in the 1970's), and the Piper Cadet (introduced in the late 1980's). Figure 1 indicates the dramatic decrease in the production of light aircraft occurring in the mid 1980's.

The problems within the GA industry associated with product liability laws and certification issues have led to the near extinction of new, single-engine aircraft in the U.S. Even the so-called newer designs, such as the Aerospatale TB9 Tampico Club represent technology that is 20 years old. Furthermore, the skills developed in flying available trainers will be of little use to the pilot of a fly-by-wire airplane having velocity vectoring and a side-arm controller such as those seen in the corporate, airline, and military sectors.⁴ Thus, the *utility* of general aviation aircraft becomes important in maintaining consistency with an expanding national airspace system.

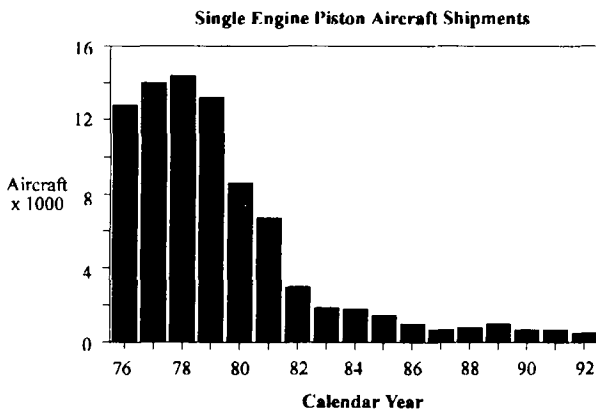


Fig. 1 U.S. Shipments of Single-Engine Primary Flight Aircraft.

Description of Project

The Advanced Design Program (ADP) at Embry-Riddle Aeronautical University (ERAU) is focused on developing recommendations for the primary flight trainer (PFT) of the twenty first century using methods of CE. Embry-Riddle has the unique opportunity to explore CE within the framework of aviation-related curricula. Students and faculty from a variety of programs such as aviation business, avionics, flight, aircraft maintenance along with engineering allow for collaborative efforts in the development of advanced primary flight trainers, representative of realistic, industry-type design projects. Thus, over the next two years, the ADP project will continue synthesizing the collective knowledge of teams comprised of engineering students, students from other degree programs, their faculty, and key industry representatives.

The development of the ADP/PFT is divided into three phases. All phases are supported by the research activities of a graduate teaching assistant visiting NASA/Langley Research Center during a summer internship. The first

phase investigates conventional trainer configurations that comply with current regulations and existing technologies; the *now* airplane. In the second phase, applications of advanced propulsion, advanced materials, and unconventional airplane configurations will be considered. Third year activities will focus on the adaptation of military and commercial technologies which are anticipated to be within the economic range of general aviation by the year 2000.

NASA Langley Research Center

The ADP at Embry-Riddle commenced with the gathering of pertinent information applicable to PFT designs driven by methods of CE. Areas of investigation included:

- Low Reynolds Number/Laminar Flow Technology
- Stall Pattern Tailoring
- In-Flight Operational Loads
- Forecasting of GA Activity
- Changes in Airworthiness Regulations
- Product Liability and Certification Issues
- Advanced Prototyping and Manufacturing Technology
- Proven Concurrent Engineering Programs

Preliminary recommendations as a result of this research activity included:

- Utilization of existing NASA NLF airfoils which have been enthusiastically accepted by the GA industry.
- Consideration of leading edge droops as an effective means for preserving aileron authority at high angles of attack and eliminating wing twist.
- Investigation of in-flight data acquisition systems for improving future designs, pilot performance evaluations, and safety.

Phase I

Over one-hundred students, faculty, and representatives from the aerospace community have been involved in design and research activities during this phase. The initial two semesters of the project (92-93 academic year) were structured to generate modern, FAR Part 23 certifiable

aircraft designs to be used as standards of comparison against the future designs of Phases II and III. This structuring was based on the fact that no existing PFT aircraft fully comply with the present FAR Part 23. By imposing design constraints such as use of certified, in-production engines, selection of proven aerodynamic configurations, and employment of proven fabrication methods, several *now* airplane designs were developed.

Embry-Riddle employs an aircraft preliminary design course and an aircraft detail design course. The preliminary design activities included concept and mission selection, configuration sizing, powerplant substantiation, weight and balance, stability and control, cost estimates, and considerations of manufacturing, repairability, and disposal of the aircraft. This past year, 22 teams were involved in preliminary design and were introduced to concurrent engineering through teleconferences and visits from engineers at NASA/Langley Research Center. In addition, instructors from non-engineering programs such as Embry-Riddle's Aircraft Maintenance Technology and Aeronautical Science departments supplied information regarding maintainability, repairability, human factors and pilot preferences essential in the design of a primary flight trainer.

For this project, a set of design parameters and mission profiles had to be tailored to fit the requirements of both the design course and a PFT as decided upon by the design course instructors. The design parameters require that aircraft:

- comply with FAR Part 23 including occupant safety and crashworthiness
- use an FAA certified powerplant currently in production.
- comply with FAA VFR standards upgradable to IFR.
- accommodate two to four occupants.
- demonstrate good spin recovery characteristics.
- assure a structural life of at least 10,000 flight hours.
- reach cruise speed of at least 120 knots.
- be able to take-off or land in no more than 3,000 feet.
- cost no more than \$50,000, excluding avionics, for production of 1,000 aircraft over five years.

Each aircraft had to satisfy one of two mission profiles. The first mission represents a general transportation scenario while the second that of a flight trainer.

Mission 1: Take-off

Climb to 5,000 ft
Cruise for 500 nautical miles
Loiter for 45 minutes with reserve
Land

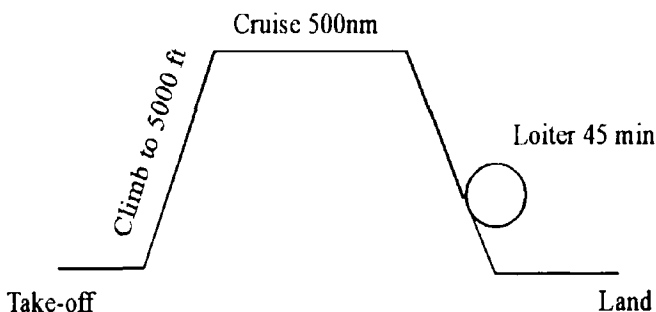


Fig. 2 Mission Profile 1.

Mission 2: Ten cycles of take-off and land (Touch and Go)

Take-off
Climb to 3,000 ft
Maneuver at 2 g's for 15 minutes
Cruise 100 nautical miles with reserve
Land

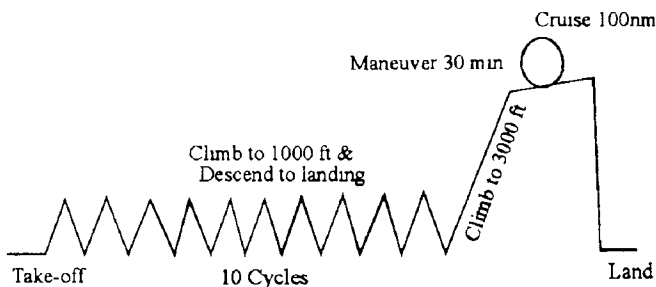


Fig. 3 Mission Profile 2.

The aircraft detail design course activities include structural design, load calculations and load path evaluation, system design and installation, material selection, manufacturing processes, and hardware familiarization. This past spring there were 14 teams assigned to conduct structural designs of the wing, empennage, and tail surfaces as well as the operation and installation of the control system. All components were designed for fatigue life and operational environments outlined in a statement of work for each project.

From the eight preliminary aircraft designs developed in the first semester of the program (Fall of 1992), two were selected for detail design. This selection was based upon the design's level of creativity, feasibility, and potential role as a primary flight trainer plus the completeness of the supporting documentation. The combined efforts of the preliminary and detail design courses have resulted in two baseline concepts, a high-wing, conventional design named Triton and a low-wing, mid-engine configuration called Viper.

The Triton Primary Flight Trainer

Configuration. The Triton Primary Flight Trainer (PFT) is a side-by-side, two-place, fixed-gear aircraft that conforms to all of the project design parameters. The aircraft has a cantilever high wing which provides excellent downward visibility, easy ingress and egress, and houses a gravity-fed fuel system. The Triton can be certified in either the normal or utility category. A single Lycoming O-235 engine enables the aircraft to attain a cruise speed of 120 knots. A summary of specifications and dimensions of the Triton are on the following page.

Design Features. The Triton has several modern design features that make it different from most of today's general aviation planes. First and foremost, the cabin was designed with ample internal volume for occupant safety and with structural reinforcement to insure increased protection. The cantilever wing eliminates the need for external strut bracing and thus reduces parasite drag and increases downward visibility. A large forward-opening "hood" to accommodate maintenance of the engine, and permits easy inspection and preflight procedures. There are inspection panels located throughout the aircraft for maintenance and inspection of control systems, flap mechanisms, wiring, and structures. Since high wing aircraft generally have poor upward visibility, a tinted window is provided between the wing spars in the cabin roof. The cargo area (42.5 ft³) in the Triton can also accommodate a third seat which would meet the requirements of the flight instruction program currently employed at Embry-Riddle. This program, called Gemini flight instruction, has two students and one instructor in the same aircraft during training. One student receives flight instruction while the other observes the process.

Versatility. Mission versatility was one of the design goals for the Triton design team. While sized for the Lycoming O-235, the engine compartment can accommodate a larger engine. Utility category certification, baggage compartment accessibility, and baggage capacity enable the aircraft to be used for cargo or

general aviation transportation. A three-passenger version configured for the Gemini flight training program is achieved without airframe changes or the need for supplemental certification. Since the high wing with the overhead window allow for excellent visibility, the Triton could also be used as an observation and reconnaissance aircraft. The high wing design and tricycle gear arrangements also permit conversion from a land-based aircraft to an amphibian.

Occupant Safety. There are several safety features employed in the Triton to maximize occupant safety and crash protection. The firewall is angled at the bottom so that the aircraft can slide along the ground without digging into the earth during a forward, falling impact. Angling the firewall also reduces the chance of fuselage buckling in the event of a crash⁵. Separate fuel tanks are set in the wing to avoid leaking and accidental puncture. The Triton is also equipped with energy-absorbing, "S-frame", JAARS⁶ passenger seats.

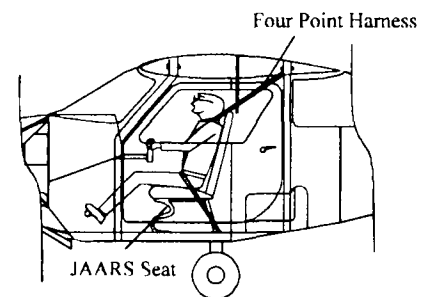


Fig. 4 Triton Cockpit layout.

The seat tracks are rigidly fastened to the floor structure so that they can absorb crash loads without dislodging from the airframe. Finally, four-point occupant restraint harnesses are attached at the floor and the wing carrythrough structure.

Configuration Sizing and Aerodynamics. Before any configuration sizing was done, the preliminary weight and fuel fractions were calculated for each of the two missions to determine which of these yielded the highest gross take-off weight. A weight of 1,785 lb came from the first mission (see **Mission Profiles**) and was used throughout the conceptual design phase until weight and balance was completed. The weight was further reduced after completing the structural design of certain parts of the aircraft (see **Structure**).

Following the take-off gross weight (TOGW) determination, the cruise power required was calculated to demonstrate that the Lycoming O-235 (rated at 118 hp)

would be sufficient for the mission profile. The preliminary sizes of the fuselage, wing, tail surfaces, and control surfaces were then determined from the gross weight, and the wing planform was designed for desired flight characteristics as agreed upon by the design team. These characteristics include mild stall progression, aileron authority at stall, induced drag reduction, tip vortex distribution, flap effectiveness, wing twist, and incidence angle. A summary of aerodynamic coefficients for the Triton, based on the preliminary weight and sizing results are zero lift drag coefficient of 0.026, cruise lift coefficient

of 0.303, maximum lift coefficient of 1.35 clean and 1.7 flapped, and a stall angle of attack of 10.7° clean and flapped.

After the wing configuration was finalized, the engine compartment and firewall section were proportioned to accommodate the engine and accessories. This task included the design and arrangement of a Dynafocal engine mount, exhaust manifold layout, carburetor intake duct, cabin heating system, and cooling air pathway. Further calculations sized the propeller to deliver the desired

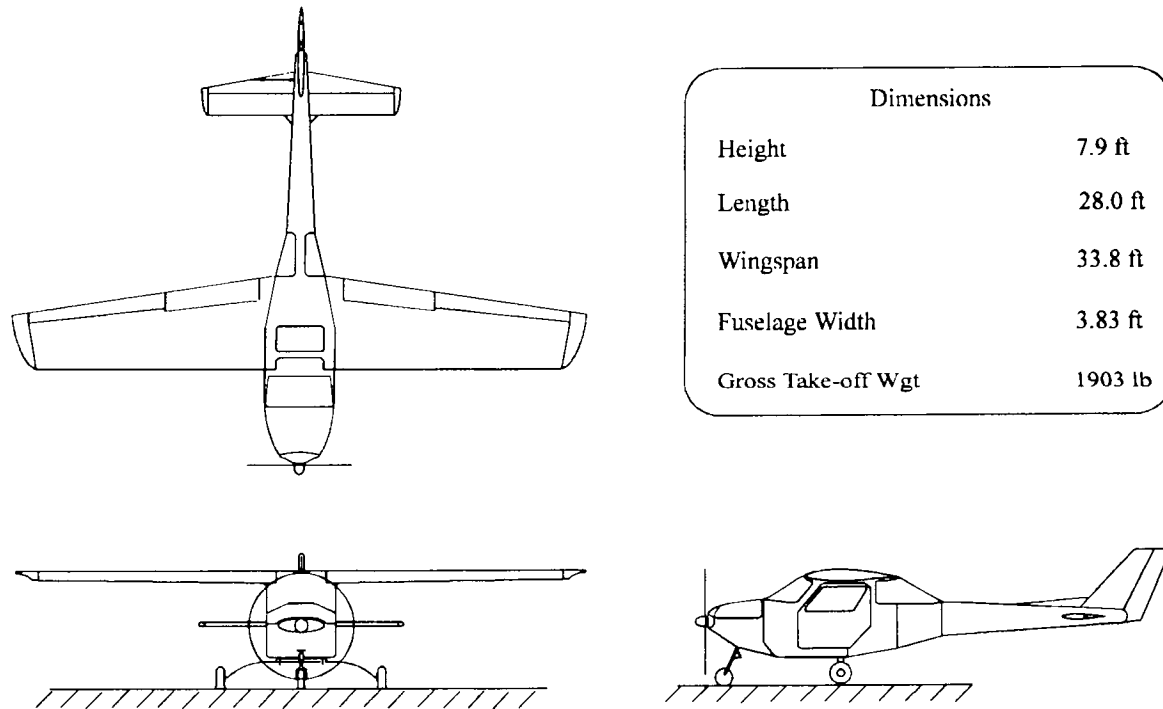


Fig. 5 Triton General arrangement

Triton Size/Configuration

Length (ft)	28.0	<u>Vertical Tail</u>	
Height (ft)	7.9	Span (ft)	4.0
<u>Wing</u>		Wing Area (sq ft)	12.8
Span (ft)	33.8	Aspect Ratio	1.25
Area (sq ft)	150.6	Taper Ratio	0.30
Aspect Ratio	7.4	Airfoil	NACA 0009
Taper Ratio	0.56	<u>Performance</u>	
Airfoil	NACA 64 ₁ -A212	Engine Type	(Lyc) O-235
<u>Horizontal Tail</u>		Horse Power	118
Span (ft)	12.25	Prop Diameter (in.)	74
Area (sq ft)	25.0	Rate of Climb SLS (fpm)	724
Aspect Ratio	6.0	Max. Velocity SLS (kts)	128
Taper Ratio	0.56	Cruise Velocity (kts)	120
Airfoil	NACA 0009	Stall Velocity (kts)	53

performance and meet the far-field noise level as described in FAR Part 36.

The landing gear of the Triton was then positioned to satisfy the tipback angle, static tail down angle, maximum stall angle, and overturn angle requirements. To accomplish this, a rough estimate of the center of gravity location had to be assumed from aircraft geometry. Landing and braking loads, strut deflection, and tire size for each wheel was then determined. The Triton can use differential braking, a steerable nosewheel or both to maneuver on the ground. A redesign of the initial engine mount was required to accommodate the final nosewheel mount.

Airframe and Structure. Triton's airframe is designed to be constructed using traditional metal fabrication employing flat wrap construction. The primary structure of the aircraft consists of fuselage frames, wing and tail surface ribs, doublers, longerons, and stringers all surrounded by an aluminum skin. The cross-section of the aircraft begins square at the firewall and remains such until just behind the door, where it transitions into a circular section at the tail cone. The cabin floor is raised four inches above the lower skin by several C-section stiffeners to which the landing gear strut, seat tracks, and occupant harnesses are attached. Also in this space are the fuel selector valve, control system pulleys, and trim wheel assembly, all located between the two seats and serviced by a removable floor panel. The instrument panel, firewall, and doors are rigidly mounted to the longerons and stringers which shape the 46-inch wide (internal) cabin.

The Triton wing (Figure 6) has two spars, several stringers, ribs, and skin that are constructed from aluminum using extrusion and flat wrap construction methods. The complete structure is joined with NAS or MS standard, aviation fasteners. The spars are assembled from two altered T-sections riveted to a sheet aluminum web forming an I-beam. Each spar is one continual piece to ease construction and save weight by eliminating multiple spar assembly points. The wing skin varies in thickness depending on the shear and torque loads encountered in each panel. Provisions were made for easy access to the fuel tank and inspection of the flap and aileron controls. The entire wing is attached to fuselage cabin bulkheads with eight bolts.

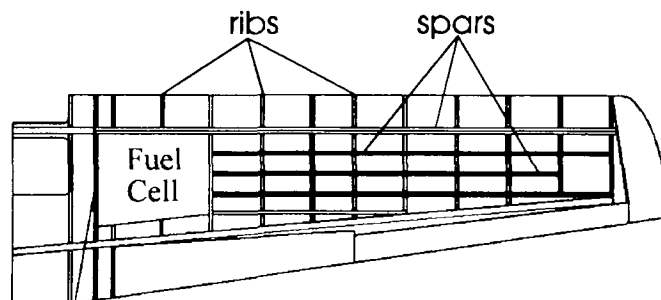


Fig. 6 Triton wing structure.

The tail surfaces are composed of ribs, stringers, and two spars wrapped with aluminum sheeting to form a NACA 0009 airfoil section. The flight loads to which the surfaces were designed were calculated using the methods found in FAR Part 23. The summation of the worst case loads was then used to design the empennage structure. The horizontal stabilizer and vertical fin have similar construction, as do the elevator, trim tab, and rudder. Each surface is bolted to the empennage using mating interface connectors. All components in each surface are designed to meet a 10,000 flight hour fatigue requirement.

The empennage consists of several ring-shaped formers held in place by eight stringers and an aluminum skin. The stringers were sized to transmit any bending and axial loads developed by the tail surfaces into the fuselage and the skin thickness was sized for the torsional loads. The frames were then placed to reduce stringer and panel buckling under the applied loads. Similar fatigue assessment was done on the components at both the fuselage and tail surface interface locations. Access panels and a ground tie provision were also incorporated in the design.

In addition, subassembly determination and assembly decomposition, snow load reactions, moisture drainage provisions, and system corrosion resistance were considered in the Triton design. After the size and strength of each component were determined, any fasteners integrated with the parts were also sized and documented.

Weight and Balance. A preliminary center of gravity location was estimated during the conceptual design phase but was later refined after approximating weights for most of the aircraft's structure and major components. Any weights not obtained from calculation or other sources were estimated. A spreadsheet program was used to evaluate various pilot, baggage, and fuel weights to determine the c.g. range and approximate locations. The new c.g. position was used to recalculate the landing gear

requirements and was also used in the stability and control calculations.

Stability and Control. The Triton's static stability and control parameters were estimated. Longitudinal, directional, and lateral stability were evaluated, as were roll rate and spin recovery. For longitudinal evaluation, the neutral point location, static margin, horizontal tail incidence, and elevator deflection were determined. Directional criteria included $C_{N\beta}$ and ample rudder deflection to maintain control in an 11.5° crosswind, while lateral parameters included $C_{l\beta}$, roll rate using the preliminary aileron size, and spin recovery behavior. All values except $C_{N\beta}$ and $C_{l\beta}$ were acceptable for this type of aircraft. A dynamic stability calculations was also performed on the aircraft for long and short period longitudinal modes, rolling mode, spiral mode, and dutch roll tendencies. Although the Triton is statically stable and controllable, a divergent long period phugoid mode (Figure 7) was predicted. While this is acceptable under FAR Part 23, such dynamic flight characteristics may cause liability problems and could result in unnecessary lawsuits.

Phugoid Mode

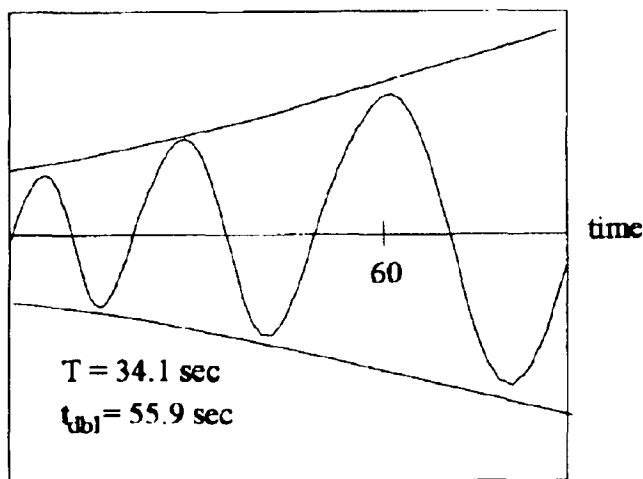


Fig. 7 Triton in phugoid mode.

The control system of the Triton is all cable-actuated from the yoke to the control surfaces. This was done primarily to keep the system weight within the prediction stated in the weight and balance calculations. The system was designed to deliver maximum control surface deflection without failure even if the pilot limit loads exceed those determined by FAR Part 23. Adequate maintenance provisions were incorporated into the design, as were considerations for thermal expansion, dust/dirt intrusion, corrosion, and component wear.

Cost. Both the production and operating costs of the Triton were evaluated using two computer programs. The production cost program determined whether 1,000 aircraft could be produced over five years with a ten percent profit margin while staying under the \$50,000 per aircraft limit (less avionics and liability insurance). This schedule yields an overall production cost of \$46,020 and therefore meets the design parameter. The operating cost program required yearly flight hours, loan values, and ownership type. With a schedule of 1,000 yearly flight hours, a 90 percent loan value, and company ownership, the operating cost is slightly over \$36 per flight hour. This value compares with current aircraft rental rates and shows that the Triton would be competitive with all primary flight training aircraft.

The Viper Primary Flight Trainer

Configuration. The Viper is a two person, low wing, low tail configured primary flight trainer with fixed tricycle gear. The most unique feature of the Viper's design is its mid-mounted Lycoming O-235 engine. The Viper is designed to be certified under FAR Part 23 in the utility category.

Design Features. Viper's mid-mounted engine concept was chosen for several reasons. The mid-engine presented a potential for a smaller frontal area which should reduce drag. Since the placement of the engine produces a smaller moment arm in the center of gravity calculations, this allows the wing to be positioned rearward which improves downward visibility. The engine is serviced by removing a horseshoe-shaped hood over the engine, through an underside access panel, or through small preflight inspection panels around the engine. The Viper's tricycle landing gear allows for good visibility over the nose during ground operations. There are two doors on each side of the Viper. The top door is a gull-wing door that allows head clearance during entry while the lower door swings down and acts as a step to enter the aircraft. The lower door grants access to the cockpit control system, the underside of the instrument panel, and contains part of the engine cooling ducts.

Versatility. The Viper can be used in roles beyond those of a flight trainer. Its performance makes it attractive as a small business plane and its visibility makes it ideal for observation in law enforcement, wildlife preservation, or traffic-reporting.

Occupant Safety. The Viper was designed to conform to current FAR Part 23 crashworthiness requirements. Its JAARS seats will withstand the 26g forward loads required by FAR 23.562. Occupants are restrained by four-point

harness systems. The engine is mounted in a truss-type mounting box which isolates it from the passenger compartment in the event of a crash. The propeller shaft, contained in the armored console, has three support bearings along its length and uses frangible couplings at both ends for safety if a crash were to occur. The shaft also has a dry clutch at the engine attachment to provide safer, smoother flight. Since the engine is behind the cabin, the exhaust is prevented from entering the cockpit with the aid

of a venting system located behind the cabin; gases exit into a low-pressure portion of the slipstream.

Configuration Sizing and Aerodynamics. In examining the mission profiles for the Viper, the 500 nautical mile cruise mission consumed the most fuel, approximately 200 lb. The initial sizing was done based on this fuel weight. The required horsepower for the mission was 83.9 which is within the limits of the 97 HP Lycoming O-235. The total weight estimate was 1642 lb.

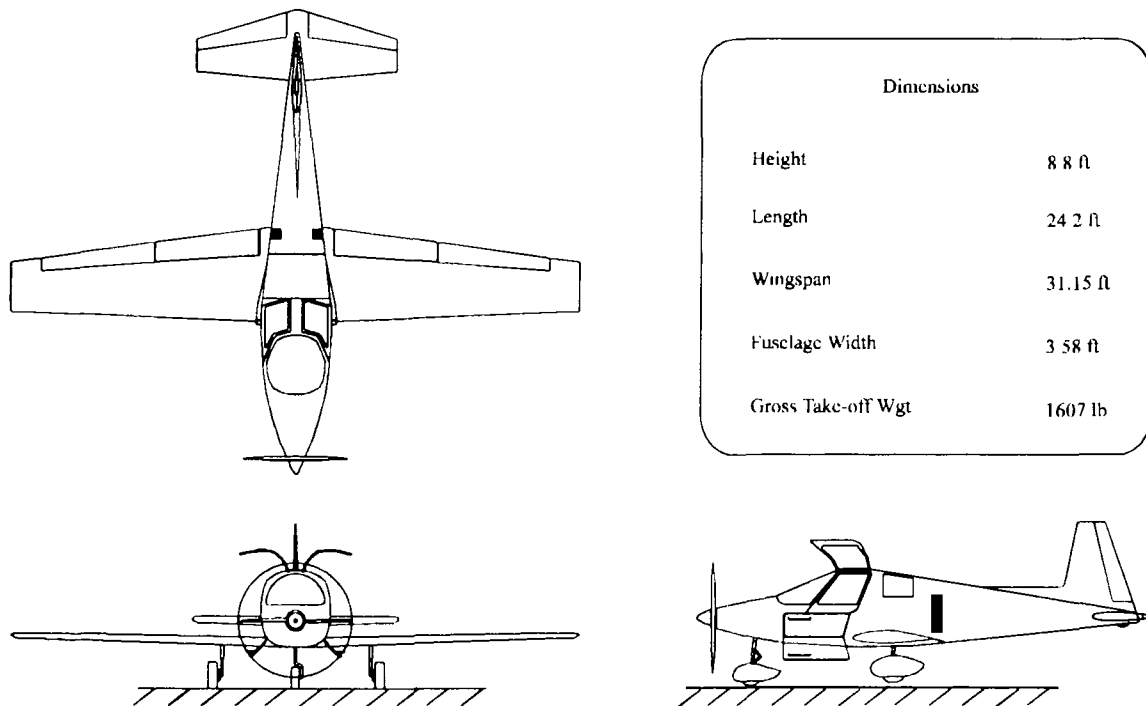


Fig. 8 Viper general arrangement.

Viper Size/Configuration

Length (ft)	24.2
Height (ft)	8.8
<u>Wing</u>	
Span (ft)	31.15
Area (sq ft)	124.4
Aspect Ratio	7.98
Taper Ratio	0.45
Airfoil	NACA 64 ₂ -415
<u>Horizontal Tail</u>	
Span (ft)	10.95
Area (sq ft)	30.0
Aspect Ratio	4.0
Taper Ratio	0.45
Airfoil	NACA 0012

<u>Vertical Tail</u>	
Span (ft)	4.5
Wing Area (sq ft)	12.9
Aspect Ratio	1.57
Taper Ratio	0.40
Airfoil	NACA 0012
<u>Performance</u>	
Engine Type	(Lyc) O-235
Horse Power	118
Prop Diameter (in.)	74
Rate of Climb SLS (fpm)	1,140
Max. Velocity SLS (kts)	140
Cruise Velocity (kts)	136
Stall Velocity (kts)	46.5

Using these values and the Raymer text, the wing, stabilizers, and fuselage was then sized⁵. The wing airfoil chosen was the NACA 64₂-415 with a platform area of 124.4 sq ft and a 31.15 foot span. The aerodynamic coefficient for Viper are as follows, zero lift drag coefficient of 0.027, cruise lift coefficient of 0.400, maximum lift coefficient of 1.3 clean and 1.8 flapped, and stall angle of attack of 12° clean and flapped.

The Dynafocal engine mount is placed in a mounting structure to transfer the engine loads into the aircraft structure. For adequate engine cooling, two 60 sq in ducts were designed into the aircraft, one on either side of the cabin. Carburetor intake will also be from these inlets. To insure an even distribution of cool air, the left inlet cools the front cylinders while the right inlet cools the rear cylinders. The fixed-pitch propeller far-field noise calculations were less than the FAR Part 36 maximum of 70 dB. The landing gear was designed using criteria for static loads, braking requirements, gear stroke, dynamic loads, and tire selection.

Airframe and Structure. The forward fuselage of the Viper is made up of longerons along the bottom with stringers and formers used to reinforce the cabin. The seats and harnesses fasten directly to the floor longerons. Sections around the doors and access panels were reinforced. The aluminum-tube propeller shaft is covered by a shroud where it runs through the cabin. Yoke control system routing is done under the shroud.

The structures of all lifting, stabilizer, and control surfaces consist of ribs, spars, stringers, and flat wrap skin. All non-moving and permanent parts are riveted together while removable sections are fastened by bolts. Each section was calculated for shear and buckling loads and fatigue life.

The wing spar is composed of two units joined by four rivets. The spars consist of L-section caps and a linearly tapered web. The wing has no angle of incidence and a 1.6° dihedral angle. The wing was designed to handle the worst case loading scenario of a vertical 3g landing with fully extended flaps and ailerons. The wing carrythrough structure is composed of a two C-sections riveted to the fuselage airframe. The wing/fuselage interface consists of mating the C-sections to the front and rear spars using twelve bolts each.

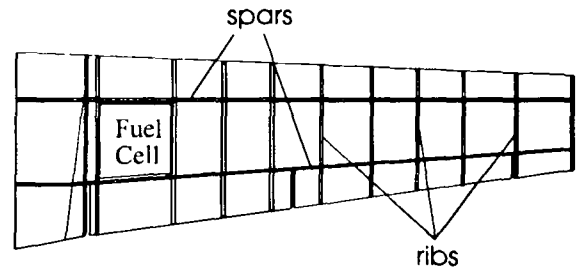


Fig 9. Viper wing structure.

The empennage is composed of the vertical and horizontal stabilizers and the tailcone. The stabilizers are similar in design to the wing with front and rear spars, ribs, stringers, hinges and torque tubes for the elevator and rudder assembly. The vertical stabilizer skin panels are beaded to reduce panel buckling. The tailcone assembly consists of 8 stringers and 3 ring frames. The last frame located at the point of the tailcone is made of cast aluminum and has a small hoop which will act as the tie down. The remaining frames are made from hydroformed aluminum blanks. Since the skin carries all of the torsional loads, while panel buckling criteria was used for sizing.

Access panels and lightening holes aid in the assembly or disassembly of the stabilizers, wing, and tailcone. These panels also provide for control system installation, maintenance, and inspection.

Weight and Balance. The weight and balance began with a detailed weight evaluation of the aircraft components. Actual component weights were used whenever possible. When these weights were not available, estimations were made using Raymer's statistical weight equations. The center of gravity was evaluated for a variety of loading conditions by varying the fuel load, number of passengers, and amount of baggage. The overall c.g. travel is 13.8% mean aerodynamic chord (MAC). The most forward position is 19.6% of MAC

Stability and Control. It is necessary that a plane possess the natural tendency to return to its original attitude, yaw, bank, and speed after a disturbance. To ensure this, several stability and control parameters were examined. For static stability, the neutral point and static margin were calculated. As a result the neutral point for Viper is 43.4% MAC and the static margin is 10%. Other calculations done to verify stability were incidence angles, directional stability, and lateral stability. Calculations were done for elevator deflection, directional and roll control, and spin recovery. In all cases, the Viper has adequate stability and control. A dynamic stability evaluation was conducted by a group of graduate students as a continuation

of Phase I and concluded that the Viper also has good dynamic stability except in the phugoid mode. In this mode, the Viper has a divergent trend with a period doubling in 500 seconds. This is acceptable in normal conditions, but may pose a liability problem if a crash were to occur.

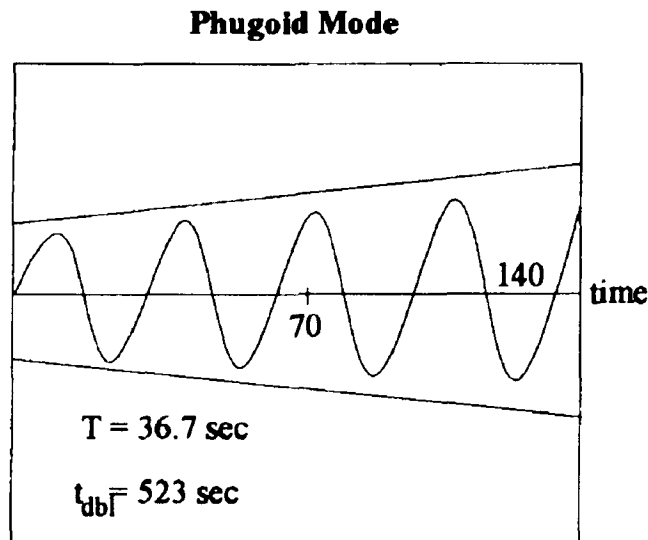


Fig. 10 Viper in phugoid mode.

The design of the control system provides a simple, reliable assembly that will withstand a training environment without excess cost or weight. An adjustable yoke in the cabin is connected to an all push-pull rod control system. Push-pull rods were selected for pilot feel and thermal expansion. The rudder control system provides both rudder and nosewheel deflection as well as differential braking. The elevator control system was designed using the loading conditions listed in FAR Part 23 and human factors specifications given in MIL-STD-1472.

Design substantiation was done for all control system components. Calculations consisted of Margin of Safety calculations, pilot limit loads, ultimate loading cases, and fatigue life. The current design provides a simple effective cockpit control system meeting FAR Part 23 specifications and will allow for comfortable flying.

Cost. The cost of the Viper was determined by using the LITECOST computer program developed at Embry-Riddle by Professor Charles N. Eastlake. This program uses the following parameters in determining cost: airframe weight, avionics cost, engine horsepower, production rate, number of aircraft produced, time to completion, and profit percentage. The Viper will cost \$41,978 for a production

of 1000 aircraft at 17 per month with a 15% profit. This price does not include avionics or liability insurance.

Materials, Manufacturing Methods, and Hardware

The primary construction material for both Triton and Viper is 2024-T3 aluminum. This material is either cast, extruded, or used as sheet to construct various components of the aircraft. Some parts are made of other aluminum alloys such as 7075 and 6061 depending on the stresses and loads in the part. Steel alloys such as 4130 are used for some highly-stressed critical components.

All components and assemblies for each aircraft are to be made from traditional manufacturing methods such as brake and hydropress forming, flat wrapping, and basic machining operations. Operations like stretch forming, double-action press forming, and spin forming were avoided due to expense, tooling complexity, and manufacturing time.

Parts are assembled using various aviation rivets and AN or NAS type bolts, nuts, and washers. The quantity and size of the fasteners were determined depending on the part load, assembly method, and orientation. Safety wire restraint is used on some bolts to eliminate loosening due to vibration or part motion.

Avionics

The statement of work for this phase required that all aircraft designed have at least visual flight rules (VFR) equipment aboard. This includes a communication transceiver, an emergency locator transmitter (ELT), and a transponder. The option to upgrade the aircraft to instrument flight rules (IFR) capability was considered. This would require adding an automatic direction finder (ADF), encoding altimeter, and distance measuring equipment.

Phase II

The design courses in phase two of the project will incorporate the use of thermoset structural composites, new powerplants, and Natural Laminar Flow (NLF) airfoils. The use of resin transfer molding increases the production rate of composite parts and lowers the manufacturing cost. Composite parts reduce weight and allow compound curves making the process suitable for the production of aerodynamic shapes such as natural laminar flow airfoils.

Several new powerplants are emerging that have great potential for use in general aviation aircraft. The water and oil/air-cooled Rotax 914 is half the size, weight, and cost of

the Lycoming O-235. The multi-fuel, 4-cylinder, Zoche Aero-Diesel has a 2000 hour time between overhaul (TBO) and runs with turbine smoothness. The six-cylinder Dyna-Cam, certified in 1960, has a unique 4-stroke design that provides 210 hp at 2000 rpm and 650 ft-lb of torque at 1200 rpm. The newly certified, fuel-injected, air-cooled, Teledyne/Continental IO-240 is based on an engine originally developed by Rolls-Royce. Other powerplants that could be considered for use in the aviation field are converted automobile engines, rotaries, and stratified charge diesels. Alternate fuels such as automotive gas, alcohol, and diesel are being considered for aviation use.

Although NLF airfoils have less drag and better overall performance than existing airfoils, their acceptance may suffer from a history of disappointing results from the general aviation use of the NACA 6-series airfoils, known as the first generation of laminar flow airfoils. With the newly developed NLF-0414, laminar flow can be maintained back to 70 percent of the chord, which allows for a significant decrease in drag.

Phase III

Phase three of the project will explore advanced flight controls, cockpit displays, flight load monitoring, and structural thermoplastic composites. Advanced flight controls and cockpit displays include heads-up display, side stick control, CRT flat panel displays, and GPS navigation. To defuse the speculation in liability claims, a microprocessor-based flight load monitoring/recording system could be used to monitor the flight loads applied during the aircraft's life and indicate possible structural failure. The use of thermoplastic composites such as polyether-ether-ketone (PEEK) will allow for faster fabrication compared to thermoset composites. The advantages of thermoplastic composites over thermoset composites are low moisture absorption, high fracture toughness, and delamination resistance under low-energy impact conditions⁸. Also, thermoplastic material can be recycled, while thermosets cannot.

Recommendations and Conclusions

In 1992 the United States general aviation industry produced approximately 900 aircraft, including turboprops and jets. Of those 510 were single engine piston⁷. A decade ago the numbers were three times higher. The aircraft produced today still use technology from the 1970's. None of these currently comply with the current Federal Aviation Administration airworthiness regulations. Not one single engine piston aircraft produced in either the United States or broad employ state-of-the-art technology currently available in commercial and military aircraft.

Applications of such technology could improve product reliability, operational safety and skill level attainment for the student pilots involved. The vehicles students currently use for primary flight training are technologically decades apart from the aircraft they will use as commercial pilots. As our national airspace system continues to expand, maintaining a parallel growth in the general aviation aircraft sector becomes increasingly more important.

The primary flight trainer aircraft market has the potential to be a multi-billion dollar per year industry in the United States. This can only be achieved if new material and manufacturing technology are explored along with significant changes in our liability laws and certification procedures. Improved methods for teaching design in engineering education can also contribute in a positive way. Concurrent Engineering at the undergraduate design level has proven to be successful as a means to bolstering student enthusiasm and interest during Phase I of this project. Student interaction on teams with input from other interested groups like engineers from industry and other previous preliminary design teams and flight instructors from ERAU's Aeronautical Science department has yielded better designs than previously accomplished in the capstone activities. The use of leading edge technology to form of stereolithography to produce models of student projects has led to a better understanding of design and manufacturing. Phase I exceeded the parameters set forth in this document. The program not only designed a better performing aircraft than required but it went in-depth in dynamic stability, cost manufacturing, engine selection for Phase II and safety constraints.

The Triton and Viper designs are important in that they represent a modern way of accomplishing an airplane design.

Acknowledgments

This project was made possible through efforts of the 121 students of the Fall 1992 and Spring 1993 classes of AE420 Aircraft Preliminary Design and AE421 Aircraft Detail Design. Special thanks go to Dr. James Cunningham, Dr. Joel Crispin, Scott Ariotti, Chris Bartlett, Todd Burroughs, Al Cepeda, Kaishun Chu, Andy Dayton, David Fitzgerald, Melissa Hall, Robert Harvey, Brian Kaplan, Chuck Klein, Brian Marchessault, Greg Meholic, Garrett Sager, George Schneider, Mark Shilladay, Mike Singer, Russ Snow, Todd Weishaar, and Mike Zable.

A special note of appreciation is due to NASA and USRA for their sponsorship.

We are grateful for all the guidance and wisdom we received from NASA/Langley and Lockheed personnel.

References

1. Roskam, Dr. Jan, Airplane Design, Vol. 1-8, Roskam Aviation and Engineering Corporation, 1988.
2. Eastlake, C.N. and Ladesic, J.G., "The Next Generation, General Aviation, Primary Flight Trainer", AIAA 93-3954.
3. Nicolai, L.M., "An Industry View of Engineering Design Education" AIAA 93-0328.
4. Stewart, R.J., and Stickle, J.W., "General Aviation - A Transportation System in Transition"
5. Raymer, D.P., Aircraft Design - A Conceptual Approach, AIAA Education Series, New York, 1989.
6. "General Aviation Aircraft Crash Dynamics", Society of automotive Engineers, SP-716, General Aviation Aircraft Meeting and Exposition, Wichita, KA, 1987
7. Reporting Points, Flying, April, 1993, pp 25-26
8. Hoskin, B.C., and A.A. Baker, Composites Materials for Aircraft Structures, AIAA Education Series, New York, 1986.

Integrated Design and Manufacturing for the High Speed Civil Transport

Georgia Institute of Technology
School of Aerospace Engineering
Atlanta, GA 30332-0150

Professor Daniel P. Schrage, Dr. Dimitri N. Mavris (Faculty Advisors)
Mark Hale and Peter Rohl (Teaching Assistants)
Reginald Abel and William Marx (Team Leaders)

Abstract

In June 1992, Georgia Tech's School of Aerospace Engineering was awarded a NASA University Space Research Association (USRA) Advanced Design Program (ADP) to address "Integrated Design and Manufacturing for the High Speed Civil Transport (HSCT)" in its graduate Aerospace Systems Design courses. This report summarizes the results of the five courses incorporated into the Georgia Tech's USRA ADP program. It covers AE8113: Introduction to Concurrent Engineering, AE4360: Introduction to CAE/CAD, AE4353: Design for Life Cycle Cost, AE6351: Aerospace Systems Design I, and AE6352: Aerospace Systems Design II. AE8113: Introduction to Concurrent Engineering was an introductory course addressing the basic principles of Concurrent Engineering (CE) or Integrated Product Development (IPD). The design of a total system was not the objective of this course. The goal was to understand and define the "up-front" customer requirements, their decomposition, and determine the value objectives for a complex product, such as the High Speed Civil Transport (HSCT). A generic CE Methodology developed at Georgia Tech was used for this purpose. AE4353: Design for Life Cycle Cost addressed the basic economic issues for a HSCT using a robust design technique, Taguchi's Parameter Design Optimization Method (PDOM). An HSCT economic sensitivity assessment was conducted to address the robustness of the basic HSCT design. AE4360: Introduction to CAE/CAD permitted students to develop and utilize CAE/CAD/CAM knowledge and skills using CATIA and CADAM as the basic geometric tools. AE6351: Aerospace Systems Design I focused on the conceptual design refinement of a baseline HSCT configuration as defined by Boeing, Douglas, and NASA in their system studies. It required the use of NASA's synthesis codes FLOPS and ACSYNT. A criterion called the Productivity Index (P.I.) was used to evaluate disciplinary sensitivities and provide refinements of the baseline HSCT configuration. AE6352: Aerospace Systems Design II was a continuation of Aerospace Systems Design I in which wing concepts were researched and analyzed in more detail. FLOPS and ACSYNT were again used at the system level while other off-the-shelf computer codes were used for more detailed wing disciplinary analysis and optimization. The culmination of all efforts and submission of this report conclude the first year's efforts of Georgia Tech's NASA

USRA ADP. It will hopefully provide the foundation for next years' efforts concerning continuous improvement of Integrated Design and Manufacturing for the HSCT.

Course Sequence

Figure 1 illustrates the sequence of Aerospace Systems Design courses offered as Georgia Tech's NASA USRA ADP.

Each course, with the exception of the CAE/CAD course, required students to work as multi-disciplinary teams. During the Fall and Winter Quarters, two separate 4- and 5-member teams worked on the required projects and submitted separate reports. For the Spring Quarter, the two teams were combined into one nine-member team in order to achieve more depth in the research and analyses. A Request for Proposal (RFP) was given as a handout at the beginning of each quarter stating the required tasks and deliverables. An oral presentation and submission of the final written report concluded each course.

Aircraft Systems Design

Over the years, aircraft research has evolved into distinct disciplines: aerodynamics, structures, propulsion, performance, controls, and others. With the distinction came isolation, as each discipline concentrated on activities related to its own concerns. This isolation has created at least two problems in the incorporation of advanced analysis techniques into the design process. First, disciplines have come to view production of their analysis results as a final product. Second, a discipline may require data from another discipline as input to an analysis, but may develop or acquire capabilities to generate these data locally. While this approach maintains independence from a multidisciplinary design group, it may not benefit from the total expertise of this group or their most recent improvements in each disciplinary area.

As industries and governments around the world refocus to achieve major quality improvements to become more competitive in the world marketplace, the term Concurrent Engineering (CE), or Integrated Product Development (IPD), is being used to express the desired environment. A major realization of this refocusing is that opportunities to improve quality are greatest early in the design process. CE has been defined as a systematic approach to the integrated, concurrent design of products and their related processes, including manufacture and support.

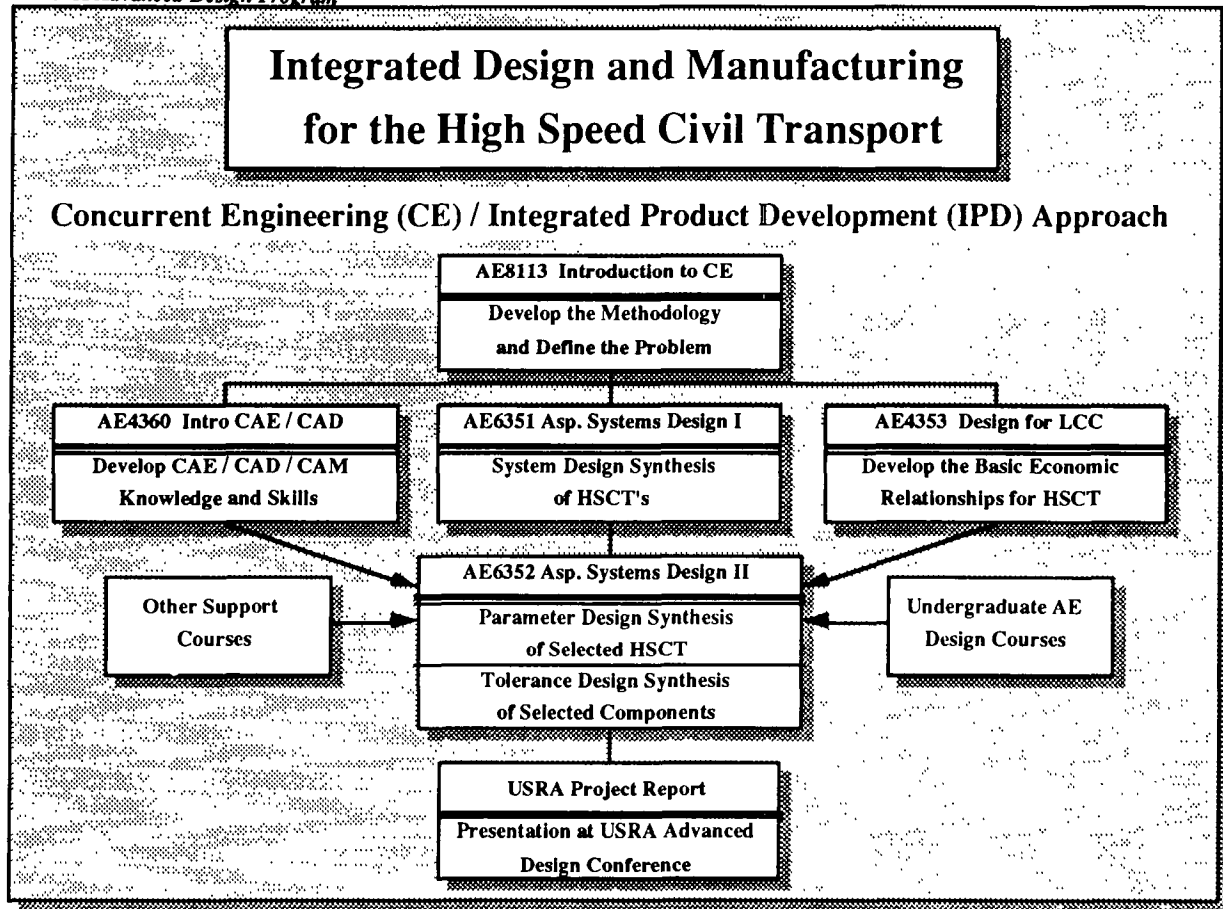


Figure 1: Georgia Tech NASA USRA ADP

CE has been called the implementation arm of the Total Quality Management (TQM) strategy. It has also been called a modern treatment of systems engineering which combines quality engineering methods in a computer integrated environment. Integrated Product Development (IPD) and the use of an Integrated Product Team (IPT) is the form of CE being applied in most of the aerospace community. For the purposes of this report, CE and IPD will be used synonymously. A next generation of CE or IPD, termed Integrated Product and Process Development (IPPD), is evolving and is specifically addressing affordability and the business processes to achieve it. One major goal of the research associated with this effort is to provide a framework for the aerospace community to move into IPPD.

The generic methodology used by Georgia Tech in its NASA USRA ADP as well as other pilot projects is illustrated in Figure 2. The basis of Georgia Tech's methodology is built on the belief that CE includes the interaction of four key elements: Systems Engineering Methods, Quality Engineering Methods, a Top Down Design Decision Support Process, and a Computer Integrated Environment. Beneath the umbrella at the top of Figure 2 are the interactions of the four key elements. The Computer Integrated Environment is also located at the top of the umbrella to emphasize its importance in providing a mechanism for integration of the other three elements.

Since CE is the concurrent design of products and processes, both product and process design must be integrated. This is accomplished through the incorporation of both Systems Engineering Methods (product design driven) and Quality Engineering Methods (process design driven). Systems Engineering focuses on system decomposition from system to component to part, while Quality Engineering focuses on system recomposition from part to component to system.

The heart of the CE methodology is a Top Down Design Decision Support Process. Though decision support is not explicitly addressed in other evolving CE methodologies, it is an essential element, particularly for management, that is used to focus efforts on the design goals. It supplies a logical, rational means for including factors that must be considered when making a decision. The structure is not designed to restrict thinking, but to organize it and ensure its completeness. Since design can be viewed as an iterative decision making process, it can be described as a sequence of steps. The first course in the design sequence, Introduction to Concurrent Engineering, consisted of presenting the overall methodology and addressing the first three elements of the Top Down Design Decision Support Process:

- Establishing the Need,
- Defining the Problem, and
- Establishing Value Objectives.

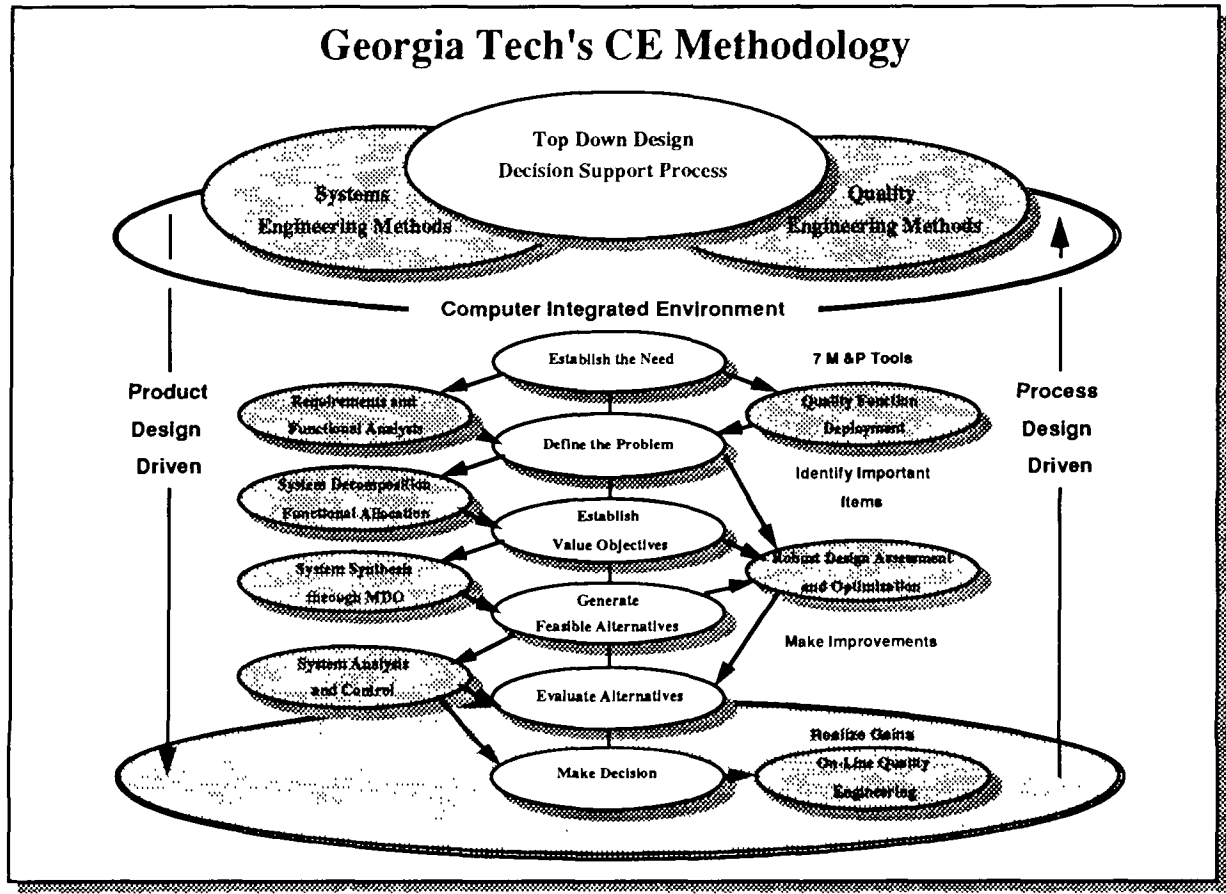


Figure 2: Georgia Tech's Concurrent Engineering Methodology

The follow-on capstone design courses (AE6351 and AE6352) were aimed at completing the second half of the Top Down Decision Support Process, especially with system synthesis through Multidisciplinary Design Optimization (MDO), both at the system level and component level (wing). Trades at the component level using information from part level trades are considered essential if an integrated design and manufacturing approach is to take place. There are two principal reasons for this required approach. First, a complex system like an airplane is not manufactured at the system, or even component level. A prime-sub-supplier relationship is always involved, with the prime aircraft manufacturer being the final assembler. Second, the complexities and interactions involved in understanding the total decomposition and recomposition of design and manufacturing of a total aircraft system is overwhelming for both industry and government, let alone academia. Therefore, choosing one primary component, such as a wing, is the only viable approach for a pilot project.

Intro to Concurrent Engineering - AE8113

The CE approach is intended to cause the developer, from the outset, to consider all elements of the product life cycle from concept through disposal, including quality, cost, schedule, and user requirements. The design of a total system was not the objective of this course. The goal was

to understand the overall generic CE methodology (see Figure 2) and define the "up-front" requirements, their decomposition, and the value objectives for a complex product such as the HSCT. This first education/research project consisted of three tasks, with deliverables for each.

The first task consisted of defining the HSCT problem by developing an initial Quality Function Deployment (QFD) Matrix that related the HSCT customer requirements to key product and process characteristics. This is usually called the Product Planning Matrix. Some of the Seven Management and Planning Tools (and Systems Engineering Tools (Requirements and Functional Analysis) were used to identify and decompose the customer requirements into key product and process characteristics.

The second task was the Establishment of Value Objectives for the HSCT. Value Objectives consist of setting feasibility constraints and establishing a Criterion Function describing a weighted relationship of pertinent criteria. The task consisted of deploying the key product and process characteristics of the first QFD Matrix to a second QFD Matrix.

This second QFD Matrix showed the relationships between the key product and process characteristics of the first QFD Matrix and the criteria that could be used to generate a criterion function and feasibility constraints. Some of the Seven Management and Planning Tools and Functional Analyses were used for brainstorming and to

decompose the characteristics and criteria to secondary and tertiary levels.

The third task was the Oral Presentation on December 2, 1992, of the results to an External Advisory Board (EAB) consisting of selected members of industry and academia. Submission of the final report was also a part of this task. Finally, an Activity Network Diagram was used to develop a schedule of events for the remaining NASA USRA ADP design courses.

As a result of this course, the team members had defined the customer requirements and key product and process characteristics, as well as determined their interrelationships with the use of QFD Matrices. Value Objectives were established for the HSCT, again using QFD. Upon reviewing both matrices, it was evident that those key product and process characteristics that had the strongest correlation with the customer requirements (in the first QFD Matrix) also had the strongest correlation with the criteria used to determine the value objectives (in the second QFD Matrix). The teams now had the capability to generate a criterion function which could be used to evaluate design alternatives to be generated in the first Aerospace Systems Design Course, AE6351. However, since the purpose of this first sequence of courses was to develop and exercise the CE design methodology (Figure 2), and the Boeing/Douglas HSCT baseline configuration was selected as the baseline concept; the criterion function was limited to the Productivity Index to evaluate alternative designs from the baseline. Maximization of the Productivity Index (P.I.) became the overall system objective function. Also, Life Cycle Costs (LCC) were included and were addressed in the Design for LCC course, AE4353.

Design for Life Cycle Cost - AE4353

During the mid - 1960s, the United States actively pursued the supersonic transport (SST) concept. In 1971, however, the U.S. Government canceled the prototype program because of increasing concerns over its economic and environmental viability. For an airplane to be economically viable, it must offer a value to the airline that is equal to or more than the price charged by the manufacturer to cover manufacturing costs. Economic viability occurs when a market size justifies the investment and risk that both the manufacturer and an airline undertake when deciding to develop or purchase an airplane.

As the budgets of aircraft manufacturers and airlines become tighter, the total cost of a product becomes extremely important. Also, as the CE/IPD methodology in industry matures, the inclusion of business practices and "Re-engineering the Enterprise" have marked the progress toward true Integrated Product and Process Development (IPPD). This total cost or Life Cycle Cost (LCC) is defined as the total cost of a system over its full life. This includes the cost of development, acquisition, operation, support and disposal. The life cycle cost of the system has to be addressed during the design process. The ability to design around potential problems through essential cost effective trades from the beginning can reduce or eliminate

the need for major "show-stopping" changes in the future. This benefit is realized in reduced development cost, reduced delays, redesigns, and inherent product development cycle times, as well as more marketable products. These benefits translate into improved business practices such as reduced overheads, better "make or buy" decisions, and elimination of "hidden factories."

The major focus of the Design for Life Cycle Cost Course AE4353 was to conduct a sensitivity assessment of the HSCT, focusing on the Airline and Manufacturer Return on Investments (ROI). ROI was chosen as a first attempt to include business practices into the CE design methodology (figure 2), and move to an extended CE methodology, IPPD. There are several methods to achieve this goal. One Quality Engineering method which is now used extensively in both the United States and Asia is Taguchi's Parameter Design Optimization Method (PDOM).

One of the most important things in LCC analysis or Economic Sensitivity Assessment (ESA), the term being used for the HSCT, is to understand the significant cost drivers early in the design process. These cost factors can be divided into two categories - control factors and noise factors. Control factors are those factors which a design engineer can control during the design process. Noise factors on the other hand are those critical factors, such as the external environment, over which the designer has no control, but which will have a major influence on his design decisions and on the viability of his product. In the airline industry, for example, the cost of fuel is a critical noise factor. To conduct the HSCT economic sensitivity assessment, the Taguchi PDOM was used in conjunction with a fixed baseline configuration and Quality Function Deployment (QFD). The outline of this process is illustrated in figure 3.

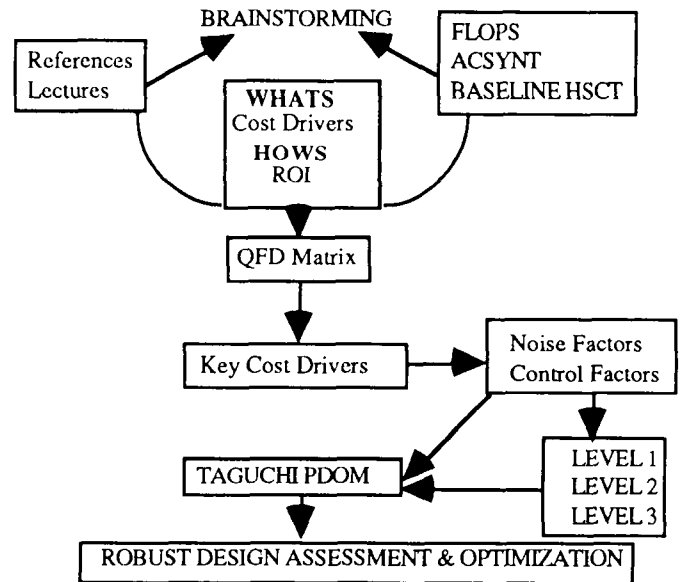


Figure 3: HSCT Economic Sensitivity Assessment.

The process began with Quality Function Deployment. This was used to determine the Key Cost Drivers for the HSCT manufacturer and airline industry. These cost drivers were separated into control and noise factors which were subsequently used to conduct the Taguchi PDOM.

The cost drivers for the airline were determined to be:

- Acquisition Cost
- Depreciation
- Insurance
- Fuel Cost
- Load Factor
- Facility/Building Cost
- Maintenance Cost
- Flight Equipment Maintenance

For the manufacturer, we determined that the important cost drivers were:

- New Manufacturing Techniques
- Engine Development
- Material Development
- Profit Margin
- Raw Materials

The second preliminary step was to determine the return on investment (ROI) criteria for both groups. This ROI criteria relates to business practices and overall productivity. It is simply a listing of the important issues that determine the level of profit for the groups.

For the airline:

- 1) Ticket Price
- 2) Labor and overhead rates
- 3) Aircraft Performance
- 4) Turnaround times

For the manufacturer:

- 1) Production Cost
- 2) Research and Development Cost
- 3) Aircraft Selling price
- 4) Airline Payment schedule
- 5) Warranty Obligation

This information was then placed in the QFD House of Quality to determine the key cost drivers. The key cost drivers were determined following the weighting scheme implemented in the QFD matrix. The key cost drivers were found to be:

Airline

- Acquisition cost
- Fuel cost
- Flight Equipment maintenance
- Load Factor
- Overall Maintenance cost

Manufacturer

- Material development cost
- Engine development cost
- Profit margin
- New Manufacturing Techniques

These cost drivers were divided into control factors and noise factors. These were then used as inputs to the ACSYNT[®] aircraft synthesis program. The economics module of ACSYNT was used as the simulation model for

exercising Taguchi's PDOM. The Boeing/NASA HSCT baseline configuration was used as a fixed input to this economics module for the cost sensitivity analysis.

ACSYNT Analysis

The ACSYNT input variables used in this study represented the best effort made to match the cost drivers output by the QFD matrix. For the manufacturer, the control factors specified to ACSYNT were: Engineering Labor Rates (material development), Manufacturer Fee (profit margin) and the Construction Factor (new manufacturing techniques). The noise factors were the Production Quantity and the Average Price Index. For the airline, the control factors were the Maintenance Labor Rates (maintenance cost), the Maintenance of Flight Equipment, and Flight Operations Costs. The noise factors were the Cost of Fuel, and the Load Factor. These factors were then varied in accordance with the orthogonal arrays of the Taguchi PDOM.

Using these Taguchi orthogonal arrays, the optimum control factors which maximized the ROI for the manufacturer and the airline were determined. These optimum factors were:

1-1-1 Airline

Lower Maintenance Labor Rates
Lower Maintenance Flight Equipment
Lower Flight Operation Cost

2-3-3 Manufacturer

Lower Engineering Labor Rates
Highest Fuselage Construction Factor
Highest Manufacturer Fee

These optimum input results were combined and executed to verify, if indeed, this "optimum" combination would result in higher ROI's when compared to the baseline aircraft.

The results indicated that the airline is directly affected by the manufacturer and **not** vice versa. For the ACSYNT analysis, the airline ROI went down and the manufacturer's return increased. This is due to the input and analysis structure of ACSYNT. In ACSYNT the results of the manufacturer is directly coupled to the airline. There is no automated coupling loop from the airline back to the manufacturer. Thus, the optimum of the airline has no effect on the manufacturer. To investigate the coupling that exists between these two parties, an off line analysis has to be conducted.

Although the identification of the optimum control factors in itself is not earth-shattering, the fact that an open loop system exists in the ACSYNT economic analysis between the manufacturer and its primary customer, the airline, demonstrates that CE and IPPD in particular is not implemented in this commonly used synthesis and analysis tool.

Computer Aided Design and Manufacturing

CAD/CAM/CAE technology has undergone enormous changes in the past 25 years. CAD systems, which began as two dimensional automated drafting systems, were used for

computer aided drafting, not computer aided design. As hardware became more powerful and numerical algorithms were improved, three dimensional wire frame systems evolved. In the past, although design work could be accomplished on these systems, the challenge existed in integrating them into the analysis and manufacturing processes. Today, CAD/ CAM tools can not only perform analysis while the design is being developed; they can also allow the design data to be passed directly to the user for access to numerical controlled manufacturing machines.

As an integral part of the Concurrent Engineering approach, CAD/CAE provides the computer integrated atmosphere which encompasses this methodology. This evolving capability makes the feasibility of conducting MDO a reality. Creating a digital product model enables electronic data sharing by all parties involved in product definition. This common database eliminates duplication efforts, and provides everyone with access to current data. With the improvements in 3-D modeling, design information can be relayed with great detail. Simulating product performance helps the designer to understand, before the product is fabricated, how it will perform. Simulations can be used early in the design process and the results incorporated during the development cycle. Digital mockups can be used to simulate the hardware assembly, thereby reducing the need for expensive physical mockups.

The capabilities of CAD/CAE are tremendous. Using today's common database approach, the designer can create a 3-D model that can be used for numerous activities. Analysts can construct finite element models from the design geometry data set. This data set can also be used to construct configuration models which are used to determine part interferences and fit. Tooling and access platforms can also be developed from this database, allowing the early identification of problems usually not found until fabrication. Additionally, traditional drawings can be created by taking 2-D views of the 3-D models and letting the computer automatically add the necessary dimensions.

CAE/CAM at Georgia Tech - AE4360

The fundamentals of Computer Aided Design were taught in the AE4360 class as part of the Concurrent Engineering/ Integrated Product Design course sequence outlined earlier. The purpose of this class was twofold. First, it presented the primary concepts behind the computational representation of objects. Second, it introduced two primary design and analysis tools.

These were:

- 1) Professional CADAM®
- 2) CATIA™

Professional CADAM is an interactive computer aided design system that is currently supported by the IBM Corporation. It is used primarily for 2-D geometric representation, and can be used for several analyses. CADAM was used to create the three view orthographic drawings of the aircraft used in this study. It was also used to illustrate the CG location of major aircraft components.

CATIA is a *Computer-graphics Aided Three-dimensional Interactive Application* system. CATIA, developed by

Dassault, has become an industry standard throughout most of the aerospace community. It is used to create three dimensional geometric models using wireframe, surface and solid modeling constructions. Additional application modules incorporated with CATIA provide capabilities for kinematics, robotics, Finite Element Modeling mesh generation, NC mill and lathe programming, structural member design and image generation. CATIA was used to ensure that the primary structure designed to support the wing would fit within the volume generated from the aerodynamic study.

Aerospace Systems Design I - AE6351

This first capstone design course addresses "System Synthesis through Multi-disciplinary Design Optimization (MDO)." Two closely related projects were associated with this course. The first was the conceptual design refinement of a baseline HSCT configuration defined by Boeing and Douglas in their systems studies. This project was essentially individual in nature and was intended to familiarize the team members with conceptual design systems synthesis trade-offs for the HSCT. The second project was team oriented and was intended to introduce students to sensitivity analysis and some analytical methods and tools used in preliminary design. NASA's synthesis codes FLOPS and ACSYNT were the primary tools used for these studies. One of the two teams used ACSYNT and the other used FLOPS. The same initial configuration and mission profile were modeled in both.

This project was modeled after the producibility technology studies that the Lockheed-California Company conducted in the mid-1970s. The purpose of the studies, funded by NASA's Langley Research Center (LaRC), was to assess materials and producibility methods for the design of the primary structure of a supersonic cruise aircraft. Emphasis was placed on an integrated design and manufacturing approach to develop low-cost producible structural configurations by identifying potential materials and fabrication technologies that would be available in the 1980s and 1990s for advanced technologies. While the studies are somewhat out of date, they served as a good foundation for Georgia Tech's first efforts, and introduced students to the methods and tools used in industry.

The criterion used to evaluate the initial baseline configuration was the Productivity Index (P.I.). This criterion addresses the relationships between optimum aircraft performance and various economic and technical design constraints. The development of an economically viable supersonic cruise aircraft is primarily dependent upon the successful integration of interactive advanced technologies involving:

- aerodynamics / performance,
- propulsion / integration, and
- structures / materials / manufacturing.

Parametric variations were performed on key design parameters in these three areas. These variations were related to the Productivity Index (P.I.) and ideas for modification of the initial baseline configuration were generated individually

by team members in each of the four respective areas. Upon culmination of all ideas and efforts, a final revised baseline configuration was selected to be used for the next quarter's capstone preliminary design course, Aerospace Systems Design II, AE 6352.

Criterion Selection

The paramount issue in the decision process is whether an ecologically suitable HSCT can be developed with acceptable risk that will provide safe and profitable operation. The pivotal concerns regarding any future HSCT are noise and pollutant emissions (both on the ground and at altitude), performance, cost, and development risk. Recently, an assessment was conducted of the mission performance benefits associated with the technology improvements and goals of NASA's HiSAIR Program. Advanced technologies in the areas of structures, propulsion, flight-deck systems, and aerodynamics were applied to a representative Mach 2.4 vehicle concept based on 1990 technology. The payoffs associated with each particular discipline were broken down to identify the result from the proposed major elements within each discipline. For each technology, a sizing thumbprint was generated, including selected constraints. The focus of these efforts was on minimizing the aircraft's TOGW by applying advanced technologies to key parameters within each discipline.

Our approach is similar to that used by NASA for their study. While minimizing TOGW is often used as a criterion, or objective function, it is often not a complete measure and does not relate completely to economic considerations. Instead of concentrating efforts on minimizing the TOGW, the objective of this analysis was to consider a criterion one step above the TOGW in the hierarchy of design variables: the Productivity Index (P.I.) was selected as the target variable of this study. The Productivity Index does indeed incorporate the aircraft's TOGW, as well as other important parameters in an explicit manner such as the payload, empty weight, fuel weight, and block speed. The Productivity Index is a commonly used criterion that relates pertinent product and process parameters to overall affordability. The Productivity Index relates design parameters to economic parameters and is defined as:

$$P.I. = \frac{P.L. \times V_B}{W_E + W_F}$$

where: $P.L.$ = Payload W_E = Weight Empty
 V_B = Block Speed W_F = Fuel Weight.

Traditionally, productivity has been a measure of relating a commercial aircraft's capability to economic viability. Thus, our selection of the productivity index as an analytical measure to evaluate alternative configuration refinements directly corresponds to an aircraft meeting its technical design goals, as well as being an economical success.

Baseline Productivity Index

As discussed in the previous section, the Productivity Index constitutes four design variables: payload, block speed, empty weight, and fuel weight. The baseline P.I. for our concept(s) modeled in FLOPS and ACSYNT were calculated as follows:

Payload:

294 pax x (170 lbs/person + 30.2 lbs baggage/person)
+9 stewardesses x (170 lbs/person + 30.2 lbs bagg./person)
+2 galley crew x (170 lbs/person + 30.2 lbs bagg./person)
+3 crew x (225 lbs/crew member)

TOTAL PAYLOAD = 61,736 lbs

Block Speed:

Block Speed = (Block Range / Block Time)
= (5000 nmi / 4.31 hrs)

BLOCK SPEED = 1160 kts (output from FLOPS)

EMPTY WEIGHT = 295,744 lbs (output from FLOPS)

FUEL WEIGHT = 305,612 lbs (output from FLOPS)

These values lead to an initial Productivity Index for the FLOPS baseline of:

$$P.I._{(Initial/FLOPS)} = 119.1 kts$$

The values for block speed, empty weight, and fuel weight output from ACSYNT lead to an initial Productivity Index of essentially the same value as that calculated with the parameters output from FLOPS. A comparison of the HSCT baseline P.I. with two other aircraft is provided in Table 1.

* Default values for person and baggage weights from ACSYNT.

Results

Two teams performed sensitivity analyses with respect to the Productivity Index in our three critical design areas: structures, propulsion, and aerodynamics. Both teams made recommendations for all three sections. At the end of the quarter, it was mutually agreed upon by the two teams to model the changes with respect to structures and propulsion in FLOPS, and to model the recommendations made with respect to aerodynamics in ACSYNT.

Structures and Propulsion Changes in FLOPS

Three parameters in FLOPS were changed in our initial baseline configuration based on our new sensitivity analysis with respect to the Productivity Index. An aggressive use of composites [mainly] in the wing, an increase in the engine overall pressure ratio, and a decrease in engine turbine inlet temperature all increased the Productivity Index. The variable FCOMP was used to model the use of composites

in the wing. After changes, 22,564 lbs of composites were used in the revised baseline (20,637 lbs in the wing) as compared to none in the initial baseline. The percentage of the composites used can be broken down as follows: (91.4%) wing, (7.1%) landing gear, (1.1%) controls, (0.2%) horizontal tail, and the remaining (0.2%) in the vertical tail. This addition of more than 22,500 lbs of composites, coupled with an increase in engine overall pressure ratio (from an initial value of 18 to a final value of 22) and a decrease in turbine inlet temperature (from 3360 degrees Rankine to 3200 degrees Rankine) resulted in 21,629 lbs less fuel required to meet the 5000 nmi range requirement. *These changes increased the baseline P.I. from 119.1 kts to 127.5 kts.*

Aerodynamics Changes in ACSYNT

To determine the effect of Hybrid Laminar Flow Control (HLFC) technology on the productivity index of the baseline aircraft, the ACSYNT laminar to turbulent factor, SFWF, was used. This factor enables the tailoring of the aerodynamic performance of major aircraft components. In essence, an 11 percent reduction in the SFWF factor resulted in a corresponding reduction in turbulent drag. Based on NASA studies, it was determined that this 11 percent reduction would require full wing HLFC. If only leading edge HLFC was employed, this would result in a reduction of approximately 6 percent. In addition to determining the effect of HLFC on the Productivity Index, the wing area was varied to observe its effect as well. The baseline area of 7700 square feet was varied between 6800 and 8500 ft², while keeping the aspect ratio and wing sweep constant. The lower limit of 6800 ft² was set because the ACSYNT sizing program was unable to reliably perform a mission for a configuration below this limit. For this particular study, the range and Mach number of the baseline was held constant. Based on the area and HLFC changes, it was found that the maximum P.I. occurred when the wing area was 7700 square feet, and full wing HLFC was employed. The Productivity Index increase was from 117.4 knots to approximately 121.8 knots.

Having determined the maximum P.I. based on these changes, the "revised" baseline was analyzed to verify that it met the necessary constraints. The FAR 25 landing constraint for this vehicle is 11,000 feet. It was determined that all HLFC configurations with wing areas in excess of 7600 ft² conformed to this rule.

From the disciplinary sensitivity analyses conducted in AE6351, it was determined that improvements could be obtained in the baseline HSCT configuration using the Productivity Index (P.I.) as the Criterion Function (Figure 4). However, these improvements can not be achieved if the resulting manufacturing considerations are not taken into account. Therefore, a major focus for AE6352 would be to address integrated design and manufacturing issues at the wing level to close the loop and include system product and process trades.

AIRCRAFT	Concorde (acsynt) (3424 nmi mission)	Boeing 747-200 (5000 nmi mission)	HSCT- base (acsynt) (5000 nmi mission)
Gross Weight (lbs)	399,051	773,800	727,291
Block Speed (knots)	1124.46	463.86	1169.43
Payload (lbs)	25,000	90,710	61,735
Empty Weight (lbs)	169,060	365,800	294,524
Block Fuel (lbs)	167,258	269,600	320,638
PRODUCTIVITY INDEX (Knots)	83.58	66.22	117.35

Table 1. Comparison of Aircraft Productivity Index

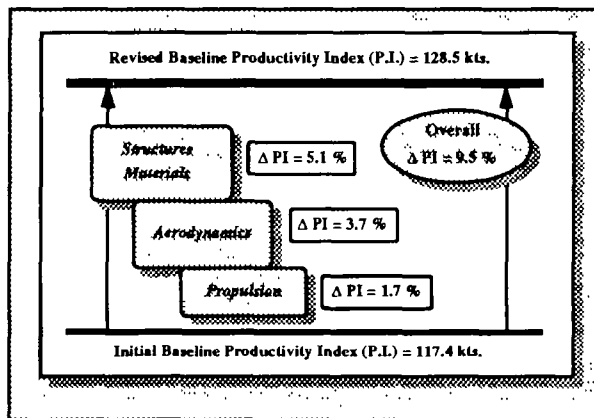


Figure 4: Overall Productivity Index Increase

Aerospace Systems Design II - AE6352

Methodology

The methodology used for the final quarter's work builds heavily upon what was learned the previous quarters. At the beginning of the quarter, some of the Seven Management and Planning Tools learned in Introduction to Concurrent Engineering were used to enable the team members to understand the design processes related to wing concept selection before analyses were attempted.

Tree Diagrams, Affinity Diagrams, Interrelationship Diagrams, and a QFD Matrix were generated at the beginning of the quarter. The Concurrent Engineering Tools were used to determine the relationships between several key

design areas and the cost analysis parameters used to make a wing concept selection.

Wing Concept Selection Methodology

Figure 5 shows the methodology that was used for the research and analysis of wing concepts for the HSCT.

The mission and performance requirements influence the system at two levels. First the mission and performance requirements are used by the synthesis codes FLOPS and ACSYNT for vehicle sizing. Second, some of these same mission performance requirements, in addition to others particular to certain disciplines, are used in the disciplinary trade-offs conducted at the wing level. Other disciplines, such as Layout / Mass Analysis and Airframe / Propulsion Integration, may only begin after some of the initial vehicle sizing has been completed.

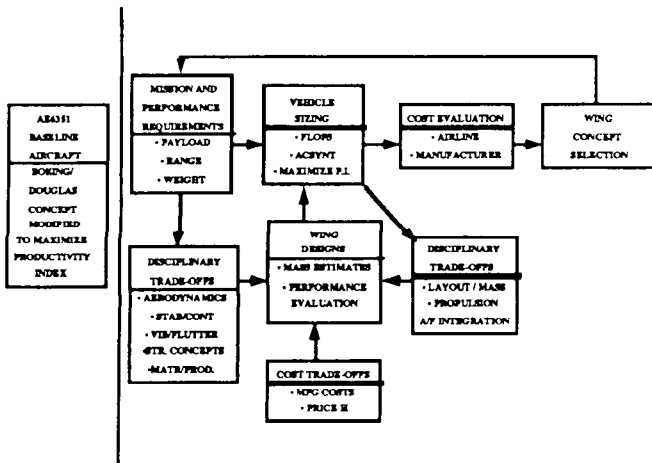


Figure 5: Wing Concept Selection

A designer's non-recurring (NR) manufacturing cost trade-off tool was used at the wing level to determine relative manufacturing costs associated with different wing concepts generated by the multidisciplinary trade-off studies. Once the parameters describing a new wing concept are determined, they can be inserted back into FLOPS and ACSYNT for overall vehicle performance estimation as well as airline and manufacturer cost estimation. Finally, the wing concept selection can be made based upon recommendation by the disciplines at the wing level and based upon vehicle performance and cost at the system level.

Results

The work completed for AE6352 entailed research and analysis focusing on the HSCT wing. Some of the Seven Management and Planning Tools were used early in the quarter to help the team determine the complex interrelationships among the various disciplines. Tree Diagrams, Interrelationship Diagrams, and QFD Matrices were used to determine the relationships between several key design areas and the cost parameters used to make a wing concept selection.

DESIGNER'S PRODUCTION COST TOOL

<i>Material</i>	<i>Cost</i>
All Aluminum	\$10,714,065
All Titanium	\$13,978,704
All Composite	\$14,477,161

Figure 6: Example Production Cost Results.

Analysis tools were identified and used for many of the design areas. FLOPS and ACSYNT were used at the system level. Other off-the-shelf codes were used for more detailed wing analysis. ASTROS was used for wing structural analysis and optimization. VORLAX and WINGDES were used for aerodynamics analysis. Several cost estimation tools were used for wing concept manufacturing cost estimates. Figure 6 shows an example of this estimate.

A methodology and database were established that can be used and expanded by next year's design teams.

Conclusions

The sequence of Aerospace Systems Design Courses addressing Integrated Design and Manufacturing for the HSCT has been completed for the first year. This report is submitted to summarize and document the results of the research and analyses conducted in these courses. More detailed results are provided in Reference 26.

Overall, the results of the year's efforts can be summarized as follows:

- A methodology and framework for Integrated Design and Manufacturing has been established.
- Analysis tools for the fundamental disciplines have been identified and are functional in most areas.
- A Computer Integrated Environment is being established to facilitate Multi-Disciplinary Design Optimization (MDO) and Integrated Product Development (IPD).

Acknowledgments

The editors of this report were Reginald Abel and William Marx. The Design team consisted of Tom Taylor, Chandra Purnawan, William Austin, Brian Byrd, Weidong Chen, Chang-Yul Song and Dave McCreary.

References:

1. High Speed Civil Transport Study, NASA Contractor Report 4233. Prepared for NASA Langley Research Center, Contract NAS1-18377, 1989

2. Carlson, Harry W., Mann, Michael J., Survey and Analysis of research on supersonic drag-due to lift minimization with recommendations for wing design. NASA Technical Paper 3202, September 1992.
3. Miranda, Luis R., et al, A generalized vortex lattice method for subsonic and supersonic flow considerations. NASA Contractor report 2865 Vorlax Report. Contract NAS1-12972, December 1977
4. Radkey, R.L., Welge, H.R., Roensch, R.L., Aerodynamic design of a Mach 2.2 supersonic cruise aircraft. AIAA paper 76-955, 1976.
5. Carlson, Harry W, Darden, Christine M, Mann, Michael J., Validation of a computer code for analysis of subsonic aerodynamic performance of wings with flaps in combination with a canard or horizontal tail and an application to optimization. NASA Technical Paper 2961, 1990
6. Messina, A.F., et al., NASA CR-132575: Substantiating Data Report: Arrow Wing Supersonic Cruise Aircraft Structural Design Concepts Evaluation. Vol 1 Section 3, 1977
7. Etkin, Bernard, Dynamics of Flight Stability and Control Second ed. 1982, John Wiley & Sons, Inc.
8. Ganley, G. A., "Concorde Development. Powerplant Installation and Associated Systems." SAE Technical Paper Series 912180, 1991.
9. Kulfan, Robert M., "Application of Favorable Aerodynamic Interference to Supersonic Airplane Design." SAE Technical Paper Series 901988, 1990.
10. Luttgeharm, Clint, "Selecting Materials for Complex Aircraft Structures," vol. 11 Aerospace Engineering, April, 1991.
11. McGaral, W. and K. Campbell, "Development of Composite Materials Applications to Production Nacelle Component Structures." SAE Technical Paper Series 902017, 1990.
12. Kerrebrock, Jack L., Aircraft Engines and Gas Turbines. The MIT Press, 1977.
13. McCloy, R.W., The Fundamentals of Supersonic Propulsion. The Boeing Company, 1967.
14. Oates, Gordon C., Aircraft Propulsion Systems Technology and Design. American Institute of Aeronautics and Astronautics, 1989.
15. Advanced Materials by Design. Summary Report, Congress of the United States, Office of Technology Assessment, OTA-E-352, June, 1988.
16. Bhatia, Kumar G., and Wertheimer, Jiri, Aeroelastic Challenges for a High Speed Civil Transport. AIAA-93-1478, 34th AIAA/ASME/ASCE/AHS/ASC Structures, Structural Dynamics, and Materials Conference, La Jolla, CA, April 1993.
17. Dovi, A.R., et al, Multidisciplinary Design Integration System for a Supersonic Transport Aircraft. AIAA-92-4841, 4th AIAA/USAF/NASA/OAI Synopsium on Multidisciplinary Analysis and Optimization, Cleveland, OH, September, 1992.
18. Messina, A.F., et al, "Vibration and Flutter", Section 10 of Arrow Wing Supersonic Structural Design Concepts Evaluation. NASA CR-132575, 1977.
19. Sakata, I.F., and Davis, G.W., Evaluation of Structural Design Concepts for an Arrow-Wing Supersonic Cruise Aircraft. NASA CR-2667, May, 1977.
20. Douglas Aircraft Company, "Study of High-Speed Civil Transport", NASA-CR-4235, 1989.
21. Arrow Wing Supersonic Structural Design Concepts Evaluation. NASA CR-132575, 1977.
22. Niu, Michael C.Y., "Airframe Structural Design ", Conmilit Press Ltd., 1988.
23. Roskam, J., "Airplane Design - Part I: Preliminary Sizing of Airplane", Roskam Aviation and Engineering Corporation, 1989.
24. Roskam, J., "Airplane Design - Part V: Component Weight Estimation", Roskam Aviation and Engineering Corporation, 1989.
25. "Code of Federal Regulations 14" FAR 25
26. Marx, William J., and Abel, Reginald W., Integrated Design and Manufacturing for the High Speed Civil Transport. Final Documentation of the 1992/1993 Georgia Tech NASA USRA ADP.

OPERATIONAL DESIGN CONSIDERATIONS FOR AN OBLIQUE ALL-WING SUPERSONIC TRANSPORT

University of Kansas
Aerospace Engineering Department
Lawrence, Kansas

Dr. Jan Roskam
Valerie Jones, Teaching Assistant
Troy Downen, Steve Smith

Abstract

The design of an Oblique All-Wing (OAW) supersonic transport presents several unique problems relating to the integration of the passenger cabin, landing gear, engines, and structure into the airplane. Because the airplane is a flying wing, the cabin height determines the wing dimensions. Doors for passenger and cargo loading and unloading, as well as emergency exits, must be located in the leading and trailing edges of the aircraft, requiring that the spars be cut. The engines and landing gear of the Oblique All-Wing often conflict during taxi and take-off ground run conditions. Burst plane locations and cabin noise also affect the placement of the engines. Directional control of the OAW is provided by drag rudders.

Introduction

The OAW concept first gained widespread attention because of the work done by R.T. Jones¹ in 1952. Because it distributes lift over a longer streamwise distance, Jones concluded that the Oblique All-Wing configuration would result in significantly reduced wave drag compared to traditional swept wing configurations for supersonic aircraft. Interest in the OAW has been renewed in the past decade as the need for large capacity supersonic transports has become apparent.

The emphasis of this design has been on the operational feasibility of the OAW concept due to the integration of such items as the passenger cabin, landing gear, engines, and cargo. Preliminary configuration decisions for the KU OAWT were based on the Oblique All-Wing developed by Mark Waters².

Internal Cabin Design

Typically the design of the internal cabin arrangement for an aircraft would be a routine process. The unique configuration of the oblique flying wing makes the cabin design for the KU OAWT somewhat

less than routine however. The passenger seating arrangement has to be specially designed to meet the FAR requirements. Passenger and cargo loading is unique due to lack of a fuselage on the OAWT, and design of emergency exits requires special attention because of the all-wing design.

Passenger Seating Arrangement

The KU OAWT was designed to take off and land at a 37.5° angle of slew. This decreases the effective span of the aircraft as it sits on the runway and therefore reduces the risk of striking buildings or aircraft on neighboring runways. This angle of slew is also required for the landing gear to fit onto the runway. However, taking-off and landing at an angle of slew presents a unique problem for the cabin arrangement.

According to the AE 622 design team's interpretation of the Federal Airworthiness Regulation (FAR) Part 25.561, passengers may be subjected to the following maximum inertial forces during a worst case crash scenario:

- Forward g limit, 9.0g
- Lateral g limit, 4.0g

Assume for a moment that the passengers are sitting facing the leading edge of the wing (this would be considered facing forward if on board a conventional aircraft). The wing takes off and lands at an angle of 37.5°, thus the passengers are also seated at this angle during take off and landing. If the aircraft should crash during take off or landing (at 37.5°), a forces calculation indicates the passengers will experience the following inertial forces:

- Forward, 4.71g
- Lateral, 8.65g

The conventional cabin arrangement violates the FARs' limit on lateral inertial forces in a worst case crash scenario.

To remedy this situation the passengers are arranged in the cabin to face the direction of take off and landing. Figure 1 shows the KU OAWT cabin with the passenger seats arranged at a 37.5° angle.

Passenger Ingress/Egress

A traditional fuselage allows for passenger ingress/egress through the side of the aircraft. Since the OAWT does not have a fuselage the passengers are limited to exits through the top, bottom, leading edge and trailing edge of the wing. Each of these methods of regular ingress/egress were examined in turn.

If the normal passenger loading were through the top or bottom of the aircraft, some arrangement with ladders, steps, or escalators would be required. This would limit access to the aircraft by the very elderly, the very young, and the handicapped. Airlines would probably be reluctant to invest in an aircraft with limited access or in an aircraft that would require the additional expense of purchasing stairs, escalators, etc. Conducting regular loading of passengers through the leading edge of the aircraft would pose several problems. Machining tolerances would create mismatches between the doors and the rest of the aircraft leading edge. Furthermore, wearing of the door seals with time would also create mismatch. This mismatch over the leading edge would tend to disrupt the airflow over the leading edge and degrade the performance of the aircraft. The superior performance of the OAWT is the reason the aircraft is being considered as a SST alternative, and should thus be preserved in every design phase. Also, the high dynamic pressures encountered at the leading edge during supersonic cruise would require a heavy door structure and the accompanying weight penalties. Instances of high angles of attack, where suction forces act on the leading edge (creating "wing thrust"), would also require a heavy door structure.

To avoid weight penalties and restricted access, the regular passenger exits were designed into the trailing edge of the aircraft. Figure 2 shows one possible method of passenger ingress and egress in which the trailing edge opens, clamshell-like, as the standard airport ramp backs up to the aircraft. Note that foreign object damage (FOD) could be a problem between the trailing edge and the airport ramp. Figure 1 shows the location of the trailing edge doors on the cabin. The location of the doors is highly dependent on the landing gear bay locations, something that is unique to the OAWT.

Cargo/Baggage Loading

Determination of locations for cargo/baggage doors follows a similar process to the passenger doors. Cargo access doors on the leading edge were rejected for the same reasons passenger doors were not designed into the leading edge. Cargo doors on the top of the aircraft would require the airlines to purchase special cranes to load the cargo. The infamous "last two bags" checked in by the last minute passenger would require the use of the crane just as much as loading the LD3 containers. Airlines would, again, be hesitant to purchase an airplane that requires large additional investments in support hardware.

Cargo could be loaded through the bottom of the aircraft. Again, a special cargo loader would be required for this method of loading, to lift the LD3 containers into place. To avoid the extra expense of special cargo loaders, doors in the trailing edge (similar to the passenger doors) would facilitate the use of airlines' current scissorbed cargo trucks. Figure 3 shows how the trucks could back up to the clamshell opening to load LD3 containers on board the aircraft. Note again that FOD problems with the trailing edge and the cargo truck could occur.

Emergency Exit Design

According to the FARs, the KU OAWT would require more than a dozen type I emergency exits, in addition to the 5 passenger ingress/egress type A doors already located in Figure 1. Only 5 pairs of type A emergency exit doors would be required for a seating capacity of 500 passengers. The 10 type A doors were chosen as emergency exits to reduce weight penalties and the reduce the number of cabin crew required during an emergency situation.

Crash Scenarios

The location of the emergency exits is dependent on the various crash scenarios of the OAWT. The first of these possible crash scenarios is an emergency landing with the landing gear down. In this scenario any emergency exits located on the top, bottom, leading edge or trailing edge of the aircraft would be equally accessible by the passengers.

Another possible scenario is an emergency crash on land but with the landing gear still retracted. In this situation, any emergency exits located on the bottom of the aircraft could not be used by the passengers. Because of the inertial distribution of the

OAWT, the wing is just as likely to crash upside-down as it is to crash upright. In that situation, any emergency exits on the top of the aircraft would be useless to the passengers.

The intercontinental mission profile of the OAWT indicates that a major portion of flight time will be spent over water. For this reason emergency ditching of the OAWT in water must also be considered. Two possible ditch scenarios are possible. An upright ditch in water would result in the bottom exits being inaccessible and an inverted ditch would result in the top-located exits being inaccessible. A study was conducted to confirm what the attitude of the OAWT would be while floating in water. The KU OAWT floats at about a 2° angle between the chordline and the waterline, both upright and inverted.

A review of the various crash scenarios indicates that at some point top and bottom located exits might be inaccessible to passengers. Additionally, top or bottom exits would require passengers to use ladders in an emergency, which would not be acceptable during an evacuation. This design team made the decision to locate all passenger emergency exits either in the leading or trailing edges of the aircraft, despite the penalties for placing doors in the leading edge. These exits should be exclusively emergency exits and should not be opened under normal conditions for any reason. Some sort of removable panel should cover the door on the outside leading edge of the aircraft to keep the leading edge smooth and prevent disruption of the airflow. These panels could be quickly removed during an emergency by use of pyrotechniques or some mechanical means. Later the panels could be replaced so the aircraft could return to regular service.

Figure 4 shows the locations of the emergency exits.

Landing Gear Design

Preliminary landing gear design of the KU OAWT is critical to its success. A takeoff weight of greater than 1.4 million lbs requires special attention be paid to surface compatibility. The size of the aircraft presents several problems also; including ground maneuverability, runway fit, and gear retraction volume.

Strut Locations and Loads

As determined in Reference 1, a nine strut layout is employed for the OAW. Five struts are positioned along the front spar, and four along the

rear spar. The methods of Reference 3 were used to calculate the static strut loads and the maximum dynamic braking load on a single nose strut:

- $P_n = 156,500$ lbs
- $P_m = 154,400$ lbs
- $P_{nDYN} = 184,000$ lbs

The maximum single tire dynamic load was calculated:

- $P_{SWmax} = 38,300$ lbs

It should be noted that this value accounts for: 1) a 25% increase in weight due to future growth of the aircraft, 2) the required 7% safety factor for FAR25 certification, and 3) an additional 10% safety factor due to the unconventionality of the landing gear arrangement.

Tire Selection

Candidate tires for the KU OAWT were selected from tables of Reference 4 with the following criterion:

- Maximum Static Loading:
 $38,300 \text{ lbs} < P_{max} < 40,000 \text{ lbs}$

This assumption is based upon an assumed six wheel per bogey layout. The tire that was selected is a 44x16 in., type VII tire. It has a maximum loading of 38,400 lbs. and a maximum speed of 200 mph.

Bogey Layout

As previously mentioned, a tri twin-tandem layout is assumed for each bogey of the landing gear. Determination of bogey dimensions requires the calculation of grown tire sizes and minimum required tire clearances to surrounding structure. The following tire growth factors were assumed:

- Width, $f_W = 1.04$
- Diameter, $f_D = 2.14$ (pg 6-15, Ref. 2)

The 'grown' tire dimensions are:

- $W_g = 16.64$ "
- $D_g = 45.82$ "

The minimum required clearances to surrounding structure, as determined from Figure 6-14 of Reference 2, are:

- Sidewall: 2.95"
- Radial: 1.89"
- Shoulder: 2.42"

The grown tire dimensions and minimum clearances lead to the following bogey characteristics:

- Total Bogey Length: 141"
(grown dimensions)
- Total Bogey Width: 51.2"
(grown dimensions)
- Wheel Base: 47.7"
(front axle to shock centerline)
- Wheel Track: 34.5"

Runway Fit

Research of Reference 1 specifies standard runway width to be 150 ft. FAR 25 Certification requires 25 feet of clearance on each side of the aircraft wheel track. The KU OAWT does not meet this requirement. In fact, the 2.5 ft clearance on each side may not be sufficient even if fully automated operations are assumed. This problem must be further researched.

Gear Strut Length

Strut lengths of conventional aircraft are frequently dictated by lateral clearance requirements. As determined by Reference 3, the required height to the wing chord plane to satisfy a 5 degree lateral clearance at 37.5 degrees slew is 9.7 feet. Serviceability requires a minimum clearance of 10.5 ft beneath the aircraft¹. The 10.5 ft minimum clearance will dictate the gear strut length.

Additional Considerations

Preliminary landing gear design for the KU OAWT requires further research in the following areas:

- ground maneuvering
- gear rotation scheduling
- gear placement

Ground Maneuverability

Maneuverability of the KU OAWT on the

ground will require a complex system to independently rotate each strut assembly. However, the friction forces in such a rotation, may be too large to overcome by a simple rotation of the strut. Additional measures, such as independent steering of wheels, may be necessary.

Gear Rotation Scheduling

Simultaneous rotation of all nine struts to the retracted position may not be feasible from an aircraft controllability standpoint. For this reason, scheduling of gear rotation may be required for the proposed gear layout to be acceptable.

Gear Placement

The chosen landing gear placement is acceptable from the standpoint of load distribution. However, location of the retracted gear may be critical to the effective emergency evacuation of the aircraft. The effects of placement of the landing gear at different locations must be evaluated. Emergency evacuation and the effects of load distribution on the aircraft and runway must be accounted for.

Engines

For the oblique all wing aircraft, the engines are a major design issue. The requirement that the engines must pivot during the flight creates operational problems.

Engines Beneath the Wing

Six engines were chosen for the KU OAW aircraft with the pivots located under the front spar of the wing. (To compensate for the large span of the flying wing on conventional taxi ways, it has been proposed to taxi the aircraft in the spanwise direction). However, as can be seen from Figure 5, this presents a problem for the engine placement. Assuming an engine pivot of 65 degrees and thrust vectoring up to 25 degrees, interference occurs between engine exhausts, landing gear, and other nacelles. One solution to this problem could involve using only the outboard port engine for taxi. However, in the event of engine failure, the aircraft would be unable to taxi.

Figure 6 displays a staggered engine configuration. This eliminates exhaust interference and allows two additional power sources in the case of engine failure. The staggering of the engines also

allows the pivots to be moved inboard from their initial positions in Figure 5.

Figure 7 displays potential problems with the staggered engines mounted under the wing. During the take-off ground run, one or two of the engines could experience Foreign Object Damage (FOD) from the landing gear. This is thought to be operationally unacceptable.

Engine Placement for the KU OAWT

One possible solution to the FOD problem is to mount the engines above the wing. The same engine placement can be used on top of the wing as below the wing, as shown in Figure 7. This eliminates the danger of FOD damage to the engines.

Another potential problem concerning the engine placement is turbine burst plane interference. With the engine configuration shown in Figure 7 (engines above the wing), the turbine planes of the engines are directly above the fuel tanks. Containment rings, increased local skin thickness, and fuel dry bays could help prevent fuel tank damage in the case of turbine failure. The turbine plane and

fuel tank interference could be avoided all together by placing the engines above and behind the passenger cabin as shown in Figure 8. The outboard port engine has been asymmetrically staggered to allow for dual engine operation during spanwise taxi. With the engines in close proximity to the passenger cabin, excessive noise and vibration in the passenger cabin could also occur.

Directional Control

Traditionally directional control is handled through the vertical tail(s) and rudder. However, due to the unique configuration of the OAW, directional control was handled through the use of drag rudders.

The engine which produces the largest (in magnitude) yaw moment was determined to be the trailing engine in slew. Windmilling drag on the failed engine was estimated using the methods of Reference 4, Eq. 4.67. Table 5.1 summarizes the various yaw moments which must be counter-acted by the directional control system.

Table 5.1: KU OAWT Yaw Moments in Various Flight Conditions

Flight Condition	Yaw Moment (about c.g.)
Subsonic flight at 37.5° slew, all six engines operating	-2.15 x 10 ⁶ ft-lb
Supersonic flight at 67.5° slew, all six engines operating	-3.10 x 10 ⁶ ft-lb
Subsonic flight at 37.5° slew, single critical engine out	-17.51 x 10 ⁶ ft-lb
Supersonic flight at 67.5° slew, single critical engine out	-11.66 x 10 ⁶ ft-lb

A single drag rudder capable of counter-acting these yaw moments was sized. The drag

rudder area required for various flight conditions is given in Table 5.2.

Table 5.2: Drag Rudder Sizes Necessary for Directional Control in Various Flight Conditions

Flight Condition	$\Delta C_{D_{airplane}}$	SDR (ft. ²)
37.5° slew, all six engines operating	0.0056	151
67.5° slew, all six engines operating	0.0045	122
37.5° slew, one critical engine out	0.0450	1213
67.5° slew, one critical engine out	0.0170	459

A drag rudder size of 1213 sq ft (i.e. 607 sq ft on the top half and 607 sq ft on the bottom half of the split flap) will not fit onto the OAWT. Therefore some alternative must be found for the single engine-out directional control other than using solely a drag rudder.

OEI Corresponding Engine Shutdown

If one engine fails in flight, a solution to the directional control problem may be to shut down a corresponding engine on the other airplane wing.

This would decrease the yaw moment that must be fought by the drag rudder (or vertical tails). If the critical engine fails, the corresponding engine would

be the leading engine on the starboard wing. Table 5.3 gives the yaw moments that must be countered with the corresponding engine shut down.

Table 5.3: Drag Rudder Sizes for One Engine Failure and Corresponding Engine Shut Down

Flight Condition	Yaw Moment (about c.g.) to be countered (ft.-lb.)	$\Delta C_{D_{airplane}}$	S_{DR} (ft. ²)
37.5° slew, critical and corresponding engine failed	-1.43 x 106	0.0037	100
67.5° slew, critical and corresponding engine failed	-1.97 x 106	0.0029	77

Table 5.3 shows that putting a routine into the control software of the OAWT to shut down a corresponding engine would be advantageous (the in-flight yaw moment with all 6 engines operating would become the critical yaw moment to counter).

Conclusions

The unique problems associated with the design of an Oblique All-Wing supersonic transport can be overcome. The cabin must be laid out with the seats at an angle, in order to meet FAR crash force requirements. The passenger and cargo doors are located in the rear spar, and additional emergency exits are located in the front and rear spars. Nine landing gear with six-wheel bogeys are required to support the OAW. The engines are placed over the wing in order to avoid FOD damage, and in a staggered configuration in order to avoid flame out caused by ingesting another engine's exhaust. Directional control is provided by drag rudders, with a corresponding engine shut down in the case of an engine failure.

References

1. Jones, R.T., Wing Theory, Princeton University Press, Princeton, N.J., 1990.
2. Waters, Mark, "Structural and Aerodynamic Considerations for an Oblique All-Wing Aircraft", AIAA paper 92-4220.
3. Currey, Norman S., Landing Gear Design Handbook, Lockheed Corp., Jan. 1992.
4. Roskam, Jan, Airplane Design Part IV, RAEC, Ottawa, KS, 1986.

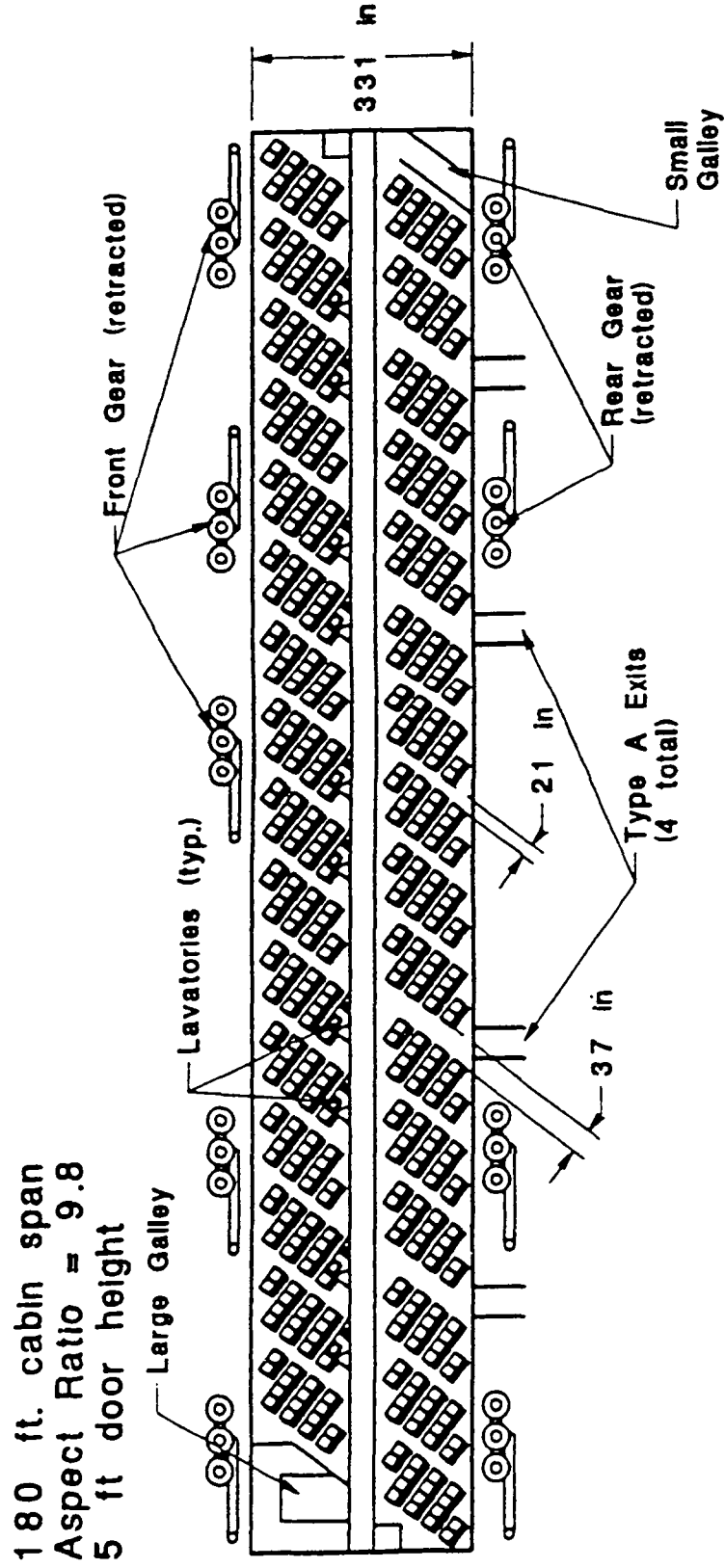


FIGURE 1: PLANFORM VIEW OF KU OAWT INTERNAL CABIN ARRANGEMENT

6 foot figures to scale

Proceedings of the 9th Summer Conference
NASA/USRA Advanced Design Program

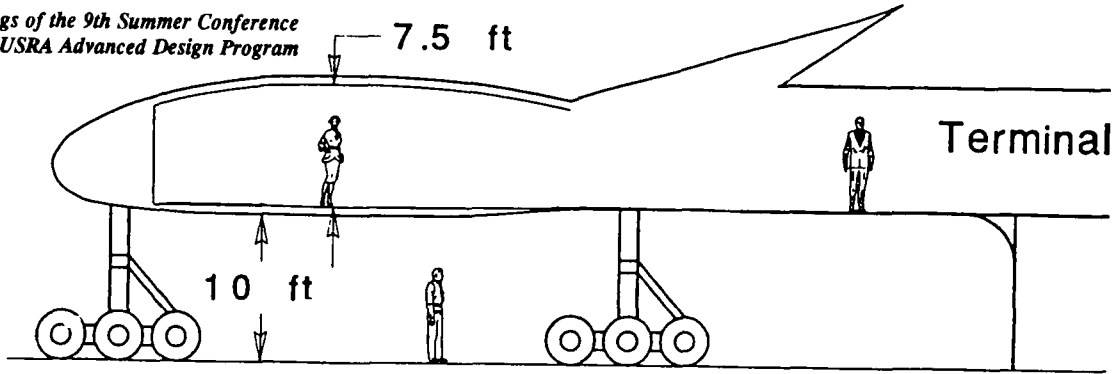


FIGURE 2: SIDE VIEW OF PASSENGER LOADING

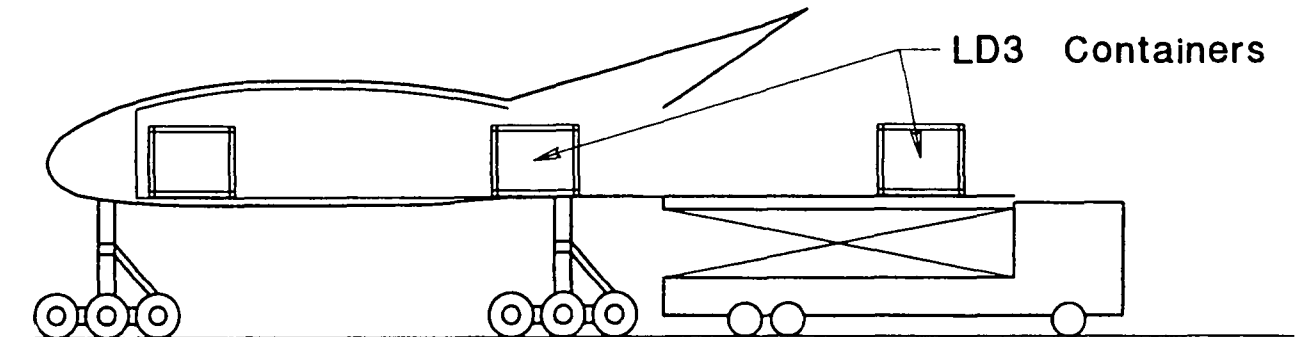


FIGURE 3: SIDE VIEW OF POSSIBLE CARGO LOADING SCENARIO

180 ft cabin span
Aspect Ratio = 8.27
6' 2" door height

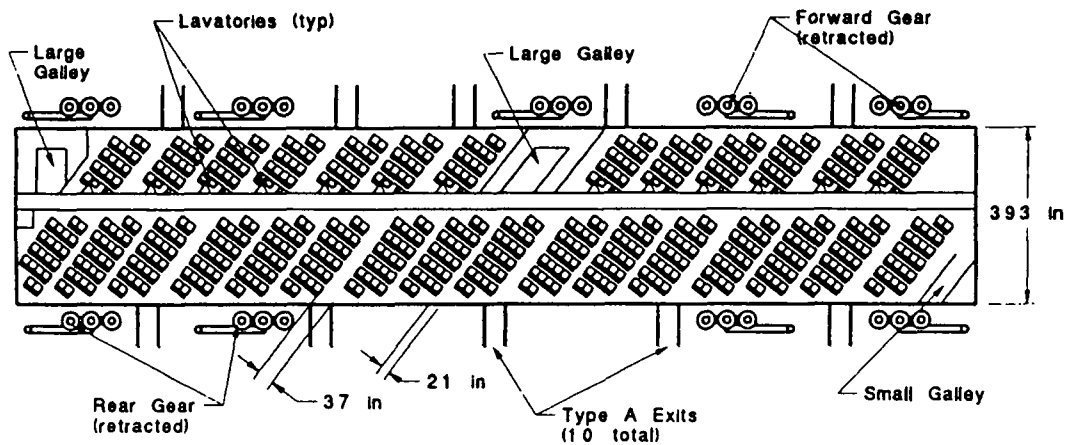


FIGURE 4: CABIN ARRANGEMENT WITH 6'2" DOOR HEIGHT

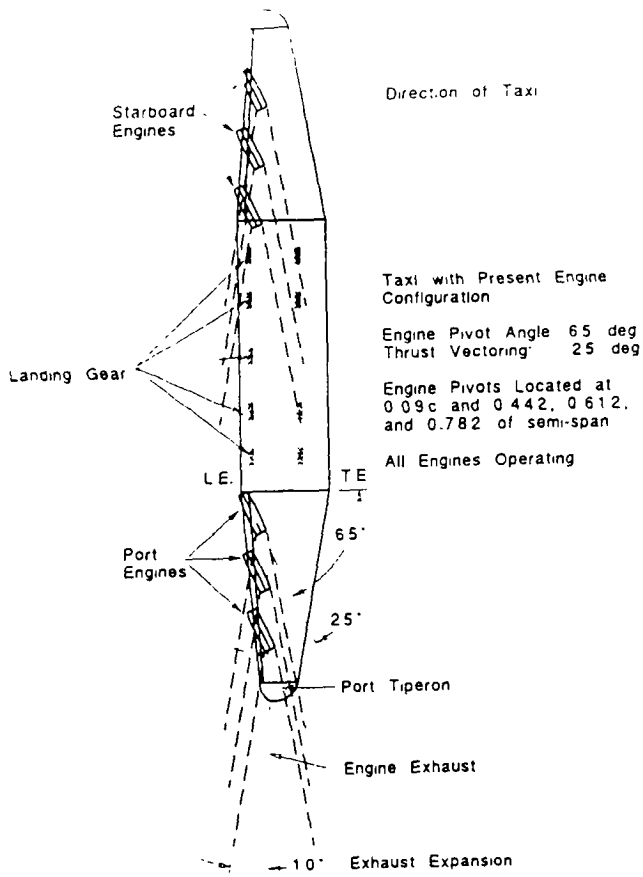


Figure 5 Taxi with Waters' Engine Configuration

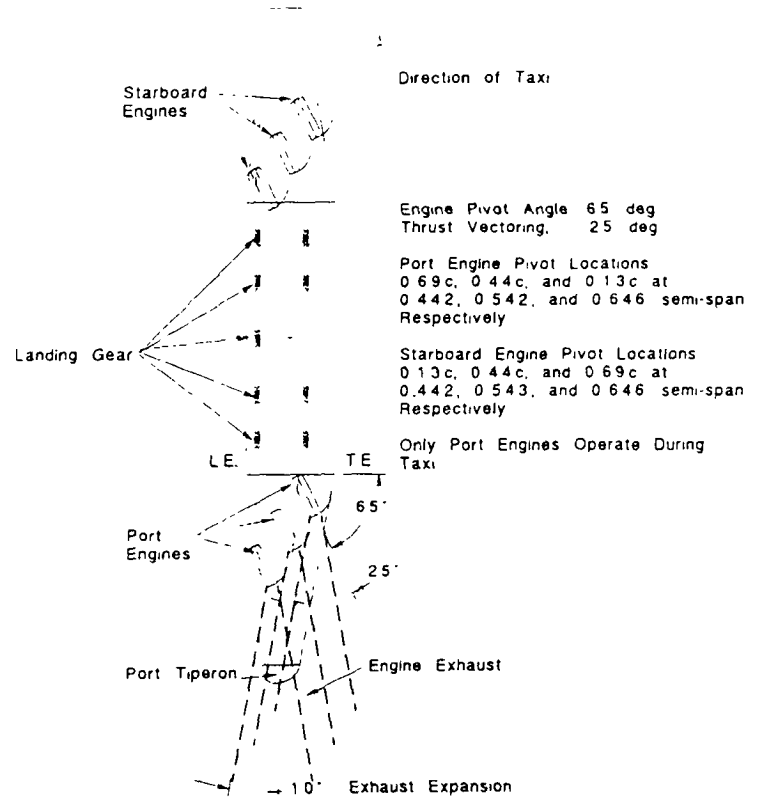


Figure 6 Taxi with Asymmetrical Engine Configuration

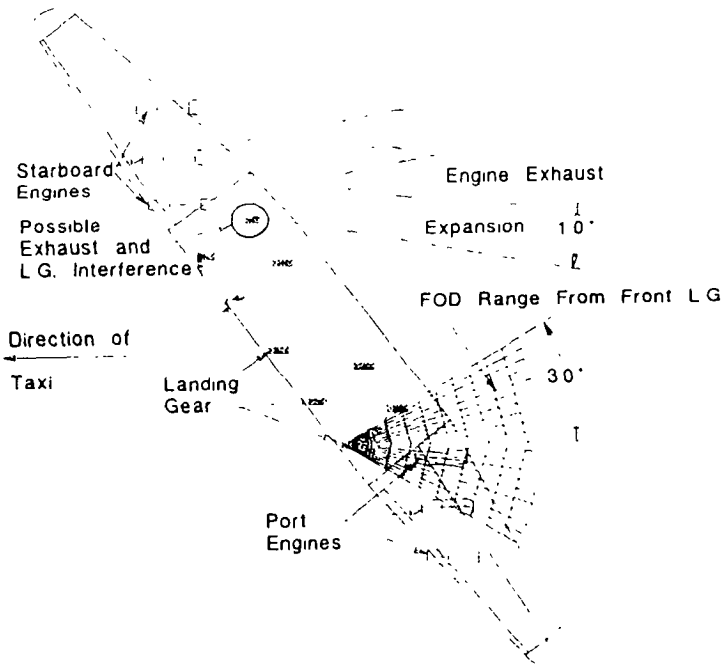


Figure 7 Take-off Taxi with Asymmetrical Engine Configuration

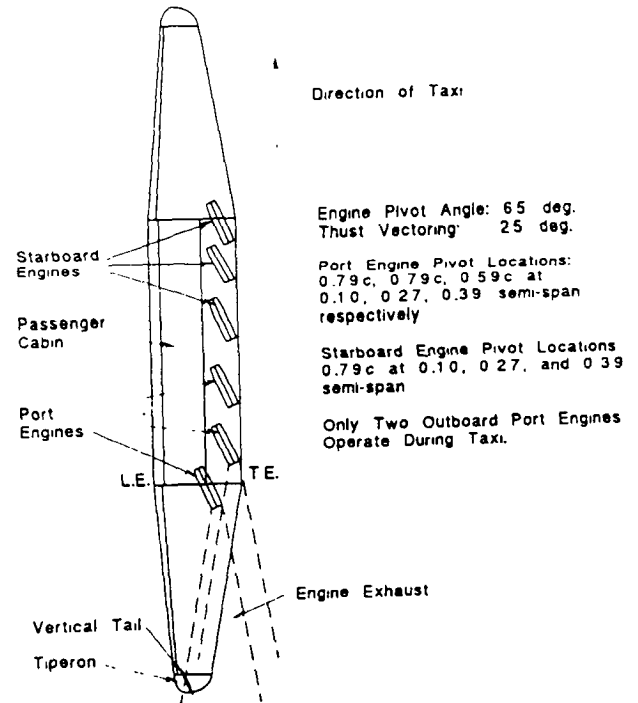


Figure 8 Taxi with Engines Above and Aft of Passenger Cabin

DESIGN OF AN AIRBORNE LAUNCH VEHICLE FOR AN AIR LAUNCHED SPACE BOOSTER

University of Michigan
Department of Aerospace Engineering
Ann Arbor, Michigan

Professor David W. Levy
John W. Blow, Teaching Assistant
Stefan M. Poth, Jr., Chin H. Chao, Scott A. Cohen,
Brian J. Dumont, and Mauricius A. Gibin

Abstract

A conceptual design is presented for a carrier vehicle for an air launched space booster. This airplane is capable of carrying a 500,000 pound satellite launch system to an altitude over 40,000 feet for launch. The airplane features a twin fuselage configuration for improved payload and landing gear integration, a high aspect ratio wing for maneuverability at altitude, and is powered by six General Electric GE-90 engines. The analysis methods used and the systems employed in the airplane are discussed. Launch costs are expected to be competitive with existing launch systems.

Introduction

One way of reducing the total weight of a space booster is to launch the booster from an airborne platform. This results in a lower booster vehicle weight for the same payload capacity. Among the advantages to this approach are that the kinetic and potential energy of the airborne platform are added to that of the space booster and that the launch takes place above a substantial portion of the atmosphere so that aerodynamic drag is reduced. One current design which takes advantage of this approach is the Pegasus, manufactured by Orbital Sciences Corporation. The Pegasus has a total weight of 41,000 pounds and a payload weight of 900 pounds. It has been carried aloft and launched by a Boeing B-52 and future launches are planned from a modified Lockheed L-1011.

In the future, there may be a market for an air launched space booster an order of magnitude larger. A space booster of this size would be capable of placing one or more satellites into geosynchronous earth orbit or a heavy payload into low earth orbit. Such a large booster would require a new airplane to be purpose built for its launch since no current airplane could carry a space booster of this size to any significant altitude.

Class history

In the fall of 1992, the University of Michigan Aerospace 481 Airplane Design class undertook the design of an airplane to carry a large air launched space booster. A preliminary design was formulated by each of the 35 students in the class. The space booster weight was set at 250,000 pounds to verify the feasibility of this project. Then, the class split into two groups to continue the design process, with one group pursuing a conventional design and the other group pursuing a more unusual design. The airplanes designed have a payload capacity of 500,000 pounds since the viability of this payload weight goal was proven with the individual design projects.

In the winter term, seven students elected to continue this design project under Aerospace 490/590 Advanced Airplane Design, a directed study class with the goal of presenting a more fully defined design at the USRA summer conference. Three designs were evaluated in the early portion of the class. First was a conventional design with the payload suspended beneath the fuselage. Second was a twin fuselage configuration with the space booster suspended beneath the wing. Last was a flying wing. The flying wing was an appealing configuration since it removed the fuselage volume which is wasted in the other two configurations. This design was eliminated after the discovery that it was not the best design for this mission from a stability and control standpoint. For the best landing gear and payload integration, the final design is based on the twin fuselage concept.

Overview

The University of Michigan Aerospace 490/590 Advanced Airplane Design class has designed the Eclipse, an aircraft whose primary mission is to act as a launch platform for a space booster weighing 500,000 pounds. Other mission requirements include:

- mission radius of 750 statute miles
- launch altitude of at least 40,000 feet
- the ability to use existing airport facilities
- reliance on components, subsystems, and processes currently used in production or which will be in the very near future
- the ability to perform 2.2g post-launch maneuver at altitude

Market studies concluded that six launch missions per year would be a realistic design goal. A ten year life span for the launch system is anticipated as this would reach until the introduction of the next planned launch systems. Only two airplanes will be built. The first will be a fully functional aircraft while the second will act as a structural spare. The design mission profile is shown in Figure 1.

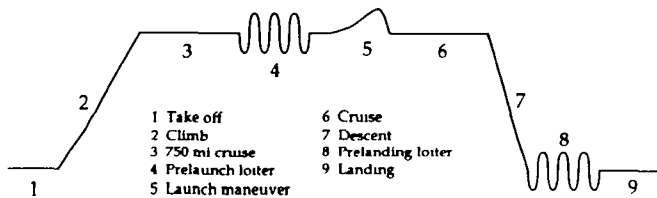


Fig. 1 Mission profile

Two other mission profiles were studied as well. The ferry mission, which consists of flying the maximum distance possible with the empty space booster, and a minimum fuel mission, which consists of a climb to maximum altitude, loiter, launch, and descent. The lack of fuel for the cruise portions results in a higher launch altitude. The design mission and maximum altitude mission performance calculations assume an aborted launch scenario. This is the worst case from a vehicle design standpoint due to the extra drag and weight of the booster which is attached for the return portion of the mission.

The final configuration of the Eclipse is presented in Figure 2 which is a configuration overview. Some of the important parameters are tabulated in Table 1. The most obvious aspect to this design is the twin fuselage configuration. This allowed for straightforward payload and landing gear integration. The high aspect ratio wing was necessitated by the need for controlled flight at high altitude. There are six engines to provide the thrust needed to attain altitude. Two vertical tails are positioned with the horizontal tail between them in a cruciform layout. This configuration keeps the tails out of the wake of the wing, payload, and engines while keeping the horizontal tail below an area susceptible to deep stall.

The airplane which is the closest in comparison to the Eclipse is the Antonov An-225 with a take off weight of 1,323,000 pounds. Available data for the An-225 indicates it could carry a 551,000 pound payload. It is doubtful, however, that it could meet the requirements of this mission since the heaviest payload carried to date is 344,000 pounds for a 3 1/2 hour mission whereas the design mission for the Eclipse calls for carrying a 500,000 pound payload almost seven hours.

Table 1 Eclipse parameters

Take off weight	1,227,000 lbf
Payload weight (U. of Michigan Gryphon)	479,000 lbf
Fuel weight (including ramp fuel)	241,000 lbf
Operational weight empty	541,000 lbf
Wing area	11,750 ft ²
Wing span	368 ft
Overall length	188.6 ft
Overall height	62.4 ft
Take off thrust (w/o extractions)	600,000 lbf
Thrust-to-weight ratio	0.489
Take off field length (to 35 ft)	4,300 ft
Landing field length (from 35 ft)	3,400 ft
Wing aspect ratio	11.53
Wing quarter chord sweep angle	22.1°
Wing loading	104.4 lbf/ft ²
Vertical tail area (each)	950 ft ²
Horizontal tail area	3700 ft ²
Cruise velocity	515 mph
Launch altitude (design mission)	43,300 ft

The remainder of this paper is an overview of the analytical work which was done for this design project. The propulsion, aerodynamics, structures and weights, stability and control, performance, and several airplane systems are studied. Finally, the results of the wind tunnel testing are discussed. Further details of the design can be found in *Design of an Airborne Launch Vehicle for an Air Launched Space Booster*, the Aerospace 490/590 class report.¹ This report contains detailed descriptions of the design work.

Propulsion

The engine selected for the Eclipse is a planned growth version of the General Electric GE-90 which will be rated at 100,000 pounds take off thrust. Six of these engines will be used to provide the thrust needed to attain altitude. The growth version of the GE-90 was selected because it is the only engine which will be commercially available in the near future which meets the thrust requirements for this airplane. The high lapse rate of thrust with altitude makes the airplane highly overpowered at take off and during a large

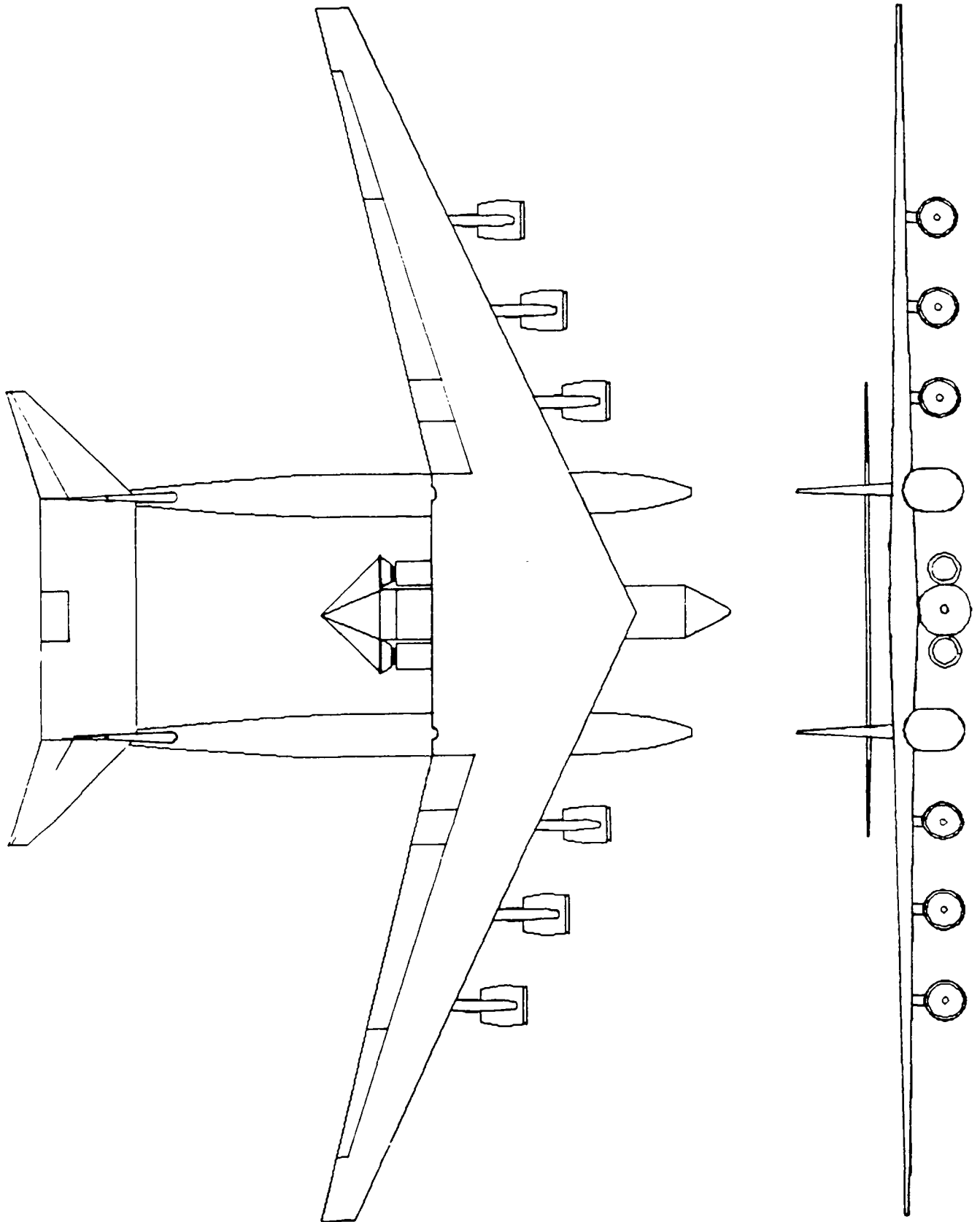


Fig. 2 Configuration overview

portion of the climb. Thrust specific fuel consumption and uninstalled thrust available (including ram drag) data was supplied by the manufacturer.² Installed thrust levels were obtained using empirical models for estimating extractions.³ Figure 3 shows the installed thrust available curves which have been extrapolated across the entire Mach number range.

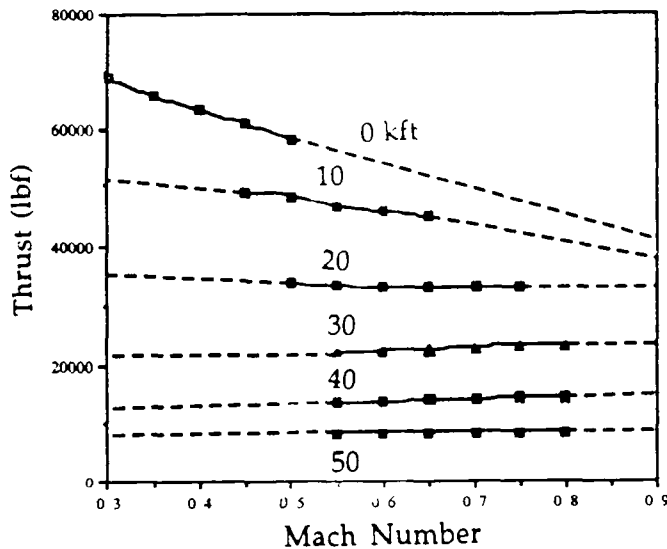


Fig. 3 Installed thrust available

Nacelles were sized using semi-empirical methods based on experience and wind tunnel testing.⁴ The engines are located with a diameter and a quarter between each engine and from the fuselage. They are mounted below and in front of the wing. This location was chosen to minimize the losses associated with installation and therefore improve altitude performance.

Aerodynamics

The wing airfoil is a NASA 14-percent thick supercritical airfoil.⁵ A supercritical airfoil was chosen to minimize wave drag and therefore increase cruise speed. To further increase the critical Mach number, the wing has a leading edge sweep of 25°. This raises the critical Mach number to 0.78, or roughly the cruise speed of the airplane. The vertical tails are NACA 0012 airfoils while the horizontal tail is a NACA 0008 airfoil for the inboard section, to raise critical Mach number where there is no leading edge sweep, and a NACA 0010 airfoil outboard of the vertical tails. The outboard sections have a leading edge sweep of 40°. This results in a higher critical Mach number for the horizontal tail than the wing, as required for stability and control purposes.

Drag polars for the airplane were found using semi-empirical methods.³ Along with this, the interference drag from the payload, i.e. the space booster, was accounted for by adding ten percent of the wing drag to the area which is directly affected by the flow around the payload. An additional five percent is added to the final drag number to account for interference in the rest of the airplane.⁶ Typical drag polars are listed in Table 2.

Table 2 Drag polars

Flight Condition	Drag Polar
Cruise h = 40,000 ft M = 0.78 w/ payload	$C_D = 0.0170 - 0.0012C_L + 0.0390C_L^2$
Cruise h = 40,000 ft M = 0.78 w/o payload	$C_D = 0.0150 - 0.0011C_L + 0.0364C_L^2$
Loiter h = 44,000 ft M = 0.78 w/ payload	$C_D = 0.0146 - 0.0016C_L + 0.0397C_L^2$
Loiter h = 10,000 ft M = 0.45 w/o payload	$C_D = 0.0144 - 0.0052C_L + 0.0414C_L^2$

A single slotted Fowler flap with an area of 1346.4 ft², covering 30 percent of the chord and from 23 to 32 and 38 to 70 percent of the half span, is utilized to lower the take off and landing speed to acceptable levels. No leading edge devices are employed. For take off, $C_{Lmax} = 2.06$ with a flap deflection of 20° and for landing, $C_{Lmax} = 2.65$ with a flap deflection of 45°.

Structures & Weights

A V-n diagram was constructed to determine the loads acting on the aircraft during flight. Between the maneuver load and gust induced load plots, the maximum loads on the airplane can be deduced. These showed a limit load of 2.5g which implies, with a factor of safety of 1.5, a ultimate load of 3.75g.

The majority of component weights were found using semi-empirical methods.⁷ These values were calibrated using a production aircraft part of similar dimensions and configuration. Engine and nacelle weights were supplied by General Electric.² Wing weight was calculated using an analytical method developed specifically for twin fuselage aircraft.⁸ This method calculates the structure required to resist the shear and bending moments associated with the distributed and point loads acting on the wing. Semi-empirical models are then used to give weights for non-load bearing surfaces and trailing edge devices. The analytical method results in a wing group weight percentage of gross take off weight which is in line with that of current production airplanes.

The longitudinal center of gravity was calculated by assigning each component a center of gravity and then calculating the weighted average. All measurements are made from a reference datum 50 feet in front of the forward most point of the wing. The payload and fuel centers of gravity are collocated with the airplane center of gravity to minimize center of gravity shifts during the flight and launch maneuver. Table 3 is a breakdown of the airplane weights and centers of gravity.

Table 3 Component weight and center of gravity

Component	Weight (lbf)	CG (ft)
Fuselages (both)	85,200	107.33
Horizontal tail	28,100	214.03
Vertical tails (both)	14,800	202.05
Crew and mission specific equipment	2,000	45.00
Space booster	479,000	103.43
Engines, nacelles, and pylons (all)	138,000	83.90
Forward landing gear	7,100	45.00
Main landing gear	64,200	110.43
Fixed equipment	50,100	80.00
- Flight controls	12,500	
- Hydraulics and pneumatics	10,000	
- Electrical systems	6,000	
- Avionics, electronics, and instrumentation	11,000	
- Auxiliary power	4,000	
- Oxygen	100	
- Air conditioning, pressurization	1,500	
- Payload specific systems	5,000	
Mission fuel	207,000	103.43
Main Wing	151,900	97.17
Total	1,227,400	103.43

Several structural issues were considered on a qualitative level in the design. The fuselage has an oblong shape so that the landing gear can be fully retracted within the fuselage and still allow for a large closed section. This large closed section significantly stiffens the structure. There is a pressurized compartment in the left fuselage for the crew. This pressurized section is a cylinder which fits inside the exterior contour of the airplane. A cylinder was chosen to minimize the possibility of fatigue due to pressure cycling. The wing has four main spars located at 17, 38 (maximum airfoil thickness), 54, and 70 percent of the chord. In addition, between the fuselages a fifth spar runs parallel to and 12.5 feet in front of the trailing edge of the wing. This spar aids in the distribution of the loads from the space booster. Two reinforced ribs are used for the mounting system for the booster. These ribs start at the first spar and extend out the back of the wing to provide attachment points

for the payload. The twin fuselage design with a horizontal tail spanning the two fuselages has an added advantage of creating a large shear cell. This should significantly lower the structure needed to carry the loads. This would be seen in a weight savings over a comparable single fuselage design. The two forward horizontal tail spars intersect the two rear vertical tail spars. This minimizes the extra structure needed to carry the tail loads.

Stability & Control

Stability and control calculations are based on semi-empirical methods.³ Longitudinal stability calculations focused on three areas. First, the airplane must be able to rotate about its main gear for take off. This did not size the horizontal tail. It did, however, size the elevators. Second, the airplane must be trimmable during cruise. Last, the airplane must meet a static margin requirement during cruise. The third criteria sized the horizontal tail. Ideally, the tail would be positioned such that all three criteria would be met simultaneously. This is not the case with the Eclipse and the tails are therefore larger than they might otherwise be. This is acceptable since the shorter fuselages which are associated with the larger tail allow for a shorter landing gear to meet the tip over and rotation requirements. Also, fuselage weight and tail weight are almost an equal trade off so there is a minimal weight penalty associated with the larger tail surface with shorter fuselages.

Take off rotation and trim calculations were estimated by summing the moments acting on the airplane. In the first case, by summing around the median point of the main gear contact points and in the second case by summing around the center of gravity. The landing trim requirement was not evaluated. Static margin calculations are done through the use of an x-plot. The design is for five percent static margin. This value was chosen as a point where there is sufficient margin for safe pilot control without making the tails extremely large. With only a five percent static margin, a stability augmentation system will be necessary to ensure controlled operations of the airplane. Static margin at take off is high due to the large tails needed for an acceptable static margin at cruise.

The critical condition for lateral and directional stability and control is a one engine inoperative condition on take off. This criteria sized the vertical tails. The two engine inoperative condition was also analyzed. Meeting the two engine out criteria required either a very high speed or excessively large vertical tails to maintain control. Since meeting this criteria would be detrimental to airplane performance, the one engine out condition was selected as the design condition. Table 4 is a summary of the lateral and directional stability and control parameters.

Table 4 Conditions for one engine out stability and control

Minimum control speed	231 ft/sec
One engine out bank angle	4.0°
One engine out sideslip angle	5.0°
One engine out aileron deflection	7.4°
One engine out rudder deflection	25.4°

Performance

Airplane performance was calculated for the three mission scenarios: the normal launch mission, the minimum fuel mission, and the ferry mission. The calculations for the two launch missions assume an launch abort at the last possible moment, which is the worst case scenario. Calculations were based on analytical models of airplane performance.⁹ The Gryphon, an air launched space booster designed by the University of Michigan Aerospace 483 Aerospace System Design class, is used as the payload for the performance calculations.

Upon launch, a minimum radius turn is conducted at constant altitude. This maneuver should give maximum separation between the vehicles in a given amount of time.

For the design mission, the mission profile was broken up into nine segments (see Figure 1), and each one of these segments was further broken up to increase the accuracy of the calculations. The fuel weight required for this mission was used for the sizing of the airplane. Take off and landing distances are the distance to clear a 35 foot obstacle from or to a complete stop, respectively. The final values for this analysis are presented in Table 5.

Table 5 Design mission performance

Take off distance	4,300 ft
Landing distance	3,400 ft
Launch altitude	43,300 ft
Launch turn load factor	2.2g
Launch turn radius	9200 ft
Mission time	6 hr 55 min

Performance for the other two missions was calculated in a similar fashion, but it was limited by the airplane configuration which was determined by the requirements for the design mission. The minimum fuel mission removed the cruise segments. Final values are contained in Table 6. The ferry mission was limited in range by the fuel tank capacity, which was designed for up to 350,000 pounds fuel weight. Also, the booster is assumed to be unfueled for this mission. Table 7 lists the performance values for this mission.

Table 6 Minimum fuel mission performance

Take off weight	1,143,000 lbf
Fuel weight (including ramp fuel)	157,000 lbf
Launch altitude	45,800 ft
Launch turn radius	11,500 ft
Mission time	4 hr 11 min

Table 7 Ferry mission performance

Take off weight	1,135,000 lbf
Payload weight	278,000 lbf
Cruise altitude	35,000 ft
Range	4,300 mi
Mission time	11 hr 14 min

Systems

Six systems of the airplane were designed. Along with these, several issues regarding the comfort and safety of the crew were considered.

Payload Integration

The University of Michigan Aerospace 483 Aerospace System Design class completed the payload integration work. This team designed the Gryphon, a space booster which could be carried and launched by the Eclipse. The integration mechanism is based on the system used in attaching the Orbital Sciences Corporation's Pegasus booster to the L-1011 carrier vehicle. It features an eight point attachment using hooks and pins which are simultaneously released using a set of hydraulic actuators. These eight points are all located on the large ribs in the wing of the Eclipse and the loads are distributed from there to the spars. Further details of this system can be found in the Gryphon project report.¹⁰

Landing Gear

The landing gear is a quadracycle configuration. This layout allows for all six gear trucks to fully retract into a fuselage without interfering with the payload. The main gear consists of four struts, each with an eight wheel landing gear truck in a dual-twin-tandem configuration. Each nose gear is steerable and has three wheels in a triple configuration. The main gear retract forward and aft and the nose gear retracts aft.

The main gear are located such that the airplane can rotate about the median point between the trucks by extending one shock absorber and compressing the other. The struts are long enough to ensure that the airplane meets all clearance

and tip-over requirements. The nose gear are located so that a sufficient amount of the airplane weight rests upon it to allow for effective steering.

The large number of wheels allow the airplane to operate from any concrete runway and in the case of an abort immediately after launch, to return and land on a runway which is used by modern wide body transport aircraft. Using the steerable nose gear and differential braking, the Eclipse needs a 73 foot radius circle of concrete to turn. With a margin for safety to keep the airplane on the concrete, this requires a wider taxi area for the airplane than is available at existing commercial airports.

Hydraulic System

A conventional hydraulic system is employed. A conventional system was chosen over a electromechanical system because of the size, volume, and performance losses associated with the electromechanical system. A conventional system was chosen over an electrohydrostatic system due to the expense associated with the electrohydrostatic system. There are four independent hydraulic systems to insure complete redundancy of the system to all airplane systems.

The hydraulic system operates at a pressure of 5,000 psi. This was chosen as a compromise between volume and weight requirements of a lower pressure system and the sealing requirements of a higher pressure system. In addition, the 5,000 psi system is the standard used on large commercial transports today.

For safety, four levels of redundancy are employed with each of the primary flight control surfaces (aileron, rudder, and elevator) with each section of the control surface powered by three separate systems. Secondary control systems employ only two levels of redundancy. The high level of redundancy is called for since only two airframes are being built and any hull loss would be devastating to the program.

Electrical System

The electrical system for the Eclipse is sized using the requirements of an airplane of similar dimensions, the Boeing 747. This is done because the actual electrical loads of the systems are not known until a more detailed design for the airplane systems is carried out.

Three engine driven generators are used for normal airplane operations. There is an extra generator connected to the auxiliary power unit and an emergency generator connected to a free-fall ram air turbine. Batteries are incorporated into

the system to maintain DC system voltage under transient conditions, to supply power for short term heavy loads, and to supply power in an emergency. In addition, there is a ground connection point for ground operations.

Flight Control System

A mechanical signaling system is used for the flight controls in this aircraft. All flight controls are irreversible. A mechanical signaling system was chosen, despite the weight penalty and higher maintenance, to avoid the cost and difficulty associated with the development of either a fly-by-wire or fly-by-light control system.

Two separate mechanical systems are employed for redundancy with the primary flight controls, while the secondary controls use only one level of redundancy.

Fuel System

The fuel system has a capacity of 260,000 pounds in the primary tanks. This value is a direct result of the performance calculations for the design mission. In addition, there are auxiliary tanks with a capacity of 90,000 pounds which brings total fuel capacity to 350,000 pounds. This extra fuel volume is used when ferrying the airplane, either with or without the payload, from place to place. All tanks are located in the outboard section of the wing between the first and third spars.

Pumps are sized for one and a half times the maximum fuel flow. The pumps have a through flow of 473 pounds per minute. The lines are two inches in diameter. Surge tanks are located outboard of the main tanks.

In order to keep the center of gravity of the fuel constant, several fuel cells are used with flow valves and pumps which are computer controlled to maintain a constant center of gravity.

Crew Issues

The crew of the Eclipse consists of three people, the pilot, copilot, and a launch officer. The pilot and copilot control the flight of the airplane while the launch officer performs the space booster system checks, performs the launch, and verifies separation after launch through telemetry sent to the aircraft from the booster.

The crew are in the forward section of the left fuselage in a pressurized compartment. The pilot and copilot are on a raised platform to enhance visibility with the launch officer behind them. A galley and lavatory are also provided for crew comfort during the mission.

A ground based simulator is needed for this airplane to maintain pilot proficiency. Since this airplane will only be used once every other month for missions, the pilots need other flight time to remain proficient. This could be attained through use of the airplane itself for training, but this risks loss of the airplane. Instead a six degree of freedom trainer could be used to train the pilots for flight and to keep them proficient in the airplanes flight qualities. One other option is available for training, the flying simulator. This concept was rejected due to the cost associated with maintaining the aircraft.

Cost Analysis

The cost analysis was performed using empirical methods.¹¹ The price was determined in 1993 dollars. Since only two airplanes are being built and the weight of the Eclipse is so large, the precision of these values remains uncertain.

The cost to acquire the two airplanes is estimated at \$1.72 billion. This includes all costs associated with the design, testing, manufacturing, flight testing, profit, and financing. This cost is much higher than buying an airplane such as the Boeing 747, but this is due to the small number of planes over which the development cost is spread.

The cost per mission for a 60 mission life time is \$28.6 million. The cost of a typical space booster, such as the Gryphon, is estimated at \$22.1 million. This brings the total launch cost to \$50.7 million. The original per launch cost goal for the airplane was to be under \$10 million. The low number of missions is what drives it higher. As seen in Figure 4, by increasing the number of missions to 100, the per mission cost is \$17 million which is more in line with the goal. This increased number of missions could be accomplished in several ways: by increasing the number of missions per year, by lengthening the life span, or by finding alternate missions. Finding alternate missions would be a last resort since it risks loss of the airframe.

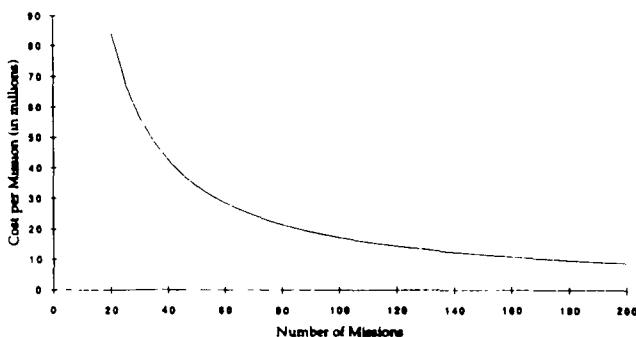


Fig 4. Cost per mission

The mission cost of the airplane is still competitive with existing launch systems and can be made even more so by increasing the number of missions. However, the initial cost of producing the airplanes may make the program infeasible.

Wind Tunnel Testing

A 1:120 scale model of the Eclipse was tested in the University of Michigan 5'x7' subsonic wind tunnel. To accurately model the supercritical airfoil, it was necessary to mill the wing. Using the SDRC I-DEAS software package, a computer model of the wing was generated and converted into tool cutter paths. These paths were then used to drive a Bridgeport computer numerically controlled (CNC) mill. The three axis CNC mill cut the wing from a one inch thick aluminum plate. The fuselages were made from wood. The tails were made of balsa wood with an aluminum core. The nacelles were made from wood and the pylons were made from aluminum. Unfortunately, the pylons could not be attached securely enough to the wing for wind tunnel testing and had to be removed.

The model was tested with and without the Gryphon attached. The tunnel was run at two speeds, 120 and 150 miles per hour. This data was then scaled to $Re = 39.4 \times 10^6$ for comparison with the analytical data.

As can be seen in Figure 5, the clean predicted and test drag polars are similar. Unfortunately, due to the scale of the model, there was very bad interference between the Gryphon and the Eclipse. This led to a much worse zero lift drag for the model than was anticipated. Due to the low speed of the test, the assumption of zero angle of attack for the payload was not valid. The model lift curve slope, however, is in good agreement with the analytical value.

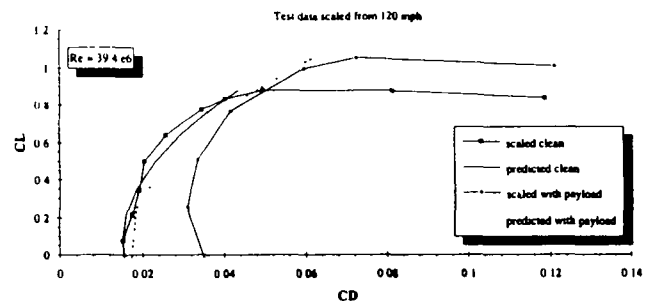


Fig. 5 Wind tunnel drag polar results

Conclusion

A design has been presented outlining an airborne launch vehicle for an air launched space booster. The airplane has a

twin fuselage layout for payload and landing gear integration. The wing has a high aspect ratio for increased altitude performance. This design meets or exceeds all of the goals which were set at the start of the design process:

- Payload capacity = 500,000 lbf
- Launch radius = 750 mi
- Launch altitude = 43,300 ft > 40,000 ft
- Can operate from existing airport facilities
- Relies on current production methods and equipment
- Can perform 2.2g post-launch maneuver

The propulsion, aerodynamics, structures and weights, stability and control, and performance analysis methods used in designing this airplane have been presented. The payload integration, landing gear, hydraulic, electrical, flight control, fuel, and crew systems designed for the Eclipse have also been presented. In addition, the results of wind tunnel testing have been presented and discussed.

It is technologically feasible to design an aircraft which can carry an 500,000 pound air launched space booster to an altitude over 40,000 feet and launch it. The stumbling block, however, is the initial cost associated with acquiring the airplanes. The per mission cost can be made reasonable, if a large enough number of missions is flown.

Acknowledgments

We would like to thank the following people for their help with the project: Dr. Levy for so graciously giving his time to help us with this project. Rich Choi and Rob Jorden, the other members of the design team and to everyone who was in Aerospace 481 with us. Prof. Anderson for his help with the analytical wing weight model. Prof. Washabaugh and Mr. Terry Larrow for their help with manufacturing the model wing. Mr. Warren Eaton for always being there to help out in all stages of model construction. Mr. Dennis Berry and Mr. Ron Bengelink of Boeing for their help with technical issues of the design.

References

- ¹ Poth, S.M., Jr., et al., *Design of an Airborne Launch Vehicle for an Air Launched Space Booster*, University of Michigan, Ann Arbor, Mich., July 1993.
- ² Lewis, R.J., Sr., *Big Engine Data*, General Electric Aircraft Engines, Evendale, Ohio, Unpublished, Nov. 16, 1992.
- ³ Roskam, J., *Airplane Design Part VI: Preliminary Calculation of Aerodynamic, Thrust, and Power Characteristics*, Roskam Aviation and Engineering Corp., Ottawa, Kansas, 1989.

- ⁴ Berry, D.L., *Civil Aircraft Propulsion Integration: Current and Future*, Boeing Commercial Airplane Company, Seattle, Wash., Unpublished, Nov. 12, 1992.

- ⁵ Harris, C.D., "Aerodynamic Characteristics of a 14-Percent-Thick NASA Supercritical Airfoil Designed for a Normal-Force Coefficient of 0.7," NASA-Langley Research Center, Hampton, Virginia, NASA TM X-72712, July 1975.

- ⁶ Bengelink, R., Boeing Commercial Airplane Co., Seattle, Wash., Personal Conversation, Feb. 1993.

- ⁷ Roskam, J., *Airplane Design Part V: Component Weight Estimation*, Roskam Aviation and Engineering Corp., Ottawa, Kansas, 1989.

- ⁸ Udin, S.V., and Anderson, W.J., "Analytical Method for Wing Mass Calculation of Twin Fuselage Aircraft," *Journal of Aircraft*, Vol. 29, Sept.-Oct. 1992, pp. 907-914.

- ⁹ Vinh, N.X., *Aerospace 440 Vehicle Systems Performance Unpublished Lecture Notes*, University of Michigan, Ann Arbor, Mich., Jan.-May 1993.

- ¹⁰ Fisher, M.A., et al., *Project Gryphon: Air Launched Space Booster*, University of Michigan, Ann Arbor, Mich., June 1993.

- ¹¹ Roskam, J., *Airplane Design Part VIII: Airplane Cost Estimation: Design, Development, Manufacturing, and Operating*, Roskam Aviation and Engineering Corp., Ottawa, Kansas, 1989.

AIRCRAFT DESIGN AT THE NAVAL POSTGRADUATE SCHOOL: TACTICAL WAVERIDER/LONG-RANGE CARGO AIRCRAFT

Naval Postgraduate School
Department of Aeronautics and Astronautics
Monterey, California

Professor Conrad F. Newberry

Abstract

The graduate program of the Department of Aeronautics and Astronautics at the Naval Postgraduate School uniquely supports a comprehensive design program in aircraft, avionics, spacecraft, missile, helicopter, and engine design. This paper is focused on four aircraft configuration designs proposed by AA 4273 Military Aircraft Design course team members. The AA 4273 course is, in turn, supported by a growing research program to enhance and further develop the methodology of aircraft design. This design effort has received considerable support from the NASA/USRA Advanced Design Program in Aeronautics. Specifically, two design solutions for a long-range, carrier based, tactical, waverider configured fighter/interceptor aircraft are reviewed herein, as are two solutions for a global range military transport. Both types of aircraft were developed as a graduate student team response to specific design RFPs.

Introduction

The Naval Postgraduate School (NPS) exists for the sole purpose of increasing the combat effectiveness of the U.S. Navy and Marine Corps. This purpose is achieved by providing military officers and defense officials with a quality education which supports the unique needs and interests of the Defense establishment. Although the NPS programs are developed for Navy and Marine Corps personnel, the student body consists of U.S. officers from all branches of military service, international students from allied countries and civilian employees of the United States Federal Government.¹ Eleven academic departments and four academic groups provide a wide spectrum of degree programs for nearly 1800 students. Nearly half of the students receive advanced degrees in disciplines different from their undergraduate areas of study.

The Department of Aeronautics and Astronautics offers the Degrees of Master of Science in Aeronautical Engineering, Master of Science in Astronautical Engineering, Master of Science in Engineering Science,

Aeronautical and Astronautical Engineer, Doctor of Philosophy and Doctor of Engineering. Doctoral programs are available in the fields of gas dynamics, flight structures, flight dynamics, propulsion, aerospace physics and aerospace vehicle design.

There are approximately 180 students distributed across the aeronautics, astronautics and avionics curricula supported by the Department of Aeronautics and Astronautics. Departmental design requirements are supported by aircraft, missile, aircraft engine, helicopter, avionics and spacecraft design courses or course sequences. The aeronautical and avionics programs are accredited by the Accreditation Board for Engineering and Technology (ABET).

The aircraft design course, AA 4273 Military Aircraft Design, is a single, twelve-week quarter course offered twice a year (summer and winter quarters). The course enrollment typically supports two 7-10 member design teams. These design teams typically respond to a Request-for-Proposal (RFP), which specifies requirements for a military aircraft.

NASA/USRA Advanced Design Program

During the fall of 1984, the National Aeronautics and Space Administration (NASA) developed the Advanced Design Program (ADP) as a national pilot project initiative to encourage and nurture engineering design education in the universities and to supplement NASA's internal efforts in the advanced planning for space system design. In 1986 the ADP was expanded to include aeronautical design activities. The ADP is administered by the Universities Space Research Association (USRA), which consists of some 75 academic institutions, supported by grants from NASA Headquarters. Some 44 academic institutions are currently participating in this program. Of the 44 participants, twelve are pursuing aeronautical design initiatives, while the remainder are investigating space related design concepts.^{2,3}

The author of this paper developed an undergraduate^{4,5} ADP effort in the mid-to-late 1980s and proposed to develop a graduate ADP effort at NPS during the most recent NASA/USRA ADP proposal period.⁶ Based on a competitive selection in 1992, the Naval Postgraduate School was selected to participate in the NASA/USRA Advanced Design Program in order to pursue waverider design initiatives. These waverider design initiatives were concerned with the development of tactical, carrier compatible, military aircraft. Once these waverider initiatives received appropriate consideration in any given year, other design topics could be addressed, if there was sufficient student interest and if class enrollment could support additional aircraft design teams.⁶

During the past year, student enrollment in AA 4273 Military Aircraft Design supported four design teams. Two teams elected to pursue waverider configurations and two elected to pursue subsonic, long-range, heavy-lift-capability configurations. The design teams were composed of either seven or eight members, depending upon the particular academic quarter. One waverider team (SABOT) was comprised of eight members, while the second (LONGBOW) was comprised of seven members. Similarly, one subsonic transport design team (DUMBO) was comprised of eight members, while the second team (HUGO) was comprised of seven members. The efforts of these four design teams are reported herein.

In the following discussion of these four aircraft designs, samples of the design effort will be presented herein. However, no effort will be made to compare the performance, life-cycle-cost or other parameters of any two similar aircraft. Instead, methodology and design results will be stressed.

Waveriders

Initially, waveriders were conceived as aerodynamic configurations that could be designed inversely to fit known flowfields. Nonweiler⁷ proposed a wedge-based configuration similar to that shown in Fig. 1. Cone-based configurations may result in planforms similar to that shown in Fig. 2.⁸ The XB-70 may well have been the first practical waverider configuration.⁹

The waverider Request-for-Proposal (RFP), to which the design teams responded, was developed by the author and consisted of few but stringent requirements. The present National Security Strategy reflects resized Naval forces that can effectively support joint warfighting scenarios in the littoral regions of the

planet. For the Navy, this new strategic direction represents a shift away from open-ocean warfighting on the sea, toward joint operations conducted from the sea.¹⁰

In keeping with this new warfighting direction, a hypothetical scenario was suggested by the author, wherein a carrier force was deployed sufficiently far at sea to preclude any land-based aircraft threat, yet able to support joint operations in the nearest littoral zone. The design question was whether or not a waverider configured aircraft could be developed as a plausible tactical aircraft capable of operating from such a carrier, yet able to provide significant support for joint operations in littoral zones of conflict.

One approach was to suggest that such an aircraft should have a large radius of operations, a high speed capability to traverse that radius and reach the littoral zone of conflict and then spend an acceptable residence time in the littoral zone, in order to provide sufficient support for joint operations. The vehicle should be able to carry acceptable quantities of ordinance and armament for that support as well as be able to provide adequate self-protection. Within this framework, the design team was free to refine and otherwise supplement these requirements.

The specific waverider air-superiority/fighter/interceptor requirements consisted of the following:

1. 1500 nm unrefueled range
2. Waverider planform
3. Cruise at $3 \leq M \leq 6$
The cruise Mach number should be dependent upon a design team trade study
4. Carrier suitable
5. Major system considerations (not necessarily in the order of importance)
 - a. Fuel fraction
 - b. Cost
 - c. Maintainability
 - d. Structures
 - e. Propulsion
6. 100 page final report.

There were two responses to these six requirements. The SABOT interceptor approximates the waverider planform, but is not a true waverider configuration. The

LONGBOW configuration closely approximates a true waverider configuration.

SABOT

Fig. 3 presents a three-view of the SABOT aircraft. The trailing portion of the wing swings forward for low-speed flight. The aircraft has a length of 63.9 feet, a height of 14.2 feet and a span of 32.5 feet (swept forward wing position, 50.6 feet). Based upon a constraint analysis, the thrust-to-weight was determined to be $T/W = 0.55$ with a corresponding wing loading of $W/S = 105$ psf. The cruise configuration leading edge sweep angle was determined to be $\Lambda = 70$ degrees. The design team considered a maximum weight limit of 85,000 lb_f for carrier suitability requirements. The maximum weight of the SABOT vehicle is 76,036 lb_f. Since this is somewhat less than the 85,000 lb_f projected limit, there is some growth potential.¹¹

Fig. 4 presents the SABOT weight statement. Weight relationships from the Nicolai¹² and Raymer¹³ texts were used to generate these weight estimates. It should be noted that the fuel fraction is approximately 51% of the gross takeoff weight. The combined fuel and ordnance weight fraction is approximately 55%. The corresponding (large) c.g. travel varies from 23.8% to 83.5% of the mac.

Fig. 5 illustrates the carrier approach and landing characteristics for the SABOT. As can be seen in Fig. 5, operations under no-wind conditions are limited to full flap landings at weights under 43,000 lb_f. The deck handling characteristics of the SABOT are in compliance with MIL-STD-805A.¹⁴

Fig. 6 illustrates the SABOT zero-lift drag coefficient variation with Mach number. USAF DATCOM¹⁵ methodology was used to compute the subsonic, transonic and supersonic C_{D_0} values. Fig. 7 illustrates representative drag polars for the SABOT aircraft.

The propulsion system features a variable bypass turbofan engine with afterburner. Automatic controls vary the bypass ratio from 0 (turbojet), at high Mach numbers, to 1 at subsonic speeds. The maximum turbine inlet temperature was assumed to be 3200 °R.

The SABOT V-n diagram for sea level operation is shown in Fig. 8. This diagram is based on guidelines set forth in FAR Part 25¹⁶ and in MIL-A-8861(ASL).¹⁷ A similar diagram was developed for the SABOT at

50,000 feet of altitude. The gust load lines all fall within the operating envelope. Fig. 9 presents the flight envelope for the SABOT aircraft.

The SABOT flying qualities are compared with MIL-F-8785C¹⁸ class IV, level 1 requirements in Table I. As can be seen, the SABOT exceeded all requirements except for a small excursion in exceeding the maximum roll rate time constant (τ_{roll}). All stability derivatives were calculated by USAF DATCOM methodology. The waverider stability sensitivity, together with the large center-of-gravity travel, requires the utilization of a three-axis stability augmentation system.

Development, Test and Evaluation (DT&E) costs together with production costs were considered to result in a unit cost of \$ 89.1 million (FY 2000 dollars) for the SABOT. This unit cost was based upon a 100 aircraft purchase, with a production rate of one SABOT per month and was based upon cost estimation methods provided by Nicolai.¹²

Table II permits a comparison of the SABOT performance with the RFP requirements. It can be seen that the SABOT meets or exceeds the design goals set for the aircraft.

LONGBOW

The LONGBOW was essentially designed to the same RFP specifications as the SABOT. Fig. 10 presents a three-view of the LONGBOW aircraft. As with the SABOT, the LONGBOW features a swing-wing configuration for low-speed, subsonic flight. The LONGBOW has a 14 foot height, a length of 57 feet and a cruise configuration wing span of 57 feet (low speed span of 76 feet). The cruise configuration has an approximate leading edge sweep angle of 67 degrees.¹⁹

The constraint analysis for the LONGBOW is illustrated in Fig. 11, which indicates that the design point has a thrust-to-weight ratio of $T/W = 0.55$ and a corresponding wing loading of $W/S = 120$ psf. It should be noted that the maintainability and reliability constraint relationships are based upon historical data. This constraint analysis is consistent with the mission profile of the LONGBOW shown in Fig. 12.

Turbojet, turbojet with afterburner and ramjet engine cycles were considered for the primary propulsion system. The result of several studies by the design team suggested that the afterburning turbojet should be the cycle of choice. Accordingly, the ONX, OFFX computer programs of Mattingly²⁰ were used in the optimization

of the cycle pressure ratio. Tsfc, specific thrust and aerodynamic heating trade studies resulted in the selection of $M_\infty = 3$ for the cruise portion of the mission.

A detailed static and dynamic stability analysis was conducted for the Mach 0.2 powered approach (configuration PA) and at the Mach 3 cruise (configuration CR). The USAF DATCOM¹⁵ and Etkin²¹ methodologies were used to compute the requisite stability derivatives. Stability augmentation was used as needed to ensure compliance with all of the stability requirements of MIL-F-8785C.¹⁸

Fig. 13 illustrates the results of the aerodynamic heating analysis. This analysis is based on a eleven element model of a typical section of the leading edge. Element 1 is the leading edge element, elements 1 and 2 comprise the leading edge heat sink. Elements 3,4,5,6,7 and 11 are skin temperatures near the leading edge. Elements 8 and 10 are spar caps and element 9 is a spar web. Element 20 is an isolated skin element six feet aft of the leading edge. The analysis suggests that the skin temperatures are acceptable for the materials selected for aircraft construction, without using an active cooling system. Painting the skin black typically reduced the titanium skin temperatures by some 35 degrees (°F).

The maximum structural loads on the wing were considered to be associated with a 6g, Mach 3 turn at 50,000 and 65,000 feet of altitude on a standard day. A finite element model was developed with MSC/PAL2 software. Stress levels were acceptable for this design condition. The swing-wing is fully swept aft at Mach numbers above $M_\infty = 0.8$. Thus, the swing-wing was designed for a maximum load factor of $n = 3$ at a Mach number of $M_\infty = 0.8$.

Based on the acquisition of 250 aircraft, the unit cost of the LONGBOW (DT&E and production) is estimated to be \$ 46.9 million (FY 1993). Based on ten years of operation, the life-cycle-cost per unit is estimated to be \$ 55.3 million.

Global Range Military Transport

The world is rapidly changing from one with two major military powers in which most countries were more or less aligned with one or the other of the so-called superpowers, to one with many downsized military powers. In this changing world environment, the United States can no longer count on the availability of worldwide operational bases that can be used by American forces responding to international crises. It is

recognized that there is an increasing need to rapidly transport large numbers of both troops and equipment from the continental United States (CONUS) to potential crisis centers throughout the world. To respond to this perceived need, the national AIAA/McDonnell Douglas Corporation Graduate Student Team Aircraft Design Competition for 1992-93 addresses this global range military transport requirement.²²

This design study was, as required, performed in two phases. Phase I was performed to formulate the mission performance specifications for range, speed and payload that will maximize the amount of material that can be transported in 72 hours (3 days). Phase II of the study was performed to develop an optimum aircraft design capable of meeting the performance specifications developed in Phase I. The minimum designated unrefueled range requirement was 6,000 nm and the corresponding minimum designated payload was 400,000 lb_f (at a 2.5g maneuver load factor). The mission specification for this heavy lift system is as follows:

1. Warm-up and taxi for 15 minutes
2. Takeoff and climb to best cruise altitude
3. Cruise at best cruise altitude and Mach number to the mission mid-point
4. Descend on course and land
5. Taxi/idle for 30 minutes, off-load full payload
6. Load 15% of full payload, takeoff and climb to best cruise altitude
7. Return at best cruise altitude and Mach number
8. Loiter 15 minutes (15 minutes reserve fuel)
9. Descend, land and taxi 10 minutes

The specifications further stipulated that the aircraft must be able to operate from existing domestic airbases and use existing airbases or sites of opportunity at the destination. Takeoff and landing rules (critical field length) were also required.

There were two NPS responses to these requirements. It should be noted that the competition requirements were not finalized until mid-to-late August of 1992 (midway through the course). The initial specified payload requirement was 800,000 lb_f, in contrast to the

final payload requirement of a minimum of 400,000 lb_f. The DUMBO design responded to the 800,000 lb_f payload requirement while the HUGO was designed for a payload of 450,000 lb_f.

DUMBO

The solution space for the DUMBO design is shown in Fig. 14. The constant speed climb, takeoff and landing tend to define the solution space. The point design thrust-to-weight ratio is $T/W = 0.21$ and the corresponding wing loading is $W/S = 140$ psf.²³

Quality Function Deployment (QFD) was used to identify significant design related attributes of the DUMBO aircraft. One of the corresponding House of Quality diagrams is shown in Table III. The 800,000 lb_f payload was considered the most important attribute of DUMBO. A plus sign indicates a strong positive relationship between the design (aircraft characteristics) parameters; a minus sign indicates a strong negative relationship. For example, the $M_{CRUISE} = 0.77$ customer requirement is shown as having a strong positive relationship with L/D .

Lambda, conventional tail, canard, two wing and three wing configurations were considered for this aircraft. The final DUMBO configuration is shown in Fig. 15 with a span of 239 feet, length of 295 feet and a height of 64.5 feet.

The DUMBO configuration features a front loading raised cab visor nose; a canard; six unducted propfans mounted on the underside of the main wing comprise the propulsion system; a landing gear of six main struts and two nose struts; a flight crew of pilot, copilot, flight engineer, navigator and two load masters; and a primarily composite airframe. The weight estimates are based upon the statistical (historical) weight methodology provided by Nicolai.¹² The maximum gross weight of DUMBO is approximately 4,000,000 lb_p, with a fuel fraction of 0.425. The static margin is approximately 13.8% of the mac. The largest shift in the c.g. occurs when the required 60,000 payload drop is completed. However, the c.g. is always within acceptable limits.

Turbojet, turboprop, turbofan and unducted fan (UDF) engine cycles were considered for the DUMBO propulsion system. The mission requirements eliminated the turbojet and the turboprop. The UDF was selected for fuel savings and life-cycle-costs. The UDF core engine has a maximum pressure ratio of 45, sfc of 0.21 per hour and a compressor frontal area of 6.7 ft². To

meet the thrust requirements of DUMBO, counter-rotating (10 blades per each of the two discs) fans with a 24.2 foot diameter were selected. At sea level takeoff conditions, the propfan will have a disc loading of 120 SHP/D² and a tip speed of 800 fps. For cruise conditions, a disc loading of 36 SHP/D² and a tip speed of 789 fps are optimal.

The DUMBO wing features an NASA SC(2)-0714 airfoil. Leading and trailing edge flaps are employed to achieve a $C_{L_{MAX}} = 3$. The wing lift curve slope

is $C_{L_{\alpha}} = 5.51/\text{rad}$ at $M_{\infty} = 0.5$. The wing aspect ratio is $AR = 10$ with a cruise lift-to-drag ratio of $L/D = 21$.

The DUMBO V-n diagram was determined to ensure compliance with MIL-A-8861B.¹⁷ The maximum wing loading condition (3.75g at cornering speed) results in a wing shear of 4.3×10^6 lb_f and a corresponding bending moment of 3.75×10^8 ft-lb_f at the wing root. The corresponding wing shear and bending moment distributions are shown in Fig. 16.

On a standard day, the DUMBO can takeoff in 7833 feet (8767 feet on a hot day). The corresponding landing distances are 8798 feet on a standard day and 9396 feet on a hot day. The critical field length is estimated to be 8675 feet on a standard day and 9570 feet on a hot day.

The longitudinal dynamic characteristics of DUMBO are shown in Table IV. Stability augmentation about all three axes, using state variable feedback design techniques, is employed.

The main cargo deck of DUMBO is 200 feet long and 33 feet in width. At the center it is 15 feet high, tapering to a height of 10.5 feet at the sides. The upper cargo deck is 20 feet wide and 185 feet long. The entire upper deck can be rigged with jump seats for approximately 500 personnel. The DUMBO kill tree is shown in Fig. 17.

The cost analysis for DUMBO was computed using the methodology presented in Nicolai.¹² It was determined that only 13 aircraft would be required to meet the global airlift requirements; one test aircraft and twelve operational aircraft. Based on these assumptions, the unit cost of each DUMBO aircraft is \$ 6.29 billion (FY 1992).

HUGO

The HUGO configuration was designed as a global

mobility platform. The mission profile for HUGO is shown in Fig. 18.²⁴ As with DUMBO, Quality Function Deployment (QFD) was used to identify significant design related attributes of the HUGO aircraft.

Table V shows a comparison of subsonic and supersonic aircraft delivery capability. Speed is shown to have little influence upon the total delivered payload quantity. The life-cycle-cost analysis shown in Table VI indicates that the subsonic, single fuselage HUGO concept has the lowest life-cycle-cost.

The HUGO constraint analysis is shown in Fig. 19, where the design point thrust-to-weight ratio is $T/W = 0.265$ and the corresponding wing loading is $W/S = 135$ psf. A three-view of HUGO is shown in Fig. 20.

The NASA SC(3)-0615 supercritical airfoil was chosen for the wing root section, while the NASA SC(3)-0609 section was chosen for the wing tip section. The wing thickness ratio versus the wing semispan is shown in Fig. 21. The extra thickness inside the 40% semispan break-point is used to balance M_{CRT} across the span, to hold fuel and to match required bending moments.

The HUGO cargo bay loading configuration is shown in Fig. 22. Various civilian and military cargo payloads were investigated. It was found that civilian cargo container size dominated the selection of the cargo bay width, while the military cargo requirements dominated the cargo bay height selection.

The HUGO configuration has a gross takeoff weight of $W_{GTO} = 1.367$ million pounds, with a payload of 450,000 lb_f and a fuel load of $W_f = 500,000$ lb_f. The fuel fraction is $W_f/W_{GTO} = 0.366$. Cruise is at a Mach number of $M_\infty = 0.8$, at 35,000 feet on a standard day, with a corresponding $(L/D)_{MAX} = 17$.

The cargo bay is 160 feet in length, 13.5 feet in height and 35 feet in width. The wing span is 300 feet and the wing planform area is 10,080 ft², with a taper ratio of $\lambda = 0.38$ and an aspect ratio of $AR = 8.93$. The wing quarter chord is swept aft by 22.6 degrees.

The c.g. shift due to payload and fuel usage is shown in Fig. 23. The maximum c.g. travel is 23% of the mac (mac = 35.27 feet) and maintains a static margin of less than 15% of the mac. The cruise and ultimate wing shear and bending moment distributions are shown in Fig. 24 and 25, respectively.

Although several engine cycles were considered, as

shown in Fig. 26, the AIAA ATF competition engine was selected for the HUGO. Six pylon mounted engines provide power for the HUGO aircraft.

The HUGO stability augmentation system (SAS) longitudinal and lateral stability characteristics are shown in Tables VII and VIII, respectively. The augmented Dutch-Roll response [roll/yaw rate (deg/sec) versus time] is shown in Fig. 27.

Life-cycle-cost (LCC) estimates were based on methods on methods outlined by Nicolai¹² and Earles.²⁵ The results of the cost trade study indicated that a fleet of 37 HUGO aircraft, with a payload of 450,000 lb_f each, was optimal for a continuous logistic operation over the range specified by the RFP. The unit cost per pound is \$ 303. The LCC analysis based on Nicolai's methodology resulted in a LCC per production HUGO aircraft of \$ 325 million.

Waverider Research

Graduate thesis work also supports the waverider design work performed by the AA 4273 design class. Based upon a 1000 nm combat radius, Price²⁶ developed an optimum waverider configuration for a cruise Mach number of $M_\infty = 6$ using ethylene (C_2H_4) for fuel. The mission profile for this vehicle is shown in Fig. 28. An eight inch (long) model is currently being prepared for water tunnel flow visualization tests. A somewhat larger eighteen inch (long) model is being prepared for low-speed wind tunnel tests. These test results are expected to be available in mid-1994.

Conclusions

1. The twice yearly offered graduate AA 4273 Military Aircraft Design course typically supports four aircraft design teams. Although waverider configured aircraft provide a principal focus for these design teams, other aircraft needs can also be addressed. Typically, two design teams can address each aircraft RFP and thereby provide some perspective to the possible design choices for these different aircraft.

2. NPS participation in the NASA/USRA Advanced Design Program for Aeronautics increases the support primarily for the AA 4273 Military Aircraft Design course. However, during the 1992-93 academic year, the ADP also provided some support for other aeronautical design related classes. It is expected that during the 1993-94 academic year, participation in the ADP will provide more balanced support for all of the aeronautical related design classes.

3. Four graduate student aircraft design configurations are summarized herein. Two solutions are proposed for the high-supersonic, carrier suitable, tactical waverider. Two solutions are also proposed for a 6,000 nm global range military transport.

4. The design classes also provide the impetus for considerable graduate level research in aircraft design methodology. An optimum $M_\infty = 6$ tactical, carrier suitable, waverider configuration was developed as part of this thesis effort. Water and wind tunnel models of this configuration will be tested in the near future to provide support for future tactical waverider design efforts.

Acknowledgements

The author takes this opportunity to thank Ms. A. Sherri McGee at NASA Headquarters for her constant support of the ADP and Messrs. Gary C. Hill and Jeffrey V. Bowles of the NASA Ames Research Center for their gracious willingness to provide time, suggestions, presentations and other support for the AA 4273 Military Aircraft Design class, in particular, and the NPS waverider design program, in general. In a similar manner, the author takes this opportunity to thank the USRA Advanced Design Program staff, particularly Mr. John R. Sevier, Dr. Vicki S. Johnson, Ms. Barbara A. Rumbaugh, Ms. Sue A. McCown and Ms. Cissy M. Novak for their constant concern and their untiring efforts to facilitate the administrative adventures of NPS participation in the ADP, and, in general, for their constant efforts to improve the ADP. The author also thanks Mr. Antonio M. Cricelli for his efforts to free the students from their many entanglements with the various software and computer codes utilized in this project. Lastly, the author thanks all those graduate students in the AA 4273 Military Aircraft Design class who contributed to the completion of this paper.

References

1. _____, 1993 Naval Postgraduate School Catalog, Naval Postgraduate School, Monterey, California, 1992.
2. _____, "Minutes of the NASA/USRA University Advanced Design Program, Third Annual Summer Conference," National Aeronautical and Space Administration/Universities Space Research Association, Washington, D.C., June 17-19, 1987.
3. Rumbaugh, Barbara A., Personal Communication, August 5, 1993.
4. Newberry, Conrad F., "The Impact of the NASA/USRA Advanced Design Program on Aerospace Engineering Design Education at Cal Poly, Pomona," 97th annual American Society for Engineering Education (ASEE) Conference Proceedings, volume 2, Lincoln, Nebraska, June 25-29, 1989, pp. 582-584.
5. Newberry, Conrad F., "The NASA/USRA Advanced Design Program at California State Polytechnic University, Pomona: An Infusion of Curriculum Strength and Innovation," The International Journal of Engineering Education, volume 8, number 2, 1992, pp. 114-125.
6. Newberry, Conrad F., "The NASA/USRA University Advanced Design Program in AERONAUTICS at the Naval Postgraduate School," Naval Postgraduate School, Monterey, California, January 15, 1992.
7. Nonweiler, T.R.F., "Delta Wings of Shape Amenable to Exact Shock-Wave Theory," Journal of the Royal Aeronautical Society, volume 67, number 1, January, 1963, pp.39-40.
8. Bowcutt, Kevin G., "Optimization of Hypersonic Waveriders Derived from Cone Flows," Ph.D. Dissertation, Department of Aerospace Engineering, University of Maryland, College Park, Maryland, 1986.
9. Ward, Lauren, "Riding the Shockwave," Skyline, North American Aviation, volume 19, number 1, March, 1961, pp. 7-12.
10. O'Keefe, Sean, Kelso, Frank B. II and Mundy, Carl E. Jr., "...From the Sea, Preparing the Naval Service for the 21st Century," Naval Institute Proceedings, volume 118, number 11, November, 1992, pp. 93-96.
11. Dober, Dave, Al-Hashel, Waleed, Baldocchi, Bob, Berg, Tim, Dunbrack, Harry, Lindsay, Curt, McAtee, Arron, and Sergeant, Dan, "SABOT High Speed Interceptor, AE 4273 Aircraft Design," Naval Postgraduate School, September, 1992.
12. Nicolai, Leland M., Fundamentals of Aircraft Design, Mets, Inc., San Jose, California, 1975.
13. Raymer, Daniel P., Aircraft Design: A Conceptual Approach, American Institute of Aeronautics and Astronautics (AIAA), Washington, D.C., 1989.
14. MIL-STD-805A.

15. Hoak, D.R., USAF Stability and Control DATCOM, Flight Controls Division, Air Force Flight Dynamics Laboratory, Report 0410, April (revised), 1976.
16. _____, "14 Code of Federal Regulations, Aeronautics and Space, Part 25 - Airworthiness Standards: Transport Category Airplanes," Revised, pp. 231-407, U.S. Government Printing Office, January 1, 1986.
17. MIL-A-8861B.
18. MIL-F-8785C, "Military Specification, Flying Qualities of Piloted Airplanes," ASD/ENESS, Wright-Patterson AFB, Ohio, 45433, November 5, 1980.
19. Stoney, Bob, Baker, Matt, Capstaff, Joe, Dishman, Bob, Fick, Greg, Frick, Steve, and Kelly, Mark, "LONGBOW Supersonic Interceptor, AE 4273 Aircraft Design," Naval Postgraduate School, March, 1993.
20. Mattingly, Jack D., Heiser, William H., and Daley, Daniel H., Aircraft Engine Design, American Institute of Aeronautics and Astronautics (AIAA), Washington, D.C., 1987.
21. Etkin, Bernard, Dynamics of Flight - Stability and Control, Second Edition, John Wiley & Sons, Inc., New York, New York, 1982.
22. _____, "AIAA/McDonnell Douglas Corporation Graduate Team Aircraft Design Competition, RFP: A Global Range Transport for Global Mobility," 1992/1993 AIAA Undergraduate & Graduate Student Design Competitions and Engineering Contest, American Institute of Aeronautics and Astronautics, Washington, D.C., July, 1992, pp. 31-35.
23. Riestler, Peter, Ellis, Colleen, Wagner, Michael, Orren, Scott, Smith, Byron, Skelly, Michael, Zraggen, Craig and Webber, Matt, "Global 'Heavy Lifter' Transport Aircraft, 'Dumbo'," Naval Postgraduate School, Monterey, California, September, 1992.
24. Johnston, Tom, Perretta, Dave, McBane, Doug, Morin, Greg, Thomas, Greg, Woodward, Joe and Gulakowski, Steve, "HUGO Global Range/Mobility Transport Aircraft," Naval Postgraduate School, Monterey, California, March, 1993.
25. Earles, Mary Eddins, Factors, Formulas, and Structures for Life Cycle Costing, Second Edition, Eddins-Earles, Concord, Massachusetts, 1981.
26. Price, David R., "Optimization and Performance Analysis of a Supersonic Conical-Flow Waverider for a Deck-Launched Intercept Mission," Master's Thesis, Naval Postgraduate School, June, 1993.

Group Weights and Moments Statement

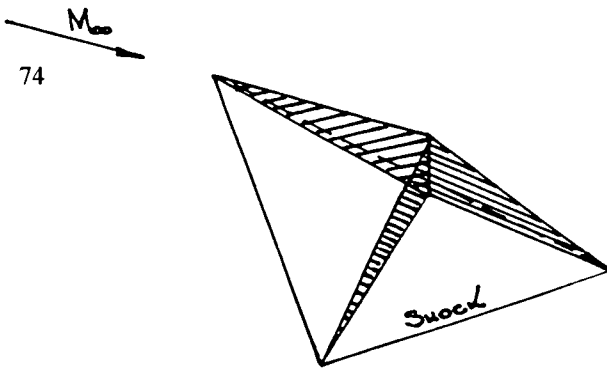


Figure 1
Wedge-Derived Waverider

Structures Group	Weight (lb)	Centroid Location (ft)			Ixx (slug ft ²)
		X	Y	Z	
Wing	8,617.11	30	0	2	35.49
Horizontal Tail	663.14	57	0	0	26.62
Vertical Tail	318.87	55	0	5	376.61
Fuselage	8,098.11	29	0	1	1,262.32
Arresting Gear	408.29	55	0	1	65.66
Catapult Gear	152.07	14	0	1	16.41
Main Landing Gear	1,589.46	48	0	4	405.10
Nose Gear	255.05	14	0	4	115.98
Inlet Ramps	834.05	37	0	1	936.53
Propulsion Group					
Engines	6,000.00	40	0	2	68,073.68
Engine Controls	48.79	40	0	1	
Starting System	264.18	37	0	1	704.43
Fuel System	1,676.78	25	0	2	8,020.30
Equipment Group					
Hydraulics and Flight Controls	2,006.71	38	0	2	613.55
Electrical	572.74	20	0	0	22.99
Avionics	1,039.15	10	0	2	305.75
Ejection seat	290.65	10	0	2	88.87
Air conditioning/ECS	230.58	25	0	1	32.71
Total Empty Weight =					34,306.35
Useful Load Group					
Pilot	210.00	10.00	0.00	1.00	57.94
Fuel	19,000.00				
Ordnance	2,800.00	40.00	0.00	2.00	57.94
Takeoff Gross Weight					
Flight Design Gross Weight =					76,836.35

Figure 4
SABOT Weight Statement

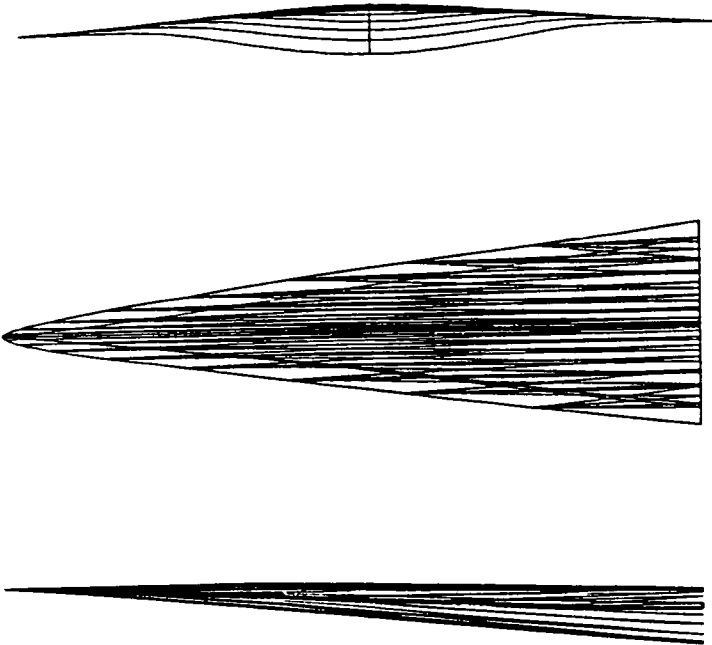
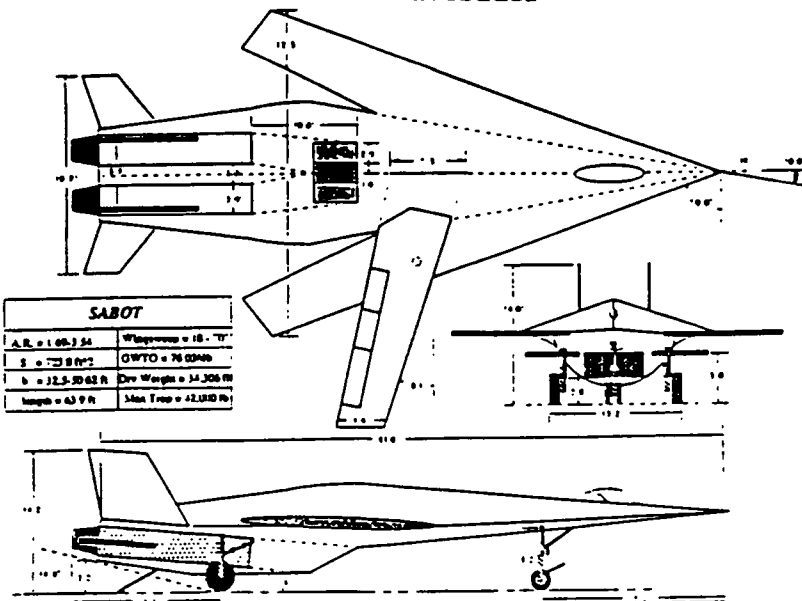


Figure 2
Cone-Derived Waverider



SABOT	
A.R. = 1.08:1.54	Wingspan = 18.00 ft
S = 723.8 ft ²	OWTO = 76,000 lb
b = 32.5-30.63 ft	Dry Weight = 34,306 lb
Length = 43.9 ft	Max Thrust = 42,000 lb

Figure 3
SABOT Aircraft

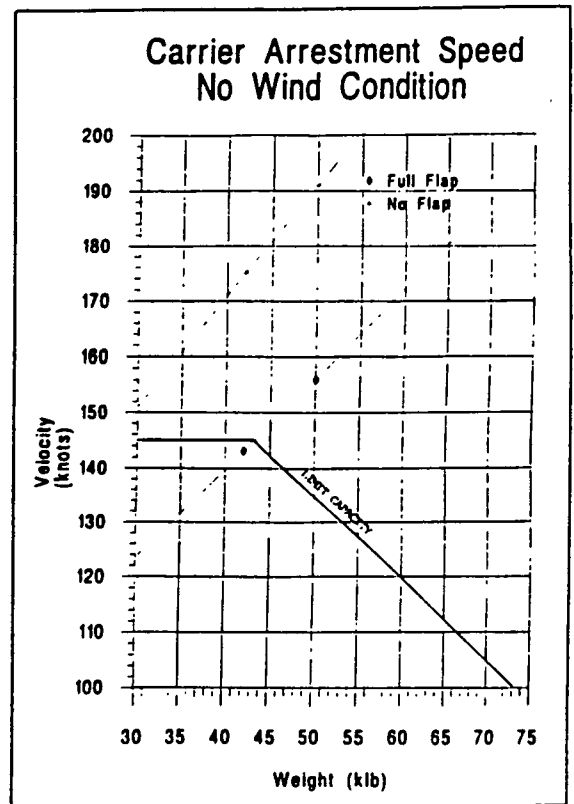


Figure 5
SABOT Carrier Approach and Arrestment Speeds

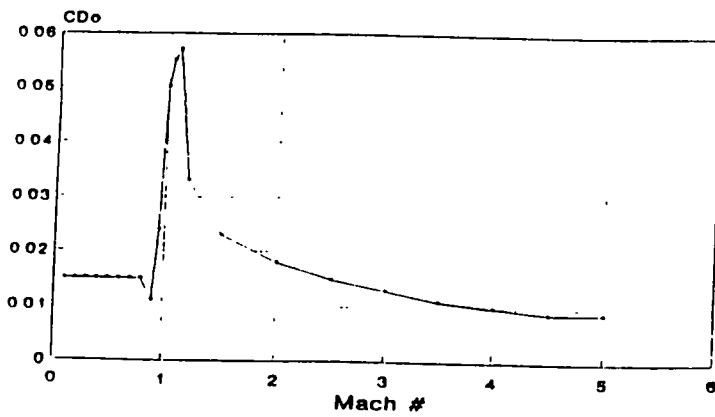


Figure 6

SABOT Zero-Lift Drag Coefficient Variation With Mach Number

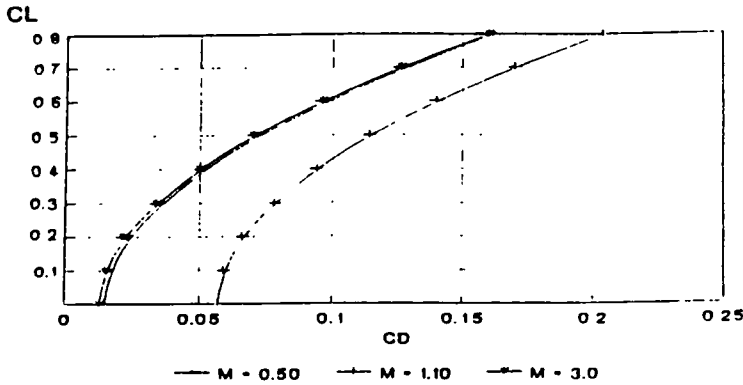


Figure 7

SABOT Drag Polars

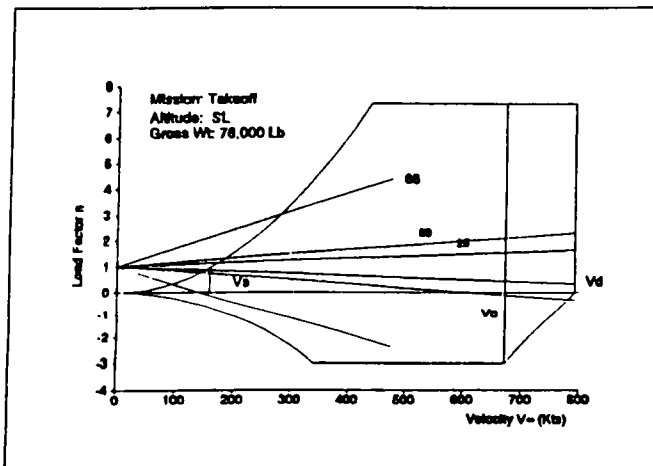


Figure 8

SABOT V-n Diagram

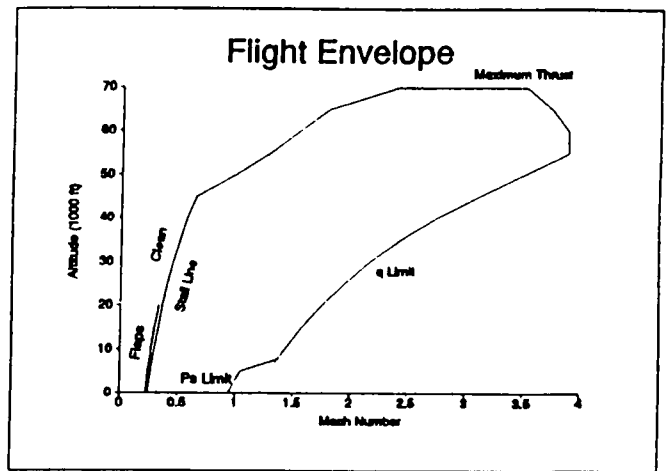


Figure 9

SABOT Flight Envelope

Flying Qualities	Sabot	MIL-F-8785C
Longitudinal-Short Period		
ζ_p	7.2143	n/a
ζ_{sp}	0.4043	$0.35 < \zeta < 1.3$
Longitudinal-Phugoid		
ζ_p	0.6204	n/a
ζ_p	0.0621	> 0.04
Lateral-Dutch Roll		
ζ_{DR}	3.5347	> 1.0
ζ_{DR}	0.1938	> 0.19
Lateral-Roll		
τ_{roll}	2.0851	< 1.0
Lateral-Spiral		
τ_{spiral}	21.142	> 20.0

Table I

SABOT Flying Qualities Summary

Specification	Required	Sabot
Minimum Radius	700 nm	762 nm
Dash Mach Number	<5	3
Missile Carriage (Internal/Conformal)	4	4
Cycle Time	1+00 (Min) 1+30 (Des)	1+00
Sustained Turn	2g or 4g	4g
Maximum Gross Weight	<85,000	76,036

Table II

SABOT Performance Comparison With RFP

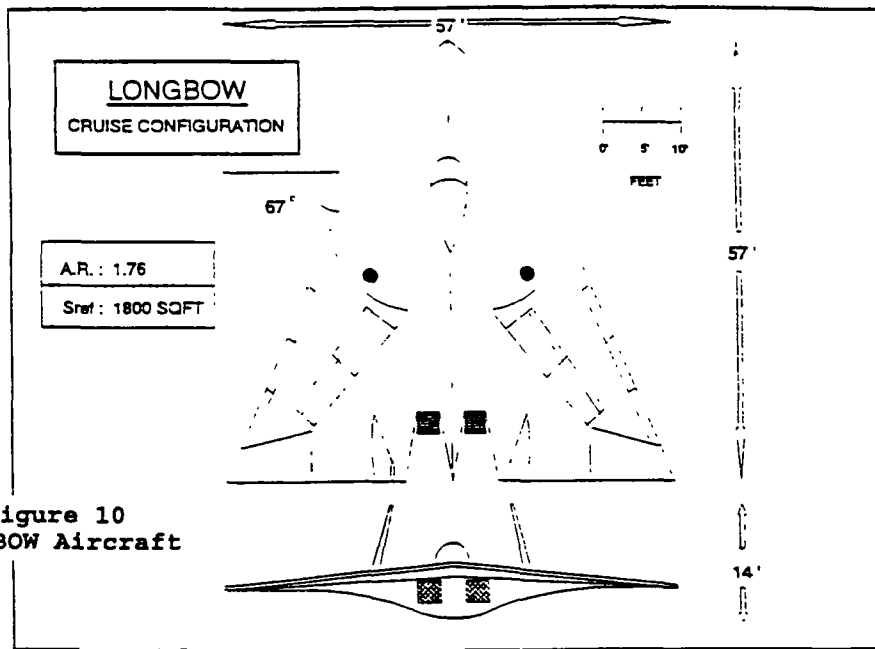


Figure 10
LONGBOW Aircraft

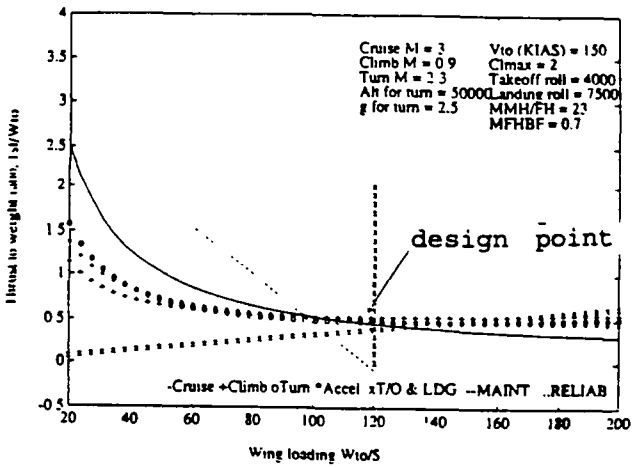


Figure 11
LONGBOW Design Solution Space

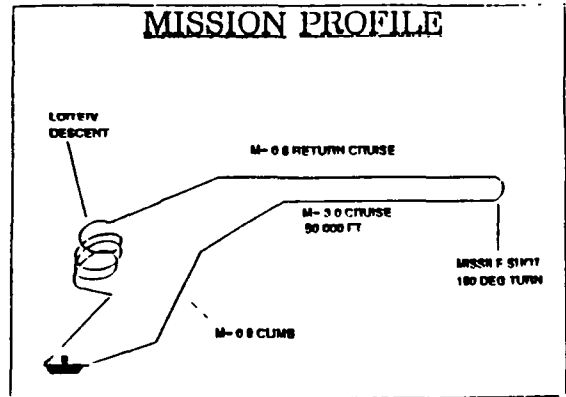


Figure 12
LONGBOW Mission Profile

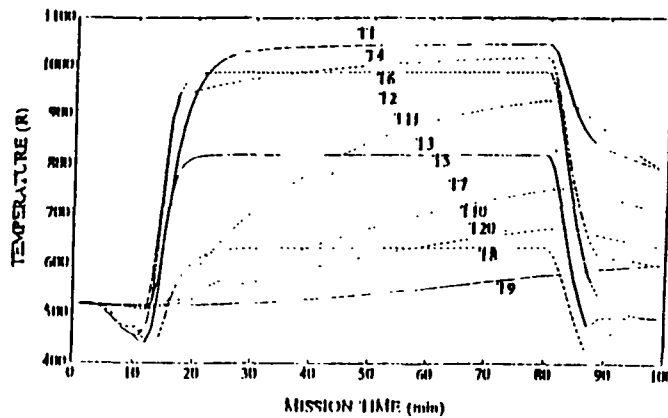
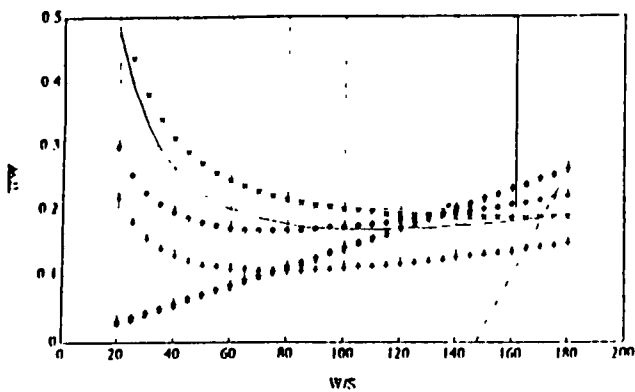


Figure 13
LONGBOW Transient Temperature Distribution Analysis



- 1) High Speed (cruise at 1100 77 & 351 ft/sec)
- 2) Constant Speed Climb at 1100 51 & 154 ft/sec
- 3) Sustained Turn at 120's & 204 ft/sec
- 4) Level Accel Rm at 304 ft/sec
- 5) Takeoff Performance (Nicotol)
- 6) Landing Performance (Nicotol)
- 7) Maintainability (1100 11-25)

Figure 14
DUMBO Design Solution Space

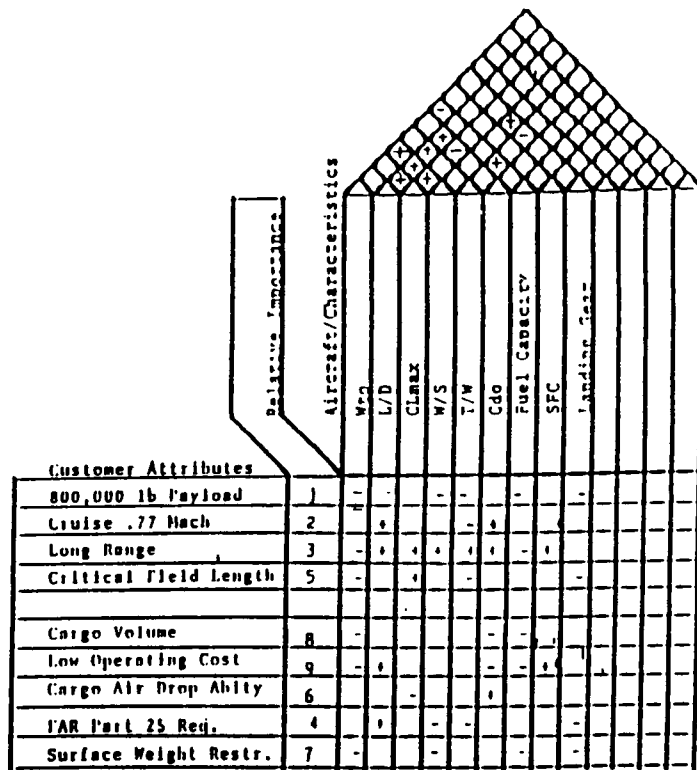


Table III
DUMBO House of Quality of Customer Attributes

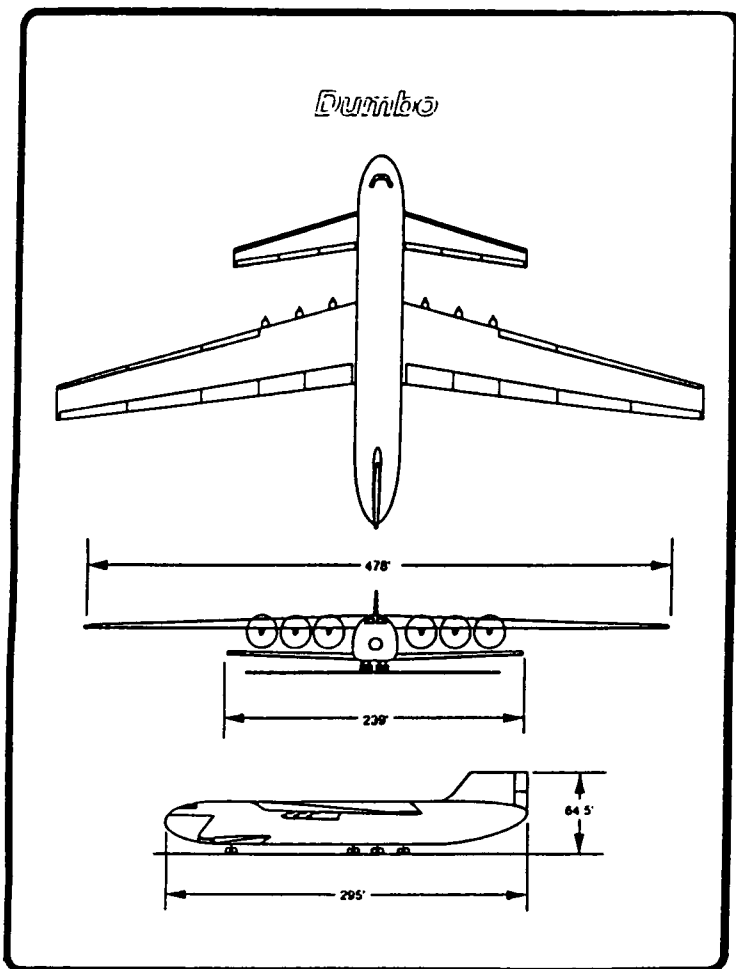


Figure 15
DUMBO Aircraft

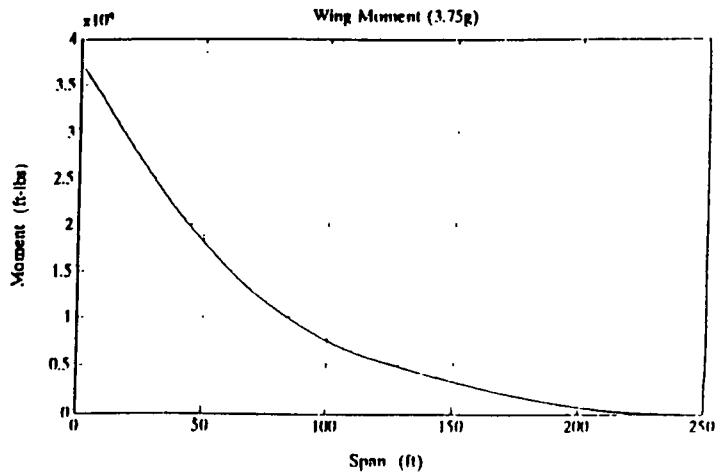
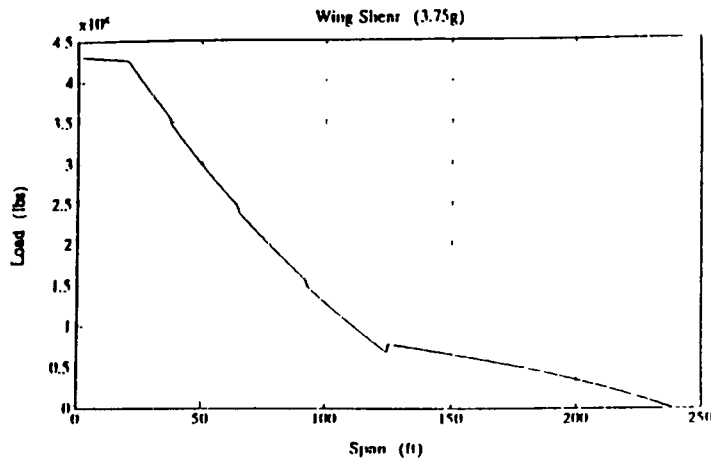


Figure 16
DUMBO Wing Shear and Bending Moment Distributions

	Mach = 0.2 Unaugmented	Mach = 0.2 Augmented	Mach = 0.77 Unaugmented	Mach = 0.77 Augmented
S.P. roots	-.351+.588i	-.9+.71	-.435+.179i	-.95+.71
S.P. damping	.5125	.7894	.3465	.8051
S.P. nat. freq.	.6849	1.1402	1.2568	1.18
L.P. roots	-.012+.1912i	-.017+.191	-.002+.0608i	-.004+.0671
L.P. damping	.0626	.0626	.0329	.0596
L.P. nat. freq.	.1916	.1916	.0608	.0671

Table IV
DUMBO Longitudinal Stability Characteristics

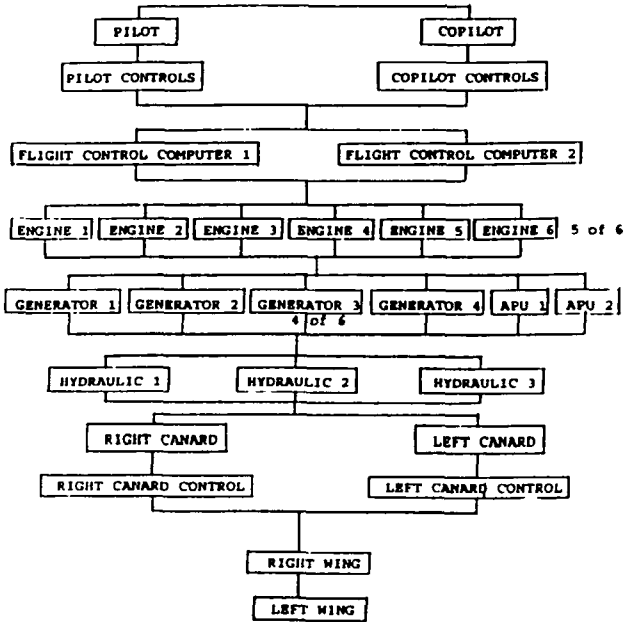


Figure 17
DUMBO Survivability Kill Tree

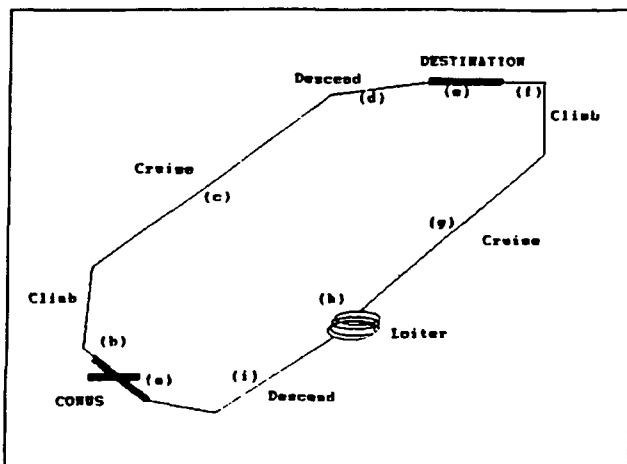


Figure 18
HUGO Mission Profile

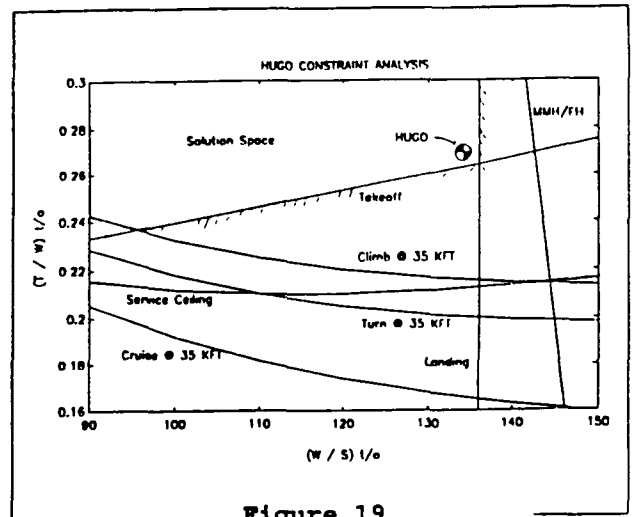


Figure 19
HUGO Design Solution Space

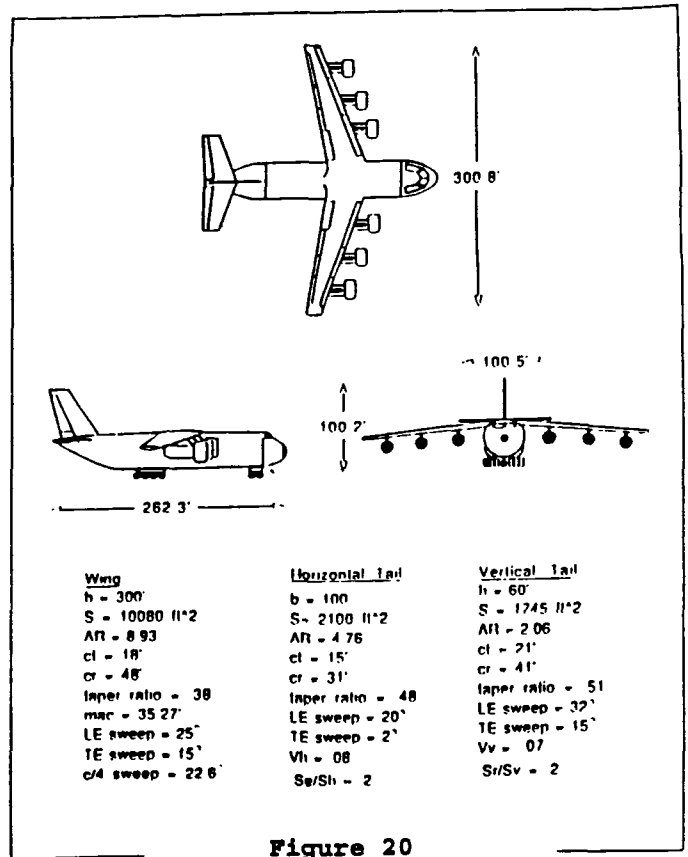


Figure 20
HUGO Aircraft

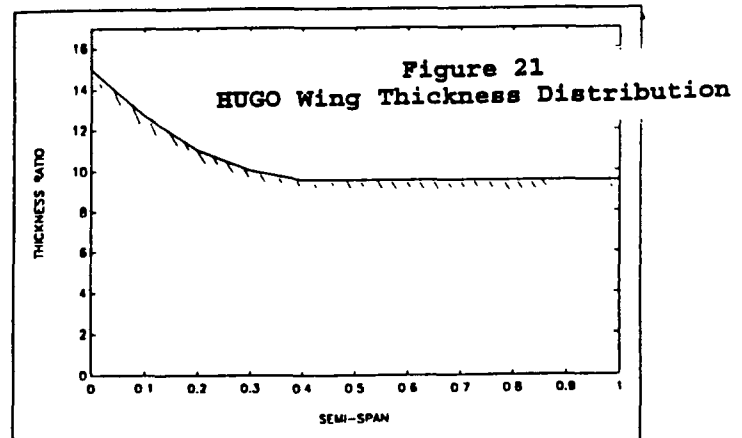
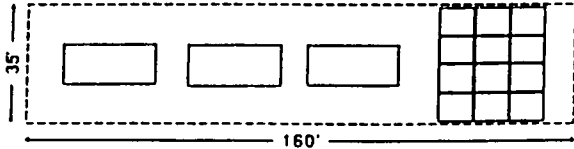
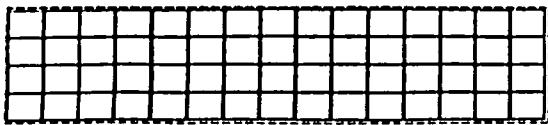


Figure 21
HUGO Wing Thickness Distribution



35ft cargo bay allows
3 vehicles side by side

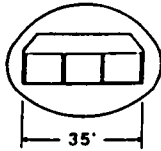


Figure 22

HUGO Cargo Bay Loading Configuration

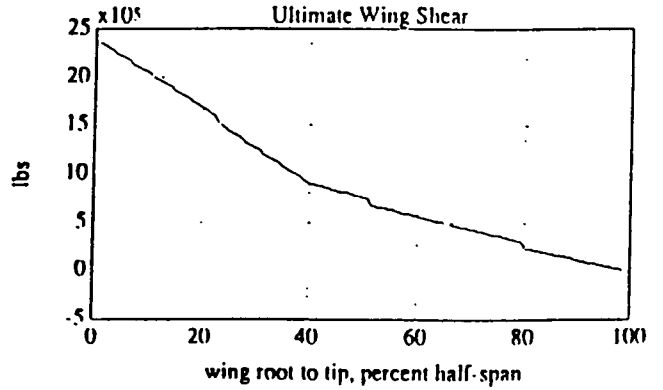
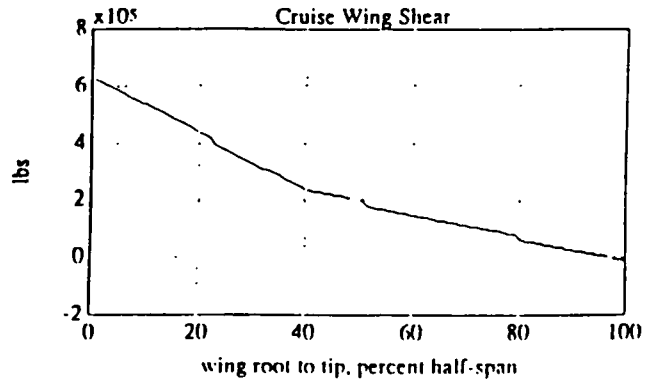


Figure 24
HUGO Wing Shear Distributions

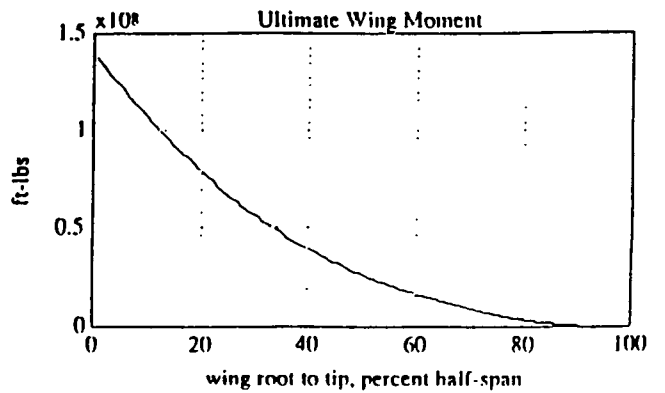
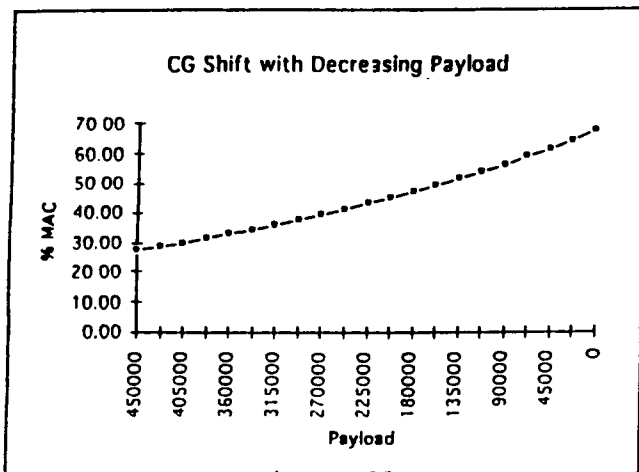
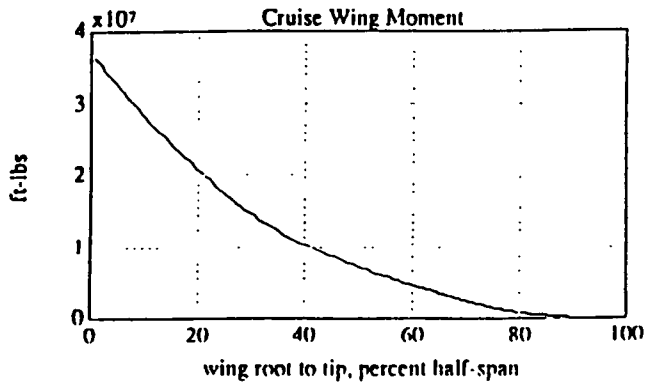
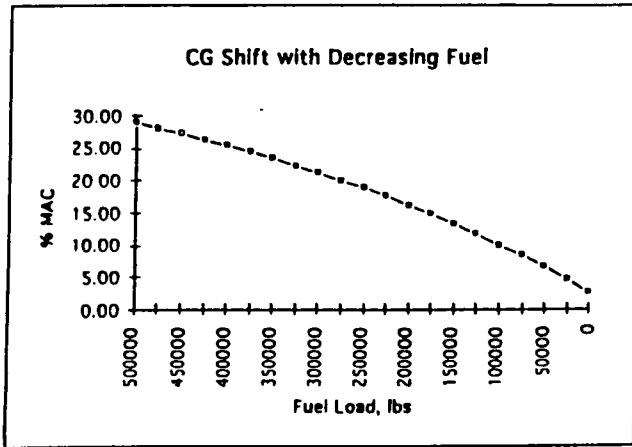


Figure 23
HUGO Center-of-Gravity Shift

Figure 25
HUGO Wing Bending Moment Distributions

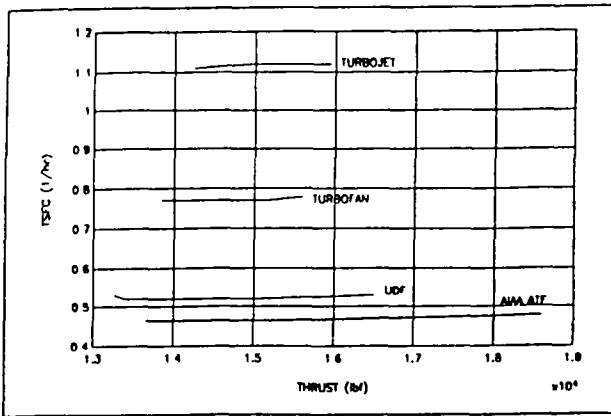


Figure 26
Engine Cycle Trade Study for HUGO

Concept Design	Cruise Time (Hrs)	Trip Time (Hrs)	MIN / REQ A/C	MIN / Buy	Ave Trips/ A/C	Total / Trips	Total Tons moved
SUBSONIC (1330 3400 0 M - .6 P 35 REF. TSFC= .41)	9.07	22.81	46	58	2.7	125	28,125
SUBSONIC (1446 3400 0 M - .8 P 35 REF. TSFC= .47)	6.72	18.11	37	46	3.5	130	29,250
SUPERSONIC (1510 3400 0 M - P 3 & 40 REF. TSFC = 1.9)	2.5	9.67	20	25	6.9	138	31,050

Table V
Effect of HUGO Speed Capability on Payload Delivery Capability

	MACH = .2	MACH = .8	MIL-F-8783C
Short Period Roots	-.401±.226i	-.405±1.051i	Negative
Short Period Damping	.870	.360	.35-1.30
Short Period Natural Frequency	.461	1.126	NA
Phugoid Roots	-.039±.181i	-.009±.069i	Negative
Phugoid Damping	.213	.134	> .04
Phugoid Natural Frequency	.185	.069	NA

Table VII
HUGO Augmented Longitudinal Stability Comparison

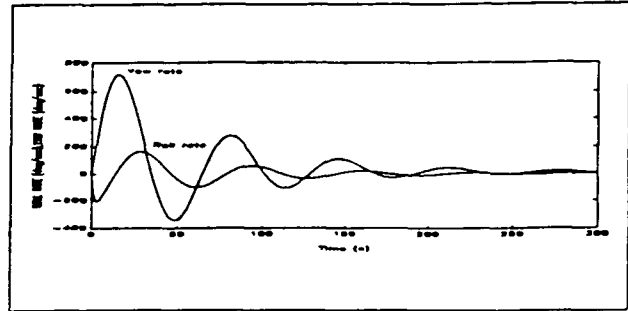


Figure 27
HUGO Augmented Dutch-Roll Response

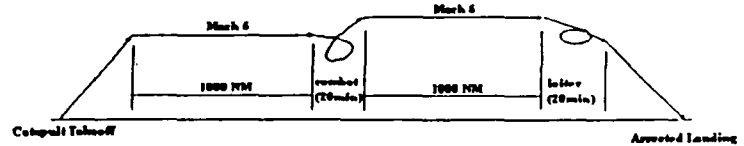


Figure 28
Hypersonic Waverider Mission Profile

	SUBSONIC TWIN FUSELAGE	SUBSONIC SINGLE FUSELAGE	SUPERSONIC LOW AR HIGH SWEEP
Airframe	1280	1067	4889
Development	502	419	2826
Flight Test A/C	2414	2012	10060
Flight Test Operations	236	197	985
Total DT&E	4434	3696	18760
Engine & Avionics	1316	1197	598
Manufacturing	3348	3044	3285
Material	663	603	663
Engineering	1926	1751	1926
Tooling	1905	1732	1905
QA	595	541	595
Total Production	9754	8871	8972
Fuel	261	234	371
Maintenance	25	22	32
Crew	15	15	11
One Year O&M Total	301	271	414
20 Year O&M Total	6020	5420	8280
Total LCC	\$ 20,200	\$ 18,000	\$ 36,000

Table VI
Life Cycle Cost Trade Study for HUGO (Millions 1993 Dollars)

	MACH = .2	MACH = .8	MIL-Y-8783C
Dutch Roll Roots	-.0202±.097	-.0118±.292i	Negative
Dutch Roll Damping	.2041	.0405	Minimum .08
Dutch Roll Natural Frequency	.0988	.2918	
Roll Root	-.8977	-1.223	Negative
Roll Natural Frequency	.898	1.223	
Roll Mode Time Constant	1.114	.818	Maximum of 1.4
Spiral Response Roots	-.0091	-.0439	NA
Spiral Natural Frequency	.0091	.0439	
Minimum Time to Double Amplitude	76	15.8	Minimum of 12

Table VIII
HUGO Augmented Lateral Stability Comparison

GAINING THE COMPETITIVE EDGE: DESIGN FOR MANUFACTURING

Department of Aerospace and Mechanical Engineering
University of Notre Dame
Notre Dame, IN 46556

Dr. Stephen M. Batill
Jim Pinkelman and Richard Sellar, Teaching Assistants

Abstract

The successful design of a commercial aircraft which is intended to be in direct competition with existing aircraft requires a market analysis to establish design requirements, the development of a concept to achieve those goals, and the ability to economically manufacture the aircraft. It is often the case that an engineer designs system components with only the perspective of a particular discipline. The relationship of that component to the entire system is often a minor consideration. In an effort to highlight the interaction that is necessary during the design process, the students were organized into design/build teams and required to integrate aspects of market analysis, engineering design, production and economics into their concepts. In order to facilitate this process a hypothetical "Aeroworld" was established. Having been furnished relevant demographic and economic data for "Aeroworld", students were given the task of designing and building an aircraft for a specific market while achieving an economically competitive design. Involvement of the team in the evolution of the design from market definition to technical development to manufacturing allowed the students to identify critical issues in the design process and to encounter many of the conflicting requirements which arise in an aerospace systems design.

Introduction

The primary goal of this design course was to introduce the students to the process of system design. The majority of the undergraduate education has been devoted to learning basic technical concepts and principles, and using this information to solve problems of limited scope. This course was structured to enhance the students' ability to approach and solve a problem with a very wide scope by integrating diverse technical and non-technical areas. The skills necessary for success in this class included communication, scheduling, teamwork, self-evaluation, budgeting, and personal responsibility. The main objectives of the course were to:

- Introduce design methodology relevant to an aircraft system.
- Illustrate the interface between individual technologies introduced in previous technical courses.
- Develop an understanding of the planning, coordination, and communication necessary in a team design effort.

These objectives have led to a design project which is effective because of two unique aspects. First, the students exper-

rienced all phases of the design process: they developed system requirements from a market analysis, performed concept definition and selection, completed trade studies and detailed design, presented their results in a design review and documented the results in a proposal, and finally manufactured a prototype and performed flight tests. Second, the project required the design teams to integrate a variety of mission, cost, and manufacturing requirements with technical disciplines such as propulsion, aerodynamics, structures, and stability and control.

This paper contains a discussion of the organization of the course and the results of the students' design efforts this year. The first major section of this paper, The Design Project, contains a discussion of the requirements for the design project as presented to the students at the beginning of the semester. The next section, The Design Process, describes the major steps the design teams went through during the aircraft design. The resulting aircraft designs of the six teams are summarized in the third section, The Design Results. Finally, the last section of this paper contains a brief discussion of the significant observations and conclusions from the project.

The Design Project

Course Requirements

The course is primarily a group effort and the success of the final product was dependent upon a coordinated team approach. However, certain milestones were provided both for the groups and for individual students. In the early stages of the design many course requirements were imposed on individuals to allow the group to become used to working with each other, and to aid in the brainstorming of ideas. These requirements included an individual mission assessment, a concept description, and design trade studies.

As design decisions were made and the basic aircraft concept was selected, the members of the groups selected specific technical areas in which they became "experts". The remaining course requirements for the project were group milestones. The next three sections provide some of the specific requirements which were supplied to the design teams. The Request for Proposals (RFP) contains the overall project requirements and guidelines, the market data contains the transportation system requirements for the aircraft, and the cost section contains the guidelines for developing cost estimates for the aircraft.

Request for Proposals

The objective of this project was to gain some insight into the problems and trade-offs involved in the design of a commercial transportation system and the role that manufacturing plays in the design process. In order to do so in the limited time allowed for this single course, a hypothetical world ("Aeroworld") has been developed along with pertinent information on geography, demographics and economic factors. The project is formulated in such a fashion that design teams were asked to design an aircraft configuration which would be able to compete with an existing, successful aircraft. The project not only allowed them to perform a systems design study, but provided an opportunity to identify those decisions in the design process which most significantly impact the manufacturing of the product. This project allowed for the opportunity to fabricate the prototype in order to experience firsthand the influence of conceptual design on system manufacturing.

The project goal was to design a commercial transport which could compete for (and win) a market share from the HB-40, the aircraft that was the first entry in the commercial aviation market of "Aeroworld". Market data for "Aeroworld" was provided to the design teams so that they could determine aircraft characteristics (e.g. range, capacity) for this market. This required a market analysis to identify which segment of the market showed particular promise. Additionally, a number of aircraft concepts to help meet these market needs were developed. Of particular concern was the development of a concept for which manufacturing costs including materials, tooling and man-hours would be minimized while still meeting performance and operating economy targets.

The HB-40 is a 40 passenger aircraft with a range of 17000 ft and a Direct Operating Cost, DOC, of approximately 0.9¢ per passenger seat/1000 foot when operating at maximum capacity for its design range (note that length, time and costs are a bit unusual in "Aeroworld"). The HB-40 was designed as the first entry into the commercial transportation market in Aeroworld and has been enthusiastically received. Due to the growth of the air transportation industry, new entries into the market are desirable. Since this single transport design cannot efficiently compete in the wide range of payload/range markets available the design teams were tasked with considering additional entries into the commercial transportation market.

The following information was to be used to define special technical and economic factors for this design:

1. Passengers: The standard Aeroworld passenger is similar in size and weight to a ping-pong ball (D=1.5 in, W=2.5 gm). Each aircraft must also contain an appropriate flight crew based upon number of passengers. Two person flight crew and one attendant per 40 passengers are needed. Passenger space requirements are considered to be 8 in³ in coach and 12 in³ for 1st class.
2. Range: distance traveled in feet.
3. Fuel: battery charge measured in amp-hours.

4. The typical runway length at the city airports is 40 feet. This length is scaled by a runway factor in certain cities.
5. Time scale: "Aeroworld day" is 1 hour.
6. Propulsion systems: Propeller driven aircraft using electric propulsion systems are considered state-of-the-art in Aeroworld. Alternative propulsion systems can be proposed but approval from management is required.
7. Handling qualities - To be able to perform a sustained, level 60' radius turn at flight speeds of 25 feet/second.
8. Loiter capabilities - The aircraft must be able to fly to the closest alternate airport and loiter for one minute.
9. Aircraft Life - Fatigue life of the materials used in Aeroworld can be determined based upon the total number of flight hours for the aircraft. Current technology allows for a design life of 50 hours. Safe-life design philosophy must be used for all structural components.

Market Data

The design teams were required to design and build an aircraft to outperform an existing aircraft (the HB-40). The market which the HB-40 currently services is a subset of the entire "Aeroworld" air transportation market. The market requirements are based on passenger transportation needs between a number of cities in "Aeroworld". There are three major aspects of the market:

- 1) The characteristics and locations of the airports in "Aeroworld",
- 2) The number of passengers who need to be transported each day, and
- 3) The frequency of flights between the cities.

Figure 1 is a map of "Aeroworld" which gives the location of each city. Table 1 below shows the number of passengers who travel between each pair of "Aeroworld" cities daily. Each latitude and longitude degree increment represents 500 feet in "Aeroworld". Figure 1 and Table 1 provide all the necessary information in order to perform a market analysis of "Aeroworld" upon which concept aircraft are based.

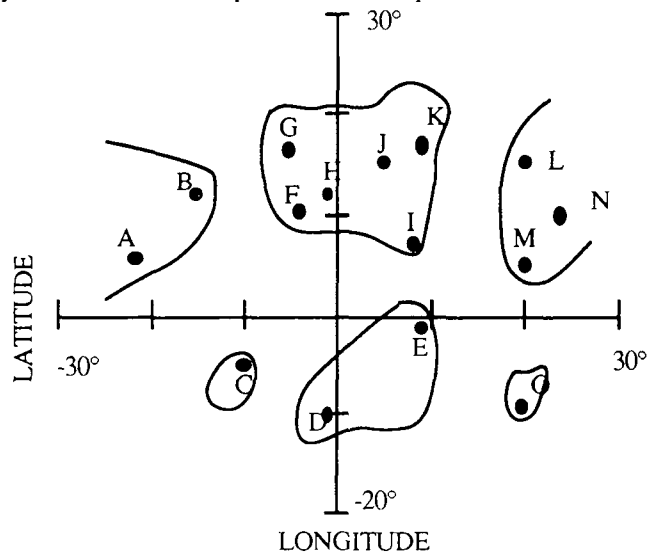


Figure 1. "Aeroworld" Geography

Table 1. "Aeroworld" Daily Passenger Traffic

	A	B	C	D	E	F	G	H	I
A	0	500	400	40	40	500	350	50	200
B	500	0	600	350	200	450	300	450	100
C	400	600	0	500	300	380	500	50	30
D	40	350	500	0	150	60	40	30	90
E	40	200	300	150	0	475	30	40	350
F	500	450	380	60	475	0	800	50	300
G	350	300	500	40	30	800	0	700	600
H	50	450	50	30	40	50	700	0	550
I	200	100	30	90	350	300	600	550	0

Origination City - Columns Destination City - Rows

Frequency of flights was the final consideration which had to be included in a complete market analysis. Because airline transportation competes with various forms of ground-based transportation, the major advantage of air travel is the speed at which passengers can travel long distances. The length of time people are willing to wait for air transportation is related to the distance being traveled. There is a resulting relationship between distance to be traveled and the need for frequency of flights. The need for frequency of flights between two locations is inversely proportional to the distance between the two locations. For this class this relationship was expressed as:

$$\text{Flights per Day} = \frac{30000}{\text{Travel Distance (ft)}}$$

Cost

Once a particular market segment (i.e. a desired passenger size and range) was selected, an initial economic analysis was performed as part of the development of the Design Requirements and Objectives, DR&O. This assisted the design teams in identifying those factors in the design process which had the greatest impact on the design and permitted the selection of certain design targets. In order to perform this analysis for "Aeroworld" the following simplified cost analysis was developed.

In most commercial transportation systems the costs can be divided into two general categories, indirect operating costs and direct operating costs. Indirect operating costs, IDC, include ground operating equipment (maintenance and depreciation), ground operations, administration, sales, etc. Though these are critical issues they were not considered for this current design project. The second category, Direct Operating Costs (DOC) usually include the cost of the flying operations such as crew and fuel as well as maintenance cost for flight hardware and depreciation of aircraft. We attempted to model each of these issues in this simplified model though one should realize that the model and associated parameters have been specially developed for this pro-

ject. The interface between economics and engineering is an important part of our profession and this brief, albeit hypothetical, exposure gave the student some insight into the complexity of the problem.

The total cost of an aircraft system is composed of many factors including basic research, design, development, test and manufacturing. Our model of the total cost per aircraft includes only a few of these factors as shown below:

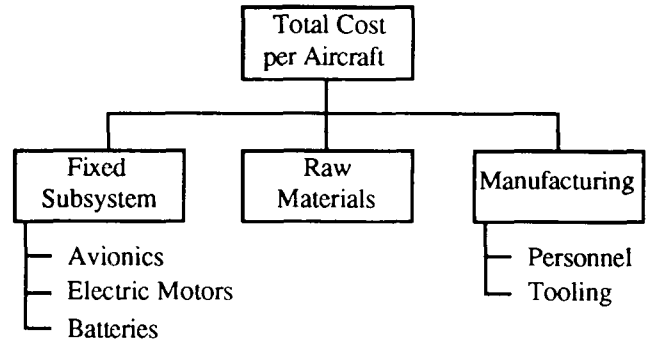


Figure 2. Total Aircraft Cost Breakdown

In addition, an expression can be developed for the direct operating cost per flight can be broken down as follows:

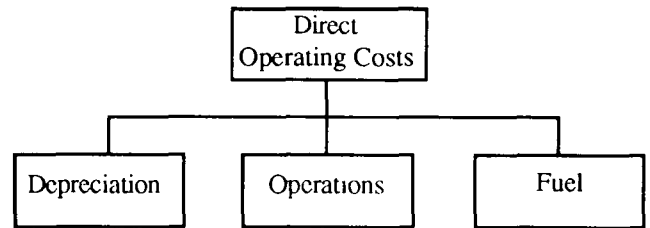


Figure 3. Direct Operating Cost Breakdown

This cost can also be expressed as a cost to move each passenger or "seat" a given distance. As a means of comparison, the following parameter will be used:

$$\text{Cost per seat per 1000 ft} = \frac{\text{DOC}}{\# \text{ of Passengers} * \frac{\text{Range (ft)}}{1000}}$$

The depreciation cost factor recognizes that the flight hardware has a limited life. In the simple "Aeroworld" model, the total cost of the aircraft must be depreciated over the aircraft lifetime. Due to the limited data available on the fatigue characteristics of materials in "Aeroworld", current technology permits a total lifetime of 50 flight hours. The depreciation cost is the cost per aircraft divided by the number of flights in the life of the aircraft. Operation costs include both the costs for the "flight crew" and the other operation/maintenance costs which depend upon the size of the aircraft and the nominal flight duration. The flight crew costs are based on the number of mechanical servos and the maintenance costs are based on the maximum number of passengers and the design flight time. The estimate of fuel

costs is complicated by the unique type of propulsion system used in "Aeroworld", i.e. electric propulsion. Fuel is measured in amp-hours of battery storage. This can be estimated using a simple estimate of the cruise power requirements since relatively little energy is expended during take-off, climb, and descent. The current draw is used with a charge per amp-hour of battery use to calculate fuel costs.

The Design Process

Because the entire aircraft design and construction was to be completed in one semester, scheduling was extremely important. The teams were provided with an overall schedule and due dates for major deliverables, and they had to develop a schedule for the specific activities. The schedule below is representative of the major activities which comprised the design project.

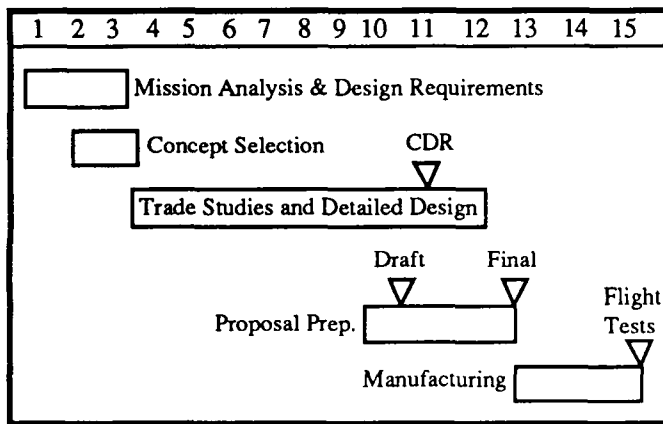


Figure 4. Aircraft Design and Production Schedule

The remainder of this section will provide some of the more important aspects of these activities.

Mission Analysis and Design Requirements

The initial steps of the design process involved the analysis of the market requirements and the establishment of resulting design requirements. The two primary aspects of the mission were the requirement to transport passengers between various locations and the cost associated with developing and building the plane and flying the passengers. The mission evaluation process was focused primarily on the analysis of how many flights and what size flights best satisfy the market demand to fly certain distances. Figure 5 details the number of passengers that desire to fly given distances in "Aeroworld".

Of primary interest was the portion of the market which the HB-40 did not currently service and therefore would be open to a new aircraft entry. The majority of the design teams opted to design aircraft which carried more passengers but had a shorter design range than the HB-40. Figure 6 (below) shows the range and size of all daily flights and the market which the HB-40 currently services.

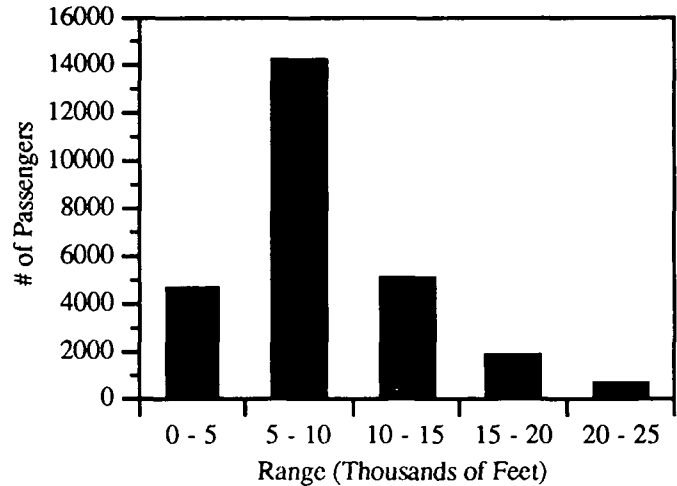


Figure 5. "Aeroworld" Market Flight Range Demand

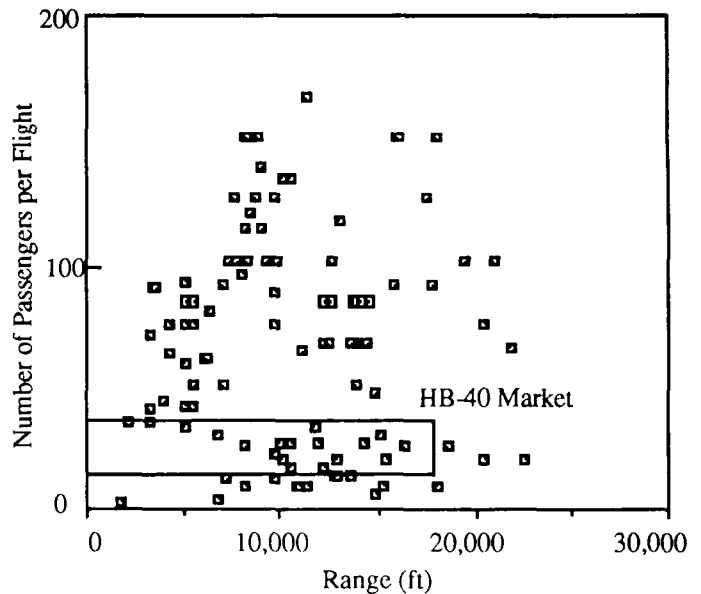


Figure 6. "Aeroworld" Air Transportation Market

The design teams used the information generated from the market analysis and flight constraints associated with "Aeroworld" to develop a high level set of design requirements and objectives for their aircraft. Typical design requirements included constraints on cruise speed, maximum speed, range, passenger capacity, and take-off distance. Many of these requirements were not technical in nature but were based on cost and manufacturing goals. Each team published a document which contained all specific requirements as well as all significant, derived design objectives. This Design Requirements and Objectives (DR&O) document provided the framework upon which all design decisions were based.

Concept Selection

Because the teams were designing an aircraft which would be in direct competition with the HB-40 they were forced to improve on some aspect of the HB-40 capabilities. With this challenge in mind, each member of the teams developed an individual aircraft concept which would satisfy the DR&O. Each design team considered these different designs and generated one team aircraft concept. In most cases, these group concepts featured a combination of characteristics from the individual designs.

Two common requirements seemed to have the most significant influence on these early design concepts. First, each group's market analysis drove them to a desirable number of passengers the plane should be designed to carry. This requirement influenced almost all of the initial aircraft sizing requirements. The number of passengers drove the passenger weight and volume, which in turn drove the size of the fuselage, the total weight of the aircraft, and the wing sizing. Although no design decisions were ultimately based only on the number of passengers, this number was essential to the first iteration of the aircraft.

The second aspect of the project which influenced early design decisions was the goal established by most groups to design for reduced manufacturing costs. As a result, many of the aircraft had features such as rectangular planform wings, flat-bottomed airfoils, and rectangular fuselages. Although the teams did not have the experience necessary to estimate the number of manufacturing hours these features might save, they were able to make qualitative design decisions to reduce manufacturing costs.

Trade Studies and Detailed Design

Next the design groups' efforts were concentrated on generating the information necessary to make detailed design decisions. During this stage of the design project the students completed a number of trade studies, both formally and informally. Each of the individual trade studies served to examine a specific area, and the information generated provided a basis upon which an informed decisions were made. Much of the effort during this phase was concentrated on the performance characteristics of the aircraft. Some decisions were made by conducting an analysis in a single technical area. Many other decisions were made by combining the results of trade studies in different disciplines, such as propulsion and aerodynamics. Quantities such as take-off distance, wing area, range, and power requirements were typical areas analyzed and compared to the requirements established in the DR&O.

The three objectives which drove the design of the aircraft for many of the groups were the desire to minimize the direct operating cost of the aircraft, the short take-off distance required at some "Aeroworld" cities, and the need to minimize the aircraft weight. To decrease the DOC of the aircraft, the majority of the design teams implemented design objectives to decrease the time to manufacture the aircraft. In general, this resulted in conservative design con-

cepts. The short take-off distance requirement drove many of the teams to consider and implement high lift devices. These high lift devices were often in direct opposition to the need to reduce the manufacturing hours. Two of the teams employed flaps on the wings for takeoff, while two of the teams used Wortmann airfoils to provide high lift at low Reynolds numbers. The desire to minimize aircraft weight resulted in decisions which directly conflicted with the need for structural integrity and the goal of minimal manufacturing hours.

Combining the results of the trade studies was an iterative process where advantages and disadvantages of the different technical areas were compared with each other. For example, airfoil selection was ultimately based on the resolution between low Reynolds number aerodynamic efficiency and manufacturing complexity. Upon completion of the major trade studies, the teams made the final design decisions. Whenever possible, the final decisions were made specifically to satisfy the design requirements and objectives established earlier in the course. Upon completing the final design the teams were required to formally present their results at a Critical Design Review.

Proposal Preparation

A major deliverable in the class was a design proposal prepared by each team. These proposals contained all of the technical details on the aircraft and the information upon which all major design decision were based. Producing a quality proposal was more important than the delivery of a successful prototype. Each group submitted a draft proposal which was thoroughly reviewed and returned. The teams then revised and resubmitted the final version of the proposals. Upon completion of the construction and flight test of the prototype, the teams wrote an appendix to the proposal which contained the relevant information from these experiences.

Manufacturing

The intent of this year's project was to emphasize the importance of including manufacturing considerations while designing the aircraft. The fact that most students had little or no experience in the manufacturing of these planes made this goal more difficult but also allowed for a great deal of learning. Given these various constraints, it was determined that the best way to encourage the considerations of manufacturing in the design process was to provide detailed costs which would be associated with the various aspects of manufacturing. By providing these manufacturing costs to the teams before the plane was designed, the students were aware of the penalties associated with designing a complicated structure which would take a significant time to manufacture.

The two primary costs of manufacturing were the materials costs and the labor costs. The estimate of materials costs was based on the amount of wood, control actuators, etc. needed for their particular design. These costs were

relatively straightforward, but risk was associated with the estimates because the students were charged disposal costs based on the amount of excess material, and any extra material needed after the construction had begun was purchased at an inflated rate. Labor costs were associated with the number of hours the students spent building the vehicle and the number of hours spent using tools (jigsaws, sanders, etc.). Because the students had little experience manufacturing such aircraft, it was difficult for them to estimate these labor hours. The manufacturing costs were the single most important component in the profitability of the aircraft. The chart below (Table 2) gives a comparison between the estimated and actual material costs and labor hours for each of the design groups.

Table 2. Comparison of Material and Labor Costs

Aircraft	Labor (\$ @ \$10/hr)		Material Cost (\$)	
	Estimated	Actual	Estimated	Actual
Airplane	1000	1350	175	112
Blue Emu	950	1600	150	150
Bunny	1000	1340	70	152
DiamondBack	1500	2710	140	234
GoldRush	1000	812.50	90	135
RTL-46	1000	1850	120	165

In almost all cases the estimated costs were lower than the actual costs. This is especially true in terms of labor hours. The overrun in labor hours was a result of design teams in which there was no systems engineer to integrate the different technical disciplines or inadequate analysis during the design phase. A substantial amount of engineering was done in the manufacturing phase of the project because the aircraft to be manufactured were still a collection of components. In other cases it was realized during construction that the initial design did not provide adequate strength or accessibility for assembly. Consequently, many of the actual aircraft weighted more than their design weight (see Table 3).

Table 3. Comparison of Actual & Design Aircraft Weights

Aircraft	Weight (pounds)	
	Design	Actual
Airplane	5.25	5.80
Blue Emu	5.30	6.70
Bunny	4.80	6.00
DiamondBack	5.40	7.22
GoldRush	4.82	5.74
RTL-46	4.90	6.00

It is particularly interesting to compare the students estimates of the costs associated with building the prototype with the cost recorded during the manufacturing process. The students estimates were primarily based on the costs incurred in previous years' projects. It is clear from Table 2 and the information provide in the Design Concepts section that the more unique characteristics the aircraft had when compared

with previous planes, the more difficult it was for the students to provide an accurate estimate of the manufacturing costs.

The Design Concepts

Because the HB-40 provided a strong competitor for the design teams, most of the designs were generally evolutionary in nature. The teams found it difficult to be able to quantitatively justify the inclusion of exotic technologies in the designs. The table below details some of the more important specifications associated with each of the aircraft.

Table 4. Aircraft Specification Summary

Aircraft	# Passengers	Range (ft)	Take-off (ft)
Airplane	70	10000	24.0
Blue Emu	60	17000	32.0
Bunny	100	10000	16.0
DiamondBack	100	15000	25.4
GoldRush	80 - 84	10000	24.0
RTL-46	100	10000	15.4

Because all of the aircraft are in the same general class, there is no wide variation in these specifications. The differences which are apparent are the result of two factors. First, the teams each made an independent decision as to the section of the market which they would fulfill. This decision led to the requirements on the number of passengers and the range the aircraft were designed to fly. Second, a team's decision to apply a particular technology (e.g. flaps, joined wing) the performance characteristics of the aircraft were directly affected. The following sections were adapted from the Executive Summaries of the students' proposals.

The Airplane

The Airplane is a moderate-range, 70 passenger aircraft. It can carry more passengers in a shorter time and at a lower cost than the HB - 40 which currently dominates the Aeroworld market. The major drivers for the design of the Airplane are economic competitiveness, takeoff performance, and weight minimization.

A critical economic feature of the design of the Airplane is the direct operating cost. This cost is greatly driven by the cost of labor and materials for the manufacturing process. By building the Airplane for less money than the HB - 40, the market may be overtaken since more seats may be filled for the flight range targeted. Fuel is conserved by transporting more passengers along a specific route in a particular time frame (i. e., smaller overall number of flights) and the added convenience of a quicker flight will attract more passengers. All of this translates into larger profit margins for airlines adding the Airplane to their fleets. In addition, the Airplane can take off at all but one of the airports which serve "Aeroworld". This is an improvement on the competition, which serves all but two airports. Finally,

the Airplane is weight efficient. This plays an important role in minimizing materials cost as well as decreasing the size of the lifting surfaces and propulsion system necessary for the Airplane to meet its range and performance objectives.

The rectangular cross-sectional fuselage houses the motor, flight deck and passenger compartments as well as the fuel and control actuating systems. The wing will be attached to the top of the fuselage as will the fuel and control actuator systems for easy disassembly and maintenance. Seats are arranged in the passenger compartment in 24 rows of three passengers on a single level. The layout calls for two seats to the right and one to the left of a single aisle. Single level construction eliminates the complexity and added weight of having two floors on the aircraft. It is feared, however, that the very wide fuselage may create strong vortices which could have a very significant effect upon the directional stability and control. The twin vertical tail concept is employed to remove the directional control surfaces from the unsteady flows.

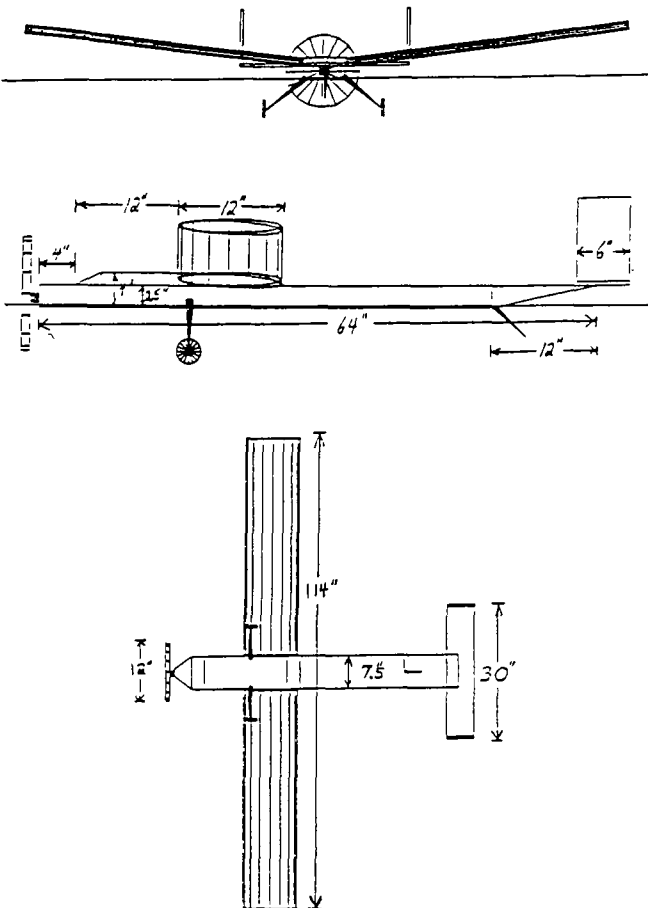


Figure 7. The Airplane

There exist, of course, weaknesses in the design of the Airplane. These include a passenger imbalance in the fuselage seating area which must be compensated for by a left-

ward shift of the battery pack. In addition, the wide fuselage of the Airplane is expected to create destabilizing vortices which leaves the aircraft controllability in doubt despite an innovative tail design. The Airplane cannot cover as large a range as the HB-40. Finally, its L/D at cruise is significantly smaller than its maximum L/D. This indicates an inefficiency which results from a required wing area to satisfy takeoff distance requirements and a desired cruise speed equal to or exceeding that of the competition.

The disadvantages are, however, overshadowed by the aircraft's many strengths. The Airplane provides more economical travel alternatives than the HB-40. It is a faster aircraft and can serve one more airport within the "Aeroworld" market than the HB-40. It can carry more passengers in fewer flights than the HB-40 and should thus reduce total fuel costs to its investors over the long term. Finally, it is less costly to operate at its own maximum range and capacity as well as at the maximum capacity of the HB-40.

The Blue Emu

The primary goal in designing the Blue Emu was to provide an airline with a cost efficient and profitable means of transporting passengers between the major cities in Aeroworld. The design attacks the market where a demand for inexpensive transportation exists, and for this reason the Blue Emu is an attractive investment for any airline. In order to provide a profitable aircraft, special attention was paid to cost and economics. For example, in manufacturing, simplicity was stressed in structural design to reduce construction time and cost. Aerodynamic design employed a tapered wing which reduced the induced drag coefficient while also reducing the weight of the wing. Even the propulsion system was selected with cost effectiveness in mind. Thus, in every aspect of the design, consideration was given to economics and marketability of the final product.

The Wortmann FX 63-137 airfoil was selected because it exhibited high lift, low drag, and favorable stall characteristics in this low Reynolds number regime. The wing size was chosen as 10 square feet to attain a desirable wing loading. The wing employed a taper ratio of 0.6 to increase the aspect ratio, which ultimately narrows the difference between airfoil section and finite wing lift characteristics, as well as approximating an elliptic wing planform. By using a tapered wing concept and thus modeling an elliptic wing shape, a 6% reduction in the induced drag coefficient over a rectangular wing was realized. Further, the wing employed by the Blue Emu produces 57% less induced drag in cruise than the HB-40. Wing design was a critical technology of the Blue Emu. This reduction in drag will improve the economic characteristics of the aircraft and allow it to successfully compete in "Aeroworld".

Longitudinal and lateral control surfaces allow the Blue Emu to maneuver. The Blue Emu utilizes a elevator-rudder, two servo control system. Ailerons were not included in the control system to avoid the complexity and weight of added servos. Flat plates were used for the horizontal and vertical tail to ease construction. The combination of rudder deflec-

tion and dihedral was the mechanism chosen to turn the aircraft. A static margin of 20% was allowed to permit the pilot longer response times when controlling from the ground.

The Blue Emu has several distinct advantages over the existing competition, the HB-40. First and most obvious, the Blue Emu has a greater passenger capacity than the HB-40. Second, the extended range of the Blue Emu adds to

flexibility in use of the aircraft. Third, the wing design offered by the Blue Emu reduces the induced drag of the aircraft. Finally, the Blue Emu has a CPSPK 34.4% lower than that of the HB-40, making it a more economical aircraft. For these reasons the Blue Emu should successfully compete in the market for which it was designed.

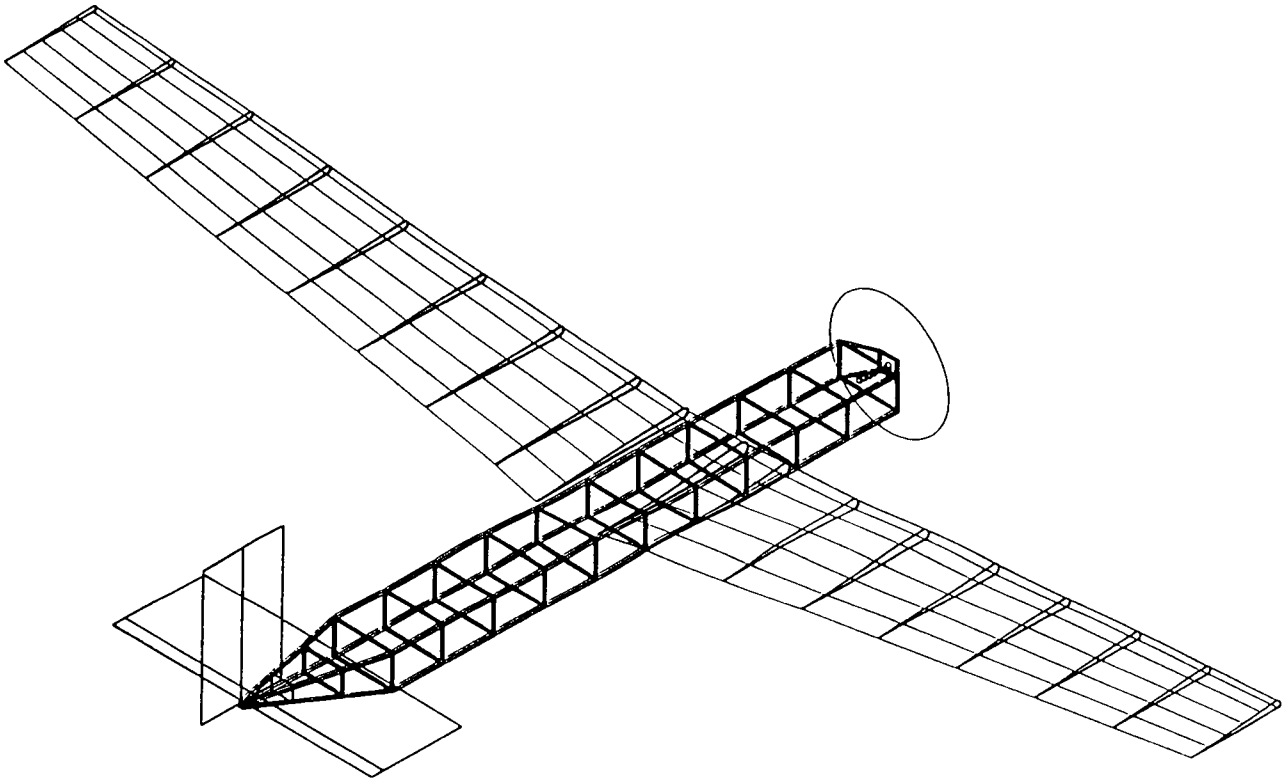


Figure 8. The Blue Emu

The Bunny

The Bunny is a single-engine, 100 passenger commercial transport designed to serve the high density short-to-medium range markets in "Aeroworld". The aircraft's design range is 10,000 feet at a cruise velocity of 30 ft/s.

The factors which had the most significant influence on the final design were the direct operating cost and the take-off distance. Since this aircraft will be in competition with the existing HB-40, it must offer "Aeroworld" airlines a distinct advantage in order to be marketable. In a competitive economic environment, the most attractive feature of a new aircraft is lower operating costs, described in terms of the cost per seat per thousand feet (CPSPK). The large capacity of The Bunny helps to reduce the CPSPK, since the total costs are divided among more revenue passengers. In addition, attempts were made to reduce the fuel costs by decreasing the overall weight and increasing the lift to drag ratio.

The aircraft features a low wing which incorporates polyhedral for roll control. Yaw and pitch control are accomplished by a rudder and elevator, respectively. Propulsion is provided by a nose-mounted Astro 15 electric motor powered by thirteen 1.2 Volt, 1000 mah batteries with a Zinger 12-6 propeller. The aircraft is structurally designed with a safety factor of 1.5 and is constructed primarily of balsa, bass, and birch wood. Passenger seating is arranged on two levels, with three-abreast on the lower level and two-abreast on the upper level. The Astro 15 motor was chosen for its light weight and low cost. The wing features a moderate aspect ratio of 8.5 in order to reduce structural weight, as well as slight taper to reduce induced drag. The Wortmann FX 63-137 airfoil has a high lift-to-drag ratio; in addition, the fuselage shape is trapezoidal to reduce frontal area and features rounded corners to reduce parasite drag. Since one of the primary missions of The Bunny is the ability to operate in all cities in "Aeroworld", take-off distance became one of the other driving factors. In order to meet a

maximum take-off distance of 20 feet, The Bunny was designed with plain flaps spanning the inboard half of the wing. In addition, the Wortmann airfoil was utilized to provide a high C_{Lmax} . With respect to this design goal, the flaps and the high-lift airfoil are critical technologies.

The primary strength of the Bunny is its ability to compete economically with the HB-40. At full capacity and mid-range fuel costs, the CPSPK of this aircraft is 25% less than the HB-40. At 75% capacity, it can operate with the same CPSPK as the HB-40 at full capacity. Thus the Bunny offers a strong economic advantage in addition to its ability to reach new markets. Another principal strength is its ability to operate in all airports in "Aeroworld". Also,

The Bunny's two-piece removable wing is an advantage from a transportability standpoint.

The Bunny also has some weaknesses which may effect its success. The manufacturing of the wing is more complicated than the competition's due to its high-lift airfoil and flaps. The inability to precisely manufacture the airfoil shape may lead to a decrease in aerodynamic performance from the design values. The use of dihedral instead of ailerons couples the roll control with the lateral/directional stability; as a result, the Bunny's roll response may be slow, although it should feature good stability. The stability and control requirements also dictated large tail surfaces; these are a weakness since they cause increased drag.

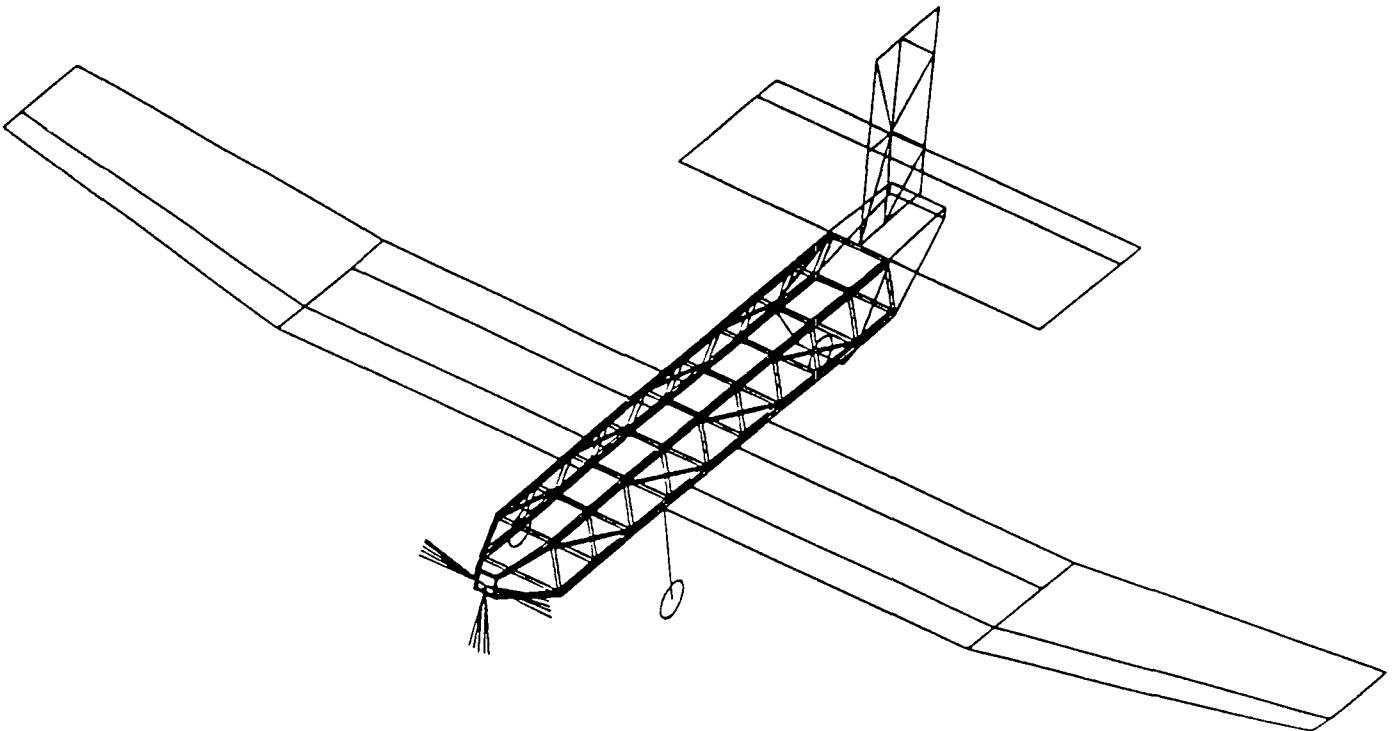


Figure 9. The Bunny

The Diamondback

Unlike conventional aircraft, the Diamondback utilizes an innovative configuration known as the joined wing. Such a design connects the wing and tail forming a diamond in both the front and plan views. For the Diamondback, the wing and tail have the same span and chord with the wing sweep equaling the tail's negative sweep. Breaking new ground, the Diamondback is the first joined wing to be designed in "Aeroworld".

The cost of operating the flight system ultimately guided many of the design decisions. Its influence was not direct but manifested itself in goals such as minimizing the drag and optimizing the propulsion system efficiency. The critical factors which had the most influence on the design were the runway length, the dihedral needed to roll the aircraft to execute a turn, and the airfoil moment about the aerodynamic center. The runway length was a significant driver of the design, requiring a high coefficient of lift to reduce the take-off speed and a high thrust to accelerate the aircraft and reduce the ground roll. The dihedral and the airfoil

C_{M0} , however, had a special significance for a joined-wing design.

Because the configuration utilized rudder and dihedral to turn, a large dihedral angle of 8° was needed. Unlike conventional designs, the wing and tail are physically and geometrically coupled such that a change in one geometry leads to a change in the other. Thus the need to obtain an effective dihedral of 8° for the Diamondback greatly determined the geometry of the wing and tail combination.

The most telling strength of the design is its cost per seat per 1000 ft (CPSPK). The best estimate of the Diamondback's operating cost reveals that at the design payload of 100 passengers the CPSPK is 0.006 \$/seat/1000 ft, less than 67% that of the HB-40 for a comparable range. The Diamondback also provides other gains over conventional aircraft. Structurally, the configuration has the benefits of increased stiffness and a possible reduction in weight of the

wing due to the additional support of the tail. Because of the diamond geometry of the wing and tail and the lifting contribution of the tail, the aircraft's neutral point and thus the center of gravity is located near the middle of the fuselage. This placement can reduce the sensitivity of the center of gravity to changes in the payload weight distribution since the distance to the payload from the empty weight center of gravity is reduced by the central location of the c.g.

Overall, however, the promising characteristics of the joined wing make the Diamondback a strong candidate for future competition against the HB-40 in the "Aeroworld" passenger aircraft market. The aircraft has not yet been optimized, and re-sizing the wing and tail with the data and insight acquired in the design process will increase the overall efficiency of the Diamondback. By blazing the path for future joined-wing designs, the Diamondback is a valuable addition to the "Aeroworld" aviation industry.

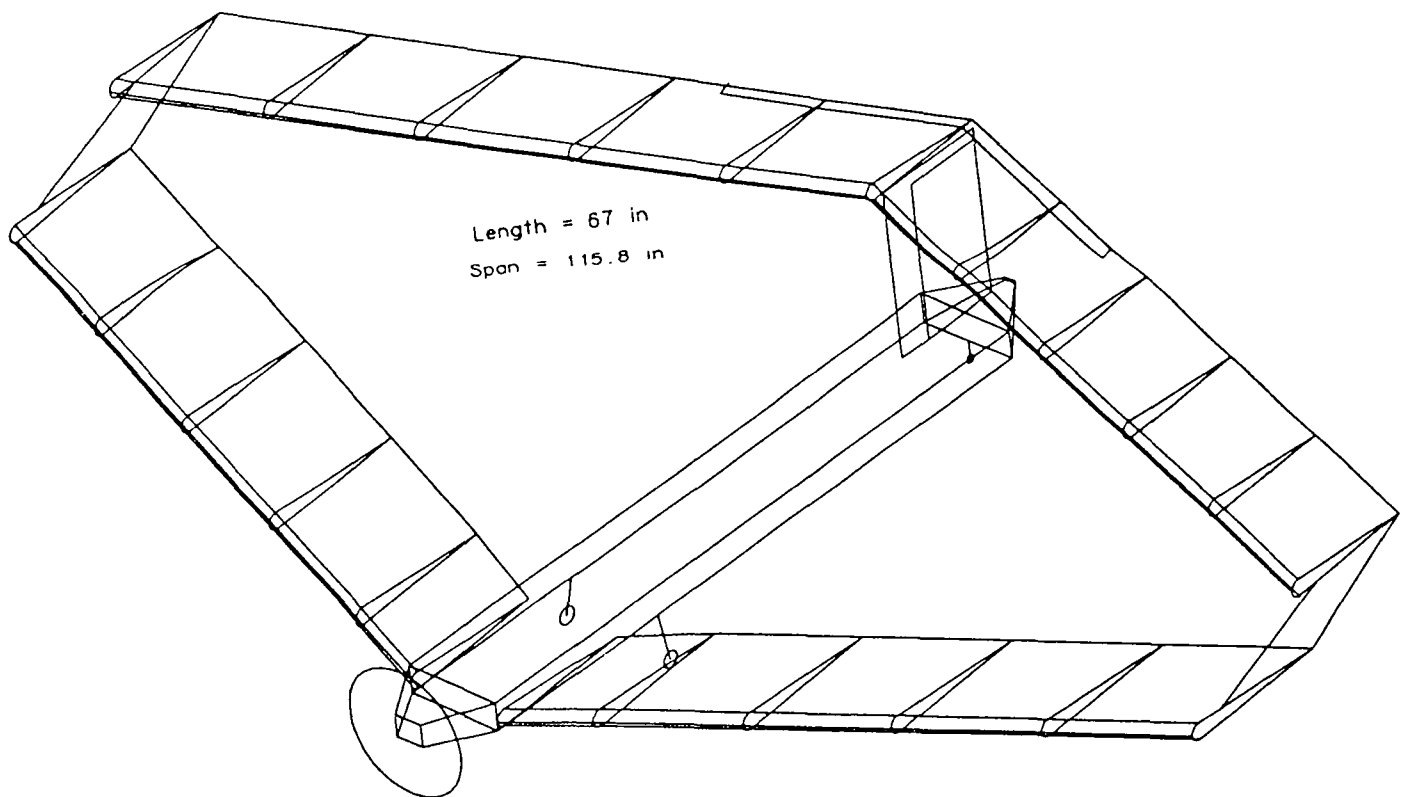


Figure 10. The Diamond Back

GoldRush

The Gold Design Group designed the GoldRush to complete the mission of transporting passengers in "Aeroworld" at a lower cost per seat per thousand feet (CPSPK) than the competition, the HB-40. To this end, the Gold Design Group selected a high traffic market to serve more effectively than the HB-40. This market consisted of

travel routes in the range of 10,000 feet. It was determined that this market would best be served by an aircraft capable of carrying 80 or 84 passengers; thus the GoldRush concept was born.

The first constraint encountered in the design was the takeoff distance of 24 feet needed to take off from the city with the shortest runway. This constraint led to the choice of a wing area of 10.9 square feet, as well as the decision to use the Astro 25 motor, which will run off of a battery pack

with a 900 mah capacity. Due to its high lift curve and excellent low Reynolds number performance, the airfoil chosen was the Wortmann FX 63-137. Also, in order to increase the Reynolds number to a higher, more desirable value, a chord of 15 inches was chosen. This led to a Re of approximately 200,000.

One way in which the design could be improved is in the area of aerodynamic drag. A less conservative drag estimation technique may have yielded the shorter takeoff distance without the need for the larger motor. Another possible area of improvement might be the ability to move the battery pack or some other method of adjusting the location of the center of gravity. The majority of the weight of the plane is in the nose which created a c.g. which was so far forward it created problems with stability.

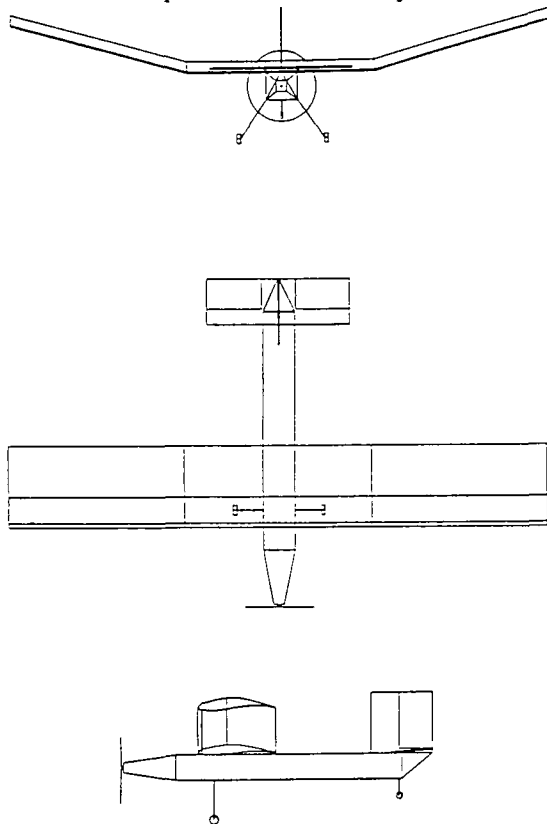


Figure 11. The Gold Rush

RTL-46

The major focus of the endeavor was to design an aircraft which would serve the Aeroworld market better than the existing aircraft, the HB-40. The RTL-46 (Reason to Live for the Six group members) is an aircraft which utilizes advanced technology to better service the air travel customers and airlines of "Aeroworld".

The driving forces behind the design for the RTL-46 were economic in nature, consisting of reducing the direct operating costs, and thus the cost per seat per thousand feet of the aircraft, and gaining a higher share of the potential market than the HB-40. The first method of decreasing the

costs and increasing the market arose through the design of an aircraft which holds 2.5 times as many passengers as the existing aircraft. The 100 passenger capacity RTL-46 decreases the cost per seat by increasing the number of seats, and achieves the increased market share goal by servicing a higher percentage of the passengers desiring flights. The second major aspect of the design, which increases the available market, consists of the use of high lift devices (full span flaps) which results in a short takeoff distance of 15.4 feet, well below the 20 foot maximum distance for service to all airports. Through structural engineering and weight analysis, these increases in the aircraft performance are achieved with only minimally greater aircraft weight than the HB-40 (less than 15% greater).

The interior of the RTL-46 is designed to maximize the comfort of every one of its 100 passengers, first class and coach. The seating arrangement provides every passenger with both a window view and aisle access from his or her seat. Passengers will be served their food from the aircraft's galley located towards the nose of the aircraft and lavatories are located in the rear. The multiple deck configuration provides each individual with enough room to move while not causing long walks to the front or rear of the aircraft to get to the lavatories or exits.

The major areas of design for the aircraft lie within the cost effectiveness through improved aerodynamics of the wing and fuselage. Although the benefits of these areas are readily apparent, their drawbacks are slightly more subtle. The increased drag of the wing with flaps down could negate the lift gain, and the increased complexity could lead to higher costs of construction than the revenue gain from the service to the shorter runway airports.

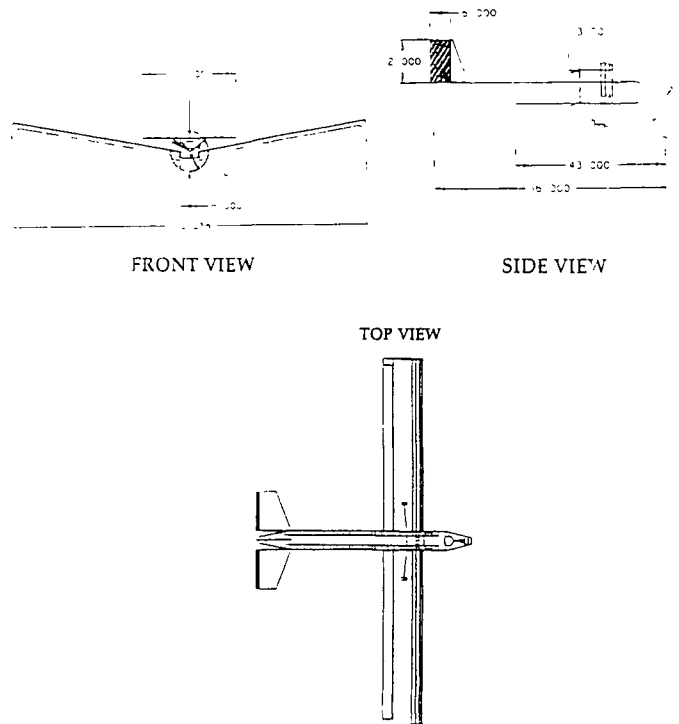


Figure 12. The RTL-46

Concept Validation

Because of the nature of this project it is possible to subject the design to a real validation. Although difficult to evaluate the design of these aircraft on paper, the requirement to build and fly the aircraft provides indisputable evaluation of the design. The final three weeks of the semester was devoted to these activities.

The teams were required to present a manufacturing plan and provide all construction materials prior to the start of construction. These requirements allowed for the evaluation of the aircraft with respect to the original manufacturing plan and the design proposal.

The flight tests were conducted in two stages. First the completed aircraft were subject to taxi tests to determine whether the aircraft could taxi adequately under remote control of the pilot. When the aircraft had adequately passed the taxi tests, they were cleared to participate in the flight tests. An experienced remote control aircraft pilot flew each of the aircraft around the flight test area.

All of the aircraft passed the taxi tests adequately, although some design modifications were necessary based on the results. One design team was forced to redesign the landing gear to attach to the aircraft more securely; one team had to redesign the wing carry-through structure when it was found that it failed under the weight of the aircraft; and one team was forced to use a larger propeller to increase the amount of thrust available for take-off.

Every aircraft flew successfully during the flight test. However, modifications were required of several aircraft before being authorized to fly or after an initial flight attempt, for example, removing twist from one wing or increasing control surface size. The Diamond Back (the joined wing aircraft) was very tail heavy and required significant movement of the center of gravity in order to fly.

The handling qualities of each aircraft were assessed qualitatively by the pilot and were used to evaluate the flight-worthiness of the aircraft.

Conclusions

This design course is evolutionary in nature. Each year the design project as presented to the students is altered to emphasize different aspects of the design process. This year the design project was expanded in three areas. First, the design teams were forced to develop a plane which would be in direct competition with an already existing aircraft. This provided the students with a bottom line, against which they would have to measure and justify their aircraft. Secondly, the teams were provided with more detailed costing methods than in the past. This allowed them a better opportunity to identify the cost ramifications of their design decisions. It also provided them with valuable lesson in the importance of cost in the development of a product. Finally, and most importantly, the project was structured in a manner which emphasized the importance of manufacturing in the the development of a successful product. The teams were required

to develop very specific plans with regard the the manufacturing process. They were required to purchase all materials prior to the start of manufacturing and they were provided with costs associated with the manufacturing labor and equipment.

The changes in the design course which were implemented this year were generally successful. Although the tight constraints on cost and manufacturing resulted in designs which were generally conservative in nature, the joined wing concept was unique. Most of the other designs had unique features such as flaps, taper, or efficient airfoils which were implemented to accomplish the requirements established by the teams in the DR&O.

Acknowledgements

This project was supported by NASA/USRA Advanced Aeronautics Design Program. Mr. Antoniewicz from NASA Dryden Flight Research Center provided technical assistance and guidance. Dr Stephen M. Batill presented the course with the assistance of graduate students Richard Sellar, Ken Cheung, and Jim Pinkelman. Finally, thanks to Mr. Joseph Mergen for his invaluable guidance in the the design and construction of the aircraft, and to Mr. Joel Preston, and Mr. Mike Swadener for their technical assistance.

THE DESIGN OF THREE EXPERIMENTAL HYPERSONIC TEST VEHICLES

The Ohio State University
 Department of Aeronautical and Astronautical Engineering
 Columbus, Ohio

Professor Gerald M. Gregorek
 Duane T. Detwiler, Graduate Teaching Associate
 Joseph C. Zuppardo, Graduate Teaching Associate

Abstract

Three different Experimental Hypersonic Test Vehicles (X-HTVs) were designed by separate student teams. These X-HTVs were designed to provide a platform to test advanced configuration and propulsion concepts under hypersonic flight conditions. The design requirements given for this project state that these vehicles must be capable of testing an airbreathing propulsion system at a speed of Mach 12-15 and an altitude of 100,000-120,000 ft. for one minute at steady state conditions. It was decided that this type of mission could be effectively accomplished by a remotely piloted vehicle. Therefore, all three vehicles were unmanned due to the hazardous nature of test flights. Three separate conceptual designs were developed to study different operational possibilities. One vehicle is a lifting-body configuration which takes off and lands as a conventional aircraft. Another is a lifting-body configuration which is vertically rocket launched and parachutes to splash-down landing. The third vehicle is a waverider which is air-dropped from another aircraft. This paper provides the details of all three vehicles along with an overview of the design process for high-speed aerospace vehicles.

Introduction

The Ohio State University (OSU) Advanced Aerospace Design Program (ADP) continues its tradition of hypersonic vehicle design with this year's project. Past projects for this program range from high speed cruise vehicles, including 250-passenger civil transports, 10-passenger executive

aircraft and military reconnaissance aircraft, to accelerating two-stage-to-orbit launch vehicles. This year's project, an experimental hypersonic test vehicle, presents its own set of unique design challenges.

There is an increasing interest around the world in developing vehicles capable of attaining low-earth-orbit in a reusable and reliable manner. The National AeroSpace Plane and its derivatives in the United States are examples. These vehicles will require advances in state of the art materials and technology to succeed.

There is always a certain amount of risk and cost involved when using new technology. For conventional flight vehicles considerable ground tests are normally carried out. However, such tests are not possible for the extreme conditions of hypersonic flight. An experimental hypersonic test vehicle provides the capability to test advanced configuration and propulsion concepts under actual flight conditions. This will reduce the risk and cost of future vehicle development. The three vehicles presented in this paper are intended for this purpose.

Project Requirements

The design requirements set for this project were intended to reflect those areas of technology advancement needed for future hypersonic vehicle development. Therefore, these X-HTVs must provide a platform capable of testing airbreathing propulsion concepts at a speed of Mach 12-15 and an altitude of 100,000-120,000 ft. for a minimum of one minute. Each vehicle was further required to carry a 1000 lb. payload of electronic data gathering equipment.

There are several operational modes possible for this type

of test vehicle. Three separate conceptual designs were developed to study these different possibilities. One vehicle was required to takeoff and land on a conventional runway. Another was to be vertically launched from a pad, making use of refurbished Minuteman boosters. The third vehicle was intended to be launched from another aircraft. This "mother" aircraft was designed by a French team from Ecole Polytechnique Feminine to release the test vehicle at Mach 2 and 50,000 ft.

All three vehicles were intended to be unmanned to eliminate the potential loss of life for the test flight. Studies showed the mission could be accomplished using a remotely piloted system. The general design requirements for all three vehicles can be summarized as follows:

Design Requirements

Test Speed	Mach 12 - 15
Test Altitude	100,000-120,000 ft.
Test Time	1 min
Propulsion	Airbreathing (Test)
Payload Weight	1000 lbs.
Payload Volume	35 cu. ft.

Design Program Outline

The Advanced Design Program at OSU consists of three separate classes over the academic year. These include a one credit hour seminar during Autumn Quarter, a four credit hour Aerospace Vehicle Design Course during Winter Quarter, and a three credit hour Advanced Vehicle Design Course during Spring Quarter.

The first course offers the students the opportunity to hear seminars from design engineers who work for NASA Lewis Research Center, Wright Laboratory, and GE Aircraft Engines. These professionals speak about the aircraft design process and some specific problems created by operating in a hypersonic speed regime.

The students were organized into three separate design teams at the beginning of the second course. These teams consisted of a team leader and members specializing in one or more core disciplines, such as aerodynamics, propulsion systems, etc. Since there is a separate structural design

course offered at OSU, no structural design was required for this project and none will be presented in this paper.

The teams were given the project requirements which they incorporated into their own design goals. The students were given access to the tools necessary to develop their designs. These included a database of related technical papers and publications, a collection of computer programs for aircraft design and analysis developed by NASA and Wright Labs, and a series of engine performance tables created by GE Aircraft Engines. Trade studies were conducted by each group dealing with different external and internal configurations, propulsion systems, and materials. The results of these studies were used to create a conceptual design for each vehicle and provide initial estimates for its aerodynamic, propulsion, and weight characteristics for an assumed flight envelope. These estimates were input into the preliminary mission analysis. The results of this analysis were interpreted and the design was accordingly altered to produce new performance characteristics. This process was repeated until a successful mission was achieved.

The design process was continued in the final course by using the iteration method to optimize the vehicle designs. Each group attempted to optimize their vehicles according to their design goals and minimize their weight and cost. The specifics of each design, such as thermal protection systems, stability and control systems, and inlet and nozzle configurations were examined. All of the design groups were required to give oral presentations on their progress and to submit a final paper at the end of both quarters.

The three design groups were designated OSU1, OSU2, and OSU3. Each group operated independently and in a spirit of friendly competition with others. The Teaching Associate functioned as a project manager making sure that all of the groups progressed accordingly.

Vehicle Designs

The OSU1 vehicle is a 50 ft. long lifting-body configuration. (See figure 1.) It reaches a test speed of Mach 12 and a test altitude of 100,000 ft. This lifting-body design was chosen for its aerodynamic performance at high speeds, its volumetric efficiency, and for ease of propulsion integration. The vehicle is powered by three RL-10 liquid

rocket engines to its test point. At this time a single hydrogen fueled scramjet is engaged. The OSU1 vehicle has a maximum gross weight of 47,800 lbs. and operates from a standard runway.

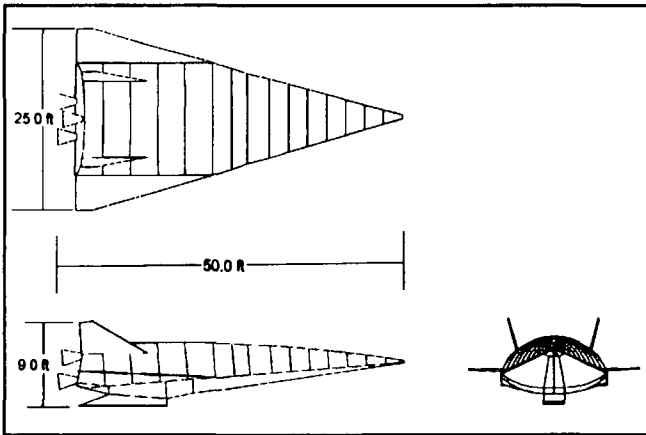


Figure 1 - OSU1 Conventional TO and Landing

The OSU2 vehicle is a 20 ft. long lifting-body configuration. (See figure 2.) It reaches a test speed of Mach 12 and a test altitude of 120,000 ft. This vehicle is rocket boosted to its test point by a two-stage Minuteman missile. The vehicle, surrounded by a protective sheath, forms the missile's third stage and nose cone. The sheath is blown away from the vehicle at the test point. The vehicle separates from the missile and its single hydrogen fueled scramjet engine is engaged. The OSU2 has a maximum gross weight of 7200 lbs. not including the rocket booster which weighs 66,000 lbs. This vehicle makes an unpowered descent until a parachute is deployed for a splash down at sea.

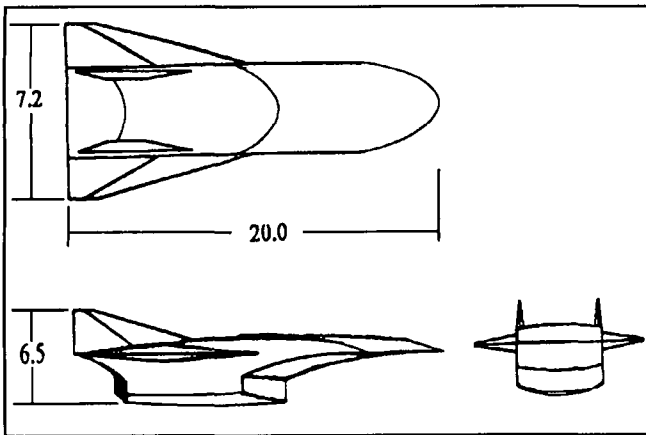


Figure 2 - OSU2 Missile Launched

The OSU3 vehicle is a 76 ft. long wave rider

configuration. (See figure 3.) It reaches a test speed of Mach 13.5 and a test altitude of 110,000 ft. This waverider configuration was designed using the exact 3-D solution of a conical flow at the test point and methods established by Rasmussen. The shock wave at the test point remains attached to the leading edge of the vehicle. This produces an optimal lift-to-drag ratio for the vehicle. While this effect is most beneficial for a cruising vehicle, the group decided their intended mission would be ideal to evaluate this concept for future use. This vehicle is carried to a speed of Mach 2 and an altitude of 50,000 ft. by another aircraft. It then separates and engages a single hydrogen fueled ramjet engine which powers the vehicle to a speed of Mach 7. At this stage a single hydrogen fueled scramjet engine is engaged to carry the vehicle to its test point. The OSU3 has a maximum gross weight of 14,260 lbs.

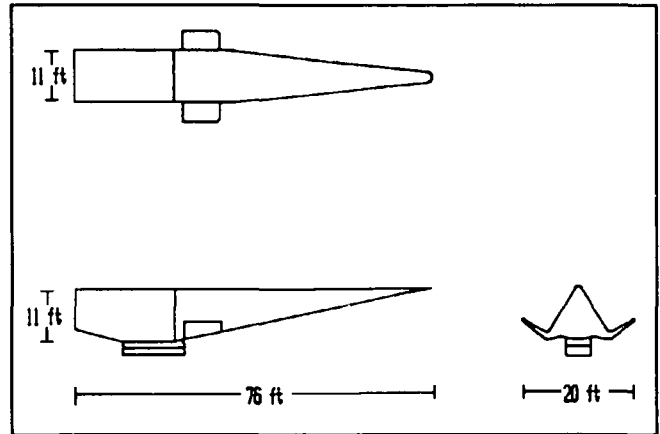


Figure 3 - OSU3 Air Dropped from Carrier Aircraft

Design Methods

The design team must satisfy the project's requirements with the best possible design according to their design goals. One major goal in all aerospace vehicle design is the minimization of overall weight. This leads to optimal performance for the vehicle. Another design goal is cost minimization. In these difficult economic times cost effectiveness must be considered in the conceptual design stage. Other possible design goals include simplicity of construction, operational flexibility, and enhanced capabilities.

The best possible design from an aerodynamic point of view is not necessarily the best for propulsion performance

or weight minimization. The design process is one of compromise between the various disciplines of aerospace vehicle design. The following sections provide details of the technical disciplines incorporated into the design process.

Propulsion

The purpose of this vehicle is to test a high-speed airbreathing propulsion system. The high internal temperatures and pressures associated with slowing airflows at speeds greater than Mach 7-8 make subsonic combustion impractical. Therefore, the only choice for an airbreathing engine system operating at speeds of Mach 12-15 is a supersonic combustion ramjet. A scramjet combusts the fuel/air mixture at speeds above Mach 1, thereby reducing the internal temperature and pressure.

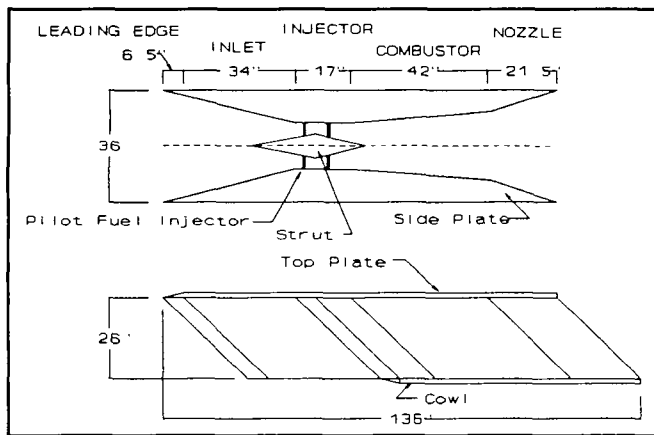


Figure 4 - Scramjet Engine Schematic for OSU3

The performance for these scramjet engines was obtained in two ways. Teams OSU1 and OSU2 scaled the data from theoretical engine performance tables provided by GE Aircraft Engines. Team OSU3 used the engine simulation program RAMSCRAM¹. Liquid hydrogen was selected by all three groups to fuel their scramjets. Trade studies showed it to be the only fuel proven capable of producing the needed amount of energy. The design teams were able to calculate maximum net thrust for the engines and the corresponding specific fuel consumptions. Figure 5 shows the performance of the scramjet drops dramatically as Mach number decreases. They may be considered unusable below Mach 6. Therefore, one or more additional propulsion systems must be used to reach the test point.

There are two types of propulsion systems capable of

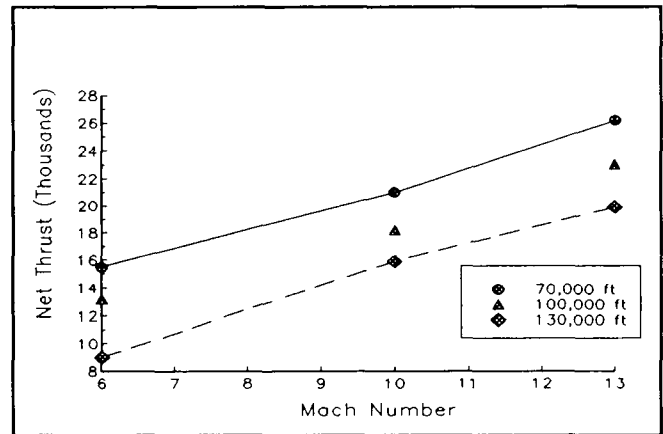


Figure 5 - Scramjet Engine Performance for OSU3

powering these vehicles to their test conditions. (See figure 6.) One is a combination of airbreathing engines and the other is non-airbreathing or rocket engines.

The efficiency of the airbreathing engines is shown to be much higher than for rockets. This means that for an equal period of time the rockets use more fuel. Therefore, the airbreathing engines can reduce the overall weight of a given vehicle. This is especially true for vehicles performing long cruising missions. The rocket engines are capable of much greater acceleration which makes them a viable option for this type of mission. Rockets are a proven and reliable technology and relatively inexpensive to purchase. They may not have the reusability of airbreathing systems.

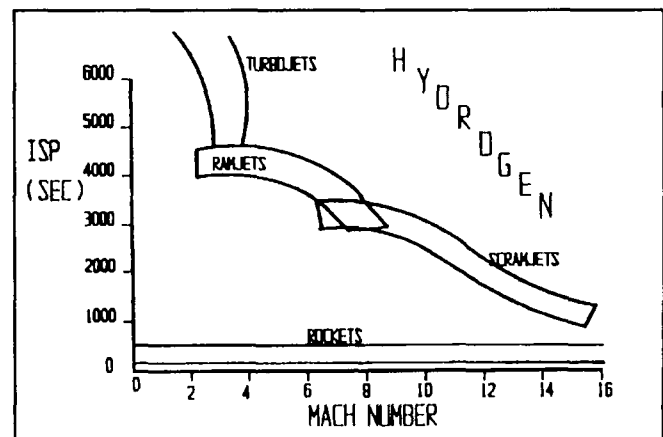


Figure 6 - Propulsion Alternatives

Two teams chose to use the rocket propulsion systems. Team OSU1 incorporated three RL-10 liquid hydrogen-

oxygen rocket engines into their vehicle. These engines weight 380 lbs. and produce 34,000 lbs. of vacuum thrust. OSU2 used a two-stage Minuteman solid rocket booster. The first stage weighs 50,500 lbs. and produces 200,000 lbs. of thrust. The second stage weighs 15,500 lbs. and produces 59,000 lbs. of thrust. The third team, OSU3, used RAMSCRAM to design a single hydrogen fueled ramjet engine for their vehicle. This engine weighs 1520 lbs. and produces a maximum thrust of 22,000 lbs. at Mach 3.

The thrust produced by each propulsion system at given speeds and altitudes was input into the trajectory analysis as thrust available. The results of this analysis were used to scale the number and size of the engines for the next design cycle. All engine data assumes mil-spec inlet and nozzle performance.

Aerodynamics

The aerodynamic analysis of these X-HTVs was conducted differently for the subsonic and supersonic/hypersonic flight regimes. Two of the vehicles have near ballistic ascent trajectories. The third is dropped off at Mach 2.2. Therefore, the subsonic characteristics are only necessary for the descent part of the trajectory. The simplified aerodynamic theories and empirical formulas outlined in the books *Fundamentals of Aircraft Design*² and *Aircraft Design: A Conceptual Approach*³ were used along with the AIREZ computer program. This program incorporates similar theories and formulas to match wind tunnel data.⁴ The vehicles were approximated as equivalent flat plate delta-wing-bodies for these methods.

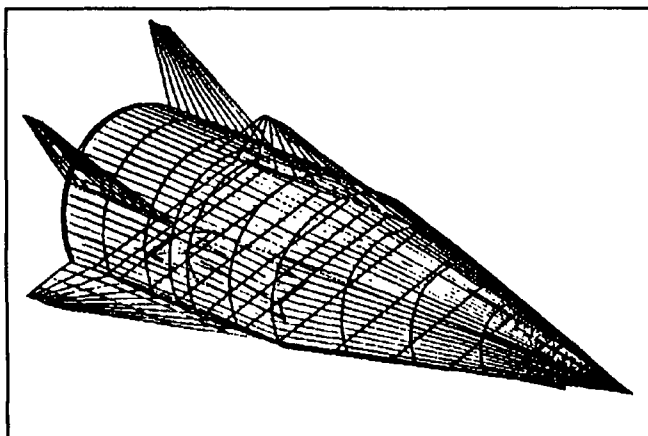


Figure 7 - APAS panel model of OSU1

In order to get more accurate results for the supersonic/hypersonic regime, each vehicle was modeled as a series of panels. (See figure 7.) The different areas of the vehicle were analyzed using different methods. These methods included Empirical Tangent Wedge and Cone, Prandtl-Meyer Shock and Expansion, and Modified Newtonian. The OSU1 group used APAS, a computer panel code developed by NASA Langley, which incorporates all of the fore mentioned methods and many others.⁵

These methods produced the aerodynamic characteristics of each vehicle with respect to free stream Mach number. The characteristics were assembled into drag polars for each vehicle. (See figure 8.) These drag polars were used along with the dimensions of each vehicle to calculate lift-to-drag ratios at given speeds and altitudes. (See figure 9.) These values were input into the trajectory analysis.

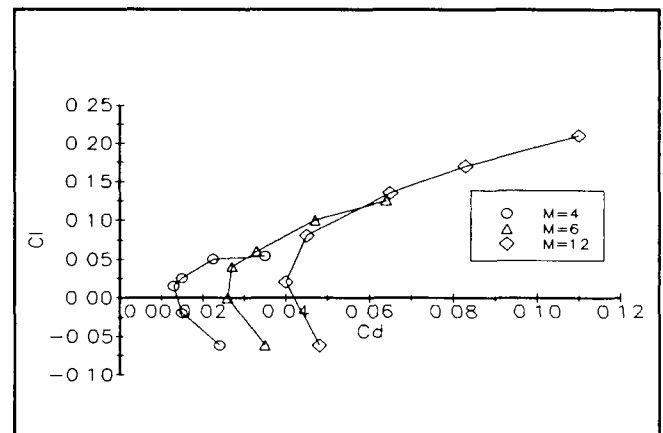


Figure 8 - Drag Polar for OSU1

The results of the trajectory analysis were then used to resize the vehicle for the next design cycle. The geometry

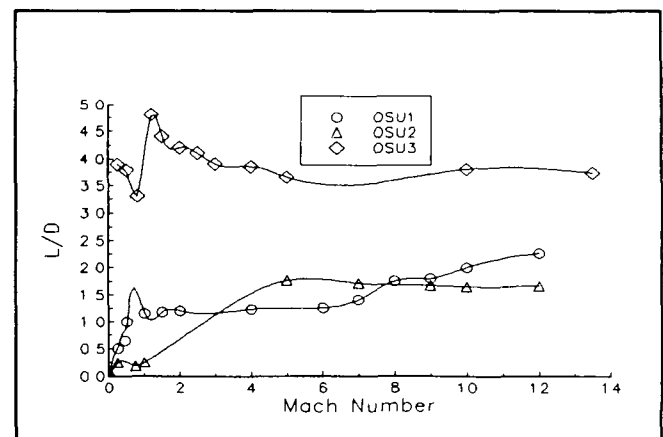


Figure 9 - L/D vs Mach Number

of each vehicle was modified to maximize the lift-to-drag ratios and meet stability constraints.

Weight and Sizing

There are two steps to the weight and sizing analysis of aerospace vehicles. The first step is the initial prediction of the weight and size of each configuration at the beginning of the design cycle. The second step is a detailed component weight and volume breakdown for each phase of the cycle.

The first step is accomplished using a fixed fraction method. The various major components of the vehicle such as structure, fuel, propulsion systems, etc. are assumed to be fixed fractions of the total vehicle weight and volume. These fractions are determined from a database of existing aerospace vehicle weight and size information. This existing data must be for aerospace vehicles similar to the one which is being designed. These fractions and an initial estimate of fuel required for the mission are used to estimate the vehicle's initial weight and dimensions.

The detailed component weight analysis for aerospace vehicles uses a statistical correlation method. This method is based on correlating existing component weight data with empirical equations. These equations can then be used to calculate the weight of new vehicle designs. The computer programs HASA and PDWAP use this method.⁶⁻⁷ These programs were used to determine a weight breakdown of each vehicle from geometric, performance, and material inputs.

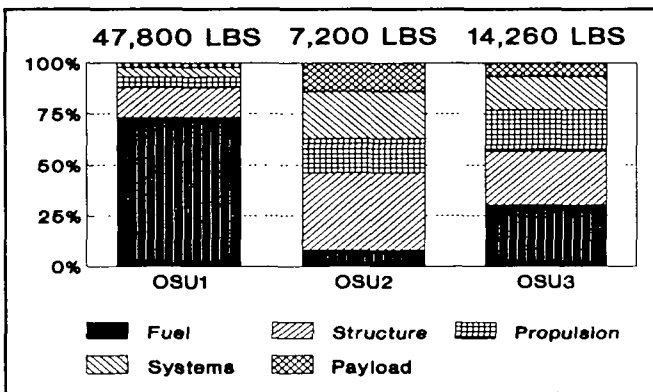


Figure 10 - Component Weight Breakdown

A component weight breakdown for the three X-HTVs is shown in figure 10. The OSU1 vehicle is the heaviest of the three. This is due to the integration of three liquid rocket engines and their fuel within the vehicle. The fuel in

this case is almost 3/4 of the total weight. The OSU3 vehicle is much lighter because it does not have to carry an oxidizer for its airbreathing ramjet. The fuel is less than 1/3 the total weight for this vehicle. The OSU2 vehicle is the smallest and lightest. It is carried to its test point by an external rocket booster. It must only carry enough fuel for the scramjet test and cooling purposes.

Once the detailed weight analysis is complete the values are used to determine a complete volume breakdown of each vehicle. These volumes are then incorporated into a 3-D model of the internal configuration of the vehicle. (See figure 11.) The vehicles dimensions may finally be rescaled for the next design cycle.

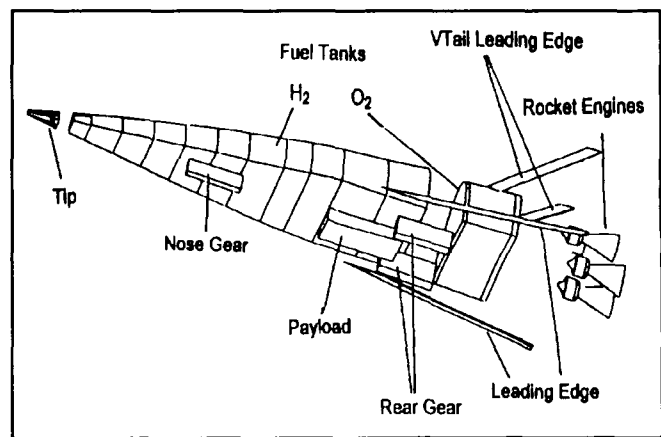


Figure 11 - Internal Configuration of OSU1

Trajectory

The trajectory analysis provides the test of the aircraft design concept. The propulsion, aerodynamic, and weight data are used as inputs to determine the aircraft's ability to meet mission requirements. If these requirements are not being met then the previous inputs must be updated and the trajectory analysis repeated until the mission is successfully accomplished. Once a vehicle that satisfies all requirements has been obtained, the vehicle can be optimized to produce the best possible design according to the group's design goals.

The trajectory analysis for the three Experimental Hypersonic Test Vehicles were based on two-degree-of-freedom methods which used five equations of motion describing velocity, flight path angle, weight, altitude, and range. The trajectory computer program ETO was used by

two of the groups.⁸ The third group wrote their own program.

The engine performance data is input as maximum thrust available. The aerodynamic drag is used to determine the thrust required for steady level flight along a determined flight path. (See figure 12.) The area between these two lines is the vehicle's ability to climb and accelerate. A successful mission trajectory requires two things. The thrust available must be greater than the thrust required at every point along the flight path. The vehicle's ability to climb and accelerate must be great enough to accomplish the mission within time constraints imposed by the specific fuel consumption of the engines and the amount of fuel available.

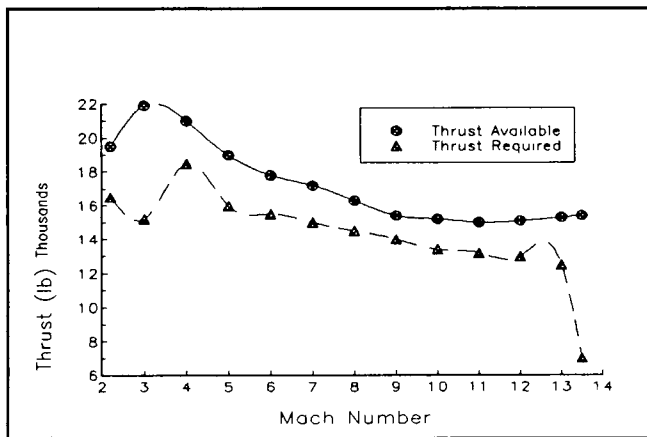


Figure 12 - Thrust vs. Mach number for OSU3

The flight path for each vehicle was determined based on selected parameters. (See figure 13.) The OSU1 vehicle performs a Rutowski climb after takeoff and then pulls up into a ballistic ascent. The OSU2 is vertically launched into a ballistic trajectory which takes it to the test point. The OSU3 vehicle makes a Rutowski climb after being dropped off. The vehicle climbs into a constant Q trajectory which it follows to the test point. All three vehicles make unpowered descents.

Conclusion

Three conceptual designs of Experimental Hypersonic Test Vehicles have been completed by independent student design teams. These aerospace vehicles were designed to provide a platform capable of testing advanced airbreathing propulsion concepts under hypersonic flight conditions. These vehicles will reduce the risk and cost of future hypersonic vehicles such as the NASP and its derivatives.

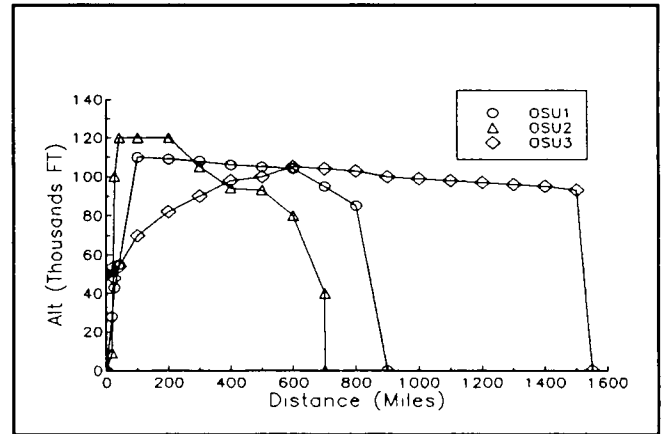


Figure 13 - Altitude vs. Range

The following table provides a comparison between the three different designs. All three concepts are inexpensive to develop and cost effective to operate. The cost analysis was based on three aircraft without propulsion systems and performing a total of ten flights. The cost analysis was performed using the method presented in *Fundamentals of Aircraft Design*². The OSU1 and OSU2 vehicles both use proven low risk rocket technology which can be purchased off the shelf. The OSU3 requires the development of a ramjet engine capable of operating at Mach 7. This airbreathing propulsion system gives the OSU3 more mission flexibility and minimizes the total system weight. These are all reusable systems with the exception of the expendable booster for OSU2. There are currently a large number of decommissioned Minuteman missiles available today.

There are still questions to be answered and details to be added to these conceptual designs. But, this project has achieved its goal. The students have discovered the cooperation and compromise necessary to conduct multidisciplinary design in a team effort.

References

1. Burkhardt, L.A., and Franciscus, L.C., "RAMSCRAM - A Flexible RAMJET/SCRAMJET Engine Simulation Program," ASME Journal, 1990
2. Nicolai, L.M., Fundamentals of Aircraft Design, San Jose, CA, METS, Inc. 1974
3. Raymer, D.P., Aircraft Design: A Conceptual Approach, AIAA 1987
4. Zeck, B., "AIREZ USER MANUAL," Seattle, WA, 1986
5. NASA Langley Research Center, "APAS Computer Software," 1991
6. Harloff, G. and Berkowitz, B., "HASA - Hypersonic Aerospace Sizing Analysis for the Preliminary Design of Aerospace Vehicles," Cleveland, OH, 1988
7. Wright Research and Development, "PDWAP - Preliminary Design and Weights Analysis Program", WPAFB, OH, 1989
8. Leingang, J.L., Donaldson, W.A., Watson, K.A., and Carreiro, L.R., Lt., "ETO - A Trajectory Program for Aerospace Vehicles," WRDC-TR-89-2023

Experimental Hypersonic Test Vehicles

	OSU1	OSU2	OSU3
Configuration	Lifting-Body	Lifting-Body	Waverider
Planform Area (sq. ft.)	625	95	720
Test Speed	Mach 12	Mach 12	Mach 13.5
Test Altitude (ft.)	100,000	120,000	110,000
Total System Weight (lbs.)	47,000	73,200	14,260
Engines	3 RL-10 Rockets 1 Scramjet	2-Stg. Minuteman 1 Scramjet	1 Ramjet 1 Scramjet
Mission Time (sec)	200	175	550
Cost (1993)	\$ 468 Mill	\$ 362 Mill	\$ 417 Mill

THE DESIGN OF AN ULTRA HIGH CAPACITY LONG RANGE TRANSPORT AIRCRAFT

Purdue University
School of Aeronautics and Astronautics
West Lafayette, Indiana

Professor Terrence A. Weisshaar
Gregory Bucci
Angela Hare
Matthew Szolwinski

Abstract

This paper examines the design of a 650 passenger aircraft with 8000 nautical mile range to reduce seat mile cost and to reduce airport and airway congestion. This design effort involves the usual issues that require trades between technologies, but must also include consideration of: airport terminal facilities; passenger loading and unloading; and, defeating the "square-cube" law to design large structures. This paper will review the long range ultra high capacity or megatransport design problem and the variety of solutions developed by senior student design teams at Purdue University.

Introduction

The objective of the senior design class of the School of Aeronautics and Astronautics at Purdue University was to provide a conceptual design for a new class of aircraft with a range of 8000 nautical miles to carry a maximum passenger load of 650 passengers, together with 30,000 pounds of cargo and to incorporate prudent amounts of advanced technology and new configuration concepts. Forecast production go ahead is 1996 with the first certificated airliners being delivered in 1999.

These large capacity airliners have been referred to as "super-jumbos", "megatransports" or "megajets." We will use the term "megatransport." The term "mega" refers to the projected take-off gross weight (TOGW) of these aircraft, a number expected to exceed 1,000,000 lbs.

Increased air travel demand that is sure to follow economic recovery will provide an opportunity for airlines to increase revenues and an opportunity for airframe manufacturers to sell airplanes. On the other hand, increased traffic may also place a burden on airports, air traffic control and airways around the world, many of which are at or near traffic saturation levels. Northern Pacific routes are already congested at prime times because there are only two airways westbound and three eastbound.

To take advantage of increased traffic, while recognizing airport and airway congestion difficulties, airlines are considering new airplanes with more than 150% the capacity of the Boeing 747-400. Predictions for the number of new

large transports needed by 2010 range as high as 550 units.^{1,2}

The last substantial increase in aircraft size occurred almost 25 years ago with the development of the Boeing 747. Megatransport designs will compete with existing Boeing 747 designs, the proposed MD-12 and possible new SST's being proposed for long range use.

This paper briefly reviews megatransport objectives and constraints, and summarizes some of the solutions developed by student design teams at Purdue University during a one semester course. It begins with a discussion of the market needs and the economic risks involved in such a project. It then summarizes some of the different approaches taken to solve the problem and the difficulties faced by the design teams. Finally, some "lessons learned" are discussed at the end of the paper.

The Request for Proposal

This was the second year that senior design teams had considered the design of a large transport. On the basis of previous experience, a Request for Proposal was generated to reflect market conditions and demand. The primary difference this year was that the range was increased to 8000 nautical miles to provide a challenge and the number of passengers was chosen to be large, but not too large compared to existing designs. The Request for Proposal is summarized as follows.

Regulations/certification

The aircraft must comply with Federal Aviation Regulation Part 25 (FAR25) and foreign equivalents. The engines must comply with Federal Aviation Regulation 36 (FAR36) and ICAO Article 16.

Mission Performance

The still air range must be at least 8000 nmi. with a full load of 650 passengers and 30,000 pounds of cargo.

Fuel reserves equal to 5% of primary trip fuel must be included in the mission.

Cruise must begin at least at 35,000 ft. and Mach 0.85. The cruise Mach number at any operational altitude must be equal to or greater than $M=0.85$.

The aircraft must be able to operate from international airports with a full passenger/cargo load using no more than 10,000 ft of runway. It must be able to land at sea level at 80% of TOGW using no more than 8500 ft. of runway.

The use of advanced materials is highly encouraged, consistent with safety, maintainability and cost requirements. Emphasis should be placed on minimal empty weight and cost.

The use of high bypass ratio turbofan engines is encouraged, consistent with cost and development considerations. It is strongly recommended that upgrades or modifications of existing engines be considered.

The use of advanced airfoils and innovative, multiple lifting surface concepts is strongly encouraged, consistent with customer acceptance and performance. Evidence of transonic area ruling must be presented in the final proposal.

The design of the fuselage must show evidence of concern for safety and for passenger comfort, loading and unloading. Compatibility with existing or slightly modified airport facilities likely to be in use in the year 2005 must be demonstrated. Carrying fuel in the fuselage is discouraged, but not prohibited. Using the entire length of the fuselage for a double deck passenger configuration is discouraged, but not prohibited because of loading and unloading and compatibility with current airports.

Cost

Acquisition and operating costs are a major factor in evaluating the suitability of the design. These costs must be determined using generally accepted data and estimation procedures.

Maintainability

The design must clearly show that maintenance and reliability have been considered.

Data requirements

The technical proposal shall be specific and complete, but must be less than 100 pages, excluding the Appendix. This proposal must demonstrate a thorough understanding of the requirements and opportunities for the design RFP.

Critical technical issues and problem areas must be clearly identified in the proposal and adequately addressed. Descriptions, sketches, drawings and analysis, method of approach and discussions of new techniques should be presented in sufficient detail to permit accurate engineering

evaluation of the proposal. Exceptions or modifications to the proposed technical requirements presented above must be identified and explained. Aerodynamic analysis using LINAIR, VORLAT and PMARK is required.

Trade-off studies must be performed and included in the proposal to describe how the final design was arrived at. A history of the design development, including possible designs that were rejected and their reasons for rejections, must be included.

The Final Proposal Report

Based on the previously stated objectives, requirements and constraints the final report must include sections and or data on the following:

- 1) Justify the final design by describing the aircraft's performance and listing its advantages compared to other existing and proposed designs. Include aircraft design and sizing trade studies.
- 2) Include a three-view drawing in the final proposal. This drawing must show important dimensions (in English and metric units), payload and passenger locations, fuel locations, crew location and crew accommodations, flight control systems and any unique or unusual features.
- 3) Weight and balance data must be provided together with a description of loads and structural materials and their location. Provide a center of gravity envelope diagram showing extreme c.g. locations relative to the aircraft aerodynamic center. This data must be provided in terms of a mean aerodynamic chord reference.
- 4) Describe techniques or methods used to determine aircraft performance, stability, control and handling qualities. Indicate the results of these techniques. Show compliance with FAR25.
- 5) Summary of design trade-offs - Describe why the final design was chosen. Describe why this design is optimal for the intended use. Describe the sensitivity of the design to changes in parameters such as aspect ratio, wing area, wing thickness, engine TSFC, range, materials choice and other design choices.
- 6) Provide cost data and sensitivity of the aircraft price to such parameters as number produced, cost of capital, take-off gross weight and government grants.

Basis of Judging

Responses to this proposal will be judged in four primary categories.

Technical Content The correctness of theory, validity of reasoning, apparent understanding and grasp of the problem.

Organization and Technical Presentation The ability to present a description of the design and to clearly communicate its advantages is an essential factor in evaluation. Organization of the design report, clarity and skillful inclusion of pertinent data are major factors in this evaluation.

Originality The design proposal should show that there was independence of thinking or a fresh approach to the problem. Does the method and treatment of the solution show imagination or extend previous efforts or is it simply a rehash of an existing solution? Evidence of team effort and participation are essential.

Practical Application and Feasibility The proposal should present conclusions and recommendations that are practical and feasible and not merely lead the evaluators into other unsolvable problems. Has the team made mention of shortcomings and made recommendations for further improvement if time permitted?

Challenges and Advantages of Megatransport Design

The design of an aircraft such as proposed in the above RFP poses some unique problems. Design addresses a customer need and then proposes a solution. The consideration of need requires an answer to the question "Is there a market for large capacity, megatransport airliners?"

During 1991 the operating losses of major airlines exceeded the total profits earned since the introduction of jet transportation in the 1950's. In 1992 airlines continued to lose money. Despite this and the worldwide economic growth problems, the demand for air travel is predicted to resume its growth within the next few years.

The number of airline revenue passenger miles (RPM) is predicted to more than double by the year 2010. Boeing predicts that the number of available seat miles (ASM) will increase by more than 180 percent to meet air travel demands in the year 2010.² Markets to consider include both domestic and international routes.

Table 1. Percentage of total available seat miles (ASM) by airlines to and from three regions (1991 value / 2010 forecast)¹

Travel to/by	US Airlines	Europe	Asian
North America	61% / 56%	32% / 26%	28% / 28%
Europe	21% / 20%	40% / 36%	17% / 28%
Asia-Pacific	12% / 20%	12% / 27%	47% / 41%

Domestic marketing concentrates on frequent flights to and from destinations. As a result, the number of passengers per flight is too small to justify a large capacity aircraft. Overseas markets with high demand, but only a few flights a day, have the most potential for generating revenue. The fastest growing markets for North America appear to be in the Pacific Rim region. The economic growth there indicates that this trend will continue. Table 1 shows a prediction of the available seat miles (ASM) categories by routes for U.S., European, and Asian airlines.¹

Airlines favor buying aircraft with a range equal to the B-747. Recent articles appear to favor aircraft ranges of between 7500 and 8000 nautical miles.³ On the other hand, each nautical mile of range increases take-off gross weight TOGW substantially and few airport pairs are located more than 7000 nautical miles from each other.

To reach out to these markets, we require a long range aircraft. The cruise portion of the flight dominates the mission of the long range transport. Estimating the fuel required for a cruise dominated mission with the Breguet range equation illustrates fuel requirements. This estimate reads:

$$W_{fuel} \equiv W_{TO} \left(1 - e^{\frac{-Rc_j}{MaL/D}} \right) \quad (1)$$

where R=range, c_j = thrust specific fuel consumption, M=cruise Mach number, a=speed of sound at cruise altitude and L/D is the estimated value of cruise lift to drag ratio.

Equation 1 shows that the fuel required for the mission approaches the TOGW as range R increases. It is not unusual for the fuel fraction (ratio of fuel weight to take-off gross weight) to be of the order of 0.45, even if the aerodynamic efficiency (ML/D) is high and the engine TSFC c_j is low.

For preliminary estimates of the TOGW, we can use the relationship of the form

$$W_{TO} \equiv \frac{W_{payload}}{1 - \bar{m}_{fuel} - \bar{m}_{empty}} \quad (2)$$

where \bar{m}_{fuel} is the fuel fraction W_{fuel}/W_{TO} and \bar{m}_{empty} is the empty weight fraction. The empty weight fraction becomes slightly smaller as TOGW increases.⁴ This occurs because the dimensions and size of the megatransport allow for more efficient use of high strength materials in the structure and

more dramatic weight savings if advanced composite materials are used.

Increased aerodynamic efficiencies may also occur because parasite drag may be reduced due to the larger Reynolds numbers at which large aircraft operate. The coefficient of friction C_f decreases because of an increase in Reynolds Number. Assuming turbulent flow over the entire wing, the C_f is approximated by⁴

$$C_f = \frac{0.455}{(\log Re)^{2.58} (1 + 0.144 M^2)^{0.65}} \quad (3)$$

where M is the Mach number and Re is the Reynolds number. Aircraft with larger characteristic lengths (wing chord, fuselage length, etc.) will have smaller friction coefficients, all other things being equal. Even with these potential advantages, the megatransport TOGW quickly grows as the range increases.

Balancing these problems, operating costs, especially fuel cost per passenger mile, decreases as passenger number increases. There will be a minimum fuel cost for a given number of passengers and a given range. This minimum fuel cost reflects the economies of scale for any given design.

Megatransport Special Design Issues

The large size of a transport with passenger capability exceeding the B-747 places demands on technology, including structures, manufacturing, landing gear and passenger configuration, to name a few items. These issues for the design of large transports are discussed in a variety of recent articles.^{5,6,7,8,9}

Airports

The long range markets with high passenger demand are currently served by B-747, DC-10 and MD-11 aircraft. Boeing 747 airplanes not only the primary competition for the megatransport, they are the standard for designing terminal facilities and runways. Increased aircraft size beyond the B747 planform may require modifications to runway widths pavement thickness, taxiways and terminal facilities.¹⁰

Several constraints arise if existing facilities are to be serviced. These include service to airport terminals built to accommodate wingspans less than 220-240 feet and fuselage lengths of the order of 220 feet. This constrains the span of the megatransport wings and makes drag reduction difficult.

Another serious problem is the logistics of quickly loading or unloading 650 passengers. This includes not only jetways, but terminals and emergency conditions.

Structural Design

Among other important issues faced by the structural designer of large transports is the so-called "square-cube law." The square cube law is a statement regarding the relationship between the loads, which are assumed to be proportional to weight, and the stresses in the structure. For similar structures of different scales, the load increases as the cube of linear dimensions and the cross-sectional areas increases as the square of the linear dimension.¹¹

If the size of the object is doubled (for instance, we simply scale up an existing design) then the stresses double. Therefore for a given material with a given ultimate stress, the square-cube law limits the size of the object. As a result, we can not simply make the aircraft larger, we have to make it different.

Recent aircraft design has focused on using new materials and structural design techniques. New materials, such as aluminum-lithium, and advanced composite materials have allowed changes in structural design. This "defeats" or at least holds off the detrimental effects of the square-cube law and allows larger aircraft to be built.

Innovative configurations can also aid in "defeating" the square-cube law. The use of such configurations as joined-wing design, three-surface designs or flying wings can overcome pessimistic predictions of the square-cube law by allowing a redistribution of weight throughout the vehicle. Finally, the weight of some items on an aircraft are not functions of scale.

Fuselage design

Containment of passengers on a large transport requires an examination of how to keep the wetted area per unit volume at a low level. This objective must be tempered by safety and comfort requirements. Fuselage design is challenging because of aircraft maximum length constraints imposed by terminal facilities and the requirements for aerodynamic efficiency of the fuselage shape. This latter feature is usually at odds with terminal requirements because short, stubby fuselages are aerodynamically inefficient.

New fuselage cross-section layouts must be considered to satisfy fuselage length limits while increasing volume and minimizing wetted area. These new layouts include multiple deck configurations, elliptical single deck configurations and dual fuselage configurations.

The largest factor constraining fuselage design is safety. There must be enough emergency exits for the passengers to escape in 90 seconds. Multiple deck configurations have emergency exits far from the ground (40 feet or more), possibly compromising safety.

Because of previous efforts in fuselage configurations, the class decided to strongly consider single deck configurations. While these configurations will have some evacuation problems, they also will have structural, aerodynamic and passenger comfort advantages. As a result, all designs described in this paper will be single deck configurations.

Wing Design

Wing design is driven by size constraints, imposed by existing aircraft terminal facilities, that limit the wing span of the aircraft. Consequently, it becomes important to consider the trades involved in wing design with the constraint of a fixed upper limit on the wing span.

The most important factor in controlling the induced drag is the wing span loading (the ratio of aircraft weight to wing span). With the span limited and the weight requirements high, one must look to new configurations. The wingspan constraint was addressed by using folding wing tips and multiple lifting surfaces, including tandem wings, canard configurations and three surface configurations.

Another key parameter in wing design is the choice of wing area. The cruise lift coefficient C_L is related to aircraft weight W and wing planform area S as follows

$$C_L = \frac{W/S}{q} \quad (4)$$

where q is the dynamic pressure. From a structural point of view the wing area should be small to decrease wing weight and empty weight. As W/S increases with decreasing wing area, C_L increases. This results in an increase of induced drag, which depends on the square of C_L as follows

$$C_{Di} = \frac{C_L^2}{\pi e AR} \quad (5)$$

where AR is the aspect ratio and e is Oswald's efficiency factor. As a result of increased induced drag, more fuel is required, so that the take-off gross weight increases even though wing weight decreases. The matter is further complicated by changes in the parasite drag as wing weight changes. Clearly there is an optimum trade-off between wing area, induced drag and fuel required.

This trade between wing area, weight, drag, and take-off gross weight exists for every type of aircraft. However, this trade is very evident in the mega-transport because of the large wing areas involved and the large take-off gross weights.

Engines

Large transports must have efficient propulsion units. These engines must meet thrust requirements, noise

standards and emission standards. Although some long range aircraft such as the Boeing 777 are powered by twin engines, the "one engine out" requirement for the megatransport requires more than two engines. All teams chose to use four engines with relatively high bypass ratios so that they could meet noise constraints and have TSFC's of about 0.55 lb/lb./hr. at cruise. One group chose a prop-fan engine with very low fuel consumption.

The team design take-off gross weights (TOGW) for the aircraft designs range from slightly below one-million pounds to about 1.2 million pounds. Although there are some large engines that may meet the requirements for megatransport propulsion, the engines used on the Purdue designs were designed to meet the special requirements of their airplane. The cycle analysis programs ONX and OFFX, developed by Mattingly and Heiser,¹² were used for engine design and performance predictions.

Large engines create design problems over and above the usual problems of finding an efficient design cycle. The large intakes require severe restrictions on ground clearance. This leaves the designer with a choice of lengthening the landing gear, adopting a high wing design or mounting the engines on top of the wing.

In addition to these problems, FAR 36 and ICAO Annex 16 (Chapter 3) have restrictions on lateral, take-off and approach noise.¹³ While these regulations permit increased noise with increased aircraft weight, the upper level of noise generation is fixed for aircraft weights greater than 900,000 pounds.

Cost and Price Estimation

The megatransport must have low operating expenses compared to existing aircraft such as the B-747 aircraft. These operating expenses translate into direct operating cost (DOC) per block hour of operation and direct operating costs per available seat mile.

The estimation of direct operating costs requires an estimate of airplane cost and fuel requirements. The production costs to build the aircraft were estimated using the DAPCA IV model discussed by Raymer⁴ This model estimates cost on the basis of aircraft empty weight, production quantity, maximum airspeed and engine and avionics cost. One problem with this estimator is that it is based on a data base heavily weighted with military aircraft. Still, the numbers generated using this model are useful.

The price of the aircraft was calculated using a cash flow analysis. This calculation considers production cost (from the DAPCA model), quantity produced over a 19 year period and the cost of raising capital (effective interest rate on borrowed money and money raised in financial markets) to initiate the program. A low cost of capital (currently near 17%) is very important to the success or failure of a

commercial venture. The production quantity was set by the teams based on what the market would support.

Direct operating costs (DOC) were estimated using a model suggested by the Association of European Airlines. The direct operating costs and the cash flow analysis required to set the manufacturers selling price were calculated, using a computer model supplied by Professor J.W. Drake¹⁴ The input to the DOC model includes mission block time, fuel requirements, cost data for labor rates, fuel prices, engine prices, aircraft purchase price, maximum weight, stage length, payload and number of crew members.

Design Resources and organization

Teams were composed of from 5 to 6 members, each with a primary responsibility. There were 4 such teams during the Fall 1992 semester and 5 teams during the Spring 1993 Semester.

The design course at Purdue is one semester long. This allows about ten weeks of group effort to produce a preliminary design after all the basic areas of effort are reviewed. In addition to the emphasis on technical effort, the requirements for communication in terms of writing quality and oral presentations are stressed.

A Summary of Configurations

This section will present four representative 1992-93 team design efforts. These designs have been selected to illustrate the range of solutions developed. Each of these designs represents a different path taken by students. The reader should keep in mind that the final results at the end of one semester are at a preliminary level. At the close of a semester the students are finally aware of the trades and are aware of where they need more effort. On the other hand, for the most part, these efforts indicate a remarkable level of understanding and effort.

The Phoenix 650

The design of the Phoenix 650 was selected and refined by its design team to be an unconventional answer to several problems and constraints posed by the RFP. This design, shown in Figure 1, uses the joined wing concept first suggested by Wolkovich. The team selected this configuration because they wanted a challenge and because they thought that this design would have lower wing weight, good transonic area distribution, low trim drag and better accessibility to existing airports. On the other hand, the team felt that the lack of a good data base for weight estimation and the challenges of doing a credible analysis were drawbacks for this selection.

The Phoenix 650 has an estimated empty weight of 505,000 lb. but has a take-off gross weight of only 750,000 lb. This low take-off gross weight is made possible by the

use of four prop fan engines with a TSFC of 0.286 lb/lb/hr. This remarkably low TSFC translates into a very low fuel weight.

This aircraft will carry 650 passengers. The length of the Phoenix 650 is 240 feet while the fuselage width is 30 feet

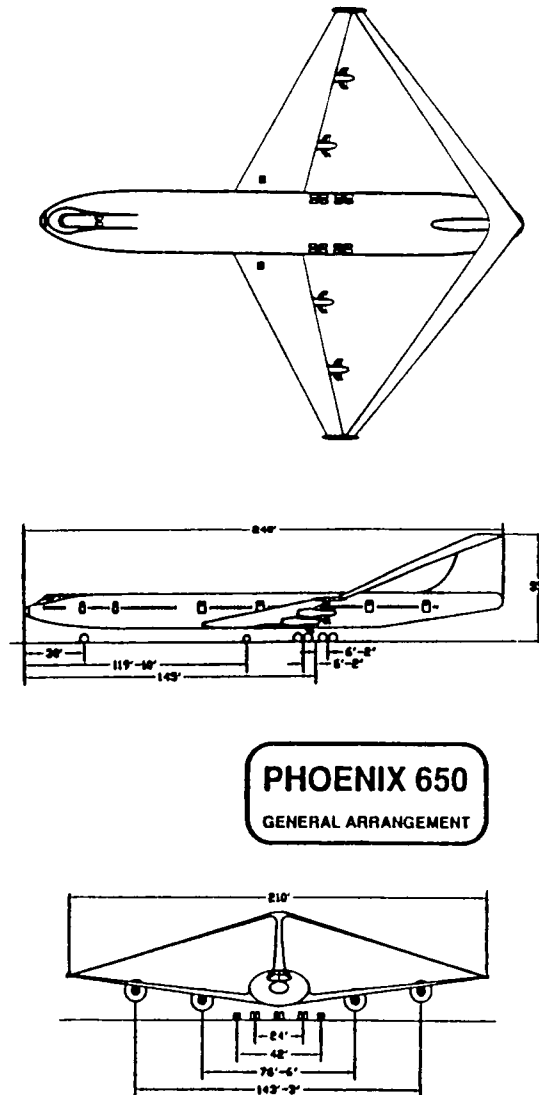


Figure 1 - The Phoenix 650

at its widest point and the fuselage height is 18 feet at the same point. The maximum L/D is estimated to be 22. The price of the aircraft is estimated to be \$140,000,000. The computer aided drawing effort for this aircraft was extremely good. A wind tunnel test model of the airplane is currently being manufactured by the Tupelov Design Bureau for delivery in September 1993 for testing.

The BWB-650 Griffin

The BWB-650 Griffin is an ultra-wide body aircraft that attempts to use the minimum of trimming and stabilizing surfaces to reduce drag. This aircraft, shown in Figure 2, has a wing span of 300 feet and a total length of 209 feet. The wing tips can be folded so that they are only 230 feet wide in their folded position. The take-off gross weight of this aircraft is 985,000 lb. with an empty weight of 450,300 lb. The aircraft price is estimated to be \$134,500,000.

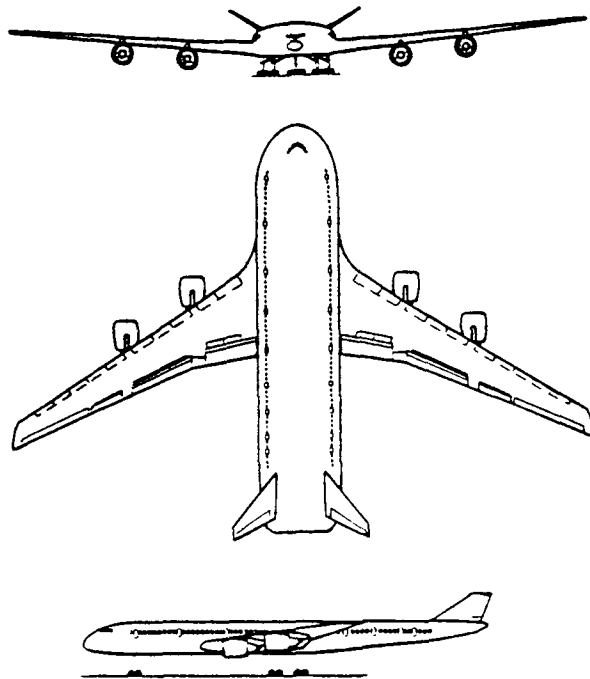


Figure 2 - The BWB-650 Griffin

The BWB-650 carries 657 passengers and has a fuselage that is 16 ft. 10 in. high and 42 ft. 2 in. at its widest point. The aircraft is powered by four high bypass ratio engines with a cruise TSFC of 0.546 lb./lb./hr. and a thrust of 81,600 lb. per engine at sea level static conditions. The maximum L/D was estimated to be 23.19 because of attempts to minimize wetted area and maximize wetted aspect ratio.

The INF Super Condor

The INF Super Condor, shown in Figure 3, is a single deck, wing/canard lifting surface aircraft that can carry 656 passengers. With a maximum span of 220 feet, the relative areas of wing and canard, as well as their placement on the fuselage, were selected with the objective of high L/D and

low wetted area in mind. The maximum L/D of this configuration is estimated to be 19.

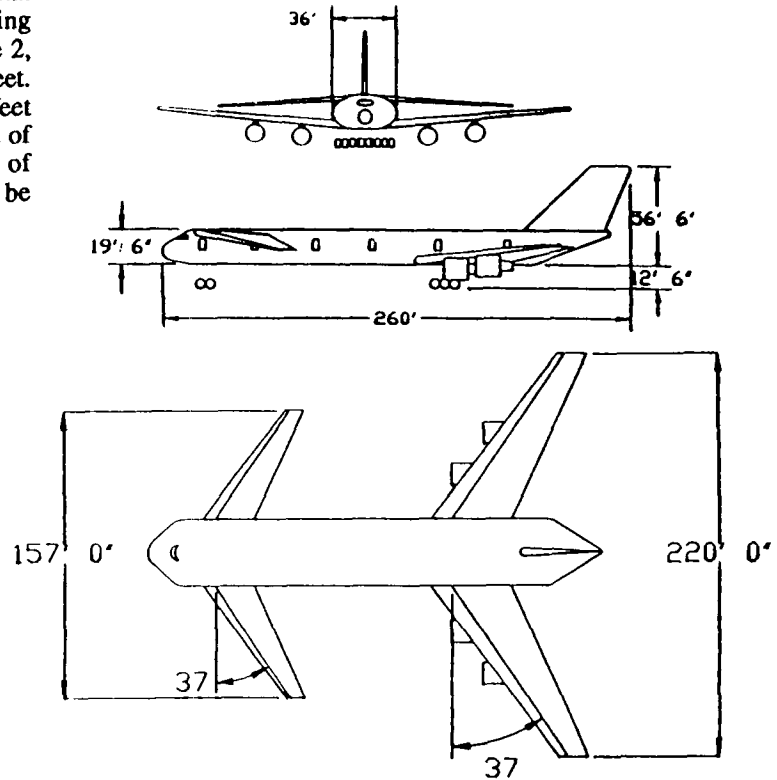


Figure 3 - The INF Super Condor

The thrust per engine is 81,000 lb. at static sea level conditions. TSFC at cruise is 0.534 lb./lb./hr. The take-off gross weight is 1,180,000 lb. with an empty weight of 539,000 lb. The price of this aircraft is estimated to be \$200,000,000. The length of the airplane is 260 ft. with a maximum fuselage width of 36 feet and a maximum height of 19 feet 6 inches.

The AMT-Condor

The AMT-Condor, shown in Figure 4, is a conventional design, again with an ultra-wide deck. The AMT-Condor team chose this design because of their concern for configuration acceptability in the marketplace. This aircraft has a take-off gross weight of 1,137,000 lbs. and an empty weight of 480,400 lb. The wing span is 275 feet and the aircraft length is 240 feet. The fuselage cross-section, with a maximum width of 33 feet and a height of 16 feet 6 inches, should help lift generation. The maximum L/D is 19.

An indication of size and efficiency of each of these aircraft is provided by the data in Table 2.

Table 2 - Design OEW, wing span, TOGW

Aircraft	OEW (lbs)	wing span (ft)	TOGW (lbs.)
BWB-650	450,300	300/230	985,000
Phoenix 650	505,000	210	750,000
AMT-Condor	480,400	275	1,137,000
INF-Super Condor	539,000	220 (2-surface)	1,180,000

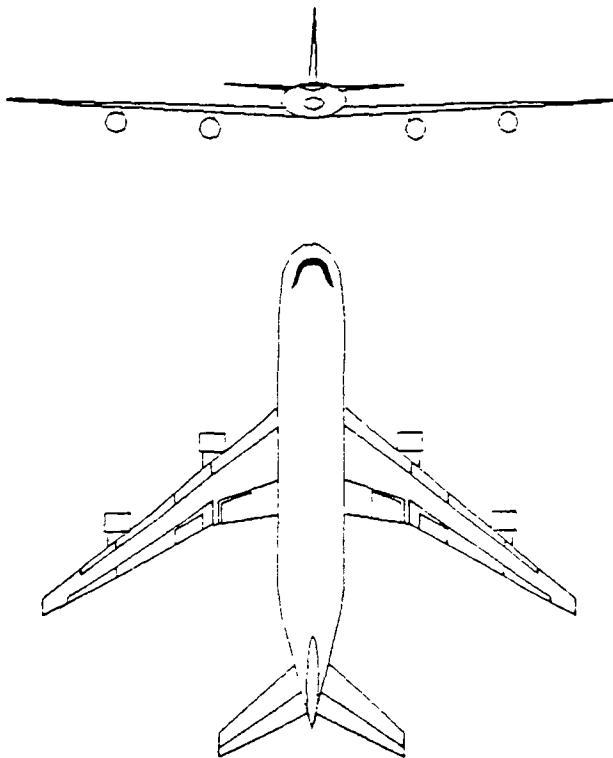


Figure 4 - AMT-Condor

Fuselage Designs and Comparisons

To the passenger, the heart of the transport aircraft is the fuselage. The aerodynamic efficiency, in terms of minimizing drag, requires a slender fuselage or no fuselage at all. One design considered initially by several groups was a flying wing. While aerodynamically efficient, the flying wing seats passengers in very wide rows. This makes it difficult to evacuate the aircraft in an emergency. It also makes it awkward to service the cabin in flight.

Fuselage designs finally centered on the single deck, "ultra-wide" configuration shown in Figure 5. Cargo storage is a design criterion, as is the ability to provide a carry-through structure. With so many passengers on board, internal traffic patterns must be considered. Also, the

requirements placed on a cargo hold to carry so much baggage are severe.

For pressurization loads there is no more efficient structural form than a circular cross-section. On the other hand, if the aircraft has two decks, then only about 1/3 of the large circular cylinder is filled with passengers. There are other related problems of increased height of the aircraft and increased landing gear length when a circular section is used.

Hitch¹⁵ assesses the trades between a "flattened" elliptical section and a circular section and concludes that a slight weight penalty is necessary to use an elliptical section, but that this increased weight is more than made up by decreased wetted area and reduced drag. It is interesting to note that the

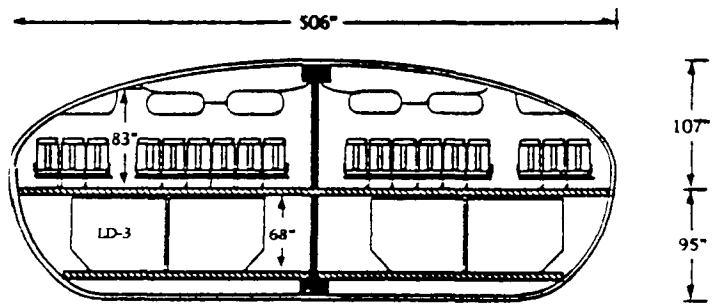


Figure 5 - Fuselage design (BWB-650 Griffin)

Tupelov Design Bureau will unveil its answer to the mega transport problem at the Paris Air Show in June 1993 and their design is rumored to be an ultra-wide-body.

Engine Design

Engine design is an integral part of the senior design course at Purdue. Each group was required to design an engine around a baseline engine provided to them. Design included the design of the engine cycle and included specifying the turbine inlet temperature, compressor pressure ratio and engine bypass ratio.

Engine design efforts were supported by the ONX and OFFX analysis programs mentioned earlier. The TSFC at cruise altitudes for turbo-fans ranged from a low of 0.52 to a high of 0.54. Bypass ratios between 8 and 10 were common. An alternative engine was proposed by the designers of the Phoenix 650. This engine was a prop-fan, shown schematically in Figure 6. This engine used the latest technology available and had a remarkably low estimated TSFC of 0.286 lb./lb./hr.

For the operator and the passenger, the fuselage is the heart of the airplane. However, for the engineer, it is the wing that makes or breaks the design. The wing design is affected by considerations of performance, such as landing,

take-off and cruise. On the other hand, the wing design must take into consideration added weight and the ability to house fuel and landing gear as well as carry engines.

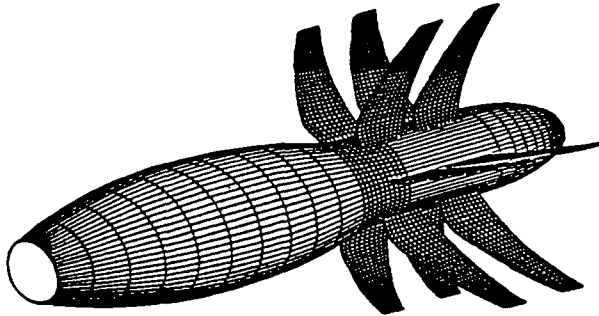


**Figure 6 - Proposed prop-fan engine
 (Oliver Debikey)
 Aerodynamics**

Most of the team designs used wing loadings near 130 lb. per square ft. This wing loading allows the aircraft to operate efficiently at cruise, however, at landing and take-off leading edge and trailing edge devices must be used to operate at the airfields specified in the RFP's.

The primary parameters for trade-off studies in wing design are airfoil thickness to chord ratio, wing area, sweep, taper ratio and aspect ratio. Wing placement on the fuselage is a consideration also. In the vertical plane of the design, the wing may be placed high on the fuselage, in the middle of the fuselage or low on the fuselage. There are advantages and disadvantages to all of these choices.^{16,17}

The megatransport designs generated by the teams used a variety of wing mounting positions. The low wing position was popular. All teams used supercritical airfoils and some used laminar flow control.

Aircraft Cost and Price Analysis

Controlling aircraft price and cost of aircraft and the cost of operations are emphasized in our design course. Cost of production and cost of operation are computed to make sure that what is being designed is cost efficient.

If the number of aircraft produced is large, then the cost per aircraft and the price per aircraft will be low. On the other hand overestimating market share can be disastrous. To illustrate this, Figure 7 shows the cash flow (profit) after 19 years of production using our computer simulation. The discount rate or cost of capital is 12% (a low estimate considering the risk) while the aircraft empty weight is 450,000 lbs.

Plotted on the horizontal axis is the manufacturer's selling price. Note that the break-even price (where the cash flow is

zero) must increase substantially if the market share is reduced from 452 aircraft to 252 aircraft.

As noted previously, the market for this type of airplane is estimated to be about 550 units by 2010. On the other hand, a company cannot be expected to capture the entire market. Design teams estimated as few as 200 units and as many as 400 units that they could sell. As a result, the prices of the aircraft varied widely depending upon their empty weights, the estimates of the number to be produced and the cost of capital estimate used for calculations.

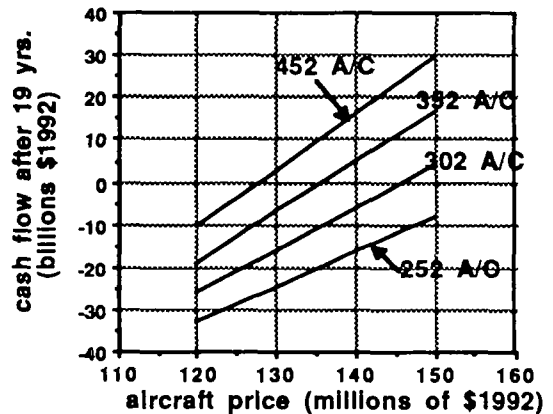


Figure 7 - Cash flow (profit) after 19 years of production vs. aircraft price; cost of capital 12%; empty weight 430,000 lbs.

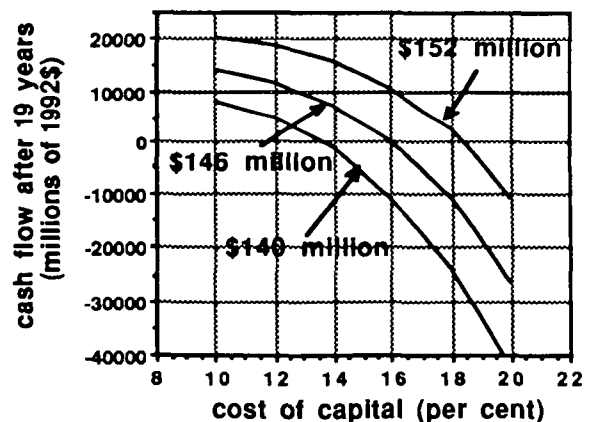


Figure 8 - The cash flow (profit) after 19 years of production vs. cost of capital at three different aircraft prices; 352 aircraft produced; empty wt. of 430,000 lbs.

Figure 8 shows the effect of cost of capital on cash flow after 19 years for three different manufacturers prices for an aircraft whose empty weight is 430,000 lbs. The production number is fixed at 352, including two test aircraft that are later sold.

From Figure 8 it is seen that financial market uncertainties, such as the increase of a few per cent in acquiring financial backing, can change a favorable return to an unfavorable return on an aircraft of this size.

Conclusions and Recommendations

Purdue design classes considered the engineering and economic tasks of designing a megatransport aircraft with 650 passengers and 8000 nautical mile range.

Due to the emphasis placed upon the use of existing airport facilities, many airplanes were of unconventional design. The use of supercritical airfoils and composite materials was considered as methods of reducing weight. The result was decreased acquisition cost and operating costs.

As aircraft grow in size, the effects of the square-cube law on the structure demands a fresh look at advanced, integrated configurations. Most teams accomplished this task, but to differing degrees. The most interesting design feature promoted by the class was the ultra-wide fuselage discussed by Hitch.

In addition, reduced weight from advanced technology, even though risky from a maintenance standpoint, requires a look at concepts such as fly-by-wire and more advanced composite materials in the primary structure.

Finally, it must be noted that the last leap forward in size occurred two and one-half decades ago. This leap involved enormous risks, but was also enormously successful. This current leap will also require vision, daring, cooperation and skill.

Acknowledgments

The opinions expressed in this paper are solely those of the authors and the students involved in this project. In addition, the authors recognize the individual and group efforts of the 55 students who participated in the project. The joys and sorrows involved with working with and teaching these students are what teaching is all about. To them - thanks for your efforts. We would also like to acknowledge the advice and estimation data provided by the Tupelov Design Bureau sponsored as part of Purdue University's globalization effort. Finally, we wish to acknowledge the support of NASA and USRA for funding provided as part of the Advanced Design Program and to Mr. Jack Morris, Langley Research Center, who provided advice and support.

References

1. "Outlook for Commercial Aircraft 1991-2010," Douglas Aircraft Company, Market Assessment, Long Beach, California, January 1992.
2. "1992 Current Market Outlook - World Market Demand and Airplane Supply Requirements," Boeing Commercial Airplane Group, Seattle, Washington, February 1992.
3. "The Biggest Influence," Flight International, 28 October - 3 November 1992, pp. 26-30.
4. Raymer, D.P., *Aircraft Design: A Conceptual Approach*, American Institute of Aeronautics and Astronautics, Washington, D.C., 1989.
5. Cleveland, F.A., "Size Effects in Conventional Aircraft Design," *Journal of Aircraft*, Vol. 7, No. 6, Nov.-Dec. 1970.
6. Lange, R.H., "Review of Unconventional Aircraft Design Concepts," *Journal of Aircraft*, Vol. 25, No. 5, May 1988, pp. 385-392.
7. Mikolowsky, W.T., Noggle, L.W. and Stanley, W.L., "The Military Utility of Very Large Airplanes and Alternative Fuels," *Astronautics and Aeronautics*, September 1977, pp. 46-56.
8. Arata, W.H., Jr., "Very Large Vehicles - To Be ...?" *Astronautics and Aeronautics*, April 1979, pp. 20-33.
9. Noggle, L.W. and Jobe, C.E., "Large Vehicle Concepts" *Astronautics and Aeronautics*, April 1979, pp. 26-32.
10. Horonjeff, R. and McKelvey, F. X., *Planning and Design of Airports*, McGraw-Hill Book Company, New York, 1983.
11. Keith-Lucas, D. "Defeating the Square-Cube Law," *Flight International*, Vol. 94, No. 3106, Sept. 1968, pp.440-442.
12. Mattingly, J.D., Heiser, W.H., and Daley, D.H., *Aircraft Engine Design*, American Institute of Aeronautics and Astronautics, Washington, D.C., 1987.
13. Smith, M.J.T., *Aircraft Noise*, Cambridge University Press, Cambridge, England.
14. Drake, J.W., Course Notes: *AAE 210 - Introduction to Air Transportation*, School of Aeronautics and Astronautics, Purdue University, West Lafayette, Indiana, 1990.

15. Hitch, H.P.Y., "Pressure cabins of elliptic cross section," *Aeronautical Journal*, June/July 1988, pp. 207-223.

16. Roskam, J., *Airplane Design; Part II: Preliminary Configuration Design and Integration of the Propulsion System*, Roskam Aviation and Engineering Corporation, Ottawa, Kansas, 1989.

17. Torenbeek, E., *Synthesis of Subsonic Airplane Design*, Kluwer Academic Publishers, Dordrecht, Netherlands, 1982.

Other useful papers include:

Bohon, H.L. and Davis, J.G., Jr. , "Composites for large transports - facing the challenge," *Aerospace America*, June 1984, pp. 58-62.

Chuprun, J., Jr., "Large Aircraft, Requirements and Capabilities," AIAA Paper 84-2505, San Diego, Calif., 1984.

Lowrey, R.O., "Evolution of Large Transport Wings," AIAA Paper 80-3038, 1980

Robinson, D.L. and Melary, M.F., "Large Airplane Derivative Development Methodology," AIAA Paper 85-3043, 1985.

Sagdeo, P.M., "Very High Capacity Medium Range Passenger Transport," AIAA Paper 91-3079, Baltimore, Md. 1991.

Verginia, F.J., Barber, E.A. and Rettie, I.H., "Parametric Design and Analysis of Large Advanced Military Transports," AIAA Paper 76-924, Dallas, Texas, 1976.

Special thanks to the following teams and team members:

AMT-Condor - Ed Caperton, Rob Gillgrist, Martin Pesut, Jason, Scheuring, Dave Semanik

BWB-Griffin - Greg Bucci, Erika Pearson, Peggy Precup, Matt Szolwinski, Kent Wiechart, Chris Wright. (This team placed first in the 1993 Thiokol Technical Communication Competition).

INF - Super Condor - Matt Fisher, Angela Hare, Bill Huston, Dan McAninch, Brian Moore, Derek Wyler

Phoenix 650 - Jerry Andrews, Eric Bates, Alonzo Brumfield, Jose Carrasco, Oliver Debikey, Brett Hoffstadt

DESIGN OF A VEHICLE-BASED INTERVENTION SYSTEM TO PREVENT OZONE LOSS

Virginia Polytechnic Institute and State University
Department of Aerospace and Ocean Engineering
Blacksburg, Virginia

Dr. William H. Mason and Professor Nathan Kirchbaum
Jacob Kay and Alexander M. Benoliel, Teaching Assistants

Sean R. Lynn (Team Leader), Deborah Bunker, Thomas D. Hesbach, Jr., Everett B. Howerton,
Gudbjörn Hreinsson, E. Kirk Mistr, Matthew E. Palmer, Claiborne Rogers,
Dayna S. Tischler, Daniel J. Wrona, Gi-ung Yum

Abstract

Reduced quantities of ozone in the atmosphere allow greater levels of ultraviolet (UV) radiation to reach the earth's surface. The 1992/1993 project goals for the Virginia Tech Senior Design Team were to 1) understand the processes which contribute to stratospheric ozone loss, 2) examine ways to prevent ozone loss, and 3) define the requirements for an implementation vehicle to carry out the prevention scheme. A scheme proposed by R.J. Cicerone, *et al* late in 1991 was selected because of its supporting research and economic feasibility. This scheme uses hydrocarbon injected into the Antarctic ozone hole to form stable compounds with free chlorine, thus reducing ozone depletion. A study of the hydrocarbon injection requirements determined that 130 aircraft traveling Mach 2.4 at a maximum altitude of 66,000 ft. would provide the most economic approach to preventing ozone loss. Each aircraft would require an 8,000 nm. range and be able to carry 35,000 lbs. of propane. The propane would be stored in a three-tank high pressure system. Modularity and multi-role functionality were selected to be key design features. Missions originate from airports located in South America and Australia.

Introduction

The discovery of an Antarctic "ozone hole" in the late 1970s led to a flurry of scientific research to determine its causes and impacts. Despite a better understanding of the processes involved, ozone loss continues and, if current predictions are correct, will continue far into the future. The potential effects of continued ozone loss on the global biosphere are devastating and this threat has created the need for methods to replace lost ozone or interrupt the processes which cause ozone loss.

Current work on an ozone loss intervention scheme builds on work by Jacob Kay.¹ Kay compiled an overview of current theories on the ozone depletion process and ideas on vehicle based intervention schemes. The 1992/93 work has dealt with selecting the best scheme to prevent or slow the ozone depletion process and defining specific vehicle requirements. The vehicle requirements will be used by the 1993/94 Senior Design Team to design the vehicle and associated systems. The work completed by the 1992/93

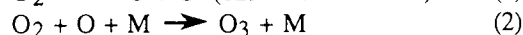
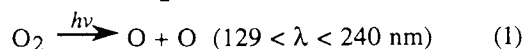
Senior Design Team includes the selection of an intervention scheme, definition of the mission profile and an analysis of the hydrocarbon injection scheme to develop requirements for the storage and injection systems. The design team concluded their work with specific requirements for a supersonic aircraft based on an in-depth mission analysis.

Ozone

Ozone (O₃) is found mainly in the stratosphere, with 90% by mass located between 10 and 50 km. The highest concentration of ozone is found between 15 and 35 km, and is called the "ozone layer."² It is a thin layer which, at sea level conditions, would be 3 mm thick. This layer is very important to the living organisms on earth. It absorbs harmful ultraviolet (UV) radiation (wavelengths from 220 to 290 nm), which causes skin cancer, cataracts, and possible immune system deficiencies.²

Ozone Chemistry

Ozone is formed by a natural photochemical process when UV radiation from the sun splits diatomic oxygen into the two oxygen atoms from which they are formed. The free O atoms then react with O₂ molecules to form O₃:²



where M represents "bath" species such as O₂ or N₂.

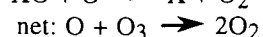
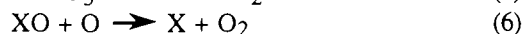
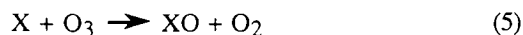
Natural ozone loss occurs by absorbing harmful ultraviolet radiation of longer wave length (220 < λ < 320 nm) through the following process:



The monatomic oxygen can then break down ozone molecules by the following reaction:



Reaction [3] is the process in which most of harmful UV is prevented from reaching the earth's surface. Other important natural ozone destruction reactions are of the form:



where X is a radical which is OH, NO, Cl, or Br (Fig. 1).³

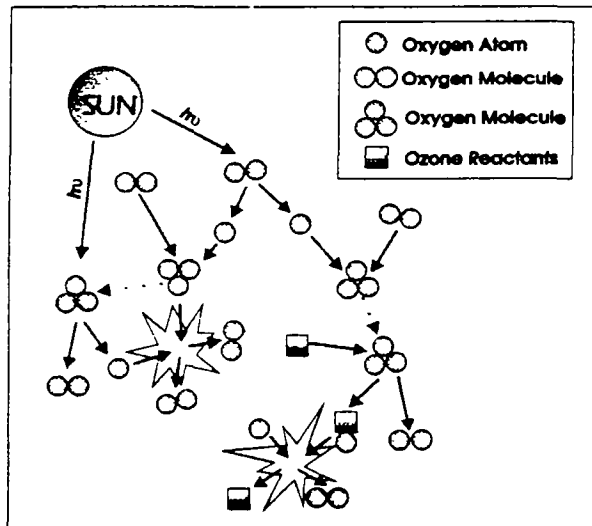


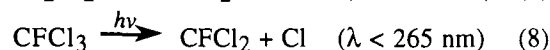
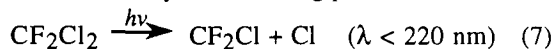
Fig. 1 Natural Ozone Creation/Destruction Process²

From reactions (1) through (6) it appears that ozone is being destroyed catalytically by oxygen atoms and radicals (X). However, there are two reasons that the catalytic ozone destruction does not occur in natural stratospheric conditions. First, O is much less abundant than O₃ in the middle and lower stratosphere. Second, the reactive species HO₂, NO₂, ClO, and BrO, from which the radicals are formed, are generally not abundant.³ This calls for additional explanations for the global ozone depletion, especially over Antarctica.

Polar Ozone Depletion

There have been many reports over the last decade that, during austral spring (autumn in the North Hemisphere), the ozone concentration over Antarctica drops to the point of almost total depletion. This decrease in stratospheric ozone is known as the "ozone hole". In 1987 and 1989, the ozone hole covered almost twice the area of the Antarctic continent.⁴ According to some researchers, severe ozone depletion may occur over the North Pole within the decade.⁵

Many scientists believe that man-made chlorofluorocarbons (CFCs) are the main cause of the depletion of the ozone layer. CFCs are used in refrigerators, air-conditioners and fast-food cartons as well as in solvents and cleaners. These chemicals are inert under most circumstances, but when they slowly rise to the stratosphere and are exposed to large amount of UV radiation, they release chlorine atoms by the following processes:



The free chlorine then reacts with ozone by the following processes:



In these reactions Cl is a catalyst, and each Cl molecule can destroy millions of ozone molecules before it combines into a stable "reservoir", described next.

Chlorine Reservoirs. Most of the atomic chlorine (Cl) released from CFCs and brought to the South Pole by stratospheric winds eventually react with hydrogen, nitrogen, and oxygen molecules to remain as reservoirs.⁶ Reservoirs are stable compounds in which ozone-depleting species are tied-up. The formations of the primary chlorine reservoirs involve the following reactions:



Polar Stratospheric Clouds (PSCs) During September and October, lower latitude air with a high concentration of CFCs is transported poleward by stratospheric winds, and is trapped inside a belt of stratospheric winds called the Polar Vortex. This polar vortex isolates the cold Antarctic stratospheric air from the warmer air of the middle latitudes. The vortex starts to form during the polar night (around June) and lasts until late September.⁷ During the Antarctic winter, temperatures inside the vortex are often well below 200 K, which allows for the formation of atmospheric particles (essentially ice) known as polar stratospheric clouds (PSCs). There are two types of PSCs. Type I PSCs appear to form at about 197 K and consist of condensed HNO₃ and H₂O. The larger type II PSCs appear to form below 187 K and consist primarily of H₂O.³ Eventually, in the spring, the vortex breaks down due to enhanced planetary wave activity.³

Heterogeneous Reactions. It has been speculated that heterogeneous reactions occurring on the surfaces of particles making up the PSCs are the possible main chemistry of the catalytic ozone destruction. Some of the important heterogeneous reactions are:



As the temperature falls below about 197 K, reactions (13) and (14) convert the reservoir ClONO₂ and HCl species to Cl₂, ClNO₂, and HNO₃. These heterogeneous reactions are likely to be the first to occur as type I PSCs form. With further cooling within the vortex, type II PSCs form and any remaining N₂O₅ and ClNO₃ react as in reaction (13), (14), (15) and (16).³ These new chemicals (ClNO₂, Cl₂, and HOCl) are rapidly converted to ClO via photolysis:



The Cl and ClO then destroy O₃ catalytically by reactions (9) and (10), and the ozone hole is formed.

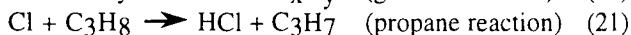
Active Intervention Schemes

Only a few science-based suggestions have been proposed for active intervention schemes to prevent or reduce stratospheric ozone loss. This is due to the lack of understanding of the atmospheric processes and dynamics within the ozone hole. Computer simulations have been used to test various hypotheses, but the complexity and chaotic nature of the atmosphere makes it impossible to accurately model all aspects of the atmospheric dynamics. In spite of the difficulties involved, several active intervention schemes have, however, been presented. Only one stands out for use in a vehicle based intervention scheme. Kay¹ has presented a survey with descriptions of various other proposals.

Cicerone Method

R.J. Cicerone, Scott Elliott, and R.P. Turco proposed a hydrocarbon injection system for binding the free chlorine in the polar vortex.⁷ Though full-scale atmospheric testing of the idea was impossible, the hydrocarbon injection scheme idea is supported by computer modelling. The results of his zero-dimensional simulations make the hydrocarbon injection scheme the most promising.

Concept. Cicerone's basic concept is to stabilize the active chlorine elements within the PSCs so that ozone will not be deteriorated. PSCs dehydrate and denitrificate the polar air so that stable chlorine reservoirs break up and attack the ozone. Injecting certain hydrocarbons into the ozone hole during PSC evaporation allows the formation of stable chlorine reservoirs. The following are some representative reactions:



The ratio of hydrocarbon to active chlorine is 1 to 1 (it takes one hydrocarbon molecule to stabilize one active chlorine species). The stability of HCl determines the effectiveness of this scheme. The presence of PSCs will free chlorine to attack the ozone.

Model. The computer simulation of the hydrocarbon injection is based on current polar stratospheric data coupled with Antarctic ozone chemistry. The calculations⁷ consisted of 130 stratospheric gas-phase photo-chemistry equations, all of the heterogeneous PSC equations, gas phase reaction rates, and ice surface reaction efficiencies based on laboratory experiments. The model is a zero-D simulation. The baseline input parameters are:

<u>Parameter</u>	<u>Baseline</u>
Altitude	15 km
Latitude	80 S
Calculations begun	8 August
Sunrise	15 August
PSC evaporation	1 September

Ethane and propane were tested for the simulated hydrocarbon injection. Two simulation versions were utilized. The versions differed by the amount of trace gases in the Antarctic stratosphere remaining after the polar night. Despite the difficulties in modelling, both models showed a possibility of increased ozone loss if the injected hydrocarbon was at a concentration less than 1.8 ppb.

Complications. Lacking extensive polar vortex data, many simplifying assumptions were incorporated in the simulation. These assumptions may cause inaccuracies and may produce misleading results. However, this method produces the best available active intervention prediction. However, the Cicerone method is sensitive to an injection time frame, due to PSC dissipation which determines the stability of the chlorine reservoirs. The simulation is also sensitive to the concentration of hydrocarbon injected. If not enough ethane or propane is injected then the ozone loss may, in fact, increase. It was recommended that a minimum of 3.6 ppb hydrocarbon be used to avert this problem.⁷

Implementation Requirements. The Cicerone method is not a permanent solution. The stable chlorine reservoirs become unstable in the presence of PSCs, and the PSCs form annually near the end of the polar night. Thus, an annual hydrocarbon injection must be performed until a safe permanent solution is found.

In our study, propane was selected over ethane as the injected hydrocarbon because of its advantageous chlorine scavenging ability. Fifty thousand tons of propane are needed to obtain 3.6 ppb in the ozone hole. The delivery time constraint requires that the propane be added in a 3 week period beginning with PSC dissipation. There must be a uniform propane distribution throughout the volume of $1 \times 10^8 \text{ km}^3$ for effective chlorine scavenging.

This is difficult due to the lack of natural atmospheric mixing within the polar vortex. The propane delivery system evolved is critical for a successful propane injection campaign.

Mission Analysis

Several types of delivery systems were considered to implement the Cicerone method. These included missiles, lighter-than-air (LTA) vehicles and aircraft. An aircraft delivery system was selected as the most appropriate. The key considerations used as the criterion for that selection are:

- Missiles have a low payload/gross weight ratio and debris problems. However, they could be used to fill gaps left by aircraft delivered propane.
- LTAs are very slow, are altitude restricted, have low payload capacity and are prone to weather damage.
- Aircraft are capable of high speeds, have high payload capacity, and are reusable, but require more extensive ground support.

Mission Parameters

The controlling factors for this mission are the volume of the polar vortex, the delivery time frame, the mission range and the delivery plume area. The polar vortex volume

is recognized as a dynamic variable in this analysis, but assumed to be constant for simplicity. The delivery time frame is set to 3 weeks as specified by Cicerone, but may be raised to a month if need arises.¹ The airport region of choice will determine the minimum mission range.

One of the main parameters in the mission analysis is the plume area. To get an idea of the plume area requirements, it is necessary to look at the delivery volume. It is 5 km in height and has a surface area of 20 million square km. That's a total of 100 million cubic km. Fig. 2 depicts the polar vortex, with a cut-out section showing the proposed delivery scheme. This drawing is not to scale, as the vortex has a diameter one thousand times its height. Untreated "holes" are a major concern of the distribution method. According to Cicerone, under-treatment may have adverse effects. Thus, the "holes" must be minimized and Fig. 2 portrays that distribution. The plumes are overlapped to maximize the mixing of the hydrocarbon, and all the untreated area is at the edges of the vortex. The radius of a single plume "sweep" through the volume is defined as the value where the propane concentration is down to 3.0 parts per billion (ppb). Using this definition, the plume radius is about 1000 m., or an area of 3.142 km², thus requiring propane delivery over three different altitude levels to achieve full coverage.

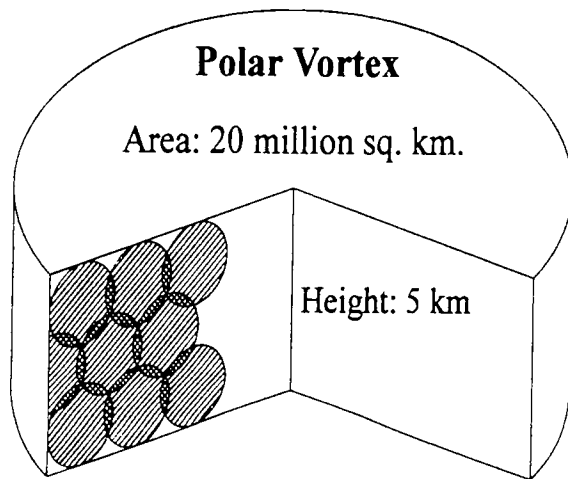


Fig. 2 Depiction of the polar vortex geometry and the proposed delivery scheme.

Mission Model

To obtain the mission requirements, a mission model was established. This model splits the polar vortex volume into equal shares for each airport region. Figure 3 depicts the model representation for two airport regions. For three airports the vortex is divided into three parts.

A FORTRAN program implementing this model was written. This program is short, but is expensive to run. It sweeps through the mission from the start to the end of the payload delivery, computing total range and delivery range.

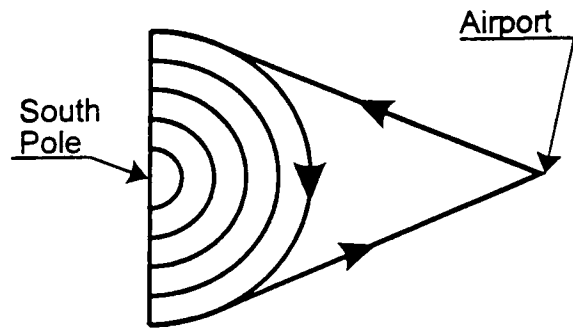


Fig. 3 A schematic of the mission model.

The number of missions depends on the aircraft range, plume area (distance between delivery paths), the size of the volume to be treated (two or three airport regions) and the distance from the airport to the polar vortex. Note that there is no Mach number dependency. The output from the code is the number of missions and the Total Mission Range (*TMR*). *TMR* is the total range of all the missions combined, but only for one stack for one airport region. Equation [22] shows the relation for the number of aircraft required.

$$\# \text{ of A/C} = \frac{TMR}{Time (sec) \cdot M \cdot a} + \frac{GT(sec) \cdot Missions}{Time (sec)} \quad (22)$$

where *M* is Mach number, *a* is the speed of sound and *GT* is the ground time per mission. This combination of a detailed code model and a short equation provides a relatively simple and cheap analysis tool.

Model Assumptions. Some assumptions were necessary to simplify the model representation. One assumption was to make the temperature over the whole mission profile equal to the lowest temperature in the polar vortex, 190 K. This is equivalent to reducing the range of the aircraft, and effectively increases the number of missions required.

Another assumption has to do with the polar vortex. Cicerone specifications treat it as a cylinder. The shape of the polar vortex has usually been that of an oval stretching from South America to Australia. This shape changes from year to year, making it difficult to model.

One implicit assumption is that the mission can be achieved in the specified manner. For instance, the distance between two delivery paths is only 1,732 m. This may be hard to maintain, resulting in non-uniform delivery.

Delivery Mission Analysis

South America, Australia and Africa were considered as locations for airport bases, in order of increasing distance to the polar vortex. Combinations of the first two bases and all three were considered. Using the model previously

established, the former combination resulted in 6006 missions versus 6066 missions for the latter combination. This is not a big difference, but enough to conclude that Africa is not a desirable airport location. The reason for this is that the larger distance from Africa to the polar vortex requires more aircraft, as well as that operating from two airport regions simplifies ground operations.

Antarctica was also considered as an airport base, but problems associated with operating an airport in an environment such as Antarctica, particularly during the middle of winter, may nullify any payoffs. However, field locations in Antarctica may be desirable as emergency airfields.

Figure 4 depicts the number of aircraft required versus Mach number, comparing different ranges. The minimum range here is 6000 nm. That is approximately the distance to the South Pole and back. As the range is increased from 6,000 to 7,000 nm. the payoffs are tremendous, and the reduction of aircraft is approximately 60%. But as the range is further increased, the reduction in the number of aircraft is less significant. As a result, the 8,000 nm. range was chosen as the baseline for this mission. That is the current limit for commercial jets and the payoffs at the higher ranges are too small to make them desirable.

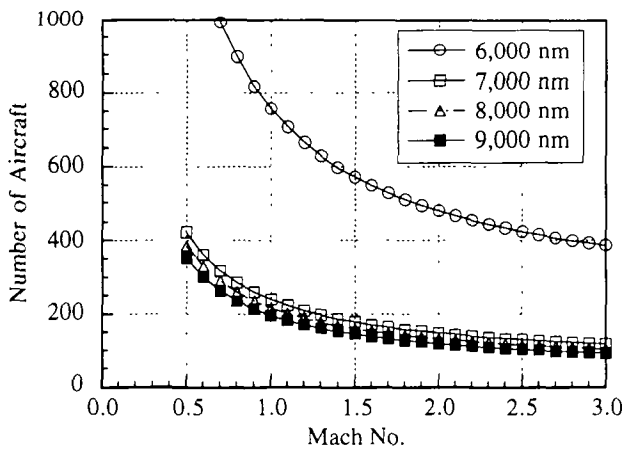


Fig. 4 Comparing different aircraft ranges. Airport locations are in South America and Australia. Ground Time is 4 hours and the plume area is 3.142 km².

Figure 5 shows the number of aircraft required versus Mach number, comparing different payloads. This is at the 8,000 nm. total range baseline. As the payload is increased, the payoffs are initially large, in terms of number of aircraft, but decrease rapidly. The difference between carrying a 35,000 lb or 40,000 lb payload is barely observable. As a result, 35,000 lb payload was determined to be the baseline.

For a given range and plume area there exists a total number of missions. As the Mach number is increased, fewer aircraft are needed to accomplish these missions. In turn each aircraft needs to be employed more often. This relationship is depicted in Fig. 6 for different ranges and does not induce any limitations on the aircraft type.

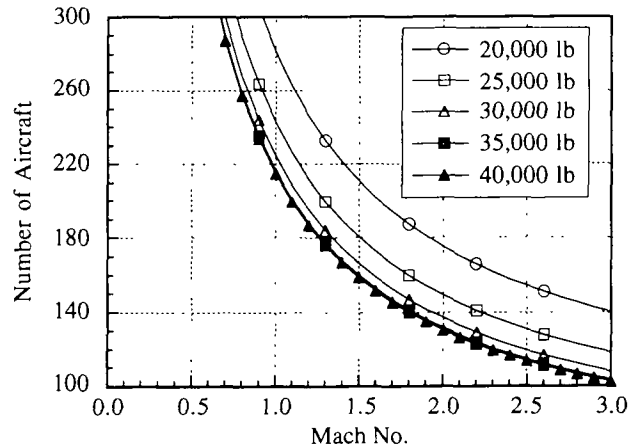


Fig. 5 Payload Considerations. Airport locations are in South America and Australia. Ground time is 4 hours and the plume area is 3.142 km². Range is 8,000 nm.

However, for fewer number of planes which are deployed more often, maintainability and reliability become more important and any misfortunes in regard to these will be more severe. For example, if one plane becomes inoperative, it will be more severe for a fleet of 50 planes than 500. This needs to be taken into consideration in the design phase. Figure 6 also shows indirectly the time of flight. For subsonic aircraft this is between 18 and 24 hours, requiring two crews to be present for each mission.

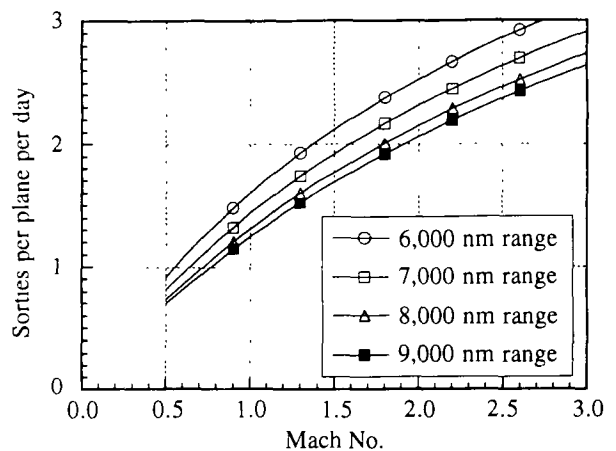


Fig. 6 Comparison of Sorties per plane per day vs. Mach number, for different ranges. Airport locations are in South America and Australia. Ground time is 4 hours and the plume area is 3.142 km².

Reloading fuel and hydrocarbon and other activity on the ground was included in terms of ground time, which is assumed to be 4 hours. Figure 7 shows that the ground time has a large effect on the number of aircraft. This is more severe at high Mach numbers; there is a difference of 18% at

M=0.8 compared to 40% at M=2.4. This shows that care must be exercised in the design process, minimizing the time it takes to reload payload, fuel, etc.

Operations at airports need to be considered. Note that the relationship between airport operations and range only depends on the number of missions, which in turn depends only on the range of the aircraft and the plume area. An operation is defined as either one take-off or one landing. At 8,000 nm range the traffic is at 286 operations per day (24 hrs.) That is at a manageable level, as discussed later.

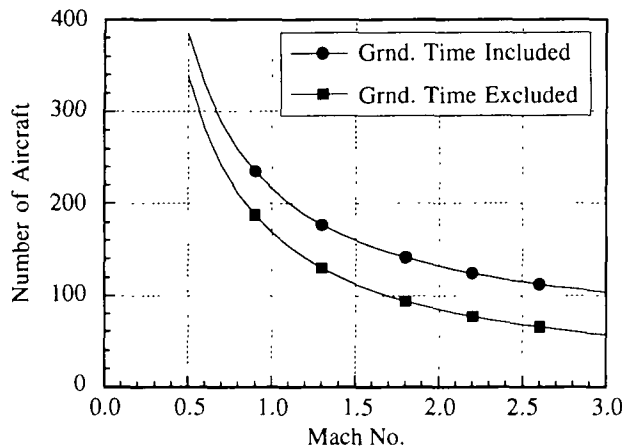


Fig. 7 Effect of Ground Time on the number of aircraft. Airport locations are in South America and Australia. Ground time is 4 hours and the plume area is 3.142 km.²

Mission Requirements Summary

The results of this analysis can be summarized as follows:

- Airports in South America and Australia
- 8000 nm. Range
- 35,000 lb. Payload
- 130 airplanes at M = 2.4

Hydrocarbon Injection and Mixing

The Cicerone scheme is based on the assumption that each aircraft can uniformly mix the propane in a cylindrical plume behind the aircraft. The hydrocarbon injection scheme requires propane to be dispersed over a plume area of 3.142 km². A mathematical model was developed to analyze the plume area estimate. The model assumes the propane is injected using a constant velocity flow turbulent jet. Figure 8 shows the basic physical representation of the model. The Cicerone method requires a uniform distribution of 3.6 ppb propane in the ozone hole. Due to mixing phenomena and aircraft range and payload limits, it is determined that an average concentration of 3 ppb is achieved. This is lower than suggested by Cicerone, but is still greater than 1.8 ppb propane concentration which may damage the ozone⁷ and thus, would be a good starting point for actual physical testing.

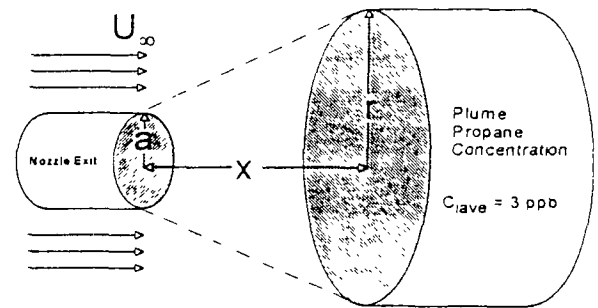


Fig. 8 Hydrocarbon Injection Model

Classical Diffusion Theory

Classical diffusion theory⁸ can be used to predict the propane concentration level after its injection from the aircraft, including turbulent mixing.⁹ The analysis was developed with the help of Dr. Joseph A. Schetz.¹⁰ A classical heat transfer integral was modified for species diffusion including the results of a turbulent mixing model:

$$C = \frac{e^{-\left(\frac{r^2}{4cx}\right)} \int_0^a e^{-\left(\frac{r'^2}{4cx}\right)} I_0\left(\frac{rr'}{2cx}\right) r' dr'}{2cx} \quad (23)$$

C = propane concentration

x = plume distance behind aircraft

r = plume radius,

a = nozzle exit radius

$I_0(rr'/2cx)$ = Bessel function,

$c = \frac{0.025}{0.8} \left| 1 - \frac{\rho_j U_j}{\rho_\infty U_\infty} \right|$, a turbulent mass diffusion coef.

ρ_j = propane injection density

ρ_∞ = air density

U_j = propane injection velocity

U_∞ = aircraft velocity

Circular Coverage Function

The integral in Eqn. (23) is the P-function, and is known as the off-set circular probability function or the circular coverage function. It simplifies the integration of some diffusion problems in cylindrical coordinates.¹¹ Here, it provides the plume size and propane concentration for the propane analysis.

Swirl was investigated as a way to increase the amount of propane mixing.¹² The exit nozzle design would include vanes to initiate the swirl effect. The swirl effect only adjusts the constant, c , which is used in the P-function, thus the turbulent mixing and swirl results are combined to maximize propane mixing.

Results

Figure 9 shows the propane concentration as a function of radius for the Mach 2.4 case. Generally, the concentration decreases as the radius increases. The slight concentration increase near the plume edge is due to the plume overlap shown in the mission analysis flight pattern. Obtaining 3.6 ppb propane concentration would more than quadruple the required aircraft payload. Therefore, an average concentration of 3.0 ppb propane is dispersed in the ozone hole. While lower than the optimum concentration, it still satisfies the requirements of the Cicerone method. The propane concentration in the inner third of the plume will exceed the Cicerone requirement. The outer part of the plume has less than the required concentration, however natural diffusion will be utilized to mix the propane.

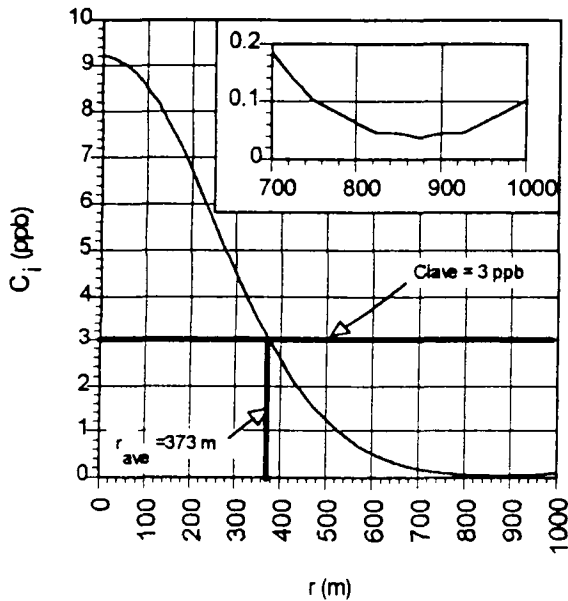


Fig. 9 Propane Concentration

Table 1 compares the Mach 2.4 and Mach 0.8 aircraft. The results are similar due to identical dispersion range, payload, and propane injection velocity compared to free-stream velocity. The only difference is the mass flow and the mixing time. Changing input parameters will not drastically adjust the mixing plume size.

Table 1
Vehicle Velocity Comparison
(note: $U_j = 1/16U$ for both cases)

	Mach = 2.4	Mach = 0.8
plume radius (m)	1000	1000
x (m)	5.9×10^6	5.9×10^6
propane (ppb)	3.0	3.0
diffusion time (hours)	2.5	7.4
propane payload (lbs)	35000	35000
propane required (tons)	100,000	100,000
mass flow @ nozzle exit (lbs/s)	0.3781	0.126

Thus for the plume radius of 1,000 meters proposed in the mission analysis, the required propane concentration level can be obtained by turbulent mixing with induced swirl. The average concentration of propane in the plume is 3.0 ppb.

Subsonic aircraft would be better if the plume area more than doubled. Plume area can not be obtained by adjusting the propane exit velocity (the only parameter which changes between the super- and subsonic cases). The plume radius may be doubled by increasing the amount of injected propane. This would require a mixing time approaching two days. The P-function injection analysis may not accurately predict the mixing beyond several hours. The inaccuracy would arise from the effect of natural dispersion in the Antarctic polar vortex. Also, the additional propane would tax the already limited range of the subsonic aircraft.

Operational Bases

Airports and ground support are vitally important to aircraft operation. Two choices for airports exist; either existing airports could be used or new airports could be constructed. However, before the selection can be made, some initial requirements must be established. The airports need to be as near the south polar vortex as possible. They will also need provisions for propane storage. Based on the mission analysis and mixing requirements it was determined that a total of 100,000 tons of propane is required for the overall mission. So, 50,000 tons of propane will need to be stored in each of the two airport regions.

Existing Airports

The two areas of interest are the southern tip of South America, including the Falkland Islands and the Australia/New Zealand region. Table 2¹³ lists civilian airports with runway lengths of at least 8,000 ft. which are being considered for bases of operation.

Table 2
Airport Locations and Proximity to Polar Vortex

Airport	Range to Polar Vortex (nm.)	Range to South Pole (nm.)
Porvenir, Chile	844.53	2206.53
Mount Pleasant, Falkland Islands	931.63	2293.63
Rio Gallegos, Argentina	943.64	2305.64
Christchurch, New Zealand	1432.21	2794.21
Puerto Montt, Chile	1555.37	2917.37
Avalon, NSW, Australia	1759.58	3121.58
Melbourne, Victoria, A-Tulamar	1781.60	3143.60
Auckland, New Zealand-INTL	1820.65	3182.65
Canberra, ACT, Australia	1922.77	3284.77
Buenos Aires, Argentina-Pistari	1952.80	3314.80
Sydney, NSW, Australia	2004.86	3366.86
Santiago, Chile	2038.90	3400.90
Rosaria, Argentina	2066.93	3428.93
Mendoza, Argentina	2071.94	3433.94
Perth, WA, Australia	2126.00	3488.00

Difficulties may arise at existing airports due to the large amount of propane storage necessary. The propane needs a large amount of storage space which may be limited, and the airports need to maintain certain safety levels. This may be resolved by building the propane storage depot in an area far enough from the airport that the danger is minimal. Trucks could then be used to transport the propane and fill the aircraft's onboard tanks.

Another limitation for an airport is air traffic. For an average international airport the maximum capacity of the entire airport is approximately 300 operations per hour, an operation being either a landing or a takeoff.¹⁴ The typical daily demand for an airport servicing larger aircraft is about 310 to 350 operations per day.¹⁵ As determined in the mission analysis, 286 operations per day are required for each region. This could be handled by one airport in each region, even with other traffic using the airport. Using only one airport would be preferable in that only one propane depot need be constructed for each region.

New Airports

Constructing entirely new airports would solve many of the problems associated with existing airports. They could be located in areas that would minimize the risk of catastrophic occurrences. A new airport would be designed to meet the minimum requirements for the mission. In doing so, the airport could also be suitable for general aviation and commuter type aircraft, or even emergency aircraft staging areas (i.e. medical, rescue, and fire fighting units). This could benefit the local community by providing jobs and encouraging business and industry to move into the area. A two runway configuration would provide an operational base of 94 operations per hour under visual flight rule (VFR) conditions and 60 operations per hour under instrument flight rule (IFR) conditions.¹⁵

It would be preferable to use existing airports for bases of operations, since the only major construction necessary would be the propane storage areas. However, if the existing airports cannot be used, then new airports would need to be constructed in locations as near the polar vortex as possible without being subjected to Antarctic winter storms.

Propane Storage

The aircraft propane storage system is an integral part of the delivery scheme. The propane will be stored in three identical, individual tanks. A multiple tank system is utilized to minimize center of gravity shift, reduce the in-flight stresses on the tanks, and provide safety in a redundant system. Each tank is to be furnished with a relief valve in case of an emergency. The tanks will be filled using check valves to prevent back flow in the lines when the pressure changes. The internal pressure of the three tanks will be utilized to disperse the propane. Each of the three tanks will be individually connected to a settling chamber with a butterfly valve to maintain a constant stagnation pressure. The stagnation pressure will be such that the flow into the air stream, after traveling through piping and an appropriate

nozzle exit area, will have the necessary velocity and mass flow rate to achieve the required plume area.

Types of Storage Systems

Two types of aircraft storage systems are feasible: a cryogenic temperature system and an atmospheric temperature system. A cryogenic temperature system would store the propane in 100% liquid form at a very low temperature (200K).¹⁶ This system would consist of the propane tank and insulation to prevent heat loss. This system requires extensive ground support systems and a cryogenic plant on site to cool the propane before it is placed on the aircraft.

An atmospheric temperature system would store the propane at atmospheric temperature, but would use a pressure of about 10 atmospheres to keep the propane at approximately 85% liquid state.¹⁷ The system would consist of a tank able to withstand the high pressure and a compressor to load it into the tanks.

Pressure Vessel Design

The pressure vessel was designed to be a cylindrical tank (length l , and radius r) with spherical end caps (radius r). This tank provides the best balance of maximum space utilization and minimum stresses. The dimensions of the tank were optimized to provide maximum volume, minimum weight, and fit within the physical constraints imposed by the aircraft.

These tanks are designed so that they would not fail due to the internal pressure and weight of the propane at a 2.5 g load, which is the standard for air transports.¹⁸ Failure would occur along the center line on the bottom of the tank when the tank is full due to weight concentration.¹⁹ A minimum thickness was determined to prevent the tank from failing according to Tresca's failure theory for 2-D stresses²⁰ with a safety factor of two.

An appropriate tank size was designed by minimizing the tank mass as a function of tank volume. A FORTRAN program was used to iterate tank radius as a function of the tank volume. Tank wall thickness was determined using Tresca's failure theory as previously stated. Furthermore, a minimum thickness of 1/8" was set to comply with the standards set by the American Society of Mechanical Engineers (ASME) for pressure vessels.²¹

Based on a three tank system, Table 3 shows the final tank design. Considering onboard requirements alone, the cryogenic approach is lighter. However, neither tank weight poses a serious problem.

Table 3
Comparison of storage systems

Dimensions	Atmospheric	Cryogenic
Radius	.5 m	.5 m
Length	12.964 m	11.596 m
Wall thickness	.004975 m	.003175 m
Mass	608 kg	348.8 kg

The cryogenic system takes up less volume and offers less tank weight. Even with additional insulation weight it would seem like the cryogenic system has the clear advantage. However, operationally, cryogenic tanks require complicated ground support and loading systems. In addition, atmospheric tanks do not involve an unreasonable payload or cargo volume penalty and its flexible loading system would decrease turnaround time. Therefore the atmospheric temperature system will be used.

Mounting within the Aircraft

Once the tank size has been set, the tank system will become an integral part of the aircraft. The propane tanks in the fuselage must be able to withstand the torsional and bending moments imparted by the aircraft as well as the weight of the propane. It is also necessary that the tanks can be removed from the aircraft with ease.

The tanks are placed in a support system whose outer shell is rigidly fixed to the airframe at one end while the other end is relatively free in order that the torsional and bending moments of the aircraft are reduced when transferred to the tanks. The three tanks are rigidly fixed to one other, and are then attached to the outer shell with a non-rigid support. The tank system would be equipped with tracks which move along airframe mounted ball bearings so that it can be removed from the aircraft.

Flight Regime and Sizing

Subsonic vs. Supersonic Cruise

To further define aircraft requirements, it was necessary to select the flight regime (subsonic or supersonic) and to set the general size of the aircraft. Mission analysis provided the following requirements for an aircraft delivery system:

- Range of 8000 nm.
- Cruise Altitude of 47,000 to 66,000 ft
- Payload of 35,000 lbs. of usable propane
- Plume area of about 3.142 km^2

This data was then used to make a comparison of supersonic cruise vs. subsonic cruise aircraft.

Advantages and Disadvantages of Supersonic Cruise. A supersonic cruise aircraft delivery system has distinct advantages over a subsonic one. These include:

- 1) A supersonic cruise mission requires fewer aircraft than a subsonic cruise mission.
- 2) A supersonic cruise aircraft provides more mission flexibility than its subsonic counterpart. Examples of potential secondary uses include civil, commercial, and military transports as well as high altitude research, for which the aircraft can be leased or purchased.
- 3) Supersonic cruise aircraft can more easily reach the required altitude than a subsonic aircraft. (Supersonic: Concorde - 60,000 ft cruise, SR-71 - 80,000 + ft cruise).
- 4) Current research is directed toward developing High Speed Civil Transports (HSCT), which are intended to cruise at Mach 2.4 and carry 50,000 lbs. payload with

a similar mission profile. The cost of development can be reduced by building on this work.

- 5) A supersonic cruise aircraft might distribute the propane more effectively due to the larger amount of energy being dissipated in the atmosphere. The supersonic aircraft will have much more drag (roughly 2-3 times as much) than the subsonic cruise aircraft. It would release more energy per sortie into the atmosphere in the form of shocks, friction and wing tip vortices and jet wake (exhaust). This would theoretically give better mixing for the supersonic cruise aircraft.
- 6) Analysis and research was conducted into the requirements of high altitude flight. It was found that a supersonic cruise aircraft like the Concorde could be constructed in existing facilities and use existing runways.

Disadvantages of supersonic cruise aircraft:

- 1) The supersonic aircraft would have to withstand heating of the leading edges of the aircraft and the resulting thermal stresses.
- 2) The supersonic aircraft would be noisier than the subsonic aircraft. The noise would come from shocks while cruising (sonic boom) and the engine noise. The aircraft will be flying over an uninhabited region, and noise should not be a problem at cruise. However, it will be difficult to meet existing noise regulations at take-off.

Advantages and Disadvantages of Subsonic Aircraft. Subsonic cruise aircraft have limited advantages over supersonic cruise aircraft:

- 1) A subsonic aircraft is likely to be more reliable, but the larger number of planes required for this mission may nullify this advantage of subsonic cruise over supersonic cruise.

The disadvantages of the subsonic aircraft are:

- 1) Larger number of planes.
- 2) More flight crew and ground support.
- 3) Difficulty reaching altitude. No subsonic aircraft has ever been built that would take 40,000+ lbs of payload (propane plus tank weight) to 66,000 feet altitude and fly 8000 nm., and not much research has been done in that area. For example, the service ceiling for civil transports is around 42-45,000 ft., while for the B-52 it is 55,000 ft. The service ceiling of an aircraft is defined as the altitude where the climb rate = 100 ft./min.
- 4) The subsonic aircraft would require a large wingspan of 270 ft, thus requiring the development of costly manufacturing techniques and facilities.
- 5) There is no existing subsonic aircraft on which to build.
- 6) The subsonic aircraft would require extremely advanced structural development. With an AR = 12 and with a sweep of approximately 30° , the structural span will be 312 feet.

Sizing

Once an aircraft delivery system was decided upon, preliminary sizing was performed. A general mission profile was defined to be the same for either flight regime. This mission profile was:

- 1) Engine start and warm-up.
- 2) Taxi and take-off.
- 3) Climb to between 47,000 and 66,000 ft.
- 4) Cruise for 8,000 nm.
- 5) Loiter 20 minutes.
- 6) Descend
- 7) Land, Taxi, and shut-down.

To compare the aircraft concepts, a subsonic and supersonic aircraft were each sized using Nicolai's sizing algorithm.²² Initial sizing studies for the supersonic cruise aircraft were also done using ACSYNT.²³ The ACSYNT model also explored the possible use of current High Speed Civil Transport aircraft (HSCT) for the propane injection mission. Notional concepts used for the sizing are shown in Fig. 10.

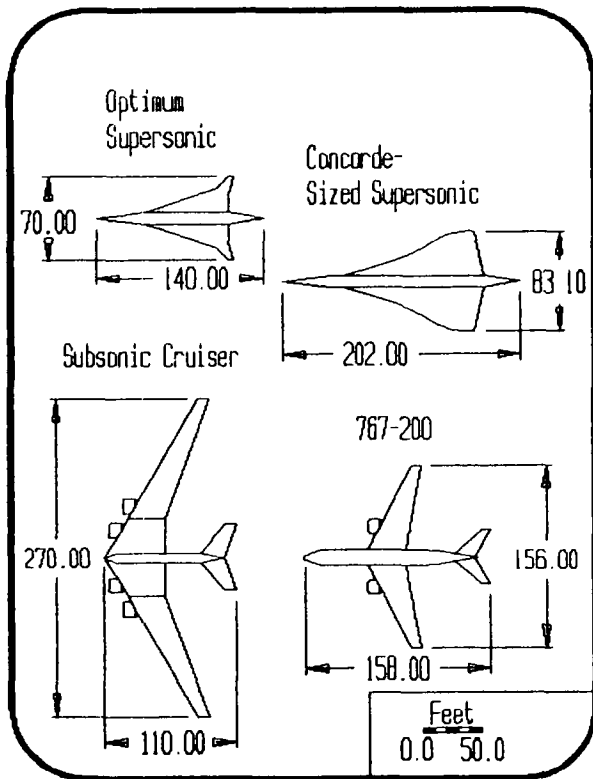


Fig. 10 Aircraft concepts for the propane dispensing system.

Supersonic Cruise. The focus of the sizing was the supersonic cruise mission because of the advantages it has over the subsonic mission, primarily the multirole adaptability and the fewer number of aircraft required.

The supersonic cruise Mach number was set to 2.4 to allow use of existing materials and to utilize existing research and technology. Supersonic cruise L/D (Lift to Drag) was varied from 9.0 to 10.5. Cruise SFC (specific

fuel consumption) was varied from 0.65 to 0.85, representative of non-afterburning, low-bypass turbo-fan engines, as discussed in the next section. [Advisor's note: Students selected the sfc range. The decision may be overly optimistic.]

The results are shown in Fig. 11. This provides an indication of the TOGW and weight of fuel required per plane (sortie) and thus some indication of the cost. The ideal case supersonic aircraft (lightest) had:

- cruise L/D = 10.5
- cruise SFC = 0.65 lbs./sec./lb.
- total fuel = 104,900 lbs.
- TOGW = 248,700 lbs.

Accounting for trapped and reserve fuel, the usable fuel/sortie is 90,000 lbs. This aircraft is almost half the size of the Concorde. Although the ideal case seems overly optimistic, it was used as an ultimate goal.

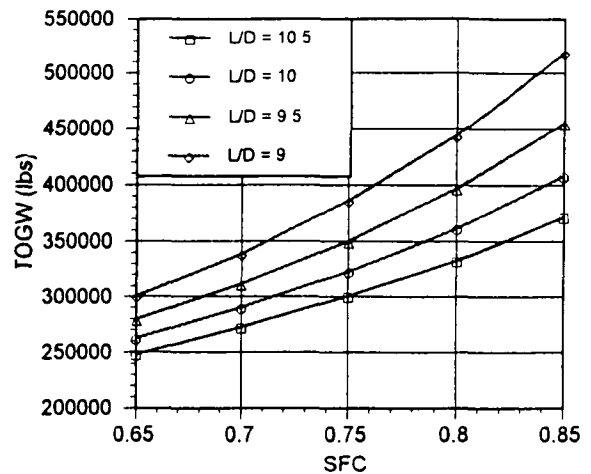


Fig. 11 TOGW Sensitivity

Subsonic Cruise. For comparison, a subsonic aircraft satisfying the mission profile was sized. Subsonic cruise, M = 0.8, was selected to optimize L/D and range. This represents current designs of civil and military long range transports.

Using an AR = 12, which is higher than modern civil transports, and other input based on Lockheed U-2 data, a reasonable weight was obtained for the subsonic aircraft. The results are:

- L/D cruise = 23.185
- Cruise SFC = 0.48 lbs./sec./lb.
- Total Fuel = 106,800 lbs.
- TOGW = 283,500 lbs.
- CL cruise = 0.894

This aircraft is almost identical in weight to the best-case supersonic cruise aircraft. However, it requires:

- Wing Area = 6074. ft.²
- Span = 270. ft.

These values are larger than equivalent weight civil transports. For example, the 767-200 has a TOGW of 300,000 lbs., and a span of 156 ft.²⁴

Based on the substantial advantages that a supersonic cruise aircraft had over a subsonic cruise aircraft, it was decided that the supersonic cruise mission would be used.

ACSYNT To verify the Nicolai sizing results, and compare the mission profile with that of the High Speed Civil Transport, the mission profile data was used in ACSYNT. ACSYNT is a software package for aircraft synthesis currently under development by the ACSYNT Institute. An available ACSYNT HSCT model was modified to fit the mission goals.

The ACSYNT engine cycle simulation produced a minimum achievable SFC of 0.98. This resulted in a TOGW of over 700,000 lb. This result, together with further analysis using Nicolai's method, will form the basis for further design work to be carried out by the 1993-94 design class.

Propulsion

Propulsive Fuel Analysis

Initially in the analysis of the design problem, much attention was focused on the propulsive fuel to be used in the aircraft. Several liquid hydrocarbon candidates were considered. After analysis of thermodynamic properties, ethane and methane were eliminated and propane was determined to be the most likely candidate. Its thermodynamic qualities nearly matched that of conventional jet fuels in several important categories. Its heating value actually exceeded that of JP-4 providing a higher combustion chamber temperature under the same fuel flow conditions.

Using propane as the propulsive fuel did pose problems with the tank design. As stated earlier, the propane to be injected into the stratosphere is to be stored in a cylindrical, standard temperature tank, mounted lengthwise in the aircraft fuselage. For the range and airspeed requirements from the mission analysis, the tank would have to be greatly modified to accommodate for the extra fuel to burn for propulsion. The volume would have to be increased by a factor of 14.7 and its radius would have to increase by a factor of 3.8. A tank wall thickness increase of approximately 1/4" would also be necessary to accommodate the extra weight of the fuel. This option would also leave the wings empty as no fuel could be stored due to the choice of pressurized propane storage tanks. One possible solution would be the use of cryogenic storage tanks to be placed in the wings for more efficient use of aircraft volume. This option would require expensive, bulky equipment, as well as increased ground support, and with current design requirements, its use is precluded.

Engine Cycle Analysis

With a range dominated mission profile, engine efficiency is of paramount importance. A supersonic cruise L/D of 10.5 was assumed. A supersonic cruising aircraft requires engines that can produce enough thrust to break

through the transonic drag rise and propel the craft into the supersonic regime. An engine that could provide enough thrust while burning dry (no afterburning) requires extremely efficient components as well as very high combustor and turbine inlet temperatures. A compressor with higher compression per stage than currently obtainable is required to generate increased thrust without a significant weight penalty. Segmented burning in the combustor and bleed air for cooling would allow for higher chamber temperatures. High technology ceramic turbine blades and state of the art Thermal Barrier Coating (TBC) would allow for much higher turbine inlet temperatures. Given the proposed flight conditions, successive iterations of a cycle analysis for a turbojet engine yielded a cruise SFC of approximately 0.65 with a thrust output of approximately 20,000 lbs.

Table 4.
Engine Parameter Requirements

Mach Number	2.4
Ambient Temperature	220K
Stagnation Pressure Ratio Across Diffuser	0.9136
Specific Heat Ratio of Compressor	1.2
Stag. Temp. Ratio Across Compressor	1.682
Specific Heat Ratio of Turbine	1.1
Stag. Temperature Ratio Across Turbine	0.786
Turbine Inlet Temperature	1900K
Stagnation Pressure Ratio Across Nozzle	0.97
Resulting Specific Fuel Consumption	18.407 mg/Ns

The parameters shown in Table 4 were determined using algorithms proposed by Gordon C. Oats.²⁵ With Mach number, ambient temperature, and efficiency ranges as input, the algorithms were successively iterated until the specific fuel consumption was minimized. The value of 0.65 lb/h/lb is the lowest realistic SFC thermodynamically obtainable. Diffuser design is of significant importance to the engine design. Its efficiency must be very high for this aircraft (0.9136). The very high stagnation pressure ratio across the nozzle also requires that its design be very efficient. These two factors have a significant effect on the specific fuel consumption of the engine in supersonic cruise.

The propulsion system will have to be powerful yet very efficient. These two requirements together appear "ideal" at first glance but with incorporation of the advancing technologies mentioned above, they are believed obtainable.

Conclusion

In our study for a vehicle intervention scheme for preventing or slowing the destruction of the ozone layer over the Antarctic, the following conclusions were drawn:

- 1) Ozone destruction is assisted by the presence of Polar Stratospheric Clouds (PSCs) and by the presence of a Polar Vortex.

- 2) A hydrocarbon injection scheme proposed by R.J. Cicerone, *et al* was found to be reasonably feasible for use as a vehicle based intervention scheme, as well as having reasonably extensive theoretical background research.
 - 3) Propane was selected for the injected hydrocarbon due to the ease of obtaining it and its greater effectiveness.
 - 4) Mission analysis determined that an aircraft would be best suited to the task. Mission analysis also provided the aircraft range, total number of sorties, aircraft payload, number of aircraft, suitable geographic regions for mission bases, and numerous other parameters.
 - 5) An aluminum high pressure system was selected for the propane storage. In addition, a tank support system was designed to minimize airframe-imparted torsion and bending moments on the tanks and to ensure tank portability from the aircraft.
 - 6) Airports and facilities were studied, based on mission analysis. Analysis concluded that only two airports were required to support the mission, one in each airport region.
 - 7) A definition of the vehicle requirements was developed and is as follows:
 - 130 aircraft required
 - Cruise at Mach = 2.4
 - Range of 8,000 nm
 - Payload Weight = 40,000 lbs
 - Takeoff Gross Weight = 250,000 lbs
 - Engine SFC = 0.65
 - Current HSCT designs and technology are applicable
 - Mission flexibility
 - Modular design
 - 8) The use of propane as the aircraft fuel was found to be impractical.
- Future work will be concentrated on the preliminary design of the aircraft and an examination of the possible adverse environmental consequences of the use of propane.

Acknowledgments

The authors would like to thank Dr. Joseph A. Schetz for his contributions to the turbulent mixing analysis. His expertise proved invaluable. Dr. Walter F. O'Brien was an excellent source of information regarding the propulsion analysis. We would also like to thank Peter Coen, NASA, and USRA for their support in this project.

References

1. Kay, Jacob, "A Review of the Stratospheric Ozone Depletion Problem and Considerations for the Development of Vehicle-Based Intervention Schemes," VPI-Aero-191, College of Engineering, Virginia Polytechnic Institute and State University. Aug 24, 1992.
2. Mims, Forrest M., III, "Ozone Layer," *Science PROBE!*, Nov. 1992. p. 34.
3. Henderson, G.S., *et al*. "Polar Ozone Depletion: Current Status." *Canadian Journal of Physics*, Vol. 69, 1991.
4. Ahrerns, C. Donald, "The Ozone Hole," *Meteorology Today*, 1991. p. 34.
5. Vogel, Shawna, "Under the Ozone Hole," *Earth*, Jan. 1993. p. 32.
6. Kawa, S.R., D.W. Fahey, L.E. Heidt, S. Solomon, D.E. Anderson, M. Loewenstein, M.H. Proffitt, J.J. Margitan, and K.R. Chan. "Photochemical Partitioning of the Reactive Nitrogen and Chlorine Reservoirs in the High Altitude Stratosphere," *J. Geophys. Res. Lett.*, 13(12), 1260-1263, 1986.
7. Cicerone, R. J., S. Elliot and R. P. Turco. "Reduced Antarctic Ozone Depletions in a Model with Hydrocarbon Injections," *Science*, Vol. 254, pp 1191-1194.
8. Carslaw, H.S., Jaeger, J.C., *Conduction of Heat in Solids*, Oxford University Press, 1959. p. 260.
9. Schetz, Joseph A., *Boundary Layer Analysis*, Prentice-Hall, Inc., 1993. p.378.
10. Conversations with Joseph A. Schetz, Department Head, Aerospace and Ocean Engineering, Virginia Tech.
11. Masters, J.L., "Some Applications of the P Function," *The Journal of Chemical Physics*, Volume 23, No. 10, October 1959, pp. 1865-1871.
12. Schetz, Joseph A., *Injection and Mixing in Turbulent Flow*, AIAA, N.Y., N.Y., 1980, pp. 111-122.
13. Boeing Aircraft Company, "Customer Analysis Document," 1992
14. Lauth, Allen, Personal Discussion, November 26, 1992
15. *Airport Capacity and Delay*, Advisory Circular, U.S. Department of Transportation, 1983.
16. Vargatille, N.B. *Handbook of Physical Properties of Liquids and Gases*, 2nd edition. p. 235.
17. Conversations with representatives of Southwestern Virginia Gas Service Corp.
18. Virginia Tech Aircraft Structures Course Notes 1990.
19. Johnson, Eric R. Personal Discussion, December 2, 1992
20. Virginia Tech Thin Walled Structures Course Notes, 1991.
21. Megyesy, Eugene F. *Pressure Vessel Handbook*. Tulsa, Oklahoma, Pressure Vessel Handbook Publishing Inc., 1983. p.23.
22. Nicolai, L.M., *Fundamentals of Aircraft Design*, METS, San Jose, 1975.
23. Jayaram, S., Myklebust, A., and Gelhausen, P., "ACSynt—A Standards-Based System for Parametric Computer Aided Conceptual Design of Aircraft," AIAA Paper 92-1268, Feb. 1992.
24. Roskam, Dr. Jan, *Airplane Design I,II,III*, Roskam Aviation and Engineering Corporation, 1985, Ottawa, Kansas
25. Oates, Gordon C. *Aerothermodynamics of Gas Turbine and Rocket Propulsion*. AIAA Education Series. Washington, D.C. 1988.

DESIGN AND ANALYSIS OF A RADIO-CONTROLLED FLYING WING AIRCRAFT

Worcester Polytechnic Institute
Mechanical Engineering Department
Worcester, Massachusetts

Dr. A. N. Alexandrou, Dr. W. W. Durgin, Dr. D. J. Olinger
Paul Crivelli, Teaching Assistant

Michelle Boucher, Hernando Carvajal, Benjamin Frank, Bruce Hill, Barry Hilliard, Matthew Jeffers, Kaan Oztuncer, Freddy Pranajaya, Jeffery Rembold, Sujay Setlur, Shilpa Shroff, Donna Villa, Yura Zhovnirovsky

Abstract

The development of new-high speed, high-capacity public air transportation is one of the challenges facing commercial aviation today. One possible solution to this challenge is a supersonic oblique flying wing aircraft. This project involves the design and construction of a radio-controlled model of such an aircraft as a means of examining some of the aircraft's unique problems, especially its natural instability. The different areas of aerodynamics, propulsion, stability, controls, and structures, are analyzed in the context of the aircraft as a whole. The design relies heavily upon computer modeling and analysis to overcome the technical challenges encountered. Since the size of the model prohibits the use of automatic control systems, the wing is designed to be as inherently stable as possible, and an airfoil is designed to provide the necessary characteristics. Finally, the optimum design is chosen and constructed using composite materials.

Introduction

A supersonic oblique flying wing aircraft is one solution to the challenges facing commercial. For instance, such an aircraft could carry as many as 500 passengers travelling at 1100 miles per hour, enabling transportation from New York to Los Angeles to be completed in under three hours. This concept was initially proposed by Robert T. Jones in 1958, but was not believed to be a feasible design due to structural and stability considerations.¹ Today, however, the technology exists to overcome these challenges.

Since the full scope of such an endeavor involves numerous difficulties, simplicity must be used to surmount these problems by examining the different aspects individually. With this approach in mind, a simplified design was developed and analyzed which studied the stability, structural and aerodynamic issues of an unswept elliptically shaped flying wing.

The result of these efforts is the *Elang*, shown in Figure 1. A description of the final configuration is summarized as follows. Due to the rather unique design requirements, the

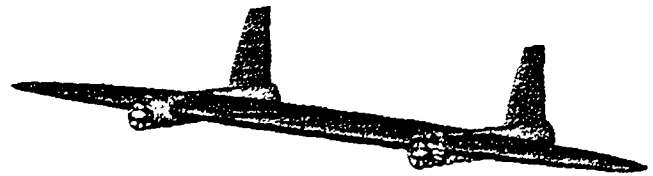


Fig. 1 The *Elang*

development of an original airfoil was necessary, resulting in the HPRS 33 airfoil section. The wing has a root chord length of 45.5 cm and a span of approximately 2.5 m, with an aspect ratio of 7. The planform area is elliptically shaped with a straight quarter-chord line.

The main control surfaces include two ailerons and one elevator which are used to stabilize the aircraft in flight. The specifications of the surfaces are as follows. The ailerons are located on each end outboard the engines, occupying 2.9 percent of the wing planform area. The elevator area is 9.2 percent of the wing planform area.

Two vertical tails are utilized, each located on the rear portion of the engine ducts. The airfoil section is the symmetric SD 8020 airfoil. The vertical stabilizers each have an effective area of 0.10716 m². Rather large surfaces were purposely employed to ensure adequate control. Only vertical tails are used, since by nature the flying wing design does not contain a horizontal tail.

The induced drag is a minimum due to the elliptical shape giving a total drag coefficient of 0.02208. The flying wing is at a geometric attack angle of 4 degrees and as a result generates a lift coefficient of 0.4355 at cruise speed of 15 m/s. The lift to drag ratio is therefore 19.69.

The wing structure is designed to be composed of a foam core wrapped with a skin of carbon fiber and epoxy. This design provides a relatively lightweight structure that can still withstand sizable loading.

A propulsion system was chosen which provides ample thrust and relatively clean aerodynamics. The system consists of two ducted fan engines, each placed 57 cm from the root chord. Operating at 22000 rpm, each engine provides 15.60 N of thrust. One centrally located fuel tank supplies both engines.

In order to achieve the final product, the group was divided into four sub-groups, dealing with aerodynamics, controls and stability, structures and propulsion. In the following sections, the analysis of each sub-group and explanations for its results are presented.

Stability

Stability is defined as the ability of an airplane to fly straight with its wings level, and remain in equilibrium without pilot assistance. It can be divided into two categories, static and dynamic, and can be analyzed along three axes, pitch, roll, and yaw.

Static stability deals with the natural ability of an aircraft to create a restoring moment after a disturbance, and return towards its initial equilibrium position. This type of stability does not give any information on how long it takes to return to its original position, and does not even insure that the plane will return exactly to its equilibrium state. A dynamic stability analysis must be performed in order to obtain this information.

Dynamic stability concerns the motion of the aircraft after the disturbance. In order for the aircraft to be dynamically stable, it must return to the equilibrium position within a certain amount of time, and thus damping is required. If an aircraft is dynamically stable, it will also be statically stable, but the reverse is not necessarily true.

There are three axes about which stability must be achieved. The rotations are about the conventional x, y, and z axes, and the motions are designated as roll, pitch, and yaw, respectively (Figure 2). These motions can be separated into two distinct groups, lateral and longitudinal. Lateral motions consist of rolling, yawing, and sideslipping. Longitudinal motions denote the movement along the aircraft's flight path, its vertical movement, and pitching.

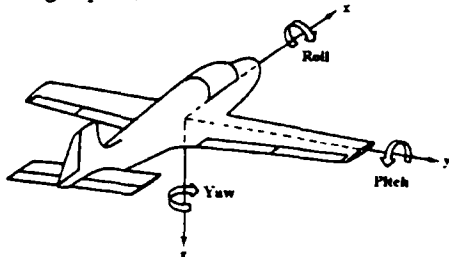


Fig. 2 Axes of Rotation

The major difficulty in stabilizing a flying wing is along the pitch axis. In conventional designs, a horizontal tail offsets the moments generated by the wing and fuselage. However, a flying wing does not have a horizontal tail. Consequently, an alternative, more advanced method for stabilizing the wing had to be utilized.

Pitch Stability

Conventional airfoils typically have a negative moment coefficient about the aerodynamic center. After analyzing a few such airfoils, it was found that to achieve static stability, the engines would have to be placed at locations which were not feasible. Thus, it was determined that an airfoil with a positive coefficient of moment about the aerodynamic center was needed. The positive moment causes the wing to have a natural tendency to pitch up. Therefore, the aerodynamics sub-group designed an original airfoil, through an extensive iterative process, which has a high lift to drag ratio along with a positive moment about the aerodynamic center.

Once the airfoil was selected, engine placement was used to obtain stability. The center of gravity for the design was calculated from the known values of the components. The weight of the wing and the location of its center of gravity along the x and y axes were generated using a solid modeling package called Aries Conceptstation Software. These values were found to be 16 N, 0.209 m, and 0.00561 m respectively. The engines each weighed 5.719 N. A fixed mass of 0.5 kg was added to allow for the receiver, batteries, and other components. This mass was placed 5 cm from the leading edge along the chord line. The center of gravity of the design was calculated by the following equations.

$$x_{cg} = \frac{x_{e_{cf}}(2 * w_e) + x_{w_{cf}} * w_w + x_{mass} * w_{mass}}{2 * w_e + w_w + w_{mass}} \quad (1)$$

$$y_{cg} = \frac{y_{e_{cf}}(2 * w_e) + y_{w_{cf}} * w_w + y_{mass} * w_{mass}}{2 * w_e + w_w + w_{mass}} \quad (2)$$

The moments about the center of gravity of the wing were analyzed, and the results led to Equation 3.

$$C_M = C_{M_{ac}} + C_{L_a} \frac{x_{cg} - x_{ac}}{c} - C_{L_b} \frac{y_{cg} - y_{ac}}{c} + C_{D_d} \frac{x_{cg} - x_{ac}}{c} - C_{D_b} \frac{y_{cg} - y_{ac}}{c} \quad (3)$$

Control Surfaces

An iterative process was conducted with Equations 1 and 3, to determine the placement of the engines along the x-axis to ensure no inherent pitching moment. Equation 2 was used to find the location of the center of gravity of the wing along the y axis. Initially, the y location of the engines was set to be six millimeters to allow placement of the engines within the wing. The calculations were carried out with lift, drag, and moment data for the cruising angle of attack of 4°.

A Moment Coefficient vs. Angle of Attack graph was generated to determine whether or not the wing was statically stable (Figure 3). By definition, an aircraft is

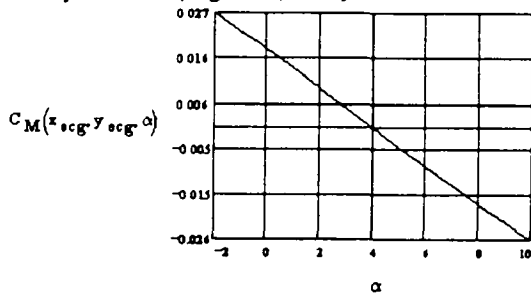


Fig. 3 Moment Coefficient vs. Angle of Attack

statically stable if it satisfies Equation 4 and as seen in Figure 3, the negative slope ensures static stability along the pitch axis.

$$\frac{dC_M}{d\alpha} < 0 \tag{4}$$

A major concern with this flying wing is the very low moment of inertia about the pitch axis, which is a result of the wing having no sweep angle. This low moment of inertia indicates that there is little time for a pilot to react to disturbances during flight. This problem, coupled with inability to guarantee exact placements and weights of the internal components of the wing, makes controllability extremely difficult for the pilot. Therefore, a gyroscope system was included as a safety precaution. The gyroscope monitors deviations about the pitch axis, and makes constant adjustments by using the elevator. The gyroscope can be utilized at the pilot's discretion, depending on flight conditions.

Roll and Yaw Stability

The stabilities in the roll and yaw directions are linked closely together. Rotation along one of these axes induces an accompanying moment along the other axis. Due to the symmetry along the x and z axes, the problem of stability in these directions is not anticipated to be present. Additionally, if the wing does roll or yaw, the moment of inertia is substantial enough to create a rate of rotation that will provide ample time for the pilot to counter the deviations.

The control surfaces consist of an elevator, a pair of ailerons, and two rudders, which control motion along the pitch, roll, and yaw axes, respectively. The analysis was performed by considering the lift, drag, and moment characteristics of each control surface. Each control system was analyzed independently of the other two. When sizing the control surfaces, they were purposely oversized, because the controllability of previous design projects has been inadequate.

Elevator Analysis

The data for the elevator was obtained by modifying the inviscid code to provide new lift, drag, and moment coefficients when the control surface was deflected. The analysis was carried out through a range of angles from -30 to 30 degrees.

Once the data for the deflected area of the wing was procured, it was combined with the previous data for the rest of the wing. From the combination of this data, a modified moment equation was developed. For these calculations, the length of the elevator was 1.4 meters at 18 percent of the cord length, resulting in an elevator area equal to 13 percent of the wing planform area. In this moment equation, Equation 5, terms with a subscript def denote characteristics from the deflected portion of the wing.

$$\begin{aligned} M_{def} = & M_{ac} + L_u(x_{cg} - x_{ac}) - L_b(y_{cg} - y_{ac}) + D_d(x_{cg} - x_{ac}) \\ & - D_b(y_{cg} - y_{ac}) + M_{ac_{def}} + L_{u_{def}}(x_{cg} - x_{ac_{def}}) - L_{b_{def}}(y_{cg} - y_{ac_{def}}) \\ & + D_d(x_{cg} - x_{ac_{def}}) - D_{b_{def}}(y_{cg} - y_{ac_{def}}) \end{aligned} \tag{5}$$

Once the moments were determined, Newton's Second Law was applied to calculate the pitching acceleration of the wing. Figure 4 shows the results of this analysis.

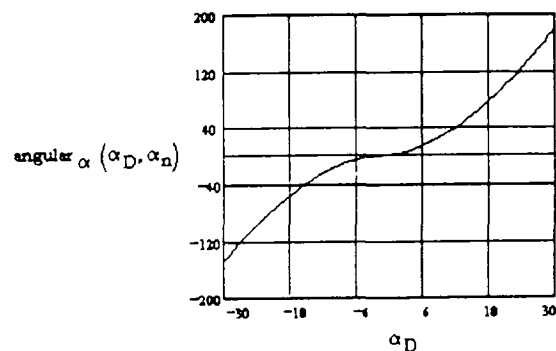


Fig. 4 Angular Acceleration vs. Deflection Angle

The values for this acceleration ranged from negative to positive 200 rad/sec². These large accelerations develop because of the small moment of inertia of the wing about the pitch axis. From this data, it was decided that the gyroscope system would be utilized to aid the pilot in controlling the wing.

Aileron Analysis

In the analysis of the ailerons, the data obtained for the elevator was applied. This similarity occurs because the elevator and the ailerons deflect in the same direction, and both occupy 18 percent of the cord length. When examining the ailerons, it was decided that they would deflect at the same rate in opposite directions. For example, if one aileron was deflected up 10 degrees, the other one would deflect down 10 degrees. Also, the rolling moment created by the drag from the rudders was neglected. The analysis produced the following moment equation.

$$M_r = L_{l_{def}} * z_{al} - L_{r_{def}} * z_{ar} \quad (6)$$

Through iteration it was determined that the each aileron would have a length of 21.8 cm, which resulted in each aileron having 2.9 percent of the wing planform area. As with the elevator analysis, Newton's Second Law was applied to generate the angular acceleration about the roll axis of the wing. The acceleration ranged from negative to positive ten radians per second squared.

Rudder Analysis

The inviscid analysis that was used for the elevator and ailerons was also used to examine the rudders. Since there is such a small moment arm for the rudders, the size of each one is considerably larger than that of conventional designs. Two rudders were selected, for symmetry, and for structural considerations. Each rudder has an area equal to 31.7 percent of the wing planform area. This sizing is accomplished by having the height 21.2 cm, the root cord 17.2 cm, and the tip cord 8 cm.

In the analysis of the rudder, it was determined that each rudder would be deflected the same amount. The moment equations were developed separately for each rudder, and then summed. These expressions are given in Equations 7 and 8.

$$M_{lr} = D_r * z_{lr} - L_r(x_{lr} + x_{ac_r}) \quad (7)$$

$$M_{rr} = -D_r * z_{rr} - L_r(x_{rr} + x_{ac_r}) \quad (8)$$

Once the moment equations were developed, Newton's Second Law was applied to calculate the angular

accelerations. A plot of these accelerations is given in Figure 5. In this graph, the maximum acceleration occurs

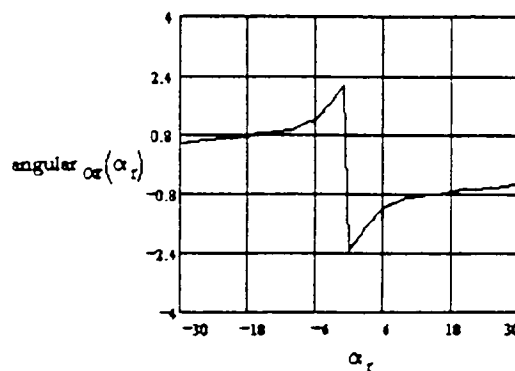


Fig. 5 Rudder Angular Acceleration vs. Angle of Deflection

close to zero. Because an inviscid analysis was used to obtain the data, drag effects are small. In reality, however, the drag effects will contribute greatly to the moment generated at large deflections.

Aerodynamics

This section discusses the aerodynamics of the aircraft, including the selection of the airfoil, airfoil characteristics, aerodynamic behavior of the aircraft, and the aerodynamic shape of the aircraft as a whole. The relationship between stability considerations and airfoil design is discussed thoroughly, since stability of the aircraft was of paramount importance. The analysis of the lift and drag characteristics for the aircraft turn out to be quite simple, since the entire aircraft is an elliptically-shaped wing.

Final Design

The airfoil section used for the wing is the HPRS 33, a custom-designed airfoil. This airfoil, presented in Figure 6, is a 15-percent thick airfoil section with a reflexed camber. The wing has a span of 2.5 meters, an aspect ratio of 7, giving a root chord of 0.455 meter and planform area S_{ref} of 0.893 m².

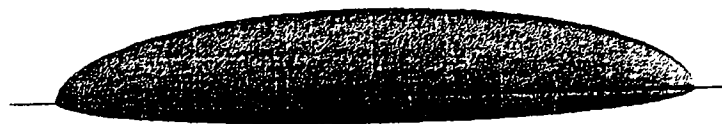


Fig. 6 Planform View of Wing

Aerodynamic Requirements

The selection of the airfoil and the design of the wing shape were dictated by the consideration that the aircraft was to be a flying wing which had to be controllable in flight by a single RC pilot. These requirements in particular were: the need for relatively high lift and low drag; the requisite of static and dynamic stability; and structural rigidity as well as the location of engines, servos, and avionics.

Since a finite wing of elliptical planform experiences a minimum induced drag, this shape was chosen for the flying wing. The wing quarter chord line is set to be a straight line, visible in Figure 6. Having this configuration avoids further complications during construction.

The requirement of static and dynamic stability without a horizontal tail necessitates the use of an airfoil with special stability characteristics. While most airfoil sections have a negative moment coefficient, the flying wing application requires an airfoil with a positive moment coefficient, as discussed previously. One way to accomplish this is to use an airfoil with a reflexed camber.

The wing must withstand the aerodynamic loads, particularly the twisting and bending loads. Also, since the aircraft has no fuselage, all components which include receiver and batteries, servos, and fuel tank, must be contained internally in the wing. These reasons led to the development of a thick airfoil, namely the HPRS 33 airfoil section.

Airfoil Design and Selection

Wing Airfoil Section. Since the flying wing has such special design requirements, it proved impossible to select an existing airfoil with the required lift, thickness, and moment characteristics. Therefore, it was necessary to develop an airfoil with the desired properties. To do this, the geometries of a thick high-lift airfoil and an airfoil with a positive moment coefficient were merged. A two-dimensional inviscid vortex panel code was utilized to calculate the lift, drag, and moment coefficients for the resulting airfoil. Points on the airfoil were then changed and inputted into the code in an iterative process until a satisfactory design was produced. The end result was the HPRS 33 airfoil, shown in Figure 7. Figure 8 presents the

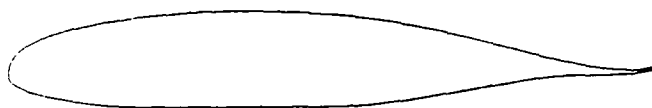


Fig. 7 HPRS 33 Airfoil Section

lift, drag, and moment coefficients versus angle of attack. Note that the drag coefficient is very low, since an inviscid approach was used.

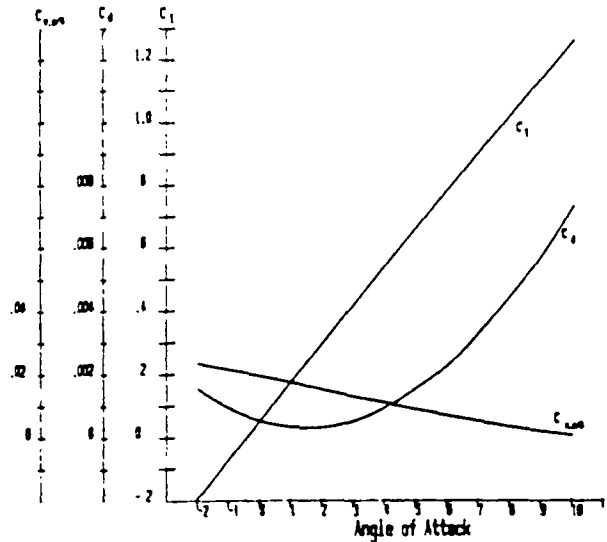


Fig. 8 Lift, Drag & Moment Coefficients vs. Angle of Attack

Vertical Stabilizer Design. The first consideration in the design of the vertical stabilizers was the shape of the airfoil to be used. After researching vertical tails on conventional airplanes, it was determined that a symmetrical airfoil was the best choice. By using a symmetrical airfoil, unnecessary moment forces caused by uneven lift distribution can be avoided. Research of thin symmetric airfoils provided the SD 8020 shape shown in Figure 9.

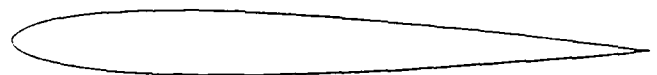


Fig. 9 SD 8020 Airfoil Section

Another important consideration in the design of the vertical stabilizers was sizing. For conventional airplanes with a fuselage, tail and vertical rudder, the area required for the vertical tail is 3% to 5% of the entire planform area of the plane. The design of the flying wing, however called for an area of more than double that percentage. Thus, it was determined that the vertical tail area was to be 12 percent of the wing planform area. With a planform area of 0.893 meter², this gives a total vertical stabilizer area of 0.10716 meter².

The final configuration of each vertical stabilizer consists of a root chord of 17.2 centimeters, a height of 21.3 centimeters, a tip chord of 8.0 centimeters and an aspect ratio of 0.85 (see Figure 7). These control surfaces provide adequate area for stabilization about the yaw axis.

Aerodynamic Calculations

The following is a very brief overview of the calculations performed to obtain theoretical data for the aircraft.

Lift. To obtain theoretical lift values for the aircraft, the slope of the lift curve for the airfoil section first had to be obtained. This calculation was obtained simply from airfoil section data; for the HPRS 33, $dc_l/d\alpha = 6.97$ per radian.

The lift curve slope for the finite wing is then given as

$$\frac{dC_L}{d\alpha} = \frac{2\pi AR}{2 + \sqrt{(AR^2/\eta^2)(1 + \tan^2\Lambda - M^2)}} \quad (9)$$

The airfoil efficiency η is approximated as 1.0. The sweep angle Λ is zero, and the flight mach number is 0.044. Equation 9 thus gives $Dc_l/d\alpha = 5$ per radian.

Integrating this expression gives

$$C_L = 5\alpha + \text{constant} \quad (10)$$

The constant is obtained by using boundary conditions, which are approximated from the section lift curve slope: at $\alpha = 1^\circ$, $c_l = 0.17$. Solving, the constant is found to be approximately 0.084. The lift curve slope for the entire wing is

$$C_L = 5\alpha + 0.084 \quad (11)$$

where the angle of attack is in radians. The lift coefficient of the wing can thus be found for various angles of attack.

Knowing the lift coefficient, the lift force can be found at any speed for different angles of attack using the following equation.

$$L = \frac{1}{2}\rho v_\infty^2 C_L S_{ref} \quad (12)$$

At cruise conditions (4° AoA, 15 m/s), the lift coefficient is 0.4355 and the total lift force is 53.55 N.

Drag. Since the inviscid vortex panel code was not capable of providing accurate drag results, an empirical method suggested by Raymer was used.²

This method depends upon the calculation of the parasitic drag, C_{D_o} , based on equivalent skin friction coefficients $C_{f,c}$,

component form factors FF_c , interference effects Q_c , wetted area S_{wetc} , miscellaneous drags $C_{D_{misc}}$, and estimated leakage and protuberance drag $C_{D_{L\&P}}$. The parasitic drag is calculated according to:

$$C_{D_o} = \frac{\sum (C_{f,c} FF_c Q_c S_{wetc})}{S_{ref}} + C_{D_{misc}} + C_{D_{LP}} \quad (14)$$

At cruise conditions (4° AoA, 15 m/s), the approximate value of parasitic drag is $C_{D_o} = 0.01346$.

The total induced drag, or drag due to lift, is given as the following expression.

$$C_{D_i} = KC_l^2 \quad \text{where} \quad K = \frac{1}{\pi A Re} \quad (14)$$

For an elliptical planform, the Oswald span efficiency factor e is unity. Therefore, $K = 0.04547$ so that, at cruise conditions, $C_{D_i} = 0.008624$.

The total drag coefficient is simply the sum of the parasitic and induced drag coefficients, so that, at cruise,

$$C_D = C_{D_o} + C_{D_i} = 0.01346 + 0.008624 = 0.02208 \quad (15)$$

The cruise drag force is therefore 2.72 N and the lift to drag ratio at cruise is $53.55/2.72 = 19.69$.

Structures

The structural design of the wing involved two primary objectives. The first was to reduce aeroelastic effects since this would alter the distribution of the forces along the wing and consequently alter the stability. Therefore the wing was designed to be as rigid as possible to minimize any bending. The second was to maintain manufacturability, since most of the construction was to be done by students using equipment available on campus.

Final Design

The absence of a fuselage posed some design limitations, namely placement and access to the electronic and engine components. Thus all the components had to be placed within the wing. In order to simplify construction most of the internal components were placed together in the mid-section of the wing, with access to them through a "trap door" placed on the top.

The engines posed a greater problem since they are the heaviest component on the wing and are placed 57 cm from the root creating regions of increased stress concentration. These connections were simplified as much as possible to

ease construction, but still maintain structural integrity. The final engine connection attaches the duct of the engine directly to the carbon shell by four screws.

Method of Construction

The wing is a sandwich construction with a carbon fiber composite "face sheet" and an extruded polystyrene "core". This type of construction makes use of the advantages offered by both the materials used in distributing the load. The "face sheet" or the carbon composite material will carry the majority of the tension and compression loading. While the "core" or extruded polystyrene will carry most of the shear as well as the compression perpendicular to the skin.

In order to construct this type of "material", a process called vacuum bagging was used since it would give the best results. The principle behind vacuum bagging is the application of an evenly distributed force, of magnitude 4-8 Newtons, being applied across the entire surface of the part. This helps reduce the presence of air bubbles as well as remove excess resin. The presence of excess resin besides increasing the weight, causes the formation of stress concentration points by inconsistency in strength. Vacuum Bagging involves placing various layers over the component to be covered.

The extruded polystyrene was chosen because it is a rigid foam therefore helping attain the desired rigidity. In addition the polystyrene is a foam that is easy to handle. The foam is initially a single oversized piece that needs to be cut and shaped to the desired shape. The airfoil section needs to be hot wired into the platform and the taper must be appropriately shaved in using coarse sandpaper. The engine connections are made through hot wiring the circular sections at a 2 degree outward canter and a 4 degree downward canter. As mentioned previously, since the absence of the fuselage forces the placement of the components in the wing, much of the mid-section will be hollowed out. A spar is placed in this area in order help regain some of the rigidity that will be lost.

Once the wing has been properly shaped, the carbon fiber skin is placed over the foam using the above described vacuum bagging procedure.

Material Selection

Many important factors had to be considered when selecting the material for the wing. Some of these were yield and ultimate strength, stiffness, resistance to fracture, density, temperature limitations, availability, and cost.

After much consideration and research, composites were decided to best meet our needs. Composites met all of the constraints and offered the largest reduction in weight.

Carbon was selected because of its high strength to weight ratio, inherent rigidity, low density, and low cost (refer to

Table 1). Carbon is also relatively easy to mold. Hexel epoxy was chosen as the matrix. Hexel epoxy was chosen primarily for its long pot life. This would make it easier to work with during construction.

Composites are very strong in tension but, they are relatively weak in compression. For this reason the composite will be supported by foam. The foam will provide a "cushioning medium" through sandwich construction. Foam will not add much weight and is much better in compression. Density was the main consideration when selecting a foam. The higher the density, the better the compression but, the heavier it would be. Polystyrene was chosen because it offered an acceptable density and was easy to form.

Table 1 Carbon Properties

	<u>High strength</u>	<u>High Modulus</u>
Tensile Strength (MPa)	3000	2000
Elastic Modulus (GPa)	275	415
Density (kg/m ³)	1900	1900

Wing Loading Analysis

One of the most important aspect of the structure of the plane was to guarantee minimum bending. If the plane were to bend or twist during flight, the distribution of forces may change greatly which would adversely affect the stability of the plane; therefore it is extremely important to maintain the shape of the platform during flight.

In order to verify that the material selected to build the wing would not bend under the loading encountered during flight an analysis of the stresses at the wing root was performed. The wing was modeled as a cantilever beam since it is symmetric along the root chord. To simplify the analysis, the cantilever beam was assumed to have a constant area cross-section unlike the actual model which has an elliptical taper.

Since the wing is of sandwich construction, which consists of two materials, it must be "transformed" into a single equivalent material. This is done by creating a ratio of Young's Modulus for the two materials involved, in this case the extruded polystyrene foam and the carbon fiber composite. This ratio then determines an equivalent area for the material. The extruded polystyrene foam is to be converted into carbon fiber composite. Below is the ratio of the Moduli of Elasticity of the two materials. As a result of this ratio being much less than one, it was concluded that the foam can be neglected in the analysis.

$$n = \frac{E_{\text{foam}}}{E_{\text{carbonfiber}}} \quad (16)$$

The loading was then applied to the beam according to those estimated for level cruising. For example, the lift was elliptically distributed along the span. Additionally the drag was uniformly distributed. The weight of the engines and thrust were placed in their appropriate position, according to the numbers obtained from the stability group. The normal stresses were determined using the following equation:

$$\sigma = \frac{P}{A} - \frac{M_x * y}{I_{xx}} + \frac{M_y * x}{I_{yy}} \quad (17)$$

The maximum stresses encountered at the root are on the order of 23.99 kPa, which is well within the limits the carbon fiber composite strength.

In addition to normal stress, the shear stress was also determined at the root. Once again the asymmetric bending was used. The airfoils section was modeled as a closed loop cross-section with a positive shear direction show in Figure 11. The shear was estimated to be 108.3 kPa. Once again well within the limits of the composite material.

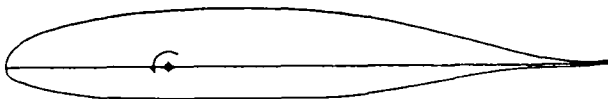


Fig. 10 Closed Loop Section

It is realized that the theoretical material strengths will be greater than those of the actual values. However, it is felt that the stresses are well within tolerance. The objective was to build a rigid yet, manufacturable wing.

Propulsion Systems

The design of the propulsion system for the flying wing was extremely complicated. Since the flying wing has no fuselage, it was important to find a method of propulsion which integrated well with the wing. Important factors that must be considered when choosing a propulsion system are engine type, method of propulsion and total systems integration. In addition, the propulsion system must produce adequate and controllable thrust to allow for a

smooth flight.

Ducted Fan Engines

Although ducted fan engines have a much more complex assembly process than regular propeller engines, their clean aerodynamic shape seemed to fit perfectly in the airfoil, producing enough thrust and yet keeping drag to a minimum.

The ducted fan engine consists of a piston engine enclosed in a cylindrical duct, with a small seven-blade rotor spinning at much higher rpm's than regular propeller engines to produce the same amount of thrust. Since the engine is completely enclosed inside the cylindrical housing, it is difficult to assemble the kit or to do any maintenance on the engines. In fact, if problems arise with the engines, the whole kit would have to be removed from the aircraft and then the engine would have to be disassembled. The assembly process is complicated because tight tolerances have to be kept in order for the fan to work properly. The rotor has to be perfectly balanced, since it rotates at speeds around 22000 rpm. The slightest imbalance can generate undesired vibrations.

Propulsion Systems Configuration

The final configuration of the propulsion system is shown in Figure 11. The three dimensional drawing clearly shows

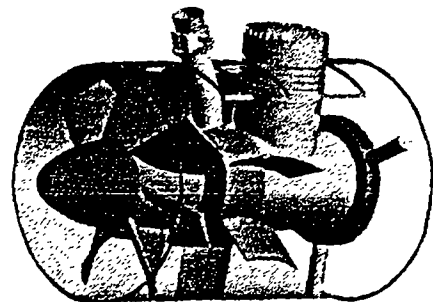


Fig. 11 Propulsion System

the shell, the rotor, the engine, the stator and all the supports. The engine's carburetor and cylinder head stick out of the duct. Each engine assembly as shown weighs 4.00 N. Both engines receive fuel from a central fuel tank located near the center of the airplane. The operating speed is approximately 22000 RPM, with a resulting thrust of 15.60 N each. The engines generate ample thrust to overcome the drag.

Conclusions

Analysis of the elliptical flying wing design has, at least in theory, demonstrated that such a configuration can be stabilized without the use of automatic control systems. This result can find significant application in the eventual design of a full size transport aircraft. Such an aircraft would have the added benefit of computerized control systems, making it a feasible design with the technology available today.

The analysis of this project can be applied to the takeoff and landing of a full size aircraft which has the ability to fly at an oblique angle for higher cruise speeds. It is hoped that next year another project would continue this work for an oblique configuration.

References

1. Jones, Robert T., "Flying Wing Supersonic Transport," Aeronautical Journal, March 1991.
2. Raymer, Daniel P., Aircraft Design: A Conceptual Approach, American Institute of Aeronautics and Astronautics (Washington D.C.), 1989.

Additional References

- Ault, H.K. & Scott, K.E., WPI CAD LAB IPI Manual of Units, Worcester Polytechnic Institute (Worcester, MA), 1992.
- Bohlmann, Eckstrom, Weisshaar, "Static Aeroelastic Tailoring for Oblique Wing Lateral Trim," Journal of Aircraft, vol. 27, no. 6, June 1990.
- Etkin, Bernard, Dynamics of Flight: Stabilities and Controls, John Wiley & Sons (New York, NY), 1992.
- Flinn, R. & Trojan, P., Engineering Materials and their Applications, Houghton Mifflin Co. (Boston, MA), 1990.
- Hobby Lobby Catalog 20 Summer/Fall 92, Hobby Lobby International, Inc. (Brentwood, TN), 1992.
- Jones, Robert T. & Cohen, Doris, High Speed Wing Theory, Princeton University Press (Princeton, NJ), 1960.
- Kalpakjian, Serope, Manufacturing Engineering and Technology, Addison Wesley Publishing Company (Reading, MA), 1992.
- McEntee, Howard G., The Model Aircraft Handbook, Robert Hale Ltd. (London, England), 1982.

Nelson, Robert C., Flight Stability and Automatic Control, McGraw-Hill Book Company (New York, NY), 1989.

O.S. Engines Catalog, O.S. Engines Manufacturing Co. Ltd. (Osaka, Japan), 1990.

RK-720 MK III Instructions and Specifications, Kress Jets, Incorporated (Saugerties, NY), 1992.

Shevell, Richard S., Fundermentals of Flight, Prentice-Hall Company (Englewood Cliffs, NJ), 1989.

Stinton, Darrol, The Design of the Aeroplane, BSP Professional Books (London, England), 1989.

Tower Hobbies 1993 Catalog, Tower Hobbies (Champaign, IL), 1992

Space Projects

WIRELESS SPACE POWER EXPERIMENT (WISPER)

**University of Alaska Fairbanks
Department of Electrical Engineering
Fairbanks, Alaska**

Professor Joe Hawkins

Brian Chouinard, Teaching Assistant

Principal Investigation Team:	James McSpadden (Leader), Sami Khouli, Eric Ruse, Christi Yearous, Tom Zietlow
Mission Analysis Team:	Mark Parrott (Leader), Jeff Alexander, Randy Meitner
Electrical Systems Design:	Clifford Murray (Leader), Tom Clark, Millicent Jones, Monty Lawler, Richard Reimers, Kanwaljeet Singh
Mechanical Systems Design:	Rajesh (Leader), Ted Hethcote, Shawn Houston, Jiong Shao, Afsar Khan

Abstract

The 1993 Advanced Design Project at the University of Alaska Fairbanks was to design a spacecraft as a technology demonstration of wireless power transmission (WPT) from earth to space. With cost effectiveness as a design constraint, a microsatellite in low Earth orbit (LEO) was chosen for the mission. Existing and near-term technologies were analyzed and selected for the project. Two methods of power beaming are examined during two separate phases of spacecraft life. The first phase will demonstrate the technology and examine the theory of microwave power transmission at 35 GHz. Special aspects of Phase I will include a highly accurate attitude control system and a 14-m inflatable parabolic antenna. Phase II will investigate the utilization of high intensity laser power using modified photovoltaic arrays. Special instrumentation on the spacecraft will measure the conversion efficiency from the received microwave or laser power to direct current power.

Introduction

WPT is simply the transfer of usable energy from one point to another without the use of wires or transmission lines. The energy is transmitted by electromagnetic waves at laser or microwave frequencies. WPT is not a new concept. Experimental demonstrations and study efforts have continued since the early 1960's. With the latest progress in transmitter and receiver technology, the next natural step is to beam power from Earth to space. This proposed flight demonstration will advance the science of power beaming and prove the viability of various applications of wireless power in space.

Throughout NASA, industry, and academia, a number of space applications for WPT technology have been proposed. As man progresses in the exploration of the solar system, WPT will likely become an integral part of the space power infrastructure. However, there is an obvious gap between

the development of WPT and space applications. The history includes a beam-powered helicopter and airplane. High efficiencies and high power transmissions have been demonstrated on Earth. A sounding rocket has carried a WPT experiment into the upper atmosphere. What is lacking is the next natural step, a demonstration of WPT from earth to space. WISPER takes that next step. The design difficulties and tradeoffs analyzed within this study will lay the foundation for the understanding of WPT on a larger scale. In accomplishing this mission, the project provides a springboard for the proposed applications and others yet to be conceived.

Microwave Power Experiment - Phase I

Microwave power transmission involves a system composed of a power source, transmitting antenna, and rectenna. The power source converts direct current (DC) power into microwave power, the antenna radiates the microwave power, and the rectenna converts the microwave power back into DC power. A unique component of the WISPER satellite is the inflatable dish that reflects the microwave power onto the rectenna. For the rectenna to perform efficiently in converting the microwave power into DC power, the incident power density must be high. The inflatable dish performs this feat by concentrating the microwave power onto the rectenna.

The major system components for Phase I consist of a 25-m antenna transmitting a 35 GHz power beam to the 14-m inflatable dish located on the WISPER satellite. The inflatable dish reflects the microwave power onto a 96-cm diameter rectenna array located at the focal point.

Operational Sequence

Microwave power beaming will begin after the WISPER satellite has achieved a stable polar orbit at 600 km. Gyrotron sources will generate approximately 400 kW of power at 35 GHz. When the satellite arrives at the ground

station horizon, communication and tracking links will commence with receivers at the ground station. Allowing time for the WISPER satellite to align itself with the transmitting antenna, power transmission will nominally occur at angles between $\pm 40^\circ$ from zenith. The separation distance is 761 km at $\pm 40^\circ$. With a direct overhead pass, approximately 2 minutes will be allowed for power beaming. At this altitude, a maximum of 105 W of DC power is expected from the rectenna under ideal weather conditions and perfect on-axis alignment between the transmitting antenna and inflatable dish. Figure 1 shows the operation sequence at an orbital altitude of 600 km.

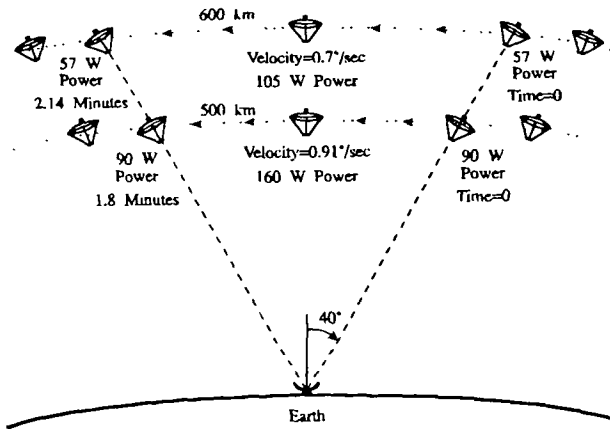


Fig. 1 Operation sequence at an orbital altitude of 600 and 500 km

Including atmospheric attenuation at 35 GHz on clear weather days and a transmitting antenna aperture efficiency of 50%, the power density of the microwave beam will be 3.22 W/m^2 at a zenith altitude of 600 km. The total atmospheric attenuation during clear weather of the microwave at 35 GHz is 0.39 dB at zenith. At 40° from zenith the total attenuation is 0.51 dB. At $\pm 40^\circ$ from zenith, the power density decreases to 1.95 W/m^2 at the WISPER satellite.

The area ratio of the 14-m inflatable dish to the 96-cm rectenna is 213. The aperture efficiency of the inflatable antenna is 47%. Taking the area ratio and aperture efficiency into account, the power density incident on the rectenna ranges from 208 W/m^2 at $\pm 40^\circ$ from zenith to 343 W/m^2 at zenith as shown in Figure 2.

The WISPER satellite will drift to a lower orbit due to the drag on the inflatable dish. The lower altitude limit for Phase I is set at 500 km. The operation sequence at 500 km is also shown in Figure 1. Using the same assumptions of clear weather and perfect alignment between the transmitter and receiver, a maximum of 160 W of DC power is expected from the rectenna. Although the power delivered

to the satellite is increased, the lower altitude results in a shorter power transmission period.

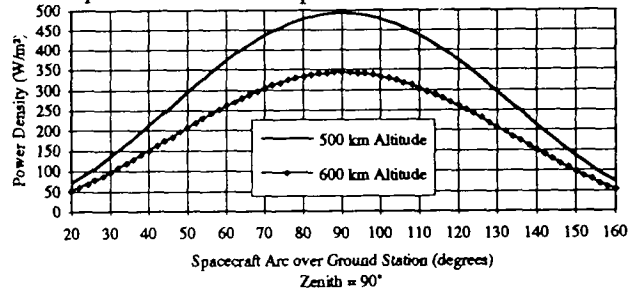


Fig. 2 Incident power density on rectenna at an orbital altitude of 500 and 600 km

The incident power density will increase due to the lower orbital altitude. The power density incident to the rectenna ranges from 296 W/m^2 at $\pm 40^\circ$ from zenith to 494 W/m^2 at zenith as shown in Figure 2.

The inflatable antenna will then be discarded to conduct laser power beaming experiments.

Experimental Objectives

The main objective of this phase is to successfully receive microwave power and convert it to useful DC power. However, an assortment of secondary investigations deserves consideration.

Conversion efficiencies of the rectenna will be determined and compared to theoretical calculations. The conversion efficiency can be measured by comparing the power density incident on the rectenna to the output DC power. The ability of the inflatable dish to focus the microwave power will be monitored. This focusing efficiency can be obtained by measuring the microwave power densities incident on the satellite and rectenna. These two efficiencies can also be measured at different power densities due to the constantly changing separation distance between the transmitter and satellite or the output power from the transmitter can be varied.

Power patterns of the transmitting antenna can be determined by a microwave detection system on the spacecraft. The ground antenna will remain fixed as the spacecraft records the pattern passing overhead.

The ground station selected for the WISPER project is the National Oceanic and Atmospheric Administration (NOAA) satellite tracking station located in Fairbanks, Alaska. This ground station is ideal for microwave power beaming because it is located in a hill valley isolated it from local inhabitants, and further, the gyrotrons power needs are available. Transmitting and receiving antennas are also available for satellite communication.

The effects of microwave power transmission at 35 GHz through a turbulent atmosphere can be analyzed. Using an existing water vapor radiometer at the NOAA tracking station allows the amount of water vapor in the atmosphere be measured. Thus, interactions of the power beam with clouds or inclement weather can be compared to clear weather transmissions and to existing attenuation models. Microwave beam propagation as a function of the ionospheric plasma density can be measured. Possible thresholds at which nonlinear effects occur in wave particle interactions with the microwave power beam may be determined. Physical effects, such as microwave defocusing or attenuation, could occur due to the nonlinear interactions.¹

Frequency Selection

The choice of operating frequency for microwave power transmission is driven by the separation distance between transmitter and rectenna, power density coverage over a certain area, and the components to support the mission using existing technology. Because the pattern of a microwave beam diverges with distance, operating frequencies are increased to reduce component sizes and to sustain high power densities. The prime candidates for the operating frequency are 2.45 GHz, 5.8 GHz and 35 GHz. The first and second frequencies are selected based on operation in ISM bands and low attenuation through the atmosphere. Recent component developments have made power transmission at 35 GHz possible.

The operating frequency of 35 GHz is selected for this project due to the ability of focusing the microwave energy onto a small spacecraft from a single transmitting antenna.

Inflatable Antenna

For the WISPER demonstration, a microsatellite was selected to minimize the cost of the demonstration. The only technology feasible for implementing the required large aperture reflector on such a small payload is an inflatable antenna. Inflatable antennas have significant advantages in mass and volume over more traditional technologies. Large aperture antennas on Earth are constructed to withstand immense gravity and wind loads. Once removed from the majority of the gravity and atmosphere of the Earth, antenna designs change significantly. Inflatable space structures utilize the different conditions to the fullest. In microgravity and near vacuum conditions, it is the nature of an inflatable structure to form curved surfaces such as a paraboloid. This allows a relatively high surface tolerance with minimum antenna structure. Also, the system mass and packaged volume are considerably less than traditional mechanical systems.²

The antenna consists of a self-rigidizing torus and three struts, a metal film surface as the reflector, a frequency transparent canopy, and an inflation system. After proper orbital injection, the struts and torus are inflated to the yield strength of the aluminum. At this point the torus becomes rigidized and the high internal pressure is no longer required. The reflector and radome are then inflated to remove any wrinkles, and the system is operational. Extra inflatant is stored on the spacecraft to replace any gas leaked due to micrometeoroid impacts. The system weight, 68 kg, includes the entire support structure, deployment mechanism and enough inflatant for a ten-year mission. The general configuration for the inflated antenna is shown in Figure 3. Not included in the drawing are inflatable struts from the spacecraft body to the structural torus. Table 1 shows the general specifications for the inflatable antenna.

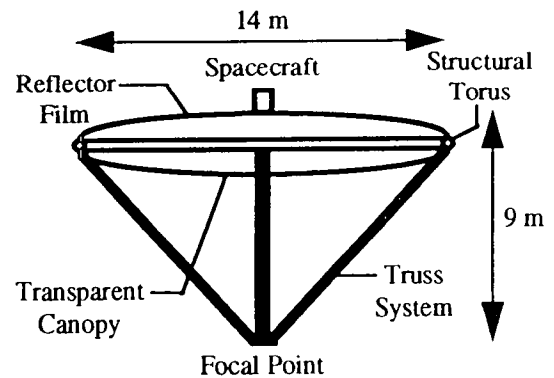


Fig. 3 Inflatable antenna configuration

Table 1. Inflatable antenna system specifications

Inflatable dish diameter	14 m
Surface tolerance	0.5 mm rms, 1/17 at 35 GHz
Aperture efficiency	47%
F/D ratio	0.65
Total system mass	68 kg

35 GHz Rectenna

The rectenna is a receiving antenna that converts microwave power into DC power. The components of the rectenna consist of an antenna, filtering circuitry, and rectifying diode. The 96-cm diameter rectenna consists of 16,848 elements that have their own filtering components and rectifying diode. Because the antenna on the rectenna is a printed half-wave dipole, the polarization is linear.

The conversion efficiency of a 35 GHz rectenna array can be simulated based on the conversion curves of a single element.³ The maximum conversion efficiency of the rectenna array is 50%. Applying the efficiency to the 96-cm

diameter array, the performance of the 35 GHz rectenna array is simulated in Figure 4.

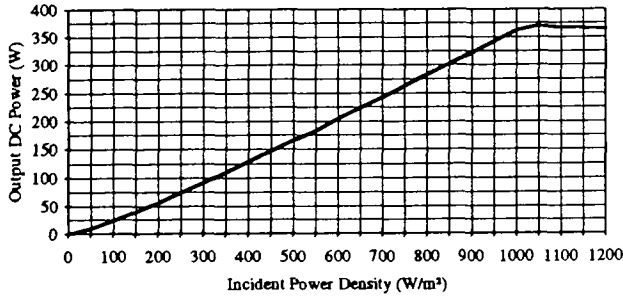


Fig. 4 DC output power of the 35 GHz rectenna with a 96-cm diameter

By comparing Figure 2 to Figure 4, the on-orbit DC power output can be estimated.

Power Density Detection

The power density at the spacecraft will be detected in two ways. One Ka-band standard gain horn antenna will be placed on the underside of the focal point platform to face the Earth. The purpose of this antenna is to detect the incident power density to the spacecraft. Two Ka-band gain horns will be orthogonally placed on the frontside of the platform to detect the focused power density from the inflatable dish. Efficiency calculations and polarization tracking can be performed using the energy collected by these two horn antennas.

Because the rectenna is linearly polarized, detection of the incoming energy on the rectenna will dictate the rotation of the microwave feed at the ground station antenna. Polarization alignment is critical to ensure maximum reception by the rectenna.

Power Patterns and Pointing Accuracy of Inflatable Dish

A design trade-off is required when deciding the diameter of the inflatable dish. To collect a large amount of the transmitted power, the dish diameter needs to be large. However, the pointing accuracy requirements also increase with diameter. Due to the large separation distance between the transmitter and satellite, the pointing accuracy of the inflatable dish is crucial. For the WISPER satellite, the power density is required to remain within 1 dB of the beam peak.

As shown in Figure 5, the power pattern of the 14 m inflatable dish is given at 35 GHz and at 600 km. The 1 dB reference occurs at 112 m from the beam axis. Thus, a 0.01° pointing accuracy is necessary.

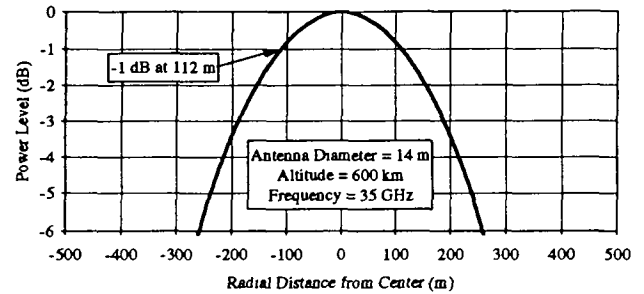


Fig. 5 Far field power pattern of 14 m inflatable dish at 600-km

Interferometer dipole sets operating in the C-band will provide pointing accuracy information for the satellite.

Monopulse Beacon

The other major component on the focal point pertains to the ground station pointing accuracy. A continuous wave (CW) and circular polarized signal at 12 GHz will be transmitted to the ground station at all times during the power beaming. The beacon consists of a power supply and traveling-wave tube amplifier (TWTA). The output power of the beacon is 14 W. A monopulse receiver at the transmitting antenna will provide a pointing accuracy of 0.001°.

Transmitting Antenna

A 25-m antenna with a high aperture efficiency is required for high frequency power beaming applications. The selection of the diameter is based on pointing accuracy requirements and the availability of the antenna. Aperture efficiency is important for power beaming applications because the total power transmitted is the product of the aperture efficiency and the power produced by the microwave power source. An aperture efficiency of 50% at 35 GHz is achievable by the Very Long Baseline Array (VLBA) radio telescope antenna.⁴

Power patterns were also computed for the VLBA with uniform aperture illumination. As shown in Figure 6, the power pattern of the 25-m dish is given at 35 GHz and at 600 km. The 1 dB reference occurs at 63 m from the beam axis. Thus, a 0.006° pointing accuracy is needed. The monopulse receiver will provide this pointing accuracy. As with the inflatable antenna, the same pointing accuracy is required at other transmission distances.

A goal for the Phase I experiments is an output of 100 W from the rectenna at an orbital altitude of 600 km. By setting this requirement, the ground station power source

could be specified to obtain this goal. Two 200 kW gyrotrons will be needed to meet the rectenna output requirement. The gyrotrons are synchronized together to produce 400 kW of power feeding the antenna.

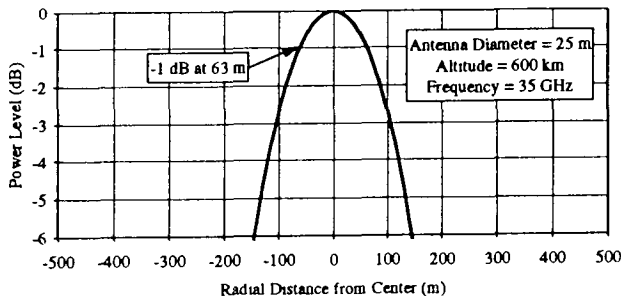


Fig. 6 Far field power pattern of the transmitting antenna

Laser Power Experiment - Phase II

The limited sources of power in space and the high cost of generating or storing that power make the Laser Power Beaming (LPB) concept attractive. Fuel and batteries for power generation and storage are important factors in determining the cost and lifetime of any spacecraft. When the satellite is in the Earth's eclipse, the solar arrays are shadowed so the batteries must supply the necessary power. This cycle of charging and discharging shortens the life of the batteries. By beaming power to the satellite during the eclipse, the lifetime of the spacecraft can be increased by alleviating the load on the batteries.

Operational Sequence

By the time the microwave power Phase I experiments have been completed, the satellite's orbit will have decayed to an altitude of approximately 500 km. At this level, the laser beaming will take place. Two 2 kW lasers, one with a 0.85 mm wavelength and the other with a 1.06 mm wavelength, will be used. These two wavelengths are selected due to atmospheric attenuation windows and efficiency curves of the monochromatically tuned photovoltaic receivers on the spacecraft. The satellite will be available to receive laser power when it is within 60° from the ground station zenith. A direct overhead pass will allow 3.0 minutes of potential lasing time for power transfer. A schematic of the operational sequence is shown in Figure 7.

Experimental Objectives

A successful completion of the laser beaming program can be summarized in the following list of mission goals:

1. Successfully receive laser power from a ground station.
2. Determine the power conversion efficiencies of both Gallium Arsenide (GaAs) and Silicon (Si) photovoltaics.
3. Perform power density measurements of the transmitted beam.
4. Measure the incident laser spot diameter.
5. Analyze the laser transmission through the atmosphere.
6. Coordinate and maintain pointing accuracy of the ground station and spacecraft.

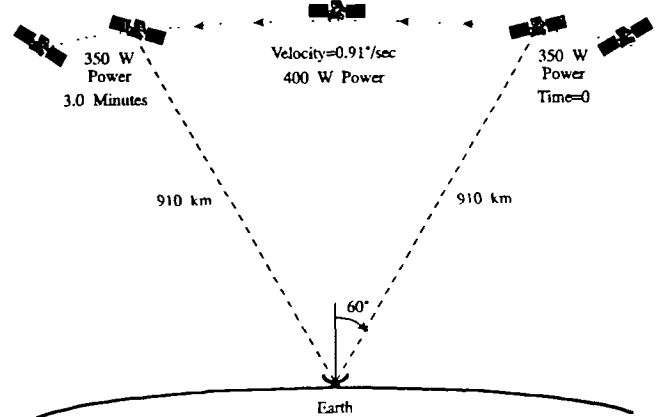


Fig. 7 Laser power beaming operational sequence

The efficiency degradation of both GaAs and Si photovoltaic arrays will be studied. The 0.85 μm wavelength laser can be directed first at the GaAs panel that has been optimized for this wavelength and then towards the Si panel. The power from each panel will be compared. Next, a similar experiment using a laser with a 1.06 μm wavelength will be pointed at each panel. The Si panel is optimized for this wavelength. The laser power can also be varied in each of the cases mentioned.

Wavelength and Laser Selection

The satellite is designed to receive power from a laser at wavelengths of both 0.85 and 1.06 mm. The criteria that determined the selection are shown in figures 8 and 9.

The radio frequency free-electron laser (RF-FEL) is the prime candidate for LPB. The RF-FEL meets two major requirements: 1) the RF-FEL is one of the few lasers that can deliver the required high power and 2) the RF-FEL is capable of operating in the wavelength range where the PV receivers are most efficient. Since the FEL is tunable to ±10% of its design frequency, a slight change in frequency will be possible for further experimentation. The RF-FEL is also used for this application because its pulse train is in the picosecond range and appears as a continuous wave to the

photovoltaic receiver.⁶

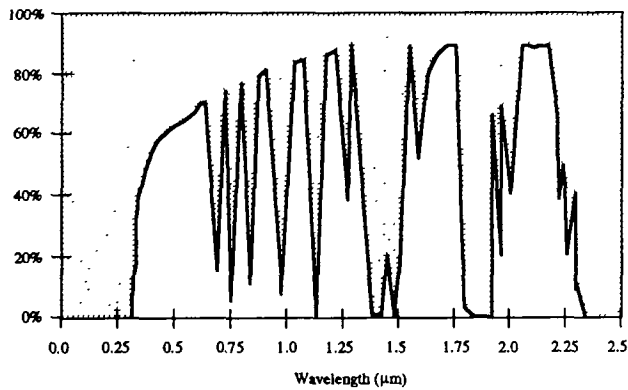


Fig. 8 Laser atmospheric transmission windows with laser located 2 km above sea level

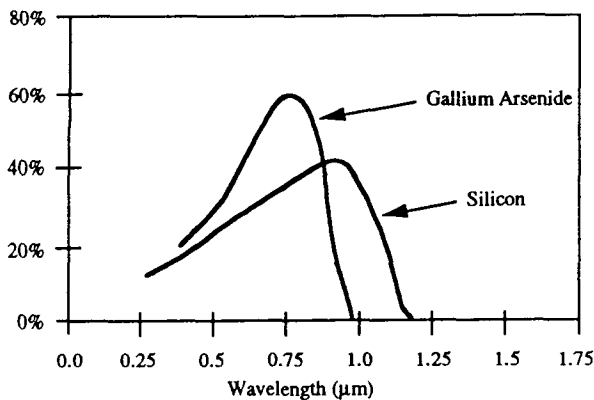


Fig. 9 Photovoltaic compensated efficiencies

Photovoltaic Receiver

Of the four photovoltaic arrays onboard the spacecraft, two will be specially designed to efficiently receive the monochromatic laser beam. One panel will be composed of specialized GaAs cells that are designed to operate most efficiently at a wavelength of 0.85 mm. A conversion efficiency of 50% is anticipated with this design. The second laser panel will be composed of a tuned Si array with an expected conversion efficiency of 40%. The actual efficiency of the two arrays must account for operating temperature. This diversity will allow for a comparative analysis of the performance of each type of cell design.

$$r_{spot} = \frac{0.61 d \lambda}{r_{lens}} \quad [m] \quad (1)$$

where r_{lens} is the radius of the mirror used to focus the beam (m), d is the source to receiver distance (m) and λ is the wavelength (m).

The spot radius is defined as the first zero in the diffraction pattern, containing 84% of the energy. For the spacecraft at an altitude of 500 km, an operating wavelength of 0.85 mm for the GaAs panel, and a 5-m diameter transmitting mirror the spot size is calculated to have a 20.5 cm diameter. The Si panel has a similar altitude and transmitting mirror, but the optimum wavelength is 1.06 mm. Thus, the spot size diameter is 25.8 cm.⁷ From the standpoint of the photovoltaics, calculation of the spot size is important for two reasons. First, it is important to have a target larger than the required spot size. Second, the spot size along with the incident power density must be known in order to address the issue of thermal management.

The first consideration should not cause problems due to the configuration of the WISPER satellite. The solar array is composed of four foldout panels, each 40.64 cm wide and 86.36 cm tall. For the GaAs panel, the spot size is half as wide and over one-fourth as tall, which should fit neatly onto the panel. The silicon spot size is slightly larger, once again there should not be a problem hitting the target panel. It should also be noted that the two panels were placed farthest away from the satellite body, so in either the GaAs or Si cases there is another panel of the same dimensions separating the photovoltaic receiver from the spacecraft. These panels should also absorb much of the 16% beam energy outside the spot area. The spot size is used to calculate the minimum size for thermal management considerations.

Thermal Management. The spot size and incident intensity of the laser beam are critical to designing a thermal management system. For the WISPER satellite with a spot diameter of 20.5 cm and output power level of 400 W, the power density is calculated to be 12.125 kW/m². This power density exceeds the normal solar incident power of 1.358 kW/m² by a factor of almost 9.

Based on a projected power density of 12.125 kW/m² at the WISPER satellite, the GaAs panel will be heated to approximately 275°C. The silicon array will be closer to 295°C. These temperatures exceed the temperatures that the panels are normally exposed to. However, due to the short exposure period, the elevated temperatures should not harm the photovoltaic receiver.

Laser Sensors. Based on the calculated incident laser spot diameter of 20.5 cm, an array of laser sensors will be positioned on the GaAs panel to provide an accurate dimension of the spot. The sensors are needed to verify the spot size and to determine the photovoltaic conversion efficiency.

The GaAs photovoltaic cells being used for the laser

power beaming have an anticipated power conversion efficiency of approximately 50% at the proposed wavelength of 0.85 μm .⁸ This efficiency can be verified with the data collected by the laser sensors. Using both the value of incident power intensity and the measured spot size, the total incident power can be compared to the power supplied by each of the panels as measured by the onboard power meter.

Ground Station Requirements

The ground site chosen for the WISPER project is the White Sands Missile Range, NM. In the near term, the availability of a 1 to 5 kW RF-FEL laser for laser power beaming purposes is anticipated. Adaptive optics will be used to compensate for the atmospheric disturbance of the beam.

Adaptive Optics. A tracking system is needed for the laser to have high pointing accuracy. A limiting factor on the spot size is the atmospheric turbulence. Atmospheric turbulence limits the resolution of an astronomical telescope to about 4 microradians. At a 500 km target distance, the turbulence contributes about 2 m to the spot diameter. This problem can be resolved by the adaptive optics technique.

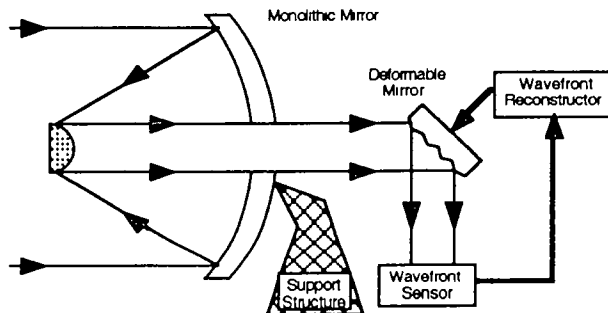


Fig. 10 Adaptive optics using a deformable array in the beacon beam path

The principle of adaptive optics involves a light source beacon at the target above the atmosphere that transmits a beam towards the earth station. The beacon source could be a distant star. As the beam propagates through the atmosphere, it experiences atmospheric distortion. The incoming beam can be detected by the wavefront sensor at the ground station. The wavefront sensor constructs a phase map of the beam. The conjugate of the distortion (i.e. the phase map of the incoming wave) is applied to the outgoing laser beam by a deformable mirror. When the predistorted

beam travels through the atmosphere and experiences the precipitation atmospheric distortion, it leaves the atmosphere nearly diffraction limited. This sequence is possible since the time scale of the atmospheric turbulence is much slower than the time it takes the beacon to get to the ground station plus the time of the deformable mirror to react.

Many methods utilizing adaptive optics exist. One method is to implement the deformable array in the path of the beacon beam before it reaches the mirror, as illustrated in Figure 10.

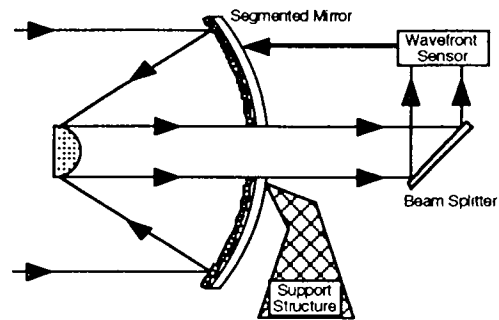


Fig. 11 Adaptive optics using a deformable mirror

Another option is to implement the deformable array on the mirror itself as shown in Figure 11. This method is known as the Phased Array Mirror, Expandable Large Aperture (PAMELA).⁹ Figure 12 shows the PAMELA concept in detail.

Since the path length through the atmosphere is a function of zenith angle, and because of adaptive optics limitations with long path lengths through the atmosphere, a limit is set for the angle off zenith to 60°.

For LEO, the distance that is separating the beacon from the satellite is large and the beacon cannot be located on the satellite. Synthetic beacons can overcome this problem where a different laser beam in wavelength and power is propagated up in the atmosphere as shown in Figure 13.

The ground station for the laser power beaming will use a synthetic beacon approach. A beacon signal will be transmitted from the ground station to the WISPER satellite. A portion of the beacon will be reflected and received at the ground station. Distortion through the atmosphere will be processed to guide the laser beam.

Laser Power Measurements

Figure 14 shows the anticipated percentage of laser power

incident upon the satellite at an altitude of 500 km.

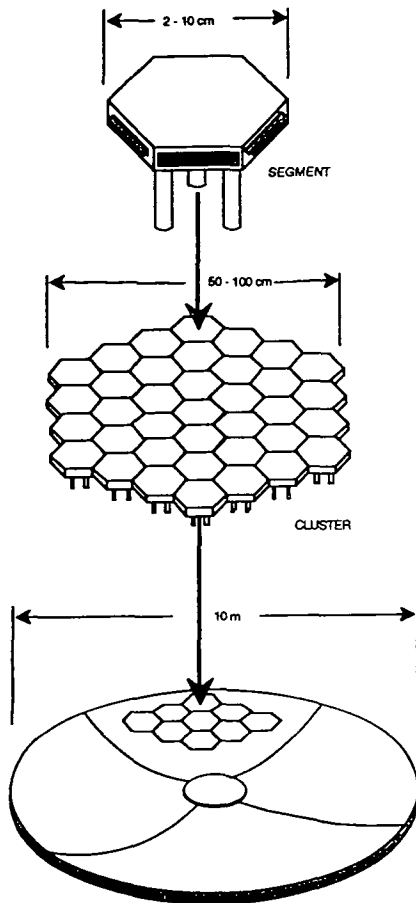


Fig. 12 PAMELA adaptive optics concept

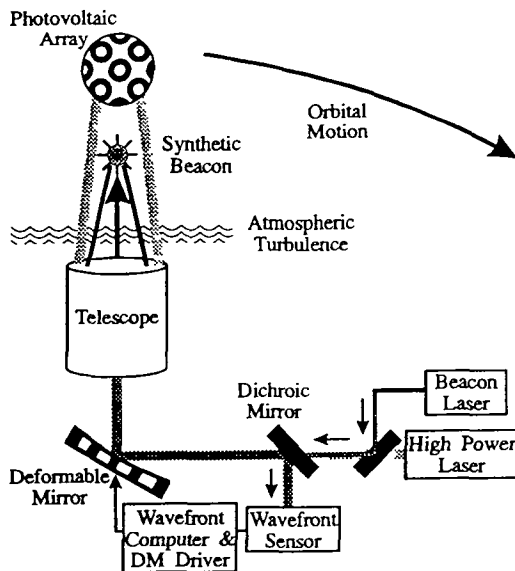


Fig. 13 Synthetic beacon configuration

Experiments will be conducted on clear days, with no precipitation or visible clouds, to allow an expected transmittance through the atmosphere of approximately 80% to 90%. With a 2 kW RF-FEL located at the 3 km altitude White Sands facility, approximately 38% of the laser power will reach the photovoltaic panel. This estimation results from a number of different tests performed on the various components involved as well as from several theoretical calculations.^{10,11} In order to validate the expected transmission efficiency, accurate laser sensors will be used to measure the incident power density.

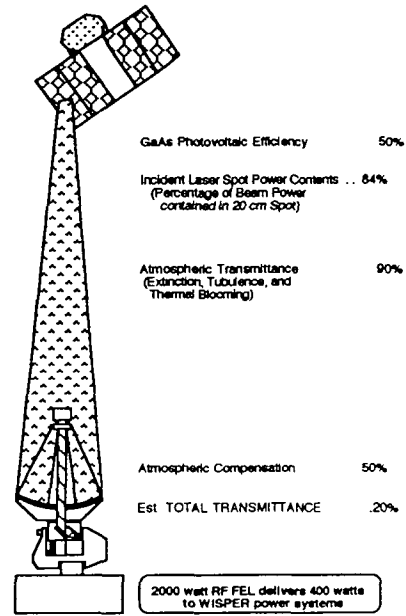


Fig. 14 Laser transmission efficiency from the 3-km altitude ground station

Taking into consideration that the PV conversion efficiency of monochromatic light is 50%, the spot power distribution is 84%, and the required atmospheric compensation loss is 50%, an overall transmission efficiency from the laser to the satellite is expected to be approximately 20%. Thus, approximately 400 W will be received from a 2 kW RF-FEL.

Command, Control and Communications(C³)

The command, control, and communications subsystem was designed with two sets of requirements in mind. During Phase I of the WISPER mission the C³ subsystem must provide a real-time communications link during the power beaming, and a relay satellite link beyond the horizon mask of the ground station. In the Phase II portion of the mission the C³ subsystem need only provide the relay satellite communications link. The C³ subsystem onboard the WISPER spacecraft is centered around the second

generation NASA Telemetry and Data Relay Satellite System (TDRSS) standard user transponder. The transponder will link with both TDRSS east and west during relay satellite links. The transponder will link with Satellite Telemetry and Data Network (STDN) equipment at the ground station in Fairbanks.

Command and Data Handling

The command and data handling subsystem was chosen such that it could interface with the C³ subsystem, provide high speed calculations necessary for the attitude and control subsystem, and provide an interface with the many sensors, instrumentation, and subsystems. The demands on this subsystem would be greater during Phase I of the mission than in Phase II, as the attitude and control is much more critical during Phase I. The computer chosen for the given requirements was the Fairchild Space 386 (FS386) computer. It includes the necessary interfaces for the mission, including a TDRSS transponder interface.

Power Storage and Distribution

The power for the WISPER spacecraft will be supplied by the solar cells that are continuously facing the sun. The power will be stored in Nickel-Cadmium(NiCd) batteries. The distribution of power and maintenance of batteries is controlled through a serial data line from the FS386 computer.

Mission Analysis

Mission analysis is the process of turning the mission statement goals into the best spacecraft and mission possible. The goal for this mission is to demonstrate wireless power beaming between Earth and space within the next 5 years. The goal is constrained by the following factors in terms of priority: cost, experimental requirements, technology development, launcher capability, communications limits, and the space environment. The best choices will optimize experimental data recovery, reliability and component usefulness.

The orbit chosen will give the highest power density at the receiver, the longest mission life, the lowest launch cost, the most sunlight for the solar cells, the most passes over the ground site, and the longest period of experiment time for each pass. The orbit parameters are:

Phase I. Microwave Experiment

Initial altitude	600 km
Final altitude	500 km
Decay time	~370 days
Inclination	97.59°

Phase II. Laser Experiment

Initial altitude	500 km
Final altitude	400 km
Decay time	> 4 years
Inclination	97.59°

The booster selection depends on the funds available, the payload requirements, the orbit parameters, and available launch sites. The Pegasus booster was selected for this mission. The Pegasus carrying WISPER would be launched from the Western Test Range into orbit for \$17 million in January, 1997.

The mission analysis design detail would begin after this initial report and would last one year.¹² The fabrication of the hardware would take 1 years to complete. Integration and testing are estimated to take 6 months under ideal conditions. The 2 phases of experimentation would each have 1 year of operation. The total cost for the mission would be \$48 million including launch. The critical path is the development of the mission equipment. However, many things can affect the schedule, such as design oversights, availability of components or testing facilities, and lack of funding.

WISPER Deployment

WISPER will be launched onboard an Orbital Sciences Pegasus launch vehicle from Eielson AFB in Fairbanks, via a B-52 bomber, into an initial 600 km low earth sun-synchronous orbit. After deployment the satellite will use onboard thrusters to account for expected insertion errors of ± 5 km. Upon acquiring orbit, stored photovoltaic arrays will unfold and the microwave antenna will inflate from the base of the satellite. Figure 15 illustrates the satellite for the microwave Phase I.

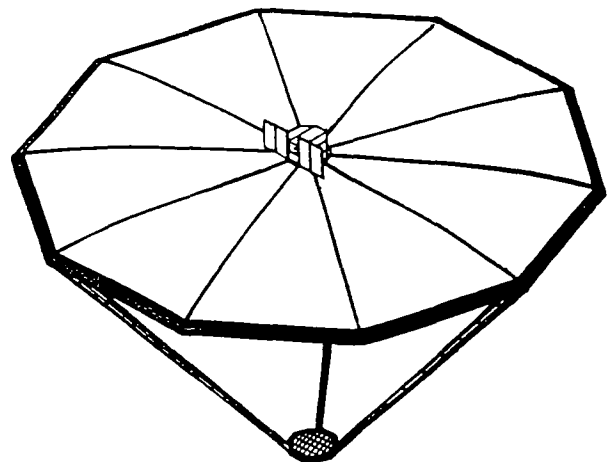


Fig. 15 WISPER Phase I configuration

Phase I will last for approximately one year as the orbit decays from 600 to 500 km. To increase the lifetime of the spacecraft, the inflatable antenna and the focal point components will be jettisoned following the completion of Phase I. The WISPER configuration for Phase II is shown in Figure 16.

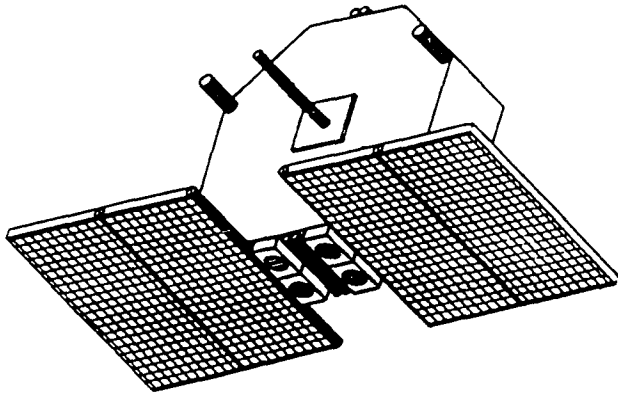


Fig. 16 WISPER Phase II configuration

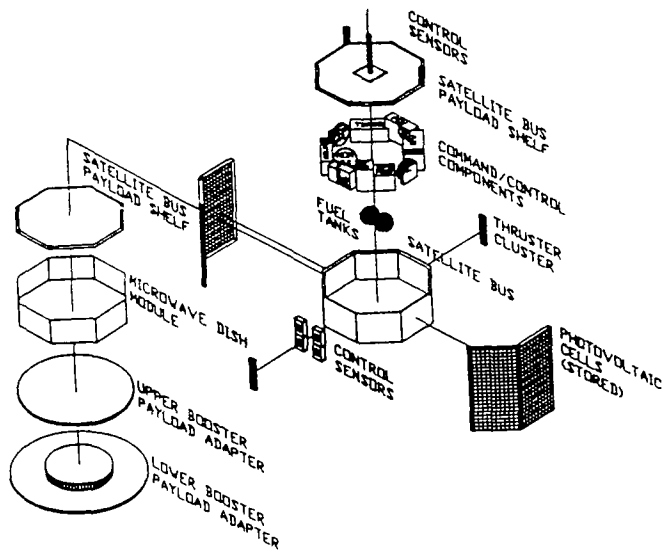


Fig. 17 WISPER component configuration

Internal Packaging

The internal packaging was constrained by the available volume inside the Pegasus launch vehicle and the size of various subsystems. A passive thermal subsystem was

selected for WISPER. Therefore, components required to be kept cool are mounted on the side away from the sun and components requiring heating are mounted on the side facing the sun. Figure 17 shows an assembly diagram of the major WISPER components.

Attitude Determination and Control

Attitude determination for the WISPER satellite will occur in two steps for Phase I and in one step for the Phase II. The two step sequence for attitude determination during Phase I is due to the tight pointing constraints imposed by the power density requirements of the rectenna. Phase II has minimal pointing requirements as the photovoltaic arrays are very sensitive to off-axis illumination.

Attitude determination for Phase I is acquired by first reading the orientation of the Earth's magnetic field with a magnetometer. The earth's magnetic field provides a 3-axis attitude frame without reference. The readings are referenced by acquiring the current relative position of WISPER with respect to Earth and the current time from a GPS receiver subsystem onboard WISPER. This information provides a space-time reference for the magnetometer readings. However, the Earth's magnetic field has random variations. As a final reference, four high accuracy digital sun sensors provide a reference for the relative position of the sun. The complete data set can then be used to provide greater than 0.03° pointing accuracy. To increase the pointing accuracy to 0.01°, an interferometer system can be used. From this high initial accuracy, interferometer antennas located on the focal point receive a C-band beacon from the NOAA ground station. The interferometer provides the needed information to the attitude control system to point the satellite within 0.01°. Some development will be needed to design a C-band interferometer with this accuracy.

Attitude determination during Phase II is accomplished by using the magnetometer and Global Positioning Satellite(GPS) data combined with data from an analog sun sensor. This system will provide better than 1.0° accuracy which is more than sufficient for the laser power beaming experiments.

The stringent pointing requirements will be achieved by 3-axis stabilization using a combination of 4 reaction wheels and 3 magnetic torque rods. Each reaction wheel will be mounted on one axis, with the fourth one acting as the redundant wheel. The reaction wheels would take care of the cyclic torque requirements. Magnetic torque rods would help dump secular torques. Magnetic torque rods have been selected instead of thrusters for this mission because of mass and volume constraints.

The spacecraft is to be constructed of Aluminum 7075. The design of the structure was influenced by structural strength, manufacturing ability, natural frequency, and packaging. A structure was designed to take care of acceleration loads of up to 6 g in the vertical axis and 7.5 g in the horizontal axes. One unique feature of the Pegasus worth mentioning is the "wing drop". At about 41,000 ft the launch vehicle is dropped from the wing of a B-52 bomber. During this vertical drop the natural frequencies of the booster and the payload should not be close to each other. The structure was designed such that its natural frequencies did not coincide with that of the launch environment.

Conclusion

As a flight demonstration, project WISPER has a number of important features that are necessary to prove WPT in space. The experiment beams power over longer distances than have been previously attempted. The distance between the transmitter on Earth and power collection and conversion receivers on WISPER varies nominally between 500 km and 1000 km for both Phase I and Phase II. Three unique features of the satellite hardware include the inflatable antenna, the space-qualified 35 GHz rectenna, and a Si 1.06 mm photovoltaic array. The microwave and laser power are transmitted through the atmosphere. Many proposed applications involve power transmitted from earth to space or space to earth. By transmitting through the atmosphere, WISPER allows experiments to examine how the high power microwave and laser beams interact with the atmosphere. These interactions can be compared with existing attenuation models. The high power levels involved in this experiment are limited by cost rather than available technology. Finally, the experiments will last a minimum of two years. This period will provide ample time to conduct campaigns of experiments, study WPT in a variety of weather conditions, and examine the operation of unproven satellite components.

Most importantly, the Wireless Space Power Experiment takes the first delicate step of using WPT in space. Once operational, WISPER will provide a reference for WPT projects in space. Simultaneously, WISPER will act as a springboard for future applications.

As shown by the large number of NASA, academic, and industry WPT experts attending the critical design review for WISPER, the project has already generated interest and support for WPT. The next step after the demonstration is a space application that utilizes WPT. The technology is rapidly developing. The advent of higher power, and lower maintenance, continuous-wave(CW) lasers will generate new interest in the WPT field. The present and near future

requires sustained interest, research, and funding for WPT. The possibilities for the future show great promise.

Acknowledgments

The WISPER project team would like to thank Lisa L. Kohout and the Space Power Integration Office at NASA Lewis Research Center, Cleveland, Ohio. Their patience and assistance with every stage of the project was appreciated. We would also like to thank those who attended the project's critical design review in Fairbanks, Alaska and provided valuable comments and suggestions for the Final Report:

Alan M. Brown	NASA Center for Space Power, Texas A&M University
William C. Brown	Microwave Power Transmission Systems
Dr. Vicki S. Johnson	USRA ADP Program Manager
Dr. Nobuyuki Kaya	Kobe University, Japan
Dr. Geoffrey A. Landis	Sverdrup Technology, NASA Lewis Research Center
Gregg Maryniak	International Space University

The WISPER project team would like to thank the many industry and academic advisors who provided support and important information throughout the project. Of special note include the following:

Bob Alper	Varian
Shawn D. Anderson	Utah State University
Dr. Costa Cassapakis	L'Garde, Inc.
Kathy Derrick	Orbital Sciences Corp.
Andy Gerber	Fairchild Space
Dr. Peter Koert	ARCO Power Technologies, Inc.
W.R. (Bill) Ray	Loral Vought Systems
Ed Reese	Radiation Systems, Inc.
Mike Simmons	GE Government Services, Fairbanks CDAS NOAA
John Wallace	Radiation Systems, Inc.

References

- 1) Matsumoto, H., and Kimura, T., "Nonlinear Excitation of Electron Cyclotron Waves by a Monochromatic Strong Microwave, Computer Simulation Analysis of the MINIX Results", Space Power, Vol. 6, 1986 pp. 187-191.
- 2) G. J. Friese and et. al., "Initial 1980's Development of Inflated Antennas, Final Report", L'Garde, Inc., Newport Beach, CA, NASA-CR-166060, Jan. 1983.

- 3) Koert P., and Cha J.T., "Millimeter Wave Technology for Space Power Beaming", IEEE Transactions Microwave Theory and Techniques, Vol. 40, June 1992, pp. 1251-1258.
- 4) National Radio Astronomy Observatory, "Very Long Baseline Array Project", Very Long Baseline Array Project Book, Version 7, p. 5-9, Oct. 1988.
- 5) Varian Microwave Power Tubes, Varian, Palo Alto, Calif., pp. 19-20, Sept. 1989.
- 6) Ponikvar, D.R., "Independent Assessment of Laser Power Beaming Options," Proceedings of SPIE, Vol. 1628, 1992, pp. 314-325.
- 7) Landis, G.A., "Laser Beamed Power: Satellite Demonstrations Applications", 43rd Congress of the International Astronautical Federation, Washington, DC, 1992.
- 8) Abraham, D.S., Anspaugh, B.E., Nesmith, B.J., Penzo, P.A., and Smith, J.H., "A Demonstration Plan for Laser-Beamed Power", Jet Propulsion Laboratory, California Institute of Tech., 1992.
- 9) Rather, J.D.G., "Power Beaming Research at NASA", Proceedings of SPIE, Vol. 1628, 1992, pp. 276-298.
- 10) Rather, J.D.G., "Project SELENE", Technology Workshop on Laser Beamed Power, NASA Lewis Research Center, Feb. 1991.
- 11) Parenti, R.R., "Technology Concept Definition for a Ground-based Power-beaming System", Lincoln Laboratory, MIT, prepared for NASA under Air Force contract No. F19628-90-C-0002, 1992.
- 12) Wireless Space Power Experiment (WISPER), Final Report, EE/ESM/ME 656 Space Systems Engineering, NASA/URSA Advanced Design Program, Department of Electrical Engineering, University of Alaska Fairbanks, Fairbanks, AK, June 1993.

AUTONOMOUS SPACE PROCESSOR FOR ORBITAL DEBRIS

University of Arizona
Aerospace and Mechanical Engineering Department
Tucson, Arizona

Professor Kumar Ramohalli
Dominique Mitchell and Nick Piagentini, Teaching Assistants
David Rowney, Zayed Alatwah, John Chan, Anwar Yousef, Seniors
Philip Cojinis, Sophomore
Visiting Russian Student from MAI, Konstantin Kulagin
Mentor, Dr. Kim Aaron, Jet Propulsion Laboratory

Abstract

This year the ASPOD project provided hands-on-hardware experience for a total of twelve students that also included independent study students. In continuing to seek economical solutions to mitigate the orbital debris problem, the robot construction was improved. The advances included: a new modern six degrees of freedom arm, a high-tech, low weight, high strength composite frame for the Fresnel lens and mirror array, and a solar tracking test bed. The test bed consists of a strong support frame that is capable of holding both arms and the entire mirror assembly. The table/platform possesses two degrees of freedom, a rotational joint, and a second tilting about an axis. These two actuators allow the table to position the lenses in order to maximize the sunlight reception. The process is controlled by hard-wired logic circuit with four phototransistors positioned on the mirror frame. This logic system directs the two mirrors and will track the sun, allowing uninterrupted cutting during solar availability.

Introduction

Since the launching of Sputnik in 1957 by the Soviet Union, and the explorer by the U.S.A. the following year, mankind has been sending spacecraft into orbit. The trend continues to this day. The remnants of these earlier launches have the potential to cause serious hazards. Some of these reenter the earth's atmosphere in a fiery manner, some have broken up in orbit and caused large numbers of junk pieces, and some pose serious threat of collision with future spacecraft. Several important organizations, including the GAO, OTA and NSA have written reports alerting us to the seriousness of the problem. Even if no future orbital debris are created, the existing ones are sufficient to pose a serious threat to our shuttle operations by 2000 A.D.

Traditional solutions, such as passive retrieval, boosting to higher orbit, etc., are not economical. Any viable solution must utilize the local resources to effectively remove the larger pieces before they break up into innumerable intractable pieces. Recognizing the abundant availability of solar energy (nearly 1.4 kW/sq.m), the microgravity that makes it easy to manipulate massive objects, and the high vacuum that quickly removes product vapors, it was decided that solar cutting of the debris would prove to be attractive. In addition, the existing databank on these large pieces indicates that we are reasonably sure of what we are dealing with; this enables us to preprogram a precise procedure to handle these debris. Also, many of these debris are in a fairly pristine state so that many of their parts are reusable. Examples include solar panels, structural members and simple circuit components. The general orbital mechanics calculations (see the 1988-89 annual report) show that the overall rendezvous and processing need not be propulsion intensive, so long as we are willing to wait approximately two years in orbit in order to process nearly ten times the launch mass of the ASPOD.

The rest is design and execution. Over the last four years, the students at the University of Arizona have designed, built and demonstrated successively improving generations of ASPOD. This year's project had the specific goal of incorporating an on-board sun tracker, reducing the mass of the basic frame and improving the arm design. All of these goals were met.

The components are described in the rest of this report. We expect rapid progress towards the completion of a high-tech lightweight robot with two coordinated arms, by the end of the 1993-94 period.

Project Description

Since the launching of Sputnik in 1957 by the Soviet Union and the Project Mercury Missions of the United States in 1961, mankind has been sending rockets and satellites into space. This trend continues even today. With this trend, the remnants of these launch vehicles are left to circle above us forever or until they decay and meet a fiery end in the Earth's atmosphere. At present, there are hundreds of scatter sections of old rocket boosters, broken satellites and smaller pieces, even down to the size of a fleck of paint, circling our planet in Low Earth Orbits (LEO) and High Earth Orbits. Near Earth Orbits are between 200 and 500 kilometers while High Earth Orbits are greater than 500 kilometers. These include the Geosynchronous Orbits. In our increasingly technological world where mass communications and scientific endeavors are king, we are facing pollution of our lands, our atmosphere, our water and now the very orbits our technology depends upon. This is especially true of the Low Earth Orbits where many of our present day satellites and manned missions are sent. Each time a space shuttle, a manned rocket or satellite is launched, it faces the risk of colliding with a piece of one of Man's past space missions. In fact, one small fleck of paint from an old Delta rocket collided with the shuttle, causing \$50,000 damage to a window. How much longer can this occur without the collapse of our system we have made for ourselves? Enter the concept of ASPOD.

ASPOD is a concept whose time is now. It is an acronym which stands for Autonomous Space Processor for Orbital Debris. This is a NASA project that is trying to clean up large space debris such as the old rocket boosters from 1960's launches of Apollo Program and later missions. The large repair bill NASA had to pay from that collision strongly illustrates the need to clean up space. It is fortunate that it was a very small fleck and not a booster rocket the size of a bus or those astronauts would not be here now. ASPOD is being developed, not to get rid of paint flecks but to get rid of those boosters before they break up to the size of paint flecks and can no longer be tracked.

Presently a Earth based prototype is being developed for demonstration purposes. The actual space model will be built later after the prototype phase is completed. It is comprised of several main parts: two robot arms which act as human arms and hands to manipulate the debris; a solar array, which consists of four gold-plated composite mirrors and five Fresnel lenses; two control boxes, one for controlling the arms' motion and the other to link the gears and motors to the solar tracker; and the solar tracking device, which acts to track the sun's motion using a photovoltaic device. The last part is the base and platform, which will have two degrees of freedom to track the sun.

ASPOD works using 6 degree of freedom robot arms, which can grab and manipulate the old space material and bring it to the focal point of the solar array. The solar array (Ramohalli, "A Robot for Retrieval of Orbital Debris, Hardware Experience," *AME Research Report 92-10*) works by reflecting the sun's light into the focal point for cutting. The solar array and the two arms have already been built. The two parts which our group has been designing are the platform and the control box that will run the mechanism of gears, motors, and the solar tracker.

Proposed Solution

The design consists, first, of an aluminum structural base. This base not only sustains both static and dynamic loads, but it also has the capacity to be easily modified in the future (welding, drilling, etc.). The solar tracking device is made from solar phototransistors which are available from local electronic supply stores at a reasonable cost. The kinematics of the table are accomplished using a power screw that offers both accuracy and rigidity for the tilt, and a pinion-gear setup for rotation. Finally, the control system not only has the ability to manage both incoming signals from the tracking device and outputs to the motors but it is flexible enough to be operated either in the automatic or manual mode.

Project Limitations and Constraints

Since ASPOD is meant to be eventually launched into space, there are many constraints on this project. There is a need to create a light but strong solar tracking table to focus sunlight in order to cut up space debris. There is also a need to have a table base that can demonstrate ASPOD's features while it is in the prototype stage of its development. The size, materials, weight, and cost of the project have been factors in our overall design.

As specified in a brief handout given to our group, the minimum constraints state that the solar tracking table will have two degrees of rotation, one horizontal and the other vertical. In the vertical, it should be able to rotate 45° either way, front or back. In the horizontal, tilting should be about 60° about the horizontal. These motions should work interdependently, with existing working parts. These parts are the two robot arms, the solar array with its mirrors, the solar tracker, and the table structure and platform. There can be no conflicts in motion between these parts.

To accomplish these tasks, the entire structure must be light and strong. There are many materials that meet these requirements, but due to cost only aluminum is economical for this project. Composites could work, but their cost and lack of structural integrity when impacted by drilling make

them infeasible for an earth-based structure. However, composites will be used when this project is eventually launched into space. For now, with a \$6,000 maximum budget of which we have decided only \$2,000-\$3,000 will be used, we will accomplish the design using aluminum. Aluminum has both the strength and lightness needed for this job.

The weights of this project are: for the base structure, less than 200 lbs, and the top of the table no more than 1200 lbs. The base will be able to support a minimum weight of 500 lbs, with a safety factor of at least 2. The 1200 lbs reflects this safety factor.

List of Constraints and Limitations

The solar tracking table must:

- Be light and movable by two individuals.
- Be strong enough to withstand static and dynamic loads.
- Not be heavier than 1200 lbs table-top weight.
- Have a base structure not exceeding 300 lbs.
- Have a factor of safety of at least 2.
- Have 2 degrees of rotation.
- Experience no interference with existing working parts.
- Not exceed the \$6000 maximum budget.

Group Limitations and Goals

- We wish to spend no more than \$2000 on the project to save the rest of the grant for future projects.
- Seek a weight for materials in the base to not exceed 200 lbs.
- Seek a deflection in the slider to not exceed 0.00001 inches. This is to insure that no bending of the power screw can occur.

Problem Definition

Design and build an Earth based solar tracking table which has a statically and dynamically stable structure, that can track the sun using a designed solar tracking device.

ASPOD Base and Structure

Selection of Materials

Due to the needs of this project, the design of the undercarriage of ASPOD had to take into account lightness and strength. It had to be able to withstand the dynamic and static loads of the moving platform. Therefore the selection of materials for this project's base structure was based on yield strength, weight, hardness for durability and finally cost. In the design we looked at steel, aluminum, and composite plastics such as fiberglass-Kevlar for materials.

We also looked at magnesium and titanium.

From Table 1-1, we decided to use aluminum as the fabricating material because of its high strength-to-weight ratio (350,000 inches), reasonable cost (about \$2-\$3 per pound), and high structural integrity. Although steel is

Table 1-1. Structure Materials, Average Values

Material	Modulus of Elasticity (PSI)	Yield Strength (KSI)	Weight (LB/in ³)	Relative Cost (\$/LB)	Hardness (HB)
Steel A-1 Structural	3 x 10 ⁶	35	0.283	0.70- \$1.00	293
Aluminum 7075-T6 (Sheet + Plate)	10.4 x 10 ⁶	70	0.101	2.00- 3.00	150
Aluminum 6061-T6 (Extruded)	10 x 10 ⁶	35	0.098	2.00- 3.00	95
Aluminum 2024-T3 (Sheet + Plate)	10.6 x 10 ⁶	50	0.100	2.00- 3.00	DATA NOT AVAIL- ABLE
Magnesium M K31A-H24	6.5 x 10 ⁶	23	0.0647	9.00- 11.00	DATA NOT AVAIL- ABLE
Titanium 6A/4V Sheet	15.9 x 10 ⁶	120	0.160	10.00- 15.00	DATA NOT AVAIL- ABLE
Fiberglass	1.8 x 10 ⁶	Ultimate 7	0.033	20-100	

Source: Engineering Mechanics of Deformations, p. 494
 and Jungstein Steel and Aluminum Company data (See Appendix A)

cheaper in cost (about \$0.70-\$1.00 per pound), aluminum has better properties in that it has the strength of steel but is almost one-third lighter. We also looked at magnesium and titanium and found that although they were reasonable in lightness and strength, they were too expensive for this project. Titanium Sales Inc. of Los Angeles gave quotes for titanium and magnesium. They quoted an average cost per pound of \$10-\$15 for titanium and about \$10.00 for magnesium. Lastly, composite materials like Kevlar and fiberglass, we found, had the strength and lightness but lacked structural integrity if at any time the frame might have to be modified (when drilling into the frame, these composites tend to lose their strength). One of the constraints of the project states that the material has to be modifiable. This is to ensure that additions to the overall project can be incorporated in the future.

The structure of ASPOD has been designed with aluminum due to its high strength and lightness. (See Table 1-1). Unfortunately, it is not as hard as steel. (See Table 1-1 for hardness comparisons). Where any moving parts are in ASPOD, they have been designed with steel in mind for

durability. The tilting shaft bar, all bolts and the powerscrew are of steel. Steel was chosen for the gears and powerscrew because of its wear properties. Any structural parts such as the I-beams, C-Channels, tubing and tilt arm are of 6061-T6 Aluminum Alloy. The reason for this is to reduce to overall possible weight of the design. The use of steel components have been minimized and are only used in the most critical areas of the structure which undergo the most stresses.

The Old Structure

The old structure of ASPOD was a table mounted on two 3" square tubing uprights with a tilting bar placed between them. This table was tilted up and down like a see-saw by a single 14 inch diameter gear which kept it from falling to the floor. This gear maintained the position of the table and was driven by a small 1/12 horsepower motor. There were several problems with this design. First, the weight of the components on the solar tracking table are precariously balanced on just this one gear, making the design very unstable. When our group was assigned this project, the tabletop was tilting under its own weight and had to be supported on the mirror side by two removable, aluminum rods on either side of the mirror array. These ran vertically from the table to the runners below. The previous designers had added the two removable aluminum bars to stabilize the structure and had mounted them on the rear of the table to the stabilizing runners. The second problem was, that the previous designers did not design ASPOD to work interdependently because each part was designed independently and with no regards to the other moving parts. These parts were then mounted to a makeshift table structure. In doing so, the center of gravity and mass were not centered because the previous designers did not take them into account in the overall design.

The Final Design

With the limitations and constraints placed upon us by this project and its backers, the design of ASPOD's present base structure necessitated that it be changed. All parts of ASPOD needed to work interdependently and the base needed to be strong and stable. In its present form, ASPOD's existing design failed on the first count and on the second count failed in the area of stability. Because of this instability, we have partially redesigned the base structure. Our design incorporates a rigid yet strong base of I-beams, a screw drive system with a C-Channel framework, a tilt table with a tilt arm, a turnstile and a lighter tabletop (See Figures 1-1 and 1-1a). Our final design has eliminated the stabilizing bars and the tilting 14-inch gear. The essence of the design of the base is mostly a design modification of the existing structure.

Structural Beams

From our calculations, the beams needed to support the table had to be made of certain cross-sectional areas. After looking at many types of beams, C-Channels and I-beams were found to satisfy this needed criteria. The I-beams chosen are of two types. One type that was chosen is 5 inches wide, while the other was 6 inches wide. Both are approximately 3 inches deep. The C-Channel is 5 inches

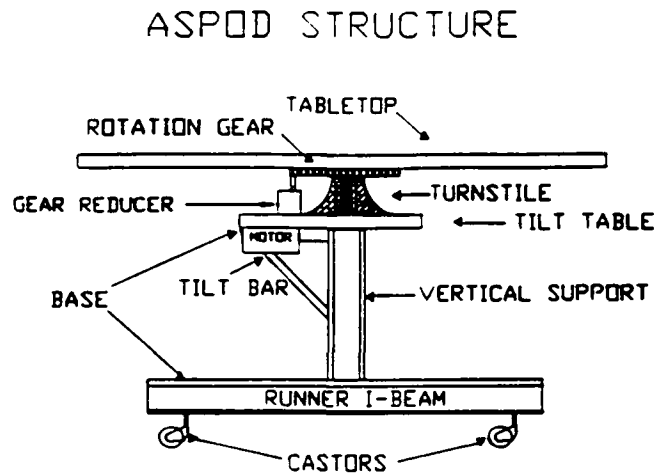


FIGURE 1-1

wide and it has 2.25 inch depth. These bars are of aluminum, as stated in the material section of this report. The old structure is adequate but unfortunately too heavy, being made of steel. This project needs to be lighter than the existing design. Therefore aluminum, which has the strength of structural steel, is best for the job. A list of beams needed for the structure is listed in Table 1-2.

(TABLE 1-2) I-Beam and C-Channel Dimensions

	Beam #1		Beam #2		C-Channel	
	Inches	lb/ft	Inches	Lb/ft	Inches	lb/ft
Weight		3.508		4.412		2.250
Width	5.00		6.00		5.00	
Height	3.00		3.30		2.25	
Thickness	0.210		0.230		0.15 web	
					0.21 flange	

As seen in Figure 1-2, the base support structure is made up of I- Beams of various dimensions. From information supplied by Jorgensen Steel and Aluminum Company of Phoenix, Arizona, we selected two Aluminum 6061-T6 Alloy I-beams and one C-Channel beam of the dimensions below.

DESIGN FOR ASPOD

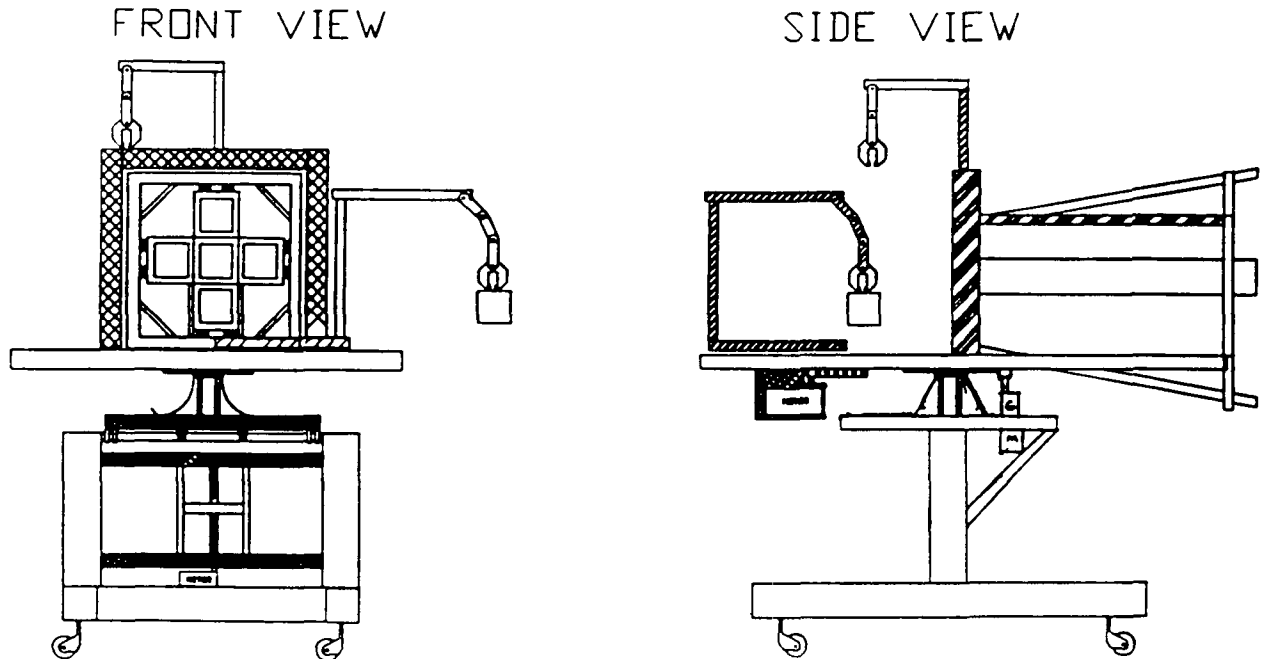


FIGURE 1-1A

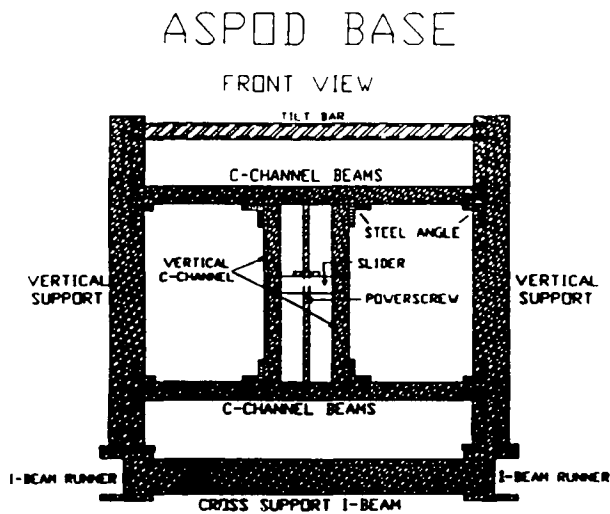


FIGURE 1-2

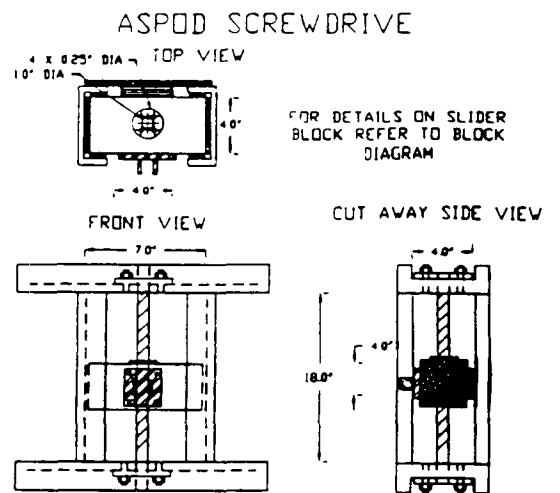


FIGURE 1-3

For this paper we will refer to the I-beam type as Beam #1 and Beam #2:

The C-Channel acts as both cross supports and as a guide for the screw drive and slider. See Figure 1-3 for further

details.

These beams and channels follow the existing design set up. There are two 34.5 inch vertical supports made up of Beam #1. These stand 36 inches apart on the two runner beams. These runners are of Beam #2 and are bolted to the bases of the vertical supports through use of 2"x 2"x 0.125" aluminum angles and 1.25"x 0.375" diameter steel bolts. These angles and bolts ensure stability of the vertical supports. They are mounted on each side of the vertical supports through eight drilled holes in each runner and through each vertical support. See Figure 1-2 for further details. To connect these supports and runners, a crossbeam of Beam #1 and a piece of C-Channel, both 40 inches long, has been placed between them and anchored inside the channel of the I-beam runners. This crossbeams is bolted in the same fashion as above. In the future, it may be welded to the base structure.

Parts Description and Uses of Beams

The Screw Drive

Six inches above the crossing I-beam is mounted the screw drive framework. See Figure 1-3. This screw drive system both stabilizes and tilts the table. This screw drive system is mounted between the two vertical I-beams. The powerscrew of this system is mounted through a slider block. This block will be connected to a tilt table through a square aluminum bar that act as a tension and compression rod to tilt the table. The screw will be mounted between 2 vertical C-Channels which maintain the slider on the screw in channel guides. It is constrained to move only up and down and not side to side using teflon and nylon plate bearings.

This framework is mounted to the supports by means of angles and bolts as in the above section. It is not welded to the supports so that the screw drive can be removed if damaged somehow. This helps in facilitating replacement of the powerscrew.

The framework consists of two, 40 inch long horizontal Channels, one mounted 10 inches up from the I-beam crossbeam while the other will be 28 inches up from the I-beam. Between these two channels will be mounted two 18 inch long, vertical Channels spaced three inches apart that will hold a 6.5"x 4"x 4" solid aluminum slider that will ride up and down on the powerscrew in the grooves of the C-Channels. This design allows for the absorbing of forces and moments into the frame and not into the powerscrew. By calculations, this design can withstand a 800 pound horizontal force and a 1800 pound vertical force, which would create a 167 foot pound moment on the slider.

The slider is made of 6061-T6 Aluminum and has been machined down to necessary dimensions to fit into the slot. It has been mounted to 1/4" thick teflon and 1/2" thick nylon bearing plates to allow for easy sliding movement up and down. In the middle of the slider, a one inch hole has been drilled through it to mount the powerscrew and a steel bearing. The bearing has been inserted into the hole to ensure the powerscrew does not damage the slider by wearing on it.

The powerscrew is made of high strength steel. It is 3/4" in diameter and 24" long. The working part of the screw is 18 inches long. The rest of the screw is used to mount through the two horizontal channels to the gears and bearings. For further information refer to Section II of this paper.

The Tilt Table and Tilt Arm

Above the screw drive, mounted to the tilt bar is a small tilting table consisting of a 27"x 36"x 0.25" aluminum plate with a support framework that tilts the ASPOD tabletop up to 60 degrees one way. This tilt table is mounted on top of the steel tilting bar.

This design was necessitated because the old design did not separate the tilting from the rotating part of the solar tracking table. A motor mounted beneath the table turned a small gear which rotated about the welded gear to turn the table. Our design eliminates this concept and creates a freer rotating axis unencumbered by any obstacle. Our design allows for a 6 inch clearance between the two tables to allow for freedom of movement in the horizontal. A motor has been mounted beneath the tilt table and is attached to a gear reducer that lies within this clearance space. See tilt table drawing. This table is made of 1" square tubing and a 25" long section of C-Channel. The dimensions of the tubing are as follows:

The channel and the tubing have been welded together. The framework forms a diamond or kite-shaped pattern and is welded to a 1/4" thick aluminum plate. The whole table is attached across its center to a 40" long, 1.75" diameter steel tilting bar by means of 4 aluminum 5.5"x 5"x 0.75" anchor plates. These plates have a 1.75" diameter hole cut through them to allow the steel tilting bar to slide through them. The plates are held in place on the bar through the use of set screws. The tilt bar is mounted to two side bearings on the base vertical supports 3" down from the top of the vertical supports. The side bearings themselves are attached to each upright support by two 1/2" diameter by 1.5" long bolts.

The tilt table is also supported by a tilt arm which runs up from the slider to the end of the tilt table. The measurements of this arm are 23"x 1"x 1". It is attached to a cross bar that distributes the forces of the tilt table to the tilt arm. This arm is able to withstand bending and buckling loads up to 4000 pounds given a factor of safety of two. Actual loads though are calculated to range from 1300 to 2000 pounds depending upon where the tilt arm is mounted in relation to the table's moment arm. When mounted at 12", the load is 1400 pounds max at 60 degree tilt.

The Turnstile

The turnstile is mounted on top of the tilt table and underneath the tabletop of ASPOD, centered in the middle of the tilt table and roughly under the front part of the mirror array. See Figure 1-1a for details. This turnstile is made out of aluminum plates and pipes. Its design incorporates both strength and lightness. The six vertical, 0.25" thick, machined plates in this design act to give support and resist bending and shearing in the aluminum pipes that hold the two inch diameter steel shaft in place. Two, 6" diameter, aluminum bearing plates are mounted to the two parts of the turnstile. The bottom part consists of a 8" base that is bolted to the tilt table and acts to distribute the weight evenly from the rotating solar tracking table to the tilt table. The top section is attached to an aluminum plate and the tabletop above where it is anchored in by bolts. These two parts face each other and allow turning through slots cut and grooved into them for placement of 1/2" thick, 3" outer diameter, teflon ring bearings. All parts of the turnstile mentioned, except for the steel shaft, have been welded together.

The Tabletop

ASPOD's tabletop is much like its original steel design but it is made of one inch square aluminum square tubing like the tilt table. This frame is 7.5 feet by 4 feet in area. Final plans are to overlay it with a 7.5'x 4.5'x 0.75" laminated plywood board. This is six inches wider than the existing table. This will be done because the front robot arm's turning diameter is 4.5 feet wide and by making the overall width 4.5 feet, this will make ASPOD more structurally sound and visually appealing. At the time of the writing of this report, this has not been done due to some modifications which are required on the mirror framework of ASPOD. In addition, the main swivel robot arm shaft has been cut down and attached to a small gear set with a five to one gear ratio. These gears control the movement of this robot arm. With these changes, this design will allow for more area in which to mount future objects.

Selection of Power Screw and Slider

A Structural Prospective

The selection of the powerscrew from a structural standpoint is based upon its ability to resist bending. As seen in Figure 1-8 a 3/4" diameter screw resists bending better than a 1/2" diameter screw. It also resists horizontal forces better. Therefore, from a structural standpoint we have used a 3/4" diameter screw. As for the slider, our group looked at three different beams to resist the forces and moments on the powerscrew. These slider shapes and the final design dimensions are shown in Table 1-4 below:

(TABLE 1-4) Slider Block Design and Dimensions

Design Type	Length Inches	Width Inches	Height Inches	Thickness Inches	Weight Pounds
4" C-Channel	8.0	4.0	2.25	0.188	1.22
Solid Slider #1	8.0	4.0	2.0		6.4
Solid Slider #2	8.0	4.0	4.0		12.8
Final Design	6.5	3.8	3.8		9.4

**0.5 AND 0.75 INCH DIAMETER SCREWS
 WITH A 2.4E-04 INCH DEFLECTION**

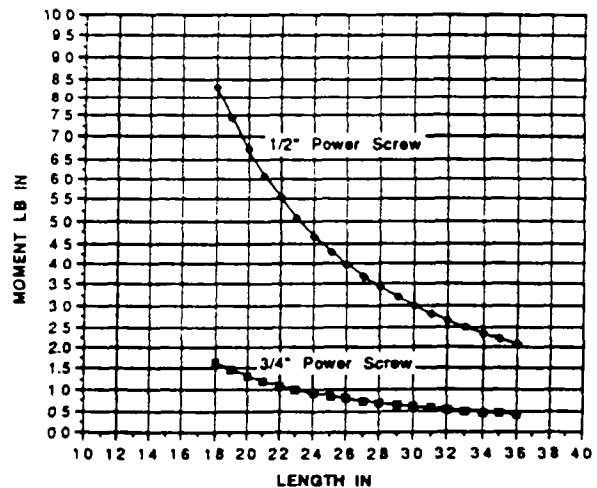


Figure 1-4

The slider block's constraints state that it has to be able to resist bending in two directions and also a vertical torque to prevent damage to the screw. To ensure this, we sought a deflection of less than 0.00001 of an inch because we wanted a stiff slider. From calculations, the best slider design that can resist the forces is a solid 3.8"x 3.8"x 6.5" block. The present vertical force in our design has a 1300 pound load acting on the slider vertically and 300 pounds horizontally. The 4"x 4" cross section satisfied our requirement and also resisted the moments on the slider very well. The lengths of the slider, we determined by varying its length from 4 inches to 12 inches. From the graphs in Figure 1-5, we found that the deflections increased with increasing length. When graphed together, the greatest deflections were in the 12 inch beam while the least was in the 4 inch beam. We sought to optimize this concept while maximizing the surface area for mounting the tilt arm. From this information, we selected a 8 inch long 4"x 4" aluminum solid slider. This design satisfied our low deflection requirement and it transmits little or no force to the screw in the horizontal. Unfortunately, this design length was found to be too heavy. For our final design, the slider was cut back to the dimensions shown in Table 1-4. See slider block diagram for specific details.

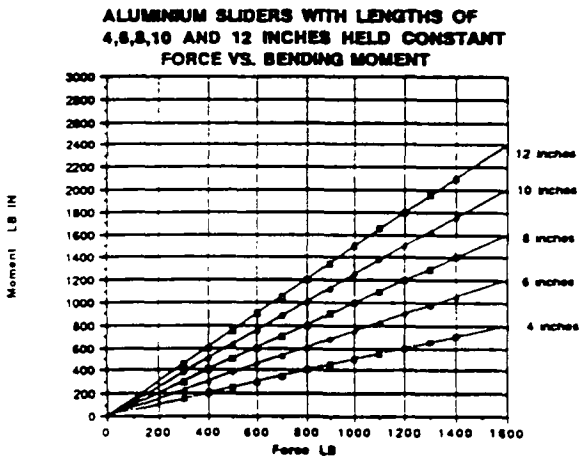


Figure 1-5

Structural Comments

The final design seems at first to be over-designed in comparison to the old ASPOD structure. This is not the case in reality. Our design takes into account all static and dynamic loads. It is partially for this reason that some of the I-beams may look out of proportion to the rest of the structure. The runners have a safety factor of 5 in bending. They were chosen more for their surface area in mounting the uprights because they required a beam with a 3.3 inch

width. Angle brackets would also be mounted to this area so as to hold the uprights in place through the use of bolts. None of these parts could be mounted without this needed surface area.

As it stands now, the runners will allow for the placement of the two arm control boxes and their computer. These will be mounted in a very well protected area between the two runners and the two crisscross smaller, Beam #1 I-beams that keep the runners together. The second crisscross I-beam was added as an addition to the structure to allow mounting of the computer and act as a pulling and steering bar for ASPOD. This can be done by adding to this I-beam a jack mount for steering purposes.

The old structure in contrast was built hastily and was originally designed to carry only the Fresnel lenses and mirrors. It was not designed to carry the robot arms and any other equipment necessary for demonstrating this project. When these parts were placed on the old structure, it started to fall apart. Our new structure is designed to handle existing and future components. This is the reasoning behind the supposed over-designed looks. It will carry the two robot arms and the mirror-lens assembly on the rotation table and two control boxes and a computer for the arms underneath the table mounted on and between the I-Beam runners. This structure needs to be durable and take into account the future of this project. Previous design projects on ASPOD were looking only at the present and were very short sighted which lead to various components being incompatible with each other. This is not the case with our design. In the limitations and constraints section of this report, we were given several limitations to overcome. In relation to the structure, we have satisfied these specifications. The following is a list of the satisfied limitations:

1. The base structure has an overall safety factor of two or greater. The design is capable of handling a 1200 pound static tabletop load without buckling or bending. The structure also takes into account dynamic loads up to 1800 pounds.
2. There are two degrees of freedom of motion in the solar tracking table. The structure satisfies the ± 45 degree rotation and the 0 to 60 degree tilting required by the specifications. The design in this area surpasses this criteria and at present can tilt from 0 to 80 degrees to allow for tracking the sun in the summer as well as in the winter. Plans are to further increase this tilting to up to 90 degrees. This is to allow the tracker to track the sun without stopping on June 21st during the summer solstice when the sun climbs above 80 degrees at high noon. This is beyond the scope of this report though and will be done at a future date.
3. There are no conflicts in moving parts in the structure.

The components are now all working interdependently. In addition, the design will allow for further additions to the structure and two tables.

4. The weight of the base and tables together are calculated to be 262 pounds. This satisfies the requirement that the overall base and skeletal table structure be less than the 300 pounds specified in the project limitations. This allows for ASPOD to be light enough to be moved by two individuals.

5. The widest dimensions of the base structure and the two tables allow for easy handling through doorways if ASPOD is being stored or being shown in an inside demonstration.

6. The overall cost of the redesign was less than the maximum \$6000 budget limit. See Cost Analysis section of this report for further details.

As one can see, this structure has been a challenging one. It required many man hours of work machining, cutting and building. Whenever possible, we have used existing materials and ordered items such as with the I-beams pre-cut to order to minimize work time. In other cases, such as with the powerscrew, slider and turnstile, this was not possible and we used the machine shop. We worked from the ground

up. We started with the base, then the tilt table and finished with the table top. This was our approach and it worked relatively well.

References

1. Ramohalli, "A Robot for Retrieval of Orbital Debris, Hardware Experience," AME Research Report 92-10".
2. Byars, Edward F., Snyder, Robert D. and Plants, Helen L., "Engineering Mechanics of Deformation", Second Edition, Harper Row Publishers, 1983.
3. Gere, James M., and Timoshenko, Stephen P., "Mechanics of Materials", Second Edition, PWS-Kent Publishing Company, 1984.
4. Askland, Donald R., "Science and Engineering of Materials", Second Edition, PWS-Kent Publishing Company, 1989.
5. Juvinall, Robert C. and Marshek, Kurt M., "Fundamentals of Machine Component Design", Second Edition, John Wiley & Sons, Inc., 1991
6. McDonald and Lowe, "Feedback and Control Systems", Reston Publishing Company, Inc., 1981

PLANETARY AND ASTEROID MISSIONS -- GETTING THERE

University of California, Los Angeles
 Mechanical, Aerospace and Nuclear Engineering Department
 Los Angeles, California

Professor Rudolf X. Meyer

ANCHORING SPACECRAFT TO ASTEROIDS

Joseph P. Melko - Teaching Assistant

Abstract

In this hardware project, the students developed ideas for attaching objects to the surface of small moons or asteroids. A device was designed, and built in the university machine shop, that uses a projectile shot into concrete, thereby attaching a model spacecraft to the landing site.

Introduction

Past exploration of the solar system has been concerned almost exclusively with large objects such as planets, the sun and our moon. However, increasing attention is now being paid to the smaller bodies, not only because of the wealth of information they may contain, but also because of their potential as propellant sources, support points for long space missions and bases of operations. Their usefulness in these areas is due in large part to their extremely low gravity which makes them very accessible and allows easy departure.

The microgravity encountered on these bodies does present some challenges, however. Not only is it easy for equipment to shift orientation or leave the surface due to internal movements, but for any action such as core-boring or drilling, a positive restraint is needed. This project seeks to address the problem of keeping probes, landers, and equipment on the surface of these tiny bodies.

Anchoring Concepts

Several ideas for anchoring devices with various capabilities were studied. Initial ideas fell into the categories of tethered projectiles, drills and hot probes. The hot probes melt into the surface, then cool down to fuse with it. The question of a deep regolith inspired ideas such as a combination of a large auger which would work its way

down to the rock and then fire a tethered projectile contained in its tip. Another idea was a "mole" machine to burrow down through the regolith letting out a cord as it went (Fig. 1.1). When it reached rock, the "mole" would fuse itself to the rock or fire a projectile. Various designs allowed multiple anchor placement without moving the lander. These systems increase complexity, but improve anchoring reliability.

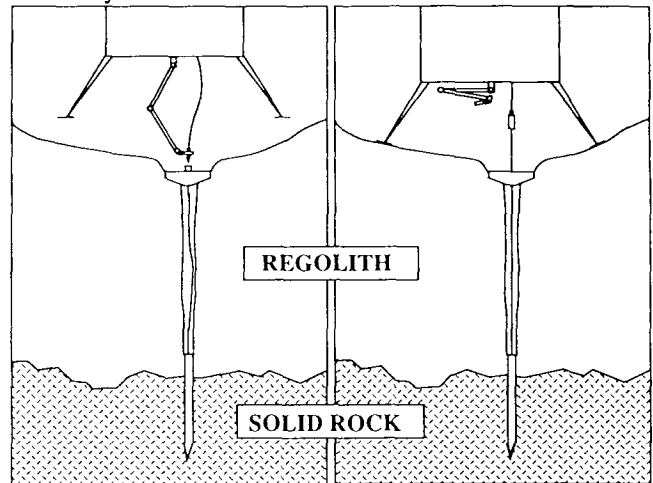


Figure 1.1: One of the various concepts for anchoring systems.

The tethered projectiles appeared to be the best choice in terms of reliability, simplicity, cost, weight, and mission flexibility. Design of the actual penetrator would be a major study in itself. Penetrators which use superheated liquid in their tip may greatly reduce velocity requirements. Recoilless penetrator systems may offer less weight and greatly decrease shock loads to the lander, but flexibility is more limited as exhaust gases must not impinge on sensitive components.

Although there were many ideas for use in outer space, few fit the safety requirements for a laboratory demonstrator. The concept chosen for demonstration was the simplest and employed common technologies which were already well proven.

Mechanical and Electrical Design

The design solution (Figs. 1.2a,b) is based largely upon a common concrete nail gun. It employs a hammer, guided by a tube and set in motion by a spring. The hammer strikes a cartridge which ignites and fires a projectile down the barrel into the surface. A motor winds up the line, which is attached to the projectile prior to insertion into the barrel. This pulls the lander to the surface and holds it there. Other major components of the design include assemblies for lowering the barrel to the surface and cocking the hammer, both of which employ a power screw driven by a motor. The trigger mechanism is operated by a solenoid.

As the device was intended to be used as a demonstrator, several support systems had to be designed and built including a tripod lander. A system of long springs was employed to simulate a weightless environment. Other systems include the safety cage, control electronics, and various simulated asteroid surfaces.

Possible Uses on Phobos

Phobos was studied as a possible near term use for this type of device. Phobos is a small moon of Mars which is receiving attention as a possible propellant source and way station for a manned exploration of Mars. Various characteristics such as composition, topology, regolith and gravity characteristics were investigated. The need to anchor equipment is evident as the gravity is roughly 1/2000th that of earth. Although most of Phobos consists of solid rock (probably carbonaceous chondrite), the presence of a regolith of variable depth (possibly up to 300 meters) raises questions about the ability of the device to work on all points of the surface. There is evidence that the regolith is very thin near recent impact areas, the tops of ridges and the rims of craters.

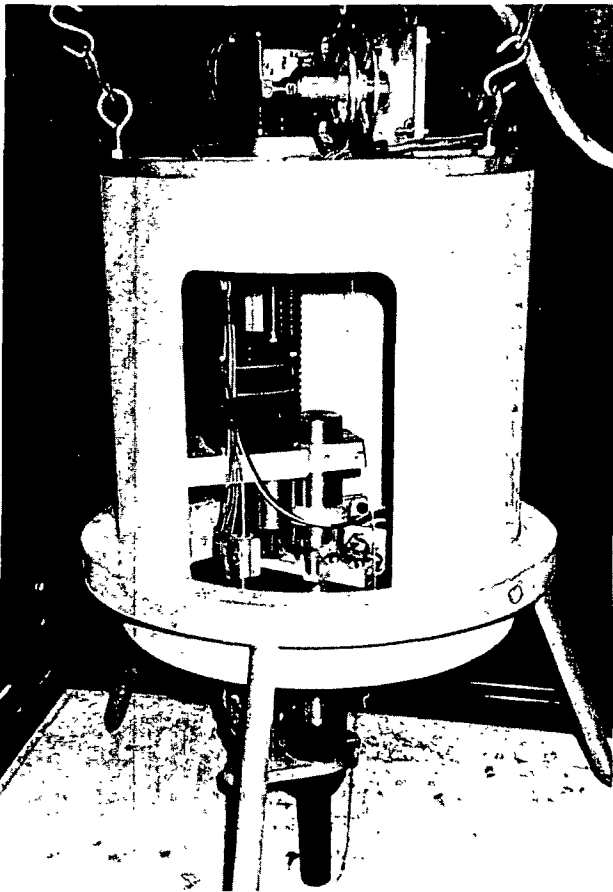


Figure 1.2a: Student-designed anchoring device shown in the firing position.

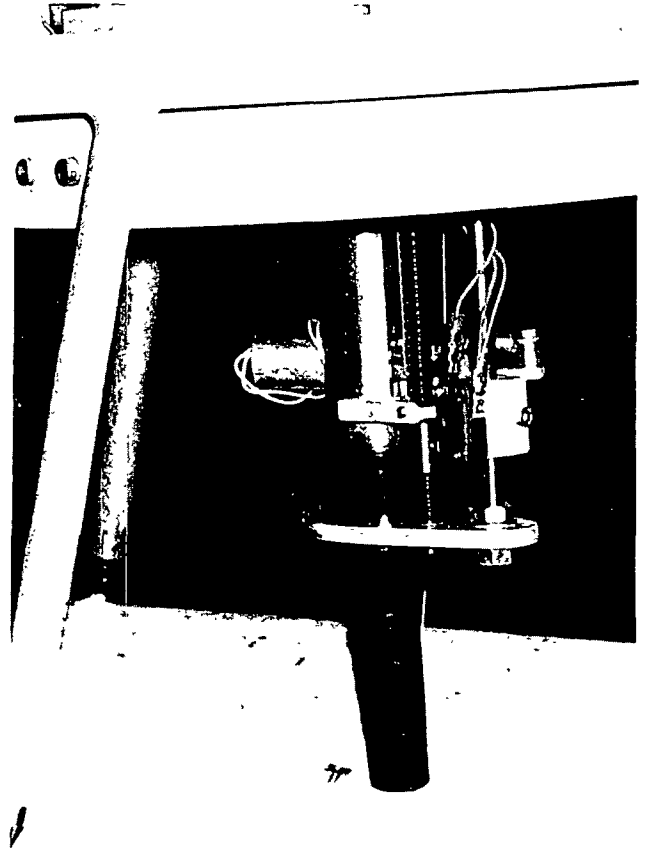


Figure 1.2b: Close-up of the barrel. The hammer has been uncocked.

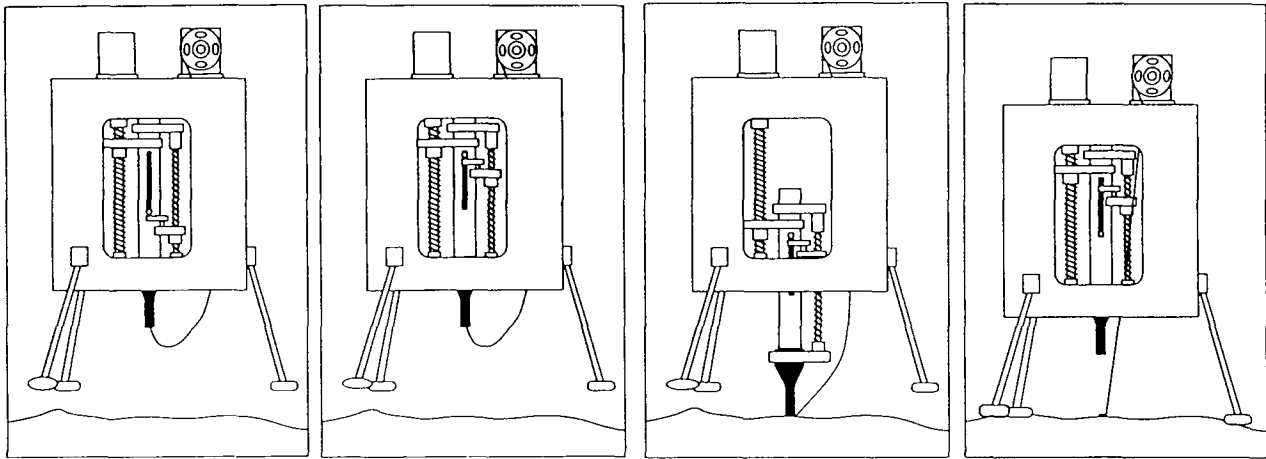


Figure 13: Operation of the final design. The spacecraft arrives at the surface(1). The hammer is cocked (2). the barrel is lowered and fired (3). The gun is raised as the spacecraft is lowered to the surface by winding the cord (4).

Conclusions

Testing has shown the device to work on concrete surfaces of various compositions. The device also works on ice if the projectile is heated prior to insertion into the barrel. Tests with ice and weaker concrete have suggested that longer projectiles would work better in these surfaces, but for reasons of laboratory safety the barrel was designed only for small nails. Only the lightest powder loads are used in the demonstrator. The construction industry uses loads up to seven times higher in nail guns of about the same size as our device. This implies that a device no larger than the demonstrator, without the housing, may be more than capable of performing the necessary anchoring on real missions. A device designed for electrically fired cartridges and lower reusability could be very lightweight and compact. Due to the variable surface characteristics of Phobos it is possible that no single device will work in all situations.

ION ENGINE PROPELLED EARTH-MARS CYCLER

Daniel Limonadi - Teaching Assistant

Abstract

The goal of this project was to perform a preliminary design of a long term (life span ≥ 15 yrs), reusable transportation system between Earth and Mars which would be capable of providing both artificial gravity and shelter

from solar flare radiation. The heart of this system is assumed to be an ion engine propelled cyclor spacecraft launched several years in advance of a manned mission. Several Mars transportation system architectures and their respective space vehicles were designed.

Introduction

General interest within the space community regarding Mars transportation system architectures has been on the rise since the mid 1980's. One class of these systems seeks to provide artificial gravity and shelter from radiation storms caused by solar flares during transit to and from Mars. Due to the expected structural constraints and large mass that an interplanetary transit vehicle meeting the above requirements is expected to have, low thrust, but very high specific impulse ion engines are assumed to power the vehicle (henceforth called the Cyclor). Several aspects of such a transportation system were investigated. They included: 1) preliminary thermal, power, propulsion, structural design, and transit time requirements of a cyclor vehicle and its particular orbital trajectory; and 2) the requirements placed on the planetary vehicles which would transport crew and cargo between interplanetary transit vehicles (the cyclors in the case of personnel transfer) and the surface of Mars and/or orbiting platforms. Emphasis was on trajectory design, the propulsion system and aerobraking.

Assumptions and Requirements

Several baseline assumptions were made which were incorporated into the various vehicle designs:

- propulsion system baseline performance ("Cycler")
 - ion drive; $I_{sp} = 10000$ sec.
 - LOX/LH2 system used on planetary vehicles ("Taxis"); $I_{sp} = 480$ sec. based on a mixture ratio of 7:1
- Nuclear reactor power to mass ratio; 8 kg/kW

•*Mars Infrastructure:* Mars infrastructure assumptions played a crucial role in defining the vehicle requirements and orbits used near the planets. The infrastructure varied from design group to design group, though a basic item which all groups included was some form of refueling station at Mars, either at Phobos or in a low orbit. Other options generally included LOX production on the surface of Mars, based on ideas presented by Zubrin¹.

•*Earth Infrastructure:* The Earth infrastructure was assumed to be in place starting at the time of the cycler vehicle assembly and generally included a space station in LEO, a vehicle assembly and servicing facility, a Moon base which supplied LOX to the transportation system, and orbital transfer vehicles (OTV's) to service the Earth-Moon system.

To help constrain portions of the vehicle design, a set of baseline requirements were made:

- The largest pressure vessel and other fabrication intensive components of any vehicle were required to be able to be placed into orbit by a launch vehicle currently in use or on the drawing boards; e.g. Shuttle, Spacelifter, Energia.
- The distance between the center of mass and crew quarters of the cycler vehicle was to be such that the Coriolis acceleration associated with a spin rate sufficient to induce 0.5g artificial gravity in the crew compartment would not be greater than 5% of the induced artificial gravitational acceleration, based on a assumed walking speed of 0.5 m/s relative to the vehicle.

Orbit and Trajectory Design

The orbits and trajectories analyzed for the Mars transportation system fall into two broad groupings: 1) interplanetary and 2) planetary (much like the vehicles that use them).

Interplanetary Orbits

One of the most important decisions to be made by the design groups was the type of interplanetary transfer orbits for the cycler spacecraft. Three classes of orbits were investigated: conjunction class minimum energy orbits; VISIT orbits; and Up/Down Escalator orbits. Table 1 shows some constraining parameters associated with these orbits. The basic trade-off between the choices focused on ΔV requirements for planetary access, frequency and regularity of cycler encounters, and crew transit time between cycler and destination planet. The final choice of the cycler orbit strongly affects both cycler spacecraft and planetary transfer vehicle design. Planetary approach velocities and transfer times especially play a defining role in design requirements for the crew/cargo planetary transfer vehicles.

The ΔV requirements required of a cycler spacecraft in conjunction orbits make it impossible to rely solely on high efficiency ion propulsion systems since these systems are inherently low thrust. Thus the main candidate orbits for cycling spacecraft are the VISIT and Up/Down Escalator orbits. However, the conjunction orbits do represent the minimum energy one way trajectory and are thus ideally suited for cargo transfer vehicles which are not restrained by requirements protecting human cargo.

Planetary Trajectories

The type of planetary trajectories executed by vehicles of the Mars transportation system are not strongly affected by the choice of interplanetary transfer orbits. However, the magnitude of the associated ΔV 's for each maneuver is strongly dependent on the type of cycler orbit chosen. Table 2 shows a sample list of trajectory sequences and associated ΔV requirements for shuttle vehicles operating between cycler spacecraft, target planet's parking orbit, and planet surface. The values given in Table 2 are based on worst case Up/Down escalator orbit encounters at Earth and Mars. Insertion into a 3600 km parking orbit is assumed at Mars, and a 6671 km parking orbit at Earth (distance taken from center of planet).

Table 1: Cyclor orbit constraining parameter comparison²

Parameters	Visit - 1	Visit - 2	Up escalator	Down Escalator	Conjunction ³
Frequency of Earth encounters [yr.'s]	5.0	3.0	2.14	2.14	
Frequency of Mars Encounters [yr.'s]	3.75	7.5	2.14	2.14	
Earth to Mars flight time [yr.'s]	0.5-3.0	1.0-2.4	.43	1.71	0.7
Mars to Earth Flight Time [yr.'s]	0.7-3.3	0.6-2.1	1.71	.43	0.7+
Earth Encounter V [km/s]	4.2-4.8	3.7-4.0	5.7-6.2	5.4-6.0	2.29-3.51
Mars Encounter V [km/s]	3.7-4.1	2.6-2.8	6.1-11.7	6.6-11.6	1.98-3.28
Earth Encounter Distance [R_E]	6.9-SOI	8.3-SOI	1.2-1.9	1.2-1.8	
Mars Encounter Distance [R_M]	1.5-40.7	2.0-18.5	1.3-29.1	1.3-9.4	
Midcourse adjustment, 15 years [km/s]	0	0	1.7	2.0	
Max. Earth access V, 14 days [km/s]*	5.5	5.2	4.8	4.7	
Max. Mars access V, 14 days [km/s]*	2.9	2.2	9.4	9.2	

* Sum of ideal injection and rendezvous maneuvers.

SOI : Sphere of influence of given body.

Table 2: Sample Trajectory Sequences at Earth and Mars for Planetary Transfer Vehicles (Calculations are based on worst case Earth and Mars encounter conditions for Up/Down Escalator orbits. Three days are allowed for shuttle transfer to Mars, and 1 day for transfer to the Cyclor at Earth.)

	ΔV [km/s]
1. Hyperbolic Earth Escape	4.69
2. Cyclor Rendezvous (Earth)	0.07
3. Transfer to Mars intercept	0.372
4. Retrofire	1.77
5. Mars aerocapture	6.39
6. Orbit circularization	0.02
7. Dcorbit	0.22
8. Ascent to parking orbit	4.4
9. Hyperbolic Mars Escape	9.13
10. Cyclor Rendezvous (Mars)	0.10
11. Transfer to Earth Intercept	0.07
12. Earth aerocapture	5.62

The most significant differences in planetary ΔV requirements arising from cyclor orbit choices are found in the hyperbolic escape requirement at Mars and the ΔV required for transfer between the hyperbolic trajectories of the cyclor vehicle and the hyperbolic trajectory required by the shuttle to intercept the target planet or return to the cyclor from a planet. A simple formula relating the ΔV cost of changing these hyperbolic trajectories is given by Friedlander³ et al¹, $\Delta V = \Delta B/\Delta T$, where ΔB is the difference in the impact parameter of the two trajectories and T is the time allowed from injection to rendezvous. Due to the large approach distances of the cyclor spacecraft traveling in Visit orbits (beyond the sphere of influence of the Earth in the worst case) relatively large ΔV penalties are required to keep the crew transfer times reasonably short i.e. less than 21 days. In the case of the Up/Down escalator orbits the approach distance is short enough to enable transfer times as short as 1 day with little penalty. The main concerns regarding transfer times in these situations deal with

minimum shuttle size to keep the crew relatively comfortable for the duration of the transfer, and more importantly, minimize the risk to crew members of exposure to radiation caused by solar flares. Although the Up/Down Escalator orbits have the advantage of a small ΔV penalty for short crew transfer time, the very large ΔV requirements for injection into hyperbolic rendezvous with the approaching cyclor spacecraft at Earth, and especially Mars, place a great demand on propulsion requirements. Unless it is required that crew transfer times for the VISIT orbit cases be reduced to much shorter time periods than one or two weeks the Up/Down Escalator orbits require more propellant.

Vehicle Design

The Vehicles comprising the Mars Transportation System can be grouped into two major categories: planetary vehicles and interplanetary vehicles. This categorization is based on where the particular vehicle carries out its principal mission. The individual vehicles and their primary roles are presented below:

Inter-Planetary Vehicles

Elements of the Mars Transportation system operating primarily in interplanetary space include the cyclor spacecraft and cargo delivery vehicles which use minimum energy orbits.

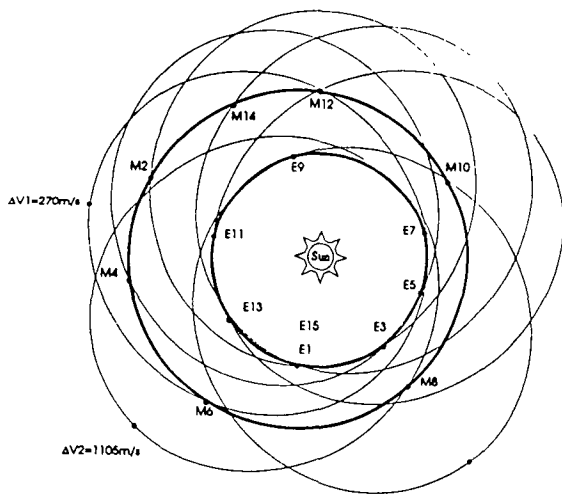


Figure 2.1: Up/Down Escalator Orbit Evolution over a 15 Year Period. Planet Encounters number in Sequence or Occurrence; E - Earth, M - Mars Encounter. (Scale 1.5 in = 1 AU).

Cyclor Spacecraft.

The cyclor spacecraft provide transportation between Earth and Mars for all personnel. Their size and trajectory choice are the primary factors which differentiate these vehicles from other proposed Mars transfer vehicles. As mentioned in the Introduction, the primary requirements for the cyclor vehicles are an artificial gravity environment and radiation storm shelters. In addition, there is need for tanks to contain the argon fuel for the ion drives, docking and possible hangar facilities for Taxi spacecraft, antennae, a nuclear reactor and associated shielding, radiators and power conversion plant, and, depending on the particular design solar arrays, greenhouses, and remote sensing equipment. Figures 2.2 and 2.3 show some Taxi, OTV, and cyclor vehicle design layouts.

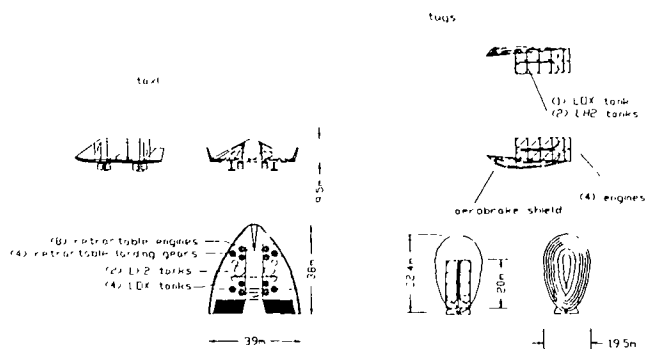


Figure 2.2: Left - Taxi Vehicle Utilizing High L/D Body Configuration. Right - Orbital Transfer Vehicle with Raked-Off Elliptical Cone Aerobrake.

Cargo Delivery Vehicles.

These vehicles are necessary to provide the ability to move large amounts of cargo between Earth and Mars. They basically consist of cargo pallets fitted into an aeroshell and provided with a propulsion system whose sole purpose is to provide attitude control, orbital correction ΔV 's to insure proper atmospheric entry geometry at Mars, and to deliver the cargo into a circular parking orbit upon completion of the aerobrake maneuvers at Mars. Some initial mission designs had the large cargo delivery carried out by cyclor spacecraft in an attempt to minimize vehicle types. Upon further analysis it was deemed that the inefficient use of propellant due to the ΔV injection requirements into higher energy Up/Down Escalator and VISIT orbits vs. those required for low energy conjunction orbits outweighed the benefits of a smaller infra-structure.

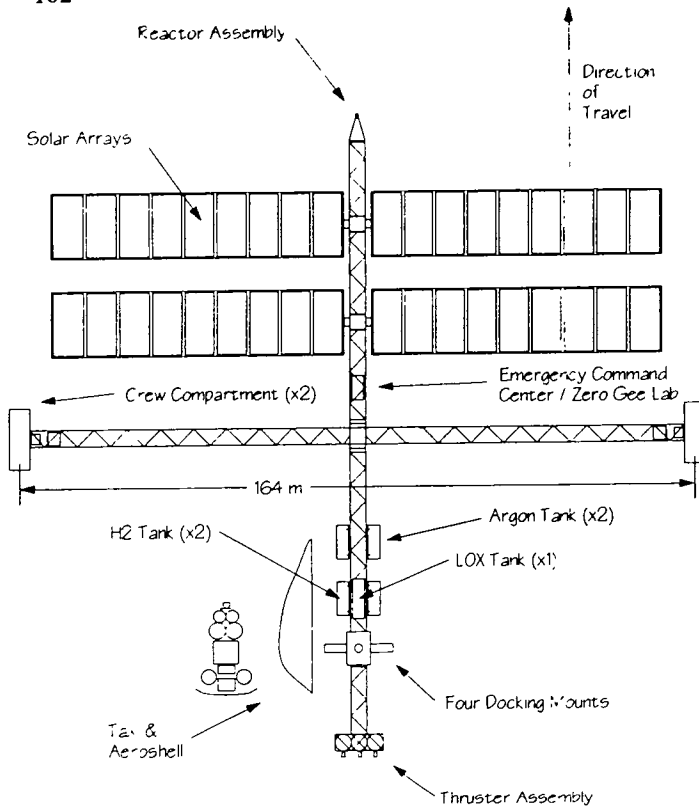


Figure 2.3: Typical Cyclor vehicle layout. Central truss structure is de-spun. Solar arrays are mounted to allow rotation about central truss and primary array axis to ensure maximum exposed surface area.

Propulsion/Power Systems

In accord with the mission statement, the primary purpose of this project was to design a cyclor spacecraft which utilized an ion propulsion system. The most important choice which had to be made by the design groups was deciding on the required level of thrust. The thrust level directly affected mass and size of the thruster array, the amount of power the vehicle electrical system needed to supply, and the length of time required to establish the cycling orbit upon launch from its assembly in the Earth-Moon system. To numerically estimate power and current requirements for the ion propulsion system the following equations were used

$$\begin{aligned} \text{Thrust} &= \dot{m} g_0 I_{sp} \\ \text{Voltage} &= (m_e I_{sp}^2 g_0^2) / (2e) \\ \text{Power} &= (I_{sp} g_0 \text{Thrust}) / (2\eta) \end{aligned}$$

where $g_0 = 9.81 \text{ m/s}^2$, \dot{m} = mass flow rate, m_e = mass of argon ion, e = elementary charge, η = efficiency of conversion. One notes that power is a linear function of I_{sp}

and thrust. For a 100 N thruster the required power is 5.45 MW. Needless to say this is a rather large requirement for a space borne nuclear reactor. Because the Cyclor spacecraft typically has a mass upwards of 600,000 kg, fully fueled thrusters in the 30-100N range will be required for reasonable orbit insertion times. It is evident that the power requirements of the ion propulsion system will drive the requirements of the vehicle power system: For comparison, a chemically propelled cyclor designed to carry 19 crew members and their associated life support and mission equipment is expected to require 300 kW of power²; this would be only 5.5% of the power required by a 100 N ion propulsion system. From these numbers it is apparent that a large part of the feasibility of developing an ion powered cyclor spacecraft rests on the ability to construct and launch a nuclear reactor or alternative power generation system that can provide these large amounts of electric power. Over the 20-30 months period required to establish a final VISIT type orbit 52,000 to 78,000 kg of argon fuel would be required. Over the 40-50 months period expected to reach Up/Down Escalator orbits, the requirement is for 104,000 to 130,000 kg of fuel. These latter numbers are dependent on how optimum a thrust angle is achieved during powered flight and are thus subject to significant variation.

It is unclear as to whether or not the ion engines are capable of providing the impulse required for the 3 mid-course adjustments of the Up/Down escalator orbits. To provide the largest single ΔV of 1.1 km/s the 100 N ion thrusters would need to operate for 76.4 days (assuming a spacecraft mass of 600,000 kg). Note that this is 9.8% of the total average 2.143 yr. period of these orbits. This point is significant to the extent that a secondary propulsion system might be required once the cyclor has reached its orbit; this could be provided by a shuttle craft docked to the cyclor or by an independent system on board the cyclor. If deemed useful only for the initial orbital insertion, it might prove advantages to remove the ion propulsion system and/or the nuclear power generator after final orbital insertion is completed. The latter point is especially applicable for cyclor spacecraft occupying VISIT orbits. An alternative, less massive, and more reliable power source such as solar panels could then be deployed to supply the roughly 300 kW of power required by the remaining vehicle systems, effectively reducing the mass of the vehicle, thereby saving fuel in the case of the Up/Down Escalator cyclor. Assuming 300 kW are required at all points of a vehicle's orbit and 17% efficiency, a gallium-arsenide solar array spanning roughly 10000 m^2 would be required to satisfy the power requirement at the aphelion of the Up/Down escalator orbits from beginning to end of life. Near Earth, large amounts of un-needed energy would therefore have to be dissipated. If the radiators used for the

nuclear generator are still available, this should not prove to be a large constraint, although some of the mass savings would then be lost.

Thermal Systems

The primary thermal aspects of the project were centered around analyzing the boil-off problems of the cryogenic propellants and designing thermal blankets and/or refrigeration systems. Also included were the design of the radiators required to dissipate the heat generated by the power system, and the analysis of the heat loads caused during the aerocapture maneuvers at Earth and Mars.

The heat flux entering the cryogenic propellant tanks is primarily a function of solar radiation intensity and incident surface area, radiating surface area, and the thermal properties of storage tank and thermal blanket. The most efficient thermal blanket design seeks to maximize reflectivity and emissivity, and minimize absorptivity at the upper surface of each layer, while minimizing emissivity, and maximizing absorptivity on the lower surface of each layer. Except for the outermost layer which is exposed to optical wavelength radiation, the lower layers should achieve these values in the thermal wavelengths. Worst case design conditions occur at closest approach to the Sun, which occurs when the cyclor flies by the Earth. Computer models were used to analyze the performance of the blankets given the thermal properties of each surface of a N-layer blanket. When the space between the layers was modeled as perfectly non-conducting, values of essentially zero heat flux were attainable with proper material selection. It became evident that the primary weakness of these thermal blankets are the spacers between layers. Assuming a worst case solar intensity of 1399 W/m^2 , a sample thermal blanket using silver-FEP teflon on the upper surface and chromium on the lower surface of each layer, with a total of 6 layers and surface area of 500 m^2 , achieved a total heat flux of .36 watts when tissue glass spacers were used. For a two year period, this magnitude of heat flux would result in a total boil-off of 50 kg of hydrogen. Assuming that highly efficient thermal blankets of this nature are realistic, it was assumed that boiloff would not be a problem. However, in case these efficiencies are not achievable, low temperature cooling systems were investigated. Reference 5 presents a good example of ideas in this field. The cooling system presented by Klein and Jones operates at 20 K, is capable of removing 0.48 watts, and weighs 31 kg. Multiple coolers of this type could be employed to accommodate the refrigeration needs of the LH2, argon, and LOX propellant tanks carried aboard the Cyclor.

The primary trade-off in radiator design centered around

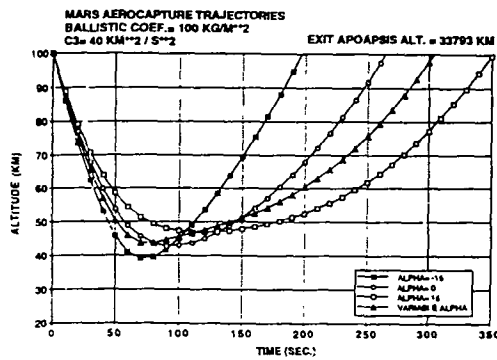
high radiation temperature and associated low relative conversion cycle efficiency and small relative radiator surface area versus low radiation temperatures and associated high relative efficiency and large radiator surface area. Radiator design played a key role in most power system designs due to the large output required (up to 5.75 MW of power). Rankine, Stirling, and thermionic power conversion cycles were some of the systems considered. Preliminary analysis seemed to indicate that Stirling cycle systems would be required to provide the megawatts of power needed with the restraint of keeping the radiator size reasonable⁶. An example power system supplying 5.75 MW utilizing the Stirling cycle, which operated with a radiation temperature of 1000 K and a Carnot efficiency of 25% required radiators covering a 575 m^2 area.

Aerobraking requirements were strongly constrained by thermal considerations in the regimes dealt with by the vehicles in the Mars transportation system^{2,7,8,9}. Current state of the art thermal protection systems (TPS), such as the reusable surface insulation TPS used on the space shuttle made up of ceramic tiles coated with a reaction cured glass, can withstand temperatures up to 1645 C. For most of the envisioned entry vehicles, especially those with L/D values above 1, aerobraking heat loads, especially those associated with Up/Down Escalator orbits, are expected to overwhelm current TPS systems. Therefore aeroshells using ablative materials were considered.

Due to the complexity of the heating analysis required for aerobraking maneuvers for Taxi, OTV, and cargo transfer vehicles entering the Mars atmosphere and the Taxi vehicle entering the Earth atmosphere, most of the analysis was restricted to what information was available in the literature. Typical loads associated with aerobrake trajectories at Earth and Mars are shown in Figure 2.4. The primary constraint on entry velocity into the Martian atmosphere seemed to be the atmosphere's ability to decrease the vehicle velocity enough in a single pass to ensure aerocapture; a quoted figure for the maximum approach velocity of an incoming vehicle is 9.97 km/s.

References

1. Zubrin, R., "In-Situ Propellant Production: The Key Technology Required for the Realization of a Coherent and Cost Effective Space Exploration Initiative," Paper No. IAF 91-668, 42nd Congress of the International Astronautical Federation, Montreal, Canada, October 7-11, 1991.
2. Nock, K.T., Friedlander, A.L., "Elements of a Mars Transportation System", *Acta Astronautica*, Vol. 15, No. 6/7, pp. 505-522, 1987.



ALPHA (DEG)	TARGET PERIAPSIS (KM)	EXIT APOAPSIS (KM)	ENTRY VELOCITY (M/S)	MIN ALT (KM)	MAX G-LOAD (g)	MAX HEAT RATE (W/CM**2)	MAX DYM PRESS (N/CM**2)
-15 0	27 0874	33793 22	8229 39	39 15	6 93	30 52	6628 69
0 0	43 4275	33791 81	8230 13	42 56	4 41	23 42	4320 30
15 0	51 9733	33810 53	8230 51	46 90	2 93	21 08	2800 86
-15 15 0	36 6991	33793 68	8229 82	43 74	4 71	26 74	4500 52

Figure 2.4: Sample aerocapture trajectories comparing angle of attack effects on flight loads, trajectory parameters, and final orbital conditions⁷.

- Friedlander, A.L., Niehoff, J.C., Byrnes, D.V., Longuski, J.M., "Circulating Transportation Orbits Between Earth and Mars," AIAA Paper No. 86-2009, 1986.
- Reports from other participating student project groups, UCLA, 1993.
- Klein, G.A., Jones, J.A., "Molecular absorption cryogenic cooler for liquid hydrogen propulsion systems," AIAA paper No. 82-0830, 1982.
- Angelo, J.A., Buden, D., Space Nuclear Power, Chapt. 13, Orbit Book Co., Malabar, Florida, 1985.
- Mulqueen, J.A., "Applications of Low Lift to Drag Ratio Aerobrakes using Angle of Attack Variation for Control," NASA TM-103544, 1991.
- Lyne, J.E., Tauber, M.E., Braun, R.D., "Parametric Study of Manned Aerocapture Part 1: Earth Return from Mars," Journal of Spacecraft and Rockets, Vol. 29, No. 6, 1992, pp. 808-813.
- Lyne, J.E., Anagnost, A., Tauber, M.E., "Parametric Study of Manned Aerocapture Part 2: Mars Entry," Journal of Spacecraft and Rockets, Vol. 29, No. 6, 1992, pp. 808-813.

University of California, Los Angeles
TRIPOD LANDING STRUCTURE

Brenda Tsiang - Teaching Assistant

Abstract

The students were asked to conceive and construct a model of a tripod landing structure for a spacecraft landing on a planet. This was an exercise in space hardware design that made the students familiar with 3-D truss analysis and the study of various structural failure modes.

Design

Each design team was composed of four members, with all teams given entire freedom in the design of their landing structure as long as the following design criteria were met: 1) The truss had to connect three strong points, (the supports for the body of the spacecraft) with three landing pads. In the model, the support points had to form an equilateral triangle with 36.6" sides. 2) A height of the model of 18.0" was prescribed. 3) A minimum 6.0" high tetrahedral exclusion zone was required to take into account rocks and other planetary debris that might be on a planet's surface. For the same reason, no horizontal members directly connecting the three foot-points were permitted. 4) All dimensions had to be maintained to within 1/16". 5) Total weight of the structure was not to exceed 7.5 lb (Figs. 3.1a-c).

With these design criteria in mind, each group set out to find the best design for their respective landing structure. Each design would be judged on the basis of two criteria: a) highest ratio of ultimate load to weight; and b) closest agreement between calculated and actual ultimate load.

In designing the landing structure, each group recognized that buckling of the compression members would be the governing failure mode. Therefore, each group developed methods of designing around this problem. Some of the solutions included additional supports from tension members to compression members, doubling and tripling compression members, employing a concentric sleeve to strengthen the compression members, and using combinations of the above ideas. In all, twelve unique tripod landing structure designs were arrived at. To analyze these increasingly complex designs, various structural analysis packages such as NASTRAN and PATRAN were available. However, to find the predicted ultimate loads, most students still pursued the traditional pencil and paper analysis.

Testing

After the designs were completed, each group was responsible for the machining of their own truss structures from 1020 carbon steel tubing with a yield strength of 65,000 psi, ultimate strength of 80,000 psi, and Young's Modulus of 2.91×10^7 psi. This tubing was available in either 1/2" outer diameter at 0.1738 lb/ft., or 3/4" outer diameter at 0.2672 lb/ft., both with wall thicknesses of 0.035". With the tubes cut to be designed lengths and the proper intersection angles, the truss structures were put together by a professional welder.

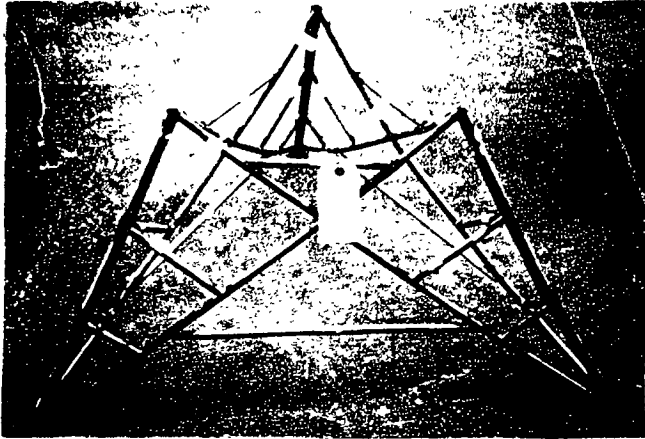


Figure 3.1a: Example of Euler Buckling.

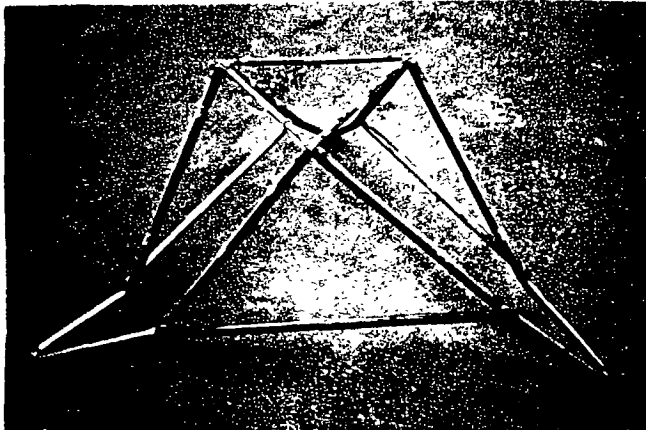


Figure 3.1b: Example of Bending in Compression Strut.

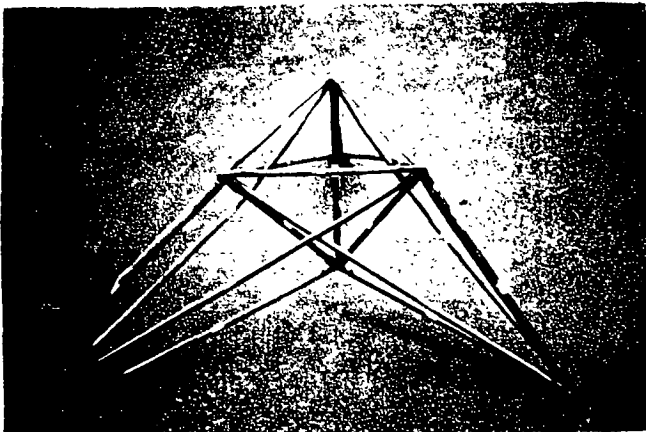


Figure 3.1c: Crack in Weld.

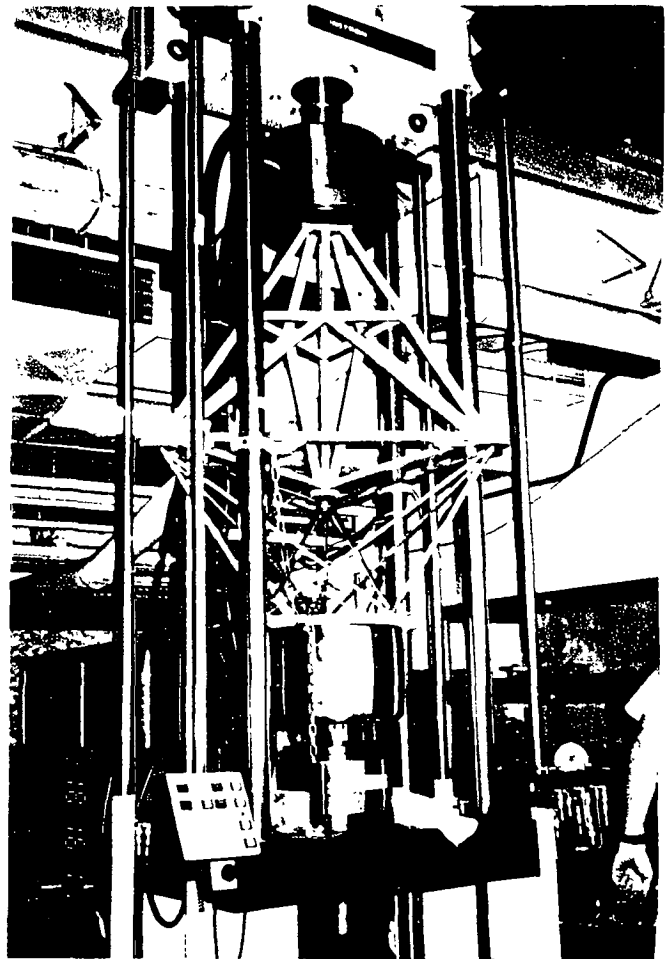


Figure 3.2: Tripod on Instron Test Machine.

To find the actual ultimate load, a 50 ton hydraulic press was utilized (Fig. 3.2). The results of the testing showed that the failures of the tripod landing structures fell into three basic categories: (a) Euler buckling; (b) thin wall buckling; and (c) cracked welds. One interesting failure mode that had occurred previously was lack of structural rigidity. In this failure mode, the structure has a tendency

to twist or rotate when compressive loads are applied due to an insufficient number of bracing members.

The testing of the tripod landing structures resulted in some interesting observations. The truss with the highest load capacity 9105 lbs, (load-to-weight ratio of 1225) failed in tension, and therefore was successful in meeting the group's design goal of strengthening the compression members. Other groups were not as adept in this area. However, even though this group had achieved the highest maximum load, it did not have the highest load-to-weight ratio. This distinction was achieved by another group (load capacity of 8499 lbs, load-to-weight ratio of 1384).

The best agreement between measured and predicted maximum load was achieved by Group 8 with a ratio of 0.926. The predicted load closely approximated the actual maximum load because it was based on a relatively simple design that included no doubled, tripled, or concentric sleeve compression members.

Not only did the students gain exposure to both theory (truss analysis) and practice (minimizing the weight of the structure), but insight was gained into how to build optimal landing structures.

Table 3.1: Results of Tripod Testing

Group	Weight (lbs.)	Predicted Max. Load (lbs.)	Measured Max. Load (lbs.)	M.M.L./wt.	M.M.L./P.M.L.	Failure Mode
1	6.71	7217	6450	961	0.894	Crack in weld
2	6.34	8767	1650	260	0.188	Bend in comp. strut
3	7.44	7000	1200	161	0.171	Fold at hinge point
4	7.25	934	8720	1203	9.34	Bending at hinge point
5	6.83	5700	4391	643	0.77	Euler Buckling
6	7.43	4161	9105	1225	2.19	Tension membrane failed
7	7.29	3500	1491	205	0.426	Bending below joint
8	6.03	4137	3830	635	0.926	Euler buckling
9	6.14	7356	8499	1384	1.16	Thin wall buckling
10	6.99	3675	1024	146	0.279	Bending
11	7.18	5414	3786	527	0.699	Euler buckling
12	5.30	3260	4835	915	1.48	Euler buckling

**DESIGN AND TESTING
OF A ONE-THIRD SCALE
SOYUZ TM DESCENT MODULE**

**SPARTAN CONVERSION PROJECT
SUPER LOKI INSTRUMENTATION**

**University of Central Florida
Mechanical and Aerospace Engineering
Orlando, Florida**

**Professor Loren A. Anderson
Graduate Teaching Assistant Pamela Kay Armitage**

Abstract

The 1992-1993 senior Aerospace Engineering Design class continued work on the post landing configurations for the Assured Crew Return Vehicle. The Assured Crew Return Vehicle will be permanently docked to the space station fulfilling NASA's commitment of Assured Crew Return Capability in the event of an accident or illness aboard the space station. The objective of the project was to give the Assured Crew Return Vehicle Project Office data to feed into their feasibility studies. Three design teams were given the task of developing models with dynamically and geometrically scaled characteristics. Groups one and two combined efforts to design a one-third scale model of the Russian Soyuz TM Descent Module, and an on-board flotation system. This model was designed to determine the flotation characteristics and test the effects of a rigid flotation and orientation system. Group three designed a portable water wave test facility to be located on campus. Because of additional funding from Thiokol Corporation, testing of the Soyuz model and flotation systems took place at the Offshore Technology Research Center. Universities Space Research Association has been studying the use of small expendable launch vehicles for missions which cost less than 200 million dollars. The Crusader2B, which consists of the original Spartan first and second stage with an additional Spartan second stage and the Minuteman III upper stage, is being considered for this task. University of Central Florida project accomplishments include an analysis of launch techniques, a modeling technique to determine flight characteristics, and input into the redesign of an existing mobile rail launch platform.

Introduction

For years, America's journey into space has demonstrated the benefits associated with working in the unique

environment of microgravity. Continuing in this tradition, an ambitious and far reaching program to further the advancement of space technology has been launched. With the space station, the United States enters an era marked by a permanent presence in space. The space station allows continuous rather than intermittent operations to be conducted in orbit. The space station opens doors to many new methods of research and experimentation. Included are better opportunities to observe the Earth and forecast future trends from a vantage point only partially exploited by previous space shuttle missions.

The space station will have a crew of four. The crew will be rotated and resupplied by flights of a space shuttle at intervals of three months. Because of the isolation and potentially hazardous conditions involved in space operations, NASA is committed to the policy of Assured Crew Return Capability for space station crews in the event (1) a medical emergency occurs and an ill, injured, or deconditioned crewmember must be rapidly transported from the space station to a definitive health care facility on Earth; (2) a space station catastrophe forces a rapid evacuation of the crew from the station; and/or (3) the Space Shuttle Program becomes unavailable, and an orderly evacuation of the crew from the space station becomes necessary.

These events, or Design Reference Missions (DRMs), can be met by a concept known as the Assured Crew Return Vehicle (ACRV). Currently, NASA is considering two classes of ACRVs: water landers and open land landers.

The project objectives detailed in this report were developed in conjunction with the Kennedy Space Center ACRV Project Manager and are focused on requirements for a water landing ACRV and post landing operations. The craft configuration is the Russian Soyuz TM Descent Module. The designs presented are as follows: an engineering test model of the Soyuz TM Descent Module; on-board flotation systems for the Soyuz TM Descent Module; and a water wave test facility. During the fall semester a one-tenth scale was used. At the beginning of

the spring semester Thiokol Corporation funded the project. Therefore, the designs were reconfigured to one-third scale and wave testing was performed at the Offshore Technology Research Center at Texas A & M University in College Station, Texas.

Universities Space Research Association (USRA) has been studying the uses of small expendable launch vehicles (SELV) for missions which cost less than 200 million dollars. To accomplish this task, military hardware would be used which has been phased out due to obsolescence or international treaties. USRA and its associates have identified the Spartan missile and the Minuteman III upper stage, which incorporates the Orbus 7 perigee motor, as possible candidates for meeting this need. "Five companies initial assessments indicate that the conversion of the Spartans is technically feasible. Two of the companies, Teledyne Brown Engineering and Orbital Sciences Corporation, extended their studies and developed preliminary vehicle designs."¹ The Spartan Conversion Project Team has investigated the Teledyne Brown Engineering Crusader2B vehicle configuration. This incorporates the integration of the original Spartan first stage and second stage with an additional Spartan second stage and the Minuteman III upper stage. An analysis of launch methods for the Crusader2B is presented. The launch methods investigated include air, land, and sea. Models to simulate the flight characteristics of the full scale Crusader2B are also presented.

In the fall of 1992, Spaceport Florida Authority (SFA), USRA and Cape Canaveral Air Force Station (CCAFS) selected a mobile rail launch platform as an economical launch method for the Crusader2B. In addition, a launch cost of between .5 to 1.5 million dollars was discussed as a target for this launch facility. To assist in the redesign of the mobile rail launch platform, the Spartan Conversion Project Team instrumented the launch rail of the Super Loki sounding rocket. This instrumentation package will be used to determine the thermal and dynamic stresses on the rail. The design and setup of the instrumentation package is presented.

Previous UCF ACRV Projects

The UCF senior-level Mechanical and Aerospace Engineering Design class has been working with the ACRV Project Office at Kennedy Space Center since 1989. During the 1989-1990 academic year, four design considerations and solutions were investigated.

The first consideration was providing crew egress and rescue personnel support subsystems to ensure the safe and rapid removal of an ill or injured crewmember from the ACRV by recovery personnel. An Emergency Egress Couch was designed to medically support a sick or injured

crewmember during the ACRV mission. To move the couch from the floor to the hatch, a Four Link Injured Personnel Egress Mechanism (FLIPEM) was developed. The second consideration was the proper orientation, attitude control, and stabilization systems required for the ACRV in the marine environment. Post landing orientation of the ACRV is achieved through the use of three CO₂ charged balloons similar to those used during the Apollo program. Attitude control systems were designed that deploy three multichambered ring segments and an appurtenance to act as a platform for the rescue personnel. Multiple underwater parachute assemblies were designed to provide motion reduction.

The third consideration dealt with providing full medical support to an ill, injured, or deconditioned crewmember aboard the ACRV from the time of separation from the space station to rescue by recovery forces. Extensive research was performed to select suitable medical support equipment and monitors as required by NASA. Equipment was integrated into unified packages and power requirements were addressed.

The fourth consideration was to provide for the comfort and safety of the entire crew from splashdown to the time of rescue. Design solutions were presented for food, water, waste management, atmosphere, contaminant/odor control, and environmental control systems.²

The format for the senior-level design class changed in the 1990-1991 academic year. The design requirement was increased from one semester to two semesters. The students design during the fall semester and build and test during the spring semester. The work continued on post landing operations for the water landing ACRV. The design objectives for this class were to determine the feasibility of the previously developed egress and stabilization systems for deployment on the ACRV. Four design teams were formed.

The first team designed, built, and tested a one-fifth scale model of the Apollo Command Module Derivative (ACMD) to be used as a test platform for the egress and stabilization systems. Test results indicated small deviations from the size and weight specifications provided by Rockwell International. Hardpoint accommodations and seal integrity were maintained throughout the water testing.

The second team worked during the fall semester investigating water test facility locations, as well as establishing designs for a permanent facility at the University of Central Florida. As a result of this investigation, stabilization testing with the ACRV model was performed at the O. H. Hinsdale Wave Research Laboratory (WRL) at Oregon State University in Corvallis, Oregon.

The third team designed, built, and tested a one-fifth scale working model of the FLIPEM optimized in the previous academic year as well as a Two Slider Support Mechanism (TSSM) for egressing the couch out the hatch. Testing was conducted in the areas of lifting force with nominal and off-

nominal loads, vertical and horizontal travel distances, redundancy characteristics of the FLIPEM and extension force, travel distance and redundancy characteristics of the TSSM. Test results indicate the design specifications for both systems were met or exceeded without interference to other systems.

The fourth team's objective was to determine, through modeling, the feasibility of reducing heave, surge, and pitch motions of the ACRV model in water using an underwater parachute system. Therefore, one-fifth scale models of the attitude ring and underwater parachute stabilization system, optimized during the previous year, were designed, built and tested. Wave testing, in simulated sea states 2 to 4, at the O. H. Hinsdale WRL, yielded results that indicate that the six-attitude sphere configuration produced minimal stabilizing effects on the ACRV model. The spheres, however, did have the effect of enhancing the flotation characteristics of the model. Numerous parachute arrangements, including single and multiple chutes per cable, increasing the weight attached, using stiff and elastic cables, and devices to partially and totally open the chutes, were tested. Results indicate that the parachutes did affect the motions induced on the model, but did not reduce or increase the frequencies out of the range that causes seasickness.³

A concept employing Rocker Stoppers was built and tested at the water test facility to determine the effect a rigid system would have on reducing the oscillations. Two Rocker Stoppers were connected, nose-to-nose, at one end of a long threaded rod. The other end of the rod was connected to a metal plate attached to the model above the break line. Four of these arrangements were connected to the model. Since the Rocker Stoppers are made of rigid plastic, they perform the same work on the upstroke as on the downstroke. This configuration was tested in a simulated sea state 4 (1.2 ft wave height, 0.45 Hz) and the response compared with that from the clean model in the same sea state. The results indicate that a rigid system in this configuration reduces the heave amplitude the model experiences.

The design projects for the 1991-1992 academic year include designs of the ACMD, the Station Crew Return Alternative Module (SCRAM) and the Emergency Egress Couch (EEC). Two teams worked on the ACMD. The first team developed a one-fifth scale model to be used as an engineering test model and test bed. The model design was similar to the 1990-1991 ACMD model, but improved the concept with a radial adjustable center of gravity (CG) and moment of inertia (MI) system. The second team designed a one-fifth scale flotation and attitude system for the ACMD. The flotation system was designed with a segmented ring constructed out of woven nylon fabric coated with butyl rubber. The attitude system provides support to the EEC and consists of a telescoping beam configuration.

The third team designed, built, and tested a one-fifth scale model of the Station Crew Return Alternative Module (SCRAM). The SCRAM consists of a cylindrical crew compartment with a conical shaped heat shield. The heat shield can either be open or closed to the water environment. The weight, CG and MI were modeled using the Adjustable Rotating Weight System. A lift attachment point system was mounted to the lid of the model. Pretests were performed to verify geometric and dynamic similitude. Wave tests took place at the Offshore Technology Research Center at Texas A & M University. Tests were completed in three wave states to determine the SCRAM's flotation characteristics as well as various methods of vehicle recovery. The test results provide the flotation and lifting characteristics of the SCRAM configuration.

The fourth team designed, built and tested a full scale model of the Emergency Egress Couch (EEC). The EEC model consisted of two basic litters, one human weight system, one medical weight system, three layers with flotation, two sets of lift attachment points and a cover. Pretesting and flotation testing were performed on the UCF campus. The dynamic testing was performed at Patrick Air Force Base with the Department of Defense Manager Space Transportation System Contingency Support Office, and the 41st Air Rescue Squadron (ARS). The test results and input from the 41st ARS provided geometric and dynamic parameters to be used in further designs of the EEC.³

1992-1993 ACRV Design Projects

During 1992 the Russian Space Agency, NPO Energia, suggested the Soyuz TM Module to NASA for use as the Assured Crew Return Vehicle from the space station. Two areas of interest identified were the flotation characteristics of the Soyuz TM Descent Module, and the stabilization characteristics of a rigidly mounted flotation system.

USRA is determining the feasibility of using obsolete military hardware to assemble and launch a Small Expendable Launch Vehicle (SELV) capable of placing a 250 to 350 pound payload into Low Earth Orbit (LEO) for under 200 million dollars. To assist with this determination, a Crusader2B configuration was used and three tasks were defined: 1) launch methods; 2) flight characteristics; and 3) stresses occurring during a mobile rail launch. Four design teams were formed and tasked as follows:

Team #1-Soyuz Model

The Soyuz Model Team was to use geometric and dynamic constraints to design, build and test a one-tenth scale working model of the Soyuz TM Descent Module. The model was required to incorporate a rigidly mounted flotation and orientation system.

Team #2-Soyuz Flotation & Orientation Model

The objective of the Soyuz Flotation and Orientation Model Team was to design, build, and test a one-tenth scale model of a flotation and orientation system for the Soyuz TM Descent Module. The team was to address location, storage, and deployment.

Team #3-Wave Test Facility

The Wave Test Facility Team was to design, build and operate a wave test channel for testing the one-tenth scale Soyuz TM Descent Module Model (SDMM). The waves were to accurately simulate the sea conditions which the ACRV may encounter. The team was to investigate the mechanics of the facility, the control system, and the data acquisition system and equipment necessary to perform the required analysis on the Soyuz TM Descent Module model.

Team #4-Spartan Conversion Project

The Spartan Conversion Project Team was given two tasks during the fall semester: 1) investigate various launch techniques for the Crusader2B; and 2) model the flight characteristics of the full scale Crusader2B. During the spring semester, the team was to determine the dynamic and thermal stresses of a Super Loki sounding rocket mobile launch rail platform.

The ACRV projects changed direction for the Spring semester. Thiokol Corporation funded the building and wave testing of the Soyuz TM Descent Module Model. The Spring tasks were to: 1) build a one-third scale model; 2) build on-board flotation systems; 3) test at the Offshore Technology Research Center (OTRC); and 4) assist Thiokol with proprietary testing. The wave test facility at UCF was not built or operated.

A one-third scale was used both geometrically and dynamically for all ACRV models. To accomplish this a Buckingham Pi dimensional analysis was performed and the Froude scaling factors were determined. These factors allow the model to accurately simulate the characteristics of the full scale craft. While the geometric dimensions of the craft scaled directly by one-third, other parameters, including volume, weight, and mass moment of inertia scaled by powers of one-third.

1992-1993 Soyuz TM Descent Module Design, Building, and Testing Results

Soyuz TM Descent Module Model

The Soyuz Model Team designed a one-third scale model of the Soyuz TM Descent Module (SDM). Current data for the geometric and dynamic constraints of the Soyuz were supplied by NPO Energia through NASA/KSC and NASA/JSC. The two areas researched were construction of the model shell and a center of gravity (CG) and mass moment of inertia (MI) system.

The crew compartment and the heat shield are constructed out of 3/8 inch thick fiberglass. The heat shield is reinforced with six wood stringers glassed to the structure in a spoke configuration. The circular access hatch of the model shell is 3/8" plate aluminum. The heat shield is fastened to the crew compartment by 16 symmetrically placed bolts. Eight symmetrically placed bolts attach the access hatch. The joints are sealed with a silicone based seal. Washers and T-nuts are used on all bolt assemblies (Figure 1).

The weight, MI, and CG were placed with an adjustable multi-axial weight system. The weight system consists of a rectangular frame, all-thread and lead weights. The outer rectangular frame is constructed of 6061-T6 aluminum. The frame members are chamfered on the ends and TIG welded together at 90 degrees, creating a four-arm system. An aluminum doughnut ring is TIG welded to the bottom of the four-arm system. The flange-ring system is sealed by compression of O-ring gaskets between the doughnut and top section flange, and silicone caulking between the doughnut and bottom section flange. One #8 all-thread screw is bolted through the top and bottom of each member of the four-arm system. Lead weights are used on the threaded rods to supply mass for adjustment of the CG and MI (Figure 2).

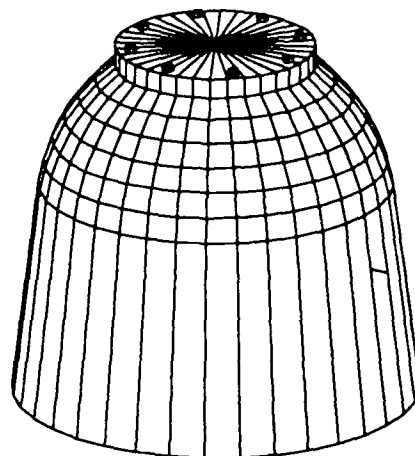


Fig. 1 Soyuz TM Descent Module Model

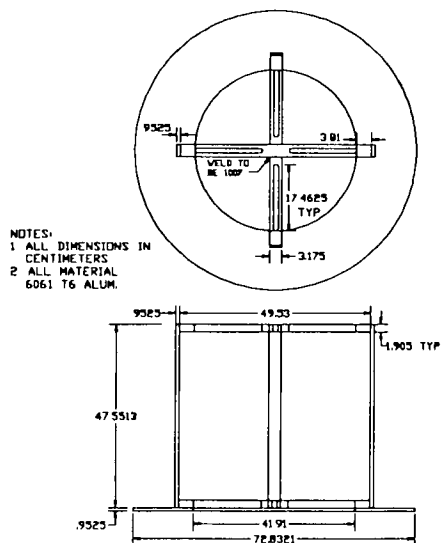


Fig. 2 Adjustable Multi-Axial Weight System

A two phase test plan was developed to evaluate the model. Phase I took place at the UCF Aerospace Senior Design Lab and consisted of a series of pre-tests to confirm the Soyuz model met its specifications. The tests included geometric similitude, model strength, water intrusion, CG and MI similitude, and flotation compatibility. Test results indicate that the model met its geometric and strength constraints. Leakage occurred during the initial testing, therefore silicone was used to supplement all seals. The CG of the model shell and CG/MI system, without the weights, is (26.8,0,0) cm with the origin located at the center point of the bottom of the model. The moments of inertia of the model shell and CG/MI system, without the weights, are $I_x = 3.42 \text{ kg}\cdot\text{m}^2$, $I_y = 3.55 \text{ kg}\cdot\text{m}^2$ and $I_z = 3.62 \text{ kg}\cdot\text{m}^2$. Using lead weights, the CG of the full scale Soyuz was modeled to within 5%, and the moments of inertia to within 28%. The flotation system integrated successfully with the model. The MI modeling could have been improved if a lighter model shell were used.

Phase II took place at the OTRC. Tests were completed to determine the Soyuz's flotation characteristics. This testing involved tethered and untethered testing of the model as well as a number of changes to the wave environment. Sea state conditions were set during the development of the model. Five wave states were modeled and evaluated (Table 1). The test results provide the flotation characteristics of the Soyuz configuration. Observations derived from the test results were also provided to the ACRV Program. These observations were: (1) the frequency of regular wave state three was approximately equal to the natural frequency of the tethered Soyuz model. Therefore, every second wave in the tethered tests damped the pitching motion of the craft.

In the untethered test, the model exhibited an oscillating rolling motion; and (2) the model in regular sea state four exhibited a significant increase in pitch in the tethered test. During the untethered test, the craft oriented itself hatch away from the on-coming waves and tracked straight in the wave direction.

Table 1 Wave States Tested

Sea State	Average Period	Average Wave Height
Regular 3	2.802 s	0.837 m
Regular 4	4.908 s	1.823 m
Random 1	1.81 s	0.2236 m
Random 2	3.073 s	0.6273 m
Random 3	4.289 s	1.328 m

Soyuz Flotation & Orientation Model

The Soyuz Flotation & Orientation Model Team designed one-third scale on-board flotation and orientation systems for the SDM. The systems form a rigid body with the SDM after deployment. Areas considered during design included: (1) required buoyancy; (2) means of rigid attachment; (3) work platform for rescue personnel; (4) feasibility for full scale Soyuz; and (5) a method of orientation.

Two flotation systems were designed and built. The four main features of the Umbrella Arm design are the locating collar, support tubes, flotation devices and the stabilization bag. The collar is made of slip rolled 6061-T6 aluminum flat stock and rigidly attaches the flotation system to the SDMM. Three studs are welded on to the collar to facilitate fastening of the support tubes. The collar is placed over the neck of the SDMM and clamped down with a bolt. This bolt tightens the collar to the SDMM. The collar is kept from rotating or slipping by installing four bolts through tapped holes and securing them with nuts. Two nut and bolt assemblies attach the support tubes onto each collar stud. Each support tube is mounted to a flotation attachment plate with a nut and bolt assembly. Using four Velcro strips an inflatable bag is attached to each attachment plate (Figure 3).

The Modular Inflatable design consists of five square inflatable bags positioned in the form of a pentagon along the water line of the SDMM. The square inflatable bags for each system are constructed of an outer layer of awning canvas with an inner plastic bladder (Figure 4).

On the SDM, either of these systems could be deflated, and stored in recessed compartments in the outer shell of the capsule. After splashdown, the system would deploy and inflate to provide stability. Each of these systems provides flotation, orientation, and a working surface for the rescue crew members.

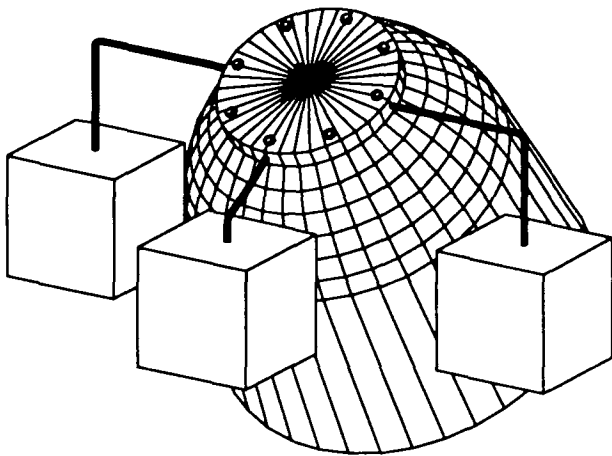


Fig. 3 Umbrella Arm Flotation System

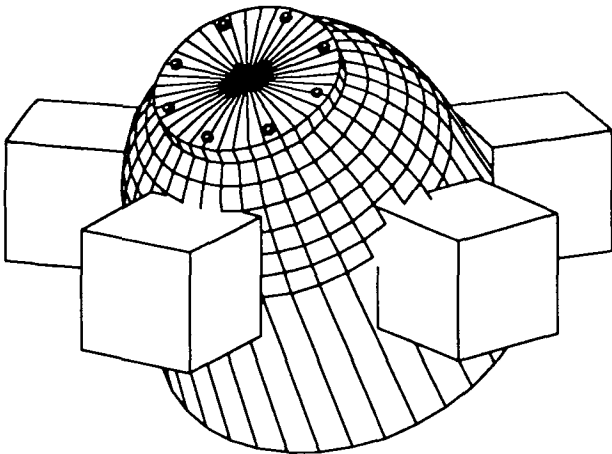


Fig. 4 Modular Inflatable Flotation System

A two phase test plan was developed to evaluate the model. Phase I took place at the UCF Aerospace Senior Design Lab and consisted of a series of pre-tests to confirm the flotation & orientation model met its specifications. The tests included safety, required buoyancy, water intrusion, dimensional verification, Velcro strength, rigid attachment, and weight verification. Test results indicate that the models were safe to use. The provided buoyancy met its specification and was sufficient to support the model. Water intrusion into the inflatable bags was negligible and did not affect the dynamic flotation characteristics. The models met their dimensional and weight constraints. Velcro strength was sufficient to resist the force of the wave motion, and each system attached rigidly to the Soyuz model.

Phase II took place at the OTRC. Tests were completed to determine the flotation characteristics of the SDMM with the Umbrella Arm system attached. This testing involved tethered tests and a number of changes to the wave environment. Sea state conditions were set during the development of the model. Three wave states were modeled and evaluated. The first was a regular sea state three with a 0.837 meter wave height and a 2.802 second period. The second was a regular sea state four with a wave height of 1.823 meters and a period of 4.908 seconds. The third wave state was a random sea state two with an average wave height of 0.6273 meters and an average significant period of 3.073 seconds. The test results provide the flotation characteristics of the SDMM craft with the Umbrella Arm system deployed. Observations derived from the test results were also provided to the ACRV Program. These observations were: (1) a small increase in the heave motion with a large decrease in the pitch motion; (2) a flotation device which provides stabilization is necessary to extract the crew from the craft; and (3) sea state three bare model pitching motion was normalized.

Wave Test Facility

The Wave Test Facility Team designed a facility to test a one-tenth scale Soyuz model. The design parameters which the group considered were: (1) kinematic scaling; (2) bottom effects; (3) portability; (4) water tank; (5) wave generation; (6) wave absorption; and (7) measurement and instrumentation.

The wave tank designed is an above ground wood tank. The rectangular tank is 6.1 meters long, 1.83 meters wide and 0.91 meters deep. The generator section occupies the first 0.4 meters of the tank. A 1.8 meter section, after the generator, is reserved to allow the wave to build to steady state prior to entering the test section. The test section immediately follows the transition section and is approximately 2.1 meters long. This provides for a 3.9 square meter test area and allows for approximately two full wavelengths of scaled regular sea state three. The final section of the wave tank is the wave absorber. This section is approximately 1.7 meters long and consists of four vertical walls of various porosity. Access to the tank is provided by a movable platform (Figure 5).

The tank is divided into five segments. The segments of the tank are composed of pressure treated plywood panels. The plywood side panels are fastened to the single floor panel by four triangular support members. The two end sections of the tank are also constructed of pressure treated plywood panels, and are connected to the sides of the tank with angle steel. The wooden rectangular tank supports the weight of the water but is not watertight. A 0.6 mm thick liner contains the water.

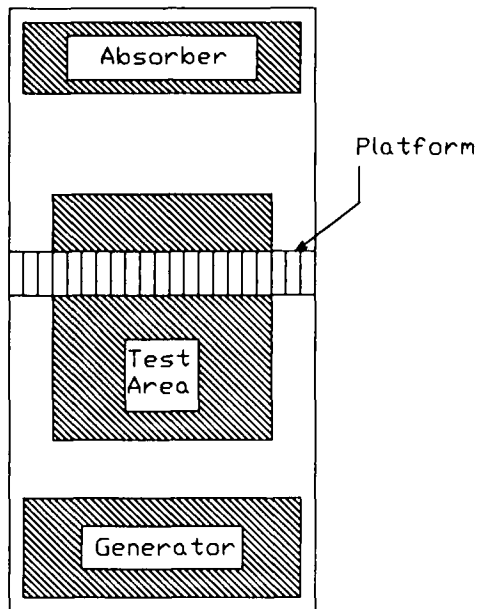


Fig. 5 Wave Test Facility Concept

The wave generator consists of a hinged flap driven by a pneumatic cylinder and linkage. This mechanism is a solid vertical surface which pivots about a mount rigidly attached to the pool bottom. The wave board is actuated by a pneumatic cylinder. The cylinder has a 5.08 cm diameter bore with a 30 cm stroke. The required air pressure for the cylinder is 275.79 kPa. The cylinder is constructed of stainless steel and aluminum. The cylinder is attached to a clevis bracket which is rigidly attached to the framework on the end of the wave tank. The cylinder rod is extended by a linkage which connects it to the top of the generator frame. The linkage consists of series of couplings and threaded rods attached to a ball joint connection located at the top of the frame.

The wave form created by the generator is managed by controlling the air supplied to the cylinder. The direction of the cylinder is controlled by switching the supplied and vented air to the cylinder. A solid state variable time relay is used to control the switching of the solenoid valve and ultimately the period of the waves generated. Stroke limiters are employed to limit the motion of the cylinder rod. The wave characteristics are determined by a fully manual measurement system, while the Soyuz model data is measured with an automatic electronic system.

Spartan Conversion Project

The Spartan Conversion Project Team focused on launch configuration alternatives for launching the Crusader2B for under two million dollars. The flight characteristics of the

full scale Crusader2B were also investigated. The launching methods considered were air, land, and sea launch.

Two air launching alternatives considered were the parachute drop, and the wing pylon launch. The parachute drop launch involves deployment of parachutes which pull the rocket out of the back of a large cargo aircraft, then stabilize its attitude with an additional set of parachutes so that the rocket is pointing upward (vertically), releasing the parachutes, and igniting the first stage motor. The wing pylon launch method involves dropping the launch vehicle from the underside of a B52 aircraft and allowing it to freefall. The aircraft veers to the side to fly clear of the launch area. The first stage motor is then ignited and the guidance system steers the rocket into the proper trajectory.

Three land launching configurations were considered. These were above ground launch complexes, existing mobile launchers, and existing abandoned silos. Modifications would need to be made to each of these launch facilities to accommodate the Crusader2B.

The sea launching techniques considered were: (1) barge tower; (2) partially submerged; and (3) fully submerged launch. Using the barge tower system, the launching structure, in the horizontal position, and integrated launch vehicle are towed away from populated areas on the barge. Once the launch site is reached, the launch structure with the integrated vehicle is raised from the horizontal to the vertical launch position and readied on the platform for launch. The support vessel with on-board control room, clean room, and support personnel moves away from the launch platform and tower to a safe location for launch. The launch sequence is then activated. The fire command is not sent until the vehicle roll and pitch rates come into specified tolerances.

The partially submerged launch involves towing the launch vehicle totally submerged, fitted with a dummy tow nosecone, and sealed in a watertight casing. When the launch site is reached, the rocket is oriented to the vertical position using flotation and ballast, exposing approximately ten percent of the rocket, by volume, above the waterline. The dummy tow nosecone is then removed and the payload, stored on-board the support vessel in a clean room, is installed onto the launch vehicle. The support vessel then moves away to a safe location and the launch sequence is started. The fire command is not sent until the vehicle roll and pitch rates come into specified tolerances.

The difference between the partially submerged launch and the fully submerged launch is that instead of flotation being attached to the rocket, the rocket is allowed to settle slightly below the ocean surface. The rocket is then ignited while completely submerged and exits the water with a considerable buoyant force.

The ability to launch for under two million dollars was an important consideration in choosing the launch method of the Crusader2B. Therefore, the parameters of initial cost and operational cost were heavily weighted in the determining

means process. The partially submerged launch method and the modification of an existing mobile launch rail allow for a simple launch method which require few modifications and provide good mobility. This mobility increases launch site selection which increases orbital range selection. The systems are also durable and require fewer range safety restrictions. These attributes lead to an inexpensive, flexible method of launching a SELV into low earth orbit.

The Aerodynamic Model (AM) required that the flight characteristics be the same as those of the full scale Crusader2B. The AMs considered were the flow table, the subsonic wind tunnel, and the supersonic wind tunnel model. These models must produce the same Reynold's number (Re), or be able to produce enough data points so that the Re can be extrapolated. The most important parameter in the selection of the method of aerodynamic testing was the Mach number. If the testing facility is unable to reach the full scale QMAX Mach number, the dynamic similarity between the full scale Crusader2B and the scaled AM is not satisfied. With the importance of the Mach number parameter, the supersonic wind tunnel testing was selected as the optimal solution for the aerodynamic modeling.

In the fall of 1992, Spaceport Florida Authority (SFA), USRA and Cape Canaveral Air Force Station (CCAFS) selected modifying an existing mobile rail launch platform as an economical launch method for the Crusader2B. In addition, a launch cost of between .5 to 1.5 million dollars was discussed as a target for this launch facility. The Spartan Conversion Project Team designed and tested an instrumentation package for a Super Loki sounding rocket launch rail to determine thermal and dynamic stresses on the rail during launch. The Super Loki launch rail (SLLR) is a twelve foot long launch rail of anodized aluminum.

The instrumentation package consists of four sections. The sensor section has two strain gauges and four thermocouples (Figure 6). These sensors are responsible for taking accurate data during the launch of the Super Loki rocket. The second section is the wires that transmit the data from the sensors to the data acquisition devices. The wires that are on the SLLR are resistant to high temperatures. The next section is the data acquisition devices. These devices include a strain indicator which converts the signal from the sensors to data that the micro-loggers record and a data logger which records the required data. The last section in the instrumentation package is the protective coverings. These coverings include the ducts that protect the wiring from data corrupting radio noise, two boxes which protect the amplifiers, and the data loggers (Figure 7).

This package is intended to acquire data on the launch of a Super Loki rocket and the effects of the launch on the rail. This includes the strains imparted on the rail by the driving fins on the dart of the rocket, and the frictional heating imparted to the rail during the launch.

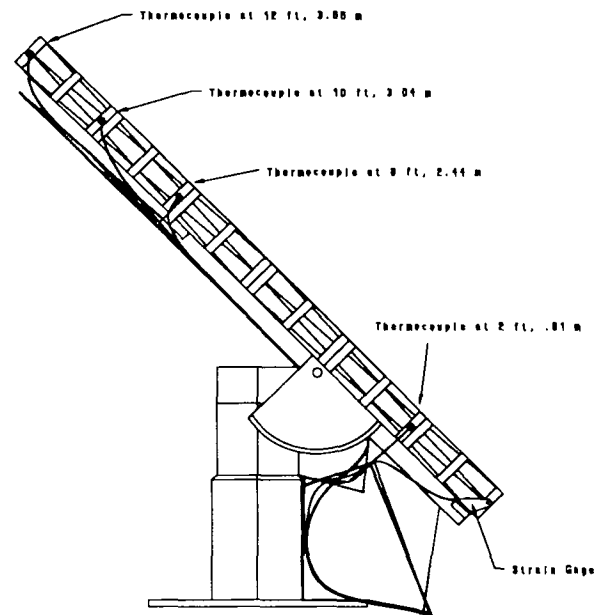


Fig. 6 Instrumented Rail

The project was separated into four phases: design, installation, pre-test, and test. During the design phase an analysis was performed in Algor to determine the location of the stresses the launch rail mounting bracket would experience during a launch. This determined the mounting location of the strain gauges on the launch rail mounting bracket.

The installation phase included the method for mounting the strain gauges and thermocouples on the rail, as well as the method for constructing protective ducts and boxes. The pre-test phase consisted of a series of tests to confirm that the strain gauges, cables, data loggers, and computers perform to specifications and within an acceptable error limit.

During the pre-test phase, tests were done to verify sensor mounting and operation, cable operation, and data logger performance and interface. The results from the tests showed that all sensors were mounted correctly and performed properly. The cables were connected securely and functioned accurately. Data recorded by the data loggers was accurate. These tests also provided data on the magnitude and linearity of the axial and torsional stresses on the mounting bracket. These stresses were found to behave linearly. Torsional stresses were found to be negligible when compared to axial stresses, therefore, the torsional stresses are neglected.

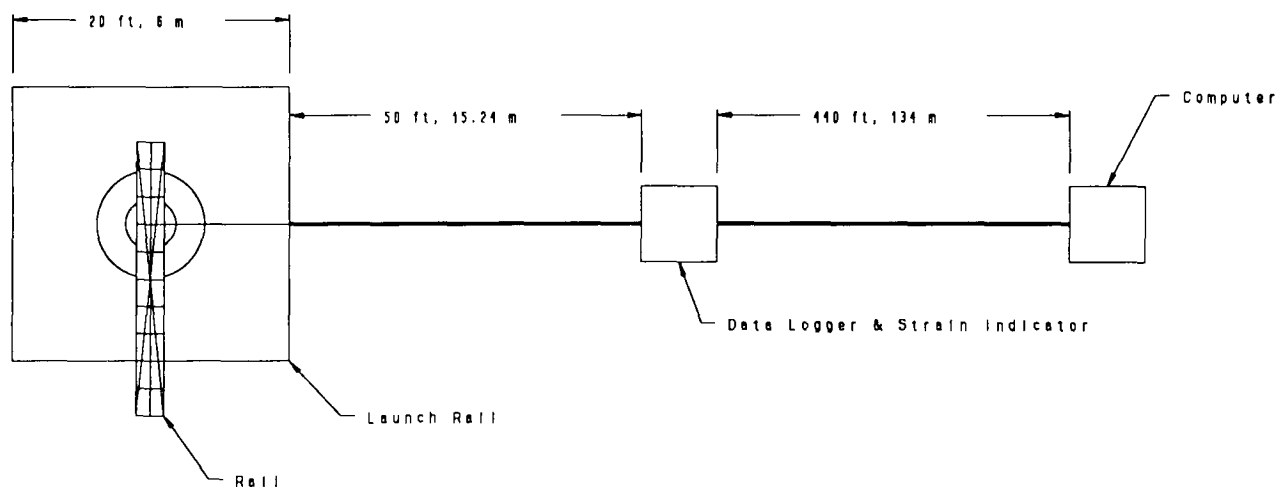


Fig. 7 Final Site Set-Up

Phase III consists of gathering the thermal and dynamic stresses from two real time launches of the Super Loki sounding rocket. These launches will be performed in conjunction with Spaceport Florida Authority at Cape San Blas, Florida. The testing has not been performed at this time.

Summary

The 1992-1993 senior Aerospace Engineering Design class completed two projects. The first project was to design, build, and test a SDMM and on-board flotation & orientation systems. The second project was the Spartan Conversion Project which included an instrumentation package for the Super Loki sounding rocket.

The objective of the Soyuz project was to determine the flotation characteristics of the SDM with and without flotation. Construction of the Soyuz model and a center of gravity and mass moment of inertia system were completed. The Flotation & Orientation project completed work in determining: required buoyancy, means of rigid attachment, a work platform for rescue personnel, feasibility for the SDM, and a method of orientation. A wave test facility to test a one-tenth scale SDMM was designed.

The objectives of the Spartan Conversion Project were to investigate various launch techniques for the Crusader2B, model the flight characteristics of the full scale Crusader2B, and provide design input into the modification of an existing mobile rail launch platform. To accomplish these objectives several launch techniques were investigated, modeling methods researched, and theoretical analyses performed on a mobile launch rail bracket

One-third scale models of the SDM and two on-board flotation & orientation systems were designed, built and tested. Testing took place in two phases. The fidelity of the Soyuz model was established from geometric and dynamic characteristic tests performed on the model in Phase I. Results from Phase I tests on the SDMM indicate that the model met its geometric and strength constraints. Leakage into the model was prevented by supplementing the seals with silicone. The center of gravity was modeled to within 5%, and the moments of inertia to within 28%. Integration with the flotation & orientation systems was successful. Phase I testing on the Umbrella Arm system and the Modular Inflatable system indicate that the models were safe to use. The buoyancy provided met specification and was sufficient to support the SDMM. Water intrusion into the inflatable bags was negligible and did not affect the dynamic flotation characteristics. The models met their dimensional and weight constraints. Velcro strength was sufficient to resist the force of the wave motion, and each system attached rigidly to the SDMM.

Phase II testing took place at the OTRC. The facility accommodated all testing configurations and the staff provided excellent support. Tests were completed to determine the SDMM's flotation characteristics with and without the Umbrella Arm system. The testing involved tethered and untethered testing of the models as well as a number of changes to the wave environment.

Five wave states were used to test the bare SDMM. The test results provide the flotation characteristics of the SDM configuration. Observations derived from the test results were provided to the ACRV Program. These observations were: (1) the frequency of regular wave state three was

approximately equal to the natural frequency of the tethered Soyuz model. Therefore, every second wave in the tethered tests damped the pitching motion of the craft. In the untethered test, the model exhibited an oscillating rolling motion. and (2) The model in regular sea state four exhibited a significant increase in pitch in the tethered test. During the untethered test, the craft oriented itself hatch away from the on-coming waves and tracked straight in the wave direction.

Three wave states were modeled and evaluated in the testing of the Umbrella Arm system. The test results provide the flotation characteristics of the SDMM with the Umbrella Arm system deployed. Observations derived from the test results were also provided to the ACRV Program. These observations were as follows: (1) a small increase in the heave motion with a large decrease in the pitch motion, (2) a flotation device which provides stabilization is necessary to extract the crew from the craft, and (3) sea state three bare model pitching motion was normalized.

A wave test facility was designed to test a one-tenth scale SDMM. The design parameters which the group considered were kinematic scaling, bottom effects, portability, water tank, wave generation, wave absorption, and measurement and instrumentation. The facility is designed to be portable. The water tank is constructed of wood in five sections. A 0.6 mm thick liner contains the water. The wave generator consists of a hinged flap driven by a pneumatic cylinder and linkage. A manual measurement system is used to determine and monitor wave motion, while an automatic electronic system is used to retrieve data from the model.

The launching methods considered for the Crusader2B were air, land, and sea launch. Two air launching alternatives were considered: the parachute drop, and the wing pylon launch. Modifications to three existing land launching configurations were considered. These configurations were above ground launch complexes, existing mobile launchers, and abandoned silos. Barge tower launching, partially submerged launching and fully submerged launching were the sea launch configurations considered. The parameters of initial cost and operational cost were heavily weighted in the determining means process. The partially submerged launch method and the modification of an existing mobile launch rail were the methods chosen to fulfill the launching requirements.

Flow table, subsonic wind tunnel, and supersonic wind tunnel modeling were investigated for use in determining the flight characteristics of the Crusader2B. Supersonic modeling was selected due to the ability to match the full scale mach number.

To determine the thermal and dynamic stresses on a mobile launch rail mounting bracket, an instrumentation package was designed and pre-tested. The instrumentation package consists of one data logger, 2 single element strain gauges, four thermocouples, high heat resistant cable, high

temperature thermocouple wire, non-shielded wire, and high temperature resistant aluminum tape.

The mounting location of the strain gauges on the launch rail mounting bracket was determined by performing an Algor analysis. The pre-tests showed that the equipment performed to specifications and within acceptable error limits. These tests also showed that the axial and torsional stresses on the mounting bracket behave linearly. Torsional stresses were found to be negligible when compared to the axial stresses and are neglected. Dynamic testing of the Super Loki sounding rocket has not been performed. Two launches are on the schedule, and data will be gathered when the rocket is launched.

References

- 1) Coleman, Jr., Paul J., "Status Report on the Spartan Conversion Project", University Space Research Association, August 10, 1992.
- 2) Hosterman, K., and Anderson, L.A., NASA/USRA Final Report 1990, "Post Landing Designs for the Assured Crew Return Vehicle," Department of Mechanical and Aerospace Engineering, University of Central Florida, Orlando, FL, 1990.
- 3) Hosterman, K., and Anderson, L.A., NASA/USRA Final Report 1991, "Design, Building, and Testing of the Post Landing Systems for the Assured Crew Return Vehicle," Department of Mechanical and Aerospace Engineering, University of Central Florida, Orlando, FL, 1991.
- 4) Hosterman, K., Thesis Report and Presentation, "Analysis of a Deployable Heat Shield Stabilization System for a Space Station-based Assured Crew Return Vehicle," Mechanical and Aerospace Engineering, University of Central Florida, Orlando, FL, Spring, 1992.
- 5) Armitage, P., and Anderson, L.A., NASA/USRA Final Report 1992, "Assured Crew Return Vehicle Post Landing Configuration Design and Test," Department of Mechanical and Aerospace Engineering, University of Central Florida, Orlando, FL, 1992.

Acknowledgments

Appreciation is expressed to the senior design students in Mechanical and Aerospace Engineering who contributed to this work. A special note of appreciation is due to Thiokol Corporation for funding the building and testing of the Soyuz model project. Thanks are due to NASA and USRA whose sponsorship made this work possible. Additional thanks go to Rockwell International, Lockheed Space Operations, the DDMS, the 41st RQS and Spaceport Florida Authority for their technical support.

DESIGN OF A LUNAR PROPELLANT PROCESSING FACILITY

University of Cincinnati
Space Engineering Research Center
with

Departments of Aerospace Engineering and Engineering Mechanics, Chemical Engineering, Civil and Environmental Engineering, Electrical and Computer Engineering, Materials Science and Engineering, and Nuclear and Power Engineering
Cincinnati, OH

Professors James Anno, Amy Ciric, Larry Cooper, Dave Greenberg, Arthur Helmicki, H. Thurman Henderson, Ray Lin, Joseph Nevin, Frank Weisgerber, Trevor Williams, and Richard Wysong
Joe Lemanski, Teaching Assistant

Abstract

Mankind's exploration of space will eventually lead to the establishment of a permanent human presence on the Moon. Essential to the economic viability of such an undertaking will be prudent utilization of indigenous lunar resources. The design of a lunar propellant processing system is presented. The system elements include facilities for ore processing, ice transportation, water splitting, propellant storage, personnel and materials transportation, human habitation, power generation, and communications

The design scenario postulates that ice is present in the lunar polar regions, and that an initial lunar outpost has been established. Mining, ore processing, and water transportation operations are located in the polar regions. Water processing and propellant storage facilities are positioned near the equator. A general description of design operations is outlined below.

Regolith containing the ice is mined from permanently-shaded polar craters. Water is separated from the ore using a microwave processing technique, and refrozen into projectiles for launch to the equatorial site via railgun. A mass-catching device retrieves the ice. This ice is processed using fractional distillation to remove impurities, and the purified liquid water is fed to an electrolytic cell that splits the water into vaporous hydrogen and oxygen. The hydrogen and oxygen are condensed and stored separately in a tank farm

Electric power for all operations is supplied by SP-100 nuclear reactors. Transportation of materials and personnel is accomplished primarily using chemical rockets. Modular living habitats are used which provide flexibility for the placement and number of personnel. A communications system consisting of lunar surface terminals, a lunar relay satellite, and terrestrial surface stations provides

capabilities for continuous Moon-Moon and Moon-Earth transmissions of voice, picture, and data

Introduction

As currently envisioned, payloads for manned missions to the moon are dominated by propellant requirements. NASA's "Report on the 90-Day Study on the Human Exploration of the Moon and Mars" estimated that the mass launched to LEO for colonization of the Moon could be reduced by several hundred tons per year if propellant were produced on the Moon. This corresponds to a savings in the \$50 billion range, which certainly justifies careful study of lunar *in-situ* propellant production. This work summarizes the design of a lunar propellant production facility and related operations by students from the University of Cincinnati.

Assumptions

This study assumes that ice containing frozen water and ammonia is present in permanently-shaded lunar polar regions.¹ The second major assumption is that a preliminary lunar outpost has been established in an equatorial region that contains established habitats, emergency medical facilities, communication facilities, offloading equipment, and other items of infrastructure useful to the construction and operation of the proposed propellant processing facility.

POLAR ICE BENEFICIATION FACILITY

Tom Cash, Tom Walker, Heather Walls

Introduction

The beneficiation facility extracts ice from the regolith by evaporation to provide the hydrogen/oxygen production plant with 563 kilograms of water mixed with 68 kilograms of ammonia per day. Due to high capillary pressures associated with removing liquids from microporous solids, only 80% of the ice can be recovered economically. A volume of 2816 m³ of regolith will be processed per day to produce the stated amount of oxygen and hydrogen.

Design Options

The technology options that were considered for the extraction process were a fluidized bed, melting, melting/vaporization/condensation, solvent extraction, and sublimation. The criteria for selecting the best extraction process consisted of process capability, processing rate, feasibility, and energy requirements. Using these criteria, the melting/vaporization/condensation process was selected.

Heating Method

Microwave energy provides a very efficient method of heating lunar regolith. The regolith can be heated with less energy than conventional methods, and the heating is accomplished in a controlled manner in much less time. This is due in part to the ability to control field intensities, heating rates, and maximum temperatures during microwave heating. Also, microwave energy tends to heat the regolith volume uniformly. High absorption rates of microwave energy are desired if the process is to be feasible.

Insulating materials such as basalt, ilmenite, and feldspars are present in the lunar regolith, with ilmenite being the most common.² Ilmenite couples with microwave frequencies of 2.45 GHz which increases microwave absorption.³ Thus, high heating rates can be achieved. With respect to lunar processing, this fact may be exploited commercially by not having to transport coupling agents into space.

Design

To obtain the amount of oxygen and hydrogen required with an 80% efficiency, a volume of 1.96 m³ must be

processed each minute. By using the dielectric properties of ilmenite at a density of 1.65 g/cm³ (dielectric constant and dielectric loss factor are 3.99 and 1.71, respectively), the amount of power output needed to heat a volume of 0.1 m³ (1 meter length x 2 meter width x 0.05 meter depth) from 100 K to 473 K is calculated as 9305 watts.⁴ This power output produces an electric field value of 4893 volts/meter. A series of twenty 15000-watt magnetrons will be used, each placed one meter apart along the length of a chamber. Each magnetron will be run at 62% of its total power output and will require a supply of 18.6 kilovolts.

Operation

Condensation is a thermodynamic process that transforms a compound and/or element from the vapor phase to the liquid phase. The constituents of this system are water and ammonia. The vapor will condense to a liquid after the required amount of heat (energy) is removed from the system. The energy to be extracted from the system to condense the vapor is dependent on the specific heat, heat of vaporization, and the mass of the vapor in the system. The rate of condensation will depend on the rate that heat can be extracted from the system. As the system is heated from 100 K, the first transformation will take place at 240 K. Here the ammonia (NH₃) will begin to vaporize until most of the NH₃ is in the gaseous phase. At this point the composition of the vapor at is nearly 100% NH₃. The system is now in a dynamic state with the temperature and pressure increasing with time. The pressure in the system will be less than the vapor pressure of water from 240 K to 473 K. At some point to be determined during this dynamic state, a valve will be opened to allow the H₂O(v) and NH₃(v) to pass through a heat exchanger starting the condensation process. The H₂O(v) will condense due to the loss of heat through the heat exchanger. The condensation will produce a thermosyphon which will be the driving force for the mass transport of vapor from the furnace to a tank. The thermosyphoning will continue until the pressure in the furnace is equal to that of the pressure in the storage tank.

The temperature in the condensate tank will be kept at a value below the boiling point of both gases. The water and ammonia will then be formed into 80-kg ice balls for transportation to the equator using the rail gun.

The beneficiation facility has a mass of 15,000 kilograms and will cost \$ 1,700,000,000. The facility does not require any personnel to operate.

DISTRIBUTED ENERGY SOURCE RAILGUN FOR LUNAR ICE TRANSPORT

John Papp

Introduction

A railgun design is chosen for bulk ice transportation from the Moon's pole to equator. Continuous transportation systems such as lunar railways, pipelines, tramways, lunar rovers, trucks, and hopping vehicles were discarded as design options due to human safety factors, maintenance, and extensive construction costs. Point-to-point methods, included ballistic and rocket transportation, were also considered. Rocket transportation proved to use more fuel than could be produced using the transported ice. Therefore, the ballistic approach of ice transportation using electric power resulted in the electromagnetic railgun design.

A railgun is very similar to a conventional canon; the major difference is the form of propulsive force. For the canon, it is the chemical reaction of gun powder and air; for the railgun, it is the simple physical principle of current loops through a magnetic field. Both achieve the same goal--supply extremely large values of propulsive force to produce high exit velocities. The components of a simple railgun are two parallel, current-carrying plates, a power supply, an armature, and the projectile. By connecting the power source to the current carrying plates and armature, a current loop is created along with an induced magnetic field. The interaction between the current and induced magnetic field produces a force on the projectile. By applying a large power supply, tremendous exit velocities of up to several kilometers per second for small masses can be attained.

Design and Operation

Multiple launches are required to reduce the tremendous amount of power that would be needed if all the necessary ice were launched at once. An optimum of ten, 80 kg ice launches per day, with three days of maintenance per Earth month, was chosen to transport the required amount of ice. The design uses a more efficient Distributed Energy Source (DES) concept with multiple powered stages rather than the conventional single-stage concept discussed above.

There are ten stages, each powered by a charged capacitor and inductor system. Ordinary differential equations describing the electrical circuit for each stage were solved using a fourth-order accurate Runge-Kutta method. The solution of these equations is represented by the calculated values below. The railgun is designed to accelerate 120 kg

module, 80 kg of which is ice, to a velocity of 1736 m/s. The powered railgun, with a bore dimension of 0.5 m square, is 121 m long, while the unpowered launch section is 200 m long. The maximum accelerating force and pressure are 2.02 MN and 8.07 MPa respectively. Values of inductance, capacitance, and voltage vary from 36.4 mH to 108.9 mH, 0.423 F to 4.23 F, and 7.65 kV to 24.11 kV respectively for the ten stages. The overall efficiency of the system is 11.7 % while the efficiency per stage is 80.9% with an overall stored energy of 361 MJ and power of 2.29 GW. The transit time of the module in the powered railgun section is 153.5 ms.

Ice projectile targeting control is achieved using reproducible methods. The ice projectile is targeted using servo controls while LED emitters and sensors measure velocity (Figure 1 and 2). Cables connected to a motor and two generators are used to reduce the module velocity accurately and predictably (B in Figure 3). Position and velocity are transmitted to a computer programmed to send a release signal once the correct velocity and position are reached (C in Figure 3). With the release signal received, the doors holding in the ice projectile are opened and the ice projectile is allowed to exit in a predetermined direction with a predetermined velocity (D in Figure 3). Pointing and velocity accuracy of the ice projectile is impossible to calculate; but, because the targeting method is reproducible, a calibration technique is used to predict landing location at varying velocities and directions.

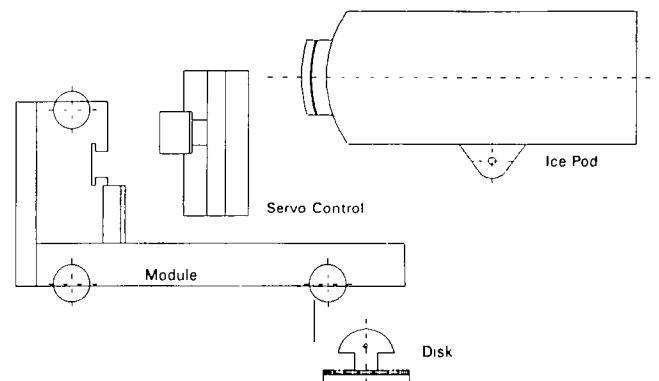


Fig. 1 Assembly view of projectile system

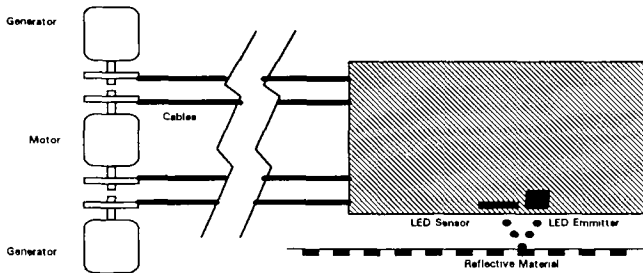


Fig. 2 Schematic of LED sensor and emitter along with braking cable system

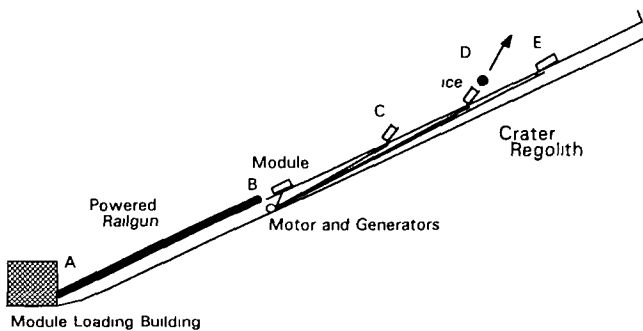


Fig. 3 Overview of typical launch scenario

MASS CATCHER

Raj Batra

Introduction

The purpose of the mass catcher is to retrieve the 80 kg ice projectiles launched by the railgun. When designing a stopping mechanism for a projectile with an incoming velocity of 1500 m/s, several criteria should be satisfied. In the interests of disposability the launched projectile, which has traversed one-fourth of the Moon's circumference, should not contain a control system nor any sort of casing. Without the control system perturbations will exist; therefore, the stopping mechanism must be mobile to accommodate for variable landing locations. In addition, the mass catcher should use minimal power and be designed for multiple catchings.

Since the mass catcher must be mobile, ideas related to stationary units such as contained crater impacts, nets, and tether systems are eliminated. Other options such as electromagnetic decelerators and orbital catchers are discarded due to the power requirements and difficulties arising from transporting ice from orbit to the lunar processing facility.

Design and Operation

What has been devised is a catching system similar to a military tank. It will be free to roam over a 1.5 km diameter paved area. The ice projectile is tracked by three ground base units. At three 10 minute intervals, the catcher will be sent information using a Laplacian method of orbit determination as to the exact impact location of the projectile. This will be sufficient time for the catcher to position itself and to allow a hydraulic jack to elevate the muzzle/funnel to a pitch angle that is aligned with the incoming projectile. The funnel is made of Kevlar-49, which has a resistive force of 344 MN and has been designed using an empirical equation calculating the critical ricochet angle. This will allow the projectile to graze the funnel, hence incurring minimal damage. The ice, upon entering the funnel, is contained by a trap door installed at the entrance of the funnel. This entrapment is required to capture the vapors produced by the imparted ice. The ice will traverse down into the belly of the catching mechanism where it will impact loosely hung chains made from MIL-12560 Armor. This will reduce part of the kinetic energy. The remnants of the projectile will then be blocked by a plate constructed from Kevlar-49 and attached to a spring-damper system.

At the end of each day, the mass catcher will be driven back to the outer perimeter of the paved surface where a pipe will be located to transport the water back to the processing facility in order to liquefy the ice. Heat supplied from the nearby nuclear power plant and ammonia extracted from ice shipments will produce a desirable chamber pressure and temperature.

PROPELLANT PRODUCTION FACILITY

Will Gareau, Larry Kruger, Bill Patrizio, Kathy Reicosky, Sherif Sakr

Introduction

The purpose of the equatorial fuel processing facility is to produce 15.22 kg/hr liquid hydrogen and 112.5 kg/hr liquid oxygen from a water/ammonia feed. These flow rates are double that of normal capacity to allow production flexibility. The plant is totally enclosed, except for storage tanks and radiative heat exchangers. This will make maintenance easier, and will protect the internal equipment from the harsh environment on the moon.

Energy costs are high, so operating the plant during the night time only would greatly reduce energy requirements. If the process were to operate during both the day and night, a separate refrigeration cycle would be needed to dissipate heat generated by the process. This refrigeration cycle would need to accommodate the nitrogen, hydrogen, and oxygen liquefaction cycles. The weight of the smaller equipment saved by operating continuously, would be less than the added weight of a large refrigeration cycle that would be needed during the daytime temperatures of 400 K.

Dissipating heat on the moon can only be accomplished by radiative heat loss. Gases to be cooled flow through radiative heat exchangers, which here are long parallel plates of glass that can be made from the regolith on the Moon, thus reducing the amount of materials needed to be transported to the Moon.

Technology Options

The feed stream from prior operations consists of an ammonia/water mixture. There are several methods which may be used to separate ammonia from water. Characteristics such as polarity and molecule size may be exploited. However, distillation was chosen because of the proven technology, the high purities needed in the effluent streams, and because of the large boiling point differences between ammonia and water. Several factors must be considered in lunar distillation design. The low gravity on the moon will result in a larger column because of the necessary residence time. Although cooling is difficult, heating is relatively cheap because heat is a major waste product of power production facilities. Heat is the main driving force in distillation, and it is more abundant than mechanical or electrical energy. The following processes were considered for the splitting of water, which is the only major native source of oxygen.

Radiolytic Cleavage

High energy radiation of water produces H^* , OH^* , H_2 , H_2O_2 , OH^- , and H^+ . Due to the production of many radicals and side products, and the large amount of energy required (approximately 2 MW), this option was eliminated.

Photocatalytic Cleavage

The irradiation of water using UV light results in the cleavage of water. This process requires two catalysts, one for hydrogen production and one for oxygen production. A sensitizing agent as well as an electron relay compound is needed for the reaction to occur. A low evolution of

hydrogen (approx. 1% of the water could be decomposed in a 28 day period) and the transportation and handling of the catalysts eliminated this option.

Thermodynamic Cleavage

The application of extreme heat (5000 K) and high pressure (10 atm) on water produces oxygen and hydrogen. Due to the low yield (max. 2.3%) and extreme material stress, this option was eliminated.

Thermochemical Cleavage

A series of chemical reactions can split water into its elements. Three separate reactions are needed, each occurring at relatively high (1200 K) temperatures and in the presence of a metallic catalyst (PtO or MgO). With the exception of water, the reactants are regenerated within the series of reactions. With a 30% conversion and up to 39% thermal efficiency, this process is the second most probable reactor system. It was not chosen due to the large amount of initial investment of transporting three reactors, their separation systems, and reactants to the moon.

Electrolysis

Electrolytic cleavage of water is accomplished by passing a current through an electrolytic substance. Hydrogen and oxygen are produced in a gaseous state at separate electrodes, which eliminates the need for a product separation system. The process itself is the simplest of the water-splitting technologies, and weighs the least. It can be transported to the Moon pre-assembled in a module. This process is currently being discussed as the future technology for obtaining hydrogen and oxygen from water by several industrial and NASA-related studies. As electrolysis is the water-splitting technology most adaptable to the Moon, it is used in this design.

Ammonia Dissociation

The ammonia will be thermodynamically dissociated by the addition of large amounts of heat. The resulting nitrogen and hydrogen streams could be separated by cryogenic distillation, absorption, or membrane separation. Cryogenic distillation, while capable of high flow rates and high purities, would only add mechanical equipment requiring maintenance to our plant. Flow rates in the ammonia subsystems are low enough that cryogenic distillation is unnecessary. Carbon beds or molecular sieves are non-mechanical, but are heavy, and would require duplicate systems for periods of regeneration. Membrane systems, in contrast, are non-mechanical, have no heat load, are low-maintenance, and have extended

lifetimes. The ammonia flow rates are small enough that a membrane system is feasible, and high purity is possible with multiple modules in series. For these reasons, a membrane separation system was chosen for the ammonia reactor outlet.

Propellant Liquefaction

The use of hydrogen and oxygen as fuels for spacecraft in NASA's space program requires the liquefaction of these gases. Liquefaction of a gas is dependent upon the temperature and pressure of the gas. In general, the lower the pressure of the gas, the lower the temperature of the gas must be for liquefaction to occur.

There are three common processes by which liquefaction can be achieved. The first of these processes involves the use of a heat exchanger to cool the gas to a temperature that is below the boiling point of the gas. This process is not feasible because it requires a cooling fluid cooler than the boiling point of the gas to be liquefied. The remaining two processes use the principle of volumetric expansion to liquefy the gas. Volumetric expansion occurs when the gas undergoes a rapid decrease in pressure. The gas maintains a constant enthalpy throughout the depressurization process while the pressure and temperature decrease. If the volumetric expansion occurs over the proper pressure range, liquefaction will occur. There are two devices that induce volumetric expansion of a gas. The first is a simple pressure release valve, known as a throttling valve, and the other is an expansion turbine. Since the valve is simpler in design and has no moving parts that would require large amounts of maintenance, it was decided that the throttling process would be the preferable expansion process.

Operation

The liquid feed stream is distilled into pure ammonia and water. The ammonia is then sent to a reactor, where heat is used to disassociate the ammonia into its nitrogen and hydrogen components. The N_2 and H_2 leave the ammonia reactor in a gaseous mixture which is separated by a membrane system. The nitrogen is then compressed and throttled to become a gaseous/liquid mixture. The gas is separated from the liquid and recycled.

The water from the distillation column is sent to an electrolysis cell that produces two product streams, O_2 and H_2 . The oxygen and hydrogen are sent to separate dryers which remove traces of water vapor. The pure oxygen stream is sent through a compressor and a radiative heat exchanger to cool it to liquid form. The hydrogen streams from the ammonia reactor and the electrolysis cell are

combined and sent to the hydrogen liquefaction process. A radiative heat exchanger is used to cool the hydrogen to ambient temperature. The hydrogen is further cooled by liquid nitrogen below 100 K. The super-cooled hydrogen is compressed and expanded to become a gaseous/liquid mixture. The gas is separated from the liquid and recycled. The liquid hydrogen and oxygen are piped to the fuel storage facility.

The major cost for the fuel production facility is from transporting the materials to the moon. The total weight of all the materials being transported to the moon is approximately 13,000 kg resulting in a transportation cost of \$1 billion. The fuel production facility is expected to require 200 kW of energy.

PROPELLANT STORAGE FACILITY

J. Matt Campbell and Chris Staneluis

Introduction

The lunar cryogenic storage facility stores liquid oxygen at a temperature of 120 K and liquid hydrogen at a temperature of 34 K. The capacity is the minimum monthly production of propellant. A modular design and parallel piping allows storage space to be increased if production is increased. Because passive means of insulation already existed in present technology, powered refrigeration was considered unnecessary even in the harsh lunar environment. Thus, insulating against the high temperature of the lunar day was the challenge.

Options

Initial designs considered whether to bury the storage tanks or to keep them above the lunar surface. Burying the storage tanks underground could stabilize the outer tank temperature to 210 K, and protection from meteorite impacts is another plus for an underground facility. Safety, maintenance, and accessibility made burying the tanks underground unfeasible. Since radiation shields would be needed for the underground facility, the safety and maintenance issues became the factors to keep the facility on the surface. Also, a heat transfer analysis considered the losses over the twenty-eight day lunar cycle. It was found that a cold lunar night balanced out a hot lunar day. The same issues existed for the pipes, so the pipes are placed on the lunar surface. The pipes, though, did not use radiation shields since product will only be shipped at night.

Storage tank design could be either cylindrical or spherical. The machining of only spherical tanks was more expensive than the cylindrical design for the facility and only offered minimal strength gains. Material selection considered weight, compatibility with each cryogenic product, availability, and price. Present commercial materials were part of this design because not enough data on light-weight plastics for this cryogenic application could be compiled nor was any of this data for the lunar environment.

Design and Operation

The final design consists of a 'Z- shaped' pipeline originating from the production facility that flows to the tank farm (Figure 4). At the tank farm, the tanks are arranged in modular form such that more tanks can be added as production is stepped up or demand lowers. The tanks are each protected by a 1 cm thick hexagonal vertical shell made of 304L stainless steel. These shells are to protect the storage tanks from any small meteorite impacts and to keep dust off the tanks' reflective surface. Centripetal pumps capable of raising pressures to 7000 kPa using 3 kW motors propel the product to the storage tanks. Along the pipeline will be the return line from the storage tanks driven by a compressor. This return line will take the boil off from the tanks back to the production facility to be recycled back into cryogenic product. The piping system is made of stainless steel. Stainless steel is chosen because of its good compatibility with both the LOX and LH, its availability and inexpensive cost, and good strength over the wide ranging lunar temperatures. Laminar flow is considered so pipe diameters are to be 0.16 m for hydrogen and 0.25 for oxygen and the minimum wall thicknesses are 7 mm for the LH line and 6 mm for the LOX line.

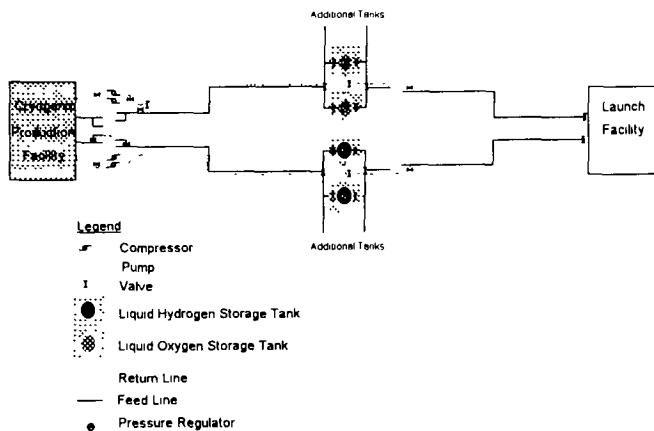


Fig. 4 Propellant Storage Facility Layout

The storage tanks are cylindrical in shape with hemispherical ends. The LOX tank is made of 304L stainless steel for the reasons stated for the pipeline. The LH tank is made of Titanium (Ti-5 Al-2.5 Sn) for its excellent strength to weight ratio and a good compatibility with hydrogen. Both tanks have a mean thickness of 1 cm. Volume for the tanks is 18 m³. This is derived from considering storage of the average of one month's production for both LOX and LH. Storage tank stress analysis is modeled on an *Ansys 4.4a* finite element program. For the Hydrogen, the tank is subjected to a maximum Von Mises stress of 3.41E8 Pa that is localized at the input pipe. The maximum Von Mises stress results in a factor of safety of 4.3. For the oxygen tank, its input pipe maximum stress is 1.42E9 Pa, which results in a factor of safety of 1.1. These results are somewhat conservative since the actual design will have a filleted input pipe and thus actual stresses are lower.

The heat transfer analysis is achieved using the Newton-Raphson numerical method. Heat transfer is minimized by using the passive method of crinkled aluminized mylar coating the storage tank's surface. By modeling the mylar as numerous heat shields, a maximum thickness for the LH tank surface is 2.15 cm and .38 cm for the oxygen tank (1cm=100 layers of mylar). Thus, the heat flux calculated for the liquid hydrogen has a total of 63.05 W/m² over the entire lunar cycle and a mean of 93.8 mW/m². For the oxygen, the total heat flux for the lunar cycle is 313.4 W/m².

POWER GENERATION SYSTEMS

Mark Gleckler, Randall Hardin, Bobbi Hartwell, Rich Listro, Chris Pickrell, Edward Schulte, Tim Taulbee

Introduction

The purpose of the power system design was to provide electrical power for the fuel processing facilities on the Moon at minimum cost and maximum reliability. We also evaluated personnel health hazards caused by radiation, developed a rough plan for the construction and implementation of the facilities, provided a remote power source for vehicles and unmanned stations, and prepared for the removal of the facilities after the mission completion.

Options

To provide power, we evaluated such options as solar, luna-thermal, chemical, combustion, radioactive decay,

fusion, and fission. After compiling the selection factors for each option, we settled upon nuclear fission as the primary source of power. This decision was based on the high specific power of fission and the ability to fulfill the mission lifetime. Research showed that many hypothetical space reactor designs existed and we decided that a modified version of the SP-100 would suit the mission well.⁵ A modular design was the goal at all levels of the design; however, differing power requirements at the polar and equatorial regions made two different designs more economical.

Design and Operation

The polar site has an overall estimated power requirement capability of one megawatt. Three reactors implemented with a thermionic topping cycle in addition to a Stirling engine and generator are used to supply the power. The equatorial site has a power requirement of only five hundred kilowatts. This is within the capability of a single reactor output. Two reactors are needed, however, for reliability reasons. The thermionic topping cycle was omitted to reduce the mass transported.

In all space environments, radiation is a health hazard. Personnel working at the processing facility can expect to receive radiation while *en route* to the moon and from a very high background radiation level on the moon. A radiation shield was needed to allow personnel to work near the reactors without exceeding the maximum dose level. The gamma and neutron shield is composed of approximately two meters of regolith, forty centimeters of lithium hydroxide, and one centimeter of steel. The final radiation level would allow a worker to travel to the moon, work at the edge of the reactors for twelve hours everyday for one hundred eighty days, and return to the Earth without exceeding the maximum allowable dose.

The polar site is the more difficult site to assemble because little equipment is assumed to already exist there, unlike the equatorial site. To construct the facility, unmanned probes will be sent first to gather data on the area. These will be followed by unmanned supply ships containing construction materials and vehicles. Personnel will finally be sent in capsules that will serve as life support modules until the habitat modules have been assembled. The entire construction process should take between three and five years.

Finally, a Dynamic Isotope Power System (DIPS) was designed to supply 2.5 kilowatts of electric power for vehicles and remote stations. The DIPS has a fifteen year lifetime to allow for use during the construction and

disassembly phases. The DIPS uses a plutonium pile to generate heat that drives a series of Stirling engines. The DIPS are maintenance free and will allow unlimited use in the fifteen year life span.

The nuclear engineers have developed a power system that accounts for personnel radiation levels and will supply the needs of the fuel processing facility throughout all phases of implementation. We have developed a rough plan for construction and use DIPS to power construction vehicles. A series of modified SP-100 reactors supply power during operation and the construction vehicles are still available for disassembly.

LUNAR COMMUNICATIONS SYSTEM UPGRADE

John Penix

Introduction

The existence of mining and propellant processing operations on the moon introduces a need for expanded communications coverage and bandwidth. The existing communications resources at the Lunar Research Center and the Lunar Industrial Park will not be sufficient to support the communication needs of the chemical processing plant and the propellant storage facilities being added to these sites. In addition, the mining operations and the beneficiation activities at the lunar pole represent an area that is not covered by the current communications system. There is also a preference to centralize the Earth-based communications center with the continued expansion of lunar activities.

By predetermining the needs of the mining and propellant processing operations, a communications system upgrade is proposed that supports the needs of the new facilities. The types of services needed between the various sites and the corresponding data rates have been taken into account. The system upgrade will consist of additional transmitters at both the equatorial and lunar pole sites as well as a lunar relay satellite to provide a link between these two sites and earth. The lunar relay satellite will reside in a halo-like orbit to provide lunar near-side coverage that will allow for communications and navigational information to be received by rovers. Coverage of the entire lunar near-side cannot be achieved with the existing Deep Space Network alone because the beam widths of the antennas are too narrow. The ability to centralize the earth based communications and control operations will be supported by the addition of two geostationary satellites working with the Deep Space Network. There will also be a need for greater redundancy

in the system due to the higher importance of the propellant processing operations.

Proposed Conceptual Design

The main assumption made in the design of the communication system is that it is an upgrade to an existing system. The basis for the specifics for the existing system and the upgrade options come from a NASA presentation outline describing the work that has been done in proposing a Telecommunications, Navigational, and Information Management (TNIM) system architecture for operations on Mars and the Moon.⁶ The assumption is made that the current operations at the Lunar Research Center are small and are of scientific, not processing or manufacturing nature, and the existing system architecture would reflect this. It is also assumed that use of the Deep Space Network will be available due to its utilization by the NASA proposal.

This level of operation would require only a minimum or moderate capability system as described by NASA. This system would involve the use of the current Deep Space Network and a single lunar surface terminal located at the research center's equatorial site. This assumption does not require any technological development beyond current levels and uses an upgrade that is currently underway for the Deep Space Network, taking it from S-band (2-4 GHz) to X-band (8-12 GHz). This minimum capability system is depicted in Figure 5.

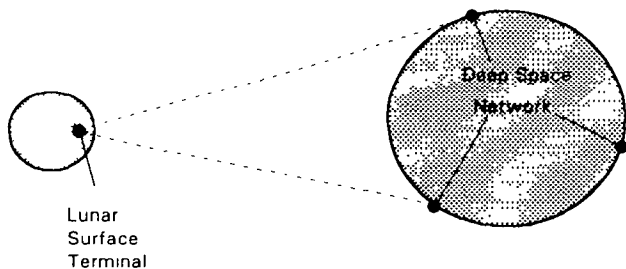


Fig. 5 Existing Lunar Research Center TNIM Architecture

The two basic objectives to be achieved by the communications system upgrade are to support the additions to the Lunar Industrial Park and the new operations at the lunar pole. Both of these requirements will be met with the addition of lunar surface terminals at the corresponding sites. These terminals will have both transmitting and receiving abilities capable of

communicating with earth and with a relay satellite orbiting the Moon.

To allow for communication between the two lunar sites and to add redundancy to the overall communications system, there will be a lunar relay satellite poised in a halo orbit over the near side of the lunar surface. This satellite will also provide the capability of covering the entire near-side lunar surface, which was not possible using the Deep Space Network. With the use of phased-array antennae, the lunar relay satellite will be able to track and monitor vehicles roving on the near-side. This may include tracking and navigational assistance for the rail-gun projectile that is being sent from the pole to the equator for further processing. The proposed upgrade of the lunar systems is shown in Figure 6.

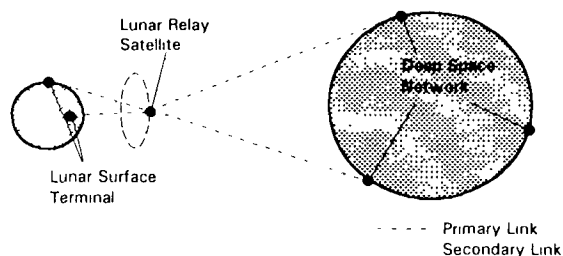


Fig. 6 Proposed Lunar Communication Support System

There may also be the preference of having a centralized command and control location here on Earth. To accommodate this preference there will have to be additional upgrades to the Deep Space Network link to the lunar end of the communication system. This addition would consist of two geostationary satellites working with one surface terminal on Earth (Figure 7). This architectural geometry would provide a constant communications link to the lunar end of the system from one earth based location.

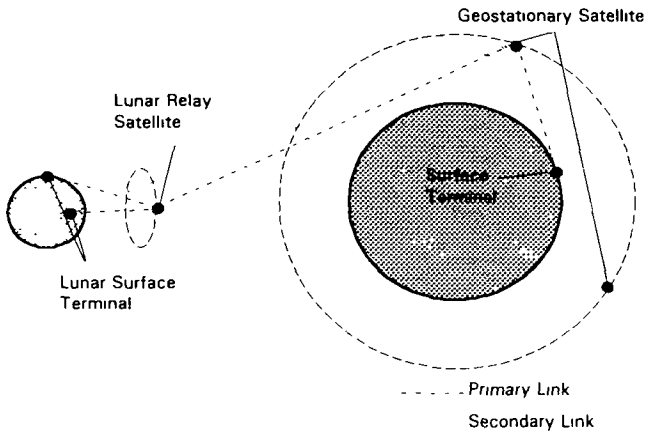


Fig. 7 Proposed communication system with centralized earth command-control location

This second system architecture could be implemented with the first system architecture as a backup for redundancy in the communication links.

Design Considerations

There are four basic system elements in the existing and upgraded communication system architecture presented. These are the Deep Space Network and their corresponding earth surface terminals, the geostationary relay satellites, the lunar relay satellite, and the lunar surface terminals.

The first of the four, the Deep Space Network, is an established communication system whose resources will be utilized for the lunar mining and propellant processing operations. At present, an upgrade is underway that would convert the Deep Space Network from S-band to K-band operations. It may eventually be necessary to convert the system to Ka-band (27-40 GHz) to facilitate even larger data requirements from the Lunar Industrial Park

The geostationary relay satellites will consist of a microwave receiver and transmitter powered by a solar array. This will require two transmitter antennae about 1-2 meters in diameter operating in the range of 50 - 100 watts, depending on the operational frequency. There will also have to be resident storage cells to insure link availability when the satellite moves through the shadow of the Earth each day. The mass of this satellite is estimated in the range of 600-1000 kilograms.

The lunar relay satellite will be very similar in configuration to the geostationary satellites. There will be the need of a third 1-2 meter transmit antenna to allow for communications between the pole, the equator and Earth

without repositioning the satellite. There is also the possible addition of a phased-array antenna to handle communications on the near-side surface. This will require an additional power source in the range of 100 watts, again depending on the frequencies desired. The mass of this satellite is estimated to be 800 - 1200 kilograms.

The lunar surface terminals will also consist of a microwave receiver and transmitter pair. These will require antennae approximately 1-2 meters in diameter, depending on the frequency of operation. The power source will be in the range of 200 watts.

During the buildup phase of the lunar sites, the system will be able to operate using only the lunar surface terminals and the Deep Space Network. The lunar relay satellite can be added when a larger bandwidth or higher frequency of communication is needed between the two lunar sites. During the operational phase, the lunar relay satellite will definitely be needed for the larger bandwidth, navigational assistance, and to introduce link redundancy. It will also be during the operational phase that the need for a centralized Earth control center may arise. This would be when the two geostationary satellites would be deployed.

The power requirement for keeping the lunar relay satellite in a halo orbit over the near-side has yet to be determined. It is also not known if the necessity of centralizing the earth based operations will be worth the cost of deploying and maintaining the two geostationary satellites.

PERSONNEL AND EQUIPMENT TRANSPORTATION

Jason Bell, John Collins, Brian Dailey, Angelique France, Charles Hamilton, Kurt Hanson, William Hull, Ken Koller

Personnel and equipment transportation will be accomplished using an innovative, reusable, chemically-powered craft called the Lunar Transport Vehicle (LTV). The LTV's 3000 mile mission from the equatorial industrial complex to the polar mining site will be accomplished via the "round-trip" method, and will occur approximately every six months. The LTV could also be used for exploratory missions.

Various systems and subsystems are incorporated in the LTV's design in order to accomplish the mission. Propulsion will be provided by four Pratt & Whitney RL10A-3-3A liquid oxygen/liquid hydrogen derivative engines, using an oxidizer to fuel ratio of 6. The structure

of the LTV is made out of Martin Marietta's lightweight Weldalite-049 alloy. The truss structure, modeled using SDRC's *I-DEAS* engineering analysis software, is designed for a maximum deceleration of 5 g and touchdown velocities of 10 m/s. Landing gear is hydraulic and able to withstand many loadings, even on the treacherous lunar terrain. The LTV is equipped with four small groups of thrusters in order to control its attitude about three axes of rotation. The guidance and navigation for the LTV includes a Hexad inertial navigational system (INS), as well as internal gyroscopes, inertial measurement units (IMU) and accelerometers. Also, the LTV will be equipped with several video cameras, recorders, and radar to provide continuous range rate data. Communication from the LTV will be transmitted at a rate of 200 kbps, and power will be supplied by fuel cells.

LUNAR STRUCTURES

Steve Hudepohl and Greg Schreppel

Introduction

The Civil Engineering Department coordinated the design of the lunar habitats and the railgun supporting structure. For both structures, various factors were considered in order to make the design as economically efficient as possible. These factors include the weight (mass) of imported materials, cargo space requirements for transportation of the structural systems, construction of the systems and required equipment, maintenance requirements, and micrometeorite and radiation protection

Lunar Habitats

The establishment of a lunar habitat early in the construction phase is vital to expediting completion of the lunar processing facility. A habitat which can accommodate any number of occupants as efficiently as possible and which can be assembled in a short period of time will be necessary. To meet these criteria, a modular design was chosen for the habitat. In this type of design, the habitat was designed to support three personnel, since this is the minimum requirement for an EVA (Extra Vehicular Activity). To accommodate additional personnel, multiple habitats, arranged in any configuration, can be established either as one large habitat at a central location or as several smaller habitats placed throughout the processing and mining sites.

Each habitat will be equipped with facilities for sleeping, eating, hygiene, and recreation, as well as facilities for

communications and research. Power will ultimately be supplied by a separate facility; however, during initial construction power must be provided by batteries and/or solar cells. These modular habitats will be transported to the lunar surface at various phases of construction until the number of habitats provided satisfies the occupant space required for operation of the completed facility.

Two habitat designs were initiated for this project. Both habitats were designed to support three personnel and sustain an internal pressure of 12 psi. To shield personnel from micrometeorites and radiation, both habitats were designed to have a 2 meter layer of regolith cover.

The first habitat alternative consists of both a flexible and rigid structure (Figure 8). The flexible or inflatable structure is made up of high strength fabric reinforced with steel cables. This structural system holds the 12 psi internal pressure. Since this structure is inflatable, a rigid structure is required to prevent the collapse of the regolith cover should the pressure be released.

The second habitat alternative (Figure 9) is made up entirely of a rigid structure. This structure resists both the internal pressure and the overburden pressure of the regolith cover. The habitat consists of five modules (5.34 m x 5.34 m) connected together by a short network of cylindrical passageways. Although identical in structure, each module serves a specific function so that together they form a suitable habitat

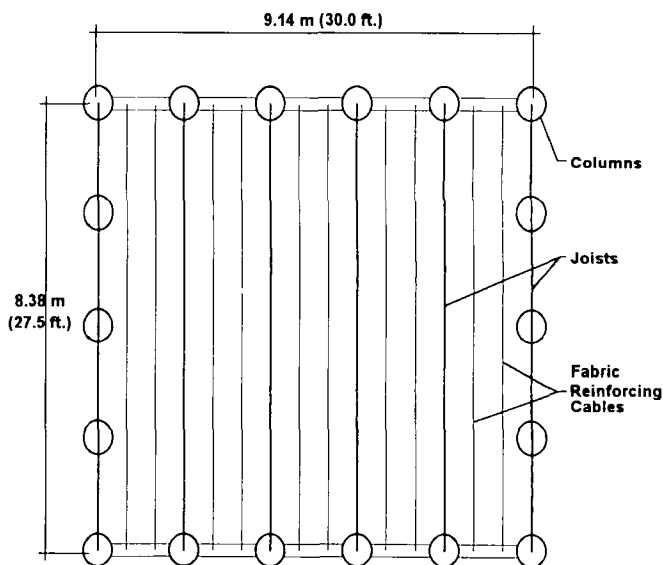


Fig. 8 Plan View of Habitat Alternative #1

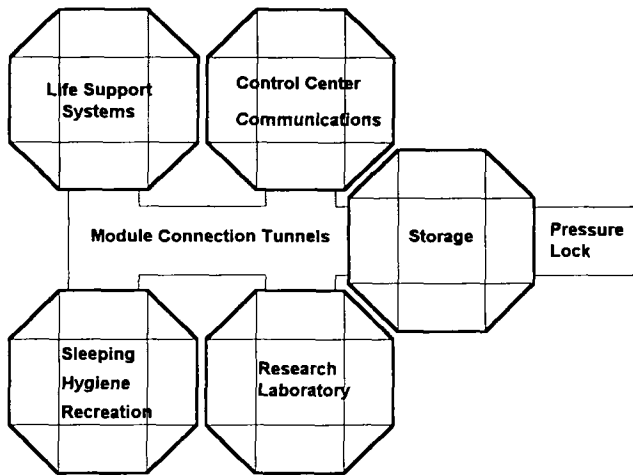


Fig. 9 Plan View of Habitat Alternative #2

Railgun Supporting Structure

Since the overall length of the railgun is about 300 meters and the required muzzle angle is about 23 degrees, the use of imported materials for the supporting structure was economically impractical. Instead, the crater wall was used to achieve the required angle. A ten meter wide path was designed and steel footings were used to transfer the railgun loads to the regolith. The path would be created using equipment capable of excavating and compacting regolith.

Acknowledgments

The students would like to thank all professors listed and unlisted whose help and guidance were invaluable to the completion of this design project. A special thanks goes to Larry Cooper, from the University of Cincinnati NASA Space Engineering Research Center, whose efforts made this project possible and exciting to work on.

Assistance was received from many industrial sources. In particular, the chemical engineering group would like to acknowledge James McElroy of United Technologies Hamilton Standard Division for his assistance on electrolyzer technology and design.

A final thanks to the USRA and center mentor Keith Henderson of NASA JSC for making this experience available.

References

- 1) Arnold, J.R., "Ice in the Lunar Polar Regions," *Journal of Geophysical Research*, Vol. 84, Sep. 1979, pp. 5661-5669.
- 2) Frondel, J.W., *A Glossary of Lunar Materials*, John Wiley, New York, 1973, p 72.
- 3) D.S. Tucker, D.T. Vaniman, J.L. Anderson, F.W. Clinard Jr., R.C. Feber Jr., H.M. Frost, T.T. Meek, and T.C. Wallace, "Hydrogen Recovery from Extraterrestrial Materials using Microwave Energy," *Lunar Bases and Space Activities of the 21st Century*, W.W. Mendell (ed.), Lunar and Planetary Institute, Houston, 1985, pp. 583-590.
- 4) Fielder, G. (ed.), *Geology and Physics of the Moon*, Elsevier Publishing Inc., Amsterdam, 1971.
- 5) French, J.R., "Nuclear Powerplants for Lunar Bases," *Lunar Bases and Space Activities of the 21st Century*, W.W. Mendell (ed.), Lunar and Planetary Institute, Houston, 1985, pp. 99-106
- 6) Zuzek J., *Space Communications Seminar - Seminar notes*, NASA Lewis Research Center, Cleveland, 1992.

RADIATION SHIELDING FOR INTERPLANETARY SPACECRAFT

**Duke University
Department of Mechanical Engineering and Materials Science
Durham, North Carolina**

**Professor Franklin H. Cocks
Seth Watkins, Teaching Assistant**

Alex Adkins, Edward Bond, J.P. Errico, Jason Garverich, Bill Goldsmith, John Gregory, Tom Harrison, Jr., Mustafa Haziq, Douglas Holt, Eric Howard, Al Johnson, Jr., Aaron Keith, Peter Laz, Jr., Doug Lindquist, Krista Olson, Graham Orriss, Vibby Prasad, Hans Steege, Alexander Vaughn, Brent Ward, David Wasik, and Brian Yamanouchi.

Abstract

The concept of using a superconducting coil for magnetic shielding against solar flare radiation during manned interplanetary missions has long been contemplated and was considered in detail in the years preceding the Apollo missions. Only lower temperature superconductors were then known, and the field coils needed to produce the protective field were limited in size to the ship dimensions. These coils were ineffective unless they carried enormous total circulating currents, and their potential use in the Apollo program was abandoned. With high temperature superconductors, it has now become realistic to consider deploying the field coils beyond the spacecraft hull and the current requirement is dramatically lowered together with the total system mass and energy requirements. Importantly, concomitant experiments are made possible with such a magnetic field generating system -- the interaction between the field of the earth and the field produced by the superconducting coil to obtain a thrust capable of increasing the mean orbital radius and the magsail. With current high temperature superconductor materials, especially wires that have been produced within the last year, a test of all these concepts now appears possible through the use of a payload small enough to fly piggyback aboard another mission.

Introduction

The ultimate objective of this work is to design, build, and fly a dual-purpose, piggyback payload whose function is to produce a large volume, low intensity magnetic field and to test the concept of using such a magnetic field (1) to protect spacecraft against solar flare protons, (2) to produce a thrust of sufficient magnitude to stabilize low satellite orbits against orbital decay from atmospheric drag, and (3) to test the magsail concept. These all appear to be capable of being tested using the same deployed high temperature superconducting coil. In certain orbits, high temperature

superconducting wire, which has now been developed to the point where silver-sheathed high T_c wires one mil in diameter are commercially available, can be used to produce the magnetic moments required for shielding without requiring any mechanical cooling system. The potential benefits of this concept apply directly to both earth-orbital and interplanetary missions. The usefulness of a protective shield for manned missions needs scarcely to be emphasized. Similarly, the usefulness of increasing orbit perigee without expenditure of propellant is obvious. This payload would be a first step in assessing the true potential of large volume magnetic fields in the U.S. space program. The objective of this design research is to develop an innovative, prototype deployed high temperature superconducting coil (DHTSC) system.

Historical Perspective

The concept of using superconducting coils to produce magnetic fields for protection from energetic particle radiation has been developed since the late 1950s. While contemplated as a means of providing radiation protection during manned missions beyond the magnetosphere, the concept gained interest in the early 1960s as a means of protecting satellites from nuclear blasts. On July 9, 1962, an explosion of a 1.4 megaton nuclear device 250 miles above Johnston Island (Project STARFISH) produced an artificial radiation belt with a peak radiation dose rate of approximately 120,000 rads per hour. This resulted in the loss of three satellites¹, and produced significant concern over satellite protection technologies. This concern led to the production of a laboratory-based prototype system which relied on low-temperature superconductors, and the idea was further developed for manned space missions. Magnetic shielding was one radiation shielding concept seriously considered for the Apollo missions, although it was later abandoned. The use of magnetic-field shielding for satellites has recently been reassessed for satellite shielding applications due to the advent of high temperature

superconductors.² With renewed interest in manned missions to Mars, magnetic shielding appears to provide the required capabilities for proper crew shielding at significant energy savings over all other designs.

Radiation Issues for Manned Spaceflight

Energetic space radiation is generally classified by three prime sources: radiation due to trapped particles in the Van Allen Belts, radiation in the form of galactic cosmic rays, and radiation due to solar particles emitted in flares, storms, and the solar wind. For interplanetary travelers, the particles that pose the greatest threat are those with high energy and fluxes. Galactic cosmic rays contain particles with the highest energies (typically greater than 1 GeV), followed by solar flare particles (10 to 1000 MeV), and finally Van Allen belt radiation. The former two forms of radiation pose potential exposures that dwarf the latter.

Historical data is commonly used to predict potential exposures, and the benchmark solar flares most often cited occurred in February of 1956, November of 1960, and August of 1972. While these flares are among the most powerful ever recorded, their magnitudes are not unique. In fact, a flare of the same order of magnitude as the August 1972 event was recorded in October 1989.³ The unshielded blood-forming-organ (BFO) dose equivalents for the three events were 62 rem, 110 rem, and 411 rem respectively.³ The BFO dose equivalents were 31.5 rem, 39.8 rem, and 50.7 rem respectively even with a 10 grams per square centimeter shield.⁴ Since the recommended rem limit for vital organs over a 30 day period for astronauts is 25 rem, and is placed at 50 rem annually⁵, significant concern must be raised for any long duration space missions. While current U.S. manned missions benefit from the natural protection afforded by the Earth's magnetosphere, interplanetary missions will require specific attention to shielding in spacecraft design. The solar cycle is a period of 11 years, and it has been noted that extremely large flares occur once or twice per cycle with lesser flares occurring every few weeks.⁶

While the Apollo missions were successfully planned to avoid periods of high solar flare activity, this will not be possible for manned Mars missions, which will last several years. In addition, the unpredictability of large solar flares forces mission designers to consider worst case scenarios for potential exposure levels. Finally, it should be recognized that the cumulative effects of smaller flares will be quite significant as well. If normal levels of solar flare activity are assumed, it has been predicted that an unprotected crew would receive an annual dose of 100 rem per year on a Mars mission.⁷

Mass Shielding

Mass shielding is generally referred to as a passive shielding concept. Simply, bulk forms of matter have inherent shielding capabilities. The major problem encountered with mass shielding is that the required shield thickness increases precipitously as the energy of the particles to be protected from increases. Furthermore, the production of energetic secondaries as a result of energetic particles interacting with the shielding material must be considered, and it should be noted that the level of production of secondary particles such as gamma rays, protons, and neutrons, is a function of the type of shielding material, and specifically increases with increasing atomic number.⁸ For a Mars mission, however, the various mass shielding concepts that have been suggested all suffer from the disadvantage of being inherently too heavy for practical implementation. This is especially the case if the most penetrating of the solar flare radiation is to be stopped. Thus, while the structural configuration of a spacecraft provides inherent shielding, additional shielding strategies must be considered in order to achieve reasonable mass levels.

Alternative Shielding Strategies

A number of active shielding concepts have been suggested, including electric, magnetic, and plasma shielding. Of these, both the electric and plasma shielding strategies suffer from severe technical problems which render their implementation infeasible. Thus, magnetic shielding, which simply involves creating a magnetic field around a spacecraft and thus deflecting charged particles, appears to be the greatest hope for use as an active shield.

Magnetic Shielding

Work on the magnetic shielding concept was initiated before manned spaceflight was even realized.^{9,10,11} Original development of the concept was, of course, limited to low temperature superconductors, at liquid helium temperatures. The use of such low temperature superconductors posed a daunting set of problems. First, even with the equilibrium temperatures attained by a spaceship in outer space, cooling to liquid helium temperatures would still be needed through mechanical refrigeration techniques in order to achieve the superconducting state. This requirement alone limited magnetic shielding designs to the use of ship-board coils¹², especially due to the power requirements for maintaining the

cryogenic temperature¹³ Second, ship-board coils required high magnetic field intensities only achievable through extremely high currents in order to shield a reasonably high volume. Third, the masses of the coils and the related supporting structures required for such coils brought into question any gains in savings over mass shielding techniques.^{12,14,15} It was found that a weight-savings was achieved when protecting against 1 bev or higher protons, and that the structural support of the shield was the main component of the total mass of the system.¹⁶

One additional concern noted with magnetic shields is the effects that such high magnetic fields might have on living organisms, especially due to long-term exposures. Studies have been undertaken as to the potential dangers to space travelers¹⁷, but no opinion has won general acceptance even today. The debate on the general topic of magnetic field interactions with living organisms still can be seen especially seen with respect to the high voltage electrical lines that are used to supply power across the country. However, with proper design the field present in the crew quarters can be reduced to values lower than normally present on earth.

With the advent of high temperature superconductors, heightened interest in magnetic shields is apparent. This interest is further fueled by recent planning for a manned mission to Mars which would directly benefit from the development of magnetic shielding technologies. A number of studies have focused on the use of the new ceramic materials which can achieve superconductivity at liquid nitrogen temperatures as well as on possible configurations for a magnetic shield. One such configuration is that of a deployed torus.¹² These new superconducting materials present a number of notable advantages, including significantly less cooling needs as well as deployed configurations for superconducting wires. The deployed configuration appears especially promising due to enormous reductions in mass and energy requirements over previous ship-board coil designs. In addition, the danger that catastrophic failure of the magnetic shield poses to a spaceship's crew is minimized by deploying the shield away from the ship as opposed to producing the necessary magnetic fields with a ship-board coil.¹²

Mathematical Basis for the Design

The concept of using deployed high temperature superconducting coils for producing magnetic fields has been developed by several investigators^{12,18}, and it is instructive to examine the basic principles behind this concept. First, it is important to establish the desired characteristics of the shield. In a practical full sized scenario, it is desired to fully protect an area of a spaceship

of 10 meters radius. With the constraint of establishing the maximum level of energetic particles, the necessary magnetic field strength can be calculated once the protected dimension is determined. This dimension, C_{st} , known as the Störmer radius, has been shown to measure the magnetically protected region¹⁹, although complete protection is only achieved in approximately 40% of that characteristic length⁹. This dimension, measured in meters, is determined as follows²⁰:

$$C_{st} = \sqrt{\frac{q\mu_o M}{4\pi P}} \quad (1)$$

where q = the particle charge
 μ_o = the permittivity of free space
 = $4\pi \times 10^{-7}$ H/m
 P = relativistic particle momentum

The magnetic moment, M , can be calculated using the relation

$$M = NIA \quad (2)$$

for which N = the number of turns in the loop
 I = the current in each turn
 A = the area enclosed by the loops forming the coil

Now, momentum is calculated as the product of the mass and the velocity of an object. However, in the case of basic particles, relativistic considerations must be made. Thus, in the case of particles approaching the speed of light, the momentum is calculated as follows:

$$P = \frac{m_o v}{\sqrt{1 - \left(\frac{v}{c}\right)^2}} \quad (3)$$

where m_o = the particle rest mass
 v = the particle velocity
 c = the speed of light
 = 3×10^8 m/s

The calculation of momentum as achieved using equation 3 may also be achieved using the relativistic relation in equation 4:

$$\gamma = \frac{1}{\sqrt{1 - \left(\frac{v}{c}\right)^2}} \quad (4)$$

Equation 4 is simply the ratio of the actual energy of the particle in question to the rest energy of that particle, as simplified in equation 5:

$$\gamma = \text{Actual Energy} / \text{Rest Energy} \quad (5)$$

In the specific case of interest, if it is desired to fully protect a radius of 10 meters, then the Störmer radius will need to be approximately 25 meters. The magnetic moment may be calculated from equation 1. A cutoff energy of 200 MeV has been suggested²¹, and to protect a Störmer radius of 25 meters from protons of this energy, the relativistic momentum must be found. Knowing that 1 MeV is equivalent to 1.6×10^{-13} joules, the kinetic energy of 200 MeV protons can be used to determine the velocity of those protons. This is achieved through solving the following:

$$K.E. = mc^2 - m_0c^2 \quad (6)$$

Here, m_0 is the mass of the proton which is 1.66×10^{-27} kg. Thus, using equation 6 with 3.2×10^{-11} joules of kinetic energy, a proton is traveling at a speed of 1.7×10^8 m/sec (approximately 57% the speed of light). The momentum of the proton can then be found using equation 3, and is determined to be about 3.6×10^{-19} kg-m/sec. Using equation 1, the magnetic moment for protection against these particles is thus found to be nearly 1.4×10^{10} ampere-turns $\cdot m^2$.

Now, the case of a ship-board coil versus deployed coils can be examined in greater detail. In particular, since the magnetic moment increases as the area enclosed by the coil it is immediately seen that the needed current, I , for a single turn coil will decrease with the radius of the coil. To obtain the dependence of the total stored electrical energy needed to activate the shield as a function of the radius of the torus, one can solve for the total current using equation 1, to give:

$$I = \frac{4\pi C_{st}^2 P}{q\mu_0 A} \quad (7)$$

Equation 7 may be solved, for example, for 200 MeV protons to approximate the current in amperes as a function of radius as :

$$I = \frac{4.5 \times 10^9}{R^2} \quad (8)$$

Here, it is interesting and important to note a relation which determines the energy required for magnetic shielding.

The energy stored in the system, E , is given by

$$E = \frac{1}{2} LI^2 \quad (9)$$

where L = the coil inductance.

If equation 7 is substituted into equation 9, and if the inductance is assumed to be a constant, then an expression for energy as a function of radius is obtained:

$$E = \frac{1}{2} L \left(\frac{4\pi C_{st}^2 P}{q\mu_0 A} \right)^2 \quad (10)$$

For the example that we have here considered (200 MeV protons, C_{st} of 25 meters), equation 8 can be substituted into equation 9 to yield:

$$E = \frac{1}{2} L \frac{(2 \times 10^{19})}{R^4} \quad (11)$$

While it should be realized that this equation, of course, varies with the energy of the particles as well as with the desired Störmer radius, the important result shown is the dependence on the radius to the minus fourth power. This shows that the smaller the radius and consequently the smaller the torus, the larger the energy required by a massive factor. This is especially relevant when considering deployed coils of much larger size, since likewise the bigger the radius and consequently the bigger the torus, the smaller the energy requirement for protecting from the same energetic particles, again by a fourth power dependence.

Torus Mass Optimization

The torus size and mass can be optimized with knowledge of the total mass as a function of the radius of the torus. First, it should be realized that the total mass (TM) is simply the sum of the wire mass (MW) and torus-tube mass (MT):

$$M_{TOT} = M_w + M_T \quad (12)$$

The wire mass is determined as follows:

$$M_w = 2\pi R a \rho \quad (13)$$

where R = torus radius
 a = total cross sectional area of wire
 = ratio of the current to the total current density
 ρ = superconductor wire density

The torus-tube mass is found as follows:

$$M_T = 2\pi R m \quad (14)$$

where m = the mass of the torus per unit length.

The optimum size in terms of the radius is finally determined by differentiating the total mass with respect to the torus radius, and then setting this to zero.

With the above procedure and previously calculated results, it is possible to now optimize the size and mass of the torus for particular constraints. First, it is assumed that the mass of the tube which forms the desired torus is 87 g/m, which is based upon the estimated total surface area required for Mylar. Assuming protection of a Störmer radius of 25 meters, equation 8 can be used to perform the optimization. Further constraints on the capabilities of the superconductor wire must be established and these can be based on recent reported properties of high temperature superconductor wire. It is claimed that a current density of 108 amps/m² can be achieved²², with a wire density of approximately 8 g/cm³. Now, if it is still desired to protect from 200 MeV protons, then the total mass can be found to be the sum of the superconductor wire mass and the torus mass using the above results.

Knowing that the critical current in a wire is simply the ratio of the current to the cross sectional area (a) of that wire, the cross-sectional area can be computed as a function of radius. Thus, using equation 8, the following approximation results:

$$a = \frac{45}{R^2} \quad (15)$$

The mass of the wire may then be calculated by simply multiplying the circumference of the wire by the cross-sectional area and the density of the wire. This results in the following:

$$M_w = 2\pi R a \rho = \frac{2.3 \times 10^6}{R} \quad (16)$$

Next, the mass of the torus-tube must be calculated, and this is found similarly as the product of the circumference and the mass of that tube per meter:

$$M_T = 2\pi R \left(0.09 \cdot \frac{\text{kg}}{\text{m}^3}\right) = 0.55R \quad (17)$$

Thus the total mass, being the sum of the wire mass and tube mass, is simply:

$$M_{TOT} = \frac{2.3 \times 10^6}{R} + 0.55R \quad (18)$$

To find the optimum size, equation 18 can be differentiated with respect to the radius and set equal to zero as follows:

$$\frac{dM_{TOT}}{dR} = \frac{2.3 \times 10^6}{R^2} + 0.55 = 0 \quad (19)$$

Solving this equation yields an optimum radius of 2036 meters. The optimum mass is then found using equation 18 to be 2240 kg for the full size (not prototype) system. It should be noted that the weight of the wire is equal to the weight of the tube in the optimum case. This problem can be easily repeated for any assumed Störmer radius, proton energy, or tube mass per unit length.

Calculation of Force and Stress in Coils

The forces and stresses involved in a deployed coil system. These characteristics may be calculated as follows. First, the magnetic force in a single wire coil may be determined from the following relation²³:

$$F_{MAG} = \frac{\mu_o I^2}{4\pi} \left[\ln\left(\frac{8R}{r}\right) - \frac{3}{4} \right] \quad (20)$$

where R = the coil radius
 r = the wire radius
 μ_o = the permittivity of free space
 = $4\pi \times 10^{-7}$ H/m
 I = the current

The wire radius must be calculated, and this is achieved once again by realizing that the area of the wire is equal to the ratio of the current (I) to the critical current density (J). Thus, the wire radius is determined using the following relation:

$$r = \sqrt{\frac{I}{\pi J}} \quad (21)$$

As an example, if the required current is 1093 amps as calculated above and the critical current density is 10⁸ amps/m², a required wire radius of 1.87 x 10⁻³ meter is found. This allows the magnetic force to be determined from equation 20, and this value is found to be 1.82 newtons, which is very low. The stress is simply the ratio of

the force to the area, as is shown below:

$$\sigma = \frac{F_{MAG}}{\pi r^2} \tag{22}$$

Using equation 22, a stress of $1.66 \times 10^5 \text{ N/m}^2$ is found.

The stress in terms of the Störmer radius and the coil radius can be calculated by combining equations 1, 20, and 22, to obtain the following relation:

$$\sigma = \frac{JC_{st}^2 P}{\pi q R^2} \left[\ln\left(\frac{8R}{r}\right) - \frac{3}{4} \right] \tag{23}$$

As an approximation, it can be seen from equation 23 that the stress increases as a function of the square of the Störmer radius and decreases as a function of the square of the torus radius, neglecting the $\ln R$ term. All of these calculations can be repeated for any chosen particle energy and Störmer radius.

Selective Emitter Calculations

With the planned use of superconducting wire, the equilibrium temperature attained by the wire in the currently envisioned deployed state¹² suggests the necessity of supplemental cooling. This is due to the fact that the superconducting conditions require temperatures below the equilibrium temperature. Even by using selective absorber and emitter coatings with an absorptivity to emissivity ratio of 6.17×10^{-2} , achievable with glass films with an internal reflecting layer of silver, the equilibrium temperature attained is still 147°K .¹² This assumes that the coil consists of 1 wire oriented with its major length perpendicular to the sun. Of course, this is well above the transition temperature of the known high temperature superconducting materials.

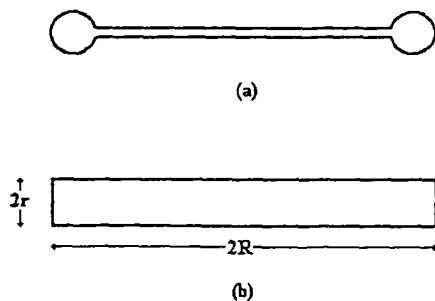


Fig. 1 Torus geometry shown in (a) cross section and (b) area projection (Note: not to scale, the sunlight is parallel to the plane of the torus)

A different approach to the problem of cooling a deployed high temperature superconducting coil is to use selective absorber and emitter coatings over a greater area of illumination. For example, by providing a mesh or Mylar sheet that has a desired absorptivity to emissivity ratio across the length of the central region inside the torus, as shown in Figure 1, and by orienting that sheet perpendicular to the sun, the area of illumination compared to the radiating area is significantly decreased.

The desirability of adding this sheet to the design may be proven by examining the energy balance between the absorption of solar energy and the reradiation of that energy. The total power absorbed by a body is governed by the following relation:

$$P_{in} = S\alpha A_1 \tag{24}$$

- where S = the solar power flux (watts/cm²)
- α = the absorptivity
- A_1 = the illuminated area

The total power radiated away from a body is found as follows:

$$P_{out} = \sigma \epsilon A_2 T_e^4 \tag{25}$$

- where σ = the Stefan-Boltzman constant
- $= 5.67 \times 10^{-12} \text{ watts/cm}^2\text{-K}^4$
- ϵ = the emissivity
- A_2 = the emitting area
- T_e = the temperature of the body

If it is now assumed that the major radius of the torus is 2036 meters and the minor radius is 0.5 meter, the illuminated area and the emitting area can be determined. First, the illuminated area is simply the product of the major diameter and the minor diameter, as indicated below:

$$A_1 = (2R)(2r) \tag{26}$$

This is calculated to be 4072 m^2 with the example we have been using. The emitting area is next found as follows:

$$A_2 = [(2\pi R)(2\pi r)] + [2\pi(R-r)^2] \tag{27}$$

This accounts for the area gained from the inner sheet of foil, and is calculated to be $2.61 \times 10^7 \text{ m}^2$ in this case. Now, by setting equation 24 equal to equation 25, the following relation is obtained:

$$T_e = \left(\frac{S\alpha A_1}{\sigma \epsilon A_2} \right)^{\frac{1}{4}} \quad (28)$$

Finally, if the same absorptivity to emissivity ratio of 6.17×10^{-2} is used, and if the solar constant is estimated to be that at Earth orbit, 1350 watts/m^2 ,¹² then the equilibrium temperature can be found using equation 26. This reveals that an equilibrium temperature of 21.9 K is achieved, which is well below the required equilibrium temperature of approximately 77 K.

Thus, it appears that a viable alternative to using mechanical cooling exists. However, numerous design problems are presented by this configuration. First, a total area of $1.3 \times 10^7 \text{ m}^2$ of foil would be required as the sheet material, and the deployment of such a foil would not be trivial. Second, this foil may present a mass penalty, but this would need to be evaluated in light of the enormous masses (and energies) required by mechanical cooling systems. A third problem is that the orientation of the torus would need to be maintained. This might be difficult due to variations in the intensity of the magnetic field, but is certainly achievable with present-day orientation and stabilization technologies developed for satellites. Fourth, it should be noted that a temperature gradient would exist across the area of the web or foil, with the coldest point being at or near the middle. This might require increasing the rate of thermal conduction in the web or foil. If a hollow web was used, this problem could be solved by allowing a gas to circulate through the matrix by forced convection. Only a small quantity of gas would be required here. Alternatively, the entire configuration could be allowed to cool naturally, as long as the necessary time for such cooling is within practical limits on such a mission. This entirely self-cooled system, with its stringent requirement on orientation, may not be practical with many designs that have already been proposed for a Mars mission. However, it does indicate the engineering possibility of dispensing with mechanical cooling entirely if the mission design can be approached with a free hand.

Shield and Spaceship Configuration

A previously published design for a manned Mars expedition took into account special considerations, such as the requirement of producing artificial gravity by rotation, and resulted in a specific ship geometry. This geometry has been adapted to incorporate a high temperature superconducting coil magnetic shield, as shown in figure 2. This geometry displays a coil of approximately a figure eight configuration in deployed state. One important design criteria is the production of a magnetic

field to protect the crew quarters, and thus a distribution of the coil wires around the exterior of those areas those areas is essential such that the magnetic field in the interior of the living quarters are substantially canceled out.

Using the Deployed Coil as a Magnetic Sail

It was first suggested by Engleberger²⁴ that the interaction between a shipboard magnetic field and the earth's magnetic field could provide a small amount of propulsion. Since this propulsive force will increase as the ship's magnetic field increases, it is evident from the magnitude of the magnetic moments discussed here that it is possible to consider this in the present case. However, detailed calculation shows that with a assumed magnetic moment of $1.5 \times 10^5 \text{ amps} \cdot \text{m}^2$ (the prototype payload scale) only 2 millionths of a pound of thrust can be obtained in this fashion. More interestingly, it has also been suggested that thrust may also be obtained due to the change in momentum of the repelled protons. Zubrin has estimated that accelerations on the order of 0.01 m/s^2 may be obtained in this fashion.²⁵ Since, in either case, what is needed is a large magnetic moment and since this is what is produced by the method described here, it is evident that both of these concepts might be tested using the same payload as that needed to test radiation shielding

Design of a Prototype System

Efforts have been focused in the current design cycle on defining the criteria for constructing a prototype system to test the magnetic shielding concept. A small, self-contained payload is envisioned, one which is capable of being launched piggyback on another mission into geosynchronous orbit. Prototype design includes the following areas:

- torus deployment system
- sensing technologies
- command, control, and communications technologies
- energy control technologies
- thermal considerations
- flexible superconducting wire

An important consideration is scaling, i.e. the sizing of the deployed coil. Detailed calculations on this matter using the equations given above have shown that with currently available high temperature superconducting wires it should be possible to use a deployed coil having a radius of under ten meters to shield a 10 centimeter zone around the torus major diameter against 50 MEV protons. The total system mass goal is 200 kg.

One highlight of the semester work was a teleconference with our NASA mentor, Don Carson, at Goddard Space Flight Center. The class is shown in figure 3, interacting during this meeting.

Acknowledgments

The assistance provided by Eric Smith, Head of the Vesic Engineering Library at Duke University, Chris Sussingham in the Duke AutoCad laboratory, and the enormously helpful input from our mentor, Don Carson, at Goddard Space Flight Center is gratefully acknowledged

Fig. 3 The senior mechanical engineering design class held a teleconference with NASA in order to discuss design parameters and strategies



- 1 Hawkins, S.R. "A Six-Foot Laboratory Superconducting Magnet System for Magnetic Orbital Satellite Shielding", in *International Advances in Cryogenic Engineering. Proceedings of the 1964 Cryogenic Engineering Conference (Sections M-U)*. Edited by K. D. Timmerhaus, Plenum Press, New York, 1965, pp. 124-136.
- 2 Vittitoes, Charles N., "Magnetic-Filed Shielding of Satellites From High-Energy-Electron Environments," *Sandia National Laboratories, Albuquerque, New Mexico, SAND--89-2956*, May 1990.
- 3 Simonsen, Lisa C. and John E. Nealy, *Radiation Protection for Human Missions to the Moon and Mars*, NASA Technical Paper 3079, 1991.
- 4 Townsend, Lawrence W., John E. Nealy, John W. Wilson, and William Atwell, "Large Solar Flare Radiation SHielding Requirements for Manned Interplanetary Missions," *Journal of Spacecraft and Rockets*, Vol. 26 (1989), pp. 126-128.
- 5 Fry, R.J. and D.S. Nachtwey, "Radiation Protection Guidelines for Space Mission," *Health Physics*, Vol. 55, No. 2, August, 1988, pp. 159-164.
- 6 Nealy, John E., Lisa C. Simonsen, Lawrence W. Townsend, and John W. Wilson, "Deep-Space Radiation Exposure Analysis for Solar Cycle XXI (1975-1986)", *SAE Paper 901347*, 1990, pp. 980-987.
- 7 Woodward, Daniel and Alcestis R. Oberg, "The Medical Aspects of a Flight to Mars", in *The Case for Mars*, Penelope J. Boston, Ed., Univelt, Inc., 1984, p. 173-180.
- 8 Kash, Sidney W. and Robert F. Tooper, "Active Shielding for Manned Spacecraft," *Astronautics*, September, 1962, pp. 68-75.
- 9 Levy, R.H., *Radiation Shielding of Space Vehicles by Means of Superconducting Coils*, Avco Corp., Avco Everett Div., Res. Lab., Res. Rep 106 (AFBSN TN 61-7), Apr. 1961.
- 10 Dow, Norris F. "Structural Implications of the Ionizing Radiation in Space", *Proceedings of the Manned Space Stations Symposium*, Los Angeles, California, April 20-22, 1960 (as cited by Levy).
- 11 Singer, S.F., "Some Consequences of a Theory of the Radiation Belt", *9th Annual Congress of the IAF*, Amsterdam, August 26, 1958 (as cited by Levy).
- 12 Cocks, F. Hadley, "A Deployable High Temperature Superconducting Coil (DHTSC) - A Novel Concept for Producing Magnetic Shields Against Both Solar Flare and Galactic Radiation During Manned Interplanetary Missions", *Journal of the British Interplanetary Society*, Vol. 44, Mar. 1991, p. 99-102.
- 13 Engleson, George A. and Glenn Murphy, "Superconducting Coils for Shielding in Space", In *American Institute of Aeronautics and Astronautics, and American Astronautical Society, Stepping Stones to Mars Meeting, Baltimore, MD, March 28-30, 1966. Technical Papers*. AIAA, New York, 1966, p. 282-287.
- 14 Brown, G.V., "Magnetic Radiation Shielding", in *High Magnetic Fields*. H. Kolm, B. Lax, F. Bitter, and R. Mills, Eds., The MIT Press, Cambridge, MA, pp. 370-378, 1962.
- 15 Dow, Norris F. Structural Implications of the Ionizing Radiation in Space, *TIS Report No. R60SD376*, Space Science Laboratory, General Electric Co., Nov. 30, 1959 (as cited in 14).
- 16 Kash, S.W., "Minimum Structural Mass for a Magnetic Radiation Shield", *AIAA Journal*, Vol. 1, June 1963, p. 1439-1441.
- 17 Kholodov, Yu. A., *Space Biology and the Magnetic Field*. Translated into English from *Kosmicheskaya Biologiya i Magnitnoye Pole, Priroda (Moscow)*, no. 4, 1966, p. 114-115, by Air Force Systems Command, Wright-Patterson AFB, Ohio, Foreign Technology Div., 31 Jan. 1967.
- 18 Hilinski, Erik J. and F. Hadley Cocks, "A Deployed High Temperature Superconducting Coil (DHTSC) Magnetic Shield", in press.
- 19 Störmer, C., *The Polar Aurora*, Oxford, at the Clarendon Press, p. 292, 1955.
- 20 Helgesen, John O. and Frank A. Spagnolo, "The Motion of a Charged Particle in a Magnetic Field due to a Finite Solenoid with Application to Sollar Radiation Protection", *American Institute of Aeronautics and Astronautics, Aerospace Sciences Meeting, 4th, Los Angeles, CA, June 27-29, 1966, Paper 66-512*.
- 21 Townsend, L. W., J. W. Wilson, J. L. Shinn, J. E. Nealy, and L. C. Simonsen, "Radiation Protection Effectiveness of a Proposed Magnetic Shielding Concept for Manned Mars Missions", *SAE, Intersociety Conference on Environmental Systems, 20th, Williamsburg, VA, July 9-12, 1990, SAE Paper 901343*.
- 22 Amato, Ivan, "New Superconductors: A Slow Dawn", *Science*, Vol. 259, January 15, 1993, pp. 306-308.
- 23 Moon, Francis C., *Magneto-Solid Mechanics*, John Wiley

& Sons, New York, 1984.

²⁴ J. Engleberger, U.S. Patent No. 3,504,868, granted April 7, 1970.

²⁵ Zubrin, Robert M., "The Use of Magnetic Sails to Escape from Low Earth Orbit", *Journal of the British Interplanetary Society*, Vol. 46 (1993), pp. 3-10.

BIOREGENERATIVE LIFE SUPPORT SYSTEMS FOR MICROGRAVITY

University of Florida
Aerospace Engineering, Mechanics and Engineering Science
Gainesville, Florida

Dr. Gale E. Nevill, Jr.
Michael I. Hessel, Jr., Teaching Assistant
José Rodriguez, Teaching Assistant

A VARIABLE GEOMETRY PLANT GROWTH UNIT

Steven Morgan, Margaret Olson, Kathryn Samuels,
Michael Schreiner

Abstract

With long-term manned space missions now technologically feasible, life supports systems for the astronauts need to become self-sustaining and durable. Such a system would require plants to recycle waste water and air. However, in the confined volume of a spacecraft, a unit to grow plants in the least amount of volume would be desirable. This report describes a Variable Geometry Plant Growth Unit (VGPGU), dubbed the "Accordion" for its resemblance to the musical instrument, which is able to stretch and contract and efficiently deliver nutrients to the plants. Although the effects of microgravity cannot be simulated on earth, the design is expected to perform better in microgravity.

Introduction

The Controlled Ecological Life Support System (CELSS) project underway at NASA/KSC is researching the possibilities for providing the astronauts with food, water and oxygen by growing plants in outer space. With space and mass at a premium, a Variable Geometry Plant Growth Unit (VGPGU) will maximize plant output in a microgravity environment. Though research is scarce in space-oriented versions of a VGPGU, the need for one is fast approaching.

Why a VGPGU?

In a spacecraft, the volume available is extremely small; therefore, making the most of the available space is absolutely necessary. A unit that can change volume -- whether it grows plants, holds water, or stores oats -- becomes valuable in such a situation.

Launching mass out of Earth's gravity well is still a costly

venture. Thus, the resources required for a massive device could outweigh the advantages the extra materials may produce. Therefore low mass designs are attractive.

Current Research

From the greenhouse to the space shuttle, controlled environments for growing plants have been extensively studied. However, research in variable geometry systems for plants has not been extensive. Ralph Prince of NASA/KSC has done the principal work in this area. He has intensively explored how plant spacing affects lettuce growth. Of the many systems examined, only two basic systems are in use; these are the tray and the trough (gully) or pipe systems. As guidelines, these designs are ideal because of their extensive use. However, for a microgravity environment neither one is practical due to their mass and free liquids.

The EPCOT Center at Walt Disney World also researches controlled environments for growing plants in The Land. Current research involves numerous nutrient delivery systems and a variety of plants from all types of climates. NASA, of course, is extremely interested in a self-sustaining life-support system for use in outer space. With the future promising extended periods of time in space -- even a trip to another planet -- preparation must be made today.

Characteristics

Ideally, a variable geometry unit of any sort should save space. A curious question arises, though: Is space being conserved? The space into which the unit will expand must still remain clear of objects. Temporary use is possible, but the space cannot be used for any permanent structures.

The mass of a VGPGU will likely be the limiting factor in its microgravity use. The cost of building one could easily be dwarfed by the price of launching one.

A VGPGU needs to be automatic and easily used so that no time is wasted by the astronauts. Many other experiments and tasks require attention.

The lifetime of a plant growth unit should be at least as

long as the lifetime of its environment. A manned mission to Mars would likely last at least two years, so the unit must have a lifetime at least as long.

Although Prince has concluded that it is impossible to create a universal variable geometry growth unit, striving for a widely versatile unit remains a top consideration. If different types of plants can be grown in one type of unit, maintenance and flexibility would be improved.

Above all, the type of unit for use in space must be usable in a microgravity environment. Water distribution, especially, will be tough to design into a weight-less system because of the behavior of liquids in microgravity. No significant leaking can be allowed. Also, the behavior of plants in weightlessness is not well known.

All these considerations are important in the design of a true Variable Geometry Plant Growth Unit.

Possible Designs

The Telescope

One candidate was a device based on the classic telescope configuration. The expansion of the system was allowed by the concentric pipes from which the plants grew. This system provided nutrient delivery inside the tubes that allow the expansion. The plants' roots grew into the tube as the leaves grew outward. This system has several serious problems. In order to slide, the pipes must have openings through which to move. Leakage and corrosion could result. Also, maintenance of the system could be time consuming and difficult.

The Tracked Wheel and The Wedge

An entirely different approach to the problem brought up two new ideas. The previous systems required that plants be planted and harvested all at the same time. Here, a system for continuous use was considered. In the tracked wheel, the plants are initially in the center of the wheel and move radially outward as they grow taller and wider. The wedge contains new plants in its narrow end which move on tracks to the wide end as they grow. Essentially, the wheel is a collection of wedges.

The tracks must move yet create a watertight seal. Leakage is quite possible as is corrosion. Maintenance could be time consuming and access to the unit would not be easy. The complexity of the tracked wheel and the wedge create many problems for space-oriented use.

The advantages of these designs, though, are intriguing. Continuous harvesting would contribute to a set routine as well as providing a constant source of food. The system is not truly variable in geometry, though, for the device itself does not change.

The Accordion

This design is shown in Figure 1. The accordion design is a pair of concentric, flexible, expandable tubes. The plants grow radially outward from the outer tube. The inner tube delivers the nutrient solution and the space between the two tubes connects to a vacuum to remove the nutrient solution before it can leak out.

This is by far the simplest design of those considered. The mass need not be high since the tubes could be made of a light polymer. Maintenance could be as simple as blasting water through the fully-extended tubes. The tubes could be arranged radially from a common point, concentrically around each other, or even just row-by-row.

The biggest drawback remains the behavior of liquids in microgravity. The solution may not be moved by the flowing air, but instead stick to the tube surfaces. However, the plants can grow radially along all parts of the tube.

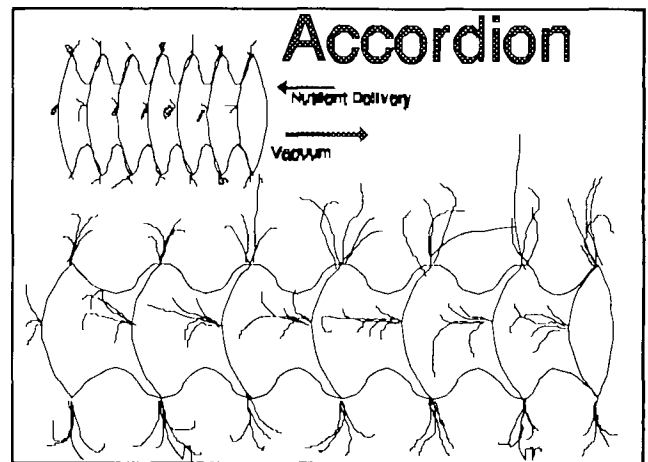


Fig. 1. The Accordion

Design Choice

After the strengths and weaknesses of each design were evaluated, no design was deemed clearly better. However, with the restrictions of time and budget, the Accordion design was selected as most promising. The largest drawback on the other designs was their complexity. Many moving parts can create havoc when only one fails.

Prototypes

The original design of the Accordion was simple enough to provide a quick and easy prototype to be built. Created by slices of PVC pipe connected by dryer hose, this design was the initial testing device. The plants grew through holes cut in the PVC slices. Everything was connected through

standard silicone caulking. The prototype's durability was never an issue since it was only intended to last long enough to conduct tests on the plants and the design. As an information-gathering device, the prototype Accordion smoothed the way for a more sophisticated version. The second version was cut from a clear plastic acrylic pipe instead of the PVC pipe used in the first prototype. In reality, a transparent system would encourage algae growth, but for testing purposes, seeing the inside of the VGPGU became important. The second system had only one row of holes -- one per plastic slice.

The Details

Plant support. With a place to hold the plants, a way to hold the plants became necessary. Sponges and peat moss, seemed impractical because of future breakdown and rotting. Rock wool used by EPCOT for most of their hydroponic systems, was not available. Therefore a neoprene system was chosen. Test results showed neoprene to be supportive and non-toxic.

Nutrient Delivery. Nutrient delivery was never intended to be a large part of the VGPGU project. However, some sort of system is necessary for testing, and any practical version requires such a system. The system used contained a three-phase pump and a delivery tube. A timer and relay controlled the time that the pump was running. Constant nutrient delivery is not necessary for plants to grow.

Originally a concentric second tube was to run inside the first one. However, the discovery of helical tubing similar to a telephone cord resulted in a new idea -- the tubing was perforated and as water was forced through the tube, the resulting water spray was more than adequate for the plants. There are drawbacks; for instance, the water spray occurs everywhere rather than concentrated on the plants. Also, as the cord-tube is expanded, it changes shape and the water holes change angle. Still, the results are very promising.

Nutrient removal. With nutrient delivery possible, some sort of water removal is necessary. For testing, simply using gravity is possible, but then the effects of microgravity may ruin the design later. Research provided information on airflow removal of the liquid nutrients, however the cross-sectional area of the tube proved too large for a simple vacuum on one end of the tube. Therefore, on the other end of the tube a fan was connected. The air-flow prevents water from attaching itself to sides or leaking beside the plant stems before being directed out of the tube and into the vacuum.

Experimentation

Plants

Due to the time constraints of the project, quick growing plants were needed. The best available plants with short growth times were lettuce and spinach. A strain of lettuce being investigated at EPCOT Center was chosen as the eventual test plants.

Small pieces of neoprene were pierced with holes in which plant seeds were inserted. For a period of a week, these seeds were left in water to test their ability to germinate. Some of the neoprene was inserted into grommets similar to the ones inserted in the VGPGU holes; some neoprene was left floating freely.

The results were only partially successful. The seeds did manage to germinate, however they did so rather slowly. A seed that managed to fall out of its own piece of neoprene germinated better than any of the others.

Results

The VGPGU succeeded at holding, feeding, and watering the plants without allowing leakage to the outside environment through the seals around the plants. The plants did manage to survive within the Accordion during changes in geometry and further experiments can help determine optimal airflow and water flow. The system as a whole proved successful at its intended purpose.

Conclusions

The VGPGU is able to adapt to different shapes to allow for different size plant spacings. Individual partitions of the VGPGU were able to change independent of the rest, and in addition, the system is also able to twist into a circular shape and expand radially instead of linearly. The geometry proved to be very versatile and adaptable.

Finally, the plants were able to live inside the VGPGU. The Accordion VGPGU appears to be a promising design for a long-term manned space mission.

References

1. Downs, R. I. and Hellmers, H. "Environment and the Experimental Control of Plant Growth." Academic Press. London, 1975.
2. Hessel, M.I., Richert, G.E., and Nevill, G.E., "Airflow-Contained Aeroponic Nutrient Delivery for a Microgravity Plant Growth Unit," Biotronics, Vol. 21, Dec. 1992, pp.33-39.

3. Schwarz, M. "Guide to Commercial Hydroponics." Universities Press, Israel, 1968.

AQUEOUS NUTRIENT SOLUTION SENSOR

Mark Dallara, Randy Hines, Scott Breneman

Abstract

The goal of this project was to design and fabricate a computer-controlled system of ion detectors that will accurately measure the concentrations of several necessary ions in solution. The project focused on the use of a sensor array to eliminate problems of interference and temperature dependence.

Introduction

NASA's Controlled Ecological Life Support System (CELSS) project centers on growing plants and recycling wastes in space. The current version of the Biomass Production Chamber (BPC) uses a hydroponic system for nutrient delivery. To optimize plant growth and conserve system resources, the content of the nutrient solution which feeds the plants must be constantly monitored. The macronutrients (>10 ppm) in the solution include nitrogen, phosphorous, potassium, calcium, magnesium, and sulphur; the micronutrients (<10 ppm) include iron, copper, manganese, zinc, and boron.

Background/Theory

In developing a sensor array to accomplish these goals, several sensor types have been examined. The most promising was judged to be Ion-Selective Electrodes (ISE). An ISE is a sensor electrode with material at one end that only allows certain ions to react electrochemically to the probe. An ISE is paired with a reference electrode and the voltage difference between the two is related to the concentration of the ion of interest by the Nernst Equation:

$$E = E_0 + ST \cdot \log(a) \quad (1)$$

The transfer function exhibits a linear range in which the electrode behaves according to the Nernst equation, preceded by a low-level non-linear range. The solutions measured in this project were well within the linear range of the electrodes.

Ideally, an ISE would only react with the selected ion, however most ISE's fall short of this goal. The voltage

difference is also affected by the presence of other ions and changes in temperature and pH. The primary effort of our project was to account for these influences in the performance of the sensor system.

Electrochemical analysis of ISE theory produces a theoretical relationship between the voltage of the ISE and the reference electrode, which is represented by the Nikolskii-Eisenmann equation:

$$E = E_0 + \frac{RT}{Fz_1} \cdot \log \left(a_1 + \sum_{k=2}^n K_{1,k} a_k^{z_k/z_1} \right) \quad (2)$$

where E is the measured voltage, E_0 is the standard voltage at a unit concentration, R is the universal gas constant, F is Faraday's constant, and z_1 is the charge of the selected ion. The summation is over the other k ions in the solution. K is an interference coefficient and z the charge of each ion. The symbol a is the activity of the ion and is directly related to the concentration of the ion.

Not all ions interfere with each ISE so some of the K's are zero. At low concentrations, similar to those found in plant nutrient solutions, the activity of the ion (a) is equal to its concentration. The interference coefficients (K_i) may also vary with temperature.

Application of Theory

The first step of the project was to prepare a data acquisition program to coordinate and use information from each electrode. The program included procedures for calibration, sampling, and the calculation subroutine which produced "first-guess" Nernstian values for concentration as well as the iterative solution based on the Nikolskii-Eisenmann equations. Once this was functional, the electrodes were calibrated and the interference constants were determined experimentally. The system was then ready to test samples with multiple ions.

Calibration Routine

Calibration of any particular electrode involved the determination of the constants E_0 and $S = \frac{R}{Fz}$ as found in the Nikolskii-Eisenmann equation.

Since these tests are carried out using only the ion for which that particular electrode is selective, the values of the activity for all other ions (a_k) must equal zero.

Calibration of each sensor begins by choosing the range over which sample data will be taken. Two samples are taken of solutions with different activities a_1 and a_2 . It

should be realized that the subscripts on the concentration (a) refer to different concentrations of the same ion, and not concentrations of two different ions. The two Nernstian equations which result from these samples can be solved simultaneously to find ST;

$$ST = \frac{E_2 - E_1}{\log(a_2) - \log(a_1)} \quad (3)$$

E_0 can be found by back substitution. The computer program used in this system carries out these calculations and saves the new calibration constants automatically. Calibration concentrations of 100 parts per million (ppm) and 1000 ppm were used to calibrate each electrode.

Equipment and Materials

Chemicals

The choice of the chemicals used came from consideration of the nutrients in the solution as well as the availability of ion selective electrodes. Since the worst problem with using ISEs is the error caused by interferant ions, the chemicals were intentionally chosen to cause maximum interference. Nutrient solutions for plant growth include calcium and potassium, both of which have commercially available electrodes. Both of these electrodes experience interference from sodium ions. Although sodium is not found in nutrient solutions, its presence as an interfering ion was important for the experimental procedure. The chemicals used were calcium chloride dihydrate, potassium chloride, and sodium chloride.

Ion Selective Electrodes

Three Orion ISE's comprised the array. They consisted of two liquid membrane electrodes and one glass membrane electrode. The two liquid membrane electrodes (calcium and potassium) were referenced to a double junction reference electrode using the standard inner-chamber fill solution. The outer-chamber fill solution was chosen because it allowed both the calcium and potassium electrodes to function normally. Using ammonium chloride solution (2M NH_4Cl) instead of the more common potassium nitrate solution (10% KNO_3) decreases the amount of interference in each electrode as the outer fill solution slowly seeps through the semi-permeable membrane of the double junction electrode.

Thermistor

An Omega 44008 Linear Thermistor Composite was used for temperature measurements. Accuracy of the thermistor at temperatures ranging from 10 C to 50 C (well within testing specifications) is ± 0.2 C.

Experimental Protocol

After calibration of each electrode, each interference constant (K_j) was determined by testing a solution which contained 100 ppm test ion and 1000 ppm interference ion. For the purposes of this project, these values were assumed to be constant for all temperatures during the life of the electrode. The calibration constants were subject to change, depending on the most recent calibration.

When running the program, the user input the known concentrations of each ion in the test solution and the A/D board then began sampling. When a sampled data channel appeared to stabilize, the user "held" the value by pressing the key for that channel and the held value was displayed below the free-floating value. Once all values were held, the user exited sample/hold mode and the program calculated and output the Nernstian "first-guess" value and the iterative value of each concentration. The testing scheme was as follows:

	Na (ppm)	Ca (ppm)	K (ppm)
Test 1	100	1000	0
Test 2	100	1000	1000
Test 3	1000	1000	0
Test 4	1000	1000	1000
Test 5	0	100	1000
Test 6	1000	100	1000
Test 7	1000	0	100
Test 8	1000	1000	100

Ionic strength adjustor (4M NH_4Cl 4M NH_4OH) was necessary for the sodium electrode in the ratio of 1 mL ISA per 10 mL test solution. The calcium electrode functioned equally well with or without ISA, so none was used.

The potassium electrode functioned well when used with ISA (5M NaCl) during initial calibration, but upon successive recalibrations the electrode slope was found to have decreased to 1 mV/decade. No amount of reconditioning changed the slope and the potassium electrode had to be discarded as a data source. The program was altered to produce a simulated data reading based on the "known concentration" inputs and the Nikolskii-Eisenmann equation. Therefore, the data output for the potassium electrode potential is a trivial value, but its effect on the calculations of the sodium and calcium ion concentrations could still be examined.

Results

Figure 2 illustrates the Nernstian output and the Nikolskii-Eisenmann iterative output as compared to the real concentration of the ion calcium. Results for sodium were generally similar but less accurate.

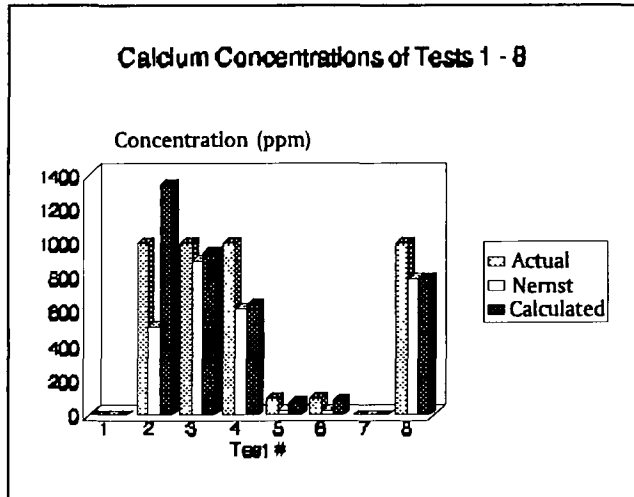


Fig. 3. Calcium Concentrations

Analysis

The iterative procedure presented in this project produced mixed results. The differences between the single-electrode outputs and the array outputs were somewhat different for each electrode. The values for calcium concentration tended to be more accurate, while the values for sodium tended to be less accurate. The potassium electrode had an insufficient response function and had to be discarded as an input.

The errors evident in some of the output values could be attributed to several different sources. As shown in Figure 3, a small difference in the calibration constants produces a rather large difference in both the Nernstian output and the Nikolskii-Eisenmann output.

Additional errors may have been introduced by inaccuracies in the output from the A/D board or the thermistor bridge circuit. All of these values (calibration constants, voltage outputs, and temperature) are part of the exponent in the Nernst equation when solved for concentration:

$$a_1 = 10^{\frac{E_1 - E_0}{ST}} \quad (4)$$

Thus both the Nernst and the Nikolskii-Eisenmann outputs are strongly sensitive to the calibration values as well as the accuracy of the voltage and temperature readings.

The ion selective electrodes used here proved to be

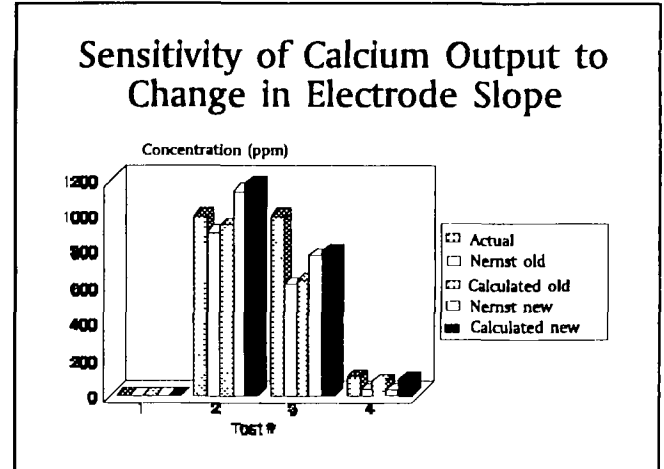


Fig. 2. Sensitivity chart

temperamental devices with a number of inherent problems. The need to use ISA for reasonable output negated one of the goals of the project - to test the solution without changing it. Without ISA, the sodium electrode illustrated a response with almost zero slope. The sodium electrode was also extremely sensitive to static charge in the room; touching the shielded BNC connector caused the voltage output to go to zero, and fluctuations in the output were repeatedly observed due to such minor disturbances as a person walking past the system setup.

It appears that a sensor array may indeed be useful for systems with multiple-ion solutions and imperfect detectors. However, the precision of the associated hardware and the method of sampling and calibration are critical to the procedure; these need to be improved upon before this system could accurately test a real hydroponics solution.

References

1. Evans, A. "Potentiometry and Ion Selective Electrodes." John Wiley and Sons, New York, 1987.
2. Schuetzle, D. "Fundamentals and Applications of Chemical Sensors." American Chemical Society, Washington, 1986.

MASS DETERMINATION DEVICE

Jeff Burke, Mark Cates, Tom Rossi, Jeff Yang

Abstract

The determination of mass in microgravity is essential for scientific research. The Mass Determination Device (MDD) group developed an instrument that utilizes centripetal force to determine the mass of solids (granular and compacted), liquids, and suspensions in microgravity. Currently, instrument's do not exist that possess this much versatility or employ the novel approach of centripetal force to determine mass. The device consists of a frame, motor, controller, transducer, and tray (for holding the mass). The transducer selected for this project applied the Hall Effect to measure displacements resulting from centripetal acceleration.

Introduction

The determination of small masses (1 to 500 grams) in microgravity is essential for scientific research in space. The mass determination methods currently used for solids and fluids have limitations. For mass measurements, a vibrating system is frequently utilized. This system may be inappropriate depending on the medium being measured. For example, the mass measurement of fluids has typically been plagued by sloshing from surface waves.

The goal of this group was to design a device that accurately measured both solids and liquids. To achieve this versatility the concept of centripetal acceleration was incorporated into the design. This concept was an important step in the development of the MDD, a working mechanism capable of measuring the mass of solids (granular and compacted) and liquids (homogeneous, heterogeneous and multiphase solutions). In addition, the MDD has few restrictions on the container for the mass being measured.

Background Information

NASA has flown a number of dedicated life sciences missions involving mass measurement technology. These missions along with NASA research centers and other institutions have primarily tested the following methods for measuring mass: acoustical, dynamic spring-mass, and pressure sensing techniques.

Acoustical Acceleration

The Jet Propulsion Laboratory (JPL) is developing an

acoustical method for the measurement of mass. This project focuses on accelerating an unknown mass in a microgravity environment using a sound wave generated pressure field. By measuring the field strength, the displacement of the mass and the time to translate the distance the unknown mass is calculated. The advantage of this method is that the mass of small solids and liquids can be determined accurately without a holding container. The main disadvantage of the acoustical method is its limitations on the size of the sample. The method is predominately for droplets of liquids and solids weighing under one gram.

Dynamic Spring-Mass

The Southwest Research Institute has developed the Small Mass Measurement Instrument (SMMI) for NASA. The SMMI is a spring-mass oscillating system that undergoes simple harmonic motion. The mass of an unknown object can be determined from the frequency.

The SMMI can determine the mass of solids over the range of 0.1 to 10,000 grams with an accuracy of 2.5%. Because the SMMI is a single degree of freedom spring-mass system, its major problems are with vibration transmission and a tendency to slosh free boundary fluids.

Fluidic Pressure Sensing

The mass of a homogeneous (constant density) fluid is acquired by rotating the fluid at a constant speed with measurements obtained of the pressure and the angular speed. Using Bernoulli's equation you can find the mass.

This method has several obvious limitations. It is not effective for solids or heterogeneous fluids. Also, pressure measurements must be made at two different radial locations.

Preliminary Designs

The conceptual stage of the design process generated numerous ideas for a mass determination device capable of performing in microgravity. The first design decision was to utilize centripetal acceleration. From this decision various techniques for the actual mass calculations evolved. Although we looked at many possible designs we will only discuss the Bearing Method, Strain Gage Method, and the Hall Effect Method

Bearing Method

The bearing method uses a piezoelectric crystal as the force sensor on the bearing. The bearings are enclosed so that minimal motion takes place in the direction of the thrust bearing. When $\theta = 0^\circ$ for the accelerated mass, the crystal is expected to supply the entire reaction force to the shaft.

Assuming the surface between the bearing and base is frictionless, or the friction is accurately measured, the crystal will provide a periodic voltage, whose peak corresponds to the maximum force transmitted by the shaft. The advantages are:

- Piezoelectric crystal technology exists
 - Simple design
 - Easy to transmit data from bearing to ground
- and disadvantage of the bearing method is:
- Friction may cause errors in force measurement

Strain Gage Method

This method uses an electrical resistance strain gage for strain measurements in the arm. From the measured strain we can calculate the mass by using stress-strain and centripetal force relationships.

Advantages:

- Strain gage technology already exists.
- Simple design.

Disadvantages:

- Transmit data from rotating shaft to ground.
- Signal is typically small.

Hall Effect Method

This method was the final choice for implementing the MDD. In general it uses a Linear Output Hall Effect Transducer (LOHET) to sense radial changes in distance of a centripetally accelerated mass.

The mass is placed at the end of a rotating arm on a leaflet spring mounted tray. As the arm is rotated the inertia of the mass will cause the tray to deflect radially outwards. By placing magnets on the tray, the LOHET can sense the displacement of the mass. The deflection is given by,

$$\Delta x = \frac{m\omega^2 r}{k} \quad (5)$$

The relationship between the LOHET's signal and Δx is not readily predictable. Because of this, the LOHET device must be carefully calibrated. This was done by creating several constant frequency calibration plots over a range of masses. From these plots the MDD is capable of making actual mass measurements.

Advantages:

- LOHET technology already exists.
- LOHET can be oriented in numerous directions to increase signal range and strength.
- High signal strength.
- Small size.

Disadvantages:

- Data must be transmitted from the rotating arm to ground.
- Must be calibrated completely.

HARDWARE DESCRIPTION

Arm Assembly

A flexible couple is used to connect the arm to the shaft. The power source (14 1.5v AA cells) for the instrumentation is located on the arm and also functions as a counterbalance for the entire system. Located at the opposite end of the arm is the spring-tray mechanism used for holding the unknown mass.

Tray Assembly

The tray consists of two aluminum plates that firmly hold the four strips of spring steel. Figure 4 shows a close up view of the tray. It should be noted that at the outset of construction, the alignment of the spring steel was thought to be crucial. However, it was found that considerable misalignment could be endured while still obtaining accurate deflection results.

A pair of magnets is attached to the side of the tray. The magnets are placed in this orientation so that the magnetic field strength would vary almost linearly. This allows the LOHET to measure deflection while attached to the spinning arm.

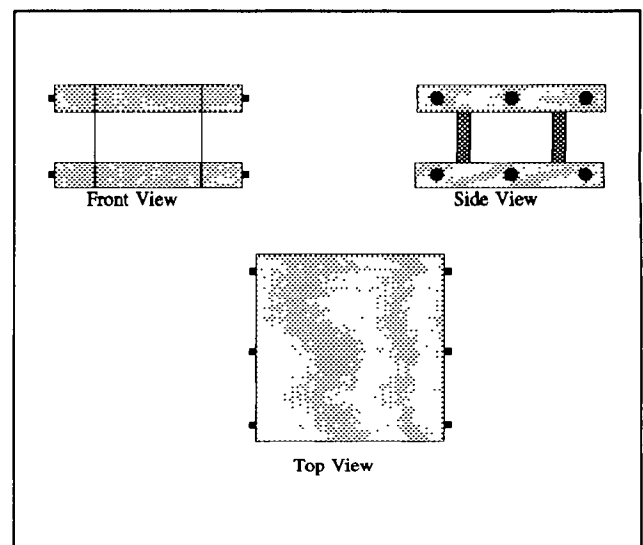


Fig. 4. Three views of tray

Instrumentation

The major requirements on the instrumentation system are to measure the angular speed of the shaft and the displacement of the mass. In addition to measuring the displacement, the information must also be transmitted from the rotating arm to a stationary readout panel.

Angular Speed Measurement. The angular speed of the vertical shaft is difficult to measure directly because of its low rotation speeds (0-2Hz). This is due mainly to fact that most modulation circuitry is expected to operate at frequencies greater than 10-20Hz. This problem was circumvented by measuring the frequency of the motor's armature, which is approximately ten times faster than the vertical shaft. The frequency of the armature was measured by demodulating a pulse train of square waves generated from an optical pick-up inside the motor. The pick-up gave an additional gain by producing 30 square waves per revolution. This amounted in a multiplication of the vertical shaft's low frequency by 300; thus, making the frequency readable by standard demodulation circuits. The demodulation was accomplished through a 4046BE phase-lock loop chip. The calibration curve for the angular speed versus output voltage, V_p , is shown in Figure 5.

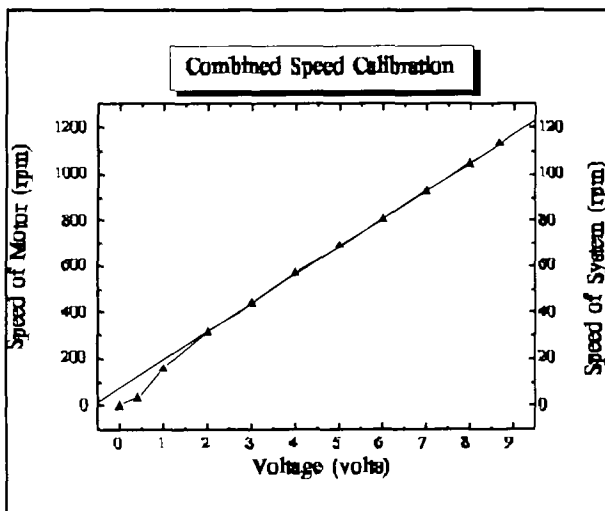


Fig. 5. Combined speed calibration

Calibration of the demodulated output was done by using a pulse counter to measure the exact frequency of the armature. This frequency was then assumed to be 10 times greater than the vertical shaft. This assumption is not exact and a more accurate measurement can be made by using another optical pick-up on the main shaft to determine the exact gear down ratio.

Displacement Measurement. The displacement of the mass was measured using a LOHET from Micro Switch Co. (Part # 91SS12-2 and 2 Indox 1 magnets (0.25" diam. and 0.125" long)). The two magnets were placed such that the north and south sides were adjacent allowing the LOHET to slide by both the negative and positive flux poles. This orientation gives flexibility to the LOHET by producing a wider voltage range (1-10VDC) and a larger range of measurable deflections (0-0.5in). It should be noted that the LOHET was also approximately 0.03125" from the magnets. At this gap distance it was noticed that small changes in gap distance (due to vibrations) cause substantial changes in the output voltage (± 0.1 VDC) of the LOHET. In retrospect this could be changed by using a more rigid support for the LOHET and more secure fasteners for the spring steel.

Signal Transmission. The voltage from the LOHET was first sent through the voltage controlled oscillator (VCO) on a 4046BE chip. After this modulation, it was then transmitted via an infrared LED across 1cm air gap to a stationary phototransistor pick-up. The signal from the phototransistor was then demodulated (using another 4046BE) to produce an output voltage, V_s . The output was then displayed on a two channel oscilloscope.

DISCUSSION OF RESULTS

With the signals V_s and V_p for the displacement and the angular speed, two single calibration curves were generated for $f = 0.8\text{Hz}$ and $f = 1.78\text{Hz}$. The low speed plot is shown in Figure 6. This plot is presented to demonstrate what the calibration procedure requires.

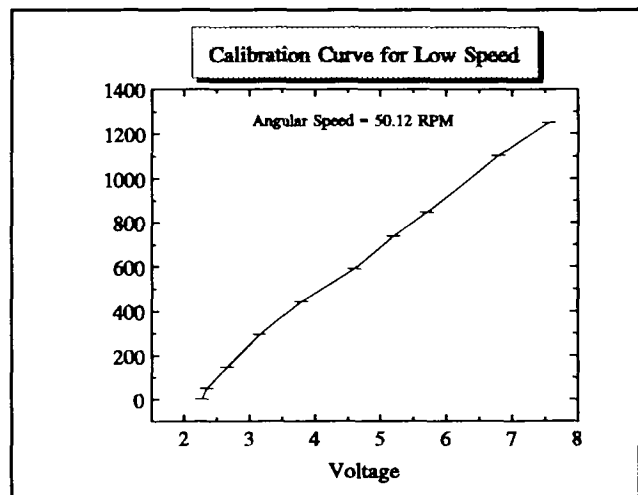


Fig. 6. Low speed calibration

Accuracy

A complete assessment of the MDD's accuracy could not be made because of the lack of calibration curves. However, information on the repeatability as well as signal steadiness can be discussed.

Repeatability

The MDD showed a high degree of repeatability for both the angular speed and displacement measurements. This claim is based on almost zero signal drift for a period of 10 hours for the angular speed. The displacement measurement repeatability also seemed rather good -- the same measurement (± 0.05 VDC) was achieved after 10 hours of continual starting and stopping of the shaft.

Signal Steadiness

Of the two signals only the displacement voltage fluctuated noticeably. The steadiness of the displacement signal is controlled by several factors, namely, oscillation of the tray, and sensitivity of the circuitry. The excessive sensitivity of the circuitry was responsible for some of the oscillations. However, some of the signals fluctuated because the mass samples were not lashed down firmly to the tray; thus causing the tray to oscillate perpendicular to the LOHET face. Although this caused substantial fluctuations in the displacement voltage, the signals were sinusoidal and so an average reading was possible. Overall, this probably introduced an uncertainty of about ± 0.05 VDC.

Changes and Improvements

Based on the experience accumulated in constructing and testing the MDD several suggestions can be made for future work.

1. As a matter of practicality the arm will always be imbalanced; therefore, small angular velocities should be used. For the MDD $f < 2$ Hz worked well.
2. A more rigid restraint for the spring steel and the LOHET should be considered. This will result in a more stable displacement signal.
3. The resolution of analog voltage measurements were also crucial especially for smaller masses where the output signal was rather high (refer to Figure 8 for $f = 1.78$ Hz). Thus a good resolution for high voltage signals is important.
4. In order to make measurements of small masses (< 50 g) it is necessary to spin the device at higher speeds. However,

the deflection of the tray for small masses is mainly dictated by the mass of the tray, and not the mass sample. Therefore, it is desirable to reduce the tray's mass for making accurate measurements of small masses.

Conclusion

The MDD illustrated that a rotational device can be used to determine mass in microgravity. The hall effect transducer served as an acceptable mechanism for calculating displacements resulting from centripetal acceleration. A computer can be incorporated into the design to make the MDD easy to use and applicable to everyday scientific research in microgravity.

References

1. Irwin, D. J. "Engineering Circuit Analysis." Macmillan Publishing Company, New York, 1989.
3. Riley, W. F. and Zachary, L. W. "Mechanics of Materials." John Wiley and Sons, New York, 1989.
4. Solberg, R. F. "Measurement of Weight in Space." Technology Today, 1991.

VARIABLE LIGHTING SYSTEM

Ed Solozobal, Tu-Ming Leung

Abstract

Light is one of the most important factors in a Controlled Ecological Life Support System -- one that is usually taken for granted. After examining the lighting system at NASA/KSC, our group decided that a more efficient design could be developed for growing plants. Before concepts were developed, it was necessary to have a full understanding of the light spectrum as well as the intensities for an average plant in order to provide the proper amount of light for growing plants. An efficiency rating was developed in order to choose the most efficient light source. Concepts were then developed, a prototype fabricated, (red LED's and miniature blue fluorescents) and tests were conducted. The design uses less power, is highly efficient in minimizing the amount of wasteful heat that must be removed, and needs less maintenance than a conventional lighting system.

Introduction

The literature on plant physiology indicates that most higher order plants need only certain wavelengths of visible light, from 400nm to 500nm and from 600nm to 700nm, with peaks at 450nm and 660nm. Plants, on average, normally absorb about 10% of their energy as blue light and 90% as red light. Therefore, a lighting system with this distribution was sought. A measure of "efficiency" was defined by dividing the light intensity of the source by the power used to operate and remove heat.

Photosynthesis

Photosynthesis is the process to absorb light energy and convert it into reductive chemical energy. The light requirements for a plant consist primarily of red (R) and blue (B) wavelengths. These are absorbed by many different pigments that vary in chemical composition and function, including the photosynthetic pigments (chlorophyll and carotenoid) and the developmental pigment (phytochrome and BAP). These pigments require different wavelengths of light, and have different absorption rates.

Intensity

The rate of photosynthesis is dependent on many factors including temperature, carbon dioxide, water, minerals, and light intensity. If all factors are held constant and light intensity is increased, the rate of photosynthesis also increases until a saturation maximum is reached. However, at these extremely high intensities, a process known as photorespiration can occur. This process competes with photosynthesis and thus limits further increases in the rate of photosynthesis. From research, we concluded that an average plant needs approximately 1600 lumens/ft², however, this value can change due to the type and size of the plant in question. Andrew Schuerger, senior plant pathologist at The Land, EPCOT Center, suggested that our group use 10 to 20% blue light and 80 to 90% red light in our design.

Various Light Sources

There are many different kinds of light sources that could be used to provide the proper amount of light to a given plant, however, some are more efficient than others. From a lighting study conducted by NASA, our group concluded that these four light sources out of 34 used the minimum power and had the longest lifetime: Standard Gro&Sho (F48T12/1500), High Pressure Sodium (LU1000), Multi-vapor Metal Halide (MVR1000/U), and the LED.

Determination of the Light Source

In our effort to determine the most efficient light sources a rating method called the ratio test was devised.

Ratio Test

Using plots of wavelength vs. intensity, the area under these curves, which represented lumens, were calculated. This was then divided by the amount of power needed to run the light source and to remove any heat produced by that source. Note:

1. The G.E. light sources have a spectrum that contains all wavelengths of visible light -- most of which is not needed by the plant. Therefore, only the areas calculated within the 400 to 500nm and 625 to 700nm were used.
2. Because the red LED's had higher ratios than the G.E. light sources when the power to produce heat was not incorporated into the ratios, it was concluded that the LEDs will still have a higher ratio if power to remove heat was not included.

It was discovered that the LEDs have a much higher ratio than the other light sources. The blue LEDs do not have as high an efficiency as their red counterparts. The miniature blue fluorescent, however, do have a slightly higher ratio than the blue LEDs.

Lighting Sources Selected

From the ratio test results, our group decided to use two light sources in our design:

1. L200CWR5k red LED (660 nm)
2. BF659-12 miniature blue fluorescent (435 nm)

The 660nm LED was preferred over the other LEDs because it has a wavelength which matches the absorption curve for chlorophyll-a which is the primary photosynthetic pigment. This LED has the highest efficiency compared with the other LEDs. The blue fluorescent was chosen primarily because the blue LEDs did not produce a high enough intensity for an average plant. Also, the blue fluorescent produced a fairly reasonable efficiency ratio in comparison to the other light sources.

Final Concept

The final design is circular (20 cm in diameter) in order to mimic the radial plant growth in the horizontal direction. The smaller fluorescent bulbs (50 mm in length) allows us to place them in a circular position so more of the bulb light

can be used to illuminate the plant. The overlap consists of three rows of LEDs at a 30 degree angle with the vertical axis, placed 5 mm apart from each other, and attached to a bread board where they are connected in parallel with each other. These boards were placed inside the supporting structure which was made out of aluminum with fluorescent bulbs attached to the underside. The device was supported by a chemistry test stand which could be adjusted to any height. Eight miniature blue fluorescent bulbs and 529 red LEDs are required for the device; however, because our group was not planning on growing any plants, it was decided to build only a pie shaped 1/8 of the device. Therefore, only 66 LEDs and one fluorescent were required for testing.

The concept is powered by a 12 volt DC power source which is reduced to 2 volts using a voltage regulator for the LEDs. This is in parallel with an inverter which converts the 12 volts into 185 volts and .004 amps making it possible to operate the fluorescent bulbs.

Testing

Two methods were developed in order to test our lighting design:

1. A light meter was used to test the relative intensities of light at 7 different locations of the test section and at 16 different heights from 2 to 18 inches (once at every inch).
2. The power to operate our device was compared to the power to operate the light sources used by NASA.

Results

Light Meter Test. The intensity of the red LEDs remain constant at each different testing area at one height. As we moved the meter away from the LEDs, the intensity decreased linearly until we reached 18 inches, after which the intensity dropped exponentially. The blue fluorescent produced different intensities in the three regions up to the 10 inch mark. The center had the highest intensity in this range because it was directly under the fluorescent. When both light sources were turned on together, the intensity equaled (one percent error) the addition of both sources' intensities that were measured separately.

Power Comparison Test. The power needed to run our light source was recalibrated in order to create a new ratio. In converting 120 volts to 2 volts for the LEDs, a resistance was needed which, in turn, produced wasteful heat. This was taken into account in order to be consistent with the

G.E. light sources which are also run off of 120 volts.

The new ratios for our system were compared to the other light sources discussed previously. It was found that the combination of the LEDs with the blue fluorescent light provides a much higher effective light spectrum to wattage ratio. The metal halide comes in second with half our design's ratio.

Conclusions

There are various light sources for plants. However since plants absorb light primarily in the blue and red wavelengths, it is important that the source provide light in that spectrum. Our group decided to use an LED (660 nm) and a miniature blue fluorescent light (435 nm) based on the fact that their efficiency ratios which were higher than other light sources. Two different types of tests were performed.

The first test showed the variation of intensities as the distance away from the design was increased. The LEDs provided a constant intensity while the fluorescent leveled off at a greater height. The second test was to compare the actual power used by our light source to the power used by the other sources. Our design lumen:watt ratio was twice as high as the next highest ratio (metal halide). Other testing could use light filters to evaluate the calculated effective spectrum as an accurate representation of the actual light spectrum being produced.

References

1. Senger, Horst. "Blue Light Response." CRC Press, Vol. 1 and 2, 1987.

UMBILICAL SUPPORT, LUNAR SURFACE EMERGENCY SHELTER AND ROBOTIC ARM FOR LUNAR SURFACE VEHICLE PROJECTS

Florida A&M / Florida State University College of Engineering
Mechanical Engineering Department
Tallahassee, Florida

Dr. Patrick Hollis
Dr. William Shields

Operational Ground Support for Lunar Lander via Umbilical System

John E. Parker (Project Manager), Fatshi
Ousib, Pedro Badillo, Dariell Morales, Pat
Kavanagh

Abstract

The purpose of this study was to develop a conceptual design of an Umbilical for Lunar Lander Support (LLS). The emphasis of the study is on the subsystems needed to fulfill each support requirement while considering environmental conditions such as thermal ranges, radiation effects, micrometeorites and lunar ejecta. These subsystems include transferring two liters of hydrogen boil-off from tanks on the lander to a storage facility to later be condensed and recycled, providing power to maintain on-board systems, and continuous transmission of video, voice and data signals. An external housing to protect each of the internal components by way of housing was designed and an interface mechanism which provides continuity between each subsystem

Introduction

The probability of an established permanent lunar base has developed to the point that serious effort is currently underway in the design of such a development. Many issues must be dealt with to insure safe and efficient operation of all aspects of the base. This study was performed to determine the requirements and design solutions involved in the support of a lunar lander via an umbilical system. This umbilical system will be located on a Mobile Transfer Unit (MTU) as seen in Fig. 1. Contained on board the MTU is a package of operational ground support equipment which includes a Hydrogen storage tank, power plant &

fiber optic transmitter. In addition, a panel controlled support boom is included to assist in the process of guiding the umbilical to its operational position.

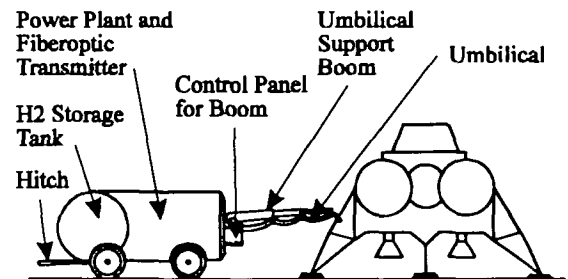


Fig. 1. Mobile Transfer Unit With Lunar Lander

Assumptions

The operational ground support for lunar lander conditions were derived from adaptations of existing lunar lander support systems.

Requirements

The design must satisfy specific requirements while operating under the conditions of the lunar environment. These requirements include:

- Gaseous H₂ boiloff from tanks on the lunar lander must be transported to a storage facility.
- Continuous supply of power is required to maintain life support and other on board systems.
- Continuous transmission of video, voice and data signals between the lunar lander and support systems must be provided.
- Housing will be necessary to protect each of the subsystems from the lunar environment.
- Adequate interface capability must be provided to insure adequate connection of subsystems.
- Manually operable.

Further, since it has been estimated that the costs is roughly \$10,000 per kilogram to deliver solid mass to a lunar base, the final design must have low mass.

Design Overview

The umbilical overall design consists a six meter long, flexible device with the following subsystem:

- Flexible high pressure gas line.
- Insulated copper power line.
- Fiber-optic communication line.
- Aluminum mesh external housing with polyethylene insulation.
- Threaded locking mechanism with dust removal apparatus.
- support boom.

Hydrogen Transfer

To prevent possible rupturing of the lunar landers LH₂ fuel tanks, gaseous boil-off must be transferred to storage tanks located on the MTU. This process is performed by initially engaging a relief valve which allows flow to travel into a stainless steel flexible hose lined with TFE which is contained within the umbilical. Proper connections are made by factory fitting permanent leak-proof ends: an angled circular nozzle fitted with a series of O-rings will be mated with its female counterpart located on the lander interface, a permanent standard integral VCO end provides semi-permanent connection to a storage tank located on the MTU. The result is a creeping flow of two liters per every 24 hour of H₂.

Power System

The power requirements were based on a 7 earth-day manned mission with a typical 0.55 kW/man and a peak maximum power requirement of 9.68 kW. In the design process, an upper limit is set on the specific mass, the power level, sink and operating temperatures, and a transmission distance of 6 m. The material chosen is standard annealed copper with an emissivity of 0.8, a conductor density of 8890 kg/m³, and conductor resistivity at 293 K of 1.724e-8 Wm. The sink temperature is assumed to be room temperature and the operating temperature is not to exceed 400 K. The upper limit set on the specific mass is 1 kg/kW. The results obtained are shown below in Table 1.

Table 1. Analyses Results

Conductor Mass	9.68 Kg
Conductor Diameter	15.20 mm
Temperature Factor	1.16e-5 (m ² /W) ²
Percent Power Loss	2.44%
Voltage	15V
Inverse Current Density	555.52 cir mils/A
Efficiency	97.56%

If the demands for load power increases due to mission requirements, then the transmission voltage can be increased to a certain degree.

Communication

A communication system for the lunar lander consists of video, audio and data signals. Fiber optic cable was enlisted for this due to several reasons: noise such as atmospheric, magnetic, and noise from power sources do not interfere, it is flexible and easily replaceable, reliable and is not affected by radiation forms currently found on the lunar surface.

Electric to Optic Conversion. The signal transmitted from the MTU is in form of an electron wave, this must be converted to a photon wave for transmission through the optic line. An LED (light emitting diode) satisfies this requirement by emitting incoherent light due to the arbitrary essence of the recombination of the hole-electron pairs. LED's typically operate on bandwidths up to 2 GHz.

Optical to Electrical Conversion. A receiver is needed to convert the optical signals to electrical. The receiver used to do so is a p-i-n photo diode. It collects incident photons and makes them generate hole-electron pairs that are detected electrically. A depletion region is exposed to the incident light and detects it.

Connectors. A connector is needed to link the optic cable from the umbilical with that on the lander. This connector serves as a non-permanent joint between the fiber and the dispersing system. The alignment of the two components is very critical and any misalignment may cause reflection losses. However, a jewel bushing connector provides the required alignment.

Dispersing System. The dispersing system divided the three signals coming from the same line. A dispersing prism-type multiplexing system is used to divide the signals where they will be delivered to the proper connector.

Housing

In order for the umbilical to remain and operate on the moon it must be protected from the harsh lunar environment. Housing for the umbilical must therefore be designed to withstand temperature differential as high as 117°C during a lunar day, and as low as -173°C during a lunar night. Also, the umbilical must be protected from Constant radiation and micro meteorites bombardments. The final design specification were met as follows. The outer layer consisting of aluminum mesh and having a thickness of one centimeters surrounds the polyethylene insulating material which is five centimeters thick. The power line, hydrogen line, and fiber optics line are embedded in additional insulating material made of glass fibers and housed in a thin layer of aluminum mesh.

Interface

Connection between the umbilical and the interface located on the lander is obviously an essential. The designed mechanism operates by first spraying each connection with Hydrogen from a pressurized tank located on the umbilical. Immediately afterward the male and female ends are connected and a rotation of 45° clockwise applies an adequate axial load for connections. At this point a self-locking mechanism is engaged to secure the connection. To release, unlock the locking mechanism by depressing a button located on the handle and simply rotate counterclockwise 45°.

Support

The umbilical and accompanying support systems are stationed on the MTU which delivers the system to and from the landing pad. Although no serious effort was applied in the design of the MTU the conceptual design contains the following: H₂ storage tank, power plant, fiber optic transmitter and an Umbilical Support Boom are located on board. A lunar Rover transports the MTU by connecting to a hitch. This transportation is necessary in order to recondition

the support systems and shelter the MTU from blast effects of the lander.

Umbilical Support Boom. In order to assist in handling the umbilical during connection and disconnection to the lunar lander an Umbilical Support Boom was designed. The basic frame of the boom was modeled and analyzed by using PAL2 finite element programs. The result is a three sectioned boom of length 2.25 m in the closed position to 5 m in the open or extended position. The large end will be electrically operated by a control panel on the MTU.

Conclusion

Each subsystem was successfully integrated into the final design and fell well within the original design perimeters. All activities involved in the design proved to be immensely educational. Not only the technical aspect of the project but the management and organizational skills acquired will prove to be invaluable in future application.

LUNAR SURFACE EMERGENCY SHELTER

Michael Render, Patrick Bilek, Robert Howard, Chris Keen, Gregory Kercher, Keith Kobetitsch, Kay Mehr, Kim Melvin, Kory Reeves

Abstract

The Lunar Surface Emergency Shelter (LSES) is designed to provide survival-level accommodations for up to four astronauts for a maximum of five days. It would be used by astronauts who were caught out in the open during a large solar event.

The habitable section consists of an aluminum pressure shell with an inner diameter of 6 ft. and a length of 12.2 ft. Access is through a 4-in. thick aluminum airlock door mounted at the rear of the shelter. Shielding is provided by a 14.9 in. thick layer of lunar regolith contained within a second, outer aluminum shell. This provides protection against a 200 MeV solar event, based on a 15 REM maximum dose.

The shelter is self-contained with a maximum range of 1000 km. Power is supplied by a primary fuel cell which occupies 70.7 ft³ of the interior

volume. Mobility is achieved by towing the shelter behind existing lunar vehicles.

It was assumed that a fully operational, independent lunar base was available to provide communication support and tools for set-up and maintenance. Transportation to the moon would be provided by the proposed Heavy Lift Launch Vehicle.

Major design considerations for the LSES were safety, reliability and minimal use of Earth materials.

Problem Statement

A shelter is to be designed to provide survival-level accommodations for up to four astronauts for a maximum of five days. Protection against ionizing radiation, and life-support must be provided. It would be used by astronauts who were caught out in the open by a solar flare event, or whose vehicle or other shelter was unable to support and protect them. Astronauts are assumed to be wearing EVA suits that provide up to six hours of life-support with a two hour extension.

Assumptions

The investigation and design of each subsystem of the LSES required that several assumptions be made concerning the technology and equipment that will be available at the time of use:

- A lunar base exists which has communication with Earth and can act as a relay station for communications from the shelter.
- Equipment at this base includes lifting machinery capable of removing the shelter from the lunar lander upon its arrival at the lunar surface. Excavation equipment and a regolith conveyor will also be required to provide lunar soil for shielding.
- Maximum required range of the shelter is set at 1000 km in any direction from the lunar base.
- Satellites and/or space stations exist for relay of communication signals.
- Launch from Earth will be aboard the proposed Heavy Lift Launch Vehicle (HLLV).

Design Overview

The Lunar shelter design was largely based on adaptations of systems currently proposed for Space Station Freedom. Whenever possible,

existing technology was considered when selecting subsystems to satisfy each requirement.

The overall design requirement was broken down into six major sections. Each of these was then analyzed separately:

- General structural design
- Mobility
- Radiation and Micro-meteorite protection
- Life Support
- Power
- Communications

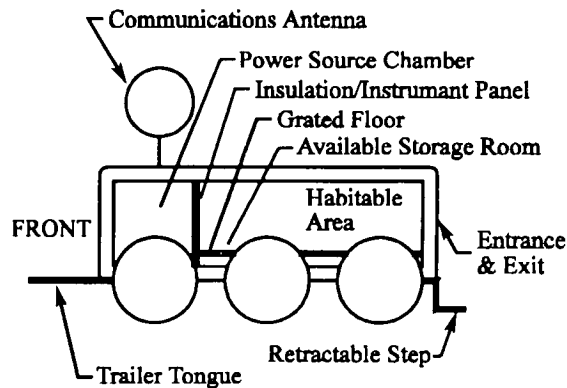


Fig. 2. Lunar Surface Emergency Shelter

General Structural Design

Decisions of general structural design determined aspects of mobility and general shape.

To satisfy given requirements, the shelter could be either permanent, temporary or fully mobile. A permanent shelter would be constructed in advance at its anticipated site. It would then act as an outpost which, although constantly available, would have limited use within a wide range. A temporary shelter would be constructed at each work-site and then dismantled when the site was abandoned. A fully mobile shelter would require no assembly on the moon but would either have to be towed or independently powered.

Assuming the permanent shelter would be buried in regolith to minimize cost, the mobile shelter would require less time to set up than a temporary or permanent shelter. Furthermore, the mobile shelter is more versatile because, unlike the temporary shelter, its systems are already intact and, unlike the permanent shelter, it is able to relocate.

Four alternatives were considered for general shape: Cubic, cylindrical, spherical and wheels (using hollow wheels as one-man shelters).

For all factors considered, the cylindrical shelter was superior or equal in suitability to the cubic shelter. The wheels were found to be unsuitable for pressurization, have little usable volume and be impractical for the required duration. A sphere was the most suitable shape for pressurization and had the minimum surface area but was found to be difficult to construct and adapt to mobility.

Therefore, it was decided to make the shelter cylindrical and fully mobile. Because of cost and weight factors involved in an independently powered shelter, the shelter would have to be towed.

Mobility

The mobility of the LSES was separated into three major systems: Tracking, suspension, and transport.

Wheels were chosen as the best solution principle for the tracking system. Wheels are mechanically efficient, can be designed into light weight systems, and provide excellent reliability. Jointed legs were ruled out because of their mechanical complexity, and a tracked vehicle was ruled out to minimize weight and add simplicity. The wheels were modeled after the design for the 1990 Lunar Articulated Remote Transportation System. This design was selected for its relative simplicity, improved ground contact for control, light weight, and dependability. The wheels are a hemispherical shell, supported on the inside by an array of curved ribs. Traction is accomplished by stainless steel wire mesh and fiberglass reinforced cleat.

A mechanical suspension system was chosen over a magnetic type. The underlying factors in this decision include weight and power minimization, cost, and simplicity. Since the LSES will not be manned when in motion, the improved comfort level associated with other technologies was not a major selection factor. The chosen suspension system is a torsion bar mechanism. This choice was based on simplicity, ease of maintenance, reliability, and ease of implementation into the overall design of the chassis. In addition, this design will allow for simple and quick modifications governed by the lunar terrain. Finally, the mechanism provides a low center of gravity necessary to prevent roll.

The transport system consists of a simple aluminum ball and socket hitch with slight modifications (curved edges) to allow some

vertical pivoting. This mobility will allow the astronauts to leave the base for extended lunar excursions with the security of having full radiation shielding and life support systems within close proximity.

Radiation and Micro-Meteorite Protection

Four designs were considered for radiation shielding against the three largest solar flare events in the last half century. The incorporation of ideas from the first three proposed designs led to the fourth and final design for the radiation shield.

The fourth design gave protection from the most pressing problems. These problems are radiation, decompression, and hypervelocity (velocities above 5000 ft/s) impacts. Even though impacts are highly improbable, they need to be addressed because the occupants of the shelter are many thousands of miles from safety.

The overall radiation shielding is a composite consisting of an 1 in thick aluminum structure, and regolith present in a 14.9 in thick polyethylene honeycomb. The combination of these materials reduces the mass of the structure while increasing the efficiency of the shielding. The honeycomb structure in combination with the regolith provides some protection, however minimal, against hypervelocity projectiles.

Life Support

Life support systems include all of the necessary systems to provide and maintain a habitable environment within the LSES. This includes any required equipment as well as integration of this equipment into the shelter. The following life support subsystems will be discussed: Environmental Control system, Thermal Control system, Fire Detection and Suppression system and the Airlock Hatch.

The Environmental Control Life Support System (ECLSS) contains components necessary for O₂/N₂ supply, atmosphere quality monitoring and maintenance, carbon dioxide removal, and humidity control. A cryogenic storage system supplies oxygen and nitrogen. This system operates under the necessary mass, volume, and power limits, and does not produce any undesirable byproducts. Cabin atmosphere quality is maintained and monitored by all solution principles considered. This consists of a particle counter monitor (PCM), a major constituent

analyzer (MCA), a trace contaminant monitor (TCM) and air filters of heavy capacity. For carbon dioxide removal, lithium hydroxide scrubbers proved to be the most efficient and reliable. Finally, humidity control is performed by a four bed molecular sieve (4BMS) which utilizes a two-media desiccant bed for water removal. The 4BMS was the most efficient alternative because of its adaptability for carbon dioxide removal.

The thermal control system is used to provide a safe and comfortable ambient temperature for the shelter personnel. The automatic system electronically monitors and controls the heating and cooling of the LSES. Heating of the shelter is accomplished through the heat transfer from onboard equipment. Cooling is performed by tubular cooling ducts within the shelter walls.

Fire is detected by utilizing photoelectric cells mounted within the ventilation system. This system was chosen because of its ability to detect smoke rather than temperature variation. Cryogenic expulsion operation is shutdown when fire is detected and a back-up safety system takes control. A carbon dioxide extinguisher is utilized to eliminate the fire. When contaminated air is evacuated, normal operating conditions are resumed.

In order to provide a safe and reliable means of accessing the shelter, an airlock hatch is utilized. The hatch creates an airtight sealing surface as well as providing required radiation protection. Many safety features are built in to ensure that pressurization of the shelter is maintained when personnel are aboard.

Power

Power system selection is generally a function of mission duration and power required. Selection was determined by studies done by NASA on multi kWe power source alternatives and on recommendations provided by Los Alamos Laboratory. The following systems were compared to provide power for the LSES: Solar dynamic, solar photovoltaic, radioisotope thermoelectric generator, nuclear reactor, dynamic isotope power source, regenerative fuel cell, nickel-hydrogen battery, and primary fuel cell (PFC).

The power system selected was required to operate continuously and safely at a rate of 10.7 kWe and for the maximum duration (5 days). Because the shelter is portable, a system was selected which could operate in close proximity to

the shelter and minimize volume, weight, and deployable area.

Although it required safety precautions during its start-up and shutdown processes, a hydrogen-oxygen fuel cell utilizing cryostorage was chosen because of its portability. The PFC required the least volume (2 cubic meters), mass (1112 kg) and deployable area than any other system considered.

Communications

The onboard communication system consists of all necessary equipment to allow communication with Earth, the lunar base, and personnel on the lunar surface in EVA suits or lunar vehicles. The system utilizes existing satellites to relay signals to appropriate locations, as well as an independent, short range UHF system for surface communication.

Integration of Internal Subsystems

To minimize the bending moment induced by the power source, the system is positioned directly over the front suspension system so that its weight is transferred directly to the wheels.

In order to shield the astronauts from the heat of the power source, a two part urethane mixture is used to form an insulative barrier between a 1/8 in aluminum divider and the power source control panel. Furthermore, the system is cooled by routing liquid oxygen to its exterior.

An aluminum floor deck is provided in the living compartment to provide a flat surface. Beneath the grating, 38.2 cubic feet of usable space is available for storage.

Finally, a retractable step is located at the base of the airlock door which can be lowered to an easy entrance into the shelter.

ROBOTIC ARM FOR LUNAR SURFACE VEHICLE

**June Clark, Anthony Cox, Robert Hall,
Oscar Hill, Jeff Mayers, Mark Nickel, Tyrene
Townesley**

Abstract

In an effort to meet NASA's goal of lunar colonization, surface vehicles will be incorporated in extensive exploration missions. These vehicles require support equipment that provides the

astronauts with the means to successfully complete tasks that would otherwise require them to exit the vehicle. There has been a need identified for a robotic arm to be mounted on the exterior of a lunar vehicle. The robotic arm is able to assist the astronauts as well as withstand the environmental conditions of the moon

Performance objectives for the robotic arm include a reach of 3 m, a positioning accuracy of 1 cm, an arm mass of 100 kg, and a lifting capability of 50 kg. The arm is able to safely complete each of three identified tasks (path clearing, equipment set-up, and cargo handling) within a reasonable amount of time, the actual time is dependent upon the task to be performed. No maintenance is required for the duration of the 28 earth day mission. Remote viewing and proximity and positioning sensors are incorporated in the design of the arm.

Introduction

Currently, the National Aeronautics and Space Administration (NASA) intends to colonize the moon by the year 2010. Provisions for such a colony include developing reliable, safe and cost effective systems to support lunar operations during an approximate time frame of 2010-2030. One such system of importance is a robotic arm which should be capable of being attached to and operated from a lunar surface vehicle. One particular design, as developed by a team of mechanical engineering students, incorporates several subsystems which provide interesting insights into the possibilities involving robotic arm concepts and their applications during lunar missions. Such systems may or may not be highly dependent upon mechanical and electrical principles. This particular design is a product of numerous concepts that apply these principles to produce a robotic arm that achieves adequate functionality, reliability, and safety; all at an acceptable cost.

Design Overview

The system is designed in such a way that it is, at minimum, able to accomplish the following performance objectives:

- have a reach of 3m with 1 cm precision
- a maximum arm mass of 100 kg
- an ability to lift 50 kg on the moon.

An additional attribute of the system includes a manual backup system such that the arm can be safely restored to its resting position in case of mobility failure. No foreseeable maintenance shall be required for the duration of a 28 earth day mission. Although remote viewing, proximity and positioning sensors were not emphasized in this particular design, they should be incorporated in the completed design.

Environmental Factors

The lunar environment is harsh and presents hazards to the reliability of the system. Therefore, the effects of such an environment have been considered in the design. The following information is needed to assure that the design is appropriate:

- Radiation: 1000 REM total during 11 year solar cycle
- Gravity: 1.62 (m/s²)
- Temperature Range: 400K to 80K
- Soil grain size: 2 to 60 micrometers, with 50% of grains less than 10 micrometers
- Pressure: 10⁻¹² Torr (1.3*10⁻¹⁰ Pa)
- Magnetic Field: no general magnetic field on the moon (dipole field is less than 0.5*10⁻⁵)

Power

The power requirements for the system are detailed by device, subsystem, and total system. The purpose of listing such information is to expedite integrating of the Robotic Arm Design into larger systems such as the Lunar Rover.

Power distribution:

<u>Subsystem</u>	<u>Peak Power</u>
Mechanical Structure	6.0 kW
[Motor (4)]	1.5 kW]
Modified Wrist Joint	4.5 kW
[Motor (3)]	1.5 kW]
Interface Subsystem	1.5 kW
[Motor (1)]	1.5 kW]
End Effector	.015 kW
[Instrument (1)]	.012 kW
Power Tool (1)	.015 kW]
System Total	12.015 kW

Subsystems

Mechanical Structure. The mechanical structure is one of the major subsystems of the robotic arm. This subsystem extends from the arm's base (which attaches to the lunar surface vehicle) to the its fourth link (where it is connected to the modified wrist joint), see Fig. 3.

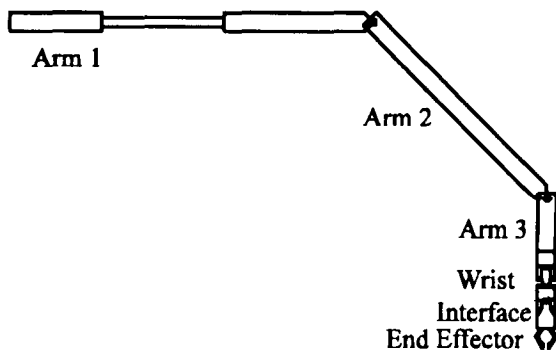


Fig. 3. Robotic Arm Design Concept

In meeting the overall system requirements, the mechanical structure supports the entire weight of the arm in addition to any external load and does not contribute an excessive mass of its own.. The following subsystem characteristics are the result of this effort to satisfy system constraints:

1. Subsystem mass does not to exceed 65% of total mass. That is, 65 kg was set as the maximum mass of the subsystem.
2. Materials make up possesses an acceptable balance between beneficial properties and weight.
3. Structure is able to withstand applied stresses and allow for the containment of cables, wires, controls, and sensors within the structure if needed.
4. Environmental effects on the lunar surface do not hinder reliability because of considerations made during material selection.

The Mechanical Structure has four degrees of freedom with four joints. Rotation at the base, one translational joint, and two revolute joints provide these degrees of freedom.

Modified Wrist Joint. Located between the primary mechanical structure and the interfacing subsystem, the modified wrist enhances the overall dexterity of the system by providing three additional degrees of freedom, see Fig. 4. This subsystem consists of three mechanisms that each provides one degree of freedom. Each mechanism, in general, is a motor-driven gear set. The significance of this design is that it very compactly integrates the motors into the system so that they deliver the proper motions effectively and simply.

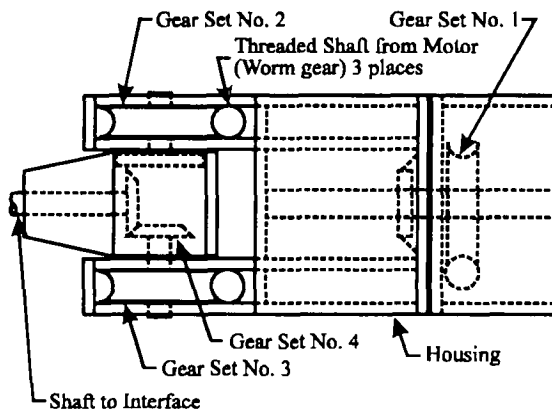


Fig. 4. Modified Wrist Joint

Structure-to-End Effector Subsystem. The purpose of the interface is to support a variety of interchangeable end effectors individually and actuate the innate functions of each end effector.

In its most basic sense, the interface consists of a cylindrical shell which encloses the fit-locking mechanism, the end effector actuation mechanism, and the motor. The interface also operates as a power outlet, channeling electrical power to the end effectors that require it, see Fig. 5.

The fit-locking mechanism is responsible for securing the fit between the end effector's outer mating surface and the inner mating surface of the shell. The fit-lock consists of the actuating link, the followers (2), and the clamps (2). Each clamp is grounded at one revolute joint. The clamps are spring loaded in such a way, that the flange portion of the clamps are restored to the closed position when no other force is applied at its follower-attached revolute joint.

The actuating link is connected to the clamps via the followers. This link slides along the unthreaded portion of the motor shaft and

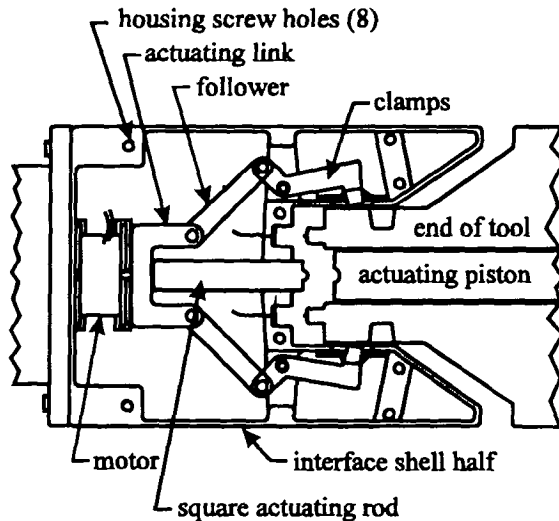


Fig. 5. Interface Subsystem

transmits the force needed to restrain the clamps in the open position. This force originates from the rotational motion of the motor shaft, which is then converted into linear motion at the threaded actuating rod. This rod in turn translates toward the motor, sliding the actuating link backward and establishing the open position of the clamps.

The open position is established prior to engagement of the end effector and constitutes disengagement of the same end effector.

End Effector Actuation Mechanism. This mechanism is responsible for the actuation of innate end effector functions. It consists of the actuating rod (of square cross-section) and the motor-driven threaded shaft.

Since some end effectors, like the small and large grippers are actuated by the displacement of their respective piston, the actuation mechanism must deliver the force necessary to induce such a displacement. This task is made possible by the conversion of the shaft's rotational motion into the translational motion of the rod. This translating actuating rod in turn performs the required work on the end effector's piston.

Controlling the precision of this rod motion and its consequential effect on the end effector involves understanding pertinent motor specifications (i.e. step size, running torque, etc.) and programming supporting controls hardware accordingly.

Motor. The motor provides the mechanical power needed to perform major subsystem functions. By operating in both directions, the motor powers the fit-locking mechanism to its open position and powers the end effector actuation as well.

Electric Power. Electric power, if required, is channeled to the end effector through the ports (2) located in the vertical mating surface of the shell. These ports also serve to align the end effector during engagement and absorb torques during operation.

Material Make Up. The Interface Subsystem is composed mostly of Aluminum 2014-T6 like the rest of the arm. Certain parts, however, are made of stainless steel. Parts such as the motor shaft and fasteners are manufactured from steel. To reduce the influence of thermal expansion at critical surfaces such as the thread to thread interface between the motor shaft and the actuating rod, they both have the same composition: stainless steel.

End Effectors. These devices are attached singularly at the end of the robotic arm and perform their function by direct contact with the object of interest. The end effectors are designed to interchangeably connect to the arm by way of the interface subsystem, as previously discussed, see Fig. 6.

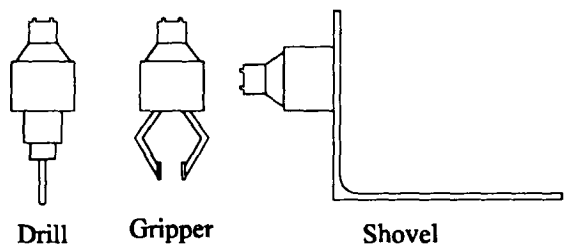


Figure 6. End Effectors

Most end effectors are designed such that they can be actuated or powered by the Interface subsystem. This involves having not only an adaptive end but also being mechanized for actuation by the translation of a rod or the power of an electrical outlet. Below are examples of such end effectors:

- Large and small grippers
- Shovel
- Power drill
- Sensors

System Controls

Proper operation of the mechanical system requires the integration of supportive hardware. Such hardware must serve a number of functions which help satisfy the performance objectives of the robotic arm. These functions include providing a means of controlling system processes.

Controls System Selection. The controls system places the functionality of the entire robotic arm in

the hands of the user. With the agitation of hand held joysticks at a computer console, the input is received, processed and delivered to the output devices by this system.

Other important factors related to the selection of an appropriate controls system are position controls for motors, velocity control requirements, acceleration/deceleration control, and indexer selection.

ENABLER: A LUNAR WORK VEHICLE

Georgia Institute of Technology
George W. Woodruff School of Mechanical Engineering
Atlanta, Georgia

Professor James W. Brazell

Abstract

Students of the George W. Woodruff School of Mechanical Engineering at Georgia Institute of Technology have researched and designed an Earth-bound concept model for a lunar work vehicle. Designated the "Enabler," the vehicle was designed to be adaptable to the harsh environment a vehicle can be expected to confront on the surface of the Moon.

The objective of the project was to design a multipurpose lunar work vehicle. In particular, the vehicle needs to provide capabilities that will be useful in remote investigation of the lunar surface, and it should provide many of the construction capabilities that will be needed for the establishment of a manned lunar base. To meet these general goals the vehicle needs to be simple, strong, light, flexible, and reliable. The Earth-bound concept model is under construction, and is scheduled for preliminary testing in February 1994.

Introduction

A number of vehicle configurations have been proposed to carry out various tasks in constructing a lunar base. Selected configurations have been evaluated against a given lunar base scenario.¹ The present design is intended to accomplish many of these tasks while offering unique features directed at minimizing life cycle costs within the total system.

Description

Enabler was designed as a six-wheel vehicle with a boom. The wheels are independently powered, and are mounted directly onto a tubular chassis. This chassis features a set of non-orthogonal articulation joints which provide for maximum maneuverability with a minimum number of parts. The boom is mounted upon the center section of the vehicle; it has three non-orthogonal articulation joints plus one revolute joint, allowing for four degrees of freedom and a large work envelope.

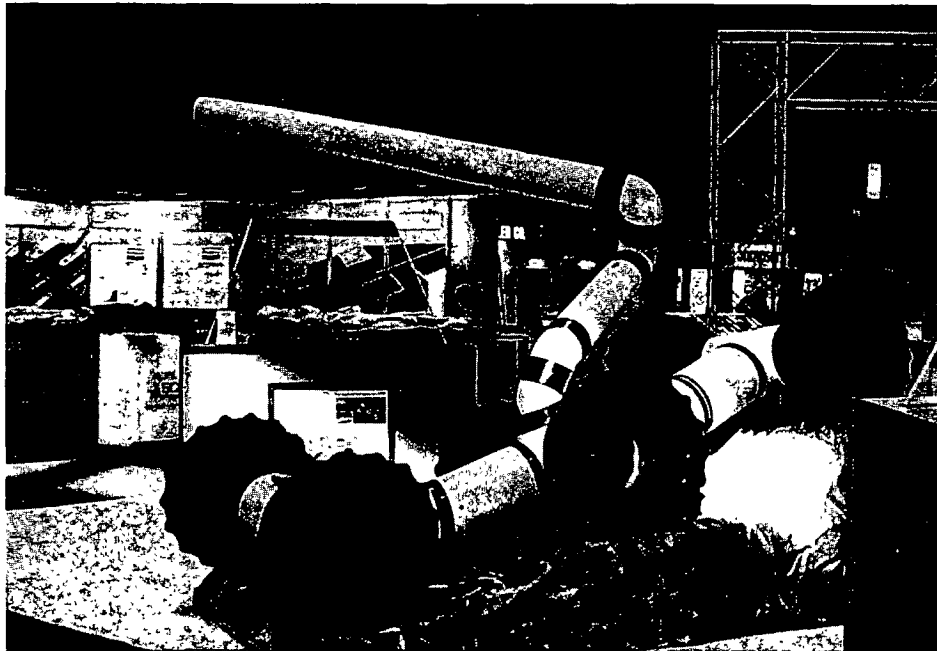


Fig. 1 The Enabler

The Enabler design has five main components (systems): the chassis, manipulator boom, power wheels, controls, and end effectors. A full-scale model of the Enabler is currently on display in the Mechanical Engineering School at Georgia Tech. An equal-size model of the vehicle was exhibited in March 1993 at the National Design Engineering Show.

Chassis

The distinguishing feature of the Enabler chassis is its set of articulation joints. The joints are designed to rotate 360 degrees, roll on a free axis, and be locked when desired. Because these joints can rotate freely, the Enabler can adjust the pitch, yaw, and roll of any individual section of the vehicle, allowing maximum maneuverability. Essentially, the vehicle has the flexibility to hug the rough lunar terrain, to overcome rocks or cracks larger than its own wheel diameter, and to remain stable through a wide range of motions.



Fig.2 Close-Up View of Articulation Joints

The modular chassis design consists of three structural elements: one forward, cylindrical T-section, a center cylindrical cross-section, and a rear T-section with an extended top area. These main sections are connected by aluminum tubes 18" long, with 12 3/4" OD. These tubes are linked at articulation joints with an angle of 15 degrees; rotation of the tubes about this joint allows each section of the vehicle to move vertically, horizontally, and rotationally through a range of 60 degrees. All of the chassis tubes are hollow to allow the installation of electrical and hydraulic lines along the centerline.

Each joint is driven by a hydraulic motor. Each of these motors is mounted to the tube, and connected to be joint with a sprocket and chain. These motors are designed to run in different directions and speeds across the joint, allowing the vehicle to turn, to lift a segment, or to otherwise adjust to the terrain. During normal operation, several of these motors will be kept in neutral in order to keep all wheels in contact with the lunar surface at all times.

This joint design allows the Enabler to perform a number of steering and positioning maneuvers: A

three-axle turn in which the front and rear axles turn with respect to the center axle to cause a change in direction; the ability to climb over obstacles in which the front, center, and rear axles raise sequentially to transfer the vehicle's weight from one axle to another as it encounters sharp irregularities in the terrain; and two-axle turning in which the vehicle essentially lifts one axle set of wheels off the ground entirely and functions like a four-wheel, skid-steer vehicle.

Wheels

The Enabler's wheel and drive system allows speeds of 8 mph on a level surface, the surpassing of one meter high objects and one meter wide crevices, and the climbing of a 30% grade. The Enabler's six wheels are individually powered by motors mounted within the wheel hubs. The wheel assemblies support the entire weight of the vehicle and provide substantial traction for lunar surfaces; in addition, their conical shape and variable spring rate provides the vehicle with an adequate suspension system. The wheel assemblies were also designed for easy removal by a lunar astronaut.



Fig. 3 Close-Up of the Enabler's Wheel System

The components of the wheel design consist of composite wheels, aluminum hubs, wheel cylinders, and bearing sprocket plates. The wheels have been fabricated using a composite material consisting of fiberglass fabric in epoxy resin. Each wheel is shaped as an approximate section of cone making a 20 degree angle with the central axis. Aluminum hubs connect the wheels to the bearings, and the motors drive the wheels directly.

Power/Motors

Power for the concept model will be provided by a Briggs and Stratton 5 hp engine, converted from gasoline to propane fuel. This engine will drive a hydraulic pump to supply hydraulic power to the six hydraulic motors in the wheels, six in the chassis articulation joints and four in the vehicle's boom.

Boom

Perhaps the most distinguishing feature of the Enabler design is its dexterous work boom, which actually performs the tasks for which the vehicle was designed. The boom features articulation joints, an end effector with an interchangeable tool

connector, and a hollow interior for the laying of cables. The design provides straight line tracking at the end effector; a full range of motion in the above-grade performance envelope; four degrees of freedom; storage space for all motors, gears, wiring, and control mechanisms, and the ability to lift a rated load; plane into a crevasse or crater; while serving as a counter balance when traversing steep slopes. The total range of motion is approximately a hemisphere above grade, with more limited extension below grade. Clemens Saur, an industrial engineering student, was instrumental in the design of the boom. His thesis² on the lunar vehicle and boom provided the necessary kinematic and dynamic analysis for choosing the exact boom configuration.

End Effectors

The vehicle's end effector system consists of a wrist and grabber mounted to the end of the boom, plus a set of tools. The wrist is driven by an electric motor and provides 360 degree rotational movement at the end of the boom. It has rotation speeds of up to 1/3 rpm.

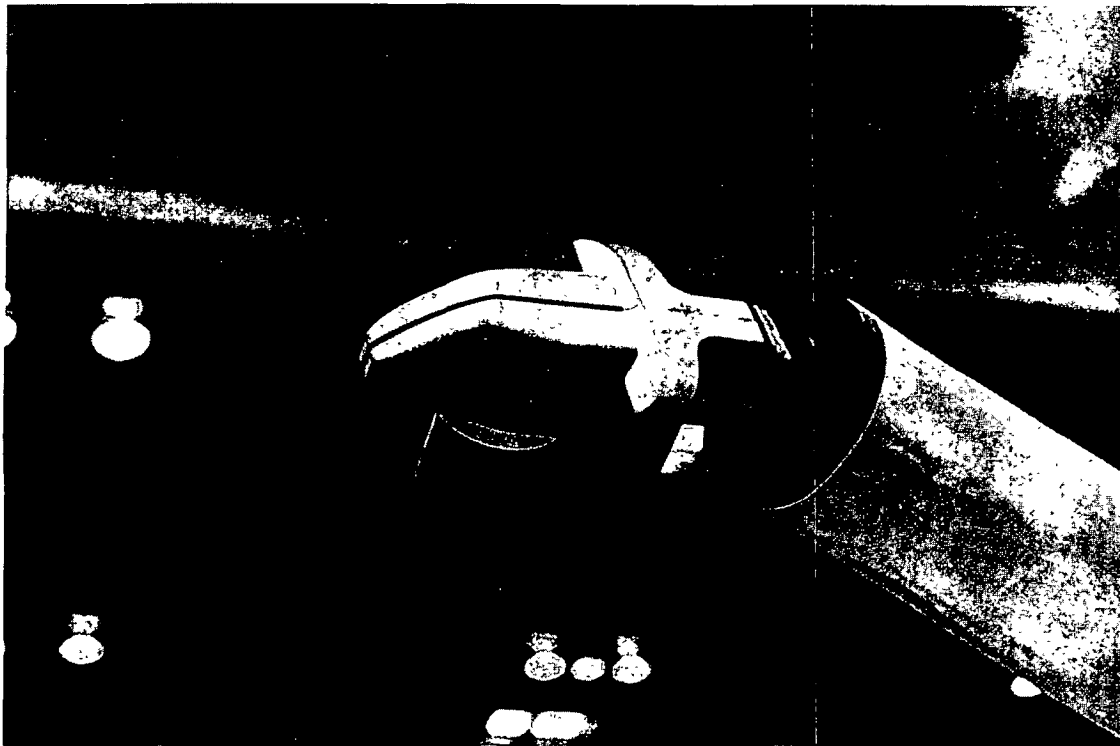


Fig. 4 Close-Up of End Effector

The work boom mounts over the center pair of wheels, and the non-orthogonal and rotating joints combine to provide freedom of movement. The boom can reach below the wheel and also has an inclination device which allows for lifting 180 degrees above the wrist. At the end of the inclination device is a gripper which provides the assembly with clamping force as well as precise positioning. The tools for the end effector assembly are designed to plug into a power source on the gripper; they are automatically activated when they are picked up.

An end effector can be picked up and used effectively only if it is provided with good positioning sensors. Here, the sensors will be optical encoders operating in quadrature. Precise positioning will be achieved with potentiometers which allow the vehicle to determine the position of the end effectors even after a power loss.

Controls

One of the critical design issues of the Enabler project is to control the vehicle and its boom and to provide a relatively simple man-machine interface. The controls were designed to allow control of each of the six wheels, the articulation joints, and the boom.

The operator of the lunar vehicle will use a control system console to command the vehicle in two different modes: articulation and steering. In the articulation mode, the operator can specify vertical or horizontal steering angles and define the front axle rotation angle. In the steering mode, the vehicle speed and horizontal steering angles can be controlled. The current steering controls consist of a set of three-position switches which specify the horizontal and vertical directions for the whole of the vehicle.

The controls system also involves a set of feedback sensors, coordinated by a Macintosh IIcx computer and reporting to the man-machine interface. Wheel velocity, for example, is measured by a set of optical encoders placed in quadrature. These velocity sensors will use bar codes printed on strips which are attached to the inside of the hubs. The articulation joints move at only one speed, but their positioning needs to be tracked; consequently, they have been fitted with 10-turn potentiometers to provide such information. In addition to tracking motion, these potentiometers can determine their orientation even after a loss of power, so the vehicle need not reorient itself to some default position after being powered down.

Status of the Project

At the National Design Engineering Show, two exhibit cases, one with a video solid model animation and another supporting the man-machine interface were displayed on each side of the vehicle. The Enabler was featured in the article "Mobility on the Moon" in *Design News* September 1992.³ The attendees at the National Design Engineering Show expressed considerable interest in the project, some mentioning that they had seen the *Design News* article.

The design stages of the project have been completed, and the Enabler is currently being made into a working machine. A major portion of the components have been assembled, and the rest are currently being fabricated. The design team is scheduled to have the chassis assembled and functioning with a preliminary control system by February 1994. The working model is scheduled to be demonstrated at SPACE '94 in Albuquerque, NM.

References

1. Boles, Walter W., "Lunar Base Construction," Dissertation, The University of Texas at Austin, Austin, Texas, December 1990.
2. Saur, Clemens M., "Evaluation of Manipulator Boom Designs for Lunar Vehicles," Thesis, Georgia Institute of Technology, Atlanta, Georgia, March 1993.
3. Boggs, Robert N., "Mobility on the Moon," *Design News*, Vol. 48 Number 17, Sept. 7, 1992, pp. 95-96, 98.

WHEELED ARTICULATING LAND ROVER: WALRUS

University of Idaho
Department of Mechanical Engineering
Moscow, Idaho

Professor Larry Stauffer

Matthew DiLorenzo and Barbara Yandle, Graduate Assistants

Students: Eric Baicy, John Barinaga, Brian Block, Wayne Bunce, John Clausen, Jay Constable, William Cresse, Travis Fulton, John Gadbois, Darryn Lunders, Jonathon Martinez, Martin Maxwell, Ron Stanley, Dave Walker, Mike Webster, Richard Williams

Abstract

The WALRUS is a wheeled articulating land rover that will provide Ames Research Center with a reliable, autonomous vehicle for demonstrating and evaluating advanced technologies. This vehicle is one component of the Ames Research Center's on-going Human Exploration Demonstration Project. Ames Research Center requested a system capable of traversing a broad spectrum of surface types and obstacles. In addition, this vehicle must have an autonomous navigation and control system on board and its own source of power.

The resulting design is a rover that articulates in two planes of motion to allow for increased mobility and stability. The rover is driven by six conical shaped aluminum wheels, each with an independent, internally coupled motor. Mounted on the rover are two housings and a removable remote control system. In the housings, the motor controller board, tilt sensor, navigation circuitry, and control board are mounted. Finally, the rover is powered by thirty C-cell rechargeable batteries, which are located in the rover wheels and recharged by a specially designed battery charger.

Introduction

The University of Idaho is providing NASA's Ames Research Center in California with an autonomous test platform for advanced technologies, such as virtual reality. This project entailed the design, construction, and testing of a land rover, nicknamed "WALRUS," which stands for Wheeled Articulating Land Rover by *Unemployed Seniors*. Several groups of computer, electrical and mechanical engineering seniors are involved in the project. This design project was divided into three sub-projects as follows: 1) The frame and wheel system. 2) The navigation and control system. 3) The power system.

Methodology

A systematic design and analysis approach was used to assure ourselves of a well designed product. Design tools such as Quality Function Deployment (QFD), decision matrixes and Failure Mode and Effects Analysis (FMEA) were used. The QFD approach gave us a better understanding of our customer's. The decision matrixes were used to help us in evaluating alternatives and making choices between different options. The FMEA analysis was used to help ensure a safe product and also to learn where improvements could be made.

WALRUS Description

The final design of the rover is a six wheeled articulating vehicle fabricated almost entirely out of Aluminum. Each of the rover's six wheels houses one motor and one battery carousel. The rover has two houses mounted on it, which house the navigation and control systems. The results of this design project are best summarized with a picture and a table. Figure 1 shows a side view of the complete rover.

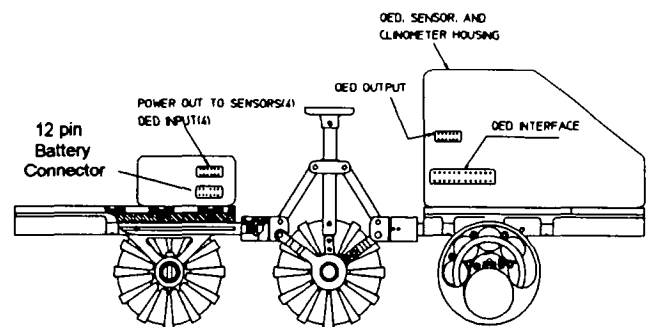


Figure 1. Rover With Housings.

Table 1 lists the final specifications and capabilities of the rover.

Length	19.7 in.
Width	14.5 in.
Height	8.95 in.
Weight	25 lb.
Center of Gravity	2.5 in. from ground
Payload Weight	5 lb.
Payload Capacity	20 lb.
Run Time	1 hr. at full payload
Charge Time	6 hr.
Turning Radius	0 in.
Climbing Ability	30 degrees
Maximum Speed	1.5 ft./sec.
Cost	\$5000.00

Table 1. Final Rover Specifications.

Wheels

The rover is equipped with six identical wheels, each containing a 35 oz-inch ($\approx .25$ N·m) 12 volt DC motor, and five C-size nickel cadmium batteries. This group of five batteries is referred to as a carousel. The two center wheels also include an optical encoder to be used to monitor the speed of the vehicle.

The aluminum wheel housing is built in two parts; a treaded cone-cylinder section and an end cap. Traction on smooth surfaces is enhanced by installing 2 o-rings onto the machined grooves of the cylinder housing section. Primary access into the wheel is gained through the end cap by releasing three half-turn fasteners. Once removed, all internal wheel components are accessible. A section view of the wheel assembly is shown in Figure 2.

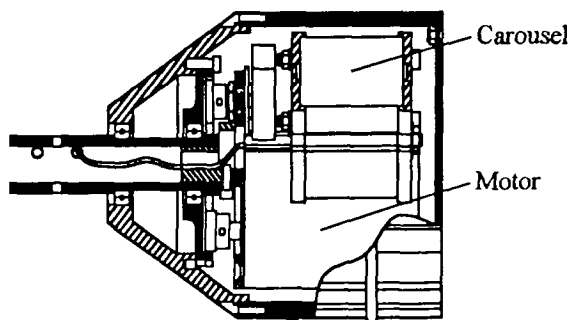


Figure 2. Section View of Wheel Assembly.

The wheel housing rotates about an aluminum shaft which is rigidly attached to the rover frame. The rotation occurs about two bearings; the first of which is connected between the shaft and the cone, the second which is

attached from the shaft to a bearing support. The aluminum bearing support is rigidly secured to the cone housing. This bearing arrangement allows us to terminate the shaft next to the bearing support, thus opening the entire wheel cavity for placement of the motor and battery carousel.

The battery carousel, optical encoder, and motor are mounted to a aluminum support plate which is attached to the shaft. The interface between the plate and shaft is a hollow, stainless steel component through which the wires are routed out of the wheel and to the control system.

The batteries in each carousel are clamped between two nylon support fixtures. This modular unit can be removed from the wheel through the end cap for easy inspection or maintenance. Also, through this primary access, the spur gear of the motor can be adjusted to properly mesh with the internal ring gear on the wheel so that gear backlash is minimized and maximum torque is transferred from the motor to the wheel.

Wheel Articulation

We found from our literature search that articulated vehicles exhibit greater mobility characteristics than vehicles of rigid body construction. The WALRUS is designed to pivot in both the longitudinal and lateral planes. This articulation mechanism allows all wheels to remain in contact with the ground while traveling across rough terrain and over obstacles.

Figure 3 shows a cross section of the rover exposing the articulation system. The mechanism is composed of three parts: two bearing assemblies, and the center shaft assembly.

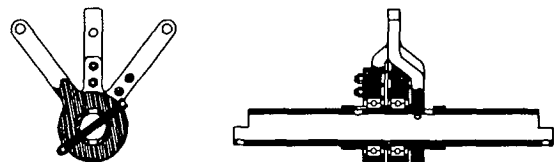


Figure 3. Center Shaft Assembly.

Longitudinal articulation occurs through the bearing assemblies. Two bearings are press fit onto a stainless steel hinge component. An external snap ring provides a redundant means of security, ensuring that the bearings remain tight. A stainless steel housing is press fit over the bearings and redundantly secured by four set screws. The front frame is connected to the mid-frame through the bearing assembly by means of a threaded fastener.

Lateral articulation occurs through the center shaft assembly. With this mechanism, the forward and rear frame assemblies are capable of a 55 degree lift, and a 45 degree drop angle. This angular path is restricted by the

bushing which slides along the camera shaft. The bushing is hinged to the lower frame by two mid frame struts. Maximum lift occurs when the bushing contacts the camera support plate. Maximum drop occurs when the bushing contacts the fastener connecting the camera shaft to the camera support arm of the center axle assembly.

In addition to increased vehicle mobility, this articulation system increases the forward-looking capability of a proposed camera that is to be mounted to the camera support plate. As the front frame assembly tilts up or down, the pitch angle of the camera is half that of the angular deflection of the front frame. For example, a 30 degree upward pitch of the front wheels will cause only a 15 degrees lift of the camera field of vision. This effect minimizes the magnitude of the intervention of the pan and tilt mechanisms controlling the camera's position, increasing the response time of any necessary camera repositioning.

The center axle assembly consists of a pivoting arm and bearing cap, a camera support with bearing cap, a fixed arm, and a center axle. The bearing caps are identical in form and function. Their purpose is to hold the bearings firmly to the pivoting arm and center shaft. The fixed arm of the axle assembly is bolted to the center shaft to provide a rigid support for mounting of the wheels. Axle shims are used to precisely locate the pivoting arm and the camera support. Additional shims are used to position the wheel on either side of the axle assembly.

Frame

Figure 4 shows the relations between the frame and wheels. The frame is symmetric about the center camera shaft. This increases the manufactureability and maintainability of the rover. The use of symmetry also promotes interchangeability of platforms allowing the rover to be used in various demonstration applications with minimal setup requirements.

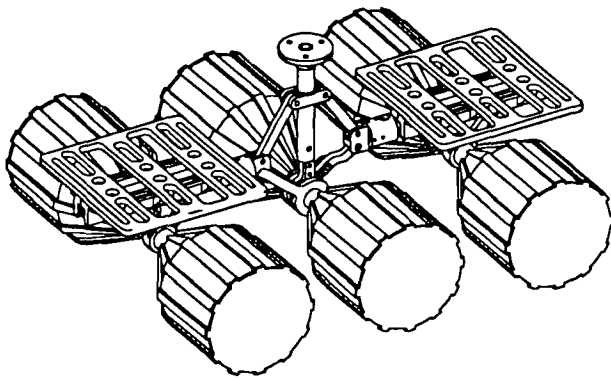


Figure 4. Schematic of Frame and Wheels.

The modular frame assembly is made of three components: two symmetrical platform supports and a top plate. The platform assembly slides onto the front frame flange and is held in place by a single clevis pin.

Main Housing

The main housing on the rover is the larger of the two housings, located on the front of the rover. Mounted in the main housing are the following devices: 1) QED board. 2) two-axis tilt sensor. 3) Global navigation circuitry. 4) Obstacle sensing circuitry. Figure 5 shows the front housing with mounting holes.

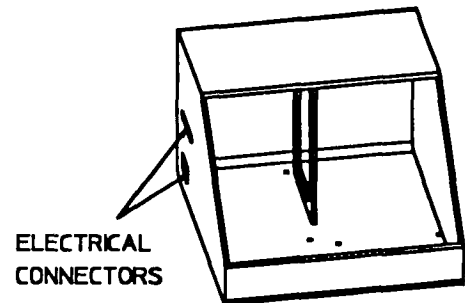


Figure 5. Front Housing.

QED. The QED board is the control unit for the rover's circuitry. This circuit board was programmed using Forth programming language in order to control the motors, ultrasonic sensors and tilt sensor. It functions well as the central processing unit for the motor control, obstacle avoidance and global navigation systems.

Tilt Sensor. The tilt sensor used was a commercially available two axis tilt sensor which is used to inform the QED of changes in the external terrain. This sensor can accurately measure angles up to 20 degrees, which is needed by the rover for avoiding unsuitable terrain.

Global Navigation Circuitry. The global navigation circuitry consists of a light beacon and microphone. The purpose of this system is to communicate with the QED board in order for it to determine its location in the test environment. The system works as follows: 1) The light beacon on the rover sends light to light sensing arrays located along the perimeter of the test terrain. 2) The light sensing arrays convert the optical signal to an audio signal which is then sent back to the rover and received by the microphone. 3) Then, through a process of timing the signals and triangulation, the QED can calculate the rover's position.

Obstacle Sensing Circuitry. The circuit board used in the obstacle detection system is a Polaroid ultrasonic sounding board. This system simply uses the principals of acoustics to detect objects near the rover and then communicates to the QED board. The QED board then enters any obstacles into it's internal map and adjusts, through the motor controller board, the course of the rover.

Rear Housing

The rover's other housing is the smaller one located at the rear of the vehicle. The reason for using two housings instead of one is twofold: 1) The circuitry located in the rear housing puts out more heat than all the circuitry in the front main housing. 2) The height of the housing was limited by the potential use of a camera located on the center post of the rover. Inside the rear housing is the motor controller circuit board.

Motor Controller. The motor controller circuitry is connected to the QED board in the main housing. Through the QED board and motor controller, the rover's six motors are controlled. The motors speed and direction, forward or reverse, is then fully adjustable.

Platforms

The mounting platforms located on the front and rear of the rover where used to mount the housings, to hold optical sensors and to interface the housings to the rover's frame. The platforms were machined from aluminum and are attached to the frame through the use of mounting rails on the frame of the rover. Figure 6 shows a schematic of one of the mounting platforms.

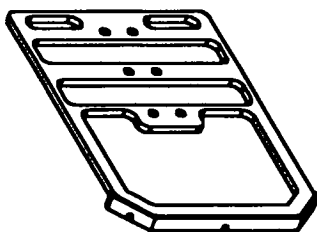


Figure 6. Mounting Platform.

Remote Control System

A Futaba two channel AM radio system will be used to calibrate the rover in it's test environment and to accomplish tasks beyond the capabilities of the semi-autonomous system.

The housing for the remote control system is mounted on the rover frame in place of either the main or rear housing.

The only difference in mounting this housing is that Velcro straps were used instead of the previously used bolts and screws. Located inside the remote control housing are the following components: 1) standard servos. 2) a standard receiver. 3) AA batteries. 4) potentiometers. 5) 1" and 3" gears.

The remote control system's transmitter is a hand held two stick transmitter. The left stick controls the speed of the rover and the right stick controls the direction of the rover. The principal of operation is as follows: The transmitter sends a signal to the receiver. Then the receiver sends a signal to the servos, which transmit a signal mechanically through gears to the potentiometers. Finally, the potentiometers adjusted electrical resistance controls the motors speed and direction (forward or reverse).

Power System

The batteries that supply power to the rover's motors and electronics are Sanyo brand 1.2 volt nickel cadmium fast charge C cell rechargeable batteries. There are a total of 30 batteries in the rover; one five battery carousel per wheel.

In order to maintain power to the rover, the batteries must be recharged when necessary. To accomplish this task, a battery charger was designed. This charger is housed in louvered aluminum box. The charger contains the following components: 1) Rover recharging cord. 2) LED display lights. 3) Illuminated power switch. 4) Standard wall outlet cord. 5) Airway hole for cooling fan. Figure 7 shows an exterior view of the charger.

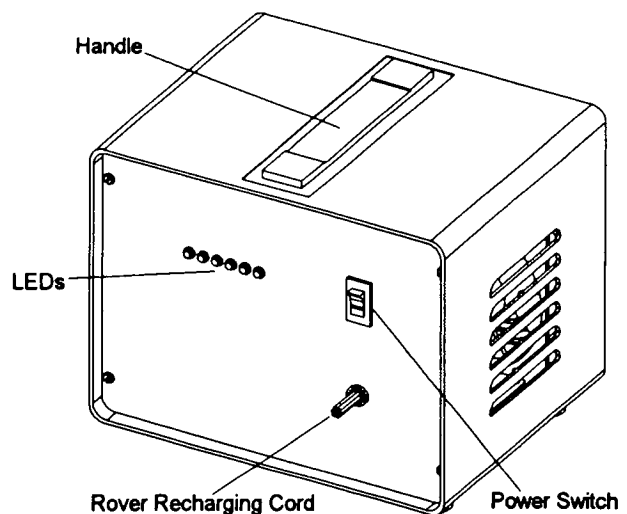


Figure 7. Overall Schematic of Charger.

The internal components of the charger constitute the electronics necessary to convert the standard 120 volt wall outlet electricity to the needed DC voltage to charge the battery carousels. The internal components of the charger

are illustrated in Figure 8. The function of these components is as follows: 1) The transformer receives and then converts the 120 volt signal to 12 volts. 2) The signal is then routed to the circuit board which controls the LED displays, rectifies the signal and amplifies the signal. 3) The signal is then routed through the capacitor, which further conditions the signal. 4) The power is then routed to the rover and connection is made through a twelve pin connector on the rear rover housing. While the batteries are charging, the fan cools the electronics in the charger housing. The charger is designed to light the six LED displays and then shut off each light as it's corresponding carousel becomes fully charged. The charger also has an automatic shut-off feature, which prevents overcharge of the batteries.

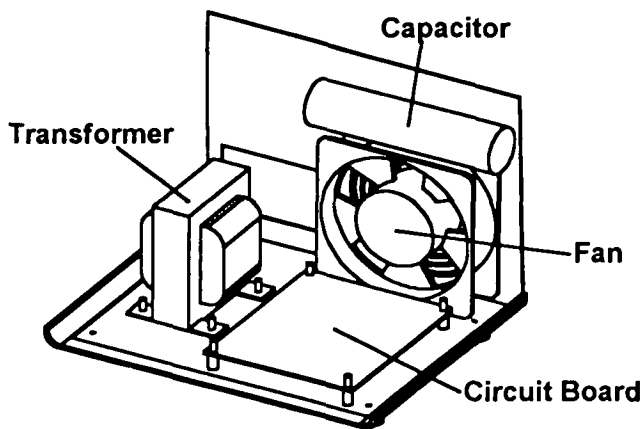


Figure 8. Internal Components of Charger.

Test Environment

In order to give NASA a fully tested and operational product, a test environment has been designed. A plywood box was erected in a university laboratory and filled with soil. A base layer of filler soil was placed in the box. The top soil will be sifted and sorted in order for it to approximate the soil at Ames Research Center. A hill will be made to approximate the desired grade. This will enable the rover's tilt sensor to be tested. The terrain will have large rocks placed around it, in order to test the rover's ultrasonic sensors. Figure 9 shows a schematic of the test terrain, including the location of the light sensing array discussed previously.

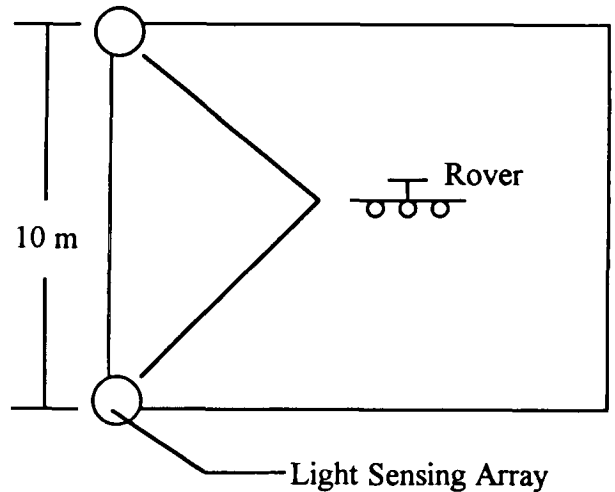


Figure 9. Test Site Layout With Detail of Light Sensing Array.

Conclusions

This design will fulfill all of our customer requirements. The design of the rover is complete but due to time and budget constraints the rover wheels are still being machined on NASA's computer numerical control machines. After the wheels have been machined, the rover will be assembled and then tested in the test terrain on campus. The rover should be delivered to Ames Research Center at the end of the summer of 1993.

Iowa Satellite Project

Iowa State University of Science and Technology
Department of Aerospace Engineering and Engineering Mechanics
Ames, Iowa

Dr. Leverne K. Seversike
Todd Kuper, Teaching Assistant

Abstract

With a few exceptions, satellite systems to date have been large and expensive. Over the past decade, there has been a growing interest in small, inexpensive satellites built and operated by universities to provide students with a 'hands on' engineering experience. It was decided that the university would design, build, and operate a satellite called ISAT-1. The primary mission of ISAT-1 is to provide a broad educational experience to Iowa citizens of all age groups and educational backgrounds. The requirements of the project are that ISAT-1 must be a small, inexpensive satellite that can be launched by mid-1996, have an operational lifetime of five years, and can be designed, constructed, and operated by university students.

This satellite will have a mass of 50 kg and will be shaped as a hexagonal cylinder 34.0 cm wide and 64.3 cm tall. ISAT-1 will be launched into a circular, low Earth orbit as a secondary payload aboard a Delta II rocket in late 1995. The satellite will be stabilized using an extendible gravity-gradient boom with tip-mass and magnetic torquers. The body-mounted solar panels and rechargeable batteries will provide approximately 25 watts of continuous power. A variety of onboard payloads are designed to accomplish the educational goal including a CCD camera with a small telescope, particle detector, Earth Radio Frequency Experiment, and a robotic arm with a miniature CCD camera to examine the exterior of the satellite. Also, a network of weather stations positioned across Iowa will send weather and soil conditions to ISAT-1 for relay to the ground station. The entire project is expected to cost \$2 million. The report gives an overview of the design effort of ISAT-1 and a detailed description of the bus, payload, and ground systems.

Introduction

Satellite systems to date have been mainly scientific, commercial, or military in nature. There are very few systems that provide students and ordinary citizens with a 'hands on' experience. The goal of the Iowa Satellite Project is to design, build, launch, and operate a satellite for a minimum of five years. The primary mission of ISAT-1 is to provide a broad educational experience to

citizens of Iowa at all levels of education. The Project will provide products, services, and activities that will be practical and useful for a large number of people. The emphasis will be on public awareness, 'space literacy', and routine practical applications.

Background

The Iowa Space Grant Consortium was established in 1989 to facilitate space education and cooperation between business leaders and the three universities in Iowa: Iowa State University, University of Iowa, and University of Northern Iowa. It was decided that the state should embark on a project that would promote space activities and provide a 'hands on' experience to university students as well as the general public. One fairly inexpensive way of doing this was to design, build, and operate a small satellite in Earth orbit. It was decided that Iowa State University would take the lead in this project.

During the spring semester of 1992, the Spacecraft Systems class at Iowa State University started the conceptual design phase. This class decided upon the mission objectives and general requirements for the project. Several configurations and payload sets were studied. A small team of undergraduate and graduate students, funded by the Iowa Space Grant Consortium and the Institute of Physical Research and Technology (IPRT), furthered the design during the summer and fall of 1992. Also during the summer, Iowa State started taking part in the University Student Researchers Association Advanced Design Program (USRA/ADP). In December 1992, a non-profit corporation called the Iowa Satellite Company was formed to be responsible for financial and legal issues. During the spring semester of 1993, the Spacecraft Systems class selected an overall configuration and payload set and also furthered the preliminary designs for the major subsystems.

Requirements

The requirements for the ISAT-1 mission were decided to be:

- have an operational orbit lifetime of at least 5 years
- have a mass less than 100 kg

- be as user-friendly' as possible
- total cost over 5 years, including launch, less than \$10 million
- to be launched by 1997
- to pass over Iowa at least 4 times per day

Payload

A number of experiments and applications that meet the design requirements and objectives comprise the payload set:

- CCD camera with a telescope
- Earth Radio Frequency Experiment
- Weather station network
- Micro meteoroid detector
- Solar cell experiment

A complete description of the purpose of each experiment and the work completed to date are discussed below. Other payloads such as a Global Positioning System receiver, seed growth experiment, robotic arm with CCD camera, and material solidification experiment are also being considered.

CCD Camera

One of the most common uses for a low Earth orbit satellite is taking pictures of the Earth. Pictures are one thing that everyone can understand and feel enthusiastic about; therefore, a color CCD camera will be included in the payload set. A small telescope, perhaps 10 cm in diameter, will be used to gain a greater resolution for the camera.

Earth Radio Frequency Experiment

The Earth Radio Frequency Experiment (ERF) will measure the intensity and spectrum of terrestrial communications signal 'leakage' through the Earth's ionosphere over the frequency range of 1.5 - 34.5 MHz. This experiment will collect data that, when analyzed on the ground, will help determine the spectrum, intensity, and temporal characteristics of this signal leakage. This data will be used to determine whether low frequency radio astronomy is feasible from Earth orbit.

Weather Station Network

The weather station network will be a network of ground transponders that will uplink stored and current weather and ground data collected by a variety of sensors connected to the transponder. The data from the entire network will

then be down-linked to the receivers on the ground. The data will be analyzed and be available to anyone that requests it. The goal is to have at least one weather station and transponder in each of Iowa's 99 counties.

Micro meteoroid Detector

While in orbit, ISAT-1 will be in an environment filled with meteoroids and orbital debris. Within 2000 km of the Earth's surface there is about 200 kg of meteoroid material, most of it smaller than 0.1 mm in diameter. While larger meteoroids and orbital debris will most likely render ISAT-1 useless upon impact, smaller meteoroids may only cause a small disturbance or vibration. The micro meteoroid detection system will be used to count the number of impacts on ISAT-1, determine where the impact occurred, and obtain an estimate of the momentum of the meteoroid before impact.

Solar Cell Experiment

A solar cell's performance degrades due to radiation, thermal stresses, and surface degradation caused by impacts with micro meteoroids. This experiment will compare the performance of gallium arsenide cells and silicon cells covered by different material films and thicknesses.

Launch Vehicle

Several launch vehicles were considered for orbiting ISAT-1, including the Space Shuttle, Ariane, Atlas, Pegasus, and Delta II. The shuttle was rejected because the shuttle could not deploy ISAT-1 in an orbit with the minimum required altitude and inclination. Because Atlas does not currently have a designated secondary payload accommodations and the primary payload cost is prohibitively high, the Atlas booster was rejected. Pegasus was summarily rejected because of the high cost. Ariane was rejected because the launch apparatus and secondary payload configuration were not compatible with the proposed ISAT-1 design. Therefore, launch on a Delta II as a secondary payload was chosen.

Configuration

ISAT-1's bus will be a hexagonal cylinder 64.3 cm in height and 34.0 cm in width. The satellite will use gravity-gradient stabilization augmented by magnetic torquers. To increase the inertia of the longitudinal axis a 6 kg mass will be attached to a 3 m long boom.

Most interior components will be placed in boxed-shaped modules. This will allow standardization of most module components and provide thermal and radiation protection. There will be two modules for the flight computers, two

Structure

modules for the two communication systems, one module for the Earth Radio Frequency Experiment, two large experiment modules, two medium experiment modules, and six small experiment modules.

The interior components will be mounted on three load-bearing shelves. The six batteries at the base of the satellite, telescope, and the two medium size experiment modules will be mounted to Shelf 1. The Earth Radio Frequency Experiment, CCD cameras, two small experiment modules, two large experiment modules, and boom will be mounted to Shelf 2. Shelf 3 will support the two flight computer modules, four small experiment modules, and the two communication modules. The bus configuration is shown in Figures 1 and 2. Table 1 shows the mass and peak power consumption of each of the components.

Orbit

The final orbit for ISAT-1 has not been finalized at this time; however, there are a few requirements that have been determined. The orbit must be near circular so that gravity-gradient stabilization can be used. To meet the 5-year lifetime requirement, the orbit must have an altitude of at least 600 km. The inclination of the orbit must be greater than 55 degrees for ISAT-1 to pass over Iowa.

The structure of the spacecraft provides the necessary physical support for all subsystems. The structure not only contains the payload and bus systems while on-orbit, but must withstand launch conditions and ensure that all of the payload and bus systems will arrive on-orbit in an operational condition.

Previous work on the ISAT structure included the selection of a hexagon shape based on solar cell power calculations. In addition, the maximum dimensions of the exterior were based on the launch vehicle payload envelope. In addition, the internal configuration was provided by the integration group.

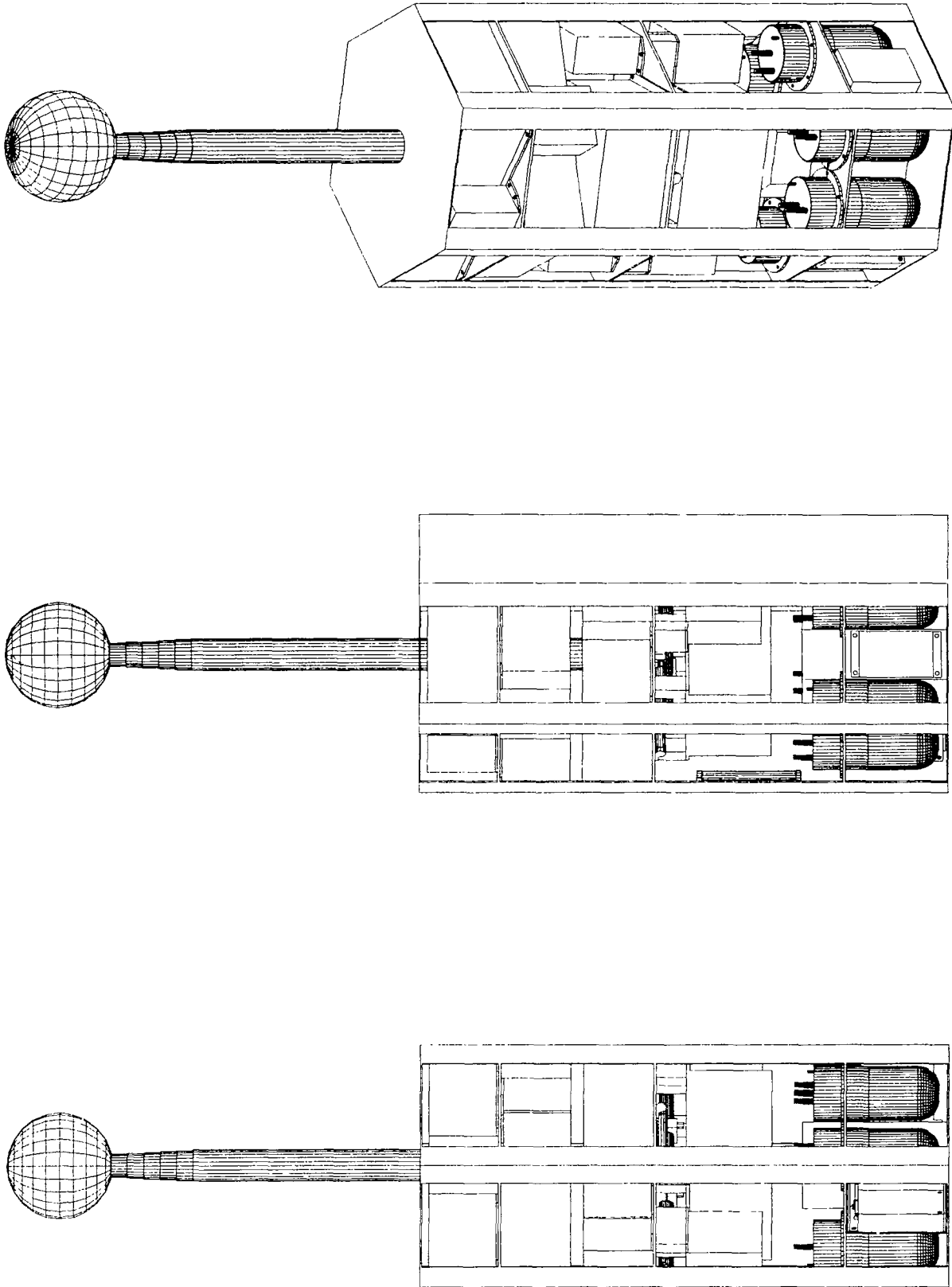
Design Considerations.

Several design criteria for the ISAT structure were developed. These included: accommodating the internal payload arrangement as specified by the integration group, providing access to internal payloads, supporting the launch adapter, providing for attitude control mechanisms, and using as little internal volume as possible. Total structural mass, cost, and ease of fabrication were also considered.

Table 1: Mass and Power Consumption of Components

Quantity	Component	Mass (kg)	Peak Power (W)
1	Structure	3.6	n.a.
1	Boom	7	n.a.
2	Communications	3	7
2	Flight Computer	3	7
2	Large Experiment Module	3	4
2	Medium Experiment Module	1.1	1.5
6	Small Experiment Module	0.9	1.1
1	Large Torquers	0.45	2
2	Small Torquers	0.1	0.25
2	Boom Tanks	0.1	n.a.
1	Earth Radio Frequency Experiment	5.4	7
1	CCD Camera	0.4	5
1	Telescope	3	n.a.
6	Battery	0.6	n.a.
6	Battery Mount		n.a.
2	Magnetometer	0.22	0.04

Figure 2



3DSTRUCT.DWG

Iowa Satellite Company

5/9/93

3-D Packing Arrangement
Delta II Secondary Payload (SPE1)

Iowa Satellite Project

ISAT-1

Mike

Drawing File

Drawn By

The internal configuration of ISAT-1 is shown in Figure 2. This arrangement shows the payload and bus systems arranged on three internal shelves. The location and arrangement of attitude control mechanisms is also shown. Most notably, the structure must be capable of transmitting control torques from the three torque-rods and from the gravity-gradient boom attached to Shelf 2.

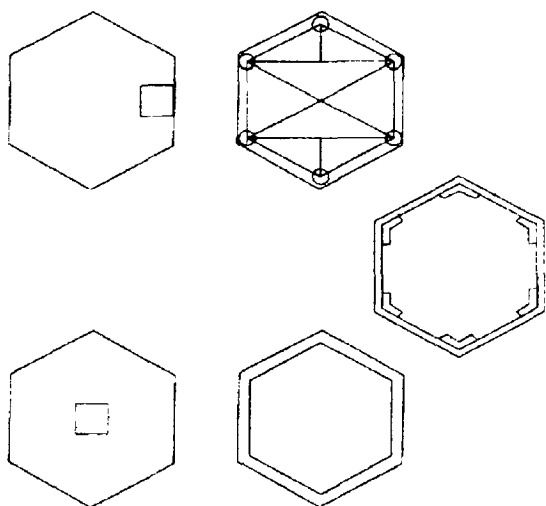


Figure 3: ISAT Structure Concepts - End View

Internal Structure

Concepts Five concepts for the internal structure of ISAT were considered. They included central support, modified central support, full monocoque, semi-monocoque, and truss. These five concepts are shown in Figure 3. These structural concepts were considered prior to determination of the internal payload arrangement.

The semi-monocoque concept would consist of skin panels attached to longitudinal stringers. The design would reduce the panel thickness while transferring more structural material into the corners of the hexagon. One panel would have to be designed to accommodate launch loads.

Selection Criteria One of the major considerations in the final selection of a structural concept was the amount of internal volume that would be required. It was felt that the semi-monocoque structure would best fulfill this criteria, as it would make the best utilization of previous unused space in the corners of the hexagon shape.

Another consideration was the ability of the structure to be adapted to the unique launch interface. The placement of the launch interface on the side of the satellite, requires that non-uniform loading be a consideration. It was felt

that the semi-monocoque structure would again adequately meet this consideration. The semi-monocoque structure can be adapted to the launch adapter by varying the stringer and panel thickness on the side of the launch adapter.

Fabrication and assembly of both the structural components and the integration of the payload was also considered. The semi-monocoque concept provides for greater flexibility in fabrication and assembly sequences than the other concepts. It should be possible to design the structure such that all segments of the payload are accessible even with the launch adapter in place.

Preliminary Structure Sizing Analysis A preliminary analysis of the structure was conducted for sizing purposes. For this case, each payload was considered to be of uniform mass, and its mass would act at its center of mass on each shelf. These loads were then transferred to the six stringers for each shelf. The details of this analysis are presented below in Table 2.

Table 2: Static Shelf Load Estimates

Bottom	0.0 N
Shelf 1	92.4 N
Shelf 2	138.5 N
Shelf 3	156.0 N
Top	t.b.d.

These loads were then used to conduct a stress evaluation of the stringers and the shear stress in the panels. A computer program was written to calculate the axial stress in the stringers and the shear stress in the panels due to the maximum shelf loading case.

Preliminary Finite Element Analysis The results from the preliminary sizing analysis were used to construct a finite-element model. The model was fixed in rotation and translation at the four launch adapter attach points. The model was loaded with the estimated shelf loads.

Structural Elements

Boom Section Selection A circular, closed-section design was chosen. This section was chosen for its torsional properties and its uniform bending stiffness. The simplicity of the deployment mechanism was also a consideration. The magnetic torquers of the attitude control system will be able to re-invert the satellite with the boom deployed, so the boom will only be deployed once.

A locking, pressure tight joint for the boom segments was developed. The design provides for a forward stop collar located on the inner wall of the outer boom section, and a series of forward segmented stops located on the outer wall

of the inner boom section. A segmented stop collar is also located on the inner wall of the outer section. A rear stop collar is located on the inner section. When pressurized, the boom extends until the forward stop collar on the outer section comes into contact with the segmented collar on the inner section. The segments on the inner section slide through the gaps in the collar on the outer section, and are then rotated to lock the boom in its deployed state. The joint design also provides for the placement of three gaskets: one each at the base of the inner section, the top and base of the rear stop collar to provide a gas seal for the pressurized deployment of the boom.

Boom Sizing A design sizing code with boom length and tip mass as control variables was written to determine an optimum length and tip mass for the satellite. The code allows the user to select the desired stability in terms of the stability criterion, σ_x as defined by the following equation

$$\sigma_x = \frac{(I_y - I_z)}{I_x} \quad (1)$$

The user also selects the desired range of boom lengths and tip masses. The code then iterates through these two variables, calculating the new mass moment of inertia I_x , and uses the new inertia to calculate the value of σ_x . The calculated value of σ_x is subtracted from the target value, and the absolute value of the difference is written to a data file along with the boom length and mass. This information can then be plotted on a contour plot. Several candidate designs meet the desired stability. The final boom size was selected to be 3 meters in length with a 6 kilogram tip mass. This represents nearly a fifteen fold increase in I_x .

Boom Section Sizing Stability considerations determined the boom length and tip mass. The diameter and thickness of each section would be determined according to the loads acting upon each section. Loads acting on the gravity-gradient boom were modeled as the Earth's gravitational force acting on the tip mass. This in turn caused forces and moments to be exerted on the boom. A sizing code was written to size the boom sections based on the known loads, the material properties of graphite-epoxy composites, and a selected factor of safety. It was not possible to accurately determine dynamic loads on the gravity-gradient boom due to insufficient source data so a large factor of safety was used.

The code was set up to allow the user to choose the desired tip mass and boom length for section sizing analysis. Once the user had completed the inputs of number of sections, minimum section thickness, gap between sections, and initial base section outer diameter, the code would size the boom sections. This entailed

determining the necessary outer diameters, section thicknesses, and inner diameters corresponding to each boom section. If the section thickness needed was found by the code to be smaller than the minimum section thickness, the code would substitute in the minimum section thickness and continue the analysis.

Results of section sizing yielded necessary section thicknesses for a number of base section outer diameters. A base section having an outer diameter of 3.81 cm was chosen based on the limited volume fraction of ISAT-1 which would be required. Table 3 shows the section sizes in terms of outer diameters, thicknesses, and corresponding inner diameters. It should be noted that in all cases the thicknesses used are the minimum section thickness, and the gap between sections is constant for ease of fabrication.

Table 3: Boom Sections

Boom Section Number	Outer Diameter (cm)	Section Thickness (cm)	Inner Diameter (cm)
1	3.81	0.102	3.71
2	3.61	0.102	3.51
3	3.40	0.102	3.30
4	3.20	0.102	3.10
5	3.00	0.102	2.90
6	2.79	0.102	2.69

Fabrication Methods

The mandrels used for curing of the boom sections consisted of two sections of steel pipe, each 0.61 meters in length. These were complemented by three rubber hose sections of 0.76 meters in length. The hoses had outside diameters 2.62 cm, 3.15 cm, and 3.61 cm. Each section was fabricated from three plies of woven graphite-epoxy composite. The composite material was cut to a length of 0.56 meters and a width equal to the circumference of the desired section. The three plies were then debulked with the edges staggered prior to being placed in the mandrel.

To avoid the added complexity and difficulties involved with co-curing the joints along with the respective boom sections, joints from separate cure cycles were epoxied in at a later time.

Modeling

The boom was modeled using ANSYS finite-element analysis. The boom was modeled as cantilevered with the tip loads acting perpendicular to the boom length. A static analysis was performed. The boom was found to have a maximum deflection at the tip of 0.05 meters (1.969 inches).

Shelving

Design Considerations Each shelf must be capable of supporting all loads and payloads. In addition the shelves must accommodate the payload boxes, including any unique interfaces (radiator, electrical connections, etc.). The internal volume of the spacecraft and the payload requirements limit the allowable deflection for each shelf. Other concerns include thermal conductivity, vibration characteristics, cost, weight, ease of fabrication, and ease of access.

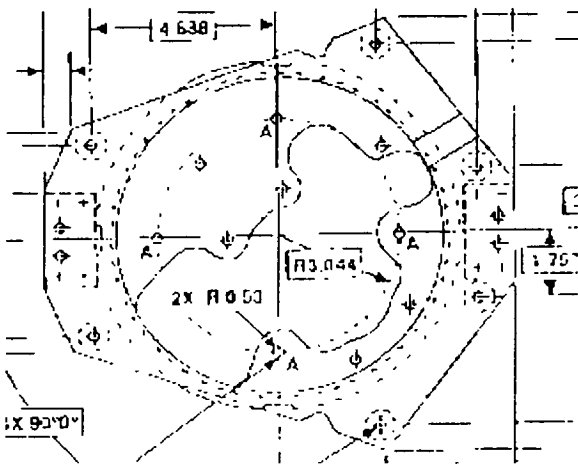


Figure 4: Payload Adapter Assembly

Launch Adapter

The launch adapter provided by McDonnell-Douglas for the SPE payload fairing on its Delta II rocket is shown in Figure 4. The launch adapter design is fixed by McDonnell-Douglas Space Systems. The adapter consists of a ring that is clamped to the launch vehicle. Six attachment bolts are provided to attach the launch adapter to the payload. The ISAT-1 structure must be designed to accommodate the given interface and be able to jettison the launch adapter when orbit is achieved. Two of the attachment bolts will not directly contact any side panel.

Several designs have been considered to meet this challenge. One possibility is the reinforcement of the side panel facing the launch adapter by addition of stringer, increasing the size of existing stringers and/or increasing panel thickness. This design may make it possible to not use the two attachment bolts not directly in contact with the panel. Further study of this design will require consultation with McDonnell-Douglas and is recommended.

Attitude Control

Because ISAT-1 will have a camera used for imaging the Earth, the satellite will need to be stabilized and controlled in a Earth-pointing orientation. The pointing requirements were set to be less than 5 degrees on the pitch and roll axis. Spin and three-axis stabilization were not considered because the pointing requirements could not justify these relatively complex and costly systems. Momentum-biased systems were considered, but rejected because of the high cost and the internal volume constraints of the spacecraft. Therefore, ISAT-1 will use gravity-gradient stabilization augmented by magnetic torquers.

Sensors

Because gravity-gradient stabilization will not give pointing control better than a few degrees on each axis, attitude knowledge requirements for ISAT-1 are less stringent than more complex systems and cannot justify massive and costly attitude sensors. It was decided that with new advances in attitude determination with magnetometers and sun sensors, these lightweight and relatively inexpensive sensors would be adequate. Two 3-axis flux-gate magnetometers mounted orthogonal to each other will measure the Earth's magnetic field and at least two sun sensors mounted on the bus surface will measure the sun angle. This will give the three-dimensional attitude of ISAT-1 to within 1 degree on each axis.

Control Hardware

A 3 meter long boom with a 6 kg mass mounted on the end will give ISAT-1 a stability ratio of 0.98 defined by equation 1. This is comparable to the stability ratios of previous gravity-gradient satellites such as Uosat-2 and Polar Bear. Three magnetic torquers will use the Earth's natural magnetic field to damp out any oscillations and correct any residual errors in the attitude. Two 1 A-m² torquers will be mounted along the pitch and roll axis and a 10 A-m² will be mounted along the yaw axis. The larger torquer will be used for re-inverting the satellite. However, current work shows that an additional 10 A-m² torquer may be needed along the roll axis.

Modes of Operation

There are four phases of attitude control to be considered:

- Despin after separation from launch vehicle
- Boom deployment
- Normal operation
- Inversion correction

Despin. Separation from the launch vehicle will induce a tumbling motion on the satellite. The magnetic torquers will be used to slow the tumble rate so that the gravity-gradient boom may be deployed. The torquers will follow the well-known control law

$$\bar{\tau}_m = -M_{sat} \left| \frac{d\bar{B}}{dt} \right| \tag{2}$$

By numerically integrating the equations of motion using this control law, it was found that tumble rates of up to 10 degrees per second on each axis can be damped out within four orbits.

Boom Deployment. Once the attitude rate has slowed sufficiently, the boom may be deployed. Assuming no roll or yaw motion, the satellite's motion can be described by the following equation

$$\left(\frac{d\theta}{dt} \right)^2 + 3\omega_c^2 \sigma_y \sin^2 \theta = c \tag{3}$$

where θ is the pitch angle, ω_c is the orbit rate for a circular orbit, and σ_y is defined by the following equation

$$\sigma_y = \frac{(I_z - I_x)}{I_y} \tag{4}$$

c is the constant calculated from the initial conditions. Using this equation and assuming boom deployment in zero time, one can find under what combination of pitch angle and pitch rate the satellite will be captured in the correct orientation, i.e boom-up, for given initial conditions. Current work is being done on the effect of roll and yaw on the capture phase.

Normal Operation. Once the boom is deployed and the attitude has been captured in the correct orientation, the magnetic torquers are used to damp out any oscillations and correct any residual attitude errors. The torquers will be controlled by the following control law

$$\tau_{m\theta} = k_p B_\phi \phi - k_n \frac{dB_\theta}{dt} \tag{5}$$

where k_p and k_n are the precession gain and nutation gain, respectively. Also being considered is a Linear Quadratic Regulator type of control law.

Inversion. Due to thermal vibration in the boom or a meteoroid impact the satellite may become inverted. It will then be required to re-invert the satellite to its proper orientation; otherwise, the camera will be useless and there will be a reduction in performance of the communications system. The procedure to re-invert the satellite is currently being studied

Power

The power system for ISAT-1 will consist of solar arrays, rechargeable battery made of six nickel-hydrogen cells, battery charge controller, and power conditioning and control unit.

Solar Array

ISAT-1 will obtain the necessary power to run the bus and payload systems by the use of solar cells mounted on the six lateral sides of the bus. The solar cells are to be arranged on panels, with each panel consisting of 32 cells each. Each panel will then have a surface area of 256 cm². Five sides will consist of 4 panels each, while the side with the launch adapter will have only 2 panels. Figure 5 shows the average power generation during one orbit as a function of sun elevation above the orbit plane and the efficiency of the solar array, e . Gallium-arsenide solar cells have beginning-of-life (BOL) efficiencies of 0.18 and end-of-life (EOL) efficiencies of 0.14. Silicon cells have BOL efficiencies of 0.14 and EOL efficiencies of 0.10. At the present time, gallium-arsenide cells have been chosen over silicon cells because of their greater efficiency; however, gallium-arsenide cells may be too expensive for this project. The results of a study in experiment scheduling will determine which cells will be used.

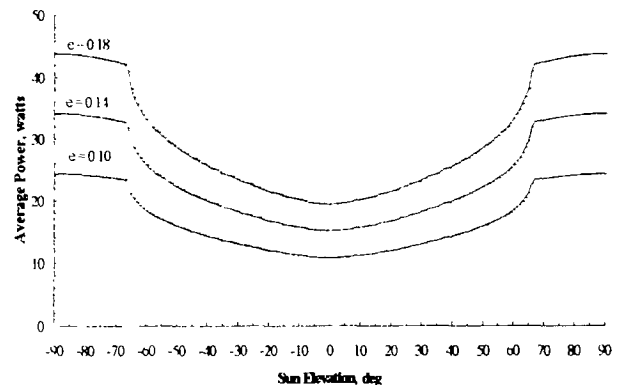


Figure 5: Average Power Generation

Power Regulation The power conditioning and control unit will have DC/DC converters to provide the required operating voltages for various satellite systems. In general, decentralized voltage regulation will be employed in order to avoid over-regulation and yet provide well-conditioned power to different systems. Control of power to various satellite systems will be handled by the flight computer software. The flight computer will monitor the battery

status and will perform the power management function under the guidance of commands from the ground station

Power Storage The satellite battery will consist of spaced nickel-hydrogen cells. Six cells connected in series will provide a nominal unregulated voltage of 15 volts.

Table 4: Cell Specifications:

Rated capacity	6 AH
Nominal voltage	2.5 V
Cell mass	0.633 kg
Diameter	6.48 cm
Length	17.15 cm
Capacity	7.1 AH
Specific energy	28 WH/Kg
Energy density	39.20 WH/l
Operating pressure	400 PSIG
Safety factor	5:1 ratio

The battery charge controller will monitor the temperature and voltage of the battery and will control the flow of current from the solar arrays, thereby ensuring maximum power transfer on one hand and avoiding over-charging of battery on the other.

Communication

The communications system for ISAT-1 will be divided into two parts called Comm-1 and Comm-2. Comm-1 will be the main communications link between the satellite and the ground station. All command and control commands will be transferred through this link. Additionally, data for bus health, payloads, and software updates will be handled by this link. Comm-2 will serve as the data link for the Weather Station Network. Comm-2 will receive weather and soil data from the ground transponders and transmit the data to the ground station upon command. In the event of failure of Comm-1, Comm-2 can act as the primary communications link. Figures 6 and 7 show a schematic of the communications system.

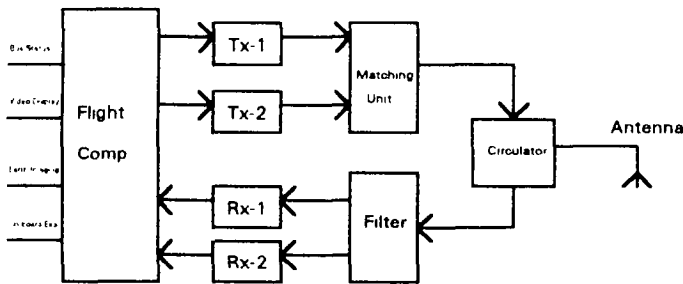


Figure 6: Onboard Communication Architecture

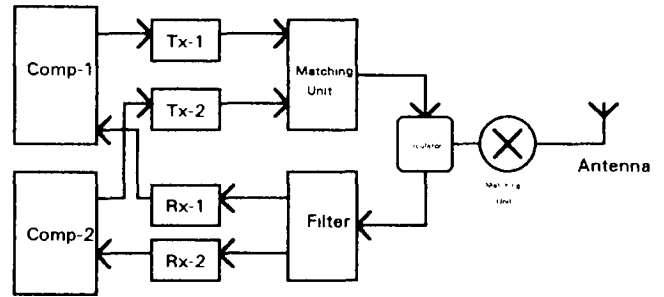


Figure 7: Ground Station Communication Architecture

On average, the satellite will be making four passes over Iowa per day with an average contact time of about 8 minutes per pass. It is expected that the data rate of 10 Kbps will be sufficient to handle the above-mentioned data on a time shared basis.

Various multiple access techniques were considered for Comm-2 and it was found that a 'packet data transfer' scheme is most appropriate. In this scheme, all the ground transponders have identical transmitters and receivers that share a common frequency band. Each ground transponder will be assigned a unique identification code and a digital logic circuit onboard the satellite will separate the data received from various ground transponders. In order to coordinate the data transfer from various transponders and avoid data clash, the satellite needs to exchange control signals with the transponders. This can be handled by either the existing downlink transmitters (Tx-1 or Tx-2) on a time shared basis or else another transmitter (Tx-3) will need to be employed.

Frequency Allocation

Keeping in view the recent radio frequency allocation by the World Administrative Radio Conference (WARC) for small satellites, two frequency bands were selected for Comm-1 and Comm-2. These are:

- 100--200 MHz VHF Band
- 400--500 MHz UHF Band

The VHF band will be used for the uplink while the downlink will operate in the UHF band. It is expected that the two bands will provide sufficient frequency isolation between the transmitters and the receivers to permit a full duplex operation.

The ultimate selection of frequency, however, is based on the allocation by the Federal Communication Commission (FCC). The process of frequency allocation by the FCC is presently in its final stage.

Antenna Design

Satellite Antenna The satellite antenna will consist of four to eight quarter-wave dipole elements attached in a symmetrical manner, perpendicular to the satellite's longitudinal axis. This will result in two symmetrical beams of about 150 degrees, one facing the Earth, while the other away from Earth.

Ground Station Antenna A Crossed Yagi directional antenna will be utilized at the ground station for transmission and reception of signals to and from the satellite. The antenna will have a beam width of about 60 degrees and will have a tracking capability of 360 degrees in the horizontal plane and 150 degrees in the vertical plane.

Ground Transponder Antenna In order to keep ground-transponder complexity to a minimum, a fixed, Crossed Yagi-array antenna is considered suitable. The antenna will have one set of reflectors, about three sets of director elements, and is expected to provide a beam width of about 100 degrees.

Command and Control

The Command and Control system will handle all telemetry to and from the ground station, schedule all the on-board experiments, collect data from various sensors and perform various other housekeeping functions. It will essentially consist of a flight computer, storage memory and the interface hardware.

Flight Computer Specifications

- DOS compatible software.
- Operating system shall be ROM based, with an automatic reload capability in the event of program crash.
- Capability of software update after launch.
- Low power CMOS technology.
- 286 or 386 motherboard with multi-tasking capability.
- On-board RAM of 4-8 megabytes.
- Multi-channel (analog and digital) data acquisition card.

Processing Requirements

Bus Functions

- *Monitoring/analysis of bus status sensors and control of satellite bus subsystems.*

- Interpretation of command data , command execution and generation of reply message.
- Periodic sanity checks.

Payload Functions

- Monitoring of payload status sensors.
- Acquisition of payload data.
- Processing of payload data.
- Storage of processed data.
- Storage of ground sensors data.
- Downlinking of payload data.

I/O Capability

- Serial input of 10K bps data from Rx-1 (Comm-1)
- Serial input of 10k bps data from Rx-2 (Comm-2)
- Serial output of 10k bps data to Tx-1 (Comm-1)
- Serial output of 10k bps data to Tx-2 (Comm-2)
- 8 bit parallel two way data transfer with storage memory.
- 2-byte (16bits) parallel two way data transfer with data acquisition card.

Reliability/Redundancy

Since the Command and Control system acts as a brain of the satellite, it has to be very reliable. The following measures are considered to achieve a high degree of reliability:

- ROM based main operating system
- Auto backup in case of failure
- Periodic diagnostic/self test(sanity check)
- Use of multiple parity bits and extensive parity checks
- Using two mother boards in a master-slave arrangement, with the slave having the ability to operate standalone in case of master's failure
- Extensive shielding of components from radio frequency interference

Thermal

The thermal analysis being done now is currently in the preliminary stages. All thermal analysis is being done by mechanical engineering students at the University of Iowa. During the Spring 1993 semester, the students created a FORTRAN finite-element analysis program to model the thermal environment and find any problem areas. Like all finite-element codes this program divides the satellite into a number of nodes which are representative of different parts of the satellite and pieces of hardware. The thermal control system can be represented by different thermal resistances between each node. By inputting orbit information, space

environment factors, and the thermal properties of the nodes, the program calculates the temperatures at each node during the orbit. At the present time only passive elements such as thermal blankets and coatings are expected to be used.

Ground System

The control center will be located in Boone, IA, a small town located about 15 miles west of Ames. The control center will be responsible for the following activities:

- Receive and archive payload data
- Receive and process bus data
- Schedule and verify all payload activities
- Verify all bus commands
- Resolve payload and bus anomalies
- Make payload data available to users
- Manage and train personnel

Figure 8 shows the layout of the ground station.

Cost and Schedule

Table 5: Project Cost Summary

Payload Hardware	\$196,286
Launch	(est.) \$500,000
Flight Hardware	\$243,540
Personnel	\$811,200
Ground Equipment	\$143,663
Miscellaneous	\$374,665
Total	\$2,269,354

Acknowledgments

The Spacecraft Systems class of 1993 continued the design of ISAT-1 with invaluable help from many sources. Most importantly, thanks go to Dr. Leverne Seversike and Bill Byrd for their guidance and encouragement, and to teaching assistant Todd Kuper. We would also like to thank Michael Lephart and Jahangir Kayani for the valuable work during the past year. This year's class of 16 students deserves recognition for the hard work that they put in this effort.

We would also like to recognize Dr. Basart and Marisa McCoy for their work on the Earth Radio Frequency Experiment. The valuable work done at the University of Iowa was done by Dr. Barry Butler, Dr. Ted Smith, Dr. Yae, Robert Windsor, and Joe Clay.

Wallace Sanders, Director of the Iowa Space Grant Consortium, and Dr. Hoffman, Institute of Physical Research and Technology, deserves our thanks for their encouragement and financial backing.

The design for the ISAT Project was continued by the 1992 summer team which included Darby Cooper, Charles Randall, Daniel Morey, Rick Zrostlik, Dale Streigle, and Steve Deaton.

We would also like to thank Jim Rodebush of Zeneca for his contribution of office equipment and Bill Fisher of the Aerospace Corporation for coming to speak to the class and for his insight

References

- Larson, W.J., and Wertz, J.R.,(ed), *Space Mission Analysis and Design*, 2nd ed., Microcosm, Inc., Torrance, California, and Kluwer Academic Publishers, Dordrecht, The Netherlands, 1992.
- Wertz, J.R.(ed), *Spacecraft Attitude Determination and Control*, D. Reidel Publishing Company, Dordrecht, Holland, 1978
- Hughes, P.C., *Spacecraft Attitude Dynamics*, John Wiley and Sons, New York, 1986.
- Stickler, A.C. and Alfriend, K.T., "An Elementary Magnetic Attitude Control System," *AIAA Mechanics and Control of Flight Conference*, 1974. AIAA Paper No. 74-923
- Roberson, R. E. "Gravitational Torques on a Satellite Vehicle", *J. Franklin Inst* 265, 1958, p. 12-33.
- Chobotov, V. A., *Spacecraft Attitude Dynamics and Control*, Krieger Publishing Company, Malabar, Florida, 1991.
- Kaplan, M. H., *Modern Spacecraft Dynamics and Control*, John Wiley and Sons, Inc., New York, New York, 1976
- Hunt, J.W., and Ray, J.C., "Flexible Booms, Momentum Wheels, and Subtle Gravity-Gradient Instabilities," 1992, AIAA Paper No. 92-1673.
- Peterson, M.R., and Grant, D.G., "The Polar BEAR Spacecraft," *Johns Hopkins APL Tech. Dig*, Vol. 8, no. 3, 1987, p. 295-302.
- Hoskin, B. C., and Baker, A. A.(ed), *Composite Materials for Aircraft Structures*, American Institute of Aeronautics and Astronautics, Inc., New York, New York, 1986.

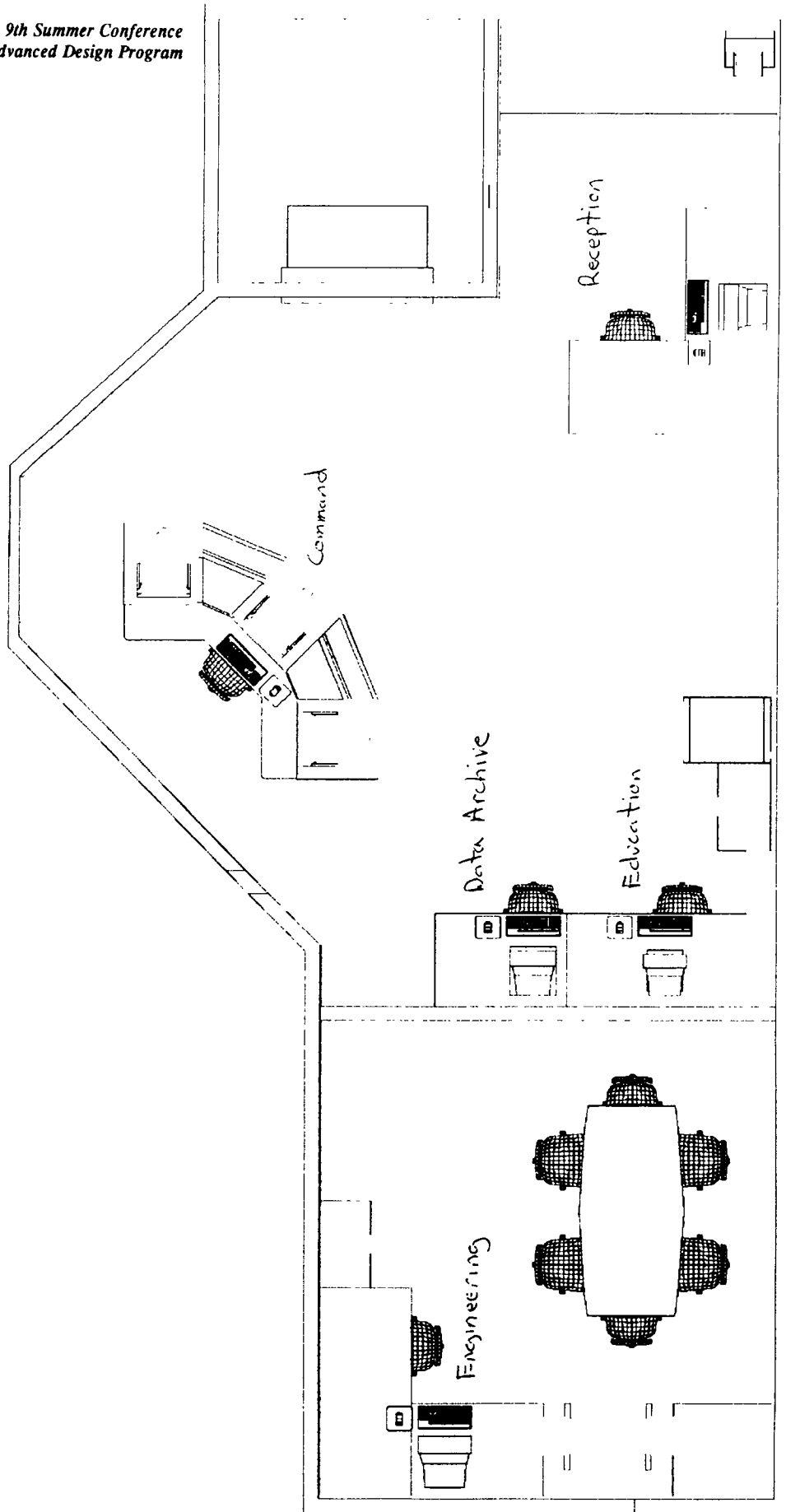


Figure 8

HUMAN-LIKE ROBOTS

Kansas State University
 Departments of Mechanical Engineering, Computer Science,
 Electrical Engineering, and Psychology
 Manhattan, Kansas

Dr. Allen Cogley,¹ Dr. David Gustafson, Dr. Warren White,
 and Dr. Ruth Dyer

Edited by Tom Hampton and Jon Freise

Abstract

The Design Team at Kansas State University has designed and built a prototype of a six-legged walking robot. This robot was designed to successfully navigate extremely rough terrain. Ultimately, the robot will be capable of near total autonomous roving and navigation with goal directed activity and self-preservation skills designed into the controlling software. The prototype is not complete, but the major phases of mechanical design and construction are complete. The electronics have been partially designed, but need much further development and implementation. The Behavior Language, developed by Rodney B Brooks at M.I.T. has been chosen to implement the high level control system.

Introduction

The present summary covers the high points of the design and construction of a six-legged, walking robot at Kansas State University in the Department of Mechanical Engineering. The first sections outline the goals and organizational aspects of the multi-disciplinary design team. The following sections on the Mechanical System go through the design process for the legs, chassis, and motor mounts. The Electronic System sections present and overview of the electrical aspects of the robot from power to computer controls. Finally, the last sections review the control scheme using Subsumption programming, a method of programming distributed decision making using local information.

Goals

Three Year

The three year goal for this NASA Senior Design Team is to design and build a walking autonomous robotic rover. The rover should be capable of rough terrain

crossing, traversing human made obstacles (such as stairs and doors), and moving through human and robot occupied spaces without collision. The rover is also to evidence considerable decision making ability, navigation and path planning skills.

When begun, this project had the title "Human like Robots in Space and Hazardous Environments". Within this scope the design team was free to choose what it felt the projects goals should be. The first group of criteria the design team picked was that the project should be some form of mobile robot, that it be as autonomous and intelligent as possible, and that some form of the robot actually be constructed. These goals were chosen as being the most interesting to the group as a whole. Several variants of these ideas were discussed:

Hazardous waste cleanup: The chernobyl accident demonstrated several instances where remotely operated or robotically controlled earthmovers would have been useful (or life saving). This idea was discarded after noting that the large equipment needed was far beyond our budget.

Planetary Rover: The ability to range widely and collect samples, data, and pictures would be of benefit for any future space exploration missions. A mobile robot was envisioned that could traverse rough terrain, carrying a variety of sensors and instruments, with enough intelligence to travel without a human operator.

Hazardous waste site scout: A mobile robot that could move freely about a disaster site, allowing human operators to assess the damage without endangering themselves was another suggested idea.

The last two ideas were combined into the current three year goal when it was noted that the same abilities to cross rough terrain on other planets would allow a rover to explore hazardous waste sites. It was further noted that if the rover could also open doors, and climb

¹Mechanical Engineering contact professor.

stairs it would be able to access almost all indoor areas that humans could reach, and those abilities became part of the goal. The choice for a legged rover design seemed best for maximizing rough terrain crossing ability. The decision for supporting an autonomous robot as opposed to a teleoperated design was to allow a rover to operate at great distances from Earth, without hindrance of lag in communications. The high intelligence factor was also supported as it would allow an operator to control several rovers.

First year

The job of the design team the first year was to pick a project goal, and then attempt to define just what needed to be done to reach that goal. It became apparent rather quickly that the design group lacked practical experience building robots, and without that experience any design would be flawed and fail. So the first year goal was set as building a working prototype of the walking robot rover for the purpose of learning as much as possible about mobile robot design.

The main criteria for the prototype were as follows:

Six legs: This was to begin the exploration into legged robot design. The choice of six legs allowed for a stable walking platform and a simpler overall control.

Three joints per leg: Three joints are the minimum needed for the robot to walk without its feet sliding or slipping.

On Board Intelligence: By restricting all processors to be on board the robot, the prototype would force realistic control schemes to be investigated.

Off Board Power: It was soon discovered that the cost of high efficiency electric motors needed to operate on battery power were out of our price range.

Stair Climbing: The prototype needed some target obstacle to test its terrain handling abilities. Stairs are a readily available obstacle in the indoor laboratory environment, and one of the needed criteria for meeting the three year goal.

The prototype was also to be designed in a modular way which allowed simple assembly and reconstruction. This requirement was to allow easy testing of various joint and leg designs, and terrain crossing abilities.

Implementation

The bulk of this report details the efforts of the design team to accomplish the first year goal of a walking

six legged robot. While each of the design teams major groups, chassis, electronics, and controls (see project organization) have each written detailed sections to explain how the prototype was implemented, here is a feel for the scope of the robot. The robot measures over 40 inches long, has a leg span of 3 feet and weighs over 60 pounds. It has three joints per leg (as specified by the goals) and one electric motor and gear train drives each joint. Modularity of design has been stressed, to the point that 10% of the robot's weight is dedicated to nuts, bolts and other fasteners. There are a total of nine microprocessors used in the control of the robot. Three of those processors will be mounted on the central body and will run the higher level behavior based motion planning software. A graphical simulation package has been written to test this software before hardware integration. The other six processors are to be mounted out on the legs of the robot to control the leg motors and gather data from a vast array of sensors. Those sensors include two types of position feedback on each joint, foot force feed back, and two types of collision detection. Again modularity has been stressed in the electronic design, so that the only connections running from the robots main body out to each leg (and through the joints) are motor power, logical power and a single serial cable. While the dozens of pages of schematic drawings, blueprints and pages of code are testimony to the amount of work that has been done so far, the NASA team realizes it has just begun to learn what is needed to reach the three year goal of a fully autonomous walking robot rover.

Project Organization

At the end of the second semester the design team had over 20 members, 7 supporting faculty, was using 4 machine shops, 2 electronics shops, and dozens of computers in several labs. The organization, managerial and communication aspects of this project soon became nontrivial. To control some of this chaos the design team created several lead positions and formed itself into subgroups. The subgroups were chosen to be:

Chassis group. which dealt with all aspects of leg, joint, and chassis design, material selection and machining.

Electronics group: which dealt with all electrical systems, including microprocessor construction, motors, motor drivers, sensor design and construction, as well as power supply to the robot

Controls group: which initially dealt with specifying sensor choices, sensor placement, specifying processor requirements, and writing all software and control algorithms.

The positions on the team were Project Lead Engineer, Control System Group Leader, Electronic System Group Leader, Chassis System Group leader, Librarian, Account Manager, and the Graduate Assistant. The responsibilities of the Lead Engineer were to coordinate the design process between the groups, aid in the design where difficulties arise, and attempt to promote the projects progress. The group leaders were responsible for helping their group members with the design and construction of their prototype sections, requesting needed supplies, equipment, and other support. The Librarians responsibilities were to file all papers, notes, journals, catalogs, progress reports and design documents. The Graduate Assistant was given the responsibility of interfacing between the students and the faculty, handling the teams budget, and purchases, and aiding in acquiring needed equipment and supplies. The Account Manager was charged with aiding new computer users while they set up their accounts and answering computer related questions.

During second semester the positions were filled as follows:

- Lead Engineer—Jon Freise (CIS)
- Chassis Leader—Paul Roesner(ME)
- Electronics Leader—Scott Shute(EE)
- Controls Leader—Tom Hampton(CIS)
- Librarian—Terri Detter(CIS)
- Account Manager—Eric Armstrong(CIS)
- Graduate Assistant—Travis Rhodes(ME)

Mechanical System

Overview

The chassis design team was responsible for the design and construction of the robot's chassis and legs to achieve the long and short term goals of the project. These goals, briefly, were to build a robot that could cross diverse terrain and climb stairs. The goal of the ability to climb stairs caused consideration of designs that would allow the legs to reach high enough and far enough away from the robot to place its legs on consecutive stairs and walk up them. An insect type design, with six legs mounted on a central chassis section, was chosen due to its high

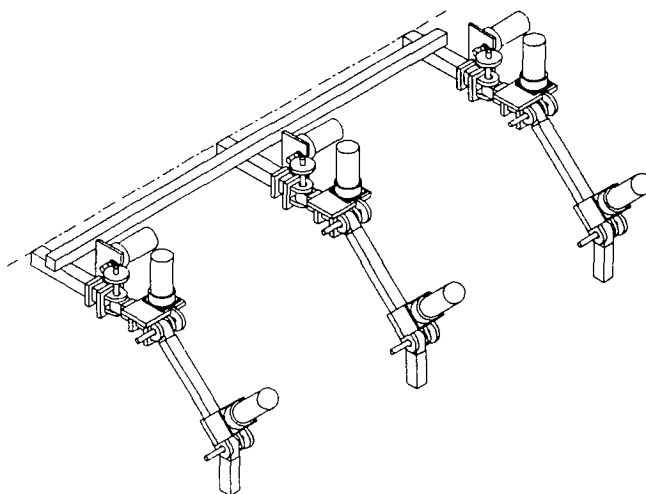


Figure 1: Robot Overview

clearance, diverse range of motion in its joints, and light weight.

The robot that was built consists of a chassis made from aluminum tubing, to which six legs were mounted. The chassis consists of two long center rails and three cross members bolted to the center rails. One leg is mounted to each end of the cross members. Each leg consists of three joints separated by lengths of aluminum tubing. The first joint (Alpha) is mounted to the end of each cross member. This joint swings in the horizontal direction. The second joint on the leg is the Beta 1 joint. It moves only in the vertical direction. The last joint, the Beta 2 joint, moves in the vertical direction as well. At each joint, an electric motor is mounted, which drives the joints through a worm-worm gear transmission. Figure 1 shows the placement of the legs along one side of the chassis, and the placement of the gears and motors at the joints.

Leg Design

Requirements. In the design of the legs of the robot, certain requirements had to be considered. First, the leg had to allow the robot to move at the original design speed of one foot per second. This speed was set arbitrarily to insure that the robot would have a fast response time in real-life applications. Next, the legs had to allow the robot to maneuver around or over obstacles in its path. The design also had to provide the robot with the ability to climb a set of stairs.

Design Considerations. Certain design parameters had then to be considered that would satisfy these

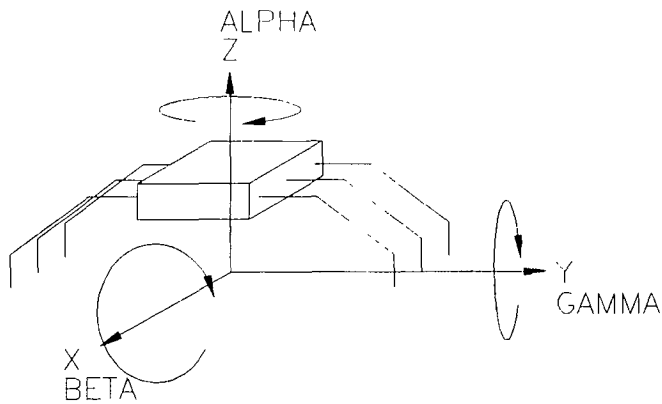


Figure 2: Base Coordinate System

requirements. These parameters were the types of motion the legs would use, and the geometry of the legs.

The types of motion that were considered for the legs were linear actuation and rotational actuation. Linear actuation would consist of leg sections that would slide inside one another to extend and contract the leg. Rotational actuation would consist of leg sections that would be attached through joints which would swing through an arc to provide leg movement. Of the two types of motion, rotational actuation was chosen because it provided a less complicated leg design.

After the type of motion was chosen, a base coordinate system for the robot was defined and can be seen in Figure 2. With the robot standing up-right, the origin of this coordinate system was chosen to pass through the center of the robot. The vertical axis of the coordinate system is defined as the Z-axis. Rotation about this axis is defined as Alpha rotation. Right to left, or from side to side of the robot is the Y-axis. Rotation about the Y-axis is defined as Gamma rotation. Lengthwise along the robot is the X-axis. Rotation about the X-axis is defined as Beta rotation.

It was then necessary to consider some aspects of leg geometry including: the number of degrees of freedom (either two or three), the number of leg joints (from one to three), and the types of rotation permitted by each joint (Alpha, Beta or Gamma). Joints with multiple types of rotation about a single joint were considered, but ruled out due to confined space requirements and the additional complexity of the joint.

Initial Design. Of the thirty designs considered, the initial leg configuration shown in Figure 3 was chosen. It has three degrees of freedom and a separate joint for each degree of freedom. One of these joints provides Alpha rotation, and while the other two joints provide

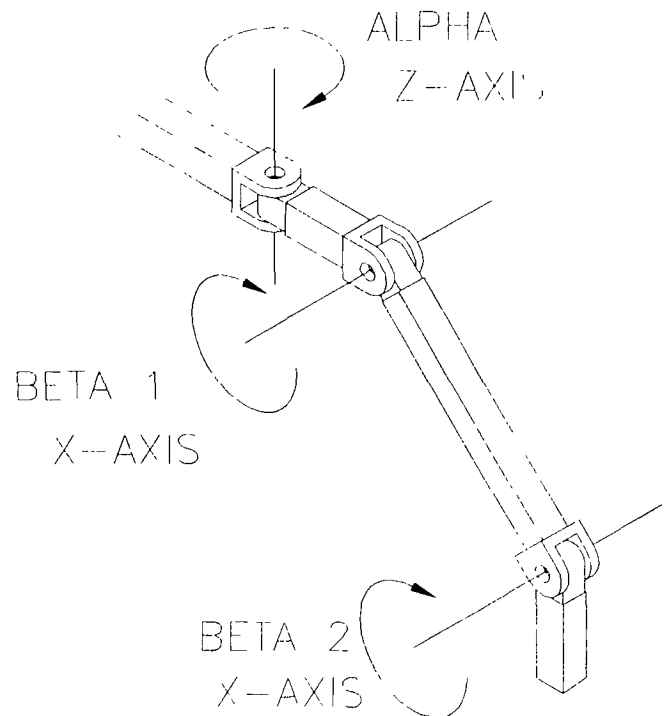


Figure 3: Initial Leg Design

Beta rotation.

The first joint, the Alpha joint, rotates about the Alpha axis and is responsible for the forward and backward motion of the robot. This means that the speed of rotation of the Alpha joint directly governs the speed that the robot will be able to move, since it is the only joint that moves in the horizontal axis.

The second joint, Beta 1, rotates about the Beta axis. The Beta 1 joint is responsible for lifting the leg and for raising and lowering the body.

The Beta 2 joint, which is the last joint, also rotates about the Beta axis. Attached to this joint is the last leg section, or foot of the robot. The Beta 2 joint is responsible for stable and controlled maneuvering of the robot. This joint rotates to keep the foot of the leg moving along a straight line with respect to the chassis as the Alpha joint rotates through an arc. This prevents the foot of each leg from having to slide relative to the chassis as the robot moves forward or backward.

This initial leg design was chosen because it provides high clearance capabilities, a large range of motion, and is a flexible design, allowing the use of variable leg section lengths between the joints.

One advantage of this design is that using two joints with Beta rotation allows lateral or sideways motion. This could be useful in tight corners where turning could be difficult or impossible. Another useful feature of this

design is that if one of the Beta joints becomes inoperative, the robot would still be able perform many of its functions with the remaining Beta joint. The use of three degrees of freedom also gives the robot the ability to probe with any of the legs. This would allow the robot to sense its surroundings using sensory devices attached to the legs.

The major disadvantage of this design is the lack of Gamma axis rotation. Gamma axis rotation would be useful in situations where the robot had flipped over and needed to maneuver on its back or attempt to right itself by flipping back over. However, the use of Gamma rotation would have led to a much more complicated design, and it was determined that it would not be necessary for our purposes.

With a very basic leg design completed, the leg joint spacings were then determined. This factor would need to be maximized to increase the amount of clearance given to the robot, as well as the speed at which the robot would travel. The joint spacing would also have to be minimized to decrease the amount of torque that would have to be supplied to the joints.

To determine the necessary leg section lengths, several robot models with different joint spacings were constructed using PVC pipe. Trials were then performed, manipulating the models by hand up a set of stairs to determine which joint spacings worked best.

The distance between the Alpha and Beta 1 joints was initially set at four inches. This distance was set at the minimum amount necessary for placement of the power transmission. The distance between the Beta 1 and the Beta 2 joints was arbitrarily set at 12 inches. This allowed about a 12 inch step as the robot moved forward. Through the trials with the models, it was determined that the last leg section should be as short as possible to allow the robot to climb the stairs. However, the longer this leg section is, the less the Beta 2 joint would have to rotate to prevent the foot from sliding. After much discussion, it was decided that this distance should be roughly one-third the distance of the middle leg section. This would provide a reasonable compromise between the amount of clearance height and the amount of rotation necessary at the joint. Therefore, the length of this section was set at four inches.

These trials also allowed the determination of the angles that the joints would need to swing through. It was determined that the Alpha joint would need to swing through an angle of $\pm 30^\circ$ from perpendicular with the chassis. The Beta 1 joint would need to swing through an angle of $\pm 60^\circ$ from parallel with the Alpha leg section. It was also determined that the Beta 2 joint would need to swing through a maximum angle of 70° down-

ward from parallel with the Beta 1 leg section, when climbing stairs.

Power Transmission

With the final leg design determined, details regarding transmission of power to the joints were addressed. Electric motors had been chosen to supply this power, requiring the design of motor mounts as well.

Gears. Proper power transmission from the electric motors to the leg joints was necessary to provide a reasonable compromise between the speed of rotation of each leg section and the torque required to rotate each joint under the weight of the robot. For this design, a large increase in the torque supplied by the motor was required to support this weight. Calculations using the weight of the robot to determine the required torque at the joints were done, and are given in the appendix. These calculations were made at the Beta 2 joint which is required to give the most support. Earlier estimates concluded that a required reduction of about 20:1 was needed, but after these calculations were done, the needed reduction was set at 30:1. This would reduce the speed of the robot somewhat, but was deemed necessary for the robot to support itself.

The types of power transmissions that were considered include worm gearing, planetary gear sets using spur gears, and chain drives. For this robot a power transmission consisting of a worm-worm gear combination was chosen. It provides a 30:1 reduction in speed of the motor and a corresponding increase in torque supplied to the leg. In this design, a single threaded worm is pinned to the motor shaft. This drives a 30 tooth worm gear that is pinned to the shaft through which the yoke and rod sections of the leg joints are connected. This shaft is free to rotate in the bearings of the yoke section, but is secured with a set screw to the rod section of the joint. Thus, rotation of the worm gear causes rotation of the rod-end leg section in all the robot's joints, and reduces the rotational speed of the leg joint to about 6 revolutions per minute.

Initial design of the power transmission for the Beta 2 joint differed from the other two joints in that the motor and worm gearing was placed further away from the joint. This design also included a chain and sprocket combination running off the worm gear shaft and driving another shaft at the joint. This design was considered because it would locate the mass of the Beta 2 motor closer to center of the chassis, increasing the stability of the robot with its legs extended. This design was not adopted for the final design, however, because it would

have added considerably to the weight and complexity of the design.

The use of worm gearing was chosen because it meets all the original design criterion. The design is very simple, consisting of only two gears, one extra shaft and two bearings. A similar transmission consisting of spur gears or chain drives would be too large, and would need several additional shafts and bearings to achieve the necessary reduction. An additional benefit of using worm gearing is that the joints are self-locking and will support the weight of the robot without any power to the motors. This feature would not be available with the use of spur gears or chain drives without additional locking mechanisms.

Various catalogs from Stock Drive Products, Berg, and Chicago Gear Works were used to make the gear selection. The worm chosen was from Chicago Gear Works. It was the only one available that was close to fitting the 8mm motor shaft. A worm gear of the same pitch and pressure angle was then chosen to meet the required gear reduction. This worm gear had a five-sixteenths inch center bore, requiring machining to fit the three-eighths inch gear shaft. The gear reduction of a worm-worm gear combination is computed by dividing the number of teeth on the worm gear by the number of threads on the worm. Therefore, thirty teeth on the worm gear gave the required 30:1 reduction for the single threaded worm.

Motor Mounts. The motor mounts for the robot were designed to hold the motor firmly to the leg joints and to allow the worm on the motor shaft to mesh properly with the worm gear. It was also designed so that it would not interfere with each joint's rotation. Another design criterion was to use the same design for all the motor mounts to ease the manufacturing process. The motor mounts were also designed to allow the addition of slightly larger worm gears so that a higher gear reduction may be used if needed.

The motor mounts consist of a flat aluminum mount plate to which the motor is secured. The mount plate is held tightly to the joints by two U-shaped clamps. The larger clamp is secured with screws to hold the mount plate to the yoke section of the leg joint. A spacer bar is used with screws in the smaller clamp to hold the mount plate against the tubing of the leg section. A small amount of clearance between the clamps and the mount plate exists, so that the motor mount may be tightened completely to the joint. Since the mount is only clamped to the leg, it may be slid back along the leg to accommodate a larger worm gear.

The design of the motor mount limits the rotation of the leg sections to a maximum of $\pm 80^\circ$. The Alpha mo-

tor mount design was changed somewhat from the other mounts to permit the Alpha joint to swing through its full range of $\pm 80^\circ$. This feature was not one of the original design criteria, but was added to increase the robot's maneuverability in stair climbing. To do this, the Alpha mount plate was lengthened by one inch to raise the Alpha motor further from the joint. This was necessary to avoid the collision of the Beta 2 mount plate with this motor as the Alpha joint rotates through this larger angle. This design change required the use of longer worm gear shafts at the Alpha joints as well.

Problems. A major drawback in using the worm-worm gear transmission is the low efficiency, or ratio of power transmitted through the gear set versus the amount of power supplied to the motor, that is associated with this type of gearing. This factor may be caused by the friction of the worm sliding across the teeth of the worm gear, or by a slight misalignment of the worm and worm gear. Through tests during the assembly of the robot, efficiencies as low as 25 percent were measured. Although the torque supplied to the joint is limited, it is still enough to lift the weight of the robot.

Solutions to this problem may involve proper lubrication of the gears, or a redesign of the motor mount to provide exact alignment of the worm and worm gear. To reduce the amount of torque required at the joints, counter-springs could be added at the joints as seen in Figure 4. Since the weight of the robot acts downward, the most torque is required of the motors when lifting the robot up. Counter-springs could be loaded to provide a couple equal or nearly equal to that produced by the weight of the robot. This would require the motors to produce more torque when raising the leg, but this torque could be balanced so that the overall torque would be less than at present. The use of counter-springs was not included in the final leg design because it was calculated that the motors would always have enough torque to lift the robot. Still, this feature could be easily added to the existing design.

Another problem with the power transmission is the excessive play of the motor shafts in and out of the motor housing. This movement allows the joints to rock back and forth under the weight of the robot. Solutions to this problem may involve a redesign of the motor mounts to incorporate thrust bearings on the motor shaft.

Electronic System

Motors

To propel the robot, a self-contained, light-weight and inexpensive source of power generation is required. DC

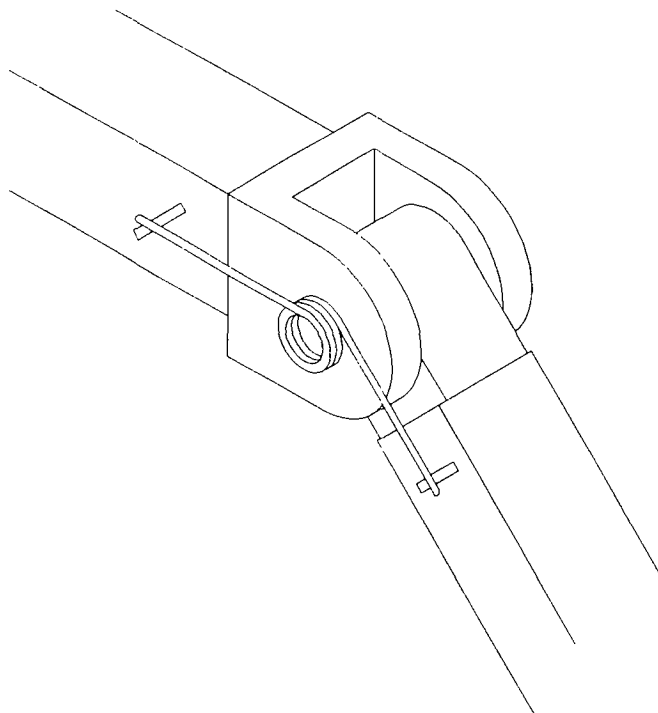


Figure 4: Counter Spring

motors were chosen for this task. For maximum efficiency and power, a motor is required at each joint of the robot, therefore 18 motors are needed. In order to determine the power required of each motor, the highest torque requirement was calculated. This worst-case load is achieved by the Beta 1 motor during the tripod gate, and is calculated to be half the weight of the robot. The required torque in this scenario is based on the following component weights (see Table 1).

Item	Weight
Aluminum tubing 1" square	6 lbs.
Hinges	6 lbs.
Motors (15 x 1.5 lbs. each) ²	22.5 lbs.
Bolts, shafts, processors, etc.	6 lbs.
Total estimated weight	40.5 lbs.

Table 1: Robot weights

To find an expected torque for this situation, the one foot link between Beta 1 and Beta 2 joints was used.

$$Torque = (1\text{ft.})(40.5\text{lbs.})(0.5) = 20.25\text{ft.} - \text{lbs.}$$

Originally, 3.8 V motors taken from cordless Black and Decker screwdrivers (model SD 2000) were included in

²In tripod gait, the weight of the three Beta 2 motors would be supported by the Beta 2 link sitting on the ground.

the design. These motors were reported by the manufacturer to have enough torque (40 ft.-lbs.) and were inexpensive (\$26 for the entire screwdriver unit). A major drawback in using the screwdriver motor was in the mounting of the motor to the robot. Because of its shape, which included the screwdriver's gear reduction system, it was very difficult to design a mount for the motor.

The motor that was chosen for the final design is a 24 V motor produced by Matsushita Electric and distributed by Servo Systems. This motor has several advantages over the 3.8 V screwdriver motor and costs about the same (\$30).

The advantages of 24 V motor over 3.8 V screwdriver motor are listed below:

- The voltage can be varied around a much larger range.
- The motor driver chips of 3.8 V are more expensive than those of 24 V (\$30 vs. \$3.00).
- The screwdriver motor and gear reduction are not one unit.
- A mounting face plate is included on 24 V motor.
- The 24 V motor includes a built-in optical encoder.

The built-in optical encoder of the 24 V motor is a major advantage, as it will be able to supply digital data relating exact relative positioning. To achieve this using the screwdriver motor would involve the installation of an optical encoder on the shaft of the motor, which would have added to the bulk of the machine and would have incurred an added expense.

The disadvantages of 24 V motor compared with 3.8 V screwdriver motor are listed below:

- The 24 V motor is heavier - 1.5 lbs. compared to 6 oz.
- The 24 V motor is larger - 7" long by 2.375" diameter compared to 3.5" long by 2.25" diameter.

The main consideration in motor choice is the torque it produces relative to its size and cost. Black and Decker claims that the model SD 2000 will produce 40 ft.-lbs. It is believed that this figure may be considered the locked rotor torque. The 24 V motor is rated for 21.8 ft. lbs. at 185 rpm, which will be the operable speed. The locked rotor torque for the 24 V motor is 33.3 ft.-lbs. The 24 V motor has a rated current of 5 A. This means that the motor is capable of safely handling $(24V)(5A) = 120$ Watts of power. To accept the same input power, the screwdriver motor would need to carry 24 A. Considering the physical size of the wire and motor from the

screwdriver configuration, the claim of 40 ft.-lbs. appears misleading

Based on the considerations mentioned above, the 24 V motor was chosen.

Power Supply

Requirements. The requirements of the power supply are determined from the operating constraints of the motors. These constraints include a voltage of 24 V and a locked rotor current of 4.5 A per motor. Power supplies capable of producing a 24 V signal are common. However, the current of 4.5 A per motor becomes significant considering eighteen such motors will be mounted on the robot. The maximum possible current occurs if all eighteen motors are locked and energized. In this case, the current would be:

$$18\text{motors} \times 4.5\text{A/motor} = 81\text{A}$$

However, it is unlikely that the robot would ever be in a situation where all 18 motors were locked and drawing 4.5A of current. What is more likely is that a few of the motors might be operating at near lock up, such as when climbing a flight of stairs. In this circumstance the robot would be using the six alpha motors to lift itself. If all six motors were to stall the robot would draw $6 \times 4.5\text{A} = 30\text{A}$ of current. Given this "worst case" estimate a 40 amp power supply was settled upon and acquired from the EECE department.

Future Interests. An option that needs to be explored in the future involves building a supply that meets the exact requirements of the robot.

One configuration is a full-bridge rectifier with a capacitive filter. A transformer would be needed to transform 120 V ac down to 24 V ac. Thyristors could also be used to allow the dc voltage to be varied.

Control System

Overview

The task of controlling a six-legged, eighteen-jointed robot is complex. There are an enormous number of tasks that must occur simultaneously. Many of these tasks have equivalent priorities. Given this, it is difficult to prioritize these tasks so that they may be executed serially and still guarantee that all tasks will be serviced in a reasonable amount of time. Therefore, it was decided to use multiple processors, and divide the essential tasks among them.

The current design is one processor on each leg which is responsible for moving the three joints on that leg

Total Machine Cycles		
50,000 × 3	150,000	Cycles for PID loop
	150,000	Cycles for PWM loop
	25,000	Cycles for send/rec
	325,000	Total Cycles

Table 2: Total machine cycles required for HC11

to given target positions. These processors will also be responsible for gathering sensor data. Between each leg pair will sit another processor that will collect this sensor data from the lower processors and make high level decisions based on this data. There will be three of these high-level processors, one for each pair of legs. These high-level processors will be capable of communicating with each other and exchanging information.

The Motorola MC68HC711E9 micro-controller was chosen for the low-level joint manipulations and sensor data gathering. The HC11 was chosen because of its compact size, on-board analog to digital converters, and built in pulse width modulation capabilities. It was shown that given its 2MHz clock the HC11 would be capable of performing the necessary 1KHz Pulse Width Modulation, Proportional Integral Derivative Control algorithm, sensor data gathering, and serial communications in each second in approximately one sixth of its 2,000,000 clock cycles (see Table 2).

The Motorola M68HC16 micro-controller was chosen for the high-level control system. It was chosen primarily for its compatibility with the HC11, its enlarged address bus, and 16MHz clock rate. The HC16 and the HC11 both have a synchronous serial communications port that is capable of baud rates approaching 2Mb/s. The HC16 also has an asynchronous line that can operate in a multi-drop mode that allows an Ethernet style protocol to be implemented. The HC16 has an address space of 1 MB in combined instruction and data mode, or 2 MB in separate instruction and data mode. This gives great flexibility in program design, and language choice, since some compactness can be sacrificed for ease of coding and readability.

Simulation

Due to the inherently long lead time on actual hardware for testing control code and the expensive nature of testing code on actual hardware, a limited simulation of the robot was developed. This simulation was limited in that it only provided for joint position feedback rather than a complete complement of sensor inputs. This sim-

ulation was used to develop and test the initial walking algorithm.

Design Criteria. This simulation was to be a static position evaluator, that took the 18 joint positions, and translated them into a 3-D wire frame of the robot. The simulation was to take commands to set new target positions for individual joints, and query the current position of any joint. There was also to be one other command that causes the simulation to increment time by some interval. As time incremented, the simulation would move the joints progressively closer to their respective targets. The simulation was also required to have a lisp interface.

Implementation. The simulation is divided into three layers:

- The Lisp interface
- The C interface calls
- The robot display routines

Library Interfaces. The Lisp interface is simply a set of primitives that make calls to the C interface. For more complete documentation on how to use the Lisp interface see the full annual report.

The C interface includes four main calls:

- `put_joint` which takes a leg and joint designation, and a target position, and sets the specified joint's target.
- `get_joint` which takes a leg and joint designation, and returns the current position of the specified joint. This is not necessarily the target position, but it is the actual position of the leg as time elapses.
- `update_simulation` which takes a length of time and moves the joints towards their targets.
- `init_simulation` which takes the complete dimensions of the robot (leg lengths, body width, height, and length, etc.), the joint limits, and the angular velocity of the joints. This initializes the graphics system, and the joint positions for the simulation.

Robot Display. Displaying the robot was done using a 3-D wire frame modeling device independent graphics library, VOGLE. This library uses a transformation matrix, and a Cartesian coordinate space to define graphic objects.

Displaying the robot can be divided into two essential tasks:

- Displaying the legs
- Displaying the body

Displaying the legs is a relatively simple task. Since they are always to be attached to the body, they are drawn relative to the body's current orientation.

Displaying the body is a more complicated task, however. Since the legs may be in any position within their limits of motion, it is necessary to determine the orientation of the body in terms of rotation and translation matrices.

There are several steps in determining the orientation of the body:

1. Determine the points in contact with the ground
2. Determine the height from the standing plane to the body
3. Determine the standing plane's rotation about the Z axis
4. Determine the standing plane's rotation about the X axis

The method used to find the points in contact with ground was to sort a fixed number of points on the body by their vertical distance from the body. The first three points not on the same side of the body are then chosen to define the standing plane.

In order to compute the height, height must be defined. The height is the perpendicular distance from the origin to the plane. It is then a simple matter to compute using 3-D vector analysis.

Theta, the rotation about the Z axis is computed by converting the Cartesian coordinates to spherical coordinates.

Phi, the rotation away from the Z axis is also computed by converting to spherical coordinates.

The body height transformation is then made by first translating the body by the height about the Z axis. The body rotation is done by rotating about Z by theta, then rotating about Y by phi, and then rotating the body back about Z by -theta. This places the body into the correct position so that the points in the standing plane will be on the "ground."

Control Background

There are many ways to control a robotic system. The most widely used method involves 3-D modelling and inverse kinematics in making decisions. This method is extremely computer intensive and requires large amounts of processing power. Dr. Rodney Brooks at M.I.T. has

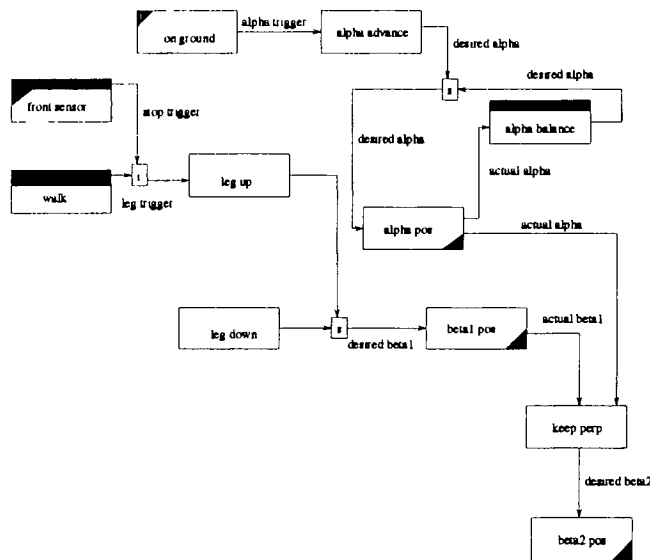
developed another approach to robotic programming called subsumption programming. The underlying assumption of this new approach is that it is rarely necessary to know everything about a given situation before any decisions are made. Therefore, a robot could "react" to certain important features of the current environment while ignoring what are deemed to be irrelevant. The burden is then placed on the programmer to then determine at what times different features are relevant or not.

Subsumption. The subsumption architecture was developed by Dr. Rodney Brooks at the MIT mobile robot lab. The basic premise of the architecture is that competence of the robot is built up in task achieving layers. Each layer reads sensor input and controls actuator output (eg. the motors). The lowest level layers handle the very basic, very general tasks, such as walking on level ground. The higher level competence would be aimed at more specific tasks such as walking on a slope, or climbing obstacles. When the higher level controls notice that the robot is in a position that their specialty applies, they take control away from (subsume) the lower levels. The lower levels are not stopped from running, they just no longer can send control messages to the actuators. This has the effect that if the higher level layers should fail, the lower level layers can take back over (with lessor ability, but at least the robot does not halt) A better description of the architecture can be found in [Brooks 1986] [Brooks 1990].

Choices. When this project began, the design team had very little experience with real time control systems. Attempting to weigh the merits of various systems was near impossible. It was decided to use the Brooks architecture as it was the most familiar, with the provision to research other systems. What follows is a listing of some of the reasons argued for subsumption.

Easily the strongest reason for choosing the subsumption architecture was that it had already been used to control two walking robots, Gengis [Brooks 1989] and Attila, and the design team wanted to evaluate its effectiveness themselves.

When subsumption was chosen the initial design weight of the robot was 12lbs (mostly motors) and there was not weight to spare for the mounting of large computer systems. To fit in the design goal of all on board computing, the control system had to be very efficient. Subsumption would appear to be very efficient, as one of the 6-legged walkers controlled 12 degrees of freedom with only 4 8bit, 2MHz processors, which was the kind of minimal control system that was needed.



The boxes without bands on top are repeated six times, once for each leg. The boxes with solid bands are unique and comprise the control. The boxes with a filled triangle in the bottom right corner control activation. The boxes with a filled triangle in the upper left corner receive inputs from sensors.

Figure 5: Subsumption Network of Behaviors for Level Ground

Further. There is no doubt that the choice of subsumption represents a compromise and a large amount of research is needed into other successful control systems. Ohio State University and Carnegie Mellon University both have built walking machines. Also at MIT, Colon Angle has published his masters thesis on Attila, which the design team has not had time to acquire.

Behavior Language

The first step in designing the upper level control system was to produce a complete, initial walking plan. The basis for the design is behaviors. Behaviors are groups of rules which become activated by certain conditions within the robot. No data structures are shared between behaviors. All behaviors are asynchronous and appear to run in parallel. Each behavior controls a specific function, and only receives the information necessary for it to function from other machines. Behaviors are connected together using inhibitions and subsumptions. These connections allow one behavior to either inhibit or subsume actions of another behavior.

2-Dimension Walking Plan

The design for walking on level ground with only two degrees of freedom is shown in Figure 5

On this diagram, each box represents a behavior. Those boxes without bands on top are copied six times, once

for each leg. Those with filled triangles in the lower corner actually control the legs. Those with solid bands are the “central control” of the robot. Those with triangles in the upper corner get their inputs from the sensors.

Walking Plan. The behaviors shown in Figure 5 work together to form a simple walking plan for level ground. Control is achieved by connecting the machines and using inhibitions and subsumptions. Not all of this walking plan was implemented due to time constraints and the lack of sensor data. Therefore, a two-dimensional walking system using only joint positions was implemented. That which was implemented is described below, and the behavior language code for it is found in the Appendix.

1. **Standing.** There are three behaviors which control the lowest level of control and interface with the motor control loop. *Alpha pos*, *beta-1 pos*, and *beta-2 pos* receive a desired position, outputs that position to the motor, and returns the actual position of the joint. There are given positions to which the joints will go when the robot is powered up so that it stands.
2. **Leg lifting.** A *leg down* machine will always output a position to the *beta-1 pos* which will place the leg in the down position. Another machine, *up-leg-trigger* subsumes the *leg down* machine when the leg is raised to walk.
3. **Leg swinging.** There is a single machine, called *alpha balance* which accepts the alpha positions from each of the legs. It then sums the alpha position, where 0 is straight out, positive is forward, and negative is backward. Based on the sum, *alpha balance* outputs a signal to each of the *alpha pos* machines which will adjust the legs to keep the body centered. If one leg moves forward, *alpha balance* will move all others backward to compensate.

For each leg, there is an *alpha advance* machine. Whenever the leg has been raised, it suppresses the *alpha balance* output to that leg, and outputs a position to the *alpha pos* machine which will swing the leg forward. So when *up-leg-trigger* raises a leg, *alpha advance* swings it forward.

4. **Walking.** Finally, a behavior must be added to trigger the *up-leg-trigger* machines in the appropriate order to produce the desired gait. For walking on level ground, the *walk* machine sends out triggers to implement the tripod gait.

Behaviors. Each behavior is described with its inputs, outputs and functions below.

- **Alpha-pos** There are six of these machines, one for each leg. Input to this machine is *signal-pos*, which is the position which the other machines signal they would like the alpha joint to be placed. The output from *alpha pos* is *current-pos* which is the actual position of the alpha joint. Its function is to interact with the lower level control loop to move the motor to *signal-pos*, and to get *current-pos* from the lower level and output it for other machines to use.
- **Beta-pos** There are six of these machines, one for each leg. Inputs outputs, and functions are exactly the same as those in *Alpha-pos* except that they control the beta-1 joint.
- **Alpha-advance** Again, there are six copies of this behavior, one for each leg. Once the robot has stood up, each *alpha-advance* machine receives a *go* input. After that, they check to see if the *beta-pos* input says that the leg has been raised. If so, the machine outputs a new *alpha-pos* to swing the leg forward.
- **Leg-down** The six copies of this machine have a simple function. As input, they take *current-beta*. If this position is not the same as the *leg-down-pos*, a constant, it outputs the new beta position in *new-beta* to put the leg down.
- **Up-leg-trigger** This machine, one on each leg, takes as input a *trig* or trigger which indicates that this leg should be raised. When the trigger has been received, the machine outputs *new-beta* to raise the leg.
- **Alpha-balance** There is only one of this machine. It takes as input the alpha positions of all six legs. Once all six have been received, it sums them to determine whether they should be altered. If the sum is greater than 0, a constant amount is subtracted from each *alpha pos*. Likewise, if sum is less than 0, a constant is added to each *alpha pos*. Output from this are all six new alpha positions.
- **Walk** This machine sends out the signals to the legs in the proper order to obtain the tripod gait. It contains monostables (timers) to keep track of which set of legs was last triggered. Once the *go* input has been received, it outputs the appropriate of the six triggers.
- **Stand** This machine makes sure that at least three of the legs are on the ground before it begins to

walk. It takes as input the beta-1 positions of the six legs, and outputs a *go* signal, if appropriate.

The behavior machines interact with each other by connecting the inputs and outputs of the machines with the *connect* statement. Connections which were used in the implementation were :

1. The output *current-pos* from beta-pos is connected to the input *beta* from stand for each of the six legs.
2. The output *go* from stand is connected to the *go* input from the walk machine, and also to each of the *go* inputs for the alpha-advance machines.
3. The outputs *signal* for each leg from alpha-balance are connected to the *signal-pos* for each of the alpha-pos machines.
4. The output *current-pos* from each of the alpha-pos machines are connected as inputs to the alpha-balance machine and to the alpha-advance machines.
5. The output *current-pos* from each of the beta-pos machines are connected as inputs to each of the alpha-advance machines.
6. The output *alpha-pos* from the alpha-advance machines are connected to the input *signal-pos* for the alpha-pos machines. These outputs also subsume all other input to alpha-pos.
7. The outputs *new-beta* from the leg-down machines are connected to the inputs *signal-pos* for the beta-pos machines.
8. The outputs *current-pos* from the beta-pos machines are connected to the inputs *current-beta* for the leg-down machines.
9. The outputs *new_beta* from the up-leg-trigger machines are connected to the inputs *signal-pos* for the beta-pos machines. Also, these outputs subsume all other input to beta-pos.
10. The outputs *trig* from the walk machine are connected to the inputs *trig* for each of the up-leg-trigger machines.

Other work

The two degree of freedom, joint position controlled implementation described above was tested on the animation program which was designed. The behavior code was translated into common lisp code, and then run on top of the animator. From this testing, we determined

that this implementation moves legs in the correct sequence and with the right timing to walk. The stand procedure was also working when the animator was started

References

- Brooks, Rodney A. 1986. A Robust Layered Control System for a Mobile Robot. *IEEE Journal of Robotics and Automation*, RA-2(April), 14-23.
- Brooks, Rodney A. 1989. A Robot that Walks: Emergent Behavior from a Carefully Evolved Network. *Neural Computation*, 1(2), 253-262.
- Brooks, Rodney A. 1990. *The Behavior Language; User's Guide*. Tech. rept. 1227 MIT AI Lab Memo.

MOOSE
Manned On-Orbit Servicing Equipment

University of Maryland, College Park
Department of Aerospace Engineering
College Park, Maryland

Professor David L. Akin, Sc.D.
Tharen Rice, Teaching Assistant

Jason Budinoff, J. Corde Lane, Nicole Leontsinis, Ram C. Singh,
and the MOOSE Development Team

Abstract

The ability to service satellites has thus far been limited to Low Earth Orbit (LEO) platforms within reach of the Space Shuttle. Other orbits, such as Geosynchronous Orbits (GEO) containing high-value spacecraft have, thus far, not been reachable by a servicing vehicle. The useful life of a satellite can be extended by replacing spent propellant and damaged Orbital Replacement Units (ORUs), forestalling the need for eventual replacement. This growing need for satellite on-orbit servicing can be met by the Manned On-Orbit Servicing Equipment (MOOSE). Missions requiring orbit transfer capability, precision manipulation and maneuvering, and man-in-the-loop control can be accomplished using MOOSE. MOOSE is a flexible, reusable, single operator, aerobraking spacecraft designed to refuel, repair, and service orbiting spacecraft. MOOSE will be deployed from Space Station *Freedom*, (SSF), where it will be stored, resupplied, and refurbished.

Introduction

MOOSE Description

The MOOSE spacecraft is an orbiting vehicle capable of sending an astronaut on three day satellite servicing missions to GEO or LEO and back to SSF. The astronaut is housed in a "shirt-sleeve" environment. Extravehicular Activities (EVAs) are not permitted from the MOOSE, since the vehicle is a single-person vessel.

In order to conduct the servicing tasks, MOOSE is equipped with a seven degree of freedom (DOF) Telerobotic Manipulator Arm (TMA), a four DOF Telerobotic Grappling Arm (TGA), and a Manual Manipulation System (MMS). MOOSE will employ a 9m reusable aerobrake in order to return rendezvous with SSF from GEO.

The MOOSE vehicle can be separated into two distinct parts. The first is the MOOSE Manned Module (MMM), shown in Figure 1 (top). It consists of the crew cabin, the Reaction Control System (RCS), spider truss, and the Manipulator/Grappler System (Man/Grapp). The second part is the MOOSE Propulsion Module (MPM), shown in Figure 1 (bottom). It consists of the aerobrake, main spinal truss, and main propulsion unit.

The MOOSE flight vehicle operates in 2 modes. The first is the primary operational configuration for servicing missions to GEO. It entails using the entire flight vehicle, consisting of MPU and the MMM fully fueled. The second is the "cab-only" mode, in which the MMM flight vehicle separates from the MPU. This configuration is used to conduct servicing missions in LEO, or in close proximity to SSF, and enables MOOSE to be more maneuverable and cost-effective.

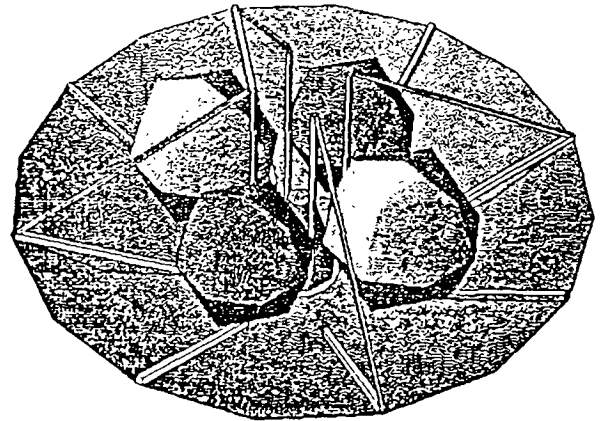
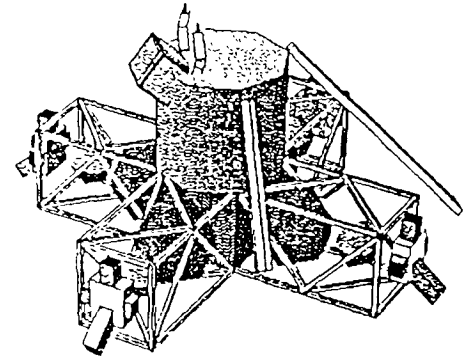


Figure 1 MMM (top) and MPM (bottom)

MOOSE subsystems are designed as ORUs which can be changed out via the SSF Remote Manipulator System (RMS). All significant systems are configured to make access, test, and change-out as simple as possible.

SSF-Based Operations

MOOSE operations increase the frequency of SSF departing/arriving spacecraft. Propellant Maneuvering Vehicles (PMVs), shuttles, and MOOSE will be utilizing SSF airspace, possibly simultaneously. A SSF traffic management scheme has been developed based upon the Johnson Spaceflight Center (JFC) Orbital Maneuvering Vehicle plan for SSF terminal control zone management.

Dedicated MOOSE support personnel on-station will be minimal. MOOSE maintenance, check-out, and refurbishment tasks will be as automated as possible. Dedicated Inter-Vehicular Activities/Extra-Vehicular Activities (IVA/EVA) would be performed by the available crew as needed.

A second crew member is required, in addition to the astronaut operating the MOOSE, to operate the SSF RMS during berthing and de-berthing operations.

Expendable Launch Vehicle (ELV) Operations

ELV operations are essential to the MOOSE mission. Regular propellant delivery must be maintained if flexibility is desired. PMVs would be delivered to SSF from their respective launch sites.

Vehicle Overview

In its standard configuration (MPU mated to the MMM), the MOOSE vehicle weighs 3067 kg (dry) and 14481 kg (wet). This configuration is the maximum weight for a three-day GEO servicing missions. For LEO missions, the MPU can be left at *Freedom*, creating a vehicle that would weigh a maximum of 1235 kg (dry) and 1980 kg (wet).

MOOSE is capable of carrying 800 kg of payload to orbits inclined up to 70° at altitudes from 185 km to 40,000 km. Consumables are provided for a nominal 3-day mission, with contingency mission duration of 10 days.

Costing Overview

<i>Develop Cost</i>			
RDT&E	\$2,374.70	M93	
First Unit	\$203.90	M93	
Flight Unit	\$203.90	M93	
<i>Development Operations Costs</i>			
ASE RDT&E	\$1,100	M93	
ELV Support	\$1,182	M93	
Ground Support	\$375	M93	
<i>Mission Operations Cost</i>			
3 sorties/year	\$294	M93	
6 sorties/year	\$432	M93	
13 sorties/year	\$780	M93	
<i>Program Cost @ IOC</i>			
	\$5,439.50	M93	
<i>Median Operations Cost/year</i>			
	\$432	M93	

Table 1 Overview of projected costs

Navigation And Tracking

Orbit and Attitude Determination

Orbit information must be accurate enough at geostationary orbit to bring the vehicle within tracking distance of the target. The working range of the selected rendezvous system will be 4.5 nmi. The error in position at GEO added to the error in the target's known position must therefore be less than this range. Using a .75 safety factor, the requirement for GEO position determination accuracy will therefore be 6 km.

At LEO and below, the main positioning requirement will be determined by the aerobraking maneuver. Non-inertial navigation systems will be blacked out during this maneuver, so inertial guidance will be need to be accurately calibrated before the maneuver. From GEO, an accuracy of 2 km will be required for the aerobraking window. On approach to the maneuver, the window will be smaller, requiring an accuracy of 100 m for necessary course adjustments.

Inertial Measurement Units (IMUs)

Two IMUs will be used on MOOSE, and will consist of sensors that measure both rotational motion (using gyroscopes) and translation motion (using accelerometers). Strapdown units will be used instead of gimballed platforms because they have less mechanical complexities and mass, while maintaining accuracy comparable to that of gimballed systems.

The Inertial Measurement Unit (IMU) was chosen as the primary navigation system for its high accuracy. The main drawback of IMUs are the time degradation that they undergo. To keep their accuracy, position and orientation information must be updated before the data is no longer useful. Immediate updates would be required immediately after large ΔV burns.

Global Positioning System (GPS)

GPS provides 25 m accuracy at LEO, but it is not designed to work above 8000 nmi altitude. This system will be used to meet the 100 m aerobrake accuracy requirement. GPS will be used in LEO for calibration of the IMUs. All LEO and GEO transfer orbits will be calculated using GPS and Kalman filtering software. A GPS update occurs at the rate of 2 updates per second. GPS information is used to verify the aerobraking maneuver approach orbit.--updates are fast enough to allow for mid-course corrections.

Microcosm Autonomous Navigation System (MANS)

This system provides 600m to 1.5 km accuracy using 2 sensors. This system is necessary for long term navigation in GEO, and to meet the 2 km aerobrake window requirement. It can provide orientation updates to an accuracy of 0.01 degrees, using the sun as a reference. For 11.4% of the time in GEO, the sun will be blocked out, but the horizon sensors will still be functional, providing an accuracy of 0.1° to 0.25°. For 4.6% of the time, no orientation updates are possible. For the first 20 hours after GPS updates are lost, the IMUs are more reliable than MANS. After this point, MANS must begin linear navigation updates at its returning frequency of 0.5 Hz.

Star Trackers

This system can provide updates to an accuracy of 0.01° when the sun's glare does not affect the sensor. Although it can be used at other points, the star trackers will definitely be able to be used during the 16% MANS blackout/partial blackout time. Star trackers are useful in increasing the accuracy of the altitude measurement, and for determining the angle and angle rate to a target for rendezvous purposes.

OMV Rendezvous Radar

Although the Orbital Maneuvering Vehicle project has been canceled, its rendezvous radar has been fully designed. This system was specifically designed to assist

the rendezvous tasks that MOOSE is required to do. It has a range of 4.5 nmi, and an accuracy of better than 20ft, or <2% of the range. It also provides a range rate accuracy of greater than 0.1 ft/sec, or 2% of the range rate.

Control Moment Gyroscopes

External torques, such as those produced by solar radiation and gravity gradients, and internal torques, such as that produced by positional uncertainty of the center of gravity, must be compensated for. A trade study was done comparing the mass of the fuel required to do orientation adjustment for a typical three day mission versus the mass of the Control Moment Gyroscopes (CMGs) required to do the same job. The required fuel mass was 150 kg for the cold gas thrusters and 242 kg of hydrazine for the RCS. This compares with a CMG mass of 76 kg.

The MOOSE vehicle was designed to use double-gimballed CMGs for three-axis control. The CMGs are located near the center of gravity for maximum performance. Three CMGs are used for redundancy considerations—should one fail, the other two will be able to maintain three-axis control. The primary RCS can be used to desaturate the CMG wheels. The impulse torques caused by gravity gradients, solar pressure, and aerodynamic effects are well below the impulse torques that the moment gyros were designed for.

The model used to design the wheels was a thin-rim, high-speed flywheel. It was found that AISI 4340 (normalized at 1600°F, quenched in oil from 1525°F) would give the smallest wheel radius and the maximum performance. For high-speed bearings, (>3000 rpm), a closed loop oil system should be used to give an active flow through lubrication system which would enhance the bearing life by continuously supplying additional oil to the spinning ball bearing at a controllable rate. A DC brushless motor will be used for its high torqueing capability. A tachometer will be used to monitor the wheel speed.

Reaction Control System

The manned module must be able to maneuver around and approach the target satellite from any angle to capture and repair it. The reaction control system is comprised of primary and secondary thrust chambers. The need to ensure a contamination-free environment about the SSF and satellite hardware drove the two-system design.

Primary RCS

The primary thrusters are utilized for attitude control, course corrections, orienting the MOOSE vehicle for proper guidance & navigation sensing and aerobrake-maneuver positioning, desaturating the control moment gyros, and collision avoidance.

The primary thrust chambers utilize monopropellant liquid anhydrous hydrazine and operate in pressure blow-down mode with helium as the pressurant gas. The hydrazine system does not require an oxidizer for combustion, it spontaneously decomposes as it flows over the Shell 405 catalyst bed and produces hot gases which are expelled through the nozzle. The selected level of ammonia dissociation is 0.6 and the resulting performance level, I_{sp} , is 240 seconds.

A total of 24 520 N (100 lbf) hydrazine thrusters will be utilized. Four thrust chambers will be on the lower truss struts, with one on each strut. Twenty thrust chambers will be on the spider truss booms with five on each boom.

The total monopropellant mass is 512 kg, and the total mass of the 24 hydrazine thrusters is 44.74 kg. The figure below is a schematic of a typical hydrazine thruster configuration.

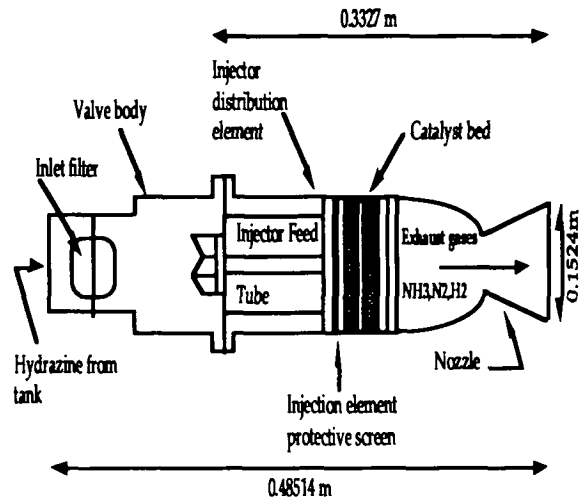


Figure 2 Hydrazine Thruster Configuration

RCS Spider Truss

The RCS Spider truss serves as a platform for the MOOSE RCS. The boom extends for only 2.6 m from the center line of the MOOSE, to protect the nozzles during the aerobraking maneuver. It houses the RCS tanks within its members and acts as a boom for the reaction control nozzles to ensure their operation as far away from the c.g. of the MOOSE vehicle as possible. The trusses and the avionics box are an integrated structure which attaches to the bottom of the MOOSE crew cabin.

The material selected for the truss is a high-strength graphite/epoxy with a 45° fiber orientation to ensure the composite's strength in bending. The resulting configuration for the spider truss consists of two different cross sections. The inner and outer cross members both have circular cross sections of outer radius 1.25 cm and inner radius of 1.0 cm. The remaining spider truss members have circular cross sections of outer radius 7 mm and inner radius 5 mm. The mass per spider truss is 9.36 kg, therefore, the total mass for all four spider trusses is 37.5 kg.

Primary RCS Tanks

Two tanks are necessary to store the hydrazine monopropellant and helium gas pressurant. The blow-down ratio is 4.2, with a beginning of life tank pressure of 420 psi and an end of life pressure of 100 psi. The total volume for hydrazine propellant is 0.5005 m³ and the helium pressurant volume is 0.1564 m³. The radius of each of the tanks is 0.428 m and the material is Al 1100-0 which is resistant to the corrosive effects of hydrazine.

Hydrazine freezes at 273K so line heaters were used to ensure the operability of the thrusters.

Secondary RCS

Due to the sensitivity of the SSF and satellite hardware to contamination from thruster exhaust products, a helium cold gas thruster system is utilized for all GEO satellite-

servicing operations and for separation and docking maneuvers. The mass of the helium for the secondary thrusters is 223 kg. The total mass of the 40 thrusters is 3.4 kg. The thrusters on the lower truss struts are grouped in threes with one grouping per strut. Seven cold gas thrusters were located on each boom of the spider truss. These thrusters produce 20 lbf (89 N) at a pressure-at-thrust of 1000 psi. The area expansion ratio is 25:1.

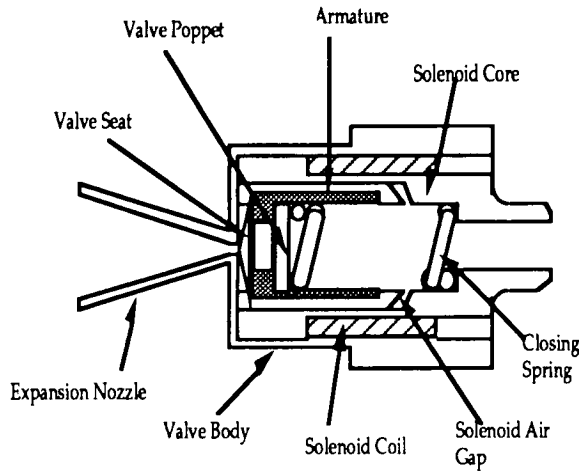


Figure 3 Single Seat Cold Gas Thruster

Secondary RCS Tanks

The helium cold gas for the secondary thrusters will be stored in four (4) Ti 8-1-1 tanks at a tank thickness of 1.66 cm and a mass per tank of 55.75 kg. The tank pressure is $41.4E6 \text{ N/m}^2$.

Main Propulsion System

The main propulsion system of MOOSE will perform four burns on a typical mission. These burns include GEO transfer injection, GEO circularization, LEO transfer injection, and LEO circularization after the aerobrake maneuver.

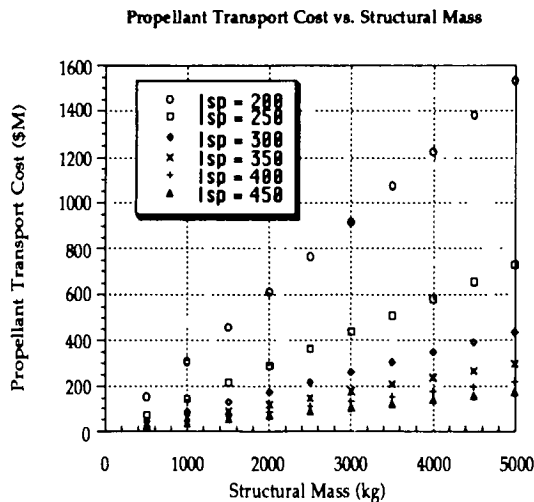


Figure 4 Propellant Transport Costs vs Structural Mass

The main propulsion system utilizes cryogenic liquid hydrogen and liquid oxygen as the fuel and oxidizer respectively. To achieve cost efficiency in propellant transport cost so the customer price tag does not exceed 100 \$Million, the performance level, I_{sp} , must be 450 seconds. The figure below demonstrates the relationship between cost and performance level. The mixture ratio is optimized at 7:1 which maximizes the I_{sp} , and assures complete combustion of the liquid oxygen while not running too hydrogen rich, where some of the hydrogen does not combust.

The dimensions of the combustion chamber are as follows: chamber diameter is 0.281 m, chamber volume is 0.022 m^3 , and chamber length is 0.355 m.

Injector Design

The injector is designed to deliver the propellants to the combustion chamber and to sufficiently mix and atomize the propellants to form a homogeneous fuel-oxidizer mixture.

The injection system selected is a coaxial non-impinging configuration which is the most common for Oxygen/Hydrogen engines, including the SSME, and provides good combustion stability. Low velocity liquid oxygen (LOX) is fed through a tube which is surrounded by high velocity gaseous hydrogen (GH_2). The GH_2 , already warmed from the regenerative cooling cycle, warms the liquid oxygen in the tube and vaporizes it. The gaseous hydrogen and oxygen then readily mix in the combustion chamber.

Ignition System

The ignition system is of critical concern for it must ensure rapid ignition of the propellant mixture and equally rapid thrust increase to the designed rating.

A spark-torch igniter was selected for the ignition system. It is highly reliable, has multiple restart capability (a must for MOOSE), and performs well at high altitude. The spark-torch igniter allows some propellant in, then supplies a spark for ignition. The flame is then ducted to various locations on the injector face to ignite the main propellant flow.

Nozzle Design

The expansion nozzle is designed to take the high temperature exhaust gas flow and expand it to allow the thermal energy of the flow to be transformed into kinetic energy, i.e. useful propulsive energy.

The MOOSE will use a bell shaped nozzle with an area expansion ratio of 40:1 at a design mach number of 4.22. This expansion ratio relates to an exit area of 0.99 m^2 and a throat area of 0.0248 m^2 .

The large heat flux to the nozzle walls from the combustion products requires a cooling process that will preserve the nozzle contour, its material integrity, and allow for an indefinite firing duration. A regenerative cooling system was selected over nozzle-material ablation since it satisfies the above mentioned requirements and the vehicle has available coolant, the LH_2 fuel. This cooling method is relatively lightweight since additional on-board cooling subsystems are not required and the desire to achieve a maximum I_{sp} , to successfully perform the MOOSE mission requirements, is achieved through augmenting the energy content in the combustion chamber

by utilizing the thermal energy picked up by the LH2 in cooling the nozzle. The high heat flux capacity, necessary for LOX/LH2 combustion, is also accounted for by the regenerative cooling system.

Turbopump Feed System / Plumbing

The pump system selected is an expander cycle turbopump feed system. An Auxiliary Power Unit (APU) is used to initiate the propellant flow to the combustion chamber. The hydrogen fuel exiting the nozzle cooling-jacket will drive both the oxidizer and fuel turbines which drive the fuel and oxidizer pumps. Once initiated, the propellant pumping process is self-perpetuating and is sustained by the turbine generating 82.7 kW of power to drive the pumps at the required pressure of $2.66 \times 10^6 \text{ N/m}^2$.

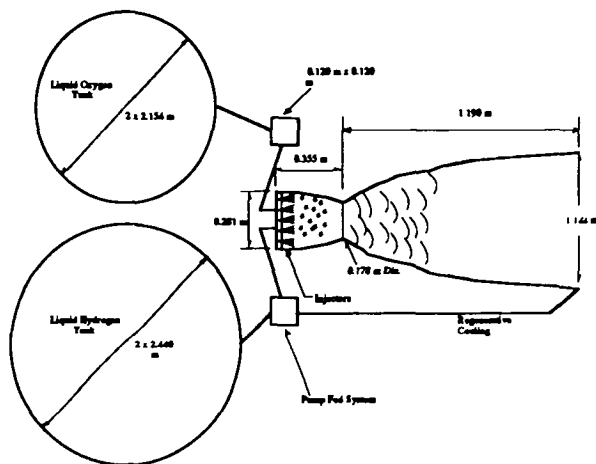


Figure 5 Main Propulsion System Configuration

Thrust Vectoring Control

Thrust vectoring will be controlled by the RCS for pitch, yaw and roll motions of the MOOSE vehicle. The thrusters are located at the ends of each boom of the spider truss and on each of the lower truss struts. The location of the thrusters will provide three axis stability.

Main Propulsion Malfunctions

The MOOSE can survive a main propulsion system malfunction if it occurs either after the first or after the third main engine burn. In the event that a malfunction occurs after the first main engine burn, the astronaut will remain in the elliptical Hohmann transfer orbit until the vehicle returns to the SSF. It will take ten and a half hours to return to SSF. The astronaut can survive this since the MOOSE is designed and equipped for a three day mission. If the malfunction occurs after the third burn for LEO injection, the RCS will handle the necessary maneuvers to return the astronaut safely to the SSF.

Malfunctions occurring after the GEO circularization and prior to the LEO transfer injection burns will require the astronaut to wait for a rescue vehicle in order to return to the space station.

Main Propulsion Tanks

The main propellant tanks will be launched empty from Earth using the NASA Space Shuttle launch platform and will be integrated with the MOOSE system on orbit at

Space Station *Freedom*. For the launch from Earth, the tanks will be pressurized to stiffen the structure against loads resulting from the launch. The tank walls will consist of Al-1100 at thicknesses of 3.5 mm and 3.0 mm for the liquid hydrogen and liquid oxygen tanks respectively, and corresponding tank masses of 178 kg and 99 kg.

The tanks will be integrated to the central support truss by a 10 cm x 5 cm, 1.1 kg Al-1100 disk threaded around its surface area and located at the top of each of the tanks. The bottom of the tanks rest on the aerobrake support arches and will be wrapped with a thermal protection foil to withstand the heat transfer from the nozzle and aerobrake maneuver and allow the Al-1100 alloy to maintain its actual yield strength. The final mass total for the liquid hydrogen tanks is 179 kg and 100 kg for the liquid oxygen tanks.

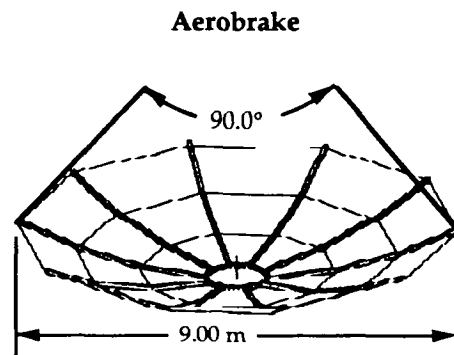


Figure 6 Aerobrake Structure

The design of MOOSE included the aerobrake used to partially reenter the atmosphere and use drag forces to modify its orbit instead of fuel, thus reducing mass. A spherical shape made of an aluminum honeycomb provided a lightweight thermally resistant structure. Ceramic thermal protection tiles were placed on the above structure. The design allowed for assembly and maintenance to easily be performed.

Trajectory

A two shallow pass trajectory was chosen instead of a single deep pass. Although the chosen trajectory speed was Mach 34, because of a shallow pass of 80 km minimum altitude, the largest aerodynamic forces were almost negligible, only a few hundred Pascals. The g forces on the brake during the two pass maneuver were less than the propulsive forces during an orbital burn, maximum of 1.5 gs.

Main Spinal Truss

This structure carried up to 2g loads. All major components the cabin, spider truss, fuel tanks, propulsion system, and aerobrake were connected to the spinal truss. The titanium longitudinal beams were welded to hard points on three spinal rings. These rings integrated the aerobrake, cabin, and fuel tanks.

Manipulator/Grapppler System

Introduction

The Manipulator/Grapppler System is essential to the execution of MOOSE's duties as an on-orbit servicer. One

of the driving requirements for MOOSE is that the astronaut should not have to do an EVA during the repair process. To accomplish this, it is necessary to equip the vehicle with a manipulation system that he/she can control from within the spacecraft. The possible components of the Man/Grasp System are: a Telerobotic Manipulator Arm (TMA), a Telerobotic Grappling Arm (TGA), and a Manual Manipulation System (MMS).

Many possible combinations of these subsystems were examined. The primary design criteria were mass, flexibility, complexity, and development/production costs. The culmination of the design process was a system that utilized all three subsystems.

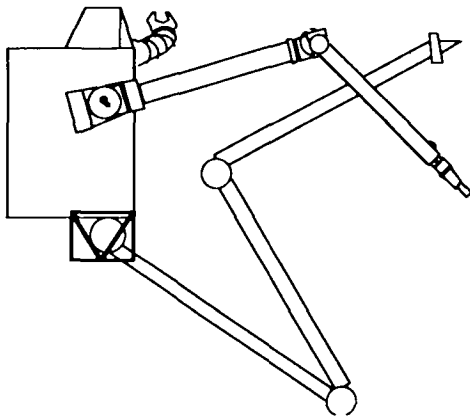


Figure 7 View of Cabin & Manipulator/Grapppler System

The TGA is a four DOF arm, with various possible end-effectors. It is necessary to have a grappling arm to maintain a fixed position and orientation, with respect to the target, during repair operations. The TGA has three links. Link 0 and link 1 are each 2 m long, while link 3 is 3 m long. It was determined that the TGA should be able to successfully maneuver a 6000 kg payload.

Spacecraft Subsystem Anomaly	Number	Percent
Timing, Control, and Command	55	9.1
Telemetry and Data Handling	112	19.1
Power Supply	56	9.2
Attitude Control	123	20.3
Propulsion	26	4.3
Environmental Control	16	2.6
Structure	6	1.0
Payload/Experiment	208	34.3
TOTAL	602	100

Table 2 Survey of 602 Satellite Failures

Degree of Failure	Number	Percent
Negligible Effect	447	74.3
Small Effect	117	19.4
1/3 to 2/3 Loss	32	5.3
2/3 to Near Total loss	5	1.0
Total Mission Loss	1	---

Table 3 Failures' Effect on Mission

Based on the data shown in Tables 2 and 3 above (Shockey 1984), it was determined that a significant number of satellites (at least 25%) can be expected to have some loss of attitude or navigational control. Therefore, it would be desirable for MOOSE to be able to grapple with

and control errant satellites, so long as the crew member is in minimal danger.

The TMA is a seven DOF arm, with interchangeable end-effectors. The TMA is expected to function as an "assistant" to the astronaut, in that it can handle massive loads, hold "handed-off" tools and equipment, retrieve ORUs from storage, etc. By providing a variety of end-effectors, it can also be used to perform simple servicing tasks, such as on-orbit refueling. The TMA should be able to handle 450 kg ORUs.

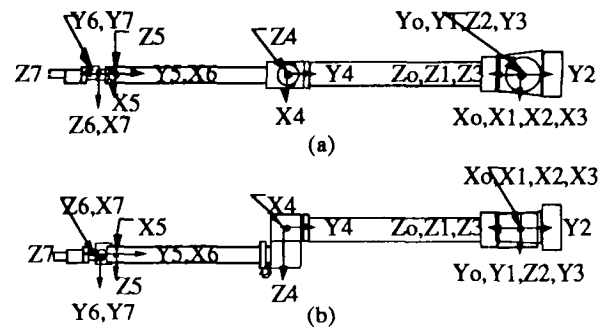


Figure 8 Side and Top View of TMA Design

The MMS is basically astronaut space suit gloves that are attached to the outside of the vessel's cabin. The astronaut has the benefit of being able to use his/her over 50 DOF arms and hands to conduct repairs, without having to leave the cabin. While this option provides the ultimate in fine dexterity, the limited workspace envelop necessitates the provision of the TMA.

Prismatic-vs-Revolute Joints

The main problem with using prismatic joints in space is the difficulty involved with sealing the linear bearings from the environment. Revolute joints are much easier to seal, and have large workspaces, and low energy and torque requirements. In spite of the added complexities of the hardware and software, the jointed manipulator design has many benefits, are well from the basis of for the MOOSE TMA and TGA.

Direct Drive-vs-Transmitted Drive

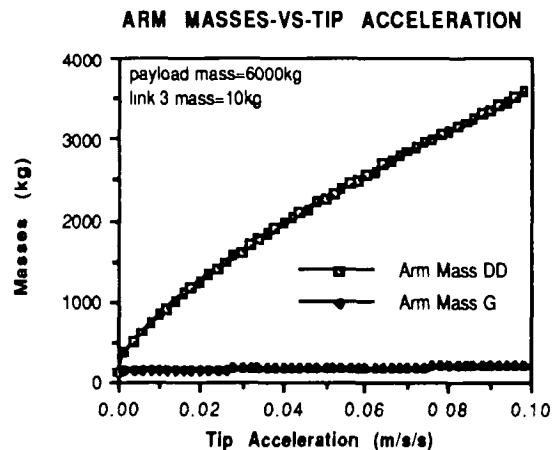


Figure 9 Arm Mass in a Direct Drive Design vs Geared Design

One of the main design drivers is that the vehicle systems have low mass. To illustrate the mass relationships of direct drive and transmitted arms, a rough cut analysis was conducted, yielding the following data. Substantial mass is saved by using a transmitted drive arm design.

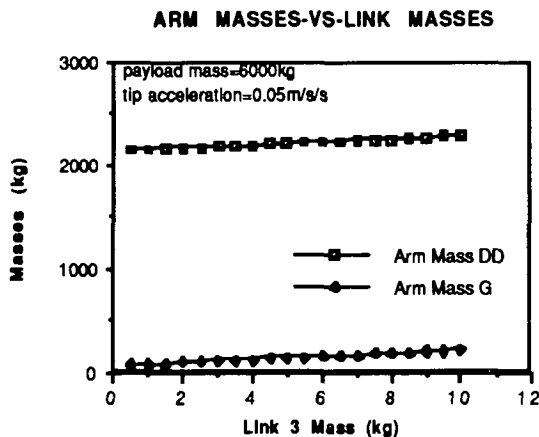


Figure 10 Arm Mass in a Direct Drive Design vs. Geared Design

Material Selection

A variety of materials with which to construct the arms were investigated. The final decision was to fabricate the main links of the TGA and TMA from Graphite/Epoxy, and the joints from Titanium (T16 A1-4 V). The major driver in this selection was the thermal expansion compatibility of the two materials, as well as their large relative strength-to-weight ratios. The resistance to corrosion of Graphite/Epoxy and Titanium was an added bonus. The TMA will be subjected to highly unfavorable conditions during satellite fluid replenishment missions.

Communications

MOOSE will not communicate with the space station directly during most of the mission. Rather, communications will be routed to SSF from ground links. If SSF were used as the main space relay link, a significant portion of its communication system would have to be devoted to MOOSE data during missions. In addition, MOOSE and SSF can be a relative position where communications are blocked by the Earth for significant periods of time, requiring the use of relay satellites. Therefore, the communication system would have to be able to communicate with earth from altitudes ranging from LEO (250 km) to GEO (39,000 km).

The uplink, from ground to MOOSE, would consist of voice and command. Voice will be used to communicate with astronaut. The ground computers can communicate with the MOOSE computer system via the command link. In the case of an emergency where ground control needs to control the vehicle, command communication will be essential.

The downlink will transmit voice, video, and telemetry information. Video information can be transmitted at any time, but may be especially useful during the repair phase of a mission. The telemetry information is essentially housekeeping data. Unlike other space vehicles, no experiments will be conducted on board MOOSE, therefore telemetry will not be as high as an STS, for instance.

Digital communications will be used instead of analog for two main reasons. One, digital signals are more reliable than analog signals. Second, several digital signals can be multiplexed onto one rf signal. For example, voice, video, and telemetry can be sent on one link.

Structure	6400	bps
Life Support	540	bps
Man/Grp	5080	bps
Propulsion	288	kbps
Attitude Control	3380	bps
Navigation/Tracking	180	bps
Reaction Control	2900	bps

Table 4 Communication Data Rate Requirements

The breakdown, according to main systems, of transmission rate requirements are shown above. Note that most of the systems will not need to transmit at the maximum rate listed above for significant periods of time during the mission. To fulfill the above requirements, the Ku-band will be used for all transmissions.

At low altitudes, links will be established through TDRSS satellites. Direct communication to the surface would not be possible due to unacceptable blackout periods, and due to the difficulty that is experienced in locking onto ground stations from low altitude orbits. When MOOSE's altitude is between 12,000 km and 39,000 km, direct ground links will be used.

MOOSE requires 20 W transmitter to send voice, telemetry, and video from a GEO orbit. The communications system will consist of two transponders for redundancy. The antennae are mounted on telescoping booms, so that they can be pulled into the protective cone of the shield during the aerobraking maneuver.

Computation And Data Management

The Computation and Data Management System (CDMS) has to provide sufficient processing power for all other systems. Computations and data transfers must be fast and reliable.

Hardware

Distributed processor architectures offer attractive benefits such as reliability, ease of growth, and parallel processing. It also allows for processors with various capabilities and requirements to work together with ease. The physical distribution of hardware on MOOSE, combined with the natural delineations and relations of tasks, makes distribution of processes and processors a natural alternative to a centralized system.

Most system processing will be invisible to other systems, but some operations (such as orbital transfer and attitude control, attitude control and manipulator/grapppler, etc.) will span several system. This would require the coordination of some highly complex computing processes over various processors. This would place a heavy burden on the lone crew member. The required level of automation is high, in order to reduce the workload for the astronaut.

Reliability has many facets, including probability of correct function over a period of time, probability of recovery (and recovery times) from minor, localized, or major systems breakdown, gracefulness of performance degradation when full service is not possible, and

assurance that critical calculations and tasks will be computed in the face of unusual computing loads.

A carefully designed distributed processing system has intrinsic benefits for reliability and secure design, including: 1. enhanced physical, electrical, and logical fault isolation., 2. convenience of configuration for redundant computing resources, 3. well-defined and protectable constraints on information flow, and 4. easy redelegation of tasks as computational priorities shift in the face of changing requirements.

MOOSE's CDMS must be able to evolve and grow over time to meet different and more complicated mission requirements. Distributed processing provides uniform physical and logical techniques for interconnecting diverse processing activities.

The main processor bus would be required to transfer 32-bits of data at high-speed. The VME-bus has a sustained data transfer rate of 40 Mbyte/s, and utilizes an asynchronous protocol, which allows for easy implementation of systems with parallel processors operating at different speeds.

A network standard was needed to interconnect the processors that were physically distributed throughout the MOOSE vehicle. Such a standard would have to have high data transfer rates, high data integrity, and low susceptibility to noise and Radio Frequency Interference/Electro-Magnetic Interference (RFI/EMI). The Fiber Distributed Data Interface provides very high transfer rates (12.5 Mbits/s, with the development of Gbit/s rates in the near future), very high data reliability, and no susceptibility to RFI/EMI. In addition, it has a low installation expense, and no sparking hazard. These benefits more than compensate for the high transmission media expense.

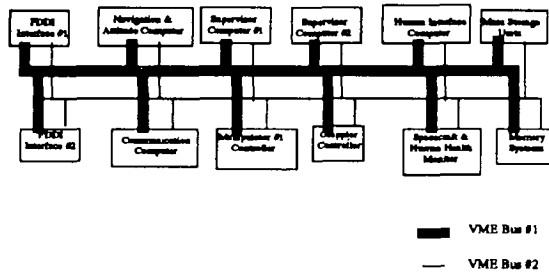


Figure 12 Double VME-bus

MOOSE will utilize a double (for redundancy) VME-bus backplane for its main processor bus. This configuration will yield a fast and mature system that is easily supported. It will also use a FDDI-based network in a double-ring architecture (to help eliminate single-point failures) to interconnect spatially distributed processors.

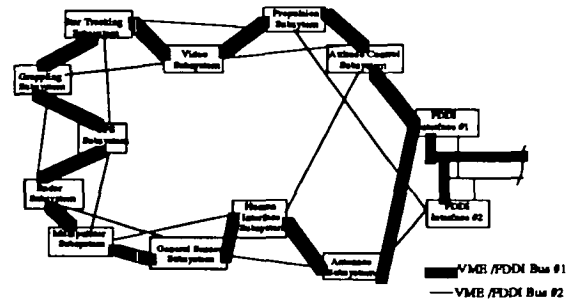


Figure 13 FDDI Double Ring Architecture

Software

True modularization of hardware design ("plug-and-play") is a well-accepted and mature idea. Attempts to do the same on the software level using traditional procedural programming methods has yielded less than adequate results. The advent of Object-Oriented Programming (OOPs) has created tools that should be used to develop and maintain MOOSE software.

Using OOPs, a real-time programmer/team of programmers can: 1. deal more effectively with complexity, 2. create a library of readily reusable code, and 3. begin the design at a much higher level of abstraction, allowing trade-offs to be effectively examined before committing to prototype development. OOPs also produces a system design and architecture that permits experts who are not programmers to contribute to the development process much easier.

There is much concern that OOPs programs suffer from performance bottlenecks. This stems from the misconception that real-time systems must be "fast". In reality, such systems need merely be "fast enough". In addition, raw speed does not necessarily equate to better performance.

Most problems with large systems have to do with the level of complexity. Programmers are not good at predicting where the bottlenecks will occur. OOPs combats this with fast development times, allowing performance data to be collected much earlier in the development cycle. The well-defined module interfaces that result from OOP practices allows for easy elimination of performance problems. This is much better than optimizing compilers. Optimizing compilers technology generally lags far behind hardware advances. They also create side effects that renders performance measurements difficult.

Power

The total available power on MOOSE is derived from the compilation of the individual subsystem power requirements. The table below outlines the system, power required, duration, and the resulting energy requirements.

System	Power Required (W)	Time	Energy Required (kW hr)
Data Recording	0120	all	8.64
Optical Sensors	0022	all	1.584
*Computer	0200	all	14.4
*Control Station and LCD Screens	0008	all	0.576
Lights	0040	all	2.88
*Inertial Measuring Unit	0030	all	2.16
*Life Support	0350	all	25.2
*Smoke Detector	0005	all	0.36
Communications	0025	all	1.8
*Rendezvous Radar (Rendezvous)	0060	1 hr	0.06
*GPS Sensors (LEO)	0006	72 hr	0.432
*Main Fuel Valves and Pumps (burne)	0020	12 min	0.004
*Star Sensor (every 8 hrs)	0003	1 hr	0.003
*Control Moment Gyros (drifting & working)	0030	4 hrs	0.72
Grappler Arm (grappling satellite)	1000	1 hr	1.0
Manipulator Arm (repairing satellite)	1000	6 hr	6.0
*Reaction Control System	0072	10 hr	0.72
Maximum Power Required	1.830 kW	Total Energy Required	66.539 kW hr
Backup Power Required	0.746 kW	Backup Energy Required	7 kW hr

Table 5 Outline of Power Requirements

The primary power source for MOOSE will be fuel cells. They will produce a maximum output of 2 kW with an allowable 10% loss due to power conditioning and full power for the mission. The fuel cells will operate on gaseous hydrogen and oxygen stored as cryogenes. The oxygen needed for life support will be stored in the same oxygen tanks as for the fuel cells. The mass of the fuel, tanks, and fuel cell will be 63 kg, including life support's oxygen mass. Fuel tanks will be stowed in the avionics box below the command module.

The lightest weight power source for the 7 kW hr needed for backup is nickel cadmium batteries. The energy density of these batteries is 0.4 kW/kg so 17.5 kg of batteries will be used.

Cabin Structure

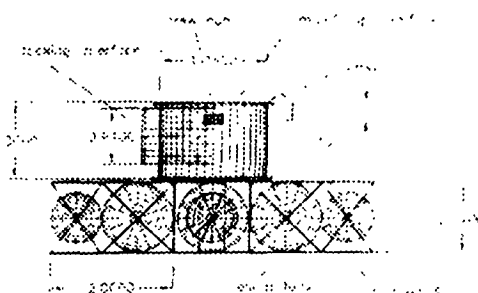


Figure 14 Main Components of the MMM

The cabin's design was a simple monocoque cylinder made from aluminum 7075. Two aluminum crossbeam gave structural support at the endplates to eliminate most deflections. The one centimeter thickness needed for radiation protection provided ample structural safety when carrying propulsive 3g loading. The stress concentration of the docking ring, also made out of aluminum, were well below material strength. A debris shield surrounding the cabin was design for a lightweight protection for the aluminum walls from micrometeor impacts. The viewport canopy, made of five centimeter Lexan plastic was designed to survive impacts without debris shielding. The base of the cylinder was mounted to

the spider truss completing the structure for the separated vehicle.

Radiation Shielding

Using NASA limits for radiation, The cabin walls were designed as one centimeter thick aluminum. The average dose for a two day mission in GEO was approximated from four to eight rem. For a LEO or polar mission the radiation dosage is below 0.2 rem.

Most radiation protection was needed during solar particle events where a dosage of 10000 rem during a day may occur. At GEO with the current shielding, the largest solar flares were able to deliver 130 to 200 rem. However since these flares have been predicted 10 to 20 hours prior to the event, the protocol allowed the crew member to take evasive maneuvers. By orienting the aerobrake toward the solar flare, more protection was offered by the aerobrake and propulsive materials. When the vehicle was directed to a lower orbit less than 50 rem dosage was delivered.

Cabin Components

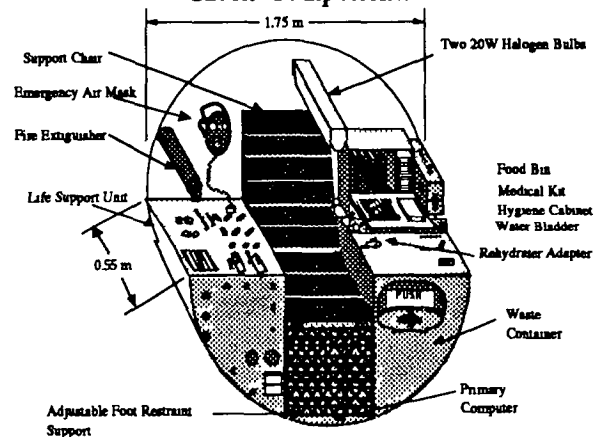


Figure 15 Cabin Layout

Oxygen And Nitrogen Supply

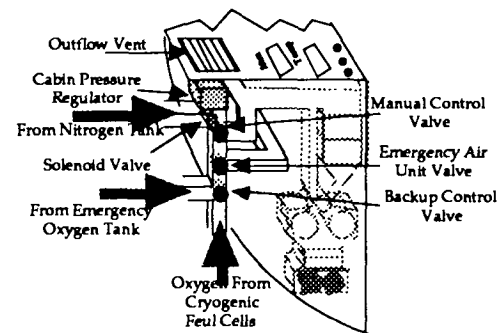


Figure 16 Oxygen and Nitrogen Supply System Layout

A 50/50 atmosphere of oxygen and nitrogen inside of the cabin had a design total pressure of 41.5 kPa (0.41 atm). This provided a low pressure, which leads to low overall mass, fire safe atmosphere, that did not affect the crew member's performance.

The oxygen and nitrogen supply system monitored the levels of oxygen in the cabin feeding gas when needed to maintain the above specifications. Pressure valves in the

cabin released air into space when necessary. The oxygen was supplied from the cryogenic fuel cells, however an emergency high pressure tank could have been used. Two other backup valves were designed to send the oxygen to the emergency air mask or directly out of the life support unit. The crew member then would have monitored the oxygen flow directly using the sensors.

Atmospheric Revitalization

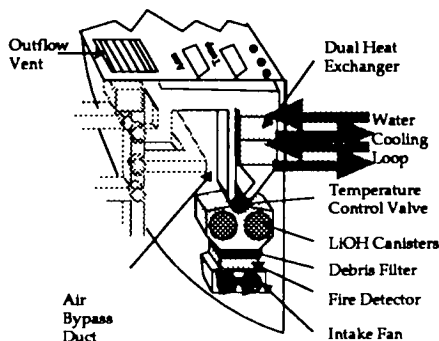


Figure 17 ARS Layout

The crew member was expected to produce 1.02 kg of CO₂, 2 kg of water vapor, and excess heat each day. The atmospheric revitalization system (ARS) was designed to extract the above and maintain an environment of less than 2000 Pa (0.02 atm) of CO₂, about 40% relative humidity, and around 21 °C.

The design for an airflow rate of 9.5 meters per minute was achieved by using either of two intake fans. The air passed through a photoelectric fire detector and debris filter. Containers holding lithium hydroxide (LiOH) and activated charcoal extracted the CO₂ and trace contaminants respectively. At the temperature control valve the flow was directed, either bypassed directly to the cabin or guided to the dual heat exchanger. Here the air was cooled, water vapor extracted, then reheated to the proper temperature the flow placed into the cabin.

Food System

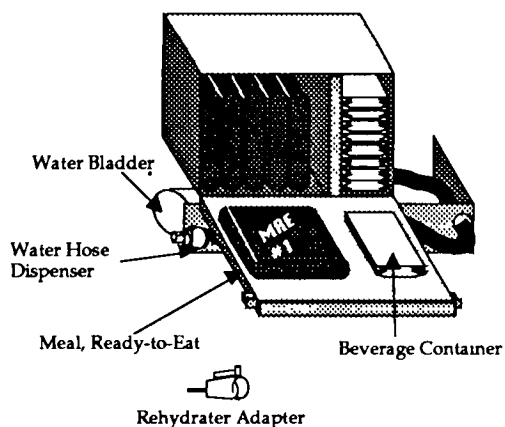


Figure 18 Food System Layout

The food system was a modified version of the MRE (Meal, Ready-to-Eat). Current used by the US Armed Forces, MREs were storable for a long duration, easy to prepare, inexpensive, compact, and were palatable with a

variety of menu selections. Beverages consisted of powdered drinks in prepackage containers. Rehydration occurred when a hose with an adapter penetrated the container, filling it with water. Beverage container can be reused for water consumption.

Hygiene And Waste

A hygiene cabinet held personal hygiene articles including wetnaps for minor clean up, toothbrush and paste, toilet paper, comb, and other amenities. Also chemically treated waste disposal bags were stored here. A urine container held a solid substance that absorbs and chemically treats the urine. A bag was provided to solid matter. After use a chemical pack was placed into the bag. The bag was then sealed and mixed.

All disposal containers were placed in the waste container. A hatch was sealed so that no fumes from the waste propagated into the cabin. The waste container was design to be able to exposed its contents to the vacuum of space as an auxiliary waste stabilization technique.

Fire Suppression

For prevention of fires, flame retardant cabin materials were integrated into the design. The small cabin interior allowed the crew member to detect most fires quickly. However, to detect smoldering fires, which are difficult to visually notice, and as a general safety precaution a photoelectric smoke detector was installed in the life support unit. These detect smoke particles precisely and were not affected by temperature or humidity that would yield false alarms.

A small fire extinguisher holding 1.13 kg of halon 1301 was placed in the cabin. This instantly cooled and smothered the fire without damaging electrical equipment. Protocol demands the crew member don the emergency air mask within five minutes after activating the halon, until the life support unit replaced the atmosphere in the cabin.

Mass Breakdown

Component	Mass (kg)
Structure	200
Cabin	355
Cabin Systems	663
Aerobrake	650
Tankage	610
Power	52
Avionics	192
Propulsion	300
ACS	41
LOX	1334
LH2	9335
Hydrazine	522
Helium	223
Crew	90
Payload	500
Dry Mass	3067
Flight Mass	15071

Table 6 Mass Budget Summary

Operations

MOOSE has the ability to perform ORU change-outs, refueling of consumables (including cryogenes), and Multi-Layer Insulation (MLI) repair to client spacecraft.

Trajectory

MOOSE can service satellites in most orbits, with the exception of polar/sun-synchronous orbits. MOOSE can execute plane changes of up to 42°. Plane changes are accomplished by a combined burn at 35,740 km apogee in order to minimize fuel consumption. A two-pass aerobraking maneuver then adjusts for the proper target altitude. All propulsive orbit transfers utilize Hohmann minimum energy transfer.

Target Proximity Operations

In the vicinity of the target, the standard closing technique is the +V-bar approach. This approach provides good target visibility.

Support Equipment

Successful MOOSE operations require a storage/refurbishment facility on SSF. The MOOSE facility can store large amounts of cryogenic for extended periods of time, possibly on the order of months. It contains berthing hardware and racks for storage of tools and payloads. The entire facility is partially enclosed with a micro-meteorite shield.

The cryogenic storage facility can store LO₂ and of LH₂. Boil-off losses are countered through the use of a Stirling cycle refrigerator. Other cryogenics are stored in the secondary cryogenic storage tank, when required. Hydrazine is contained in two other tanks. Fluids are transferred via positive expulsion, using high-pressure GHe as the pressurant. The pressurant supply also contains the GHe supply for the MOOSE flight vehicle.

The berthing area contains the lock-down and securing hardware for the MOOSE vehicle. Crew ingress/egress is provided by a retractable pressurized docking assembly. This assembly attaches to SSF at one of the resource nodes. The MOOSE vehicle, once berthed, may be rotated around the flight axis to provide the SSF RMS access to all vehicle components.

Conclusion

MOOSE was designed to fulfill a primary mission of servicing satellites in GEO, a task that can be done by no system in operation today. The MOOSE design team had the foresight to design a vehicle that can fulfill a host of secondary missions (astronaut EVA rescue, Space Station *Freedom* assembly and servicing, Hubble Space Telescope (and other LEO satellites) servicing, for instance). In addition, MOOSE can conduct multiple missions per outing, servicing two or more satellites at once. MOOSE is a small, inexpensive, and flexible system that can greatly expand the types of activities that can be conducted in space, with a minimal risk to the crew member.

References

- Shockey, Edward. *Analysis of Spacecraft On-Orbit Anomalies and Lifetimes*. PRCR-3579. February 10, 1984.
- Wertz, James R. and Wiley J. Larson, ed. *Space Mission Analysis and Design*. Kluwer Academic. Boston, MA. 1991.

Acknowledgements

J. Budinoff, J. Lane, N. Leontsinis, and R. Singh co-authored this document. The MOOSE Design Team (the

undergraduates who researched and co-authored the full MOOSE document) consisted of the following additional 24 students: K. Angelone, C. Boswell, I. Chamberlain, M. Concha, M. Corrodo, O. Custodio, S. Drennan, N. Eberly, B. Flaherty, D. Grove, C. Lash, D. Mohr, E. Pearson, T. Rivenbark, D. Roderick, S. Ruehl, J. Sabeau, A. Seaman, P. Septoff, T. Sheridan, C. Smith, M. Solfrank, G. Tansill, A. Zumburum. Barbar Flaherty deserves a special commendation for originating the name "MOOSE". We also appreciate all the extra work that Marco Concha did in preparing the computer animated video and photo-realistic stills of MOOSE.

The entire MOOSE design team would like to thank Dave, our most excellent advisor, and Tharen, his able minion and lovable sidekick. We would like to thank Dr. Mark Lewis for the sharp criticisms and welcomed praise that helped hone this project. We would also like to thank Drs. Russ Howard and Craig Carrigan for sharing their insight and know-how with us. Lastly, we would like to thank the Academy...ahem...the USRA for their continued support of this program.

PROJECT PERSEUS

A Crew Return Vehicle for Space Station Freedom

Massachusetts Institute of Technology
Department of Aeronautics and Astronautics
Cambridge, Massachusetts

Professor Stanley I. Weiss
Professor Hugh L. McManus
John-Paul Clarke (Teaching Assistant)
David E. Suzuki (Teaching Assistant)

Erik Abernathy	Richard DeChristofaro	John Hur	Lilac Muller
Amir R. Amir	Mike Dumbroski	David Kiesel	Carmen Perez de la Cruz
Edward Aron	Paul Engola	Kim Kohlhepp	John Piatkowski
Pelarin Bacos	Tri Freed	Jeff LaDelfa	Andrew Robertson
Michelle Bakkila	Bethany Foch	Kevin Lee	Birgit Sauer
Jakob Bernstein	Chris Glenn	Sam Leung	Dan Schwartz
John Brandt	Tim Glenn	Carl Livadas	Larry Smilg
Irene Budianto	Karen Gondoly	Andrew McFarland	Scott Snelling
B. Ray Conley	Homero Gutierrez	Brian Meade	Robert Wickham
Quyem Chu	Ron Harvey	Jim Miskel	Jeremy Yung

Abstract

In the wake of the Space Shuttle *Challenger* accident in 1986, NASA reassessed the safety of manned space missions. As a result, the Johnson Space Center initiated a study for an escape vehicle for Space Station *Freedom* (SSF). The objective of this vehicle is to provide astronauts onboard the station a safe and simple method of evacuation in case of an emergency. While the Russian Soyuz capsule provides an early option, it has several limitations. Two Soyuz spacecraft can accommodate only four crewmembers, whereas current planning calls for four to eight by FY 2000. For the long term, there is a need for alternative concepts.

The semester-long senior course, Space Systems Engineering, at the Massachusetts Institute of Technology undertook a design study for an alternative solution to the Soyuz capsule. Requirements were provided by the NASA Johnson Space Center. This vehicle, called PERSEUS for *Personal Emergency and Utility Spacecraft*, was designed as a lifting body with a cylindrical shape and a nose cone. The geometry provides a lift-to-drag ratio of approximately 1, allowing for a necessary cross-range capability to access seven possible landing sites, of which Eastern New

Mexico is the primary one and Stuart Plain, Australia is secondary. PERSEUS sizing is governed by the ability to be launched in pairs by the Space Shuttle or singly by a Titan IV booster from the Kennedy Space Center.

In addition to being able to safely evacuate four astronauts to earth, PERSEUS can provide a temporary "safe haven" for station personnel, capture and transport back an EVA astronaut unable to return to the station, and reach a Space Shuttle in a lower orbit if it is disabled. Parachutes are released during reentry to reduce the velocity of PERSEUS and retro-rockets are fired shortly before touchdown to provide a soft landing in an upright position. All these mission scenarios can be accomplished within a period of 24 hours, fulfilling a requirement from NASA.

Introduction

In January 1986, seven astronauts lost their lives in the tragic *Challenger* accident. As a consequence, the public suddenly increased their awareness that space missions are not yet routine and demand better safety precautions for the future. In response to that concern, NASA began to reassess the safety of

“manned” space missions. First of all, NASA acknowledged that the Space Shuttle is not as reliable as hoped and might not be available when needed. In addition, a life threatening emergency onboard the planned low earth orbit Space Station *Freedom*, without the ability to evacuate the station, would—in addition to potential tragedy—subject NASA to heavy criticism from the public. Such an incident would have a very negative impact on the agency’s image and endanger future projects. As a result, the Lyndon B. Johnson Space Center began a study in June 1986 for an Assured Crew Return Vehicle (ACRV) for the U.S. space station. In 1992, for political and economic reasons, use of the Russian Soyuz capsule was identified as a viable rescue vehicle. This solution, however, is viewed as short term; after completion of the Space Station, each of the two rescue vehicles needs to accommodate four astronauts. The Soyuz vehicle is designed to carry two, and altered to accommodate only three.

The Advisory Committee on the Future of the U.S. Space Program has classified a rescue vehicle as essential to the SSF program. In response to the ultimate need for an advanced vehicle, the senior-design course *Space Systems Engineering* in the department of Aeronautics and Astronautics at MIT undertook a design study for an advanced crew rescue vehicle during the 1993 spring semester. The goal of the designed vehicle, dubbed PERSEUS for *Personal Emergency and Utility Spacecraft*, is to be an advanced, yet simple, reliable, and affordable alternative to the Soyuz capsule. PERSEUS is a unique vehicle since it must stay in orbit for a long period of time. No reentry vehicle has spent so much time in orbit before its return to earth.

Mission Objectives

Based upon the objectives established by the Johnson Space Center for a crew return vehicle, the primary and secondary objectives for PERSEUS were established:

1. Safe evacuation of four astronauts from Space Station Freedom to earth within a period of 24 hours.
2. Return of a station crewmember in case of a medical emergency.
3. Provision of a “safe haven” for the crew of the Space Station for up to 24 hours.
4. Rescue of an astronaut engaged in an extravehicular activity close to Space Station Freedom in case of emergency.
5. Rescue of Space Shuttle crewmembers in case of an emergency of the Shuttle orbiter.

Of these five mission objectives, the first three represent the primary objectives, and the others the secondary mission objectives for PERSEUS. The mission is considered a failure if PERSEUS is unable to recover all of the astronauts involved in an emergency.

Mission Requirements

From the above objectives, the NASA ACRV Project Office established requirements for a crew return vehicle that were the basis for the PERSEUS’s functional and operational requirements. These were:

- The vehicle shall carry four crew members and provide life support for an operation of up to 24 hours.
- The vehicle shall be able to separate from Space Station Freedom within 5 minutes.
- The vehicle shall be able to perform a plane change of up to 1° and all possible phase changes to reach a disabled Space Shuttle.
- The vehicle shall be completely autonomous with the option of crew and ground control override.
- The vehicle shall not subject crew members to loads of more than 4 *g*.
- The vehicle shall provide a “soft” touchdown on land within a target area of 100 km by 40 km.
- The vehicle shall have an overall reliability of 99.5%.
- The overall mission cost shall be comparable by the Soyuz option.
- The vehicle shall be operational by Fiscal Year 1997.
- The life span of the vehicle shall be a minimum of 6 years without refurbishment and 30 years with refurbishment.
- The vehicle shall be able to communicate directly with Space Station *Freedom*, the Space Transportation System, and ground control.

Design of this vehicle was derived through a systems architecture which established eight subsystems tied to a unified design. Necessary trades were identified and configurations for each of the vehicle subsystems and their components were selected. Choices were made which best met the system requirements, always keeping *simplicity, availability, reliability, and affordability* as high level concerns.

Launch Configuration

As part of the pre-mission activity, PERSEUS is launched with either the Space Transportation System (Space Shuttle) or the expendable Martin Marietta Titan IV booster. Since PERSEUS is manned reentry vehicle with an extended on orbit stay, it was expected to be a very heavy and large vehicle. The two largest U.S. launch vehicles, the Space Shuttle with a payload capacity of 20 000 kg and the expendable Titan IV with a payload capacity of 12 700 kg to the SSF orbit, provide also the largest volume for the payload. These LV's are available at Kennedy Space Center/Cape Canaveral and thus can efficiently reach the Space Station's orbit. To minimize the cost, the Space Shuttle is used for a double launch in the initial installation and a Titan IV for a single launch after refurbishment. This choice of launch vehicles constrained both geometry and mass of the PERSEUS design.

Mission Scenarios

The mission of PERSEUS begins when it docks with Space Station *Freedom*, performs a test flight, and initiates standby operation. During the standby mode, power is supplied by the Space Station. PERSEUS is able to initialize all systems from the standby mode in less than 5 minutes in order to meet system functional requirements and separate quickly.

PERSEUS has been designed to operate in five mission scenarios. In the first scenario, the vehicle is used to return to earth a space station crewmember in need of medical attention available on the ground only. Most of the time required for this mission is necessary to achieve correct phasing for the landing site. In order to save power, PERSEUS can remain attached to the space station in standby mode until optimum separation time. The second scenario requires an evacuation of all astronauts from *Freedom* due to a massive failure of station systems. A

third scenario defines a "safe haven" in the case of an impending possible Space Station failure. PERSEUS may remain attached to the SSF or place itself 10 nautical miles away. From this location a "safe haven" is provided, allowing monitor of the Space Station to determine the cause of failure. At a predetermined time, PERSEUS must make the decision to either redock or to return to earth (in order to complete the mission in 24 hours). PERSEUS will also have the capability to rescue personnel from a stranded STS at an altitude of 180 km and normal space shuttle inclination near 28°. The STS can be up to 180° out of phase with the station and up to 1° out of plane. The final mission scenario for PERSEUS is the rescue of an astronaut during an extravehicular activity near the Space Station. The ΔV requirement for all scenarios is shown in Table 1.

Table 1: Summary of ΔV Requirements

Scenario	ΔV [m/s]
Emergency Evacuation	
Medical Emergency	242
SSF Failure	242
Safe Haven	
Return to SSF	160
Return to earth	272
STS Rescue	
Direct transfer	725
Phasing Orbits	1020
EVA Rescue	≈ 40
Maximum ΔV Required	1020

Reentry

The reentry into earth's atmosphere constitutes a critical part of the mission, especially after a long stay in orbit. After an orbital transfer, PERSEUS arrives at the upper limit of the atmosphere, 122 km, and begins the gliding phase of reentry. Most deceleration occurs during this phase due to the drag on the body. Next, the drogue parachutes open, slowing the vehicle even more and orienting it properly for landing (see Figure 1). Once PERSEUS has reached the proper altitude of about 5000 m, the main descent parachutes are opened. Because the parachutes will not decelerate the vehicle quite enough for a truly soft landing, retro-rockets are fired and the landing gear is deployed. About 32 minutes after the initial

atmospheric entry, the vehicle softly lands. To satisfy the NASA requirement of a touchdown on land, seven landing sites on land have been identified. The primary site is a plain area in eastern New Mexico close to White Sands. The secondary site is in Stuart Plain, Australia.

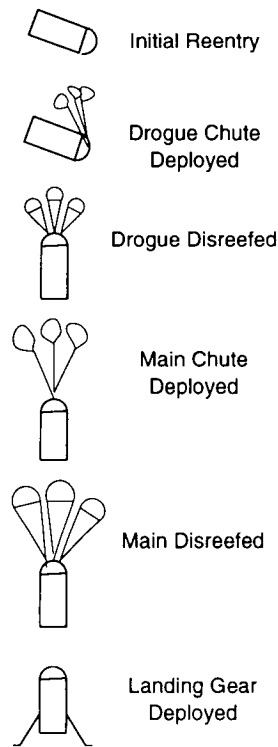


Figure 1: Parachute Configuration during Reentry.

The landing sites have been chosen in part for their nearby resources, providing immediate post-mission attention. During the last phase of reentry, the vehicle will be tracked using standard tracking procedures, allowing the search and rescue teams to quickly find the astronauts.

Vehicle Concept Selection

The three main vehicle configurations considered for the PERSEUS vehicle were conic, bicylindrical, and cylindrical designs. After a thorough trade study, driven by the requirements or primary recovery on land, the cylindrical concept was chosen. A cylindrical body is led by a blunt nose cone configured according to reentry heating and drag requirements. The maximum L/D of this configuration is 1.1, which proves sufficient for reentry cross range requirements.

A protective flared extension is included to shield the nozzles from atmospheric heating on reentry, spanning the circumference of the vehicle to provide protection during roll maneuvers. This vehicle lands on its aft end, with the drogue and main parachutes deployed from the tip of the nose. A schematic of the vehicle configuration and layout is shown in Figure 2.

In order to protect against debris on orbit, a Whipple shield was used in the structural design. In this design, two thin sheets of aluminum separated by spacers, provide protection of against debris impact while minimizing weight. Since it will be protected by the Space Station while docked, the upper surface of the vehicle is thinner in order to reduce vehicle mass. Primarily for the purpose of simplicity and weight savings, it was decided that in areas where tiles were needed for thermal protection they would also serve as the bumper for the Whipple shield.

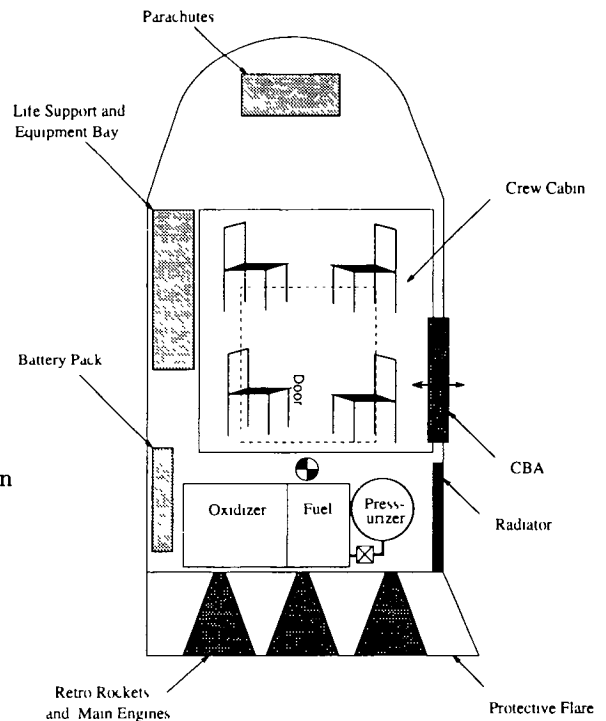


Figure 2: Schematic drawing of the selected cylindrical vehicle design.

Schedules

Schedules for the PERSEUS mission were developed with production separated into distinct phases. Integration of the entire vehicle is the final stage and

includes production of a prototype and time for burn in. Operation of the vehicle will take place after safety is ensured and the reliability specifications are met.

The On Orbit Mission of the project includes time from launch preparation to the end of vehicle life. Significant events are outlined in Figure 3.

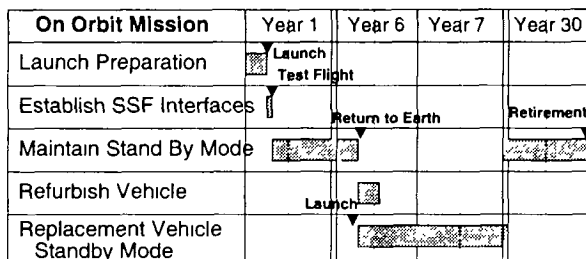


Figure 3: Schedule of mission life.

Cost

A cost analysis showed adherence to the top level concern of affordability. Total project cost is under \$800M (see Table 2), somewhat below but within scaling estimates for similar programs. The current Soyuz option will cost roughly \$400M. It is important to note that although it is twice as expensive as Soyuz, the fit-to-order quality clearly outweighs that of the much older design of the Soyuz capsule.

Table 2: Total System Cost

Phase	Cost (FY93\$M)
R&D	260
Testing and Evaluation	61.8
Production	168
Maintenance	42
Administration	55
Training and Simulation	15
Subtotal	601.8
Contingency (30%)	180.6
System Total	782.4

System Limitations

The system limitations reflect requirements or partial requirements that are not satisfied by the current vehicle design. While the current vehicle design represents a system satisfying the most requirements possible, there are still limitations to mission and vehicle performance. These must be addressed either through design refinements or operational techniques.

- **Space Shuttle Crew Rescue:** all seven shuttle astronauts cannot be rescued by PERSEUS in one mission unless two PERSEUS vehicles are sent to the shuttle, temporarily compromising the primary objective
- **Space Shuttle EVA Rescue:** a shuttle EVA astronaut does not have sufficient life support to allow time for PERSEUS to perform the worst case transfer to the Space Shuttle before expiration
- **Safe Haven:** a decision on whether the crew can return to earth must be made within seven hours of station separation in order to allow the maximum phasing time for landing of 17 hours
- **Station EVA Rescue:** rescue of an unconscious EVA member with failed MMU controls requires a suit up of a second astronaut, limiting the time allowed to reach the astronaut before life support expires
- **Touchdown:** PERSEUS must be directed to land in a relatively calm area since the vehicle will land softly and without tipping over only if the wind gusts and the parachute swing angles are within the specified range
- **Water Landing:** landing sites chosen suggest that water landing will not be necessary, however, the vehicle is watertight and stable due to its low center of gravity

PROJECT GRYPHON : AIR LAUNCHED SPACE BOOSTER

University of Michigan
Aerospace Department - Space System Design
Ann Arbor, Michigan

Professor Joe Easley
James Akers, Teaching Assistant
Mike Fisher, Asst Project Manager
Krista Campbell, Adam Nagaj, Elizabeth Hilbert, Alan Ristow, Ron Shimshock

Abstract

The Gryphon Design Team has developed a next generation 500,000 lb air launched space booster. The Gryphon is launched from a 1.2 million lb aircraft, the Eclipse, at 44,000 ft. The primary purpose is the delivery of 7,900 lb to Geosynchronous Transfer Orbit (GTO) and 17,000 lb to Low Earth Orbit (LEO). With these payload capabilities, the Gryphon is able to beat out competitor launch vehicles cost per pound by 50% which allows investors a 15% return on their investment. The design has also allowed for the ability to supply Space Station Freedom, based on the Space Shuttles capabilities. Since the Gryphon was designed to compete with existing vehicles, cost has been minimized in all areas. Therefore, only 'off the shelf' technology has used in the design process.

Introduction

The goal of the Gryphon Design Team was to develop a 500,000 lb air launched space booster with the capability of delivering 7,900 to GTO and 17,000 lb to LEO. These payload goals were determined in order to beat the competition's cost by 50% to insure investor's of a 15% return.

The task of designing the Gryphon was daunting. No project of its size and nature had been previously undertaken. OSC has begun an initial study of a similar sized launch vehicle called Pegasus III, but they have yet to decide whether they will continue. An additional challenge stemmed from the 'real world' application of the Gryphon, since there is current commercial interest. This restriction has not allowed for the design of components and systems to be developed in the 'future', or without cost constraint. With the added dimension of a 14 week semester, the Gryphon has been designed as efficiently as possible, above and beyond all of the limitations imposed.

Reason for the Configuration

Robert Lovell of Orbital Sciences Corporation presented the idea of a large air launched space booster based on his department's belief in a market opportunity between the Space Station Freedom resupply needs and the commercial communications industry. The 500,000 lb weight suggestion was based on his intuitive knowledge of available engines and their capabilities. Other than his

initial weight recommendation and stipulation of a 15% return, the entire project's development was left to the design team.

Unlike the Pegasus, which is carried underneath a L1011, the Gryphon's weight caused an entirely new aircraft to be developed in order to carry it into the upper atmosphere. The Eclipse Design Team, which designed the carrier airplane, specified a drop at approximately 40,000 ft at a speed of 500 mph. With this knowledge, the technical groups proceeded in their research and design. At the start, the Pegasus was used as a baseline and many aspects were designed as larger upgraded versions of those found on the Pegasus. However, it was quickly realized that extrapolating components from a 40,000 lb vehicle to a 500,000 lb vehicle was not always possible. Even though many aspects from the Pegasus could not be used, the Gryphon still resembles current launch vehicles. All the systems and components are currently available. Its final configuration results from a combination of cost, simplicity, and available technology. Figures 1 and 2 show a transparent view of the Gryphon and how the Eclipse and Gryphon look while attached.

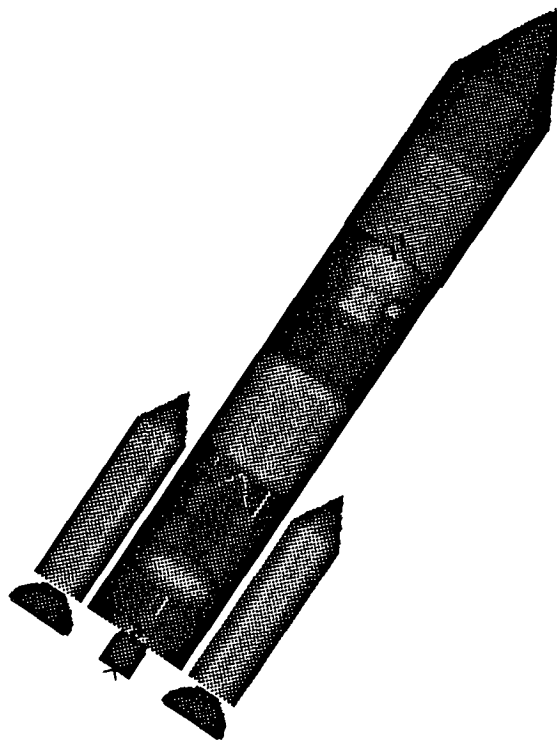


Fig 1 Transparent View of Gryphon

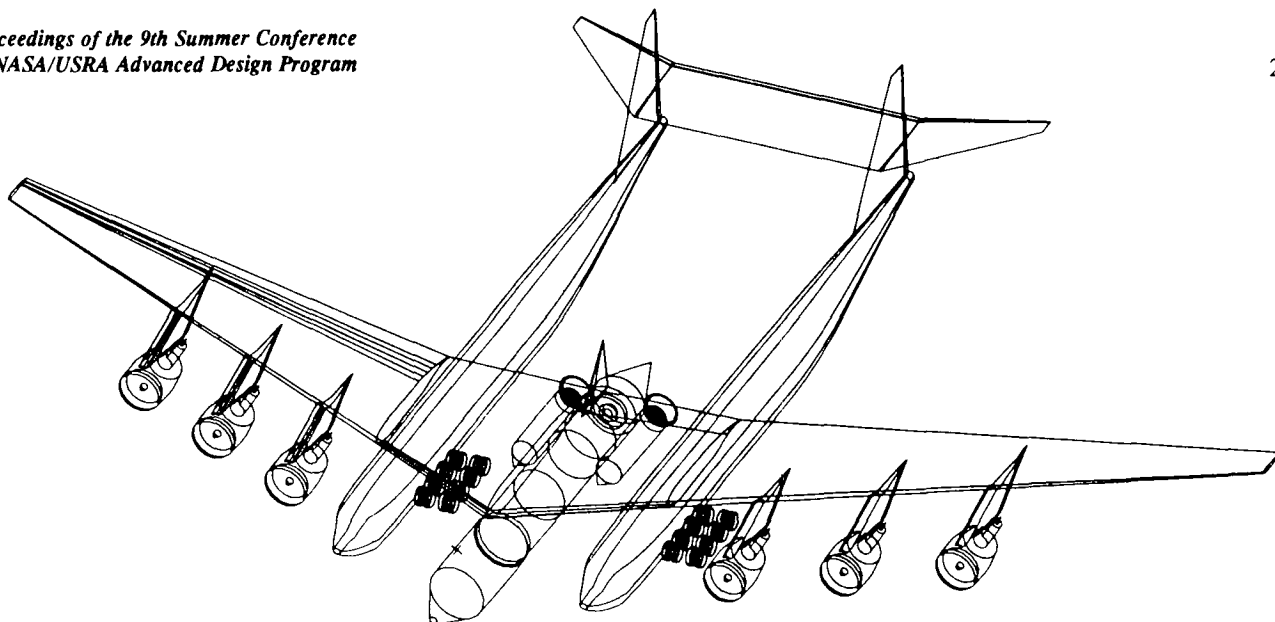


Fig 2 Gryphon and Eclipse attached

Cost Analysis

The most important aspect of this project is to give investors a 15% return on their investments. To achieve this, the cost (per pound of payload) of the Gryphon was determined in order to beat the launch prices (also per pound of payload) of chief competitors by at least 50%. This leaves the other 50% for financing, insurance, and profits while still having a competitive price.

Gryphon's main competitors in the satellite launch market are the Ariane 4, Atlas Centaur, and Titan 3. The price data for these and other launchers are listed below in Table 1. Note that Ariane prices are in 1990 dollars, Atlas and Titan prices are in 1991 dollars, and numeric figures are averages.

Table 1 Launch Prices of the Competition

Launch Vehicle	Payload Size (lb)	Launch Price	Price per Pound
Ariane 40	4,190	\$ 65 million	\$ 15,513
Ariane 42P	5,730	\$ 67 million	\$ 11,692
Ariane 44P	6,610	\$ 70 million	\$ 10,590
Ariane 42L	7,050	\$ 90 million	\$ 12,766
Ariane 44LP	8,160	\$ 95 million	\$ 11,642
Ariane 44L	9,260	\$ 115 million	\$ 12,419
Centaur	5,148	\$ 60 million	\$ 11,655
Titan 3	10,978	\$ 110 million	\$ 10,020

Using the market average price per pound of the competition derived from Table 1 and an inflation factor of 4.5% per year, a project goal cost per pound of \$ 6,200 was determined. This cost per pound translates into a payload of 7,900 lb to GTO and a per mission cost of \$49 million.

The final cost analysis is given below in Table 2. The costs given are high estimates and include a fifty million dollar development cost (which is what OSC used for their Pegasus program).

Table 2 Cost Analysis

Airplane Cost	\$ 1,000 million
Project Costs	\$ 106 million
Vehicle Cost	\$ 28 million
Airplane Operating Costs	\$ 2 million

The total mission cost was calculated by dividing the one-time costs (the airplane and project costs) by sixty launches and adding the per launch costs for the vehicle and plane operation. Sixty launches was chosen as a realistic estimate for the number of launches that would be performed over ten years. This estimate is based on the recent satellite market. Table 3 shows the final mission cost of the Gryphon. It should be noted that this cost estimate meets the project goal of \$49 million per launch.

Table 3 Cost of Gryphon

Total Mission Cost (60 launches)	\$ 48.3 million
----------------------------------	-----------------

Per Launch Cost

The per launch cost of the Gryphon is \$27.9 million, while the per launch cost of the Eclipse is \$2 million. A \$1 billion fixed cost of the Eclipse must be evenly spread over each launch. For a projected duration of 60 launches, this calculates to a total average cost per launch of \$46.6 million. The minimum price that can be charged per launch and still turn a profit in the last year is \$65.2 million. This includes an additional 18% for insurance. Disregarding the amount per launch towards insurance premiums, the Gryphon grosses \$55.2 million per launch. The net profit is the amount grossed per launch minus the total expenses per launch resulting in a net profit margin of \$8.6 million per launch.

Vehicle Configuration

The Gryphon consists of three stages for the GTO configuration. For the LEO configuration, the third stage engine and propellant tanks are removed and replaced with pure payload. Both configurations use solid and storable liquid fuels. For the GTO version, a cryogenic third stage is employed.

All of the major components on the Gryphon are listed in Table 4 and the overall parameters in Table 5. A picture detailing all of the major systems within the Gryphon is shown in Figure 3.

Table 4 Major Components

Stage 1	Stage 2
2 Castor Solid Rocket Motors	2 LR91 Liquid Rocket Motors
LR91 Liquid Rocket Motor	Gryphon-Eclipse Rings 3 - 8
Gryphon-Eclipse Rings 1 & 2	Plane Attach Rings 2 & 3
Engine Mount	External Skin
Plane Attach Ring 1	Strut Support Ring
Vertical Tail	Engine Mount
Interstage Ring	Interstage Ring
Aft Nozzle Cover	
Fairing Attach Rings	

Stage 3
1 RL10A-4 Cryogenic Liquid Fuel Rocket Motor
Payload Interface
External Skin
Engine Attach
Power/Avionics Ring
Cabling
Hydrazine/Oxidizer & Tanks
Control Thrusters
Venting System
Thermal Control
Batteries
CPU
Radar Transponder
Telemetry Transmitters
GPS
Inertial Guidance (IMU)

Table 5 Overall Parameters

Parameter	GTO	LEO
Stage 1,2,3 and ANC	479,056 lb	476,368 lb
Components on Eclipse	10,435 lb	10,435 lb
Total Gryphon Weight	489,491 lb	486,803 lb
Total Length with ANC	124 ft 3 in	104 ft 5 in
Total Length without ANC	106 ft 3 in	86 ft 5 in
Width	32 ft 2 in	32 ft 2 in
Height	30 ft 0 in	30 ft 0 in

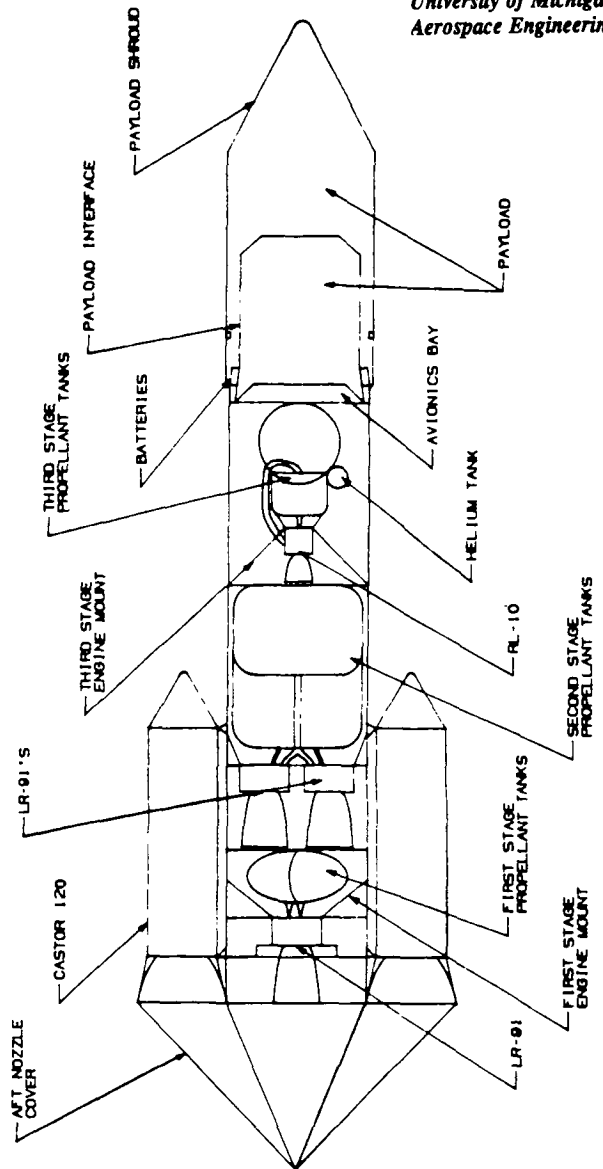


Fig 3 Internal Components

Mission Analysis

Trajectory

Analysis of the Gryphon's ascent trajectory was completed using nomographs and a series of equations. Initial vehicle parameters were read from the nomographs, and the results were substituted into the appropriate equations. A MATLAB routine was written to solve the system of equations that yielded the second stage trajectory.

Initially, the Gryphon is dropped from the belly of the Eclipse aircraft. The aerodynamic shape of the Gryphon causes it to pitch up approximately 20 degrees during the ensuing 10 second drop. At this point, the first stage engines ignite and the Gryphon begins its ascent into space.

The Gryphon pitches upward at a rate of 6.25 degrees per second until it reaches a pitch angle of 10 degrees from vertical. Pitch control is achieved by gimbaling the engine nozzles. The Gryphon pitches back down before second stage ignition, to an angle of 70 degrees from vertical. Pitch

down is achieved via a gravity turn in order to minimize gravitational energy losses.

The first stage engines burnout at an altitude of 130,397 feet and a velocity of 7,297 feet per second. Second stage ignition follows, accelerating the Gryphon to a circular parking orbit. The engines burn out at an altitude of 574,240 feet and a velocity of 24,864 feet per second. At this point, the vehicle has entered low Earth orbit (LEO). The payload shroud is jettisoned along the way, at an altitude of 200,000 feet.

The method of analysis for the second stage assumes a non-atmospheric, low altitude circular orbit and a constant pitch rate of 0.075 degrees per second.

Once the parking orbit is reached, the second stage is ejected and the Gryphon orbits until it reaches the proper position for insertion into geotransfer orbit (GTO). Finally, the third stage engine ignites, and GTO insertion is completed.

Aft Nozzle Cover Design

The aft nozzle cover (ANC) was designed to reduce the drag of Gryphon while it is being carried by the launch plane. Since the ANC is dropped into the ocean following separation from the plane, the goals for this design were to make it as light and inexpensive as possible. Initial designs have the ANC being constructed out of reinforced molded fiber glass, this should reduce weight, while giving the ANC enough strength to support its own weight and any loads incurred during the plane flight, separation and drop.

Propulsion

When designing the Gryphon's propulsion system three goals were recognized. The first goal was to assure the safety of the vehicle. This space booster is attached to an aircraft carrying crew members. Dangers of the different propellants had to be explored to minimize potential hazards to these personnel and the airplane. The second goal was to have the minimal amount of complicated connections with the Eclipse. The third goal involved the overall vehicle weight of approximately 500,000 lb. This weight required a study into high performance engines that would give as much thrust as possible for minimal propellant.

System Selection

Many various staging configurations were investigated. However, each version tested resulted in severe limitations, as seen in Table 6.

Table 6 Rejected Configurations

Configuration	Drawback
All solid fuel	Not enough payload, Too heavy
No cryogenic fuels	Not enough payload, Too heavy
Cryogenic Stage 2	Safety concerns
Extra Stage	Too expensive

Consequently, the final design resulted in a three stage system composed of:

Table 7 Propulsion Configuration

Stage	System	Fuel
1	2 Castor 120's	Solid
1	1 LR91-AJ-11	Storable Liquid
2	2 LR91-AJ-11	Storable Liquid
3	1 RL10A-4	Cryogenic Liquid

The chosen configuration allows for the Gryphon to meet its payload and ultimately its cost goals. The combination of the three fuel types allows for a successful orbit, while minimizing possible hazard.

Staging

The first stage engines include a LR91-AJ-11 mounted in the middle of the main body and two Castor 120 solid rocket boosters attached symmetrically to the sides. The elliptical propellant tanks, containing nitrogen tetroxide for oxidizer and Aerozine-50 for fuel, are mounted just ahead of the LR91. Control of the booster is provided by a vertical tail and gimbaled nozzles on all three engines.

After the Stage One engines and structure have jettisoned and a coast phase is completed, two LR91-AJ-11's ignite for the second stage. The propellants are the same for the first stage LR91 but are contained in two large, nearly cylindrical tanks. Gimbaled nozzles again provide stability.

For a GTO mission, these engines are released and after another coast phase, a RL10A-4 engine ignites and burns cryogenic propellant. Liquid oxygen is supplied from a nearly cylindrical tank just ahead of the engine and liquid hydrogen is supplied from a spherical tank attached in front of the oxidizer tank. The RL10's vectorable nozzle provides control along with RCS thrusters. For a LEO configuration, this stage is not needed and orbit can be established after the second stage. Refer to Figure 4 to see the overall propulsion system configuration.

Payloads

The Gryphon was designed with the goal of meeting several important payload delivery criterion. These payload related criterion consisted of the following:

- The delivery of 7900 lb, including payload support structures, to GTO
- The delivery of 17,000 lb, including payload support structures, to LEO
- The maximization of usable payload envelope
- The capability for multiple-satellite deployments to both LEO and GTO
- The compatibility of delivering Space Station Freedom related payload packages

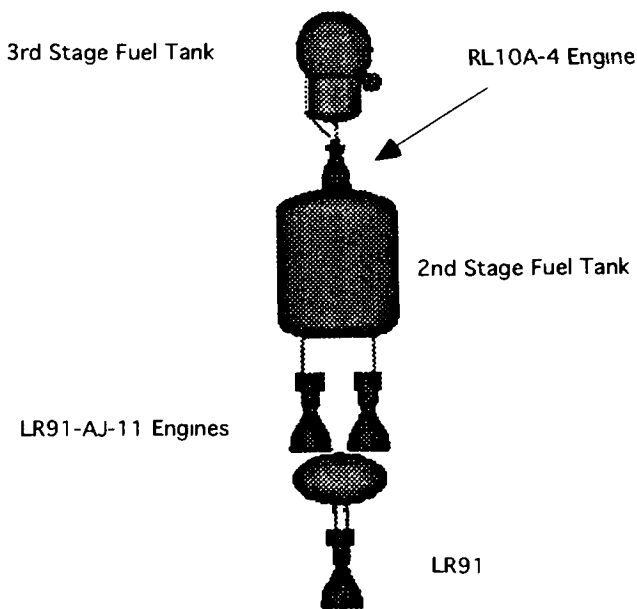


Fig 4 Overall Propulsion System

These goals acted as the driving force behind the design of the Gryphon. The delivery weights of 7900 and 17,000 lb for GTO and LEO missions were decided upon after careful consideration of the likely market demand and the cost analysis. The geosynchronous delivery limit will allow the booster to carry a large majority of the currently existing commercial communication satellites to their transfer orbits, utilizing either single or multiple payload configurations. The low earth capability will allow for the delivery of a large variety of scientific satellites, either in single or multiple configurations. This 17,000 lb limit and 15 ft diameter will also allow for the delivery of payload packages to the Space Station Freedom.

Payload Bay Dimensions

The volume of the Gryphon payload envelope was maximized in order to ease satellite design and payload configuration constraints. The maximization of the payload envelope provides several attractive features for potential booster customers. First, a large payload volume allows customers to relieve launch cost burden by participating in multiple customer/satellite deployments. Second, a large payload bay eases the design constraints which commercial and scientific satellite producers must adhere to. Third, a large payload volume, in the case of the Gryphon allows for compatibility with proposed Space Station Freedom related payload packages. These packages have a large diameter of 15 ft and lengths between 10 - 15 ft and therefore are able to be delivered by few launch systems.

Satellites are usually cylindrical in shape when in the launch configuration. They cover a large range in size, but average 7-10 ft in diameter and 8-12 ft in length. The volume of the payload bay, approximately 19,675 cubic feet, is large enough to accommodate both of these payloads in various configurations (single, double, and

possible triple stacked). The final design of the Gryphon payload envelope is shown in Figure 5.

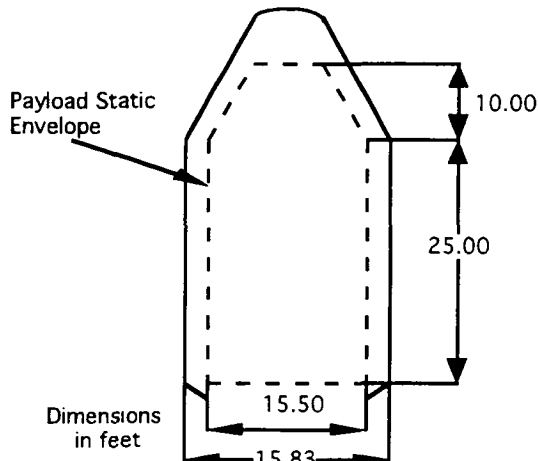


Fig 5 Payload Bay Dimensions

Space Station Freedom Options

The Space Station Freedom has been designed to be built and resupplied by the Space Shuttle. Although the shuttle may be the most efficient vehicle to boost the actual space station components into space, it is not the most efficient launch vehicle for some of the resupply missions. Therefore, the Gryphon has been designed to be capable of boosting some of the space station resupply payloads more cost effectively.

All resupply of the space station has been compacted into four main elements each designed to be held in the space shuttle payload bay. The major consideration in determining which elements the Gryphon would be able to boost was size and weight. Therefore, listed below (Table 8) are all of the elements with their respective sizes and weights (with cargo).

Table 8 Space Station Module Parameters

Module	Weight (lb)	Dimensions
PKM	34,750	Dia - 14.6 ft Length - 23 ft
MPLM	18,050	Dia - 14.6 ft Length - 12.5 ft
ULC	18,695	6.8 x 4.3 x 12.5 ft
PM	11,040	14.7 x 7.3 x 13.8 ft

Although all of the above modules are about the right size to fit into the Gryphon, the PLM is much too heavy to be considered. The PM is well below the maximum weight of 17,000 lb to LEO. The MPLM and ULC are just a little above the maximum weight. However, 41.6% of the MPLM's weight and 18.4% of the ULC's weight is in the carrier alone. If these packaging weights could be reduced by as little as 10%, the Gryphon would be able to handle these modules. Consequently, the Gryphon should be able to carry the MPLM, ULC, and PM.

Guidance, Navigation, and Control

Guidance, Navigation, and Control (GNC) is the most important responsibility of Mission Control. Mission Control must be able to accurately keep track of Gryphon's position, velocity, and acceleration in order to determine what attitude controls need to be implemented. The main areas of concern to assure the reliability of GNC are the location of Mission Control, telemetry, tracking, and command, inertial measurement, the global positioning receiver, and the on-board computer.

Mission Control. Since the Gryphon is similar to OSC's Pegasus and will be performing similar missions, there is no justification for building a new system. If the Gryphon uses the same existing ground support infrastructure the Pegasus utilizes, the missions will have already been matched to the system because of this mission similarity. Mission similarity will also have the advantage of reducing contractual negotiations required for the Gryphon.

Telemetry, Tracking and Command. The Gryphon project will employ all telemetry, tracking and command (TTC) services from the Eastern and Western Space and Missile Centers. All captive carry takeoffs from Kennedy Space Center will be supported by the eastern range, and all those from Vandenberg AFB will be supported by the western range.

Inertial Measurement Unit. Inertial reference is supplied by the strapdown inertial measurement unit (IMU), consisting of integration gyroscopes, linear accelerometers, and sensor electronics. A single gyro produces one component of the total angular inertial reference, which is known in body defined coordinates. Each accelerometer provides one component of the linear inertial constant, where each component corresponds to one body defined axis.

The Litton LR-81 system is the choice of this design. It is currently under contract for use and is thus readily available and cost effective, while providing the functions desired on the Gryphon system.

Global Positioning System Receiver. Using both cost effectiveness and reliability as primary criteria for selection, the Trimble Quadrex is the GPS Receiver chosen for use on Gryphon. Trimble also provided the six-channel GPS Receiver that was used on Pegasus, but the Quadrex is an improved version in that it includes a multiple antenna. The multiple antenna provides both better visibility and attitude determination.

Launch Panel Operator

It was decided that one additional crew member, onboard the Eclipse a Launch Panel Operator (LPO), would be needed to monitor the Gryphon's system's systems before and immediately after launch. Their responsibilities will include:

- Monitoring Gryphon and payload status
- Provide external power to Gryphon
- Switch between external and internal power (prior to launch)
- Update Gryphon IMU prior to release
- Download mission data to the flight computer and verify mission data
- Prepare and enable vehicle for drop
- Capture, record, and display data from the vehicle and payload

The LPO will be seated at a console that consisting of a ruggedized PC, display devices, a mass data storage device, and a precision IMU.

On-Board Computer

The on-board computer system interfaces with the sub-systems and determines the course of action that they should take. In short, it functions as the brains behind the Gryphon and plays a critical role in the success of the mission. Table 9 details the characteristics of the chosen computer for the Gryphon

Table 9 Characteristics of Gryphon Computer

Processor	32 bit, 68000 Motorola based
Architecture	Versa Module Europe Bus
Telemetry processor	16 bit
Weight	10 lb
Dimensions	4" x 8" x 8"
Temperature tolerance	-40 °C to +85 °C
Reliability	0.95 at end of 10-year period
Radiation protection	hardening to 1 Mrad
Vib. amplification	close to factor of 1

Communications System Overview

The Gryphon's communications system provided the link between the spacecraft and ground control after launch from the carrier aircraft. The communication system will transmit telemetry and tracking data to the ground control station and transmit termination commands, if necessary, from the ground to the Gryphon.

Tracking data will consist of position, velocity, attitude, and acceleration information received from the GPS and the IMU. If necessary, the termination command will be sent via an encoded (for security purposes) signal from the ground to be received and decoded by specific FTS (Flight Termination System) hardware on the Gryphon. All of the mission control components (i.e. the CPU, GPS, and Inertial Guidance Systems) are bolted to the top of the avionics bay (See Figure 3).

Structures

In general, each stage has the following structures:

- Engine mounts
- Propellant tank supports
- Interstage connections
- External skin with reinforcements

Additionally, the payload and avionics are supported by dedicated structures.

Investigation into the exact dimensions and structural capabilities of all of the structural components was done (where applicable) using laminate modeling, buckling analysis, ply failure analysis, stress analysis, finite element modeling and analysis and displacement analysis in SDRC I-DEAS.

Overall Structural Components

In the first stage, each Castor 120 has two sets of two attach struts which connect it to the main body of the Gryphon, which is a 1/64 in aluminum shell bolted to stringers and buckling rings. Each Castor 120 also has a conical fairing mounted on its top to reduce drag. The LR91 is held in place by an engine mount, and the LR91 and its propellant tanks are encased by a reinforced external skin. An interface ring links the skin with the interstage connector. The interstage connector sheaths the nozzles of the second stage engines.

The second stage consists of two LR91's affixed to the Gryphon by means of the second stage engine mount. The engine mount then transfers the thrust produced by the engines to the total vehicle. The reinforced external skin covers the propellant tanks and support structure for this stage. An interface ring connects the skins of the second and third stage.

The third and final stage has an engine attach which unites the RL10 with the propellant tanks. A structure mount supports the engine and fuel tanks which are designed to carry the thrust load while a payload interface attach connects the third stage with the payload area.

The volume between the power/avionics ring and the payload interface attach comprises the avionics bay. Navigational modules are attached to the power/avionics ring via an adapter plate. In the dual-satellite configuration, the first payload is mounted directly to the power/avionics ring, and the second payload is mounted to the payload interface which surrounds the first satellite. A payload shroud encloses the entire payload/avionics area. As with the Castor 120 fairing, the payload shroud conically tapers to a point to reduce drag.

For a LEO launch, the third stage is removed and the second stage interface ring is attached directly to the payload interface attach. All other structures remain the same as for a GTO launch.

Payload Shroud and Solid Booster Fairings

Both the payload shroud and solid booster fairings are constructed of the same composite materials, but with different ply orientation and core thickness. The material used is a sandwich composite of 5056 aluminum honeycomb, with piles of 0.0055 inch carbon epoxy, both of which are from the Hexcel Corporation. The choice of

this system is because of its strength, light weight, and extensive use in aerospace applications. Table 10 shows characteristics of the shroud and fairings.

Table 10 Shroud and Fairing Characteristics

	Overall Thickness	Aluminum	Carbon Epoxy	Number of Piles
Shroud	0.948 in	0.75 in	0.198 in	18
Fairings	0.485 in	0.375 in	0.11 in	10

Payload Interface

The Payload Interface (PI) supports and protects the payload during ascent. It is roughly 16 feet high and has a diameter which varies between 10 and 14 feet to adapt to various payloads. It can support two satellites with a maximum weight of 5000 lb each.

The PI consists of an aluminum skin that is 1/64" thick. The skin is reinforced with beam supports. Along the outside, eight I beams run the length of the PI. These are aluminum beams with a 1" I-beam cross section. Around the top of the PI, a ring is positioned to interface with an upper satellite. This ring was modeled as a 3" I beam section, made of aluminum. A second ring, 14' above the base of the PI, supports the structure against buckling and is a 1" I beam made of titanium. Finally, a third supporting ring is positioned 10' above the base of the structure. Again this ring mainly prohibits buckling, and is composed of titanium. The lower satellite is supported by a truss structure originating from the base of the PI, and running inside the skin. The entire structure weighs 636 lb.

Engine Mounts

Stage 1. The LR91 engine includes a 15" diameter attach ring used to join the engine to the structure. The base of the Stage 1 engine mount connects to this ring, and a tubular truss structure transmits the thrust load to the exterior hull via four attach points (see Figure 6).

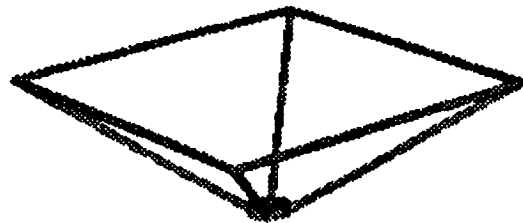


Fig 6 Stage 1 Engine Mount

The mount is constructed of A333 steel, due to its high yield strength (75 ksi), high stiffness, and availability in pipe form. Having a total weight of 349 lb, the mount is capable of transmitting 105,000 lb of thrust from an LR91 engine to the exterior hull. It has a height of 48" and fits inside the 180" hull diameter.

Stage 2. The Stage 2 Engine Mount holds two LR91 engines side by side and connects them to the external hull. The mount attaches to the engines at its base, similarly to the Stage 1 mount, and to the hull at six connection points on the top. The Stage 2 mount is shown in Figure 7.

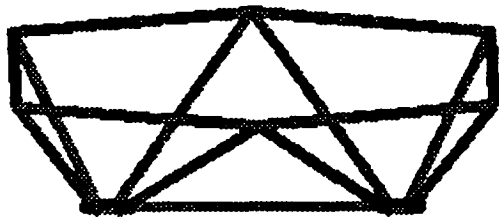


Fig 7 Stage 2 Engine Mount

The mount is constructed of A333 steel, due to its high yield strength (75 ksi), high stiffness, and availability in pipe form. With a total weight of 646 lb, the mount is capable of transmitting 210,000 lb of thrust to the exterior hull. It has a height of 40" and fits inside the 180" hull diameter.

Stage 3. The Stage 3 support structure has two primary functions. First, it supports stage 3 in the early stages of the mission and second, it connects the RL10 engine to the stage 3 spherical fuel tanks. Figure 8 shows the support structure and engine mount together.

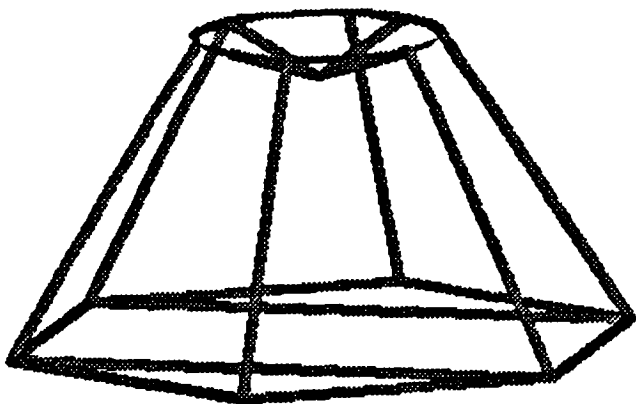


Fig 8 Stage 3 Engine Mount

During stage 1 and stage 2 burn, the structure acts as a support, carrying the 17,400 lb stage 3 under acceleration loads of up to 5 g's. After stages 1 and 2 burn out, the engine attach transmits 20,000 lb of thrust from the RL10 engine to load carrying fuel tanks. The support structure is a tubular aluminum truss with a total weight of 234 lb.

Aluminum provides a high strength to weight ratio and an acceptable stiffness for this application. The Stage 3 structure has a height of 90" in order to accommodate the RL10 nozzle inside it, and its sides slope from a diameter of 180" where it connects with stage 2, to a 72" diameter at the fuel tank interface ring.

Attitude Control

To fulfill the requirements of attitude control and payload deployment, the Reaction Control System (RCS) will use Thrust Vectoring from the main rocket engines and an additional series of small hydrazine thrusters

Free Fall

Because of the danger of an explosion when the first stage main engines are ignited, the booster must be at least a half mile (2640 ft) from the airplane before ignition can occur. To ensure the half-mile separation distance, the Gryphon must drop through a vertical distance of 1188 ft for the LEO configuration and 1258 ft for the GTO configuration. The Mission Analysis Group determined that a vertical tail will provide the required yaw control.

During the free fall period, which lasts approximately 8.5 seconds, the booster pitches up 20 degrees to allow the main engines to propel the booster into the correct trajectory after ignition. A detailed aerodynamic analysis showed that this pitch-up maneuver can be satisfactorily accomplished by utilizing the aerodynamic forces that naturally result from the free fall. The maneuver calls for the separation of the ANC from the booster as soon as enough clearance exists between the booster and the plane. For both configurations, this occurs approximately 2.25 seconds after release at an absolute distance of 261 ft from the plane. The separation of the ANC shifts the booster's center of pressure forward nearly 10 ft, greatly increasing the aerodynamic pitch-up moments that result from the booster's downward velocity.

After 8.5 seconds the booster is pitched at the correct 20 degree inclination from horizontal. The vertical drop distances mentioned above are greater than those required for the minimum half-mile separation distance. The additional drop distance was required in order to complete the pitch-up maneuver.

The analysis showed that the engines were capable of regaining control of the booster's attitude and pitch rate, and that full recovery (0 angular velocity) occurred at 14.25 seconds. The final recovery angle for the LEO configuration (84 degrees from horizontal) is higher than that for the GTO configuration (62 degrees from horizontal). Because the center of mass for the LEO booster is closer to the base of the rocket, the moment arm of the aerodynamic forces is greater for this configuration. The resulting increase in the aerodynamic pitch-up moments on the booster cause the increase in the final recovery angle.

Preliminary analysis also showed that the hydrazine thrusters have sufficient thrust (100 lb) to provide control in the roll direction for the third stage.

Hydrazine Thrusters

The Hydrazine thrusters will serve four main functions. These include:

- Spin / Despin for payload deployment or maneuvering at Space Station Freedom
- Attitude corrections during all coast periods
- Roll control on stage 3
- Reorientation before entering GTO

The MR-104 hydrazine thrusters, manufactured by the Rocket Research Company, will be located immediately above the avionics section and attach to the payload interface ring. The tanks for the fuel and oxidizer will be located in the avionics bay. Two thrusters will be placed on each of the three axes: yaw, pitch and roll.

The tanks will be made from Stainless steel 347. The oxidizer and fuel weight will equal 450 lb. This will compensate for payload deployment, coast attitude control, roll control, and any unforeseen emergencies. The approximated time of use was based on a twenty-four hour mission.

Power Systems

The on-board power systems are composed of two major sub-systems: the principal system and the ignition system. The principal power sub-system supplies power to the on-board systems (such as the computer and communications equipment) while the ignition power sub-system supplies power to the engines for startup.

Principal Power Sub-System

The principal power sub-system will consist of lithium thionyl chloride batteries. This type of primary battery (non-rechargeable) is available off-the-shelf and is packaged in individual cells, each of which operates at a specific voltage and contains a fraction of the required power. It was determined, by examining the power requirements of all the Gryphon's on-board systems (See Table 11) that Li/SOCl₂ cells with an energy density of 642 W-h/kg and an open circuit voltage of 3.63 volts would optimize the power system performance while minimizing the cost and weight of the overall system. This sub-system will consist of four modules, each containing 8 cells and providing operational power to the Gryphon for 24 hours.

Table 11 Power Requirements of On-board Systems

Components	Power (W)
Flight Computer	250
GPS Receiver	3.5
Telemetry Transmitter (x2)	98
Radar Transponder	31
Communications	323
Thrusters	200
Inertial Receivers	200
Misc.	250
TOTAL	1356

Ignition Power Sub-System

Each of the rocket engines and the two solid rocket motors require 5 amps at 28 V DC. applied to it for up to 1 second to achieve ignition. This system consists of three modules of silver zinc primary cells. Each module will be completely independent and responsible for the ignition of all the rockets in each stage of the propulsion system. In order to meet the specifications of 5 amps at 28 V DC. for one second each module will need to contain 20 high rate silver zinc cells. Each of these cells contains 1.5 W-h of energy and operates at 1.4 volts. This means that each module will supply 30 W-h of energy at 28 V DC. which is more than is needed to activate each stage.

Thermal Control Systems

It is the goal of the thermal control system to keep all components within their specified temperature envelopes while minimizing cost and weight and maintaining reliability. The thermal control system for the Gryphon is concerned with two major areas. These areas are the external structure and the avionics bay. The external structure will use ablative coatings to provide thermal protection against aerodynamic heating during the ascent of the booster. The avionics bay will use a multi-component system which includes a helium purge, a heat sink radiator, enamel coatings, and multilayer insulation. This system will maintain the temperatures of all the electronic equipment located in the avionics bay.

Thermal Control of the External Structure

Because of hypersonic speeds during ascent, aerodynamic heating becomes an important factor in the design of the Gryphon. At speeds of Mach 8.0, temperatures of 4900°F can be felt by the booster. The composite material used for the external structure has a usable realm of up to 350°F, therefore, ablative coatings will be applied to surfaces where high heat rates occur to provide thermal protection. The ablative coatings that will be used for the Gryphon will consist of Firex and Thermal-Lag, because they are relatively inexpensive and they can be applied easily. The major surfaces exposed to high heat rates have been identified as:

- the nose cone of the payload shroud
- the nose cones of the solid rocket boosters
- the leading edge of the vertical tail surfaces

A maximum thickness of 2.5 inches of ablative coating will be applied to the stagnation surfaces of each of the mentioned surfaces. The coating will then taper as the heat rates decrease along the body of the Gryphon.

Thermal Control of the Avionics Bay

Spacecraft electronics typically have temperature limits from 0 to 80°F. The Lithium Thionyl Chloride batteries must operate at temperatures below 100°F. Consequently, a thermal control system must be provided in the avionics

bay. Thermal control of the avionics bay consists of a multi-fold system. The system includes: purging with helium, heat sink radiators, enamel coatings, and multilayer insulation.

Helium will be bled from the propulsion system and purged through the avionics bay. The purge will take place until the payload shroud is deployed. The helium purge provides forced convective cooling of the flight computer, the batteries, and certain transmitters. It will also be available for use after the payload shroud is deployed if the heat sink radiator fails. Helium was chosen since it was being used by the propulsion system for fuel tank pressurization. This option eliminated the need for two separate inert gas systems.

After the payload shroud is deployed, a heat sink radiator will provide cooling for the flight computer. The radiator has a surface area of 144 in² and is made of aluminum. Its outer surface will be coated with white enamel to improve radiative heat transfer effects.

Coatings will also be applied to critical components in the avionics bay. These coatings include white enamel and black paint, and they are used to increase or decrease radiative effectiveness. These coatings are simple devices that can be used to control the temperature passively and will add little weight or cost to the project.

Finally, multilayer insulation will be used to protect important electrical boxes and the electrical wiring against any radiative heat transfer. The insulation will consist of alternate layers of aluminized Mylar and a coarse netting. Multilayer insulation is the primary insulation used on most spacecraft and was chosen for this reason.

Gryphon Integration

To design the actual systems used in the putting the Gryphon together and attaching it to the Eclipse, several tasks needed to be completed. These include:

- Gryphon Assembly Building (GAB)
- Transportation and attachment of Completed Booster
- Physical attachment of Eclipse to Gryphon

Gryphon Assembly Building

The GAB is where the vehicle is assembled from its sub-components and the payload is integrated payloads. The GAB has been designed to have one completed Gryphon finished every two weeks.

Gryphon Assembly Building Layout. After considering several different building configurations, an assembly building with two parallel assembly lines was chosen. Two independent lines were chosen to allow greater flexibility in launch scheduling. If only one assembly line were used, launches could not be easily conducted in close succession. With two independent assembly lines, the assembly schedules could be staggered to provide one vehicle every two weeks, or two vehicles in close succession if launch windows require it. Having two independent assembly lines

also allows for some protection from delays in any step in the assembly process.

The Gryphon Assembly Process. The various components are delivered to the GAB in the Stage Build-up Area. They are unloaded using an overhead crane. Each assembly line is equipped with an 80 ton overhead crane. The crane was sized at 80 tons to allow it to move the Castor 120 solid rocket boosters. These boosters weigh approximately 60 tons and are the heaviest component of the Gryphon.

Following completion in the Stage Build-up Area, the components are picked up with the 80 ton overhead crane and placed in position on the trailer in the Stage Integration area. This area of the GAB is equipped with a scaffolding system which can be pushed up close to the Gryphon being assembled to allow easier access to all areas of the Gryphon.

Following completion of Stage Integration and Integrated Vehicle Testing, the scaffolds are pushed back and the Gryphon is rolled on its trailer into the Payload Integration and Final Systems Check Area. In each line, this area is sealed off from the rest of the GAB and maintained at a class 10,000 clean room environment. This is necessary to protect the payloads from contamination prior installation of the fairing. The Payload Integration area of each line is also equipped with a 20 ton overhead crane to be used for hoisting payloads into position for integration with the Gryphon.

Following completion of the payload integration and all final systems checks, the completed Gryphon is rolled out of the GAB and to the waiting Eclipse for attachment.

Assembly Schedule. The assembly schedule of the Gryphon was based on the Pegasus's. Due to the much larger size and complexity of the Gryphon's liquid fueled stages, considerably longer times were assumed necessary for certain assembly steps. The following table compares the two assembly schedules.

Table 12 Pegasus/Gryphon Timeline Comparison

Step	Pegasus	Gryphon
Stage Build-up and Pre-Integration Testing	3 weeks	4 weeks
Stage Integration and Integrated Vehicle Testing	1 1/2 weeks	4 weeks
Payload Integration	1 week	2 weeks
Final Systems Tests	1 1/2 weeks	2 weeks
Total	7 weeks	12 weeks

Gryphon/Eclipse Interface

The main aspects necessary to attach the Gryphon to the Eclipse are the transportation trailer, the facility, and its location.

The Gryphon Transportation Trailer. The Gryphon Transportation Trailer (GTT) supports the 500,000 lb booster, transports the Gryphon to the Eclipse without

imparting undue shocks, and can make precise orientation adjustments for alignment.

The GTT was patterned after the trailer used by OSC to transport the Pegasus from its assembly building to the B-52 drop aircraft. The trailer used to transport the Pegasus is equipped with 24 standard seem-trailer wheels on 6 axles. By comparison then, the GTT would require 73 axles and 292 wheels. It was decided that the GTT should be based on a rail system to support the Gryphon's large weight.

In order to insure proper alignment of the Gryphon with the Eclipse during attachment, the GTT must be able to shift the Gryphon from side to side and also rotate several degrees. To allow for this, it was decided that the Gryphon will be supported in a cradle which rests on top of the trailer. Large screw jacks will be mounted horizontally at the front and rear and of the trailer. By operating the two screw jacks synchronously in either direction the cradle can be moved either left or right. Operating the screw jacks differentially allows the cradle can be rotated a few degrees to make the necessary adjustments.

The Gryphon will be brought out from the GAB on its trailer and rolled underneath the Eclipse from the rear. Once it is in position, it will be lifted by four hydraulic lifts (mounted in the ground). The screw jacks on the GTT will then be used to move the Gryphon either to the left or right or to rotate it to achieve proper alignment. If the fore and aft positioning is incorrect, the Eclipse can be pushed forward or backward slightly, or the Gryphon could be lowered, pushed forward or aft on the rails, and lifted up again. Once correct alignment has been achieved, the Gryphon will be raised the last few inches and the hydraulic interface mechanism closed, thus securing the Gryphon to the Eclipse. The GTT can then be lowered back onto its rails and removed.

Gryphon Facility Location

The location of the facility was based on the availability of rocket fuels on site, proximity to the equator for GEO launches, distance from large population centers, and the availability of a 10,000 ft runway.

Based upon these requirements it was decided that the Kennedy space center was the best place to locate the Gryphon Facility for GEO launches. However, a small percentage of the launches might be made to very high inclination (polar) orbits. For these orbits, Vandenberg Air Force Base was chosen as the launch site for the west coast. For these missions, a Gryphon would be ferried unfueled from Kennedy to Vandenberg by the Eclipse and then fueled and launched.

Aircraft/Booster Interface Mechanism

The best configuration was found to be two four point, attachment systems on the second stage, symmetric about the center of gravity. All of the pins lie within the second stage. With the exception of pins 1 and 2, a circular support structure had to be designed at the pin locations. The first two pins were purposefully placed at the interstage between stage 1 and stage 2 due to the structure

required there. Pins 5 and 6 are placed at the attach ring required for the struts connecting the two Castor 120 engines. Some of the key aspects of this system are shown below (see Table 13).

Table 13 Characteristics of Gryphon/Eclipse Interface

Hook Cross Sectional Area	16 in ²
Maximum Pin Length	27 in
Total System Weight	11,104 lb
Total Pin Weight	1328 lb

Pin Layout. In order to fully analyze the different possibilities, a finite element model was constructed in I-DEAS. It was determined to run different configurations using finite element models in order to find the best pin layout on the Gryphon. The parameters determining the best pin configuration were:

- Distribution of forces on pins
- Stability of configuration
- Structural Dynamics

Having approximately the same force on each pin would mean only one type of hook and pin combination had to be designed. This would greatly reduce manufacturing costs. Due to the overall need to reduce costs and ability to meet the requirement, only one combination was chosen.

Required Hydraulic Force. The hydraulic force to operate the system was calculated using a worst-case-load. It was calculated by using the forces on the pin/hook combination, the friction coefficient between the pin and hook and the geometry and the lengths of the lever arm and connecting rods. The hydraulic pressure provided by the plane was given at 5000 psi. It was noted that pumps could be added for emergency pressure loss and additional hydraulic force if needed. Using the hydraulic pressure, the pistons were sized by calculating the worst-case load force required. After completing the detailed analysis in I-DEAS the pistons cross sectional area was found to be 10.54 in².

Materials. The material used for the structural members throughout the interface system is a heat treated, quenched and tempered, steel alloy ASTM-A242. This alloy was chosen due to the fact that it is the strongest construction material in yield shear strength.

G-Force Loads. The maximum G-Force was given from the Eclipse Design Team to be 2.5. This was then multiplied by the structural factor of safety and the dynamic loading coefficient to obtain the overall system factor of safety of 4.

Conclusion

Project Gryphon is the beginning investigation of a 500,000 lb air launched space booster. This Phase I study demonstrates the viability for a venture of this type.

Ultimately, the cost effectiveness of the Gryphon will determine its future. As demonstrated in this summary, the Gryphon has the capability of providing investor's a 15% return, which would provide a corporation a profitable endeavor. As with all projects, one can expect that changes will occur as the process develops. However, the initial results definitely merit continued study into large sized air launched space boosters. For a more detailed explanation of the process and analysis that went into the Gryphon, consult the Gryphon Air Launched Space Booster Report.

Acknowledgments

The author would like to acknowledge all those individuals involved in Project Gryphon. The 40 students of Aerospace 483 Space System Design at the University of Michigan deserve the credit for the work and commitment needed on a project of this nature. Although be restrained by a tight budget was quite difficult to work with, it helped the group feel as if its endeavors were realistic and worthwhile. And everyone should be commended for sticking together to meet the budget.

Special thanks also go to Professor Joe Easley for all of his support and for providing all the resources needed to make for a technically sound project. Teaching Assistant James Akers must also be mentioned for all of his outstanding contributions. Without his guidance and support, we may have never gotten as far as was possible.

Robert Lovell of OSC presented the idea behind all of the work and must be thanked for his help. Also, Lisa Kuhout of NASA Lewis Research Center must be mentioned for providing support when needed.

TETHERED ATMOSPHERIC/IONOSPHERIC RESEARCH SATELLITE (AIRSAT)

University of Michigan
 Departments of Aerospace, Electrical, Mechanical and Nuclear Engineering
 and the Department of Atmospheric, Oceanic and Space Sciences
 Ann Arbor, Michigan

Professor Brian E. Gilchrist
 Andrew Santangelo, Teaching Assistant
 Penny Niles and Paul Doud, Student Authors

Abstract

The AIRSAT research group has designed a proof-of-concept tethered research satellite to be launched into orbit as a secondary payload aboard a Delta II rocket. Following the precedent set by the initial tethered satellite flight demonstration missions, Tethered Satellite System-1 (TSS-1) and the Small Expendable Deployment System-1 (SEDS-1), AIRSAT is proposed to be the first to deploy downward into the Earth's upper atmosphere and lower ionosphere with the intention of conducting proof-of-concept measurements of a scientific and technological nature.¹ The external and internal sensor arrays will collect information concerning electron density and temperature, ion concentration and relative ion temperature, sub-satellite surface pressure, acceleration of sub-satellite, tether tension, attitude stability, and orbital decay. The design is innovative in concept and emphasized not only low cost but also a rapid transition from design completion to flight.

Introduction

The *in-situ* exploration of the Earth's upper atmosphere and ionosphere and the development of aerodynamic technology capable of operating in this altitude regime has been both slow and difficult. The altitude is too high for aircraft and balloons and too low for extended operations by satellites (due to atmospheric drag) making research of the region a formidable challenge. However, it remains an important transition region for atmospheric and ionospheric processes and for future aerospace transportation systems.²

To address this issue, an interdepartmental class of students from five departments in the University of Michigan College of Engineering was asked to develop a complete proof-of-concept mission to evaluate and demonstrate the use of tethered satellite technology for remote exploration of the Earth's upper atmosphere and lower ionosphere as well as to conduct transition flow flight research. In addition to being a technically innovative design, the initial constraints emphasized simplicity, rapid turn-around from concept to flight, and low cost.³

Mission Overview

General Mission Specifications

- **Spacecraft Type**
 - Unmanned, downward deployed tethered satellite system
- **Launch System**
 - Secondary payload on Delta II 7925 configured for Navstar GPS Satellite as the primary payload
- **Mission Duration**
 - 24 - 30 hours

To significantly lower the overall cost, the mission is based on the secondary payload concept; the AIRSAT system will be transported into space mounted on the second stage of a launch vehicle carrying a separate primary payload. The capability for this type of design has previously been developed and demonstrated by NASA using the Delta II 7925 rocket whose primary payload is a Navstar Global Positioning System (GPS) satellite. For this reason, AIRSAT will be launched aboard a Delta II although the design could easily be modified for other launch vehicles such as the Titan II or Pegasus. On the Delta II, the secondary payloads are mounted on the guidance section of the second stage. The mounting locations are on a ring surrounding the guidance equipment, but still within the fairing. The payload envelope on the Delta II is shown in Figure 1.

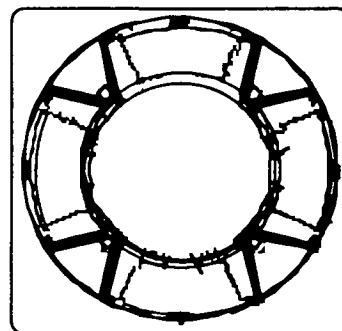


Figure 1. Top view of payload envelope of Delta II

A side view of the Delta II payload, as shown in Figure 2, demonstrates the side mounting of the AIRSAT platform on the Delta II second stage.

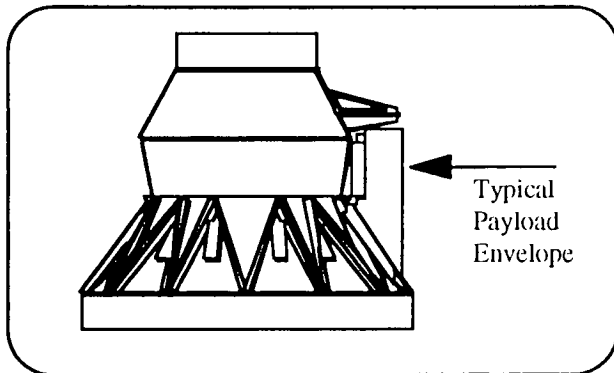


Figure 2. Side view of payload envelope of Delta II

These mounting locations present a challenging packaging task for the AIRSAT system, and present many design constraints. The AIRSAT system maximizes the Delta II secondary payload capability in both mass and volume and utilizes all four available sectors.

Table 1. Expected mission timeline

Time	Action
0 seconds	Launch
260 seconds	Delta II First Stage Burnout
380 seconds	Delta II Faring Separation
1267 seconds	Delta II Third Stage Separation
4473 seconds	Circularization/Depletion Burn
4533 seconds	Sub-satellite Ejection
8 - 24 hours of deployed operation	
Second stage decays to 175 km - tether is cut; sub-satellite and tether re-enter	

As shown in Table 1, prior to the ejection of the sub-satellite, the Delta II will undergo first stage burnout, fairing separation and finally third stage separation. After the third stage separates to carry the primary payload to its orbit, the AIRSAT mission will begin.⁴ By making use of fuel margins and the attitude control capabilities of the second stage, the orbit of the vehicle will be circularized from the initial elliptical orbit of the primary payload to the circular orbit prescribed for the AIRSAT system. Normally, extra second stage engine fuel is burnt off in a depletion burn. However, in this mission, the extra fuel will be used in the circularization to provide the needed total velocity impulse of 155 m/s to reach a circular orbit at an altitude of 215 km. After orbit circularization, a depletion burn will be instituted, but the second stage will be oriented such that

this burn will only produce a slight increase in the inclination angle - the orbit will remain circular. Next, the second stage will be oriented so that the sub-satellite is facing downward toward Earth. From this position, the sub-satellite is ejected from the launch vehicle and the attitude control system will reorient the second stage so that the tether canister and deployment mechanism are lined up with the deploying tether. Over the next five hours, the sub-satellite will be deployed toward the Earth at the end of a 60 km long, 1.3 mm diameter tether. Throughout deployment, until the attitude control fuel is exhausted, the attitude control system will be used to stabilize the second stage. When the initial altitude of 155 km is reached, the sub-satellite will experience atmospheric drag forces causing the orbit of the system to decay into the atmosphere over the next 8 to 24 hours.

Throughout the deployment (215 to 155 km) and operational periods (155 to 120 km), the sub-satellite will be taking scientific measurements of the atmosphere and ionosphere, and measuring transition flow flight characteristics as well as tethered satellite characteristics with its array of sensors. The data will be transferred from the sub-satellite to a computer in the second stage, and from there to ground stations via microwave telemetry links. When the probe reaches 120 km, the orbital decay will be very rapid, so the tether will be released from the second stage. The sub-satellite and tether will quickly descend and burn up in the atmosphere, while the second stage will remain in orbit to transmit the remaining data from the computer's memory. The second stage will stay in orbit for at least one year before its orbit decays into the atmosphere.

Scientific Research

Sensor Overview

- **Tensiometer:** Tether Tension
- **Ionization Gauges (12):** Surface Pressure
- **Thermocouples (14):** Heat flux through sub-satellite
- **Accelerometers (3):** Sub-satellite acceleration
- **Retarding Potential Analyzer:** Ion concentrations and temperature
- **Langmuir Probes (2):** Electron Density and temperature
- **GPS Receiver:** Position and orientation of sub-satellite

As was noted above, it is difficult to make *in situ* measurements and operate in the altitude regime below 150 km which is a transition region between the "vacuum" of outer-space and the Earth's upper atmosphere. However, the use of tethered satellite technology offers the opportunity to overcome some of the limitations with proper system design, instrumentation, and aerodynamics. The mission of

AIRSAT is to make fundamental ionospheric and atmospheric measurements, observe aerothermodynamic phenomena on a satellite in the transition region, acquire data which specifically describes the dynamics of a tethered satellite system (proof-of-concept measurements), and to help determine how the tethered satellite concept can be applied to scientific and engineering research in the near earth space environment.

Figure 3 is an isometric view of the sub-satellite and the sensor array. Due to mass, volume, and cost constraints in this first AIRSAT mission, the number and type of sensors is limited. For measurements of the natural environment, the primary focus is on ionospheric sensors, only requiring neutral gas measurements to characterize the immediate environment surrounding the sub-satellite. Based on the results of this first mission, it would be possible to provide a new instrument complement which emphasizes the neutral atmosphere characterization.

The ionosphere is made up of a diffuse plasma. The electrons and ions do not necessarily have the same temperatures, so there will be different types of sensors to measure each one independently.⁵ For electron temperature and density information, two Langmuir probes will be placed on the sub-satellite such that they are perpendicular to the velocity vector.

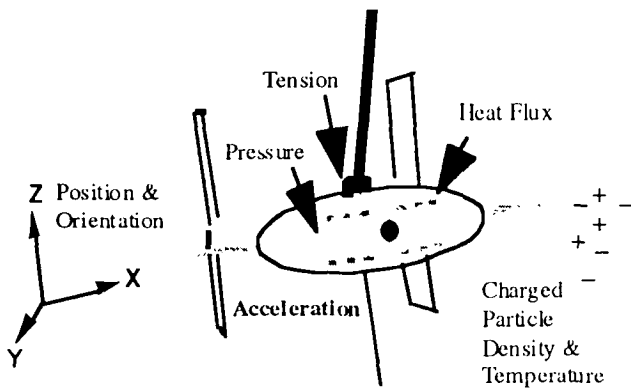


Figure 3. View of sub-satellite emphasizing sensor array

A retarding potential analyzer (RPA) will measure ion concentrations and average relative ion temperature. A complex grid system which varies with voltage allows ion collection at different rates depending upon the directed energy and mass of the particle. A two cm diameter orifice allows particles to enter the RPA for collection and is placed in the center of the leading sub-satellite surface heading into the ram direction. From these electron and ion I-V curves, fundamental ionospheric characteristics can be deduced.

Other observations will monitor the behavior of the second stage, tether, sub-satellite system. Two tensiometers provide tether tension information at the sub-satellite and the second stage. The tensiometer at the sub-satellite is made of three load cells sandwiched between two pressure plates. This also provides information on the angle which

the tether makes with the sub-satellite axis. The Global Positioning System (GPS) will be used to provide sub-satellite attitude information and general location. GPS operates by decoding precise microwave transmitted time-coded signals from various NAVSTAR satellites in high earth orbits (around 20,000 km). These signals are combined with knowledge of the orbital positions of the broadcasting satellites to triangulate the exact position of the receiving antenna. The GPS system can give very accurate attitude information by monitoring the phase differences between three different signals received at three non-collinear antennae placed at least 18 cm apart on the sub-satellite. Position of the sub-satellite can be measured to well below 100 m accuracy in the three directions. Additionally, three pairs of pressure sensors in an anemometer-type configuration will also provide attitude information while flying in the transition region.

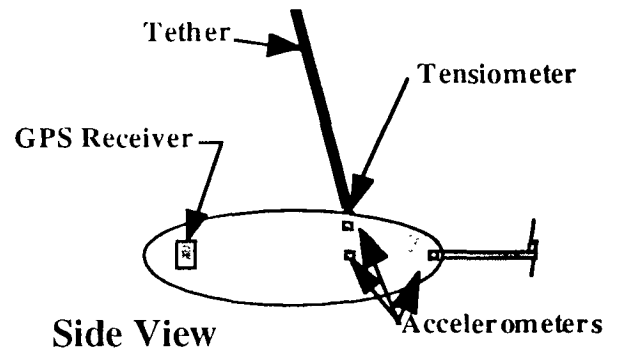


Figure 4. Internal sensor layout of sub-satellite

Finally, observations will be made to describe the aerothermodynamic behavior of the sub-satellite. These include measuring the surface heat transfer with heat flux sensors, sub-satellite surface pressure with ionization gauges, and total sub-satellite acceleration (3 axes) using miniature accelerometers. Internal placement of engineering sensors is shown in Figure 4 and external sensors in Figure 5.

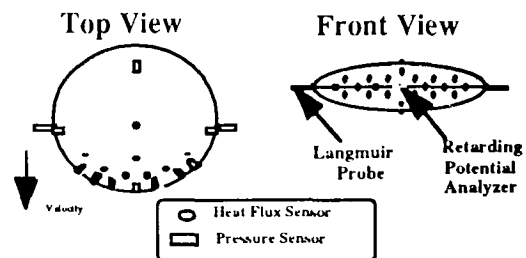


Figure 5. Sub-satellite external sensor layout

The tri-axial accelerometers within the sub-satellite will consist of three orthogonally-aligned sub-miniature linear accelerometers. Ideally, these three accelerometers should

be placed at the center of inertia of the sub-satellite. However, due to the unusual volume constraints, this is not practical. Instead, acceptable results should be obtained as long as each accelerometer is only displaced from the center of inertia in a direction along its sensitive axis (see Figure 4). In this manner, vibration of the sub-satellite should not cause undue distortion of the acceleration signal.

Fourteen heat flux sensors will be used to measure the heat transfer to the surface of the sub-satellite. This will be done by differentiating the temperature between opposite sides of the sub-satellite skin. As heat is transferred through the surface, two thermocouple junctions will generate small voltages. The difference in voltages between the two junctions is interpreted as proportional to the temperature differential. The predicted surface temperature of the sub-satellite as a function of altitude is shown in Figure 6.⁶

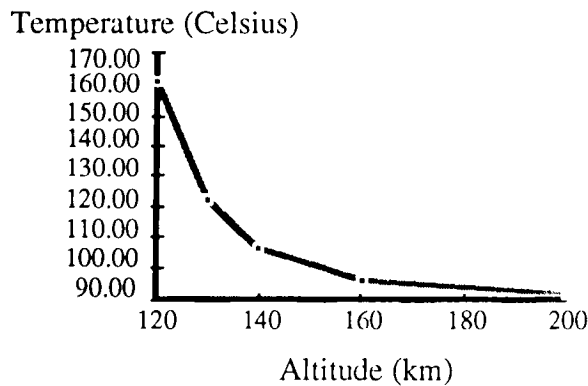


Figure 6. Surface temperature of the sub-satellite as a function of altitude

Twelve ionization gauges will measure the pressures experienced at different points on the sub-satellite surface. The Bayard-Alpert Gauge is a hot filament ionization gauge. The gauge is operated by bombarding and ionizing the gas in the gauge with electrons emitted from the heated filament. The resulting ion current collected by a collector anode is proportional to the ambient pressure in a gauge.

Structures and Payload Integration

General Sub-satellite Structures Specifications

- **Mass:** 105 kg
- **Overall Length:** 3.05 m
- **Structural Components**
 - Material:** Aluminum
- **Primary Insulation**
 - Material:** Polymide Resin RMR-15
- **Internal Propulsion:** None

The structure of the sub-satellite must be capable of containing and protecting the various scientific instruments and support devices. Since the AIRSAT mission will be launched as a secondary payload, the sub-satellite and all its support systems must fit within the limited space of the four compartments of the secondary payload area. The sub-satellite will be exposed to a wide range of temperatures and pressures. It must survive aerodynamic heating and drag forces while orbiting at 7400 m/s, as well as large forces, shocks and vibrations during launch, fairing separation, and rocket stage separation.



Figure 7. AIRSAT Conceptual Sub-satellite Design

The sub-satellite design that most accurately fulfilled all the mission requirements is shown in Figure 7. It consists of a circular ellipsoid (saucer-like) capsule and a pair of stabilizer wings that are mounted on a boom behind the capsule. The tether is attached to the top of the sub-satellite, above the center of mass. There is also a keel attached below the capsule to aid in roll and pitch stability. Figure 8 provides a side view of the tethered sub-satellite in its fully deployed configuration.

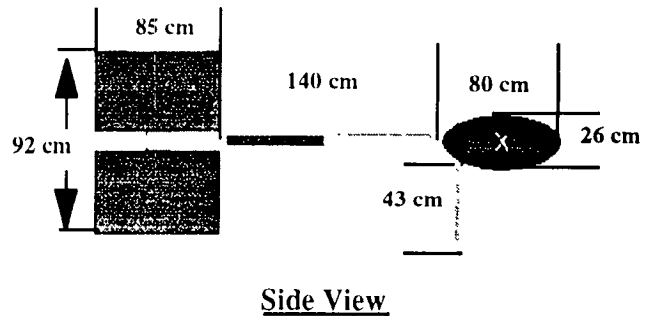


Figure 8. Sub-satellite Dimensions

The capsule contains electrical and communications devices that support the various measurement instruments that are mounted on and through the surface of the sub-satellite. All internal equipment is attached directly to a framework which is made of an aluminum "T" section. The framework is bent or machined to follow the elliptical contour of the capsule and laid out in a radial pattern. All external components, such as the boom, the tether

connection, and the keel, are also connected to the frame through the skin.

A telescoping boom connects the wing stabilizers to the main capsule. The boom needs the extra complication of a telescoping mechanism to be both short enough to fit in the allowed secondary payload volume, and long enough to provide a good moment arm for the stabilizing wings. The wing system consists of two vertical wings, each divided into two sections. Each section consists of a frame of aluminum rods that support a thin aluminum sheet. The multiple wing sections allows for a folded configuration that will fit within one of the secondary payload areas. In deployed position, the two vertical wings are set apart by a cross beam so that they will not be in the aerodynamic flow 'shadow' of the capsule.

The keel consists of an aluminum rod and endmass that aid in the stability of pitch and roll by lowering the location of the sub-satellite's center of mass. As with the boom and wings, the keel is folded to fit within the payload area.

Prior to ejection from the second stage, each component unfolds itself. All of the eight movable mechanical joints are spring loaded. The springs store enough potential energy to provide the momentum to unfold the components and lock them in place. The joints are designed to provide the desired motion and locking mechanism to secure each component's position, as well as aid in the unfolding.

The sub-satellite's frame and skin are made of aluminum. Its ease of fabrication, low cost, and low density make it a desirable aerospace material. Its electrical conductivity and its ductility make it a good skin material. The conductivity of the skin provides a consistent ground potential for measurement instruments. The outside surface is coated with aluminized Teflon to reflect solar radiation (to reduce heating), and to maintain electrical conductivity.

Some components inside the sub-satellite, such as the battery, must be protected from excessive heat. Most of the heat will come from skin friction with the atmosphere, and most of that is at the leading edge of the sub-satellite. To insulate the interior, a polyimide (PI) resin is placed inside the skin. This material has a favorable combination of thermal stability, processibility, structural reliability, and long service life. The insulation is tapered from a thick layer at the leading edge, to a thin layer at the trailing edge.

General Tether Specifications

- **Type:** Non-conductive
- **Length:** 60 km
- **Diameter:** 1.3 mm
- **Mass:** ~95 kg
- **Material:** B29/12 x 1500 Kevlar
- **Construction:** Multi-layer and braided
- **Jacketing:** None required

Many factors were taken into consideration for the specification of a tether reliable enough for the AIRSAT mission. The overall tether requirements are extremely

severe considering the upper- and lower-altitude environments. The most important characteristics required for the 60 kilometer long tether, with the lower end at a 120 km altitude include:

- High strength-to-weight ratio
- Minimum strength of 1000 N
- Maximum mass of 90 - 120 kg
- Maximum diameter not to exceed 2 mm to minimize aerodynamic drag,
- Serviceability for temperatures ranging from -100° C to 1000° C
- Ability to withstand the potential degradation of atomic oxygen flux ranging from 10^{18} to 10^{21} atoms/m²-hr; and
- Effective protection against solar ultraviolet radiation.

The operational temperature and atomic oxygen requirements vary substantially along the length of the tether. Therefore, the initial design approach is to use a tether material that remains within the other constraints of minimum mass and minimal tether diameter. The one material that met each of these requirements was the Aramid fiber with the brand name KEVLAR - 29. Kevlar has strength characteristics superior to stainless steel, has low density, and can be braided to provide flexibility with low torque. It can be impregnated to provide good resistance to abrasion and protection against ultraviolet damage and can be manufactured to AIRSAT's desired length, thereby making splicing unnecessary.

Degradation due to atomic oxygen is a major concern for the tether material. Martin Marietta, NASA, and other agencies have studied the effects atomic oxygen have on proposed tethers. These groups found that for tethers comprised of Aramid fibers such as Kevlar, the damage caused by atomic oxygen was very detrimental to the structure and the strength of the fibers. This created a major concern for the longevity of the tether. At first it was assumed that these concentrations would endanger the mission and coatings or jackets would be needed to protect the tether. The two possibilities considered were a coating of silicon or a braided jacket of Nomex. These protective coatings added considerable weight and diameter to the tether. The tether could be tapered to add thickness on the lower portion without adding unnecessary weight to the portion that is clear of the damaging effects of the atmosphere. However, the Nomex jacket put the diameter of the tether to 2.10 millimeters which was over the desired diameter of 2 mm. The silicon coated tether was only 1.73 mm, but the weight and diameter was still too large to accommodate 60 km of tether in the volume that was allowed by the tether canister. A smaller tether or alternative coating had to be determined.

According to the research completed at Martin Marietta, the AIRSAT mission's duration and the length of the tether is too short for atomic oxygen to be a problem. The biggest

problem for the tether would come from temperature effects. However, temperature will not be a problem for the tether since Kevlar works well at higher temperatures.

Another concern for the tether was the possible damage or severing of the tether by micro-meteoroids. If a solid strand of Kevlar were to be used, any damage caused by the micro-meteoroids would be critical and could cause the tether to fail. However, if a tether consisted of braided Kevlar there would be no matrix to transmit a fracture stress to other filaments in the braid. The experiment of AIRSAT length would have to have enough filaments to ensure the tether would not fail during the experiment. There are two structural changes that can toughen the structure. One is to use a larger number of strands of smaller denier, such as 48x200d. The filament size and strength are the same as fewer strands and larger denier, but a local break will allow the finer braid to close in and retain a higher percentage of original brake strength. The second method is to use a successive number of layers, called braid-over-braid to allow outer layers to act as buffers. In the case of the AIRSAT tether, it would be wise to employ both methods to ensure that the tether does not break prematurely. Manufacturers recommend that designers should allow a safety factor of three or four when determining how much Kevlar to use. The tether the AIRSAT mission will be using is at least 6 times as thick as needed.

Sub-satellite Launch Mechanism

The deployment of the tethered satellite from an orbiting platform relies on the ability of the sub-satellite to pull the tether out of its storage canister. However, when the sub-satellite is close to the platform, the force from the gravity gradient is too small for the sub-satellite to pull the tether. Therefore the sub-satellite must be accelerated away from the platform in order to initiate the deployment of the tether.

If the 105 kg sub-satellite is accelerated to 3 m/s, it will have enough momentum to separate the sub-satellite and platform such that the gravity gradient can provide sufficient force to pull the tether the rest of the way. A novel ejection mechanism concept was developed to provide this initial energy.

The ejection mechanism utilizes a spring loaded extendible boom structure. The boom extends to 5 m, from an initial folded configuration of 10 cm. As the ejection boom extends, the springs in the joints of the boom transfer 157.5 kg-m/s of momentum to the sub-satellite, driving it away from the platform. Since the acceleration is spread out over 5 m, the acceleration on the sub-satellite is far gentler than a single acceleration impulse. The sub-satellite itself has a boom and wing structure that could be damaged by very strong acceleration. The momentum of the sub-satellite from the spring loaded boom is augmented by 157.5 kg-m/s from a compression spring situated in the center of the boom. This compression spring initiates the ejection process and increases the momentum of the system to a total

of 315 kg-m/s. The sub-satellite ejection scenario and second stage rotation is shown as a series of time sequenced sketches in Figure 9.

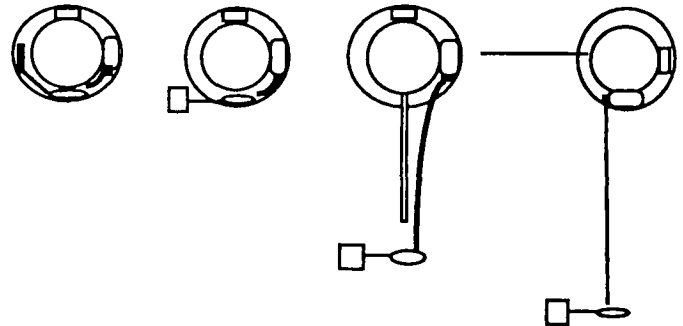


Figure 9. Sub-satellite ejection scenario

The ejection boom has another advantage besides the gentle application of energy to the sub-satellite. The boom will hold the sub-satellite in a relatively fixed attitude as it is ejected. This will minimize any 'tip off' tumbling of the sub-satellite as it begins its deployment. If tip off is excessive, the sub-satellite could become tangled in the tether.

The ejection boom is designed as series of 10 rings, connected together by 51 jointed linkages. Three evenly spaced linkages connect adjacent rings. The linkages are staggered so they will store compactly in the folded position. Each linkage has a torsion spring in its joint that provides the energy to extend the boom and eject the probe. A small section of this ejection boom has been prototyped.

Dynamics and Control

General Dynamics and Control Specifications

- **Eccentricity:** ~ 0
- **Sub-satellite Altitude:** 210 - 120 km
- **Inclination:** 32 - 34 degrees
- **Mean Motion:** 16.235 rev/day
- **Attitude Control:**
 - Active Control (210 - 180 km) Cold gas thrusters
 - Passive Control (180 - 120 km) Wing stabilization system

In order to get accurate measurements from the sensors placed in the second stage and in the sub-satellite, the system must be in equilibrium while in orbit. Therefore, an orbit must be selected that allows the system to attain equilibrium and be stable. The orbit will also be characterized to provide adequate ground coverage to ensure that the data collected from the sensors can be down linked to Earth.

The orbital mechanics for the AIRSAT mission includes the orbit selection, satellite system model, and orbital maneuvers. Since the most stable satellite system occurs when a circular orbit is achieved, the system will be placed in an orbit with an eccentricity of approximately zero.

To characterize the satellite system in terms of orbital mechanics, a dumbbell model was chosen. The dumbbell model, which is shown in Figure 10, is designed to allow the motion of the center of mass of the system to represent the motion of the entire system; this drastically simplifies the analysis of the mechanics and dynamics of the problem.

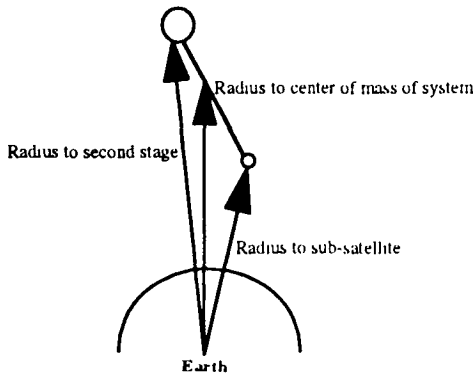


Figure 10. Dumbbell model used to characterize the tethered satellite system

The second stage of the Delta II is left in an elliptical orbit with an inclination of approximately 32 degrees after third stage separation. Since inclination change maneuvers are costly in terms of fuel consumption, the second stage will remain at that inclination. However, several orbit transfers (requiring velocity impulses) will be used to transfer the orbit to the more desirable circular orbit.⁷ The first transfer burn will occur at the apogee of the initial orbit and will have a magnitude of 3.03 m/s acting in the opposite direction of the incidental velocity vector; this slows the second stage. The effect of this impulse will be to place the second stage in a transfer ellipse coincident with the desired final orbit. Figure 11 schematically shows the first phase of the orbit maneuvers.

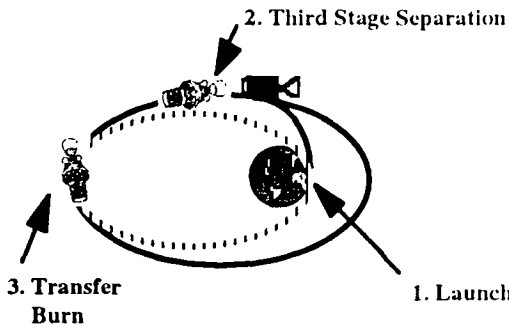


Figure 11. First phase of orbital maneuvers

The second velocity impulse occurs at perigee of the final orbit, that is, at an altitude of 215 km. The second impulse has a magnitude of 151.34 m/s also opposite to the current velocity vector and will produce the desired circular orbit at the correct altitude. Finally, a depletion burn will occur to deplete any excess fuel that remains. This burn will act only to produce a slight increase in the inclination of the orbit. Figure 12 schematically shows phase two of the orbit maneuvers.

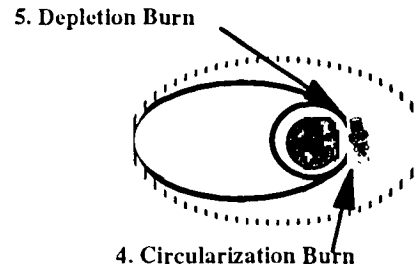


Figure 12. Second phase of the orbital maneuvers

The effects of the atmosphere on the system, aerodynamic drag and orbital decay, were also explored so that the lifetime of the mission could be maximized. The predicted aerodynamic drag on the sub-satellite as a function of altitude is shown in Figure 13. The aerodynamic drag of the second stage is orders of magnitude smaller due to its higher initial altitude even though its effective surface area is at least twice as large.

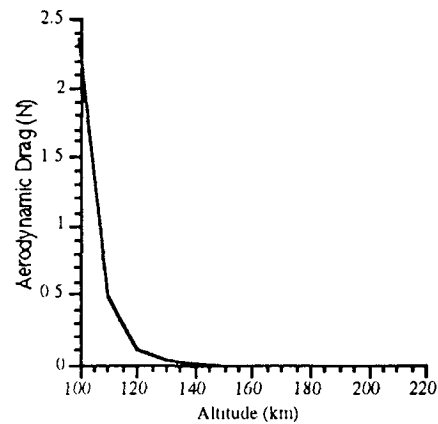


Figure 13. Aerodynamic drag on the sub-satellite as a function of altitude

The drag on the tether is an important issue in determining the dynamics of the system. To predict the maximum drag that the tether would be subjected to, the drag was computed at the center of pressure (where the drag force would be the largest) and integrated over the length of the tether. Although this value varies with altitude, in free molecular flow, the maximum drag is expected to be on the order of 10 Newtons.⁸

When these graphs are analyzed, it is apparent that the maximum lifetime of the mission can be obtained when the second stage is in a circular orbit of 215 km after the tether is deployed.

The orbital decay of the system is a direct result of the aerodynamic drag experienced by the components of the system. Under nominal conditions, the mission is expected to last from 24 - 30 hours. However, the maximum orbital decay that the system could occur as a function of altitude is shown in Figure 14.

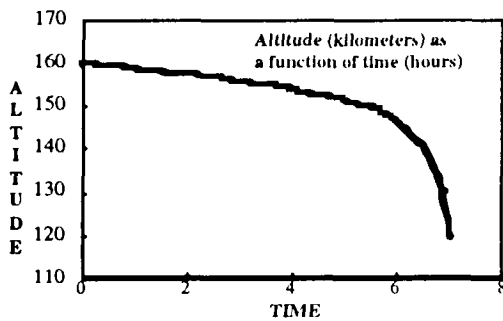


Figure 14. Maximum orbital decay

A 60 km tether will be used to deploy the sub-satellite downward into the Earth's upper atmosphere. Therefore, the sub-satellite will be at an altitude of 155 km after the tether is fully deployed. The tether will be deployed using a length rate control law. Using this law, the tether will be deployed at exponential and uniform rates and the whole deployment procedure will take approximately 5 hours.

Active and passive control systems will be used during the AIRSAT mission to provide stability and to perform some of the maneuvers required during the mission. The second stage of the Delta II has an active control system which will be used to provide stability, to rotate the rocket after the sub-satellite has been launched, and to circularize the initial orbit. Both active and passive control systems will be used to stabilize the sub-satellite. Attitude thrusters will be used when the sub-satellite is outside the atmosphere and a keel structure and the tension in the tether will be used to help provide stability in pitch and roll. When the sub-satellite is inside the atmosphere, a passive control system will be used. The passive system consists of wings attached to a boom, a keel structure, and a nutation damper. The wing configuration will provide stability in yaw, while the keel structure and tether tension will provide stability in pitch and roll. A nutation damper will be placed in the yaw plane to damp out any perturbations in the motion of the system in this plane. The attitude thrusters can also be used when the sub-satellite is in the atmosphere in case of any large perturbations in the motion of the system.

Communications

General Specifications

- **Sub-satellite to Second Stage Link:**
 - Frequency: 2.2 - 2.3 GHz
 - Data Rate: 9.6 kbps
 - Effective Isotropic Radiated Power (EIRP): 18.4 dBW
 - Bit-error-rate: 10^{-5}
 - G_r : 0 dB
- **Second stage to Ground Station Link:**
 - Frequency: 2.2 - 2.3 GHz
 - Data Rate: 38.4 kbps
 - EIRP: 4 dBW
 - Bit-error-rate: 10^{-5}
 - G_r : 54 dB

The primary task of the communications systems is to acquire all the data from the sensors and successfully down link the information to ground stations. As suggested in Figure 15, the process begins with the sensors on the sub-satellite.^{9,10} Their output is collected and processed for uplink to the second stage. The second stage then stores all the information into its memory where it is kept until it is transmitted to ground stations.

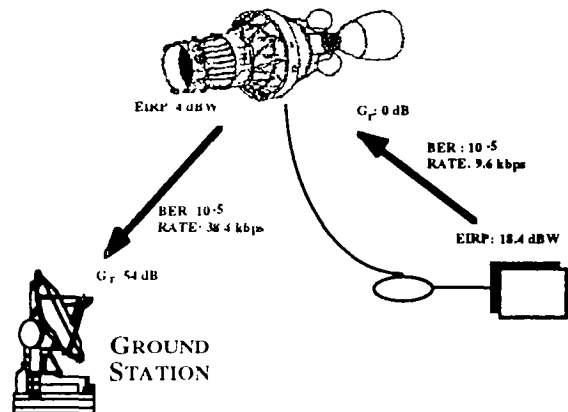


Figure 15. Communications down link overview

Due to the small size of the sub-satellite, the primary goal in the design of the communications systems was to minimize its mass and power requirements. Therefore, a direct link to Earth was ruled out because it required greater mass and power budgets within the sub-satellite. By first sending the data to the second stage, a distance no greater than 60 km, the higher powered system required for transmit to the ground can then be placed on the second stage. Figure 16 schematically shows the sub-satellite communication system.

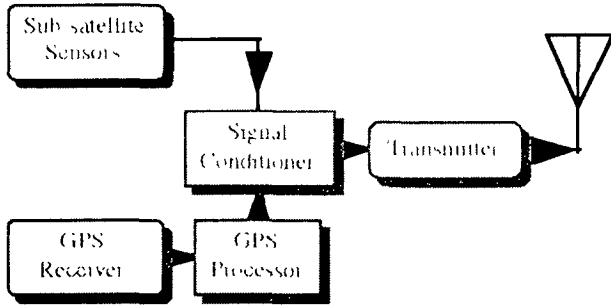


Figure 16. Sub-satellite communication system

The sub-satellite to second stage link will operate between 2.2 and 2.3 GHz with a data rate of 9.6 kbps. This rate is sufficient for the sub-satellite sensor data rate. Once it arrives at the second stage it is put into the computer's memory after going through initial data processing. This on-board processing reduces total data per orbit required to be transmitted to the ground to 500 kbytes. The memory can hold 4 orbits worth of data (see Electrical Systems) with newly archived data over-writing the oldest stored data. The computer's memory is then continuously transmitted open-loop to ground stations on Earth. This link transmits at a rate of 38.4 kbps and assures that at least two orbits worth of data can be down linked while over one ground station, which is approximately six minutes of coverage. On the average AIRSAT will pass over a minimum of one ground station per orbit. This configuration allows 100% transmission of data. The ground coverage for the mission is shown in Figure 17.

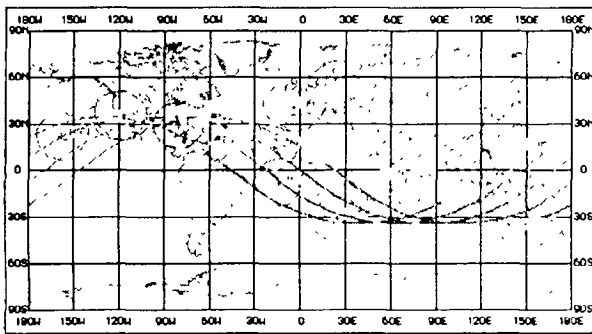


Figure 17. Mission Ground Coverage

The overall system was designed to have a bit-error-rate (BER) of 10^{-5} . This is equivalent to having ten error bits for every one million bits transmitted, resulting in a very reliable and accurate overall link. The Effective Isotropic Radiated Power (EIRP) of each link is sufficient to guarantee this BER.

Electrical and Computer Systems

Power is essential to the operation and proper functioning of the AIRSAT mission. In the design of a power supply, many factors must be considered to insure the

safe and reliable operation of the mission. A power source must fit within the mission constraints while providing adequate power to all of the systems. In addition, cost, reliability, equipment safety, size and weight must all be considered carefully. After analysis based on these criteria the decision was made to use batteries as the power source for both the sub-satellite and second stage systems. Table 2 lists the specifications of the batteries chosen for the sub-satellite and second stage.

	<i>Sub-satellite</i>	<i>Platform</i>
Chemistry	Silver/Zinc	Silver/Zinc
Cost	\$20,000	\$4,000
Nominal Voltage	29.6 V	28V
Capacity	4.1 kW-hr	7.0 kW-hr
Total Mass	33.6 kg	59.1 kg
Total Volume	23.4 L	24.7 L

Table 2. Mission battery specifications

Through research of commercially available qualified batteries, Ag/Zn batteries were chosen as the best fit within the mission's constraints while supplying adequate power. Two small - cell battery packs have been selected to provide power on the sub-satellite; with each cell providing 14.8V, a series combination provides a nominal voltage level of 29.6 V. At 140 A-Hr, this will provide a total power of 4.1 kW-Hr to all of the sub-satellite's internal systems. On the second stage, a single - cell Ag/Zn battery with a nominal voltage of 29 V will be used. It will provide 7.3 kW-Hr to all of the second stage's AIRSAT systems at an operating current of 250 A-Hr.

Not only must adequate power be supplied to all of the on-board systems, it must also be delivered reliably and efficiently. The design of a distribution system is as important as the source itself. Many of the systems requiring power need different input voltages, which must be accommodated by the distribution system. These voltages must be regulated to avoid line noise and voltage spikes which could hamper the operation of a system. Fault and surge protection must be employed to insure the reliable operation of the systems; a power failure in any system would render it inoperative, and as many of the systems are essential to the mission such a failure could cripple or even end the mission. Therefore considerable care must be put into the design of a reliable distribution system. Two main options exist for a distribution system: a centralized power source or a distributed architecture. The former uses a single voltage source and employs the use of DC/DC converters to provide the required voltage levels to the various systems, while the later relies on the use of multiple batteries at different operating voltages. Pros and cons exist for each system, but after an analysis the decision was made to use a distributed power system.¹¹ Figure 18 is a schematic diagram of the platform distribution system.

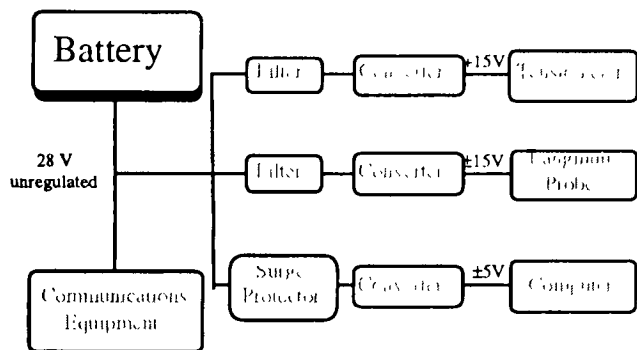


Figure 18. Platform distribution system

In addition to the power supplies and distribution systems, a computer system must be used aboard the platform to perform control functions and data handling procedures. A microprocessor based computer is needed to process and store the experimental data being uplinked from the sub-satellite, and to control the communication of this data to the ground stations. In addition to the data handling, the computer will also be responsible for the timing/sequencing of the mission, primarily to control the operations and systems control during deployment. To meet these needs as well as conforming to the mass and size requirements as closely as possible, an Embedded Micro - Controller (model EPC - 22) from Industrial Computer Systems was selected as the best option. Operating at 25 MHz, this small computer system based on the Intel 386SL processor is capable of handling the required tasks.

Future Research

Future missions can build on the results of AIRSAT. Better knowledge of the ionosphere and upper atmosphere will improve the models used for design studies, not only for scientific research and future tethered satellite missions, but also for transonic flow flight research.

Future tethered satellites can extend the work of this mission in the following ways:

- Use a polar orbit that will allow for global coverage of the Earth.
- Make measurements with instruments not included in the AIRSAT complement for logistics reasons. This could include neutral constituent and concentrations, sub-satellite surface erosion, and auroral studies.
- Test other sub-satellite shapes for their aerodynamic properties, especially for minimizing drag and increasing passive stability in thin atmosphere.
- Perform longer missions that can resist orbital decay by using thrusters on the orbiting platform. This would allow for mapping at nearly constant altitude for extended periods of time.

The AIRSAT system is a complete system, from launch to down linked data. Tethered satellites are a promising

technology for exploring the Earth's upper atmosphere / ionosphere region, and to conduct research into transition flow flight. Due to its simplicity and low cost, AIRSAT is an excellent way to prove tethered satellite technology as a science and engineering tool as well as a precursor for more complex and costly missions.

Acknowledgments

We wish to acknowledge the financial support and encouragement of the Martin-Marietta Astronautics Group, NASA Universities Space Research Association (USRA), the University of Michigan Space Grant, the University of Michigan College of Engineering, and the Center for Research on Learning and Teaching (CRLT) have also provided financial support. A special note of appreciation goes to Professor Joe Easley, University of Michigan Aerospace Engineering Department, for his close collaboration and support of this interdepartmental class. Professor John Vesecky, University of Michigan AOSS Department, provided encouragement for the class and coordination for AOSS classroom resources. Professor Sridhar Kota, University of Michigan Mechanical Engineering Department, coordinated a special "subcontract" design team of students through Mechanical Engineering 450 - Mechanical Design II. There have been many from the University of Michigan faculty, other universities, NASA, and industry professionals who patiently provided technical assistance and answered student questions. We would like to acknowledge the special assistance by Mr. Chris Rupp (NASA) and Mr. Don Crouch (Martin-Marietta). We wish to thank the following guest class lecturers: Mr. Rick Barton (NASA-JSC), Professor Vincent Coppola (UM-Aerospace Engineering), Dr. Jason Daida (UM-AOSS), Dr. Jeffrey Hoffman (NASA-JSC), and Professor Timothy Killeen (UM-AOSS). Finally, a special note of appreciation by the class for Ms. Michele Maurer for her extensive assistance in the logistics of the class.

References

- 1) Rupp, C.C., and Laue, J.H., "Shuttle/Tethered Satellite System," *Journal of Astronautical Science*, Vol. 26, Jan.-Mar. 1978, pp. 1-17.
- 2) "Space Science in the Twenty-First Century: Imperatives for the Decades 1995-2015," Report by Space Science Board, National Academy of Sciences, 1988.
- 3) Wiley, J. and Wertz, J., *Space Mission Analysis and Design*, 2nd ed., Microcosm, Inc., Torrance, California, 1992.
- 4) NASA, *Delta II Launch Vehicle Secondary Payload Planner's Guide for NASA Missions*, National Aeronautics and Space Administration Goddard Space Flight Center Orbital Launch Services Project, August 1992.

- 5) Neiburger, M., Edinger, J.G., and Bonner, W.D.,
Understanding Our Atmospheric Environment,
Freeman and Company, 1982.
- 6) Dogra, V., Wilmoth, R., and Moss, J.,
"Aerothermodynamics of a 1.6 Meter-Diameter
Sphere in Hypersonic Rarefied Flow", *AIAA Journal*,
Vol. 30, No. 7, July 1992, pp.1789-1794.
- 7) Wiesel, W., *Spaceflight Dynamics*, McGraw-Hill, New
York, 1989.
- 8) Arnold, D.A., "The Behavior of Long Tethers in Space,"
Tethers in Space, Advances in Astronautical Sciences,
Vol. 62, 1987, pp. 35-50.
- 9) Tomasi, W., *Advanced Electronic Communication
Systems*, Prentice-Hall, New Jersey, 1987.
- 10) Ulaby, F.T., and Fung, A.K., *Microwave Remote
Sensing: Active and Passive, Vol. 1: Microwave Remote
Sensing Fundamentals and Radiometry*, Addison-
Wesley, 1981
- 11) Ormond, T., "DC/DC Converters Simplify System
Power Distribution," *EDN*, December 10, 1987, pp. 195-
202.

DESIGN OF A LUNAR TRANSPORTATION SYSTEM

**University of Minnesota
Aerospace Engineering and Mechanics
Minneapolis, Minnesota**

**Professor Andrew Vano
Michael Wright, Teaching Assistant**

**Dan Kottke, Nathan Clyde, John George, Dan Edwards
Greg Gulseth, Thane Hathaway, Chay Yang, Mark McNitt,
Mike Mecklenburg, Terry Johnson, Scott Ryun, Shawn Krupicka,
Anita Westberg, Jason Gadbois, Todd Bohman, Erik Fosshage,
Swee-Beng Tan, Charles Gerlach, Tom Meier, Bob Peterson**

Abstract

A significant presence on the Moon is necessary if America is to become a spacefaring nation. This presence must not be another Apollo style "Flags and Footprints" mission; it must be a fully crewed Lunar Outpost. A major investment in a Lunar transportation infrastructure must be made in order to accomplish this mission. In order to achieve this goal by turn of the century, the University of Minnesota Spacecraft Design Team has developed a Lunar Transportation System (LTS). This reusable and cost efficient system will deliver crew and cargo to the Lunar surface well into the 2020 time period. A Lunar orbit rendezvous is used to reduce mass, which splits the vehicle into two parts, each with different mission tasks. The first vehicle is the Lunar Excursion Vehicle (LEV), which is used as a Lunar lander. This cryogenic lander has the capability of carrying a crew of six or 50t of cargo to the surface of the Moon. In addition, the piloted lander is reusable and returns to Low Lunar Orbit to dock with the LTV at the conclusion of the surface stay. The second vehicle is the Lunar Transportation Vehicle (LTV) which "ferries" the lander between low Earth orbit and low Lunar orbit. Due to the large masses of the Lunar Transportation System components an exotic but by no means new propulsion concept has been developed for the LTV: a NERVA derived Nuclear Thermal Rocket (NTR).

Introduction

In accordance with the Space Exploration Initiative (SEI) if America is to become a spacefaring nation, a significant presence on the Moon will be required. The Moon is the gateway to the solar system, acting as a transportation node as well as a source of raw materials. For this reason, a major investment in a Lunar transportation infrastructure

must be made. To help reach this goal by the turn of the century, the University Space Research Association (USRA) has asked the University of Minnesota Spacecraft Design Team to develop a Lunar Transportation System (LTS). This task has been a year long design effort, culminating in a complete conceptual design of a Lunar Transportation System. The following is a summary of this design.

Mission

The first major goal of the Space Exploration Initiative (SEI) is to establish a permanent Lunar outpost. Returning to the Moon to stay will require a series of cargo and crew missions. This objective is divided into three phases. The first phase missions will send large habitation and research modules to be assembled into a Lunar base. Several crews will be sent to accomplish this task. Once this architecture is complete, the next phase is to reach steady state operation. This involves extended stays for crews who will be resupplied on a regular basis. The last phase and long range goal is to attain a level of self-sufficiency by utilizing the Moon's resources to supply oxygen and materials for the outpost.

Design Objectives

The primary design objective of the Spacecraft Design Team was to design a Lunar Transportation System which emphasizes component reusability and commonality to promote cost efficiency. However, the safety of the crew during each phase of the mission was considered paramount. Hence, no cost reduction was permitted in aspects of the design which would compromise the safety of the crew in any way. Cost efficiency was selected as a priority for the

design due to anticipated reduced funding available for space research in the near future. In addition to designing for multi-use capabilities for certain LTS components and allowing for interchangeability of parts between vehicles in the LTS, cost efficiency in the design was also achieved by maintaining an emphasis on the utilization of existing and near term technologies.

Lunar Transportation System (LTS)

The LTS is comprised of two vehicles; a Lunar Transportation Vehicle (LTV) and a Lunar Excursion Vehicle (LEV). The LEV is used as a "Lunar Elevator" which transports crew or cargo from Low Lunar Orbit (LLO) to the Lunar surface and return crew back to LLO. There are two kinds of LEVs. A cargo LEV is used for placing cargo on the Moon, while the piloted LEV is used to land and return crew. The LTV is used as a "ferry" vehicle. Its job is to transport the LEV from Low Earth Orbit (LEO) to Low Lunar Orbit and back to LEO.

Lunar Excursion Vehicle (LEV)

The generic title Lunar Excursion Vehicle is used for both the cargo and piloted LEV (see Figures 1 and 2). The main components of the piloted LEV are the RL10 engines, LEV truss, Landing Gear, LEV Crew Module (LEVCM) and fuel tanks with descent and ascent fuel. The main propulsion for the LEV are two Pratt and Whitney RL10 engines. The LEV truss contains the LEVCM interior of the truss. All other component are on the truss' exterior. The LEVCM is where the crew stays in descent to and ascent from the Moon. It also houses the main flight deck for the LTS. The cargo LEV is comprised of a truss, Landing Gear, RL10 engines and descent fuel. A larger truss and more landing gear are used to accomodate the Habitat module cargo. The main proplusion is this LEV is four RL10 engines.

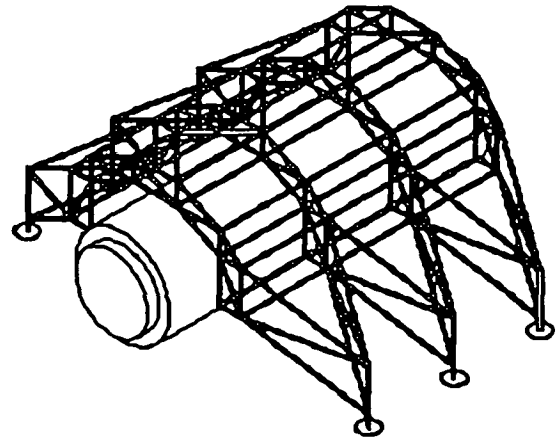


Figure 1 Cargo Lander

Lunar Transportation Vehicle (LTV)

The primary structure of the LTV is the central truss. This truss is 33 meters long, connecting the LTV Crew Module (LTVCM) to the primary propulsion system. The LTVCM is designed to support a crew of six during the transit to and from the moon. A Nuclear Thermal Rocket (NTR) was chosen as the primary propulsion system for the LTV due to it's superior performance over conventional cryogenic systems. An external radiation shield, combined with the 33 meter seperation distance provided by the LTV truss, ensures that the radiation levels in the crew module conform to NASA guidelines. The NTR uses liquid hydrogen (LH₂) as propellant. The LH₂ is stored in four tanks which are mounted to the LTV truss structure. This fuel is used during the four primary burns that the NTR performs during the mission. The LTV is detailed in Figure 3.

Earth To Orbit Vehicle

The Lunar Transportation System (LTS) has been designed to meet the goal of building and supporting a Lunar base. The first step in implementing this plan is to literally "get it off the ground."

The United States currently has no heavy lift capability. A new launch system or one derived from existing components must be developed to support the SEI requirements. It is estimated that a direct launch Lunar mission would require a 75 to 105 metric ton payload capacity at post Trans-Lunar Injection (TLI). Future Mars missions require a liftcapacity of about 250 metric tons to

Description

Transports 4 crew from lunar orbit to the lunar surface and back to lunar orbit

Sub-System Mass Table

Component	Mass (lb)
Truss	3,735
Crew Module	9,995
Primary Structure	4,270
Secondary Structure	1,633
CELSS	1,520
Commodities	600
Miscellaneous Items	1,100
Power System	1,740
Primary Propulsion	344
RL100-A (2)	1,577
Dry Tanks	613
RCS System	1724
Total Dry Mass	37794

Fuel Mass Table

Item	Mass (lb)	
Transfer from SSF		
LR2 @ 920	LOI @ 139	
Ascent	LR2 @ 6	LOI @ 18.8
Ascent	LR2 @ 12	LOI @ 18.8
Transfer to SSF	LR2 @ 800	LOI @ 844
RCS Inert Mass	40 (Hydrogen)	
Total	LR2 @ 78	LOI @ 2079

CG and Moment Table

Center of Gravity	Coordinate (ft)
(X, Y, Z)	(0, 0, 5.73)
Moment	Value (ft-lb)
Yxx, Yyy	5,264
IZZ	4,363

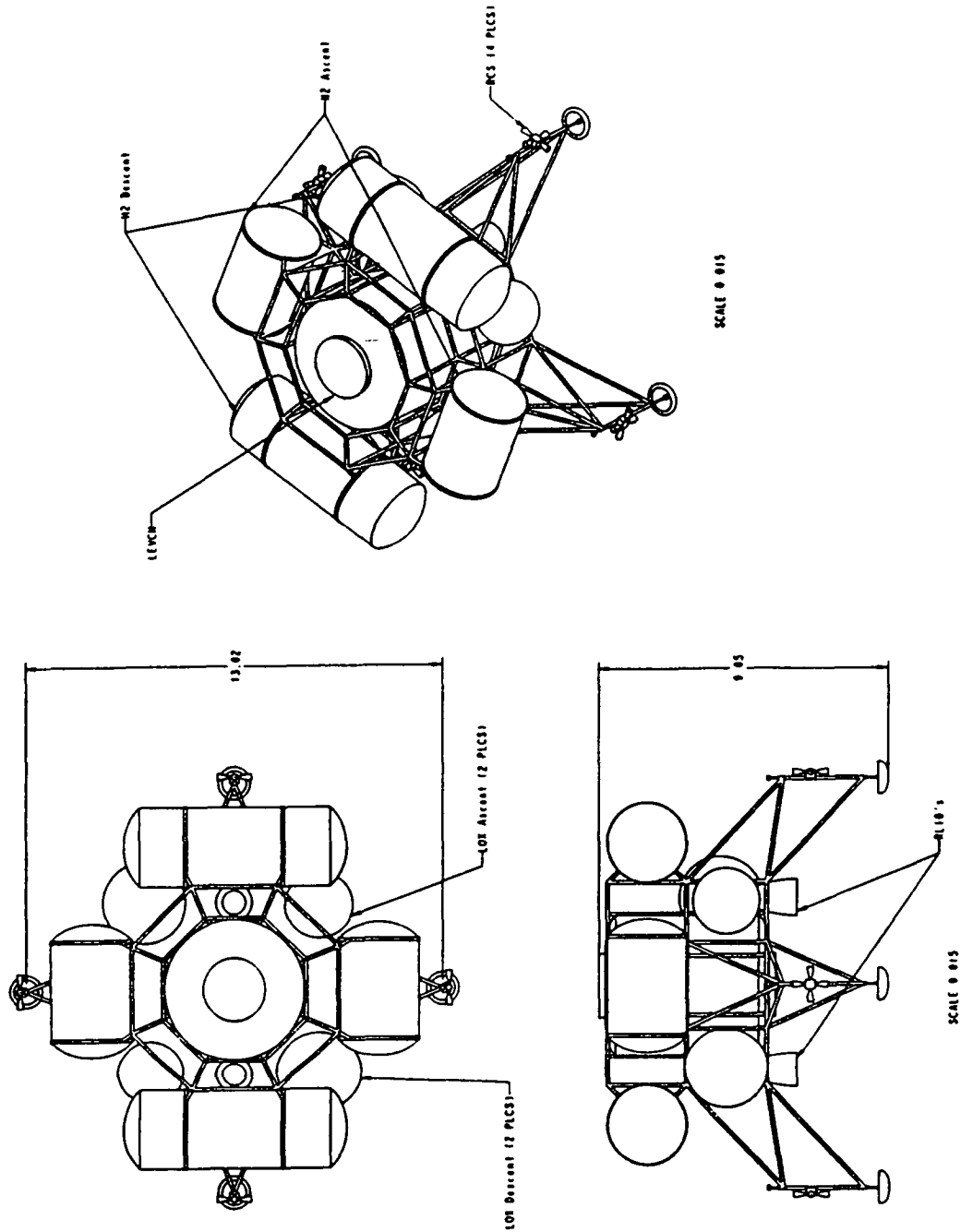


Figure 2: Piloted LEV

SPECIFICATION SHEET **Lunar Transportation Vehicle**
University of Minnesota / NASA / USRA **Lunar Transportation System**

Description

Carry the LTV and Cargo loaders to Lunar orbit and return them to LEO

Sub-System Mass Table

Component	Mass (lb)
Truss	5.5
Crew Module	10,000
Primary Structure	3,712
Secondary Structure	1,457
Internal Components	712
Crashables	1,000
Miscellaneous	2,000
Power System	3,345
Primary Propulsion	13,000
RIF	0.5
Radiation Shield	4.5
RCS System	452
Dry Load Mass	12,307
Residual Masses	0
Total	64,077

Fuel Mass Table

Item	Mass (lb)
TL1	70.2
LOI	19.99
TLI	12.39
LOC	26.50
RCS Total Mass	2,071.5 (Storage)
Total	69,727

CG and Moment Table

Center of Gravity Location	Value (in)
X - Coordinate	0
Y - Coordinate	0
Z - Coordinate	0.917
Moment	Value (lbf-in)
TL1	21,465
TLI	0.668

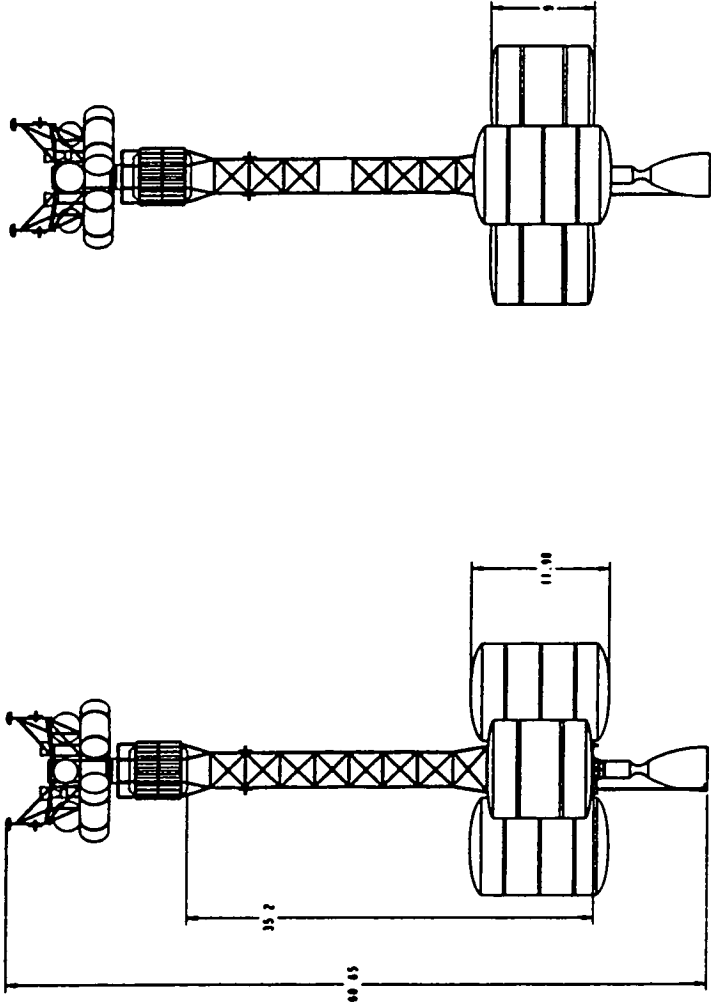
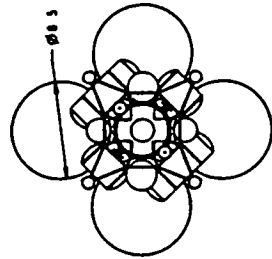


Figure 3: Piloted LTV

Low Earth Orbit (LEO). Both of these requirements can be met with the same Heavy Lift Launch Vehicle (HLLV). NASA's Marshall Space Flight Center (MSFC) has been investigating the development of a HLLV to meet these requirements.

Final Selections

The Space Transportation System (STS) derived HLLV was selected as the launch vehicle for the LTS. This vehicle in its maximum configuration provides a lift capability of 265t to LEO.¹ This design was chosen for its versatility in configurations for specific missions as listed below. Also, this design is the most cost effective and feasible launch vehicle for the near future.

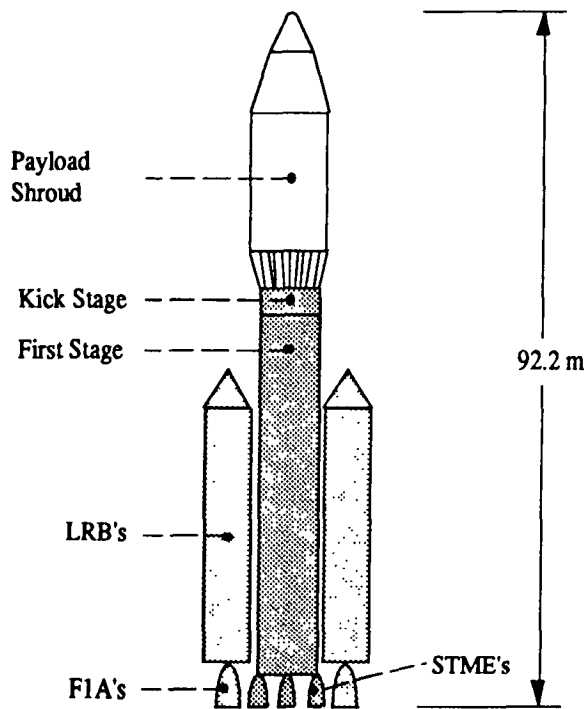


Figure 4 HLLV with 2 Liquid Rocket Boosters

The HLLV configuration in Figure 4 is capable of lifting 123t into LEO. This vehicle will be used to place the Lunar Transportation Vehicle (LTV) truss, crew module, and Lunar Excursion Vehicle (LEV) into orbit in a single launch. This vehicle will also be used to place various cargo such as the habitation module (HM) into orbit.

The baseline mission requires 130 t of Liquid Hydrogen (LH₂) fuel for the Nuclear Thermal Rocket (NTR). The density of LH₂ is 0.071 t/m³, which translates into a

volume with a diameter of 10 m (maximum) and a length of 23 m. This is too long to fit in the standard payload shroud of the HLLV, but can be accommodated by integrating the tanks into the upper stage of the HLLV. A conversation with design engineers at MSFC confirmed that this is feasible. The outside diameter of each tank is 8.4m (27.6 ft) same as the STS derived core (first stage in Figure 4).

On-Orbit Operations

Preparing for any mission requires on-orbit operations. Initially, the entire LTV must be launched and assembled. This will require two launches. One vehicle carries the truss, crew module, and LEV. The other transports the NTR. The NTR is launched separately on a Titan III for safety reasons. Assembly in a parking orbit near Space Station Freedom (SSF) follows. The major components will require minimal on-orbit construction. Instead, rendezvous and docking of the components will be all that is necessary for assembly.

Once the LTV is completed in LEO, cargo missions to the Moon will begin. Each cargo mission will require two HLLV launches. One launch will consist of LH₂ fuel, the other would deliver the heavy lander with its cargo to the LTV.

The piloted missions will involve one HLLV launch for the fuel. The crew arrives by the shuttle or a personnel launch system (PLS) to SSF and then transfer to the LTV in the LEV which will be initially docked at SSF.

Piloted Mission Scenario

A detailed account of the piloted mission scenario follows:

Low Earth Orbit At the start of the mission, the LTV is in LEO as shown in Figure 5 (following page). The fuel tanks are attached by an orbital maneuvering vehicle (OMV) from SSF. A wet tank transfer was chosen for its simplicity and level of safety. The fuel launch, attachment, and vehicle check out will take no more than one week. After the vehicle is fully assembled, the crew transfers from SSF to the LTV in the LEV. The LEV docks with the LTV for the trip to the Moon. Once the LTV has been checked out in LEO, the crew prepares for the TLI burn. Finally, the NTR is engaged and the TLI burn initiated.

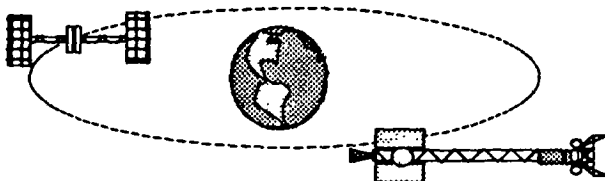


Figure 5 LTV in Low Earth Orbit

Trans-Lunar Injection The TLI burn lasts for 35 minutes, after which the LTV coasts for about three days to Low Lunar Orbit (LLO). During transit, various crew activities and experiments are performed.

Lunar Orbit Injection At this point the LTV undergoes a 9.05 minute LOI burn. This braking maneuver inserts the spacecraft into LLO.

Low Lunar Orbit Now in LLO, the LTV undergoes an orbital adjustment to the desired inclination for a landing. The crew at this time must enter the LEV. Now the LEV separates from the LTV and maneuvers to leave its orbit and descend as shown in Figure 6. At this point, the mission elapsed time is at T+ 72 hours.

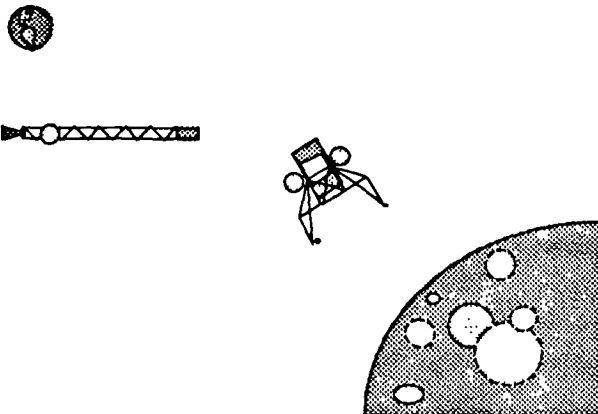


Figure 6 LEV in Low Lunar Orbit

Descent To Lunar Surface The LEV descends to the lunar surface using the RL10 engines. The burn time of descent is 17.64 minutes. Mare Cognitum (Known Sea) has been chosen as a preliminary landing site for the Lunar outpost. This is the landing site of Apollo 12 and Surveyor 3.² The coordinates are latitude: 3° 12' South and longitude: 23° 23' West. This site was selected for several reasons. The location is within the +/- 5° latitude limits set by the orbital mechanics of the mission. In addition, this site has been surveyed and photographed in detail. Finally, the Apollo 12 Lunar descent stage and Surveyor spacecraft should provide valuable data on the long term effects of the Lunar environment on materials used in the construction of the Lunar outpost.

Ascent to LLO, rendezvous with LTV After an initial stay of one lunar day (14 days), the LEV ascends to rendezvous with the LTV. The ascent burn of the RL10 engines is 10.13 minutes. Now back in LLO, the LEV rendezvous with the LTV. An orbital adjustment is made to prepare for the Trans-Earth Injection (TEI) trajectory. The NTR is prepared to be engaged for the TEI burn.

Trans-Earth Injection The NTR is engaged for a 5.15 minute TEI burn. Transit back to LEO will take about two days in which many tasks must be executed. In-transit crew activities will be performed. The LTV will execute a series of mid-course corrections. Finally, the LTV must be reoriented to the proper position needed for Earth orbital insertion (EOI). At this time determination of the status of the NTR for EOI will be performed.

Earth Orbit Insertion On approach to Earth, the EOI burn is performed placing the LTV into LEO. The EOI burn lasts for 10.82 minutes. The orbit of the LTV is adjusted to rendezvous with SSF.

Cargo Mission Scenario

The cargo scenario is very similar to the piloted case except that nothing is returned from the Lunar surface. The flight is completely automated and monitored from Mission Control at Johnson Space Center (JSC) in Houston.

Contingency Planning

Contingency plans must be made for many different system failures. Not every possible scenario could be studied in the amount of time available. Only the "worst case" scenarios which could lead to mission failure or loss of life are included.

Possible Critical System Failures

Launch The NTR will be launched separately from the rest of the LTV to reduce mission risks. In the event of a launch failure, the deep waters of the coast of Florida provides an excellent disposal option. For this reason, the launch from KSC will maintain a flight path over water up to the orbital injection point.³ Since the LTV fuel launch will consist of 2000m³ (70640 ft³) of LH₂ a launch accident resulting in an explosion on the pad would probably destroy the launch complex.

NTR: All of the following contingency plans for NTR failure refer to Figure 7.

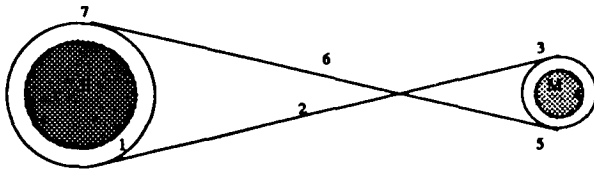


Figure 7 In Transit Contingency Plans

1. While in LEO, if a malfunction should arise before the NTR is ignited, the LTV will remain in orbit.

2. After TLI, NTR failure requires either a fly-by around the Moon and flight back to LEO in the LEV or an abort to the Lunar surface. This latter option allows the crew to complete their mission and return to Earth in the LAM.

3. In LLO prior to descent, an NTR failure requires the LEV fuel for TEI. An LEV failure requires the use of the NTR as planned to complete the trip back to Earth. Alternatively, an automated launch and rendezvous of the LAM with the LTV in LLO is also possible.

4. A problem with the LTV while the crew is on the surface requires returning to Earth in the LAM.

5. After ascent, there will be no fuel in the LEV. An NTR failure at this point requires an automated launch and rendezvous of the LAM with the LTV in LLO. The crew transfers to the LAM for the trip back to Earth.

6. After TEI, NTR failures are again considered. In the event that the NTR does not fire, there are no options for braking into LEO. The large delta V required in any type of abort at this point results in an unacceptably large mass increase on the LTV. This type of failure is considered unlikely and was deemed an acceptable risk for the mission.

7. An NTR failure in LEO also has possible solutions. The crew could be rescued with the use of an ETO such as the shuttle. In the event of a core failure, the NTR can be disposed of with the use of a specially created vehicle constructed concurrently with the LTS. This vehicle would launch the reactor core to a higher orbit with an orbital decay period on the order of thousands of years.

LEV A single engine failure on the piloted LEV can be compensated by the remaining engine and the RCS system. Descent and ascent can be accomplished with a single engine. The cargo LEV has four engines so a loss of

one is manageable, but if two or more fail the cargo LEV will crash.

Crew Modules Failure of any critical system in the crew modules are covered by redundant systems.

Delta V Requirements

Table 1 shows a summary of the delta Vs required for each stage of the LTS mission. The total mission delta V required is approximately 12.5 km/s.

Mission Phase	Delta V (m/s)
Trans-Lunar injection	3100
Mid-course correction (Earth-Moon)	10
Lunar orbit insertion	1100
Lunar descent	2000
Lunar ascent	1900
Trans-Earth injection	1100
Mid-course correction (Moon-Earth)	10
Earth orbit capture	3000
Circularization	300
Docking with SSF (minimum)	14
Total	12,534

Table 1 Required Delta V's

LTV Primary Propulsion

The primary propulsion system for the LTV is a Nuclear Thermal Rocket (NTR). The decision to pursue the development of an NTR was made after determining that the fuel requirements of an all cryogenic LTV were too massive. By using an NTR, the LTV was able to be designed to fulfill the original mission goal of providing a robust transportation system, capable of supporting a permanent Lunar outpost.

Nuclear Thermal Rockets

The use of a nuclear thermal rocket for space vehicle propulsion is certainly not a new concept. In fact, NTR propulsion has a history spanning the past 38 years. In 1955, the U.S. Air Force and the Atomic Energy Commission (AEC) began the Rover Project. Rover was directed towards the research and initial development of nuclear reactor technology for single stage Intercontinental Ballistic Missile propulsion.⁴ Several reactors were built

and tested during this program in a series of designs denoted Kiwi. In 1958, the newly formed National Aeronautics and Space Administration (NASA) replaced the Air Force as partners with the AEC as primary developer of the nuclear propulsion effort. Then, in 1959, a new program began that was to expand on the successes of the Rover Project. This new program was known as the Nuclear Engine for Rocket Vehicle Application, or more succinctly, NERVA.

At its close, the combined Rover and NERVA programs had overseen the construction and testing of twenty reactors and two complete flight engines.⁴ More importantly, these programs generated a data base that is again being reviewed by NASA, as the agency and the nation once again look towards the future of space exploration.

NTR Versus Cryogenic Systems

It is the two-fold advantage in Isp which enables an NTR to use substantially less fuel than a chemical system. This is due to the fact that the fuel mass flow rate at a specified thrust level is inversely proportional to Isp as evident in equation 1.

$$\dot{m} = \frac{T}{g_0 I_{sp}} \quad \text{Eq. 1}$$

Thus, the fuel mass flow rate required to generate a specific level of thrust is much less for an NTR than it is for a chemical system. This results in a significant reduction in the fuel required for the LTV to perform a round trip mission to the Moon. A comparison of the piloted LTV scenario is displayed in Figure 8.

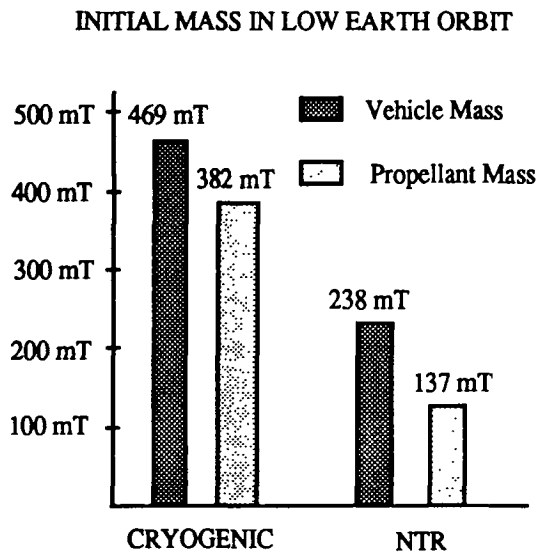


Figure 8 Comparison of Vehicle & Fuel Masses.

As can be seen in Figure 8, the use of the NTR results in a 50.7% reduction in the total vehicle mass. This translates to a reduction in the propellant mass of 64%, a savings of 245t. In steady state operation, this represents significant savings with respect to mission costs. If one estimates the launch costs for the proposed Heavy Lift Launch Vehicle at \$1000 per kilogram, the monetary savings generated through the use of the NTR surpass \$230 million dollars per launch over a comparable chemical system. The reduction of propellant mass requirements as well as mission costs are the driving forces behind the decision to employ a nuclear propulsion system for the LTV.

NTR Specifications

A modified version of the solid core NERVA flight engine is selected as the primary propulsion system for the LTV. It is estimated that a flight rated engine based on the NERVA design can be ready within six years.⁴

The NTR to be used on the LTV is an updated version of the NERVA flight engine that will be capable of an Isp of 925 seconds and 333,600 N (75,000 lbf) of thrust. The engine components consist of the nuclear reactor, turbomachinery, fuel pumps and lines, exhaust nozzle, and internal shield. The total mass of the reactor and its subsystems is approximately 8.5t. A 4.5t external radiation shield is also included to attenuate the radiation dose that the crew module will experience. This brings the NTR component mass to 13t.⁵ The internal and external radiation shielding are constructed of borated-aluminum-titanium-hydride (BATH). This shielding attenuates the neutron and gamma radiation emitted from the reactor. Hydrogen is the single propellant and is thermodynamically expanded in an Expander cycle.

End of Life NTR Disposal

Since the NTR contains radioactive material, disposal of the engine is a major concern. The end of life disposal scenario is defined with two primary considerations in mind. First, the projected service life of the LTV crew module will exceed that of the NTR. As such, any disposal scenario will have to initiate in LEO, so that the LTV crew module can be removed. Second, it is undesirable to store the NTR in any sort of near-Earth disposal location such as a high Earth orbit. For these reasons, the most likely disposal scenario consists of placing the NTR in a long-term, stable, Solar circular orbit. Additionally, the NTR could be used as the primary propulsion system for either a Mars precursor mission or a deep space science probe since at the end of the

defined NTR service life of five years, the NTR will still be capable of producing useful amounts of thrust.

LEV Primary Propulsion

While the NTR system on the LTV does an excellent job of shuttling between Earth and Lunar orbits, a second vehicle, the LEV, is required to actually send people and material to the Lunar surface. Therefore, a primary propulsion system for the LEV must also be defined.

Engine Selection

RL10A-4 engines will be used as the primary propulsion system on the LEV. The other propulsion options available for use on the LEV are quite limited. Among these options are one other cryogenic system, several storable systems and a hybrid storable/cryogenic system.

Piloted vs. Cargo LEV

Due to the differences in both mission and mass between the LEV's, they each have different propulsion systems. The unpiloted LEV must deliver 85% more mass to the Lunar surface than does the piloted LEV. Therefore, the cargo LEV will have four RL10's while the piloted LEV will have only two.

Reaction Control System (RCS)

The LTV and LEV RCS must be capable of performing both large and small maneuvers in a reasonable amount of time. These systems are limited strictly to chemical propellants. Based on the relative benefits and disadvantages of cryogenic and storable RCS options, a storable RCS is being used on the LTV and LEV.⁶ The modularity of a storable RCS greatly reduces the complexity of the entire system while also lending added redundancy.

LTV RCS Placement

It is necessary that the LTV vehicle be able to maneuver freely in all six degrees of freedom. This will be accomplished by strategic placement of eight, quad-directional RCS pods on the LTV. To improve maneuvering time of the LTV, the RCS pods will be located as far from the LTV center of mass as is practical. The pods will be placed on each face of the truss, forming two rings of thrusters at each end of the vehicle.

LEV RCS Placement

The best location for the lander RCS at this time is on the lander legs themselves. This removes the nozzle exhaust from any sensitive lander components and utilizes long moment arms to help in craft rotational maneuvering. The thruster fuel tank can be located inside the structure of the landing leg.

Fuel Requirement Breakdown

The LTS fuel mass requirements are shown Figure 9. The fuel requirements for both missions are separated into the six major propulsive phases.

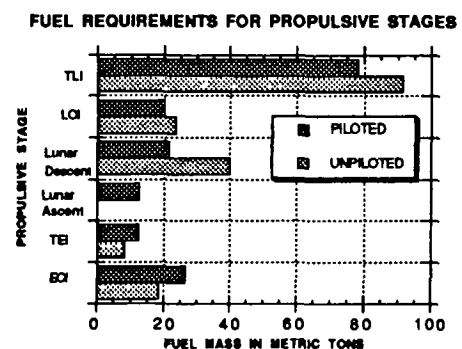


Figure 9 Fuel Requirements for Mission Phases

Figure 9 shows that the unpiloted mission consumes more fuel in TLI, TEI, and Lunar descent, while the piloted mission consumes more fuel during all return stages. This result is intuitive when one considers the large amount of mass which the unpiloted mission leaves on the Lunar surface. The total NTR fuel requirement for the piloted and unpiloted missions are 137.2 and 141.5 metric tons respectively.

LEV Truss

The truss structure for the piloted LEV is shown in Figure 10. The truss is octagonal, consisting of three tiers spaced vertically 2.5 meters apart. Each tier of the truss consists of two rings, an "inner" and "outer" ring, oriented concentrically within the tier, one inside the other. The purpose of the second concentric ring was to provide increased in-plane rigidity of the tiers. The inner rings of each tier are circumscribed about a circle of 4.5 m diameter, to provide 0.05m clearance between the truss and crew module. The outer ring of each tier is circumscribed around a circle of 6.5 m diameter. This dimension was selected so that the truss would fit within the shroud of the launch

vehicle, while maintaining reasonable mass and rigidity. The LEVCM is mounted concentrically within the truss to provide it with maximum support during landing on the Lunar surface. The crew module has a cylindrical shape with a diameter of 4.42m (14.5 ft) and a height of 5m (16.4 ft). The landing gear, fuel tanks, and the cargo are attached to the truss at the nodes where several members intersect. These nodes are called "hardpoints" and are the optimal location to attach the components of the LEV. The advantage of the hardpoints is that the tendency to induce bending moments in the truss members is minimized, which reduces the risk of buckling in the truss at loads below the critical buckling load.

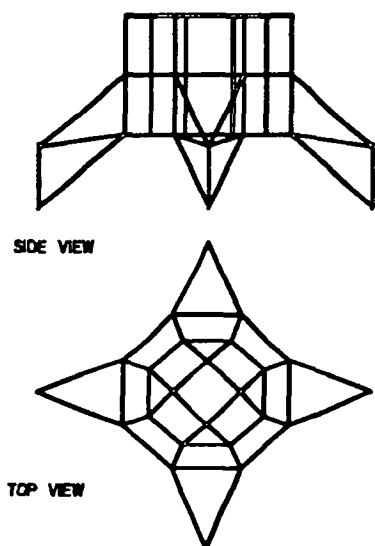


Figure 10 LEV Truss Configuration

The placement and mounting of the engines to the truss structure was considered from two criteria. First, a minimum clearance between the bottom of the engine and the Lunar surface at touchdown of 1.5m (4.92 ft) was established to ensure that the engines would not be damaged by Lunar dust and debris during landing. In addition, the distance from the bottom tier of the LEV truss to the ground was set at 3m (9.84 ft) to allow the astronauts to easily maneuver beneath the vehicle. Finally, the height of the RL-10A engines is 2.22m (7.55 ft). These constraints established a mounting location on the vehicle within the truss. Hence, the engines mounts are attached to the middle tier of the truss approximately 1 m above the bottom tier. The engine mounts are attached from the top of the RL-10A engine both to the inner and outer rings of the middle tier.

The material selected for the LEV truss structure was a particular Aluminum Lithium (ALi) alloy, known as

Weldalite 049. This material was selected because of its superior strength to weight ratio. Weldalite provides tensile strength values comparable to steel with mass density on the order of aluminum. Titanium alloys have also been considered for use on the LEV truss, particularly in areas where increased strength is a more significant factor than weight reduction, such as the landing gear and engine mounts.

LTV Truss

The primary function of the LTV truss is to maintain the LEV and LTV crew module 33 m (108.3 ft) from the Nuclear Thermal Rocket to keep the radiation exposure to the crew within acceptable limits. In addition, the truss must provide support to the fuel tanks which contain the fuel mass for the NTR. The design for the LTV truss is presented in Figure 11.

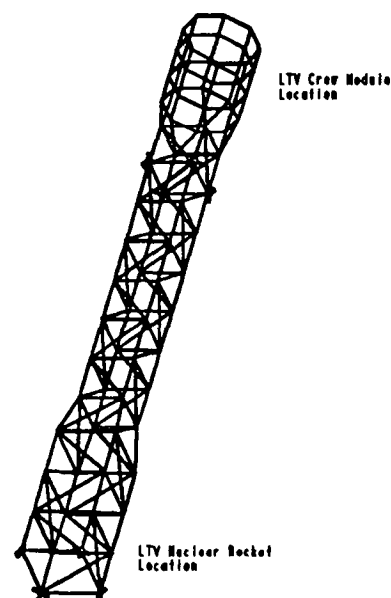


Figure 11 LTV Truss Configuration

As is shown in Figure 11, the truss consists of rectangular cross-sections spaced at three meter intervals. At the end of the truss where the fuel tanks are attached, the truss sectional dimensions are 4m (13.1 ft) by 4m (13.1 ft) to allow the tanks to mount to the truss without interference between them. Away from the fuel tanks, the truss sections reduce to three meter square sections. The end of the truss which supports the LTV crew module has an octagonal shape, both to provide structural support to the crew module and to allow for the LTV truss to butt up to the LEV truss. In addition to the rectangular members on the truss, diagonal members are also included along its

length in an alternating pattern to provide rigidity against torsion and bending. As with the LEV, the components of the LTV are attached at the "hardpoints" of the LTV truss to minimize the bending moments applied to the truss members.

Thermal Analysis

The LTS must endure a number of thermal loads during its mission scenario. While in orbit around the Earth, in transit to the Moon, in orbit around the Moon, or in return transit to Earth, the LTS experiences approximately 1400 W/m^2 incident radiation to its external surfaces at all times. In addition to direct radiation, there are also reflected radiative inputs to the vehicle from the Earth and Moon. Finally, internal heat generation sources such as the NTR and LTVCM and RL-10A engines provide additional loads as well. Effective thermal control of the LTV thus requires mechanisms to redistribute heat about the vehicle to prevent concentration of heat in one region, which might lead to thermal stress gradients in structural members, and mechanisms to exhaust heat to the surrounding space. In the absence of an atmosphere, the only active heat transfer mechanism for exhaustion of waste heat is radiation. Thus, the most important thermal control mechanism on the LTS is its external coating. Hence, the entire LTS truss and components are painted with a white paint with an effective absorptivity of 0.36 and emissivity of 0.9. This coating helps to reduce the amount of heat entering the system on radiative-input surfaces and increase the amount of radiation leaving on radiative-output surfaces of the vehicles at all times. In addition to the white paint coating, the LTV will rotate about its centerline to prevent the development of thermal gradients due to nonsymmetric solar input. Also, the LTVCM will be shielded by rotating louvers, which shield the crew module from solar radiation and allow for radiation from the crew module to space on the shadowed side of the truss. Finally, the LTVCM is also equipped with a heat pipe, which also reduces thermal stress gradients in the structure by assisting in the redistribution of heat within the surface of the crew module.

Cryogenic Boiloff

Both the LEV and LTV make use of chemical fuels which must be maintained at cryogenic temperatures to maintain liquid phase necessary for proper engine operation. Several issues arise when transporting cryogenic liquid fuels in the harsh space environment. The boiling temperatures of LH₂ and LOX are approximately 21°K and 92°K, respectively. While the ambient temperature in space is 3°K, the intense

thermal energy from the sun, radiation reflecting from the earth's surface and radiation reflecting from the moon's surface cause an effective temperature above the boiling temperature of the cryogenes.⁷ Thus, there is heat transfer from the exterior surface of the fuel tanks to the fuels within. This results in a tendency for the cryogenic fuels inside the fuel tanks to evaporate. This evaporation is known as boiloff. If the boiloff is not effectively controlled, it can jeopardize the mission by reducing the available useful fuel mass and increasing the pressure within the tanks. Losses due to boiloff are prevented with the use of Multilayer Insulation (MLI) on exterior surfaces of all cryogen tanks. The MLI serves as a thermal blanket that surrounds each tank. These blankets are attached to the tanks with velcro straps and Lexan pins.⁷ An outer jacket surrounds the MLI to protect the tanks from dust and meteoroids.

LTV Crew Module

The LTVCM is designed to support a crew of 6 for the transit between LEO and LLO. All life support systems (Environmental Control and Life Support System-ECLSS) on the LTVCM are independent of the LEVCM. In the event of a system failure, the LEV can take over life support functions. The LTVCM utilizes a Space Station Common Module (SSCM)⁸. This is done to reduce development and production costs. The external dimensions of the LTVCM are 4.42 m (14.5 ft) diameter and 5 m (16.4 ft) in length

Internal Layout

The placement of internal components is shown in Figure 12.

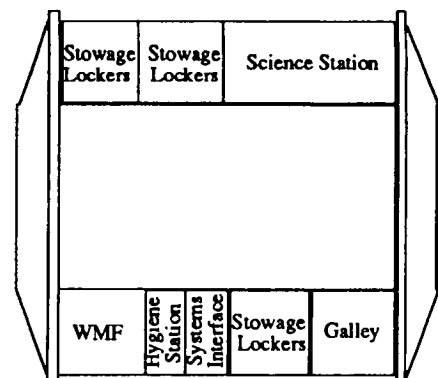


Figure 12 LTVCM Component Layout

The galley, Waste Management Facility (WMF) and hygiene station are all space station standards. The science

station will support both crew intensive and autonomous experiments.

LEV Crew Module

The LEVCM supports a crew of six for both descent and ascent operations to the Moon. It also serves as a transfer vehicle between SSF and the LTV during normal operations. The LEVCM can provide primary life support to the crew in the event of an abort due to NTR failure. Like the LTVCM, the LEVCM also utilizes the SSCM. The exterior dimensions of the module are the same as the LTVCM (see Figure 12).

Internal Layout

The dimensions of the internal usable space on the flight deck and dust containment deck (DCD), depicted in Figure 13, are 2.2m by 2.2m (7.22 ft by 7.22 ft). These dimensions were determined from the internal diameter of the module (4.22 m) and the rack depth (1.016 m). The usable length of the module is 4 m (13.1 ft). The height of the dust containment deck is 2.10 m (6.9 ft) so that a crew member can comfortably stand in the DCD while donning an EVA suit. The height of the flight deck is 1.75 m (5.74 ft).

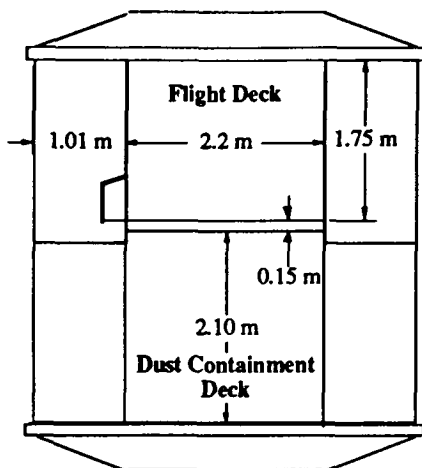


Figure 13 LEVCM Internal Dimensions

Figure 14 depicts the layout of the flight deck. The Commander (CDR) and Pilot (PLT) each have a side panel containing system interfaces. The side panels give both the CDR and PLT access to system function controls with minimal movement.

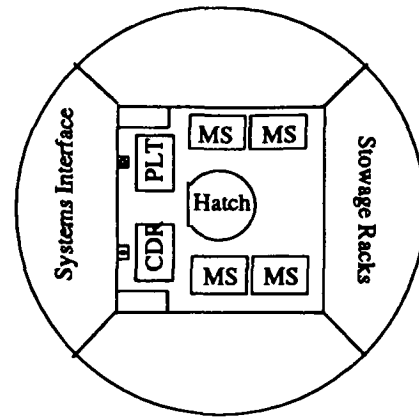


Figure 14 LEVCM Flight Deck Layout

The Mission Specialists' (MS) seats (Figure 14) were rotated 90 degrees to allow for more leg room and easier mobility in the 1/6 g environment of the Moon. The MS seats are removable and can be folded to a height of 0.28 m (11 in) for stowage.

Crew Radiation Exposure

The radiation sources that pose the greatest threat to the crew are galactic cosmic radiation (GCR), solar particle event radiation (SPE), and radiation from the NTR. The GCR at an altitude above 38000 km with no shielding is 57 rems per year. This equates to approximately 1 rem per mission. The radiation levels due to the NTR is approximately 5.48 rems per mission. Total radiation exposure for the mission fall under NASA guidelines of 25 rems in a 30 day period.⁹

LTS Avionics

In order to reach its destination, the LTS must have a system of avionics. This system will entail a set of subsystems that include communications, Guidance Navigation & Control, and data management. Failure of any of these systems can lead to a major mission catastrophe. A primary requirement of the LTS avionics is that it be useful for both piloted and unpiloted missions. All subsystems must be controllable by both pilots and ground controllers.

LTS Power Systems

In order to meet the power requirements of the LTS, power generation systems need to be included on the LTV and LEV. The power system on the LTV will consist of solar panels attached to both 6.25 meters of the octagonal truss section and 12 meters of the square truss section. The power output of the solar panels will be able to meet the 10.294 kWe demand of the LTS when the LEV and LTV are docked together. The LEV will have an additional power generation system consisting of fuel cells in order to meet the 8.041 kWe demand of the LEV when it is undocked from the LTV. On the Lunar surface additional power for long stay times will be supplied to the LEV by "plugging" it into the Lunar Habitation Module's power system. This information is summarized in the following table.

LTV Power System

Type of Power Generation: Photovoltaic

Power Available (We)	Peak Power Demanded (We)
10300	10294
Power System Mass (kg): 1345	

LEV Power System

Type of Power Generation: Fuel Cell

Power Available (We)	Peak Power Demanded (We)
10400	8041
Power System Mass (kg): 1746	

Conclusion

To reclaim the prestige of space, the United States must act now. The Moon is a valuable commodity both as a source of raw material and a stepping stone to the rest of the solar system. The Lunar Transportation System can cost effectively perform the needed task by 2005. If the United States waits too long they will be surpassed by other countries that know the value of the Moon and are willing to exploit it. Now must be the time or we will surely lose our edge.

References

- 1 Cook, Stephen and Hueter, Uwe; "Launch Vehicles For The Space Exploration Initiative", AIAA 92-1546, NASA-Marshall Space Flight Center, Huntsville, AL.
- 2 Hall, Al ed. *Petersen's Book of Man in Space. Volume V. Beyond the Threshold.* Los Angeles: Petersen, 1974.
- 3 Buden, David, *Nuclear Rocket Safety*, ACTA Astronautica, Volume 18, 1988, pp. 217-224.
- 4 David L. Black and Stanely Gunn, "A Technical Summary of Engine and Reactor Subsystem Design Performance During the NERVA Program", AIAA 91-3450.
- 5 D. Peaccio, C. Scheil, and J. Collins, "Near Term Lunar Nuclear Thermal Rocket Engine Options", 27th Joint Propulsion Conference, Sacramento, California, June 24-26, 1991.
- 6 *Lunar Module Reaction Control System*, NASA Technical Paper TN D-6740, Manned Spacecraft Center, Houston, TX, 1972
- 7 "Cryogenic Boiloff in Low Earth Orbit - A Parametric Study Utilizing Multilayer Insulation", Sverdrup Technology, Task Number 313-002, February 12, 1990.
- 8 "Space Station Freedom physical Description at Permanently Manned Capability", Boeing Defense and Space Group, Huntsville, AL, September 1992
- 9 Manned Systems Integration Standards, NASA 1989

NATSAT - A MULTI-PURPOSE LEO BUS

Naval Postgraduate School
Space Systems Engineering
Monterey, CA

Dr. Brij Agrawal

B. Clifton, M. Hecker, J. Laszakovits, B. Mathers, D. McCrorie, S. Newman, B. Urban

Abstract

In response to requirements established by the Strategic Defense Initiative Office, the Naval Postgraduate School (NPS) has designed NATSAT, a general purpose satellite for use in low and medium Earth orbits. Inexpensive and light weight, NATSAT serves as a spacecraft bus onto which a variety of small experiments can be mounted and flown. Payload masses up to 23 kg can be bolted onto an external equipment platform and receive housekeeping services that include 40 W of power, 3 axis stabilization, TT&C links, ephemeris data, and a small amount of thermal control. Orbital inclinations from zero to sun synchronous are achievable with a minimum life of one year. With a combined bus and experiment mass of 113.5 kg, NATSAT is configured to be launched from Orbital Sciences Corporation's Pegasus vehicle.

Introduction

The Strategic Defense Initiative Office (SDIO) is tasked with developing and deploying systems capable of defending against a limited ballistic missile attack. Research into the space based portion of this system requires conducting on orbit experiments in power generation, advanced materials, and radiation effects. Rather than testing complete spacecraft or prototypes, the goal of these experiments is basic research on smaller components with potential use in SDIO projects. Although several experiments could be combined into a single payload and placed into orbit using a traditional launch vehicle, SDIO has opted for a generic spacecraft bus that would supply a mounting platform and housekeeping services for a small payload. Forming a lightsat, the bus/experiment combination would be placed into orbit using the Pegasus, Taurus, or possibly a Scout derivative launch vehicle.

Through the generic bus approach, SDIO hopes to

realize cost benefits over conventional spacecraft that are custom built for each payload and launch. By procuring dozens of the satellites and storing them for future use, economies of scale can be achieved and the per unit cost of each bus reduced. In addition, use of the lightsat concept should result in savings from the reduced time and effort necessary to develop and deploy the system. The ultimate desire is to provide small payloads with quick, low cost access to near Earth space.

Based on these goals, the strawman specifications outlined in Table I were established. Payload mass, payload power, and 3 axis stabilization were hard requirements necessary to support anticipated experiments. The remaining parameters were considered desirable, but not mandatory. Rather than

Table I. Strawman Requirements

PARAMETER	VALUE
Orbit	
Max altitude	1000 km
Min altitude	400 km
Mass	
Bus	68-91 kg
Payload	23 kg
Total	91-114 kg
Power	
EOL orbital average	40 W
ACS	
Type	3 axis
Precision	0.5° attitude 0.5° knowledge
Point modes	Earth, sun, velocity
Life	12 months
TT&C	
Uplink	2 kbps
Downlink	1000 kbps
Launch Vehicle	Pegasus
Reliability	0.9 Single string acceptable
Bus	MIL-STD-1553

performance, cost was SDIO's overriding concern during the design process. Consequently, the specifications are intentionally vague; SDIO gave wide latitude in the hope that cost effective tradeoffs would be made.

Spacecraft Description

Configuration

Configured as a box, the NATSAT provides an equipment platform of .6 m² area for mounting experiments with masses up to 22.7 kg and volumes of a tenth of a cubic meter. Power comes from two deployable solar arrays and additional cells mounted on two faces of the spacecraft body. Figures 1 and 2 show the satellite with the arrays deployed and stowed for launch. The arrays are fixed and double sided with cells. Orbital average power available is 108 W with 40 W going to the payload.

Attitude control is provided by a biased momentum wheel with six hydrazine thrusters. The thrusters also provide the velocity corrections necessary to counteract orbital decay. For telemetry, tracking, and control, omni-directional antennas on two faces are utilized. Communications are via a SGLS compatible S-band transponder. Downlinking of experimental data is also accomplished through this single communications system. Command and data handling is implemented on a MIL-STD-1553 bus utilizing a single CPU for spacecraft control and bus mastering.

Thermal control is largely passive with heaters only used

on the hydrazine thrusters and fuel tank. The thermal requirements of any payload depends on the type of experiment being conducted. Therefore, no specific thermal control is provided to the experiments, although the bus is capable of providing or dissipating a certain amount of payload heat depending on orbital orientation.

Equipment Placement

Figure 3 is a top and side view of the satellite layout. The batteries, momentum wheel, spacecraft electronics, and other bus equipment are mounted directly to the +Y and -Y faces. The exterior of these faces also hold the radiators used for thermal control. The X faces hold no gear but instead have their exteriors covered with solar cells. The center of the NATSAT is occupied by the hydrazine storage tank. Four of the thrusters are located on the -Z face with the remaining two placed off centerline on the X faces. Experiments are attached to the +Z face.

Mass and Power Budget

The breakdown of mass and power requirements for the various subsystems is provided in Table II. Maximum powers represent the peak demand of a subsystem while nominal is closer to an orbital average.

Operational Envelope

The spacecraft meets the requirements given in Table I. Inclinations from zero to sun synchronous can be

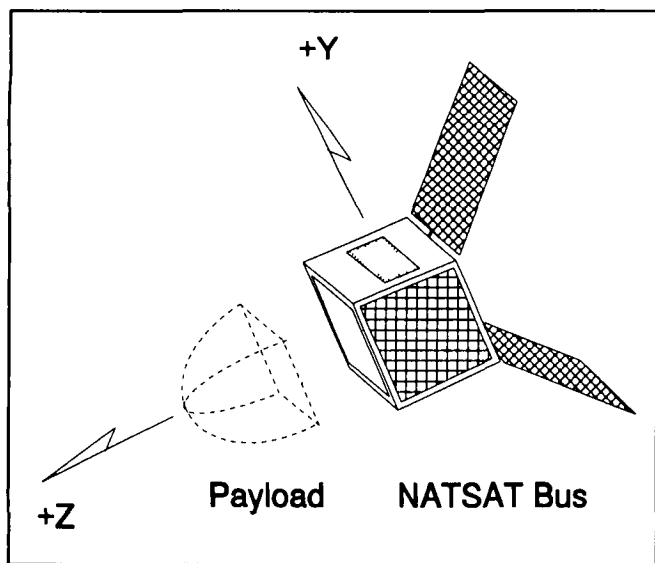


Figure 1. NATSAT deployed configuration

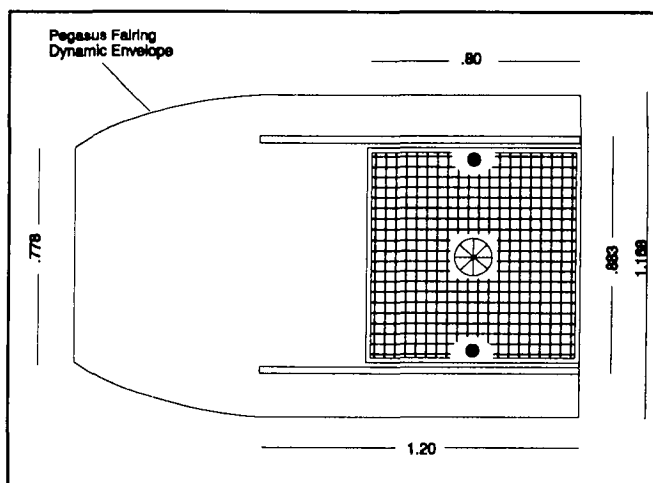


Figure 2. Stowed configuration. Dimensions in meters

accommodated. Minimum life is one year at 400 km and is limited by the amount of hydrazine monopropellant available. Longer life can be achieved at higher altitudes or by reducing payload mass and onloading more fuel. Design was based on a circular orbit; the impact of eccentricity on life and communications links was not analyzed.

Subsystem Design

The utility of a generic bus lies in the variety of payloads it can host. For the SDIO project, this translates into a spacecraft that can support the diverse orbits required by different experiments. As shown in Figure 4, inclinations from zero to sun synchronous are desirable along with altitudes from the upper atmosphere to the radiation belts. Depending on the experiment, one of three orientations is preferred: sun pointing, which keeps the payload continuously exposed to solar radiation; nadir pointing to keep the payload continuously facing the Earth; and velocity vector pointing, subjecting the payload to the oncoming

orbital environment.

The combination of inclinations, altitudes, and pointing modes produces such a variety of orbits that exhaustive analysis is not possible. Instead, each system is designed to meet the minimum requirements for a worst-case scenario and, consequently, exceed the requirements for less adverse conditions. This results in a bus with excess capability in certain orbits that a payload may be able to utilize.

In approaching the design, the NPS team made two early decisions. First, in the interest of low cost, only commercial off-the-shelf technology would be used while exotic materials and processes would be avoided. When feasible, actual parts were identified. Secondly, compatibility with only one launch vehicle, the Pegasus, was considered. While this restricts launch options, it simplified the design process and increased the available mass budget from the 114 kg envisioned by SDIO to the 140 kg available from Pegasus.¹ The design margin of 4% given in Table II is based on the original SDIO requirement. The margin using Pegasus is actually 22%, a much more realistic number for

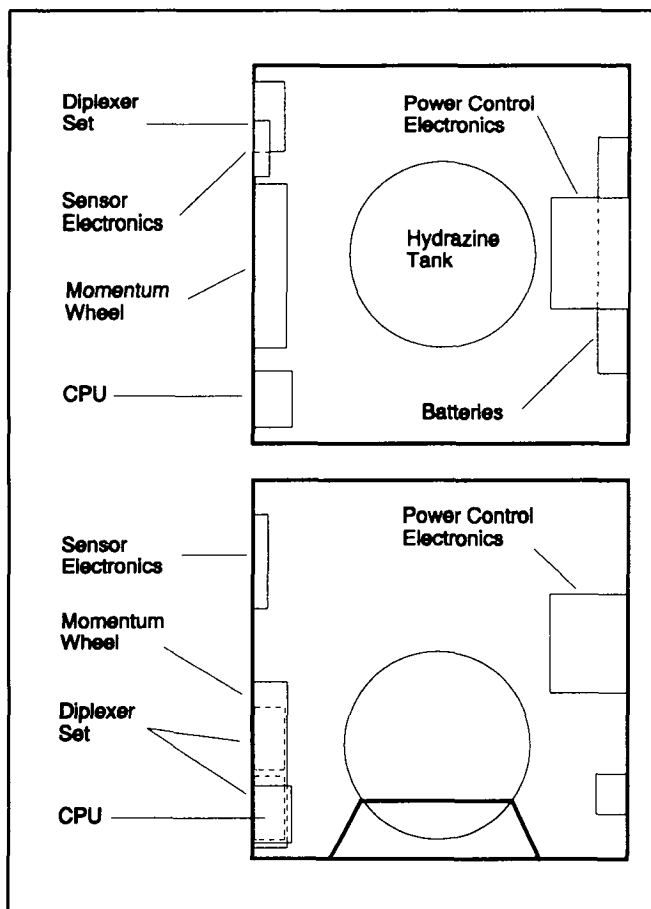


Figure 3. Top and side view of equipment placement

Table II. Mass and power budget

Subsystem	Mass (kg)	Maximum Power (W)	Nominal Power (W)
Structure			
Components	28.0	0.0	0.0
Integration	18.0		
Power	22.3	62.4	40.0
Control	4.0		
Batteries	5.7		
Arrays	12.6		
TT&C	7.7	33.0	16.0
Transmitter	2.1		
Receiver	2.1		
CPU	2.5		
Antennas	1.0		
ACS	9.9	12.0	12.0
Mom. wheel	3.8		
Sun sensors	2.5		
SS control	1.1		
Earth sensor	2.5		
Propulsion	12.4	10.0	0.0
Tank & fuel	8.4		
Plumbing	2.0		
Thrusters	2.0		
Thermal	6.0	10.0	0.0
Payload	22.7	40.0	40.0
Totals	114.0	183.7	118.8
Subtotal	109.0	167.0	108.0
Margin	5.0	16.7	10.8
Margin %	4%	10%	10%

a preliminary design.

General guidance for the design of subsystems came from references (2) and (3).

Structures

The overall shape and size of the bus was driven by solar power requirements and the need for a configuration that produces sufficient power for any of the expected orbits. To reduce mass, a truss and panel design was used with the panels serving as both the skin of the craft and platforms for mounting equipment. Twelve U-channel beams of equal dimensions form a cube onto which panels are riveted. To provide structural support to bus equipment, the Y faces are composed of 1.9 cm honeycomb. The X faces consist of thin skins which act as the substrates for the body mounted solar cells. To prevent excessive deflections of the substrates, U-channel stringers were added to the X faces. The positive Z face is another 1.9 cm panel on which the experiment payload is bolted. In order to align the

propellant mass as closely as possible with the spacecraft's principal axes, a support structure was constructed in the interior of the bus. As shown in Figure 5, it consists of four hollow tube support legs which originate at a tank waistband and attach to the upper half of an adaptor clamp on the -Z face. This adaptor acts as the upper half of a Marmon clamp and forms the structural interface between the NATSAT and the Pegasus launch vehicle.

The deployable solar panels, which fold along the Y faces when stowed in the Pegasus' payload shroud, are attached to the +Z face with explosive bolts at each corner. Preloaded, damped torsional springs extend the panels upon firing the bolts and a self-locking mechanism holds them in place once fully deployed.

Composites and light weight metals, while saving mass, were not found to be cost effective. Consequently, their use was limited to the extendable solar panels which use 3 mm graphite/epoxy for the cell's substrate. Otherwise, the entire structure is constructed from 6061-T6 aluminum. With a 1.5 design margin, acceleration loads during launch were used to determine the thickness of stringers and panel skins. Finite element analysis found the fundamental frequency of NATSAT to be 18 Hz, high enough to keep the bus dynamically decoupled from the Pegasus.

Electrical Power

More than any other subsystem, power generation drove the design of the NATSAT. Depending on the orbit, any surface may find itself continuously exposed to solar

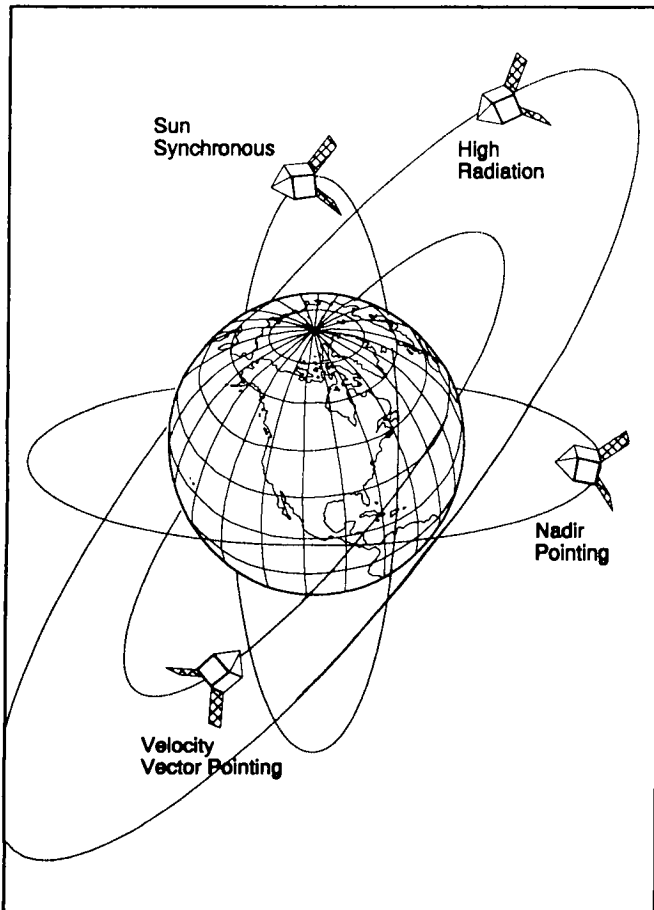


Figure 4. Potential bus orbits

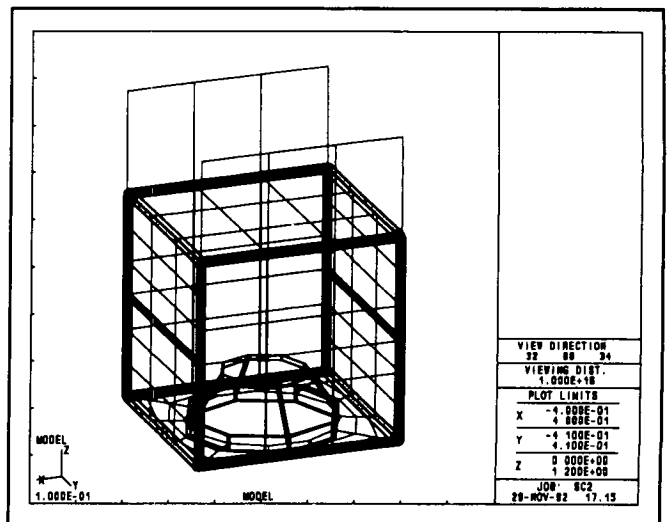


Figure 5. Finite element model

radiation or perpetually in shadow. Sun orientation (beta angles) can vary from zero to 90°. In addition, altitude and inclination combine to produce eclipse periods from zero to 34% of the orbital period. While all of these factors demand an electrical power system (EPS) of great versatility, the overall goal of designing a simple and inexpensive bus still remains. Three alternatives were considered: sun tracking arrays, fixed arrays, and body mounted cells.

Sun tracking arrays are a logical choice for the NATSAT since a single set of panels can provide power in all of the various orbital orientations. However, while this saves cost by minimizing the total number of solar cells required, it extracts a higher price in terms of system complexity and mass. By abandoning arrays and utilizing only body mounted cells, the EPS can be greatly simplified. Unfortunately, the variety of potential orbits would require every surface of the bus to be covered with cells to ensure adequate power. This makes equipment placement (thermal radiators, antennas, thrusters), payload attachment and ground handling problematic.

Ultimately, a compromise solution was adapted that uses two fixed arrays in conjunction with body mounted cells on two of the bus faces. Canted at 45° and double sided, the arrays have good solar visibility in most orbits. For those periods when the arrays are obscured or orthogonal to incoming solar radiation, the body mounted cells augment power generation.

The EPS affected the configuration of the NATSAT in two ways. Surface area requirements for the body mounted cells set the overall bus dimensions. To meet minimum power requirements, roughly .6 m² of silicon cells are needed on two faces, leading to the .8 x .8 m size. Also, although not specifically required, the cross section is square vice hexagonal or circular. While hexagonal provides greater internal volume to the bus and supports a more modular design, it complicates the analysis of power generation with all the potential orbits and beta angles. Circular cross section was ruled out because of the difficulty in mounting cells on surfaces that are not flat.

Sizing the batteries was a straight forward process based on a worst-case scenario of maximum eclipse period and power usage. Because the array output can vary from zero to 190 W, a regulated bus is required. Table IV summarizes the EPS components. A cursory glance at the table might indicate that the design is not capable of delivering 118 W of power, especially when compared with comparable spacecraft. However, the size of a power generation system is dependent on the satellite's life; the effects of radiation degradation and charge/discharge cycling mandate cell arrays and batteries to meet end-of-life, not beginning-of-life, requirements. With only one year on station, the NATSAT's beginning-of-life and end-of-life requirements are essentially the same.⁴

ADC and Propulsion

Significant cost and performance tradeoffs can be made between the attitude determination and control system (ADC) and propulsion system. The most spartan approach considered using only magnetic torque rods and a momentum wheel with no propulsion system. Although this method simplifies the spacecraft's design significantly, it was discarded for two reasons. First, a stable orbit can not be maintained at the lower LEO altitudes without some sort of thrusters. Analysis showed that, for periods of maximum solar activity, the bus would survive at 400 km for roughly six months before atmospheric drag caused reentry. Secondly, the Pegasus alone could not place the NATSAT in some of the desired trajectories, notably a sun synchronous orbit at the 1000 km range. For these instances, a propulsion system on the NATSAT is necessary to augment the ΔV provided by the launch vehicle.

Consequently, a modest propulsion system was

Table III. Electric power system components

Component	Description
Cells	
Manufacturer	Spectrolab
Model	Spectrodata K7700B
Size	2 cm x 4 cm
Deployable Arrays	
Quantity	2
Size	.8 m x 1.2 m
Cells, parallel	19
Cells, series	56
Body Mounted Panels	
Quantity	2
Size	.8 m x .8 m
Cells, parallel	19
Cells, series	37
Batteries	
Manufacturer	Gates Energy Co
Model	4280-05AB10
Type	Nicad
Quantity	1
Size	5 AMP-HR

sun sensors placed on the +Z face. The conical Earth sensor, with a 45° x 45° field of view, is able to detect the horizon in both Earth and velocity vector pointing modes.

TT&C

Figure 7 is a block diagram of the spaceborn portion of the telemetry, tracking, and control system (TT&C). To provide 360° coverage, two omni-directional antennas are used on opposite faces of the bus. A single transponder with a diplexer allows the one set of antennas to support both transmission and reception. Individual antennas for transmission and reception were not considered feasible due to the added mass and the potential for mutual interference. Omni-directional antennas provide no signal gain; however, the data transfer rates of 2 kbps uplink and 1000 kbps downlink are modest. A transmitter with EIRP of -10.1 dB is sufficient to ensure a 6 dB link margin even at the extreme orbital altitude of 1000 km (maximum of 3400 km slant range).

It was anticipated that dedicated ground resources would not be allocated to a single NATSAT mission and that a continuous link would not be maintained. Compatibility with the Air Forces' SGLS network of ground stations was incorporated so that that system can be utilized if desired. Whether a satellite will be in view on each pass depends on the orbit's orientation. At some inclinations, communications will not be possible with the satellite for several orbits, even if the full SGLS system is available.

Factors affecting the choice of transponders were SGLS compatibility, space heritage, adequate receiver sensitivity, and commercial availability. Data encryption was deemed

undesirable due to the high cost of encoding hardware and added security requirements at ground facilities. However, mass allowances were made for encoding gear in the event a mission requires it. Output for most SGLS transponders is 3 W, more than adequate for the NATSAT's communications needs.

Parametric analysis was conducted to size the computational requirements of the bus' computer. Allowances were made for command and telemetry interpretation, attitude sensor processing, thruster and momentum wheel control, and system monitoring for the spacecraft's power and thermal systems. As always, a tradeoff exists between performing processing onboard the satellite versus on the ground. It was found that if only rudimentary autonomy was provided, a single CPU could be used as a bus master and spacecraft controller. The mass and power savings realized made this a desirable choice. Consequently, ephemeris calculations are performed onboard through a simple propagation algorithm with regular updates being provided by ground controllers.

Because some SDIO experiments specifically require high radiation orbits, care was taken to protect against single event upsets and other electronic disturbances. A space proven CPU meeting MIL-STD-1750 was selected with the system kernel stored in EEPROM. Fault diagnosis and isolation are minimal and, for the most part, critical problems are handled by entering a safe state.

Data is handled onboard by a distributed network on a MIL-STD-1553 bus. This bus also provides an interface to the experimental payload and the communications system. NATSAT does not provide any data store-and-forward capability. If the mission requires saving information for later download, the payload itself must provide onboard storage.

Selected TT&C components are given in Table V.

Thermal Control

Like power generation, the design of the thermal control system was very much driven by the complex set of orbits that need to be supported. Depending on the orientation, panels end up perpetually in sunlight, continuously shadowed, or cycling between these extremes. The original desire was to utilize a completely passive thermal control system based on optical solar radiators (OSR's) and insulation. The decision to include the hydrazine propulsion

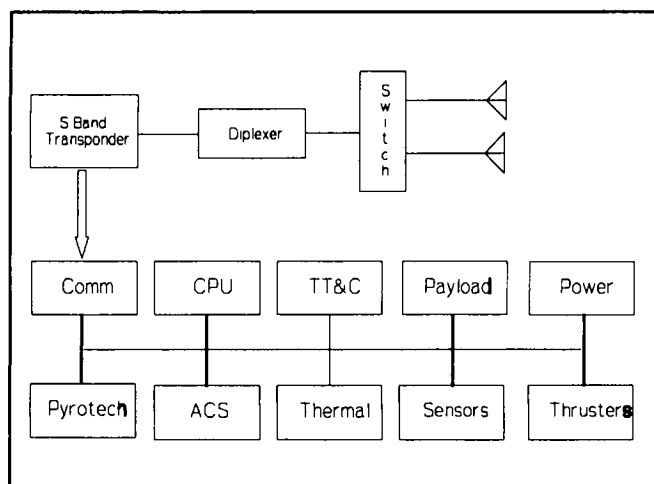


Figure 7. TT&C Block Diagram

incorporated into the design. Another trade was considered between using thrusters or magnetic torque rods for attitude control. Torque rods are appealing for roll/yaw control and momentum wheel desaturation due to their simplicity and low cost compared to thrusters. However, their mass is approximately the same as an equivalent set of thrusters and they average 40% more power to operate. Eliminating torque rods also greatly reduced spacecraft memory and processing requirements necessary for an on orbit model of the Earth's magnetic field. It is also questionable whether the rods could handle the disturbance torques encountered while firing the thrusters for orbital corrections. Ultimately, they were abandoned in favor of four more hydrazine thrusters resulting in a total of six thrusters. Two thrusters counteract orbital decay, provide desaturation for the momentum wheel, and augment orbital insertion if needed. The other four provide roll and yaw control.

To guarantee a one year life at the 400 km altitude requires approximately 7 kg of hydrazine monopropellant. The smallest commercial tank with at least that capacity comes from the Air Force's NAVSTAR program which is fielding the constellation of global positioning satellites. The actual tank can hold 10 kg, so experiments can opt to trade up to 3 kg of payload mass for additional fuel and extended satellite life.

A standard momentum wheel provides bias momentum used for pitch control. As illustrated in Figure 6, the thruster pairs about the X and Z axis supply roll and yaw control. Firing of these thrusters is controlled by a derived rate increment system and achieves identical results as a single set of thrusters offset from the YZ plane by angle α .

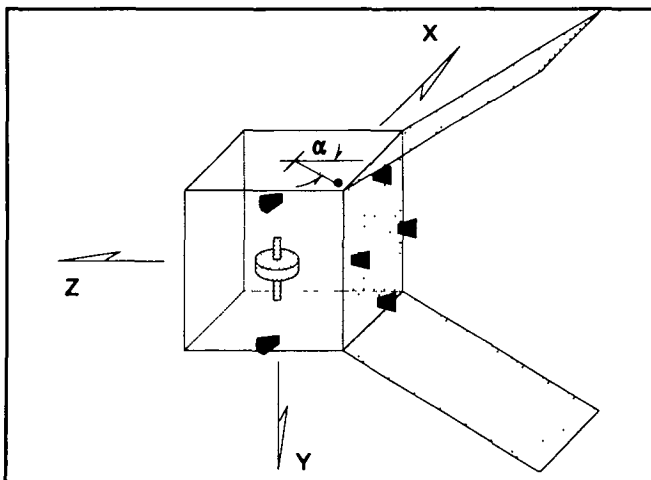


Figure 6. Thruster placement

Thrusters are not fired in pairs, therefore small perturbations will occur when they are utilized. Momentum wheel sizing and feedback control for the thrusters was computed to handle the relatively large aerodynamic and magnetic disturbance torques present in some orbits. Disturbances from solar pressure, gravity gradient, and thruster misalignments are easily controlled.

Because the size and mass of payloads is not known in advance, exact data for computing the center of mass and moments of inertia were not available. Instead, the payload was modeled by a plate distributed evenly over the +Z face. The control system is robust enough that experiments with greater inertia, while slowing down response time, should not severely impact performance. To locate the center of mass as closely as possible to the spacecraft's principal axes, equipment is mounted in the lower portion of the bus to counteract the payload.

Table IV summarizes the ADC and propulsion system. Attitude determination is achieved through a set of Earth and

Table IV. ADC and propulsion system components

Component	Description
Momentum Wheel Manufacturer Model Quantity Momentum, max Momentum, nominal	Space Sciences Corp 3005 1 10 Nms @ 6000 RPM 5 Nms @ 3000 RPM
Earth Sensor Manufacturer Model Quantity Type Field of View	Ithaco CS301A 1 Conical scan 45 x 45 degrees
Sun Sensor Manufacturer Model Quantity Field of View	Adcole 17032 3 64 x 64 (1 sensor) 180 x 180 (3 sensors)
Thrusters Manufacturer Model Quantity Size	Olin MR103C 6 .44 N
Fuel Tank Manufacturer Model Type Quantity Size	Rockwell GPS TI-6AL-4V Diaphragm 1 10 kg capacity
Control System Offset Angle (α) Control Gain Lead Time Constant	7 degrees 6.88 Nm/rad 4.49 s

system made this impossible and heaters were added for the fuel tank and each of the thrusters. However, beyond the propulsion system, no active control is used. The viability of heat pipes and louvers was explored but dismissed as unnecessary.

Internally, heat is transferred via conduction and radiation and, externally, dissipated through a set of radiators located on the Y faces. The ample internal volume of the NATSAT permitted heat generating components to be mounted directly on the spacecraft's panels to facilitate heat transfer. Radiators were sized to provide adequate dissipation during maximum irradiation from the sun and then checked to determine the resulting coldest case temperatures. OSR areas of 710 cm² and 980 cm² for the +Y and -Y faces are used. Some orbits produce wide temperature variations between opposing satellite faces and, because no active control is used, significant thermal gradients exist inside the bus. The equipment, notably the batteries, occasionally operate at temperatures considered marginally acceptable. Although this degrades their operational life, the performance was still more than adequate for the NATSAT's brief one year on orbit.

One shortcoming of the thermal analysis was an assumption that the experimental payload would be isolated from the bus and neither absorb nor dissipate any energy. Clearly, this is unrealistic. However, the variety of payloads coupled with the different orbits made meaningful analysis impossible. The NATSAT can provide some thermal housekeeping to the payload, but the amount would have to

be determined once the mission is specified.

Conclusion

Several areas of the satellite's design were not extensively explored such as safety, testability, and ease of ground handling. In addition, reliability is a concern since the subsystems have very little redundancy and single string failures could result in the loss of the bus. However, the design is mature enough to be considered feasible. Pragmatic and cost effective, NATSAT meets the goal of providing small payloads with inexpensive access to space.

References

- 1) Rye, G., *Pegasus Payload User's Guide, Release 2.00*, Orbital Sciences Corporation, Virginia 1991.
- 2) Agrawal, B., *Design of Geosynchronous Spacecraft*, Prentice Hall, New Jersey, 1986.
- 3) Wertz, J. R. and Wiley, J. L., *Space Mission Analysis and Design*, Kluwer Academic Publishers, The Netherlands, 1991.
- 4) *Solar Cell Array Design Handbook Vol I and II*, Jet Propulsion Laboratory, California, 1976.

Table V. TT&C components

Component	Description
Antennas Manufacturer Model Quantity Type Size	Watkins-Johnson WJ-48915 2 Hemispherical spiral 9 cm x 10 cm
Diplexer Manufacturer Model Quantity Type Transmit Efficiency Receive Sensitivity	Motorola SGLS 1 set S band 12.5% -104 dB @ 10 ⁻⁶ BER
CPU Manufacturer Model Quantity MIPS	Control Data Corp 444R ² 1 1.25

NEAR-EARTH ASTEROID RENDEZVOUS

Naval Postgraduate School
Department of Aeronautics and Astronautics
Monterey, California

Professors Brij Agrawal and Ed Euler

Lt Dave Price, Lt John Figuerres, Lt Greg Hand, Lt Rick Johnson, Lcdr Eric Lantto, Lt Rena Loesch,
Lt John Riggs, Lcdr Mark Wilsey, and Lt Dudley Atkinson

Abstract

The AE4871 Spacecraft Design Course is the capstone design class for the M.S. in Astronautics at the Naval Postgraduate School. The Fall 92 class designed a spacecraft for the Near Earth Asteroid Rendezvous Mission (NEAR). The NEAR mission uses a robotic spacecraft to conduct up-close reconnaissance of a Near-Earth asteroid. Such a mission will provide information on Solar System formation and possible space resources. The spacecraft is intended to complete a NEAR mission as a relatively low-budget program while striving to gather as much information about the target asteroid as possible. A complete mission analysis and detailed spacecraft design were completed. Mission analysis included orbit comparison and selection, payload and telemetry requirements, spacecraft configuration, and launch vehicle selection. Spacecraft design included all major subsystems: structure, electrical power, attitude control, propulsion, payload integration, and thermal control. The resulting spacecraft demonstrates the possibility to meet the NEAR Mission requirements using existing technology, "off-the-shelf" components and a relatively low-cost launch vehicle.

Introduction

This design project was completed as part of course the Advanced Spacecraft Design course at the Naval Postgraduate School. The purpose of the mission is to send a satellite into a Near Earth Asteroid Rendezvous that will gather as much useful information about the asteroid as possible, while keeping the cost down. Cost efficiency is achieved by designing a flexible spacecraft bus which is capable of performing follow-on missions.

Target Asteroids

Four target asteroids and interplanetary trajectory solutions were provided in the supplementary data package. Table 1 lists the target asteroids and characteristics.

Asteroid	Seleucus	1982 XB	McAuliffe	Orpheus
Max solar dist (AU)	2.750	2.640	2.460	1.600
Max Earth dist (AU)	3.430	3.600	2.180	2.580
C3 (km ² /sec ²)	36.880	27.799	38.745	17.72
v (m/s)	1.804	1.458	1.336	1.458
Delta Payload Max (kg)	605	725	580	895
Launcher	Atlas IIA	Delta II	Atlas IIA	Delta II

Table 1. Target Asteroids

Design Criteria

The spacecraft is required to reach the asteroid within three years of launch and remain for at least one year. The launch must occur between 1996 and 2006, within a ten day launch window. The spacecraft must be capable of mid-course and rendezvous maneuvers, and a total Δv of 1.85 km/s. It should be capable of maneuvering in the asteroid vicinity. This design orbits the asteroid in order to reduce fuel consumption and lower sensor range. The satellite must be able to communicate via the NASA Deep Space Network and be capable of autonomous operation for seven days. Sensors should be capable of measuring mechanical and chemical properties of the asteroid.

Mission Description

The mission is divided into six phases of flight. During the *Launch Phase* (booster ignition to spacecraft separation) all systems are dormant except the battery, which is functioning to maintain loads. The *Eclipse Phase* (separation to exiting Earth's shadow) will not exceed 30 minutes. The battery is specifically designed to provide the requisite power for this period. The solar array remains stowed and the spacecraft slowly spins with the momentum imparted by the launch system. The Delta third stage fires for transfer orbit insertion. During the *Post-Eclipse Phase* (shadow exit to solar array deployment) one third of the

solar array is used to relieve the battery during transition to three-axis stabilization. The reaction wheel system is started and spin is removed by thrusters. The solar arrays are deployed once attitude control is gained. The spacecraft transits to rendezvous during the *Cruise Phase*. A mid-course trajectory burn is performed if required. As the satellite approaches rendezvous, the *Acquisition Phase* begins. Relayed images allow for a refined orbital solution and the satellite is inserted into orbit about the asteroid. Once in orbit, the *Mission Phase* begins.

The Mission Phase is subdivided into the Science and Communications Phases. During the Science Phase the +X face of the satellite is pointed at the asteroid to gather data while the solar arrays point to the sun. When the maximum data collection is reached or when commanded from Earth, the satellite slews to point the High Gain Antenna to Earth to begin the Communication Phase.

Payload Description

The payload consists of the Science Payload, RF Communications, and Command and Data Handling (C&DH) systems. The C&DH subsystem is further divided into Telemetry, Tracking, and Control (TT&C) and data storage.

The mission of the payload is to gather, store, and transmit remote sensing data of the asteroid. The payload will maintain two-way X-Band Doppler through the mission as well as Doppler and range-tracking simultaneously with command and telemetry. The RF Communications Subsystem handles command, ranging, and telemetry functions in uplink or downlink mode in conjunction with the Deep Space Network (DSN).

Science Payload

The purpose of the Science Payload is to examine the asteroid and infer the chemical properties. It consists of a visible imager, an IR spectrometer, a laser altimeter, and a magnetometer. This subsystem is controlled by the main processor, which operates the instruments and directs the data stream.

Visible Imager. The main science instrument is the Visible Imager. The imager is required to obtain six color images with resolution of 6 m per pixel pair. The science mission must be scheduled to obtain low resolution images with two inbound and two outbound images exceeding 300 m per pixel pair resolution at thirty minute intervals for five hours preceding closest approach of full face. The Visible Imager will be a government furnished (GFP)

camera developed to support science and navigation requirements of the Near Earth Object Missions. It has a 1024 x 1024 pixel CCD detector. The GFP camera has adequate sensitivity or integration to obtain science images in a single exposure or scan and navigation images of objects brighter than visual stellar magnitude nine in the same field of view as the target body.

IR Spectrometer. The IR Spectrometer has an object field-of-view (FOV) of approximately 4° and a wavelength range of 0.9 μm to 2.7 μm . The signal-to-noise ratio (SNR) will be greater than 15 dB at the poorest performance point with an integration time of greater than or equal to 1.0 sec. Radiative plate cooling is possible, but temperatures will probably be no lower than 150 K. The IR spectrometer will be a match with the camera system with respect to data processing and data fusion. The IR Spectrometer is connected to a control unit and processor, which serves as the interface between the instrument and the data handling interface in the main processor.

Laser Altimeter. The laser altimeter provides ranging information to the satellite. This instrument will be used for topographical mapping and for attitude control during close orbits of the asteroid. The operational range of the laser altimeter is 20 km with a resolution of 50 cm. Global coverage at this accuracy would yield a volume determination with an accuracy of less than 0.2% for the asteroid McAuliffe.

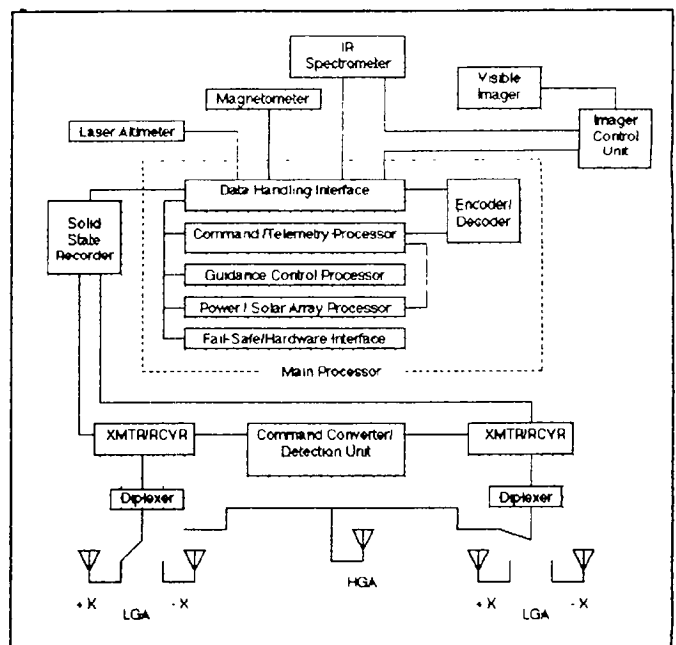


Figure 1. NEAR Payload

Magnetometer. The purpose of the magnetometer is to study the intrinsic magnetic field of the asteroid. The range for operation is 10 asteroid radii. Cancellation circuitry will be built into the sensor to cancel out any residual spacecraft magnetic fields.

Science Data Interface. The science payload data will be downloaded to the solid state recorder via the data handling interface in the main processor. The visible imager and imaging spectrograph data stream will be processed in their joint control unit/processor and then will be read out to the data interface. The data interface will control and monitor all phases of storage and data transmission.

RF Communications

The RF Communications subsystem is a fully redundant system with the exception of the HGA. The power amplifiers can be switched between a 10 W and 5 W transmission signal. Each set of equipment is connected to the Main Processor. The Main Processor continuously monitors, controls, and processes all data received by the system. In case of system failure, the Main Processor will switch from the primary to the backup communication system.

The communication system will operate in X-band frequencies. The spacecraft will be capable of simultaneous X-band radiometric tracking, telemetry, and commanding.

Antennas. The satellite will have omnidirectional uplink capability using four low gain antennas (LGA), which will be used during emergencies, near-Earth orbits, and during the periods when the high gain antenna (HGA) is not pointed at Earth. The HGA will be used for high data rate downlink. The HGA is an X-Band parabolic dish antenna with a diameter of 1.5 m and a f/d ratio of 0.4. The antenna was designed to have a 1° beam width and a gain of 40 dBi. The narrow beam width and the high gain will allow the high data rates required for uplink and downlink operations at 3 AU. The HGA will be a fixed antenna and must be pointed at Earth in order to transmit and receive data. The primary function of the LGAs is to act as receivers and as transmitting antennas if the HGA fails. During emergencies or system failure, two LGAs will be automatically switched on to act as receivers. Each is placed on opposing corners to achieve hemispherical coverage.

Command and Data Handling

The C&DH subsystem will act as the interface between the Science Payload and RF Communication subsystems. It will collect the information relating to satellite health and status, monitor all system programming; receive, decode, process, and distribute spacecraft commands. It will then gather, format, store, and transmit all telemetry data. In the case of a disabling failure, a fail-safe mode is planned to disengage the data streams, align the solar arrays with the sun, enable the LGAs, and await instructions from Earth.

Main Processor. The Main Processor will control all activities aboard the spacecraft. It will be a single processor that will handle TT&C, data handling, guidance and control, and coding and decoding of communication, plus other onboard functions discussed in other sections.

Science Data. The data retrieved from the science instruments will enter the data handling interface (DHI) of the main processor. The DHI will store the information in the solid state recorder. When instructed by the Command/Telemetry Processor that the communications system is in the transmission phase, the DHI will retrieve the data from the solid state recorder and send the data to the encoder. The data will then be prepared for transmission.

Command and Telemetry. The status (health) of all systems will be monitored by the main processor. Each piece of equipment will be connected to the command/telemetry processor. The telemetry data will be stored in the solid state recorder until it can be transmitted back to Earth. All systems will be updated based on equipment status and spacecraft needs.

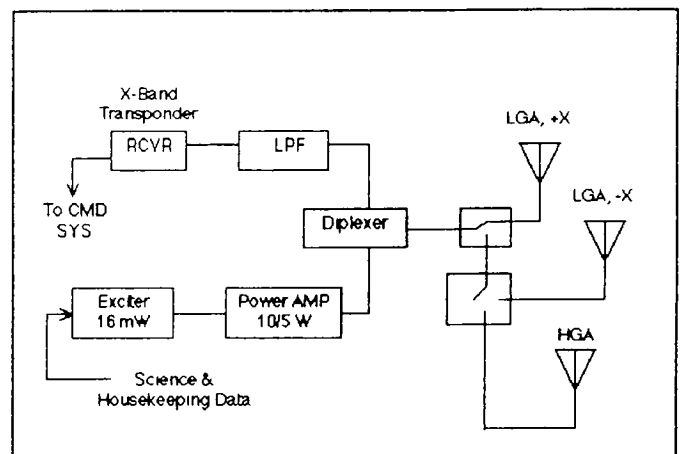


Figure 2. RF Communication Subsystem

System Integration

The RF Communication subsystem will receive the uplink X-band carrier transmitted from the Deep Space Network (DSN) to the spacecraft. The uplink is received by one of the two transponders via the Low Gain Antennas or by the narrow-beam High Gain Antenna. The command data and the phase modulated ranging signal is demodulated. The command stream is submitted to the C&DH subsystem for decoding and processing.

The downlink carrier is phase modulated with a square-wave subcarrier on which the housekeeping telemetry and science data is PSK modulated by the C&DH subsystem. The science data is retrieved from the solid state recorder via the data handling interface. The housekeeping telemetry is utilized for monitoring the operating conditions of the RF Communication subsystems as well as the status of the rest of the spacecraft. The downlink signal is amplified (10 W or 5 W depending on the mission phase) and then transmitted via either the LGA or the HGA. The RF Communications subsystem permits control of the subsystem by ground command. The ranges utilized in the link budget analysis support all missions. For simplification in measurements for the link budgets, the range for the spacecraft was set at the mean range (from Earth) for each phase: the Eclipse and Post Eclipse phases were designated to take place at a range of 1 AU, the Cruise phase was a range of 2 AU and the Acquisition phase and Mission Phase were at a range of 3 AU. The range of 3.6 AU is assumed to be the worst case. The distance limits the data transmission rate.

Deep Space Network (DSN). All uplink communications will utilize the DSN 34m (HEF) antenna. This is the only type that supports X-band frequencies. Downlink communications will be split between the 70 m and the 34m (HEF) antennas. The 70m antenna will be required for the emergencies and when the spacecraft is outside the 3 AU range. The 34 m (HEF) antenna will be utilized for normal downlink between the HGA and Earth.

Payload Operation

Normal Operations. Normal operations change with the mission phase. During Launch, Eclipse, and Post-Eclipse Phases, the Main Processor is performing and monitoring housekeeping operations. The solid state recorder is on and storing telemetry information for commanded relay. The command receivers are on and switched to the LGAs. All science instruments are off. During the Cruise phase, the transmitter power amplifier is turned on to provide a 5 W

transmission signal, the antennas are switched to the HGA for transmission and all science instruments are still off.

The Acquisition Phase consists of two sub-phases: science and transmission. During the science phase, the Visible Imager will be photographing the approaching asteroid target, the transmitter power amplifier will be off and the receiver will be switched back to the LGAs. All data from the Visible Imager is stored in the solid state recorder. After accumulating enough data, storage is stopped and the transmission phase is entered. During the transmission phase, all science instruments will be off, the transmitter power amplifier will be on and the output will be switched to the HGA. The science data will be coded and multiplexed with the telemetry and ranging information and downlinked via the HGA to DSN on Earth.

The Mission phase also consists of two sub-phases: science and transmission. During the science phase, all science instruments will be on and data will be stored in the solid state recorder. The power amplifier will be off and the LGAs will act as receivers. This continues until a command to transmit is received. During the transmission phase, all science instruments will be off and the HGA will be pointed to Earth. These two phases will be cycled for one year: 14 hours of the science phases and 8 hours for transmission.

Autonomous Operations. The spacecraft must have the capability to operate without ground contact for 7 days. The TT&C subsystem of the Main Processor will be capable of controlling all spacecraft operations. All telemetry will be stored in the solid state recorder for future transmission.

Launch Vehicle Selection

To achieve all four missions, the launch vehicle is required to provide a C3 of $40 \text{ km}^2/\text{s}^2$, with an earliest launch date of 1996. The Delta II was selected over Ariane, Atlas, and Titan for political, cost and availability considerations. The Delta is capable of lifting the required mass for two of the missions at much reduced cost and was chosen as the launch vehicle on which this design is based.

Delta II Description/Performance

The Delta II 7925 is a three-stage launch vehicle manufactured by McDonnell Douglas. The Delta II will provide $27.90 \text{ km}^2/\text{s}^2$ with a 725 kg payload. The Delta will provide the necessary C3 for 1982XB and Orpheus missions, but the Atlas IIA would be needed for the McAuliffe and Seleucus missions. The satellite is designed for a 37 inch diameter launcher interface which fits both

Delta and Atlas. By designing the spacecraft to fit inside the fairing of the Delta II, compatibility with the larger Atlas is assured.

Spacecraft Description

Spacecraft Configuration

The primary considerations in designing the NEAR spacecraft configuration were size constraints for the Delta II launch vehicle, power and communication requirements, internal component placement, and structural integrity. In order to minimize moments of inertia, the propellant tanks were clustered symmetrically about the origin, centered on the solar array axis. A detailed accounting of mass, dimensions and moments of inertia was completed using a computer-based spreadsheet program.

To maximize packing efficiency and minimize moments of inertia, the oxidizer tanks are mounted inside the Central Tube Assembly. The fuel tanks are situated in opposite corners of the spacecraft. Mounting and axial support are provided by two struts each. Lateral support is provided by the center deck. The two small N_2 tanks are located in a similar manner.

Equipment/Instrumentation. For thermal control reasons, most spacecraft equipment is mounted internally on the plus and minus Y faces. These equipment panels receive very little sunlight during all normal operating modes of the spacecraft. The Reaction Wheel Assembly is mounted internally using struts. Payload instrumentation used for direct observation of the asteroid is mounted on the plus X face.

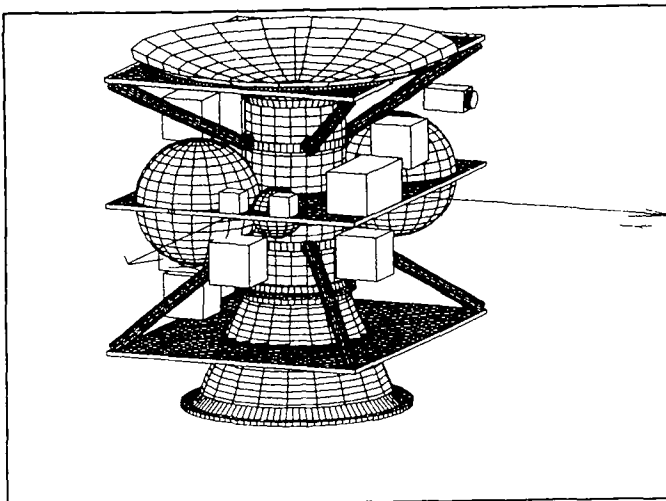


Figure 3. Internal Configuration

Structure Subsystem

The structure subsystem must provide mechanical support to all other subsystems, meet subsystem position and alignment requirements and protect subsystems from launch loads. The structure is designed to meet the frequency and load requirements of the Delta II launch vehicle.

The structure uses a central tube assembly as the primary load carrying member supporting two main side equipment panels, three decks, and two lighter sides via a network of strut assemblies. The structure was designed to support a spacecraft separation mass of 725 kg with a design load factor of 1.5. Properties for 6061-T6 aluminum were used in all calculations. Total structure subsystem mass is 10.6 percent of the spacecraft separation mass.

A series of 8 struts connect each corner of the spacecraft to mounting points on the central tube. The struts provide load paths for the equipment panels and axial mounts for the fuel tanks.

The sides and decks of the spacecraft are made of aluminum honeycomb sandwich material designed to support equipment loads. Each panel is connected to the strut assembly at all four corners. The top and bottom decks are designed primarily to close the spacecraft interior for thermal control. The top deck provides some lateral support for the high gain antenna. The center deck provides lateral support for the fuel and nitrogen tanks.

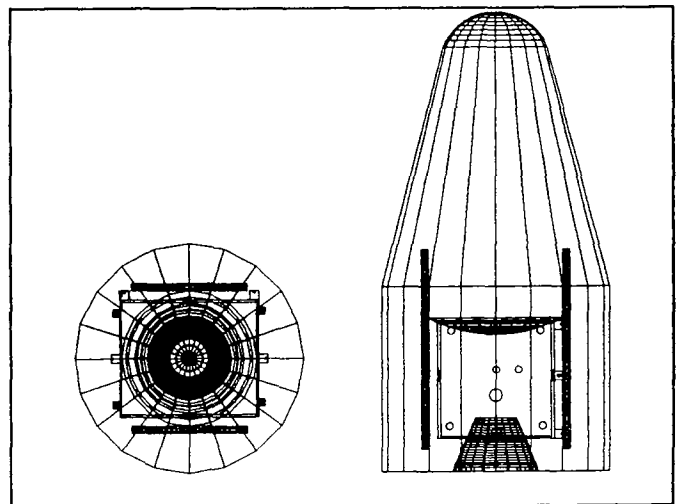


Figure 4. Delta II Launch Configuration

Launch Configuration

In the stowed configuration, one panel of the solar array is folded under and one over the center panel of each wing to allow power production during the Post-Eclipse Phase. In this configuration, the spacecraft is designed to fit inside the Delta II 9.5 foot fairing.

Electrical Power Subsystem (EPS)

The electrical power subsystem (EPS) utilizes a centralized, fully-regulated design to provide a $28 \pm 4\%$ DC bus voltage through end-of-life (EOL). The power required depends on the mission phase. The greatest power demand is 221 W during the Acquisition Phase. While in this phase and the Mission Phase, the base power will be provided by the solar array, with power peaks floated by the battery.

No redundancy is employed in the power sources due to mass constraints. If the battery or a portion of the solar array is lost, the EPS will go into a degraded mode. In the degraded mode, the C&DH processor will autonomously prioritize power distribution to the spacecraft's subsystems based on a pre-programmed hierarchy. The ground station will have the capability of overriding or changing the hierarchy.

The power source is a silicon cell solar array supplemented by a single Eagle-Picher 25AH NiH₂ battery for peak load periods. Two wings of three panels each produce the power required by the spacecraft. The solar array wings are capable of full rotation about one axis. The array was designed to provide 34.2VDC bus voltage at 192W maximum power at end of life.

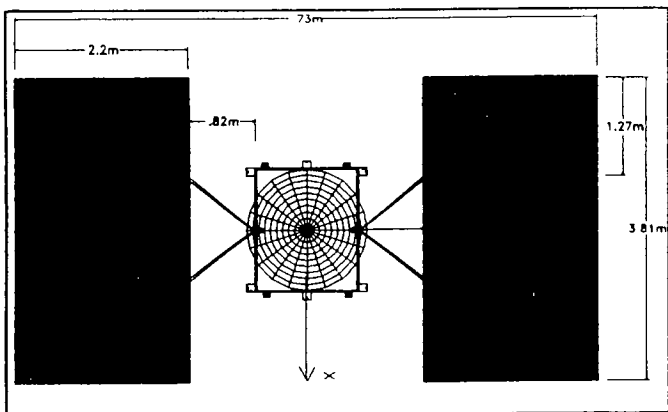


Figure 5. Deployed Configuration

The battery is capable of furnishing the entire 221W for sun reacquisition for up to 1.77 hours. It will take about 7.6 hours to recharge. The ground station can shorten or lengthen the recharge time.

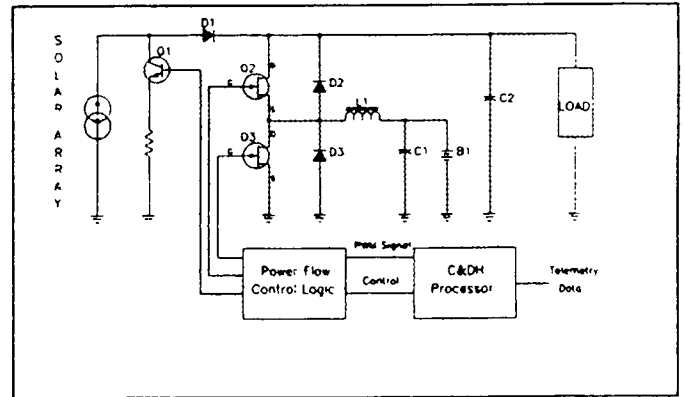


Figure 6. NEAR Power Regulation

Attitude Control

The Guidance and Attitude Control System (GACS) maintains the correct spacecraft attitude during the mission. The operational requirements are as follows.

- Three axis stability with slew capability for sensing and transmission modes.
- Antenna pointing accuracies of $\pm 0.1^\circ$ about any axis.
- Sun tracking solar arrays.
- Minimum slew rate of $6^\circ/\text{min}$.

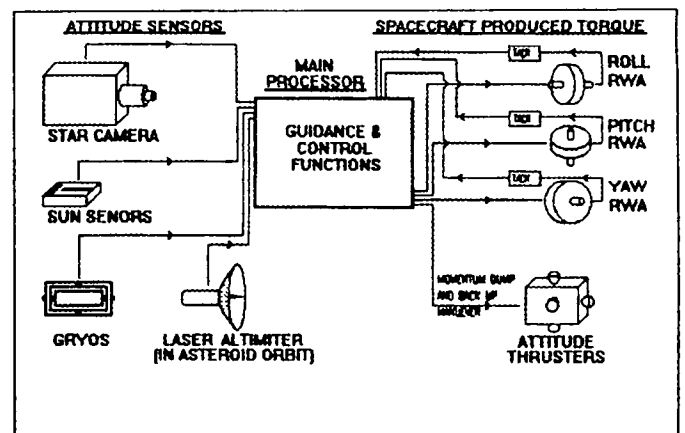


Figure 7. Attitude Control Subsystem

Three orthogonal Reaction Wheel Assemblies (RWA's), one along each body axis, allow independent control of rotation about each axis. In the event of an RWA failure, the skewed fourth wheel will be used. Momentum dumping is accomplished by twelve orthogonal attitude control thrusters. Normal operations call for pairs to work simultaneously to rapidly desaturate the RWAs before slew maneuvers and to periodically activate to keep the RWA bias low. The propulsion system will give limited three-axis stability in the event of multiple RWA failure.

Propulsion Subsystem

The propulsion subsystem must be capable of executing a mid-course trajectory correction maneuver and a rendezvous/capture maneuver with a total delta-V of 1.85 km/sec. The spacecraft must also be able to maneuver in the vicinity of the asteroid for a minimum of one year. The propulsion system will provide attitude control during large Δv maneuvers.

The propulsion system consists of one 468-N (105 lbf) thruster used for Δv maneuvers and twelve 4.5-N (1 lbf) thrusters for attitude control and small maneuvers. The large thruster will be used whenever possible for Δv maneuvers because of its higher specific impulse. The 468-N thruster utilizes bi-propellant fuel while the 4.5-N thrusters are monopropellant. There are four titanium alloy propellant tanks, associated fill, drain and isolation valves, filters, pressure regulators, pressure transducers, and fuel lines.

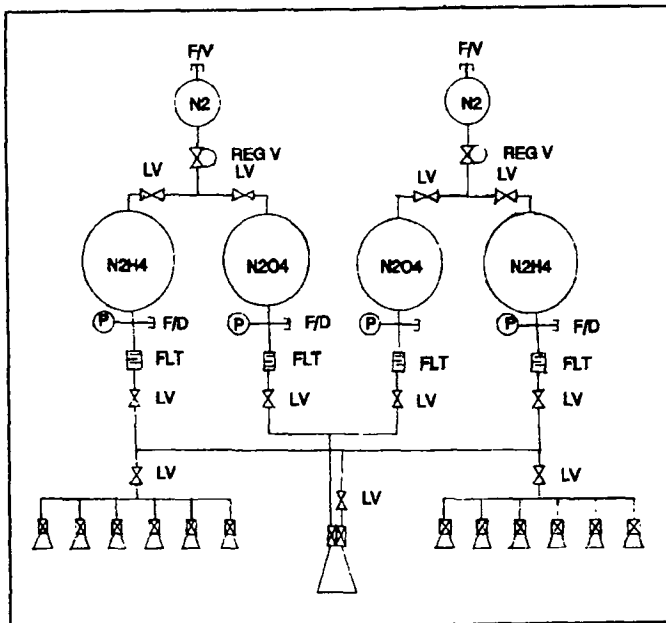


Figure 8. Propulsion System

Thermal Control Subsystem

The Thermal Control Subsystem ensures that the spacecraft and its internal components are maintained at the required operating temperatures. Locations of components in relation to the boundaries of the spacecraft and to each other affect the ability of the system to maintain the required temperatures.

The spacecraft's entire exterior (except areas required for instruments and the thermal radiator) will be covered with MLI to minimize heat transfer across the surface panels. It will also be used to insulate fuel and oxidizer tanks and lines to prevent freezing. The insulation will consist of twenty layers of aluminized kapton on the exterior surface and mylar insulation between the kapton and the surface of the spacecraft.

Heat is rejected to space via optical solar reflector (OSR) material, located on the same faces as the solar array drive motors to avoid direct sunlight. They are thermally coupled to the equipment attached to the interior surface of the structure at the OSR panel. This includes the TWTA's, the communications equipment, and battery. Electric heaters will be used to maintain temperatures of key components. These include the fuel tanks and lines, thruster valves, momentum wheels, and battery. Each fuel tank, oxidizer tank, and battery require one five watt heater, for a total of five heaters.

A steady-state thermal analysis for the NEAR spacecraft was performed using the PC-ITAS software program, developed by ANALYTIX Corporation. The thermal model consisted of the surfaces where heat is generated, surfaces thermally coupled to the heaters, structural members, and the OSR. The exterior was assumed to consist either of MLI or OSR and the interior surfaces were assumed to be painted black to help effectively radiate heat away from the components. The results show that the instruments and equipment will remain within the allowed operating ranges.

Conclusion

This spacecraft design was completed using a very straightforward approach to mission analysis and component selection/design. All systems were designed using proven methods. The structure is a fairly standard configuration and constructed of low-cost materials. The electrical system uses existing technology and low-cost solar cells to accomplish its mission. Thermal control is accomplished easily by standard means such as the use of heaters and OCRs. The use of off-the-shelf components keeps the cost of the payload, communications, and

propulsion systems down. The attitude control system is used to accomplish all required pointing tasks for communications and data acquisition and also assists in solar array pointing. This reduces the complexity of those systems. Redundancy is designed into the attitude control system to minimize the chance of a disabling failure in this system. Discipline in keeping the spacecraft separation mass down makes relatively low-cost launch by the Delta II possible.

It is concluded that careful determination of mission and performance requirements, close attention to target asteroid and orbit selection and the use of off-the-shelf components and existing technology, results in a flexible, capable and low-cost spacecraft able to complete the NEAR mission.

References

1. *Supplemental Data Package for A Near-Earth Asteroid Rendezvous (NEAR) Mission*, AIAA Graduate Student Design Competition, 1992/1993.
2. *Delta II Commercial Spacecraft Users Manual*, McDonnell Douglas Astronautics Company, 1987.
3. Agrawal, B., *Design of Geosynchronous Spacecraft*, Prentice-Hall, 1986.
4. Martin Marietta, *Discovery Program - Near Earth Object Spacecraft Study: Rendezvous Mission*, Martin Marietta, June 1991.
5. Applied Physics Lab, *Near Earth Asteroid Rendezvous: Report to Discovery Science Working Group NASA Solar System Exploration Division*, The John Hopkins University Applied Physics Lab, May 1991.

INTERNAL COMBUSTION ENGINES ON THE MARTIAN SURFACE

Old Dominion University
Department of Mechanical Engineering & Mechanics
Norfolk, VA 23529-0247

Faculty Advisors: Dr. Colin P. Britcher & Dr. Robert L. Ash

Keith Davis, Scott Hoover, Stephen Lauer, Lori Lawrence,
Christos Paparistodemou, Douglas Taylor, Michael Uenking, Wesley Wigginton,

Teaching Assistant: Daniel Neff

Abstract

Previous design teams at Old Dominion University have studied the feasibility of oxygen production by dissociation of the Martian atmosphere and the use of this oxygen to operate internal combustion engines. In combination, this provides a practical option for motive power on Mars, that is the generation of oxidizer (and fuel) from indigenous resources and on-demand shaft power generation. The emphasis in 1993 has been on the refinement of experimental facilities in both areas. Specifically, the Mars Oxygen Processor team has designed a new furnace/vacuum chamber and the Mars Methane Engine team has developed a new engine and test-bed.

Since the Martian atmosphere is mostly CO_2 , studies are underway to utilize this component to provide oxygen to support Martian surface operations and earth-return missions, thereby providing large savings in payload from earth. In cooperation with the University of Arizona, ODU is developing an oxygen processor using a zirconia cell. A high temperature chamber has been designed that can operate at pressures equivalent to the Martian surface. The design consists of an alumina shell with internal alumina baffles and tubing and a stainless steel cap. The stainless steel cap will be at a sufficiently low temperature to permit standard fittings to be used. The five alumina tubes will be used for feed and waste gas, oxygen extraction, wiring and instrumentation leads.

Since it is feasible to generate oxygen on the Martian surface and since there exist significant sub-surface ice deposits, it is considered relatively straightforward to synthesize methane, from water and CO_2 feedstock, as a fuel. The goal of the Mars Methane Engine team is to develop the technology required for operating internal combustion engines on the Martian surface, fueled by methane and oxygen and using CO_2 as a diluent. A new test-bed has been commissioned, using a standard single-cylinder 4-cycle engine, with a modified carburetor and extensive instrumentation. Preliminary operating data has been obtained, using gasoline-air, methane-air and methane-oxygen-carbon dioxide.

Introduction

Over the past thirty years, research has been carried out to determine what would be necessary to successfully land, explore, and return from the planet Mars. It had appeared that launch vehicles able to travel to the planet, land, and return to earth would be unreasonably large. Another problem was that the Earth-produced supply of oxygen for life support (and as an oxidizer for rocket propellant) could accidentally be depleted in such a way that a return to Earth would be impossible and the ability to sustain manned exploration would be lost. Since the major constituent of the Mars atmosphere is CO_2 , this feedstock is prevalent. Therefore, current research is being done to extract usable oxygen from Mars atmospheric carbon dioxide using a solid electrolyte process. This approach has the potential to substantially reduce round trip cost for Mars missions.

As missions to Mars advance, it will be desired to operate internal combustion engines for uses such as generators and operating small machinery. The options of transporting fuel or utilizing the Martian atmosphere for fuel & oxidizer have been investigated and the latter case has been accepted and considered feasible.

The Martian atmosphere contains more than 95 percent carbon dioxide, which can be synthesized with water to produce methane. As already discussed, oxygen can also be obtained from carbon dioxide by thermal decomposition. The ultimate goal of this portion of the project is to effectively operate and obtain results from an internal combustion engine operating on methane, carbon dioxide and oxygen. These three constituents will compose the test case in the experiment. Prior to testing of the three gases, a base case of methane and air will be examined for comparative results.

The Mars Oxygen Processor

Background

Studies are underway to determine what is needed to sustain a successful mission to the planet Mars. As mentioned previously, one of the problems that is faced is the high cost incurred due to the amount of propellant and life support consumables that would be needed to sustain such a mission. Sridhar and Iyer¹ report that more than 80% of a spacecraft's mass is due to the propellant; therefore, if a propellant production system could be installed on the planet's surface, the Earth launch mass requirement would decrease substantially and cost, in turn, would be

greatly reduced. One way to achieve this is through the use of an in-situ oxygen production system that produces oxygen from carbon dioxide. Since carbon dioxide makes up about 95.32% of the Mars atmosphere (Viking probe data) extraction of oxygen from carbon dioxide is very attractive. A demonstration oxygen processor has been constructed and tested previously by research teams at Old Dominion University. A team at the University of Arizona has developed a sample solid electrolyte cell using 8% yttria stabilized zirconia as the solid electrolyte and have tested it to produce a noticeable flowrate of oxygen. The ODU processor has been designed to use this cell. However, the existing furnace and vacuum chamber had poor temperature profile characteristics and vacuum leaks. Therefore, current research aims to correct these problems by designing a new furnace and vacuum chamber combination that will permit simulated Mars oxygen production at sub-atmospheric pressure.

The Zirconia Cell

Vaniman et al.², at the University of Arizona, has performed several tests on a zirconia test specimen at an elevated temperature (approx. 1000°C) and at atmospheric pressure. To further emulate the true operating conditions on the Mars surface, it is necessary to reduce the cell pressure to around 0.1 atm. Therefore, a vacuum chamber was required which could accommodate the existing zirconia cell design and satisfy the operating temperature and pressure requirements.

As mentioned previously, the cell is constructed of 8% yttria-stabilized zirconia and consists of a 1.150" dia. x 1.575" long x 1/8" thick cylindrical zirconia crucible and a 1.150" dia. x .025" thick zirconia disk that is connected to the crucible via a fired ceramic paste (Fig. 1). Platinum electrodes are pasted to the disk, to provide a means to maintain an electric potential across the disk. A 1.8" dia. alumina tube is pasted to the crucible to provide an exit port for the removal of oxygen inside the crucible.

The carbon dioxide, when heated to the prescribed temperatures, is dissociated into CO and O⁺⁺ ions. Because of the properties of yttria-stabilized zirconia at this elevated temperature, application of a voltage across the crystal lattice of the zirconia allows the oxygen ions to be conducted ionically through the material. After passing through the matrix, these ions release two electrons which are removed by the interior -electrode and returned to the power supply and then the remaining oxygen atoms recombine to form O₂.

Furnace Specifications

In order for the Mars Oxygen Processor System to operate, the CO₂ must be elevated to approximately 950°C to 1000°C and maintained for the dissociation of the CO₂ to occur. The use of a vacuum chamber to simulate the Mars atmospheric pressure requires that a heat source be selected that is capable of maintaining the entire chamber at these temperatures while the process occurs.

An existing commercial furnace, manufactured by the Lindberg Corporation, that was already available at O.D.U. was found to be suitable. Figure 2 shows the basic dimensions of the furnace, which has a maximum temperature capability of 1250°C.

In order to determine the position of the vacuum chamber inside the furnace, a thermal profile was obtained for the cavity. The interior of the furnace was instrumented with thermocouples positioned at equal distances from the bottom of the unit and set near the wall. The furnace was operated at several temperature ranges to obtain the steady-state temperature profiles of the unit. Figure 3 shows the basic set-up for the test.

The time required for the furnace to reach the required temperature of 950°C was approximately 2 hours. Figure 4 shows the temperature distributions recorded when each individual thermocouple registered 950°C, with increasing time. The temperature profile for the furnace's centerline is shown in Figure 5. The profile shows a smooth temperature rise for the furnace vs. the time required to reach the operational temperature of 950°C.

The furnace temperature sensor was found not to be very accurate when compared to the internal thermocouples. While the thermocouples recorded a temperature in excess of 950°C, the furnace's unit read only 750°C. This discrepancy could be due in part to the location of the sensor within the furnace itself. However, no attempt was made to disassemble the unit and locate the sensor position. Therefore, it will be necessary for sensor units to be recalibrated for future operation. Also, the temperature controller used in the furnace is a simple on-off control type and it simply cycles power on and off the heating elements. The installation of a more modern microprocessor based controller will allow for greater control and accuracy within the unit.

The Lindberg Furnace meets the performance requirements needed for the operation of the Mars Oxygen Processor. Given its design and type of controller, it will be a simple unit to operate and give good service. However, the installation of a new controller will be required if finer temperature control is needed. Also, a thermal heat load test should be conducted with a dummy vacuum chamber installed to further characterize the capacity of the furnace and document a baseline for future operations of the unit.

The Vacuum Chamber

As stated earlier, the operating conditions for the oxygen processor are a pressure of approximately 0.1 atm and a temperature between 900°C and 1000°C. The primary purpose of the vacuum chamber is to maintain vacuum integrity and while allowing heat transfer from the furnace to the carbon dioxide atmosphere inside the chamber. Several designs were considered for the chamber. The initial design is shown in Figure 6. It was a very simple hollow cylinder with the zirconia cell located in the center of the cylinder. Concerns about the structural integrity of the zirconia cell supports and heat transfer problems resulted in a series of modified designs. Figure 7 shows the interim chamber design. Some of the features of this design are the addition of radiation baffles, extension of the gas tubes further from the top of the chamber, and the use of simple shapes for the individual parts. The radiation baffles were added to reduce the radiation heat transfer in the direction of the cap and to make the assembly stronger. The tubes were extended to provide better cooling and the shapes of the individual parts were kept simple because of construction difficulties and cost related to complex geometries.

The final design, shown in Figures 8 & 9, performs well in thermal analyses and a vendor was found that stocked many of the parts required to construct the chamber. The thermal analyses revealed that the length of tube extending from the chamber could be eliminated and that than originally expected. The results are shown in Figure 10. Several individual parts that were required to construct the chamber were eliminated because a single dome assembly was found that could replace all the parts.

The chamber consists of two major assemblies. The external assembly is a canister that maintains vacuum integrity. This assembly can be reused for different geometry zirconia cells without modification. The internal assembly is a series of tubes and plates. The purpose of the internal assembly is to provide for plumbing connections (carbon dioxide inlet, oxygen outlet, waste gas outlet), instrumentation passages (thermocouples and power leads), and a seat for the zirconia cell. The cap (flange) is part of the internal assembly and double O-ring seals maintain the vacuum integrity between the two assemblies. Since several components are joined with high temperature adhesives in the internal assembly, that equipment probably cannot be reused if the zirconia cell fails. The inability to reuse this portion of the pressure vessel requires that a great deal of care be used during handling.

The material selected for the majority of the chamber is alumina. This selection was based on its high operating temperature range and to match the thermal expansion of the oxygen exit tube from the zirconia cell. The major drawbacks of this material are its cost and machinability. The material costs are high, so the design needs to be optimized in order to reduce waste. Alumina is permeable to gas in all conditions except the fully sintered state. Unfortunately, in the fully sintered state, it is too hard to machine with carbide tooling, the only suitable tooling being diamond chip tooling. Only a few companies offer this type of machining service and it is very expensive. Alumina is also very brittle and easily broken. Extreme caution must be exercised when handling this material.

The cap is a 300 series stainless steel. This series of stainless steel is suitable for high temperature applications and is readily available. The transition from alumina tubes inside the chamber to stainless steel tubes outside the chamber occurs in the cap. A 1/8" diameter tapered pipe thread is provided for each tube to install a fitting suitable to attach to external tubing. For the final design, Coors Ceramics Company provided the estimate for the alumina parts and Aremco Materials provided the estimate for the adhesives. The total estimated cost for two complete chambers, less assembly, was \$2800. It is intended that one of the chambers be assembled without the internal assembly and used as the dummy chamber for the thermal heat load test. This will determine the optimum position of the zirconia cell in relation to the furnace and the length of the internal tubes can be adjusted if necessary.

Thermal stresses are an important consideration. Both alumina and zirconia will crack if heated or cooled too rapidly. The temperature profile of the furnace during heating and cooling has been determined, but it may be necessary to control the rate of temperature rise and cooling time manually to prevent cracking.

Two operational problems have been identified that need to be addressed. First is the over-pressurization of the vacuum chamber during heating. The operating temperature is four times room temperature (on the absolute scale), therefore, the internal pressure will increase to four times the atmospheric pressure if the chamber is not vented. Alumina has excellent strength characteristics in compression, but its strength characteristics in tension are poor. Therefore it is recommended that the chamber be vented during heating. The second problem is damage to the zirconia cell by unequal pressures on the input and output sides of the wafer. The maximum allowable pressure differential is set at two pounds per square inch. An allowable pressure differential of one psi is desirable. In order to protect the cell during all phases of operation, a two-way pressure relief valve can be placed between the waste gas line and the oxygen exit line. Data would be lost if a pressure differential existed that caused the valve to operate, but the cell would not be damaged.

The Mars Methane Engine

Background

The Mars methane engine project has been ongoing for the past two years. Previous design teams had experienced many difficulties in their work and were not able to obtain any substantial test results. In particular, the main problem encountered by last semester's team was the internal combustion engine being used. The one-cylinder Megatech lab engine was not able to perform adequately under the required conditions. The higher temperatures resulting from the combustion of methane and poor tolerances in the cylinder caused fracture of the cylinder. The team designed and machined a stainless steel cylinder but still experienced difficulties.

After encountering these problems, the previous team decided to initiate the construction of a new test bed, including purchasing a new engine and all equipment needed. This included 1) a new Honda GX120 4Hp engine^{3,4}, 2) an AVL 8QP500C pressure transducer⁵, 3) an AVL charge amplifier, 4) three Cole Parmer variable area flowmeters, 5) a Lucas Ledex K3 Series incremental encoder, and 6) an Omega K type thermocouple probe. The new engine required a larger dynamometer which was available in the thermodynamics laboratory. In addition, an existing PC-based data acquisition workstation was obtained.

Engine Modifications

In order to operate the engine on methane, carbon dioxide and oxygen, the existing air-fuel carburetor, throttling mechanism and fuel system were removed. The required fuels are supplied by pressurized tanks and controlled by regulators and flowmeters to a mixing chamber, shown in Fig. 11. The mixing chamber has eddy generators to promote mixing. A pressure gage was connected to a tap in the mixing chamber to monitor inlet pressures.

The engine also needed modifications to both ends of the driveshaft. A fitting was installed to the end of the shaft connected to the dynamometer. The other end was also adapted for connection with the incremental encoder.

It is required that gas samples and temperature readings be taken at the exhaust of the engine. For this reason, an exhaust

extension was designed and manufactured. This extension also relocated the muffler, allowing more access to the cylinder head for the mounting of the pressure transducer.

Finally, the most important modification made to the engine was the installation of the pressure transducer. This was a difficult process that required a great deal of thought and precise measurements. The pressure transducer was mounted onto the cylinder head to measure pressure in the combustion chamber as a time history. In determining the location of the transducer in the cylinder head, three criteria were suggested by the manufacturer:

1. If possible, at least 50% of the diaphragm surface area should lie over the combustion chamber.
2. The measuring position should not lie in the immediate vicinity of the exhaust valve.
3. Installation of the pressure transducer should be as perpendicular as possible to the cylinder head face and a safety clearance of at least 0.5 mm should be maintained.

The limited space within the combustion chamber made it difficult to fully meet all three criteria. Approximately 60% of the diaphragm surface area lies directly over the chamber, the location is in the general vicinity of the exhaust valves, (Fig. 12) and the transducer is mounted at an angle of approximately 30 degrees.

Test-Bed

The overall setup of the system is shown in Figure 13. A mounting stand was constructed to secure the dynamometer, engine, and encoder. A 12V battery supplies DC power to the dynamometer and to start the engine. While testing, it is necessary to water-cool the pressure transducer. It was recommended that a distilled water cooling system be used but due to time limitations and the limited use of the transducer, a simple open loop water cooling system was connected from a water supply line in the laboratory. The instrumentation (thermocouple, pressure transducer, and incremental encoder) are connected to the data acquisition system via an analog and digital input/output board.

The AVL 8QP5000C pressure transducer utilizes the piezoelectric effect for measuring pressure. The effect involves the use of quartz crystal, affected by a pressure disturbance, to act upon a water-cooled diaphragm and a stiff intermediate element. The pressure transducer is shown in Fig. 14. The crystal transforms a pressure signal into an electric charge signal. This electric charge signal is then fed through a coaxial cable (with high impedance isolation) to a charge amplifier where it is then transformed into an electrical voltage. This voltage is then fed to the data acquisition system.

To establish the crankshaft angular position as a function of time, the team will be using an incremental encoder. The encoder that was chosen is a LUCAS K3 Series Modular Rotary Encoder. As the encoder disk rotates in front of a stationary mask, it shutters the light from an LED light source. The light is received by a photodetector which produces pulses in the form of a square wave output. This encoder also includes a single marker that provides one pulse every 360 degrees of mechanical rotation. This pulse is a reference to determine a home-base position. A drawing of the components of the encoder is shown in Fig. 15.

The software used in conjunction with the data acquisition system is LPCLAB by Data Translation. The software consists of numerous subroutines that can be programmed in various languages, with FORTRAN being chosen for this application.

The program 'MARS' consists of three main subroutines that allow for all required measurements to be made. The first subroutine involves the temperature of the thermocouple. The next subroutine (for the pressure transducer) is slightly more complicated. A burst of A/D conversions is made at a specified (high) rate, with the program execution suspended until completion. The final subroutine, which represents a high-speed digital interface to the crank angle encoder, is not yet complete.

Engine Operation

In order to determine the chemically correct mixture of methane, carbon dioxide, and oxygen required, many thermodynamic calculations must be made^{6,7,8}. To begin with, several assumptions must be made for the combustion process, including steady flow of the mixture, ideal complete combustion, and adiabatic conditions. From these assumptions a chemically correct combustion equation can be derived and the appropriate flowrates of fuel and oxidizer can be injected to obtain complete combustion.

Prior to testing of the base case (methane-air) and test case (methane, CO₂, O₂), it was necessary to obtain preliminary results from the engine operating on unleaded gasoline. This testing was performed as a basis for familiarizing the team with the ranges of the dynamometer and for comparison of torque and brake horsepower versus rpm.. Results can be seen in Fig. 15.

Upon completion of the modified engine setup and programmed data acquisition system (for temperature and pressure readings), testing of the base case and test case was performed. Since this was the first time realistic testing was to be performed on the Mars methane engine, procedures had to be developed. Many possibilities and options exist in order to establish comparable base and test cases. The team felt that an adequate preliminary test constraint was to hold the inlet (manifold) pressure constant in both cases. When operating the engine on methane and air, the aspiration plug is removed from the end of the mixing chamber to allow for air flow. This air flow is not regulated by a flowmeter. Therefore, the inlet pressure for the base case was atmospheric. When operating the engine on methane, carbon dioxide, and oxygen, the flowrates were adjusted to the same inlet pressure (approximately 1.0 atm.). With the inlet pressure held constant, similar rpm and torque values could be set for each test. Temperature and pressures were then sampled by the data acquisition system and an exhaust gas sample was taken. These operating procedures will now be summarized:

Preliminary Base Case Testing:

1. Turn on water cooling supply for pressure transducer.
2. Set supply tanks to a back pressure of 60 kPa.
3. Ensure CH₄ flowmeter is closed.
4. Connect 12V battery to dynamometer and turn on AC power supply.
5. Turn on engine switch.

6. Set dynamometer to Start Operational Mode, CW Field Mode, and HIGH Load Range.
7. Increase Field Load adjustment on dynamometer until shaft rotates.
8. Increase flowrate in methane flowmeter until combustion occurs.
9. Set Operational Mode to desired field load
10. Monitor flowrate, Field Load, and rpm until desired conditions are met.
11. Perform data acquisition for exhaust temperature and cylinder pressure.
12. Follow steps 1-7 in section 6 (exhaust gas analysis) for exhaust sample.
13. Reduce flowrate until combustion process ceases.
14. Turn off dynamometer, supply tank pressure.
15. Allow engine to cool (5-10 minutes minimum before disconnecting water supply to pressure transducer.

Preliminary Test Case Testing:

1. Repeat Steps 1 through 3 for all three gases and flowmeters. (above)
2. Repeat Steps 4-7. (above)
3. Supply excess amount of carbon dioxide to the mixing chamber along with required amounts of methane and oxygen.
4. Slowly decrease CO₂ (diluent) until combustion occurs.
5. Repeat Steps 9-15. (above)

Results

A set of results was obtained for both the base case and test case. These results include exhaust temperature, cylinder pressure as a function of time, and one exhaust sample for each case. Testing was performed while the engine operated at an inlet pressure of 1.0 atm., 2700 rpm, and a torque of 20 in-lbs. Results are shown in graphical form in Fig. 16 and tabulated in Fig. 17. Pressure histories are shown in Fig. 18. As indicated from the base case results, peak pressures ranged from approximately 220-240 psig. Results also show that the pressure inside the combustion chamber had a minimum pressure of approximately -5 psig.

As shown from the test case results, peak pressures ranged from approximately 130-170 psig. These values of pressure are slightly lower than the base case results.

The exhaust temperature for the base case was about 570 (Celsius) and the test case was about 750 (Celsius).

From the exhaust gas analysis, it was found that the base case results show that the engine was operating with an excess of fuel. The exhaust gas analysis of the test case has not yet been completed.

Conclusions

The first part of the project concentrated on the design and analysis of the vacuum chamber/tube furnace combination. Three design improvements were required as analysis results and refinements were made. There appear to be no problems with structural integrity, vacuum integrity, thermal stress, and heat transfer. All materials and hardware have been purchased or acquired to construct the vacuum chamber, however there was not enough time to assemble and test the chamber this semester. This semester has marked a turning point for the Mars Methane Engine project. The installation of a new reliable engine will provide the accurate testing and results necessary for future design teams to build upon and draw conclusions. The engine has been modified and is capable of operating on the base case of methane and air as well as the test case of methane, carbon dioxide, and oxygen. Calculations for required air-to-fuel ratios of methane and air have been performed as a basis for future testing. Programming of the data acquisition system has been completed, with the exception of the incremental encoder. Preliminary testing of the base case and test case have been performed for comparative results. Exhaust samples have been taken and to be analyzed. The successful completion of each of these aspects of the overall project will allow future teams to focus on testing of the test case.

References

1. Iyer, Venkatesh A. and Sridhar, K. R., "Thermal Analysis, Optimization and Design of a Martian Oxygen Production Plant," NASA Space Engineering Research Center for Utilization of Local Planetary Resources, Annual Progress Report, 1990-1991.
2. Vaniman, B., et al., "Oxygen Production on Mars and the Moon," Annual SERC Report, 1991-1992
3. GX120K1 Shop Manual, Honda Power Equipment, 1991 Honda Motor Co., Inc.
4. American Honda Motor Co., Inc., P.O. Box 100021 Duluth, Georgia 30136-9421. Phone: (404) 497-6400.
5. Charles Elias, Technical Sales Manager - AVL North America, Inc., Novi, Michigan. Phone: (313) 477-3399. Fax: (313) 477-6043.
6. Ferguson, Colin R., Internal Combustion Engines, John Wiley and Sons, Inc., New York, 1986.
7. Campbell, Ashley, S., Thermodynamic Analysis of Combustion Engines, Robert E. Kreiger Publishing Company, Malabar Florida, 1986.
8. Arcoumanis, C., Internal Combustion Engines, Academic Press, San Diego, Calif., 1988.

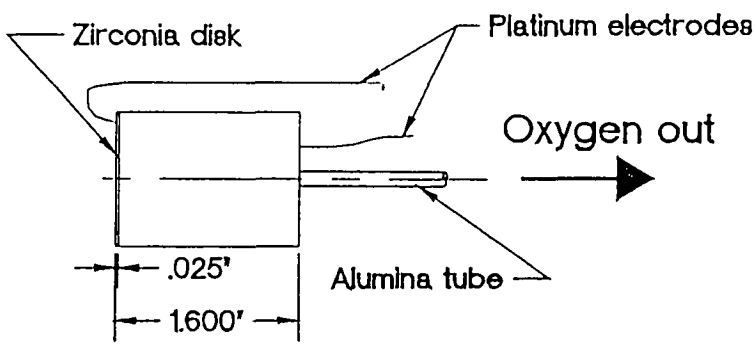


Figure 1 Schematic of Zirconia Cell

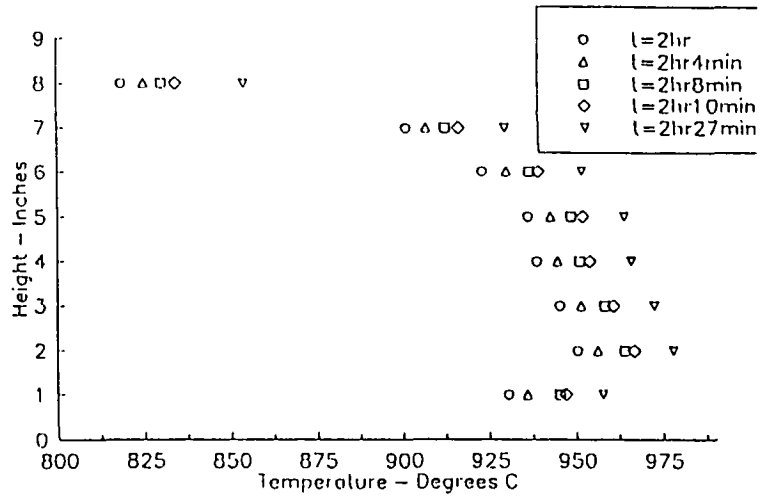


Figure 4 Temperature Profile of Furnace

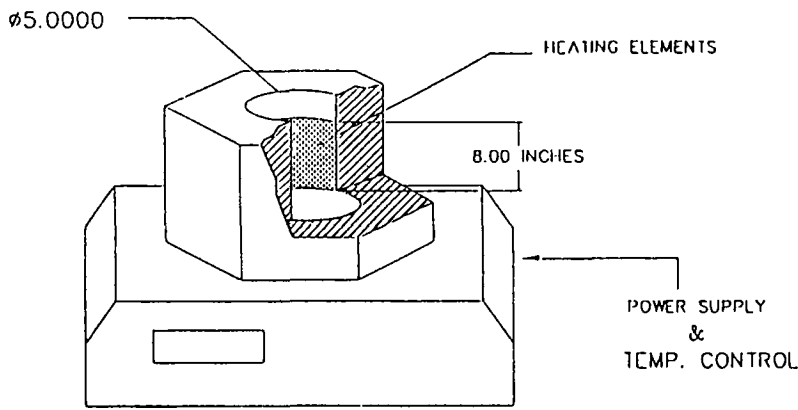


Figure 2 Schematic of Zirconia Furnace

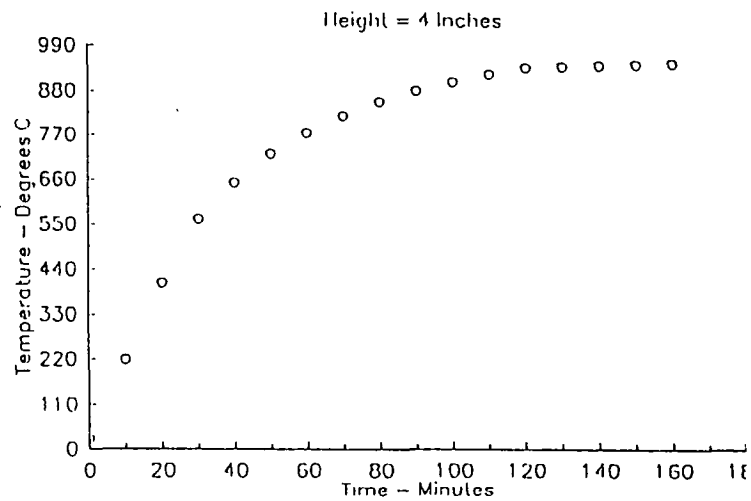


Figure 5 Temperature Rise on Furnace Centerline

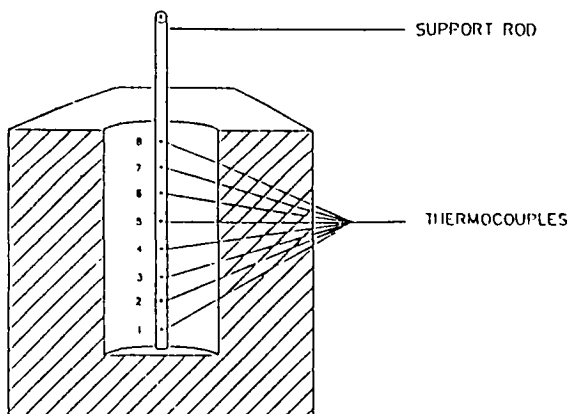


Figure 3 Temperature Profile Test Set-Up

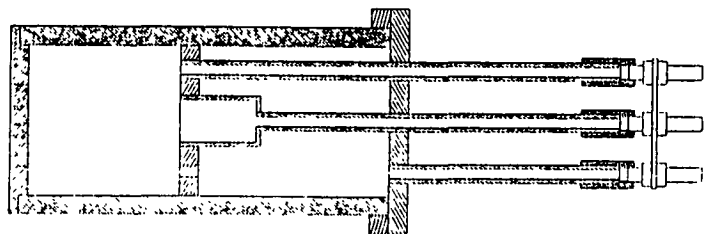


Figure 6 Initial Vacuum Chamber Design

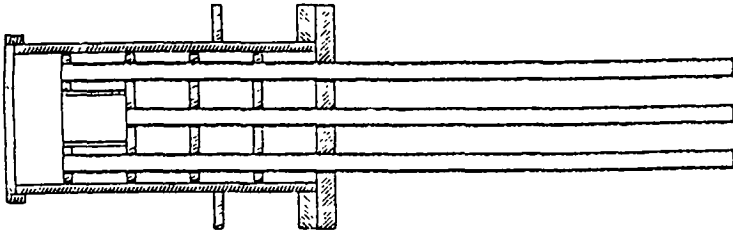


Figure 7 Interim Vacuum Chamber Design

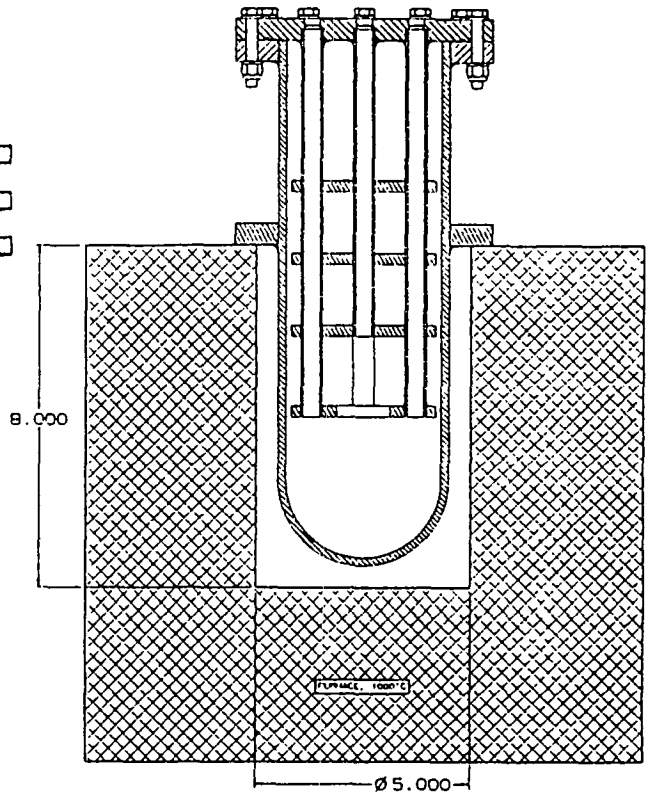


Figure 9 Final Design Installed in Furnace

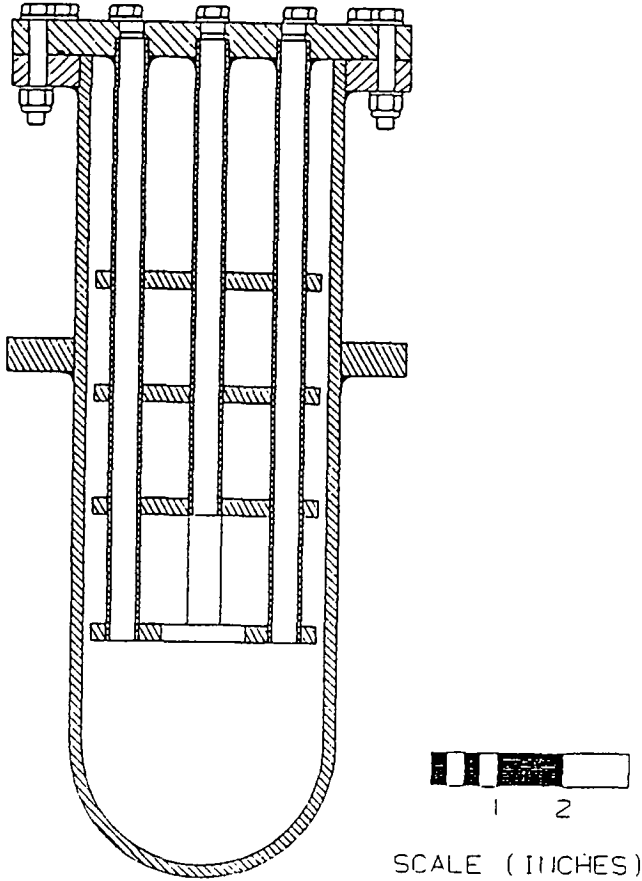


Figure 8 Final Vacuum Chamber Design

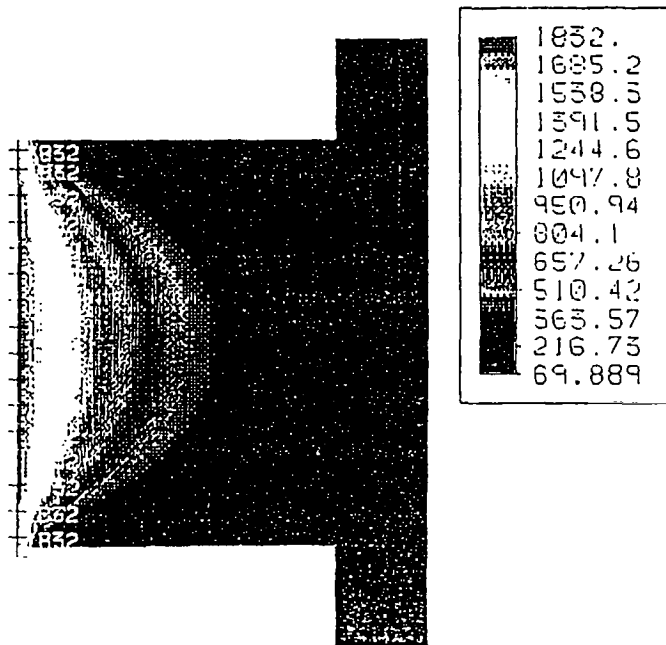


Figure 10 Temperature Profile of the Exposed Portion of the Vacuum Chamber

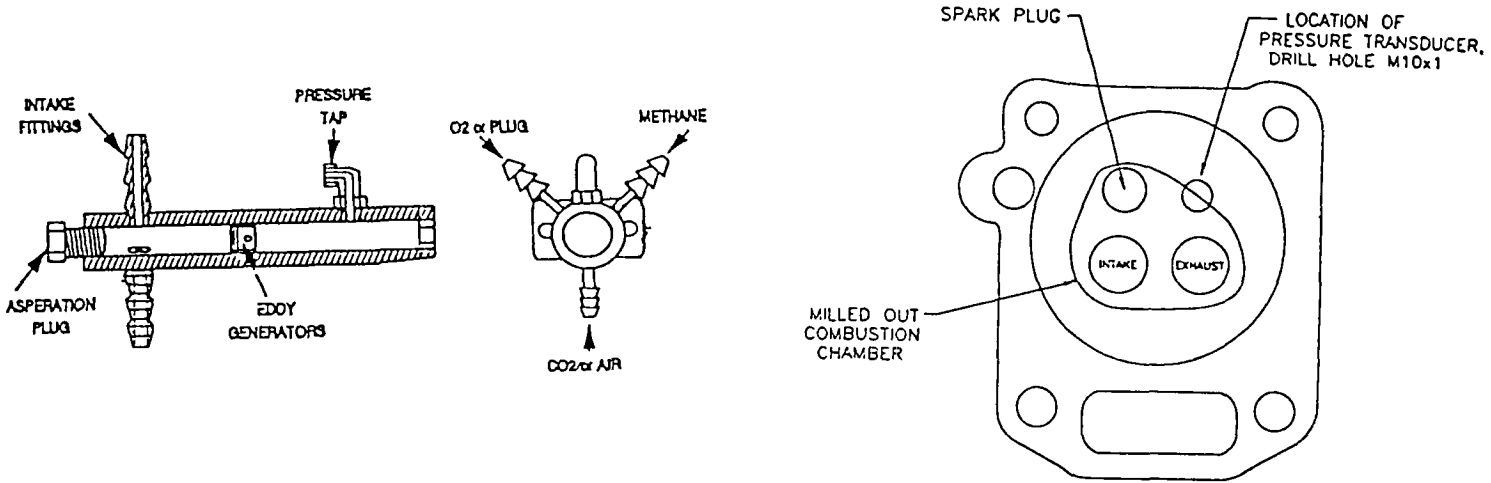


Figure 11 Carburetor for CH₄ + O₂ + CO₂ Mixing Operation

Figure 12 Location of Pressure Transducer in Cylinder Head

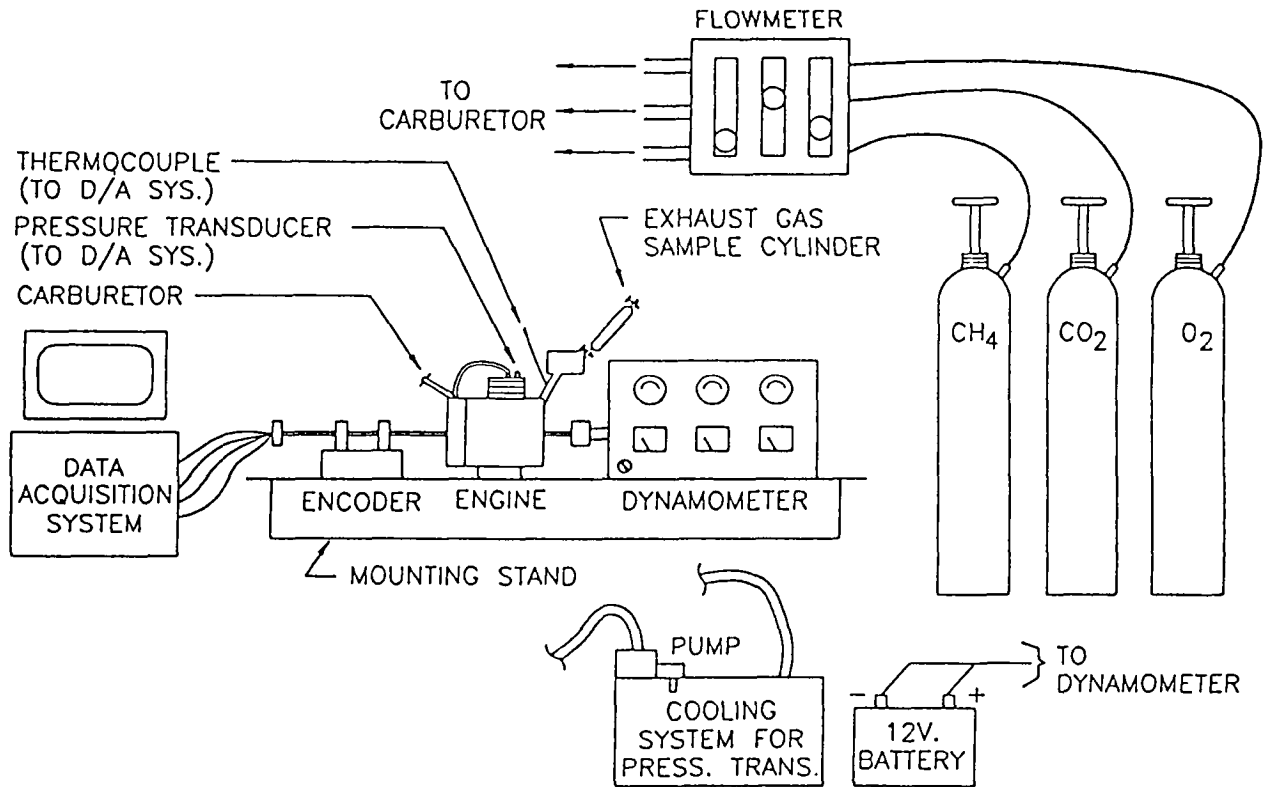


Figure 13 Schematic Diagram of Engine Test-Bed and Set-up.

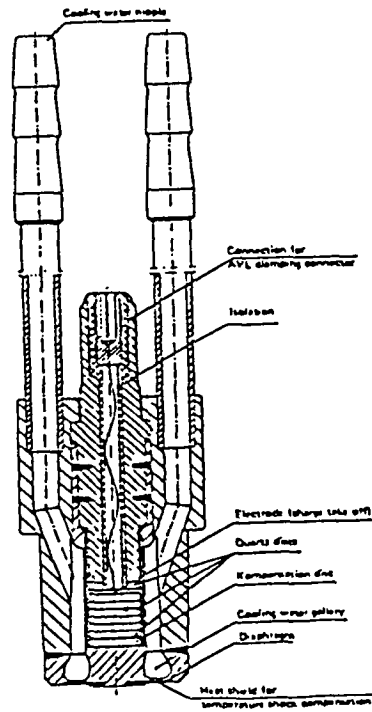
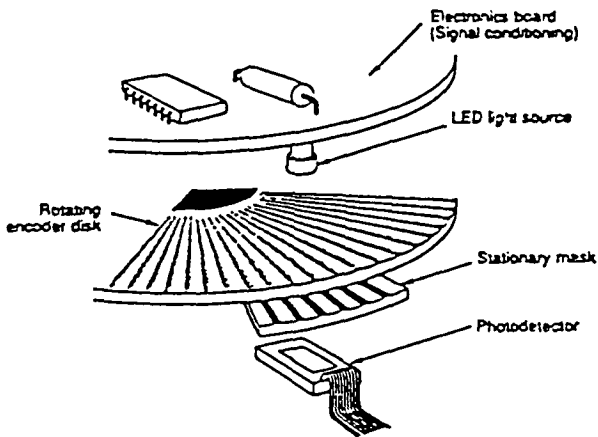


Figure 14 AVL Pressure Transducer



Dual Channel - Quadrature Encoders

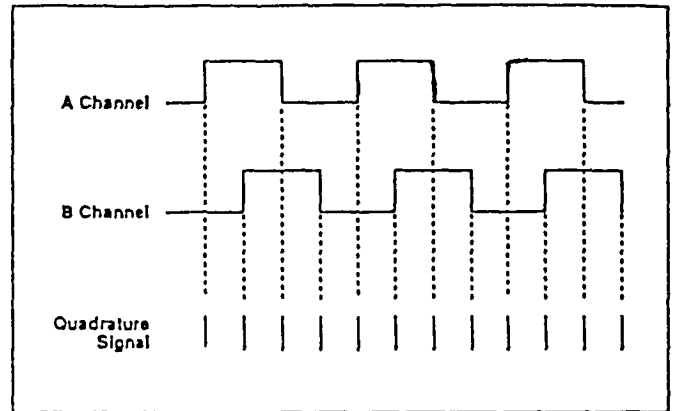


Figure 15 LUCAS K3 Rotary Encoder

Performance Curves for Honda GX120 Full Throttle

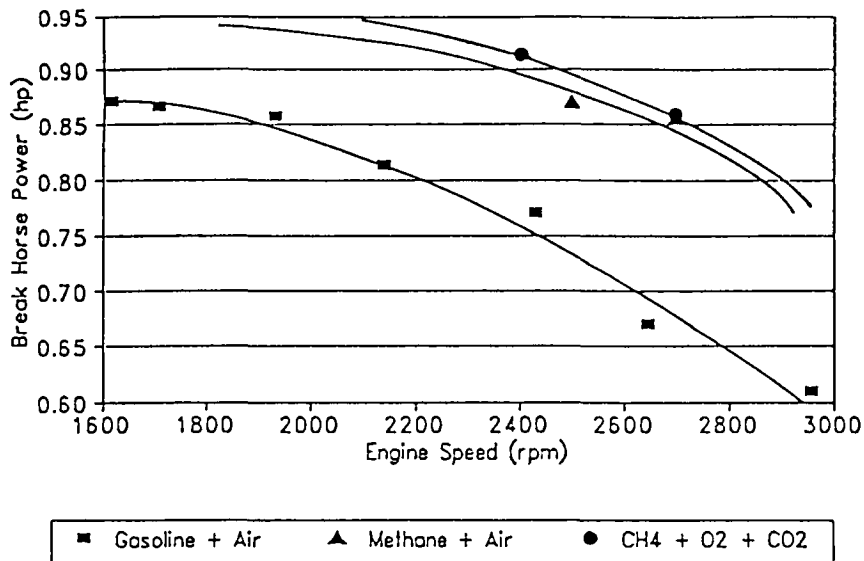


Figure 16a Power versus RPM, various cases

MODIFIED DATA

HONDA GX120 ENGINE (FULL THROTTLE)

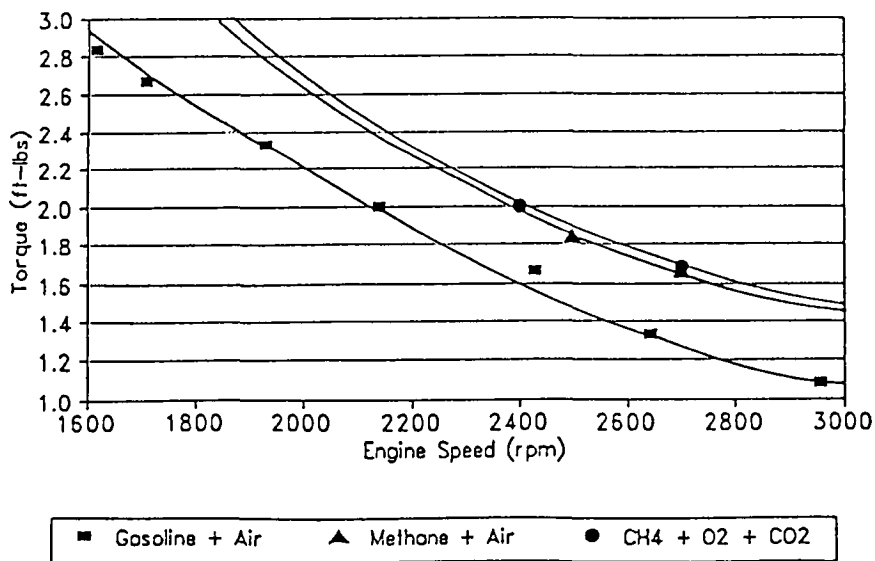
FUEL: UNLEADED GASOLINE

RUN	N (RPM)	TORQUE (in-lbs)	TORQUE (ft-lbs)	BEP (hp)
1	2957	13	1.083	0.6097
2	2643	16	1.333	0.6708
3	2430	20	1.667	0.7713
4	2140	24	2.000	0.8149
5	1932	28	2.333	0.8582
6	1708	32	2.667	0.8673
7	1617	34	2.833	0.8722

FUEL: METHANE + AIR

RUN	N (RPM)	TORQUE (in-lbs)	TORQUE (ft-lbs)	BEP (hp)
1	2700	20	1.667	0.8564
2	2500	22	1.833	0.8722

Performance Curves for Honda GX120 Full Throttle



FUEL: METHANE + OXYGEN + CARBON DIOXIDE

RUN	N (RPM)	TORQUE (in-lbs)	TORQUE (ft-lbs)	BEP (hp)
1	2700	20	1.667	0.8564
2	2400	24	2.000	0.9135

Figure 16c Tabulated Results

Figure 16b Torque versus RPM, various cases

DATE APRIL 16, 1993

R.P.M.: 2700

TORQUE 20 in-lbs (LOAD #1)

FLOWRATES CB4: 8mm

INLET PRESSURE <1 atm

EXHAUST TEMPERATURE (C) 572.4749

VOLTS (volts)	DIGITAL	TIME (sec)	PRESSURE (psig)	PRESSURE (psig)
0.87647	2407	0.002	128.81	163.61
0.34668	2190	0.004	50.95	85.95
0.13184	2102	0.006	19.38	54.38
0.06592	2075	0.008	9.69	44.69
8.00000	2055	0.010	2.51	37.51
-0.16846	1979	0.012	-24.76	10.24
-0.24414	1948	0.014	-35.88	-0.88
-0.25391	1944	0.016	-37.32	-2.32
-0.26367	1940	0.018	-38.75	-3.75
-0.26123	1941	0.020	-38.39	-3.39
-0.16846	1979	0.022	-24.76	10.24
-0.29297	1928	0.024	-43.06	-8.06
-0.28809	1930	0.026	-42.34	-7.34
-0.28809	1930	0.028	-42.34	-7.34
-0.28809	1930	0.030	-42.34	-7.34
-0.27344	1936	0.032	-40.19	-5.19
-0.26367	1940	0.034	-38.75	-3.75
-0.24414	1948	0.036	-35.88	-0.88
-0.17578	1976	0.038	-25.83	9.17
-0.00488	2046	0.040	-0.72	34.28
0.55420	2275	0.042	81.45	116.45
1.29883	2560	0.044	190.88	225.88
0.77637	2366	0.046	114.10	149.10
0.30518	2173	0.048	44.65	79.65
0.10254	2090	0.050	15.07	50.07
0.03662	2063	0.052	5.38	40.38
-0.01221	2043	0.054	-1.79	33.21
-0.17334	1977	0.056	-25.48	9.52
-0.23193	1953	0.058	-34.09	0.91
-0.23682	1951	0.060	-34.80	0.20
-0.23438	1952	0.062	-34.45	0.55
-0.22949	1954	0.064	-33.73	1.27

DATE APRIL 16, 1993

R.P.M.: 2700

TORQUE 20 in-lbs (LOAD #1)

FLOWRATES CB4: 50mm

CO2: 50mm

O2: 30mm

INLET PRESSURE <1 atm

EXHAUST TEMPERATURE (C) 750.1325

VOLTS (volts)	DIGITAL	TIME (sec)	PRESSURE (psig)	PRESSURE (psig)
-0.15869	1983	0.002	-23.32	6.68
-0.18789	1971	0.004	-27.63	2.37
-0.19287	1969	0.006	-28.35	1.65
-0.19287	1969	0.008	-28.35	1.65
-0.18066	1974	0.010	-26.55	3.45
-0.17334	1977	0.012	-25.48	4.52
-0.14893	1987	0.014	-21.89	8.11
-0.13184	1994	0.016	-19.38	10.62
-0.06836	2020	0.018	-10.05	19.95
0.11963	2097	0.020	17.58	47.58
0.61279	2299	0.022	90.06	120.06
0.86670	2403	0.024	127.38	157.38
0.72022	2343	0.026	105.85	135.85
0.53711	2268	0.028	76.94	108.94
0.31494	2177	0.030	46.29	76.29
0.19775	2129	0.032	29.06	59.06
0.03418	2062	0.034	5.02	35.02
-0.11475	2001	0.036	-16.86	13.14
-0.13428	1993	0.038	-19.73	10.27
-0.13184	1994	0.040	-19.38	10.62
-0.12451	1997	0.042	-18.30	11.70
-0.11719	2000	0.044	-17.22	12.78
-0.14893	1987	0.046	-21.89	8.11
-0.14648	1988	0.048	-21.53	8.47
-0.16602	1980	0.050	-24.40	5.60
-0.17090	1978	0.052	-25.12	4.88
-0.16846	1979	0.054	-24.76	5.24
-0.16602	1980	0.056	-24.40	5.60
-0.14893	1987	0.058	-21.89	8.11
-0.12695	1996	0.060	-18.66	11.34
-0.05859	2024	0.062	-8.61	21.39
0.14160	2106	0.064	20.81	50.81

Figure 17 Tabulated Results for one cycle

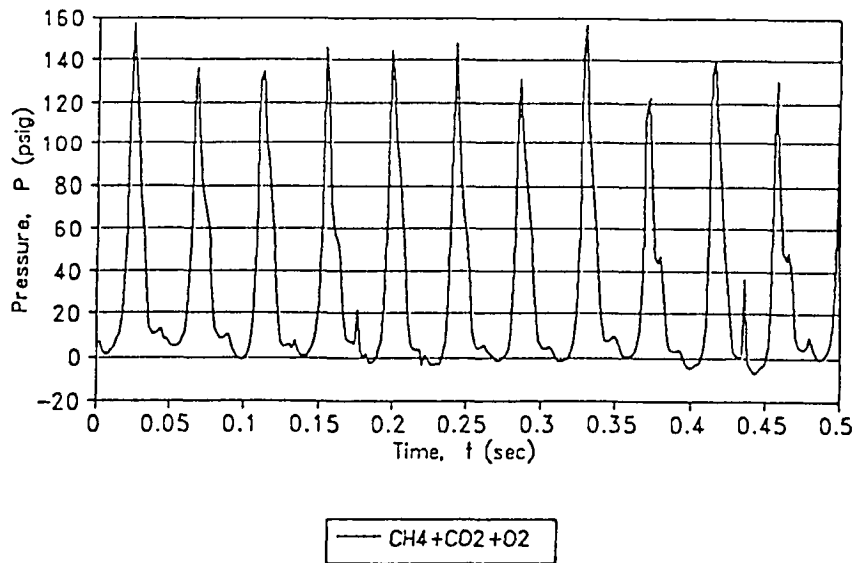
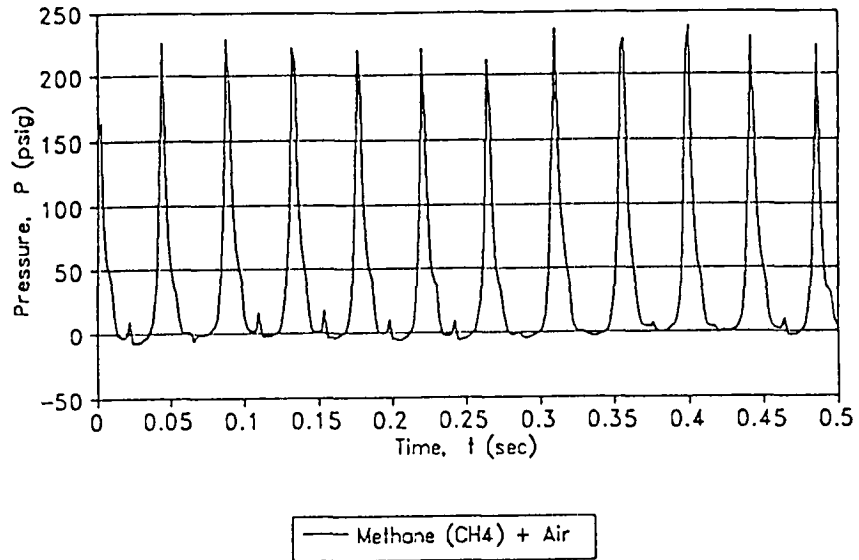


Figure 18 Typical Cylinder Pressure Histories

A MISSION TO MERCURY AND A MISSION TO THE MOONS OF MARS

The Pennsylvania State University
Department of Aerospace Engineering
University Park, Pennsylvania

Dr. Robert G. Melton and Dr. Roger C. Thompson
Thomas F. Starchville, Jr., Teaching Assistant

PROJECT FIREFLY: MISSION TO MERCURY

Kimberly Clemons, Kevin Gallagher, Jeffrey Gray,
Shane Kessler, Rick Sleutaris, George Truman

Abstract

The primary objective of this mission is to study the planet Mercury and advance the findings of Mariner 10. A proof of concept for use in later missions is a solar sail used during the spacecraft's interplanetary trajectory. Once at Mercury, the sail will detach and the planet will be mapped paying particular attention to regions of interest (the Caloris Basin, the hilly and lineated terrain, the intercrater plains, and the smooth plains) for possible landing sites. In order to avoid the extreme temperatures and radiation at the surface of Mercury, the probes will land on the dark side to perform their analyses. The scientific study on the surface will include seismic and tectonic activity and in-situ analysis of the regolith.

Introduction

Mariner 10's observations of the planet Mercury started to answer many questions about the planet closest to the Sun. However, partial mapping of the planet and quick flybys left many questions unanswered. Since its mission in the early 1970's, many more questions have arisen. Are there prospects of using Mercury's resources to relieve Earth's dwindling supply? Could Mercury support a laboratory for closer study of the Sun? Are there polar ice caps on Mercury? What is the make-up of the surface regolith?

Specifically, the scientific study of the planet by Project Firefly includes sending four landers to the surface to analyze seismic and tectonic activity, thermal conductivity of the soil, regolith composition, ice experiments, and mapping of the planet. This project also investigates the feasibility of propulsion via solar sail using a spiraling orbit to Mercury, composite systems to reduce thermal stresses, communication in an area of high solar activity, communication with an inflatable antenna, and thermal control challenges of keeping the spacecraft and its landers

within an acceptable range while temperatures vary from -183°C to $+467^{\circ}\text{C}$ on the planet's surface.

This report summarizes final work on the mission to Mercury. Specifically, a mission scenario is presented along with the spacecraft and lander configuration, final cost estimate, and the individual subsystems' mass and power requirements.

Mission Objectives

Project Firefly is designed to send multiple landers to Mercury, conduct experiments, and map the planet. The primary objective is to study different regions of Mercury in an effort to understand their formation. Secondary objectives are to study the efficiency of a solar sail for interplanetary travel and to map, within a few decimeters, the entire planet.

Since various regions of Mercury show different evolutionary characteristics, it is important that as many of these regions as possible be studied. The differences in region formation may enlighten scientists as to the creation of the solar system. Also, Mercury may contain ice deposits from passing comets. Regolith analysis and seismic and tectonic studies will give insight into Mercury's evolution.

A secondary objective is to determine the feasibility of solar sail travel. Since the solar sail is relatively new in practice, Project Firefly will give insight into the practicality of interplanetary solar sail applications. The effects of sail angle, spacecraft trajectory and sail deployment will be helpful in understanding the physical constraints of the solar sail. Solar sails may prove to be a cost-effective means of future unmanned space transportation.

Another secondary objective is the total mapping of Mercury within a few decimeters. Upon Mercury capture, the spacecraft will map the entire surface with a resolution of 21 meters. A laser altimeter will generate a three-dimensional map of each landing area with a resolution of 50 cm. After the landers are deployed, three-dimensional mapping of the entire planet will be attempted. This will occur while the orbiter transmits to the landers or to Earth.

Mission Profile

The mission profile can be divided into two phases. The first phase includes those events occurring from Earth's

surface to Mercury. The second phase includes actions taken in low Mercury orbit and on the planet itself. Figure 1 shows the mission scenario for Project Firefly.

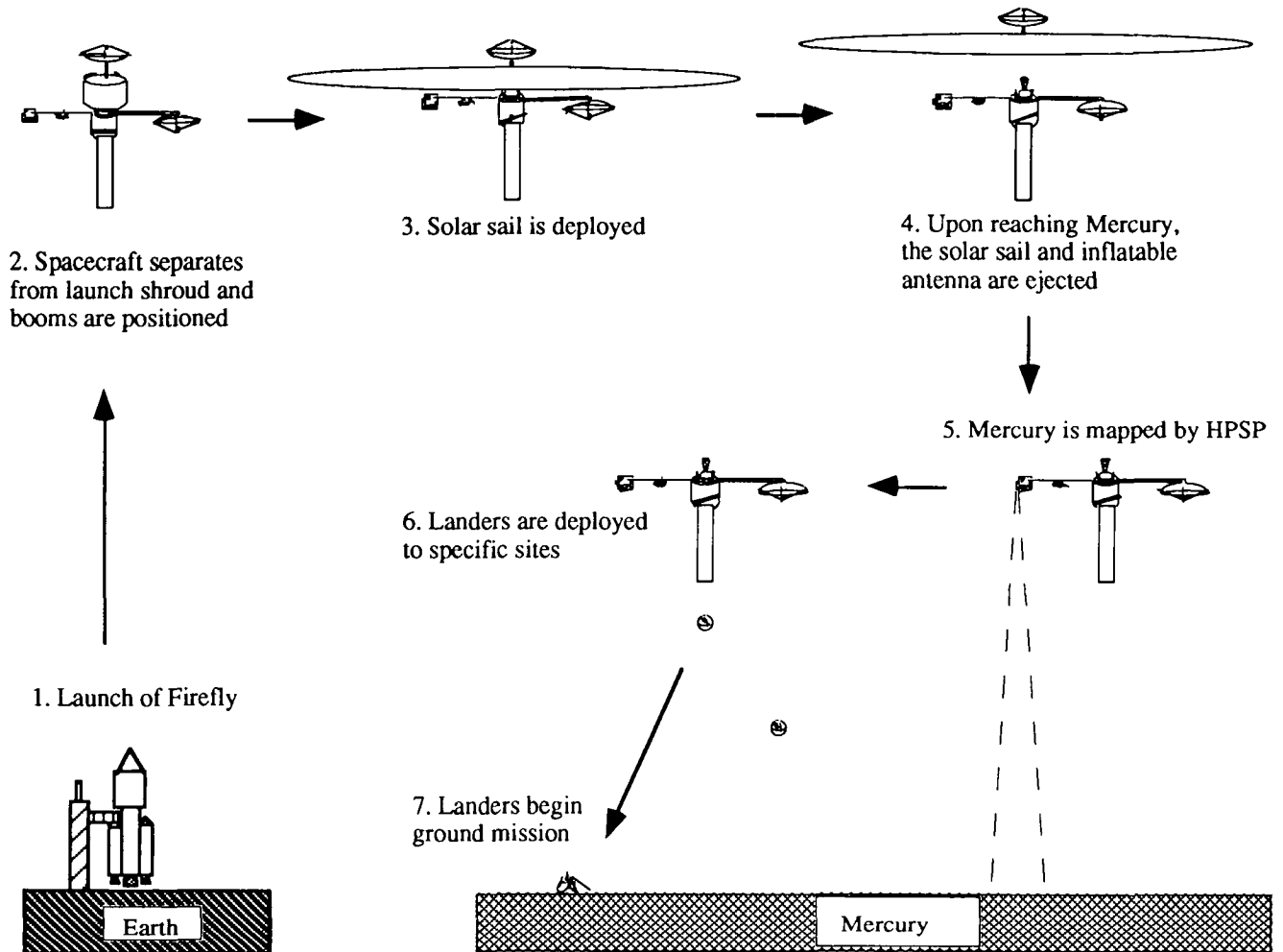


Fig. 1. Project Firefly Mission Scenario

Phase One -- From Earth to Mercury

Due to the length and the large mass of the SPF-2000 spacecraft, many of the previously studied launch vehicles were eliminated. The only launch vehicle that would fit the specified spacecraft dimensions is the Titan IV. This vehicle will boost the craft from Earth to LEO where a systems check will be performed and the solar arrays and communication antennae deployed, as shown in Figures 2 and 3. The spacecraft will then use an RL-10A rocket motor

for escape to an interplanetary transfer orbit. While on this hyperbolic escape orbit, the spacecraft will be spun and the solar sail deployed from a canister 4.84 m in diameter and 6 m long. Once the sail is completely unfurled, the spacecraft begins its spiral toward Mercury. This will take approximately 3.5 years. Once the spacecraft reaches Mercury's orbit, it will be turned 180 degrees, aligning itself for the eventual firing of the XLR-132A capture motor and insertion into a 500 km orbit above the surface of the planet.

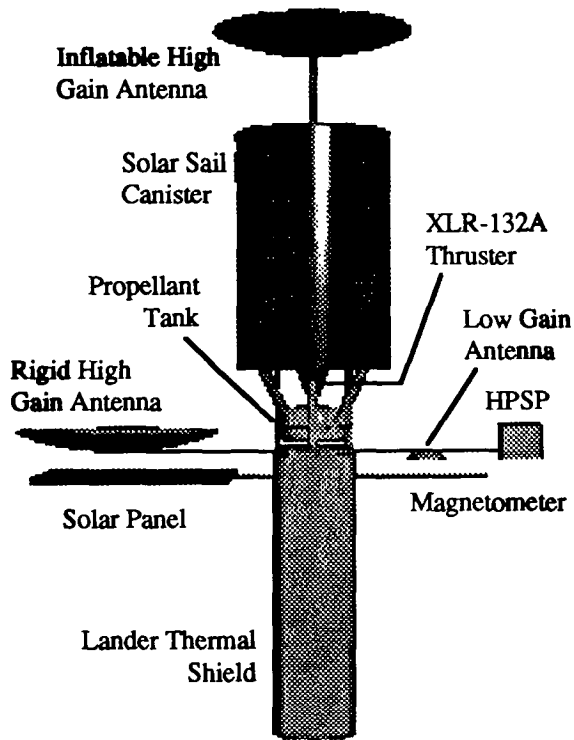


Fig. 2. SPF-2000 Spacecraft

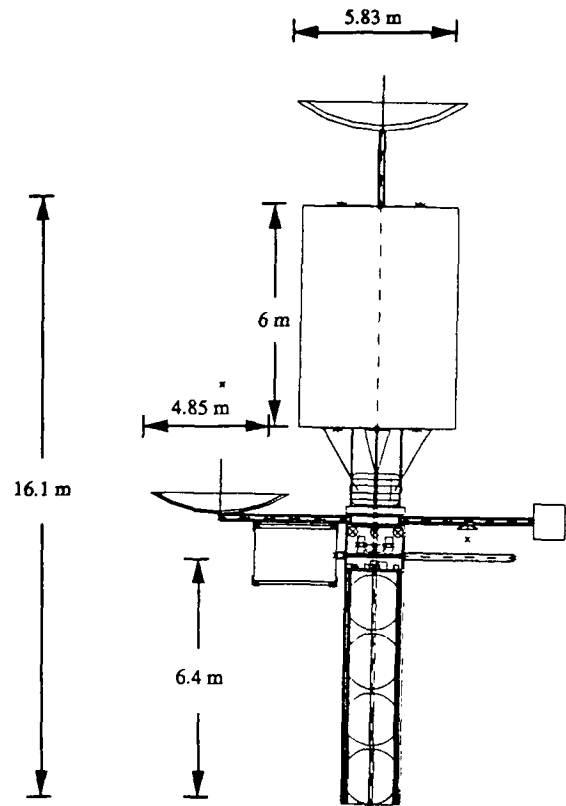


Fig. 3. Side View Schematic of Spacecraft

Phase Two -- Mercury Orbit and Landings

After capture at Mercury, the spacecraft begins mapping the planet with its High Precision Scanning Platform (HPSP), as shown in Figure 4. After mapping is completed, the four predetermined areas are scanned for suitable landing sites. Suitable 20 km by 20 km regions in the Caloris Basin, Hilly and Lineated Terrain, the crater Bernini, and the Smooth Plains are determined by a ground support team. The main C&DH computer (the Rockwell RI-1750 A/B) then calculates the required trajectory for the landers to reach their sites. Once this is done, small attitude thrusters place the spacecraft in the necessary orientation and the first lander is ejected via explosive bolts. The spacecraft then adjusts to the next location and the second lander is released. The same procedure is used for the third and fourth landers. (This mission is designed to place each lander on the surface near the dusk terminator so as to take advantage of the prime thermal conditions.) After the landers have been ejected, the orbiter will be used to store and relay information between Earth and each lander. It also continues to map the planet with cameras and a radar altimeter as well as determine the temperature changes over some significant portion of a local solar day. A

magnetometer, extended from a boom on the orbiter, will be used to study the magnetosphere of the planet.

Once a lander leaves the spacecraft configuration, an S3K engine will fire to orient and land each vehicle. As the lander falls toward Mercury, a Leros 20 thruster pack atop the lander will fire to slow its descent and aid in orientation. When the lander is close to the surface, the extendible positioning system slowly opens the shell, as in Figure 5. The lander contacts the surface, adjusts to the local terrain, and begins ground tests. A seismometer is transferred from the lander to the surface via the surface sampler arm. Regolith studies determine temperature conductivity, magnetic properties, and elemental composition. Cameras photograph the local landscape, while the seismometer monitors local tectonic and seismic activity. Each lander relays its information to the orbiter which, in turn, relays it back to Earth. Waste heat from the RTGs is used to keep the landers within their prescribed operational temperatures. Assuming a solar day of 88 Earth days, each lander will last for a maximum time of 136 Earth days. The lander is configured as shown in Figures 6 and 7.

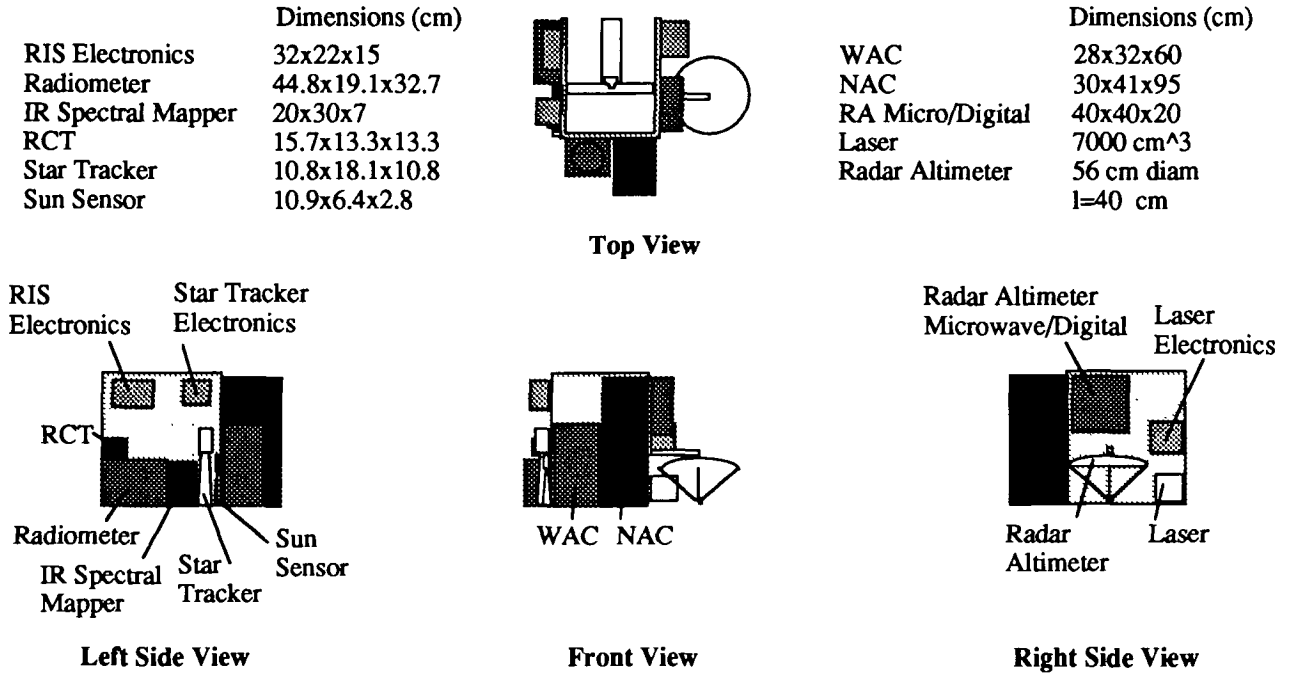


Fig. 4. High Precision Scan Platform (HPSP) Configuration

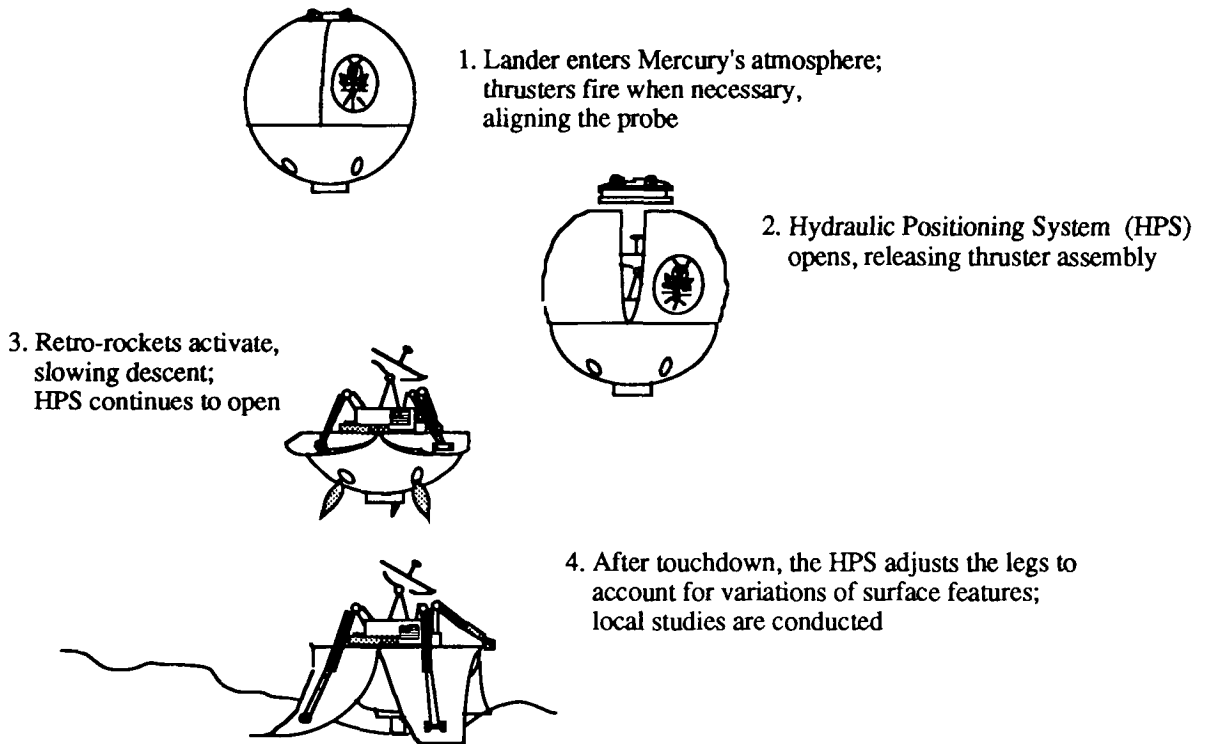


Fig. 5. Landing Sequence

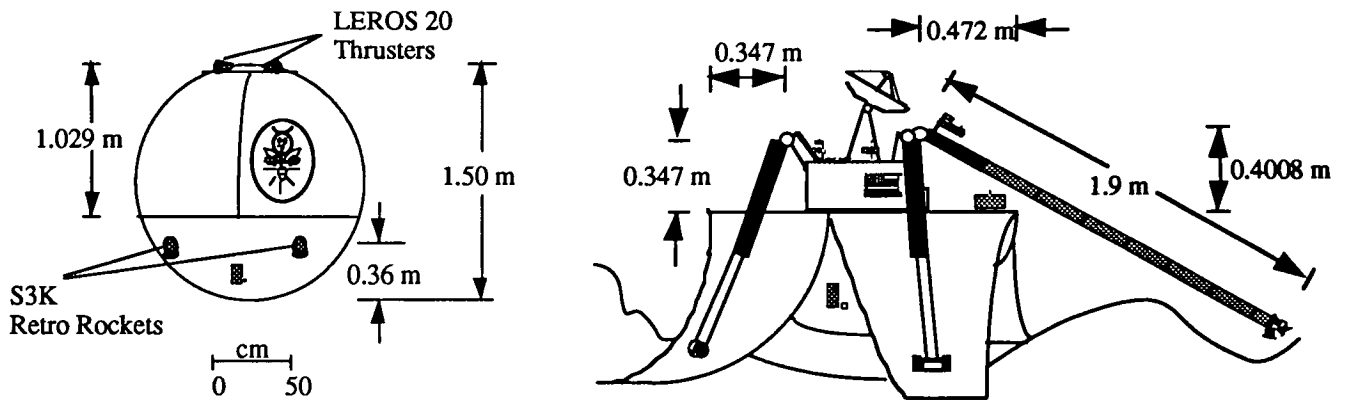


Fig. 6. Lander Dimensions

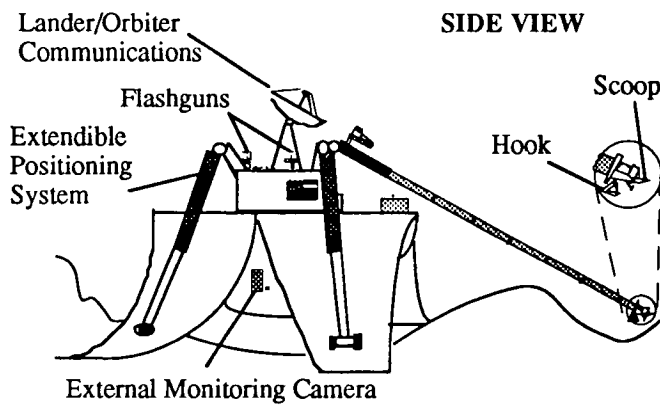
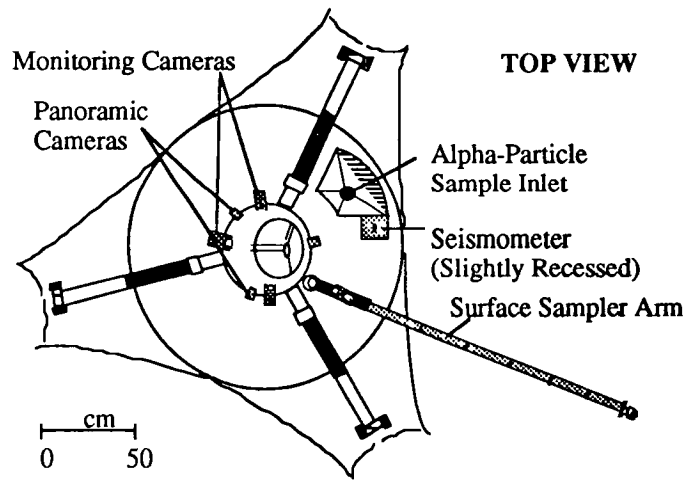


Fig. 7. Lander Components

Summary of Mass, Power, and Cost

Using the "Cost Estimation Methods for Advanced Space Systems" by Kelly Cyr [1], the cost of each major component of the subsystems previously described was found. It should be noted that unless specified, the following costs are not *absolute* estimates for any of the systems. It is strictly a qualitative estimation based on

weight, year of initial operation, and generation. Tables 1 and 2 list each subsystem and their respective masses, power requirements, and costs for the orbiter and landers. Subsystems with proven space worthiness, such as structures and scientific instruments, are assumed to be in an *nth* generation at the time of launch. Other subsystems, such as propulsion, are designated as first generation models.

Table 1. Total Subsystem Mass, Power Requirements, and Cost (FY2005) for the Orbiter

Subsystem	Mass (kg)	Power (Watts)	Cost (M\$)
Communications	120	165	118.3
C & DH	15	10	16.9
Power	50	0	3.3
Thermal Control	158	56	242.3
Structure	1408	0	852.9
Scientific Instruments	93	197	134.3
Propulsion	3792	0	1956.5
GNC	93	582	154.3
TOTAL	5729	1177	3478.8

Table 2. Total Subsystem Mass, Power Requirements, and Cost (FY 2005) for the Landers

Subsystem	Mass (kg)	Power (Watts)	Cost (M\$)
Communications	15	65	14.4
C & DH	10	50	11.0
Power	36	0	25.5
Thermal Control	9	(Negligible)	37.0
Structure	30	0	68.2
Scientific Instruments	28	82	61.0
Propulsion & GNC	429	0	260.2
TOTAL	557	197	\$477.3

Conclusion

Project Firefly will be ready for launch in early 2005. The spacecraft is an orbiter containing surface landers in tandem. Newly developed subsystem components such as inflatable

antennas, a solar sail, and composite structural materials make Project Firefly unique. Multiple landers will provide redundancy in surface sampling while the increase in landing sites and study of those areas will give a better overall understanding of the planet's evolution. This

understanding will prove to be valuable as insight into the makeup of Earth and the other planets in the Solar System. This project's cost comes to \$5.388 billion in fiscal year 2005. The cost of this project, considering the first generation solar sail and other first generation components is reasonable. Many of the systems used in this project are proven systems, and reduce the risk of sending such a spacecraft to Mercury. This limited risk, accompanied with the wealth of scientific information it will gain, makes this a project worthy of consideration.

PROJECT ARMA: MISSION TO THE MOONS OF MARS (PHOBOS AND DEIMOS)

Bob Colbert, Kelly Jandrisovits, Kent Mitterer, Simon Nagel, Brock Spigelmyer, Brian Wanger

Abstract

A limited amount of scientific information is known about the moons of Mars. Two former Soviet Union probes sent to study Phobos fell short of achieving their goals. Still, there is considerable interest in returning to the Martian satellites. The goals of this mission include: (1) achieving a better understanding of the geology, geophysics, and climatology of the moons; (2) providing information about their origin and history, (3) achieving a more accurate determination of the moons' positions, and (4) determining a better understanding of the interactions between the moons and the solar wind. An orbiter and two landers (one lander includes a penetrator) will be sent to the Martian system. Entry into a Martian orbit will be facilitated through the use of an aerobraking system. Upon completion of the aerobraking maneuver, the orbiter will release the lander for Deimos, transfer to Phobos, and deploy the last lander. Surface mapping and regolith analysis are to be performed by the orbiter, while the landers record measurements pertaining to temperature, seismic activity, and solar radiation over a complete solar cycle. A penetrator will be fired into Phobos exposing the subsurface material to the instruments housed in its structure.

Introduction

Very little is known about the moons of Mars, Phobos and Deimos. Many previous missions to Mars have primarily focused on retrieving information about Mars with little attention to the moons. Some of these missions include Viking, Mariner 9, and the recently launched Mars Observer. Of all the missions to the Mars system, only one has focused on Phobos. This was performed by the former Soviet Union which launched two satellites, Phobos-1 and Phobos-2, to study the moon. Unfortunately, contact with

Phobos-1 was lost during interplanetary transfer, and contact with Phobos-2 was lost shortly after Mars capture. With Mars being a destination for future manned missions, propellant and other raw materials will be needed. If Phobos and Deimos have oxygen and hydrogen as expected, propellant for return trips to Earth can be extracted from the two moons [2]. Thus, a scientific mission to Phobos and Deimos (Project Arma) has been developed to analyze regolith and other moon properties, which may be of concern for future manned missions.

Mission Objective

The primary goal of Project Arma is to perform an in-situ analysis of each moon's regolith. Other goals of Project Arma include: (1) achieving a better understanding of the geology, geophysics, and climatology of the moons [3]; (2) shedding light on the origin and early history of the moons and the solar system [4]; (3) achieving a more accurate determination of their orbital characteristics; (4) obtaining a better understanding of the interactions between the moons and the solar wind [5]; and (5) studying the effects of one complete solar cycle in the absence of an atmosphere.

Mission Profile

Project Arma will be launched on a Proton rocket in the year 2010. The spacecraft consists of one orbiter, one lander per moon, and one penetrator. Upon arrival at the Mars system, an aerobraking maneuver will be implemented to slow the spacecraft and place it in an orbit about Mars. After capture into a Martian orbit, the orbiter will transfer to Deimos, map its surface, and perform other regolith analyses from orbit. When the orbiter finishes its mapping and regolith analysis of Deimos, the orbiter will release the first lander to the surface. The orbiter, second lander, and penetrator, will then transfer to an orbit about Phobos.

At Phobos, the orbiter will map and perform regolith analysis. Upon completion, the orbiter will release the second lander and the penetrator to Phobos' surface. The orbiter will then transfer to a final parking orbit between Phobos and Deimos. From the parking orbit, the orbiter will perform long-term measurements of the Martian system and act as a communications link between the landing packages (landers and penetrator) and Earth. The mission scenario is depicted in Figure 8. Due to extensive mapping data, the limitations of the communications subsystem requires the landing packages to perform limited analyses until the orbiter completes mapping both moons. All parts of the spacecraft, except the penetrator, are designed to last a full solar cycle (11 Earth years). Figures 9, 10, and 11 illustrate the primary configuration of the orbiter, lander, and penetrator respectively.

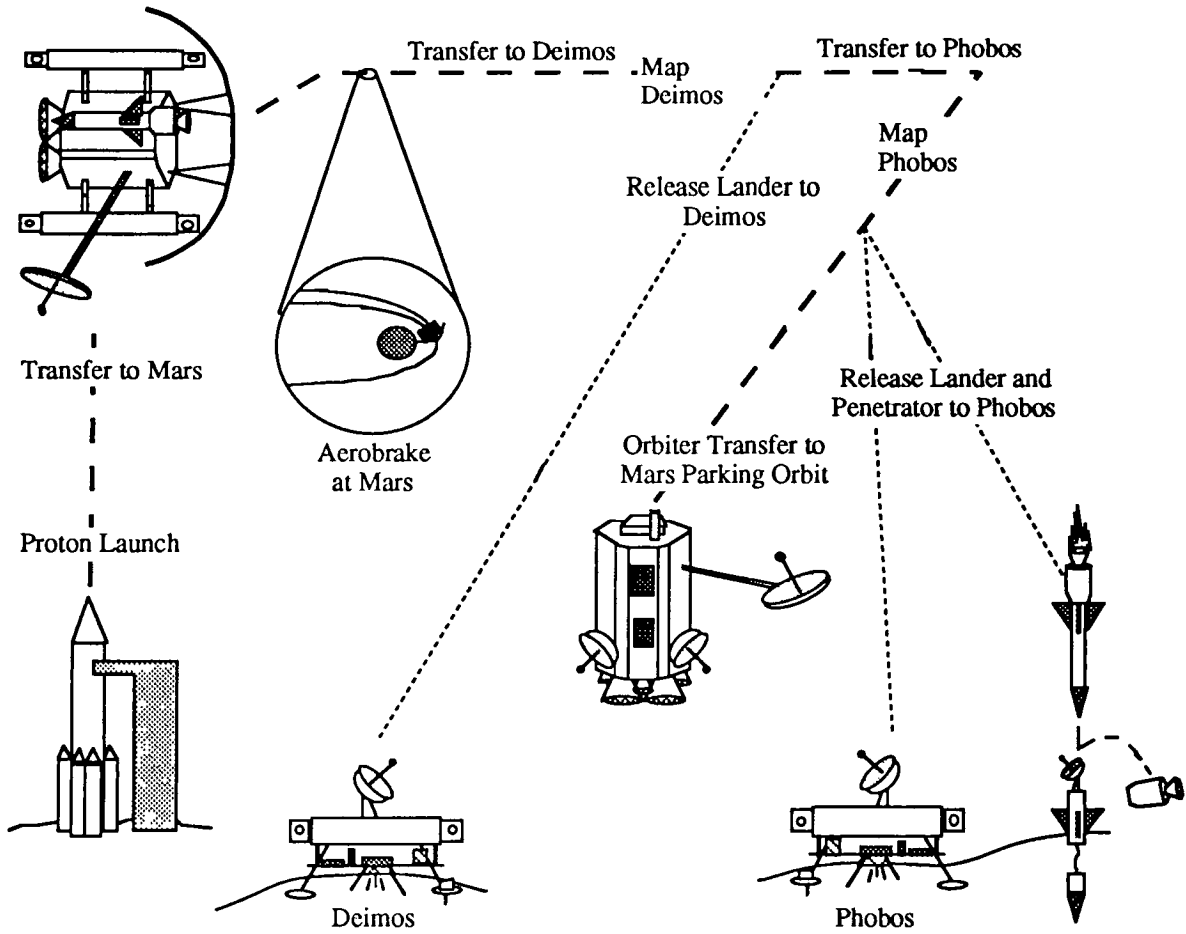


Fig. 8. Project Arma Mission Scenario

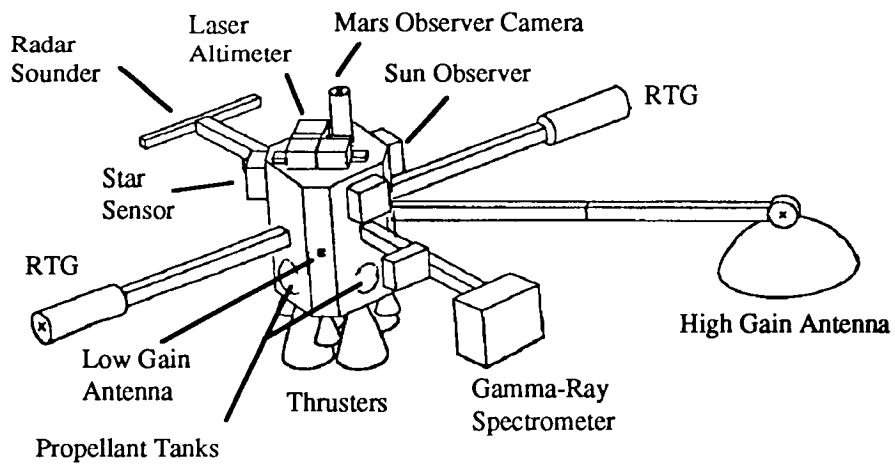


Fig. 9. Arma Orbiter Configuration

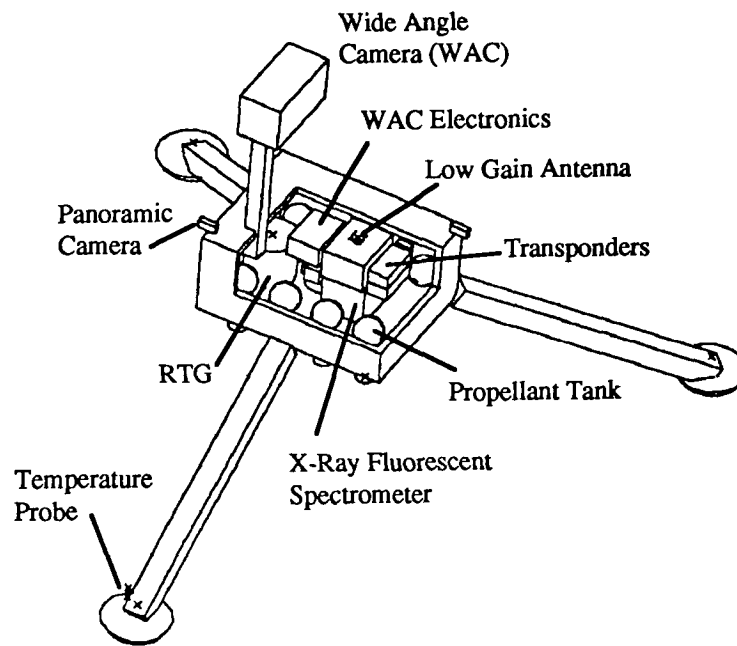


Fig. 10. Arma Lander Configuration

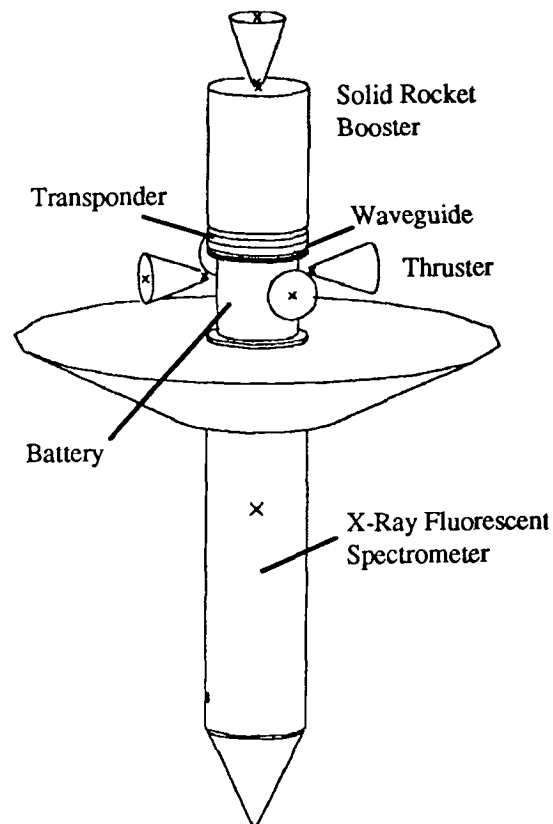


Fig. 11. Arma Penetrator Configuration

Orbiter Function

The orbiter has three functions. The first function is to map and perform a regolith analysis on the moons, while in orbit about each. Mapping will consist of visual photography, radar sounding, gravity, magnetic field, temperature, and surface altitude measurements. The radar sounding will be used to determine the internal structure of each moon. During the mapping phase, a regolith analysis will also be conducted. The regolith analysis will determine surface history and surface composition of each moon. The scientific instruments are listed below in Table 3.

The second function of the orbiter is to act as a communications link with Earth. The orbiter receives and transmits all information to and from the Martian system through a high-gain antenna. Low-gain antennas provide communications between the orbiter and the three landing packages (Deimos lander, Phobos lander and penetrator).

The third, less vital, function of the orbiter is to perform long term Martian system observations. The observations will be conducted from an orbit about Mars and will obtain information on solar wind interaction with Mars as well as magnetic, gravitational, and temperature measurements.

Table 3. Orbiter Scientific Instruments

Instrument	Purpose
Laser Altimeter Near-IF Mapping Spectrometer Magnetometer Gamma Ray Spectrometer Mars Observer Camera Radar Sounder Retarding Potential Analyzer Mass Spectrometer DION	Mapping a landing site Calculating Temperature Profiles Determining moons' magnetic properties Defining moons' elemental composition Visual photography and mapping Determining moons' internal structure Determining moons' magnetic properties Analyzing regolith composition Investigating moons' surface history

Lander Function

The two landers have three identical functions. The first is to perform an in-situ regolith analysis, via an X-Ray Fluorescence Spectrometer. The second function is to record temperatures, seismic activity, and radiation levels for a full solar cycle. These measurements will aid in

understanding the effects of the Sun's cyclic activity on all celestial objects. The third function is to obtain visual pictures of the moons' surfaces. The only difference between the landers is that the Phobos lander will also photograph Mars, using a wide angle camera. The scientific instruments are listed in Table 4.

Table 4. Lander Scientific Instruments

Instrument	Purpose
Radiation Experiment Temperature Probe Panoramic Camera Seismometer X-Ray Fluorescence Spectrometer Wide Angle Camera (Phobos)	Determining radiation Obtaining temperature variations Surface visuals Determining ground wave characteristics Analyzing regolith composition Surface visuals of Mars

Penetrator Function

The penetrator consists of a surface and subsurface section. To insure the safety of the penetrator's subsystems, the communication components and other electronics will be allowed to remain on top of Phobos' surface, yet remain connected to the embedded tip of the penetrator, by means of an extendible cord. This configuration will protect the subsystems from the energy of the impact.

The penetrator has two functions. The first is to perform an analysis of the subsurface composition of Phobos by an X-Ray Fluorescence Spectrometer. This analysis is important since scientists speculate that the surface dust is contaminated by meteor impacts, and will therefore not indicate the moon's true composition. By comparing the penetrator's regolith analysis to the orbiter's and lander's analysis, the homogeneity of the moon's surface and internal composition can be verified.

The second function of the penetrator, is to act as an experimental prototype. Using penetrators is of current interest for future Mars missions, since NASA has yet to successfully obtain a core sample from a celestial body. Thus, the operational data obtained from this penetrator will aid in the future technological development of such devices.

Design Overview

The mass, power, and cost of individual subsystems for the orbiter, landers, and penetrator have been calculated and are tabulated in Tables 5, 6 and 7, respectively. Many of the subsystem costs were not available, thus a cost estimation program developed by Kelly Cyr [1] has been utilized. The inputs of the cost estimation program were: total wet mass (5141.9 kg), launch year (2010), and the type of spacecraft

(exploration). Using this cost estimation package, a total cost of approximately \$1.48 billion in 1993 dollars has been obtained and in the launch year of 2010, the cost is projected to be \$2.41 billion.

The total spacecraft wet mass is 4285.0 kg, including the orbiter, two landers, and penetrator. With a generous 20% added for items such as the aerobrake heat shield and mass contingencies, the total wet mass is 5141.9 kg. This total mass is well below the Proton launch vehicle limit of 6200 kg.

The mass and power estimates for the orbiter are listed in Table 5. The orbiter's total wet mass is 3539.9 kg. The aerobraking maneuver will yield a considerable mass savings by reducing the propellant needed, by as much as 25%, to achieve Mars capture orbit. The total power is estimated to be 601.4 Watts, while the peak power consumption is estimated to be 596.9 Watts, and 657 Watts with a 10% design margin. The power discrepancy exists because instruments used to study Mars will not be operational until the orbiter is placed into its final parking orbit.

The total wet masses for the Deimos and Phobos landers are 256.6 kg and 280.2 kg, respectively. The total power requirements for the Deimos and Phobos landers are 72.6 Watts and 88.9 Watts, respectively. With the exception of the cameras, all instruments will record data at 30 second intervals. Also, the wide angle camera will be used only at Phobos and will be used for long term observation of Mars. Table 6 lists the mass and power, estimates for the landers.

Project Arma's penetrator has a total wet mass of 208.3 kg, and a total power requirement of 37.4 Watts. Table 7 lists the mass and power estimates for the penetrator's subsystems.

Table 4.1: Orbiter Mass and Power Estimates

Subsystem	Mass (kg)	Power (W)
Propulsion	2892.5	60.0
Communications	24.9	75.0
C & DH	73.2	29.0
Power	86.6	—
Structure	145.4	—
GNC	174.0	221.0
Scientific Instruments	115.7	189.4
Thermal	27.7	—
TOTAL	3539.9	601.4

Table 6. Lander and Penetrator Mass and Power Estimates

Subsystem	Lander		Penetrator	
	Mass (kg)	Power (W)	Mass (kg)	Power (W)
Propulsion	116.0	20.0	137.0	6.0
Communications	8.5	15.0	6.8	15.0
C & DH	35.0	9.6	2.5	6.6
Power	26.3	—	0.3	—
Structure	46.1	—	30.8	—
GNC	5.0	—	5.0	—
Scientific Instruments	43.0	44.3	20.0	8.0
Thermal	8.8	—	6.4	1.8
TOTAL for Phobos Lander	256.6	88.9		
TOTAL for Deimos Lander	280.2	72.6		
TOTAL for Penetrator			208.3	37.4

Conclusion

A mission to study the Martian moons (Phobos and Deimos) has been proposed. Project Arma will send a lander to each moon, with the Phobos lander containing a surface penetrator. An orbiter will map each surface and act as a communications relay to Earth. Among the technology demonstrations are the use of an aerobrake maneuver and the Phobos penetrator. Furthermore, by using a Russian Proton launch vehicle, international space relations could be greatly enhanced and strengthened. Scientific study of the moons could provide scientists with valuable insight into the formation of the solar system, as well as possible raw materials for use in rocket propellants. The success of Project Arma could be a positive first step to a manned mission to the Martian system.

References

1. Cyr, Kelly, "Cost Estimation Methods for Advanced Space Systems," NASA Johnson Space Center, 1988.
2. Mulqueen, J., "Manned Mission Transfer from Mars Parking Orbit to Phobos and Deimos," Manned Mars Mission Working Group Papers, Vol. 1, NASA Marshall Spaceflight Center, Huntsville, AL, May 1986.
3. Blume, W., Dodd, S., and Whetsel, C., "Mars Observer Mission Plan," *Journal of Spacecraft and Rockets*, Vol. 28, No. 5, October 1991.
4. Glasstone, S., *The Book of Mars*, NASA Office of Technology Utilization, 1986, p. 72.
5. Zaitsev, Y., "The Success of Phobos-2," *Spaceflight*, November 1989, pp. 375-777.

LEO, LUNAR AND MARS PROJECTS

The University of Texas at Austin
 Department of Aerospace Engineering and Engineering Mechanics
 Austin, Texas

Dr. George W. Botbyl
 Professor Wallace T. Fowler
 Anthony Economopoulos, Teaching Assistant

AUTONOMOUS EXTRAVEHICULAR ROBOTIC CAMERA

Greg Cabe (Team Leader)

Chris Gallagher, Alexa Maurer, Jaime Nualart, Dan Stern, James Rehfeld, Xuan-Trang Le, Brian Wilson

Introduction

Degobah Satellite Systems (DSS), in cooperation with the University Space Research Association (USRA), NASA - Johnson Space Center (JSC), and the University of Texas, has completed the preliminary design of a satellite system to provide inexpensive on-demand video images of all or any portion of Space Station Freedom (SSF). DSS has narrowed the scope of the project to complement the work done by Mr. Dennis Wells at Johnson Space Center. This three month project has resulted in completion of the preliminary design of AERCAM, the Autonomous Extravehicular Robotic Camera

The final report begins by providing information on the project background, describing the mission objectives, constraints, and assumptions. Preliminary designs for the primary concept and satellite subsystems are discussed in detail. Included in the technical portion of the report are detailed descriptions of an advanced imaging system and docking and safing systems that ensure compatibility with the SSF. The report concludes by describing management procedures and project costs.

Design Objectives

Video access to any structural component and Orbital Replacement Unit (ORU) of the Station is an essential aid for crew operation and maintenance of Space Station Freedom. Versatile viewing capabilities also offer unique opportunities for enhancing the public image of the SSF program and its vital role in space exploration.

The video system currently baselined for use on SSF is composed of up to 14 cameras positioned in fixed locations throughout the Station truss. The cameras offer limited viewing angles and require extensive data and support cables. Though some of the cameras can be moved, this operation requires support from the Space Station Remote Manipulator System (SSRMS) and extravehicular activity (EVA) crew members. The system is therefore cumbersome, limited in its mobility, and complicated to service or modify.

The DSS design team has, consequently, undertaken the design of a system more appropriate to space applications and based on advances in a number of technical areas. A few major goals and constraints were established at the beginning of the project to guide the design. The primary task of the AERCAM system, as determined by DSS, is to provide on-demand detailed video access to all or any portion of SSF. In order to accomplish this task, a number of important design objectives were identified. These objectives were ultimately met by the final AERCAM design. The following is a brief list of those objectives:

Satellite Operations

A brief list of the Satellite Operations objectives is the following:

- Provide observation of the entire Station from orbit
- Provide observation of small components in great detail
- Provide the ability to translate and hold position relative to SSF at various distances
- Provide the ability to revolve around SSF in an apparent sub-orbit for wide angle viewing
- Allow for both autonomous and user-controlled maneuvering and operation

Safety

A brief list of the Safety design objectives is the following:

- Integrate a highly automated safing and proximity detection system
- Meet SSF safety and outgassing requirements for proximity operations
- Maintain continuous Station avoidance capability
- Ensure negligible damage to the SSF, through some method of energy attenuation, in case of collision

Satellite Bus

The following is a brief list of the Satellite Bus design objectives:

- Maintain an inexpensive, long life satellite system
- Design the satellite to be retrievable, refuelable, and serviceable
- Design simple, modular components for servicing
- Remain compatible with SSF communication and computer protocols

Imaging System

The following is a brief list of the Imaging System design objectives:

- Provide capability for both high resolution and a wide field-of-view
- Provide zoom, tilt, and pan capabilities for the camera
- Allow for viewing in all lighting environments

The DSS design team made three major assumptions, each of which implies that AERCAM will be a dedicated element of the SSF baseline. The first assumption is that there will be dedicated human support for control of the satellite. The second assumption is that limited scarring of the Station will be allowed and some SSF resources (propellant and power) will be available to AERCAM. Finally, the AERCAM will require some communication and data handling support from SSF.

Concept Selection

The DSS design team studied four design concepts before selecting a final design. The concepts were evaluated heavily on their safety, reliability,

simplicity, and the viewing detail they could provide.

A self-reboosting satellite was considered a possibility for a long-life satellite that would not require modifying the Station truss for a satellite support structure. Although the system would require very little maintenance and retrieval, the mass would have to be greater than 200 lb., and the satellite would require a stand-off orbit greater than a kilometer, reducing the resolution and versatility of the imaging system.

A disposable satellite was also considered. For this concept, an inexpensive satellite would orbit the Station in a manner similar to the self-reboosting satellite, and then re-enter the atmosphere by means of a drag balloon after one or two SSF reboosts (~200 days). Hardware that is inexpensive enough not to prohibit disposal would not be of a high enough quality to provide adequate imaging or maneuvering systems, however; and storage and deployment of replacement units was also a problem.

To avoid scarring of the Station truss, while allowing for a re-usable satellite, DSS studied using an independent docking platform designed to orbit behind the Station on the SSF velocity vector. The added costs of an external docking platform, which would need periodic maintenance, and the added complexity of multiple autonomous vehicles interacting with the docking platform resulted in the rejection of this concept.

DSS ultimately decided to base the preliminary design on a satellite which would nominally dock to the Space Station truss structure, either autonomously or with human assistance, for periodic servicing. This satellite could be smaller due to reduced propellant requirements, and more weight and power could be dedicated to improving imaging and maneuvering systems. This concept was also evaluated to be the most reliable.

The Concept

The AERCAM has been designed as a refuelable, free-flying spacecraft, based from a docking/servicing platform on the SSF truss and housing an advanced imaging system. The spacecraft bus weighs about 130 lbs. and is 0.7 cubic meters in volume. It is powered by NiH₂ batteries, which provide 40 Watts of power for up to 4 hours of

operation at peak usage. Portions of the exterior panels of the satellite are removable to provide access to a number of modular components, including the imaging system. The spacecraft features a docking mechanism compatible with the Space Station arm end effectors and a cold-gas propulsion system using compressed waste gas from the Station. The spacecraft is shown in Figure 1, including a front view, a view of the docking mechanism on the right and a view of the interface to the SSF arm end effector on the left.

Though configured for remote control by a user, AERCAM is fully capable of autonomous orbiting and safing. It features three fault tolerant components and an array of sensors and artificial intelligence for proximity sensing and contingency safing operations. The bus is also equipped with a passive energy attenuation system to prevent damage to the Station in the event of a collision.

The imaging system for AERCAM is a self-contained infrared and visual camera package, housed within a removable, spherical encasement. It provides 40° panning in all directions and zooming. Coupled with a number of flight modes ranging between 10m and 500m from the Station, the imaging system can provide a resolution as detailed as 1mm/pixel and can provide a field of view which includes the entire Station.

Operational Concept

AERCAM is nominally docked to the Space Station truss, on a dedicated docking platform, until it is needed by a crew member. The docking structure is a standard attach platform used for SSF ORU's, modified to include a power and propellant interface to refuel and recharge the satellite while it is docked.

Once AERCAM is launched from its platform, it is capable of a number of flight modes. The satellite can be controlled by a hand controller and command console onboard the Station. The Station command console can control the operation of the imaging system, maneuvering system, and the internal functions of the satellite. The satellite is also capable autonomous flight modes. It can hold its position at any location with respect to the Station, including holds on the velocity vector and the radial vector. Nominally, the satellite is designed to translate and position hold ten meters from the Station, allowing for an adequate safety zone. In

addition, it can maintain a sub-orbit about the SSF at one half a kilometer from the Station. Though capable of user-controlled operation, the satellite calculates its own trajectories and propulsion and attitude requirements, and it is actively aware of a dynamic environment, allowing for operation independent of constant human control.

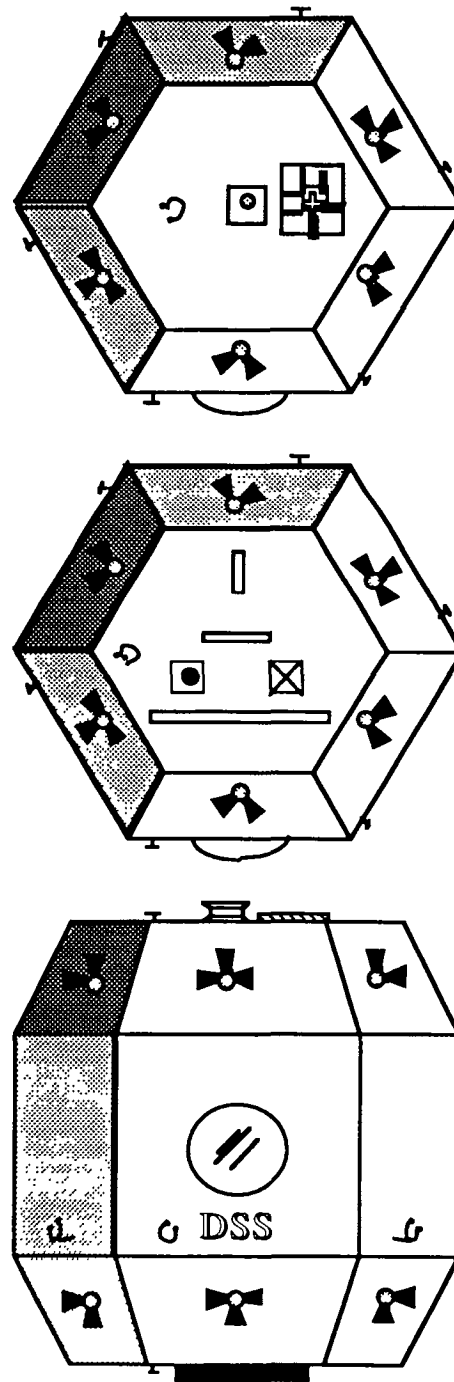


Figure 1. Satellite Concept.

Imaging System

The imaging system is housed in an independent, spherical encasement, capable of panning up to 40° in all directions. The imaging system housing has two locking gimbals, coupled with two small actuators and gimbal stops, to provide the required pointing at a rate of 10° per second. The housing weighs approximately 10 lb., occupies 1.77 ft.³, and the system requires approximately 15 Watts during peak operation. The system is modular and easily accessed through a removable panel and detachable latches at the gimbals.

The imaging system features a small light, providing illumination for nearby viewing in dark conditions. It also features a flash shield, reactive in 2 milliseconds, designed to protect the camera components from intense radiation.

The cameras are based on digital charged coupled devices (CCD's) and produce digital images using a matrix of 2048 by 2048 sensors. A series of mirrors and filters separate the incoming electromagnetic radiation into two streams, one directed to a visual camera and the other to an infrared (IR) camera. The visual camera responds over a spectrum from 0.45 μm to 1.1 μm, and the IR camera responds over a spectrum from 1.1 μm to 15 μm.

The imaging system is designed to provide a resolution of 1 mm / pixel at a distance of ten meters from the Station, which corresponds to a field of view 2.048 meters. The imaging system can also provide a field of view as wide as 128 meters at 500 meters from the Station, which corresponds to a resolution of 62.5 mm / pixel.

Images are produced at a rate of 3 frames per second, generating at least 4.5 Megabits (Mbps) of data each second. This data is processed and compressed using a computing system derived from the Kodak DCS 200 and processors used for the Brilliant Pebbles system.

The performance of the AERCAM imaging system is summarized in Table 1.

Communication System

In order to provide adequate communications support, the satellite is capable of transmitting 100 Mbps of telemetered data and of transmitting and

receiving 10 Kbps of commanding, health, and status data. In order to reduce the amount of data telemetered from the imaging system, AERCAM offers a number of data reduction and compression techniques, including Vector Quantization - a patented compression technique that can reduce data in a lossless manner by up to a factor of 12.

Table 1. AERCAM Performance Characteristics.

Spectral Response.....	0.45 μm to 15 μm
Maximum Resolution.....	1 mm / pixel
Maximum Field of View.....	128 meters
Frame Size.....	2048 pixels X 2048 pixels
Frames Per Second.....	3 (nominal)
Maximum Data Compression.....	12 to 1

The AERCAM communication system is based on a space-to-space communication system originally designed for Space Station Freedom. It employs twelve antennas on the satellite and ten antenna arrays on the Space Station. Each antenna is a circular loop antenna, one wavelength in diameter. The satellite antennas draw 0.5 Watts of power for transmission, and the Station antennas draw less than 2 Watts. The carrier frequency ranges between 14.0 GHz and 14.9 GHz. Based on a transmission path length of 1 kilometer, the AERCAM link budget predicts a signal-to-noise ratio of 25 and a transmission margin of 18.5 dBWatts, both excellent characteristics for a communication system.

Satellite Bus

The satellite bus is a 20 sided hexagonal structure, shown in Figure 1, composed of an internal support structure and 20 external panels, 8 of which are removable. The structure is designed for modularity and ease of access to the internal components. The propulsion system includes a 0.5 cubic foot tank, containing compressed carbon dioxide. It provides up to 150 ft/sec of ΔV. Twenty-four NiH₂ cells supply 40 Watts of power, and can operate up to 4 hours at peak usage. Twenty Watts are allocated to the imaging system for nominal operation, and the computer system and propulsion/attitude control systems are always guaranteed 20 Watts, respectively, for emergency operations.

One end of the satellite is equipped with a docking mechanism compatible with the standard attach

platform, and the opposite end of the satellite is equipped with a standard SSF grapple fixture to allow for grappling and maneuvering using the Special Purpose Dexterous Manipulator. The docking mechanism provides interfaces with a power fixture and propellant valve to allow recharging and refueling of the satellite while it is docked.

Safety is one of the most important elements in the AERCAM mission. In order to maintain autonomous proximity detection and collision avoidance, the spacecraft is equipped with an intelligent logic system, capable of adapting to a dynamic world model. To support this system and to generate the dynamic world model, the satellite is equipped with sensor clusters on each face of the satellite. These clusters provide both ranging and relative velocity information for the satellite.

The following critical components of the satellite have been designed for three fault tolerance: computer system, thruster/propulsion system, and power system. Key elements in the communication system have also been designed for fault tolerance.

Should the satellite collide with the Station, the bus has been equipped with an energy attenuation device. The method of energy attenuation which DSS chose to implement requires that the vertices of the satellite be fitted with compartmentalized "bumpers," filled with an inert gas. These bumpers represent a passive system, and therefore will always be operational, despite other failures within the spacecraft.

The insurance of safety is perhaps the most significant hurdle to overcome for acceptance of a satellite of this nature. Therefore DSS has been committed to identifying the most reliable methods of operation, control, and safing. We believe that the satellite's design will offer reliability and safety measures which will be acceptable to the SSF program.

Recommendations

Due to the limited duration of the project and the scope of work which the DSS design team undertook, some areas of design have been left for future work. Some crucial areas of future design work are listed below:

- Design of proximity sensor arrays
- Design of a remote user control station

- Selection of an energy attenuating material for the spacecraft skin
- Analysis for low impact scarring of the SSF truss to support servicing and communications
- Testing and simulation for contingency operations
- Miniaturization of spacecraft components

Conclusion - The AERCAM Advantages

Advances in automation, robotics, and microtechnology, as well as the modern proficiency for designing inexpensive, reliable systems with multiple fault tolerance offer a unique opportunity to take a large step forward in space imaging and servicing technology. The current baseline video system for SSF uses the same design philosophy used for video surveillance on Earth - multiple, fixed cameras linked through a large system. While this design philosophy is a proven one, Degobah Satellite Systems believes that a new technology, more appropriate to space application, is not only feasible, it is also more versatile and powerful and represents a stepping stone to automated robotic maintenance in space.

The AERCAM is a more mobile system than the fixed video system. It can be moved more rapidly and does not require crew or SSRMS support to change locations. Its viewing is not limited by physical obstacles, and access to all or any portion of the Station is available on very short notice. It offers much greater versatility in its viewing options, and can even be attached to the SSRMS as additional mode of viewing.

AERCAM requires only a single platform for docking and servicing, and two (as opposed to 14) units must ever be modified or serviced. It also offers superior imaging through higher resolution, wider spectral response, and a larger field of view.

AERCAM's application can be extended far beyond the SSF project. The camera, even based from the Space Station, can be used to provide imaging for nearby spacecraft and to assist in any docking or proximity operations of multiple spacecraft. Further, an easily modified or replaced docking panel and the advanced proximity detection and maneuvering capabilities of the satellite make it adaptable to use on future orbiting facilities.

Finally, if AERCAM were implemented, it would represent the first major step toward using fully

automated robotics for space maintenance. The imaging, proximity detection and maneuvering, and intelligent logic systems are the major design hurdles in developing advanced space robotic devices. AERCAM's "hands-off" viewing operations offer an excellent opportunity to safely test these three crucial systems before progressing to actively interacting with Station hardware. It is then a small step to equip one or more of AERCAM's unused external panels with robotic arms and end effectors for use as an autonomous maintenance system. Such robotic systems will be invaluable in terms of reducing crew work time and increasing crew safety.

MARS GRAVITY FIELD DETERMINATION MISSION

David W. Reed (Team Leader)

Paul Bolton, Susan Elliott, Doug Hamilton, Stewart Lilley, James Nickelson, Artemus Shelton, Melinda Sirman

Introduction

With the downturn of the world economy, the priority of unmanned exploration of the solar system has been lowered. Instead of foregoing all missions to our neighbors in the solar system, a new philosophy of exploration mission design has evolved to insure the continued exploration of the solar system. The "Discovery-class" design philosophy uses a low cost, limited mission, available technology spacecraft. The "Voyager-class" design philosophy uses a "do-everything at any cost" spacecraft. The "Voyager-class" philosophy is no longer feasible. The Percival Mission to Mars has been proposed by Ares Industries as one of the new "Discovery-class" of exploration missions. The spacecraft will be christened Percival in honor of American astronomer Percival Lowell who proposed the existence of life on Mars in the early twentieth century.

The main purpose of the Percival mission to Mars is to collect and relay scientific data to Earth suitable for designing future manned and unmanned missions to Mars. The measurements and observations made by Percival will help future mission designers to choose among landing sites based on the feasibility and scientific interest of the sites. The primary measurements conducted by the Percival mission include gravity field determination, surface and atmospheric composition, sub-surface soil composition, sub-surface seismic activity, surface weather patterns, and surface imaging. These

measurements will be taken from the orbiting Percival spacecraft and from surface penetrators deployed from Mars orbit.

Percival has been designed as a follow-up mission to the Mars Observer (MO) spacecraft that is currently in route to Mars. As a follow-up mission, it will augment the Mars Observer mission by improving the gravity field map created by MO and by supporting the Visual and Infrared Mapping Spectrometer (VIMS), which was originally planned for the Mars Observer mission. In addition, images and data taken by MO will be used to determine the desired impact sites for the three surface penetrators included within the Percival mission.

As a secondary mission, Percival will support the Mars Balloon Relay (MBR) communications system, similar to the one used on Mars Observer. This system is a separate communications package directed towards the surface of Mars to receive and transmit data from surface landers. During the science phase of the Percival mission, this system will be used for data relay between the surface penetrators and Earth. After the completion of the science phase of the mission, the MBR will be used to support future Mars landers.

The Percival mission scenario consists of the following elements:

- Launch using modified Delta-class launcher.
- Use a broken-plane Hohmann transfer trajectory between Earth and Mars.
- Insert into a low altitude, circular, sun-synchronous Mars orbit.
- Determine gravity field using gravity gradiometer and Doppler-shift measurements as a backup.
- Release each penetrator individually from Percival in Mars orbit.
- Use the Mars Balloon Relay communications system for data relay from surface penetrators and future surface missions.
- Support both real-time and store-and-forward data transmission to Earth.
- Conduct scientific measurements for approximately 1-2 Martian years.

The design work for the Percival Mission to Mars has been divided among four technical areas: Orbits and Propulsion System, Surface Penetrators, Gravity and Science Instruments, and Spacecraft Structure and Systems. This overview summarizes the results for

each of the technical areas followed by a design cost analysis and recommendations for future analyses.

Orbits and Propulsion System

The main objective of the orbits and propulsion group was to develop the best combination of launch system and transfer trajectory that would maximize the allowable mass in Martian orbit. The design of the final Mars orbit was designed to accommodate the gradiometer, the VIMS, and the relay communications packages. The spacecraft propulsion system was designed to provide transfer trajectory corrections, Mars orbit insertion, and end-of-mission boost burns.

The choice of launch system and the design of the transfer trajectory was heavily impacted by the low cost objective of the Percival mission and the Delta-class launch vehicle constraint stated in the Request For Proposal. The Delta launch system is one of the less expensive launch systems, but it is also one of the lower performance vehicles among those capable of supporting an interplanetary payload. To maximize the amount of mass that can be placed into a Martian transfer trajectory, a Delta 7925 with an additional upper stage motor has been chosen. The first two stages of the Delta will place the boost stages and the spacecraft into Earth orbit, while the two Star-48B motors will provide the thrust for the Mars transfer injection burn.

To compromise between minimal energy transfer and time of flight, a broken-plane Hohmann transfer, shown in Figure 2.3, was chosen. This trajectory requires a 3576 m/s ΔV , provided by the Star 48B's, for transfer insertion. The plane change burn is performed at a true anomaly of 90°, requiring a 258 m/s ΔV to change the orbital plane by 0.53°. Course corrections will also be made during this burn. The Mars insertion burn will require a 2178 m/s ΔV by the spacecraft propulsion system. The time of flight will be approximately 11 months.

The design of the final Mars orbit was driven by the instrument packages onboard Percival. To increase the accuracy and precision of the gradiometer data, a low-altitude (179.4 km), circular orbit was chosen. To increase the groundtrack coverage of Mars, a high inclination orbit was necessary. A sun-synchronous orbit was chosen for this reason as well as to reduce thermal variations on the spacecraft. The sun-synchronous orbit also minimizes the pointing requirements of the high-gain

antenna used to communicate with Earth. The period of the Martian orbit will be 108 minutes. The groundtrack for this orbit allows for communication with each penetrator every two to three days and allows for a complete VIMS mapping cycle in 82 days.

Percival's propulsion system is designed to provide the plane change burn, course corrections, Mars orbit insertion, and end-of-mission orbit boost. These maneuvers will require a ΔV of 2436 m/s. The resulting propulsion system will have approximately 60 kg of hardware mass and 730 kg of propellant mass.

Surface Penetrators

The surface penetrators group was tasked to design the penetrator system, which includes deployment methods, deceleration methods, impact and stress analysis, structural design, subsystem design, and scientific instrumentation of the penetrators. The purpose of the penetrator system is to provide scientific data from the surface and sub-surface of Mars as an aid to designing future manned and unmanned missions. The data returned by the penetrators will help determine the feasibility of a landing site and the scientific interest of a site.

Each of the three penetrators will be deployed separately from Martian orbit and impact at a different location on the Martian surface. The deployment and deceleration system uses a spring for the initial separation from Percival, a 500 m/s ΔV deorbit motor for entry, and a 1.14 m diameter drag chute for deceleration and stability through the atmosphere. The transfer from Mars orbit to impact takes approximately 4.5 minutes and results in a 235 m/s impact velocity.

Upon impact the forebody and afterbody of the penetrator separate as shown in Figure 3.1. The umbilical cord connecting the two sections of the penetrator contains power and communications lines. Both hard and soft soil models were used to analyze the impact. The forebody must penetrate deep enough to isolate the seismic instruments from surface wind disturbances, but must not separate from the afterbody farther than the umbilical cord will allow. The penetration of the afterbody must be minimized so that the communications and surface instruments will remain on the surface. The results of the penetration analysis are summarized in Table 3.2.

Each penetrator contains instrumentation that will carry out four scientific objectives: planetary science, imaging, soil analysis, and meteorology. Planetary science is the determination of the interior structure of Mars. This involves the study of the surface structure, global seismology, and the magnetic field of the planet using a seismometer and a magnetometer. Imaging systems on the penetrators will provide information on the geology of the Martian surface. Two imaging systems will be on each penetrator: a descent imager located on the nose of the penetrator and a panoramic imaging system located in the top of the afterbody. Soil analysis is the study of the chemical composition, water content, and physical properties of the subsurface soil. The physical properties of the soil include the subsurface temperature and conductivity. A meteorology package containing four distinct instruments will measure the temperature, pressure, humidity, and wind speed and direction of the local atmosphere.

The necessary subsystems for each penetrator are power, communications, and thermal control. The power subsystem is composed of a 0.5 W Radioisotope Thermoelectric Generator (RTG) and a 20 W Nickel-hydrogen battery. The RTG handles all continuous power requirements and recharges the battery. The battery will provide for peak power requirements, such as transmission of data to Percival. This type of power system provides for a penetrator with an operating life of one year. The communications system uses a helix antenna on the penetrator afterbody for receiving and transmitting data. The thermal system uses thermal blankets and excess heat from the RTG to keep the battery in the proper temperature range. The remainder of the excess heat is transferred to the soil using a heat pipe. Figure 3.3 shows a layout of the penetrator subsystems and instrumentation. Table 3.6 shows a breakdown of the mass and power requirements of the penetrator.

Gravity and Science Instruments

Two of the main objectives of the Percival mission are to augment and improve the gravity field mapping being done by MO and to serve as a support platform for scientific instrumentation that was originally planned for MO. The gravity and science instruments group chose the instruments to accomplish these objectives and developed the constraints that the instruments placed on the Percival spacecraft.

Mars Observer will be using radioscience techniques (Doppler shift measurements) to carry out gravity

mapping of Mars. Percival will improve upon the accuracy of the MO gravity map by using a two-axis gravity gradiometer, sensitive in the radial and transverse directions. This instrument uses highly sensitive accelerometers to measure the local gravity field. It is expected that an accuracy of 1 Eotvos will be obtained by using the gradiometer without cryogenic cooling. Since gradiometers have never been used in space, Percival will also have the capability to support radioscience techniques. Doppler shift measurements will still augment the gravity map created by MO, though the accuracy of the map will not be improved.

To achieve the desired accuracy and sensitivity of the gravity field map, mechanical vibrations and accelerations generated by the spacecraft must be eliminated or minimized. The gradiometer also requires that attitude position and rates be known very precisely. Table 4.1 summarizes the requirements placed on the GN&C system. While attitude maneuvers are being conducted, the gradiometer will not make gravity field measurements.

The Visual and Infrared Mapping Spectrometer (VIMS) will also be flown on Percival. This instrument, originally designed for MO, will determine the composition of the Martian atmosphere and surface. The VIMS mapping mission requires the Percival spacecraft to maintain a nadir orientation. This type of orientation requires the spacecraft to maintain a constant revolution rate of one revolution per orbit. This rotation rate is not high enough to significantly affect the gradiometer measurements. A more sensitive, cryogenically-cooled gradiometer would need to take the rotational acceleration terms into account. With an orbital altitude of 179.4 km, one VIMS mapping cycle of Mars will take 82 days.

Spacecraft Structure and Subsystems

The Spacecraft group was responsible for designing the basic structure and the subsystems of the Percival spacecraft. To eliminate the need for a complete redesign of the spacecraft bus, the Percival spacecraft bus was based on a scaled down version of the Planetary Observer bus used for the MO mission. Systems design was done for the communications, power, thermal, and GN&C subsystems.

The communications system consists of a high-gain antenna and a backup low-gain antenna for

communication with Earth. The high-gain antenna will transmit at a frequency of 8.4 GHz with a data rate of 150 kbps. Since Percival will not be able to transmit at all times, the capability to store data in addition to real-time transmission will be used. Ares Industries expects that Percival will receive an allocation of Deep Space Network (DSN) time roughly equivalent to the 8 hours per day that MO receives currently. During the 8 hour period, Percival would be able to transmit approximately 1622 megabits of data.

For communications with the surface of Mars, Percival will use the Mars Balloon Relay (MBR) communications system currently used on MO. This system consists of a low-gain antenna pointed towards the surface of Mars. The antenna will transmit at 401 MHz and receive at 406 MHz with a data rate of 8 kbs. This communications system will support the surface penetrators during the science phase of the Percival mission. Beyond the science phase, the MBR system will support other future surface missions.

An RTG and battery combination was chosen to provide power for the Percival spacecraft. The RTG was chosen for its good mass to power rating (5.4 W/kg) and for its ability to generate power without repointing as solar panels are required to do. The battery would be used to provide power during peak power consumption phases of the mission. Today's RTGs use Plutonium 238 as the radioactive isotope. This isotope is not commonly available, making the RTG very expensive. A less expensive alternative would be to make RTGs that utilize a more readily available isotope, such as Strontium 90. This isotope is a common daughter isotope in all nuclear reactors. In the past, Strontium 90 has been used for SNAP reactors on spacecraft.

The thermal control methods will be based primarily on passive methods to reduce the mechanical noise produced by the system. Passive methods of thermal control will include thermal blankets and surface coatings. The active thermal control methods used will include freon radiators and heaters.

The Guidance, Navigation, and Control system consists of sensors and thrusters to determine and control the spacecraft's position, velocity, and attitude. The GN&C system is designed to be completely autonomous with the capability of ground override. Attitude and position determination will be done using a sun sensor and a fixed-head star

tracker. Rate determination will be done using a ring laser gyro. The control system will use 24 reaction control jets divided among two independent systems. One system will use hot gas, while the other will use cold gas. The cold gas thrusters will allow the spacecraft to be controlled more precisely than the hot gas thrusters will allow.

Recommendations

As designed, the Percival spacecraft is not capable of supporting all mission objectives. The constraint of the Delta launch vehicle has limited the allowable mass of the spacecraft to 460 kg dry mass at Mars. This is 75 kg higher than the mass estimate for Percival of 535 kg. To come within the mass budget, one or more mission objectives may have to be eliminated or a higher performance launch vehicle must be used. It may also be possible to take advantage of larger GEMs (Graphite-Epoxy Motors) to provide the additional boost, if they become available in the future.

A preliminary estimate of the development and production cost for the Percival mission has shown that, as designed, Percival exceeds the desired "Discovery-class" budget of \$150 million. The current estimate of \$270 million includes the development, production, and launch costs for the Percival mission. The cost estimate does not include program costs, operation costs, or other long term management costs. Ares Industries has concluded that the numerous mission objectives of the Percival mission make it unsuitable for a true Discovery-class mission. If a Discovery-class mission is required, one of the three major scientific objectives, gradiometer, penetrator, or the VIMS, should be chosen as the single, primary mission objective.

To design the Percival Mission to Mars beyond the preliminary design phase, detailed design must be done for all portions of the project. The following issues must also be considered. For the propulsion system, the type of propellant must be chosen to give a more precise estimate of the fuel mass required. The penetrator system requires the accuracy of the penetrator targeting to be determined in addition to the effects of winds on the entry trajectory and attitude of the penetrator. Also, the susceptibility of the penetrator structure to failure during an oblique impact must also be considered. The feasibility of increasing the data rate of the Mars Balloon Relay should be determined. For the spacecraft power system, the feasibility of using a Strontium 90 RTG

should be further analyzed. The GN&C system of Percival should be analyzed in more detail to determine if it satisfies the position and rate determination and control requirements defined by the gradiometer.

LEO SATELLITE FOR DEEP SPACE NETWORK CALIBRATION

Dennis McWilliams (Team Leader)

Joe Araiza, Michael Clavenna, Jason Jones, Pat Lett, Cassidy Norman, Clint Slatton, John Opiela, Mark Tedesco, Michael Wortman

Overview

Mankind's quest for knowledge of space has led scientists to loft expensive, complex space probes that gather a multitude a data. Current spacecraft can gather more data than their communication system can transmit during limited transmit times. In order to increase efficiency as well as the amount of data a satellite can retrieve, faster data transmission methods must be found. The fastest data transmission rates now occur over X-band. However, a debate by scientists currently focuses on whether NASA should switch to another radio frequency, like Ka-Band, or if they should move on to a more advanced scheme such as laser communication. Mockingbird Designs hopes to aid the debate by studying Ka transmissions. Although the Ka-Band could offer higher data transmission rates, the effect of the atmosphere on the signal is unknown. Therefore Mockingbird designed and plans to produce a small satellite, named BATSAT, that will transmit a test signal over both Ka and X bands to study atmospheric signal attenuations.

Satellite Bus

The BATSAT satellite incorporates small satellite design principles to provide a simple, low-cost design ideal for university production and testing. The satellite is an 0.64 m diameter space-frame truss structure built of 6061-T6 aluminum truss members. The skin panels will be built of a honeycomb sandwich material, which will be mounted the outer truss structure using locking bolts. In lieu of an axial strut to support launch loads, an inner strut configuration will provide stiffness. The inner strut design also provides more space inside the spacecraft for component placement. The components will be placed in an insulated disk that will be isolated from the structure using nylon cords. Using a NASTRAN structural model, Mockingbird found that the

spacecraft has a large structural design margin while maintaining a low mass. This could be very beneficial if one wished to increase the component mass by adding scientific instruments. The mass budget for the final design is shown in Table 2.

Table 2. BATSAT Mass Budget.

No.	Element	Comments, Heritage	Unit Mass	Total Mass
Communication				4.85 kg
1	Ka Transmitter	SURFSAT, pre-tested	1.00 kg	1.00 kg
1	X Transmitter	SURFSAT, pre-tested	0.70 kg	0.70 kg
1	S Transmitter	SURFSAT, pre-tested	0.42 kg	0.42 kg
8	X Antenna	SURFSAT, pre-tested	0.06 kg	0.48 kg
8	Ka Antenna	SURFSAT, pre-tested	0.08 kg	0.64 kg
8	S Antenna	SURFSAT, pre-tested	0.08 kg	0.64 kg
0	Ku Antenna	SURFSAT, pre-tested	0.10 kg	0.00 kg
	Cables		0.97 kg	0.97 kg
Power				8.07 kg
1	Peak Power trkr.	Off the shelf, space qual	3.00 kg	3.00 kg
1	Solar Array	Lockheed space qual. Si	1.95 kg	1.95 kg
2	Ni-Cad Batteries		1.40 kg	2.80 kg
	Cables		0.32 kg	0.32 kg
Thermal & Radiation				8.20 kg
1	Blankets		3.00 kg	3.00 kg
2	Strip Heaters	Minco	0.10 kg	0.20 kg
1	Shielding		5.00 kg	5.00 kg
Command Sys				2.60 kg
1	X Receiver	SURFSAT, pre-tested	0.60 kg	0.60 kg
1	Logic Circuits		2.0 kg	2.00 kg
Structure				16.60 kg
Payload				0.00 kg
0	Grav Meter		10.00 kg	0.00 kg
0	Radiation Meter		10.00 kg	0.00 kg
0	Voltage Meter		3.00 kg	0.00 kg

Margin	20%
--------	-----

S/C Dry Weight	48.4 kg
Launch Adapter	17.0 kg
Boosted Weight	65.4 kg

Total Launch Mass =	65.4 kg
---------------------	---------

Subsystems Design

The communication system includes Ka and X-Band transmitters that are used to carry the test signal. Mockingbird also plans to include an S band transmitter that will be used to help train DSN personnel. By purposely turning certain antennae off, DSN trainees could determine the attitude motion of the satellite via blinking techniques. The spacecraft will transmit the 1 mW test signal over four omnidirectional antennae provided for each band. The

increase in signal interference due to these antennae can be compensated for using filter techniques available at DSN, but most importantly these effects are distinguishable from atmospheric effects. Commands will be up-linked via an X-Band transponder and a step logic circuit will change the spacecraft configuration for different subsystems. Also, to insure that the satellite can always be in a known state, a reset command was designed to return the satellite to an initial state.

Thermal control is often a problem for small satellites. To compensate, Mockingbird Designs cold biased the BATSAT satellite. The outer surface will be covered with solar arrays, and all remaining surfaces will be painted white. This prevents the satellite from exceeding hot temperature limits. To prevent certain satellite components from getting to cold, small thermal strip heaters with a thermostat will be used to heat up components. Since all components will be placed in a circular disk, components can also be warmed via thermal blankets. Also, the circular disk can be radiation hardened to increase satellite reliability.

When the satellite is transmitting over both X and Ka-Bands with heaters on, it will need 8.6 W of power. This maximum power requirement will be fulfilled using silicon solar arrays and nickel-cadmium batteries. The solar arrays will be surface mounted to the honeycomb skin structure to offer omni-directional solar flux coverage. A peak power tracker will be used to smooth out the power from the arrays. Both the solar arrays and the batteries are designed for a 10 year lifetime. Four batteries will be used: one for the first five years, one for the second five years, and two redundant batteries.

Operational Concept

The BATSAT satellite will be lofted into an 1163 km, 70° orbit by the Pegasus launch system. This orbit fulfills the DSN dish slew rate requirement of .4 deg/s while also keeping the satellite out of the heaviest regions of the Van Allen radiation belts. Currently, only the Goldstone, California DSN dish can receive in Ka-Band, but the Canberra, Australia and the Madrid, Spain dishes will soon be upgraded. Each of the three DSN stations capable of receiving Ka-Band (Goldstone, Canberra, and Madrid) will have an average of 85 minutes of view-time per day. A seven day repeating groundtrack will allow for easy planning and view time estimates. The Pegasus launch system by Orbital Sciences Corporation will

provide the launch services for BATSAT. Pegasus offers the lowest priced commercial launch option while providing many performance options that decrease satellite complexity. While the Pegasus system is relatively cheap (around \$9 million), Mockingbird Designs is researching cheaper options such as shared launch and military surplus. Figure 2 shows the Pegasus payload fairing dimensions.

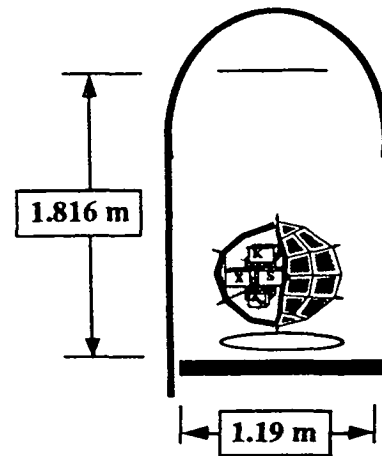


Figure 2. Pegasus payload fairing dimensions.

Conclusions

The current BATSAT design offers an excellent spaced-based platform for testing the merits of Ka-Band transmissions. The satellite fulfills the mission goals while keeping complexity and costs down. However, the most important aspect of the BATSAT satellite is its receptiveness to university design. By using students to design, fabricate, and test the satellite structure, costs can be kept to a bare minimum. Many of the electronic components have been built by other university groups and can be adapted to the BATSAT design. Even though this satellite was designed specifically for the DSN/JPL testing project, the small satellite can easily be modified to carry scientific instruments. Mockingbird hopes that other missions will wish to use the BATSAT design for their small satellite applications.

MANNED LUNAR LANDER FOR FIRST LUNAR OUTPOST

David Garza (Team Leader)

Nikola Babic, Matt Carter, Donna Cosper, David Goodine, Eloy Gonzalez, Edward Hirst, Ray Li, Martin Lindsey, Tony Ng

Operational Concept

Selenium Technologies has been conducting preliminary design work on a manned lunar lander for use in NASA's First Lunar Outpost (FLO) program. The resulting lander is designed to carry a crew of four astronauts to a prepositioned habitat on the lunar surface, remain on the lunar surface for up to 45 days while the crew is living in the habitat, then return the crew to Earth via direct reentry and land recovery. Should the need arise, the crew can manually guide the lander to a safe lunar landing site, and live in the lander for up to ten days on the surface. Also, an abort to Earth is available during any segment of the mission. Table 3 shows the approximate Δv numbers corresponding to the worst-case geometry between the Earth and the Moon.

Table 3. Δv Budget for Worst-Case Earth-Moon Geometry.

Event	Δv (m/s)
Translunar Injection	3200
Outbound Midcourse Corrections	30
Lunar Orbit Insertion (LOI)	890
Deorbit	20
Descent	1850
Ascent	1830
Lunar Orbit Circularization	20
Trans-Earth Injection	850
Inbound Midcourse Corrections	30

Subsystems Design

The main propulsion system consists of a cluster of four modified Pratt and Whitney RL10 rocket engines that use liquid methane (LCH_4) and liquid oxygen (LOX). Four engines are used to provide redundancy

and a satisfactory engine out capability. Differences between the new propulsion system and the original system include slightly smaller engine size and lower thrust per engine, although specific impulse remains the same despite the smaller size. Concerns over nozzle ground clearance and engine reliability, as well as more information from Pratt and Whitney, brought about this change.

The power system consists of a combination of regenerative fuel cells and solar arrays. While the lander is in flight to or from the Moon, or during the lunar night, fuel cells provide all electrical power. During the lunar day, solar arrays are deployed to provide electrical power for the lander as well as electrolyzers, which separate some water back into hydrogen and oxygen for later use by the fuel cells. Total storage requirements for oxygen, hydrogen, and water are 61 kg, 551 kg, and 360 kg, respectively.

Lander and Crew Module

The lander is a stage-and-a-half design with descent propellant, cargo, and landing gear contained in the descent stage, and the main propulsion system, ascent propellant, and crew module contained in the ascent stage. The primary structure for both stages is a truss, to which all tanks and components are attached. The crew module is a conical shape similar to that of the Apollo Command Module, but significantly larger with a height and maximum diameter of 6 m. Figure 3 shows the configuration of the lunar lander.

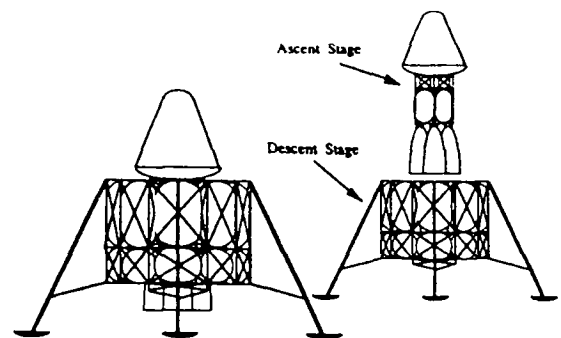


Figure 3. Lunar Lander Configuration.

The descent truss is composed of cylindrical aluminum members, with titanium end fittings for additional support. The structure holds all the fuel and oxidizer necessary for descent. This fuel will be

linked to the ascent stage, connecting to the RL10 engines. The truss also houses the mission cargo and extra area for any life support or power equipment that cannot be contained within the crew module or in the ascent truss.

As shown in the figure, the descent stage has a platform on top of it so that the astronauts can walk around the module when they are on the surface of the Moon. Mounted on this platform are two solar arrays that will be deployed during the lunar surface stay to provide power. These solar arrays are shown retracted in the figure, but they will be extended outwards to form a square with 6.2 m sides. There is also an elevator mechanism shown in this figure. The mechanism allows the astronauts to descend to ground level and go back up, without using the ladder that is mounted on one of the legs. The mechanism uses a small platform to go up and down that fits within the descent truss structure. The platform is lowered or raised with cables that are connected to winches mounted on top of the descent stage. The whole mechanism is powered electrically, but there are handles in the winches as a mechanical backup system in the case of power failure.

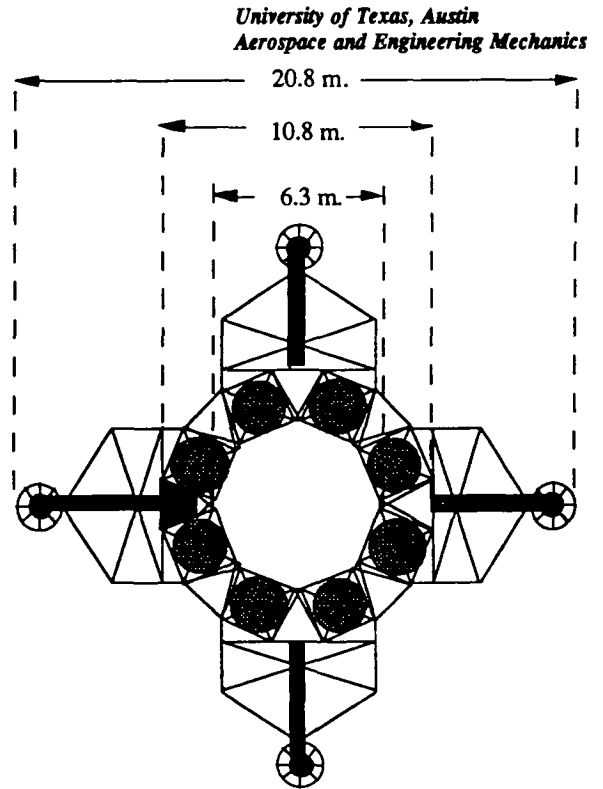


Figure 4. Descent Truss Top View

SPACE ENGINEERING PROJECTS IN DESIGN METHODOLOGY

The University of Texas at Austin
Department of Mechanical Engineering
Austin, Texas

Dr. R. Crawford, Dr. K. Wood, and Dr. S. Nichols

C. Hearn (Teaching Assistant), S. Corrier, G. DeKunder, S. George, C. Hysinger,
C. Johnson, K. Kubasta, R. McMahan, J. Salinas, C. Triplett, and T. Zizelmann

Abstract

NASA/USRA is an ongoing sponsor of space design projects in the senior design courses of the Mechanical Engineering Department at The University of Texas at Austin. This paper describes the UT senior design sequence, focusing on the first-semester design methodology course. The philosophical basis and pedagogical structure of this course is summarized. A history of the Department's activities in the Advanced Design Program is then presented. The paper includes a summary of the projects completed during the 1992-93 Academic Year in the methodology course, and concludes with an example of two projects completed by student design teams.

Introduction

The Department of Mechanical Engineering at The University of Texas at Austin offers an ABET-accredited undergraduate degree in mechanical engineering. The department currently has approximately 1400 undergraduates enrolled in the program leading to an undergraduate degree in mechanical engineering. In order to complete the requirements for graduation, each student must successfully complete a design methodology course and a capstone design course, usually in the last two semesters prior to graduation. Both of these design courses provide students with opportunities to combine and integrate material covered in the undergraduate curriculum in order to solve open-ended engineering design problems. Since 1989 the department has been a member institution of the NASA/USRA Advanced Design Program, where the program has focused on space-related design projects in the capstone design course. Twenty-four projects have been successfully completed, and three internships at NASA centers have resulted. This paper summarizes the philosophical foundation of the UT design sequence, the implementation of this philosophy with NASA/USRA ADP, recent projects in the capstone design course, and ongoing projects in the design methodology course.

During the period covering the Fall of 1986 through the Spring of 1993, ADP projects have been used in the capstone design course and in the graduate program. Since the Fall of 1992, ADP projects are being introduced to the undergraduate design methodology course. This allows the faculty to present space related design concepts to a larger

number of students and introduces the material at an earlier time in the undergraduate curriculum. Students in the course experience each phase of the design process, since each ADP project focuses on a different phase of the process, ranging from conceptual design to embodiment design. Participation in ADP has also encouraged cooperation between ME and ASE. The two departments have participated in joint design efforts and have identified interdisciplinary projects (education and research).

Approach

Annual conference reports of the ADP program indicate a broad spectrum of approaches by various departments and universities in developing their design programs. In fact, the ASE and ME programs take significantly different approaches in how they teach engineering design at The University of Texas at Austin. ME generally teaches the ADP material in the undergraduate design sequence required of all mechanical engineering students. The Department graduates approximately 200 undergraduate students a year. ADP material has also been taught in the graduate program.

The design sequence consists of nine semester credit hours of work taken over two semesters. The first course in the sequence (ME 366J) is a three semester-hour credit course which presents design methodology. ME 366J generally gives students the opportunity to complete several design assignments throughout the semester in order to apply the design tools discussed in lecture. The second semester of the design sequence involves two courses taken concurrently, a four hour lecture course (ME 466K) and a two hour lab course (ME 266P). The combination of these two courses are frequently referred to as "K". Students registered for K are divided into three person design teams to work on sponsored design projects.

During the last three years, the undergraduate senior-level course "Mechanical Engineering Design Methodology (ME 366J)" has been developed. In its current form, this course includes the following components: in-depth instruction in Pahl and Beitz's¹ functional-based methodology, student participatory case studies on fluid-thermal and mechanical system design, decision-making, cost evaluation, scheduling, and mathematical design techniques (e.g., quality methods, design optimization, and computer-aided engineering). The example problems given in lecture emphasize not only concept generation (in which the students participate enthusiastically), but also comparing

alternatives through technical feasibility, incorporation of empirical data, etc.

Students entering this course have had limited exposure to open-ended, market-driven problems and the necessary skills to attack such problems. The design methodology is structured to address these deficiencies. An initial case study is used to motivate the need for a systematic approach to engineering design. Following the introductory case study, creativity is presented as a recognized facet of design. Two types of creativity are explored, i.e., creativity as spontaneous idea generation and creativity as accumulation of existing ideas and composition of these ideas to meet specified goals.² Techniques such as brainstorming are taught and practiced by the students. Following the general topic of creativity, a particular design methodology is introduced. This methodology, created by Pahl and Beitz¹, is founded on the concept that design is a process of developing functional descriptions of design solutions, transforming these functional descriptions to form (or physical) descriptions, and finally choosing the most feasible design for further development and construction. This methodology is generally characterized as a decomposition strategy — the design problem is decomposed into subproblems. Five general process steps comprise Pahl and Beitz's design methodology: (1) problem definition and clarification (including the generation of initial design specifications); (2) process description and functional description, generation of solution variants to the design subfunctions, and combination of solution variants into overall configurations; (3) developing preliminary layouts, selecting the most feasible configuration, and embodying this configuration; (4) optimizing the selected configuration; (5) and finally detailing the solution for production or fabrication. Case studies, example problems, and group design projects are used as vehicles for learning this methodology.

During the 1992 Fall semester, the USRA ADP sponsored the establishment of a design methodology program for space engineering. The program was implemented in the existing design methodology course as described above; however, the design problems developed through the addition of the NASA/USRA ADP provided a unique vehicle for applying the design principles taught in the course. These principles include, in part: function sharing and multi-function capabilities, design for quality, and design for small-batch manufacturing. Function sharing, or the concept that devices should perform multiple functions, is a common theme in space applications. Previously, this principle was taught in the design methodology course based on simple mechanical components, such as using a worm gear to replace the combination of spur gears and a bevel gear to achieve a 90° offset and speed reduction. Broader scope problems that exhibit this need for function sharing are typical in NASA systems. Of course, the underlying idea is to reduce the size, complexity, and cost of components and systems, a recognized goal of all space

engineering. Design for quality is another design principle taught in the design methodology course. Little data is available from industry for exercising quality techniques, such as the Taguchi method, statistical process control, and factorial design. Through the NASA/USRA program and contacts at NASA centers, such data was solicited and provided realistic case problems for the students. Likewise, NASA representatives benefit from the student's analysis. Design for small batch manufacturing was another principle emphasized in the design methodology course. This principle focuses on reducing uncertainties in manufacturing due to set up, tooling, fixturing, etc., and to enable quick changes in process lines. This is an important problem to NASA in that most systems developed for space missions are fabricated in small batches. Through the NASA/USRA program, students are provided with design problems based on such systems, requiring the application of the concept of designing for small batch production.

The design methodology for space engineering course is structured around design projects. This course features four projects that emphasize different stages of the design process. Each student in the course works on three different design problems via three project assignments. The first two project assignments are oriented toward the conceptual design phase. The first assignment requires problem clarification, generation of specifications, and a functional decomposition. The second project requires the development of variant designs for subfunctions and their combination into a complete concept variant. Both of these projects require group collaboration for problem clarification, specification generation, and functional decomposition. Students then complete individually written reports of their work on each of these projects.

The final project assignment in the course focuses on the embodiment stage of design. This assignment is completed by teams of three to five students. The teams are given a choice of two projects, with at least three concept variants provided by the instructors. Students generate one additional design concept, perform comparative evaluation of all alternatives, and select one alternative for embodiment. The results of this project include a design report, complete with working drawings of the design solution, and an oral presentation of the project.

Projects Completed During the 1992-1993 Academic Year

The remainder of the paper addresses eight of the projects completed in the 1992-1993 Academic Year. The projects are discussed briefly and highlight the key issues associated therein. (The NASA/JSC contacts are noted as well.)

Topic 1: Specifications and Function Structure for an EVA Glove Tester (Contact: Glenn Klute)

Before a NASA astronaut uses a pair of EVA gloves in space, NASA spends at least \$100,000 in design and manufacturing iterations to obtain an acceptable pair of gloves. The NASA EVA gloves are prebent when manufactured. In other words, there is a natural curvature to the gloves. This curvature and the contour of the glove can cause a glove misfit upon EVA space suit pressurization. As a result, the gloves are custom designed for each astronaut, and the gloves are manufactured until the astronaut finds an acceptable pair. This process is quite costly. To reduce these costly design iterations, NASA has proposed a device that can measure the torque needed to open and close the fingers and thumb of the glove. The design teams were required to develop design specifications and a function structure for such a device.

Topic 2: Conceptual Design for a Ammonia Leak Detection System (Contact: Dave Belenger)

Ammonia will be used in the cooling system on the Space Station Freedom. NASA has been directed to use variation in system parameters, such as temperature and pressure, to detect leaks in the ammonia system. However, these changes may be so minute as to make detection extremely difficult. The design teams were asked to develop concepts based upon that and other techniques for detection.

Topic 3: Design of Autonomous Regolith Throwing Device for Radiation Shielding of Lunar Habitats (Contact: Dennis Wells)

NASA is considering establishing a fully equipped manned outpost on the moon by the year 2015. Regolith (lunar soil) will probably be used to shield habitats from radiation on the lunar surface. The regolith must be excavated and placed on the habitats. The purpose of this project was to prove the feasibility of throwing regolith onto lunar habitats. Low gravity and lack of a lunar atmosphere may allow regolith to be thrown accurately over large distances with a low power requirement. Throwing solutions were compared to traditional, Earth-based methods for moving lunar soil. It was shown that throwing is a feasible method of regolith placement, and an embodiment design of such a device was developed.

Topic 4: Design of a Radiator Shading Device for a Lunar Outpost (Contact: Mike Ewert)

NASA is designing a thermal control system for an outpost to be placed permanently on the Moon. One of the functions of the thermal control system is to reject waste heat, which can be accomplished through a radiator. At the lunar equator, a conventional radiator absorbs more heat than it rejects during the lunar midday. This problem can be solved by either increasing the temperature of the radiator

by means of a heat pump or by reducing the radiation incident on the radiator. The incident radiation can be reduced passively by using a shading device. The design teams developed concepts for radiator shading devices and for deploying and retracting the radiator and shade system. The design includes the embodiment and analysis of support structure, mechanical and thermal stress, and thermal performance. In addition, the teams addressed ideas for removing lunar dust from the shading device.

Topic 5: Specifications and a Function Structure for a Full Body Dynamometer (Contact: Glenn Klute)

NASA has performed studies on various Skylab and shuttle missions with respect to the effects of microgravity on the human body. They have found that human soft tissue begins to atrophy and weaken during prolonged exposure to microgravity. As a result, many of the astronauts returning from space missions experience difficulty performing motor tasks that are affected by gravity. To maintain or monitor the strength of the astronauts, a resistive training apparatus should be used to exercise the whole body. NASA intends to use this device for all future missions by adding the full body dynamometer to the space station and to the space shuttles when long periods in microgravity are of significant concern. While considering the human factors and the test environment, the design teams were required to develop the design specifications and a function structure for the dynamometer.

Topic 6: Conceptual Design for a Device to Measure Flight Hand Anthropometry (Contact: Glenn Klute)

NASA has given special attention to the development of their EVA gloves. An acceptable pair of EVA gloves cost on the order of \$100,000. This high cost results from two problems: the gloves are custom designed for each astronaut, and gloves are manufactured until the astronaut finds an acceptable fit. Despite these costly design iterations, these gloves have been shown to reduce effective grip strength significantly upon space suit pressurization. During an extended EVA, this may result in significant hand fatigue. The problems do not end there; micro-gravity environments introduce more variables with respect to the gloves' design. Studies by NASA have shown that two liters of fluid evacuate the lower body in micro-gravity experiments and some of that fluid goes into the hands causing them to swell. The design teams were required to conceptually design a method and/or device that can measure the swelling of hands in micro-gravity. Special consideration was given to the expected accuracy and repeatability of the readings. Also, the teams addressed the capabilities of measuring the swelling between the fingers.

Topic 7: Design of a Space Shuttle Reentry Couch (Contact: Phil Mongen)

NASA is currently planning collaborative space missions with the Russians to the Space Station Mir. The Mir will accommodate a crew of three astronauts for a period of ninety days. After their stay, the astronauts will be shuttled back to Earth via a space shuttle. Due to the physical deconditioning effects associated with prolonged exposure to microgravity, the astronauts may experience fainting and dizziness during reentry. As a result, NASA suggests a recumbent position for the space station astronauts to insure their safe return. In addition to general comfort, the couch must be able to withstand the effects of hard landing and crash situations. In order to implement the couch successfully, the following constraints must be considered: astronaut anthropometry, geometry, and center of gravity, shuttle floor strength, and assembly. The design teams were responsible for developing an embodiment design for the couch while also addressing the deployment and modularity of the couch.

Topic 8: Design of a Resistojet Thrust Control (Contact: Joe Riccio)

NASA needs a propulsion system that can provide small amounts of thrust to space stations and satellites. The thrust provided by the system would be used to maintain and control the orbital position of the space vehicle. The resistojet is a rather effective and inexpensive alternative for this objective. The resistojet uses a resistive element to heat compressed waste gases from the vehicle. Upon leaving one of the vehicle's storage tanks, the waste gases are heated and expanded through a nozzle. In order for the thruster to perform its task, it has to generate 50-350 millipounds of thrust over a period of several hours given only 500 Watts and a predetermined amount of waste gas. Additionally, the resistojet must be able to simply ventilate waste gases while generating little or no thrust. The design teams were responsible for developing an embodiment design for the layout and control of the resistojet.

Example Designs of a Reentry Couch and a Resistojet

The embodiment phase of the design process highlights the students' abilities to exercise their skills in analysis and modeling. Up to this point in their studies, students have had limited opportunities to utilize these skills on such open ended problems. For the final project assignment, the design teams used the conceptual design methodology before pursuing the embodiment phase. Without the experience of the previous conceptual design problems, their efforts through the embodiment would be less coordinated. The skills acquired through the first two project assignments facilitate the embodiment effort in the following ways:

- * The design specifications have thoroughly defined the requirements of the design.

- * The functional decomposition portrays the interaction of functional components and their roles within the design.
- * The solution variants for each main function of the design have been qualitatively defined and fulfill the specifications.
- * The solution variants interact in a technically feasible manner.
- * The resulting concept variant is defined and has been selected to best satisfy the mitigating design parameters.

To illustrate the results of the final project assignment, the designs of a Space Shuttle Reentry Couch and a Waste Gas Resistojet will be summarized.

Conceptual Design of the Space Shuttle Reentry Couch

Specifications. The first step in solving any design problem is developing a complete list of specifications. The specifications encompass the functional requirements and constraints for the reentry couch. Instead of listing all of the specifications noted by the design teams, a list of the most critical specifications are listed in Table 1.³

Table 1. Key specifications of reentry couch.
Must withstand emergency landing load factors 20 g forward in a 20 degree cone area 3.3 g aft 3.3 g right 3.3 g left 10 g down 4.4 g up
Must accommodate 5th percentile female to 95th percentile male
C.G. < 16" from middeck floor with occupants
C. G. < 6" from floor in stowed position
Weight < 180 lbs. without occupants
Must withstand fatigue from vibration 20 - 150 Hz @ 6.00 dB/Octave 150 - 1000 Hz @ 0.03 g ² /Hz 1000 - 2000 Hz @ -6.00 dB/Octave
Assembly without tools
Restrain all occupants
Comfortable

Another specification worth noting relates to the size constraints of the middeck floor of the space shuttle. See Figure 1 for an overhead view of the middeck floor and the mounting points for the couch. The load carrying capabilities of points 1 through 12 are very critical constraints of the design since the couch's floor connectors

must be relegated to these points. These additional specifications are highlighted in Table 2.³

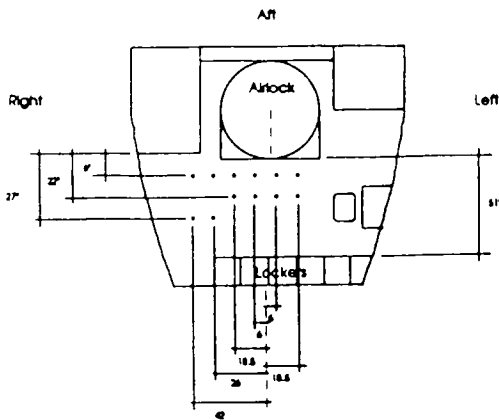


Figure 1: Overhead view of the middeck floor.

Table 2. Additional specifications for couch/floor interaction.
Couch connections are limited to points 1 through 12
Points 1 - 12 are limited to 5000 lbs. in the horizontal direction
Points 9 - 12 are limited to 80 lbs. in the vertical direction
Points 1 - 8 can feasibly accommodate all vertical couch loads

Function Structure. The function structure is a visual description of what the couch does. Before any such description can be developed, all the system's inputs and outputs should be identified. See Figure 2 for this representation. The system is lumped into one box that explains the couch's role: to provide support during reentry for astronauts suffering from muscle atrophy (due to prolonged exposure to microgravity). The inputs and outputs are identical in this case and are represented by the style of the line used, where bold lines represent materials, thin lines represent energy, and dashed lines represent signals.

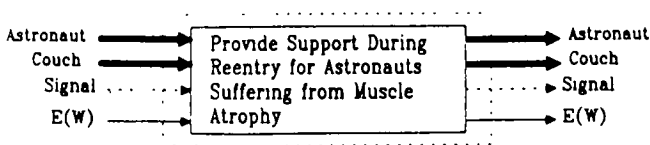


Figure 2: I/O diagram for the reentry couch.

Figure 3 illustrates a detailed function structure. The couch (bold line) enters the system to be assembled. This requires energy (thin line) and signals (dotted line) to insure proper couch setup. The couch then supports the astronaut

(bold line). The astronaut remains in the couch for reentry and is protected from normal and possible crash loads. An additional signal is used in case of a crash to release all restraining devices for astronaut evacuation.

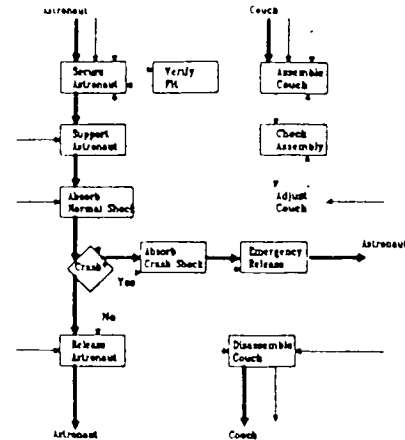


Figure 3: Function structure for the reentry couch.

Main Functions. The design teams developed solutions for the main functions of their function structures. The consensus of teams resulted in the main functions featured in Table 3.

Table 3. Main functions of reentry couch.
Assemble/Disassemble Couch
Secure Couch to Middeck Floor
Support Crew via Couch Structure
Absorb Shock
Secure Crew

Solution Variants. Since the couch had to be assembled and disassembled without tools, many assembly techniques were addressed. Most of the teams considered the following solution variants: hand screws, latches, shear pins, rigid structure (no fasteners), and notched bars.

Securing the couch structure to the middeck floor is a critical issue when considering the force limitations of points 9-12. As a result, many teams developed two sets of solution variants for this function. For points 1-8, the solution variants included: preinstalled floor bolts fastened to wing nuts, wing bolts screwed into a drilled and tapped floor, clevis joints, latches, floor-mounted mushroom studs, and floor-mounted spring-loaded shear pins. For points 9-12, most of the solution variants included a technique that uses a short (not touching the floor) shear support resting inside a floor-mounted journal. Additionally, many teams

decided not to use the points 9-12 at all due to the lack of floor strength in the vertical direction.

The couch structure supports the crew and should be strong enough for all expected loads. Therefore, the configuration of the couch with respect to the astronaut must be supported by an underlying structure. The solution variants for the couch support included: a solid platform, an enclosed fluid mixture, struts, and a magnetic field.

To absorb shock, many different solutions were explored. Some of the resulting solutions included combinations of the following solution variants: linear dampers and springs, torsional dampers and springs, airbags, magnetic damping, crushable or extruded materials, couch rotation, and adjustable seat cushions.

The safety of any device involving humans and inertia must include a restraint system. The solutions for crew restraint were as follows: 4-point safety belts, 5-point safety belts, air bags, and lap belts.

Concept Variants. Although a variety of solutions exist for each main function, it is impossible to combine all of the solutions from one main function with all of the solutions from another. Invariably, some solutions are technically incompatible with others. Also, some solutions cannot adequately satisfy the requirements defined by the specifications. As a result, the concept variants were determined through combinations of technically compatible and sufficient solution variants.

The concept variant embodied in this summary was derived after investigating many, but not all, of the solutions mentioned previously. This concept is represented by Figure 4. The couch is assembled with notched support bars. This technique is strong, holds without slippage, and is easily disassembled. The couch must be connected to the middeck floor. Shear/cotter pins were chosen because they can be assembled and disassembled easily without tools. With proper embodiment, they can survive the loads noted in the specifications. The couch structure utilizes struts. Struts can be connected and disconnected with little effort and can connect easily to the energy absorbing spring/damper setup and the adjustable cushions. Finally, the crew members are restrained by 5-point harnesses based on their proven effectiveness in helicopter crash seats.

Embodiment Design of the Space Shuttle Reentry Couch

The embodiment design process concentrates on the analysis and layout of the couch. The steps for embodying the concept depicted in Figure 4 were quite numerous and detailed. A summary of the following couch attributes will be presented: geometric layout, materials, springs and dampers, and the couch floor mounts.

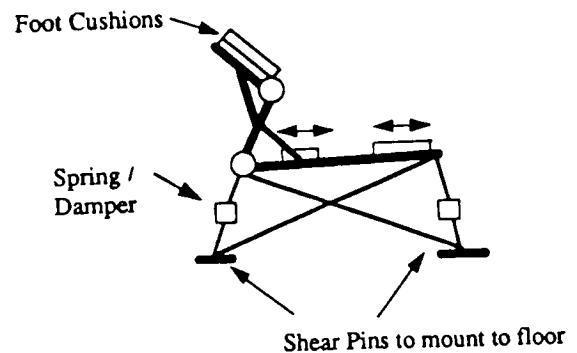


Figure 4: Concept selected for the reentry couch.

Geometric Layout. Since the couch must accommodate from the 5th percentile female to the 95th percentile male astronaut and there is limited space on the middeck floor, the astronauts must lie with their knees and waists bent. An excess length of 1.5 inches at the head and 1 inch at the foot have been left for spring and damper motion.

The angles and lengths of the supporting struts were selected based upon the center of gravity limitations of the couch. As a result, the back support of the couch is placed 9 inches from the floor. See Figures 5 and 6 for the side and bottom views of the couch, respectively. Notice that floor mounts 9-12 are not used in this design. To damp shock in all directions, all struts attached to shock absorbers are placed at an angle of 45 degrees from the floor.

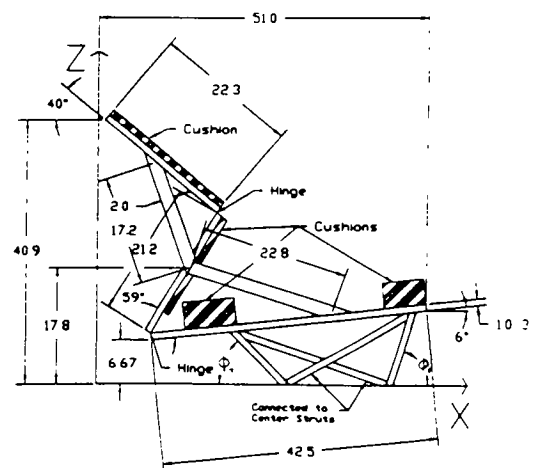


Figure 5: Side view of the reentry couch.

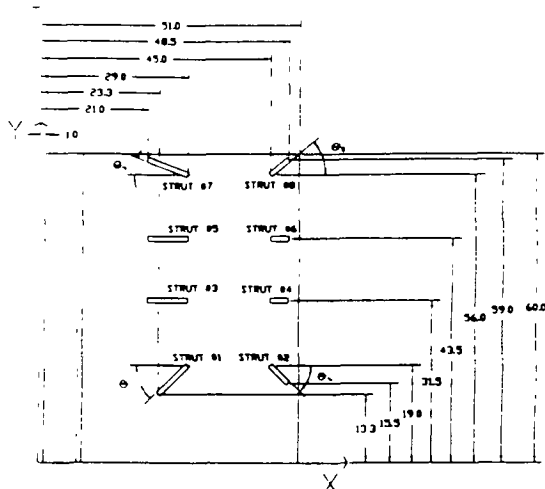


Figure 6: Bottom view of the reentry couch.

Materials. A light material was selected for choosing the couch structure material due to a weight limitation of 180 lbs. Fire-lam was selected based upon Ciba-Geigy's (the manufacturer) performance specifications.⁴ Also, this honeycomb material is flame retardant, hypo-allergenic, non-corrosive, and does not off-gas. The frame of the structure has members no larger than 1 inch square. The manufacturer has designed special inserts for hinges that can accommodate the cushions and assist during collapse and storage.

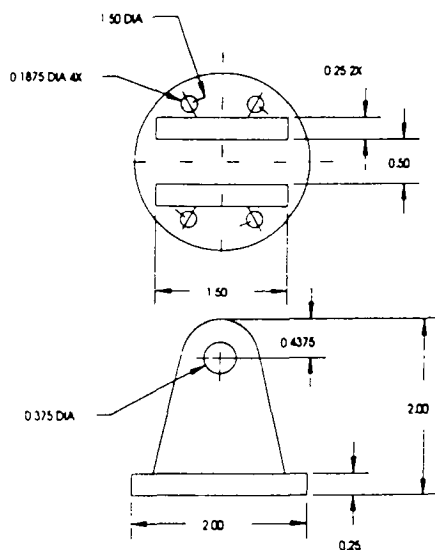


Figure 7: Floor and couch mount.

Spring and Damper. The spring stiffness and damping characteristics of the shocks were determined through a model incorporating the translational load factors in Table 1. A stroke range of four inches was allowed in the design, assuming a maximum amplitude of two inches in either direction. A spring constant of 11000 N/m coupled with a damping coefficient of 5000 Ns/m was calculated. All struts are designed according to these values. However, more

sophisticated analysis may reveal a more optimal value for each shock absorber.

Couch and Floor Mounts. After the spring and damper values were chosen, the mounts for the couch struts were designed. See Figure 7 for the floor mount. A couch strut is placed into the mount and secured with a shear pin.

Conceptual Design of the Waste Gas Resistojet

Specifications. The specifications of the resistojet highlight its functional requirements and constraints. The most critical specifications are listed in Table 4. The contents of Table 4 concentrate on waste gases that are stored in a tank external to the resistojet. These waste gases consist of the following compounds and elements: CO₂, N₂, Ar, H₂O, and air.

Table 4. Key specifications of resistojet. ⁵
Operational lifetime of 10,000 hours
Generate 50-350 millipounds of instantaneous thrust
Materials must withstand temperature and pressure ranges of operation
Operate with a peak power of 500 Watts
Heat waste gases up to 1600° C
Must withstand input gas pressures of 80-1000 psia from a storage tank
Must utilize storage tank gas mixtures
No adverse interaction between exhaust plume and space vehicle

Function Structure. The function structure, shown in Figure 8, is a visual description of what the resistojet does. The inputs are defined as the following: exit pressure signal, exit temperature signal, waste gas, DC power, and storage tank pressure. The outputs are the following: heat loss from heating the gas, heat loss from the tank, exit temperature data, DC energy loss, thrust, and exhaust. According to the flow of the inputs and outputs, the system's thrust can be controlled if pressure, temperature, and thrust are monitored at various locations in the resistojet.

Main Functions. Many of the design teams focused on the control aspects of the resistojet. As a result, the main functions dealt with the flow of the waste gases. Table 5 lists main functions considered by many of the design teams.

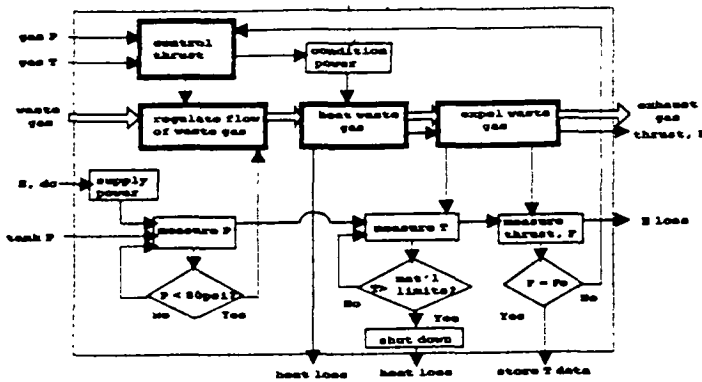


Figure 8: Function structure of the resistojet.

Table 5: Main functions of resistojet.
Regulate Flow of Waste Gas
Heat Waste Gas
Expel Waste Gas
Control Thrust

Solution Variants. Since waste gases enter the resistojet from an external storage tank, the first function of the resistojet is to regulate flow. The design teams investigated several techniques for this function. These techniques include: a simple orifice, a mechanical pressure regulator, an electrical pressure regulator, a fixed valve, and a variable valve.

The waste gases must be heated to generate any significant thrust. Most design teams addressed two basic approaches to heating the waste gases. The first approach suggests that the waste gases make actual contact with a heating element. The teams considered both straight line gas motion and helical gas motion over the heating element. The heating elements could be a variety or combination of geometries: shells, coils, spheres, cylinders, or fins. The second approach involves isolating the heating element from the waste gases to avoid contamination. The same gas motions were considered for an external heating element such as a heating coil or a rod array isolated by a shell.

Once the waste gases are heated, they exit the resistojet and generate thrust. Most teams thought a nozzle of a particular or a combination of geometries would perform effectively. The following nozzle geometries were explored by the design teams: divergent, convergent, conical, bell, and combinations of these.

The thrust is the key factor for determining whether a resistojet is functioning properly. The solution variants for controlling thrust were: a flow transducer, a pressure transducer, a pressure and flow transducer, a load cell, and a variable geometry nozzle.

Concept Variants. The concept variant embodied in this summary was derived after investigating many, but not all, of the solutions mentioned previously. This concept is represented by Figure 9. The concept selected by the design team regulates the flow with an electric pressure regulator. The waste gases are then heated by an internal helical coil wrapped around a thin tube and covered by an insulating cylinder. Upon leaving the heat exchanger, the gases enter a converging-diverging nozzle. Thrust is controlled by an on-board computer monitoring various temperature and pressure values at specific system locations.

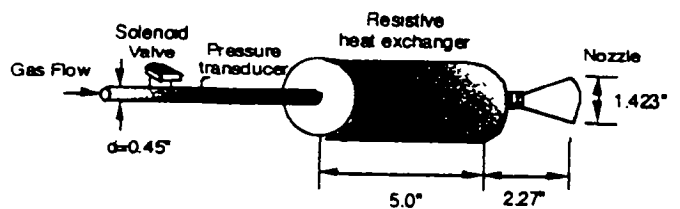


Figure 9: Concept selected for the resistojet.

Embodiment Design of the Waste Gas Resistojet

The embodiment design process concentrates on the analysis, materials and layout of the resistojet. The steps for embodying the concept depicted in Figure 8 were quite numerous and detailed. A summary of the following resistojet attributes are presented: pressure regulation, geometric layout, performance, and materials.

Pressure Regulation. In selecting an electronic pressure regulator, critical specifications must be addressed. For example, the waste gases stored in the tank may have pressures up to 1000 psia at 490°R (30.33°F). A solenoid valve with a pressure transducer was selected based upon its ability to satisfy the specifications and provide a means of pressure conditioning.

Solenoid valves are constructed from three basic parts: the valve, the body, the electrical coil, and the coil enclosure. Valve bodies are normally made from stainless steel and brass for greatest media compatibility. Each electric coil is encased in a protected encapsulated material to resist extreme environmental conditions. In a direct solenoid

valve, the magnetic force of the solenoid acts directly on the valve's sealing mechanism. Therefore, the pressure and flow capabilities of these valves are limited by the power of the solenoid.

Geometric Layout. The overall geometric layout is depicted in Figure 9. The heat exchanger is five inches long. The gas flows through the 0.45 inch diameter tube. The overall tube length is dependent upon the distance of the resistojet from the external storage tank. The outside of the tube is surrounded by a helical heating element. Extended, the heating element is 0.107 cm in diameter and is 383 cm long. The outside diameter of the heating chamber has not been determined. It will depend on a heat transfer analysis of the insulating materials covering the heating coil/gas tube assembly.

The most critical component of the resistojet is the nozzle. A good nozzle will give the maximum amount of thrust for a given mass flow. A schematic of the resistojet nozzle is shown in Figure 10.

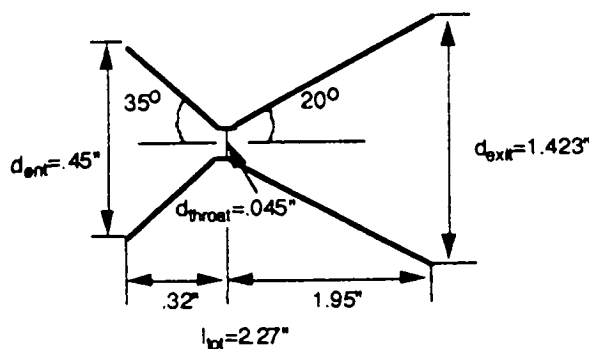


Figure 10: Resistojet nozzle dimensions.

The primary issues involved in designing the nozzle are throat area, exit area, entrance area, and nozzle shape. Using an iterative process with various gases flowing through the nozzle at different temperatures and pressures and assuming choked supersonic flow, a throat area of 0.00159 square inches was chosen. For a conical nozzle, this gives a throat diameter of 0.045 inches (1.143 mm). In an ideally expanded nozzle, an exit area is chosen that will lower the pressure of the gas flow to the ambient pressure. Since the ambient pressure for the resistojet is zero, this is not possible. To lower the exit pressure to about 0.001 percent of the stagnation pressure in the nozzle, an area ratio (exit area/throat area) of 1000 was chosen. This gives an exit area of 1.590 square inches and an exit diameter of 1.423 inches (25.4 mm). The entrance area to the nozzle was chosen sufficiently large to keep the gas flow upstream of the nozzle at a speed below 8 m/s so that proper heat transfer can take place in the heat exchanger. An area ratio of 100 was chosen to ensure that for the worst case situation the upstream gas speed is at most 8 m/s. This nozzle entry area ratio gives an entrance of 0.159 square inches and an entrance diameter of 0.45 inches (11.43 mm).

The most important consideration for determining the shape of the diverging part of the nozzle is ensuring that the flow will not separate from the nozzle wall, since this will cause large losses in thrust and unwanted vibrations. The simplest shape for the nozzle is a circular cone. This shape has the advantage of being easier to produce, which is important due to the small size of the nozzle, the materials from which it is made, and the small tolerances needed near the throat. A more complex shape would make the production of the nozzle considerably more complicated. Also, a more complex shape would add more nozzle mass for a very small increase in efficiency. Therefore, a circular cone geometry was selected.

With a back pressure of zero, a divergence angle of 20 degrees can be used without fear of gas flow separation. In the converging (entrance) section of the nozzle, a convergence angle of 35 degrees is used, since gas flow separation in the convergence region of the nozzle is much more difficult. This gives the nozzle an overall length of 2.27 inches (57.69 mm).

A consideration in the resistojet design is the impact of the exhaust plume on the space station environment. Placing any object in the path of the exhaust plume is undesirable, since the exiting gas will tend to collect on any surfaces encountered. Also, vision can be impaired by the exhaust plume. However, this effect is small since the mass exiting the nozzle is small and will disperse quickly.

To determine the shape of the exhaust plume, Prandtl-Meyer expansion theory was employed. By knowing the exiting gas Mach number (about 11 in the worst case), an exhaust plume angle of 85 degrees was calculated. This determined the cone of waste gases exiting the nozzle.

Performance. The performance will vary as the geometry of the resistojet changes. The layout of the resistojet satisfies the requirements without excess size or weight. Since the dimensions of the resistojet nozzle and heater were established, a detailed analysis of resistojet's thrust was performed.

To understand the system performance, a qualitative approach will be developed. As the gases exit the external tank and enter the heat exchanger, the power dissipated by the heating element heats the gases. The outlet gas temperature is increased by an increase in the heater power, a decrease in the specific heat of the gas, or a decrease in flow rate. The gases then flow into the nozzle. The nozzle is assumed frictionless with no back pressure. The flow is choked at the nozzle throat and is supersonic at the nozzle exit.

The gases chosen for analysis were pure argon, pure carbon dioxide, air, and an arbitrarily chosen mixture of 40% CO₂, 30% argon, and 30% air. Water was neglected due to the complexity of its phase changes. The inlet stagnation pressure (at the pressure regulator) was varied

from 20 to 120 psi, and the heat addition was incrementally set. The maximum power of 500 watts was not used in the analysis to allow 50 watts for powering the pressure regulators, solenoids, and the rest of the control system. See Figure 11 for the results.

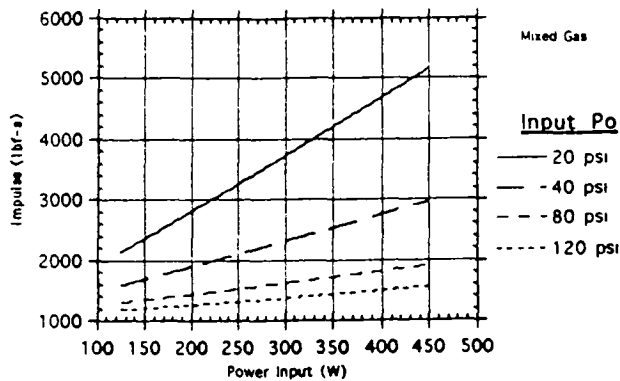


Figure 11: Resistojet impulse as power and pressure are varied.

Figure 11 represents the important results of the analysis. The thrust is increased by increasing the inlet stagnation pressure, but is barely affected by the amount of heat addition. The thrust falls into the specification range of 0.05 to 0.35 pounds force given by NASA for a relatively small power requirement of 125 Watts.⁴ See Figure 12 for these results. The rather modest power requirement is intended to reserve plenty of power for other systems.

Materials. One of the key issues addressed in the design of the resistojet was the material used for each of the system components. The difficulty in selecting appropriate materials rested in the extreme variation in temperatures that the resistojet had to withstand (-273°C to 1600°C). All selected materials satisfy the requirement for high melting point and the potential for use at cryogenic temperatures.

For the heat exchanger of the resistojet, many different material properties were investigated. The magnitude and the duration of exposure (up to eight hours) to the upper temperature limit (1600°C) was a major concern. Another criterion in material selection for the heat exchanger was the thermal conductivity of the material. A thermal conductivity approaching or exceeding 400 W/mK is necessary to maximize the amount of heat delivered to the gas flowing through the heat exchanger. Workability, or more specifically, weldability was also a factor in the material selection, since the heat exchanger was decided to be welded to the nozzle. For these reasons, a platinum-rhodium alloy (Pt-10Ro) was selected for the heat exchanger. Rhodium by itself has a high thermal conductivity (627 W/mK), but it oxidizes at temperatures above 1200°C; it was also one of the most infusible metals.⁶ Combining rhodium with platinum (with a thermal conductivity of 305 W/mK) into this particular alloy

increases the high-temperature strength of platinum.⁶ This alloy was also chosen for the piping of the system. Since the coiled heating element used in the resistojet is essentially a pipe heater, and the heat exchanger itself is really just an extension of the resistojet piping, the two components are made of the same material to eliminate the need for welding, thus simplifying the manufacturing process.

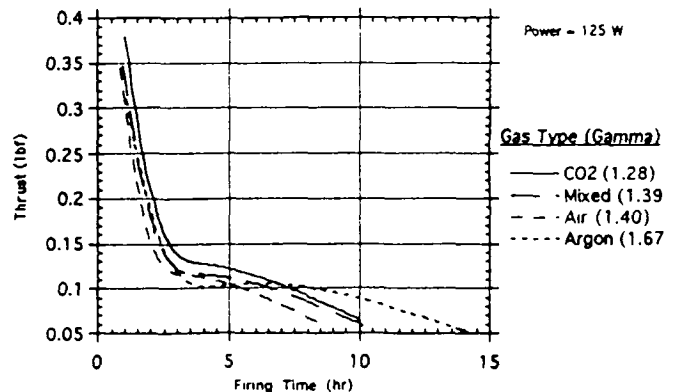


Figure 12: Resistojet thrust vs. time at 125 Watts.

The nozzle posed a more complex material problem. One end the nozzle is exposed to the high-temperature gases leaving the heat exchanger, while the other end of the nozzle is exposed to the cold of space. The material comprising the nozzle must withstand both the high and the low temperature limits simultaneously. A material with a low thermal conductivity is needed to protect the nozzle from radiation to space. Also, since the throat diameter of the nozzle is so small, absolutely no material oxidation can occur. Single-crystal tungsten was selected for the nozzle.⁷

A cylindrical insulation and radiation shield is needed for the outside of the heating coil. Reinforced carbon carbon (RCC) with a silicon carbide coating is used behind the heating element. It is not an insulator, but it can withstand temperatures up to 1760°C for an extended period of time, and it bears the load caused by the vibrations of the resistojet when in operation.⁸ Behind the RCC is a layer of multi-layer insulation (MLI). MLI is a blanket-like material consisting of layers of metal foils that are spaced apart.⁸ Behind the MLI, Lockheed Insulation 2200 (LI-2200) tiles are bonded onto a titanium alloy (Ti-6Al-4V) casing. These tiles are capable of withstanding temperatures up to 1650°C for an extended period of time. The tiles are bonded to the inside of the titanium casing (so the bonds face space, and their surfaces face the heat coming from the MLI). The SIP is then attached to the titanium casing by another layer of RTV adhesive. The intent of the SIP is to expand and contract with the titanium, thereby isolating the tiles from this expansion, and preventing them from "popping" off. The reason for bonding the tiles facing the heat is to prevent

the RTV from exceeding its temperature limit of 343°C. MLI blankets are then wrapped around (or attached to) the outside of the titanium casing to protect the RTV bond on the inside of the titanium casing from the cold temperatures of space, and to act as a second radiation shield.⁸ All of the insulation materials described are existing technology, and all are flight certified.

Conclusion

NASA and USRA have developed a university based program (ADP) to support space design education. ADP allows participating universities sufficient flexibility to fit the program to support each institution's individual curriculum. The program provides the Department of Mechanical Engineering at The University of Texas at Austin with the opportunity to expose students and faculty to the challenges and opportunities of space related design problems and to improve the design education experience of its students.

The Department would like to thank NASA and USRA and the project sponsors for their support. The Department hopes to continue such participation and contribute in any fashion to promote new ideas and broaden the education experience.

References

- 1) Pahl, G. and Beitz, W., *Engineering Design*, Springer-Verlag, Design Council, 1984.
- 2) Adams, James L., *Conceptual Blockbusting: A Guide to Better Ideas*, 3rd ed., Addison-Wesley, Reading, MA, 1986.
- 3) Mongan, Phil, NASA/JSC Engineer, phone interview, March 28, 1993.
- 4) Ciba-Geigy Composite Materials, Product Catalog, 1993.
- 5) Riccio, Joe, NASA/JSC Engineer, phone interview, March 21, 1993.
- 6) Brady, G. S. and Clauser, H. R., *Materials Handbook*, 13 ed, McGraw-Hill, 1991.
- 7) Waterman, N. A. and Ashby, M. F., *CRC-Elsevier Materials Selector*, vol. 2, CRC Press, 1991.
- 8) Pham, V., NASA/JSC Engineer, phone interview, April 30, 1993.

REMOTE UNIVERSAL NAVAL TRANSPONDER

United States Naval Academy
Aerospace Engineering
Annapolis, MD

Dr. James Severns, Professor
Karl Schultz, Matthew Finney, David Tandy, Lori Perkins

Abstract

The United States Naval Academy Space Systems Design Team has designed a digital transponder for use by U.S. Navy and commercial vessels for accountability and communication. The Remote Universal Naval Transponder, or "RUNT", was designed as a follow on to MACSAT and modeled loosely after PANSAT. The main benchmark when designing RUNT was cost. The overall goal was to produce a less expensive source of communication for naval vessels without sacrificing reliability. The RUNT will operate in a 881 km polar orbit. The spacecraft will be placed into this orbit, two at a time, by the SCOUT launch vehicle, which is capable of placing 130 kg into a 900 km orbit. The total lift off weight of both RUNTs, and all accompanying structure totals 84.4 kg. Total earth coverage could be accomplished with 32 satellites. However, with only eight satellites, a satellite would pass over any point on earth, at least every forty minutes. By using a gravity gradient boom, and a directional antenna, transmissions can be accomplished with less than 1 Watt eirp from the RUNT.

Systems

Introduction

The need for reliable, inexpensive, long-range communications can not be overstated. With satellites playing a larger role in long range communication, we must find ways to make satellites less complicated and expensive without sacrificing dependability. Development of inexpensive satellites began with the Oscar series, amateur satellites designed and built by

Ham radio operators. These satellites started out as very simple radios in space, but since then, as more money and resources became available to amateurs, the Oscars have evolved into more complex and more expensive communications satellites, not unlike many commercial satellites.

Recently, there has been a newfound interest in small satellites. The Microsat series, MACSAT, and PANSAT are all examples of the fresh attention being given to these smaller, less capable versions of commercial communications satellites.

The need for fleet accountability took a different route. Large scale use of satellites for fleet accountability began with the introduction of the Global Positioning System (GPS) which allowed a unit to determine its position within a few meters with a box no bigger than a walkie-talkie. While this greatly aids the unit possessing GPS, it does not provide anyone else with knowledge of that unit's location.

This problem was addressed by Commander Robert Bruninga of the Naval Academy's Satellite Earth Station. Commander Bruninga recognized the need for the Academy to keep track of its fleet of YP ships during the summer months while the boats are deployed along the east coast. CDR Bruninga then developed software and hardware for a High Frequency system, to be used in conjunction with GPS which allows a single Command Station to locate and track all of the assets within its command.

Since the current system is limited by the range of the HF tracking station, the next logical step is to provide an overhead relay from the fleet assets to the command station and, if necessary, from the Command Station to the individual assets.

It is with this in mind that the RUNT was designed.

It is capable of transmitting digital messages in either real-time or store-and-forward mode. This message can carry location information, tactical data, or emergency text messages. The RUNT can be fitted with the capability to transmit scrambled data in tactical situations. Since it is fitted with a high gain, circularly polarized antenna, a unit can use RUNT with a small, hand-held unit and without tracking the satellite.

The development of the RUNT has shown that a simple, inexpensive satellite can be designed, constructed and utilized without sacrificing practicality or reliability.

Operations and Data Flow

The RUNT Ground Accountability System consists of various fleet assets and one or more Central Processing Stations which will receive, analyze and plot the positions of the assets involved. The RUNT can also be used as a real-time digital repeater or a store-and-forward digital bulletin board by any user who can operate using AX.25 protocol. The RUNT mission operations and data flow is shown in Figure 1.

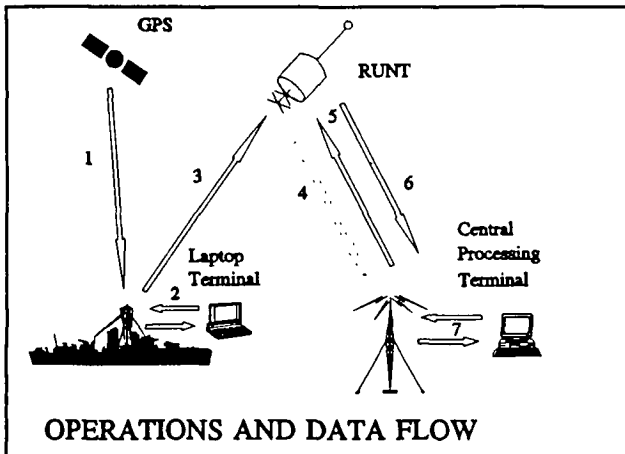


Figure 1

The system works as follows:

- a) GPS sends message to naval vessel
- b) Laptop on board processes signal
- c) Message is transmitted to RUNT
- d) Message is received and stored by RUNT
- e) Command station sends message to send the entire message

- f) RUNT transmits message
- g) Information is analyzed and plotted at the central processing terminal

Orbital Analysis

When selecting an orbit, cost was the underlying factor. A high altitude orbit would require too much transmission power thus driving up the cost. An orbit which is too low would have a small footprint, necessitating the use of more satellites for full earth coverage.

The 881 km circular orbit selected was chosen because it provides an acceptable compromise between low power budgets and large footprint area and it allows the spacecraft to pass over the same position on the earth each day. The 90 degree inclination was chosen to achieve total earth coverage.

Each RUNT will cycle through 14 full orbits each sidereal day. This will place the satellite over the same spot each day, but since a civil day is four minutes longer than a sidereal day, the RUNT will pass over each point four minutes earlier than it did the day before.

With the given altitude and assuming a usable inclination of five degrees above the horizon, the max slant range is determined to be 2954 km and the footprint width is 5325 km. With those dimensions, eight satellites would fill an orbit with some overlap. Four of such orbits would allow for total earth coverage.

Since launch of 32 satellites would take a large amount of time, an intermediate configuration is to put two satellites, 180 degrees apart, into each of the four polar orbits. With an orbital period of 102 minutes and 13 usable minutes per pass, the maximum time between passes is 38 minutes.

Scout Launch Vehicle

The launch vehicle most suitable for the RUNT mission is the Scout. This vehicle is 22.9 meters long with a 0.86 meter diameter. It is capable of placing a 100 kg load into a 1000 km orbit or 130 kg into an orbit of 881 km. The proposed payload fairing is the 3.65 m

long, 0.86 m diameter configuration since this fairing is capable of placing two RUNT satellites into orbit along with support structures. See Figure 2

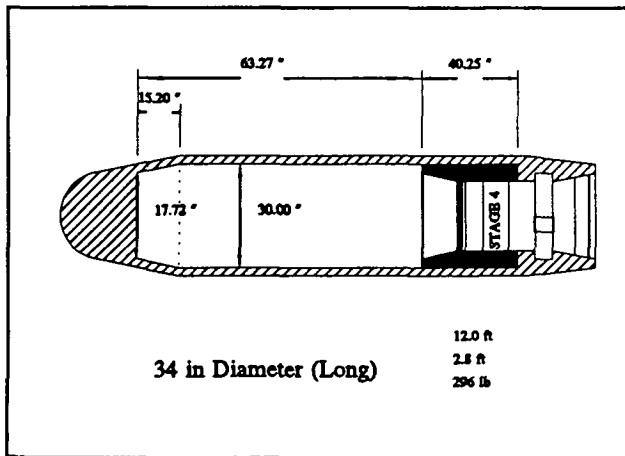


Figure 2

The satellites and accompanying structures will be fastened to the Scout by three equally spaced hard points with bolts and explosive actuated nuts. Release from the launch vehicle will occur then the nuts are fired and the third stage is simultaneously backed away. This separation occurs at $t+10$ minutes 11 seconds. Final burnout takes place 40 seconds later when the fourth stage burns out. At this point, the two RUNT satellites, still connected, should be spinning at 150 rpm in a 881 km circular orbit.

Power

Requirements

The RUNT's power subsystem requirement is to provide a +28 volt, 5.0 watt continuous orbital average load bus for an orbit life of approximately 7 years. A +28 volt bus was chosen because most systems flown in the U.S. have used close to a +28 volt DC system. Most hardware is designed around this type of system, and since one of our satellite's requirements is to use off the shelf components, this was determined to be the best option.

The satellite will have two different phases of power requirements. Initially, the power requirements will be significantly lower to bring the satellite into full operation (Transition Stage). This stage will include

deploying the gravity gradient boom, deploying the antenna, and other tasks. After the satellite is fully operational, all systems will be running continuously during daylight hours and eclipse time (Operational Stage).

System Specifications

Power Source	Solar Panel Arrays Secondary Batteries
Power Subsystem	Direct Energy Transfer System
Power Regulation	Unregulated Subsystem using Shunt Regulator
Bus Voltage	27.50 V Average (24-33 V)
Transmission Power	4 Watts
Battery Type	22 2 A-hr Cell Commercial Aviation NiCd
Battery Capacity	55 W-hr (Redundant Batteries)
Battery Weight/Volume	3.6 kg/1900 cm ³
DOD/# of Cycles	10 percent /26000-36000 cycles
Solar Cell Type	Silicon (12 mil cover slip/back reflector)
Solar Panel Area/Weight	5574.2 cm ² /4.10 kg

Solar Cell Array Design

The RUNT will derive its power from body-mounted solar arrays using silicon solar cells with a 21 mil cover slip and back surface reflectors similar to those incorporated in MICROSAT. This will produce a 15% power conversion efficiency at BOL. The cover slip will provide protection against radiation damage. The RUNT's orbit of 881 km is safely out of the Van Allen Radiation Belts (1600-1800 km). Silicon cells were used instead of Gallium-Arsenide in order to minimize cost.

The solar cell arrays are mounted on the top of the satellites as well as on the sides. There are three panels on the top and one on each of the twelve sides. The cells are arranged in series in order to provide voltage of approximately 33 V. This is necessary in order to ensure the batteries are charged. The arrays need a higher voltage than the batteries due to partial shading, swings in bus voltage and efficiency losses.

Using JPL curves for this particular orbit it was

determined that each cell will produce 0.430 volts and 31.4 mA/cm² after seven years. Therefore, 77 cells must be placed in series to achieve the proper voltage. There are 77 2x4 cm² cells in each of the top panels and 80 2x2 cm² cells in each of the side panels. The layout for the side panels is a simple rectangular array, placed onto the center of each side. The layout for each of the top arrays is shown below.

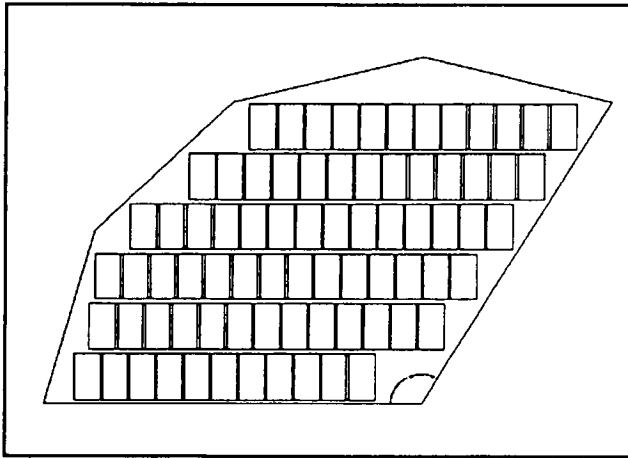


Figure 3

Power Budget

There are two separate power budgets. The first is for the transitional stage when the satellite is released from the Scout launch vehicle until the satellite becomes fully operational. The second is the Operational Stage.

The Transitional Stage is necessary because the satellite is not in its optimal orientation to receive maximum power from its arrays and will depend more on the batteries during the early stages of flight. Different subsystems will also be in operation. These include deployment of the gravity gradient boom, ignition of rocket motors, and the firing of ordnance.

In the Transitional Stage, the transponder will require a constant 0.5 watt power supply. The transmitter will draw 0.05 watts since the satellite will be tracked by a 12 meter dish during this phase. Other miscellaneous subsystems will draw an average of 0.5 watts. At this rate, the satellite can sustain itself for 55 hours before an exterior source of power will become necessary. It

should be noted that other systems such as the rockets and explosive devices may draw power as well, but for very short periods of time (less than 0.5 seconds).

The operational stage will rely entirely on the solar arrays to charge the batteries to the necessary levels to meet the satellite's power requirements. These requirements will be the running of various subsystems such as the transponder and the transmitter which will require the vast majority of the power.

In the Operational Stage, (once the yo-yo devices, boom, and antenna are deployed) the data rate will be increased to 9600 Baud. The transponder will still run at 0.5 Watts, but the transmitter will be run at full power of 4 Watts (0.8 Watts eirp). Miscellaneous subsystems will still draw a constant 0.5 Watts.

Orbital Power Analysis Graphs

Below is a diagram showing the model used to determine available power at each point of various orbits. The latitude of the satellite is Theta(θ) while the angle the orbital plane makes with the sun is denoted by lambda(λ). Following Figure 4 are some graphs displaying the power available from side and top panels during each orbit.

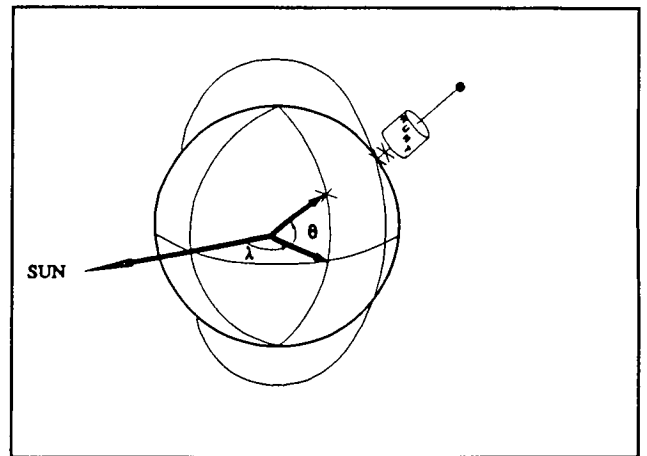
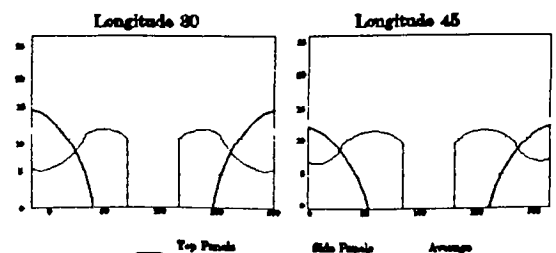


Figure 4



Propulsion

Due to the compact size of the RUNT, two satellites are able to be launched by a single Scout launch vehicle. However, once the desired altitude of 881 km is reached, both satellites, when released from the scout, lie next to each other in the same orbit. This is obviously no use. In order to obtain continuous global coverage using a minimum of satellites, the eight satellites in each orbital plane must be evenly spaced. This calls for a separation of 45 degrees between satellites.

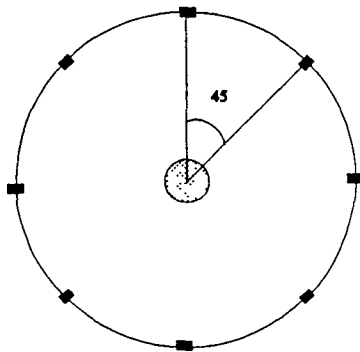


Figure 5

In order to separate the two satellites after release from the SCOUT, one satellite must be boosted by a propulsion mechanism to a position which will eventually result in the required 45 degree separation from its partner. At a point in the initial orbit, one satellite will be boosted by a small, solid fuel Morton-Thiokol Star 5A rocket motor. The velocity imparted to the boosted satellite will change its orbit from the original circular polar orbit to a new orbit which is slightly elliptical. This new elliptical orbit will have a period slightly longer than the 881 km circular orbit resulting in an increasing separation as the two satellites, now in different orbits, continue to circle the Earth. After the boosted satellite becomes 45 degrees separated "behind" its partner, a delta velocity will be imparted to the transfer satellite dropping it back into the necessary 881 km circular orbit. The Figure 6 shows this.

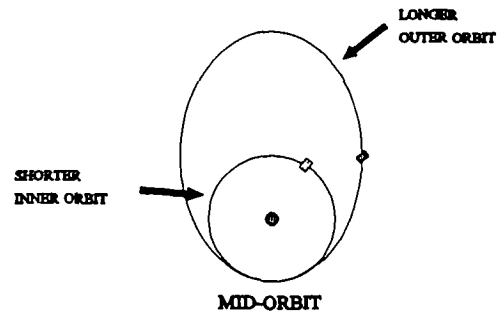


Figure 6

Specifics

The Star 5A has a sufficient total impulse to impart a delta velocity of 100.3 m/s to the RUNT. With this delta velocity, the transferring satellite will be moved into an elliptical orbit with an eccentricity of approximately 0.027. This orbit will have a period of 6411 seconds compared to the 881 km circular orbit's period of 6155 seconds. The difference of 256 seconds will separate the two satellites by 15 degrees for each orbit the boosted satellite makes. Therefore, after three orbits made by the boosted satellite, the desired separation of 45 degrees will exist between the two satellites. When the boosted satellite approaches its perigee (which is the only common point of the two orbits) the Star 5A will be fired and the velocity of the transfer satellite will be slowed 100.3 m/s dropping it back into the 881 km circular orbit.

Star 5A

The Morton-Thiokol Star 5A is an ideal choice for the booster rocket motor needed by the RUNT. Its small size, light weight and adaptability meet the requirements necessary to separate the two RUNT satellites launched with each Scout. A total impulse of 519.4 kg-sec is needed to boost the RUNT into and out of its transfer orbit. The Star 5A has a maximum total impulse of 590 kg-sec but the fuel load, and consequently the total

impulse of the Star 5A, can be off-loaded by as much as 20% or nearly 0.455 kg. The total impulse range of the STAR 5A limits of the weight of the satellite ranging from a minimum of 46.5 kg to a maximum of 57.2 kg. Additionally, the simplicity of the solid rocket motor in conjunction with the small power requirements to fire the rocket mesh with the RUNT design criteria of simplicity and reliability well.

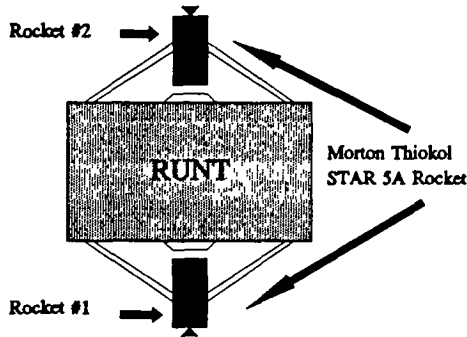


Figure 7

Spacecraft Structural Design

The structural configuration of the RUNT is based upon two things. The first is the need to sufficiently support all subsystems through launch, separation, and operation and to point the antenna toward the earth. Since cost is of primary concern, the best way to achieve this is through a gravity gradient boom. With the boom pointed away from the earth, the antenna will have an unobstructed view. Both the antenna and the boom will extend from the center of either end of the satellite in order to avoid torquing moments due to asymmetric mass distribution. All other components will be housed within the structure.

The second requirement which the structure must meet is to have sufficient area upon which the solar arrays will be fitted. This was, in fact, the determining factor when deciding how big the satellite was to be.

Launch Loading

The loads placed upon the satellite at lift-off are by

far the most critical. Frequency vibrations from the launch vehicle come from both internal and external sources. The internal sources are disturbances such as engine vibration while the external sources come from aerodynamic effects. By designing the satellite structure to have different natural frequencies than the launch vehicle, resonance can be avoided, and much of the frequency induced load will be erased. The natural frequencies of the Scout are 18 Hz and 20 Hz axially and laterally respectively. By varying the construction and material thickness of the RUNT, different natural frequencies can be obtained.

Another, perhaps more apparent source of launch loading is due to the axial acceleration of the launch-vehicle. The weight of the overall structure will decrease as the propellant is expelled, thus the acceleration will slowly increase. The maximum axial acceleration of the SCOUT is 9.5 times the normal force of gravity. The mid-deck of the RUNT will hold the majority of the weight, and thus bear the largest load. At maximum acceleration, the load acting on the mid-deck is calculated at just under 3000 N, which translates into 10,280 Newton's per square meter. This load will be more than adequately accounted for since Aluminum 7075, the design material, has an Ultimate Tensile Strength of 524 million Newtons per square meter.

Pyrotechnic Loads

Pyrotechnic shock is another load which the structure must be designed to withstand. Pyrotechnic shock comes from the explosions of separation apparatus. The RUNT will use a total of five marmon clamps to be separated by exploding bolts. One clamp will join both satellites to the satellite interface, two will connect the satellites to one another, the remaining two will hold the nozzles in place until after the orbital transfer is completed. Pyrotechnic bolts will also be used to release the yo-yo mechanism used to de-spin the RUNT.

Booster Rocket Loads

The final event which will demand structural integrity

beyond the operational requirements is the firing of the STAR 5A rockets to change the orbital orientation of the satellites. This burn produces much smaller accelerations than the launch vehicle, therefore the forces have been thoroughly accounted for when designing for launch.

Structural Configuration

The structural design of the satellite is a 12 sided cylinder. Its internal framework is composed of 12 vertical and 36 horizontal "L" spars, as shown in Figure 5.1. The second layer of material, composed of 15 inch by 6.2 inch Aluminum 7075, provides a base for the placement of the external honeycomb support.

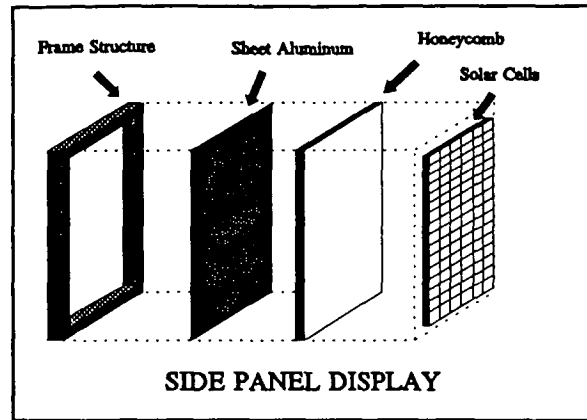


Figure 9

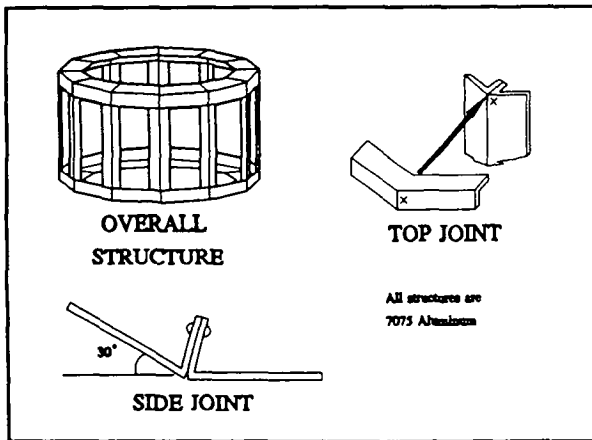


Figure 8

The side panels are constructed as shown below.

The total weight of the satellite structure is 18.39 kg. This brings the total weight per satellite to 32.27 kg. More mass was added to the launch configuration as the satellite interface and separation apparatus were accounted for. Those structural members along with the engine mounting devices add a mass of 10.53 kg. There is also the additional weight of the two STAR 5A solid fuel booster rockets. This is a total of only 52.10 kg for one satellite and all of the supporting hardware. This relatively low weight allows two satellites to be launched per launch vehicle. The total mass of the two satellites, the rockets, and the separation structures comes to 84.37

kg.

The layout in which the launch vehicle will be loaded is shown below.

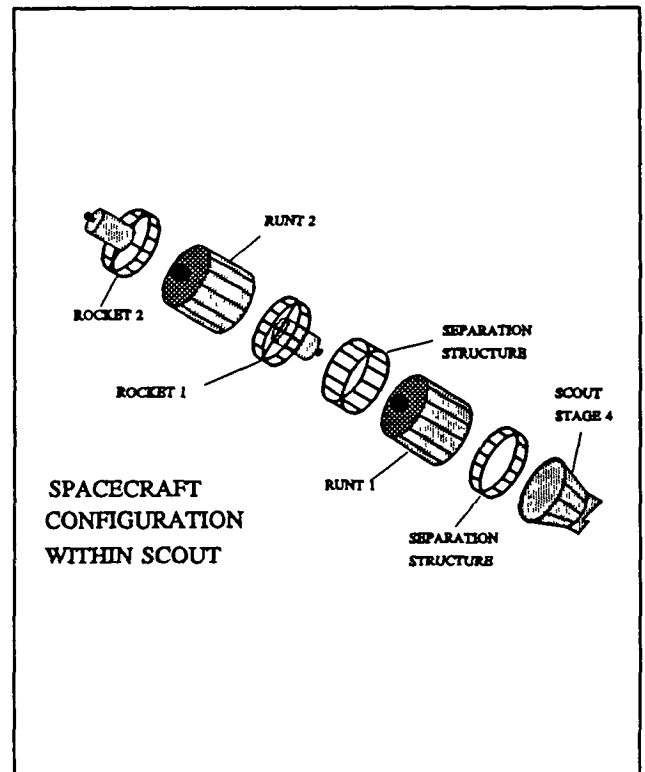


Figure 10

Thermal Design

One very important aspect of satellite layout is thermal design. By using different materials and coatings, each with different absorptivity (α) and emissivity (ϵ) the temperature of the spacecraft can be determined. These characteristics cause the surface to hold various equilibrium temperatures when illuminated by sunlight. The interaction of all of the surfaces determines the final equilibrium temperature of the spacecraft.

Although every machine has an optimum operating temperature, temperature is especially important when dealing with electronics components. By exploiting the different α and ϵ of various materials, the spacecraft can be designed to operate at nearly any desired temperature.

This method operates on the premise that, at equilibrium, power into the satellite is equal to power out of the spacecraft. Power into the satellite is defined by the following equation:

$$P_i = (\alpha) (S) (a) (\cos X)$$

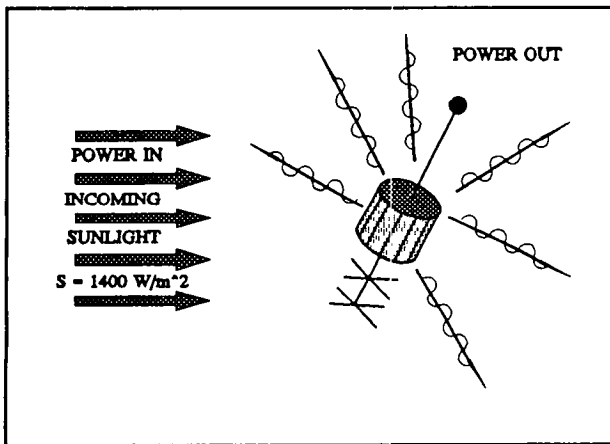


Figure 11

Power out of the satellite can be found using this equation:

$$P_{out} = (\epsilon) (A) (\sigma) (T^4) + P_{gen}$$

- α = Absorptivity
- S = Sunlight Intensity (1400 W/m²)
- a = Area
- X = Pitch Angle
- ϵ = Emissivity
- σ = Stefan Boltzman's Constant (5.6705 x 10⁻⁸)
- A = Area
- T = Temperature (Kelvin)
- P_{gen} = Power Generated

Notice that the two areas are different. Area *a* is the area being hit by sunlight while area *A* is the total surface area of the spacecraft which radiates heat into space.

The resultant temperature can be found by setting power out equal to power in plus power generated by the spacecraft and solving for T.

This has been done assuming gold to be the coating on all areas not covered by solar cells. The graph below shows the temperature of the satellite as it spins in relation to the sun. An angle of zero means that the side is directly facing the sun. An angle of 90 means that the top is facing sunward.

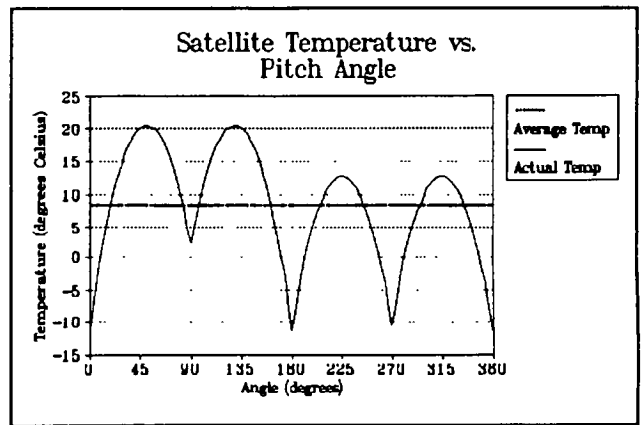


Figure 12

Using this graph as a guide, it is apparent that the satellite will operate at temperatures ranging from -10 degrees to +20 degrees Celsius. This range is a safe and efficient range for all components used, including all transmission, electronic, and solar equipment.

Communications

Because the primary purpose of RUNT is the relay of information , the choice of uplink and downlink frequencies, power requirements, antenna design and data rate are vital to mission success. Additionally, the need for relative simple design, compatibility with present systems, and the need for small size were fundamental design criteria.

During the transition from launch to final orbit position, the RUNT's communication's antenna will not be deployed. Furthermore, the satellite's available power will be limited. Timers on board the satellite will control the majority of satellite functions required during the transition phase, such as firing the booster rockets. However, there is still a need to maintain communications with the satellite in order to monitor its progress and status.

The RUNT's small size and small power budget limited the transmitting power available to the transmitting antenna. In order to minimize errors in data transmission, a signal-to-noise ratio of 13 dB was required. At this ratio, an error of one bit per 100,000 bits will be obtained. Additionally, a 6 dB gain cross dipole antenna with a reflector will be used as the satellite's transmitting and receiving antenna. The antenna's small size, gain, low cost and low weight meet the satellite's driving design criteria. A half-wave dipole with again of 2.1 dB was assumed as the antenna to be used on the ground.

An ambient noise level of 1.242×10^{-16} Watts on the ground was calculated:

$$\text{Noise} = (\text{Boltzmann's constant})(T)(\text{bandwidth})$$

$$\text{Noise} = (1.38 \times 10^{-23} \text{ W/Hz/K})(300\text{K})(3 \times 10^4)$$

$$\text{Noise} = 1.242 \times 10^{-16} \text{ Watts}$$

From this noise level and a signal-to-noise ratio of 13 dB, the receiver needed to receive a signal 2.478×10^{-15} Watts in strength.

$$\text{Power Transmitted} = \frac{P_{rec} (4\pi)^2 R^2}{G_t G_r \lambda^2}$$

- where P_{rec} = signal power at the receiver
- R = distance between transmitter and receiver
- G_t = gain of the transmitter
- G_r = gain of the receiver
- λ = wavelength of signal

the minimum transmitter power needed over the maximum slant range of 3400 km (881 km circular polar orbit) to give a signal-to-noise ratio of 13 dB at the receiver was 0.56 Watts.

	<u>Transitional Stage</u>	<u>Operational Stage</u>
Baud Rate	1200	9600
Bandwidth	4000 Hz	30000 Hz
Ambient Noise	1.65×10^{-17} Watts	1.24×10^{-16} Watts
Transmitter Gain	0 dB	6 dB
Receiver Gain	25 dB	2.1 dB
EIRP	0.01 Watts	0.86 Watts
Uplink Frequency	300 MHz	300 MHz
Downlink Frequency	259 MHz	259 MHz

Table 1

Antenna Design

The antenna system on the RUNT is critically important. The antenna chosen for the RUNT is a dual dipole. The dual dipole will be used on both the ship and the satellite. The reasons for this choice are:

- a. The dual dipole antenna provides a gain of 6 dB.
- b. It has a simple mechanical structure.
- c. It is not as fragile as a parabolic dish.
- d. It takes up less space during launch.
- e. The antenna is lightweight.
- f. The antenna is inexpensive.

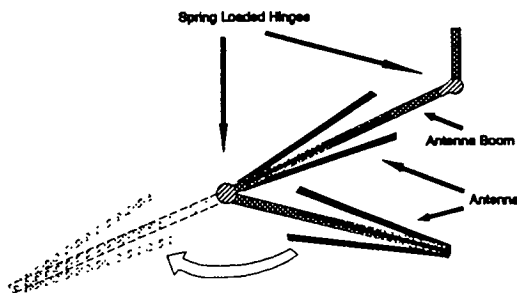


Figure 13 Antenna Fold Up Design

During launch, the antenna boom itself will be folded up using 2 hinges with springs in order to minimize space. At a certain point in the launch sequence the antenna will be unfolded using explosive bolts. The springs hinges will ensure the boom extends fully.

Protocol

Introduction

Given that the basic concept behind RUNT is to have a simple, accurate, and cost-effective method for relaying vital information from all U.S. Navy ships to some command center in the United States. The tool for achieving this goal is a modified amateur packet

radio system. RUNT will be equipped with the Digital Radio Systems, Inc. DPK-2 Packet Radio Terminal Node Controller (TNC). The system will use the AX.25 Version 2.0 protocol.

Procedure Overview

Each navy ship will be equipped with a simple computer and radio transmitter that can be easily interfaced with the current Global Positioning System (GPS). The computer will transmit the ship's latitude, longitude, course, and speed every ten minutes automatically.

Also, a brief message can be sent with each transmission. The DPK-2 will store all information. As each satellite passes over a command center, an operator at the center will transmit a command requesting to receive stored messages. Once the information is received, the operator will transmit a command to erase this data in order to make room for more incoming messages.

The operator can also command the DPK-2 to transmit or erase specific messages instead of all of them at once. This is accomplished by giving each message a code to differentiate it from all others. Finally, the operator can be replaced and the system completely automated with the introduction of a computer at the command site.

Detailed Protocol

RUNT will use the AX.25 protocol. The DRSI DPK-2 utilizes the first two layers of the International Standards Organization (ISO) layered network model. First, the physical layer is concerned only with the transmission and reception of data on the bit level. Specifically, the physical layer ensures compatibility and proper interface between hardware devices. For example, it checks for voltage compatibility of a transmitted signal.

The second layer is the data link layer and its purpose is to pass on an error-free stream of data. Level two partitions data into individual frames based on the High Level Data Link Control (HDLC) protocol defined by the ISO. Each frame possesses its own error detection

field and frame identification field.

The receiving system recomputes a FCS based on the data received and compares it to the FCS transmitted. If a discrepancy exists, the receiving system rejects the data. Therefore, bad data is not passed to the receiving operator and a retransmission of that single message is all that is required.

Although transmission data is not always required (i.e. Link control frames), the mission of RUNT requires all data fields to have the same format when they are transmitted.

The combination of ship's code and time of transmission will serve as a method for categorizing messages. No two messages can have the same ship designator and time of transmission.

Transmissions of time, latitude, longitude, course, and speed can all be automated by interfacing with current GPS systems. All the operator on board ship would have to do is enter any text that the commanding officer desires. However, free text is not required for accurate transmission.

Command Station Locations

The following map shows the location of the eleven global command stations.



Figure 14

1. Honolulu, Hawaii
2. San Diego, California
3. Corpus Christi, Texas
4. Bermuda
5. Azore Islands
6. Sigonella, Italy
7. Incirlic, Turkey
8. Diego Garcia
9. Melbourne, Australia
10. Guam
11. Marshall Islands

WHEELED EXPERIMENTAL SURFACE LUNAR EXPLORER (WESLE)

Utah State University
Mechanical & Aerospace Engineering
Logan, Utah

Dr. Frank J. Redd

Jeff Gessaman, Teaching Assistant

Lynn Adams, Travis Bishop, Stephen Clarke, Val Crook, David Henderson, Bret Holman, Scott Jensen,
Don Jones, Scott Kessler, Phillip Larson, Paul Mueller, Jim Nelson, Shawn Nielson, Todd Rindlisbaker,
Peggy Roskelley, Craig Rupp, Stephen Shepherd, Travis Sip, Rik Stallings, Ryan Yamauchi

Abstract

The Utah State University 1992-1993 Advanced Space Systems Design Team focused its design effort on a long range lunar rover. The Wheeled Experimental Surface Lunar Explorer (WESLE) was designed such that transport to the Moon could be done with the Artemis Common Lunar Lander which has been conceptualized by a team at the Johnson Space Center. Scientific instruments on board each WESLE include: an alpha-proton-x-ray spectrometer, a visual spectrometer, and an electromagnetic sounder. With these instruments the rovers will be capable of detecting all elements except hydrogen, analyzing the crystalline structure of lunar samples, and mapping sub-surface geologic features. The WESLE relies on six conical wheels for mobility and will turn using the "skid-scuff" method, similar to tanks. The semi-autonomous operations for maneuvering requires that an earth-based operator send the rover to a spot that is visible. The rover will be capable of maneuvering over or around various obstacles with an increase in uncertainty of location relative to the point of destination for every obstacle encountered. The rover will telemeter Earth for further information when it has reached the desired location, the uncertainty level has exceeded a preset value, or the rover encounters an obstacle that it cannot negotiate. The WESLE is designed to operate over a range of 1,000 kilometers for approximately one year.

Introduction

The Moon is the closest astronomical body to the Earth and, at this time, is the only one that can be explored by manned missions. Through exploration of the Moon, we can gain knowledge about space travel and habitation which will enable extension of human exploration to Mars. Such exploration could be made more viable if we were able to mine lunar resources and produce such things as propellants and supplies for life support systems instead of requiring that they be lifted out of the large gravity well of the Earth. Also, the Moon's surface is not protected or changed by an

atmosphere; consequently, astronomical events that have influenced the Earth-Moon system over billions of years are recorded in its ridges, regolith, and craters.¹ Studying lunar geological characteristics may unlock questions about the origin of the Earth, Moon, and even the universe. These are just a few arguments in favor of man's return to the Moon.

Before man returns to the Moon, robot missions will map and explore the lunar surface. Global mapping will be performed by orbiting space craft. Exploration and detailed resource mapping will be conducted by semi-autonomous surface rovers. These surface rovers will fall into two classes: site rovers which will extensively explore a localized area, and long range rovers which will travel hundreds of kilometers while exploring the Moon. The Johnson Space Center has conceptualized a delivery system, the Artemis Common Lunar Lander, that will be capable of delivering these rovers as well as other unmanned payloads to a user specified location on the lunar surface.² The 1992-93 Advanced Space Systems Design class at Utah State University has designed a long range lunar rover to be delivered to the lunar surface by the Artemis.

The Wheeled Experimental Surface Lunar Explorer (WESLE), nicknamed the Moon Weasel, was designed to give valuable data about the lunar surface and to minimize cost in both hardware and operational requirements.

Top Level Requirements

Before design began, several top level requirements were set to assure that the design could produce a valuable product. The following six requirements were established with the assistance of engineers who have had experience in rover design and testing:^{3,4,5}

- Three rovers will be delivered on each Artemis Common Lunar Lander.
- Rovers will be designed to operate for one year.

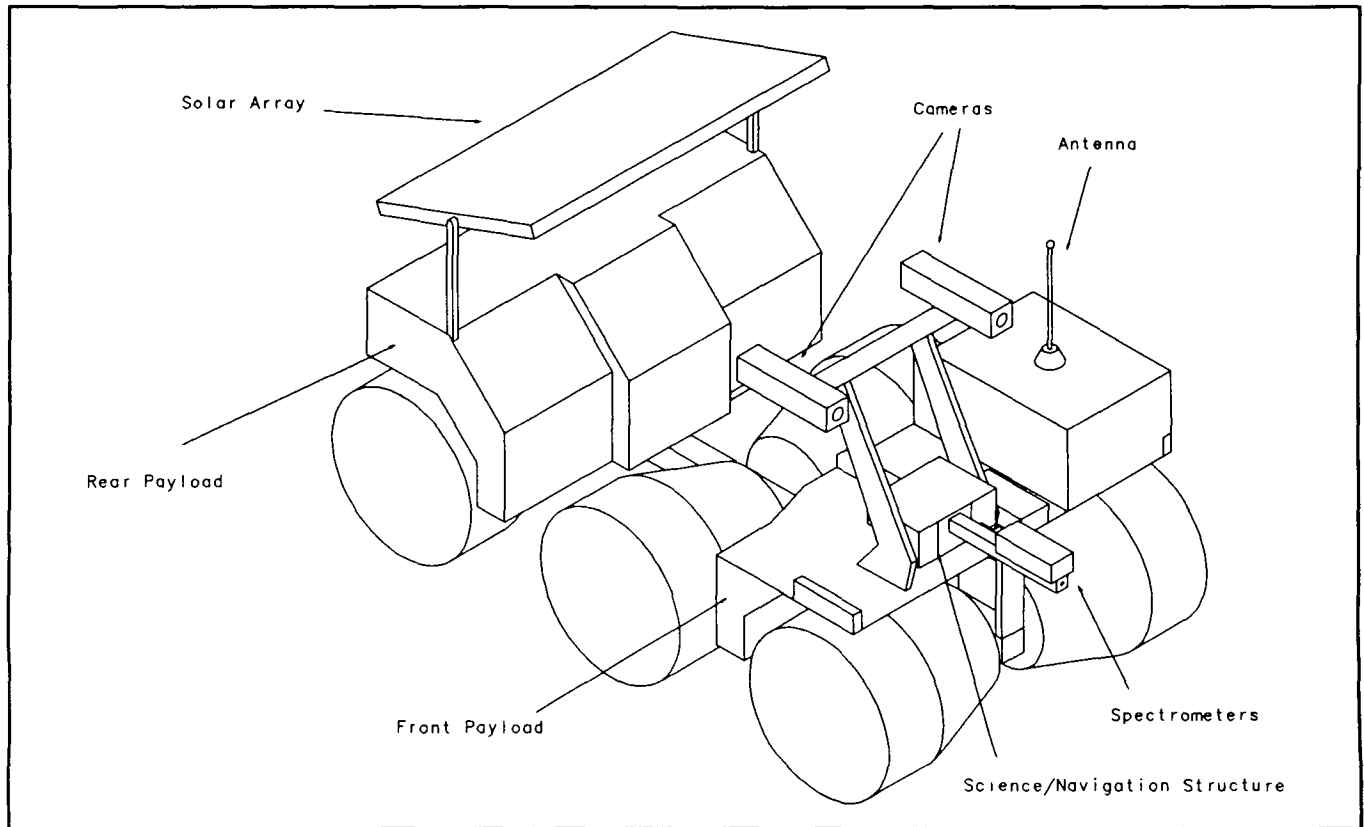


Fig. 1 Isometric view of a WESLE

- Rovers must be able to travel 1,000 kilometers
- Maximum speed of travel will be 1 kilometer/hour
- Accuracy of location must be known to within 100 meters relative to lunar maps.
- Operation will be semi-autonomous.

Design Overview

Configuration

Figure 1 shows an isometric view of a WESLE. It may be noticed that this design is not entirely original. Because there are no analytical methods for the design of a mobility system for a rover, we studied designs that have been proven in the field and combine what we feel to be optimal for our mission. Many ideas originated with the Russian rover that is slated for the Mars 1996 Mission, while others came from the Rocky IV rover that the Jet Propulsion Laboratory (JPL) is working on.^{3,4,5}

Operator Requirements

The level of autonomy is such that the rover will require aid from an earth-based operator only when it encounters trouble or has reached the operator specified destination.

This allows for a minimum number of personnel on the earth-based operations team while in the operations mode. The WESLE will operate only during the lunar day; during the 350 hour lunar night the rover will go into a survival mode and no communications will be made between the rover and Earth. Therefore, although operators will be required around the clock during the lunar day, there will be no requirement for an earth-based operator during the lunar night.

Lunar Environment

In any design the operating environment must be considered. The lunar environment differs greatly from what we experience on Earth. The three primary areas of concern when designing a mechanism to operate on the lunar surface are radiation, regolith, and temperature.

The Earth, unlike the Moon, is protected from radiation by the Van Allen belts. Therefore, electrical components on Earth do not require special protection from bombardment by solar winds, galactic cosmic rays, and solar cosmic rays from solar flares. However, in order for equipment to operate correctly on the Moon, it must be protected from this radiation, or the use of redundant instruments must be considered.

A rover traversing the lunar surface will constantly be kicking up regolith or lunar soil which is much like very fine grain volcanic ash. The high abrasivity of regolith will quickly wear down a moving part that is not protected. Therefore, the number of moving parts must be minimized and those that cannot be eliminated must be designed to be protected from the regolith.

Because of the twenty-eight day lunar cycle (350 hour day and 350 hour night), temperature variations are extreme. During the Apollo missions, temperature variations of 282°C were measured with a low of -181°C and a high of 101°C.¹ Temperatures will vary with location, but the temperature extremes have proven to be quite a difficult thermal management problem to overcome.

Other environmental factors include low gravity (1/6 Earth) and the lunar vacuum.

Artemis Delivery Capabilities

The mass that the Artemis is capable of delivering to the lunar surface is dependent upon the launch vehicle used to deliver it to low Earth orbit. The Atlas II launch vehicle was our choice to deliver three rovers and the hardware required to interface with and deploy the rovers from the Artemis. Using the Atlas II allows an Artemis payload of 200 kg. At this point in the design, the WESLE payload and Artemis interface hardware totals 155.7 kg, giving a 28.5% mass contingency. The 28.5% contingency is to allow for unexpected increases in the mass as design and manufacture of the system proceed.

Possible Landing Sites

As part of the Artemis Common Lunar Lander design, ten landings were dedicated to rover excursions. Because this number will include both site rovers and long range rovers, we selected three possible landing sights. Although travel would be much easier over the mare (lunar flatlands), past studies indicate that there is a much greater diversity in elemental composition near the ridges and craters.¹ Thus, the chosen landing sites allow for travel on or near the mare as well as study of the more diverse terrain. The selected landing sites are: Montes Apenninus (28°N, 5°E), Copernicus (7°N, 21°W), and Sinus Iridum (40°N, 32°W).

Structure

The Structure subsystem is responsible for secure placement of all components on the WESLE. The overall structure is shown in Figure 1.

Component Location

Components are located on either the front or rear payload. The front payload contains: the Science Payload and Navigation structure (cameras and spectrometer package); Operations Control's proximity sensors, IR LEDs, and microcontroller; and Communications' amplifiers, signaling equipment, and antenna. The rear payload contains the batteries, solar array, and electromagnetic sounder. Inclinometers are located on both payloads.

The location of the center of gravity of the rover was a major factor in the design of the structure. The location of the center of gravity was a direct function of the mass, dimensions, and preferred location constraints of each component placed on the rover. It was desirable to distribute the masses of the components so as to position the center of gravity towards the rear of the rover and as low as possible. The payload envelope was determined to ensure that the components contained within the envelope would not interfere with the mobility of the rover.

Rover Structure

The structure of the WESLE consists of three main components: baseplates, supports, and encasements. The baseplates were designed to provide a stable platform for all subsystem equipment to be mount to, while minimizing the amount of material required to perform this task. Vertical and horizontal supports are used to provide rigidity to the structure. Four vertical beams are used to support the upper portion of the plates. Angle brackets are used to connect the baseplates to the encasements. The encasements provide environmental protection (e.g. from radiation, regolith, etc.) for the rover. The rear encasement covers the batteries and provides thermal protection from the solar array, which is a large heat source during the lunar day.

Mobility

Configuration

The WESLE mobility system consists of six conical wheels with each axle being fixed to a central shaft comprised of 3 bars. The central shaft is hinged forward and aft of the two center wheels to allow for pitch and roll. Figure 2 shows a top view of the Mobility subsystem.

Steering

The mobility design employs skid-scutt steering, such as is used in military tanks. This method eliminates the need for steering linkages and motors, hence, the modes of

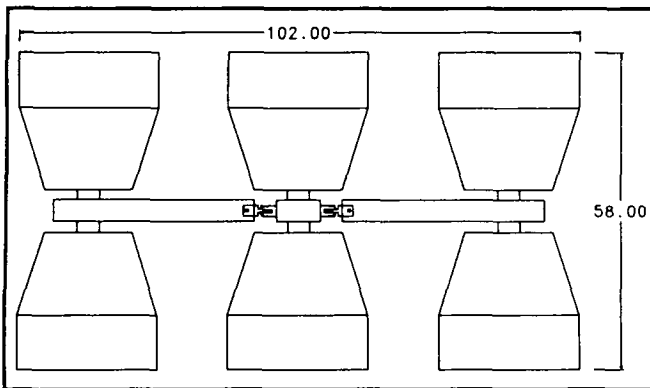


Fig. 2 Top view of rover (dimensions in centimeters)

failure are reduced. Also, skid-scoff steering enables the rover to turn in very tight quarters.

Materials

Composites and metals were investigated in materials selection for the Mobility subsystem.^{6,7} The composites considered have been proven in space and maintain their properties to temperatures reaching 230° C. The primary advantages of composites are their low coefficient of thermal expansion and high specific strength. Composites, however, have poor abrasion resistance which is a great concern in the design of a rover that will be traveling over the abrasive regolith. Aluminum and titanium were both considered for the Mobility structure. Aluminum was chosen because it is much less expensive to purchase and machine. Also, it has a high thermal conductivity to allow for an even temperature distribution over the rover.

Motors

The power to maneuver the rover over the lunar surface is provided through one electric motor in each of the six wheels. The power requirements for these motors were calculated by modeling a six wheel vehicle traveling at a constant speed up an incline. The slope of this incline ranged from 5° to 30° with power output requirements per motor of 0.4 watts to 2.3 watts respectively. The minimum inclination of 5° accounts for losses due to wheel bearing friction, rolling resistance, and soil compaction while traversing level ground. The maximum angle of 30° was selected by evaluating the performance of current rover prototypes. The motors selected are Pittman 30 mm² with a 144:1 gear reduction drive.^{6,7}

Wheel Design

Figure 3 shows a cross sectional view of a wheel motor assembly. The dashed lines represent the envelope that the

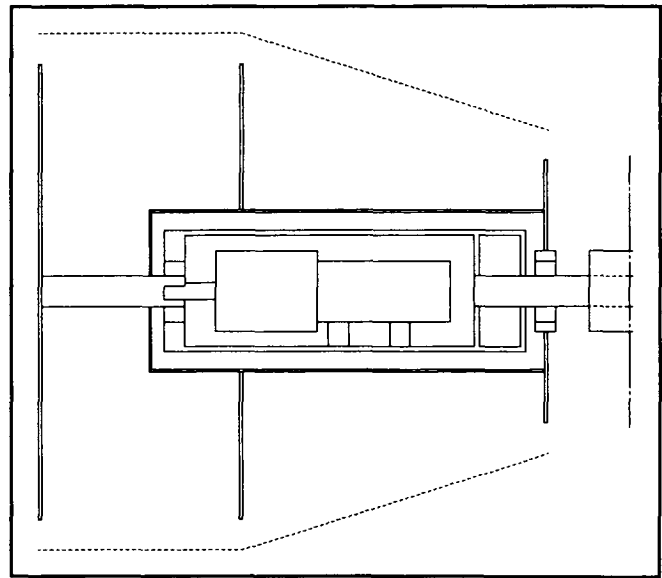


Fig. 3 Cross-section of the wheel/motor assembly

not yet designed spring steel outer skin must stay in. The three vertical lines are aluminum rims that will support the outer skin. The motor, which will not rotate, is housed in an aluminum casing for protection against regolith. JPL has developed a rover (Rocky IV) with a spring steel skin on its wheels.⁴ The thin steel deforms allowing more of the wheel to contact the terrain. Unfortunately limited time prohibited the design of this part of the wheel.

Science Payload

The Science Payload subsystem chose to concentrate on lunar geology, specifically on elemental composition and subsurface structure. To accomplish this, the science payload will consist of an alpha-proton-x-ray (A-P-X) spectrometer, a visual spectrometer, and an electromagnetic sounder. The science payload spectrometer package is shown in Figure 4. The A-P-X spectrometer detects all elements except hydrogen.^{8,9,10,11} A gamma-ray spectrometer could be used to detect hydrogen and to complement the A-P-X spectrometer, but there are currently no gamma-ray spectrometers small enough for our mission. The visual spectrometer will be used to investigate small-scale surface morphology (crystalline structure). The electromagnetic sounder (EMS), mounted under the rear payload area, will be used to map sub-surface structure to a depth of 10 to 20 meters depending on material density. The EMS can also detect subsurface ice.

Alpha-Proton-X-Ray Spectrometer

The A-P-X spectrometer uses a radioactive source that emits radioactive waves which excite the molecules of the

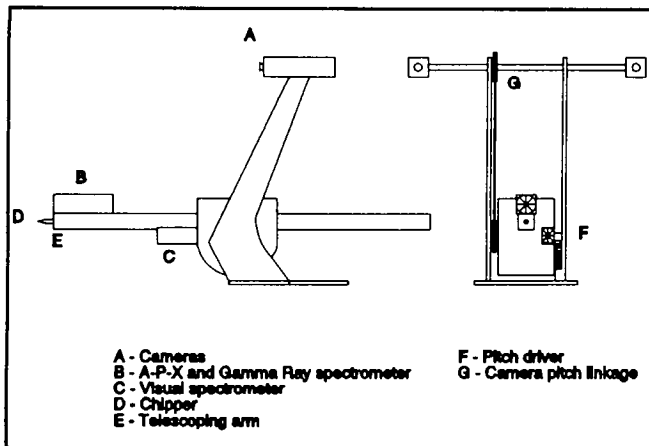


Fig. 4 Science payload spectrometer package

sample being studied.^{8,9,11} These molecules in turn emit alpha waves and subatomic particles. Every material has a characteristic intensity and wavelength of emissions. Scientists on Earth can then compare the results of these tests to known materials tested on Earth before the rover was sent to the Moon. Because the lunar surface is constantly being bombarded with very tiny particles, the rock surfaces are not necessarily the material of the rock. Because of this, a chipper will be used to clear away the rock surface in order to get to the more valuable information below the surface for spectrometer readings. This chipper will be carried in the telescoping arm that also holds the A-P-X spectrometer.

Visual Spectrometer

A visual spectrometer refracts the reflected light into a light sensing array which then records the intensities of the light spectrum.^{10,11} The visual spectrometer is able to help identify the atomic structure of a material. It will identify a body-center cubic, face-center cubic, tetrahedral, or amorphous structure of the material.

Electromagnetic Sounder

The EMS consists of an emitter which sends out an electromagnetic wave of approximately 500 Mhz.^{8,11} The receiver antenna is a dipole antenna, basically consisting of a long wire. The electromagnetic waves will penetrate the lunar surface much like a radar wave. Differing structures and material densities will reflect the waves back to the surface. The receiver antenna will pick up the return signal which will be stored with the rovers location to later be sent to Earth.

Artemis Interface

The Artemis Interface group is responsible for designing hardware that will allow safe transport of the rovers via the Artemis Common Lunar Lander and deployment of the rovers from the Artemis to the lunar surface after landing.^{2,12,13}

Platform

The Artemis payload guidelines require that the center of mass be 65 cm above the mounting pad.¹³ Because the rovers center of mass are much lower than 65 cm, an elevated platform was needed to meet this requirement. This platform is designed to be made of an aluminum honeycomb-G10 sandwich mounted on a G10 support ring.

Rover Attachment

Each rover will be secured to the platform by running cables over each axle. Support blocks will be placed under the central bar of the rovers. Upon tiedown the tension in the cables will deform the spring steel skin of the wheels drawing the rovers firmly against the support blocks. After landing pyrotechnics will sever the cables allowing the rovers to drive free.

Deployment Ramp

The platform the rovers are secured to during launch and translunar flight is nearly 2 meters above the lunar surface; therefore, a ramp is required for rover deployment after landing. Figure 5 shows the ramp in flight configuration (left) and after the Artemis has safely landed (right). The ramp will be constructed from the same aluminum honeycomb-G10 sandwich as the elevated platform.

Multiplex (Mux) Bus

The Multiplex (Mux) Bus was incorporated into the rover design to allow for simplified internal communication and control interfaces among the various subsystems.

Description

The Mux Bus idea was taken from the standard military serial digital multiplex bus used in the F-16 C/D and F-15 E aircraft.¹⁴ The purpose of the Bus is to provide internal communication for the subsystems of the WESLE. The Bus contains all words of interest to the subsystems in each operating mode. The Bus is not a memory device, but it acts as one because the words present on the bus, in the form of digital signals, are updated many times a second.

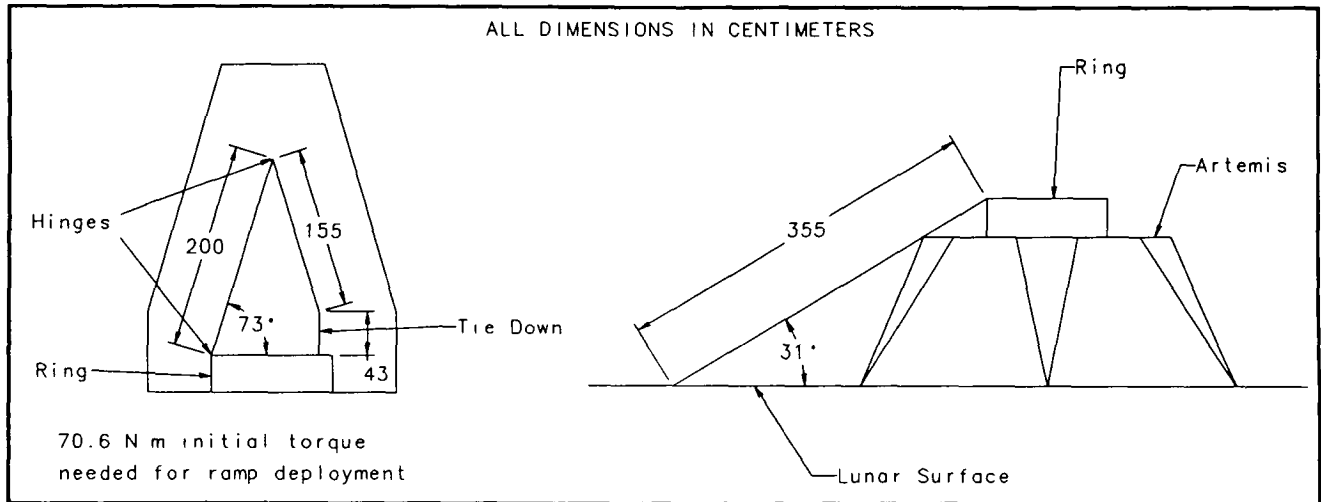


Fig. 5 Folded and extended ramp

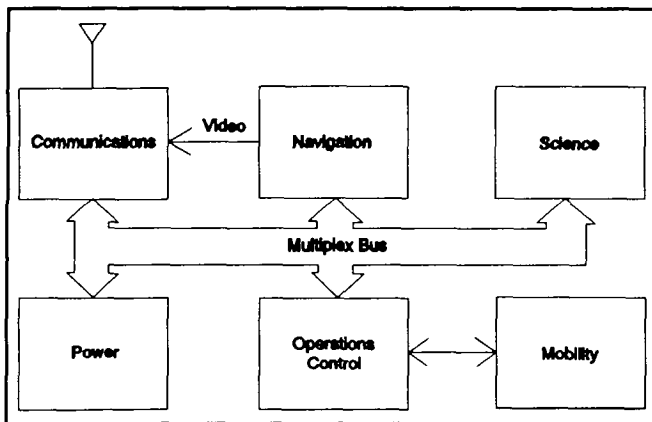


Fig. 6 Mux Bus schematic

As can be seen in Figure 6, all rover internal communications are carried out over the Mux Bus with two exceptions. The video frames are sent directly from the Navigation subsystem to the Communication subsystem for relay to Earth due to the large bit volume in the video images and the fact that no other subsystems need video images to perform their functions. The communication between the Operations Control subsystem and the Mobility subsystem also does use the Mux Bus. This is because the Mobility subsystem is directly controlled by Operations Control.

Operations Control

The Operations Control subsystem is responsible for maintaining the integrity of the Mux Bus, obstacle negotiation, calculating the wheel positions and/or velocities for navigation, and monitoring the other subsystems to ensure proper operation. The main processor for the rover will be the Intel 8096BH microcontroller.¹⁵

Mux Bus Integrity

The Mux Bus is controlled by the Operations Control subsystem. All commands to the subsystems will be sent by Operations Control. For example, if the Power subsystem determines that the batteries need recharging, it will notify Operations Control and Operations Control will command each subsystem to stop its activities and go into the "Recharging" mode. This ensures that control of the rover is centralized in Operations Control, thus avoiding the possibility of contradictory commands coming from different subsystems. Operations Control also maintains control of the Mux Bus by determining which subsystems can update which words on the Bus. This is to prevent a malfunctioning subsystem from being able to change words on the Bus outside its responsibility.

Obstacle Negotiation

The Operations Control subsystem controls the motors of the Mobility subsystem. Motor control will be achieved through the use of a chip set from National Semiconductor that has been designed specifically for use in precision motor control.¹⁶ The rover will cruise blindly over the lunar surface in a direct heading towards the desired destination until it senses it has encountered an obstacle that cannot be negotiated. Inclinometers located in the front and rear payload areas will be triggered when such an obstacle is encountered.¹⁷ The WESLE will then back off of the obstacle and use infrared proximity sensors to find a possible escape route around the obstacle.¹⁸ A highly collimated beam of infrared light will be emitted from the front of the rover. This light will reflect off an obstacle in its path. The scattered light will be refocused, through a lens, onto the surface of a series of position sensing devices (PSD). The distance to the object can then be calculated using optical triangulation techniques. There will be a

minimum as well as a maximum distance that can be measured. There will be multiple PSDs on the front of the rover as well as an array of infrared light emitting diodes (IR LED). Starting with the IR LED on the far right of the rover, each IR LED will be strobed, and the distance to any obstacle in its path will be calculated. There will always be a minimum of two PSDs used to calculate the distance to an obstacle. This allows for redundancy as well as a comparison of the distance measurements.

Once a possible escape route is detected, the rover will turn and proceed in the direction indicated by the proximity sensors for a distance required to get "parallel" with the obstacle (see Figure 7). At this point, Operations Control will obtain a new heading from the Navigation subsystem in order to reach the desired destination and will then return to the cruise mode.

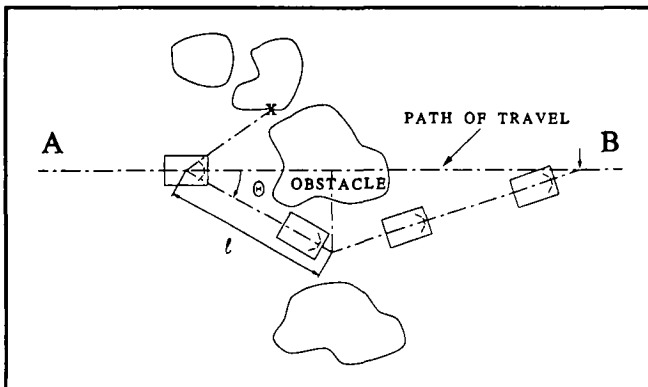


Fig. 7 Obstacle negotiation

Data on Wheel Position and Velocity

The Navigation subsystem receives direction and distance to the desired destination from the Earth based operator. Through wheel position and velocity which is sent from Operations Control, Navigation can determine if the destination has been reached. Data on wheel position and velocity are determined using the National Semiconductor motor control chips.¹⁶

Monitoring of Subsystems

As mentioned above, the Operations Control subsystem "watches over" the words on the Mux Bus. If a subsystem begins to put words on the Bus that do not match the norm for the current operating mode, Operations Control will stop normal operations, notify the earth-based operator, and wait for further commands.

In order to develop lunar rovers capable of semi-autonomous operation, the various scenarios in which the rovers must operate needed to be developed. Once the

operating scenarios were decided upon, the development of basic algorithms for each scenario began. The development of these algorithms provided us with a model of how the Mux Bus subsystem will function in regards to its operating modes, or exactly what type of information can be updated and when it can be updated. Figure 8 is a flow diagram illustrating the basic operating modes and how the algorithms relate.

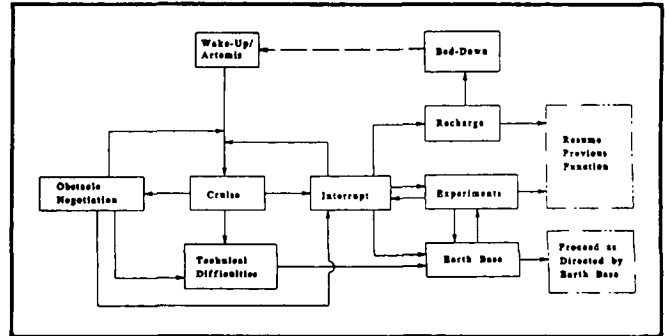


Fig. 8 Operating modes

Navigation

The Navigation subsystem is responsible for tracking the rover throughout its mission on the lunar surface. Tracking refers to knowing the approximate location of the rover, in addition to navigating the rover from place to place for different science experiments. In order to assure proper navigation primary and secondary navigational methods were investigated. Landmark navigation was selected as the primary method with Differential Very Long Baseline Interferometry (DVLBI) as the secondary method.

Landmark Navigation

Landmark navigation uses the existing peaks, high points, and mountains in a given terrain as navigation points. Anything that appears on metric overhead imagery from a satellite or other space mission qualifies as a landmark. Because of the rovers small size, significant testing will need to be performed to determine what will show up as landmarks to the WESLE cameras. Two Sony XC-999 stereo imaging cameras will be attached to each rover.¹⁹ These are high resolution cameras capable of performing in harsh environments such as the Moon.¹⁰

Navigation Logic

Figure 9 represents the basic logic schematic for WESLE navigation. A step sequence will be used starting from earth base and looping back for various scenarios. The objective for using this logic is to reach the desired destination with minimal error.

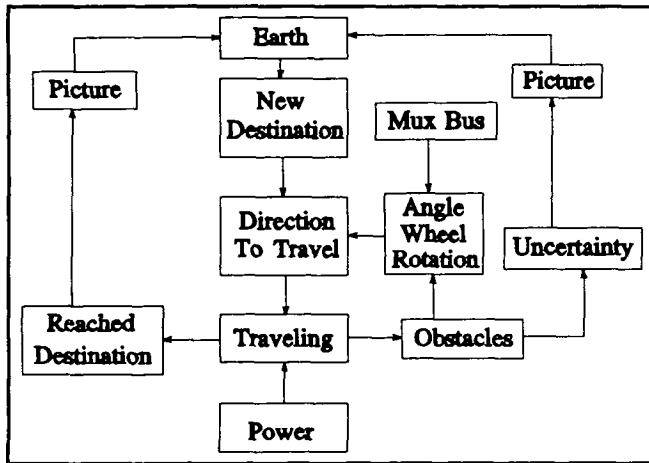


Fig. 9 WESLE logic schematic

The WESLE will receive the coordinates of a new destination from Earth over the Mux Bus. Using the coordinates, the rover will attempt to travel in the correct direction and reach the new destination.

In its traverse, the rover may encounter obstacles. If this occurs, the Operations Control subsystem will negotiate the WESLE around the obstacle and then provide the Navigation subsystem with the angles turned and the distances traveled while negotiating the obstacle. Using these angles and distances, navigation algorithms will calculate a new direction to travel in order to reach the desired destination (see Figure 7).

While traveling, the wheel rotations will be monitored to determine if the appropriate distance has been traveled in order to reach the desired destination. When the desired destination is supposedly reached, the rover will stop and take a picture. If it is indeed the desired destination based on the image telemetered to earth base, the Science Payload subsystem will then conduct the appropriate experiment. If the desired destination is not reached, the rover's path can be retraced using the wheel rotations and angles turned to avoid obstacles. Again, coordinates from earth base will be sent to direct the WESLE in the proper direction. This sequence will be repeated for the entire duration of the mission.

While the rover is traveling, a certain degree of uncertainty will accumulate. Uncertainty may arise from encountering small rock obstacles, side hills, or by the rover not precisely turning the specified angles (i.e. turning only 40 degrees when 45 degrees was specified). Once an unacceptable level of uncertainty is reached, the rover will stop, take a picture, and send it to earth base for determination of a new destination or direction of travel. The level of uncertainty is an extremely important detail;

acceptable and/or unacceptable levels of uncertainty will have to be determined through extensive testing of a WESLE prototype.

The rover traverse may also be interrupted by the Power subsystem for recharging the batteries. When this occurs, travel will simply halt until the recharging is complete. The rover will then continue traveling in the direction of the desired destination.

Secondary Navigational Methods

Both laser navigation and DVLBI were explored as possible secondary methods of navigation.

Laser Navigation. Laser navigation would involve place a number of retroreflectors on each WESLE. An earth-based laser would fire at the WESLE, and the retroreflectors would reflect the laser directly back on the same path. Sufficient light photons could then be collected from the reflected laser beam via a telescope, and location of the rover could be determined through angle sensors. The required surface area and mass of the retroreflectors were well above the area and mass available on the rover so this method was abandoned.

DVLBI. The concept in DVLBI is that of radio waves.³ A precision transponder would be used to telemeter the radio waves to the rover on the lunar surface, the WESLE could then send a signal back. With precision receivers on Earth extremely accurate angular measurements may be taken. Due to time constraints the DVLBI method was not developed to the point of placing it in our official design.

Communications

The primary function of the Communications subsystem is to efficiently communicate with Earth. This includes transmission of science, position, video, and other data collected by the rover to the Earth, and reception of command and control data from Earth.

Communications Design

The communications design utilizes a transmitter carrier frequency of 2 GHz and a receiver carrier frequency of 3 GHz. Phase Shift Keying (PSK) type modulation was implemented in two forms: Quadrature (QPSK) on the transmitter, and Binary (BPSK) on the receiver. Data compression, buffering, and strobed transmitter power are employed to the streamline data transfers. A single, duplexed, omni-directional, vertical monopole antenna is used for both transmitting and receiving. The

Communication's system power of 40 watts provides a data rate of 100 kilobits per second and requires a 35-meter parabolic dish, earth-based antenna available at various scientific institutions, including, but not limited to, NASA's Deep Space Network (DSN).

Power

Power Requirements

The goal of the Power design team was to develop a power system that would survive a one year mission life while maximizing power availability and reliability and minimizing mass and cost. The average power used by the rover will be between 13 and 25 watts (W) depending on the operating mode. The maximum instantaneous power requirement will be approximately 75 W.

Selected Power Scheme

Secondary batteries were chosen to provide a power storage system in conjunction with a gallium arsenide solar array as the power source.

Battery. The battery used on the WESLE consists of 11 individual nickel hydrogen cells which provide 1.25 volts (V) and 20 amp-hours per cell.²⁰ The cells are connected in series to provide a total of 13.75 V at 20 amp-hours, for an overall capacity of 275 watt hours.

Solar Array. Gallium arsenide (GaAs) solar cells were chosen for the power source. The GaAs cells have an efficiency of 18.3% compared to 15% for the best silicon solar cell. As temperature increases, the efficiency of silicon cells drops twice as fast as GaAs cells.²¹ Thus, at high temperatures the GaAs cells behave considerably better. A solar array area of 1620 cm² is needed to meet the power requirements. The solar array will be allowed to rotate with one degree of freedom to allow the array to achieve the best angle of incidence with the Sun. For the GaAs solar cells, a string of 20 (2x4 cm) cells in series will provide 17.5 V. The specified array area will allow for 10 strings placed in series and will provide 2.25 Amps.

Power Profile

Figure 9 shows the power profile for a typical 24 hours of operation in conjunction with the charge of the battery when the solar array is operating at 65% of capacity. At zero power the battery is fully charged. The negative slope indicates that the rover is using more power than the solar array is able to provide. The positive slope indicates that the batteries are being charged.

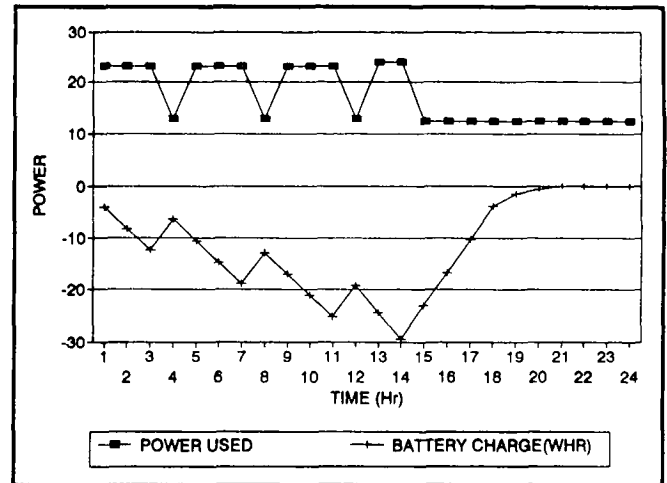


Fig. 10 Power profile and battery charge

Thermal Management

The most difficult part of this thermal management problem is not the extremely hot temperatures or the extremely cold temperatures, but the large temperature fluctuation (-181°C to 101°C) and the fact that the rover must be designed for both.

Hot Case

With the body painted white and radiators mounted on the solar panel, cameras, and communications box, each component will function below its specified upper temperature bound with the exception of the battery. The average steady state temperature of the rover is approximately 55°C. Since the battery has a maximum operating temperature of 30°C, there is no heat sink available to dump the excess battery heat. A method for managing the thermal conditions of the battery is a follow-on effort to this study that needs to be conducted.

Cold Case

The rover's cold case presents an entirely different set of constraints. The rover will be in a dormant mode with no internal heat generation. The rover's exposed surface will radiate to deep space ($T = -270^{\circ}\text{C}$) and to the lunar surface ($T = -181^{\circ}\text{C}$). A further challenge occurs because the rover has a emissivity of 0.9 to meet the hot case. Changing the emissivity of the rover for the cold case would be extremely impractical. Some possible sources for heat are resistive heaters, plutonium buttons, and the Moon itself.

Resistive Heaters. The batteries are capable of delivering a mere 0.55 W for the duration of the entire

lunar night. This would only heat one or two components at best.

Plutonium Buttons. Plutonium is a radioactive material that produces heat as it decays. It has a number of adverse effects including possible damage to electrical components, the fact that it cannot be turned off (it would continue to produce unwanted heat during the lunar day), and possible negative environmental impacts.

Heat From the Moon. At a depth of 30 cm the temperature of the Moon is approximately $-22^{\circ}\text{C} \pm 3^{\circ}\text{C}$.¹ This heat could be tapped and funnelled to the components that require it.

Conclusions

The design concept for the WESLE consists of three identical rovers per Artemis Common Lunar Lander. The rovers are 58 cm in width by 102 cm in length, with a mass of 43.6 kg each. Each rover uses six conical wheels for mobility, each with independent drive and speed control. The chassis is hinged in two places to allow flexibility between the wheel pairs in both pitch and roll. It is designed to scale an obstacle with a maximum height of 30 cm, though prototype testing will be required to verify this capability.

The WESLE is designed for a top speed of 1 km/hr on a flat surface. Its mission lasts one year with no operation during the lunar nights. This mission duration and the top speed translate into an estimated 1000 kilometer total distance travel capability. Operating power is provided by nickel hydrogen batteries, which are recharged periodically by a gallium arsenide solar array on the rear of the rover.

Landmark navigation is the means by which the WESLE (with a lot of help from the earth-based operators) will determine its location at different points along its path. There are two concerns with relying on landmark navigation for position determination. The first is that current maps of the lunar surface have a resolution only down to 60 meters. This relatively poor resolution will make landmark navigation more difficult and less accurate; 12-meter resolution maps would make the concept much more feasible. The second concern with landmark navigation is that it is possible that the WESLE can find itself in regions of the Moon where distinct landmarks are rare and become lost. This can be avoided by mission planning, but it limits the ability to explore these regions with the WESLE.

In current lunar and Mars rover designs, the algorithm designs for navigation and obstacle negotiation are some of

the most difficult problems. The WESLE design concept does not presume to have solved these problems; as with any rover, substantial testing and modification of the navigation and obstacle negotiation algorithms is expected before a working rover could be sent to the Moon.

Efforts have been made in the design of the WESLE to avoid the use of moving parts wherever possible because of the risk of jamming of the moving parts by lunar dust, differential heating, or other causes. However the use of some moving parts was unavoidable, specifically the wheels, science mechanisms, and solar array pointing devices. A concern remains that these moving parts could become jammed, disabling the WESLE.

The use of an RTG would help solve many of the thermal control problems. When the original power tradeoff study was conducted, the power needed by the rover was estimated to be between 100 to 300 W. This would have required an RTG of about 20 to 35 kg. However, by using high efficiency components, the power requirement was lowered to an average of 25 W. This fact opens the possibility of using an RTG having a mass of 10 to 15 kg. The battery-solar array system works well in providing power to the rover, however, in light of the new information the option of using an RTG should be reevaluated to determine which system would provide more advantages to the overall design.

Although several concerns remain with the conceptual design of the WESLE rover, it meets its overall design requirements and, if further developed and deployed, would contribute significantly to our understanding of the Moon, planetary science, and our understanding of the solar system and universe in general.

References

- 1) Heiken, G.H., Vaniman, D.T., and French, B.M. (editors), *Lunar Sourcebook: A User's Guide to the Moon*, Cambridge University Press, Cambridge, UK, 1991.
- 2) NASA Johnson Space Center, "Artemis, Final Presentation: Results of the Engineering Feasibility Study," NASA Johnson Space Center, Houston, TX, September 17, 1991.
- 3) Burke, James D.: Jet Propulsion Laboratory and The Planetary Society. Personal Communication, October 1992 - May 1993.
- 4) Aaron, Kim: Jet Propulsion Laboratory. Personal Communication, September 1992 - April 1993.
- 5) Powell, George: Electrical Engineer, Space Dynamics Laboratory, Utah State University. Personal Communication, January - May 1993.

- 6) Pittman, "PITTMAN ELCOM Brushless D-C Servomotors, Series 3100 - 30 mm square cross section," Pittman, a Division of Penn Engineering & Manufacturing Corp., Harleysville, PA, March 1989. (Technical assistance by Randy Rhoad, Applications Engineer).
- 7) Pittman, "Planetary Gearheads," Pittman, a Division of Penn Engineering & Manufacturing Corp., Harleysville, PA, September 1990.
- 8) Budney, C.J., "Science-Engineering Analysis, 1989 Final Instrument Catalog," JPL Document D-6836, Jet Propulsion Laboratory, California Institute of Technology, Pasadena, CA, October 20, 1989.
- 9) Plescia, Jeff: Jet Propulsion Laboratory. Personal Communication, March-May 1993.
- 10) Crisp, Joy: Jet Propulsion Laboratory. Personal Communication, January, March-April 1993.
- 11) Jet Propulsion Laboratory, "SEI Science Payloads, Descriptions and Delivery Requirements," Jet Propulsion Laboratory, California Institute of Technology, Pasadena, CA, 1991.
- 12) NASA Johnson Space Center, "Artemis, Common Lunar Lander: Phase 2 Study Results for External Review," NASA Johnson Space Center, Houston, TX, March 10, 1992.
- 13) Binder, A. and Holdenbach W., "Artemis Payload Planner's Handbook, Version 1.0," NASA Johnson Space Center, September 30, 1991.
- 14) U.S. Department of Defense, "Aircraft Internal Time Division Command/Response Multiplex Data Bus," MIL-STD-1553B, U.S. Department of Defense, Washington DC, 21 September 1978.
- 15) Intel Corporation, "16-Bit Embedded Controllers" (order number 270646-002), Intel Corporation, Mt. Prospect, IL, 1989.
- 16) National Semiconductor Corporation, "Special Purpose Linear Devices: LM628/LM629 Precision Motion Controller," National Semiconductor Corporation, Santa Clara, CA, 1992.
- 17) Spectron Glass and Electronics Incorporated, "Two-Axis Electrolytic Tilt Sensor SP5000," Spectron Glass and Electronics Incorporated, Hauppauge, NY.
- 18) EG&G Judson, "J1L and J2L Series PSDs: Position Sensing Detectors from SiTek® Electro-Optics" (Bulletin #2030), EG&G Judson, Montgomeryville, PA.
- 19) Sony Image Sensing Division: Sony XC-999/999P CCD Color Camera Module Specifications Sheet.
- 20) Eagle Picher, Electronics Division, "Nickel Hydrogen System Technical Data Sheet," Eagle-Picher Industries, Inc., Joplin, MO. (Technical Assistance from Robert Brown, 417/623-8000, January-March, 1993).
- 21) Agrawal, B.N., *Design of Geosynchronous Spacecraft*, Prentice-Hall, Inc., Englewood Cliffs, NJ, 1986.

STIFFENING OF DEPLOYABLE SPACE BOOMS AND AUTOMATED PROTEIN CRYSTAL GROWTH

Vanderbilt University
Department of Mechanical Engineering
Nashville, Tennessee

Dr. Thomas Cruse
Susan E. Ward, Teaching Assistant

STIFFENING OF DEPLOYABLE SPACE BOOMS

Vincent Baria, Lynne Coleman, Craig Driscoll,
Jay Dyer, David Everson, Greyson Gallaher,
Kevin Graham, Ken Johns, Spencer Lisenby,
Don Nordin, Wayne Oetinger, Chris Rehberg,
John Rich, Jason Seay, David Sims, Scott
Shepard, Brett Susany, Becky Turner

Abstract

The future of space structures rely upon the use of deployable trusses. The vibrations induced by these highly flexible booms are potentially damaging to possible remote experiments. By stiffening the trusses, and therefore increasing the fundamental frequency, the vibrational effects will be reduced. MSFC is developing a space and ground integrated test facility for study of vibrational control of deployable trusses. The Vanderbilt design team developed a system of stiffening using spreaders and tensioning cables attached to the trusses. The passive control system is designed to attach to either a Lanyard or Nut deployed truss and deploy along with the truss. The truss/cabing system will stow in a canister which will attach to an Eagle platform and launched via a minuteman rocket. After launch and deployment, an end mounted vibration system will excite the free and stiffened system. Accelerometers will measure the first modes of vibration. The data will be relayed to earth for analysis and comparison to an earth base experiment at MSFC. The results of the testing will aid future application of deployable, flexible space trusses.

Introduction

Dr. Henry Waites and Angie Bukley in the Dynamics and Controls area of Marshall Space Flight Center introduced the 1992-93 Vanderbilt design team with a new concept in deployable, flexible space truss stiffening using spreaders and tensioning cables. The project is specifically for the Low-cost Active Structural Control (LASC) flight experiment. The purpose of the experiment is to place a flexible, deployable space truss

with an active or passive control system in place for simple control testing. The results will be compared with a similar 1-g test facility. The goal for the design teams was to develop a deployable stiffening system which raised the natural frequency five to ten times of the space truss. The group was split into three teams. Two of the teams investigated stiffening for either the Lanyard or Nut deployed trusses. The third team was responsible for system integration of the truss systems with the Eagle platform and Minuteman as well as the information and data systems.

Assumptions and Requirements

The initial mission requirements were set by MSFC/NASA Dynamics and Controls group. The facility must:

- Increase the fundamental frequency of the boom five to ten times.
- Deploy spreaders and cable system with deployment of the truss.
- Be proven through prototypes or calculations.
- Be a scalable design which can be applied to a range of trusses from 12 ft to 300 ft.
- Employ a cable deployment mechanism which can be integrated into the holding canister of the boom.
- Cable tension must have the ability to be adjusted and sensed to 0.5 Newton increments.
- Use of off the shelf items for design and development.
- Launch from the Minuteman rocket.
- Use the Eagle space platform with sun synchronous solar panel configuration.
- Have a lifetime of 1 year.
- Have a five pound end mass on the end of the boom.
- The operating temperature range is defined as -100° to 100° C.

For the Lanyard Deployed Boom (LDB) group:

- Design a spreader/cable configuration such that the frequency is increased accordingly for a Lanyard deployed boom.
- Use the 5 meter long model LDB with 23 cm diameter, manufactured by the Astro Aerospace Corporation for testing and development.

For the Nut Deployed Boom (NDB) group:

- Design a spreader cable configuration such that the frequency is increased accordingly for a Nut deployed boom and will accommodate the canister design needed for deployment.
 - Design using the dimensions and properties for the ABLE continuous longeron nut deployed boom.
- For the Systems Integration Team (SIT):
- Determine the attachment of the space boom to the Eagle spacecraft to withstand launch and vibrational loads.
 - Supply instrumentation and power to the experiment.
 - Determine accelerometer placement on the deployed boom such that the first ten modes of the structure with and without the cable in tension can be determined. Placement refers to both number and position of accelerometers.
 - Transmit data to Earth for analysis.
 - Design of excitation devices for testing of control system.

Analyses

To determine the most effective stiffening system for the trusses, analyses of the booms must be completed first. The differences between the two boom teams only effects the method of deployment. The boom is the same once the system has been fully deployed. Therefore, the analysis that was performed was applied to both teams. The boom was analyzed in several ways. These methods included finite element analyses, a mathematical examination and optimization of the spreader and cable system, and an experimental analysis of an available prototype boom.

Finite Element Analysis

Initially, a simple cantilever beam model was constructed using ANSYS 4.4A to model the unstiffened boom. The beam consisted of 35 nodes and 34 3-D beam elements. Node 1 was constrained in all directions and master degrees of freedom (MDOFs) were included for all other nodes. Effective boom values were used for material and geometric properties.

A modal analysis of the model was performed, and natural frequencies and mode shapes were determined. The first mode of bending was determined to be 2.85 Hz.

Mathematical Analyses

A numerical analysis was performed using Mathcad. The increased boom stiffness needed to be calculated for varying spreader positions and lengths.

Analysis shows that the stiffness is maximized when the angle between the cable and the boom is 45°. However, with one spreader on the boom, the a spreader length of $L/2$ is large and impractical for larger booms. This led to a double spreader design shown in Figure 1.

Analysis incremented the spreaders from the end to

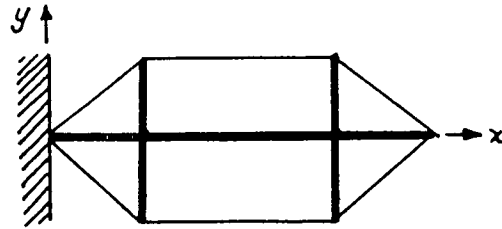


Figure 1: Double Spreader Configuration

the center of the boom while the spreader lengths were similarly incremented to determine the best configuration.

The Mathcad iterative solution tries to maximize stiffness while minimizing the effective mass in order to increase the natural frequency. Examination of the model shows that the length of the spreader must be equal to the distance of the spreader to the end of the boom, thus ensuring the 45° angle between the cables and the boom and a maximum normal force component of the tension in the cables.

Experimental Rap Test

Experimental data was gathered in the form of a rap test. In this test, the Astro LDB obtained from Dr. Garcia was fully deployed and energy was imparted to the structure in the form of an impact to excite the lower frequencies. The boom's response was monitored with accelerometers. Two accelerometers were placed at the top of one of the longerons. The accelerometers were positioned measure the accelerations in the x and y directions.

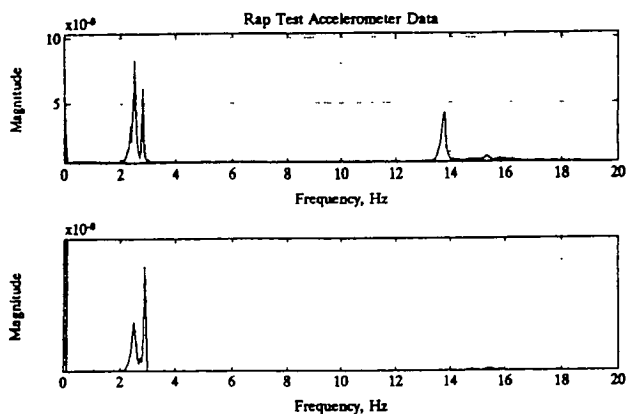


Figure 2: Rap Test Accelerometer Data

A typical response is shown in Figure 2. This is a trace of the x (2a) and y (2b) accelerometer signals. Both plots show three peaks from 2.45 to 2.85 Hz. These are the first bending mode about the three faces of the boom. The peak at 13.8 Hz in the x direction does not exist in the y direction and can be assumed to

be a torsional mode. This test shows that the boom has both bending and torsional modes under 20 Hz. Both must be raised to over 20 Hz to achieve the design objective.

Lanyard Deployed Boom Design

The lanyard deployed boom is held in place by the lanyard which holds the boom in its various positions. As the lanyard is unwound by the motor found in the base, the boom deploys. Figure 3 shows the deployment of the lanyard boom from its canister. The design of the stiffening system must take into consideration the deployment of the lanyard system. The longeron rotates about 90 degrees during deployment and therefore adds

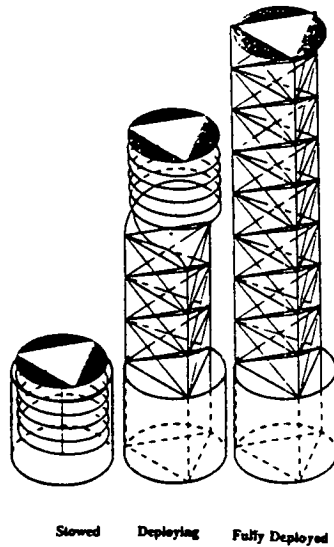


Figure 3 : LDB Deployment Stages

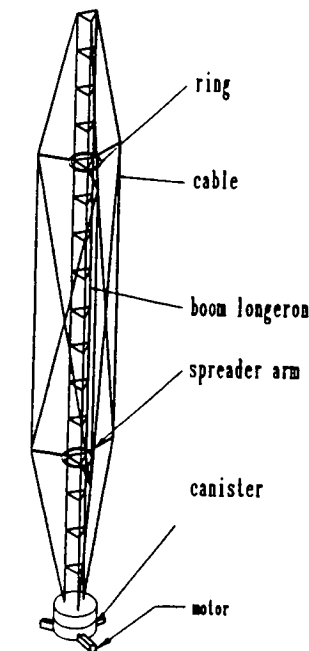


Figure 4 : Stiffening System for LDB

difficulty to the design. The change in diameter of the deploying structure also must be considered.

In developing the cable/spreader configuration proposed by NASA, it was determined that cables would run the length of the boom between the spreaders to stiffen the LDB. The boom has a triangular cross section and bends about each face. The cables are tensioned by motors and are attached to the ends of spreaders mounted to the boom in a triangular orientation (Figure 4). During bending in one direction, the cable on the opposite side of the boom will be brought into tension and thus reduce

the actual bending of the boom. By this method, the cable tension will reduce the amount of bending the boom undergoes and thus raise the vibrational frequencies. The details of the design are in the following sections

Rings

Rings were developed as the mounting interface between the spreaders and the boom. Each ring has three spreaders mounted to it, and it in turn is mounted to the boom (Figure 5). The purpose of this arrangement is to establish a rigid connection between the spreaders and the boom without affecting the structural integrity of the boom.

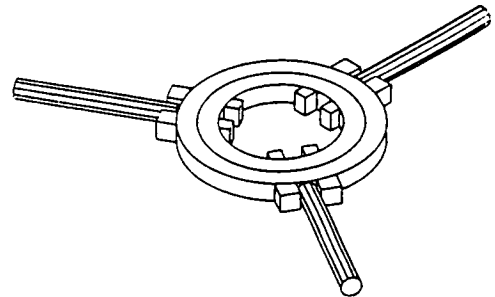


Figure 5 : Ring with Spreaders

The circular rings serve several purposes. The round shape allows for the coiled longeron to fit inside during deployment, the circular shape reduces stresses imparted to the boom as well as reducing stress in the ring itself, and the circular shape allows for the rotating double ring design discussed later.

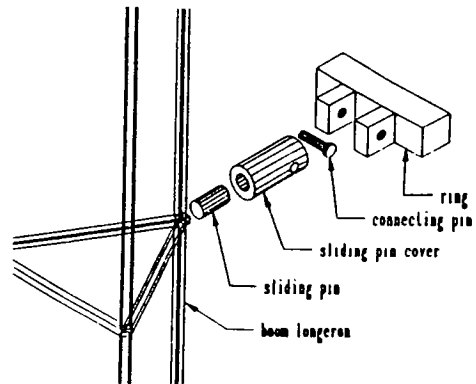


Figure 6 : Boom-Inner Ring Interface

These rings are mounted to the boom by simple pins. Hinges on the longerons of the boom at designated positions will have pins projecting outward. These pins will interface with holes in the inner edge of the mounting ring (Figure 6). In addition to providing a rigid mount for the rings, the pins allow for the reduction of the cross section of the boom as it deploys.

The spreaders are mounted to the rings in a pinned hinge arrangement. The pins are attached to the ring by simply-hinged tabs, and allow the spreaders to rotate 90°. The spreaders rotate from parallel to the boom's longitudinal axis during storage to perpendicular to the boom while deployed.

Due to the rotation of the boom during deployment, a split ring which allows for rotation of the outer ring avoids the tangling of the cables. The benefits of the stiffening system would not be realized if the rings were allowed to rotate once the boom is deployed. Therefore, a locking mechanism was added to the rings and top plate to prevent the swivel mechanisms from rotating.

Spreaders

The spreaders are long thin tubes of graphite. They are stiff, and hollow to allow for cable routing inside. The outboard ends of the spreaders have teflon inserts to allow for smooth passage of the cables through the tips. The inboard end of the spreaders are mounted in aluminum sleeves for added support and strength while pinned to the mounts on the outer ring. The curved surface on the pinned end of the sleeve allows the spreader to rotate 90° during deployment, but no further.

Cables

The cables are made of Kevlar, a space-proven material high in strength and very low in weight, creep and elasticity. The Kevlar cables are susceptible to atomic oxygen removal, as are the spreaders and rings, so a proper coating would also have to be used to protect the cables.

Stiffening Mechanism Kinematics

The method of deployment developed involved a parallelogram-type pivoting action. While stored, the spreaders are folded against the boom to minimize the diameter of the stored payload. During deployment, the spreaders are rotated 90° into their deployed positions, perpendicular to the boom. This is accomplished by tensioning the cables at their bases, thus pulling the spreaders from a "flattened parallelogram" state into a rectangle.

Prototype - proving deployment kinematics

A prototype of the deployable stiffening concept was constructed to test the kinematics of deployment of the spreaders and cables. The prototype was built on an Astro lanyard deployed boom. The prototype was mechanically similar to the design concept in almost every way.

The model included two rings with three spreaders each, and axial cables. Available materials were used for construction. The prototype was useful in design verification.

Analysis of Design

The stiffened boom was analyzed by the FEM adding spreaders, cables, and lumped masses for rings to the original analysis model. The first mode of bending from this analysis was found to be 18.67 Hz, a 7 times increase.

Nut Deployed Boom Design

The nut deployed boom deploys in a different manner than the lanyard. The boom's canister is made up of three sections--the boom storage section, the transition section, and the nut section. (see Figure 7)

The nut section contains the actual deployment mechanism which is highly complex. In order to avoid interference with this mechanism another section was simply added to the top of the NDB canister. This section is

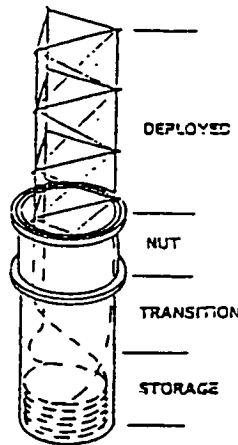


Figure 7 : NDB Deployment

called the spreader section and consists of three main parts: the top plate, spreader plates, and the locking plate. This device is shown in Fig. 8 with the end mass representing an experiment.

Locking and Spreader Plates

The detailed design of the locking and spreader mechanism is better shown in Figure 9a and Figure 9b. The locking plate is rigidly attached to the canister and secures the spreaders via pins.

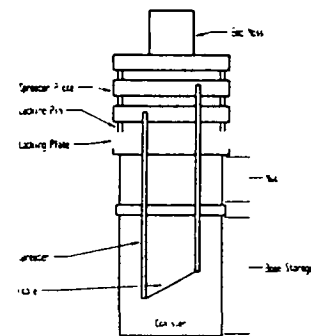


Figure 8 : NDB Stiffened Boom System

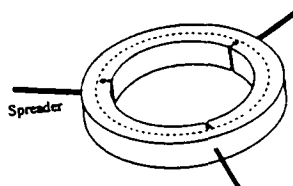


Figure 9 a : Spreader Plate

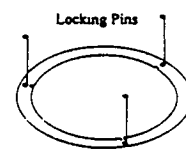


Figure 9b : Locking Plate

The spreader plate's detailed design is circular to allow for nesting of the spreaders along side the NDB canister. To minimize the volume of the overall package, the spreaders were folded down along the sides of the NDB canister and each successive ring is rotated a few degrees to keep the spreaders from tangling.

Attachment of Cables

The cables for the boom will be rigidly attached to the ends of the spreader arms. The lowest spreader arm on the boom will have spools attached on the upper and lower ends of the arm.

Tensioning of Cables

The tension for the cables will be provided by the boom itself. As the boom is deploying, the cables attaching the spreader arms will reach their maximum length just before the boom is fully deployed. When the boom length is increased, the cables will pull taut, thereby tensioning the cables.

Prototype

A prototype of the locking mechanism as discussed above was developed. The prototype was made of wood and accurately models the locking of the spreader collar to the top of the canister. The prototype was built to enhance understanding of the mechanism involved in unlocking the spreader plated from the canister and attaching them to the deploying boom.

Instrumentation

The instrumentation with which this design is concerned is comprised of triaxial accelerometers and strain gauges. The accelerometers are to be mounted approximately every fifth bay along the length of the boom, and will be used to map out the mode shapes of the boom during excitation. The strain gauges will be mounted on the tensioning motor support and will be

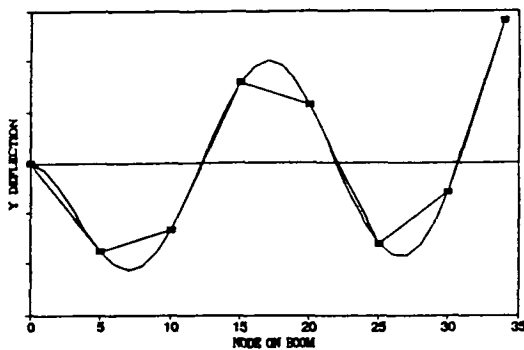


Figure 10 : Accelerometer Placement Using Highest Bending Mode

used to derive the tension in the cables.

The desired locations of the accelerometers on the boom were determined using a FEA model. To identify mode shapes, it is desirable to record data on each side of every peak for the highest vibrational mode of concern. Figure 10 indicates that for the ninth mode of the unstiffened model, this spacing requirement is approximately every fifth bay. Wiring for the accelerometers will be run down one continuous boom longeron and will pass through the canister at the point designated by the systems integration group.

System Integration

The system integration team was responsible for providing a platform for the booms and excitations of the system. The lanyard and nut deployed booms will be encased in canisters which will be attached to the Eagle spacecraft and launched into space by the Minuteman rocket. The pre-launch configuration of the Eagle system is presented as Figure 11. The boom will

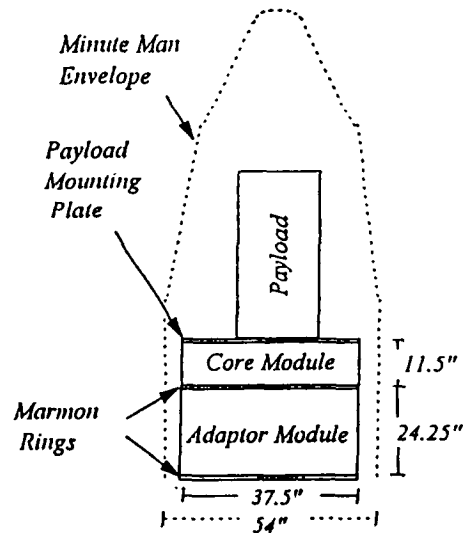


Figure 11 : Eagle Satellite

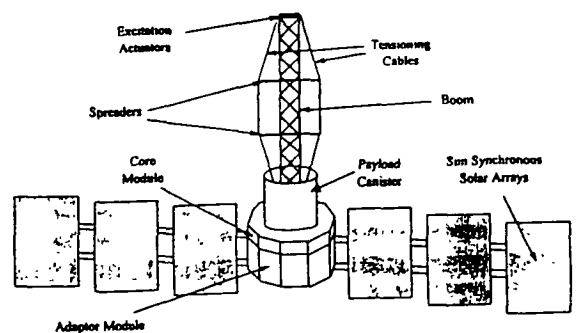


Figure 12 : Orbiting Configuration of Eagle Satellite

then be deployed and excited for testing. A schematic of the orbiting satellite including the deployed boom can be seen in Figure 12, although it is not to scale. Once stiffened, the computer on board must be able to monitor the first ten modes of vibration. Therefore the excitation device will be designed to create vibrations ranging from 0 to 1000 Hz. The information will then be relayed back to Marshall Space Flight Center to be analyzed and compared to an identical boom under the same stiffness in a 1 g environment. NASA requires that the stiffening device be able to increase the fundamental frequency of vibration by at least five times, and preferably ten.

Boom to Space Bus Interface

It was determined that bolting was the best method of attachment because of its reliability. Calculations of the forces expected resulted in a design with six carbon steel bolts with one centimeter diameter.

In both designs, lanyard and nut deployed, the retracted boom will be packaged in a storage canister that protects the boom during launch and shroud separation. This canister will be made with a filleted flange on the bottom to reduce stress concentration.

Eagle Satellite Support Systems

The Eagle satellite was selected as the support system for the stiffened space boom experiments. This satellite is an excellent choice because of its flexibility in design. The Eagle satellite is a Space Test Experimenters Platform (STEP) satellite designed for modularity and quick reusability. Each STEP satellite is unique because it is designed around the specific requirements of a particular mission. The Eagle's structure consists of a core module, various subassemblies, and solar arrays.

The core module is driven by a software based system, which controls all communications, data handling, power, and experimental needs of the satellite. The core module acts as the intelligence of the Eagle design and is required for each mission.

Subassemblies can be included with the core module as required by the experimenter. These subassemblies include a deployment module, a payload module, and a propulsion (or adaptor) module. The deployment module is a separable platform used to assemble and test payload deployables. The payload module is simply an enclosed volume dedicated for user payloads. The propulsion or adaptor module includes facilities for orbit maintenance, orbit raising, and maneuvers.

The solar arrays of the Eagle satellite also exhibit great flexibility. For this experiment, the sun synchronous assembly was chosen.

Core Module Systems

The core module on the Eagle Satellite can be divided into three basic sections: the electrical power subsystem, the control and data handling facilities, and the core module software. The electrical power subsystem is responsible for generating, storing, regulating, and distributing power to the required drains. The control and data handling subsystem is responsible for processing, storing, and handling all experimental data. The core module software is used to control all spacecraft commands. There are two different pieces of software required for each mission: the spacecraft software subsystem (SSS): controls all spacecraft, including payload actions, after launch; and the ground operations support software (OSS): experiment specific software for interfacing with the experimenter from the ground.

Adaptor Module

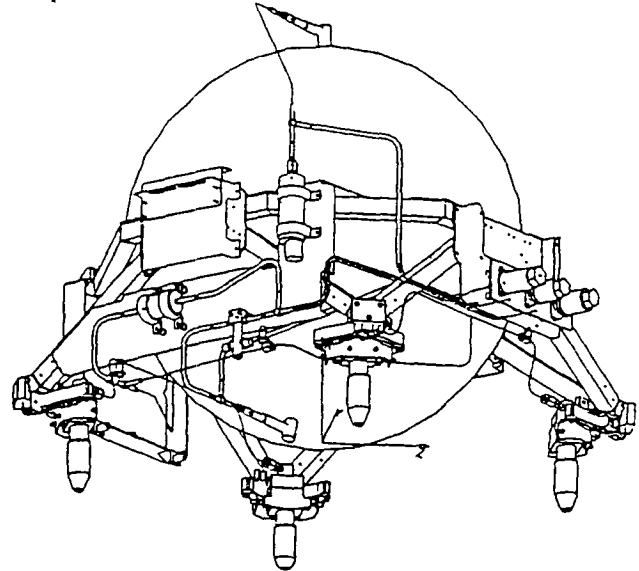


Figure 13 :Reaction Control System

Due to concerns about base stability, the Reaction Control System (RCS) has been included in the design of the Eagle satellite. This system is responsible for the attitude determination and control of the space bus and will ensure that any vibration experiments performed on the boom will not adversely affect the trajectory of the satellite. An additional section, termed the Adaptor module, is required to house the RCS and can be seen in Figure 13 along with the core module.

The Reaction Control System consists of five basic elements: propulsion system, torquods, reaction wheels, scan wheels, and a magnetometer. The five elements give the system the vibrational control for stability during experimentation

Solar Arrays

Solar arrays are an essential part to the Eagle satellite. These arrays provide all the electrical power required by the spacecraft. For the stiffened boom mission, the sun-synchronous solar array configuration will be used. This configuration provides plenty of power, is low weight, and reliable. The solar arrays begin folded down along the circumference of the eagle to comfortably fit into the Minuteman launch vehicle.

Boom Excitation

A reaction mass actuator (RMA) has been selected to generate vibrations in the deployable booms. A reaction mass actuator can be designed to be very lightweight and still generate a wide range of frequencies. The RMA designed provides excitation in the range of 1 to 1000 Hz.

Conclusions

A stiffening system was designed for the lanyard deployed boom which took into consideration the specific problems of the LDB. The design consisted of a linearly scalable cable and spreader mechanism. The spreaders were attached to the boom with a ring system which reduced stresses on the boom as well as allowed for the rotation of the boom during deployment. A working prototype was developed which proved the design concept. An ANSYS finite element model was developed of the design which showed that the first mode was increased by a factor of 7.

The design for the nut deployed boom was successful in that it addressed the specific problems of the NDB deployment system. The rings which the spreaders and cable were attached to were on the top of the canister and were picked up as the boom deployed. An effective locking/unlocking mechanism was designed and prototyped for the picking up of the rings. The designers investigated the stiffening of the boom, and analysis showed the concept to be a valid one.

The attachment of the boom to the Eagle space bus was designed with safety in mind. The canister will be bolted to the Eagle platform. The support system for the experiment was studied and determined that the electrical, data management and control systems provided by the Eagle is adequate for the mission. Excitation of the boom during experimentation is provided by the reaction mass actuator developed. These elements provide a stable, complete base for the experiment to be successfully launched, deployed and completed.

Recommendations

Recommendations for this design project are mainly in the area of further investigation of the design feasibility and further prototyping for design verification. The lanyard deployed boom could be

modeled more accurately with mathematical models, therefore testing the design concept, also, the prototype that was built could be refined and rebuilt with greater precision. The nut deployed boom needs to be prototyped for design verification, but this design would also benefit from more mathematical analysis. The system integration team needs to verify the design of the reaction mass actuator as well as study the adaptor module vibration suppression effectiveness.

Acknowledgements

This design project would not have been possible without the suggestion of a passive damping system for flexible boom from Dr. Henry Waites at Marshall Space Flight Center. This idea was developed into the three specific teams which addressed the problem from different angles. Angie Buckley was also critical in the gathering of information and contacts for the students.

At Vanderbilt, Dr. Tom Cruse was the driving force behind the development of the designs as well as the investigation of the concepts which govern them. Dr. Ephraim Garcia helped greatly in the understanding of the dynamic principals as well as lending the students the Astromast boom for prototyping. Ms. Susan Ward helped the students throughout the year and prepared the conference papers and presentations.

AUTOMATED PROTEIN CRYSTAL GROWTH

Clayton Alves, Chris Apple, David Anderson,
David Beckham, John Bryan, Christopher
Chandler, Andrew Cocks, Melissa Cross, Stephen
Erdmann, Mike Fowler, Ken Givens,
Allegra Lewis, Robbie Loveless, Joe Martinez,
Sabina Mohyuddin, Jason Pierson, Braxton Sealy,
Brian Weston

Abstract

The scientific value of experimental protein crystal growth has been well established in recent years. For full three dimensional growth of crystals, the zero gravity environment of space has been found to be an improvement to normal laboratory environments. The Automated Protein Crystal Growth Facility was designed to provide a fully automated protein crystal growth facility that is fully compatible with the Space Station Freedom (SSF).

The precipitant, protein, and quenching solutions are pre-mixed, pre-loaded, and contained in the chamber. Growth is induced and terminated through the use of an automated robot. The rack was designed to optimize the space available in the ISPR (International Standard Payload Rack) by using an octagonal shape with a combination of storage and active growth sites.

The automation of this experiment uses both a robotic arm and an end-effector designed to interface with the crystal growth chambers. The end-effector operates plungers and grasps chambers through the use of attachments to the end effector.

The experiment is supported by an integrated environmental control and data management system. The data management system offers continuous groundbased control of the experiment through the use of optical sensors (fiber optics and photo transistors), heat sensors (thermocouples), and heat generators (electrical resistance heating coils).

Introduction

Since completion of the first crystallographic study of a protein crystal structure (myoglobin) in 1960, crystallography has become a valuable tool for revealing the structure and functional relationships that are of major importance in understanding how macromolecules operate in biological systems. More recently, pharmaceutical, biotechnological, and chemical industries have become interested in crystallographic studies of proteins because of their promise in protein engineering, drug design, and other applications to biological systems.(1)

Gaining the three dimensional structure of the protein can be done in a variety of ways. Due to the effects of gravity on the growth of the crystal on earth, it is

difficult to grow a crystal which has not been affected. Thus the growth of crystal in reduced gravity would ease the study of the crystals.

Background

The Preliminary Design Branch at Marshall Space Flight Center has been investigating the possibility of developing a fully automated protein crystal growth facility. Currently, the space program on the shuttle supports a partially automated facility. The idea which Melody Herrmann suggested was to develop a facility which would require no human interaction and therefore could be placed in the Space Station Freedom during the tended period.

Melody Herrmann, Frederick Herrmann, Elaine Hinman-Sweeny and others had developed an automated system using a Zymark Zymate II robot.(2)(3) The system was designed to utilize the robot for manipulation of the chambers which would hold the crystals during transport and growth. That design was the basis for the design of the students.

Assumptions and Requirements

The goal was to develop an automated protein crystal growth facility for use on space station. During a meeting on January 21, 1993 at Marshall Space Flight center with Melody Herrman and Elaine Hinman-Sweeny, the specifications of the project were determined.

- The experimental facility must fit within an ISPR payload rack.
- A minimum of 500 protein crystals must be grown during the 90 day un-tended period between shuttle flights.
- Each protein must be individually controlled with respect to temperature and time of growth.
- The control and monitoring of the growth process may be done from a remote location.
- The final crystal must be encased such that it can be returned to earth successfully.
- Viewing of each crystal is required.
- The facility must be completely safe and comply to space station requirements for astronaut interaction.
- All experimental equipment placed within the rack must be space qualified and meet launch requirements.
- The experiment must not interfere with any other experiments on board.

These specifications were used to guide the students to a successful design of an automated protein crystal growth facility.

Vapor Diffusion Method

A common and rather simple method of growing protein crystals is the vapor diffusion method. This is the method that will be employed in the Space Station Freedom facility. In this method, The difference in concentration of protein solution combined with

vaporization of the solutions causes nucleation within the drop. The growth process continues until a quenchant solution is introduced into the chamber.

Protein Crystal Growth Experimental Facility

The advantages of growing crystals in space prove the need of designing a protein crystal growth chamber capable of producing crystals in micro gravity without any human interaction. The design of the chamber incorporates several key design specifications. Key specifications include preparing the chamber for growing the crystal, minimizing waste from the chamber, and controlling and monitoring the crystal growth. Since the experimental facility will be automated, minimizing robot interaction with the chamber is also a key specification.

The protein crystal growth chamber has a robotic chamber locking device located on the bottom where the robotic end-effector will attach to the chamber for movement and storage. The keyway tabs on the side of the chamber secures the chamber within the slot.

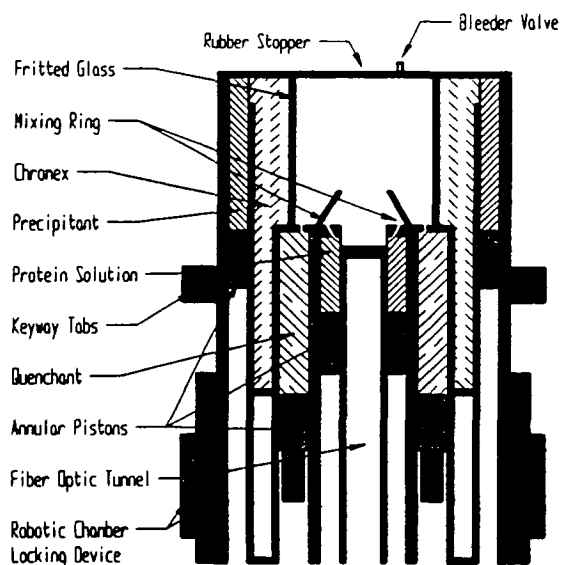


Figure 1 : Protein Crystal Growth Chamber

Figure 1 shows a sectional view of the proposed chamber. The chamber has pre-loaded protein/precipitant, precipitant, and quenching solutions. These solutions are separated from each other and are contained in the chamber before usage. The order of actions performed on the chamber by the robot are as follows: (1) move chamber to active site; (2) simultaneously plunge protein solution, optical pedestal, and precipitant solution in outer annulus; (3) monitor crystal growth through optical tunnel; (4) quench crystal

growth; (5) return chamber to storage site. Some key design features of these actions are: (1) Key way tabs for securing chamber in active and storage sites. (2) The mixing ring above the protein solution mixes the solution before it is placed on the pedestal. The precipitant solution is pushed into the chromex (steel wool substance) so that vaporization may occur. (3) The optical tunnel is the pedestal which the crystal grows on, therefore reducing mistaken readings. Crystal growth is monitored through the use of light diffraction. The light is shone down the tunnel and an optical sensor at the base of the chamber within the active site monitors crystal growth. (4) The quenchant solution suspends the crystal for return to earth.

Each chamber has the ability to be individually thermally controlled. Temperature is the major variable which effects the rate of vapor diffusion of the crystal. Therefore, individual chamber temperature control gives the user the ability to develop a range of growth rates. The thermal control is implemented by the use of an electrical resistance heated wire wrapped around the conical section of the chamber and extended to the top of the chamber. A thermocouple is placed on the conical section above the heating wire.

Geometry of Experimental Facility

The experimental facility had to adhere to the constraints of the robot end effector while maximizing the space allotted and promote and store protein crystals. Space within the experimental facility was allotted for data acquisition devices, HVAC units, as well as other environmental or data control hardware. Additional considerations were taken to ensure room for any wiring and an opening for an emergency door on the front of the facility.

Robot accessibility was a high priority in designing the facility geometry. By mounting the robot on the back wall, it could reach all the chambers because it has the ability to extend approximately 22.8".

Maximization of number of locations for growth was a consideration when choosing a experimental geometry. An experimental facility in the shape of an octagon with cylindrical removable storage shelves was design. The final overall design is shown in Figure 2.

The design chosen has four active growing region while it also has fourteen cylindrical shelves where chambers are stored before or after growth.

Active Sites

There are four locations for the active sites. The angled corners of the experiment facility house the active sites. Each of the four shelves contain 33 experiment sites; thus, there are a total of 132 active sites. The environment of each chamber is isolated and can be easily controlled. The active sites have more space between them than the storage sites to account for

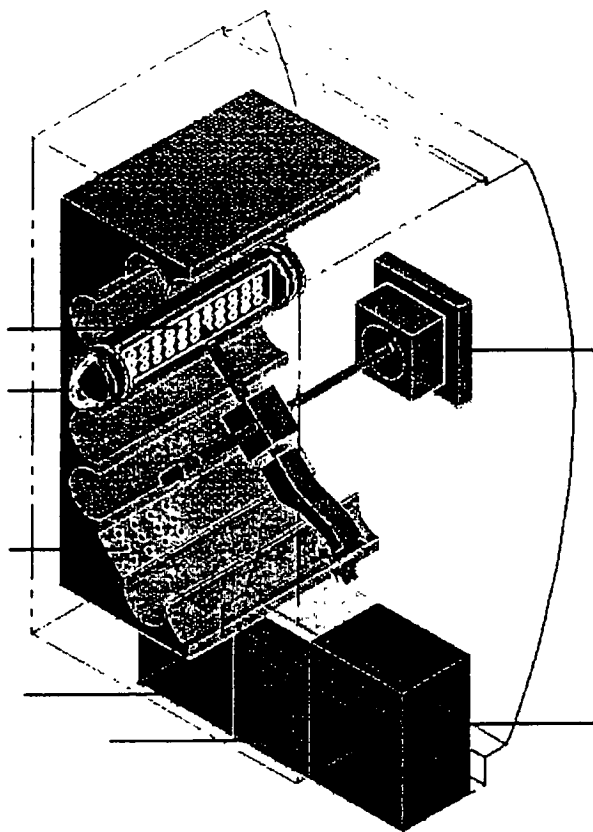


Figure 2 : Experimental Facility

the environmental control and monitoring.

Storage Sites

There are fourteen locations for storage sites in the automated protein growth facility. The storage sites are located along the top, bottom, and sides of the facility. The storage sites reside in removable trays housed in drawers. Each tray can hold 45 chambers for storage, thus there are 630 storage sites.

Once a tray is full of chambers, the drawer can be retracted, and the tray replaced by another with new chambers. The chambers are locked in place by keyways and springs as with the active sites.

Robot End Effector

The Zymate II is a laboratory robot that has been used in medical experiments in the past and therefore has proved its reliability in that area. The Zymate's small size allows for efficient use of space in the experimental facility, but its reach is still sufficient to access all areas of the rack. The Zymate II also has acceptable repeatability. The Zymate II has 6 degrees of freedom, two in the end effector. See Figure 3.

The most prominent feature of the end effector is its tetrahedron-shaped tool head which rotates to orient different tools. One of the four faces of the tetrahedron

is connected via spider gear to a MicroMo motor and gearbox which provides rotational motion. The various tools required for protein crystal growth are mounted on the other three faces of the tetrahedron. These tools include two plungers and a screw top gripping apparatus. The

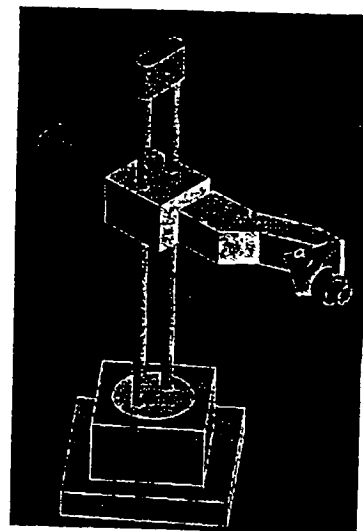


Figure 3 : Zymark II Robot

The active tool on the tetrahedron is located along the centerline of the robot arm, and the inactive tools are oriented back and away from the active tool. Thus, the two tools which are not in use will not interfere with the operation of the active tool and will not collide with the rack wall when the active tetrahedron face rests flatly against it. There is a timing and locking system that allows the active tool to be properly oriented to perform the necessary functions and maintains that orientation while these functions are being performed. The tools themselves are stationary in that they do not provide any motion on their own. The end of the end effector is also equipped with a light source for use in retrieving data from the crystals. An overall two-dimensional picture of the end effector is provided in Figure 4.

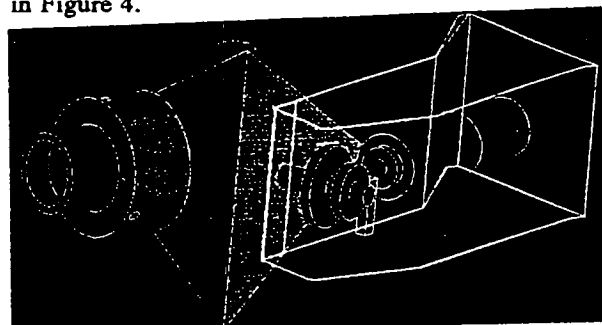


Figure 4 : End Effector for Robot

Screw Top Gripping Concept

In order to grasp the crystal growth chambers, the end effector utilizes a locking thread that screws onto a collar at the end of the chamber. Sufficient safety to prevent breakage of the chamber were designed into the

screw top locking mechanism.

Plunger Design

The primary functions of extruding the protein solution and quenchant for crystal growth are accomplished through the use of a two plunger system. The plungers will accomplish the task of extruding the solutions by depressing annular pistons. They are cylindrical in shape and are stationary. Therefore the robot provides the plunging motion that depresses the pistons. The plungers were designed to meet the tolerance of the chambers in order to interface with all chambers.

Gearbox and Motor

A motor was chosen with appropriate torque and gearing for the application.

The Timing and Locking Mechanism

The purpose of the timing and locking mechanism serves the dual purpose of providing correct orientation for the active tool as well as locking the tetrahedron in place to maintain proper orientation during use. The mechanism accomplishes these tasks through the use of a wheel with three notches, one for each tool, that are equally spaced about the circumference of the wheel. The wheel is locked by the locking mechanism to prevent slipping.

Robosim Robotic Movement Visualization

A robotic simulation of the movements of the robot was completed using the ROBOSIM robotic simulation package. The simulation shows the Zymark Zymate II robot rotating into position and grasping a chamber. The chamber is then moved from the storage position into the active site and twisted to secure it. The simulation was completed for visualization purposes.

System Integration

One of the first major concerns in the development of the Automated Protein Crystal Growth Facility is the maximization of the experimental volume. The two major constraints for the experimental volume are the AAA environmental control device and the Zymate II robotic components. With these limitations considered, the maximum experimental volume was determined. Within this volume is the entire experimental facility, which consists of an octagonal shaped area, oriented in the same manner as a common clothes dryer. The active and storage sites (which are located outside of the octagon) are also placed within the experimental volume.

Placement of the interior components were carefully studied to determine the most effective placement of all components taking into consideration human interaction, launching conditions and spacial restrictions.

Human Interface

To extend the life of the experiment, the removable drawers containing the storage trays and completed

experiments were designed for the best human interface conditions. The interior of the rack was also defined as separate environments, therefore the idea of a cylindrical drawer was then developed. This drawer could be made with an o-ring seal to separate the two environments and still be easily removable by an astronaut. A sleeve was created to seal the inside of the experimental facility from the SSF environment during the removal of the storage trays. The key way system was developed to reduce the possibility of the drawer floating out of position in microgravity.

The emergency access doors are the final human interface concern. These doors provide the astronauts with access to the interior of the experimental facility. The requirements for the door are: must maintain an airtight seal, be light weight, withstand vibrations due to shuttle launch, have long life with little maintenance, allow easy access to the facility, consume very little space, be transparent, not protrude into the space station corridor, and allow for the use of space gloves. A regular door with an o-ring was chosen to fit these design requirements. Two separate doors are used in order to avoid any intrusion upon the space used for the robot running bars.

Data Management

The Automated Protein Crystal Growth Facility has a computer system which controls the Zymate II robot, the data collection system, and the heating of the facility. The computer commands the robot to retrieve an inactive crystal chamber and activate it. After activation, the computer checks the growth of the crystal and ultimately commands the robot to quench the crystal and replace the finished crystal in storage.

A 386/486 computer and accompanying workhorse were chosen for control of the robot and collection of the data. The computer control also allows for the individual control of each chamber. The temperature as well as the viewing of the crystal growth will allow the ground controller to customize each crystal growth experiment for best growth.

Environmental Control

A major systems integration issue is environmental control. This consists of providing the proper lighting, temperature, humidity, and pressure to support the experimental project. In the case of the automated protein crystal growth facility, systems integration was responsible to design a system that would individually control the temperature of the growing crystal at each of 132 active experimental sites. The growing crystals must be kept within .5° C of the desired temperature. The system must be able to detect the temperature of the growing crystal, and respond automatically to maintain the preset temperature if the detected temperature is not satisfactory. As mentioned before,

the chambers are sealed and coated, which not only prohibits mass transfer into and out of the chamber, but also prevents radiation heat transfer from taking place. Thus, with respect to the chambers, the objective of the environmental control system is to regulate temperature only. Isolation of the system from the Space Station provides the safety which the Freedom astronauts require.

The system must combine a heating and a cooling system to maintain each individual site temperature. These requirements are met by providing general cooling of the facility (below 4 C) and providing individual site heating.

The base hardware offered by NASA and Boeing for environmental control is called the Avionics Air Assembly (AAA). This hardware may be connected to the Space Station's low-temperature loop, which will enable the facility to reach the desired ambient temperature.

The heating of the individual sites will be accomplished through electrical resistance heating. In an effort to reduce temperature gradients within the chamber, and to lower the necessary power consumption of the system, the heating wire is placed inside the chamber and wrapped around the pedestal. Additionally, a thermocouple is placed on the pedestal, as close as possible to the growing crystal. Electrical connection of the heating wire and the thermocouple is made via the metal spring connection outside the chamber.

Conclusions

Protein Crystal Growth Experimental Facility

The objective of this design effort was to create a suitable chamber design that could sustain crystal growth in a controlled environment. It was also to establish a rack design that could encompass the stipulations set by protein crystal growth experiments, and integrate these factors with the chosen Zymate robot and the new chamber design. The chamber and rack designs, according to the design objective, meet all of the required specifications.

The chamber design, much like the rack, meets all of its design criterion. It is easy to manipulate by the robot by requiring only pushing motions, as well as integrated with the facility through the temperature control and crystal growth monitoring.

The experimental facility design exceeded the requirements by providing 630 experiments during the 90 untended period on the SSF. The ability to change out experiments also exceeds the requirements of the facility.

Robot End Effector

The robotics group has successfully developed an end-effector for the existing Zymate II robotic system

that allows for the development of an integrated, fully autonomous protein crystal growth facility. The final end-effector design is a tetrahedron. One side connects the end-effector to the drive shaft, allowing rotational movement. The other three faces of the tetrahedron hold the "tools" which perform actions on the protein chambers. There is a screw-top attachment, a double plunger, and a single plunger.

System Integration

The experimental volume in the ISPR was maximized using the dimensions of the Zymate II robot and support equipment as constraints. The environment of the experimental area is completely sealed from the SSF environment through the use of cylindrical storage drawers which function as airlocks.

The APCGF contains an IBM 386/486 control system that provides direct system analysis for all systems. The environmental control system will maintain an ambient facility temperature of 4° C by using the standard AAA/REP package, equipped with a dehumidification device, connected to the low temperature loop on the Space Station.

Recommendation

Though the design objectives of this protein crystal growth facility were completely achieved, there are some details that could be explored in furthering this design effort. The sensor used for detecting the growth of the crystal is for the most part unidentified. The manufacturability of the entire facility must be considered. The exact placement and configuration of the optical data retrieval system needs to be determined. The sizing of the electronic data gathering components (Workhorses) should be investigated. Another issue that calls for further design is the vacuum system safety valve. The general cooling/dehumidification has yet to be fully developed. A full prototype of the entire facility should be built to validate the design.

References

- 1) DeLucas, Lawrence J., Bugg, Charles E., "Protein Crystal Growth in Space". *Advances in Space Biology and Medicine*, Volume 1, pp 249-278, JAI Press Inc., 1991.
- (2) Dike, Paul H. *Thermoelectric Thermometry*. Philadelphia: Leeds and Northrup Company, 1954.
- (3) Incropera, Frank P. and DeWitt, David P., *Introduction to Heat Transfer*. New York: McGraw-Hill, 1981.

Virginia Polytechnic Institute and State University
Department of Aerospace and Ocean Engineering
Blacksburg, Virginia

Professor Antoni K. Jakubowski
Hazim Youssef, Teaching Assistant

Abstract

Two 1992-93 Space Design student teams designed UV/Optical/IR long-baseline interferometric arrays to be emplaced on the far side of the moon. The array's primary objectives will be to detect and characterize extrasolar planets up to 10 parsec away and to carry exploration of the structure and evolution of the universe with an angular resolution 3 orders of magnitude better than Hubble's designed goal and over a greatly increased spectral range (up to 10 μm). Addressing requirements established by NASA, the student teams developed two proposals named LOLA (Lunar Optical Long-baseline Array) and LOITA (Lunar Optical/Infrared Telescope Array). Both designs use maximum baseline of 5 km and will be capable of imaging with an angular resolution of 20 microarcsec at 500 nm. LOLA is an array of twenty seven 1.5 m telescopes arranged in a Y-configuration. A two-stage, coarse and fine, optical delay system controlled by the laser metrology equalizes the optical path lengths of all 27 beams. Scientific instruments provide pupil plane imaging and spectroscopic analysis with fields of view ranging from 15 arcsec to 10^{-3} arcsec. A planet detection module operating in IR utilizes an achromatic nulling interferometer and single mode fiber optics. For continuous communication with Earth, a satellite orbiting L2 libration point is used. LOITA is composed of eighteen 1.75 m alt-azimuth telescopes arranged in a circular geometry and uses a three-stage delay system to equalize optical path lengths to within a few wavelengths. To ensure high IR sensitivity at wavelengths up to 10 μm , the optics and some detectors are cooled to about 70 K temperature. The array science instruments will allow: (a) wide-to-medium field imaging utilizing various beam combiners and large format mosaics of CCDs with 10^8 to 2.5×10^9 pixels, (b) direct planet detection by starlight suppression at a level of 10^8 , (c) astrometric measurements providing 0.1 microarcsec accuracy, and (d) single telescope option for direct imaging in the focal plane. A relay satellite at the L4 libration point will serve communications with Earth. LOITA will be constructed in 3 phases of 6 telescopes each. The combined mass of the array is estimated at about 77,000 kg.

Introduction

The astronomical frontiers of the next century will require space observations using giant filled-aperture tele-

scopes and interferometric arrays with multi-kilometer baselines. The moon offers a nearly ideal site for these observatories. It has effectively no atmosphere allowing perfect transmittance in all wavelengths and very long life of fully efficient exposed optical surfaces. The moon's dark and cold sky permits infrared astronomy and the absence of wind combined with low gravity and minimal seismic activity (10^{-8} that of Earth) ensures stability for interferometric arrays with even the longest baselines, and allows accurate pointing and smooth tracking. On the moon, we have an unlimited supply of raw material for shielding from solar storm and cosmic radiation. The long lunar night and slowly varying thermal environment permit long exposures when observing faint sources and excellent dimensional stability. Also, compared with free space, the moon with its small gravity offers a better and healthier environment for a manned crew involved in periodic tending of the observatory.

A conceptual/preliminary design of a back-side lunar UV/optical/IR long-baseline interferometric array has been selected as the 1992/93 space design project at the Virginia Tech. The array's primary objectives and design requirements were set by the Space Exploration Initiative Office at NASA Langley; the array must be able to:

- resolve Earth-type planets orbiting stars at distances of up to 10 parsec
- cover wavelength spectrum of 5 nm to 5 mm
- use identical array elements with maximum 2 m aperture
- provide a signal - to - noise ratio of no less than 10 at 500 nm
- use the lunar far side within 10° N and S, no closer than 15° to either limb
- minimize mass

Several recent studies have examined the feasibility of the design and operation of a lunar-based optical interferometric arrays.¹⁻⁵ These studies concluded that high resolution optical interferometry on the moon is possible, but they often do not explore the array design beyond that of the overall concept and/or major component design.

Two Virginia Tech student teams, working mostly inde-

pendently, developed two design proposals, named LOLA (Lunar Optical Long-baseline Array) and LOITA (Lunar Optical/Infrared Telescope Array). Early in the design process, both teams have realized that it was not really feasible to design an array that covers a spectral range from 5 nm to 5 mm while consisting of identical 2 m diameter elements. Also, it was realized that using near-term technology it will be extremely difficult to resolve Earth-like planets in the visible light.

LOLA: LUNAR OPTICAL LONG-BASELINE ARRAY

Tony Guinta (team leader), Daniel Bronte, Joanne Chaney, Christine Curran, Keith Ferguson, Eric Flint, Duane Knill, Daniel Levesque, Donald Lyon, Sean Murphy, Christopher Shively, Angela Wesner, and Thomas Yablonski.

Array Configuration

The LOLA's team selected a Y array configuration which when compared with a circular array, has several advantages such as a simpler delay line scheme, simplified layout of the power and signal cables, relative ease of maintaining image rotation and signal polarization, and greater potential for expansion in the future by adding additional elements along the Y arms. The array consists of 27 telescopes, nine per each arm of the configuration (Fig. 1). The 2.9 km arms point north, southeast and southwest providing a 5 km maximum baseline and a 220 m minimum baseline. The selected orientation allows maximum exploitation of the moon's rotation, termed rotation synthesis required for imaging of complex objects. The array will be constructed in two stages. The initial stage will consist of 9 telescopes providing 36 baselines. The second stage will add 18 telescopes to provide a total of 351 baselines.

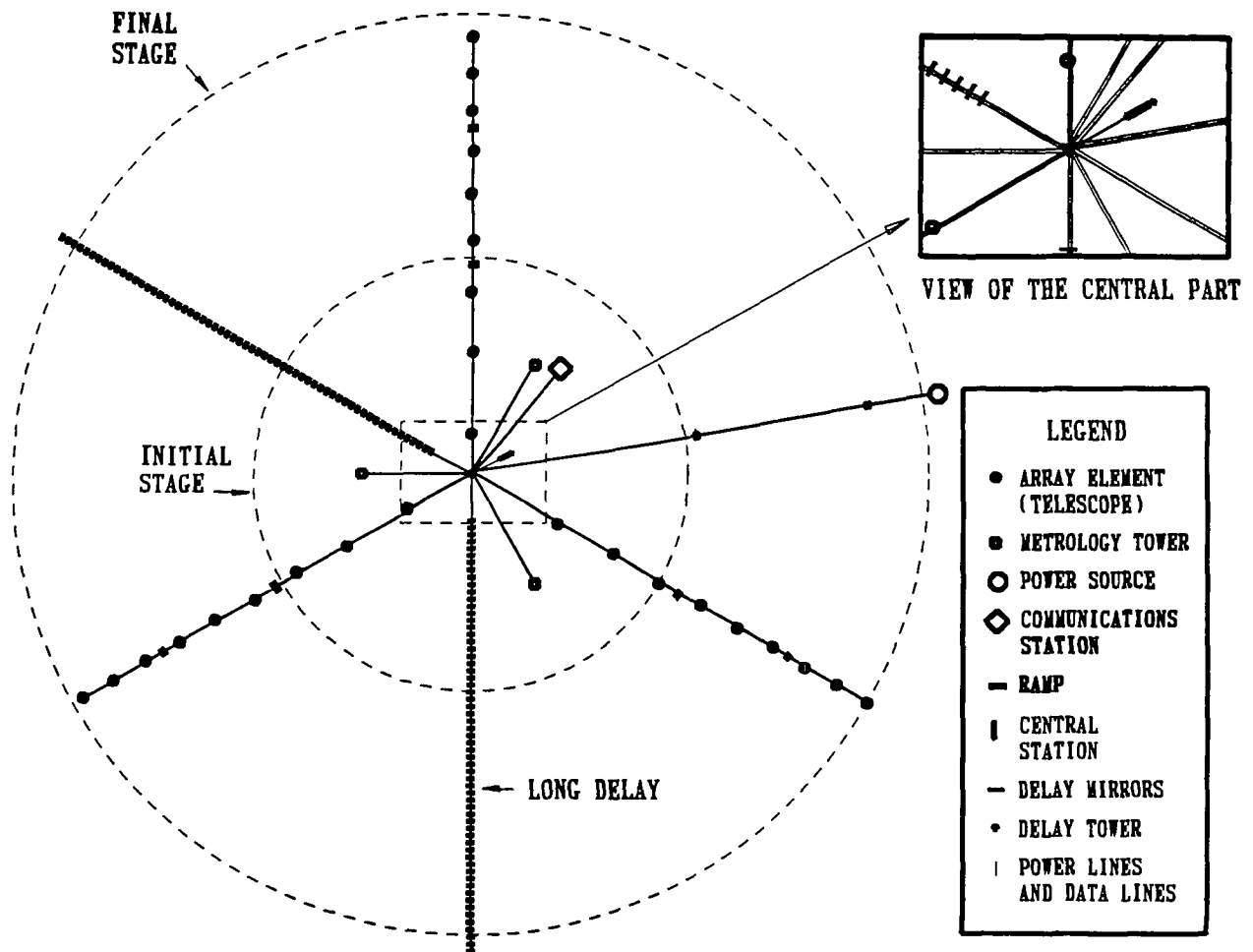


Fig. 1 LOLA array layout

The final array layout and telescope spacings were established on the basis of $u-v$ plane* coverage computations for a variety of layout/spacings arrangements and for the array equatorial locations. Four spirals of varying tightness were overlaid on the Y configuration to produce baseline non-redundancy (while still retaining some near redundant baselines required to retrieve optical phase information) and create the required baseline length taper. The final spacings of the array (Fig. 1) display good $u-v$ plane coverage even with only 9 initial telescopes (Fig. 2).

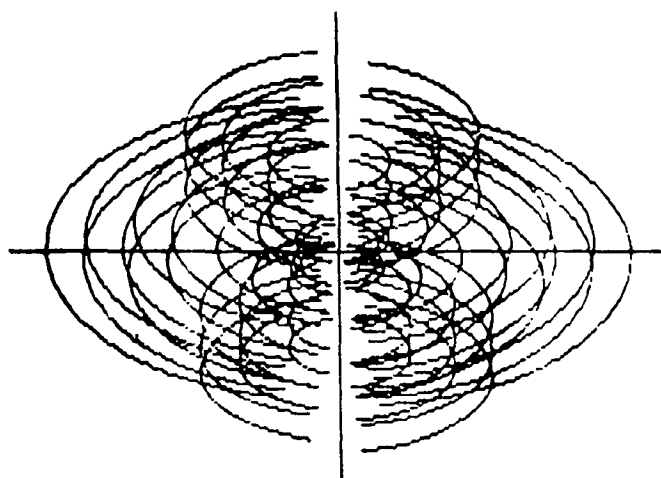


Fig. 2 $u-v$ coverage at 45° target declination with 9 telescopes

Optical Layout/Considerations

Selection of the mirror diameter of 1.5 m resulted from the considerations of the optical performance, fabrication costs and weight. The collecting area of 45.8 m^2 was initially sized so as to accomplish the most difficult task of detecting visible (500 nm) light of an Earth-like planet 10 parsecs away with a signal-to-noise ratio (S/N) of 10. It was assumed that the light of the parent star can be mostly canceled, the mirrors will have a $\lambda/100$ surface finish and the integration time can last up to 10 Earth days. However, it will be extremely difficult to satisfy these conditions and, therefore, visible light detection of extra-solar planets will be very unlikely when using the LOLA array. Extra-solar planet detection in the visible light may actually require a collecting area one order of magnitude greater, i.e., an array consisting of hundreds of telescopes, a highly unrealistic solution for the moon based interferometer. Comparison of the emission of an extra solar planet at visible and IR (around $10 \mu\text{m}$) wavelengths shows that by moving to IR the contrast ratio between the star and planet reduces by 3 orders of magnitude, and the photon flux actually increases. Therefore, the LOLA's planet detection scheme is designed to operate at $10 \mu\text{m}$ which will require to keep the entire optical

train at a temperature of 77 K or less during the lunar night. The collecting area of 45.8 m^2 was accepted as satisfactory for majority of scientific objectives (including planet detection at IR) and as a reasonable compromise between the requirements of sufficient number of telescopes (for good $u-v$ coverage), large collecting area (to increase S/N and reduce integration time) and telescope sizes below 2 m (for economical/fabrication reasons).

The LOLA's observable spectrum spans from 200 nm to $10 \mu\text{m}$ with the visible spectrum from 400 to 700 nm as the region of primary interest. Fig. 3 illustrates variation of S/N with the wavelength when observing solar system-like planets during 1 day integration time.

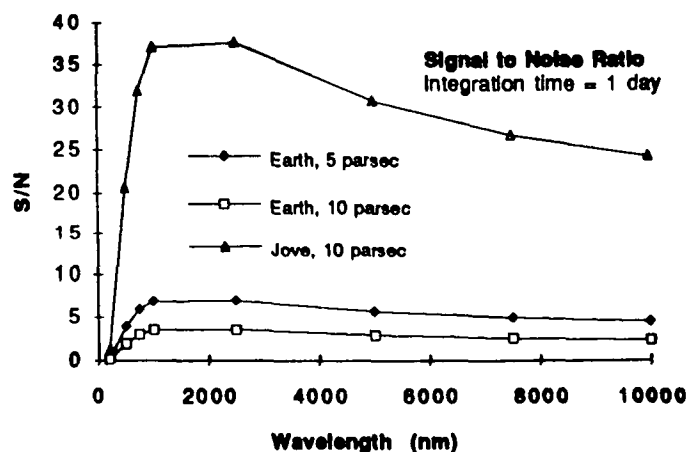


Fig. 3 Signal-to-noise ratio vs wavelength

The optical path of a beam from a source through a telescope and long delay lines to the central station is illustrated schematically in Fig. 4. The 1.5 m primary mirror and the 25 cm secondary mirror are paraboloidal with a focal number of 2.46. Structural considerations made it necessary to have the secondary mirror plane at the same height or lower than the pupil plane. This made it impossible to reduce the remaining field curvature and distortion to zero. The tertiary mirror directing light out of the telescope cylinder is elliptical (25 cm by 35.5 cm) and is 3rd order curved to remove distortion and field curvature. The 25 cm diameter of the beam leaving the telescope was chosen as a compromise between diffraction effects and complexity/cost of large size of delay lines optics. Because of the long beam path length at large baselines the quality of the received signal begins to drop off gradually for longer wavelengths.

* The (u, v) coordinates correspond to the baseline coordinates on a plane normal to the source direction.

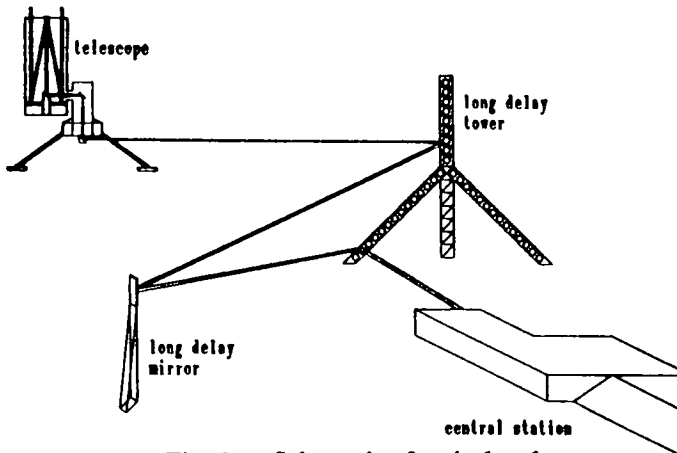


Fig. 4 Schematic of optical path

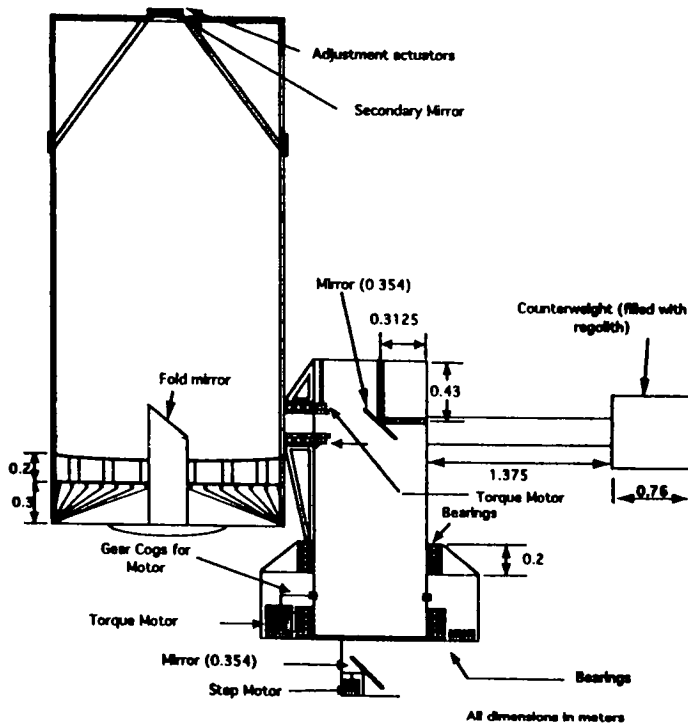


Fig. 5 LOLA telescope

Telescope/Mirror Structure

The telescope design was selected after a series of trade studies of several options which were compared on the basis of mass, size, optical performance, stability, simplicity, reliability, power required and cost. The telescope is shown schematically in Fig. 5. For this conceptual design, boron/epoxy laminates (with metal joints) were selected for the telescope structure. Metal matrix composites would have been an excellent choice for the telescope, however, they are still under development and cannot be adequately characterized. A preliminary structural and deformation analysis was performed and indicated maximum deformations in the μm - range.

The telescopes use spudcan footings which are usable in a variety of soils, are self-installing and allow excellent lateral stability. These footings are filled with lunar regolith to increase their stability and then driven into the soil by vibratory pre-loading. Torque motors (Inland Co.) are used for both the side arm and the base rotation as they allow "infinite precision" positioning of the telescope.

The honeycomb-type primary mirror will be made of Schott Glasswork's Zerodur glass/ceramic material and it will have 2 cm-thick top and bottom substrates with a honeycomb thickness of 15 - 20 cm. The mirror surface should be finished to a $\lambda/100$ accuracy. A silver dielectric coating is chosen as the reflecting film (98 -99% reflectivity beyond 500 nm). Boron/epoxy supports are required underneath the mirror to reduce possible deflections. Maximum deflection calculations of the primary mirror due to self-weight were performed for three different load scenarios: moon's gravity, 3 g (shuttle launch), and 6g (expendable launch vehicle). The maximum deflection on the moon was found to be acceptable 3nm. The total mass of the telescope is 1882 kg.

Optical Delay Lines

To equalize the optical path lengths of all 27 beams before they reach the instrumentation, a two-staged, long and fine delay system is used. Taking into account possible movement of telescopes to achieve baseline redundancy, the maximum required total delay line is 5400 m. The long delay system consisting of the central long delay tower, fixed mirrors and small steering mirrors, equalizes the path lengths to within 90 m. The remaining difference is removed by the fine delay system which also compensates continuously for lunar rotation. Prior to entering the fine delay lines, the beams are compressed down to 4 cm diameter using a Cassegrain system. Each fine delay line is folded within a 55.5 m distance and uses a mobile mirror transported on a small cart and controlled by PZT actuators to adjust for possible vibrations in the optical structures. Computer algorithms taking target declination, azimuth, baseline and optical path length data, calculate the needed delay for each telescope and direct the controllable mirrors of the long and fine delay systems to achieve that delay. Both the mobile and the fixed mirrors will have a near $\lambda/100$ surface finish and will be sized to accommodate both the incident beam and metrology beams utilized to ensure positioning accuracy. All 27 fine delay lines will be housed in a sealed structure placed in the central receiving station, which provides radiation, thermal, and dust protection.

Metrology

The equalized beams exiting the fine delay lines are directed to the beam combiners and instruments. First, the

beams are split; one branch continuing to the science instruments, while the other beam is split again and directed to the laser metrology and the pointing/control system. The metrology system is divided into two main subsystems, the optical delay path metrology (ODPM) and the baseline metrology (BM). The ODPM measures the delay path through whole optical path length and should provide nanometer length corrections to the fine delay system. This will require a solid-state laser stability of 1 part over 1 trillion (10^{-12}). Two laser beams originating in the metrology housing travel back through the beam splitters, the fine delay lines, long delay lines and into each telescope. At the telescopes, the beams hit retroreflectors located near the opposite edges of the secondary mirror and are reflected back along the optical path to the metrology housing (Fig. 6).

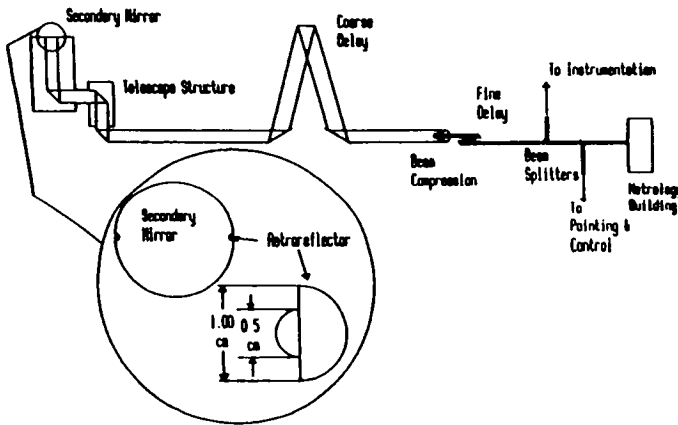


Fig. 6 Optical delay path metrology

The baseline metrology (BM) provides accurate measurements of each telescope's position (with μm precision) and orientation. This can be accomplished by combining measurements from an upgraded Mark III - type laser system located at the base of each telescope with nominal baseline measurements made from three metrology towers.

Pointing and Control

LOLA array employs pupil plane interferometry which allows to significantly relax the requirements on accuracy of the pointing the telescopes during most of the observational tasks except for astrometry and the planet detection using destructive interference to cancel the parent star light. The schematic of the pointing and control system is shown in Fig. 7.

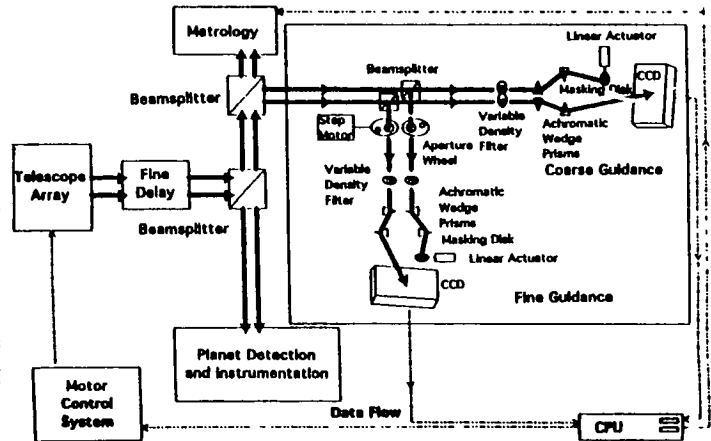


Fig. 7 Pointing and control schematic

Instrumentation

There are four scientific instruments for imaging and spectroscopic analysis over a spectral range from about 200 nm to $10\ \mu\text{m}$, and a module system for IR planet detection. The lower wavelength limit of about 200 nm is imposed by several factors including the attainable quality of optical components and the problems with maintaining high UV throughput through the large number of reflections. The upper limit of $10\ \mu\text{m}$ is produced by thermal emissions of the optical components (assumed to be kept near 70 K during the lunar night) and diffraction effects. The instruments and their spectral regions are:

UV Imager	200 nm - 300 nm
UV - Visible-IR Imager	200 nm - $1\ \mu\text{m}$
UV-Visible-IR Spectrometer	200 nm - $1\ \mu\text{m}$
IR Imager/Spectrometer	$1\ \mu\text{m}$ - $10\ \mu\text{m}$

The field of view for the instruments may be varied from 15 arcsec down to 10^{-3} arcsec through 27 focusing aperture wheels located downstream of the beam splitter.

These instruments are contained in a cylindrical carousel which can be rotated to position any of the four instruments in the beam path from the beam combining optics. Normally, the carousel will be held fixed on one instrument. A semi-concurrent use of two or three instruments may be accomplished by rotating the carousel between the selected instruments, for instance every 60 sec, and multiplexing to the computer system.

The instrumentation housing is covered by a 5 m thick blanket of compacted regolith and provides shielding from lunar dust, micrometeoroid impacts, radiation, and the thermal extremes of the lunar day.

Thermal Control

To detect IR signals at wavelengths up to 10 μm , all elements in the optical path must be maintained at a temperature of 77K or lower. Without either passive or active cooling, this temperature cannot be reached during the lunar night. In the Large Lunar Telescope study⁶ it was estimated that 98% of the radiative heat transfer from the regolith to the structure occurred within a 100 m radius of the telescope. This result was utilized in the heat transfer analysis of the LOLA telescope. To provide passive cooling during the lunar night, the telescope is wrapped with a Teflon multilayer insulation (MLI). Additional passive cooling is provided through the use of 30-layer, 5 mm thick MLI surface radiation shield which surrounds the base of the telescope with an outer radius of 7 m and an inner radius of 1 m.

Lunar-day thermal protection for each telescope is provided by a collapsible, hemispherical dome having a radius of 7 m and using aluminized Teflon MLI. The dome also protects the telescope from dust contamination and provides limited protection from micrometeoroid impacts.

Both active and passive systems are needed for thermal control of instrumentation. An active system is employed to cool the IR Imager/Spectrometer, while passive systems are used for the other instruments. The active system may be modeled after the cryogenic (liquid helium) cooling techniques applied on the Space Infrared Telescope Facility (SIRTF) or, alternatively, a closed loop mechanical system proposed for the Large Lunar Telescope⁶ can be used. The other instruments may be maintained at or below 300 K and can be cooled by a passive heat pipe system. Because the floor and walls of the instrumentation room will remain at a constant temperature of around 250 K, the heat pipes can utilize the regolith as a heat sink.

Communications

The communications network consists of the lunar communication center, the lunar relay satellite and the Earth-based Deep Space Network. Three network options were studied: (a) a lunar surface link from the observatory to a near-side direct transmitter, (b) three satellites in polar orbits at 120 degrees intervals, and (c) one satellite placed in a halo orbit. The halo orbit relay satellite orbiting the L2 libration point was chosen as a practical, cost-effective solution for the far-side, real time continuous communications and data transfers.

The communication system operates in the X-band and provides 100 Mbps downlink (9 GHz) and 50 Mbps uplink (10 GHz) data rate (Fig. 8). Should the data rate requirement increase to over 350 Mbps after compression, a Ku-band would be necessary and possibly a dedicated network of LEO satellites similar to Advanced Tracking and Data Relay Satellite System (ATDRSS).

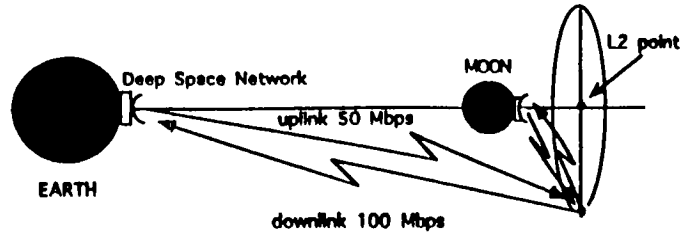


Fig. 8 Communications Scheme

Power

Three types of power systems were investigated to provide 10 kW electrical power required for LOLA's operation: solar array/regenerative fuel cells, dynamic isotope power system (DIPS), and the Topaz II nuclear reactor. The DIPS using plutonium 238 as the heat source in a closed Brayton cycle was selected as the most attractive candidate.

The aluminum transmission lines (1000 V) will be buried to a depth of at least 10 cm. This should significantly reduce exposure to temperature variations and radiation dosage. To connect all the array telescopes and the power supply approximately 14 km of lines will be needed. Two main power converters will serve to divide and regulate the power.

Launch and Transfer to Lunar Surface

The total weight to orbit required for the LOLA project is estimated at 253 mt, which includes 83,500 kg of the LOLA array systems as well as the weights of the Lunar Transfer Vehicle (LTV), Lunar Excursion Vehicle (LEV), lunar construction vehicles and fuel tanks. After comparing various options for cargo transfer to the lunar surface, it is proposed to launch the LOLA into LEO by two Shuttle C Blk II's (7.6 m shroud X 27.4 m payload envelope and a 61,000 kg capacity) and two Shuttle C's (4.6 m shroud x 25 m payload envelope and 71,000 kg capacity). A single LTV/LEV transfer vehicle hauls the LOLA cargo from LEO to LLO (Low Lunar Orbit). The LTV drops its expended fuel tanks, the LTV and LEV detach, and the LEV descends on the lunar surface.

Construction

The construction of the LOLA will take place in two phases. The first phase will establish the power system, the central station, the communications, and 9 telescopes. The array will operate on a limited scale until the second phase brings 18 additional telescopes.

The build-up strategy for the first phase has three stages: site preparation, assembly, and calibration. The LOLA report outlines a plan and a time table for the entire construction process of the array, identifies the necessary vehicles, machinery and equipment, and gives workload estimates for all major operations. Also included is brief discussion of routine system checks, alignment adjustments, and replacement of degraded equipment during the yearly maintenance operations. The LOLA is designed to be fully operational by 2010.

LOITA: LUNAR OPTICAL/INFRARED TELESCOPE ARRAY

Geoffrey Pierce and Neil Thomas (team leaders), Set Chiaramonte, Sheri Davis, David Grubb, Brian Hartt, Marc Luek, Timothy Mahoney, Kevin Martin, Kelly Matney, Scott Schorn, Gregory Sheppard, and Kevin Wood.

Overall Configuration

The LOITA team proposes a circular array providing the maximum baseline of 5 km and consisting of 18 unevenly spaced telescopes as shown in Fig. 9. Resolution of an Earth-like planet at 10 parsec away (initial NASA requirement) in visible light (500 nm) requires a baseline of 10 km. To keep the cost and complexity of the facility at manageable levels, the 5 km max baseline was selected for LOITA. This will still permit resolution of planets around hundreds of nearby stars, including Earth-like planets at distances up to 5 parsec.

The circular arrangement of the telescopes was primarily determined by the u-v coverage studies. A carefully selected, unevenly spaced circular design may be superior to the conventional Y-type configuration, providing a good tapered sampling density from the center to the edge and a near circular region of coverage.

The required combined collecting area of the array was determined through analysis of signal-to-noise (S/N) ratio and collecting area required for detecting planets at different distances using various wavelengths and observation times. This analysis was carried for a similar set of assumptions as those used in the LOLA project. Figure 10 shows that for an S/N of 10, the total collecting area (assuming CCD efficiency of 70%) of 38.5 m² is needed to detect an Earth-like planet at 5 parsec away with an exposure of 3 days at 500 nm.

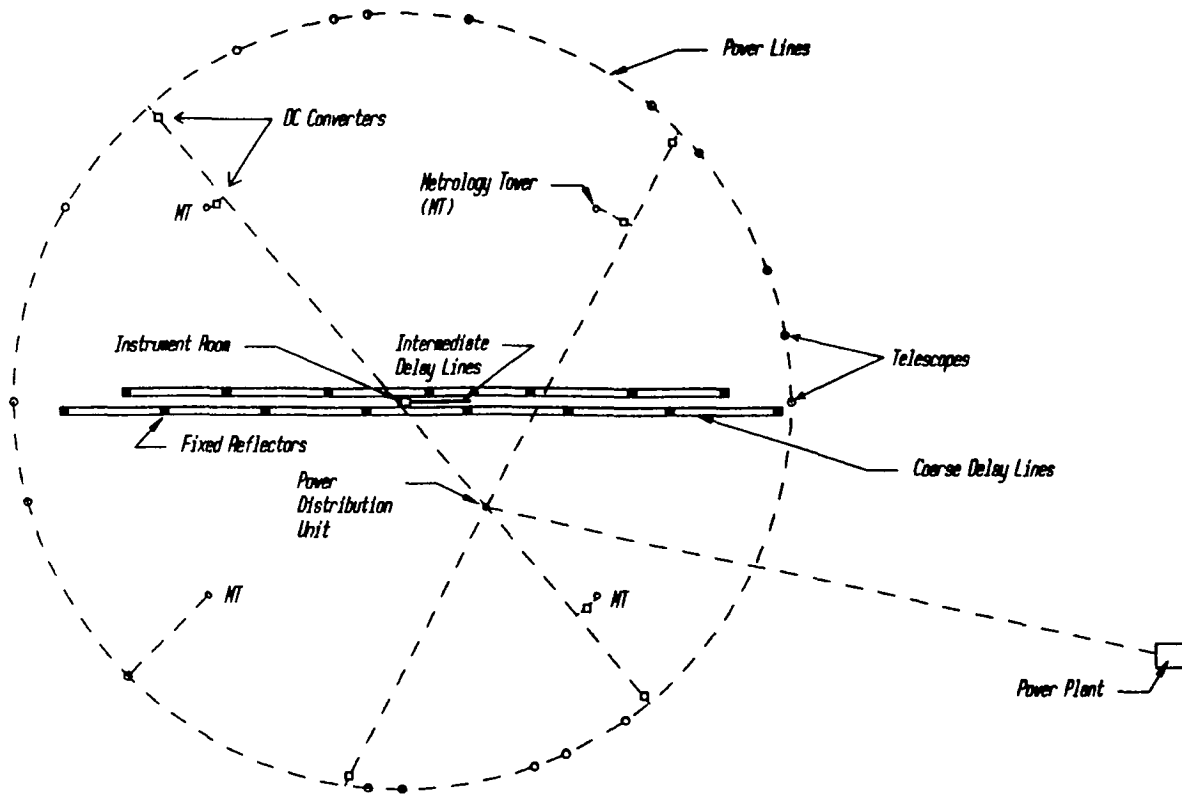


Fig. 9 LOITA array layout

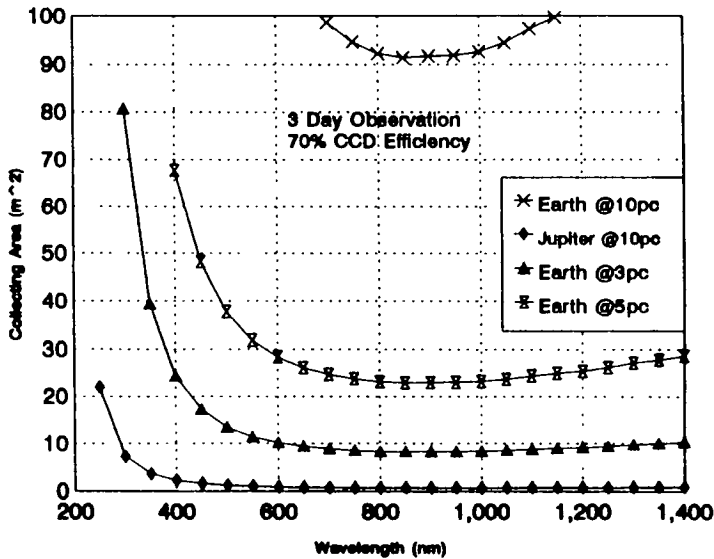


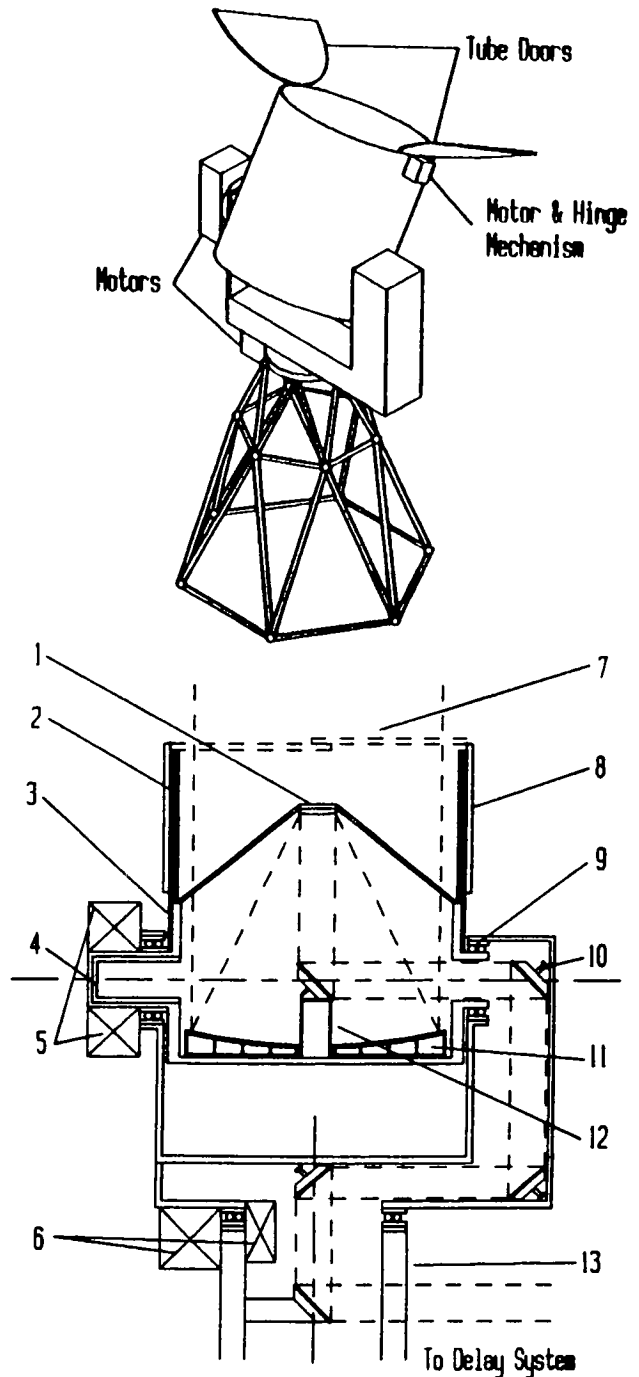
Fig. 10 Array collecting area vs wavelength

The telescope primary mirror of 1.75 m was selected through the use of a mass minimization trade-off study. The number of the telescopes (18) and the final collecting area of 42.5 m² resulted from considerations of u-v coverage and the area blocked by the secondary mirror (24 cm diameter). The observable spectrum of the array extends from 200 nm to 10 μm.

The LOITA array will be constructed in three phases. The first (initial) phase will establish 6 telescopes, the power system, communications, and the central control/instrumentation station, allowing the initial operation of the array. The second and third phases will each emplace six additional telescopes.

Optical Train

The telescope (Fig. 11) uses a standard Cassegrain design with paraboloidal primary and secondary mirrors. The telescope creates an afocal beam which will be able to propagate across path lengths up to 7.5 km with only small losses in fringe visibility due to diffraction. Once reflected off the secondary mirror, the beam is bounced through four reflections to the telescope base and then enters the delay lines. To maintain signal polarization, the delay lines are designed such that each beam strikes the same number of mirrors and is



- | | |
|------------------------------|---|
| 1. Secondary Mirror | 8. Shield Door |
| 2. Thermal Shielding (MLI) | 9. Bearing |
| 3. Al Radiation/Light Shield | 10. Mirror Mount With Ceramic Actuators |
| 4. Thermal Insulation | 11. Primary Mirror |
| 5 & 6. Fast & Slow Actuators | 12. Light Baffle/Mirror Support |
| 7. Door in Closed Position | 13. Base Support Leg |

Fig. 11 LOITA telescope

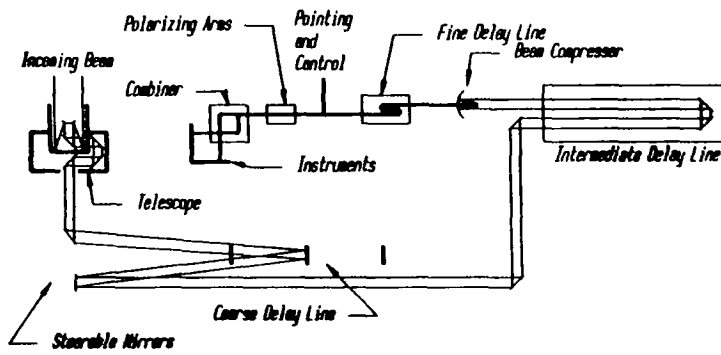


Fig. 12 Optical delay lines

deflected through the same angles. The maximum path difference which must be removed is about 7.5 km. This task is accomplished by a three-tiered delay system: coarse, intermediate, and fine (Fig. 12). The coarse delay lines arranged in two east-west bands reduce the path difference to within 600 m. The intermediate delay lines reduce path length difference to less than 2 m. The fine delay system uses beam compression to a diameter of 2 cm and positionable reflectors controlled to nm accuracy. The beams leaving the delay system encounter a beamsplitter which bleeds off approximately 7% of the light to the pointing and control system. The remaining light enters the beam combiner and is directed to the various detectors.

Beam Combiners and Instruments

LOITA will accommodate beam combiners/instruments for imaging, direct planet detection, and astrometry.

Imaging

The first approach to wide-field imaging will use fixed mirrors and beam splitters to equally divide each of the eighteen incoming parallel beams into pairs of beams (Fig. 13). An arrangement of beam splitters/combiners movable to preset locations provides a means for interfering any beam with any other beam. There may be two such combiners: one designed to process the beams in the wavelength range of 200 - 1100 nm, and the other coated for the range from 1 to 10 μm . The second approach will use more complicated schemes for combining three or more beams for closure phase imaging. Beams leaving the combiner are directed via prismatic deflectors into various instruments/detectors.

LOITA will utilize pupil plane interferometry which offers a variety of detection schemes. Fringe detection and visibility measurements can be most easily accomplished in the pupil plane because imaging the fringes in that plane allows increased tolerance to the path length errors. Note that

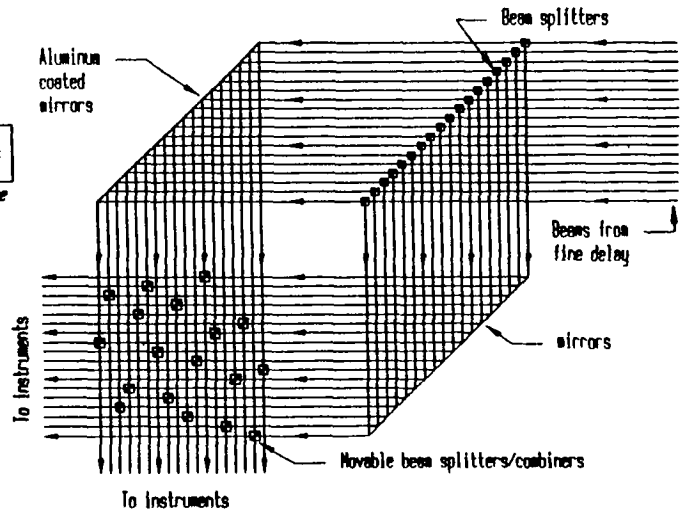


Fig. 13 Beam combiner

in order to resolve fringes in the focal plane of a system with a focal length f , it must be possible to resolve a distance of $f\lambda/B$, where B is the baseline length. Assuming 4 μm pixel size, resolving fringes at 500 nm would require an $f=40$ km!

For imaging and spectroscopic analysis, LOITA instruments/detectors will be specialized for the spectral ranges of 200-400 nm (UV), 400 nm - 1 μm (visible - near IR), and 1 μm - 10 μm (IR). The field of view (FOV) will vary from a few arcsec to around 1 milliarcsec depending on the bandwidth of the detected signals ($\text{FOV} \sim (\lambda/\Delta\lambda)(\lambda/B)$). Very large format CCDs will be needed for the wide-field imaging. A 1 arcsec field in the visible light (20 microarcsec resolution) will require $50,000^2$ pixels. Assuming 4 μm pixels, the detector size will be at least 20 x 20 cm and it will be constructed as a mosaic (at least in the east-west direction) of monolithic CCD detectors. To minimize gaps in sky coverage due to inevitable small spacings between CCDs, the largest possible CCDs ($10,000^2$ or larger) will be utilized. To accommodate possible field curvature introduced by the optics in the image forming plane, the CCDs can be bent. To maintain reasonable readout times, multiple simultaneous outputs will be incorporated. Because the interferometer angular resolution is reduced in the infrared, the IR detectors will need fewer pixels. At 10 μm , the 4 arcsec field requires $10,000^2$ pixels.

Direct Planet Detection

The beam combiner for the direct detection of the extra-solar planets will employ a scheme devised by Shao and Colavita⁸. Their design is based on a concept of starlight suppression using a combination of a four-element polarization-compensated achromatic nulling interferometer and single-mode spatial filters. Very deep nulling of the starlight

is achieved by interference of four wavefronts. Single-mode optical fibers are used to clean up the wavefront by removing light scattered from imperfections in the surface of the optics. Such a system would be able to achieve starlight cancellation at a level of 10^8 enabling it to detect in the IR Earth-size planets orbiting nearby stars. For detection at a wavelength of $10 \mu\text{m}$, the required pointing/tracking accuracy will be 40 microarcsec (10% of the angular resolution).

Astrometry

For astrometry, the LOITA interferometer has the potential to provide extremely high accuracies approaching 0.1 microarcsec. Achieving this level of astrometric accuracy with a 5 km interferometer will require: (a) 2.5 nm accuracy in baseline measurements, (b) maintaining the angle between the telescopes used for astrometry to 0.1 microarcsec accuracy, and (c) extreme precision in fabrication and assembly of retroreflectors and optical components involved in the path length and baseline metrology. Therefore, the interferometers selected for astrometry would be furnished with specialized metrology and tracking/pointing systems and/or optical components capable of providing required levels of accuracy. Development of these systems entails significant technical challenges.

Wide-angle astrometry will use three or more connected interferometer baselines and a dedicated pupil-plane beam combiner. The phase and amplitude of the fringes will be measured using path length modulation over a wavelength in one interferometer leg. The detectors will be broad-band photon counters (avalanche diodes). It may be pointed out that 0.1 microarcsec astrometric accuracy should allow an indirect detection of an Earth/Sun - like system up to a distance of 12 parsec.

Single Telescope Option

One of the telescopes will be capable of an optional operation in complete independence of the array. The telescope will perform direct imaging in the focal plane after removal of the tertiary (fold) mirror. The instruments would be housed beneath the primary mirror. The telescope would offer significantly better performance than the Hubble Space Telescope because of the excellent stability, long observation times and improved pointing/tracking capability allowed by the lunar location. Conceivably, this telescope could even detect large planets around nearby stars by using long exposures, photon-counting mode, coronagraphic masks and electronic image subtraction when the telescope is rotated about its optical axis to various angles on the detector. The process of image subtraction would remove the pattern of stray light while leaving the planet image at various angles corresponding to those at which exposures were made.

Metrology

LOITA utilizes interferometric internal metrology to control equality of the optical path lengths from each telescope through the delay lines and on to the beam combiner. Maintaining the path lengths within three or less wavelengths should provide adequate fringes for quality image reconstruction through Fourier analysis of the combined light beams. A system using a 600 nm laser with instabilities below 10^{-12} will be capable of equalizing path length to less than $\lambda/5$. The internal metrology will utilize small hemispherical retroreflectors placed in the center of the secondary mirror of each telescope.

The external metrology system establishes the topocentric baseline vectors of every possible pair of telescopes. These baseline vectors are constantly changing in the celestial sphere as the moon rotates relative to the observed source. Ergo, on exact determination of these baseline vectors will be required for u-v plane analysis. The accuracy of the measurements will be less stringent than the accuracy required for internal metrology. Four metrology towers will be positioned within the circular array and a single hemispherical retroreflector (8 cm diameter) will be placed on the base of each telescope (Fig. 14).

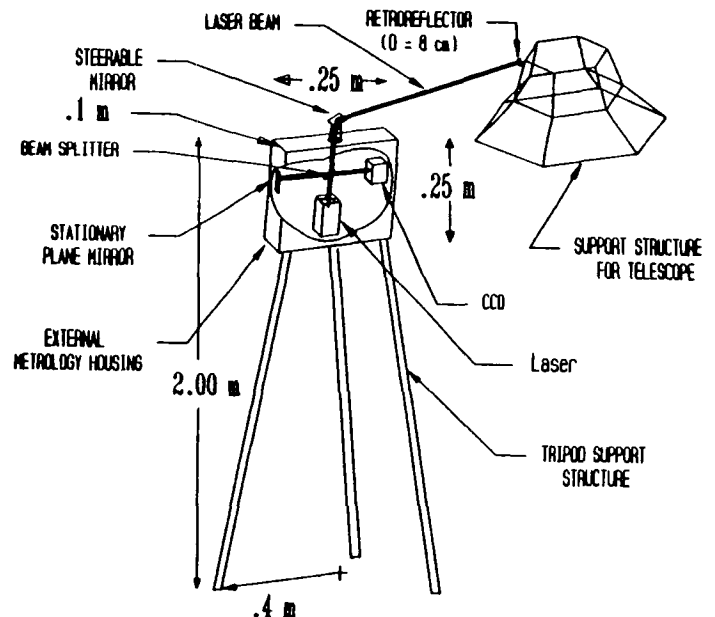


Fig. 14 External metrology tower

The three (or more) telescope pairs selected for astrometry will require significantly higher accuracies of measurements of the path lengths, baselines, and telescope orientations (see Beam Combiners and Instruments). These telescopes will be provided with specially developed metrology systems.

Pointing and Control

For many observational tasks, the pointing and control accuracy of 10^{-5} arcsec or even 10^{-4} arcsec will be adequate. However, astrometric measurements impose a very stringent requirement of sub-microarcsec accuracy. For the acquisition of the initial target coordinates, the control system must maneuver each telescope in a combined 180° base rotation and 80° vertical rotation in 15 minutes. The pointing and control system is driven by a control command center which also serves as an interface between ground control and the telescope array. The objectives of the fine pointing are met through the use of a special charge coupled device (CCD) image sensor-driven system to detect the pointing error, incremental updating of the predetermined tracking rates of the telescopes (through the motor driven mechanisms) and/or adjusting the two steerable mirrors in the coarse delay system. A simplified diagram of the pointing and control system is given in Fig. 15.

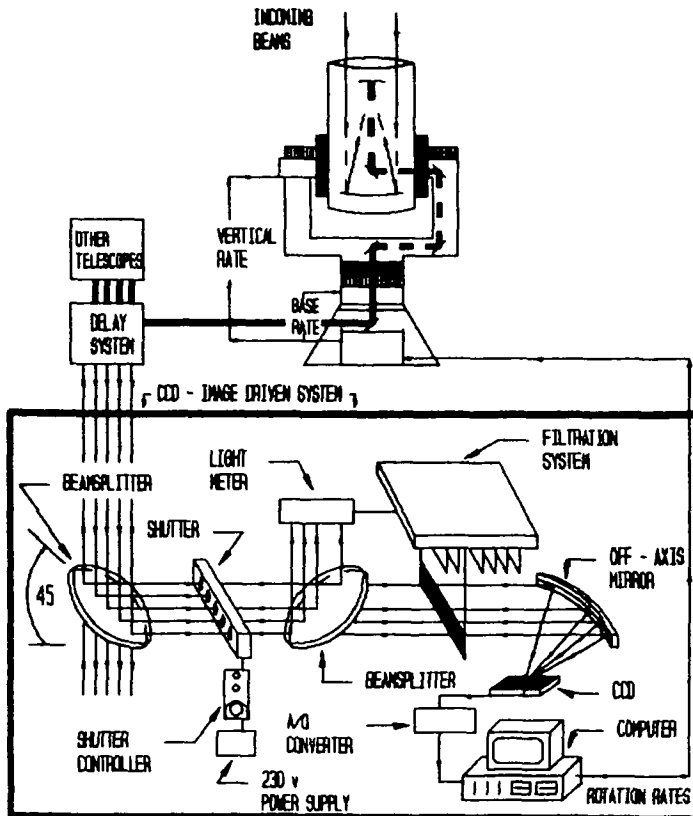


Fig. 15 Pointing and control schematic

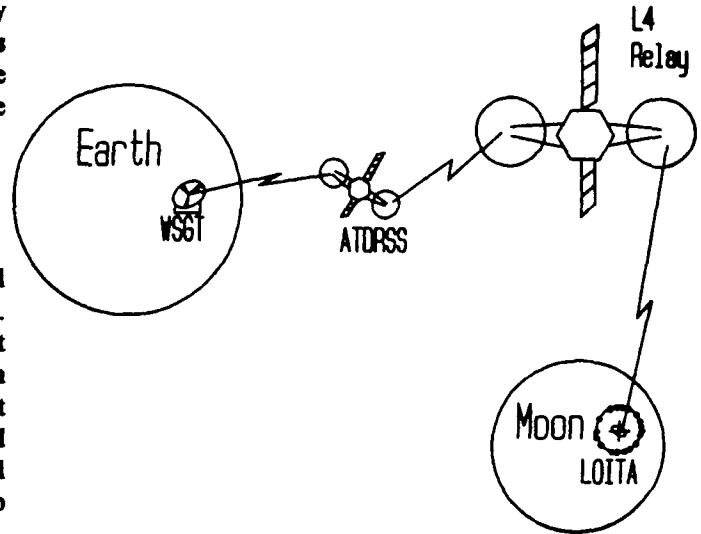


Fig. 16 LOITA communications scheme

To achieve sub-microarcsec accuracy required by astrometry, a parallel interferometer sharing the optical path of the astrometric interferometer can be used to track the target. The system would require a bright unresolved counterpart.

Communications

Several schemes for a communication link with ground were examined: (a) one low-altitude lunar satellite, (b) three mid-altitude lunar satellites, (c) one geostationary lunar satellite, and (d) a satellite placed at either L2 or L4 libration point. The L4 was judged to be the optimal location for the relay satellite between LOITA and the Earth. The relay will be used in conjunction with the Advanced Tracking and Data Relay Satellite System (ATDRSS) and operate in the Ka-band (Fig. 18). The system will be able to handle the massive amount of data collected during observations. The data rate may range from 50 Mbps to perhaps as high as 250 Mbps.

Power

The power required to operate LOITA is estimated at about 10 kW. The following power sources were examined as possible candidates: a scaled-down SP-100 nuclear power, Soviet Topaz reactor, and photovoltaic solar arrays. A 15 kW scaled-down version of SP-100 was chosen to power LOITA for a duration of 10 years, providing large margin for any contingencies. The aluminum transmission lines will be deployed at a depth of about 10 cm.

Telescope Structure

The telescope design is schematically shown in Fig. 11. The cylindrical tube housing the primary and secondary mirrors is supported by a fork-type mount which in turn is supported by a truss base. The alt-az fork mount utilizes existing technology with proven reliability and minimal maintenance. It also provides a rigid structure which can be passively balanced. A graphite epoxy composite was selected as the primary structural material for the telescope. Among several properties, the low coefficient of thermal expansion and high stiffness of the graphite epoxy composite were considered particularly important as the precise alignment of the optical components demands that the structural members supporting the primary and secondary mirrors do not deflect more than about 3 nm. Structural analysis was carried out for all major elements of the telescope.

The telescope tube structure will be comprised of the structural graphite epoxy mirror mount, tubing from the primary to secondary and primary to stationary exit mirrors. An aluminum shell will protect the optics from dust and radiation, as well as shield the aperture from stray light. Affixed to the end of the cylinder tube will be a graphite epoxy aperture door.

To meet the stringent pointing accuracy requirement, specially developed motors will be needed, one set for fast and slow azimuth rotation and one for fast and slow elevation. Among possible options, low power direct drive DC torquing motors may be considered.

Instrument Room

The line delay system, scientific instruments and detectors, computers and communication equipment are housed within the instrument room which is made up of two level structure (Fig. 17). The structure will be made of aluminum and it will be covered with a thick layer of lunar soil.

Thermal Control

An approximate thermal analysis was used to determine: (a) the equilibrium temperature of the telescope structure for both lunar day and night with and without the use of radiation shields, and (b) transient temperature of the telescope structure throughout the lunar cycle. The results of this analysis led to selection of the exterior surface coatings (magnesium oxide aluminum oxide paint) and radiation shielding allowing the telescope temperature to remain near or below 70 K during night.

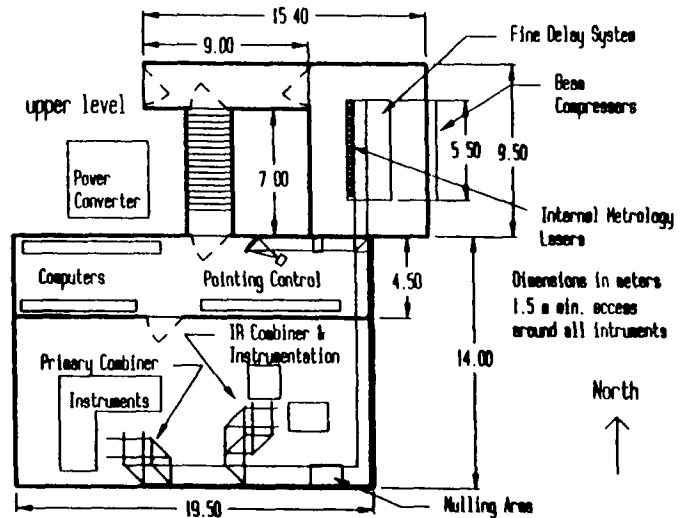


Fig. 17 Instrument room floor plan

To cool optical components and several instruments housed in the instrument room, four cooling modules based on the Stirling cycle are proposed. Each module works by coupling cold hydrogen gas to a copper plate within the instrument box through stainless steel heat pipes utilizing nitrogen. The copper plate is maintained at a temperature of 70 K. All instruments within the casing are thermally coupled to the copper plate. As a thermal sink, another stainless steel heat pipe using Freon-12 and operating at 295 K is coupled to 300 K hydrogen gas. This pipe radiates heat into the 250 K housing environment. To eliminate vibrations, the Stirling refrigerator is isolated by elastic seals and an additional heat exchanger.

Launch, Construction and Cost

The total mass of the array and its supporting systems required for the initial operation (phase 1) is 59,000 kg. The total mass of the fully assembled array (phase 3) is 77,000 kg.

Launch scenario is based on three basic requirements. First, the manned space station (SSF) must be operational and useful as a transfer point for lunar transit. Second, a heavy lift vehicle (HLV) capable of launching a 70,000 kg payload must be operational. Third, a new lunar lander and a lunar excursion vehicle (LEV) must be developed. The proposed launch and transfer to lunar surface sequence for the construction and initial operation of LOITA (phase 1) includes a total of 12 launches or transfers using Atlas II/Centaur, Titan IV/Centaur, Shuttle, HLV and LEV. All sensitive equipment, including the telescopes is first transferred to SSF. Once at SSF, the equipment could be examined for any damage and any necessary repair could be made. Astronauts would not be

placed on the lunar surface until all equipment was in place.

Construction and assembly scheme will be designed to minimize the necessary man-hours and equipment, thereby reducing cost. The major equipment will consist of a personnel and pressurized rovers, and a utility vehicle. Construction will be a seven-phase endeavor: (1) start up, (2) power activation, (3) instrument room, (4) telescopes, (5) delay lines, (6) metrology towers, and (7) testing.

Cost analysis started from creating a Work Breakdown Structure (WBS). The WBS serves as an outline of the LOITA program from construction through operations. The LOITA program was broken into 9 primary areas. As with any space-born system, the primary cost incurred is due to transportation. In this analysis, launch/transfer costs are assumed to be \$10,000/kg. Labor costs on the moon are assumed \$440/h (due to EVA). The estimated initial cost of LOITA (Phase 1) is \$8.9 billion which includes \$5 billion for research and development.

References

1. Burke, B., "VLBI at Optical and Radio Wavelengths," European Space Agency paper SP-226, Proceedings of the Colloquium on Optical Arrays in Space, 1985, pp. 177-183.
2. Simon, R., et al, "Big Optical Array: An Imaging Interferometer," Naval Research Laboratory, 1990, pp. 4-6.
3. Labeyrie, A., Lemaitre, G., Thom, C., and Vakili, F., "Steps Toward an Optical Very Large Array," pp. 669-693.
4. Colavita, M., "A Strawman Lunar Interferometer," Presented at the JPL Workshop on Technologies for Space Interferometry, 1990, pp. 233-242.
5. Burke, B. F., "Astronomical Interferometry on the Moon," Mendell, ed., Lunar Bases, pp. 281-291.
6. Large Lunar Telescope (LLT) Report, LLT-001, NASA Marshall Space Flight Center, March 1991.
7. Colavita, M. M., Shao, M., Hines, B. E., Levine, B. M., and Gershman, R., "Optical System Design for a Lunar Optical Interferometer," SPIE Conference 1494, 1991.
8. Shao, M. and Colavita, M.M., "Long-baseline Optical and Infrared Stellar Interferometry," Annual Reviews Astron. Astrophys., 1992, 30, pp. 457-498.

**PROJECT HYREUS: MARS SAMPLE RETURN MISSION
UTILIZING *IN SITU* PROPELLANT PRODUCTION**

University of Washington
Department of Aeronautics and Astronautics
Seattle, Washington

Professor A.P. Bruckner

Brian Thill, Teaching Assistant

Anita Abrego, Amber Koch, Ross Kruse, Heather Nicholson,
Laurie Nill, Heidi Schubert, Eric Schug, Brian Smith, Keith Stokke, Pat Sweeney,
Lee Thrush, Dave VanNoy, Leo Warmuth, Richard Warwick, Andre Williams, Mark Yee

Abstract

Project Hyreus is an unmanned Mars sample return mission that utilizes propellants manufactured *in situ* from the Martian atmosphere for the return voyage. A key goal of the mission is to demonstrate the considerable benefits of using indigenous resources and to test the viability of this approach as a precursor to manned Mars missions. The techniques, materials, and equipment used in Project Hyreus represent those that are currently available or that could be developed and readied in time for the proposed launch date in 2003. Project Hyreus includes such features as a Mars-orbiting satellite equipped with ground-penetrating radar, a large rover capable of sample gathering and detailed surface investigations, and a planetary science array to perform on-site research before samples are returned to Earth. Project Hyreus calls for the Mars Landing Vehicle to land in the Mangala Valles region of Mars, where it will remain for approximately 1.5 years. Methane and oxygen propellant for the Earth return voyage will be produced using carbon dioxide from the Martian atmosphere and a small supply of hydrogen brought from Earth. This process is key to returning a large Martian sample to Earth with a single Earth launch.

Introduction

Project Hyreus is an unmanned Mars sample return mission that utilizes *in situ* propellant production to reduce the amount of mass that needs to be launched from Earth. In other words, the propellant necessary for the return trip is produced using materials from the Martian environment. The demonstration of propellant production from indigenous sources is an important precursor to manned missions to Mars. In addition to demonstrating the technology of *in situ* propellant production, the unmanned return of Martian soil/rock samples will prove invaluable for scientific discovery.

From the time of fictional stories about Martian life forms to the excellent photo surveys performed by the

Mariner and Viking spacecraft, and to the current Mars Observer mission, human interest in Mars has remained strong. The Mars Observer mission started a new phase in Martian exploration that will continue with Mesur, ESA's Marsnet, and Russia's Mars 94 missions. Eventually, these missions will lead to successful manned exploration of Mars.

The idea to use *in situ* propellants for a Mars direct mission approach as presented by Zubrin^{1,2} could drastically reduce mission costs; thus expediting a manned mission. Project Hyreus takes the technology of *in situ* propellant production and places it in a cost effective mission scenario that lays the groundwork for advancements in future missions to Mars.

In 1992, the NASA/USRA design team from the University of Washington presented Project Minerva.³ This proposal called for a series of manned expeditions to Mars which would rely on propellant produced from the Martian atmosphere and a supply of imported hydrogen. A cost analysis of this mission design indicated that its cost would be approximately 55 billion dollars, i.e., 10% of the conventional missions that NASA has been studying. Even the much reduced cost of such a mission would represent a very large national investment, in terms of money, resources, time, and personnel. Therefore, an unmanned precursor mission should be performed to prove the viability of this mission architecture. Project Hyreus is a proposal for such a mission.

The two primary mission goals of project Hyreus are successfully delivering a large Martian soil sample to Earth and demonstrating that *in situ* propellant production allows a significantly larger payload mass than traditional sample return missions. In addition to the primary mission goals several other goals exist. These include: learning more about the Martian environment, determining if and where water exists on Mars, and showing that *in situ* propellant production leads to significantly lower mission costs than traditional mission methods.

The Project Hyreus mission goals are accomplished through the following: a rover is placed on Mars to explore the area around the landing site using a variety of attachments such as scoopers and manipulator arms to collect the samples for the sample return. The rover also carries an assortment of scientific instruments for non-sample return related studies. Additional scientific instruments are mounted directly on the Mars Landing Vehicle (MLV). A satellite with a ground penetrating radar (GPR) system is placed in sun-synchronous orbit around Mars. The GPR is used to explore the Martian subsurface landscape and detect any available underground sources of water/ice. In addition, the satellite's payload includes communication and weather-monitoring systems.

The mission scenario (Fig. 1) begins with a single Titan IV launch of both the spacecraft and a Centaur upper stage into low Earth orbit (LEO). The Centaur then injects the MLV into a transfer orbit to Mars. The MLV is equipped with a raked-cone aerobrake. The vehicle is slowed into a low Mars orbit (LMO) through aerobraking maneuvers, during which time the satellite is released into Mars orbit. Additional aerobraking maneuvers are used to slow the MLV sufficiently to deploy parachutes. Retro-rockets are used to perform the final soft landing maneuver in the Mangala Valles region.

Once the MLV is in place, the Mars surface portion of the mission begins. The propellant production plant is activated and begins producing fuel and oxidizer for the rover and for the return trip. Through a coupled Sabatier and electrolysis process methane and oxygen are produced by reacting carbon dioxide from the Martian atmosphere with liquid hydrogen imported from the Earth. The product gases are liquefied and stored in the initially empty tanks of the Earth return vehicle (ERV). Rover surface missions are begun once sufficient amounts of methane and oxygen have been produced to meet the needs of the rover's methane-burning thermophotovoltaic power system. The rover then explores the Martian surface, gathering rock and soil samples. Scientific experiments are conducted throughout the stay time on Mars and approximately 25-30 kg of soil and rock samples are collected.

Approximately 1.5 years after arrival, the ERV launches from the MLV support structure and returns for Earth. The ERV is a single-stage vehicle which first ascends into LMO, and then performs the burn that places it in the Earth transfer orbit. Once the vehicle reaches the vicinity of Earth the payload capsule detaches and performs an aerocapture maneuver in the atmosphere. The ERV itself continues on a hyperbolic trajectory back to deep space. The payload

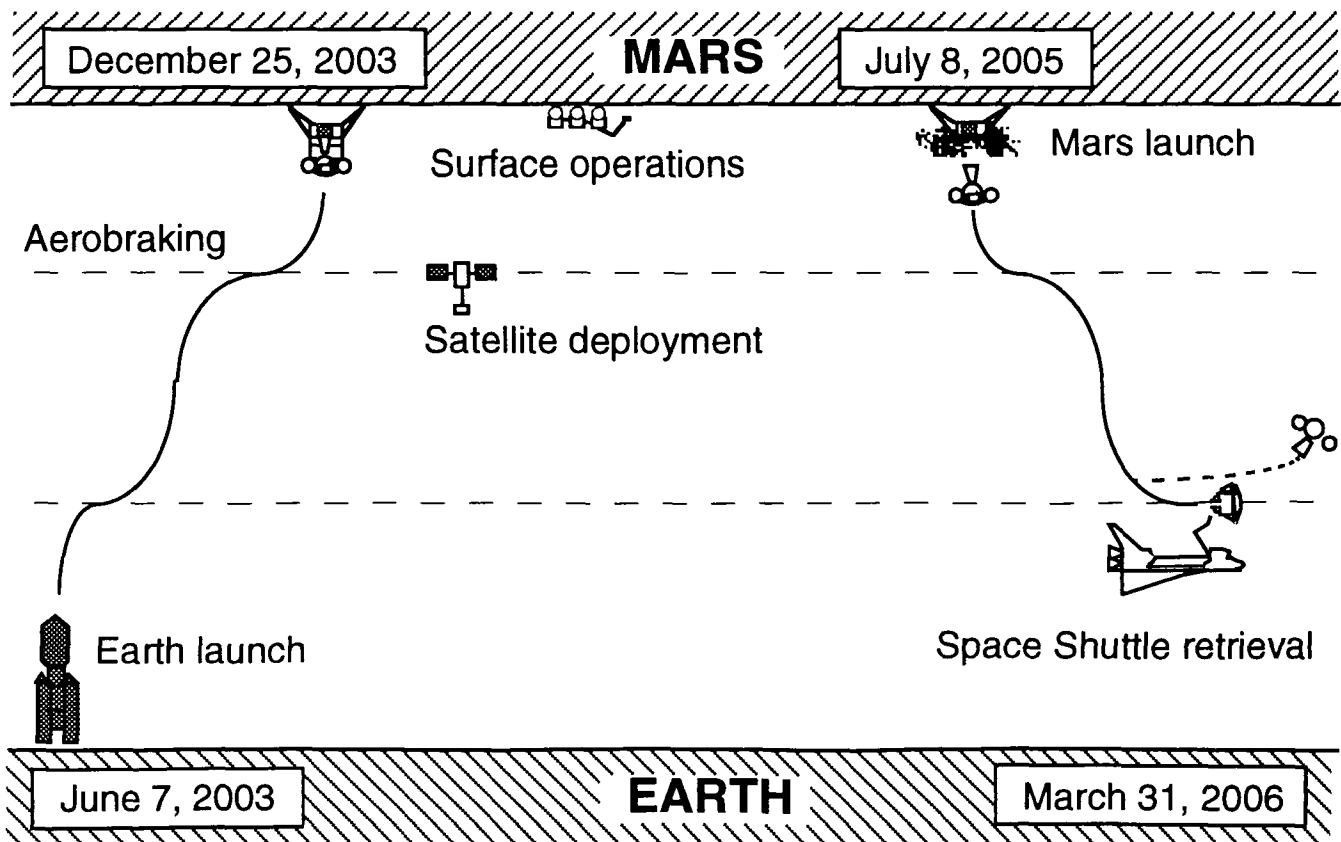


Fig. 1 Project Hyreus mission summary

capsule's orbit is circularized to LEO, by aerobraking and a rocket burn, where it is subsequently retrieved.

Project Hyreus' mission architecture and main components are presented here in the following format: The design and configuration of the MLV and ERV are discussed first. Next, the launch system, astrodynamics, and aerobraking/landing aspects of the mission are presented. Then, Martian surface operations are discussed: propellant production, planetary science, rover, satellite. Lastly, the Earth return scenario and conclusions are given.

Vehicle Design

The vehicle is composed of two main parts: the MLV and ERV. The ERV is actually part of the MLV until it detaches during Mars launch back to Earth. The configuration and structure of both vehicles are discussed concurrently in the following section. In addition, the landing engines and reaction control system (RCS) on the MLV and the methane rocket engine on the ERV are described. The masses of the major components are shown in Table 1.

Table 1 MLV component masses

Component	Mass (kg)
Truss Structure (MLV & ERV)	700
MLV Thrust Structure	60
Centaur Adapter	160
Mars Aerobrake	735
Landing Engines	75
Landing Propellant Tanks	10
Landing Propellant	300
Landing Gear	62
Parachutes	250
Propellant Plant	385
Power and Control	530
Radiators	60
H ₂ Tank	55
Seed H ₂	158
Science Equipment	230
Sample Loading Arm	8
Rover	200
Satellite	280
ERV Thrust Structure	100
Earth Aerobrake	37
ERV Engines	100
ERV Propellant Tanks	55
Payload Module	100
Total	4650

Configuration

Figures 2 and 3 show the configuration of the MLV. It consists of a central truss frame with necessary equipment mounted where needed. The location of the payload within

the spacecraft is determined by several requirements: to achieve a suitable vehicle center of mass location, to keep all payload within the aerobrake envelope, to place certain components in close proximity, and to minimize launch fairing size. The center of mass of the MLV should be as close to the centerline of thrust as possible, in order to minimize control problems. It should also be as close to the Centaur interface plane as possible to avoid having to use a structural upgrade on the Centaur. The payload must all be contained within the aerobrake (not shown, for clarity) in order to be shielded from the heat of atmospheric entry at Mars. Certain components must be kept close to each other because of their interaction. One example is that the seed hydrogen tank should be kept close to the propellant manufacturing plant, in order to minimize piping.

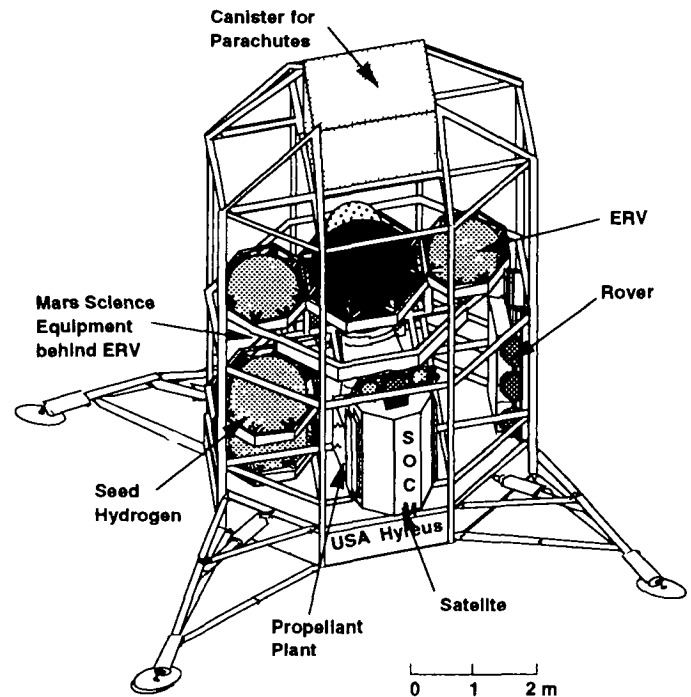


Fig. 2 Isometric view of MLV, with radiators and aerobrake deleted for clarity

The payload of the MLV is located in two main sections. These sections can be seen in Fig. 3, labeled A-A and B-B. Centered around the space that the ascent engine of the ERV occupies, the lower section (B-B) contains the propellant manufacturing plant, the satellite, the Mars science equipment, the seed hydrogen tank, and the rover. These four components are similar in mass and therefore are fairly well balanced. The upper section (A-A) contains the Dynamic Isotope Power Source (DIPS) and the ERV. The configuration of the ERV is discussed below. The parachutes for landing on Mars are located at the top of the vehicle.

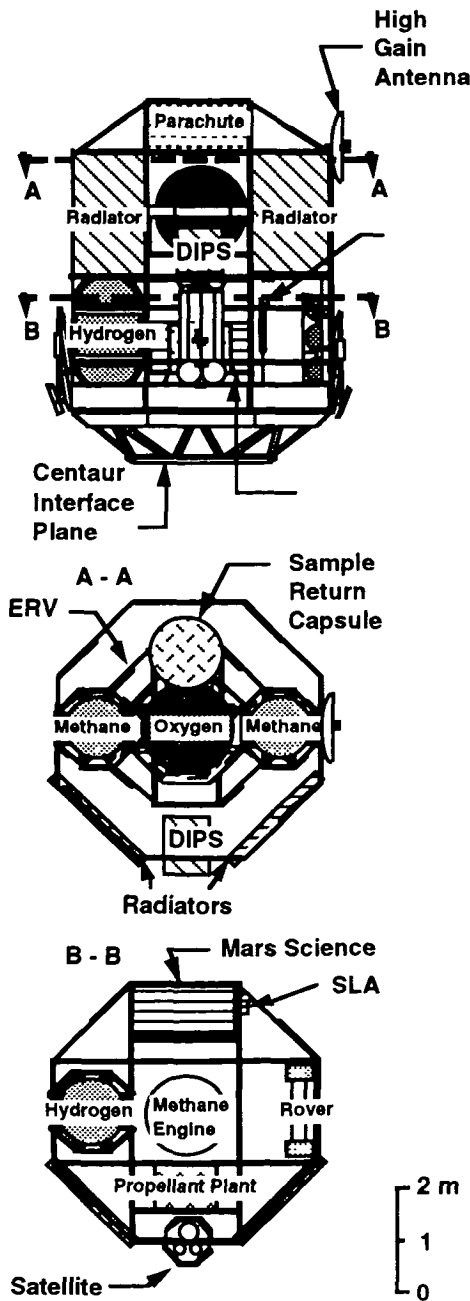


Fig. 3 Mars Landing Vehicle configuration. The aerobrake shell is not shown

Figure 4 shows the ERV, which is composed of a thrust frame with a gimbaled methane ascent engine, two methane tanks, one oxygen tank, and the sample return container with supporting structure. There is also an aerobrake that is attached to the sample return container. The tanks are arranged in such a way as to keep the ERV

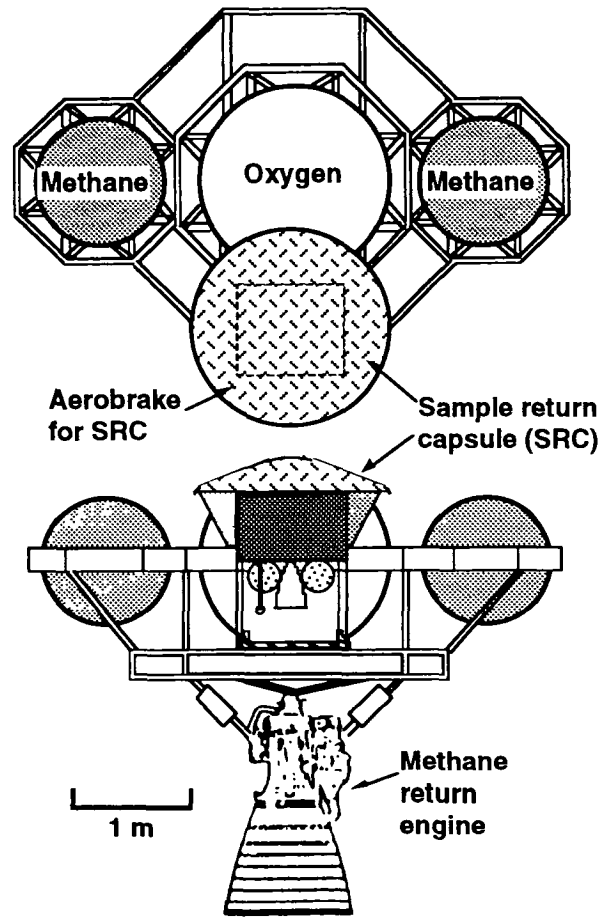


Fig. 4. Earth Return Vehicle configuration

center of mass along the centerline of the engine. The sample return container shifts the center of mass only slightly.

MLV and ERV Structure

The structure of the MLV consists of a central truss frame, a thrust structure, a Centaur adapter, and various supporting struts where needed. Some parts of the structure, such as the adapter, are expendable. When separations are needed, pyrotechnic bolts are used.

The central truss frame is made of aluminum-lithium 2090-T83 structural tubing with a 4 cm O.D. and 2 mm wall thickness. Where welding cannot easily be done, connections are made with titanium tube end fittings and pins. The structure of the frame is made up of five octagonal-shaped rings with interconnecting elements. Cross-members are added for extra stiffness. The truss frame acts as the primary load bearer. The thrust structure is a modified Boeing design made of stiffened web construction.³ The Centaur adapter, and support struts are all also made of

aluminum-lithium 2090 alloy in various shapes and sizes. The propellant tanks are made of Weldalite™ because of its better welding strength.

The Centaur adapter is connected to the thrust structure with pyrotechnic bolts. After Centaur firing, the adapter is separated from the thrust structure. The thrust structure is actually like the fifth ring of the truss frame, and is welded onto the bottom of the truss frame. The support structure for the satellite is discarded after the satellite is released, in order to allow the parachutes to be deployed. When the parachutes have served their purpose, their supporting structure is also released to keep the path of the ERV clear for the launch back to Earth.

The ERV structure (Fig. 4) is also made of the same aluminum-lithium alloy as the MLV. It consists of an octagonal ring with a thrust frame welded to its inside and support struts for the sample return container and propellant tanks. The thrust frame is made of 4 cm OD tubing and supports the methane return engine at the gimbal point. The support struts for the sample return capsule are designed to release it for its reentry to LEO.

Aerobrake

Using aerobraking at Mars allows for a large reduction of the required Earth launch mass, compared to all propulsive braking, thus allowing the Hyreus mission to be accomplished using a single launch from Earth.

As shown in Fig. 5, the geometry of the Mars aerobrake is that of a raked sphere-cone. This design is able to provide the required L/D of 0.4. The dimensions of the aerobrake are 11.3 m by 9.4 m in order to shield and decelerate the MLV. To fit inside the 7.5 m launch vehicle fairing, the aerobrake is hinged to allow it to fold closely around the MLV.

Mission requirements subject the aerobrake to high heating and pressure loads, especially at the stagnation point. For thermal protection, the majority of the outside aerobrake shell consists of FRCI-12 ceramic insulation, coated with RCG, a highly emissive glass (see Fig. 6).^{4,5} In the stagnation region, the material used is reinforced carbon/ carbon composite, which can withstand higher heat loads and surface temperatures than FRCI-12. The backing structure of the aerobrake shell consists of three layers: first is a thin sheet of graphite epoxy, followed by a layer of aluminum 2024 honeycomb. The bottom layer, or backwall, is a graphite epoxy/aluminum 2024 sandwich.

When the Centaur fires for the trans-Mars injection, the aerobrake must be able to hold its own weight at this loading, approximately 48 kN, which is larger than the

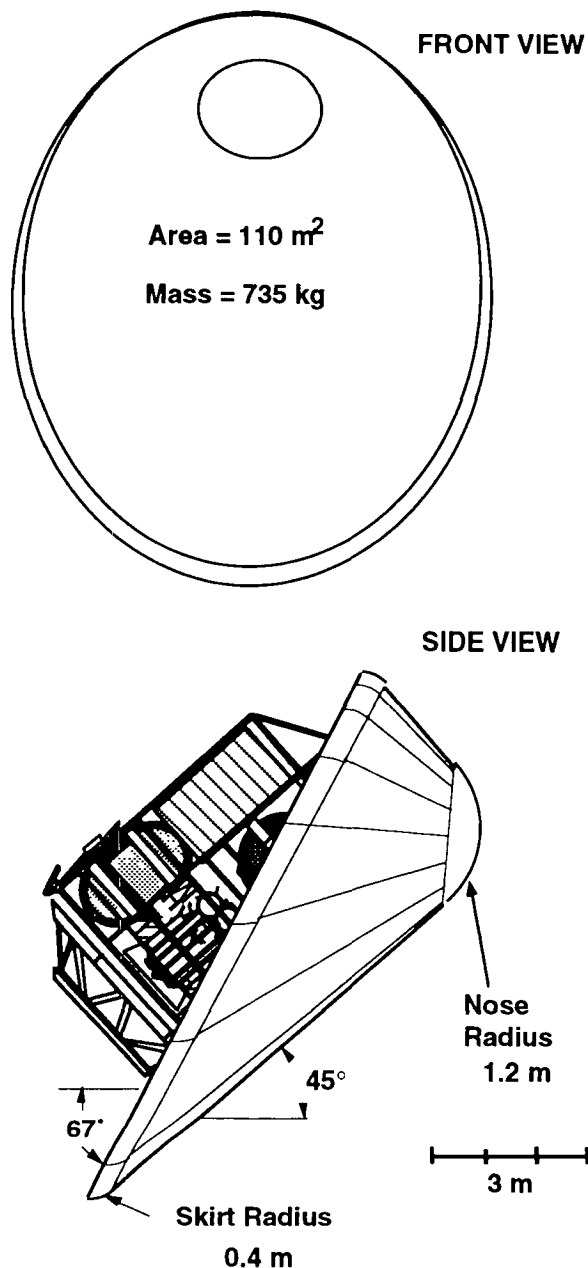


Fig. 5 Aerobrake configuration

33 kN force on the shell during aerobraking passes. The supporting framework is designed to direct the forces to the MLV structure. Anchor ribs, 1 cm thick, on the inside of the shell connect the supporting struts to it. The struts are tubular, 4 cm dia x 0.5 cm wall thickness, and are attached to the MLV structure with pyrotechnic bolts. The struts and ribs are constructed of aluminum-lithium 2090, the same material used for the MLV structure.

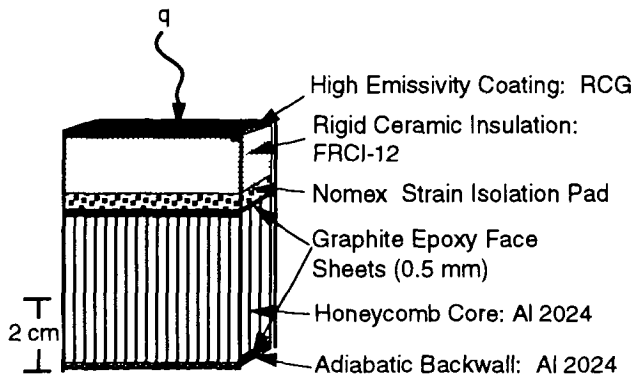


Fig. 6 Composition of Mars aerobrake shell

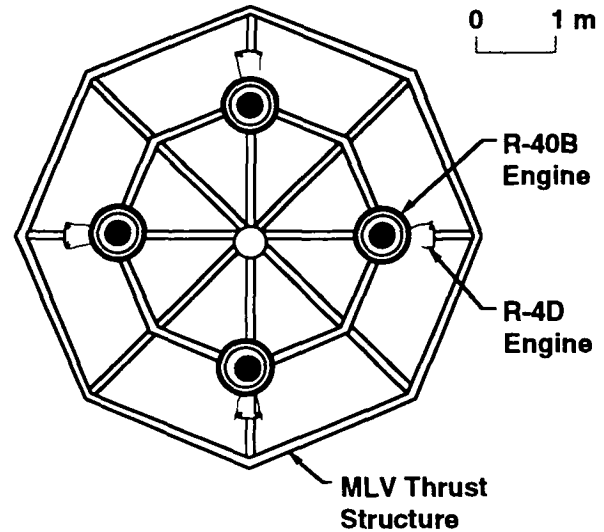


Fig. 7 Bottom view of MLV, showing descent and RCS engine arrangement

Landing Engines and Reaction Control System

Several different types of rocket engines were examined for the retrorocket system and the reaction control system (RCS). The criteria used in selecting an appropriate package were:

- Propellant must be easily storable.
- Engines must be simple and reliable.
- Must have minimum net thrust of 16,000 N (for a landing thrust/weight ratio of 1.2)
- Low mass and high specific impulse.
- Use same propellant in retro engine as in RCS.

With these requirements in mind, the Marquardt R-40B and R-4D engines were selected.⁶⁻⁸ Both are currently in production and both use the same propellants. Relevant specifications are shown in Table 2.

Table 2 Landing and RCS engines

Engine	Thrust (N)	I _{sp} (sec)	Propellant*	Mass (kg)
R-40B	4000	303	N ₂ O ₄ /MMH	7.26
R-4D	490	312	N ₂ O ₄ /MMH	3.75

* MMH is monomethyl hydrazine

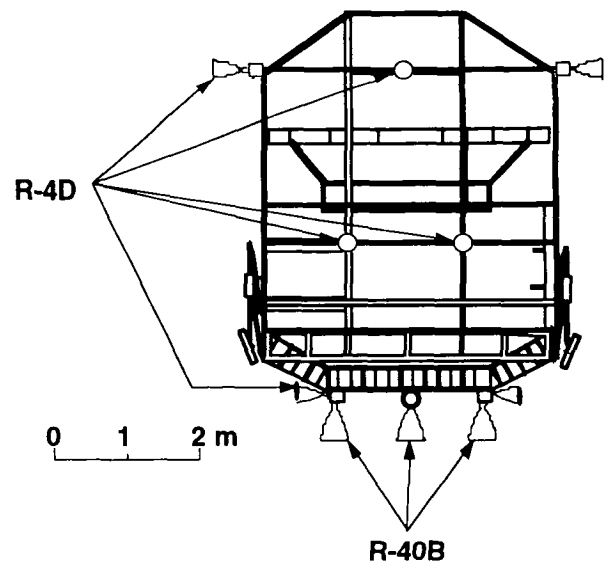


Fig. 8 Side view of MLV showing placement of engines for RCS

With a nominal thrust of 4,000 N, four Marquardt R-40B engines are needed to meet the required net thrust of 16,000 N for the Mars final descent. As shown in Fig. 7, these four engines are spaced evenly on the bottom of the MLV. Four R-4D thrusters are mounted in close proximity to the descent engines Fig. 7. These RCS engines point out radially from the center-line of the vehicle and provide maneuvering control during the descent.

Other R-4D engines are placed on the MLV as shown in Fig. 8, to complete the RCS. Their location and thrust provide a maximum angular acceleration of 5 deg/sec².⁹

Methane Rocket Engine for Mars Ascent

For the past 28 years, methane and other light hydrocarbons have been examined for their applicability in Earth-to-Orbit vehicles^{10,11}. The last two years have seen an increased interest in methane's potential for Mars *in situ* propellant production missions.^{1,3} Exploiting this potential was a motivating factor for the selection of the liquid-methane/liquid-oxygen (LCH₄/LOX) rocket engine for Mars ascent.

The criteria used in designing this engine were:

- Thrust level close to 20,000 N.
- Ability to restart.
- Record of reliability.
- Existing technology.

Because there are no existing spaceworthy LCH₄/LOX engines known to have been built to date that satisfy these criteria, the methane engine used for project Hyreus is a new design but utilizes as much existing and proven technology as possible.

Existing Technology. The methane engine designed for project Hyreus operates on an expander cycle. This cycle was chosen for its simplicity, proven technology, and potential for adaptability to a throttleable engine. The expander cycle is used in such engines as Pratt & Whitney's RL-10. Because oxygen has better heat transfer characteristics than methane, it is used as the regenerative coolant.¹²

Copper would be the preferred metal to line the combustion chamber, due to its high thermal conductivity.¹³ However, because methane is known to react with copper at high temperatures,¹⁴ it was not used in the combustion chamber. Instead, graphite is used to line the chamber wall. This configuration has been tested by Aerojet and has proven to work "very successfully in the test program."¹⁵

Because LH₂/LOX engines already exist, it is assumed that a LOX turbopump can be easily redesigned for use in a methane engine. A turbopump for methane was designed, fabricated, and tested in 1989 by Rockwell International.¹⁶

Injectors for LCH₄/LOX have been designed, built, and tested by Aerojet, Pratt & Whitney, and Rockwell International's Rocketdyne Division.^{14,15,17} All injectors were coaxial and achieved stable combustion, demonstrating the viability of injectors for LCH₄/LOX engines.

Engine Design. By combining all the above stated existing technologies, the major constituents of the LCH₄/LOX engine can be built. The mass of the engine was estimated from the engines used by the Space Shuttle Orbital Maneuvering System (OMS). The OMS engines have a thrust comparable to the design thrust of the LCH₄/LOX engine, thus, the methane engine mass was approximated to be the same as that of a single OMS engine, i.e., 100 kg.¹⁸

The design of the methane engine was based on four assumptions/criteria:

- Thrust = 20,000 N
- Combustion Chamber Pressure = 3447 kPa (500 psia)
- Exit pressure = 800 Pa
- Propellants enter combustion chamber at their respective boiling temperatures

The thrust level was selected to provide a thrust to Mars weight ratio of 2:1 at lift off. The exit pressure is approximately equal to Mars surface pressure. The chamber pressure was selected as being reasonable for efficient expander cycle operation.¹⁹

Given the chamber pressure and initial propellant temperatures, the properties of the combustion products were determined by the computer program EQLBRM.²⁰ By assuming an isentropic nozzle and using common rocket engine design equations, the characteristics of the LCH₄/LOX engine were calculated.¹³ These are summarized in Table 3.

Table 3 Methane rocket engine characteristics

I _{sp}	371 sec
Thrust	20,000 N
Propellant Mass Flow	5.49 kg/s
Propellant Exit Velocity	3,643 m/s
Combustion Chamber Temp	3,505 K
Nozzle Exit Temperature	1,214 K
Combustion Chamber Pressure	3,447 kPa
Nozzle Exit Pressure	800 Pa
Nozzle Area Ratio	296
Throat Diameter	0.06 m
Exit Diameter	1.03 m
Engine compartment Diameter	1.2 m
Engine Height	1.9 m

The engine was assumed to occupy the approximate space of a circular cylinder whose dimensions were found in the following manner: A diameter slightly larger than that of the nozzle exit was chosen to allow room to gimbal the engine upon takeoff from Mars. The total engine length was approximated by scaling it after another expander cycle engine, the RL-10.¹⁹

At Mars take-off the ERV will follow a gravity turn trajectory. Thrust vectoring, by gimbaling the engine, will be used to provide the necessary impulse for the tip-over maneuver of this trajectory.

Flight Sequence

Project Hyreus will be launched from a Titan IV into LEO. The Centaur upper stage boosts the MLV into a

conjunction class intercept with Mars. Upon reaching the planet, the MLV aerocaptures in the Martian atmosphere. The launch system, astrodynamics, and aerobrake maneuvers are discussed below.

Launch System

Several launch systems were evaluated for use with Project Hyreus.²¹ Among them were the Delta, Titan III, Titan IV, Proton, Zenit, Energia, Ariane V, and the Space Shuttle. The Delta and the Zenit are not capable of launching the Hyreus spacecraft. Of the remaining systems, analyses of the Proton, Titan III, and Ariane V produced results that were closer to the mission ΔV requirement than the probable error in the analyses. Since the Russian rockets are integrated and fueled horizontally, the necessary structural upgrade to the spacecraft could raise the payload mass above the Proton's capacity. The Ariane V will not fly until 1995, making an accurate analysis difficult. Analysis of the Titan III, with a TOS upper stage carrying a payload of 4,647 kg, indicated a ΔV capability less than 200 m/s above the mission requirement. Although the Space Shuttle is capable of launching Hyreus, it is the most costly launch system, at \$245 M for a dedicated flight. The Energia, while certainly the most powerful launch vehicle considered, also has the problem of horizontal integration. Furthermore, with only two flights and a 50% success rate, it was not felt to be suitable.

The Titan IV/Centaur was chosen for its availability and reliability. Table 4 shows the ΔV budget for the Titan IV/Centaur.

Table 4 ΔV Budget for Titan IV/Centaur (m/s)

Velocity at parking orbit insertion	7,898
Velocity penalty due to drag	68
Velocity penalty due to gravity	823
Transfer Orbit Injection ΔV (max)	3,649
ΔV gain from Earth rotation	- 407
TOTAL	12,031

The payload mass of 4,647 kg is well within the capability of this launch system. It should be noted that the Russian systems would be a lot cheaper than a Titan IV. If the payload mass were reduced, the Russian Proton could launch Hyreus for approximately one third the cost of the Titan IV.

Astrodynamics

The transfer trajectories for project Hyreus were designed with payload maximization in mind. This required that the

transfer trajectory energy requirements be minimized. The lowest energy launch opportunities and trajectories were used. The transfer trajectory variables which define the orbit were obtained from Jet Propulsion Laboratory publication 82-43.²² The year 2003 was selected for the start of the mission, due to its favorable C_3 values.

The Earth to Mars transfer is a Type I trajectory, a conjunction class trajectory with a true anomaly less than 180° . The launch window defined by a maximum departure energy value of $C_3 = 10 \text{ km}^2/\text{sec}^2$ and a Mars arrival date of December 25, 2003, opens on May 22, 2003 and closes on June 20, 2003. The optimal launch date is June 7, 2003. The total velocity increment required to reach Mars from LEO ranges from 3.596 km/sec to 3.649 km/sec. The time of flight ranges from 188 days to 217 days.

The Mars to Earth transfer is a Type II trajectory, a type of conjunction class trajectory whose true anomaly exceeds 180° . The launch window, defined by a maximum C_3 of $14 \text{ km}^2/\text{sec}^2$ and an Earth arrival date of March 31, 2006, opens on June 25, 2005, and closes on July 21, 2005. The optimal launch date is July 8, 2005. The total velocity increment required from the Mars surface to LEO ranges from 5.958 km/sec to 6.024 km/sec. The time of flight ranges from 253 to 280 days.

The total trip time of project Hyreus is approximately 2.8 years, with a Martian surface stay time of approximately 1.5 years.

Aerobraking At Mars

When the MLV arrives at Mars, it is in a hyperbolic trajectory. As it enters the atmosphere at an altitude of 125 km, it has a velocity of 5.7 km/sec and a flight path angle of 10.1° (Fig. 9). Then it proceeds with a lifting atmospheric pass which puts it into an orbit with an apoapsis of 2500 km.^{23,24} Next, it performs an apoapsis burn to place it into a 2500 km by 250 km parking orbit. The MLV waits in this orbit until the landing site is in proper alignment, at which point it does a burn to decrease its periapsis to make a second pass through the atmosphere. The total ΔV for these two burns is about 100 m/s. The second pass reduces the apoapsis to 580 km, where the satellite is deployed. The satellite's orbit is circularized using a small ΔV supplied by its onboard reaction control system. The MLV continues its trajectory down into the atmosphere to perform the final entry and landing. When the aerobrake has reduced the velocity to 350 m/s, it is jettisoned and parachutes are deployed to further slow the MLV. The final soft landing is effected by means of the retrorockets described earlier. The landing site selected for this mission is Mangala Valles; 148.1°W , 13.8°S ,²⁵ as described later in this paper.

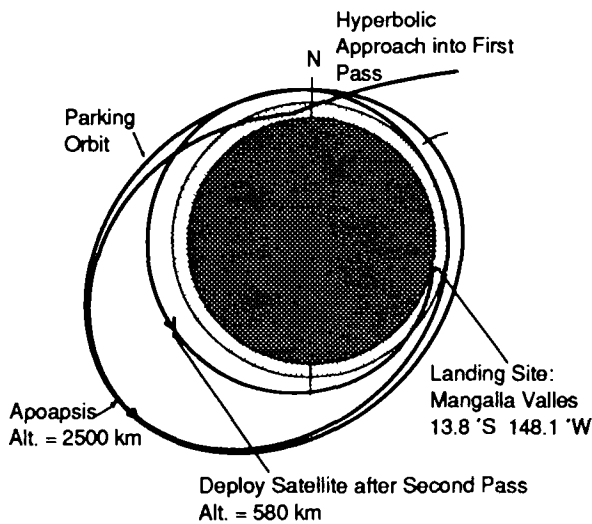
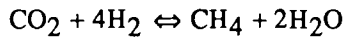


Fig. 9 Aerobraking at Mars

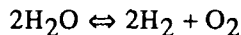
In Situ Propellant Production Plant

This mission requires 480 kg of methane and 1921 kg of oxygen to be produced during the 1.5 year stay on the surface of Mars. These propellants are manufactured in the Propellant Production Plant (PPP), using carbon dioxide found in the Martian atmosphere and hydrogen imported from Earth.

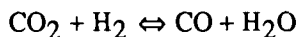
The production of methane is performed through the Sabatier reaction:¹⁻³



Many reactors have been made to perform this reaction reliably, including the one chosen for this mission which is produced by Hamilton Standard.²⁶ The oxygen is produced through two means. The first is the electrolysis of the water product in the Sabatier reaction. The electrolysis breaks the water down into hydrogen and oxygen:



The hydrogen is recycled into the Sabatier reaction, to minimize the amount to be imported from Earth. However, the Sabatier and electrolysis reactions produce only half the required oxygen. Thus, oxygen production is supplemented using the reverse water-gas shift (RWGS) reaction:



This reaction produces carbon monoxide as a waste product that is released into the Martian atmosphere.

The PPP, shown in Fig. 10, is designed to produce the needed propellant in approximately 1.4 years, to allow for any delays in the landing sequence at Mars and for any necessary plant shutdowns which may occur due to dust storms. Methane is produced at a rate of 0.94 kg/day and oxygen at 3.76 kg/day. Martian atmospheric gases are drawn into the PPP at a rate of 8.25 kg/day.

The Martian atmosphere is composed of 95.3% carbon dioxide, 2.7% nitrogen and 1.6% argon.²⁷ Dust is also present. The filter system, composed of a hydrocyclone and a membrane filter in series, is designed to remove the dust. The hydrocyclone removes dust particles as small as 5 μm, and the membrane filter removes the remaining fine dust. Dust particles removed via the hydrocyclone are collected as a return sample. Following filtration, the carbon dioxide is purified by removing nitrogen and argon. This is accomplished by compressing the atmospheric gases to 1.3 MPa, condensing the carbon dioxide at ambient Martian temperatures, and bleeding off the trace gases. A portion of the liquefied carbon dioxide is stored at 1.3 MPa and ambient temperature for use on the rover as a diluent.

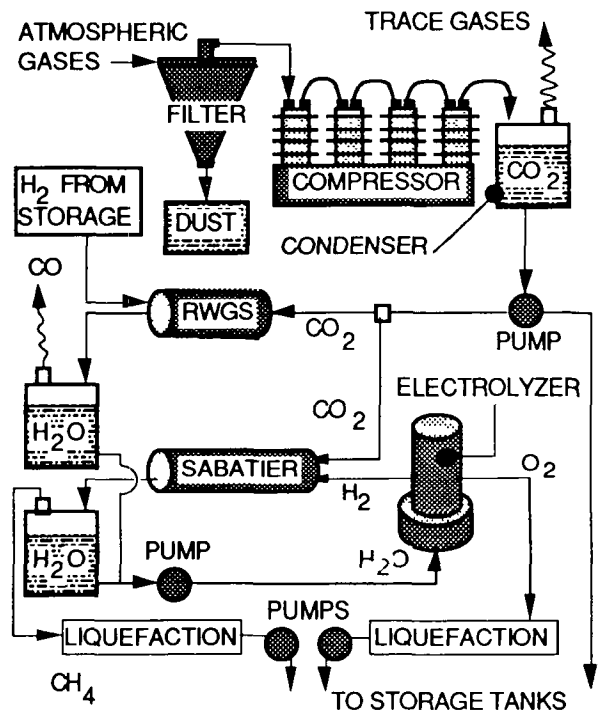


Fig. 10 Propellant production plant schematic.

The purified carbon dioxide is pumped to the Sabatier reactor and the RWGS reactor. The Sabatier reactor produces methane and water, and the RWGS reactor produces carbon monoxide and water. The water is condensed out of both the carbon monoxide and the methane, and is pumped to the electrolyzer. The carbon monoxide is vented to the atmosphere, and the methane is pumped to the liquefaction

cycle. The water from the two reactors is pumped through the electrolyzer at a rate of 4.29 kg/day. The hydrogen product is pumped to the Sabatier reactor and the oxygen is pumped to the liquefaction cycle.

In the liquefaction cycle, the methane and oxygen are compressed, cooled in heat exchangers, and liquefied through Joule-Thompson expansion in a throttling valve. Methane is pumped into two tanks aboard the ERV, to be stored at 1.0 MPa and 135 K. Oxygen is pumped into the remaining tank on the ERV, to be stored at 0.71 MPa and 108 K. The storage tanks and the seed hydrogen tank are all insulated by Multi-Layer Insulation (MLI). The MLI reduces the heat flux into the tanks to a total of 8 W. To prevent boiloff and propellant loss, this heat is removed from the tanks by a refrigerator.

The PPP requires 1215 W of electric power to operate at the required production rate. This power requirement plus the power requirements of the Mars science package, will require the use of one Dynamic Isotope Power System (DIPS). The DIPS unit has a mass of 370 kg and provides 2.5 kW of electric power. Table 4 summarizes the component masses and power requirements of the PPP.

Table 5 Propellant production plant masses and power requirements

Component	Mass (kg)	Steady State Power(W)	Start-Up Power (W)
Filter system	5	0	0
Pumps/Compressors	140	500	500
Sabatier reactor	43	0	200
RWGS reactor	43	60	400
Water electrolyzer	15	55	55
Condensers	10	0	0
Liquefaction unit	30	300	300
Refrigerator	30	300	300
Storage insulation	60	0	0
Radiator	10	0	0
Power Supply (DIPS)	370	-	-
TOTAL	756	1215	1755

The procedure for plant start-up begins with the operation of the inlet compressor and the subsequent accumulation of liquid carbon dioxide. Next, the RWGS reactor heats up to its operating temperature of 400 K by its turned on to produce hydrogen and oxygen. The oxygen liquefaction begins at this time, and the Sabatier reaction is started using the hydrogen from the electrolyzer. The methane product is liquefied. Refrigeration of the storage tanks begins when the oxygen and methane begin to accumulate. Once steady state operation is achieved, the Sabatier reactor, which is exothermic, produces most of the

heat required by the RWGS reactor. Only 60 W of additional heating is required. The power requirements for the start-up of each individual component are shown in Table 4, where they can be compared to the steady state power requirement.

Special Planetary Observation Transport (SPOT)

Sample collection on the Martian surface is accomplished by the special planetary observation transport (SPOT). This is a semi-autonomous robotic vehicle equipped with a remote manipulator arm and having a range of approximately 45 km.

SPOT is a six-wheeled vehicle with three individual sections in tandem, shown in Fig. 11. Each section's frame is 1 m wide and 0.44 m long, and has a wheel attached to each side via a double wishbone suspension. SPOT's design includes a remote manipulator arm with tools, sample storage, controls, communications antenna, power source, and a driller. Of the three sections, only the front two have powered wheels. The trailer has 4 hydraulic arms for stabilization during drilling.

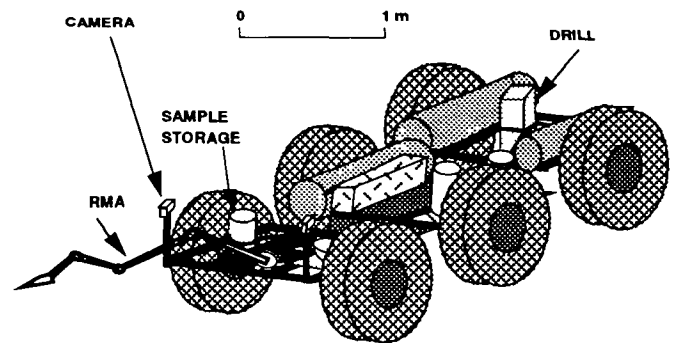


Fig. 11 Isometric view of SPOT rover (Waste heat radiator not shown, for clarity)

The material used for SPOT's primary chassis is Aluminum 7079-T6, chosen because it is lightweight, and has the highest yield and ultimate stresses of the different types of aluminum alloys considered. Another factor considered in the choice of aluminum alloy is its ability to withstand radiation. This radiation resistance ability was determined through examination of aluminum parts of the Long Duration Exposure Facility (LDEF).²⁸ The chassis has a mass of approximately 25 kg.

Composites are used for secondary structures, such as propellant tank supports. Composite materials were not selected for the primary chassis because they are more susceptible to environmental effects, such as radiation.

The tires have a design based on the Apollo LRV.^{28,29} At 0.5 m in diameter, they are 38% smaller than the

originals and have a mass of approximately 4 kg each. The upper and lower wishbones of the suspension system are connected by an angled beam that is attached to SPOT's tubular chassis, and also are attached to a shock absorber and spring. A second angled member connects the lower corner of the suspension to the chassis

Power Source

The power source chosen for SPOT is a thermophotovoltaic (TPV) generator system utilizing mechanically stacked two-junction GaAs/GaSb cells, in tandem with an infrared emitter burning gaseous methane, and oxygen, diluted with CO₂. The TPV unit is shown in Fig. 12. The concept is currently being developed by the Vehicle Research Institute at Western Washington University in Bellingham, WA.³⁰

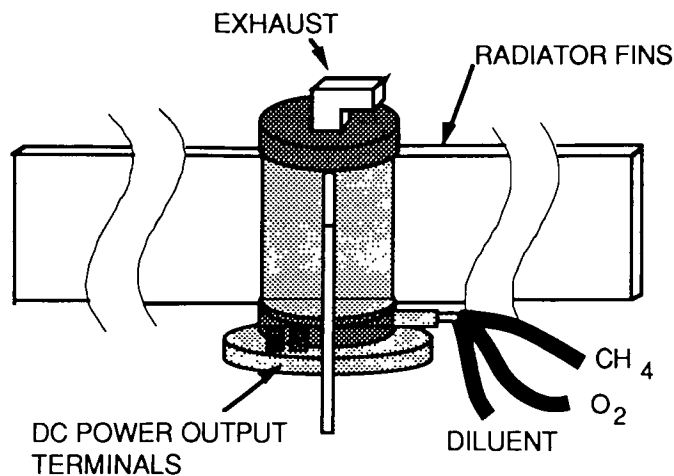


Fig. 12 Thermophotovoltaic generator

The methane burns with oxygen and carbon dioxide at a molar ratio of 1:1:0.1 inside a 1 cm dia. tungsten tube, heating it to a temperature of approximately 2000 K. The infrared radiation emitted by the hot tube peaks at a wavelength of $\sim 1.5 \mu\text{m}$. Because silicon and GaAs solar cells are mostly transparent in this bandwidth, the GaSb cells are the key to the high efficiency (30%) of the TPV unit. Another advantage of the GaAs/GaSb solar cells is their resistance to degradation from radiation. This resistance is due to the relative thinness of the photon gathering portion of the cell. This is a major consideration, as silicon cells degrade rapidly without heavy radiation shielding. The infrared emitter is located inside a 15 cm diameter cylindrical enclosure tube which is lined with the photovoltaic cells, and whose end walls are highly reflective. This configuration produces 1 kW of electrical power for the rover. The combustion process is continuous rather than intermittent, as in the batch firing of a typical internal

combustion engine, resulting in a more complete combustion and a drastic reduction of exhaust emissions.

Nearly 3 kW of waste heat must be rejected by the TPV. This is accomplished by using heat pipe radiators extending radially outward and upward from the TPV unit. At an operating temperature of 373 K these radiators require a total surface area of 3.4 m² for waste heat dissipation.

The TPV unit continuously charges onboard batteries which actually drive the electric motors in each wheel hub. Nickel metal hydride batteries were chosen because of their high energy density (215 Whr/liter) and cycling ability (1000 cycles).³¹

Controls

The remote distance of a Martian rover provides challenging problems for the control systems designer. SPOT uses semi-autonomous navigation (SAN) wherein the rover has a high level of autonomy.^{32,33} SPOT collects information and constructs its own local world map. Onboard processors plan a path and determine if the map is traversable. If SPOT needs assistance, it sends all available information to Earth for human intervention.

Equipment for the control system includes two charge-coupled device (CCD) cameras mounted on gimbals for a stereo image of the Martian terrain. Two laser range finders are mounted below the CCD cameras to help determine exact ranges. Inclinometers are included for a cost-effective warning of rover stability. These will prevent the rover from exceeding rollover stability requirements. Potentiometers are also installed in each wheel alongside the motors to enable the processor to know if a wheel is stuck and not rotating at the same rate as the others.

Design objectives of SPOT consisted of maneuverability, weight, collection and transport of samples, and avoidance of obstacles. Table 5 shows the mass inventory of the rover.

Satellite for Observation and Communication at Mars (SOCM)

A small orbiter, Satellite for Observation and Communication at Mars (SOCM) is placed in a sun synchronous orbit around Mars by the MLV. The primary mission objective of SOCM is to look for subsurface water deposits (ice) using a ground penetrating radar (GPR) system. Also, the satellite is equipped with a weather monitoring system (wide-angle camera) to warn the rover of impending Martian dust storms. In addition, SOCM provide a communication link between the rover and the MLV. SOCM has two arrangements, the initial launch configuration and the final orbital configuration (Fig. 13).

Table 6 SPOT rover mass inventory

Component	Mass (kg)
Frame	25
Cameras(2)	0.25
Lasers(2)	8
AHARS	2.2
Controls	20
Electric Motors(4)	4
TPV's(2)	8
Batteries	20
Wheels(6)	21
Antenna	0.5
Fuel Tanks(3)	9.6
Hydraulic Legs(4)	20
RMA	4
Suspension	15
Coolant System	27.7
Total	180

In the initial launch configuration the satellite is compactly stored in the MLV. The satellite is deployed while in the folded launch configuration. Upon orbital insertion, solar panels are deployed, and a lattice-type exten-

dible boom separates the two sections of the satellite for gravity gradient stabilization. The total wet mass of SOCM is 280 kg, and the dry mass is 260 kg.

SOCM's payload consists of a GPR system, wide-angle camera and a communication system. The wide-angle camera provides a weather warning system for the rover and Mars science experiments, while the GPR system conducts a survey of the Martian subsurface landscape. This survey serves as valuable insight into the characteristics of the Martian subsurface, such as composition and ground water/ice content. Discovery of water or ice sources on Mars would be highly beneficial for future missions.

SOCM has a dual control system: gravity gradient control and three axis stabilization. The first job of the attitude control system is to place SOCM in its operational orbit through a propulsive unit. This requires active control using attitude sensing and control devices. A sun sensor provides attitude sensing, and hydrazine thrusters provide three-axis control. Once placed in operational orbit, SOCM is controlled by gravity gradient, a passive method of control. Gravity gradient stabilization works by the fact that the longitudinal axis of an elongated structure tends to align itself with the gravity field. This method results in a Mars-pointed orientation of the satellite. There are three main advantages of using this type of control method: surface orientation of payload, low propellant, and low power requirements for attitude control. The three-axis stabilization system is used for occasional orbital maintenance and attitude adjustment.

SOCM is placed in a Sun-synchronous orbit, an orbit inclined to keep the orbital plane at a constant angle with respect to the Sun. This is done by matching the variation in the right ascension of the ascending node of SOCM's orbit to Mars' motion around the sun. Thus, the satellite continuously sees the sun, providing a constant power source. The Sun-synchronous orbit is almost polar, with an inclination of approximately 88°, therefore, most of the planet's surface is covered by the satellite's camera and ground penetrating radar. SOCM is deployed from the MLV after the spacecraft has aerobraked for landing. The satellite is deployed at the apoapsis of the landing orbit (580 km) and does a burn with its four hydrazine control thrusters simultaneously to circularize the orbit ($\Delta V = 100$ m/sec).

The Sun provides power to SOCM by means of solar arrays which are deployed after the orbital maneuver. The arrays fold around the octagonal body of the satellite for compact storage in transit from Earth to Mars. The orientation of the arrays is continuously controlled by a sun sensor so, that they remain pointing towards the sun as the angle of SOCM's orbit plane with respect to the sun changes. Gallium arsenide (GaAs) solar cells (efficiency = 22%) have been chosen. With a solar constant at Mars of 592 W/m^2 , the total power requirement of 350 W is generated with a solar array area of 2.7 m^2 .

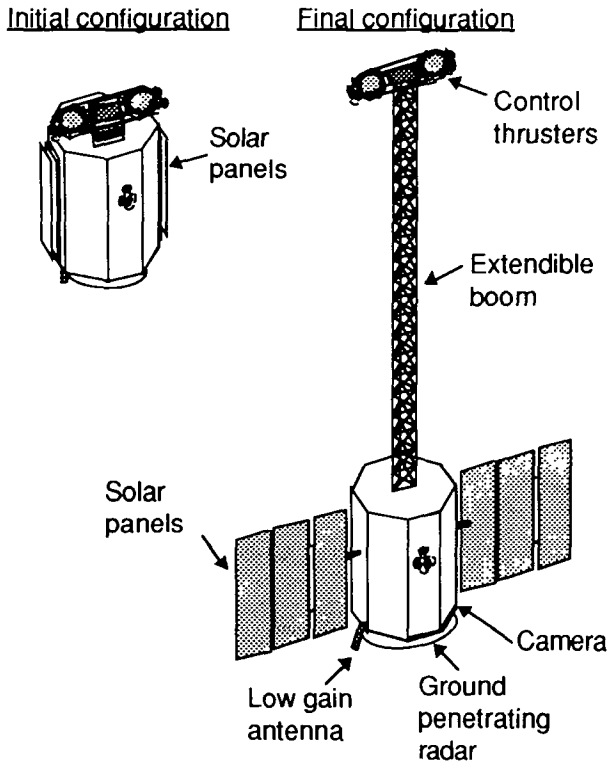


Fig. 13 Configuration of SOCM

SOCM does not communicate directly with Earth. Instead, the satellite dumps data to the MLV which relays the information to Earth (Fig. 14). The MLV is equipped with a low-gain antenna for in-transit communication on both the incoming trip to Mars and the return to Earth voyage. Upon landing on the Martian surface, the MLV deploys a high-gain antenna for Mars/Earth communications. Both the rover and the satellite have a low-gain antenna for communication with the MLV. If the rover/MLV communication link is blocked by terrain, the rover can still communicate with the MLV via SOCM.

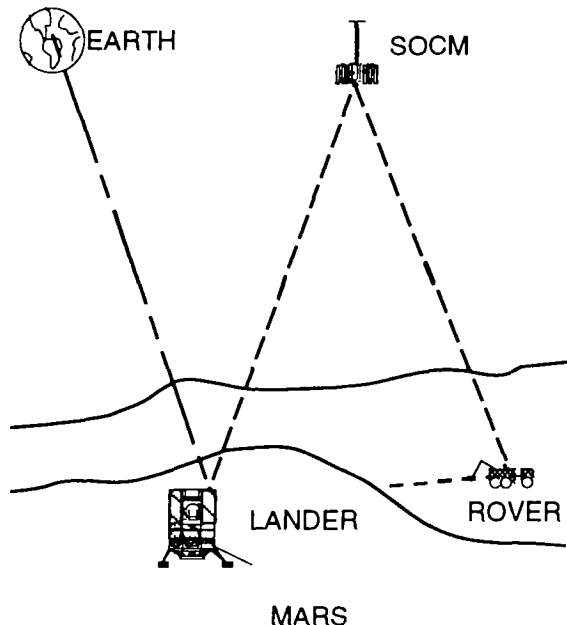


Fig. 14 Communications architecture

Mars Science

Our knowledge of Mars is the driving factor in future planning. In the Hyreus mission, there are two main scientific objectives to be accomplished: bringing 25 to 30 kg of Martian samples back to Earth and locating water deposits on Mars.

Landing Site

The primary landing site is Mangala Valles, located at 148.1°W, 13.8°S.³⁴ (see Fig. 15, Site #1). Mangala Valles offers a variety of physical features within short distances of each other, which enables the rover to obtain a variety of samples for return to Earth. Features at Mangala Valles include young volcanoes, dry river channels, crustal rock, and craters.

The backup sites considered are Vallis Marineris, at 63°W, 16°N, and Chryse Planitia, at 45°W, 20°N. (see Fig. 15, Sites #2 and #3)

Scientific Package

A variety of scientific investigations, including exobiology, meteorology, and seismology are to be conducted. The satellite is equipped with a Ground Penetrating Radar (GPR), which searches for water deposits on Mars. In addition, the satellite houses a low-resolution camera.

The rover uses a Remote Manipulator Arm (RMA) with various attachments to acquire samples. The "scoober" is a scoop and grabber integrated into one device capable of being used on the RMA (see Fig. 16). The rover also carries an infrared spectrometer for studying the surface composition of the planet.

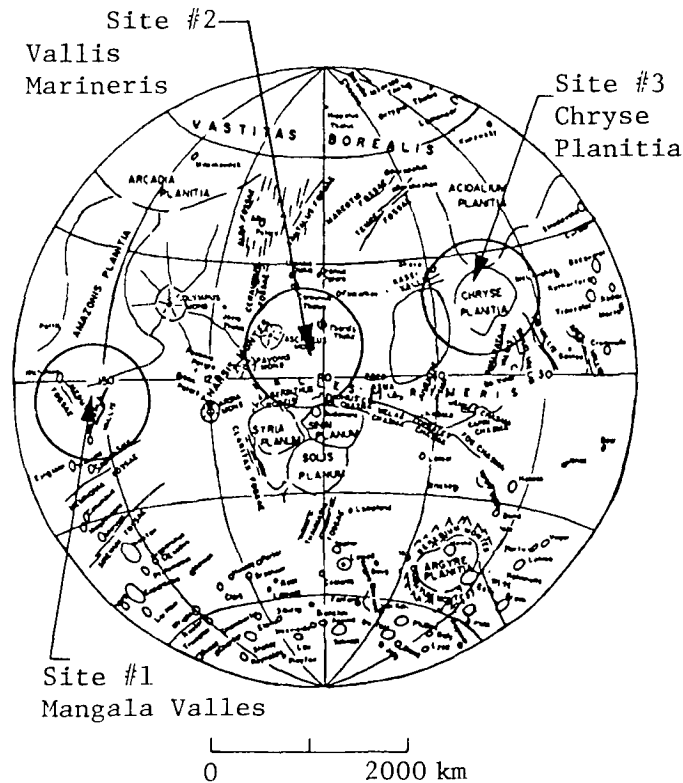
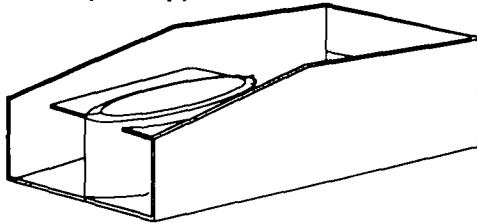


Fig. 15 Potential landing sites

The lander houses the Sample Return Capsule (SRC), the exobiology experiments, a seismometer, and a meteorology package. Samples tested on the lander will be acquired either through material returned by the rover, or material retrieved with the lander Remote Manipulator Arm (RMA), which is provided for redundancy to ensure sample acquisition.

Closed (Scoop)



Open (Grabber)

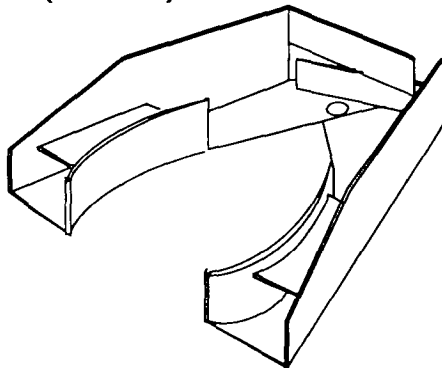


Fig. 16 "Scoobber," integrated scoop and grabber

The samples are returned in the SRC, which has a thermal management system to keep the samples at conditions as close to Mars ambient as possible during the return trip in order to preserve the abundance and distribution of volatile components for analysis on Earth. The returned capsule is separated from the ERV as Earth is approached. Aerobraking and a small rocket burn place the capsule into LEO, where it is accessible with the Space Shuttle. The samples will undergo preliminary analysis in LEO, in order to ensure that Earth quarantine is not broken. If deemed safe, the samples will then be brought to the surface for further extensive analysis.

Earth Return Scenario

Shortly before the launch window for return to Earth opens, the propellant plant ceases operation and the last samples are loaded aboard the ERV. When all systems are ready, the methane ascent engines ignite and the ERV lifts off the Martian surface. The ΔV budget for the Mars launch and Earth return is given in Table 7.

Table 7 ΔV budget for Mars launch (m/s)

Velocity at parking orbit insertion	3412
Velocity penalty due to drag	< 5
Velocity penalty due to gravity	146
Transfer Orbit Injection ΔV (max)	2693
ΔV gain from Mars rotation	- 232
TOTAL	6,024

Sample Return

The Martian samples returned to Earth are extremely valuable because they can be extensively analyzed with sophisticated instruments that cannot be flown to Mars. The proposed samples include lava, sediment from riverbeds, underground soil, crustal rocks, and top soil, all of which are available near the proposed landing site, Mangala Valles. Figure 17 shows a possible rover traverse.²⁷

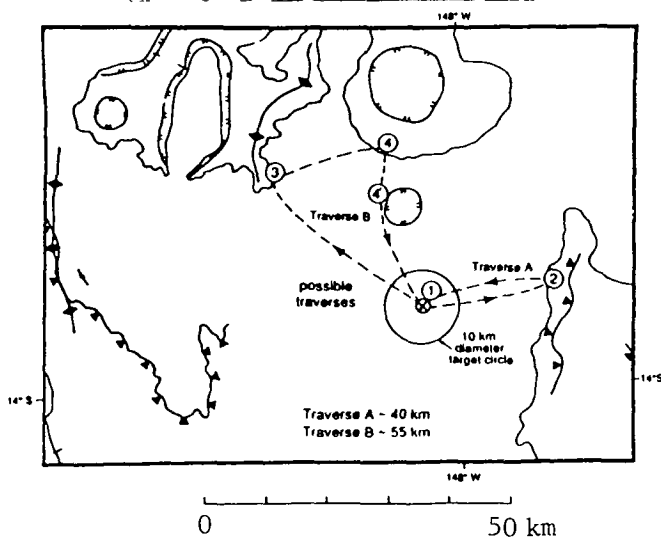


Fig. 17 Proposed rover traverses

Upon achieving a low Mars orbit of 300 km altitude, the ERV coasts until it reaches the burn point for the interplanetary transfer orbit injection. The methane engines fire again and boost the ERV through the velocity increment required to send it to Earth. Once the ERV is in transit to Earth, the vehicle orients itself so that the small aerobrake on the Earth return capsule shades the sample container. This maneuver alleviates the need for a large and elaborate refrigeration system that would otherwise be required to reject the heat from the sample canister due to the solar flux. Temperature control is essential for maintaining Mars ambient conditions in order to preserve the state of volatile components of the samples.

When the ERV reaches the Earth's sphere of influence, the Earth return capsule, which consists of the sample canister, an ablative aerobrake and a small control system, detaches from the rest of the ERV. The ERV then performs a contamination and collision avoidance maneuver (CCAM) which moves it away from the Earth return capsule. During the CCAM, the ERV reorients itself so that the thrust vector is away from the Earth return capsule, yet the exhaust does not impinge on the capsule. The appropriate RCS thrusters fire to depletion. The ERV coasts away from the capsule for a brief time. When the

ERV is a safe distance from the Earth return capsule, the remaining primary propellants are burned in the main engine. This provides the small boost required to prevent the vehicle from re-entering the Earth's atmosphere and burning up. The ERV swings by Earth in a hyperbolic orbit and continues back out to deep space.

The Earth return capsule, now powered by internal batteries, re-enters the Earth's atmosphere at an entry angle of 11.8° and an entry velocity of 11.2 km/sec using an Apollo style ablative heat shield for the aerocapture pass. This maneuver decelerates the capsule to a velocity of 7.27 km/sec. Once the aerobraking is completed, the orbit is circularized at 340 km with a ΔV of 490 m/sec, provided by a small monopropellant RCS system. The capsule is then reoriented to shade the sample container from sunlight, and awaits retrieval by the Space Shuttle. As an alternative, the capsule could be picked up at either Space Station Freedom or Mir, provided one of them is in orbit at the time. Preliminary analysis of the samples can be conducted in orbit to determine if there is any danger of biological contamination. If deemed safe, the samples can be returned to Earth. If for some reason the decision is made not to return the samples to Earth's surface, the samples can either be sterilized and disposed or the sample container can be attached to a payload assist module and boosted to a quarantine orbit or back into deep space.

Conclusions

This paper has presented Project Hyreus, a Mars rover sample return mission that utilizes the Martian atmosphere as an indigenous resource to manufacture methane and oxygen as the propellants for the trip back to Earth. The primary goals of the mission are to demonstrate the considerable benefits of *in situ* propellant production and to test the technical viability of this approach as a precursor to future manned missions. Additional goals are to robotically explore the surface of the planet, and to return a large quantity of Martian surface and subsurface material. All the hardware and technology used in this mission are either currently available or could be easily developed in time to meet the projected launch date in 2003. The mission includes a Mars-orbiting satellite whose task is to make extended observations of the planet using both an optical camera and a ground penetrating radar system, the latter to search for subsurface ice/water deposits. This satellite will complement and build on other missions, such as Mars Observer. Surface exploration will be performed with a large rover that will allow a variety of locations to be examined to give diversity to the collected samples. Hyreus will bring back approximately 25-30 kg of Martian soil and rocks to Earth. This represents an increase in yield of 5-100 times over conventional sample return missions currently being considered, and is a direct consequence of the use of indigenous Martian resources.

Acknowledgments

The authors are deeply indebted to the NASA/USRA Advanced Design Program for the grant that supports the space systems design courses at the University of Washington.

Numerous people have provided valuable information and help that contributed in a major way to the successful completion of this design project. Diane Linne and Mary Wadel of NASA Lewis Research Center were invaluable for their help with information on rocket engines designed for using indigenous propellants. Tom Callahan, Phil Ginser, and Mike Holquin of General Dynamics provided copious and prompt data on the Titan Centaur. Ed Parsons of the Air Force Public Affairs Office and Capt. Kevin Klonoski of the Titan IV Program Office were extremely helpful and Lt. Tim Dickinson even provided his home number in the event we needed to reach him after hours. Peter Nolan of the University of Arizona provided much useful information about indigenous propellant plants.

We are very grateful to Dana Andrews and Jeff Cannon of Boeing for their advice at our preliminary design review. Their dose of reality was instrumental in improving our design. Thanks are also due to John Jordan of Boeing, who was able to fill in the gaps of our knowledge about the Russian Energia launch vehicle. Robert Hartmann of General Electric promptly sent information about the MOD-RTG space power system. Clarence Quan of McDonnell Douglas was able to answer all our questions about modifications to the Titan payload fairing, and Tim Voght of Martin Marietta provided the Titan IV launch simulations we requested. We are also deeply indebted to everyone else who provided technical assistance to this project.

Many thanks are due to Dean J. Ray Bowen for helping to make possible our travel to the NASA/USRA Advanced Design Summer Conference in Houston, and to the Department of Aeronautics and Astronautics for its support of the project.

Finally, we would like to express our special gratitude to Professor Adam Bruckner and to our teaching assistant, Brian Thill, both of whom made this class one of our best experiences at the University of Washington.

References

1. Zubrin, R.M., Baker, D., and Gwynne, O., "Mars Direct: A Simple, Robust, and Cost Effective Architecture for the Space Exploration Initiative," AIAA Paper No. 91-0326, 29th Aerospace Sciences Meeting, Reno, NV, Jan 7-10, 1991.
2. Zubrin, R.M., "In-Situ Propellant Production: The Key Technology Required for the Realization of a Coherent

- and Cost-Effective Space Exploration Initiative," Paper No. AIAA 91-668, 42nd Congress of the International Astronautical Federation, Montreal, Canada, October 5-11, 1991.
3. "Project Minerva: A Low-Cost Manned Mars Mission Based on Indigenous Propellant Production," Final Report, AA420/421 Space Systems Design, NASA/USRA Advanced Design Program, Department of Aeronautics and Astronautics, University of Washington, June 1992, p. 3-20.
 4. Kourtides, D.A., Chiu, S.A., Iverson, S.A., and Lowe, D. M., "Thermal Response of Rigid and Flexible Insulations and Reflective Coating in an Aeroconvective Heating Environment," NASA TM 103925, Ames Research Center, 1992.
 5. Williams, S.D., Gietzel, M.M., Rochelle, W.C., and Curry, D.M., "TPS Design for Aerobraking at Earth and Mars," NASA TM 104739, Johnson Space Center, August 1991.
 6. Griffin, M.D. and French, J.R., *Space Vehicle Design*, American Institute of Aeronautics and Astronautics, Washington, D.C., 1991, pp.172, 292-309.
 7. Larson, W.J., and Wertz, J.R., eds., *Space Mission Analysis and Design*, Second Edition, Microcosm Inc. and Kluwer Academic Publishers, 1992, pp. 646, 657.
 8. *Rocket Engines and Propulsion Systems*, Kaiser Marquardt, Revised: 1985.
 9. Powell, R.W. and Braun, R.D., "A 6-Degree of Freedom Guidance and Control Analysis of Mars Aerocapture," AIAA Paper No. 92-0736, 30th AIAA Aerospace Sciences Meeting and Exhibit, Reno, NV, January 6-9, 1992.
 10. Masters, A.I., "Investigation of Light Hydrocarbon Fuels with Flox Mixtures as Liquid Rocket Propellants," Final Report, NASA CR-54445, Pratt & Whitney Aircraft, Sept. 1, 1965.
 11. Martin, J.A., "Hydrocarbon Rocket Engines for Earth-to-Orbit Vehicles," *Journal of Spacecraft and Rockets*, Vol. 20, 1983, pp. 249-256.
 12. Kramer, R., and Martin, J., "Undeveloped Rocket Cycle Applications to Advanced Earth-to-Orbit Transportation," AIAA Paper No. 90-2438, 26th AIAA/SAE/ASME/ASEE Joint Propulsion Conference, Orlando, FL, July 16-18, 1990.
 13. Sutton, G.P., *Rocket Propulsion Elements: An Introduction to the Engineering of Rockets*, Sixth Edition, John Wiley & Sons, Inc., 1992, p. 93.
 14. Cook, R.T. and Kirby, F.M., "LOX/Hydrocarbon Combustion and Cooling Survey," NASA Technical Report N89-12648, Rockwell International/Rocketdyne Division, 1989, pp. 472-473.
 15. Mercer, S.D., and Rousar, D.C., "Aerojet Tech Systems Company Contribution to LOX/HC Combustion and Cooling Technology," NASA Technical Report N89-12646, Aerojet Tech Systems Company, 1989, pp. 396, 398, 404-405.
 16. Nielson, C.E. and Csomor, A., "Advanced Launch System Propulsion Focused Technology Liquid Methane Turbopump Technical Implementation Plan," NASA CR-183681, Rockwell International/Rocketdyne Division, May 25, 1989.
 17. Masters, A.I., Visek, W.A., and Carroll, R.G., "Survey of LOX/Hydrocarbon Combustion and Cooling," NASA Technical Report N89-126471, Pratt & Whitney Aircraft/ United Technologies Corp., p. 445.
 18. "Spacecraft Subsystems," NASA/USRA Advanced Design Project, Department of Aerospace Engineering and Engineering Mechanics, The University of Texas at Austin, Sept., 1991.
 19. *Titan/Centaur Evolution Plan 1993*, General Dynamics, Space Systems Division, 1993.
 20. Pratt, B.S. and Pratt, D.T., "An Interactive Code for Calculation of Gas-Phase Chemical Equilibrium: EQLBRM", NASA CR-168337, Department of Mechanical Engineering, University of Washington, April 1984.
 21. Isakowitz, S.J., *International Reference Guide to Space Launch Systems*, American Institute of Aeronautics and Astronautics, Washington, DC, 1991.
 22. Sergeyevesky, A.B., Snyder, G.C., and Cunniff, R.A., *Earth to Mars Ballistic Mission Opportunities, 1990-2007*, Publication 82-43, Jet Propulsion Laboratory, Pasadena, CA, 1983.
 23. Regan, F.J., *Vehicle Re-Entry Dynamics*, American Institute of Aeronautics and Astronautics, Washington, DC, 1984, pp. 100-1.
 24. Tauber, M., et al., "Aerobraking Design Studies for Manned Mars Missions," AIAA Paper No. 91-1344, 26th AIAA Thermophysics Conference, Honolulu, HI, June 24-26, 1991.
 25. Corliss, W.R., "The Viking Mission to Mars," NASA SP-334, 1974, pp. 20-21.

26. McElroy, J.F., "The Status of SPE Water Electrolyzers in Support of Space Energy Systems," Hamilton Standard Division, United Technologies Corporation, April 1992.
27. Carr, M.H., *The Surface of Mars*, Yale University Press, New Haven, CT, 1981.
28. Rao, N.S. and Wallace, B.E., "Considerations for the Design of Lunar Rover Structures and Mechanisms for Prolonged Operation in the Lunar Environment," AIAA Paper No. 93-0993, February 1993.
29. "Project: Apollo 15", *NASA News*, Release No. 71-119K, July 15, 1971.
30. Seal, M., Western Washington University, Bellingham, WA, Personal Communication, March 11, 1993.
31. Ovshinsky, S.R., Fetcenko, M. A., and Ross, J., "A Nickel Metal Hydride Battery for Electric Vehicles," *Science*, Vol. 260, April 9, 1993, pp.176-181.
32. Lavery, D. and Bedard, B.D. Jr., "NASA Planetary Rover Program," NASA TN91-20651, Washington, DC, Jan. 1991.
33. Cooper, B.K., Cameron, J.M., Salo, R.A., and Wilcox, B.H., "Planetary Rover Mobility Control," *Mobile Robots*, Vol. 727, 1986, pp. 330-335.
34. Greeley, R., ed., *Mars Landing Site Catalog*, NASA Reference Publication 1238, 1990.

VARIOUS APPLICATIONS OF NASA'S CAPACIFLECTOR PROXIMITY SENSOR

**West Virginia University
Department of Electrical and Computer Engineering
Morgantown, West Virginia**

**Dr. Robert McConnell
Michael Manzo, Teaching Assistant**

Abstract

A capacitive proximity sensor (capaciflector) developed at NASA (Goddard Space Flight Center) depends upon detecting changes in capacitance when an object is brought within range. This sensor, which is sensitive to conductive and dielectric materials, consists of a capacitive sensing element (sensor) backed by a reflector element (shield) to reduce the effects of stray capacitance. Through the use of the capaciflector several systems were developed at West Virginia University that include: A multiplexing scheme for addressing thirty two separate sensors, An Automatic Docking System for Space Based Orbital Replacement Units (ORU's), An Image Scanning system, and A Robot Controller with Visual and Tactile Feedback.

Introduction

Researchers at Goddard's Tele-Robotics lab have developed an automatic docking system for space based ORU's using the capaciflector shown in Figure 1. With the success of that project, it was thought that the capaciflector had many other applications as well. During the 1992-1993 school year, a group of sixteen students designed and constructed a complete sensor system. The system is capable of accessing 32 separate sensors. The information collected is then manipulated by each group to facilitate the desired response (i.e. Visual Display or Robot Command).

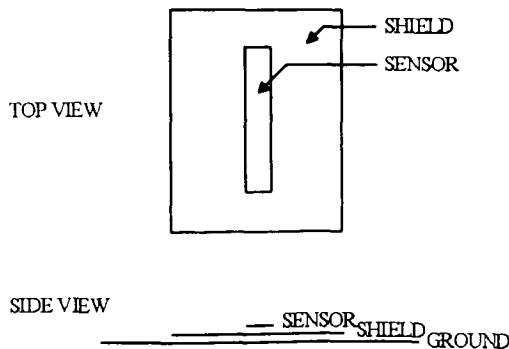


Fig. 1 Capacitive Reflector 'Capaciflector' Geometry

Capaciflector Background

The sensor shown in Figure 1 depends upon detecting changes in capacitance when an object is brought near by. As can be seen from Figure 2, there is a substantial amount of stray capacitance when just a single plate, the sensor, is placed between the object and ground. Most of the sensitivity is lost due to stray capacitance coupling with the ground and very little coupling with the object. To reduce the stray capacitance, a conductive plate, driven at the same instantaneous voltage (and phase) as the sensor, is placed between the sensor and ground so as to 'shield' the effects of ground coupling. As can be seen from Figure 3, this shield greatly decreases the path to ground as observed in Figure 2, and subsequently reduces stray capacitance and enhances the coupling between the sensor and object.

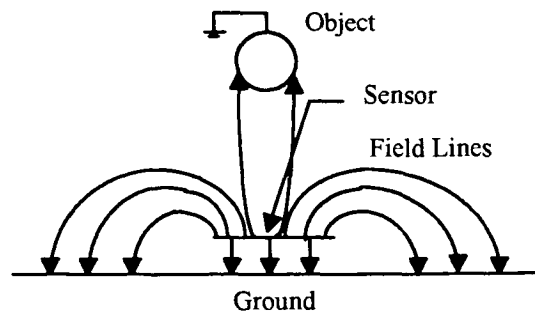


Fig 2. Sensor Without Shield

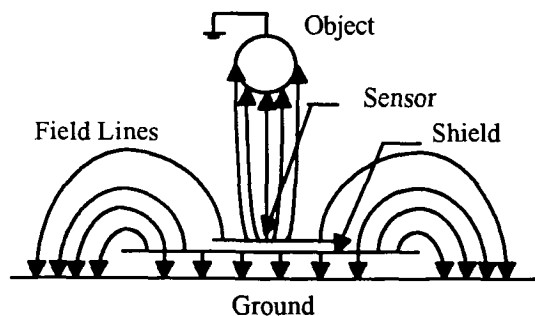


Fig3. Sensor With Shield

This shield is used to reflect the electric field lines of the sensor away from the ground plane and direct them outward toward an incoming object. In essence, the shield is reflecting the field lines outward, hence the name 'capaciflector' (Capacitive Reflector). To approximate this sensor in the classical sense, the sensor plate comprises one electrode of a 'virtual' capacitor. The incoming object can then be looked upon as the second plate of the capacitor. This 'virtual' capacitance in turn controls the frequency of oscillation of a relaxation oscillator, where frequency is proportional to the inverse of the capacitance. As the object gets closer to the sensor plate, this capacitance increases, resulting in a decrease in frequency at the output.

Sensor Electronics

The description of operation for this system includes two main topics: Communications (data transfer between the sensors and the computer interface, see Figures 4 and 5) and the actual operation of the sensor electronics.

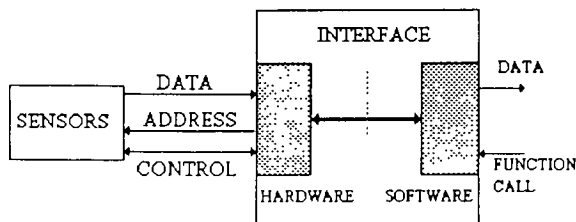


Fig. 4 Handshaking

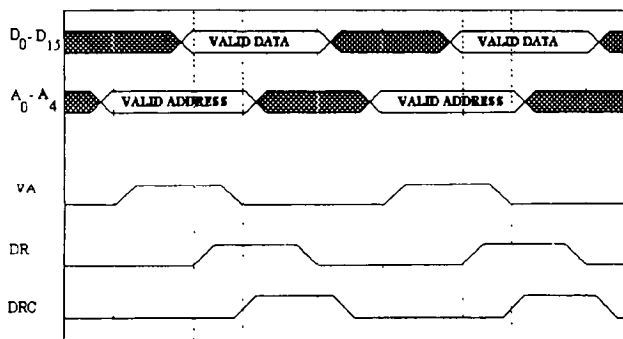


Fig. 5 Timing Diagram

The address lines ($A_0 - A_4$) contain a binary number representing a particular sensor. This is the sensor from which a measurement is being requested. The Valid Address control line (VA) is used to initiate a reading of the sensor. After the reading has been taken, the data will be present on a 16-bit output port from the analog to digital converter. The second control line, Data Ready (DR), is used to inform the interface that valid data is available. When the interface has secured the data, the third control

line, Data Received (DRC), will inform the sensor electronics that a successful acquisition has occurred. This action will disable the sensor electronics until a new address is placed on the lines. In the "handshaking" process, the sensor system controls the data line (digital voltage level) and the data ready control line. The interface controls the address lines, valid address control, and the data received control. The operation of the sensor electronics is shown in block diagram form in Figure 4 shown. Operations are initiated at the control lines of the Demultiplexer (D-MUX) chips. These D-MUX chips receive the 5-bit digital address of the selected sensor and send a signal to the sensor driver that will charge the addressed sensor. Application of this voltage induces a charge between the sensors and any adjacent conducting objects. This induced charge will change as the distance between the sensor and the adjacent object changes. The sensor driver circuit will then use the induced charge to produce a voltage level to be sent to the analog to digital converter. This is accomplished by using the principle that charge is equal to the capacitance multiplied by the voltage in a circuit. The sensor driver uses the sensor as a capacitor in a circuit with known voltage sources and resistors. As the magnitude of the capacitance changes, the voltage in the resistors will vary. As this voltage changes, opamps placed in the circuit measure this voltage and transform it to an analog voltage level. A different distance between sensors and adjacent objects will produce a different and unique charge and thus a different and unique voltage level. The analog to digital converter will use this voltage level to create a 16-bit binary number. Figure 3 shows these lines as $D_0 - D_{15}$. A different binary number will be given to each unique voltage level. At this point, the handshaking signals will complete a full cycle of communications as outlined above. The entire process, handshaking and sensor electronics operation, will be repeated upon request from the interface in the form of a 'high' on VA.

Specifications

- Operating temperature range is 0 to 70 degrees Celsius.
- Data will be presented to the computer as a 16-bit binary number.
- Precision will be one part in ten thousand.
- The circuitry will allow for 32 operating sensors.
- The maximum time to deliver the reading from a random sensor to the PC is 100 seconds.
- Sensor will detect conductive objects at a distance of two times the width of the shield.

Automatic Docking

The automatic docking system solves the ORU docking problem by automating the docking process through the use of computer control, thereby, minimizing the necessary manual manipulation of the device. Reducing the amount of manual manipulation required provides a twofold solution to the problems associated with ORU docking. First, the automated system allows the ORUs to be docked more precisely and more easily. Second, the amount of time spent docking the ORUs is reduced, allowing the astronauts more time to engage in other activities.

Figure 6 depicts the interconnection of the primary subsystems required by the automated ORU docking system and indicates the data flow between them. A sensor interface is necessary for communication between the sensor electronics and the computer. A robot interface is also needed to pass robot commands from the computer to the robot. Finally, an automated docking software module is required to process the sensor information and generate the robot commands necessary to automatically dock ORUs.

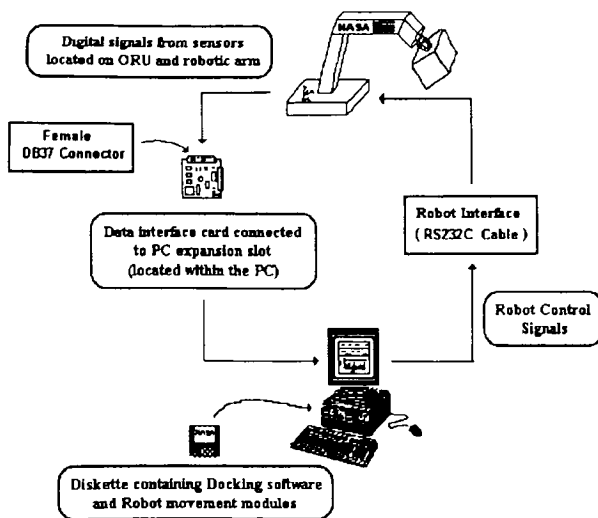


Fig. 6 Data Flow Diagram

Figure 7 illustrates the locations for the sensors on the ORU. It has been determined that these 20 sensors will provide all necessary information concerning the environment surrounding the ORU. In addition, there will be four sensors strategically placed on the robot arm for purposes of collision avoidance.

To use the automated docking system, the operator must run the program by entering the command "autodock" at the DOS prompt. Next, the operator may elect to enter optional information at the command prompt concerning the current population status of the pallet, such as "PALLET FULL" or "PALLET EMPTY". This information will be used to simplify the scanning process. The operator must then place the ORU within sensor range

of the pallet using manual controls, which will consist of the cursor keys to control motion in the x-y plane, and the + and - keys to control the position in the z-direction. Once the ORU is positioned above the pallet, the operator must enter the command "DOCK" at the command line prompt to initiate the docking procedure. The docking algorithms will then take control of the robot and begin systematically moving the ORU around the pallet scanning for an opening. When an available opening is found, the docking system will place the ORU into the opening. No user interaction is necessary once the docking process has begun; however, if the operator wishes to regain control of the robot arm during automatic mode, pressing the escape key will manually override the system and return control to the operator.

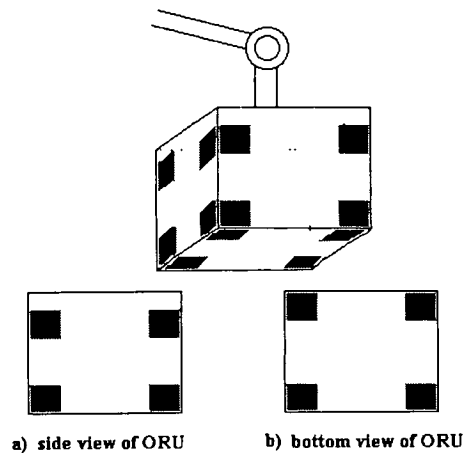


Fig. 7 ORU Sensor Location

If, at any time during the docking procedure, the rate of closure between either the ORU or the robot arm itself and an object indicates that the object is threatening to impact the ORU or the arm, the collision avoidance system will be engaged. The collision avoidance will also engage if, during manual control, the operator moves the ORU or the arm too close to a stationary object.

When the collision avoidance mechanism is triggered, a warning will be displayed on the screen, an audible alarm will sound, and all movement of the ORU will cease. User involvement will then be necessary to avoid the incoming object and remove the ORU from danger. Once it is deemed safe to continue, the operator can resume the docking procedure. The system, though, will not continue the docking procedure from the point where the object was encountered, but will restart the entire automated docking process because the ORU may have been moved by the operator thus corrupting the algorithms.

During both the manual and automatic modes, the user will be presented with a visual display screen depicting all of the information necessary to alert and inform the user of

the current system status. The screen will consist of three distinct sections: 1) warning messages, 2) command section, and 3) bar graphs representing sensor to object distances. Figure 8 illustrates the visual display screen.

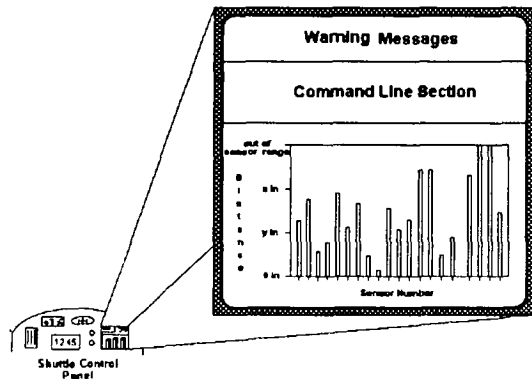


Fig. 8 Visual Display Screen

Any warnings which might be generated during the docking procedure, such as an impending collision, will be displayed in the warning message window. Warning messages will be accompanied by their own distinct auditory alarm in conjunction with the visual alert. The command section will be the area in which the prompt is displayed and the operator enters commands. The graph section of the screen will contain a separate bar for each individual sensor. As the distance between a sensor and an object decreases, the corresponding bar will become shorter. To increase the visual effectiveness of the bar graph display, the bars will change colors as the distance moves through various pre-defined ranges.

Specifications

- **Docking System**
 - Maximum Docking Time : 10 minutes
 - Maximum Distance Between ORU's : 1.125 inches
- **Collision Avoidance System**
 - Minimum Safe Distance : 2 inches
- **Sensor-PC Interface**
 - Data Lines : 16
 - Address Lines : 5
 - Control Lines : 3

Image Scanning

Some of the many tasks that the astronauts aboard the space station will do routinely include work done on an external storage pallet. Most of these duties will be accomplished with the use of a robot arm. This arm will be remotely controlled by an astronaut located in the protection of the space station's control room. To see the way to maneuver this arm and any load that it may be

carrying, such as an Orbital Research Unit (ORU), the operator will have only limited video riposte to indicate the relative locations of objects on the pallet. This lack of adequate visual feedback would tend to make it difficult to maneuver payloads around other objects that may already be on the pallet. To remedy this, a more complete feedback system was developed. This system is able to provide the operator with the necessary information to complete these tasks more efficiently. One method of accomplishing this is to provide a more complete visual image of the external pallet.

By interfacing low cost sensors to a personal computer, an image of the pallet is created. The data collected from the sensors is stored in such a manner so that the user can view the pallet from any perspective. This enables the operator to obtain a more complete visual understanding of the pallet and the elements contained on it.

When the user selects the scan option from the main menu bar, a pull down menu appears allowing the selection of the start command. This option initiates the robot control software to scan the pallet area. When the scanning starts, the robot arm moves the ORU from its current location on the pallet to the reference position (Figure 9). From here, the robot arm proceeds to follow the basic scanning motion outlined in Figures 10. Starting at the initial position, the sensors are checked to verify the existence or absence of an ORU at each of the positions available for the placement of ORUs (i.e. the dots). The sensor location on the ORU and sensor size are similar to those shown in Figures 7. Depending on the data received from the scan, a 0, 1, or 2 to indicate the number of ORUs in the current pallet position is written in the array location that corresponds to the current position on the pallet. This continues until every available location on the pallet has been scanned.

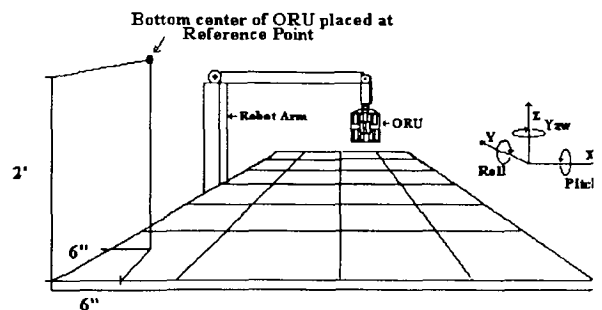


Fig. 9 Initial Position of ORU

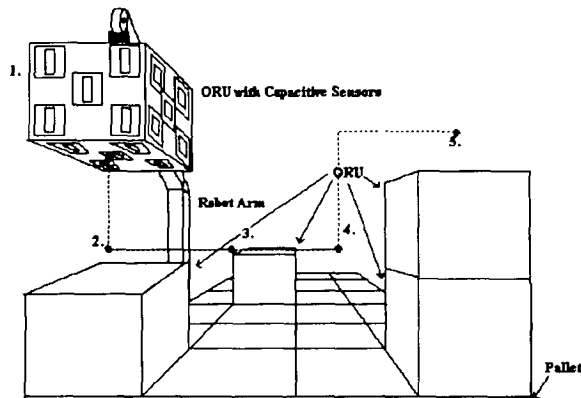


Fig. 10 It is with this type of scanning algorithm that a three dimensional view can be constructed. Through the use of software controls, the image can be viewed from almost any angle. The user has the option to rotate the image 360 degrees in fifteen degree increments. Figure 11 shows a representative view after the image data has been processed.

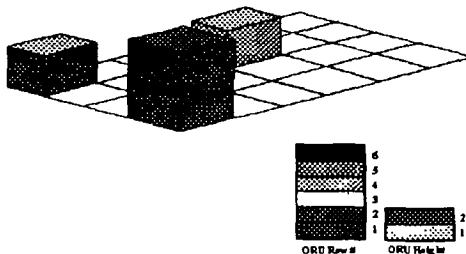


Fig. 11 Partially Rotated 3 Dimensional View of Pallet

As can be seen from the above figure, a distinct pattern of ORU's can be seen on the screen. All an astronaut has to do is rotate the image counter clockwise to see 'behind' a stack of ORU's. This greatly enhances perception when trying to place an ORU in its mounting fixture.

Specifications

To perform the calculation for the approximate image scanning time, a worst case analysis will be performed using the information supplied by product manufacturers and other groups involved in the NASA/USRA project.

Each time the robot moves, it moves approximately one foot. The manual for the robot arm, supplied by General Electric, states that the robot can move 59 inches in one second. Therefore, the time that it takes the robot to move one foot is approximately 200 ms. This time will be taken as 1 second, to account for starting and stopping the robot, general estimation error, and a certain degree of safety for

those standing near the pallet at the time the scan takes place.

To move the robot from the furthest location on the pallet to the reference position, the maximum distance that the robot will have to travel is 3 feet in the X direction, 3 feet in the Y direction, and 5 feet in the Z direction. Using the above estimate for robot travel, the maximum time to move the robot to its reference position is $(3+3+5) * 1 \text{ s} = 11$ seconds.

To gather the data from the sensor will take between 50 ms and 100 ms according to the sensor design group in the NASA/USRA project. The largest estimate will be used in the calculations.

To process the data gathered from the sensors will take a maximum of 1000 clock cycles of the CPU to accomplish. For a 16 MHz machine, this translates 10 under 10 us to complete. To account for varying machine speeds and estimation error, a value of 2 ms will be used in calculation.

The pallet arrangement for the worst scanning time is one where the possible ORU spaces alternate between being stacked 2 high and empty. In this case, the robot has to move 2 locations in the vertical direction at every location. In this scenario, the robot repeats the following process: It reads the sensors, processes the data, drops 1 foot, reads the sensors, processes the data, raises 1 foot, moves 1 foot in the current direction (either X or Z), reads the sensors, processes the data, moves another foot in the current direction and repeats. Since there are 24 possible locations on the pallet, this process is repeated 12 times. The total scan time will then be:

$$[12 (100 + 2 + 1000 + 100 + 2 + 1000 + 1000 + 100 + 2 + 1000\text{s}) + 11000] \text{ ms} = 62.67 \text{ s} = 1.045 \text{ minutes}$$

Tactile Feedback Robot Controller

Due to limited storage inherently associated with a space station, experimental data collection hardware can be stored outside of the orbiting craft.

The equipment used for each experiment will be placed in a space based ORU. The two foot cubes are attached to the pallet, which in turn is mounted on the space station. As was the case in previous systems, a one inch tolerance exists between adjacent ORUs.

ORUs are stored and retrieved by a remotely controlled robot arm. Visibility of the storage rack from the space station is limited to cameras mounted on the robot arm or a view from a window. Since it could be disastrous for an ORU to collide with the pallet or other objects, a method of carefully controlling the exact placement of the ORU during the docking and retrieving process is needed. An operator must adjust the position of the ORU using data obtained from visual sources and computer displays.

During the docking procedure, direct observation and television displays may not provide sufficient information, and precise manipulation of the ORU may be hindered.

The operator must visually monitor the movements of the ORU during docking, and avoid collision of the ORU with other objects. The control unit designed will allow the user to manipulate the movements of the ORU, while being assisted by visual and tactile feedback. This in turn would allow an operator to closely control the placement of the ORU during the docking procedure. With a computer supplying visual and tactile feedback based on data obtained from a telemetry system, placement of an ORU on the pallet can be greatly simplified.

An integrated docking system including a manual control unit with tactile feedback, a computer generated visual representation of an ORU, and both controlling routines and data collection software was developed. The system interprets data from sensors mounted on the ORU, takes movement commands from the control unit, and generates tactile and visual feedback, during manual control of the robot.

The integrated system designed and constructed allows an operator to dock an ORU on the pallet with no detailed direct visibility of the actual ORU. The operator, through tactile feedback from a control panel and visual feedback from a computer monitor, will be able to guide the ORU around obstacles and place it on the pallet.

The complete system, consists of a robot arm, an ORU with sensors, a control unit providing tactile feedback, an interface card for the Tactile Control Unit (TCU), a display providing visual feedback, and a computer controlling the system. The sensor electronics, robot arm, and their interfaces have been previously explained.

The operator must first move the ORU within the sensor range of the desired docking site. Then, using the visual feedback and the TCU, the ORU's position will be adjusted so that proper docking can proceed. As the ORU moves closer to the surface of the pallet, tactile feedback through the TCU will inform the user of the proximity to the pallet as well as other ORU's. The feedback consists of impulses having a frequency inversely proportional to the distance of the ORU from the object. The feedback begins at a range of 6 inches and a frequency of 1 Hz. As the distance of the ORU to the object decreases, the frequency of the feedback increases. The directional switch (for that particular direction) is deactivated via software and the feedback frequency will be 10 Hz, if the ORU is in danger of collision. The presence of an object within 0.75 inches of the ORU or 6 inches of the robot arm is considered dangerous. There are four sensors placed on the robot arm to monitor this.

The TCU consists of three multidirectional switches that will control the position of the ORU. Each

switch rocks at the center so that opposing directions of any given degree of freedom cannot be depressed at the same time. Beneath each arm of each switch there is an electromechanical device to provide the tactile feedback. Feedback is activated by commands from the controlling software.

Data which represents the switch positions is conveyed to the PC. Data from the ORU's sensors is used to generate a visual image, to decide if the desired movements will cause a collision, and to determine if feedback is necessary. If collision is imminent, the motions will not be relayed to the robot, and the feedback to the required switches on the TCU will become continuous.

The visual feedback is viewed as a grid on the PC monitor screen. A box-shaped image will represent the field of view of the ORU, rather than the ORU itself. Each surface of view is 6 inches from its corresponding side of the ORU.

Four sensors are placed on each of five sides of the ORU, the sixth side being attached to the robot arm. Each intersection of the dashed lines on the grid will correspond to the center of a sensor on that face. As the ORU approaches a surface, the visual feedback will be modified to reflect the objects surrounding it. This effect creates a better sense of the ORU orientation with respect to the object being sensed.

As the ORU is moved closer to the pallet, the grid will start to reflect this change. As the ORU moves closer, each intersection representing a sensor (that senses an object) will begin to disfigure in the direction of an imaginary force perpendicular to the face of the object. As the grid is registering an impeding object, a depth gauge is updated that represents the imaginary exertion force.

Below is a list of the color scheme giving each color used and the distance range (depth) it represents. All distances are in inches.

0 to 1	-	dark red
1 to 2	-	red
2 to 3	-	dark orange
3 to 4	-	orange
4 to 5	-	dark yellow
5 to 6	-	yellow
> 6	-	white

Specifications

- **Tactile Control Unit**

- Six degrees of freedom.

- Two degrees of freedom from each switch

- Three four way switches

- Tactile feedback through an impulse, applied in the opposite direction of each movement of each switch.

- **ORU and Robot**

- Experimental 1 foot square box.

Four sensors located in corners of each of five faces

Total of 20 sensors

Four sensors, one on either side of robot arm at two feet and four feet from ORU

- **Docking Software**

Visual representation of field of view of sensors.

Collection of sensor data.

Collection of control stick data.

Control of tactile stick feedback.

Control of robot arm movement.

THE PRELIMINARY DESIGN OF A UNIVERSAL MARTIAN LANDER

West Virginia University
Department of Mechanical and Aerospace Engineering
Morgantown, West Virginia

Dr. Timothy L. Norman, Asst. Prof
Mr. David Gaskin, NASA/USRA Grad TA
Mr. James Simpson, Systems Integrator

Mr. Sean Adkins
Mr. David MacDonnell
Mr. Enoch Ross

Mr. Kouichi Hashimoto
Mr. Loran Miller
Mr. John Sarick

Mr. Jonathan Hicks
Mr. Andrew Parlock
Mr. Scott Wenger

Abstract

As part of the NASA/USRA program, nineteen West Virginia University students conducted a preliminary design of a manned Universal Martian Lander (UML). The WVU design considers descent to Mars from polar orbit, a six month surface stay, and ascent for rendezvous. The design begins with an unmanned UML landing at Elysium Mons followed by the manned UML landing nearby. During the six month surface stay, the eight modules are assembled to form a Martian base where scientific experiments are performed. The mission also incorporates hydroponic plant growth into a Controlled Ecological Life Support System (CELSS) for water recycling, food production, and to counteract psycho-logical effects of living on Mars. In situ fuel production for the Martian Ascent and Rendezvous Vehicle (MARV) is produced from gases in the Martian atmosphere. Following surface operations, the eight member crew uses the MARV to return to the Martian Transfer Vehicle (MTV) for the journey home to Earth.

Introduction

America needs a systematic approach towards the exploration of our solar system. It began with the first suborbital flight of an United States astronaut in late 1959. In the years that followed, the critical steps needed to land humans on the moon were mastered. More than a decade of intense preparation and sacrifice culminated in the momentous day when Neil Armstrong became the first human to set foot on the moon. Like a young child learning to walk, Americans became more confident living in the strange new environment. New adventures began with Skylab and later with the reusable Space Shuttle. Space Station Freedom will be the next stepping stone to even grander adventures. A permanent base on the moon and then a first manned mission to Mars¹.

The Space Exploration Initiative (SEI) was enacted by President Bush to continue the systematic approach to

explore our solar system. His announcement of the SEI came as a bold challenge to do what must be done if America is to remain a leader in space sciences.

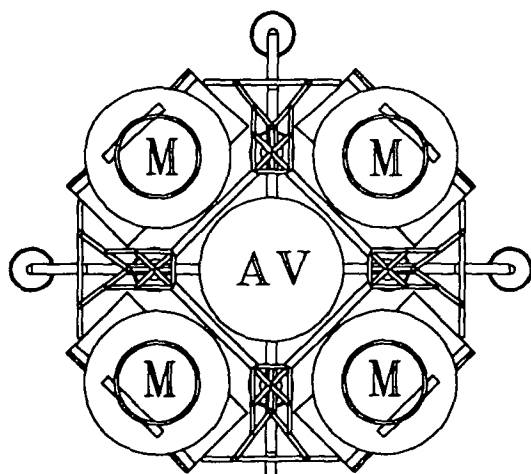
In the next 25 years, mankind will be undertaking yet another giant leap forward in the exploration of the solar system: a manned mission to Mars. This journey will provide important information on the composition and history of both Mars and the Solar System. A manned mission will also provide the opportunity to study how humans can adapt to long term space flight conditions and the Martian environment. The design of a vehicle to transport humans and equipment to Mars should be versatile while being low cost. The UML's design will provide a "universal" platform, consisting of four modules for living and laboratory experiments and a liquid-fuel propelled MARV. The distinguishing feature of the UML is the "universal" design of the modules which can be connected to form a network of laboratories and living quarters for future missions thereby reducing development and production costs. The UML will be able to provide America that opportunity to journey to Mars. The UML combines new technology, new thinking, and an ambitious approach to the challenge of the Space Exploration Initiative.

Within this summary report, the different subsystems and components of UML will be discussed. First, the structure of the truss and the modules are reviewed. This will be followed by a discussion of the different phases of the UML mission. This discussion begins with orbital parameters and the communication satellites used for the descent to the surface of Mars. The descent phase is discussed beginning with the stability maneuvers in orbit, aeroshield, parachute, and the finally the landing gear for touchdown on the surface. Features of the surface stay are discussed including the landing site selection, Universal Habitat Module (UHM) deployment, power systems, radiation concerns, fuel production, life support, environmental control, extravehicular activity, and physiological/psychological effects. The ascent phase is

then described by the aerodynamics and power systems of the MARV, ascent maneuvers, and rendezvous with the Martian Transfer Vehicle (MTV). The project costs are estimated in cost analysis. Finally, the conclusions will cover the unique attributes of the UML.

Structure

The configuration of the manned and unmanned UML's was designed with the following factors in mind. The two UML's needed to fit completely assembled into the Extended Heavy Lifting Launch Vehicle (EHLLV), which has a cylindrical cargo hold with a diameter of 14 meters (46 feet) and a height of 30.5 meters (100 feet). A limit of 75,000 kg was put on the weight of each lander, to keep the total weight of the two landers below the maximum lifting capacity of the EHLLV, which is 150,000 kg. The design



M=Module
AV=Ascent Vehicle

Figure 1. The planform view of the Universal Martian Lander with the landing gear deployed..

load for all structures (except the aeroshield) was the limit of 3 Earth g's, set by NASA for the astronauts, multiplied a safety factor of 2.

The Universal Martian Lander consists of four universal modules placed evenly around an ascent vehicle (Figure 2), with a truss structure used to support the modules and the ascent vehicle (Figure 1). The truss consists of over 550 tube-elements made of Boron-Aluminum. In the design of the truss it was assumed that each module would weigh 15% of the total weight (11,250 kg) and the ascent vehicle would weigh 30% of the total weight (22,500 kg). It was modeled on I-DEAS (Integrated Design Engineering Analysis

Software), where stress and buckling analysis were performed. The truss was optimized to its final form (Figure 3).

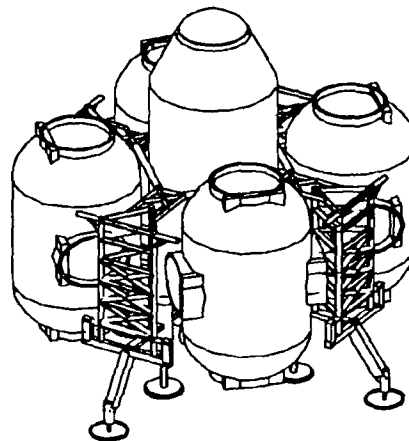


Figure 2. Overall configuration of the universal martian lander.

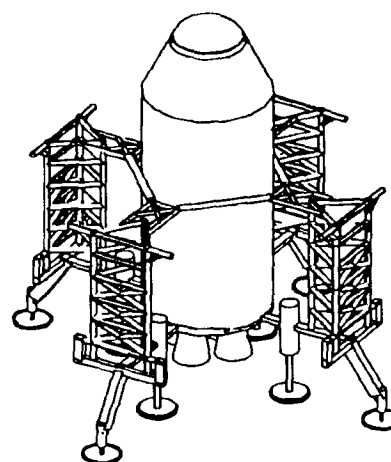


Figure 3. Diagram of the truss structure and the ascent vehicle after the modules have been removed.

The modules are 9.09 meters long and have a 4.25m diameter. Each module has 4 hatches, one on each end and one on each side (Figure 2). The structure of the modules is semimonocoque, using an aluminum 2219 skin with a thickness of 6 mm and Boron-Aluminum 4 cm x 8 cm x 1 cm box beam ribs.

Orbital Parameters

The MTV will orbit Mars during the mission; thus, the first consideration was to determine its orbit parameters. The MTV will be parked in a 250 km circular polar orbit about Mars with an inclination of 90°. The orbital period of the MTV was computed to be 1.84 hours. The orbital velocity was calculated to be 3.45 km/s.

The time of decay for the MTV in its 250 km orbit was calculated to ensure that the orbit would not substantially decay over the duration of the mission. Assuming a worst case scenario, the decay lifetime was calculated to be 1.89×10^8 years³.

Mars, like Earth, bulges at its equator. This bulge leads to 2 major effects on a low orbit. The first effect is the regression of the nodes. Calculations show that the node only regresses a maximum of -0.00885 radians after approximately 9 months. Therefore, the effect of the regression of the nodes on the MTV parking orbit of 250 km is negligible. The second effect of the equatorial bulge is the advance of the perigee⁴. The MTV orbit will be circular, therefore the advance of the perigee can be neglected.

Scan System

It was necessary to develop a communication and navigation network for the crew during the length of the Mars mission which would provide a continuous link with the MTV and Earth. The Satellite Communication And Navigation System (SCANS) configuration (Figure 4) was developed for this purpose.

Two satellites were designed to be carried on the MTV and launched into orbit after entering the polar orbit and prior to launch of descent vehicle to the surface. The satellites would then enter a geosynchronous orbit around Mars⁵. The orbit radius was determined to be 20,468.07 km. Once in a geostationary orbit, one satellite would be

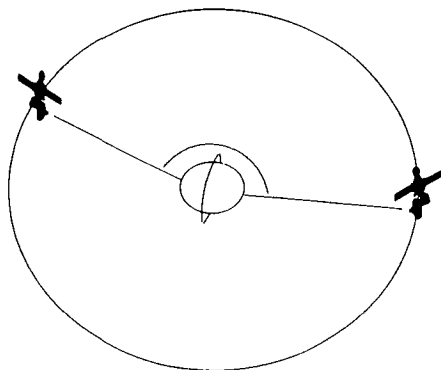


Figure 4. Schematic of SCAN satellite parameters.

positioned over the landing site. The second satellite would be 163° from the first one. This would allow for a continuous link between surface and the MTV. Information could be relayed from one to the other without interference from the planet. Therefore, there would be continuous communication link independent of the transfer vehicle's location.

The SCAN system served two main purposes. The first was for navigation during all stages of the mission. While on the Martian surface, the crew could use the SCAN while operating the rover. In the case of a sudden, blinding dust storm the satellites could relay navigation information to a rover so it could pin-point its location and determine the direction to the base. The second purpose was for communication. Communication to Earth could be obtained through the Deep Space Network (DSN) currently in operation. Contact between the crew members and the MTV or DSN satellites could be obtained through a network concept design (Figure 5). The network uses workstations on the surface and does major computing and data storage with a supercomputer left on the MTV.

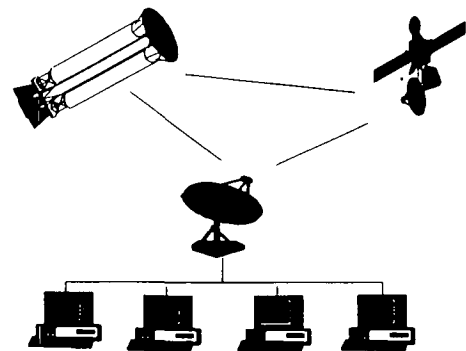


Figure 5. Schematic of network concept for communication.

Descent

Stability Maneuvers

Upon release from the MTV, the manned landing vehicle (MLV) and the unmanned vehicle go through a series of orbital maneuvers so to correctly orientate themselves for safe atmospheric penetration. After being released, the MLV will perform a gravity gradient stabilization maneuver, in order to orientate itself in a gravity gradient stable configuration. This maneuver will consist of one ninety second 957.4 N burn about the Y-axis, which is the orbit normal axis, to begin the MLV rotating and another identical burn to stop the rotation once the vehicle is in its stable configuration. These burns are

performed using the Reaction Control System, (RCS). To begin descent, the MLV will perform a deorbit burn. This deorbit burn will have a velocity change (ΔV) of 0.035 km/s. The burn will place the MLV into an elliptical orbit and allow the MLV to begin atmospheric penetration at 60 km above the Martian surface, with a atmospheric penetration velocity of 3543 m/s. A first-order approximation of ballistic entry for Mars descent was used to find the velocity and deceleration as the UML enters the atmosphere. The density of the atmosphere was based on data from the revised COSPAR (Council on Space and Research) data⁶.

The maximum deceleration of 3 Earth g's (29.43 m/s²) was satisfied with the final MLV configuration at an entry

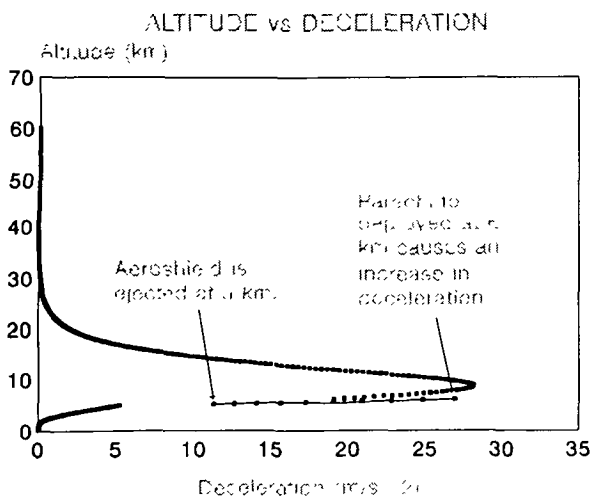


Figure 6 UML deceleration as a function of altitude.

angle and velocity of -2.25° , with respect to the atmospheric tangential, and 3540 m/s, respectively (Figure 7). The deployment of the parachute (26.9 m/s²) and the ejection of the aeroshield (11.3 m/s²) can be seen as discontinuities in the curve.

The plot of velocity versus altitude without the use of engines is shown in Figure 7. As seen in this figure, the velocity at surface impact was calculated to be approximately 8.5 meters per second. With this relatively low velocity, a successful landing is obtainable with the use of engines.

Descent

The aeroshield was designed to protect the UML's modules and truss from impinging flow and aerodynamic heating during atmospheric entry. The symmetry of the aeroshield allows the UML to perform a ballistic entry, however when an angle of attack is introduced a lift is created allowing maneuverability.

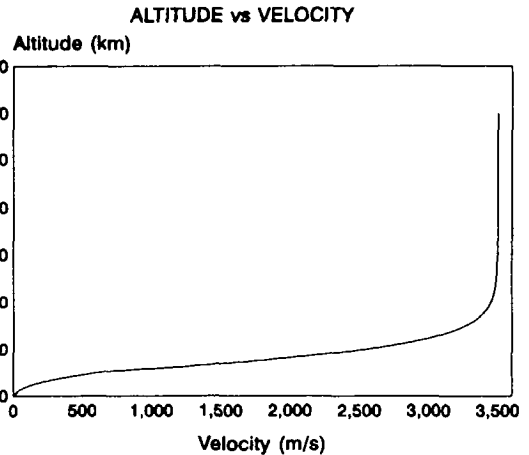


Figure 7 Altitude versus velocity for the final UML configuration.

The aeroshield structural design is based on the flexible/deployable aerobrake design performed at the Marshall Space Flight Center⁷. The shield was designed to fold and fit into the EHLLV. Twenty ribs were used to support the Tailorable Advanced Blanket Insulation (TABI). Four ribs are used to support the thin aluminum shell that makes up the rigid core. The final size and shape are shown in Figures 8 and 9.

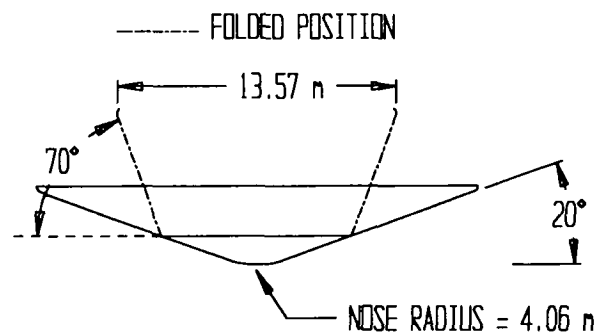


Figure 8. The aeroshield in its unfolded and folded position.

The Thermal Protection System (TPS) of the aeroshield used two different materials. The TABI will serve as TPS for the flexible/deployable outer ring and will be 2 cm thick. For the rigid core, it will have 0.5cm of ablative material, SLA-561 covering the Aluminum shell. According to a design by Marshall Space Flight Center, Aluminum-Lithium Alloy should be used for the ribs and the thin aluminum shell that makes up the rigid core. After

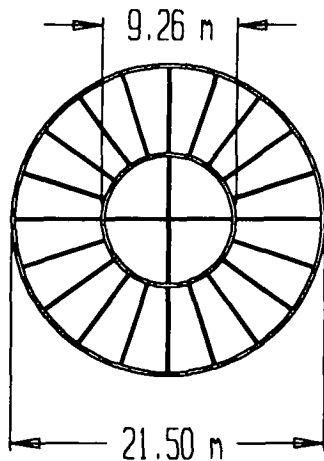


Figure 9. Overhead view of the aeroshield, looking at the inside structure.

researching Aluminum-Lithium alloys, a decision was made to use Aluminum 2090.

The maximum heat flux occurs at 32.2 km with a radiative heat flux of 256.511 kW/m^2 and a convective heat flux of 6.147 kW/m^2 . These values were dependent on the TABI thermal conductivity and emissivity. After reviewing hypersonic data, it was determined that the temperature ratios of a calorically perfect gas would be adequate⁸. Allowing for an angle of attack of ± 10 degrees. The impinging flow was calculated to be 22° toward the payload⁹ (Figure 10). Based on the impinging flow, the diameter was determined to be 21.5 meters.

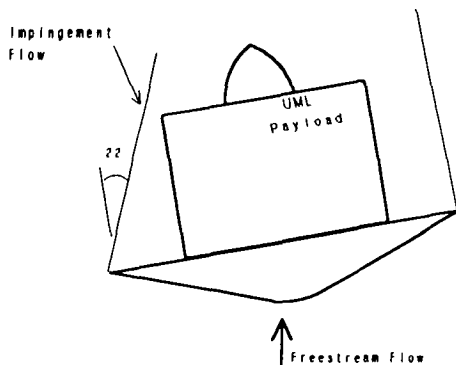


Figure 10. Impinging flow at a 10° angle of attack.

A parachute with a diameter of 15 meters will be deployed at 6000 meters above the surface. The parachute is made of dacron and will be ejected from the UML with the use of an explosive charge. The suspension line length for the parachute was determined to be 25.5 m^{10} .

The final descent sequence will begin with ignition of the four primary system's landing rockets. For simplicity,

weight and space savings it was desired that the same propulsion system was used for both the descent phase and the ascent phase. Each engine was designed to use in situ propellant. It was determined that four engines, each with a thrust of 334 kN (1340 kN total), a specific impulse (Isp) of 305 seconds, and a weight of 641.8 kg (2567.33 kg total) are needed for the descent phase. Throttleable engines were needed to ensure adequate control for the UML. Liquid carbon monoxide and oxygen were chosen as the propellants¹¹.

Landing Gear

The lander was designed with eight landing gear based on a Oleo-Pneumatic shock absorber (Figure 3). The stroke needed to safely land the UML was calculated to be 40 cm. For safe landing and blast off operation of the engines, a

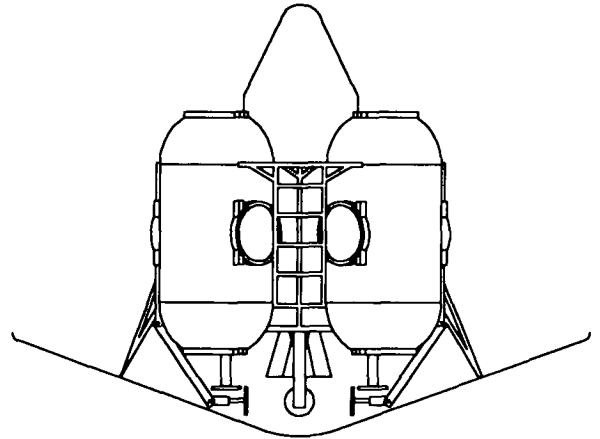


Figure 11. UML configuration for descent, landing gear stowed and aeroshield still attached.

distance of 1.2 m between the nozzle and the surface was needed. Based on this, the landing gear was designed with a 1.42 m length and a 15 cm diameter.

The final design of the landing gear needed to be able to fold up in order to allow the aeroshield to be attach to the truss structure (Figure 11).

Power Systems

The power requirements during the descent stage are estimated as 17.8 kW for the operation of the life support system and for the avionics.

The operation time of the descent stage power system consists of two phases. It is estimated that it will take 2 hours from lander release at the 250 km Martian orbit to touch-down on the Martian surface. Three days of Martian surface stay were allowed before the full operation of the

Martian-base power system for safety reasons. Thus, the descent stage power system was designed to fulfill the power requirements for both. Table 1 shows the power requirements for the 8-person crew systems during the descent stage.

The power sources for the descent stage are Silver-Zinc

Table 1: Power Requirements for Descent Stage.

Component	Power Requirement
Life Support	2.0 kW / Astronaut
Avionics	1.8 kW
Total	17.8 kW

(Ag-Zn) batteries and Hydrogen-Oxygen(H₂-O₂) fuel cells (Figure 12). Ag-Zn batteries are a reliable, quick reaction, and low maintenance power source for short periods, these batteries were the primary power source of the APOLLO Lunar Lander^{12,13}. H₂-O₂ fuel cells are a reliable and environmentally clean power source, which are used as the primary power system in Space Shuttle Orbiter. The total weight of the descent stage power system is 1329.3 kg.

Electrical power requirements during the ascent stage are considered to be the same as the power requirements during the descent stage. The operation time is estimated as 5 hours until the rendezvous at 250 km Martian orbit.

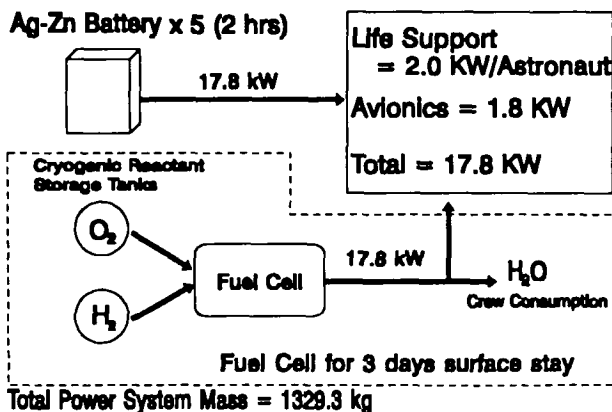


Figure 12 Power Distribution Schematic for Descent Stage

Surface Activities

Landing site

There were three criteria used in determining the landing site: safety, climate and experimental value. The area known as Elysium Mons in the Northern hemisphere was chosen as the landing site. This site is in a plain region of medium altitude approximately 26° N and 216° W. For safety a low altitude and flat area was desired¹⁴. The lower altitude would allow for the UML to be exposed to the atmosphere longer, providing more drag and longer time for the parachute and aeroshield to be more effective for deceleration. The Northern hemisphere is also noted for having longer summers and less violent wind and dust storms. The topographic features of the landing site are accessible by a rover and would make surface experiments accessible. Near the site there is a large volcano and several lava overflow channels¹⁵. There are several small craters, large channels or canyons possibly formed by water, and tectonic troughs.

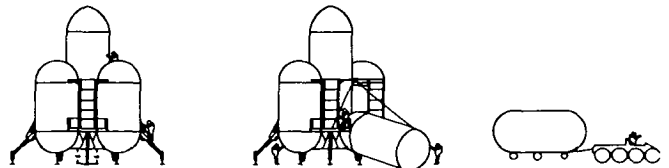


Figure 13 Sequence of steps in Habitat Module Deployment.

UHM Deployment

Once on the surface the astronauts will exit the ascent/descent module and rendezvous with the Unmanned Martian Lander for Universal Habitat Module (UHM) deployment. The detachment of the Manned Unmanned Martian Explorer (MUME) will take place first. The detachment of equipment and UHMs will follow the same procedure. Four electrically driven winches will be located on the truss near the connection of the interior landing gear. Each winch will have a cable connected to the top of each UHM. Once the winches are proven operational, the explosive bolts holding the cylinder to the Main Truss will be activated. This will disconnect the top of the UHM completely and leave the UHM supported by the two rotational shafts on the lower connection and the cable from above. The UHM will then be lowered to the surface. Once the top of the cylinder is lowered to the ground, the cable will be manually removed and reattached to the bottom end of the UHM. The rotational shafts will be

detached from the Main Truss and the UHM will be lowered to the ground.

The MUME will transport the cylinder into a designated position to be connected to the next UHM lowered. This will be repeated for each UHM removal (Figure 13). Once the UHM's are removed they may be joined in several different ways. An example of one way is shown in Figure 14.

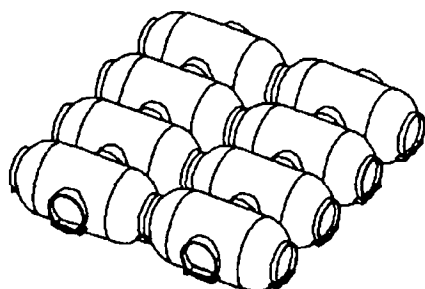


Figure 14. Layout of a possible module configuration for a martian base.

Power Systems

The power requirements for the habitat module during the Martian surface stay are estimated as 54.9 kW during daytime, and 19.7 kW during night. Table 2 shows the power requirements for the habitat module of the eight on crew systems. A deployable type solar array is selected rather than a rigid array configurations for the Martian daytime power source. In the interest of lowering the total array deployment costs, the same type of mast as used for the OAST-1 wing was chosen¹⁵. Although the OAST-1 wing was designed for the zero-gravity environment, the application for the Mars mission is still considered to be possible. The power produced by the solar array needs to fulfil both the daytime power requirements and stored power requirement for night use. The 102.3 kW of electrical power is required from the solar array to fulfill both 54.9 kW of daytime power requirement and the 47.4 kW for RFC systems. An area size of 2361.2 m² is required to produce sufficient amount of electrical power on the Martian surface. The total power system mass is 6904.7 kg. The power system for the habitat modules during the Martian surface stay was illustrated in Figure 15 and the solar wing in Figure 16.

The CLEFT GaAs/CuInSe₂ Tandem with deployable solar array system was selected for the power source during Martian daytime. Cleavage of Lateral Epitaxial Film for Transfer (CLEFT) Gallium Arsenide (GaAs) with Copper

Indium Selenide (CuInSe₂) array shows the highest efficiency (23.1%) ever-reported for thin-film photovoltaic cell¹⁶, and this is the reason for the selection. The hydrogen-oxygen regenerative fuel cell (RFC) with a cryogenic reactant storage system was selected for the power source for the nighttime power production.

Table 2: Power Requirements for Habitat Module.

Day Time:

Component	Power Requirement
Life Support	2.0 kW / Astronaut
CDMS	2.2 kW
Science	5.0 kW
Rover	0.5 kW
Fuel Production	31.2 kW
Total	54.9 kW

Night Time:

Component	Power Requirement
Life Support	2.0 kW / Astronaut
CDMS	2.2 kW
Science	1.0 kW
Rover	0.5 kW
Total	19.7 kW

samples, assemble, maintain, repair, inspect, and service their habitat and user systems. Three major components of an EVA are: Airlocks, Decompression, and EVA suits. There are 2 identical airlocks installed for the UML which accommodate EVA suits with 2 crew members and a CO₂ shower. The CO₂ will be used to blow off debris gathered on the suit during an EVA.

Decompression sickness is an extremely dangerous injury. If a pressure change forms on the body too rapidly, nitrogen in the blood will bubble. This bubble can cause extreme pain and even death. The airlock provides a means of controlling the pressure change and therefore, preventing decompression sickness.

Decompression times are primarily based on how long a person has been subject to a particular pressure, the partial pressure of oxygen at that pressure, and what is the required pressure change. To minimize decompression times in the modules, it was decided to decrease the pressure difference between the habitat modules and suit environments. When the cabin pressure is decreased, the oxygen partial pressure drops. This is corrected by increasing the percentage of oxygen in the module environment from a typical 21.0% to 40.0%. In doing so, decompression times decrease. The final time needed for decompression will be approximately 30 minutes²⁰.

The EVA suit allows a person to survive in a hostile space environment. Today's suits are extremely reliable and have an expected life of 15 years. In order to reduce mission costs, existing suits are suitable for the UML. Slight modifications may be made as suit technology unfolds. One such modification will be to incorporate suit monitoring of the EVA in a heads-up-display (HUD). This allows the person in the suit to read the information faster and more accurately. The best feature in the HUD will be its compass navigation system which is fixed to the UML's ascent vehicle. This will keep the EVA member oriented to "home" via directional and distance indicators.

Twelve suits will provide each of the 8 crew members with one suit each. The remaining 4 suits will be used in case of an emergency and/or spare parts.

The detection of fire is performed in 3 ways: visual detection, smoke detection, and heat detection. Fire extinguishers are strategically placed and are readily available. Self contained oxygen tanks (SCOT) will also be easily accessible. Once a fire is detected CO₂ from the Martian atmosphere is pumped into the compartment and extinguishes the fire. CO₂ was chosen because of its effectiveness against fires and because it requires no storage.

Physiological/Psychological Effects

During the mission to Mars the astronauts will be in a micro-gravity environment as well as a near zero gravity environment during flight for an extended period of time.

A mission to Mars is a quantum leap for the space program. Therefore, the physiological and psychological needs of the astronauts place an extremely important role in planning a Mars mission.

Micro-gravity environment has a number of effects on human body. These effects include muscle and bone atrophy, body fluid shifts, and cardio-pulmonary problems, which include heart shrinkage, blood pressure fluctuation, and blood cell changes. Motion sickness affects only some astronauts²¹. Little information is available that addresses physiological effects during long duration space flight and return to a gravity environment. Current research suggests that one way to help counteract the effects of microgravity is to have a rigid exercise regime. Throughout the duration of the mission the crew members will adhere to an exercise program regularly. Astronauts chosen for this Mars mission will be in top physical condition.

A dedicated mini-gym will include a treadmill, a rowing ergometer, and weight machines. Additionally, a "Penguin suit", as used by Russian cosmonauts can be used. Exercise not only serves as a physiological need, but also as a form of recreation.

A Health Maintenance Facility (HMF) was incorporated into the UML and is designed to handle emergencies that can be treated by an emergency room on Earth²².

Psychological needs are extremely important for a mission that is the length of the Mars mission. Windows have been included in the modules²³. The windows give the astronauts the chance to reflect on home life and also reduce "cabin fever"²⁴.

Ascent

Structure

The ascent vehicle is 12m tall and has a diameter 4.25m. It contains the crew module, a kick motor, the main engine and the fuel (Figure 17). It was designed after a

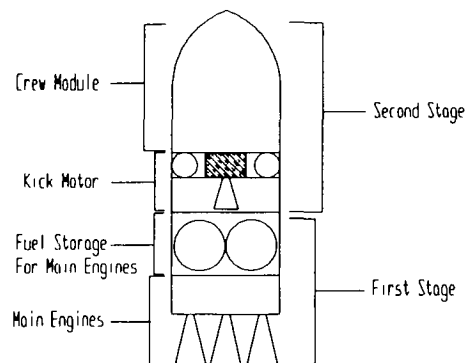


Figure 17. Schematic of the ascent vehicles major components.

aircraft fuselage with stringers and ribs using aluminum 2219 as the material. For added control during the ascent flight, moveable fins were placed at the base of the ascent vehicle. Once the modules are removed, the truss structure will act as a launching pad for the ascent vehicle (Figure 3).

Aerodynamics

The ascent phase was modeled in a computer program using Milne's Method of integration²⁵. The program modeled a rocket which accelerated vertically with no gravity turn. The module must be throttled down from full thrust of 1,340 kN to avoid excessive g loading. The total MARV weight, including fuel, is 31,204 kg. The nose cone geometry was selected to be an ogive configuration with a radius of curvature of 3.25 meters. This nose cone gives the module more space for equipment and crew. The wave drag and the skin friction drag coefficients were calculated in the program using equations for an ogive nose cone²⁶.

According to the program the time until burnout for the ascent module is 87.5 seconds. If the module were to accelerate straight upward, it would reach an altitude of 105 kilometers, and the velocity would peak at 2.5 km/s. The module does not reach 100% thrust because of the 3 Earth g limitation. The ascent module will have to be throttled down even more due to acceleration from a gravity turn. This gravity turn places the ascent module in a circular orbit around Mars.

A secondary system engine is needed to boost the ascent vehicle to an altitude of 240 km. An engine similar to Rockwell's RS-41 is used to provide a thrust of 12 kN²⁷. A storable liquid propellant called nitrogen tetroxide/monomethylhydrazine is used to fuel the secondary engine with an Isp of 320 seconds. With a length of 1.88 m and a nozzle diameter of 0.98 m, the secondary upperstage engine weighs 68.95 kg.

Ascent Maneuvers

The ascent analysis was started by selecting the proper pre-rendezvous orbit from which to park the MARV. The "below and behind" geometry will be used in order to allow proper phasing of the rendezvous procedure²⁸. The MARV will have to park in a lower orbit before parking in a pre-rendezvous orbit of 240 km due to the fuel and thrust constraints. A gravity-turn trajectory would be used to obtain a preliminary 60 km orbit. After the MARV has been in flight for 50 seconds, it will be rotated at a constant rate of 2.4 rad/s for the remainder of the burn time, or 37.5 seconds. The MARV will then circularize in a 60 km orbit. The velocity at burn-out was calculated to be 3.54 km/s. A small ΔV of 0.956 km/s will be needed using the RCS at the instant of main engine burn-out in order to successfully park the MARV in a 60 km orbit. Then the MARV would

move into a 240 km orbit to prepare for docking with the MTV using a secondary engine. The time to reach the 240 km orbit from 60 km was 52.8 minutes.

Rendezvous

The MARV will move from the 240 km orbit to the 250 km and "catch" the MTV. The ΔV needed for this maneuver was 0.00476 km/s. The coast time was found to be 54.95 minutes. A thrust of 46.92 N for rendezvous maneuvers was calculated. The thrust needed for rendezvous was estimated by assuming that all of the 18000 kg of fuel will be consumed in reaching the 60 km orbit and the mass of the MARV was 15,600 kg. The velocity was estimated by calculating an average velocity between the 240 km and 250 km orbits. COSPAR data was used to obtain a density of 250000 kg/km³ at a 245 km orbit. A C_d of 1.0 and a frontal area of 14.19 m² for the MARV were used.

All maneuvers are controlled by a fully autonomous Guidance, Navigation, and Control computer system with pilot override. The flight computer would gather information from an inertial measurement unit, radar, position sensors, and navigation beacons. Then determine trajectory, attitude, and flight path and make adjustments or deploy devices as needed.

Cost Analysis

The UML hardware development and production cost will be \$8.70 billion in 1993 constant value dollars. This estimate is based on existing flight hardware cost estimates or from developing new technologies to produce new flight hardware. This analysis uses primarily cost estimates from a Lunar Lander cost analysis. This Lunar Lander analysis used previous cost data from the Apollo and Space Station Freedom programs²⁹. This cost analysis also looks at the manned UML only. The unmanned UML will differ from the manned lander UML because the unmanned UML will be remotely piloted from the orbiting MTV.

This analysis estimates the cost to design, test, build, and integrate the various UML subsystems. Each phase has a development and production phase. Analysis is broken down into these 8 different phases: Developmental drafting, design, project management, manufacturing, Production drafting, design, project management, and manufacturing. The cost analysis allows for any portion of the project cost to be defined carefully.

Earth-based integration and testing will provide a method of verifying proper functioning of the UML. The integration will consist of all subsystems in the UML testing together for an operational readiness test. This testing will provide the engineers the means of finding errors in the assembling of subsystems. This test will help to ensure mission success.

Conclusions

This design will adapt to many future Mars mission requirements. The UML uses modular design to allow flexibility in Martian base setup configuration. The UML has a standard pressurized or unpressurized vessel which can be used for a variety of needs. Each module is the same as other modules, with the exception of equipment modules which may have a large swinging door to allow the deployment of small transport vehicles. These swinging doors will be resealable. Each module can be attached from all 4 sides and to form a base. Each module hatch can be pressurized or unpressurized for changing base needs.

The same vehicle is used to provide final deceleration and complete transport to Martian orbit during ascent. Just prior to touchdown on Mars, the main engines will be used to slow the UML to landing velocity. Once the fuel tanks are refueled with in situ propellant, the same motors will be used for ascent and rendezvous with the orbiting MTV. Having only one set of engines will greatly reduce mass and cost of the UML.

The recycling of vital resources helps reduce mass of the UML. By recycling all water, the amount of mass saved is several thousand kilograms. This saved mass will allow more scientific payloads to be taken to Mars. This is the same case for replenishing air. Without recycling resources such as water and air, the mission would be greatly hampered.

The UML design has attempted to minimize psychological effects on a closed environment. There are 8 windows per module which will give the crew members the feeling of an open environment. The UML design calls for individual sleep chambers for privacy and multiple rooms to create the feeling of a large living space. Through the use of ECLSS, the hydroponically grown plants (wheat, lettuce) will provide the crew members a change of scenery that is reminiscent of Earth.

References

1. Aldrin, Buzz, McConnell, Malcolm, Men From Earth, Bantam, New York, 1989.
2. Stafford, Thomas P., America at the Threshold: America's Space Exploration Initiative, Synthesis Group, Arlington, VA, 1991.
3. Wiesel, William E. Spaceflight Dynamics. McGraw-Hill, Inc. 1989. p.85
4. Ibid., p.87
5. Agrawal, Brij N. Design of Geosynchronous Spacecraft. Prentice-Hall, Inc. Englewood Cliffs, New Jersey. 1986
6. Tartabini, Paul V., and Suit, W.T., "Aerobraking Characteristics for Several Potential Manned Mars Entry Vehicles", NASA Langley Research Center, Hampton, VA, N90-14272, Nov. 1989.
7. Dickerson, Tom, "LTV Aerobrake Assessment", NASA Marshall Space Flight Center, Huntsville, AL, July 1990.
8. Anderson, John D., Jr., Hypersonic and High Temperature Gas Dynamics., McGraw-Hill, New York, 1989, pp. 507-513.
9. Dickerson, Tom, "LTV Aerobrake Assessment", NASA Marshall Space Flight Center, Huntsville, AL, July 1990.
10. Bendura, R.J., Lundstrom, R.R., Renfroe, P.G., and LeCroy, S.R., "Flight Tests of Viking Parachute System in Three Mach Number Regimes," NASA Langley Research Center, Hampton, Virginia, NASA TN-7734, Nov. 1974, pp. 4-56.
11. Roncace, E.A., "In-Situ Propellant Rocket Engines for Mars Mission Ascent Vehicle", NASA Lewis Research Center, Cleveland, Ohio, N91-24305, June 1991.
12. The National Aeronautics and Space Administration Manned Spacecraft center, APOLLO SPACECRAFT NEWS REFERENCE, Grumman Aircraft engineering corporation, Pg EP-1
13. Griffin, M.D. & French, J.R. Space Vehicle Design, AIAA.
14. Masursky, Harold & Crabill, Norman. Viking Site Selection and Certification. NASA Scientific and Technical Information Branch. Washington, D.C. 1981. p.9
15. Carr, Michael H. Surface of Mars. Yale University Press. New Haven, Connecticut. 1981. p.106
16. N. P. Kim, R. M. Burgess, R. A. Mickelsen, and B. J. Stanbery, Progress in GaAs/CuInSe₂ Tandem Junction Solar Cells, N91- 19190
17. William E. Simon, Donald L. Nored, Manned Spacecraft Electrical Power Systems, Proceedings of the IEEE, vol.75, No.3, March 1987

18. Armstrong, Elizabeth S., "Cooling of In Situ Propellant Rocket Engines for Mars Mission", NASA TM-103729, NASA Lewis Research Center, Cleveland, OH, January 1991.
19. Skoog, A. I., BLSS: A Contribution To Future Life Support Adv. Space Rec. Vol. 4, No. 12, pp. 251-262, 1984
20. Extravehicular Activity System and Airlock Comprehension. Mission Operations Directorate, Matt Lindsey, Nov. 1991.
21. Gannon, Robert "The Unbearable Lightness of Space Travel," Popular Science March 1993, pp 74-79.
22. Design of a Fast Crew Transfer Vehicle to Mars. Scientific and Technical Aerospace Report, The Mars Company, May 1988, N89-15968.
23. Human Performance Issues Arising from Manned Space Station Missions. Scientific and Technical Aerospace Report, N88-25156
24. Design of a Fast Crew Transfer Vehicle to Mars. Scientific and Technical Aerospace Report, The Mars Company, May 1988, N89-15968.
25. James, M.L., Smith, and Wolford. Applied Numerical Methods for Digital Computation., 3rd Ed., Harpers and Row, 1985.
26. Chin, S.S., Missile Configuration Design., The Martin Company, Orlando, FL, McGraw-Hill, New York, 1961.
27. Rockwell International, "A Past to Build a Future On," Rocketdyne Division, Canoga Park, CA, 1991.
28. Griffin, M.D. & French, J.R. Space Vehicle Design. AIAA. p.57
29. Eagle Engineering, Inc. "Lunar Base Scenario Cost Estimates," Eagle Engineering, Inc., Houston, Texas, N89-15286, Oct.1988.

Association, West Virginia University, University of Minnesota, Rockwell International Corporation, Redstone Scientific Information Center, Remtech Inc., and U.S. Army Missile Command at Redstone Military Arsenal.

Acknowledgements

The MAE 120/236 design class wishes to acknowledge the following for their tremendous contributions. Their contributions were vital to the completion of this design: Frank Swalley, program monitor at NASA - George C. Marshall Space Flight Center, Langley, L.B. Johnson Space Flight Center, and University Space Research

JUPITER EXPLORATION USING FUSION ROCKET INTEGRATION (JEFRI)

The University of Wisconsin-Madison
Department of Engineering Mechanics and Astronautics
Madison, Wisconsin

Ronald E. Thomson, Instructor
Dr. John F. Santarius, Senior Scientist
Anthony Kellicut, Teaching Assistant

Theodore Zach (team leader), Christopher C. Drews, Bryan C. Davis, Ned Finnell, Michael J. Hernandez, D. Andrew Pierpont, William D. Strauss

Abstract

This project encompasses the design of a spacecraft for a three year round trip mission to collect data on the environmental and geological conditions of the Jovian moons. The design emphasizes the propulsion aspects and environmental control of the fusion engine, structure and shielding, dynamics, and habitat design. The spacecraft is configured about its spin axis which passes through the major axis of a cylindrically shaped engine and the center of a torus which houses the living modules and science platforms. Artificial gravity is created by rotation of the torus, which houses the astronauts in shielded and ergonomically-designed living modules. The type of fusion engine used is the Field Reversed Configuration. The engine is high-velocity-low thrust, and can utilize three different propulsion options: direct, mass-augmented, and NERVA-mode exhaust. The hydrogen propellant is stored as a liquid and frozen before injection. Deuterium and Helium-3, the fuel, is injected into the engine at its midpoint from external storage tanks. The engine is enclosed in a bioshield and rejects waste heat via a liquid drop radiator that uses sheets of liquid aluminum, which is piped in a continuous loop from an external emitter to a collector for heat rejection.

Introduction

Spacecraft carrying humans to the planets of the outer solar system, because of the large distances involved, require the high velocity performances achieved through the use of fusion propulsion. For a mission to Jupiter, a chemical rocket would reach the planet in 3 years, whereas a fusion rocket carrying an equivalent payload is capable of reaching the planet in approximately 1 year.¹ Fusion rockets are able to achieve such high velocities because of the extremely

high temperatures produced by their reactions and the low molecular weight of their exhaust products. The temperature of the fusion products can reach 10^9 K,² and the molecular weight of the primary exhaust product, the proton, is 1.0. The resulting maximum I_{sp} is 10^6 seconds,² which is more than a thousand times the specific impulse of chemical propulsion systems.

Previous Designs

Senior design classes of 1989 and 1991 completed designs of fusion powered rockets that served as bases for the 1993 JEFRI design.^{3,4} However, differences do exist in the original specifications between this year's and the previous projects. Namely, both 1989 and 1991 teams used another type of engine, the tandem mirror, as the basis for the design.

In addition, the previous designs have focused on orbital analysis, flight plans, the tandem mirror propulsion system, and life support systems. This year's design team chose to focus on propulsion systems of the FRC, structure, and shielding.

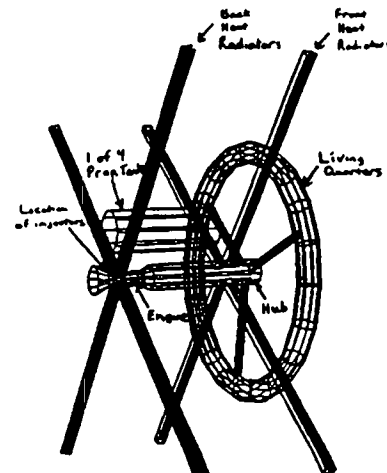


Fig. 1 JEFRI Rocket

Mission Analysis/Environmental Design

Radiation

For the duration of the three year mission, the living quarters requires shielding against both solar flare particles (SFP) and galactic cosmic rays (GCR). The expected dose for SFP is 53 rem/year⁵ to 331 rem/month and the expected dose for GCR is 45.1 to 120.6 rem/year. For shielding, a material with a low atomic mass number and a significant hydrogen content is desired.⁶ Aluminum 2024-T3 with a low amount of silicon was chosen for the walls of the living quarters, with a thickness of 11.4 cm. This would reduce the GCR dose to 35 rem/year during solar flare (SF) minimums. During SF maximums, the crew will stay in a saferoom, which contains an extra 10.4 cm of shielding.

Space Debris

The flux of meteoroids in low earth orbit is described the logarithmic distribution:⁷

$$\text{Log}_{10}(N) = -14.41 - 1.22 \cdot \text{Log}_{10}(m) \quad (1)$$

where N is the meteoroid flux is number/m²s and m is the mass in grams of the meteoroid particle. This equation is valid for meteoroids with a m ranging from 10⁻¹² to 10 g. In interplanetary space, the flux correspondingly increases and a correction factor needs to be applied to the flux:⁸

$$N_{i.p.} = N \cdot m^{-0.9} \quad (2)$$

where Ni.p. is the flux in interplanetary space. The number of impacts per mission can then be solved for using:

$$\# \text{ impacts} = N_{i.p.} \cdot A_p \cdot t \quad (3)$$

where A_p is the projected area of the target in m² and t is the time of exposure in seconds of the target over the duration of the mission. Using this equation, the probability of the torus colliding with a meteoroid of 0.0293 g was determined to be 100% and for a meteoroid of mass 2.2545 g, 0.01%.

Operations Support

Implementation of Artificial Gravity

Artificial gravity is necessary in this application for both health and productivity reasons.³ To induce

this condition within the craft, the torus (which houses the living modules) must be rotated.

There are many short term physiological effects which result from improper levels. Therefore, the rotational velocity of the craft must fall within limits to prevent the onset of these symptoms. These limits are defined by the Coriolis effect.

Coriolis effect. The Coriolis forces will either add to or subtract from a person's weight depending on their direction of locomotion within the spinning torus.

The Coriolis force is calculated as a percentage of the person's weight.

$$\%C = \frac{2 \cdot \omega \cdot v_{rel}}{r \cdot \omega^2} \cdot 100 \% \quad (4)$$

According to human factors data: a Coriolis percentage of over 20% will cause the occupant discomfort ; a spin rate greater than 4.0 rpm will cause motion sickness in the crew.⁹

From reasonable Coriolis percentage (%C) ranges, their corresponding radii¹⁰, and the limitations on the radius of the torus, a radius of 35 m and a gravity ration of 0.41g was determined to be necessary.

Design of the Living Quarters

The living area, shown in Figure 2, was designed to supply maximum comfort, to meet the criteria of minimum living area per person, and to follow previously defined and human factors constraints.

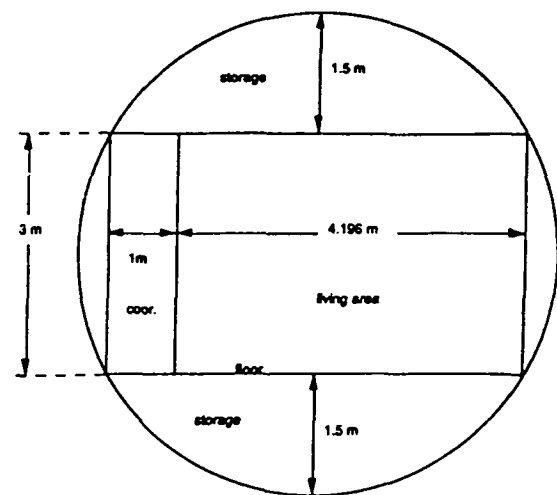


Fig. 2 Cross section of Living Modules

Results. Design Parameters are shown in Table 1.

Table 1 Design Specifications for Living Modules

Percentage of Torus for Living Area	25
Number of Cabins	12
Volume of Living Space/person (m ³)	44
Volume of Recreational Area (m ³)	163

The area marked "Storage" in the Figure 2 is designated for storing equipment, food, and water, and also contains piping for the habitat.

Shielding and Structure

Interior of the Torus

Materials Selection of the Interior. Previous astronautics projects and research clearly indicates that the best choice for interior supports of the spacecraft are be a glass-fiber reinforced plastic (GFRP), due to its high strength to weight ratio.¹⁰

The possible resins for GFRP are limited due to this particular application. The space environment has high levels of radiation that limit options to three choices: epoxies, polyesters, and phenolics.¹¹

Beacuse these supports are internally located, they will not experience any pressure or temperature extremes. For pressures of one atmosphere, room temperature, and slight radiation exposure, polyester is the best base resin. The specific laminate chosen is Paraplex P-43 due to its high flexural strength.

Impact Plate for the Torus

Two types of impact plates for meteoroid shielding were examined, one a single solid sheet of metal or composite with a low density and high Brinell hardness and the other a bumper shield with three sheets of material for shielding. It was determined that the bumper shield was the best choice to keep shielding mass to a minimum. The equations for the three bumpers is given by:¹²

$$t_1 = \frac{0.13 \cdot d_p \cdot \rho_p}{\rho} \quad (5)$$

$$t_2 = 0.3 \cdot t_1 \quad (6)$$

$$t_3 = \frac{4.85 \cdot e^{-5} \cdot f \cdot m_p^{0.367} \cdot \rho_p^{0.133} \cdot V_p^{0.667}}{H_3^{0.25} \cdot \rho_3^{0.167}} \quad (7)$$

where

t_1, t_2, t_3 = the thickness of the 1st, 2nd and 3rd walls, cm

ρ_1, ρ_3 = density of the 1st and 3rd walls, g/cm³

d_p = diameter of the projectile, cm

ρ_p = density of projectile g/cm³

m_p = mass of the projectile, g

V_p = velocity of impact in cm/s

f = the finite sheet factor, 1.8

H_3 = Brinell hardness of target material

The seperation of the 1st and 2nd bumpers h_1 , and h_2 , in cm, are calculated by:¹²

$$h_1 = 30 \cdot d_p \quad (8)$$

$$h_2 = \frac{h_1}{2} \quad (9)$$

Using a density of 2.8 g/cm³ for an average meteoroid, and a maximum impact velocity equal to the maximum velocity of the rocket, the thicknesses of the bumpers could be determined. The first wall consists of 0.16 cm of aluminum, the second wall of 0.07 cm of Kevlar, and the third wall is 4.73 cm of Kevlar.

Nuclear Fusion Rocket Engine Shielding

The purpose of the engine shield is to protect the inhabitants of the fusion rocket from the harmful emissions of the engine-- the radiation, etc.

Previous Design of Engine Shield. The 1991 design analyzed two options for the engine shield: a reactor shield and a shadow shield.⁴

The conclusion of 1991 design is that the shadow shield's mass was too large, and that the reactor cover shield would be the best in terms of weight, which is considered to be the most important optimization variable in the design.⁴

Original Specifications. The specifications for design are shown in Table 2.

Table 2 Specifications for the Engine Shield

Neutron Power Emitted	80 MW ¹³
Temperature on Outer Surface	Can be changed ¹³
Radiation Tolerance Limit for Torus	15 rem/year
Radius of Engine	1.27 m ¹³
Length of Engine	10 m ¹³

Radiation Attenuation (n-g). As stated previously, the engine emits neutron flux. As the nuclear reactions occur within the plasma, protons, neutrons, and by-products of Helium and water are released.¹⁴ The engine magnets and the first layer of shielding can contain the protons due to their charged nature, and Helium and water by-products due to their larger masses. Two kinds of "waste power" are emitted in the form of Bremsstrahlung power, and neutrons.¹³ The Bremsstrahlung, gamma ray production caused by beta particle deceleration and positron annihilation, is absorbed by metals in the engine core.¹⁵ The neutrons are not absorbed by this shield and must therefore be absorbed so the radiation levels are below appropriate limits (see Table 2).

As the neutrons come into contact with matter (the shield), the neutrons collide with the atoms, and either an inelastic or elastic event may occur. In the case of an elastic event, the neutron rebounds off of the atom with a decrease in velocity (energy). In the case of an inelastic event, the energy from the collision and the binding energy of the atom is released in the form of gamma rays.¹⁴ This gamma ray flux must also be attenuated to tolerable levels.

This radiation flux is a constraint for design. Using the radiation tolerable levels, the flux at the core, one can use one of the methods below to find a suitable shield for radiation attenuation.

There are three methods that were considered for the analysis of flux from the engine: point kernel integration, Moment Transfer, and Monte-Carlo.¹⁴

Point kernel integration methods are analytical integration methods. These use simple flux equations, accounting only for uncollided flux, which are integrated over the entire length of the engine core.¹⁶ Since the application of the theory of uncollided flux is an unrealistic one, a buildup factor

would be used in the case of flux through shielding (this acts as a sort of safety factor).

The moment transfer method is a computational method for the analysis of flux. This project was already used in 1991 design- the 1991 designer was provided results from a computational model by the Department of Nuclear Engineering and Engineering Physics and the Fusion Technology Institute. The tandem mirror engine was the radiation source in this model.¹⁷ Since the fluxes and dimensions were similar, so the data from this model was used in the JEFRI design. This computational model was performed using five popular shielding materials: H₃BO₃ (Boric Acid), Borated water, Lead, Aluminum, and Titanium.

The point kernel integration method was used for the calculation of flux through free space (between the shield and the torus).

Results of Shield Calculations for Radiation Attenuation. Using the radiation limits as a constraint for design, the results showed that Boric acid at a thickness of 2.17 m and a mass of 427 Mg fit the constraints best with the lowest thickness and mass.

In retrospect, the Boric acid is the most likely candidate for shielding among these five materials (the Borated water was very close to these results). Water or aqueous solutions of a high acidic content are among the best for neutron shielding due to their lower atomic mass/high Hydrogen content (it is more likely for an elastic event and energy absorption through collision).¹⁵ A borated material has a high macroscopic cross section-- this property characterizes the lower gamma ray emission after collision.¹⁵

In the moment transfer model, the shield of Boric acid (and borated water) included a stainless steel container (SS204), which is 5% of the mass of the shield.¹⁷ Its dimensions will be discussed in later section.

Of great importance is the maintenance of the state of Boric acid. Orthoboric acid is a solid that must be ground into powder and dissolved in water (an aqueous solution). The computational model used a solution of 5% Boric Acid, and therefore must be maintained above 273 K to maintain its solubility.¹⁸ If the temperature of the solution is too

high or low, the water will change phase and the Boric acid will precipitate out. This will result in a lower radiation shielding capacity.

Heat Transfer Calculations. The radiation flux through the shield is the source of internal heat generation. This can be modeled using the Fourier equation of heat transfer; this is a second order differential equation, so two boundary conditions must be set.

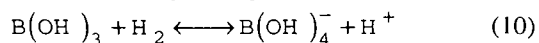
First we assume that the minimum temperature is at the outer radius of the liquid shield. With this assumption an isothermal condition is set with the temperature at 273 K, due to the solubility requirements of the boric acid.

Secondly, the heat flux is set as a constant at the inner radius, calculated from the neutron flux at the outer radius of the engine core.

Heat Transfer Results and Related Concerns. As a result, the inner boundary must be maintained at a temperature of 451 K. From the original specifications, the outer wall of the magnet can provide this condition.

This temperature presents a problem with regard to maintenance of the necessary state of the Boric Acid. Therefore, a pressure of 1.15 MPa must be maintained in the steel container in order to maintain the liquid phase of the solvent. A pump can added to maintain the solubility by mixing the solution.

Radiation Damage. As stated previously, radiation damage can be a concern in the design of the shields. Firstly, the solution's equilibrium can be characterized by the equation:¹⁸



The boric acid, when exposed to radiation, will disassociate into H, OH pairs, and boron, when exposed to thermal neutron radiation, will follow this equation:¹⁵



Although this neutron interaction above will result in a degradation of the Boric Acid:

1) Boron is the best material in this case for thermal neutron capture and lowest for gamma ray emission, and this damage is and expected part of the gamma ray capture;¹⁵

2) Although there will be a decrease in the amount of Boron, there will be an increase in the Helium content, whose low atomic mass is excellent for neutron shielding.¹⁵

As far as the disassociation into H, OH pairs, the equilibrium will be somewhat shifted, but this can be cared for by a pump (stated previously for the solubility problem).

The outer shield (the steel container and any structural shield needed) may be damaged differently. However, due to the boric acid shield, the structural shields (if made of Al, Ti, etc.) are not subjected to levels of radiation that would lead to damage. Therefore, this damage is considered negligible if these metals are used. If these metals are not used, the radiation damage would have to be incorporated qualitatively into the design. However, damage would have to be considered as an optimization variable and not a constraint, due to the small experimental data base.

Outer Shield Design. In view of the problems of the shielding presented above, one can summarize the needs/specifications of the outer shield surrounding the steel container. First, the outer shield is not responsible for radiation shielding. The liquid shield resolves that constraint. Secondly, a pressure of 1.6 MPa must be maintained inside this shield, with the outside set at near zero pressure. Thirdly, the heat flux at the boric acid-outer shield boundary is low enough to be considered negligible. Finally, there is the impact problem (due to particles in the atmosphere and space).

Therefore, the governing relations are: thick cylinder stress calculations which utilize the nature of composite shells (the internal stresses between the two shells can reduce the thickness of the outer shield needed to maintain a pressure)¹⁹, theories of failure, and empirical impact relations and fluxes.⁸

The results are that the steel container needs a thickness of 1.5 cm and a mass of 21 Mg (based on the specifications of the computational model of the liquid shield), and the pressure between the steel container and the impact shield is 1.6 MPa.

The materials used for the shield are based on ability to absorb impact, the density, the hardness, and the yield strength. An initial calculation was done which showed that the driver for the thickness would be the impact relation. According to this

relation, the density would be the prime factor. The choice of the material was also based on a qualitative judgement of its impact resistance. Based on these criteria, the chosen material was Aluminum (2.5% Li alloy), with a thickness of 16 cm and a mass of 175 Mg. Table 3 lists the the shield's cross sectional dimensions.

Table 3 Dimensions of Engine and Shield

Layer	Dimension (cm)
Radius of Engine Core	127
Thickness of Boric Acid Shield	216.7
Thickness of Steel Container	1.5
Thickness of Aluminum Shield	16
Total Radius of Shield	234.2

Finite Element Analysis of the Spokes

The purpose is to design the spokes, which act as support structures for the torus and link the torus to the main body of the spacecraft. The design will use finite element analysis, normally used as an analysis tool for checking stresses and displacements in a structure.

General Procedure. An iterative process will be used, in which an initial structure will be tested, and the results from the test will be analyzed for the formation of a new structure. The new design is then tested using FEA, and the analysis continues until specifications are met.

The job results chosen for analysis were nodal values for Von Mises stress-- although there are more exact techniques for determining failure, the Von Mises stresses were considerably less than the yield stress (10 times less), that another method of analysis was not needed.

The software used is MARC, a FEA package for the HP-risc machines (Apollo series 710).

Original Specifications. The initial specifications of the spacecraft follow:

- The loadcase includes two inertial loads. The maximum acceleration of the craft is 0.98 m/s^2 , and the rotation of the living modules is 0.35 rad/s .

- The torus, spokes and hub are made of Aluminum, with a elastic modulus of 69 GPa, a Poisson's ratio of 0.3, and a density of 2700 kg/m^3 .

- The torus and the hub act as containers-- the torus contains the living modules, and the hub contains the astronics equipment.

- The spokes must also house astronics equipment and transmission lines to the life support system in the living modules. Since they must act as containers and truss cross sections (for bending), it was decided that they should be hollow members, instead of flanged cross sections (I-beams, T-beams) or solid cross sections.

- The radius for the torus is 35 m, the radius of the living modules is 2 m, and the radius for the hub is 8 m. The thickness of the walls is 0.3 m.

Geometry and Mesh Generation. Each model is comprised of three sections: the torus, the hub, and the spokes. Each of these components has been modeled using plates. The only part of the torus and the hub modeled is the wall.

The spokes, the subject of the design, must be modeled to fit the specified loadings. The rotational velocity will cause tension radially in the spokes, and the translational acceleration will cause bending of the spokes. Thus the spokes, like many other space structures, should be of a similar construction as truss members. The aspect ratio of the elements to best model a beam subjected to bending was used-- elements length that is perpendicular to the loading plane was kept as small as possible by refining the mesh.²⁰

Bilinear thick shell elements (Mindlin four-node plate elements) are used-- MARC element 75. These elements have membrane and bending capabilities, but best model bending deformation and transverse shear. They were also used due to the thickness of the walls in the model, and with regards to CPU time, they are very inexpensive.²¹

The element has six degrees of freedom (x, y, z displacement, r_x, r_y, r_z rotation). It uses bilinear interpolation for the coordinates, displacements, and the rotations. In some cases, the bilinear shell was collapsed to a triangular element for transition purposes.²¹

Symmetry is used in the model. Since there are three spokes, and loading is uniform in 120 degree

sections, a 120 degree section is modeled with the spoke at the center of the section.

Boundary Conditions. There are five boundary conditions (Table 3).

Table 3 Displacements and Loadings

Location (of Nodes)	Boundary Condition
0 degree boundary on hub and torus	Zero disp. in y-direction; zero rot. about z-axis
120 degree boundary on hub and torus	Zero disp. tangent to curve; zero rot. about z-axis
Front curve of hub	Zero disp. in z-direction
All nodes	Rotational velocity and Acceleration as Inertial Loads

See Figure 6 for one of the models analyzed.

Results and Analysis. The first model had a circular cross section. The deflection and the stresses were in acceptable ranges, but later it was changed to a rectangular cross section, which would better fit the nature of the loadings (bending). The stresses in the model were under the yield stress.

The second model had a rectangular cross section of the same area of the circular cross section, but a moment of inertia (about the bending axis) three times that of the previous model. The stresses were higher due to the corner-hub intersection, stress concentrations that were not present in the circular cross section. The deflections lower in the z-direction due to an increased moment of inertia. The stresses in the model were under the yield stress.

Since the stress concentrations are expected and could easily be decreased by a rounding of the corners at the intersection, a third model again used a rectangular cross section but of a smaller area. This model yielded stresses higher than the circular cross section (again due to the stress concentrations), but lower than the rectangular cross section. The z-direction deflections were lower than the circular cross section, but higher than the large rectangular cross section. Since stress and deflection values were of a reasonable values and the mass is smaller, this model's geometry will be used.

The geometries modeled are shown in Table 5, and the resulting z-direction deflections are listed in Table 6.

Table 5 and 6 Geometries and Deflections

Cross Section	Area (m ²)	Moment of Inertia (m ⁴)
Circular	12.56	12.56
Large Rectangular	12	36
Small Rectangular	8	10.67
Cross Section	At end of spoke (cm)	At ends of section (cm)
Circular	2.57	2.54
Large Rectangular	2.0	1.94
Small Rectangular	2.42	2.36

See Figure 3 for stress contours of the model with the small rectangular cross section.

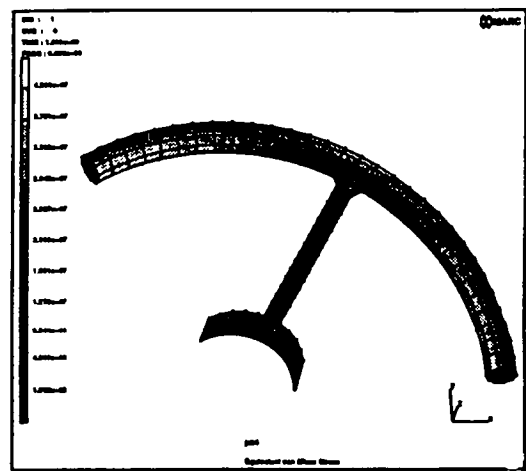


Fig. 3 Equivalent Von Mises Stress Contours for Model with Small Rectangular Cross Section (stresses are in Pa, with the yield stress for the material at 520 MPa)

Propulsion System and Engine Design

Thrust Performance. Fusion systems are capable of operating in a large range of thrust to weight ratios, 5×10^{-5} to 10^{-1} .¹ The variance of thrust can be achieved through three different thrust modes (see

Figure 4). The fuel exhaust mode has the lowest thrust/weight, 5×10^{-5} , and the highest I_{sp} , 10^6 sec. In this mode the ions are directly exhausted out the nozzle. The ions are moving very fast but are also very lightweight, so the resultant thrust is the lowest. The mass-augmented mode has thrust/weight ratios of 10^{-4} to 10^{-2} and I_{sp} 's of 10^3 to 3×10^6 . In this mode, solid propellant is added to the exhaust stream and is ionized. The added exhaust mass decreases the velocity of the exhaust stream and increases the resulting thrust.

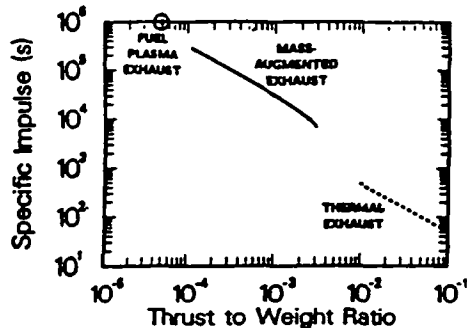
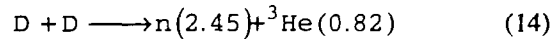
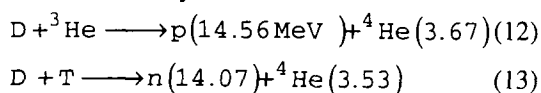


Fig. 4 Range of Specific Impulses and Thrusts for Thrust Mode Options of Fusion Propulsion Systems¹

The highest thrust mode is the thermal exhaust mode which has thrust/weight ratios of 10^{-2} to 10^{-1} and I_{sp} 's of 50 to 1000 seconds. In this mode, liquid propellant is run through tubes in the first wall of the reactor and is heated to a gas by the radiating heat from the engine, much in the same way that fission thermal systems achieve thrust.

For the JEFRI mission to Jupiter, the mass-augmented and thermal exhaust modes will be used. The mass-augmented mode will be the primary mode, and will be used for the transfer between earth and Jupiter. The thermal exhaust mode will be the secondary mode, and will be used to turn the ship around during the deceleration phase, and for transferring between the moons of Jupiter, which requires greater thrusts.

Fuel / Fusion Cycle. The choice of fuel is dependent on the amount of power available for thrust produced by the fusion cycle, the amount of neutrons produced, and the availability of the fuel. The most notable fusion cycles are:¹³



The amount of thrust power available is directly related to the amount of charged particles produced in the fusion reaction, in the form of protons (p) and alpha particles (${}^4\text{He}$). The neutrons produced cannot be used for thrust and must be shielded, raising the mass of the overall system. Considering the above cycles, the D- ${}^3\text{He}$ cycle is the best choice for propulsion because nearly 3/4 of its total energy is available for thrust, and less than 1/10 of the total energy is the form of neutrons produced by the secondary D-D cycle.¹³ It is much more efficient than the D-T cycle which produces less than 1/4 of its total energy in the form of thrust and more than 3/4 in the form of neutrons.¹³ As far as availability is concerned, ${}^3\text{He}$ is rare on earth but is expected to be mined in large quantities from the moon some time in the twenty-first century. For these reasons D- ${}^3\text{He}$ was chosen as the fuel for JEFRI.

Engine- The FRC. Many concepts for fusion rocket engines have been conceived and are described in reference 2. The engine chosen for JEFRI is the field reversed configuration (FRC), shown in Figure 5. In this fusion system, the hot plasma is confined to the central region through two sets of magnetic field coils. A certain amount of cold plasma is bled from the core and is directed out of the rocket using a magnetic nozzle. Downstream of the core the propellant is injected to provide thrust. The parameters for the FRC are listed in Table 7 (next page), along with some of the parameters for the tandem mirror configuration, which was used on the previous mission configurations (1989 and 1991 reports).^{3,4}

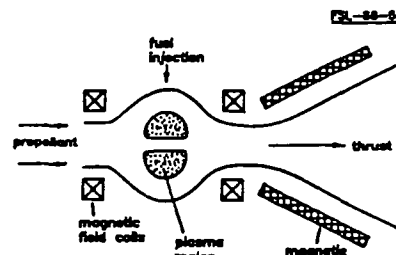


Fig. 5 FRC Engine¹

The most important parameters in choosing a system are the specific power and the plasma temperature. The specific power is the total amount

of power available for thrust divided by the total mass of the engine including shielding and radiator mass. It is a measure of the efficiency of the thrust delivery of the system. Because low mass is a major requirement in space, it is important that a system have a high specific power. In comparing the FRC with the tandem mirror, the tandem mirror had twice the thrust power, but more than ten times the total mass. The FRC had the larger specific power, 5.5 kW/kg, compared to the tandem mirror 1.6 kW/kg.

Table 7 D-³He Fusion Rocket Model Parameters for FRC and Tandem Mirror 1,13

Parameters	FRC (1993)	Tandem Mirror (1989,1991)
Plasma Temp., keV	55	105
Thrust Power, MW	600	1500
Total Mass, Mg	109	1250
Specific Power, kW/kg	5.5	1.6

Temperature is an important parameter because it is directly related to the maximum specific impulse achieved by the rocket. The plasma temperature of the FRC is 55 keV, which is only half of what the tandem mirror achieves, 105 keV. However, because the specific impulse varies with the square root of temperature, the maximum specific impulse of the FRC is only 30% less than the maximum specific impulse of the tandem mirror. Therefore, if the maximum specific impulse of the tandem mirror for the mass-augmented mode was 300,000 seconds, the maximum specific impulse of the FRC is approximately 220,000 seconds.

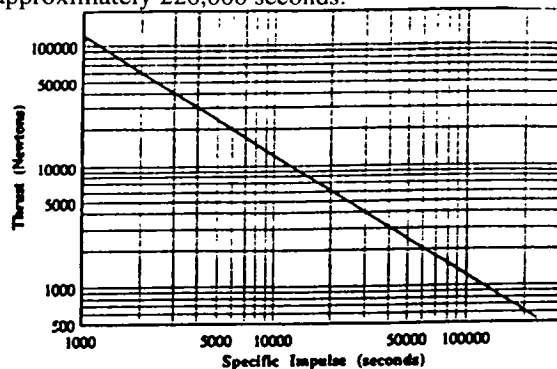


Fig. 6 Range of Specific Impulses and Thrusts for the FRC

The range of thrust and specific impulse was determined for the FRC in the mass-augmented mode and is shown in Figure 6. From the graph it can be seen that at maximum specific impulse the rocket delivers 0.5 kN of thrust and at maximum thrust the rocket delivers over 100 kN at 1000 seconds of specific impulse. The thrust values were not derived for specific impulses of less than 1000 seconds, where it becomes more thrust efficient to use the thermal exhaust mode.

JEFRI Propulsion System

Propellant Requirements. The primary mass-augmented mode is considered to be a low-thrust mode. For this reason, the rocket must thrust continuously, rather than impulsively, throughout the mission to build up to its maximum velocity. The amount of propellant burned will depend on how quickly it is desired that the rocket accelerate to its top speeds, and therefore how long of a transfer time is desired.

Table 8 is a list of four equal one-way mission travel time increments, and their corresponding exhaust velocities and required propellant masses. From the table, it can be seen that as travel time increases the amount of burned propellant decreases since the rocket is able to thrust at lower rates. For low propellant mass requirements, it is desirable to have longer travel times, however, for human consideration shorter travel times are desirable. It was eventually decided that a one-way travel time of one year was the most beneficial for both propellant mass consumption and mission duration.

Table 8 Earth-Jupiter Propellant Mass for 5 kW/kg Specific Power

One-Way Time (days)	Exhaust Velocity (m/s)	Propellant Mass (Mg)
180	2.0×10^5	800
365	3.9×10^5	410
730	6.8×10^5	280
1096	9.7×10^5	200

Propellant Storage, Consumption, and Injection. Table 9 (next page) is a list of the propellant storage and injection requirements for JEFRI for a round trip mission to Jupiter.

From table 8 it was determined that 850 Mg would be required for a round trip mission. The propellant used would be hydrogen, because its low molecular weight gives the maximum specific impulse. The hydrogen would be injected in the form of solid hydrogen (SH₂), where the high energy density of a solid is required to receive the velocity performance of the mass-augmented mode. The SH₂ is injected as pellets approximately 1.2 cm in diameter, and the mass flow rate of pellets required for maximum thrust is 1 kg/sec.²² The pellets will be injected into the plasma stream downstream of the core, and must be travelling at speeds of at least 1.0 km/sec in order to penetrate the center of the stream.²³ 1800 injectors are required for maximum flow rate.

Table 9 Propellant Storage and Injection

Storage Requirements	Injection Requirements
propellant mass: 850 Mg	injected as (phase): SH ₂ pellets
total volume: 12000 m ³	pellet diameter: 1.2 cm
volume per tank (4): 3000 m ³	temperature: 14 K
tank radius: 6 m	pressure: 0.068 MPa
tank length: 30 m	velocity: 1.0 km/sec
stored as (phase): liquid H ₂ (LH ₂)	mass flow rate: 1 kg/sec
temperature: 19 K	no. injectors: 1800
pressure: 0.068 MPa	pressurization: H ₂ gas at 297 K, 10.7 MPa
pressurization	4.13 Mg of H ₂ gas (GH ₂) at 297 K, 0.3 MPa

The propellant will be stored in the form of a liquid for both ease of storage and withdrawal. The total amount of liquid volume required is 12000 m³, stored in four cylindrical tanks of volume 3000 m³, 6 m radius, and 30 m length. The tanks will be pressurized using evaporated propellant, gaseous hydrogen (GH₂) at 297 K and 0.3 MPa.

The tanks will be mounted radially along the axis of the ship above the engine and fuel tanks, and between the front and back heat radiators as shown in Figure 1. This configuration has the benefit of providing additional meteoroid shielding for the engine. The injectors will be mounted radially

around the axis between the back heat radiators and the nozzle.

The injection process proceeds as follows: the propellant injection process begins with a portion of LH₂ being drawn out of the storage tanks and fed into a heat exchanger on the engine, where it is evaporated to GH₂ at 297 K, 0.068 MPa.; the gas is compressed to 0.3 MPa and sent into the tanks and forced against a membrane, which pumps the LH₂ out of the tanks, continuing the cycle; the larger portion of the liquid hydrogen is run through a liquid helium cooled freezer, where it is frozen to a temperature of 14 K; the SH₂ is then fed into the injectors where it is cut into pellets and blown into the plasma stream at the desired flow rates; the injectors are pressurized by a portion of GH₂ at 297 K, and 1.07 MPa, which is obtained by running LH₂ through the engine heat exchanger and a compressor.

Injectors

Performance. Table 10 is a list of the performance requirements for the injectors, and pellet dimensions.

Table 10 Parameters for Pneumatic injectors

Pellet speed (km/s)	1.0 ²³
Pellet mass (g)	0.11 ²³
Barrel diameter (mm)	13.2
Barrel length (m)	6.5
Breech length (cm)	20.0 ²³
Propellant gas pressure (bars)	10.7
Repetition rate (Hz)	0-5 ²³
Mass flow rate/gun @ 5 Hz (g/s)	0.55
Pellet diameter, initial (cm)	1.32
Pellet diameter, final (cm)	1.20
Pellet length (cm)	1.2
Pellet erosion (%)	30 ²³
Maximum acceleration (m ² /s)	4.8 x 106 ²³

The pneumatic injector, also called a gas gun, is shown in Figure 7 (next page). These injectors are mechanisms which are used for fueling the cores of fusion reactors during experiments. To integrate it into the JEFRI propellant injection system, where mass flow rates are much higher, many more injectors would be needed (1800). The injector works by first receiving LH₂ into a freezer, where it frozen into SH₂. The SH₂ is then fed into a gun barrel by a piston. At the entrance of the barrel is a mechanical pellet cutter which cuts the pellets into cylinders. The pellets are blown down the gun barrel and into the plasma stream by a hydrogen gas charge.

The task of the injectors is to allow the pellets to penetrate the center of hot plasma stream, before being completely vaporized. For temperatures of 10^8 K, this requires a velocity of at least 1 km/s.²³ Because the maximum speed of the pellet is dependent on the speed of sound of the pressurant gas, it is desired to use a gas with the lowest molecular weight to achieve the highest speeds, which is why hydrogen is chosen. In addition, raising the temperature of the hydrogen gas can correspondingly increase the velocity of the gas, allowing for larger sized pellets to be used.²³ This is not believed to be desirable, as increasing the pellet mass would result in more mass being eroded along the gun barrel, more volume of gas required to pressurize the pellets, and lower pellet repetition rates. More as-stored propellant mass would be required to satisfy these conditions, adding to the overall mass of the rocket.

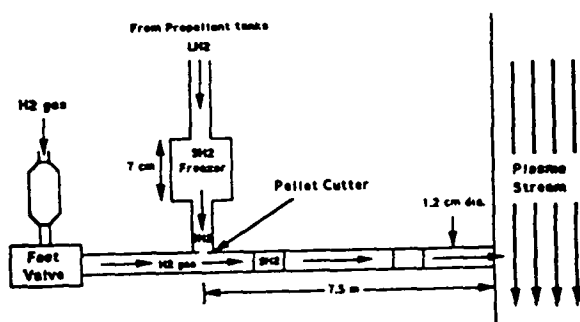


Fig. 7 Lateral View of Injectors and Engine

Propellant Tank Design

Materials Selection. For the propellant tanks, a material that was both lightweight and strong at a variety of temperatures was desired. Aluminum alloy 2219-T87 was chosen for its good properties of strength and ductility at both cryogenic and elevated temperatures.²⁴

Loads and Environment. The greatest internal stress was the ullage pressure, which is required to be greater than the sum of the pressure of liquid propellant, plus the pressure needed to overcome all losses in the lines in which the propellant is fed. For pressure fed liquid hydrogen evaporated propellants, as is used in JEFRI, reference 25 gives a maximum value of 0.3 MPa for the ullage pressure. This value turns out to be large compared to the fluid inertial forces. The largest load was due to meteoroid impact, where it was determined that there was a

100% probability of the tanks being struck by a meteoroid with an energy of 10 MJ.

Tank Thicknesses. The wall thicknesses for the tanks were solved for using a design stress of 305 MPa, corresponding to the stress to produce 0.1% creep at 300 K and 20,000 hours for Al 2219. Meteoroid armor was designed for the outside of the tanks, where Kevlar was chosen for the material because of its properties of high strength and low density. The tank thicknesses were 6.7 mm of Al 2219 for the sides and 4.8 mm for the ends. The required meteoroid shielding was 7.2 mm for the sides and 4.9 mm for the ends. The total fully loaded mass of all four tanks was 1500 Mg. A view of one tank mounted on the JEFRI rocket is shown in Figure 1.

Liquid Droplet Radiator

The engine of JEFRI produces 400 MW of waste heat that must be rejected into continuously throughout the mission. There are several radiator concepts such as heat pipes, dust radiators, and belt radiators that may be employed to reject this heat. However, a rectangular liquid droplet radiator (LDR) was chosen for two main reasons. One, the nature of the LDR minimizes mass by exposing the radiating medium directly to space. Two, the use of liquid metal as the radiating medium allows high rejection temperatures that minimize surface area for a more compact design. Other advantages include easy deployment due to reduced mass and compact storage, and relative immunity to micrometeoroids that will pass harmlessly through the radiating surface area. A partial schematic of the LDR being employed on the fusion rocket is shown in Figure 8. Figure 8 shows one of four droplet sheets that extend radially from the longitudinal axis of the rocket. The working fluid is heated in the engine, and pumped forward and out to the droplet generators. The generators form billions of droplets and pumps the fluid back to the engine to complete the cycle.

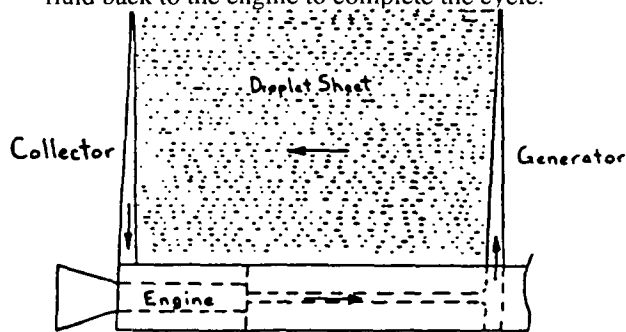


Fig. 8 LDR Schematic for JEFRI Rocket

LDR Components. The LDR can be broken down into three main systems, the generator, the collector, and the piping system.

The generators form the droplet sheets by breaking up a liquid jet using an imposed periodic disturbance. The technology is very similar to ink jet printers that use a Raleigh breakup to produce as many as 250,000 droplets per second from a single orifice.²⁶ This technology is well developed, and can be applied directly to the LDR generators. However, modifications are made to accommodate the high temperature liquid metal that the LDR will use. In addition to forming these droplets the generator must focus the droplets with enough accuracy to prevent excessive collision and coalescence during the flight time. The coalescence of the two droplets reduces their combined surface area by 21% and therefore a large number of collisions will reduce the radiative performance of the droplet sheet.

The collector the fusion rocket LDR employs is called a linear passive collector. The opening of the collector is slightly larger than the droplet sheet thickness. An auxiliary film is injected on the impact surfaces to prevent backflow and help direct the flow to the collector pump. The droplet collector must collect essentially all incoming droplets to achieve an acceptable mass loss for the duration of the mission. Acceptable droplet loss rates are on the order of one lost droplet per 10^8 incident droplets.²⁷

The piping system consists of pipes and pumps. Both must operate in the space environment without the benefits of gravity or gas pressure. The components must also be able to handle high temperature (1000 K) liquid metal.

The piping is made of a titanium alloy similar to that used in the high temperature application of turbine engines. Titanium alloys also have a high strength to weight ratio that helps minimize mass of the conical pipes that extend radially. The pipe that carries the liquid metal from the engine to the generators runs through the center of the rocket along side the fuel and coolant tanks. In order to minimize the heat transfer from this pipe to the tanks, the pipe is lined with a thin ceramic layer on the inside and is plated on the outside with highly polished silver. The polished silver provides a highly reflective surface and thus a low emissivity (0.02) that minimizes

radiative heat transfer. A series of pumps consisting of a screw pump in each of the collectors and generators along with a gear pump just forward of the engine keep the liquid metal cycling through the system.

Droplet Sheet Radiative Behavior. One of the reasons for selecting the LDR was to eliminate the need for metallic radiating surfaces and expose the working fluid directly to space in the form of trillions of tiny droplets. This concept takes advantage of a sphere's high surface area to volume ratio to create a radiator with a low specific mass (radiator mass/radiating area). This, along with interdroplet reflections to increase the effective emissivity, results in a low mass radiator for space applications.

The emissivity of the droplet sheet is described by Brown and Kosson²⁸ to be a function of the droplet emittance (approximately 0.2 for liquid metals) and a sheet geometry parameter. Their relationship is shown in Figure 9 where for JEFRI's LDR:

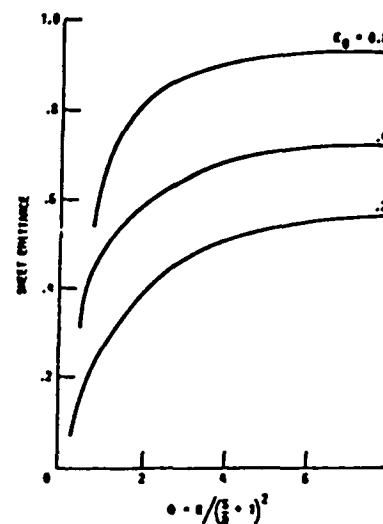


Figure 9 Dependence of Sheet Emittance on Droplet Emmissivity and Sheet Geometry Parameters²⁷

ϕ = sheet geometry parameter = 4.8

N = number of droplet layers = 30

S = spacing between droplets = 0.3 mm

D = droplet diameter = 0.2 mm

For a pure liquid metal the effective sheet emittance (ϵ_0) is approximately 0.5. By dispersing a high emissivity powder, such as carbon black, on the

surface of the liquid the emissivity can be enhanced to approximately 0.5 resulting in an effective sheet emittance of about 0.8. It follows that to dissipate 400 MW of heat using a liquid metal operating in a temperature range of 945 K to 1030 K, the fusion rocket LDR droplet sheets must have 9200 m² of radiating surface area. Four droplet sheets (30 m x 40 m) make up this surface area.

Working Fluid. The main drivers for selecting the working fluid for the fusion rocket LDR are low mass and compact design. Many fluid properties contribute to a low mass LDR, such as density, emissivity, vapor pressure, and operating temperature range. However, only emissivity and operating temperature affect the compactness of the design by minimizing the surface area of the radiator.

Liquid aluminum was determined to be the best candidate. In the liquid state aluminum's density is relatively low (2300 kg/m³), it has an effective operating temperature range of 940 K to 110 K, and its emissivity is about 0.2 (typical of liquid metals). The only drawback of liquid aluminum is that its vapor pressure is a high for long term missions, as shown in Figure 14. However, the fusion rocket mission is only 2-3 years, so even though the inventory of extra aluminum will initially double the mass of the LDR the other benefits justify its use.

LDR Performance. The performance of all space applicable radiators are based on the heat radiated to radiator mass ratio (kW/kg). For the fusion rocket LDR this ratio depends on the mission length since evaporative losses play such a significant role in the total mass of the LDR. The goal was to reject 5 kW/kg from the radiator. Based on a 2 year mission, the fusion rocket will be able to reject 6.4 kW/kg by the end of the mission.

Another performance concern is droplet collection. Any linear accelerations perpendicular to the droplet sheets or angular velocities of the rocket will cause the droplets to miss the collector. Neither of these would be present during normal operation except the angular velocities of the transfer orbit that would be negligible (approximately 10⁻⁸ rad/s). However problems can result during maneuvering. One solution would be to temporarily bypass the LDR and make the maneuver as quickly as possible. The feasibility of this would depend on the heat capacity of the fluid and the time to make the

maneuver. Another possible solution would be to design the collector so that it can expand or move just enough to collect the drops when maneuvers are made very slowly.

Bibliography

- 1) Santarius, J.F., "Lunar 3He, Fusion Propulsion, and Space Development," Presented at the Second Symposium on Lunar Bases and Space Activities of the 21st century, 5-7 April 1988, Houston, Texas, (Revised August 1988).
- 2) Santarius, J.F., "Magnetic Fusion for Space Propulsion: Capabilities and Issues," Prepared for the American Nuclear Society Topical Meeting on Nuclear Technologies for Space Exploration (August 1992), July 1992.
- 3) Brantmeyer, M., Buchanan, D., Chan, A., Gile, V., Godleski, T., Hayes, T., Irizarry-Quinones, H., Kisslinger, E., Newmann, D., Radzanowski, M., Schlick, F., Williams, M., "Fusion Rocket Design," Department of Engineering Mechanics/Astronautics, University of Wisconsin-Madison, 1992.
- 4) Buscholtz, J. Freuh, J. Hendrick, E. Jensen, P. Ward, "Proposal for a Jupiter Manned Fusion Spaceship," Department of Engineering Mechanics/Astronautics, University of Wisconsin-Madison, 1990.
- 5) McKay, M. F., McFay, D. S., Duke, M. B., "Space Resources: Social Concerns," NASA SP-509, vol. 4, 1992.
- 6) Townsend, L.W., Nealy, J.E., Wilson, J.W., Simonsen, L.C., "Estimates of Galactic Cosmic Ray Shielding Requirements during Solar Minimum," NASA TM-4167, 1990.
- 7) Sukey, M., "A Review of Micrometeoroid Flux Measurements of Models for Low Orbital Altitudes of the Space Station," NASA TM-86466.
- 8) Cadle, R.D., *Particles in the Atmosphere and Space*, Reinhold, New York, 1966.
- 9) Woodson, Tillman, Tillmann, *Human Factors Design Handbook*, McGraw-Hill, New York, 1992.

- 10) *Materials for Missiles and Spacecraft--Engineering and Science Extension Series*, McGraw-Hill, New York, 1963.
- 11) Goetzel, C.G., Rittenhouse, J.B., Singletary, J.B., ed., Lockheed Missiles and Space Company, *Space Materials Handbook*, Addison-Wesley, Reading, Mass., 1965.
- 12) Richardson, A.J., Sanders, J.P. "Development of Dual Bumper Wall Construction for Advanced Spacecraft," *Journal of Spacecraft and Rockets*, Vol.9 no.6.
- 13) Santarius, J.F., Logan, B.G. , "Generic Magnetic Fusion Rocket Model", "Generic Magnetic Fusion Rocket Model Parameters," Updated for JEFRI, Jan. 1993.
- 14) Jaeger, R.G., Blizard, E.P., Chilton, A.B., Grotenhuis, M., Hoenig, A., Jaeger, Th. A., Eisenlohr, H.H. ed. *Engineering Compendium of Radiation Shielding*, Vol.1 & 2, Springer-Verlag, New York, 1975.
- 15) Harrison, J.R., *Nuclear Reactor Shielding*, Temple, London, 1958.
- 16) Blizardi, E.P., Abbot, L.S. ed., *Reactor Handbook: Shielding*, Vol. 3 Part B, 2nd ed., John Wiley and Sons, New York, 1962.
- 17) H. Khatar, "Reaction Rates for Response Functions," Department of Nuclear Engineering and Engineering Physics, University of Wisconsin-Madison, 1990.
- 18) Othmer, D.F., ed., *Encyclopedia of Chemical Technology*, Vol. 3, 3rd ed., John Wiley and Sons, New York, 1978.
- 19) Cook, R.D., Young, W.C., *Advanced Mechanics of Materials*, Macmillan, New York, 1985.
- 20) Cook, R.D., Malkus, D.S., Plesha, M.E., *Concepts and Applications of Finite Element Analysis*, 3rd ed., John Wiley and Sons, New York, 1989.
- 21) MARC Analysis Research Corporation, "MARC Reference Library", *Element Library*, Vol. B, 1992.
- 22) Chapman, R., Miley, G.H., Kernbichler, W., and Heindler, M., "Fusion Space Propulsion with a Field Reversed Configuration," *Fusion Technology*, March 1989.
- 23) Gouge, M.J., St. Onge, K.D., Milora, S.L., Fisher, P.W., and Combs, S.K., "Pellet Fueling System for ITER," *Fusion Engineering and Design*, Vol. 19, 1992.
- 24) Kreimendahl, R., "Propellant Tanks and Storage Systems," Presented in EMA 601 Spacecraft Transportation and Propulsion, University of Wisconsin-Madison, 1992.
- 25) "Pressurization Systems for Liquid Rockets," NASA Space Vehicle Design Criteria (Chemical Propulsion), National Aeronautics and Space Administration, Oct. 1975
- 26) Sweet, R. G., "High-Frequency Oscillography with Electrostatically Deflected Ink Jets," Stanford Electronic Laboratories, SEL-64-004, Mar. 1964.
- 27) White, A.K., "Liquid Droplet Radiator Development Status," NASA Technical Memorandum 89852, July 1987.
- 28) Incropera, F.P., DeWitt, D.P., *Introduction to Heat Transfer*, John Wiley and Sons, New York, 1985.

**UW-3S900 Dark Horse
Joined Wing Global Transport**

**University of Wisconsin-Madison
Department of Engineering Mechanics
and Astronautics
Madison, WI**

**Mr. Ron Thomson
Mr. David Corr, Teaching Assistant**

**Mark Fleming, Daniel Jones, Chris Lewis, Andrew McLandress,
Marcelle Millan, Brad Marthaler, Ryan Roloff, Laura Rudolph**

Abstract

A global transport is needed to meet the needs of the military to rapidly deploy large numbers of troops and equipment from the continental United States to potential trouble spots throughout the world. The primary mission profile is to fly 6,500 nautical miles with full payload (typically 800,000 pounds), off load, and return with 15% of payload without refueling and while using existing military and commercial facilities for takeoff and landing.

To meet the design requirements, a tri-surface transport has been designed. The three lifting surfaces, the canard, the fore wing, and the aft wing, are mounted on the front of the elliptical fuselage, mid-fuselage, and tip of the tail, respectively. To meet the stringent takeoff requirements, nine GE-90 ultra-high bypass turbofan engines are employed to generate 900,000 pounds of thrust. The aft wing tip joins the fore wing at 70% of its span, with an engine located between each set of wings. The resulting configuration, resembling a joined wing and a biplane hybrid, reduces interference effects and structural complexity at the joint and provides an increase in wing stiffness and a reduction in weight. The remaining engines are mounted underneath the fore wing with one in the tail.

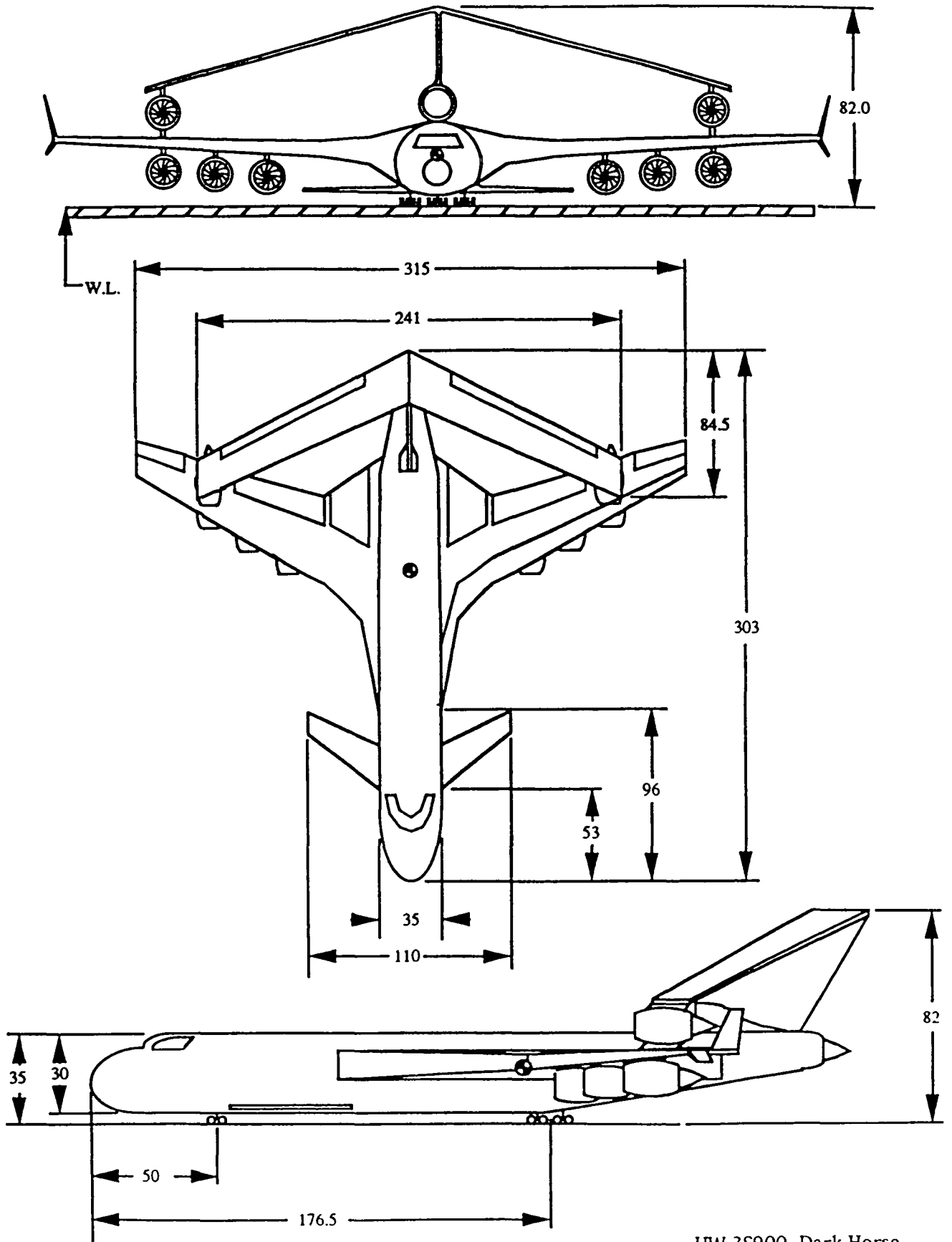
Introduction

A global transport is necessary to meet the needs of the military to rapidly deploy large numbers of troops and equipment from the continental United States to potential trouble spots throughout the world. The UW-3S900 meets this challenge. The mission profile is to

fly 6500 nautical miles with full payload (typically 800,000 pounds), off load, and return with 15% of payload, without refueling, while using existing military and commercial facilities for takeoff and landing.

To meet the design requirements, a tri-surface transport has been designed. The three lifting surfaces, the canard, the fore wing, and the aft wing, are mounted on the front of the elliptical fuselage, mid-fuselage, and tip of the tail, respectively. The joined wing with canard (hereafter referred to as the joined wing) has several advantages over conventional designs. First conceptualized by the late Julian Wolkovitch, the joined wing consists of two wings joined together to form diamond shapes in the plan and front views. The fore wing is similar to a conventional wing. The aft wing, which extends from the tail to the joint on the fore wing, provides another lifting surface and stabilizes the boundary layer over the fore wing increasing the allowable angle of attack.

To meet the stringent takeoff requirements, the UW-3S900 needs nine GE-90 ultra-high bypass engines to generate the 900,000 pounds of thrust. The aft wing tip joins the fore wing at 70% of its span. At the joint of the UW-3S900, the vertical separation between the wings is 20 ft. This allows the placement of an engine in the joint while maintaining the structural advantages of the joined wing. Therefore, this design is not a true "joined wing," because the wing tips do not join, but the aircraft is referred to as a joined wing transport. The resulting configuration, resembling a joined wing and biplane hybrid, reduces drag effects and structural complexity at the joints. The joining of the wings serves to reduce the bending moment and stresses by a truss support of the two independent lifting surfaces, therefore increasing the bending strength of the pair of wings in the in-plane



UW-3S900 Dark Horse
University of Wisconsin

direction. The vertical separations also reduce interference effects between the fore and aft wings. The remaining six engines are mounted underneath the fore wing, with one engine in the tail.

It is difficult to compare the UW-3S900 with current aircraft because of the extreme differences in size and configuration. To satisfy the mission requirements, the calculated takeoff weight is 2.86 million pounds. This weight is about three times the takeoff weight of the currently used C-5 transport.

Although the UW-3S900 is not a true joined wing, much of the information used on the design is from the joined wing research completed by Julian Wolkovitch. Other areas of information include Roskam's Airplane Design, Parts I-VIII and Abbott's Theory of Wing Sections. Through studies of the joined wing, certain assumptions are made for the UW-3S900. These assumptions, as well as other important design features, are discussed in the following sections: Mission Requirements, Weights, Lift, Boundary Layer Control, Drag, Stability, Control Systems, Structures and Materials, Landing Gear, and Cost. All of the calculations in the sections can be found in the complete report and appendix, which is available upon request.

Assumptions and Mission Requirements

The mission requirements for this design meet all of those suggested by AIAA:

- "The payload = 800,000 pounds at a 2.5g maneuver load factor"
- "The Primary Radius Mission is to fly 6,500 nautical miles with full payload, off load and return with 15% of fuel load, without refueling."
- "The Secondary Radius Mission is to fly 8,000 to 12,000 nautical miles with at least 75% payload, land and return empty, without refueling."
- "For both missions the critical field length for initial airfield is 10000 ft at sea level and for midpoint airfield the critical field length is 8000 ft at 4000 ft elevation and 95° F."

Weight

The weight of the airplane resulting from the above requirements, is a driving factor in the overall design. Two weights proved crucial to the design: empty weight and takeoff weight. Using conventional airplane equations, these weights are 1,076,265 lbs and 2,859,432 lbs, respectively. These values are conservative since weight savings due to the joined wing is not considered due to unavailability of information. Research on the joined wing suggests savings up to 65-78% for the weight of the wings. Considered weight savings are due to high performance materials, mainly aluminum lithium and some composites used on the fore and aft wings, the vertical tail, and the nacelle.

Table 1. Class II Weight Summary

Structural Weight	790500 lb
Powerplant Weight	152600 lb
Fixed Equipment Weight	133200 lb
Empty Weight	1076300 lb
Payload Weight	800000 lb
Crew Weight	3000 lb
Fuel Weight	980200 lb
Takeoff Weight	2859500 lb

Lift

The UW-3S900 needs large lift forces for takeoff and landing. To achieve the lifting force of 2.86 million lbs., the three surface "joined" wing configuration is an ideal choice. The addition of an extra wing and a canard increased the planform area as compared to classical configurations. In addition, the joined wing configuration has a maximum coefficient of lift of 4.86 for the entire airplane, which is comparable to a typical monoplane configurations with a maximum coefficient of lift of 3.0. The use of high lift devices is a major asset in increasing the maximum coefficient of lift.

Table 2 is a summary of the overall aircraft characteristics. The relationship between these variables and the coefficient of lift curve is noted in Fig. 1.

Table 2. Overall Aircraft Characteristic Information

Flaps Up	
C_{L_0}	0.1390
$C_{L\alpha}$	7.6148/°
$C_{L_{max}}$	1.4164
α_{0L}	-1.05°
$\alpha_{C_{L_{max}}}$	13°
α^*	7°
Flaps Down	$\delta_f = 40^\circ$
ΔC_L	1.8265
$(C_{L\alpha})_\delta$	7.5459/°
$\Delta C_{L_{max}}$	2.8371

The choice of the joined wing configuration is based on many facets of the design mission, but a major deciding factor is the ability to increase the planform area while keeping wing moments at a reasonable level. The joined wing and canard configuration has three wings contributing to the airplane's total lift as compared to one for monoplane configurations. Consequently, each joined wing would normally have a much shorter chord length than compared to monoplane configurations that require the same lift. However, since lift is a function of planform area, altitude, velocity and the coefficient of lift, the aircraft requires an extremely large planform and thus chord length to keep the other variables within acceptable ranges for takeoff. The total planform area of the

design is 23,400 ft² which is distributed between three surfaces. The fore wing contributes 51% of the overall lifting surface of the aircraft. The aft wing supports 37% of the lifting force of which 20% is designed for the purpose of a horizontal tail and the canard supports only 5% of the total planform area with the rest of the lifting force being generated by the elliptical fuselage. With the planform area already determined and by multiplying the stall velocities by 1.20, the approach and takeoff velocities 200 ft/s and 250 ft/s, respectively.

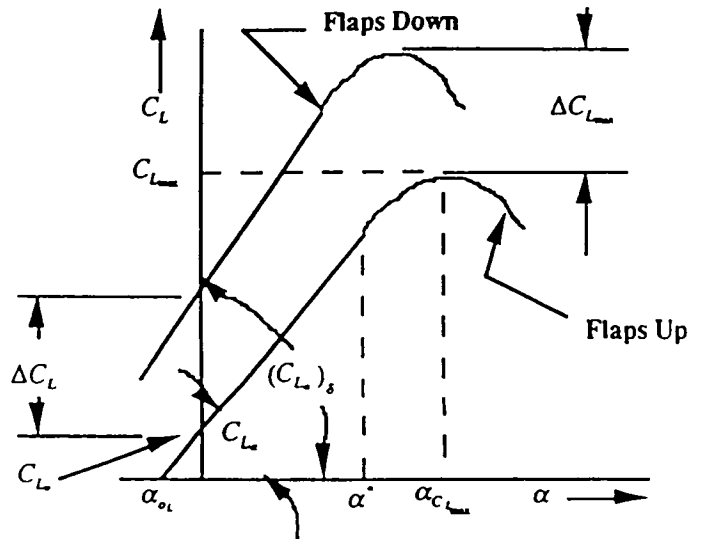


Fig. 1. Fundamental Airplane Lift vs. Angle of Attack Curve with Flaps Up and Down.

High Lift Devices

Incorporating various high lift devices into the design of the UW-3S900 assists in stall prevention at high angles of attack associated with takeoffs and landings (See figure 2). The use of fowler flaps and leading edge slats are standard on current aircraft and their use is continued. The incremental lift coefficient for the double slotted fowler flaps is 2.04. The leading edge slats increase the lift coefficient by 0.4. More lift augmentation is gained through the use of boundary layer control systems. Both leading edge suction and trailing edge flap blowing is used. In flap blowing, high energy air is injected into a "tired" boundary layer thus re-energizing the flow. The leading edge suction is to arrest the increasing size of the boundary layer along the wing chord and to reduce the adverse pressure gradient acting on the retarding fluid particles which tends to cause eventual flow

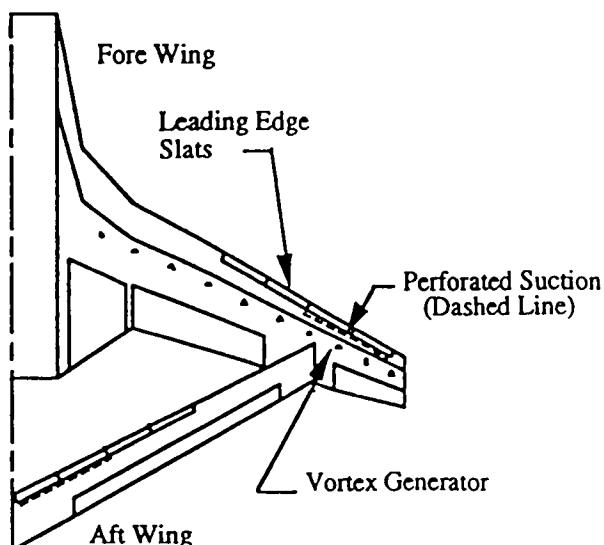


Figure 2. Location of Leading Edge Slats, Perforated Suction, and Vortex Generators

separation. These systems combined increase the coefficient of lift by 1.0 and greatly decrease the required takeoff and landing distances. The joined wing configuration with canard can also lend itself to some natural lift augmentation, as the canard sheds vortices that help maintain flow attachment over the fore wing. Due to the relatively large size of the main lifting surfaces, (i.e. fore and aft wings) space exists for the implementation of a combined blowing and suction boundary layer control system.

The system used in the UW-3S900 provides a substantial amount of increased lift (even for the conservative analysis); prevents stall at the leading and trailing edges; decreases required takeoff and landing distances; and allows steeper climbs over obstacles (Chang, p. 300). The boundary layer control system is meant to be used at takeoff and landing only, and vortex generators help prevent flow separation during cruise. These devices create tip vortices that draw high energy air from outside the boundary layer into the slower moving air close to the skin (Northrop, p. 69). Drag does increase slightly but the prevention of separation and slight lift increment normally outweigh this.

Drag

The drag of the aircraft is divided into profile and induced drag. The drag on the UW-3S900 used conventional aircraft techniques that

yield conservative estimates. The total drag of the entire airplane is the sum of the individual components and the interference drag that each component imposes on the other.

Theory from Wolkovitch suggests that the joined wing actually reduces induced drag and trim drag. The closer the joint to the tips the larger the reduction in drag. In this configuration, the span efficiency is at a maximum and will yield a maximum lift over drag ratio. However, this configuration increases the weight of the wing. The balance between structural weight and aerodynamic efficiency placed the joint of the wings of the UW-3S900 at 70% span of the fore wing. The chosen position of the joint allows for a small reduction in weight and an increase in a theoretical lift efficiency of about 2%. Theory from Wolkovitch also does not account for wing overlap. The UW-3S900 differs from any current joined wing theory in that the joint includes an engine. Because of the lack of research in this area, the specific effect on drag of this configuration is unknown. The best estimate is made.

Stability

The stability of the aircraft is another important aspect of this design. The two aspects of stability considered are static and dynamic stability. The static stability of the UW-3S900 is larger than most aircraft with a static margin of -0.15 to -0.22. Since the aircraft has a center of gravity movement of 7.5 ft., ample allowance in the static margin is provided to assure static stability. The large elevator on the aft wing compensates for the larger than normal static margin, thus alleviating any disadvantages associated with the margin.

Dynamic stability of this aircraft is excellent. The longitudinal and lateral modes are all stable except the Spiral Divergence mode that is slightly unstable and correctable by the pilot. The aircraft will not need a complex automatic control system. Therefore this will lower cost and raise reliability. Reliability is a major concern especially for a 50 hour round-trip over oceans and uninhabited areas without emergency ejection capabilities.

Control Systems

Two areas of control systems considered in the design of the UW-3S900 are the flight system and the fuel system. A reversible, hydraulically and mechanically actuated system selected for the flight system proved to be the most cost efficient system. A fly by wire control system selected for deflection of the spoilers allows response to movements to be quick and precise. The effect of the joined wing creates no additional considerations except the addition of extra elevators on the aft wing.

The fuel system includes fuel lines, fuel pumps, vents, and fuel management systems. The main driving factor in designing the system is the fuel tanks. The tank used self-sealing bladders. This is very important in military transports that fly in combat areas and are vulnerable due to the resulting fuel loss and the danger of fire.

Wing Structure

One major criterion in the design of any airplane is the overall structure of the wing and fuselage. The joined wing proved to be very beneficial to the entire structure of the UW-3S900. The largest advantage is the wing's high stiffness. The joined wing, as stated earlier, forms a diamond truss structure that resists the bending moments from the lift and drag forces in the in-plane direction. The in-plane direction is the surface that connects the quarter chords of the fore and aft wings. To increase the strength in the out-of-plane direction, the asymmetrical wing box concentrates bending resistant material near the upper leading edge and the lower trailing edge of the wing from the wing root to the wing joint. From the wing joint to the wing tip, a cantilever structural wing box optimizes the bending strength of the wing. Composite materials are used for most of the wing structure. These materials combine small weight advantages and the ability of designing composites to resist large bending and shear stresses in one direction.

The joint, composed of stiffened cylindrical frame structures, attaches to the wings with strengthened pylons. The engine is placed in the center of the stiffened joint.

The fore wing's profile has a lift distribution beneficial to the structure of the aircraft. The section of the fore wing near the fuselage produces the largest lifting force. By decreasing the resultant moment arm of the lift force, the moment about the longitudinal axes reduces. This reduction in moment corresponds to a reduction in the amount of required bending resistant material and therefore a reduction in weight. The root of the wing has the largest thickness. This allows for a thickening of the spars at the wing root that resists the large shear and bending forces at the wing-fuselage connection. The thickened wing area can also contain more fuel than conventional design.

Fuselage Structure

Another aspect of structures is the arrangement of the fuselage. The joined wing configuration greatly helps the structural integrity of the connections between the fuselage and wings. While standard cantilever wing airplanes have huge bending moments resulting from a fuselage supported in the center, a joined wing with a canard has three supports. This lowers the maximum bending moment in the fuselage. According to Wolkovitch, lateral and torsional fuselage loads may also be reduced since the joined wing provides additional load paths to withstand rolling and yawing moments applied by gusts or by control surfaces. Both of these effects allow the use of lighter frames.

The fuselage consists of frames, stiffeners, and skin. It consists of two separate cabins: the upper cabin that contains the troops' seats and flight deck, and the lower cabin that contains the cargo. Cargo is loaded from the front and the rear. The frames and skin/stiffeners are made of aluminum alloys. The frame spacing determined by using a non-dimensional analysis relates frame deflection to skin/stiffener panel buckling, as discussed by Shanely. The frames have a "Z" cross section and the skin/stiffeners have a blade cross section. The stiffened skin concept is selected because of its excellent stress carrying capabilities. The mid section of the airplane incorporates a carry through wing box that carries the wing loads and joins the wings to the fuselage. The pressurized upper cabin uses fail-safe titanium straps that bond to the skin.

Propulsion

One of the requirements for the design of the UW-3S900 is that it uses commercial and military runways. The 9 ultra-high bypass turbofan engines each produce 100,000 lbs of thrust that meet the noise requirements for both the civilian and military specifications. The ultra-high bypass engines also reduce the specific fuel consumption to allow for more efficient use of fuel. The plane satisfies the takeoff and landing requirements and completes the required 180 turn-around radius on a runway.

Landing Gear

One final design area is the landing gear. The main criterion in the design of landing gear is the loads produced upon landing. The loads on landing require multiple strut-multiple wheel combinations to support the large loads. Sensory materials employed allowed early detection of cracks or the yielding of material. High quality Type VII tires are selected based on loading capabilities and pressure. In the landing gear analysis, the joined wing was not a consideration with the exception of the center of gravity placement located in the center of the wing box. This proved to be too far aft to allow retraction into the wings due to the placement of the flaps. Therefore, the landing gear retracts into the fuselage.

Cost Evaluation

Cost of the airplane program, while not a critical area is an important feasibility requirement. Life Cycle Cost includes all those costs associated with three phases: the research phase, the acquisition phase, and the operation phase. Each of these has several assumptions based on graph interpolation and data specific to the UW-3S900. From these assumptions and calculations the Life Cycle Cost is 5.8 billion dollars assuming 100 planes. This gives a cost per airplane of approximately 900 million dollars and is comparable to other aircraft that also need extensive research.

Conclusion

From the performance evaluation of the completed UW-3S900, the aircraft can complete both the primary radius mission and the secondary radius mission that the AIAA proposed. The emphasis of the design is on static and dynamic stability, wing and fuselage frame design, as well as overall soundness and compliance with proposal requirements. This design is for feasibility study purposes only. There are areas of optimization in every section. However, from this feasibility study and performance evaluation, this aircraft meets the needs of the military to rapidly deploy large numbers of troops and equipment from the continental United States to potential trouble spots throughout the world.

Acknowledgment

The design team extends its gratitude to the following people, without whose support and guidance this project would not have been completed. Our thanks to: Professor Thomson, Design Instructor; Professor Lovell, Dept. Chairman; Professor "Bud" Schlack, Aerodynamic Guru; David "Lucious" Corr and Tony Kellicut, Teaching Assistants and Foosball Coaches; and Rita Martinson, Department Secretary. A special thanks to Mr. Gary Rudolph, Solid Modeling Consultant and Kim Aarons from JPL. A final thanks to USRA for their support, AIAA and General Dynamics for sponsoring the project and any others whom we have regrettably forgotten.

References

- Abbott, I. H., and A. E. Von Doenhoff. Theory of Wing Sections, Dover Publications Inc., New York, 1959.
- Chang, Paul K., Control of Flow Separation: Energy Conservation, Operational Efficiency, and Safety, Hemisphere Publishing Corp., New York, 1976.
- Northrop Institute of Technology, Basic Science for Aerospace Vehicles, 3rd ed., McGraw-Hill, New York, 1963.

Roskam, Jan. Airplane Design. Parts I-VIII,
Roskam Aviation and Engineering Corp.,
Ottawa, Kansas 1987.

Shanely, F. R. Weight-Strength Analysis of
Aircraft Structure. Dover Publications, Inc.,
New York, New York, 1960.

Wolkovitch, Julian. "Joined-Wing Research
Airplane Feasibility Study." AIAA-84-
2471, Oct. 31 - Nov. 2, 1984: 1 - 13.

Wolkovitch, Julian. "The Joined Wing: An
Overview." AIAA-85-0274 Jan. 14 - Jan.
17, 1985: 161 - 178

**DOMUS I AND DYMAXION:
TWO CONCEPT DESIGNS FOR LUNAR HABITATS**

University of Wisconsin-Milwaukee
Department of Architecture
Milwaukee, Wisconsin

Gary T. Moore, Project Director/Faculty Advisory
Janis Huebner-Moths, Teaching Assistant
Christine M. Brinlee, David S. Erdmann, Lydia H. Matheson, Wayne A. McCambridge, Steve M. Schmidt,
and Augustus J. Wellings

Abstract

Two concept designs for lunar habitat missions were explored and developed. In contrast to other work on lunar habitat designs, the driving force was habitation objectives and habitation performance requirements based on human factors/environment-behavior considerations. Attention was given to site selection and site planning requirements, first lunar outpost requirements, and initial operating configuration design requirements (both quantitative and qualitative). After review of 5 technological options and 12 previously published lunar habitat concept proposals, it was decided to further explore two concepts. The first is a pressurized self-supporting membrane structure (PSSMS) proposed by Chow and Lin, and the second a dymaxion dome structure based on the work of Buckminster Fuller. The master plan, construction sequencing, building system, technical subsystems, and interior configuration of one of the concepts is presented in this paper. *Domus I* consists of three entrance/EVA modules connected to a rigidized, inflatable torus containing all research laboratories and mission control, and a domed interior of an rigidized, inflatable ellipsoid containing all crew quarters and the crew support facility. (*Dymaxion* consisted of three hard module research laboratories/EVA chambers, a mission control core, and a two-floor habitation inflatable.) The relative advantages and limitations of the PSSMS concept are briefly reviewed. In summary, the concept seems extremely feasible and deserves most serious exploration by the various lunar program offices at NASA.

Introduction: Project Goals

A final mission design has as yet to be determined by NASA for either the First Lunar Outpost (FLO) or the first Permanent Lunar Habitat (PLH). Open to a wide variety of conceptual suggestions, NASA looks to internal ideas as well as to those from industry and academia. The

Advanced Design Program in Space Architecture at the University of Wisconsin-Milwaukee hopes to make an impact. Students play the pivotal role participating in a combined educational and research process resulting in a variety of aerospace design proposals. Each proposal is presented not only in the USRA conference proceedings, but also in a series of technical reports, monographs, technical papers, and, when possible, at NASA seminars and technical interchange meetings.

In the broadest sense, the priority of a lunar base proposal is to provide a safe, productive environment to sustain human habitation and experimentation. To achieve this end, materials should be of near-term technology requiring minimal extravehicular activity (EVA) time for crewmembers. A lunar base represents humankind's ability to expand its own horizons, challenge technology that currently exists, and push the same technology to address unique situations. There is potential, as has been demonstrated by shuttle missions, of utilizing new advances to better life on Earth. We are upon the threshold of achieving the goal of permanent settlement on another celestial body. Estimates of commencing this venture vary, yet many feel that within the first decade of the new century, the goal is within reach.

The project goals were to research available concept options, evaluate them and select the most promising for further study, develop detailed habitation performance requirements, and study the feasibility of outfitting the most promising concepts following those requirements for human habitation on the moon. The resulting final product was two complete lunar base designs based on the two most promising concepts (only one concept is developed here; for the second, see the monograph by Huebner-Moths, Rebholz, & Moore, 1993). *Domus I* is available as a complete AutoCAD slide program, rendered in Animator-Pro and 3-D Studio programs. An animated fly-through provided a brief overall perspective of the base exterior and interior components.

Assumptions and Constraints

The surface mission objectives for a permanent lunar presence including the following:

- advance scientific knowledge in microbiology, life sciences, astrophysics, geomorphology, botany and plant growth, and astronomy with on-site laboratories and human participation as well as telerobotic research
- study effects on humans of a lesser gravitational field and of various protective measures against temperature extremes, environmental vacuum, and radiation hazards

To support these surface mission objectives, the following are the key, high-level requirements for lunar habitation:

- support a crew of 12 international astronauts for stay times up to 9 months, with first launch around 2005
- support the crew being able to perform command and control functions, science objectives, and habitat maintenance
- minimize life-critical and mission-critical risks associated with solar storms, radiation, fire, contamination, and depressurization, physical deconditioning, and stress and other psychosocial performance factors
- address what have been called "mission-discretionary" psychological and sociological issues (Cohen, 1993) related to long-term isolation and confinement, including but not limited to space for shelter, privacy, and recreation, space for rest, relaxation, exercise, and entertainment, and psychological support, e.g., communications home, and other factors leading to improvements in productivity and the quality of life for the crew

The principle technological constraints are the following (based in part on Moore & Campbell, 1993):

- utilization of FLO as a starting point for PLH
- minimum construction operations, and especially minimum EVA operations
- construction technology exhibiting advancements in material design, weight reductions, and compactability for transport
- ability to reconfigure/expand the habitat where/when applicable

Alternative Technological and Design Concepts

A large number of technological alternatives for lunar habitats and an equally large number of architectural design concepts have been published in the aerospace literature and in internal NASA documents (cf., for

example, the references in Moore, Huebner-Mohts, Rebholz, Fieber, & Paruleski, 1992, and the comparative analysis of five design concepts in Moore & Rebholz, 1992). Unfortunately, all too often engineering or architectural designers proceed as if they were the only ones with decent ideas, paying no critical attention to the concepts that have been published and critically reviewed in the scientific and engineering literatures.

To not repeat this unfortunate precedent, the study team collected and critically reviewed 5 different technological options and 12 different concept designs. Each design concept was evaluated in terms of ease of construction, simplicity of design, near-term technology, minimizing EVA involvement, number of facility components, volumetric allowances for specific functions, and habitability.

The technological options for lunar habitats include the following:

- membrane structures
- tents and screens
- laminated bladder systems
- resin foam-rigidized structures
- aluminum alloy hard-modules

The alternative design concepts published to date include the following:

- inflatable and hard-module concept
- LEO-assembled hard-module concept
- pillow-shaped tensile concept
- pre-assembled hard module concept
- suspended inflatable concept
- earth-sheltered family home concept
- hard-module rack concept
- linear underground hard-module concept
- hybrid triangular inflatable and hard-module concept
- hybrid underground inflatable and hard-module concept
- dymaxion dome concept
- pressurized self-supporting membrane structure concept

The full details of this evaluation are given in Huebner-Mohts et al. (1993; for an earlier more detailed evaluation of five concepts, see Moore & Rebholz, 1992).

Habitability Performance Requirements

There will be four major elements to the PLH base: the solar panel collection fields, nuclear power facility, the habitat, and the launch and landing site.

Site Requirements

Permanent landing pads should be located between 3 and 5 km from the habitation zone, and no further than 5 km away from FLO. The base should have a north-south axis, the habitat centrally located within this axis, with the power and landing areas on opposite ends of the axis. This will allow a protective envelope for the habitat guarding against spacecraft fly-over and potential hazard. The nuclear power facility should be located 1 km from the habitat, accessible by road along the axis. This allows for a measure of safety while limiting the distance current must travel. The solar fields should be located where little exploration is expected, limiting dust contamination. Future field operations and lunar scenery should be taken into consideration.

According to the latest NASA thinking and requirements (Carpenter, 1992; Perkinson, Adams, et al., 1992), a large number of detailed human factors/environment-behavior (EB) habitability performance requirements must be met in the design of the habitat of any FLO or PLH. Details are given in Carpenter (1992), Perkinson et al. (1992); salient performance requirements for the design of the habitat itself (i.e., excluding technical requirements for hatches, scientific surface mission operations, transportation vehicles, etc.) have been extracted and summarized in Huebner-Mothes et al. (1993).

General Human Factors/EB Requirements

A few, sample, high-level requirements for the habitat/research laboratories as a whole include the following:

- the architecture should be configured to accommodate evolution of the outpost, e.g., potential additional volumes including future integration of an additional pressurized volume to provide for outpost expansion, airlocks, logistics containers, other habitats, etc.; growth should accommodate spatial adjacency between similar activity centers and not jeopardize crew well-being
- the architecture should be designed for simple interfaces, modularity, and replacement; this modularity should provide quick disconnect for hardware and electrical equipment
- to overcome the stresses induced by the mission environment, mental health should be preserved by providing appropriate design and psychological support
- the architectural layout should insure that adjacent volumes are set aside for similar or compatible activities and that interfering activities be separated, e.g., compatible activities such as hygiene and waste

management functions can be adjacent, while interfering activities such as food preparation and waste management should be separated

- the architecture should provide a marked emergency route for contingency operations
- the habitat should support internal operations by space-suited crewmembers, e.g., emergency cases will require suited crewmembers to operate inside habitable elements
- the architecture should accommodate unimpeded translation and circulation paths within the habitat; traffic paths should be sized according to activities, location of crew stations, and size of cargo/crew; a range of scenarios that focus on the size of equipment and crew moving through the habitat need to be addressed
- the intra-vehicular activity (IVA) architecture of the habitat shall provide a minimum of 10.0 cubic meters of habitable volume per crewmember (by habitable volume is meant free volume that the crew can access for working, sleeping, eating, personal hygiene, recreation, exercise, etc.)
- external viewing shall be provided for the crew; windows or video are essential for crew use in observing their external environment
- the architecture should provide multipurpose/flexible activity centers and volumes; multipurpose utilization will increase the efficiency of the habitat, e.g., the wardroom can fold away to create an open area for exercise equipment
- the architecture should provide a consistent orientation throughout the habitat, to provide a familiar and comfortable living and working environment for the crew
- the habitat shall provide two independent paths for crew egress; in the event of fire or other emergency which may block crew access to the airlock, a minimum one emergency exit (hatch) must be provided for crew egress

Research Functions

At the present time (Carpenter, 1992), it is expected that the primary mission operations for FLO and by extension for the first PLH will consist of four primary research functions:

- space physics and astrophysics including telerobotic monitoring of at least three remote astronomy telescopes: Lunar Ultraviolet Transit Telescope (LUTT), Small Research Telescope (SRT), and Small Solar Telescope (SST; Eppler in Carpenter, 1992)
- engineering research including tests on the lunar surface, in-situ resource utilization (ISRU) demon-

stration, evaluation of subsystems and prototypes of future equipment, demonstration of prototypes for future lunar surface processes, and test-bed functions for new materials and construction processes for future Mars missions

- life sciences including botany, microbiology, plant growth, health maintenance, and monitoring of human performance and biomedical parameters, and for operating experiments in human physiology, exobiology, and gravitational biology
- geosciences including geomorphology, monitoring geophysical activity and environmental characterization and regional exploration of the lunar surface

In all phases of the mission, the crew will be interacting with various workstations. Designing these stations around crew capability can maximize productivity (Brown & Bond in Carpenter, 1992). Adequate and appropriate space for these scientific mission operations (both crew-tended and telerobotic) must be provided. Crew size, viewpoint, reach, and restraint should be considered. The gravity environment, required visual data, room to use tools and equipment, and location of task should be considered to maximize crew capability.

Crew Functions and Crew Support Requirements

For the crew to be able to perform these scientific and engineering functions at full productivity, adequate and suitable crew spaces and crew support spaces must be provided in the PLH. These include space and appropriate design for each of the following:

- safe haven
- centralized command and communications center
- mission operations laboratories and workstations
- health maintenance facility capable of emergency surgery and critical care
- exercise countermeasures facility
- wardroom for all eating, meetings, and passive recreation, including adequate space for 12 crewmembers to be seated, share meals and celebrations, and conduct briefings, table able to be reconfigured to seat fewer numbers, especially 6 at one time, communication system for teleconferencing, lighting to allow for task and general illumination, and materials to permit easy maintenance and cleaning
- galley for all food preparation and stowage of consumables, cleanup post-mealtime, and waste management, including space for more than one crewmember to prepare food, food stowage compartments, refrigerator/freezer, microwave/convection oven, food preparation equipment and stowage, food consumption utensils, sink, trash management container, cleanup supplies and stowage, material

surfaces conducive to easy maintenance, and illumination for tasks and general activity

- recreation area dedicated to crew relaxation and communication including audio/visual projection system, stowage compartments for video or audio tapes and compact discs, seating for smaller groups of crew members, seating to accommodate quiet activity like reading, space for game playing, space designed for small group casual conversation, and stowage for hard-copy printed books for leisure
- sleeping quarters for both single and double crew occupancy for sleep, privacy, and retreat, including horizontal sleeping space (bed), personal work space, personal stowage compartments, controls for communications and caution/warning system, and accessibility to hygiene facility
- personal hygiene facility and limited hygiene facility near the exercise countermeasures facility and research laboratories, including hand, face, eye cleansing capability, toilet, shower and full body cleansing, mirror, stowage for general supplies, ventilation for humidity control, adequate volume to allow donning and doffing of clothing and drying off after shower, and lighting system for proper visual acuity for personal hygiene
- laundry
- trash management facility
- logistics-stowage area for consumables (oxygen, nitrogen, water, food, refrigerated/frozen food, etc.) and equipment
- suit stowage and maintenance area
- suit donning/doffing area, dust-off, and EVA/IVA compression chamber/airlock

Detailed performance requirements for all of the above and for modular rack components, furnishings and equipment, illumination, and materials, colors, and finishes are given in Huebner-Moths et al. (1993).

Building System Requirements

Detailed building system requirements have been developed for each of the following (and are reported in detail in Huebner-Moths et al., 1993):

- materials
- construction system
- structural system
- connections
- hazard shielding
- energy considerations
- construction sequencing
- expandability and retrofit

For example, the structure system requirements were the following:

- internal pressure of 101.4 kPa
- sustain load from regolith cover or ability to withstand radiation exposure
- survive impact of micrometeoroids
- support internal rack systems
- handle live loads
- support entrance and exit points
- withstand radiation exposure
- flexible
- easily erected and retrofitted

Based on these performance and technical requirements, and on the evaluation of 12 different concepts, a FLO concept was selected, and two concept designs were developed in sufficient detail to learn if the concepts were feasible in terms of research operations and habitability considerations.

First Lunar Outpost (FLO)

In response to requirements like those above, we have chosen to incorporate a FLO scheme developed in the Advanced Design Program at the University of Puerto Rico for several reasons:

- based on the strengths and limitations of an earlier NASA-JSC scheme
- particular attention to human factors in its design
- proposes interesting ways of handling radiation protection/safe havens for short duration stay-times without regolith covering

The scheme is a vertical pressure vessel habitat designed to be integral with the FLO lander, in fact the habitat is embedded within the lander legs and fuel and oxygen tanks rather than being a horizontal habitat resting on top of the lander and tanks as in the earlier NASA-JSC concept (cf. Perkinson et al., 1992). This arrangement provides some radiation protection for the habitat and research spaces. The safe haven is the second lowest level of the habitat.

FLO is divided horizontally into four floors. The lowest level is the airlock and ingress/egress module. The second level is the crew quarters, double-functioning as a safe haven. The third level is the research level. The top level is the crew support facility.

While this scheme has some limitations (e.g., awkward zoning from public entry to private crew quarters to semi-private work spaces to public recreation spaces), it has the

distinct advantages of being protected by the structure and tanks of the lander and providing a natural safe haven.

With the proximity of the FLO module(s), the astronauts will have the capacity to reside in FLO while conducting the construction of *Domus I*, or *Dymaxion*.

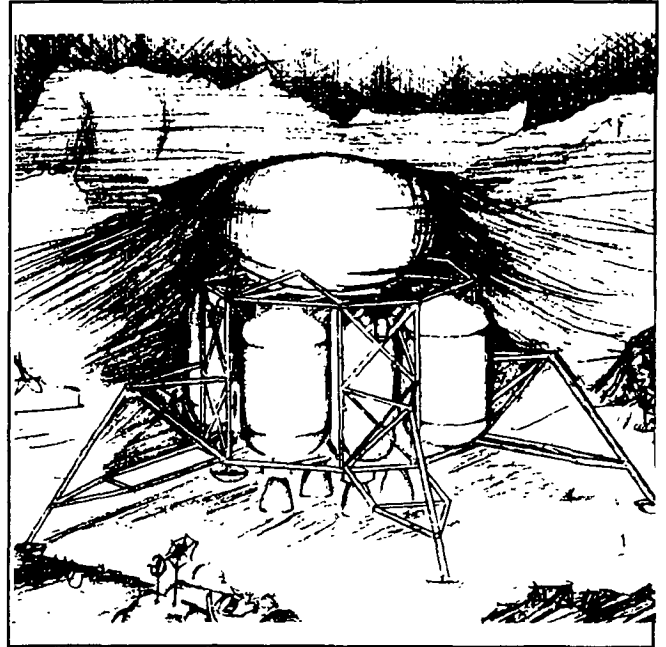


Figure 1. First Lunar Outpost, designed by the University of Puerto Rico Advanced Design Program.

Domus I Lunar Habitat and Research Facility

Initial Operating Configuration (IOC) will be achieved with the outfitting of all interior spaces of the PSSMS concept. After inflation and hardening of the rigidized foam, the structure will be depressurized, allowing easy movement of partitions, equipment, and furnishings into the habitat and research areas. Wall partitions, mechanical systems, hatches, scientific equipment, and all other equipment and furnishings for the research spaces, mission control, crew quarters, and crew support facility will be moved into the structure, deployed, and put into operational mode. Once completed, the three major ingress/egress hatches will be closed and the entire structure repressurized, thus achieving IOC.

The habitat will be organized as the center of a linear base plan. This central habitation zone will consist of the PSSMS habitat connected to FLO along with a solar collection field.

There are two major component that comprise the habitat. These include three airlocks and a pressurized, rigidized ellipsoid with perimeter torus.

The primary airlock will have a dust-off entry system. The other airlocks, positioned to provide egress capability from the ellipsoid and torus, have rover docking collars. Each can be used for emergency egress with or without a rover docked to it.

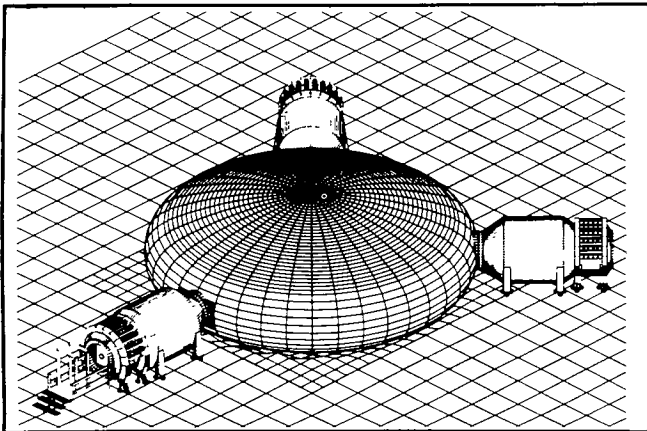


Figure 2. Overall axonometric view of *Domus I* shown without regolith radiation protection system.

To support mission directives, a single-floor semi-public/semi-private outer torus houses life and physical science laboratories, the health maintenance facility (HMF), and the Mission Command and Communications Center (MCCC).

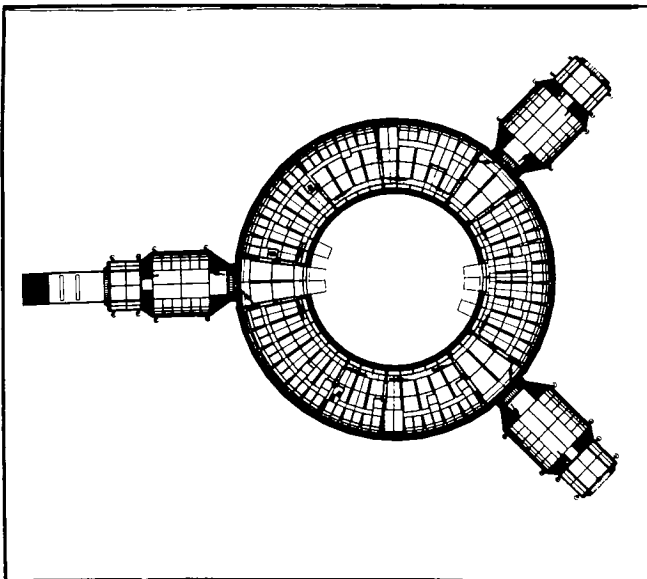


Figure 3. "Mezzanine" level floor plan of *Domus I* -- research laboratories, mission control, and the three airlocks.

The domed portion of the ellipsoid is two-floors--separating the private crew quarters (lower level floor) from the public crew support facility (upper level floor).

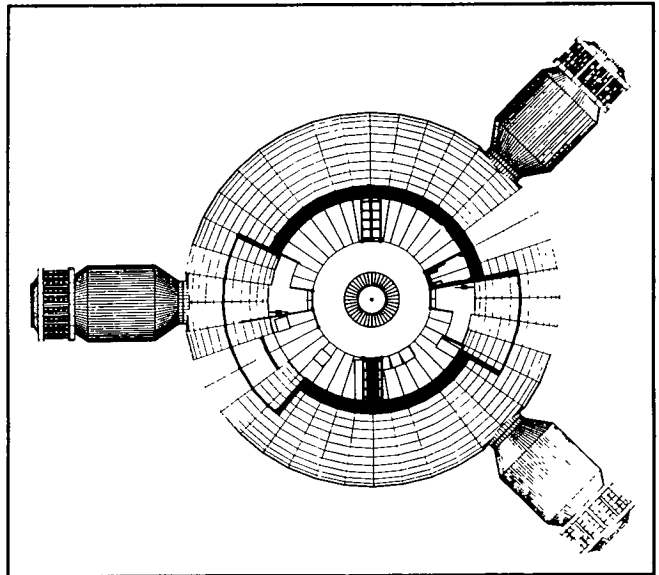


Figure 4. Upper level floor plan of *Domus I* -- crew support facility (wardroom, galley, library, recreation, exercise facility).

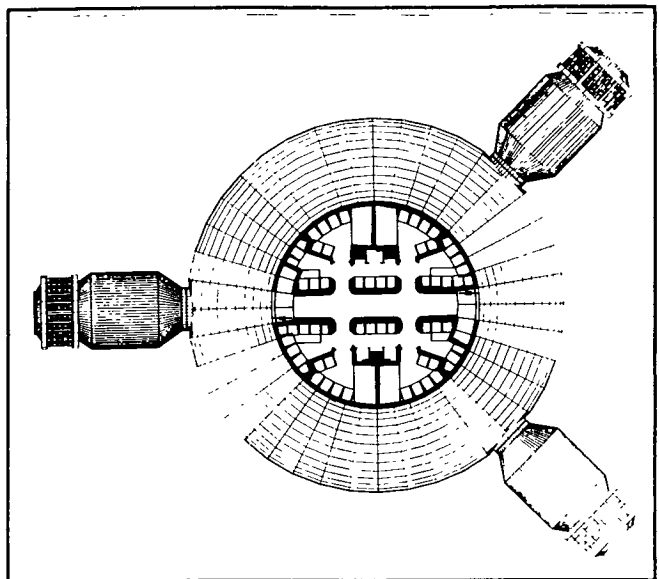


Figure 5. Lower level floor plan of *Domus I* -- crew quarters and personal hygiene facilities.

Kit of Parts, Racks, and Workstations

There are three basic types of workstations that were designed for Domus I. Each workstation is a derivative of a basic rack. The basic rack was divided into a 2 by 8 matrix so that a standard "kit of parts" could fit into this rack. The MCCC workstation, laboratory workstations, and the backup workstation utilized this standard matrix.

The rack dimension is 2.3 m high, 1.2 m wide, and 1.2 m deep. This rectangle is bisected twice. The rear storage rack is bisected into halves. The front rack is divided into 2 equal unit mods horizontally and 8 units vertically. These are designed as interchangeable parts with different inserts to accommodate various stowage requirements.

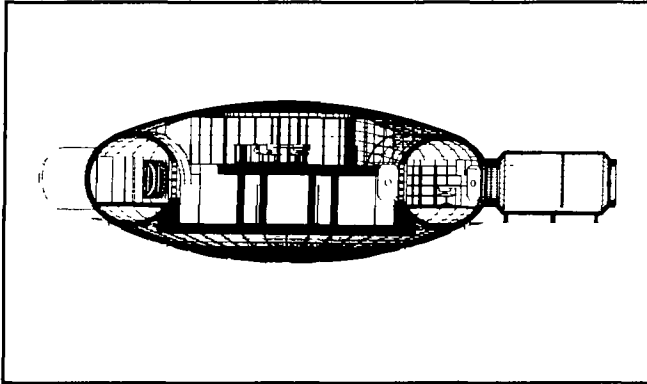


Figure 6. Section through *Domus I* showing the research labs (outer), crew support facility (upper), and crew quarters (lower).

Research Laboratories

The torus is divided into three functional crescents. The laboratories are allocated into the crescents by function and similarity. The human sciences crescent contains microbiology, life sciences, and the HMF. The physical sciences crescent contains two geomorphology labs, botany, and the plant growth chamber. A third crescent contains Mission Control and Communications.

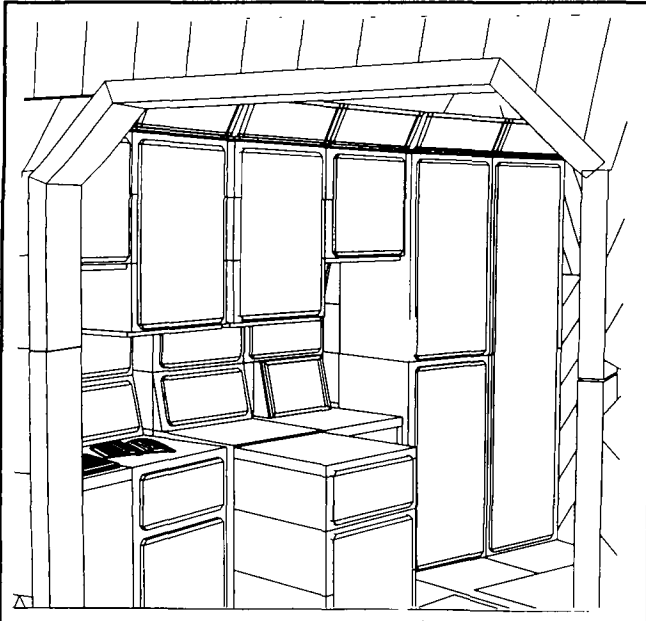


Figure 7. Part of the life sciences laboratories showing the modular rack system and workstations.

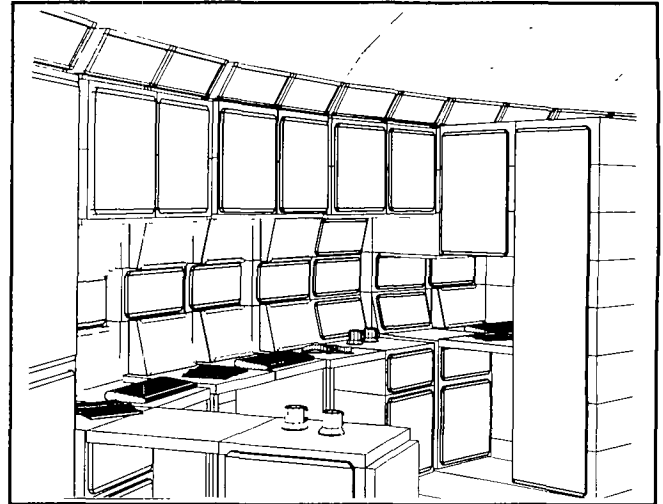


Figure 8. Mission communications and control center in the torus.

Crew Quarters

The crew quarters of *Domus I* are located on the lower floor of the domed interior of the ellipsoid. They are designed to accommodate a crew of 12, with four double and four single crew compartments. These are paired with two full hygiene facilities. Throughout the area, curved bulkheads have been introduced as a safety feature for movement. All the doors are retractable, requiring no additional volume for stowage or opening and closing. Crewmembers will have the option of personalizing their quarters with a number of interchangeable components and color choices.

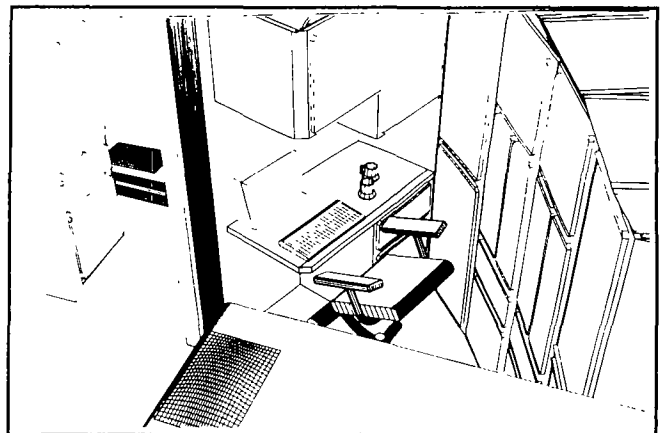


Figure 9. View into one of the single crew quarters looking down at the personal workstation and stowage compartments from the raised bed.

The crew quarters can be isolated from the balance of the habitat at the bounding platforms. The crew floor, being the most protected both by regolith and by the remainder of the ellipsoid and torus with their stowage

racks, is the designated safe haven for the crew. This floor can be isolated by airlock hatches from the torus. Caution and warning systems as well as mission control capability are integrated into the personal quarters.

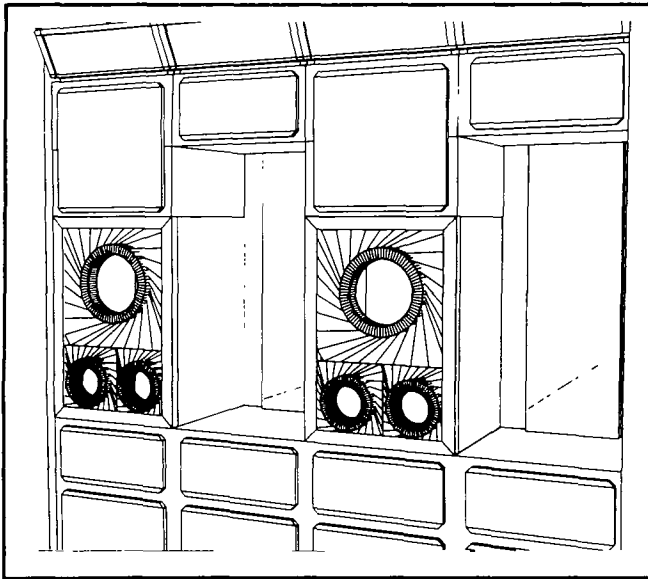


Figure 10. Part of the personal hygiene facility showing the hand and face washing system, mirrors, and personal stowage compartments.

Crew Support Facility

To respond to requirements for privacy and social interaction, the crew support facility provides semi-public meeting places as well as semi-private recreation spaces. Contained in the upper-floor crew support facility are a central wardroom surrounded by an entertainment center, library, exercise facility, galley, and limited hygiene facility. Bounding platforms connect the crew support facility with the research labs and the lower crew quarters.

The wardroom will serve as a central focal point for all the crew's leisure activities and celebrations as well as double function for group briefings and mission telecommunications. The dominant feature is the wardroom table. This table has the ability to be configured in a number of ways to allow for a flexible seating program. With panels stowed in the floor compartments directly below the table's perimeter, a crewmember will be able to easily access the panel and install it on the existing pedestal. The table can also be completely removed to allow the entire space to be open. The chairs that have been designed for the habitat are mobile and can be drawn up to the table to provide seating.

From this central point within the crew support area, the projection screens of the entertainment center are visible. A crew member can prepare a meal in the galley

and may use the table for eating. Small groups or the entire crew can be seated comfortably with generous surface space for working. A lighting system in the center of the table will provide task illumination for the crew. There will be a power supply and cable access to install laptop computers. Circumscribing the wardroom space, an illumination light ring will provide general illumination. The key feature of this interior volume is the reconfigurability and allowance for crew involvement in its spatial arrangement.

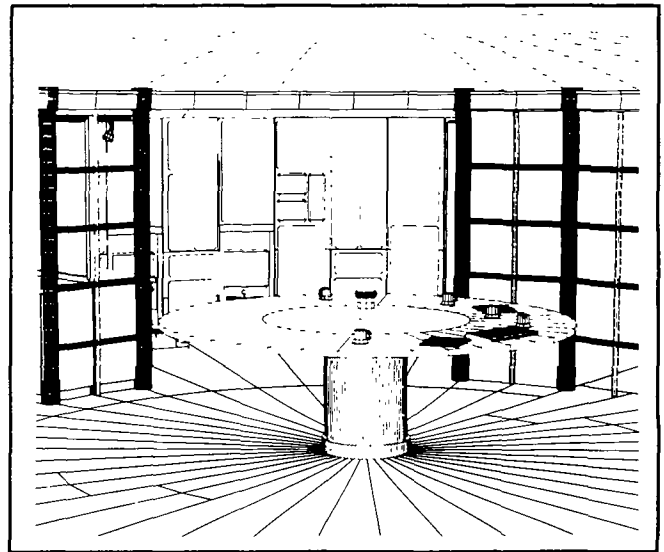


Figure 11. Wardroom view illustrating the wardroom table fully deployed.

The galley is designed for efficiency in food preparation with ample and convenient stowage for consumables and cooking implements. Foods will be stored in ready-to-eat form, dehydrated, thermostabilized, or freeze-dried. Storing additional food will be accomplished by using refrigeration/freezer units. Fixed appliances designed into the rack system are the sink, dishwasher, and microwave/convection oven, along with a hand and face-wash system. Cleanup will be easily accomplished. Counter space has been designed as working surfaces. Lighting is built into the wall rack system. Surface colors and textures as well as the illumination type will compliment the space.

A quiet library location has been provided to access personal choices of reading material. The choices can be electronic as well as hard copy. The library is adjacent to the galley, yet divided by a rack component system. The torus has a window emplaced and provides a viewing port into the plant growth laboratory. Comfortable seating, desk space, and computer capability are provided. Stowage for hard copy and electronic information is included.

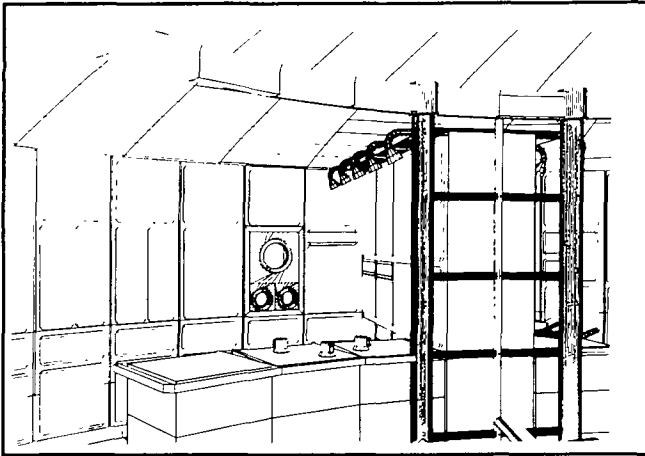


Figure 12. Galley as seen from the wardroom.

Stowage components have been included to allow room for tapes and any additional equipment deemed necessary for listening to music or watch the monitor. The floor space was purposely left open to allow the crew the option to bring a chair into the space or to lounge on the floor.

Exercise countermeasure equipment that dual functions has been included in this area. Visually, the crewmember will focus on the wall ahead of the machines. In this space, projection monitors have been installed to provide a variety of settings in which to exercise. The equipment itself is capable of being stowed in the upright position, compacted into the wall rack system. This removes the equipment should additional space be required for crew functions. Although full hygiene facilities are located just below the crew support level, a limited hygiene facility was designed adjacent to the exercise area.

Bounding Platforms

Bounding platforms, rather than stairs or polls, will allow easy access in 1/6th reduced gravity between the three levels of the habitat (see the section in Figure 6 above). The bounding platforms have been designed to accommodate a fully-suited crewmember. Visual access is permitted by the split level positions of the platforms. From the research areas in the torus, a crewmember can see into the crew support facility. Translating down one platform, visual access is gained to the central hallway of the crew quarters area, but not to the crew compartments or hygiene facilities. Lighting of the platform and hand-holds are provided to assist locomotion.

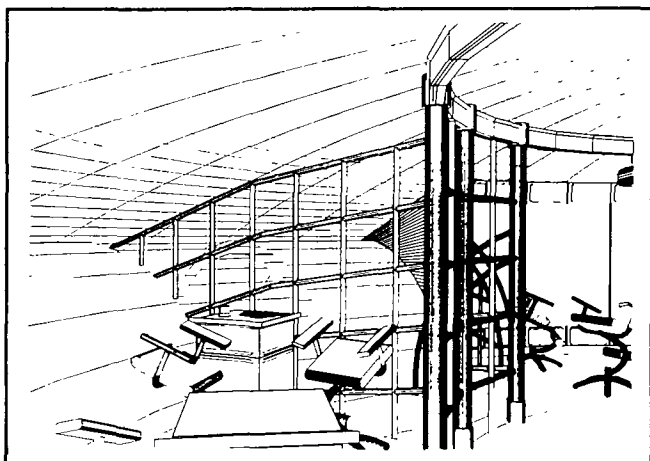


Figure 13. Library and small group recreation area.

A recreation area has been designed with a large projection screen as the focal point. A rack component spatially divides the recreation area from the exercise countermeasure facility. Yet this entire space is clearly visible from most points within the upper floor of the habitat. The design was driven by the proximities of the galley and wardroom, and the desire to allow the crew to enjoy a video or a viewing of the surface of the Moon during relaxation, while eating or preparing their meals, or while exercising. A major benefit of the large screen system is the ability to conduct full-crew, unobstructed briefings with all seated at the wardroom table. The projection system is located above the table, attached to the light ring.

Conclusions: Critical Design Features -- Strengths and Limitations

Domus I is the result of a feasibility study of the Chow and Lin PSSMS concept on the lunar surface. The results of this design analysis indicate the concept is very feasible from habitability, human factors, and environment-behavior considerations. The PSSMS structure is easily able to be made habitable. The torus versus the inner part of the ellipsoid allows easy separation of work from living areas. The two floor possibility in the ellipsoid allow separation of public crew support spaces from private crew quarters. Orientation and circulation are clear. Translation pathways allow for unobstructed movements of components and crew. Dual egress is assured. Variety of space within tight quantitative space limitations is accomplished. Creating two separate environments within one envelope--the torus and the domed center of the ellipsoid--lessens the number of materials interfacing with one another.

Some additional critical design features of this concept. *Domus I* allows separate work and relaxation realms within the habitat. The separation of work and relaxation may be vital to the well-being of crewmembers. It is a feature found in terrestrial architecture and allows the human being time to refresh and regroup. As productivity is a major component in the success of a lunar mission, creating a positive work environment is essential.

Another feature of *Domus I* addresses the visual and spatial variety of the habitat. Though there are only three major levels of operation--laboratories, crew quarters, and crew support levels are designed with spaces that flow and blend with one another, while being distinctly different in style and character. The torus portion, dedicated to the laboratories, differs in geometry, color scheme, and workstation arrangement from other parts of the habitat. Work spaces are open; walls have windows emplaced to promote a visual sense of spaciousness. Those areas dedicated to the crew are in the central domed ellipsoid. Some spaces, like crew quarters, have curved outer walls. Translation spaces in the crew quarters are rectilinear, centrally located, and clearly connected to the bounding platforms. The ceiling of all crew support social spaces is slightly domed, giving a more spacious feeling for these relative large group spaces.

The crew has a choice of single or double quarters, in agreement with various aerospace professionals who encourage spaces be designed that will allow a crewmember to be alone for some period of time. Personalization is encouraged with interchangeable panels of differing colors, and privacy when needed is assured.

The crew support facility is separated from the private crew quarters. It is designed as an open-plan arrangement with a larger central volume to serve the entire crew and supporting facilities on the perimeter. This area allows visual and social interaction among the crewmembers.

Safety is a prime requirement of any structure housing human life. All levels and spaces in the habitat have been designed with dual means of egress and the ability to "lock down" a specific area in the event of a system failure or solar flare. Communication and computer systems can be accessed in numerous locations throughout the habitat. Provisions for short-term stays in the safe haven area--the crew quarters--have been included.

The rack component system allows for change-out and can be shifted within several areas. These designs respond to the change in the anthropometric alignment of the body in the 1/6th g of the Moon.

The construction method of the habitat has not been perfected. Yet, it appears that the construction may be relatively easy to achieve. Site preparation that requires little EVA time for the crew will be beneficial.

Outfitting the interior of the habitat in a shirt-sleeve environment will permit the crew to work without the bulk of spacesuits. There are few components to the entire facility. This fact will allow for easy expansion at the airlock locations. Fewer components means fewer interfaces or potential points of failure.

The volume of the habitat is not expansive, yet every effort has been made to have the geometry appear as though it is. When coupled with the component system flexibility, these spaces should serve a variety of individuals who will inhabit the facility during their tours of duty in a diversity of different spatial settings.

As yet, widespread testing of inflatable technology--and of the PSSMS system in particular--has not been accomplished. The theory behind inflatables, e.g., great volume attained with a reduced amount of packing volume, less weight at liftoff relative to great amount of resultant space, etc., are important characteristics dictating further promotion of the technology. Adding the use of rigidizing foam to enhance the structural integrity is of considerable value added.

With the technology of inflatables still in the discovery stage, *Domus I* has been developed under the assumption that living within a pressurized, reinforced-fabric envelope is not only feasible, but practical. Still to be determined is the method of packaging the envelope and the best strategy to deploy the habitat on the surface of the Moon.

The major limitation of *Domus I* lies in the currently uncorroborated technology of the construction methods and materials. The construction process will demand the use of various types of equipment yet to be developed. In the interior portion of the habitat, further testing will be required to evaluate locomotion within a torus (in 1/6 g). Post-occupancy evaluation (POE) will be vital as lunar bases of the future are constructed and inhabited for any length of time.

In summary, the PSSMS *Domus I* concept seems extremely feasible and deserves most serious exploration by the various lunar program offices at NASA.

References

- Carpenter, J. (1992). First Lunar Outpost: Detailed assumptions. Working draft, Mission Analysis and System Engineering, Exploration Programs Office, NASA-Johnson Space Center, Houston, TX, June.
- Carpenter, J. (1992). First Lunar Outpost: Requirements and guidelines. Working draft, Mission Analysis and System Engineering, Exploration Programs Office, NASA-Johnson Space Center, Houston, TX, June.
- Chow, P.Y. (1992). Construction of pressurized, self-supporting membrane structure on Moon. *Journal of Aerospace Engineering*, 5(3), 274-281.
- Cohen, M.M. (1993). Mars 2008: Surface habitation study. Final review draft, Center for Mars Exploration, NASA-Ames Research Center, Moffett Field, CA, May.
- Huebner-Moths, J., Rebholz, P.J., & Moore, G.T. (1993). *Domus I and Dymaxion: Two Proposed Concepts for a Lunar Base Habitat*. Milwaukee: University of Wisconsin-Milwaukee, Center for Architecture and Urban Planning Research, Space Architecture Monograph No. 6.
- Moore, G.T., Huebner-Moths, J., Rebholz, P.J., Fieber, J.P., & Paruleski, K.L. (1992). Lunar base requirements for human habitability. In W.Z. Sadeh, S. Sture, & R.E. Miller (Eds.), *Engineering, Construction, and Operations in Space III: Space 92, Proceedings of the Third International Conference*. New York: American Society of Civil Engineers. Vol. 1, pp. 224-239.
- Moore, G.T., & Rebholz, P.J. (1992). Aerospace architecture: A comparative analysis of five lunar habitats. Paper presented at the American Institute of Aeronautics and Astronautics 1992 Aerospace Design Conference, Irvine, CA, February, Paper AIAA 92-1096.
- Moore, N., & Campbell, P. (1993). Mars mission habitats: Reference implementation concepts. Mars Exploration Workshop II, Flight Crew Support Division, NASA-Johnson Space Center, Houston, TX, May.
- Perkinson, D., Adams, A., et al. (1992). First Lunar Outpost: Lunar habitat documentation. Preliminary Definition Study by Program Development, NASA-Marshall Space Flight Center, Huntsville, AL, May.

**EVALUATION OF THE
MICROGRAVITY IGNITION EXPERIMENT
PREPARED FOR THE GASCAN II PROJECT**

**Worcester Polytechnic Institute
Mechanical Engineering Department
Worcester, MA**

**Professor James Duckworth
Professor Vahid Motevalli
Richard Smith, Teaching Assistant
Timothy Johnson (ECE), Richard E. Parker (MEA)**

Abstract

As flight durations increase, the risk of occurrence of fires also increases. It is important to better understand the physics of a fire in a microgravity environment so that the fire can be detected and suppressed as quickly as possible. The Microgravity Ignition Experiment is designed to answer fundamental questions regarding time to ignition.

The purpose of this project was to perform ground-based testing of the prototype version of the Microgravity Ignition experiment chamber and finalize the electrical and mechanical design of the experiment. A preflight procedure has been developed for preparation of the experiment for launch, assembly, and final check. Finally, the combustion chambers have been constructed and will be assembled. Any modifications of the procedure or instrumentation based on results of the prototype testing will be implemented.

The current experiment consists of exposing a sample of alpha-cellulose paper to a radiant flux and measuring the changes in ambient temperature and pressure in the chamber and the rise in fuel temperature.

The ground based experiments in 1-g have resulted in ignition occurring within approximately thirteen seconds. In microgravity, it is anticipated that the two competing mechanisms of increasing surface temperatures and reduced oxygen near the fuel surface, both caused by reduced convective flows, will significantly change the time to ignition.

Background

The Micro-gravity Ignition Experiment was designed to simulate ignition in a space vehicle in microgravity to determine how microgravity affects ignition time. This is an important concern for long duration space flight for several reasons. The main and most important reason is the commitment to a continued manned presence in space. Space Station Freedom is scheduled to begin operations by the early

part of the twenty-first century. Given the national attention and investment in the station, the safety of the station is important.

Ignition and fire in a microgravity environment will not behave the same as on earth. Several important forces drive terrestrial combustion which are not present in space. Most of these factors involve heat transfer.

There are three ways in which heat is transferred into or away from an object. These are radiation, conduction, and convection.

On Earth, convection currents are the result of density differences in gases caused by temperature changes. The temperature of the air near a hot substance, such as a burning piece of paper, rises. As a consequence it becomes less dense than the air around it. These air molecules then rise and cooler air falls into the resulting space. This gives rise to currents around objects that are warmer than the surrounding area. (See Fig. 1.)

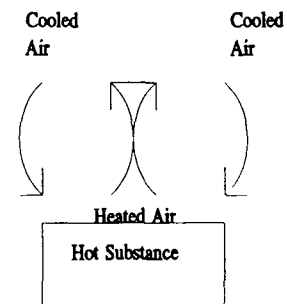


Figure 1

Convection is responsible for carrying away hot combustion products which aid in detection of fire, cause the fire to spread, and foul the environment around the fire. Convection also acts to bring heavier, cooler, oxygen-bearing air to the fire. In

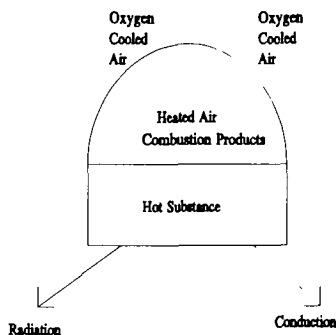


Figure 2

space, convection currents are very small since the accelerations that drive them are very small. Gravitational accelerations are almost exactly balanced by other accelerations resulting in very small forces on air molecules. (See Fig. 2.)

This leads to a number of interesting problems. Since the combustion mechanism is altered in microgravity, what is the most effective method of fire detection? Will ignition occur and how? How long will a fire burn? Will it go out due to oxygen starvation? Will the fire accelerate and spread as easily as it does on earth? What is the most effective method of extinguishing a fire once it starts? This project focuses on the ignition issue in the microgravity environment.

Objective

The goal of this project at its inception was to develop an experiment to perform the simulation of ignition in low gravity. An experimental approach was developed by several project groups. This approach was refined and hardware was constructed to implement this approach. The approach developed by the first project team was as follows.

1. Use a radiative source to ignite a sample of combustible material.
2. Measure the changes in conditions around the sample.
3. Determine how long the sample took to ignite.
4. Compare the ignition data in microgravity to the 1-g data.

The present prototype is the final refinement of these original ideas and is shown in Figure 3. It consists of an aluminum chamber sealed at both ends. One end houses a high flux soldering lamp. At the other, a teflon support holds the sample in position along with a stand containing three thermocouples. A fourth thermocouple is positioned at the back face of

the sample to measure the fuel temperature.

Two valves are placed on either side of the support to purge the chamber with dry air since it was discovered that moisture content affected the sample's ignition time. Finally, a pressure transducer is included in the chamber to measure the pressure changes in the chamber.

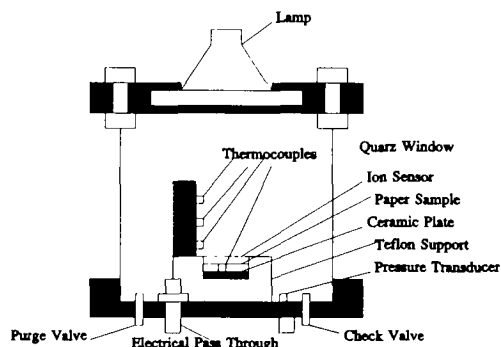


Figure 3

Review of Previous Projects

The microgravity ignition experiment has been an ongoing project, with the goal of producing flight-ready hardware for the GASCAN II project to be launched in 1995 on the Space Shuttle. The first Major Qualifying Project (MQP) on this project was completed in 1986. This project set the goals for this experiment and developed a prototype. In addition, the project group investigated various types of sensors to be used to gather data in the experiment (Blacker, et al., 1986).

Later MQPs focused on the material to be used as a test sample for the experiment. M. N. Forget, E. E. Mattor, and J.S. Siemasko (1990) eventually settled on National Bureau of Standards α -cellulose paper as the best material for the experiment. This paper was chosen for its relative consistency in properties and the relatively small amount of heat required to ignite a sample (Forget et al., 1990).

Previous projects also considered several different heat sources. An Argus type 44 infrared heat lamp with reflector was eventually chosen for the heat source in 1991. The 1991 group designed an alignment apparatus to verify the correct positioning of the lamp. This allowed the maximum flux to be placed on the target sample (Maranghides, Roy, 1991).

Experiment Sequence

The actual experiment consists of four chambers, three of which are ignition chambers containing paper samples. The fourth is a control chamber which only contains a teflon support and flux gauge to measure the energy output of the lamp. There is some concern that the lamp may be affected by the microgravity environment. Furthermore, as the experiment runs, the lamps may cause an excessive drain on the 24-volt current string, causing a drop in bulb output. The control chamber containing the flux gauge will be run once before and once after the experiment to determine if the bulb output has been affected.

The experiment begins with the control chamber being powered on. This chamber runs for five seconds during which the flux gauge measures the energy output of the lamp. After this canister shuts down, there will be a five second rest period for battery recovery. Then the first ignition chamber will run. This stays on until ignition is detected by an ion sensor or until thirty seconds have elapsed. In either case, the GASCan data-acquisition and control system will continue to sample data. An experimental timeline follows in Fig. 4.

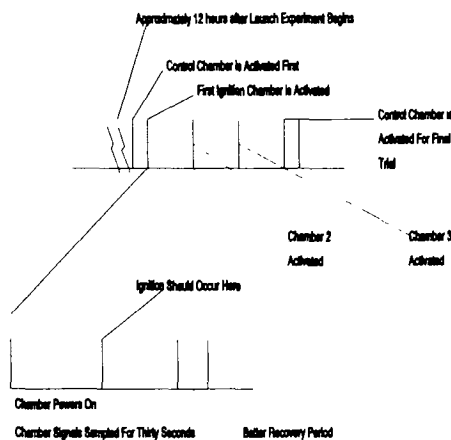


Figure 4

Instrumentation

Four different sensors are currently in use in the latest version of the microgravity ignition package. One of these is an ion sensor. This sensor is used to determine actual time of ignition. Mounted above the test sample are two stainless steel wires which form an open electronic circuit powered by 12 volts. When

the sample burns, it produces ions. These ions complete the circuit between the two wires allowing current to flow. Once the ion sensor circuit voltage has increased above a threshold value, the lamp is turned off. This also marks the ignition time.

Four thermocouples are used to measure temperatures within the chamber during the experiment. One is positioned at the sample backface and the other three are positioned on a stand at three different distances from the sample. These are K-type thermocouples with teflon insulation.

The thermocouples and the ion sensor wires are fed through a pressure sealed connector. The wires are crimped into connector pins for reliable connections. In an effort to reduce signal noise, shielded and teflon insulated thermocouple extension wires are used to connect the thermocouples in the chamber to the micro-controller.

Experiment Revisions

Problems with sealing the chamber resulted in a change in the endplates used to seal the canister. Due to the success of the design of the bottom endplates, the top endplates were changed to match them. Previously, four bolts were screwed into threaded holes in the second top plate to hold plate one and the lamp in place and to apply sufficient pressure to the gaskets which sealed the quartz window located below the lamp. However, due to problems with this configuration, the holes in the number two plate were drilled through. Nuts will be added to the end of the bolts for the top plates because of the greater amount of force that can be applied to tighten them and seal the chamber. Furthermore, use of epoxy to better hold the gaskets in place for the top end plates resulted in an excellent seal.

The seal of the bottom endplates was improved by moving the location of the check valve to a point closer to the teflon support. The check valve interfered with the proper seal of the endplate since it was located under the edge of the cylinder.

Finally, the issue of the thermocouple support had to be addressed. As designed by the 1992 MQP group, the support was only a temporary measure. It would not handle excessive vibrations. A new stand for the flight-ready canisters was developed. The previous configuration used a copper tube with two slots cut lengthwise in opposite sides. An arc shaped copper piece and a small plug with holes drilled through them were used to hold the thermocouples in place. This system had the benefit of being adjustable. However, the time has come to set the final heights of the thermocouples.

The new design also uses a length of copper tubing. However, instead of a long slot, single holes are drilled in the tube at a distance of 1/8". The thermocouples drawn through ceramic bead insulators are secured to the tube by set screws.

Test Results and Discussion

Several experiments were run to define the experiment's baseline characteristics at 1 g. The experiment controller was successfully used, after some modification, to acquire the data. These figures display the temperature changes in the canister with respect to ambient temperature. In 1992 it was suggested that this thermocouple be mounted against the surface of the paper. When this was done, the thermocouple tracked the temperature changes experienced by the paper before, during, and after ignition extremely well. Some changes to this thermocouple still have to be made, since the thermocouple still does not reach the peak temperature. Currently, the back of the paper is simply open to the air and the back face thermocouple is pressed against the paper. Figure 5 shows a comparison of the back face thermocouple readings from five consecutive experiments.

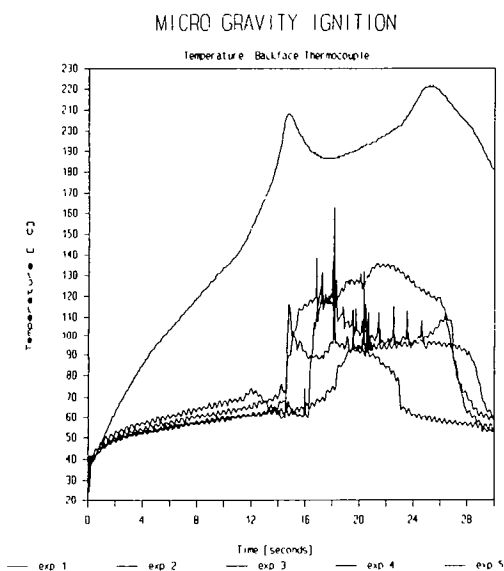


Figure 5

As can be seen, in four out of the five cases, a consistent ignition time can be pinpointed. Furthermore, in those four cases, the sample consistently begins to flame after the lamp has been shut off. The flaming is noted by the sudden rise in temperature and erratic fluctuations. The magnitude of the temperature, however, is low due to poor contact between the paper and the thermocouple. We

believe that the temperature response can be improved by improving contact between the back-face thermocouple and the sample. As the paper burns away from the thermocouple, a hole develops around the thermocouple and the temperature it senses begins to decline. This can be clearly seen in all but one of our trials. Experiment four seems to be an anomaly. We do not detect a distinct ignition of the paper from the temperature. Instead we have a gradual ramping up of the temperature of the sample. When the lamp is shut off, we have a slight decline, and then a slight upturn towards the end of the experiment. Finally, the thermocouple temperature curve drops dramatically, though still not as sharply as in the other four trials. This is a problem that should be investigated further.

Figures 6 through 11 show that the ion sensors register the ignition consistently within a 1.5 second window around the 14 second mark. In these figures, the ion sensor voltage is plotted against time. These plots show that the experiment is repeatable in several important aspects. The experiment consistently runs to conclusion at approximately the same time, even in the case of experiment four. The experiment achieves a consistent burn-through of the sample. The other sensors consistently show ignition at the same time the ion-sensor detects ignition. This is an important concern and is discussed later. The main problem with the data seems to be a problem in achieving consistent temperature measurements at the back face thermocouples. The back face thermocouple is one of our most important measurements, since it tells us what temperature the paper sample experiences. It is critical that we achieve a consistent means of contact with the sample that insures consistent data; otherwise a great deal of data may be lost.

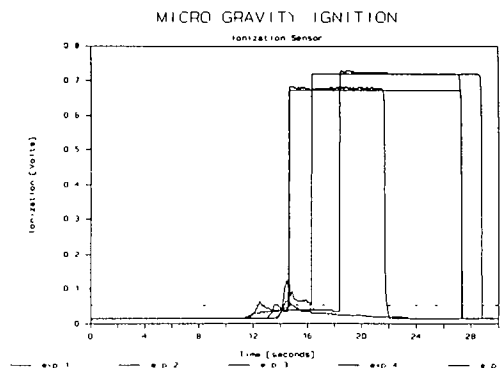


Figure 6

Figure 6 shows some data that may be of importance in setting the final ignition detection

scheme. The present scheme relies solely on the voltage across the ion sensor. If this voltage reaches a threshold value, then the micro-controller turns the lamp off. Several of the MITRE Corporation critical design review team led by Lawrence R. Moschini have expressed concern that pyrolysis may become a more important factor under low-g conditions and may result in a premature shut-down of the lamp. A second, though lesser, concern is that the lamp may remain on longer than necessary if combustion products don't reach the ion sensor soon enough. Therefore MITRE has asked that alternative ignition detection schemes be examined. One such approach involves the use of chamber pressure rise. There is a definite peak when ignition is reached in all five cases as can be seen in Figure 7. When ignition occurs, a definite pressure wave is created. This effect can be measured at the pressure transducer and is a secondary means of detecting time to ignition. This wave occurs very nearly simultaneously with the ion sensor's detection of ignition in our 1-g trails, as can be seen in the plots. This issue should be examined more closely by the next project team.

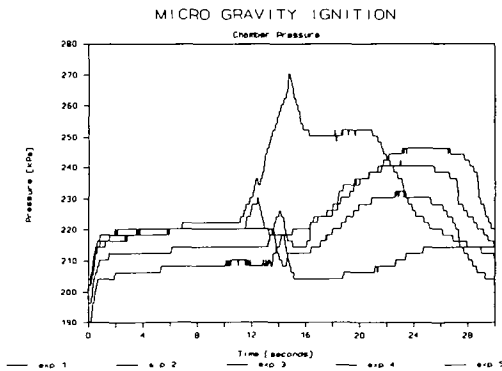


Figure 7

Our final data in figures 8-12 show the temperature data plots for each of the five experiments. These plots are used to compare data from different experiments.

Conclusion

The determination of time to ignition using the ion sensor is reliable and to some extent repeatable. The pressure wave generated by ignition is a weak signal and although a good indicator, is difficult to use as primary ignition detection, especially to effect a lamp shutoff. However, it can be used to check the ion sensor performance for the microgravity experiment. Further experiments may result in switching to a modified scheme using either the pressure transducer or ion sensor signals to determine ignition and cause

a lamp shutoff. The back-face temperature measurement needs improvement.

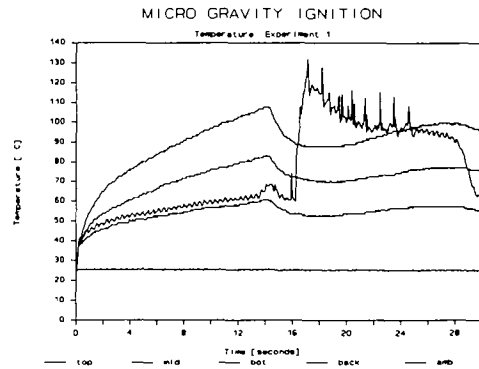


Figure 8

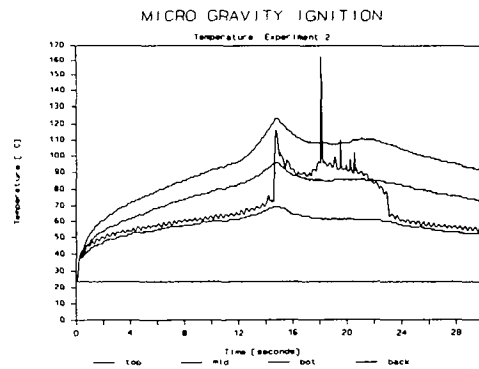


Figure 9

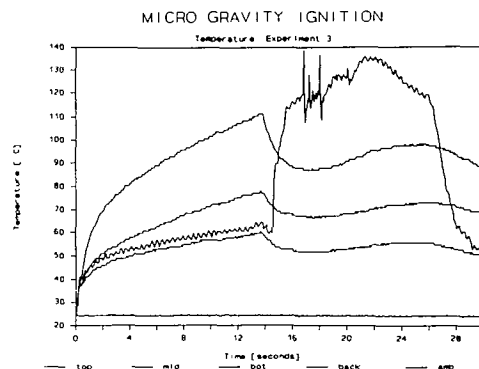


Figure 10

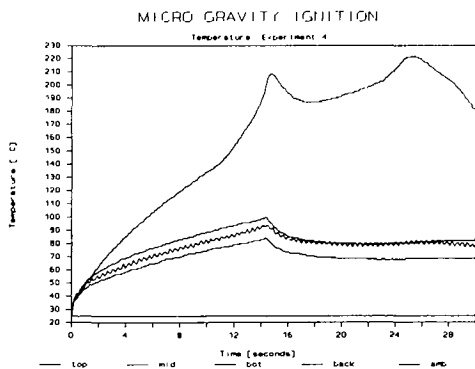


Figure 11

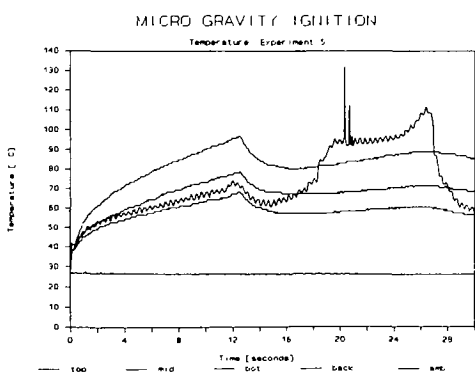


Figure 12

References

Blacker, P. L.; Dilorenzo, J.E.; Tucker, J.H.; Vlangas, C.P., Shuttle Project II-Micro Gravity Ignition, Worcester Polytechnic Institute, Major Qualifying Project, 1988.

Buckley, R.F.; Rousseau, M.P., Microgravity Combustion, Worcester Polytechnic Institute, Major Qualifying Project, 1987.

Crochiere, J.F.; Sickles, G.D.; Tondora, C.M., Micro-Gravity Combustion WPI/Mitre GASCAN II, Worcester Polytechnic Institute, Major Qualifying Project, 1987.

Enos, J.J., Shuttle Project II-Micro Gravity Ignition, Worcester Polytechnic Institute, Major Qualifying Project, 1988.

Forget, M.N.; Mattor, Ethan E.; Siemasko, J.S., Micro Gravity Ignition Experiment, Worcester Polytechnic Institute, Major Qualifying Project, 1990.

Goldmeier, J., Jumper, G., Motevalli, V., and Haghdoost, M., "Determination of the Natural Convection Coefficient in Low-Gravity", 30th Aerospace Sciences Meeting & Exhibit, Jan. 6-9, 1992, AIAA 92-0712, Reno, Nevada.

Goodspeed, C.G.; Hall, J.G.; Maylott, D.J.; Motyka, M.M.; Ryder, P.A., Effects of Micro-G on Ignition Energy: Prototype, Worcester Polytechnic Institute, Major Qualifying Project, 1986.

Haghdoost, M.H., Experimental Evaluation of Transient Natural Convection Coefficient, Worcester Polytechnic Institute, Master's Thesis, 1991.

Maranghides, A.; Roy, P. Micro-Gravity Ignition Report, Worcester Polytechnic Institute, Major Qualifying Project, 1991.

Garrant, K.; Lusk, A., Microgravity Ignition, Worcester Polytechnic Institute, Major Qualifying Project, 1992.